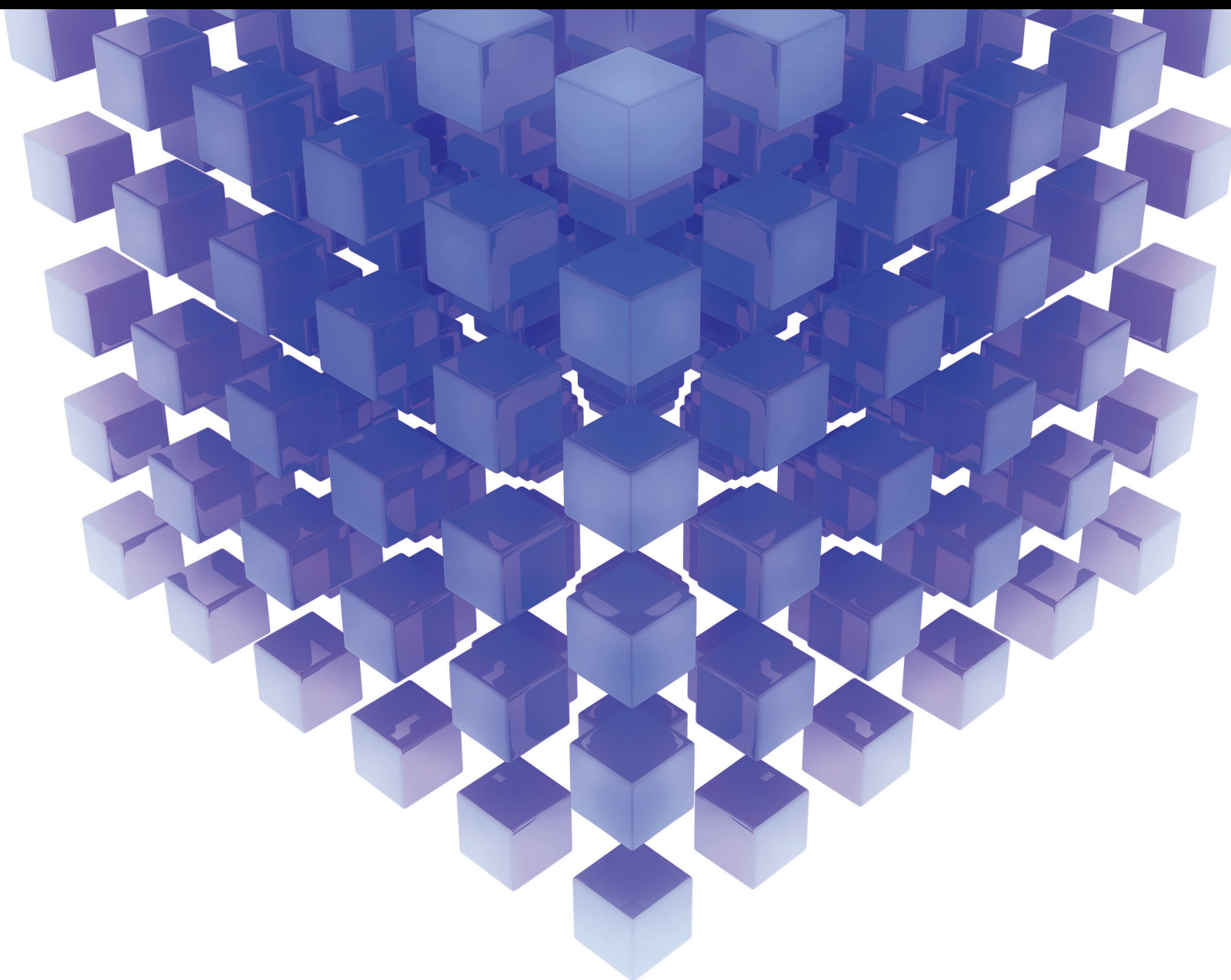


Mathematical Problems in Engineering

New Trends in Networked Control of Complex Dynamic Systems: Theories and Applications

Guest Editors: Huaicheng Yan, Xudong Zhao, Hak-Keung Lam, Huiping Li, Yang Shi, and Lixian Zhang





New Trends in Networked Control of Complex Dynamic Systems: Theories and Applications

Mathematical Problems in Engineering

New Trends in Networked Control of Complex Dynamic Systems: Theories and Applications

Guest Editors: Huaicheng Yan, Xudong Zhao, Hak-Keung Lam, Huiping Li, Yang Shi, and Lixian Zhang



Copyright © 2014 Hindawi Publishing Corporation. All rights reserved.

This is a special issue published in “Mathematical Problems in Engineering.” All articles are open access articles distributed under the Creative Commons Attribution License, which permits unrestricted use, distribution, and reproduction in any medium, provided the original work is properly cited.

Editorial Board

- Mohamed Abd El Aziz, Egypt
Eihab M. Abdel-Rahman, Canada
Rashid K. Abu Al-Rub, USA
Sarp Adali, South Africa
Salvatore Alfonzetti, Italy
Igor Andrianov, Germany
Sebastian Anita, Romania
W. Assawinchaichote, Thailand
Er-wei Bai, USA
Ezzat G. Bakhoum, USA
José Manoel Balthazar, Brazil
Rasajit Kumar Bera, India
Jonathan N. Blakely, USA
Stefano Boccaletti, Spain
Stephane P. A. Bordas, USA
Daniela Boso, Italy
M. Boutayeb, France
Michael J. Brennan, UK
Salvatore Caddemi, Italy
Piermarco Cannarsa, Italy
Jose E. Capilla, Spain
Carlo Cattani, Italy
Marcelo Cavalcanti, Brazil
Diego J. Celentano, Chile
Mohammed Chadli, France
Arindam Chakraborty, USA
Yong-Kui Chang, China
Michael J. Chappell, UK
Kui Fu Chen, China
Kue-Hong Chen, Taiwan
Xinkai Chen, Japan
Jyh-Horng Chou, Taiwan
Slim Choura, Tunisia
Cesar Cruz-Hernandez, Mexico
Erik Cuevas, Mexico
Swagatam Das, India
Filippo de Monte, Italy
Yannis Dimakopoulos, Greece
Baocang Ding, China
Joao B. R. Do Val, Brazil
Daoyi Dong, Australia
B. Dubey, India
Horst Ecker, Austria
M. Onder Efe, Turkey
Elmetwally Elabbasy, Egypt
Alex Elías-Zúñiga, Mexico
Anders Eriksson, Sweden
Vedat S. Erturk, Turkey
Moez Feki, Tunisia
Ricardo Femat, Mexico
Robertt Fontes Valente, Portugal
Claudio Fuerte-Esquivel, Mexico
Zoran Gajic, USA
Ugo Galvanetto, Italy
Xin-Lin Gao, USA
Furong Gao, Hong Kong
Behrouz Gatmiri, Iran
Oleg V. Gendelman, Israel
Paulo Batista Gonçalves, Brazil
Oded Gottlieb, Israel
Fabrizio Greco, Italy
Quang Phuc Ha, Australia
Tony Sheu Wen Hann, Taiwan
Thomas Hanne, Switzerland
Katica R. Hedrih, Serbia
M. I. Herreros, Spain
Wei-Chiang Hong, Taiwan
Jaromir Horacek, Czech Republic
Gordon Huang, Canada
Huabing Huang, China
Chuangxia Huang, China
Yi Feng Hung, Taiwan
Hai-Feng Huo, China
Asier Ibeas, Spain
Anuar Ishak, Malaysia
Reza Jazar, Australia
Zhijian Ji, China
Jun Jiang, China
J. J. Judice, Portugal
Tadeusz Kaczorek, Poland
Tamas Kalmar-Nagy, USA
Tomasz Kapitaniak, Poland
Hamid R. Karimi, Norway
Metin O. Kaya, Turkey
Farzad Khani, Iran
Ren-Jieh Kuo, Taiwan
Jurgen Kurths, Germany
Claude Lamarque, France
Usik Lee, Korea
Marek Lefik, Poland
Stefano Lenci, Italy
Roman Lewandowski, Poland
Shihua Li, China
Ming Li, China
S. Li, Canada
Jian Li, China
Teh-Lu Liao, Taiwan
Panos Liatsis, UK
Kim Meow Liew, Hong Kong
Yi-Kuei Lin, Taiwan
Shueei M. Lin, Taiwan
Jui-Sheng Lin, Taiwan
Wanquan Liu, Australia
Bin Liu, Australia
Yuji Liu, China
Paolo Lonetti, Italy
Vassilios C. Loukopoulos, Greece
Chien-Yu Lu, Taiwan
Junguo Lu, China
Alexei Mailybaev, Brazil
Manoranjan K. Maiti, India
Oluwole Daniel Makinde, South Africa
Rafael Martínez-Guerra, Mexico
Driss Mehdi, France
Roderick Melnik, Canada
Xinzhu Meng, China
Jose Merodio, Spain
Yuri Vladimirovich Mikhlin, Ukraine
Gradimir Milovanović, Serbia
Ebrahim Momoniat, South Africa
Trung Nguyen Thoi, Vietnam
Hung Nguyen-Xuan, Vietnam
Ben T. Nohara, Japan
Sotiris K. Ntouyas, Greece
Claudio Padra, Argentina
Bijaya Ketan Panigrahi, India
Francesco Pellicano, Italy
Matjaž Perc, Slovenia
Vu Ngoc Phat, Vietnam
Maria do Rosário Pinho, Portugal
Seppo Pohjolainen, Finland
Stanislav Potapenko, Canada
Sergio Preidikman, USA
Carsten Proppe, Germany
Hector Puebla, Mexico

Justo Puerto, Spain
Dane Quinn, USA
Kumbakonam Rajagopal, USA
Gianluca Ranzi, Australia
Sivaguru Ravindran, USA
G. Rega, Italy
Pedro Ribeiro, Portugal
J. Rodellar, Spain
Rosana Rodriguez-Lopez, Spain
Alejandro J. Rodriguez-Luis, Spain
Carla Roque, Portugal
Rubén Ruiz García, Spain
Manouchehr Salehi, Iran
Miguel A. F. Sanjuán, Spain
Ilmar Ferreira Santos, Denmark
Nickolas S. Sapidis, Greece
Evangelos J. Sapountzakis, Greece
Bozidar Sarler, Slovenia
Andrey V. Savkin, Australia
Massimo Scalia, Italy
Mohamed A. Seddeek, Egypt
Leonid Shaikhet, Ukraine
Cheng Shao, China
Bo Shen, Germany
Jian-Jun Shu, Singapore
Zhan Shu, UK
Dan Simon, USA
Luciano Simoni, Italy

Grigori M. Sisoiev, UK
Christos H. Skiadas, Greece
Davide Spinello, Canada
Sri Sridharan, USA
Hari M. Srivastava, Canada
Rolf Stenberg, Finland
Changyin Sun, China
Xi-Ming Sun, China
Jitao Sun, China
Andrzej Swierniak, Poland
Yang Tang, Germany
Allen Tannenbaum, USA
Cristian Toma, Romania
Gerard Olivar Tost, Colombia
Irina N. Trendafilova, UK
Alberto Trevisani, Italy
Jung-Fa Tsai, Taiwan
Kuppapalle Vajravelu, USA
Victoria Vampa, Argentina
Josep Vehi, Spain
Stefano Vidoli, Italy
Yijing Wang, China
Cheng C. Wang, Taiwan
Dan Wang, China
Xiaojun Wang, China
Qing-Wen Wang, China
Yongqi Wang, Germany
Moran Wang, China

Youqing Wang, China
Gerhard-Wilhelm Weber, Turkey
Jeroen Witteveen, The Netherlands
Kwok-Wo Wong, Hong Kong
Ligang Wu, China
Zhengguang Wu, China
Gongnan Xie, China
Wang Xing-yuan, China
Xi Frank Xu, China
Xuping Xu, USA
Jun-Juh Yan, Taiwan
Xing-Gang Yan, UK
Suh-Yuh Yang, Taiwan
Mahmoud T. Yassen, Egypt
Mohammad I. Younis, USA
Bo Yu, China
Huang Yuan, Germany
S.P. Yung, Hong Kong
Ion Zaballa, Spain
Ashraf M. Zenkour, Saudi Arabia
Jianming Zhan, China
Yingwei Zhang, China
Xu Zhang, China
Lu Zhen, China
Liancun Zheng, China
Jian Guo Zhou, UK
Zexuan Zhu, China
Mustapha Zidi, France

Contents

New Trends in Networked Control of Complex Dynamic Systems: Theories and Applications,
Huaicheng Yan, Xudong Zhao, Hak-Keung Lam, Huiping Li, Yang Shi, and Lixian Zhang
Volume 2014, Article ID 316395, 5 pages

Event-Triggered Average Consensus for Multiagent Systems with Time-Varying Delay, Zhaoxia Wang,
Minrui Fei, Dajun Du, and Lili Shang
Volume 2014, Article ID 131586, 14 pages

Guaranteed Cost Control for Multirate Networked Control Systems with Both Time-Delay and Packet-Dropout, Qixin Zhu, Binbin Xie, and Yonghong Zhu
Volume 2014, Article ID 637329, 9 pages

The Research on Modeling and Simulation of TFE Polymerization Process, Jing Gao Sun and Qin Cao
Volume 2014, Article ID 365486, 10 pages

Monitoring of Multimode Processes Based on Quality-Related Common Subspace Separation,
Yunpeng Fan, Shipeng Li, and Yingwei Zhang
Volume 2014, Article ID 487582, 7 pages

H_∞ Control of Supply Chain Based on Switched Model of Stock Level,
Junzhi Luo and Wanly Yang
Volume 2014, Article ID 464256, 8 pages

Information Exchange rather than Topology Awareness: Cooperation between P2P Overlay and Traffic Engineering, Jia Zhao, Jianfeng Guan, Changqiao Xu, Wei Su, and Hongke Zhang
Volume 2014, Article ID 792563, 12 pages

An Overview of Networked Control of Complex Dynamic Systems, Huaicheng Yan, Sheng Yan,
Hao Zhang, and Xudong Zhao
Volume 2014, Article ID 794096, 10 pages

Design and Stability Analysis of Uncertain Networked Predictive Control Systems with Multiple Forward Channels, Hongbo Song
Volume 2014, Article ID 403137, 11 pages

Fault Detection for Network Control Systems with Multiple Communication Delays and Stochastic Missing Measurements, Jie Zhang, Ming Lyu, Hamid Reza Karimi, Jian Zuo, and Yuming Bo
Volume 2014, Article ID 690461, 9 pages

Impact of Social Network and Business Model on Innovation Diffusion of Electric Vehicles in China,
D. Y. Kong and X. H. Bi
Volume 2014, Article ID 230765, 7 pages

A Novel Mathematical Formula for Retrieval Algorithm, Yuping Qin, Hamid Reza Karimi, Aihua Zhang,
and Qiangkui Leng
Volume 2014, Article ID 859157, 5 pages

Coarse-Grain QoS-Aware Dynamic Instance Provisioning for Interactive Workload in the Cloud,

Jianxiong Wan, Limin Liu, Jie Lv, and Zhiwei Xu

Volume 2014, Article ID 215016, 11 pages

A Bayesian Network Method for Quantitative Evaluation of Defects in Multilayered Structures from

Eddy Current NDT Signals, Bo Ye, Hongchun Shu, Min Cao, Fang Zeng, Gefei Qiu, Jun Dong,

Wenying Zhang, and Jieshan Shan

Volume 2014, Article ID 405707, 15 pages

Multiagent and Particle Swarm Optimization for Ship Integrated Power System Network

Reconfiguration, Zheng Wang, Li Xia, Yongji Wang, and Lei Liu

Volume 2014, Article ID 280345, 7 pages

Output-Feedback Controller Design of a Wireless Networked Control System with Packet Loss and

Time Delay, Zhen Hong, JinFeng Gao, and Ning Wang

Volume 2014, Article ID 206475, 7 pages

Phoenix: A Collaborative Location-Based Notification System for Mobile Networks, Yongping Xiong,

Yubo Deng, Wendong Wang, and Jian Ma

Volume 2014, Article ID 307498, 12 pages

Group Synchronization of Nonlinear Complex Dynamics Networks with Sampled Data, Man Li, Bo Liu,

Yuqing Zhu, Lijun Wang, and Mei Zhou

Volume 2014, Article ID 142061, 8 pages

An Improved Car-Following Model in Vehicle Networking Based on Network Control,

D. Y. Kong and H. Y. Xu

Volume 2014, Article ID 857965, 6 pages

Optimal Placement of Actors in WSAWs Based on Imposed Delay Constraints, Chunxi Yang, Xinyu Wu,

Jian Huang, and Lingyun Huang

Volume 2014, Article ID 410363, 7 pages

Design of Attitude Control System for UAV Based on Feedback Linearization and Adaptive Control,

Wenya Zhou, Kuilong Yin, Rui Wang, and Yue-E Wang

Volume 2014, Article ID 492680, 8 pages

Nonlinear Disturbance Observer Based Robust Tracking Control of Pneumatic Muscle,

Youssif Mohamed Toum Elobaid, Jain Huang, and Yongji Wang

Volume 2014, Article ID 872093, 8 pages

Fast Consensus Tracking of Multiagent Systems with Diverse Communication Delays and Input Delays,

Chun-xi Yang, Wei-xing Hong, Ling-yun Huang, and Hua Wang

Volume 2014, Article ID 253806, 10 pages

Robust Decentralized Adaptive Neural Control for a Class of Nonaffine Nonlinear Large-Scale Systems

with Unknown Dead Zones, Huanqing Wang, Qi Zhou, Xuebo Yang, and Hamid Reza Karimi

Volume 2014, Article ID 841306, 10 pages

Fundamental Issues and Prospective Directions in Networked Multirate Control Systems,

Wang Zhiwen and Guo Ge

Volume 2014, Article ID 513506, 10 pages

Fault Diagnosis System Based on Multiagent Technique for Ship Power System, Zheng Wang, Li Xia,

Yongji Wang, and Lei Liu

Volume 2014, Article ID 370246, 7 pages

Robust H_∞ Filtering for Networked Control Systems with Random Sensor Delay, Shenping Xiao,

Liyan Wang, Hongbing Zeng, Lingshuang Kong, and Bin Qin

Volume 2014, Article ID 710952, 7 pages

Steady Modeling for an Ammonia Synthesis Reactor Based on a Novel CDEAS-LS-SVM Model,

Zhuoqian Liu, Lingbo Zhang, Wei Xu, and Xingsheng Gu

Volume 2014, Article ID 168371, 18 pages

Identification of LTI Time-Delay Systems with Missing Output Data Using GEM Algorithm,

Xianqiang Yang and Hamid Reza Karimi

Volume 2014, Article ID 242145, 8 pages

Eddy Current Inversion Models for Estimating Dimensions of Defects in Multilayered Structures, Bo Ye,

Jun Dong, Gefei Qiu, Siqu Li, Fang Zeng, Tanghua Yang, Biao Bai, and Zhangzhou He

Volume 2014, Article ID 649608, 11 pages

A Local and Global Search Combined Particle Swarm Optimization Algorithm and Its Convergence Analysis, Weitian Lin, Zhigang Lian, Xingsheng Gu, and Bin Jiao

Volume 2014, Article ID 905712, 11 pages

Cultural-Based Genetic Tabu Algorithm for Multiobjective Job Shop Scheduling,

Yuzhen Yang and Xingsheng Gu

Volume 2014, Article ID 230719, 14 pages

Switched Quantization Level Control of Networked Control Systems with Packet Dropouts, Shuo Wang,

Mei Yu, Hangfei Wang, and Wen Tan

Volume 2014, Article ID 890543, 8 pages

Event-Triggered H_∞ Control for Networked Control Systems with Time-Varying Delay, Huaicheng Yan,

Sheng Yan, Hao Zhang, and Hongbo Shi

Volume 2014, Article ID 874823, 7 pages

Optimal Distributed Controller Design for Nonlinear Coupled Dynamical Networks, Hao Zhang,

Huaicheng Yan, and Qijun Chen

Volume 2014, Article ID 790643, 7 pages

Metric Learning Method Aided Data-Driven Design of Fault Detection Systems, Guoyang Yan,

Jiangyuan Mei, Shen Yin, and Hamid Reza Karimi

Volume 2014, Article ID 974758, 9 pages

A New Mechanism for Network Monitoring and Shielding in Wireless LAN, Jiujun Cheng, Liufei Hu, Junjun Liu, Qingyang Zhang, and Chendan Yan
Volume 2014, Article ID 620926, 8 pages

Residual Generator-Based Controller Design via Process Measurements, Zenghui Huang, Shen Yin, and Hamid Reza Karimi
Volume 2014, Article ID 290371, 8 pages

Design of a TFT-LCD Based Digital Automobile Instrument, Yunsong Xu, Shen Yin, Jinyong Yu, and Hamid Reza Karimi
Volume 2014, Article ID 549790, 8 pages

Distributed Multitarget Probabilistic Coverage Control Algorithm for Wireless Sensor Networks, Ying Tian, Yang Ou, Hamid Reza Karimi, Yan Tao Liu, and Jian Qun Han
Volume 2014, Article ID 421753, 8 pages

The Finding and Dynamic Detection of Opinion Leaders in Social Network, Baocheng Huang, Guang Yu, and Hamid Reza Karimi
Volume 2014, Article ID 328407, 7 pages

A Discrete Group Search Optimizer for Hybrid Flowshop Scheduling Problem with Random Breakdown, Zhe Cui and Xingsheng Gu
Volume 2014, Article ID 621393, 11 pages

Sampling Based Average Classifier Fusion, Jian Hou, Wei-Xue Liu, and Hamid Reza Karimi
Volume 2014, Article ID 369613, 6 pages

Effects of Surfactants on the Performance of CeO₂ Humidity Sensor, Chunjie Wang, Aihua Zhang, and Hamid Reza Karimi
Volume 2014, Article ID 723050, 6 pages

A New Three-Dimensional Indoor Positioning Mechanism Based on Wireless LAN, Jiujun Cheng, Yueqiao Cai, Qingyang Zhang, Junlu Cheng, and Chendan Yan
Volume 2014, Article ID 862347, 7 pages

Impulsive Consensus Tracking of Multiagent Systems with Quantization and Input Delays Using Position-Only Information, Hong Zhou, Yu-Zhen Qin, Kuo Feng, Wen-Shan Hu, and Zhi-Wei Liu
Volume 2014, Article ID 781048, 10 pages

Bayes Network Based Collaborating Control Algorithm in Active Multicamera Network with Applications to Object Tracking, Rui Zhao, Zhihua Wei, Yan Wu, Cairong Zhao, and Duoqian Miao
Volume 2014, Article ID 219367, 8 pages

Attitude Stabilization Control of a Quadrotor UAV by Using Backstepping Approach, Xing Huo, Mingyi Huo, and Hamid Reza Karimi
Volume 2014, Article ID 749803, 9 pages

New Strategy for Analog Circuit Performance Evaluation under Disturbance and Fault Value,
Aihua Zhang, Yongchao Wang, Chen Chen, and Hamid Reza Karimi
Volume 2014, Article ID 728201, 8 pages

Whether and How to Select Inertia and Acceleration of Discrete Particle Swarm Optimization Algorithm: A Study on Channel Assignment, Min Jin, Xiangyuan Zhong, and Xudong Zhao
Volume 2014, Article ID 758906, 6 pages

State Feedback Control for Stochastic Feedforward Nonlinear Systems, Liang Liu and Ming Gao
Volume 2013, Article ID 908459, 6 pages

Editorial

New Trends in Networked Control of Complex Dynamic Systems: Theories and Applications

**Huaicheng Yan,^{1,2} Xudong Zhao,³ Hak-Keung Lam,⁴
Huiping Li,⁵ Yang Shi,⁵ and Lixian Zhang⁶**

¹ Key Laboratory of Advanced Control and Optimization for Chemical Processes of Ministry of Education, Shanghai 200237, China

² School of Information Science and Engineering, East China University of Science and Technology, Shanghai 200237, China

³ College of Information Science and Technology, Bohai University, Jinzhou 121013, China

⁴ Centre for Robotics Research, King's College London, UK

⁵ Department of Mechanical Engineering, University of Victoria, Victoria, BC, Canada

⁶ Research Institute of Intelligent Control and Systems, Harbin Institute of Technology, Harbin 150080, China

Correspondence should be addressed to Huaicheng Yan; hcyan@ecust.edu.cn

Received 12 May 2014; Accepted 12 May 2014; Published 4 June 2014

Copyright © 2014 Huaicheng Yan et al. This is an open access article distributed under the Creative Commons Attribution License, which permits unrestricted use, distribution, and reproduction in any medium, provided the original work is properly cited.

In recent years, networked control systems (NCSs) have been extensively studied in both academy and industry and used in many fields, such as telerobotics, smart grids, intelligent transportation systems, and even in medical, military, and aerospace applications. NCSs offer great advantages, such as low cost, high reliability, simple installation and maintenance, and reduced weight and power requirements. In the meantime, the common shortcomings of the communication networks, such as transmission delays, packets drops and disorder, and data quantization, also appeared in the loops of the networked systems. During past decade, plenty of studies have been carried out in the literature to address the network-induced problems for given dynamic systems that are relatively simple. However, more challenging mathematical problems such as network-based control of more complex dynamics, including time delay, parameter variations, uncertainties, and nonlinearities, are still largely open and necessitate further investigations to enable wider and more successful applications. This special issue aims to provide a timely discussion on the trends and challenges of networked control of complex dynamics systems. Both theoretical and application-oriented papers are sought for, addressing the issues and mathematical techniques of network-based control, sensing, multiagent control of complex dynamic systems, and so forth.

This special issue contains fifty papers, the contents of which are summarized as follows.

“Identification of LTI time-delay systems with missing output data using GEM algorithm” by X. Yang and H. R. Karimi considers the parameter estimation for linear time-invariant (LTI) systems in an input-output setting with output error (OE) time-delay model structure. The problem of missing data is commonly experienced in industry due to irregular sampling, sensor failure, data deletion in data pre-processing, network transmission fault, and so forth. To deal with the identification of LTI systems with time-delay in incomplete-data problem, the generalized expectation-maximization (GEM) algorithm is adopted to estimate the model parameters and the time-delay simultaneously.

“Guaranteed cost control for multirate networked control systems with both time-delay and packet-dropout” by Q. Zhu et al. presents a new stabilization method for multirate NCSs. A multirate NCSs with simultaneous consideration time-delay and packet-dropout is modeled as a time-varying sampling system with time-delay. The proposed Lyapunov function decreases at each input signal updating point, which is largely ignored in prior works. Sufficient condition for the stochastic mean-square stability of the multirate NCSs is given, and the cost function value is less than a bound.

“Fault detection for network control systems with multiple communication delays and stochastic missing measurements” by J. Zhang et al. considers the fault detection problem for a class of network control systems (NCSs) with multiple communication delays and stochastic missing measurements.

The missing measurement phenomenon occurs in a random way and the occurrence probability for each measurement output is governed by an individual random variable. Besides, the multiple communication delay phenomenon reflects that networked control systems have different communication delays when the signals are transferred via different channels.

“Effects of surfactants on the performance of CeO₂ humidity sensor” by C. Wang et al. In this paper, nanosized CeO₂ powders were synthesized via hydrothermal method with different types of surfactants (polyethylene glycol (PEG), cetyl trimethyl ammonium bromide (CTAB), and sodium dodecylbenzene sulfonate (SDBS)). X-ray diffraction, Raman spectroscopy, and transmission electron microscopy were utilized to characterize the phase structures and morphologies of the products. The sample with CTAB as surfactant (CeO₂-C) has the largest specific surface area and the smallest particle size among these three samples. The humidity sensor fabricated by CeO₂-C shows higher performance than those used in the other two samples.

“Attitude stabilization control of a quadrotor UAV by using backstepping approach” by X. Huo et al. investigates the modeling and attitude stabilization control problems of a four-rotor vertical take-off and landing unmanned air vehicle (UAV) known as the quadrotor. The quadrotor’s attitude is represented by the unit-quaternion rather than Euler angles to avoid singularity problem. Taking dynamical behavior of motors into consideration and ignoring aerodynamic effect, a nonlinear controller is developed to stabilize the attitude. The control design is accomplished by using backstepping control technique.

“Optimal distributed controller design for nonlinear coupled dynamical networks” by H. Zhang et al. presents the optimal distributed impulsive controller design for globally exponential synchronization of nonlinear dynamical networks with coupling delay. By the Lyapunov-Razumikhin method, a novel criterion is proposed to guarantee the global exponential synchronization of the coupled delayed network with distributed impulsive control in terms of matrix inequalities. The sum of coupling strength of the distributed impulsive control is minimized to save the control effort.

“A novel mathematical formula for retrieval algorithm” by Y. Qin et al. proposes a method to retrieve mathematical formula in LaTeX documents. Firstly, it represents the retrieved mathematical formula by binary tree according to its LaTeX description, normalizing the structure of the binary tree and obtaining the structure code. And then it searches the mathematical formula table that is named by the structure code and the formulate elements of the first two levels of the binary tree in the mathematical formula database.

“Event-triggered H_∞ control for networked control systems with time-varying delay” by H. Yan considers the H_∞ controller design problem for event-triggered networked control systems (NCSs), where the next task’s release time and finishing time are predicted based on the sampled states. A new model of NCSs that involves the network conditions, state, and event-triggered communication strategy is proposed. Based on this model, some novel criteria for the asymptotic stability analysis and H_∞ state feedback controller design of the event-triggered NCSs with time-varying delay

are established to guarantee a prescribed H_∞ disturbance rejection attenuation level.

“State feedback control for stochastic feedforward nonlinear systems” by L. Liu and M. Gao considers the state feedback stabilization problem for a class of stochastic feedforward nonlinear systems. By using the homogeneous domination approach, a state feedback controller is constructed to render the closed-loop system globally asymptotically stable in probability.

“Output-feedback controller design of a wireless networked control system with packet loss and time delay” by Z. Hong et al. investigates the problem of modeling and stabilization of a wireless networked control system (NCS) with both time-varying delay and packet-dropout. And the time-varying delay can be more or less than one sampling period. The wireless NCS is modeled as an asynchronous dynamic system (ADS) with three subsystems. Sufficient condition of the closed-loop NCS to be stable is obtained by using the ADS approach.

“Residual generator-based controller design via process measurements” by Z. Huang et al. proposes a scheme which embeds a residual generator into control loop based on realization of the Youla parameterization for advanced controller design. Basic idea of the proposed scheme is constructing the residual generator by using the solution of the Luenberger equations as well as the well-established relationship between diagnosis observer (DO) and the parity vector. And the core of the above idea is straightly using the process measurements to obtain the parity space based on the Subspace Identification Method (SIM), rather than establishing the system model.

“Design of a TFT-LCD based digital automobile instrument” by Y. Xu et al. proposes a design of a TFT-LCD based automobile instrument. With a 7-inch TFT-LCD and the 32-bit microcontroller MB91F599, the instrument could process various information generated by other electronic control units (ECUs) of a vehicle and display valuable driving parameters on the 7-inch TFT-LCD. The function of aided parking is also provided by the instrument. The significant contribution is to point out basic principles to be obeyed in circuits designing under on-board environment.

“Metric learning method aided data-driven design of fault detection systems” by G. Yan et al. proposes a metric learning based fault detection framework in fault detection. Meanwhile, a novel feature extraction method based on wavelet transform is used to obtain the feature vector from detection signals.

“Sampling based Average Classifier Fusion” by J. Hou et al. empirically investigates the behavior of soft labels and classifiers in average fusion and finds that by proper selection of soft labels and classifiers, the average fusion performance can be evidently improved. This result presents selection based average fusion as a better baseline, that is, a newly proposed classifier fusion algorithm should at least perform better than this baseline in order to demonstrate its effectiveness.

“Distributed multitarget probabilistic coverage control algorithm for wireless sensor networks” by Y. Tian et al. investigates the problem of multitarget coverage based on probabilistic detection model and proposes a distributed

probabilistic coverage algorithm for the WSN with multiple static targets. This algorithm is robust to the change of network size, and all the targets can be monitored at the requirement of network coverage probability.

“*The Finding and dynamic detection of opinion leaders in social network*” by B. Huang et al. presents a dynamic opinion rank algorithm to find out the opinion leaders in Chinese news. The proposed network model explicitly takes explicit and implicit links into account. Moreover, the proposed algorithm is able to conclude that the most influential comments and the opinion leaders were time-varying.

“*New strategy for analog circuit performance evaluation under disturbance and fault value*” by A. Zhang et al. proposes a novel strategy for analog circuit online performance evaluation based on fuzzy learning and double weighted support vector machine (DWMK-FSVM). First, the double weighted support vector regression machine is employed to be the indirect evaluation means, relied on the college analog electronic technology experiment to evaluate analog circuit. Second, the superiority of fuzzy learning also is addressed to realize active suppression to the fault values and disturbance parameters. Moreover, the multikernel RBF is employed by support vector regression machine to realize more flexibility online such as the bandwidths tuning.

“*Whether and how to select inertia and acceleration of discrete particle swarm optimization algorithm: a study on channel assignment*” by M. Jin et al. proposes a strategy scheme and the selection of inertia and acceleration on whether the inertia section should be abandoned and how to select the appropriate acceleration in order for DPSO to show the best convergence performance. They are verified to have the advantage to channel assignment in three respects of convergence rate, convergence speed, and the independency on the quality of initial solution.

In “*New strategy for analog circuit performance evaluation under disturbance and fault value*” by A. Zhang et al., the authors design a peer-to-peer location based notification system Phoenix and focus on the design of the key component message controller. The results show Phoenix can satisfy the user-specified notification performance with the low transmission overhead.

In “*Coarse-grain QoS-aware dynamic instance provisioning for interactive workload in the cloud*” by J. Wan et al., The authors investigated the coarse-grain QoS-aware dynamic instance provisioning problem for interactive workload in the cloud computing. For self-similar traffic in internet they studied the percentile delay constraint. To solve the problem, they proposed a dynamic instance provisioning algorithm and a learning algorithm to design the instance rental policy. The effectiveness of the algorithms was verified by simulations.

“*Fast consensus tracking of multiagent systems with diverse communication delays and input delays*” by C.-X. Yang et al. investigates the consensus tracking problem for discrete-time multiagent systems with input and communication delay. A sufficient condition is obtained over a directed graph based on the frequency-domain analysis. A fast decentralized consensus tracking conditions based on increment PID algorithm is discussed for improving convergence speed of the multiagent systems.

“*Optimal placement of actors in WSNs based on imposed delay constraints*” by C. Yang et al. The authors find a method to determine the accurate number of actors which enables them to receive data and take actions in an imposed time-delay. The k -MinTE and the k -MaxTE clustering algorithm are proposed to form the minimum and maximum size of cluster, respectively. In those clustering algorithms, actors are deployed in such a way that sensors could route data to actors within k hops. Then, clusters are arranged by the regular hexagon.

“*Information exchange rather than topology awareness: cooperation between P2P overlay and traffic engineering*” by J. Zhao et al. The authors investigated cross-layer conflict between P2P overlay and ISP underlay and proposed a solution to use cooperation rather than hyperselfish topology-awareness. They illustrate the suboptimal profit of hyperselfish initiator based on two dynamic game models. Simulation results demonstrated that the SC model with path classes can improve costs for both layers and decrease the computation time of achieving the stable equilibrium.

“*Robust decentralized adaptive neural control for a class of nonaffine nonlinear large-scale systems with unknown dead zones*” by H. Wang et al. investigates the problem of robust decentralized adaptive neural stabilization control is investigated for a class of nonaffine nonlinear interconnected large-scale systems with unknown dead-zones. In the controller design procedure, RBF neural networks are applied to approximate packaged unknown nonlinearities and then an adaptive neural decentralized controller is systematically derived without requiring any information on the boundedness of dead-zone parameters. Simulation study is provided to demonstrate the effectiveness of the developed control scheme.

In “*An overview of networked control of complex dynamic systems*” by H. Yan, the authors focus on network imperfections and review the related studies, paying special attention to those carried out since the publishing dates of the surveys referred to. Some future research is also proposed. The main objective of the paper is to provide readers with an overview of the NCSs and a vision for future development. The other objective is to provide a tutorial on NCSs.

In “*Design of attitude control system for UAV based on feedback linearization and adaptive control*” by W. Zhou et al., the feedback linearization and model reference adaptive control (MRAC) are integrated to design the attitude control system for a fixed wing UAV. Simulation results indicate that the system performance indexes including maximum overshoot, settling time (2% error range), and rise time obtained by MRAC are better than those by PID.

“*The research on modeling and simulation of TFE polymerization process*” by J. Sun et al. deals with the problem of modeling and simulation of TFE polymerization process. The authors use the emulsion polymerization method at background to carry out a semibatch reactor system. Upon the actual production conditions, simulation process under the steady state conditions is used to analyze the effects of the changes on operating conditions; the corresponding dynamic model is created to analyze the impact of the changes of conditions on the entire system.

“*Design and stability analysis of uncertain networked predictive control systems with multiple forward channels*” by H. Song, is concerned with the design and stability of networked predictive control for uncertain systems with multiple forward channels. The delays and packet dropouts are distributed such that the classic networked predictive control (NPC) needs modifications to be implemented. An improved control signal selection scheme with distributed prediction length is proposed to increase the prediction accuracy and hence achieve better control performance.

“*Impact of social network and business model on innovation diffusion of electric vehicles in China*” by D. Y. Kong and X. H. Bi uses the theory of network control to analyze the influence of network forms on EV diffusion in China, especially focusing on the building of EV business models (BMs) and the resulting effects and control on the diffusion of EVs. They can find the appropriate network forms and BMs for EVs which is suitable to the local market conditions.

In “*An improved car-following model in vehicle networking based on network control*” by D.-Y. Kong and H. Y. Xu, a car-following model using vehicle networking theory is established, based on network control principle. The car-following model, which is an improvement of the traditional traffic model, describes the traffic in vehicle networking condition. The impact that vehicle networking has on the traffic flow is quantitatively assessed in a particular scene of one-way, no lane changing highway. The examples show that the capacity of the road is effectively enhanced by using vehicle networking.

“ *H_∞ control of supply chain based on switched model of stock level*” by J. Luo and W. Yang is concerned with the problem of H_∞ control for a class of discrete supply chain systems. A new method based on network control technique is presented to address this issue. Supply chain systems are modeled as networked systems with stochastic time-delay. Sufficient conditions for H_∞ controller design are given in terms of a set of linear matrix inequalities, based on which the mean-square asymptotic stability and H_∞ performance are satisfied for such systems.

“*Bayes network based collaborating control algorithm in active multicamera network with applications to object tracking*” by R. Zhao et al. considers the problem for an active camera network framework is designed for human detection and tracking by optimizing the cameras collaborating control. A multicamera collaborating control algorithm is proposed based on Bayes network. The proper human feature selection is also concerned to improve the tracking precision. Experimental results on real world environment indicate the effectiveness and efficiency of proposed framework and algorithm.

“*A Bayesian network method for quantitative evaluation of defects in multilayered structures from Eddy current NDT signals*” by B. Ye et al. proposes to evaluate defects quantitatively from Eddy current NDT signals using Bayesian networks (BNs). BNs are a useful method in handling uncertainty in the inspection process, eventually leading to the more accurate results. The domain knowledge and the experimental data are used to generate the BN models. The models are applied to predict the signals corresponding to different

defect characteristic parameters or to estimate defect characteristic parameters from Eddy current signals in real time.

“*Multiagent and particle swarm optimization for ship integrated power system network reconfiguration*” by Z. Wang et al. establishes the simplified network model and reconfiguration mathematical model of SIPS. PSO and multiagent technology are analyzed. Regional feeder agents are defined. Combining with multiagent and PSO, MAPSO is presented. In this algorithm, regional feeder agents communicate with adjacent agents to accomplish SIPS network reconfiguration.

In “*Fault diagnosis system based on multiagent technique for ship power system*” by Z. Wang et al., a multiagent fault diagnosis system is established with FED-Agent and other functional agents. Considering the characteristics of agent, the multiagent system processes both autonomy and interactivity. It can solve fault diagnosis problem of ship power system effectively.

In “*Eddy current inversion models for estimating dimensions of defects in multilayered structures*” by B. Ye et al., two effective approaches have been proposed to estimate the defect dimensions. The first one is a partial least squares (PLS) regression method. The second one is a kernel partial least squares (KPLS) regression method. The comparison results demonstrate the feasibility and validity of the proposed two methods.

“*A new three-dimensional indoor positioning mechanism based on wireless LAN*” by J. Cheng et al. proposes a hybrid approach in this paper using k -medoids algorithm to partition the set of fingerprints into several subsets first and then we reduce the dimension of fingerprints of every subset on which a multicategory SVM is used to train, outperforming the approach just using SVM to train on all large-dimension fingerprints, in terms of error distance resolution.

“*Event-triggered average consensus for multiagent systems with time-varying delay*” by Z. Wang et al. investigates average consensus for multiagent systems with time-varying delays. A reducing dimension multiagent systems model is presented firstly. Using event-triggered strategy to reduce network load, a comprehensive model is then proposed, which considers communication delays and triggered issue. Further, the event-triggered average consensus stability of multiagent systems with fixed directed/undirected graph is analyzed, and sufficient conditions are provided.

In “*Steady modeling for an ammonia synthesis reactor based on a novel CDEAS-LS-SVM model*” by Z. Liu et al., a steady-state mathematical model is built in order to represent plant behavior under stationary operating conditions. A novel modeling using LS-SVR based on Cultural Differential Evolution with Ant Search is proposed. LS-SVM is adopted to establish the model of the net value of ammonia. The modeling method has fast convergence speed and good global adaptability for identification of the ammonia synthesis process.

“*Group synchronization of nonlinear complex dynamics networks with sampled data*” by M. Li et al. considers the group synchronization of complex dynamical networks with sampled data. Using the Lyapunov method, the group synchronization of the nonlinear complex networks is analyzed. All the nodes in each group can converge to own synchronous

state asymptotically, if the sampled period satisfies some matrix inequality conditions.

In “*Monitoring of multimode processes based on quality-related common subspace separation*” by Y. Fan et al., the authors aimed at developing a new monitoring approach for multimode processes based on quality-related common subspace separation. In the model, the data set forms a larger space when the correlation between process variables and quality variables are considered. The whole space is decomposed as quality-related common subspace, quality-related specific subspace, and the residual subspace. The effectiveness of the proposed approach was verified by simulations.

“*A new mechanism for network monitoring and shielding in wireless LAN*” by J. Cheng et al. investigates various issues about wireless security, analyzing numerous problems in implementing the WLAN. They implemented an actual wireless LAN monitoring system to monitor the network data transmission, allowing users to understand the situation of device. What is more, the system analyzes and records ARP, RARP, IP, UDP, TCP, ICMP, and other protocols efficiently and flexibly.

In “*A discrete group search optimizer for hybrid flowshop scheduling problem with random breakdown*” by Z. Cui et al. The authors introduce the hybrid flowshop scheduling problem with random breakdown (RBHFS) together with a discrete group search optimizer algorithm (DGSO). In particular, two different working cases, preempt-resume case and preempt-repeat case, are considered under random breakdown.

In “*Cultural-based genetic tabu algorithm for multiobjective job shop scheduling*” by Y. Yang et al., the authors propose a novel quad-space cultural genetic tabu algorithm (QSCGTA) to solve such problem. This algorithm provides a different structure from the original cultural algorithm in containing double brief spaces and population spaces. They also present a bidirectional shifting for the decoding process of job shop scheduling.

“*Fundamental issues and prospective directions in networked multirate control systems*” by W. Zhiwen and G. Ge has introduced and reviewed the fundamental issues and prospective directions for NMCSSs. One can draw the conclusions that the introduction of multirate sampling in NCSs, on the one hand, will make the modeling, analysis, and synthesis of NCSs more complicated and challenge the achieved theoretical results; on the other hand, it will bring opportunities toward some higher goals for NCSs.

“*Nonlinear disturbance observer based robust tracking control of pneumatic muscle*” by Y. Mohamed et al. proposes nonlinear disturbance observer based control law (NDOBC) providing a relatively new thread for the control of PMA. The advantage of this method not only is reflected in its high accuracy, but also manifests itself in convenience. The proposed approach represents a simple, yet robust mechanism for guaranteeing finite time performance of zero error condition.

“*Robust H_∞ filtering for networked control systems with random sensor delay*” by S. Xiao et al. investigates the robust H_∞ filtering problem for a class of network-based systems with random sensor delay. Using the Lyapunov function and Wirtinger’s inequality approach, the sufficient conditions are

derived to ensure that the filtering error systems is exponentially stable with a prescribed H_∞ disturbance attenuation level and the filter design method is proposed in terms of LMIs. The effectiveness of the proposed method is illustrated by a numerical example.

“*A local and global search combined particle swarm optimization algorithm and its convergence analysis*” by W. Lin et al. presents a LGSCPSO algorithm, and simulations show that it is effective. The performance of the new approach is evaluated in comparison with OPSSO algorithm for eight representative instances with different dimensions and obtained results show that LGSCPSO algorithm is effective for solving optimization problems.

“*Switched quantization level control of networked control systems with packet dropouts*” by S. Wang et al. investigates the relationship between the maximum allowable dropout bound and the quantization density. The NCS is described as a time-delay switched system with constrained switching signals. A switched dynamic output feedback controller with prescribed disturbance attenuation level is designed via a cone complement linearization approach. A novel stability criterion is obtained by switched system theory.

“*Impulsive consensus tracking of multiagent systems with quantization and input delays using position-only information*” by H. Zhou et al. investigates the consensus tracking problem for second-order multiagent systems without/with input delays. Randomized quantization scheme is considered in the communication channels, and impulsive consensus tracking algorithms using position-only information are proposed. Based on the algebraic graph theory and stability theory of impulsive systems, sufficient and necessary conditions for consensus tracking are studied. It is found that consensus tracking for second-order multiagent systems without/with input delays can be achieved by appropriately choosing the sampling period and control gains which are determined by second-/third-degree polynomials.

Of course, the selected topics and papers are not a comprehensive representation of the area of this special issue. Nonetheless, they represent the rich and many-faceted knowledge that we have the pleasure of sharing with the readers.

Acknowledgments

We would like to express appreciation to the authors for their excellent contributions and patience in assisting us. The hard work of all reviewers on these papers is also very greatly acknowledged.

Huaicheng Yan
Xudong Zhao
Hak-Keung Lam
Huiping Li
Yang Shi
Lixian Zhang

Research Article

Event-Triggered Average Consensus for Multiagent Systems with Time-Varying Delay

Zhaoxia Wang,^{1,2} Minrui Fei,¹ Dajun Du,¹ and Lili Shang¹

¹ Shanghai Key Laboratory of Power Station Automation Technology, School of Mechatronics Engineering and Automation, Shanghai University, Shanghai 200072, China

² School of Electrical Engineering and Automation, Qilu University of Technology, Jinan 250353, China

Correspondence should be addressed to Dajun Du; ddj@shu.edu.cn

Received 6 December 2013; Accepted 13 March 2014; Published 4 May 2014

Academic Editor: Huaicheng Yan

Copyright © 2014 Zhaoxia Wang et al. This is an open access article distributed under the Creative Commons Attribution License, which permits unrestricted use, distribution, and reproduction in any medium, provided the original work is properly cited.

The paper investigates average consensus for multiagent systems with time-varying delay. A reducing dimension multiagent systems model is presented firstly. Using event-triggered mechanism to reduce network load, a comprehensive model is then proposed, which considers communication delay and triggered issue. Furthermore, the event-triggered average consensus stability of multiagent systems with fixed directed/undirected graph is analyzed, and sufficient conditions are provided. Moreover, the upper bound of time-varying delay can be obtained conveniently. Finally, simulation results confirm the feasibility and effectiveness of the proposed method.

1. Introduction

Recently distributed coordination of multiagent systems has attracted significant interest of many researchers. It is becoming increasingly important in multivehicles, sensor network, and formation flying [1–5]. Consensus (or synchronization) problem [1, 6–8] is one of the most important issues of multiagent systems. In practice, it is very important for multiagent systems to achieve average consensus [9].

With the development of industrial large-scale dynamical multiagent systems, the agent is responsible for collecting a lot of information from its neighboring nodes and transmission signals in the shared wireless communication network are massive. However, computing resources of each agent and the bandwidth of wireless network are limited. Therefore, it is necessary to study communication mechanism of multiagent systems [10], which is one of the most important issues in the implementation of average consensus algorithms. Moreover, communication networks are not always reliable, and communication delay is inevitably introduced [11–14]. It is well known that time delay may degrade the system performance or even cause the system instability [15–19]. Therefore, it is necessary to investigate the average consensus

problem with time delay. Some researchers have investigated the average consensus problem for multiagent systems with time delay and communication scheme, respectively.

Considering the average consensus problem with time delay, there are some research results that have been reported [9, 20–23]. For an undirected network with fixed/switching graphs, an upper bound of communication time delays was obtained [20, 21]. Average consensus problem for directed networked multiagent systems with fixed/switching graphs and constant/varying time delays was investigated based on the LMI method [22, 23]. A necessary and sufficient condition was derived for multiagent systems with heterogeneous time delays to achieve average consensus [9]. The average consensus problems have been investigated with time delays and other issues such as noise [24–26]. Moreover, some researches have investigated consensus or average consensus for high-order multiagent systems with time-varying delays [27–30]. However, how to get the quantitative relationship between maximum time delay and system stability for directed networks with fixed/switching graphs is still an open issue.

For communication schemes, the event-triggered mechanism has been proposed [31–34]. Compared with traditional time-triggered mechanism (i.e., the fixed sampling period),

the event-triggered mechanism can reduce the communication burden. This is because the signal can be transmitted only when the triggered condition is satisfied. Event-triggered mechanism has been employed in multiagent systems [10, 35–37] without time delay, which was an effective methodology for multiagent systems with limited computational and communicational resources. Furthermore, based on event-triggered mechanism, a tracking control problem of leader-follower multiagent continuous-time systems with communication delays was investigated [38], and the consensus problem of discrete-time multiagent systems with random communication delays was studied [39].

In this paper, the event-triggered average consensus problem for continuous-time multiagent systems in a directed network with time-varying delay is studied. The main contributions include the following. Firstly, a reducing dimension multiagent systems model with event-triggered average consensus protocol and time-varying delay is provided. Secondly, a Lyapunov-Krasovskii functional is constructed, and sufficient conditions are obtained, and all the agents can achieve the average consensus asymptotically. Different from [38, 39], an upper bound of time-varying communication delay is derived in this paper.

The paper is organized as follows. Section 2 presents the background and system model. The proposed approach is provided in Section 3. Section 4 gives the main results of the paper. Simulation results are described in Section 5. Section 6 concludes the paper.

2. Background and System Model

2.1. Preliminaries of Graph Theory. Let $G(V, E, A)$ be a weighted digraph of order n , with the set of nodes $V = \{v_1, \dots, v_n\}$, and set of edges $E = \{e_{ij} = (v_i, v_j)\} \subseteq V \times V$, where $e_{ij} = (v_i, v_j)$ is ordered, v_i is the edge's tail, and v_j is the head. The set of neighbors of node v_i is denoted as $N_i = \{v_j \in V \mid (v_j, v_i) \in E\}$. The node indexes of G belong to a finite index set $I = \{1, 2, \dots, n\}$. $A = [a_{ij}]$ is a weighted communication adjacency matrix with nonnegative adjacency elements a_{ij} , where $a_{ii} = 0$ and $a_{ij} > 0$ if and only if $v_i \in N_j$. The in-degree and out-degree of v_i are defined as

$$d_{\text{in}}(v_i) = \sum_{j=1}^n a_{ji}, \quad d_{\text{out}}(v_i) = \sum_{j=1}^n a_{ij}. \quad (1)$$

The degree matrix $D = [d_{ij}]_{n \times n}$ is a diagonal matrix with

$$d_{ij} = \begin{cases} d_{\text{out}}(v_i), & i = j, \\ 0, & i \neq j. \end{cases} \quad (2)$$

The graph Laplacian of G is defined as $L = D - A = [l_{ij}]_{n \times n}$. It can be easily obtained that the element l_{ij} of L satisfies

$$l_{ij} = \begin{cases} \sum_{j=1}^n a_{ij}, & j = i, \\ -a_{ij}, & i \neq j. \end{cases} \quad (3)$$

By definition, every row sum of L is zero and thus $\mathbf{1}_n = [1 \ 1 \ \dots \ 1]^T \in \mathfrak{R}^n$ is an eigenvector of L associated with the eigenvalue $\lambda = 0$. This therefore means that $\text{Rank}(L) \leq n - 1$.

Definition 1 (balanced graph [20]). We say the node v_i of a graph $G(V, E, A)$ is balanced if and only if $\sum_{j=1}^n a_{ij} = \sum_{j=1}^n a_{ji}$. A graph $G(V, E, A)$ is called balanced if and only if all of its nodes are balanced. Obviously any connected undirected graph is balanced.

Definition 2 (balanced matrix [22]). A square matrix $M \in \mathfrak{R}^{n \times n}$ is said to be a balanced matrix if and only if $\mathbf{1}_n^T M = 0$ and $M \mathbf{1}_n = 0$.

It is easy to know that the Laplacian L of a balanced graph G satisfies $\mathbf{1}_n^T L = 0$ and $L \mathbf{1}_n = 0$.

Lemma 3 (see [22]). *Consider the matrix*

$$A = \begin{bmatrix} n-1 & -1 & \cdots & -1 \\ -1 & n-1 & \cdots & -1 \\ \vdots & \vdots & \ddots & \vdots \\ -1 & -1 & \cdots & n-1 \end{bmatrix}. \quad (4)$$

The following statements hold.

(1) The eigenvalues of A are n with multiplicity $n - 1$ and 0 with multiplicity 1 . The vectors $\mathbf{1}_n^T$ and $\mathbf{1}_n$ are left and the right eigenvectors of A associated with the zero eigenvalue, respectively.

(2) There exists an orthogonal matrix O such that

$$O^T A O = \begin{bmatrix} n I_{n-1} & 0_{(n-1) \times 1} \\ 0_{1 \times (n-1)} & 0 \end{bmatrix}, \quad (5)$$

and O is the matrix of eigenvectors of A . For any balanced matrix $B \in \mathfrak{R}^{n \times n}$

$$O^T B O = \begin{bmatrix} * & 0_{(n-1) \times 1} \\ 0_{1 \times (n-1)} & 0 \end{bmatrix}. \quad (6)$$

Remark 4. For the Laplacian L of a connected graph G , it is easy to have the following equation by Lemma 3:

$$U^T L U = \begin{bmatrix} U_1^T L U_1 & 0_{(n-1) \times 1} \\ 0_{1 \times (n-1)} & 0 \end{bmatrix}, \quad (7)$$

where U is an orthogonal matrix of eigenvectors of L , and we define it as $[U_1 \ (1_n/\sqrt{n})]$, in which $U_1 \in \mathfrak{R}^{n \times (n-1)}$ is the first $n - 1$ columns of U .

2.2. System Model. Suppose that the network system consists of n agents. Each agent is regarded as a node in the graph G . Let $x_i(t) \in \mathfrak{R}$ denote the state (or value) of node v_i . The value of a node might represent physical quantities including position, temperature, and voltage. Moreover, assume that each node is an agent with dynamics:

$$\dot{x}_i(t) = u_i(t), \quad \{i \in I = 1, 2, \dots, n\}, \quad (8)$$

where $u_i(t)$ is the control input (or protocol). The consensus control protocol without communication time delay in [20] was given by

$$u_i(t) = \sum_{v_j \in N_i} a_{ij}(t) (x_j - x_i). \quad (9)$$

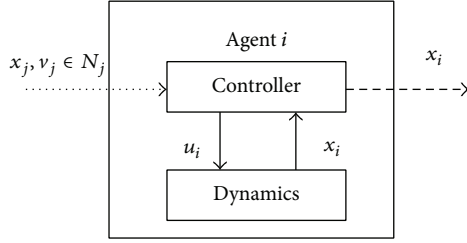


FIGURE 1: Agent with the consensus protocol.

Here with the consensus protocol, each agent consists of a controller and dynamics as shown in Figure 1.

We say the nodes of a network have reached a consensus if and only if $x_i = x_j$ for all $i, j \in I, i \neq j$. Whenever the nodes of a network are all in agreement, the value of all nodes is called the group decision value. Particularly, for all $i, j \in I$, if there exists

$$\lim_{t \rightarrow \infty} x_i(t) = \frac{1}{n} \sum_{j=1}^n x_j(0), \quad (10)$$

protocol $u_i(t)$ asymptotically solves the average consensus problem.

Further, the consensus control law with communication time delay was given by [9]

$$u_i(t) = \sum_{v_j \in N_i} a_{ij}(t) (x_j(t - \tau_{ij}^c) - x_i(t - \tau_{ij}^s)), \quad (11)$$

where $\tau_{ij}^c \geq 0$ is the communication time delay with which the state of node v_i passes through a channel e_{ij} before getting to node v_j . $\tau_{ij}^s \geq 0$ is the self-delay, which occurs when node v_i compares its self-information and information of node v_j over the network.

In this paper, we consider the case that the self-delay τ_{ij}^s is equal to the communication delay τ_{ij}^c , that is, $\tau_{ij}^s = \tau_{ij}^c = \tau_{ij}$, which is discussed in [9, 20, 22, 23]. Then the consensus control law (11) becomes

$$u_i(t) = \sum_{v_j \in N_i} a_{ij}(t) (x_j(t - \tau_{ij}) - x_i(t - \tau_{ij})). \quad (12)$$

Given protocol (9) and (11), the network dynamics of agent n is summarized as

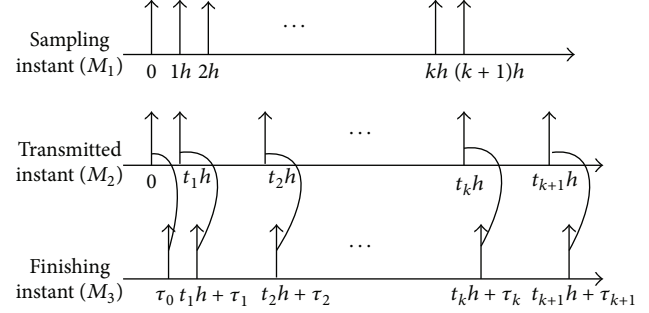
$$\dot{x}(t) = -Lx(t), \quad (13)$$

$$\dot{x}(t) = -Lx(t - \tau_{ij}), \quad (14)$$

where $x(t) = (x_1(t), x_2(t), \dots, x_n(t))^T$ denotes the value of all nodes and L is the Laplacian of graph G .

The system (13) without communication time delay under event-triggered strategy has been investigated in [36, 37].

In the following section, we will redefine protocol (12) and model (14) to take into account event-triggered mechanism. The consensus control formulation and problem statement for centralized event-triggered cooperative control are described in the following section.


 FIGURE 2: The relationship between M_1, M_2 , and M_3 .

3. The Proposed Approach

3.1. Event-Triggered Mechanism and Modeling of Multiagents Systems with Communication Time Delay. Each agent of multiagent systems is equipped with a small embedded microprocessor and regularly sampled with period h by microprocessor in practice, where the monotone increasing sampling sequence is described by the set $M_1 = \{0, h, 2h, \dots, kh\}$, $k \in \mathbb{N}$. Using event-triggered mechanism, only the successful transmitted signals are available, where the successful transmitted instants sequences $M_2 = \{0, t_1h, t_2h, \dots, t_kh\}$ satisfy $0 = t_0 < t_1 < \dots < t_{k-1} < t_k < \dots, t_k \in \mathbb{N}$. Considering the bounded delay $\tau_{t_k} \in [0, \bar{\tau}]$, which denotes the time delay at successful transmitted instant t_kh , the transmitted finishing instant is described by the set $M_3 = \{0, t_1h + \tau_{t_1}, t_2h + \tau_{t_2}, \dots, t_kh + \tau_{t_k}, \dots\}$. Moreover, the control input is generated by a zero-order holder (ZOH) with the holding time $t \in [t_kh + \tau_{t_k}, t_{k+1}h + \tau_{t_{k+1}})$. The relationship between M_1, M_2 , and M_3 is shown in Figure 2.

Remark 5. Specially, if $M_1 = M_2$, it means that all sampled data are transmitted, that is, a time-triggered transmission scheme. If $M_1 \subset M_2$, it means that not all sampled data are transmitted; that is, the numbers of sampled data are reduced. Therefore, the event-triggered scheme can reduce communication burden.

3.1.1. Centralized Event-Triggered Mechanism. The state measurement error is defined by

$$e(kh) = x(kh) - x(t_kh), \quad (15)$$

where $e(kh)$ is the error between the current sampled value $x(kh)$ and the latest transmitted sampled value $x(t_kh)$.

The event-triggered transmission mechanism in [40, 41] is designed as

$$f(kh, t_kh) = e^T(kh) \Phi e(kh) - \gamma x^T(t_kh) \Phi x(t_kh) > 0, \quad (16)$$

where Φ is a positive definite matrix and $0 < \gamma < 1$ is a given and bounded positive scalar parameter.

When the local state measurement error signal exceeds the given threshold, that is, condition (16) is satisfied, the current sampled information $x(kh)$ is transmitted. Obviously,

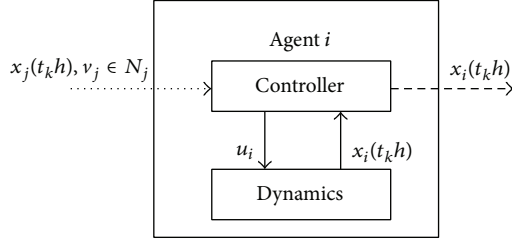


FIGURE 3: Agent with event-triggered consensus protocol.

the current successful transmitted state value $x(kh)$ is the subsequences of the latest transmitted sampled value, which is denoted by $x(t_{k+1}h)$. Then each agent with event-triggered consensus protocol is shown in Figure 3.

Remark 6. The event-triggered mechanism (16) is characterized by the parameters γ , Φ , and h . Specially, if $\gamma = 0$ in (16), this leads to $t_{k+1}h = t_k h + h$, and it becomes a time-triggered transmission mechanism.

3.1.2. Modeling of Hybrid Event-Triggered Multiagent Systems. Here we considered the system (12) with fixed topology G and time-varying delay. We know that the input $u_i(t)$ is held constant in a control period; that is,

$$u_i(t) = u_i(t_k h), \quad t \in [t_k h, t_{k+1} h). \quad (17)$$

The proposed event-triggered control law of (12) in the centralized case is defined as

$$u_i(t) = \sum_{v_j \in N_i} a_{ij}(t_k h) (x_j(t_k h - \tau_k) - x_i(t_k h - \tau_k)), \quad (18)$$

so that

$$u(t) = -Lx(t_k h), \quad t \in [t_k h + \tau_k, t_{k+1} h + \tau_{t_{k+1}}). \quad (19)$$

The network dynamics of system (14) is then given by

$$\dot{x}(t) = -Lx(t_k h), \quad t \in [t_k h + \tau_k, t_{k+1} h + \tau_{t_{k+1}}). \quad (20)$$

Obviously, $t_{k+1}h + \tau_{t_{k+1}} \geq t_k h + h + \tau_k$ and $t_k h + h + \bar{\tau} \geq t_k h + h + \tau_{t_{k+1}}$.

Next, two cases are discussed.

(1) If $t_{k+1}h + \tau_{t_{k+1}} \geq t_k h + h + \bar{\tau}$, there exists $l \geq 1 \in \mathbb{N}$, satisfying

$$t_k h + lh + \bar{\tau} \leq t_{k+1} h + \tau_{t_{k+1}} < t_k h + (l+1)h + \bar{\tau}. \quad (21)$$

For a detailed timing analysis, consider the following interval:

$$\begin{aligned} \Omega &= [t_k h + \tau_k, t_{k+1} h + \tau_{t_{k+1}}) \\ &= [t_k h + \tau_k, t_k h + h + \bar{\tau}) \\ &\cup \left\{ \bigcup_{i=1}^{l-1} [t_k h + ih + \bar{\tau}, t_k h + ih + h + \bar{\tau}) \right\} \\ &\cup [t_k h + lh + \bar{\tau}, t_{k+1} h + \tau_{t_{k+1}}) \\ &= \bigcup_{i=0}^l \Omega_i, \end{aligned} \quad (22)$$

where some sets Ω_i are defined as follows:

$$\begin{aligned} \Omega_0 &= [t_k h + \tau_k, i_k h + h + \bar{\tau}), \quad i = 0, \\ \Omega_i &= [i_k h + \bar{\tau}, i_k h + h + \bar{\tau}), \quad i = 1, 2, \dots, l-1 \\ \Omega_l &= [i_k h + \bar{\tau}, t_{k+1} h + \tau_{t_{k+1}}), \quad i = l, \end{aligned} \quad (23)$$

and $i_k h = t_k h + ih$, $i = 0, 1, 2, \dots, l$.

Define

$$\eta(t) = t - i_k h, \quad t \in \Omega_i, \quad i = 0, 1, 2, \dots, l. \quad (24)$$

From (23) and (24):

$$\begin{aligned} \tau_k &\leq \eta(t) \leq h + \bar{\tau}, \quad t \in \Omega_0, \quad i = 0, \\ \bar{\tau} &\leq \eta(t) \leq h + \bar{\tau}, \quad t \in \Omega_i, \quad i = 1, 2, \dots, l-1, \\ \bar{\tau} &\leq \eta(t) \leq h + \bar{\tau}, \quad t \in \Omega_l, \quad i = l. \end{aligned} \quad (25)$$

From (25), it can be obtained that

$$\eta_1 < \eta(t) \leq \eta_3, \quad t \in \Omega_i, \quad i = 0, 1, 2, \dots, l, \quad (26)$$

where $\eta_1 = \inf\{\tau_k\} > 0$ and $\eta_3 \triangleq h + \bar{\tau}$.

Define the state measurement error

$$e(i_k h) = x(i_k h) - x(t_k h), \quad t \in \Omega_i, \quad i = 0, 1, \dots, l. \quad (27)$$

(2) If $t_{k+1}h + \tau_{t_{k+1}} < t_k h + h + \bar{\tau}$, define $\eta(t) = t - t_k h$, $t \in [t_k h + \tau_k, t_{k+1} h + \tau_{t_{k+1}})$.

It is clear that $\tau_k \leq \eta(t) \leq h + \bar{\tau}$; that is, $\eta_1 < \eta(t) \leq \eta_3$, $t \in [t_k h + \tau_k, t_{k+1} h + \tau_{t_{k+1}})$. Then there exists $e(i_k h) = x(t_k h) - x(t_k h) = 0$.

According to the definition and analysis of the aforementioned two cases, it is seen that (19) and (20) can be equivalently written as

$$\begin{aligned} u(t) &= -Lx(t - \eta(t)) + Le(i_k h), \\ \dot{x}(t) &= -Lx(t - \eta(t)) + Le(i_k h), \\ t &\in \Omega_i, \quad i = 0, 1, 2, \dots, l, \end{aligned} \quad (28)$$

where $i_k h = t_k h + ih$ and $0 < \eta_1 < \eta(t) \leq \eta_3$. The initial conditions of system (28) are assumed to satisfy $x(t) = \phi(t)$,

$t \in [-\eta_3, 0]$, $\phi(0) = x(0)$. Moreover, between $t_k h$ and $t_k h + ih$, no control signal is triggered; that is,

$$\begin{aligned} f(i_k h, t_k h) \\ = e^T(i_k h) \Phi e(i_k h) - \gamma x^T(t_k h) \Phi x(t_k h) \leq 0. \end{aligned} \quad (29)$$

Therefore, in the event-triggered formulation, the event time $t_{k+1} h$ is defined by

$$t_{k+1} h = t_k h + \min_i \{ih \mid e^T(i_k h) \Phi e(i_k h) \geq \delta \wp\}, \quad (30)$$

with $\wp = x^T(t_k h) \Phi x(t_k h)$, $0 < \gamma < 1$, $i \in \mathbb{N}$.

3.2. Problem Setting. The following task is to find the conditions for system (28) to reach average consensus with the event-triggered communication mechanism (29). Considering a directed network system (28) with fixed graph G that is strongly connected and balanced, denote $\alpha(t) = \text{Ave}(x) = (1/n) \sum_i x_i(t)$ by the average of the agents' states. Due to the balanced graph of G , the Laplacian L satisfies $1_n^T L = 0$ from Definition 2. For system (28), it implies $1_n^T \dot{x} = 1_n^T u = -1_n^T L[x(t-\eta(t)) - e(i_k h)] = 0$; that is, $\sum_{i=1}^n \dot{x}_i(t) = \sum_{i=1}^n u_i(t) = 0$. Then the time derivative of $\alpha(t)$ is given by $\dot{\alpha}(t) = (1/n) \sum_i \dot{x}_i(t) = 0$. So that $\alpha = \text{Ave}(x) = \text{Ave}(x(0)) = (1/n) \sum_i x_i(0)$; that is, $\alpha = \text{Ave}(x)$ is an invariant quantity. Then the state vector $x(t)$ can be decomposed as [20]

$$x(t) = \alpha 1_n + \delta(t), \quad (31)$$

where $\alpha = \text{Ave}(x)$ and $\delta(t) \in \mathfrak{R}^n$ satisfies $\sum_i \delta_i(t) = 0$. For a strongly connected digraph, the vector $\delta(t)$ belongs to an $(n-1)$ -dimensional subspace called the disagreement eigenspace of L .

Submitting (31) to (28), system (28) is equivalent to

$$\begin{aligned} \dot{\delta}(t) &= -L\delta(t - \eta(t)) + Le(i_k h), \\ 0 &< \eta_1 < \eta(t) \leq \eta_3. \end{aligned} \quad (32)$$

Moreover, between $t_k h$ and $t_k h + ih$ ($i = 1, 2, \dots, l$), no control signal is triggered; that is,

$$\begin{aligned} f(i_k h, t_k h) \\ = e^T(i_k h) \Phi e(i_k h) - \gamma x^T(t_k h) \Phi x(t_k h) \leq 0. \end{aligned} \quad (33)$$

Because Φ is a positive definite matrix, there exists invertible matrix W satisfying $\Phi = W^T W$. Substituting $\Phi = W^T W$ into (33) yields

$$\begin{aligned} e^T(i_k h) W^T W e(i_k h) - \gamma x^T(t_k h) W^T W x(t_k h) \leq 0, \\ \|We(i_k h)\| \leq \sqrt{\gamma} \|Wx(t_k h)\|; \end{aligned} \quad (34)$$

that is,

$$\begin{aligned} \|We(i_k h)\| &\leq \sqrt{\gamma} \|W(\alpha 1_n + \delta(t_k h))\|, \\ \|We(i_k h)\| &\leq \sqrt{\gamma} \|\alpha W 1_n\| + \sqrt{\gamma} \|W\delta(t_k h)\|. \end{aligned} \quad (35)$$

So when the condition satisfies

$$\begin{aligned} \|We(i_k h)\| &\leq \sqrt{\gamma} \|W\delta(t_k h)\|, \\ \|We(i_k h)\|^2 &\leq \gamma \|W\delta(t_k h)\|^2, \end{aligned} \quad (36)$$

$$e^T(i_k h) W^T W e(i_k h) - \gamma \delta^T(t_k h) W^T W \delta(t_k h) \leq 0,$$

one can get

$$e^T(i_k h) \Phi e(i_k h) - \gamma \delta^T(t_k h) \Phi \delta(t_k h) \leq 0. \quad (37)$$

Between $t_k h$ and $t_k h + ih$ ($i = 1, 2, \dots, l$), no control signal is triggered, where

$$e(i_k h) = \delta(i_k h) - \delta(t_k h), \quad t \in \Omega_i, \quad i = 0, 1, 2, \dots, l. \quad (38)$$

For system (32), it follows that, from Remark 4,

$$\begin{aligned} U^T \dot{\delta}(t) &= -U^T L U U^T \delta(t - \eta(t)) + U^T L U U^T e(i_k h) \\ &= - \begin{bmatrix} U_1^T L U_1 & 0_{(n-1) \times 1} \\ 0_{1 \times (n-1)} & 0 \end{bmatrix} U^T \delta(t - \eta(t)) \\ &\quad + \begin{bmatrix} U_1^T L U_1 & 0_{(n-1) \times 1} \\ 0_{1 \times (n-1)} & 0 \end{bmatrix} U^T e(i_k h) \\ &= - \begin{bmatrix} \tilde{L} & 0_{(n-1) \times 1} \\ 0_{1 \times (n-1)} & 0 \end{bmatrix} U^T \delta(t - \eta(t)) \\ &\quad + \begin{bmatrix} \tilde{L} & 0_{(n-1) \times 1} \\ 0_{1 \times (n-1)} & 0 \end{bmatrix} U^T e(i_k h), \end{aligned} \quad (39)$$

where U is an orthogonal matrix of eigenvectors of L , and we define it as $[U_1 \quad (1_n/\sqrt{n})]$, in which $U_1 \in \mathfrak{R}^{n \times (n-1)}$ is the first $n-1$ columns of U . Denote $\tilde{L} = U_1^T L U_1$.

Noting that $\sum_i \delta_i(t - \eta(t)) = 0$, $\sum_i \delta_i(t) = 0$, we have

$$\begin{aligned} U^T \dot{\delta}(t) &= [* \dots * 0]^T = \begin{bmatrix} \tilde{\delta}^T(t) \\ 0 \end{bmatrix}^T, \\ U^T \delta(t - \eta(t)) &= [\tilde{\delta}^T(t - \eta(t)) 0]^T, \\ U^T \delta(t_k h) &= [* \dots * 0]^T = [\tilde{\delta}^T(t_k h) 0]^T, \\ U^T e(i_k h) &= [* \dots * 0]^T = [\tilde{e}^T(i_k h) 0]^T. \end{aligned} \quad (40)$$

Then, system (32) is equivalent to

$$\begin{aligned} \dot{\tilde{\delta}}(t) &= -\tilde{L} \tilde{\delta}(t - \eta(t)) + \tilde{L} \tilde{e}(i_k h), \\ t &\in \Omega_i, \quad i = 0, 1, 2, \dots, l, \\ 0 &< \eta_1 < \eta(t) \leq \eta_3, \end{aligned} \quad (41)$$

where $\tilde{L} \in \mathfrak{R}^{(n-1) \times (n-1)}$ and $\text{Rank}(\tilde{L}) = n-1$.

Condition (37) is equivalent to

$$\begin{aligned} [\tilde{e}^T(i_k h) 0] U^T \Phi U [\tilde{e}^T(i_k h) 0]^T \\ - \gamma [\tilde{\delta}^T(t_k h) 0] U^T \Phi U [\tilde{\delta}^T(t_k h) 0]^T \leq 0; \end{aligned} \quad (42)$$

that is,

$$\begin{aligned} & \tilde{e}^T(i_k h) \tilde{\Phi} \tilde{e}^T(i_k h) \\ & - \gamma \tilde{\delta}^T(t_k h) \tilde{\Phi} \tilde{\delta}^T(t_k h) \leq 0, \end{aligned} \quad (43)$$

where $0 < \tilde{\Phi} \in \mathfrak{R}^{(n-1) \times (n-1)}$ and $\tilde{\Phi} = U_1^T \Phi U_1$.

Lemma 7. *If $\lim_{t \rightarrow \infty} \|\tilde{\delta}(t)\| = 0$, then $\lim_{t \rightarrow \infty} \|\delta(t)\| = 0$.*

Proof. From $\sum_i \delta_i(t) = 0$, we have $U^T \delta(t) = [\tilde{\delta}^T(t) 0]^T$, and then $\delta(t) = U[\tilde{\delta}^T(t) 0]^T$. Therefore, Lemma 7 is obtained. This completes the proof. \square

Lemma 8 (see [42]). *Let G be a balanced digraph; then G is strongly connected if and only if G is weakly connected.*

Remark 9. The requirement of graph G that we discuss is strongly connected, but it can be obtained that it should be weakly connected based on Lemma 8.

Definition 10 (see [43]). Let $\Phi_1, \Phi_2, \dots, \Phi_N : \mathfrak{R}^m \mapsto \mathfrak{R}^n$ be a given finite number of functions such that they have positive values in an open subset D of \mathfrak{R}^m . Then, a reciprocally convex combination of these functions over D is a function of the form

$$\frac{1}{\alpha_1} \Phi_1 + \frac{1}{\alpha_2} \Phi_2 + \dots + \frac{1}{\alpha_N} \Phi_N : D \mapsto \mathfrak{R}^n, \quad (44)$$

where the real numbers α_i satisfy $\alpha_i > 0$ and $\sum_i \alpha_i = 1$.

For a reciprocally convex combination of scalar positive functions $\Phi_i = f_i$, Lemma 11 is obtained by Definition 10.

Lemma 11 (see [43]). *Let $f_1, f_2, \dots, f_N : \mathfrak{R}^m \mapsto \mathfrak{R}$ have positive values in an open subset D of \mathfrak{R}^m . Then, the reciprocally convex combination of f_i over D satisfies*

$$\min_{\alpha_i | \alpha_i > 0, \sum_i \alpha_i = 1} \sum_i \frac{1}{\alpha_i} f_i = \sum_i f_i + \max_{g^{i,j}(t)} \sum_{i \neq j} g_{i,j}(t) \quad (45)$$

subject to

$$\begin{aligned} & \min_{\alpha_i | \alpha_i > 0, \sum_i \alpha_i = 1} \sum_i \frac{1}{\alpha_i} f_i = \sum_i f_i + \max_{g_{i,j}(t)} \sum_{i \neq j} g_{i,j}(t), \\ & \left\{ g_{i,j} : \mathfrak{R}^m \mapsto \mathfrak{R}, g_{j,i}(t) \triangleq g_{i,j}(t), \right. \\ & \left. \left[\begin{array}{cc} f_i(t) & g_{i,j}(t) \\ g_{j,i}(t) & f_j(t) \end{array} \right] \geq 0 \right\}. \end{aligned} \quad (46)$$

Lemma 11 can be applied to handle the double integral terms of the Lyapunov-Krasovskii functional for time delay systems.

4. Main Results

Theorem 12. *Considering a network system of n agents, the network has a balanced and weakly connected weighted*

*digraph G with uncertain time-varying communication delay. For some given positive constants η_1, η_3 , and γ , under the event-triggered mechanism (43), the system (41) is asymptotically stable, if there exist positive definite matrixes $P, \tilde{\Phi}, S, R_i$ ($i = 1, 2, 3$) $\in \mathfrak{R}^{(n-1) \times (n-1)}$, matrix Q_i ($i = 1, 2, 3$), U_j ($j = 2, 3$) with $(n-1)$ dimensions and $\begin{bmatrix} Q_1 & * \\ Q_3 & Q_2 \end{bmatrix} > 0$, $\begin{bmatrix} R_j & * \\ U_j & R_j \end{bmatrix} > 0$ ($j = 2, 3$), such that*

$$\begin{bmatrix} \Gamma_{11}^j & * \\ \Gamma_{21} & \Gamma_{22} \end{bmatrix} < 0 \quad (j = 2, 3), \quad (47)$$

where

$$\Gamma_{11}^2 = \begin{bmatrix} \Pi_{11} & * & * & * & * & * \\ \Pi_{21} & \Pi_{22} & * & * & * & * \\ \Pi_{31} & \Pi_{32} & \Pi_{33} & * & * & * \\ 0 & \Pi_{42} & \Pi_{43} & \Pi_{44} & * & * \\ 0 & 0 & \Pi_{53} & \Pi_{54} & \Pi_{55} & * \\ \Pi_{61} & 0 & \Pi_{63} & 0 & 0 & \Pi_{66} \end{bmatrix},$$

$$\Gamma_{11}^3 = \begin{bmatrix} \tilde{\Pi}_{11} & * & * & * & * & * \\ \tilde{\Pi}_{21} & \tilde{\Pi}_{22} & * & * & * & * \\ \tilde{\Pi}_{31} & \tilde{\Pi}_{32} & \tilde{\Pi}_{33} & * & * & * \\ 0 & \tilde{\Pi}_{42} & \tilde{\Pi}_{43} & \tilde{\Pi}_{44} & * & * \\ 0 & 0 & \tilde{\Pi}_{53} & \tilde{\Pi}_{54} & \tilde{\Pi}_{55} & * \\ \tilde{\Pi}_{61} & 0 & \tilde{\Pi}_{63} & 0 & 0 & \tilde{\Pi}_{66} \end{bmatrix},$$

$$\Gamma_{21} = \begin{bmatrix} 0 & 0 & -\eta_1 R_1 \tilde{L} & 0 & 0 & \eta_1 R_1 \tilde{L} \\ 0 & 0 & -\eta_{12} R_2 \tilde{L} & 0 & 0 & \eta_{12} R_2 \tilde{L} \\ 0 & 0 & -\eta_{23} R_3 \tilde{L} & 0 & 0 & \eta_{23} R_3 \tilde{L} \end{bmatrix},$$

$$\Gamma_{22} = \begin{bmatrix} -R_1 & * & * \\ 0 & -R_2 & * \\ 0 & 0 & -R_3 \end{bmatrix},$$

$$\Pi_{11} = \tilde{\Pi}_{11} = S - R_1, \quad \Pi_{21} = \tilde{\Pi}_{21} = R_1,$$

$$\Pi_{22} = \tilde{\Pi}_{22} = -S - R_1 - R_2 + Q_1,$$

$$\Pi_{31} = \tilde{\Pi}_{31} = -\tilde{L}^T P, \quad \Pi_{32} = R_2 - U_2,$$

$$\Pi_{33} = U_2 + U_2^T - 2R_2 + \gamma \tilde{\Phi},$$

$$\tilde{\Pi}_{33} = U_3 + U_3^T - 2R_3 + \gamma \tilde{\Phi},$$

$$\Pi_{42} = Q_3 + U_2, \quad \tilde{\Pi}_{42} = Q_3 + R_2,$$

$$\Pi_{43} = R_2 - U_2, \quad \tilde{\Pi}_{43} = R_3 - U_3^T,$$

$$\Pi_{44} = \tilde{\Pi}_{44} = Q_2 - R_2 - R_3 - Q_1, \quad \tilde{\Pi}_{53} = R_3 - U_3,$$

$$\begin{aligned}
 \Pi_{54} &= R_3 - Q_3, & \tilde{\Pi}_{54} &= U_3 - Q_3, \\
 \Pi_{55} &= \tilde{\Pi}_{55} = -R_3 - Q_2, \\
 \Pi_{61} &= \tilde{\Pi}_{61} = \tilde{L}^T P, & \Pi_{63} &= \tilde{\Pi}_{63} = -\gamma \tilde{\Phi}, \\
 \Pi_{66} &= \tilde{\Pi}_{66} = \gamma \tilde{\Phi} - \tilde{\Phi},
 \end{aligned} \tag{48}$$

and $\tilde{L} = U_1^T L U_1$, $U_1 \in \mathfrak{R}^{n \times (n-1)}$ is the first $n-1$ columns of U , and U is an orthogonal matrix of eigenvectors of L .

The proof of Theorem 12 is presented in the appendix.

Corollary 13. Consider system (28) with the conditions (29), and assume that the network has a balanced and weakly weighted digraph G with uncertain time-varying communication delay. Then, the system asymptotically achieves average consensus; that is,

$$\lim_{t \rightarrow \infty} x_i(t) = \alpha = \frac{1}{n} \sum_i x_i(0). \tag{49}$$

Proof. Using Theorem 12, we have that $\lim_{t \rightarrow \infty} \tilde{\delta}(t) = 0$. According to Lemma 7, $\lim_{t \rightarrow \infty} x(t) = \alpha 1_n + \lim_{t \rightarrow \infty} \tilde{\delta}(t) = \alpha 1_n$, so we have $\lim_{t \rightarrow \infty} x_i(t) = \alpha = (1/n) \sum_i x_i(0)$. This completes the proof. \square

From Remark 6, when $\gamma = 0$ in (29), the event-triggered mechanism becomes a time-triggered sampling mechanism. The following Corollary 14 provides the results for this case.

Corollary 14. Considering a network system of n agents, the network has a balanced and weakly connected weighted digraph G with time-varying communication delay. For some given positive constants η_1, η_2 , the system (28) asymptotically achieves average consensus, if there exist positive definite

matrixes P, R_i ($i = 1, 2, 3$), $S, \tilde{\Phi} \in \mathfrak{R}^{(n-1) \times (n-1)}$, $\begin{bmatrix} R_j & * \\ U_j & R_j \end{bmatrix} > 0$

($j = 2, 3$), $\begin{bmatrix} Q_1 & * \\ Q_3 & Q_2 \end{bmatrix} > 0$ and matrix Q_i ($i = 1, 2, 3$), U_j

($j = 2, 3$) with $(n-1)$ dimensions, such that

$$\begin{bmatrix} \Xi_{11}^j & * \\ \Xi_{21} & \Xi_{22} \end{bmatrix} < 0, \quad (j = 2, 3), \tag{50}$$

where

$$\Xi_{11}^j = \begin{bmatrix} \Theta_{11} & * & * & * & * \\ \Theta_{21} & \Theta_{22} & * & * & * \\ \Theta_{31} & \Theta_{32} & \Theta_{33} & * & * \\ 0 & \Theta_{42} & \Theta_{43} & \Theta_{44} & * \\ 0 & 0 & \Theta_{53} & \Theta_{54} & \Theta_{55} \end{bmatrix},$$

TABLE 1: Comparison of maximum allowable delays.

γ	0.00	0.10	0.30	0.50	0.80
τ_{\max}	0.3645	0.3452	0.3044	0.2582	0.1244

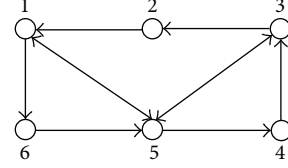


FIGURE 4: A directed graph.

$$\Xi_{21} = \begin{bmatrix} 0 & 0 & -\eta_1 R_1 \tilde{L} & 0 & 0 \\ 0 & 0 & -\eta_{12} R_2 \tilde{L} & 0 & 0 \\ 0 & 0 & -\eta_{23} R_3 \tilde{L} & 0 & 0 \end{bmatrix},$$

$$\Xi_{22} = \begin{bmatrix} -R_1 & * & * \\ 0 & -R_2 & * \\ 0 & 0 & -R_3 \end{bmatrix},$$

$$\Theta_{11} = S - R_1, \quad \Theta_{21} = R_1,$$

$$\Theta_{22} = -S - R_1 - R_2 + Q_1,$$

$$\Theta_{31} = -\tilde{L}^T P, \quad \Theta_{32} = (3-j)(R_2 - U_2),$$

$$\Theta_{33} = U_j + U_j^T - 2R_j,$$

$$\Theta_{42} = Q_3 + (3-j)U_2 + (j-2)R_2,$$

$$\Theta_{43} = R_j - (3-j)U_2 - (j-2)U_3^T,$$

$$\Theta_{44} = Q_2 - R_2 - R_3 - Q_1,$$

$$\Theta_{53} = (j-2)(R_3 - U_3),$$

$$\Theta_{54} = (3-j)R_3 + (j-2)U_3 - Q_3,$$

$$\Theta_{55} = -R_3 - Q_2,$$

(51)

and $\tilde{L} = U_1^T L U_1$, $U_1 \in \mathfrak{R}^{n \times (n-1)}$ is the first $n-1$ columns of U , and U is an orthogonal matrix of eigenvectors of L .

Remark 15. It is known that any connected undirected graph is balanced by Definition 1. Therefore, the proposed Theorem 12 and Corollaries 13 and 14 can be applied to the connected undirected network.

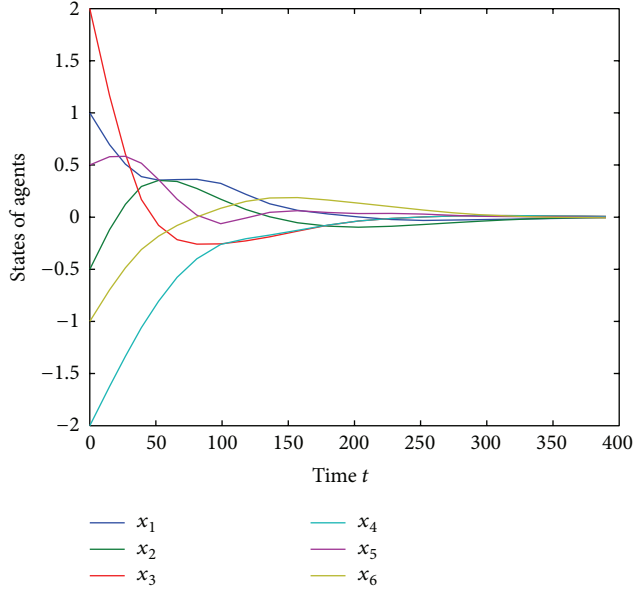


FIGURE 5: State trajectories of the network with $\gamma = 0.1$, $\eta_1 = 0$, $\eta_3 = 0.30$.

$$\tilde{\Phi} = \begin{bmatrix} 0.6811 & -0.0578 & 0.0297 & -0.0494 & -0.0685 \\ -0.0578 & 0.7583 & 0.0240 & -0.0303 & -0.0035 \\ 0.0297 & 0.0240 & 0.8437 & -0.0933 & -0.1292 \\ -0.0494 & -0.0303 & -0.0933 & 0.7566 & 0.0349 \\ -0.0685 & -0.0035 & -0.1292 & 0.0349 & 0.8766 \end{bmatrix},$$

$$\Phi = U_1 * \tilde{\Phi} * U_1^T = \begin{bmatrix} 0.6166 & -0.1657 & -0.1087 & -0.1499 & -0.1298 & -0.0625 \\ -0.1657 & 0.6262 & -0.0956 & -0.1338 & -0.1168 & -0.1143 \\ -0.1087 & -0.0956 & 0.6863 & -0.2101 & -0.1995 & -0.0724 \\ -0.1499 & -0.1338 & -0.2101 & 0.6497 & -0.0182 & -0.1378 \\ -0.1298 & -0.1186 & -0.1995 & -0.0182 & 0.7074 & -0.2432 \\ -0.0625 & -0.1143 & -0.0724 & -0.1378 & -0.2432 & 0.6302 \end{bmatrix}. \quad (52)$$

The state trajectories of the network are shown in Figure 5. It is seen obviously that average consensus is asymptotically achieved. Figure 6 shows the event-triggered time instant and time intervals. It is seen that the sampled data that need be transmitted reduce importantly. Evolution of the error norm is seen in Figure 7. It is seen that

5. Numerical Example

To verify the effectiveness of proposed method, numerical example was operated on.

Example. Considering a directed network of six agents as shown in Figure 4, it has balanced and weakly connected digraph with 0-1 weights. Set the initial condition $x(0) = [1; -0.5; 2; -2; 0.5; -1]$; then $\alpha = \text{Ave}(x(0)) = 0$.

Set $\gamma = 0, 0.10, 0.30, 0.50, 0.80$, using Theorem 12, and maximum allowable delay τ_{\max} can be easily gained. Simulation results are listed in Table 1. It is found that the maximum allowable delay decreases with the increasing of γ .

For the first case $\gamma = 0.1$, $h = 0.01$, $\eta_1 = 0$, $\eta_3 = 0.30$, using Theorem 12, the corresponding feasible solution is

the solid line represents the evolution of $e^T(t_k h)\Phi e(t_k h)$, which stays below the specified state-dependent threshold $\gamma x^T(t_k h)\Phi x(t_k h)$ which is represented by the dotted line.

For the another case $\gamma = 0.3$, $h = 0.01$, $\eta_1 = 0$, $\eta_3 = 0.30$, using Theorem 12, the corresponding feasible solution is

$$\tilde{\Phi} = \begin{bmatrix} 2.1939 & -0.7841 & -1.2138 & -1.2540 & 0.8663 \\ -0.7841 & 5.3061 & 0.5101 & -0.0073 & -0.5493 \\ -1.2138 & 0.5101 & 4.3940 & -1.8528 & -0.2296 \\ -1.2540 & -0.0073 & -1.8528 & 5.6745 & 0.7017 \\ 0.8663 & -0.5493 & -0.2296 & 0.7017 & 6.1132 \end{bmatrix}.$$

$$\Phi = \begin{bmatrix} 3.2067 & -1.3028 & -1.0731 & -1.4047 & 1.0093 & -0.4355 \\ -1.3028 & 4.2036 & -0.2639 & -0.7973 & -1.5763 & -0.2634 \\ -1.0731 & -0.2639 & 4.4228 & -2.2695 & -0.2068 & -0.6096 \\ -1.4047 & -0.7973 & -2.2695 & 5.0211 & 0.5312 & -1.0808 \\ 1.0093 & -1.5763 & -0.2068 & 0.5312 & 2.3404 & -2.0979 \\ -0.4355 & -0.2634 & -0.6096 & -1.0808 & -2.0979 & 4.4871 \end{bmatrix}, \quad (53)$$

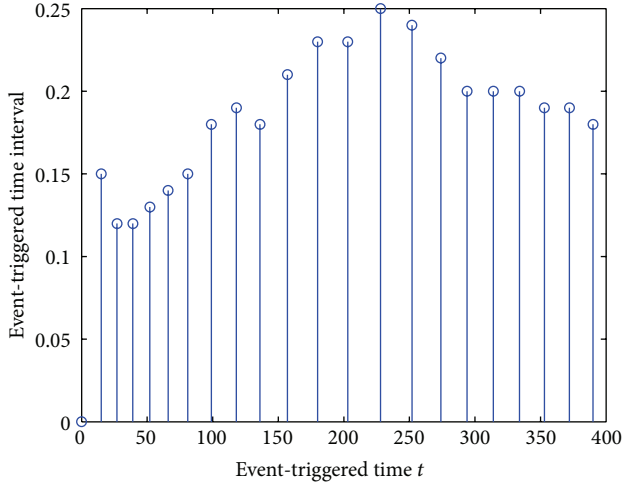


FIGURE 6: Event-triggered time and time intervals with $\gamma = 0.1$, $\eta_1 = 0$, $\eta_3 = 0.30$.

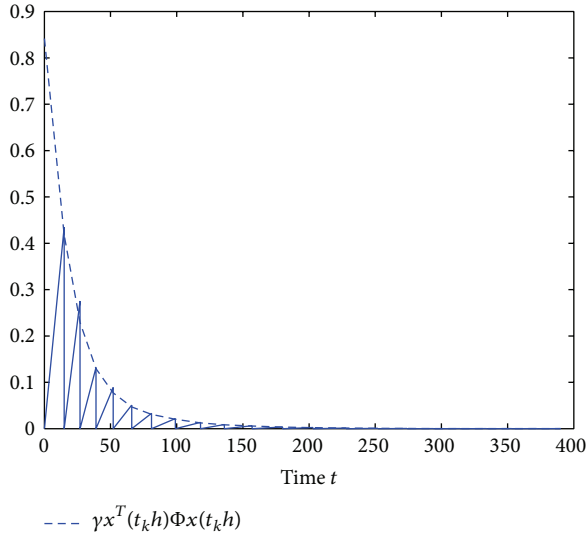


FIGURE 7: Evolution of $e^T(t_k h)\Phi e(t_k h)$ with $\gamma = 0.1$, $\eta_1 = 0$, $\eta_3 = 0.30$.

Similarly, Figure 5 shows the state trajectories of the network with $\gamma = 0.3$, $\eta_1 = 0$, $\eta_3 = 0.30$. The network also asymptotically achieved average consensus. Event-triggered time instant and time intervals are shown in Figure 8.

It is found from Figures 6 and 9 that the numbers of event-triggered time instant reduce and the average value of event-triggered time intervals increases with the increasing of γ . Simulation results are listed in Table 2. Therefore, the proposed event-triggered mechanism can reduce much signal transmission and thus reduce the multiagent network load.

6. Conclusions

This paper has mainly investigated the event-triggered average consensus problem in a directed/undirected network for

TABLE 2: Simulation results for different γ with $\eta_1 = 0$, $\eta_3 = 0.30$.

γ	Event numbers	Average value of event intervals	Max. (min.) value of event intervals
0.1	22	0.1890	0.26 (0.12)
0.3	13	0.3075	0.38 (0.18)

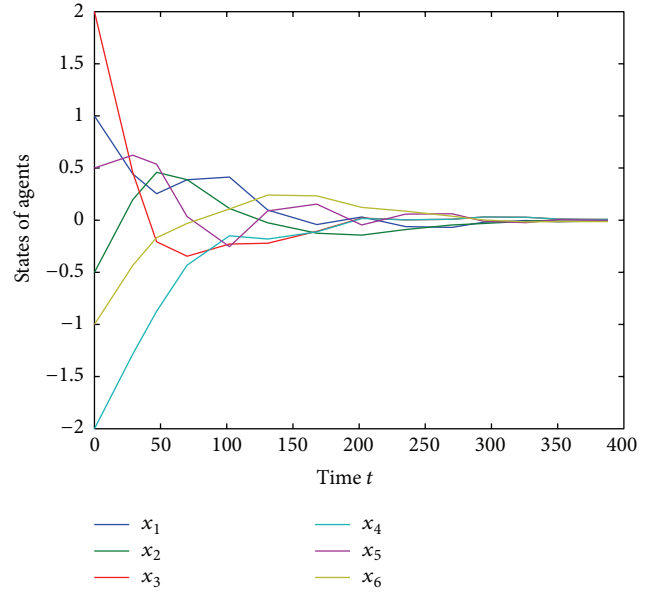


FIGURE 8: State trajectories of the topology G with $\gamma = 0.3$, $\eta_1 = 0$, $\eta_3 = 0.30$.

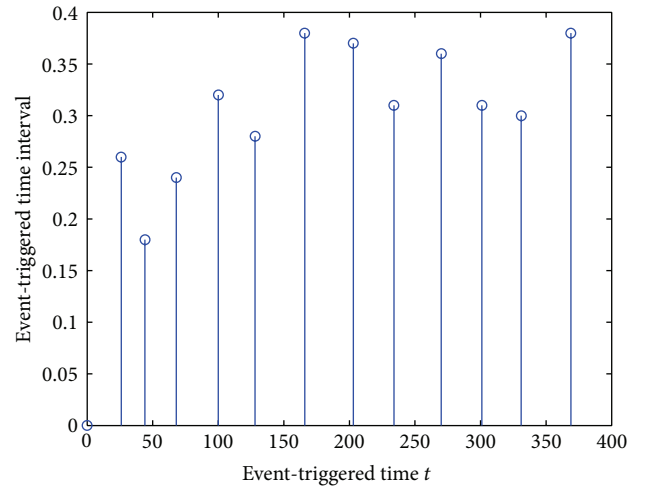


FIGURE 9: Event-triggered time and time intervals with $\gamma = 0.3$, $\eta_1 = 0$, $\eta_3 = 0.30$.

multiagent systems with fixed topology and time-varying delay. Sufficient conditions for average consensus are presented, and an upper bound of time-varying communication delay is derived. Furthermore, due to unreliable information channels and limited bandwidth, communication between agents may produce data packet dropout and out-of-order. Considering these issues, how to study the average consensus

problem is the further work. Moreover, how to solve decentralized event-triggered mechanism with networked-related nondeterministic issues is another important direction in the future.

Appendix

Proof of Theorem 12. The system (28) is equivalent to (41). Based on the system (41), we construct a Lyapunov-Krasovskii functional candidate as

$$\begin{aligned} V(t) = & \bar{\delta}^T(t) P \bar{\delta}(t) + \int_{t-\eta_1}^t \bar{\delta}^T(\alpha) S \bar{\delta}(\alpha) d\alpha \\ & + \sum_{i=1}^3 (\eta_i - \eta_{i-1}) \int_{-\eta_i}^{-\eta_{i-1}} \int_{t+s}^t \dot{\bar{\delta}}^T(v) R_i \dot{\bar{\delta}}(v) dv ds \\ & + \int_{t-\rho}^t \zeta^T(\beta) Q \zeta(\beta) d\beta, \end{aligned} \quad (\text{A.1})$$

where P, R_i ($i = 1, 2, 3$), $S \in \mathfrak{R}^{(n-1) \times (n-1)}$ are positive definite matrices:

$$\rho \triangleq \frac{\eta_3 - \eta_1}{2}, \quad \eta_0 = 0, \quad \eta_2 \triangleq \frac{\eta_1 + \eta_3}{2},$$

$$\zeta(\beta) \triangleq \begin{bmatrix} \bar{\delta}(\beta - \eta_1) \\ \bar{\delta}(\beta - \eta_2) \end{bmatrix},$$

$$Q \triangleq \begin{bmatrix} Q_1 & * \\ Q_3 & Q_2 \end{bmatrix} > 0, \quad Q_i \ (i = 1, 2, 3) \in \mathfrak{R}^{(n-1) \times (n-1)}. \quad (\text{A.2})$$

Define

$$\begin{aligned} V_1(t) &= \bar{\delta}^T(t) P \bar{\delta}(t), \\ V_2(t) &= \int_{t-\eta_1}^t \bar{\delta}^T(\alpha) S \bar{\delta}(\alpha) d\alpha, \\ V_3(t) &= \sum_{i=1}^3 (\eta_i - \eta_{i-1}) \int_{-\eta_i}^{-\eta_{i-1}} \int_{t+s}^t \dot{\bar{\delta}}^T(v) R_i \dot{\bar{\delta}}(v) dv ds, \\ V_4(t) &= \int_{t-\rho}^t \zeta^T(\beta) Q \zeta(\beta) d\beta. \end{aligned} \quad (\text{A.3})$$

Then $V(t) = V_1(t) + V_2(t) + V_3(t) + V_4(t) + V_5(t)$.

The derivative of (A.1) with respect to t is

$$\dot{V}(t) = \dot{V}_1(t) + \dot{V}_2(t) + \dot{V}_3(t) + \dot{V}_4(t), \quad (\text{A.4})$$

where

$$\begin{aligned} \dot{V}_1(t) &= 2\bar{\delta}^T(t) P \dot{\bar{\delta}}(t), \\ \dot{V}_2(t) &= \bar{\delta}(t)^T S \dot{\bar{\delta}}(t) - \bar{\delta}^T(t - \eta_1) S \dot{\bar{\delta}}(t - \eta_1), \end{aligned} \quad (\text{A.5})$$

$$\begin{aligned} \dot{V}_3(t) &= \sum_{i=1}^3 \dot{\bar{\delta}}^T(t) (\eta_i - \eta_{i-1})^2 R_i \dot{\bar{\delta}}(t) \\ &\quad - \sum_{i=1}^3 (\eta_i - \eta_{i-1}) \int_{t-\eta_i}^{t-\eta_{i-1}} \dot{\bar{\delta}}^T(v) R_i \dot{\bar{\delta}}(v) dv, \end{aligned} \quad (\text{A.6})$$

$$\dot{V}_4(t) = \xi^T(t) Q \xi(t) - \xi^T(t - \rho) Q \xi(t - \rho). \quad (\text{A.7})$$

Define

$$\begin{aligned} \eta_{21} &\triangleq \eta_2 - \eta_1, \quad \eta_{32} \triangleq \eta_3 - \eta_2, \\ \chi(t) &= \begin{bmatrix} \bar{\delta}^T(t) \bar{\delta}^T(t - \eta_1) \bar{\delta}^T(t - \eta(t)) \bar{\delta}^T(t - \eta_2) \\ \times \bar{\delta}^T(t - \eta_3) e^T(i_k h) \end{bmatrix}^T, \\ t &\in \Omega_i, \quad i = 0, 1, 2, \dots, l, \\ e_1 &\triangleq [I \ 0 \ 0 \ 0 \ 0 \ 0]^T, \\ e_2 &\triangleq [0 \ I \ 0 \ 0 \ 0 \ 0]^T, \\ e_3 &\triangleq [0 \ 0 \ I \ 0 \ 0 \ 0]^T, \\ e_4 &\triangleq [0 \ 0 \ 0 \ I \ 0 \ 0]^T, \\ e_5 &\triangleq [0 \ 0 \ 0 \ 0 \ I \ 0]^T, \\ e_6 &\triangleq [0 \ 0 \ 0 \ 0 \ 0 \ I]^T, \\ e_7 &\triangleq (-\tilde{L}e_3^T + \tilde{L}e_6^T)^T. \end{aligned} \quad (\text{A.8})$$

Then the system (41) is rewritten as $\dot{\bar{\delta}}(t) = e_7^T \chi(t)$.

Using Jensen's inequality [44] to handle the integral items in (A.6). Next, two cases are discussed.

(1) When $\eta_1 < \eta(t) \leq \eta_2$, $t \in \Omega_i$, $i = 0, 1, 2, \dots, l$, we can get

$$\begin{aligned} & \eta_1 \int_{t-\eta_1}^t \dot{\bar{\delta}}^T(v) R_1 \dot{\bar{\delta}}(v) dv \\ & \geq \eta_1 \times \frac{1}{\eta_1} \sum_{k=1}^n \dot{\bar{\delta}}^T(\varepsilon) \Delta t_i R_1 \sum_{k=1}^n \dot{\bar{\delta}}(\varepsilon) \Delta t_i \\ & = (\bar{\delta}(t) - \bar{\delta}(t - \eta_1))^T R_1 (\bar{\delta}(t) - \bar{\delta}(t - \eta_1)) \\ & = \chi^T(t) (e_1 - e_2) R_1 (e_1 - e_2)^T \chi(t), \end{aligned} \quad (\text{A.9})$$

$$\begin{aligned}
& (\eta_2 - \eta_1) \int_{t-\eta_2}^{t-\eta_1} \dot{\delta}^T(v) R_2 \dot{\delta}(v) dv \\
&= \eta_{21} \int_{t-\eta(t)}^{t-\eta_1} \dot{\delta}^T(v) R_2 \dot{\delta}(v) dv \\
&\quad + \eta_{21} \int_{t-\eta_2}^{t-\eta(t)} \dot{\delta}^T(v) R_2 \dot{\delta}(v) dv \quad (\text{A.10}) \\
&\geq \frac{\eta_{21}}{\eta(t) - \eta_1} \chi^T(t) (e_2 - e_3) R_2 (e_2 - e_3)^T \chi(t) \\
&\quad + \frac{\eta_{21}}{\eta_2 - \eta(t)} \chi^T(t) (e_3 - e_4) R_2 (e_3 - e_4)^T \chi(t),
\end{aligned}$$

$$\begin{aligned}
& (\eta_3 - \eta_2) \int_{t-\eta_3}^{t-\eta_2} \dot{\delta}^T(v) R_3 \dot{\delta}(v) dv \\
&\geq \frac{\eta_3 - \eta_2}{\eta_3 - \eta_2} \chi^T(t) (e_4 - e_5) R_3 (e_4 - e_5)^T \chi(t) \quad (\text{A.11}) \\
&= \chi^T(t) (e_4 - e_5) R_3 (e_4 - e_5)^T \chi(t).
\end{aligned}$$

Applying Lemma 11 to (A.10) yields

$$(\eta_2 - \eta_1) \int_{t-\eta_2}^{t-\eta_1} \dot{\delta}^T(v) R_2 \dot{\delta}(v) dv \geq \chi^T(t) \Lambda_2 \chi(t), \quad (\text{A.12})$$

where

$$\begin{aligned}
\Lambda_2 &= \begin{bmatrix} (e_2 - e_3)^T \\ (e_3 - e_4)^T \end{bmatrix}^T \begin{bmatrix} R_2 & U_2^T \\ U_2 & R_2 \end{bmatrix} \begin{bmatrix} (e_2 - e_3)^T \\ (e_3 - e_4)^T \end{bmatrix}, \\
&\quad \begin{bmatrix} R_2 & * \\ U_2 & R_2 \end{bmatrix} > 0. \quad (\text{A.13})
\end{aligned}$$

Substituting (A.9)–(A.11) into (A.6) yields

$$\begin{aligned}
\dot{V}_3 &\leq \sum_{i=1}^3 (\eta_i - \eta_{i-1})^2 \chi^T(t) e_7 R_i e_7^T \chi(t) \\
&\quad - \chi^T(t) (e_1 - e_2) R_1 (e_1 - e_2)^T \chi(t) \quad (\text{A.14}) \\
&\quad - \chi^T(t) \Lambda_2 \chi(t) \\
&\quad - \chi^T(t) (e_4 - e_5) R_3 (e_4 - e_5)^T \chi(t).
\end{aligned}$$

Substituting (A.5), (A.7), and (A.14) into (A.4) yields

$$\begin{aligned}
\dot{V}(t) &\leq \chi^T(t) [e_7 P e_1^T + e_1 P e_7^T] \chi(t) \\
&\quad + \chi^T(t) e_1 S e_1^T \chi(t) - \chi^T(t) e_2 S e_2^T \chi(t) \\
&\quad + \sum_{i=1}^3 (\eta_i - \eta_{i-1})^2 \chi^T(t) e_7 R_i e_7^T \chi(t) \\
&\quad - \chi^T(t) (e_1 - e_2) R_1 (e_1 - e_2)^T \chi(t) \\
&\quad - \chi^T(t) \Lambda_2 \chi(t) \\
&\quad - \chi^T(t) (e_4 - e_5) R_3 (e_4 - e_5)^T \chi(t) \\
&\quad + \chi^T(t) \begin{bmatrix} e_2^T \\ e_4^T \end{bmatrix}^T \begin{bmatrix} Q_1 & * \\ Q_3 & Q_2 \end{bmatrix} \begin{bmatrix} e_2^T \\ e_4^T \end{bmatrix} \chi(t) \\
&\quad - \chi^T(t) \begin{bmatrix} e_4^T \\ e_5^T \end{bmatrix}^T \begin{bmatrix} Q_1 & * \\ Q_3 & Q_2 \end{bmatrix} \begin{bmatrix} e_4^T \\ e_5^T \end{bmatrix} \chi(t). \quad (\text{A.15})
\end{aligned}$$

Since, between $t_k h$ and $t_k h + ih$, no control signal is triggered, then condition (43) is satisfied; that is,

$$\begin{aligned}
& \tilde{e}^T(i_k h) \tilde{\Phi} \tilde{e}^T(i_k h) - \tilde{e}^T(i_k h) \tilde{\Phi} \tilde{e}^T(i_k h) \\
&\leq \gamma \tilde{\delta}^T(t_k h) \tilde{\Phi} \tilde{\delta}^T(t_k h) - \tilde{e}^T(i_k h) \tilde{\Phi} \tilde{e}^T(i_k h) \quad (\text{A.16}) \\
&= \gamma \chi^T(t) (e_3 - e_6) \tilde{\Phi} (e_3 - e_6)^T \chi(t) \\
&\quad - \chi^T(t) e_6 \tilde{\Phi} e_6^T \chi(t).
\end{aligned}$$

Substituting (A.16) into (A.15) yields

$$\begin{aligned}
\dot{V}(t) &\leq \chi^T(t) \left[e_7 P e_1^T + e_1 P e_7^T + e_1 S e_1^T - e_2 S e_2^T \right. \\
&\quad - (e_1 - e_2) R_1 (e_1 - e_2)^T - \Lambda_2 \\
&\quad - (e_4 - e_5) R_3 (e_4 - e_5)^T \\
&\quad + \begin{bmatrix} e_2^T \\ e_4^T \end{bmatrix}^T \begin{bmatrix} Q_1 & * \\ Q_3 & Q_2 \end{bmatrix} \begin{bmatrix} e_2^T \\ e_4^T \end{bmatrix} \\
&\quad - \begin{bmatrix} e_4^T \\ e_5^T \end{bmatrix}^T \begin{bmatrix} Q_1 & * \\ Q_3 & Q_2 \end{bmatrix} \begin{bmatrix} e_4^T \\ e_5^T \end{bmatrix} \\
&\quad \left. + \gamma (e_3 - e_6) \tilde{\Phi} (e_3 - e_6)^T - e_6 \tilde{\Phi} e_6^T \right. \\
&\quad \left. + \sum_{i=1}^3 (\eta_i - \eta_{i-1})^2 e_7 R_i e_7^T \right] \chi(t). \quad (\text{A.17})
\end{aligned}$$

Since

$$\begin{aligned}
& \sum_{i=1}^3 (\eta_i - \eta_{i-1})^2 e_7 R_i e_7^T \\
&= \sum_{i=1}^3 (\eta_i - \eta_{i-1})^2 (-\tilde{L}e_3^T + \tilde{L}e_6^T)^T \\
&\quad \times R_i (-\tilde{L}e_3^T + \tilde{L}e_6^T) \\
&= \Gamma_{21}^T \Gamma_{22}^{-1} \Gamma_{21},
\end{aligned} \tag{A.18}$$

based on the Lyapunov theory, the system (41) is asymptotically stable such that

$$\begin{aligned}
& e_7 P e_1^T + e_1 P e_7^T + e_1 S e_1^T - e_2 S e_2^T \\
&\quad - (e_1 - e_2) R_1 (e_1 - e_2)^T - \Lambda_2 \\
&\quad - (e_4 - e_5) R_3 (e_4 - e_5)^T \\
&\quad + \begin{bmatrix} e_2^T \\ e_4^T \end{bmatrix}^T \begin{bmatrix} Q_1 & * \\ Q_3 & Q_2 \end{bmatrix} \begin{bmatrix} e_2^T \\ e_4^T \end{bmatrix} \\
&\quad - \begin{bmatrix} e_4^T \\ e_5^T \end{bmatrix}^T \begin{bmatrix} Q_1 & * \\ Q_3 & Q_2 \end{bmatrix} \begin{bmatrix} e_4^T \\ e_5^T \end{bmatrix} \\
&\quad + \gamma (e_3 - e_6) \tilde{\Phi} (e_3 - e_6)^T - e_6 \tilde{\Phi} e_6^T \\
&\quad + \Gamma_{21}^T \Gamma_{22}^{-1} \Gamma_{21} < 0.
\end{aligned} \tag{A.19}$$

Finally, using Schur complement, (A.19) is equivalent to (47) ($j = 2$).

(2) Similarly, when $\eta_2 < \eta(t) \leq \eta_3$, $t \in \Omega_i$, $i = 0, 1, 2, \dots, l$, in the same way, we get

$$\begin{aligned}
\dot{V}(t) &\leq \chi^T(t) \left[e_7 P e_1^T + e_1 P e_7^T + e_1 S e_1^T - e_2 S e_2^T \right. \\
&\quad - (e_1 - e_2) R_1 (e_1 - e_2)^T \\
&\quad - (e_2 - e_4) R_3 (e_2 - e_4)^T \\
&\quad - \Lambda_3 + \begin{bmatrix} e_2^T \\ e_4^T \end{bmatrix}^T \begin{bmatrix} Q_1 & * \\ Q_3 & Q_2 \end{bmatrix} \begin{bmatrix} e_2^T \\ e_4^T \end{bmatrix} \\
&\quad - \begin{bmatrix} e_4^T \\ e_5^T \end{bmatrix}^T \begin{bmatrix} Q_1 & * \\ Q_3 & Q_2 \end{bmatrix} \begin{bmatrix} e_4^T \\ e_5^T \end{bmatrix} \\
&\quad + \gamma (e_3 - e_6) \tilde{\Phi} (e_3 - e_6)^T - e_6 \tilde{\Phi} e_6^T \\
&\quad \left. + \sum_{i=1}^3 (\eta_i - \eta_{i-1})^2 e_7 R_i e_7^T \right] \chi(t),
\end{aligned} \tag{A.20}$$

where

$$\Lambda_3 = \begin{bmatrix} (e_4 - e_3)^T \\ (e_3 - e_5)^T \end{bmatrix}^T \begin{bmatrix} R_3 & U_3^T \\ U_3 & R_3 \end{bmatrix} \begin{bmatrix} (e_4 - e_3)^T \\ (e_3 - e_5)^T \end{bmatrix}, \tag{A.21}$$

$$\begin{bmatrix} R_3 & * \\ U_3 & R_3 \end{bmatrix} > 0.$$

If $V(t) < 0$, the system (41) is asymptotically stable. So we have

$$\begin{aligned}
& e_7 P e_1^T + e_1 P e_7^T + e_1 S e_1^T - e_2 S e_2^T \\
&\quad - (e_1 - e_2) R_1 (e_1 - e_2)^T - \Lambda_2 \\
&\quad - (e_4 - e_5) R_3 (e_4 - e_5)^T \\
&\quad + \gamma (e_3 - e_6) \tilde{\Phi} (e_3 - e_6)^T - e_6 \tilde{\Phi} e_6^T \\
&\quad + \begin{bmatrix} e_2^T \\ e_4^T \end{bmatrix}^T \begin{bmatrix} Q_1 & * \\ Q_3 & Q_2 \end{bmatrix} \begin{bmatrix} e_2^T \\ e_4^T \end{bmatrix} \\
&\quad - \begin{bmatrix} e_4^T \\ e_5^T \end{bmatrix}^T \begin{bmatrix} Q_1 & * \\ Q_3 & Q_2 \end{bmatrix} \begin{bmatrix} e_4^T \\ e_5^T \end{bmatrix} \\
&\quad + \Gamma_{21}^T \Gamma_{22}^{-1} \Gamma_{21} < 0.
\end{aligned} \tag{A.22}$$

Finally, using Schur complement, (A.22) is equivalent to (47) ($j = 3$). This completes the proof. \square

Conflict of Interests

The authors declare that there is no conflict of interests regarding the publication of this paper.

Acknowledgments

The work was supported by the National Natural Science Foundation of China (Grant no. 61104089), National Key Scientific Instrument and Equipment Development Project (Grant no. 2012YQ15008703), the National High Technology Research and Development Program of China (Grant no. 2011AA040103-7), Science and Technology Commission of Shanghai Municipality (11jc1404000), and Shanghai Rising-Star Program (13QA1401600).

References

- [1] W. Ren, R. W. Beard, and E. M. Atkins, "Information consensus in multivehicle cooperative control," *IEEE Control Systems Magazine*, vol. 27, no. 2, pp. 71–82, 2007.
- [2] N. Maréchal, J.-M. Gorce, and J.-B. Pierrot, "Joint estimation and gossip averaging for sensor network applications," *IEEE Transactions on Automatic Control*, vol. 55, no. 5, pp. 1208–1213, 2010.
- [3] J. Hu and G. Feng, "Distributed tracking control of leader-follower multi-agent systems under noisy measurement," *Automatica*, vol. 46, no. 8, pp. 1382–1387, 2010.

- [4] X. Y. Luo, N. N. Han, and X. P. Guan, "Leader-following consensus protocols for formation control of multi-agent network," *Journal of Systems Engineering and Electronics*, vol. 22, no. 6, pp. 991–997, 2011.
- [5] Y. Cao and W. Ren, "Distributed coordinated tracking with reduced interaction via a variable structure approach," *IEEE Transactions on Automatic Control*, vol. 57, no. 1, pp. 33–48, 2012.
- [6] L. Cheng, Y. Wang, Z.-G. Hou, M. Tan, and Z. Cao, "Sampled-data based average consensus of second-order integral multi-agent systems: switching topologies and communication noises," *Automatica*, vol. 49, no. 5, pp. 1458–1464, 2013.
- [7] U. Münz, A. Papachristodoulou, and F. Allgöwer, "Consensus in multi-agent systems with coupling delays and switching topology," *IEEE Transactions on Automatic Control*, vol. 56, no. 12, pp. 2976–2982, 2011.
- [8] E. Nuño, R. Ortega, L. Basañez, and D. Hill, "Synchronization of networks of nonidentical Euler-Lagrange systems with uncertain parameters and communication delays," *IEEE Transactions on Automatic Control*, vol. 56, no. 4, pp. 935–941, 2011.
- [9] K. Sakurama and K. Nakano, "Necessary and sufficient condition for average consensus of networked multi-agent systems with heterogeneous time delays," *International Journal of Systems Science*, 2013.
- [10] E. Garcia, Y. Cao, H. Yu, P. Antsaklis, and D. Casbeer, "Decentralised event-triggered cooperative control with limited communication," *International Journal of Control*, vol. 86, no. 9, pp. 1479–1488, 2013.
- [11] H. C. Yan, H. B. Shi, H. Zhang, and F. W. Yang, "Quantized H_∞ control for networked systems with communication constraints," *Asian Journal of Control*, vol. 15, no. 5, pp. 1468–1476, 2013.
- [12] H. Zhang, H. C. Yan, T. Liu, and Q. J. Chen, "Fuzzy controller design for nonlinear impulsive fuzzy systems with time delay," *IEEE Transactions on Fuzzy Systems*, vol. 19, no. 5, pp. 844–856, 2011.
- [13] M. R. Fei, J. Yi, and H. S. Hu, "Robust stability analysis of an uncertain nonlinear networked control system category," *International Journal of Control, Automation and Systems*, vol. 4, no. 2, pp. 172–177, 2006.
- [14] H. J. Gao, T. W. Chen, and J. Lam, "A new delay system approach to network-based control," *Automatica*, vol. 44, no. 1, pp. 39–52, 2008.
- [15] X. D. Zhao, M. X. Ling, and Q. S. Zeng, "Delay-dependent robust control for uncertain stochastic systems with Markovian switching and multiple delays," *Journal of Systems Engineering and Electronics*, vol. 21, no. 2, pp. 287–295, 2010.
- [16] W. H. Deng, M. R. Fei, and H. S. Hu, "A linear matrix inequality approach to system stabilization over constrained channels," *Transactions of the Institute of Measurement and Control*, vol. 35, no. 1, pp. 83–91, 2013.
- [17] H. C. Yan, Z. Z. Su, H. Zhang, and F. W. Yang, "Observer-based H_∞ control for discrete-time stochastic systems with quantisation and random communication delays," *IET Control Theory & Applications*, vol. 7, no. 3, pp. 372–379, 2013.
- [18] L. X. Zhang, H. J. Gao, and O. Kaynak, "Network-induced constraints in networked control systems—a survey," *Transactions on Industrial Informatics*, vol. 9, no. 1, pp. 403–416, 2013.
- [19] H. Zhang, H. C. Yan, F. W. Yang, and Q. J. Chen, "Quantized control design for impulsive fuzzy networked systems," *IEEE Transactions on Fuzzy Systems*, vol. 19, no. 6, pp. 1153–1162, 2011.
- [20] R. Olfati-Saber and R. M. Murray, "Consensus problems in networks of agents with switching topology and time-delays," *IEEE Transactions on Automatic Control*, vol. 49, no. 9, pp. 1520–1533, 2004.
- [21] Y. G. Sun, L. Wang, and G. M. Xie, "Average consensus in networks of dynamic agents with switching topologies and multiple time-varying delays," *Systems & Control Letters*, vol. 57, no. 2, pp. 175–183, 2008.
- [22] P. Lin and Y. Jia, "Average consensus in networks of multi-agents with both switching topology and coupling time-delay," *Physica A: Statistical Mechanics and its Applications*, vol. 387, no. 1, pp. 303–313, 2008.
- [23] J. H. Qin, H. J. Gao, and W. X. Zheng, "On average consensus in directed networks of agents with switching topology and time delay," *International Journal of Systems Science*, vol. 42, no. 12, pp. 1947–1956, 2011.
- [24] Y. Z. Sun, W. Li, and J. Ruan, "Average consensus of multi-agent systems with communication time delays and noisy links," *Chinese Physics B*, vol. 22, no. 3, Article ID 030510, 2013.
- [25] A. V. Proskurnikov, "Average consensus in networks with nonlinearly delayed couplings and switching topology," *Automatica*, vol. 49, no. 9, pp. 2928–2932, 2013.
- [26] F. L. Sun, Z.-H. Guan, L. Ding, and Y.-W. Wang, "Mean square average-consensus for multi-agent systems with measurement noise and time delay," *International Journal of Systems Science*, vol. 44, no. 6, pp. 995–1005, 2013.
- [27] L. Rong, S. Xu, B. Zhang, and Y. Zou, "Accelerating average consensus by using the information of second-order neighbours with communication delays," *International Journal of Systems Science*, vol. 44, no. 6, pp. 1181–1188, 2013.
- [28] Q. J. Zhang, Y. F. Niu, L. Wang, L. C. Shen, and H. Zhu, "Average consensus seeking of high-order continuous-time multi-agent systems with multiple time-varying communication delays," *International Journal of Control, Automation and Systems*, vol. 9, no. 6, pp. 1209–1218, 2011.
- [29] H. C. Yan, Y. C. Shen, H. Zhang, and H. B. Shi, "Decentralized event-triggered consensus control for second-order multi-agent system," *Neurocomputing*, vol. 133, no. 1, pp. 18–24, 2014.
- [30] H. Y. Zhu, Y. R. Cong, X. K. Wang, D. B. Zhang, and Q. Zhang, "Consensusabilization for continuous-time high-order multi-agent systems with time-varying delays," *Mathematical Problems in Engineering*, vol. 2013, Article ID 527039, 12 pages, 2013.
- [31] Y. Tipsuwan and M.-Y. Chow, "Control methodologies in networked control systems," *Control Engineering Practice*, vol. 11, no. 10, pp. 1099–1111, 2003.
- [32] H. A. Thompson, "Wireless and Internet communications technologies for monitoring and control," *Control Engineering Practice*, vol. 12, no. 6, pp. 781–791, 2004.
- [33] P. Tabuada, "Event-triggered real-time scheduling of stabilizing control tasks," *IEEE Transactions on Automatic Control*, vol. 52, no. 9, pp. 1680–1685, 2007.
- [34] W. P. M. H. Heemels, J. H. Sandee, and P. P. J. van den Bosch, "Analysis of event-driven controllers for linear systems," *International Journal of Control*, vol. 81, no. 4, pp. 571–590, 2008.
- [35] S. G. Loizou and K. J. Kyriakopoulos, "Navigation of multiple kinematically constrained robots," *IEEE Transactions on Robotics*, vol. 24, no. 1, pp. 221–231, 2008.
- [36] D. V. Dimarogonas, E. Frazzoli, and K. H. Johansson, "Distributed event-triggered control for multi-agent systems," *IEEE Transactions on Automatic Control*, vol. 57, no. 5, pp. 1291–1297, 2012.

- [37] G. S. Seyboth, D. V. Dimarogonas, and K. H. Johansson, "Event-based broadcasting for multi-agent average consensus," *Automatica*, vol. 49, no. 1, pp. 245–252, 2013.
- [38] J. P. Hu, G. R. Chen, and H.-X. Li, "Distributed event-triggered tracking control of leader-follower multi-agent systems with communication delays," *Kybernetika*, vol. 47, no. 4, pp. 630–643, 2011.
- [39] X. X. Yin and D. Yue, "Event-triggered tracking control for heterogeneous multi-agent systems with Markov communication delays," *Journal of the Franklin Institute*, vol. 350, no. 5, pp. 1312–1334, 2013.
- [40] S. L. Hu and D. Yue, "Event-triggered control design of linear networked systems with quantizations," *ISA Transactions*, vol. 51, no. 1, pp. 153–162, 2012.
- [41] C. Peng and T. C. Yang, "Event-triggered communication and H_∞ control co-design for networked control systems," *Automatica*, vol. 49, no. 5, pp. 1326–1332, 2013.
- [42] C. D. Godsil and G. Royle, *Algebraic Graph Theory*, Springer, New York, NY, USA, 2001.
- [43] P. G. Park, J. W. Ko, and C. Jeong, "Reciprocally convex approach to stability of systems with time-varying delays," *Automatica*, vol. 47, no. 1, pp. 235–238, 2011.
- [44] K. Gu, V. L. Kharitonov, and J. Chen, *Stability of Time-Delay Systems*, Birkhäuser, Boston, Mass, USA, 2003.

Research Article

Guaranteed Cost Control for Multirate Networked Control Systems with Both Time-Delay and Packet-Dropout

Qixin Zhu,^{1,2} Binbin Xie,² and Yonghong Zhu³

¹ School of Mechanical Engineering, Suzhou University of Science and Technology, Suzhou 215009, China

² School of Electrical and Electronic Engineering, East China Jiaotong University, Nanchang 330013, China

³ School of Mechanical and Electronic Engineering, Jingdezhen Ceramic Institute, Jingdezhen 333001, China

Correspondence should be addressed to Qixin Zhu; bob21cn@163.com

Received 26 November 2013; Revised 8 February 2014; Accepted 9 February 2014; Published 17 April 2014

Academic Editor: Xudong Zhao

Copyright © 2014 Qixin Zhu et al. This is an open access article distributed under the Creative Commons Attribution License, which permits unrestricted use, distribution, and reproduction in any medium, provided the original work is properly cited.

Compared with traditional networked control systems, the sampling rates of the nodes are not the same in the multirate networked control systems (NCSs). This paper presents a new stabilization method for multirate NCSs. A multirate NCSs with simultaneous considering time-delay and packet-dropout is modeled as a time-varying sampling system with time-delay. The proposed Lyapunov function decreases at each input signal updating point, which is largely ignored in prior works. Sufficient condition for the stochastic mean-square stability of the multirate NCSs is given, and the cost function value is less than a bound. Numerical examples are presented to illustrate the effectiveness of the proposed control scheme.

1. Introduction

Feedback control systems where in the control loops are closed through real-time network are called Networked Control Systems (NCSs) [1]. Compared with the traditional control architecture, NCSs have many advantages such as high reliability, simple installation, and lower cost. Although the NCSs have many advantages, the applying of NCSs makes the system more complicated to analyze. Since the data is transmitted via network, there are two major problems of NCSs. Firstly, the network-induced delay occurs while transferring data between devices and shared medium. Secondly, unreliable network transmission may lead to packet dropout.

For these reasons, it is vital to study NCSs with network-induced delay and packet dropout. Up to now, many good achievements have been investigated to deal with these problems. For the issue of time delay, the stability of NCSs with short random time delay was studied in [1]. The achievement in [1] was expanded for the situation of long time delay in [2]. The system was modeled into switch systems to investigate the stability of networked control systems in [3]. Packet dropout not only exists in time delay progress but also in transmission loss. For the problem of packet dropout,

the stabilizing of controller was investigated in [4–18]. The models of NCSs in prior papers were divided into three cases: switch linear systems [6], asynchronous dynamical systems [9], and jump linear systems [13]. It is more complex to deal with the modeling and analysis for NCSs with both delay and packet dropout, compared with separately considering each other. In [15], the method of switched linear systems was applied in modeling for the NCSs of both packet dropout and network-induced delay in NCSs. Sufficient conditions for stochastic stability were discussed in [16]; what is more, packet dropout on both sides of sensor-to-controller and controller-to-sensor was modeled as two Markov chains.

It is important to ensure that the system possesses a strong robust performance. The guaranteed cost control is a good way to deal this problem, which guarantees the system performance affected uncertainty bellow the given performance index bound. The guaranteed cost control was first mooted in [19]. These years it has been applied to networked control system with time delay, and many issues have been developed for this item in [20–25].

Unfortunately, most aforementioned conclusions are under the following assumption: the sampling rates of each node in NCSs are the same. This brings convenience for the

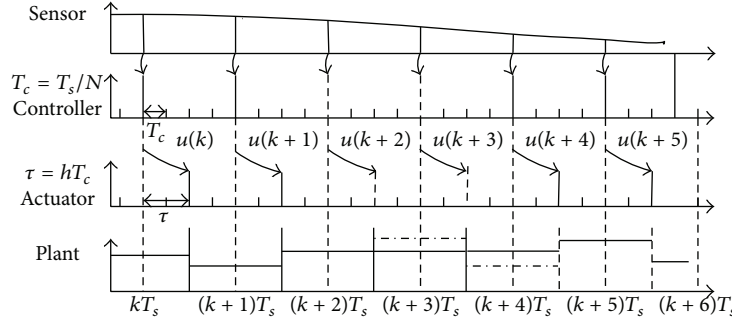


FIGURE 1: The timing diagrams of multirate NCSs.

theoretical research of NCSs; however, the sampling rate of each node is not identical in practical application. For the multirate network, the rates are not the same, the sampling period of sensor is T_s , and sampling period of the controller is T_c , $T_s \neq T_c$. In recent years, the investigations of multirate control system have made a great progress [26–36]. The NCSs are modeled as switched systems by using multirate method, when sensor, controller, and actuator are all event-driven, in [26], and the stability was analyzed. The exponential stability of multirate NCSs was analyzed including three cases of perfect transmission, delayed transmission, and time-varying transmission, in [28]. In [32], the condition of stabilizing controller of multirate NCSs was discussed by the way of using a V-K iteration algorithm. Controllability and observability of networked control systems with short time delay are analyzed in [35, 36].

It is nice to see that the network control systems theory has been widely applied to practical area. Two online schemes based on the data-driven fault-tolerant control (FTC) systems on the benchmark Tennessee Eastman process are presented in [37]. A subspace-aided data-driven approach for batch processes is proposed in [38]. A comparison between the basic data-driven methods for process monitoring and fault diagnosis (PM-FD) is provided in [39].

Published literature shows that many questions about guaranteed cost control for multirate NCSs with both time delay and packet dropout should be investigated. The main contributions of this paper are as follows. (1) A multirate NCSs with simultaneous consideration time delay and packet dropout are modeled as a time-varying sampling system with time delay. (2) The Lyapunov function decreases at each input signal updating point, which is largely ignored in prior works. Compared with traditional NCSs methods, it can yield less conservative. (3) State feedback controller of multirate NCSs, which render the multirate networked control systems stochastic mean square stable, is proposed. And the cost function value is less than a bound.

This paper is organized into four sections including the Introduction. Problem formulations and main assumptions were presented in Section 2. In Section 3, the guaranteed cost control of NCSs was discussed. The controller is proved to render the system stochastic mean square stable. An illustrative example is provided in Section 4.

Notations. The superscript “ T ” stands for the transpose of a matrix. R^n and $R^{n \times m}$ denote the n dimensional Euclidean space and the set of all $n \times m$ real matrices, respectively. $\|\cdot\|$ stands for the Euclidean norm. I and 0 stand for identified matrices and zero matrices with appropriate dimensions, respectively. The notation $X > 0$ ($X \geq 0$) means that the matrix X is positive definite (X is semipositive definite). I is the identity matrix of appropriate dimensions. $\begin{bmatrix} X & Z \\ * & Y \end{bmatrix}$ denotes a symmetric matrix, where $*$ denotes the entries implied by symmetry.

2. Problem Formulation

It is assumed that the controlled process is a linear time-invariant system, which can be expressed as

$$\begin{aligned} \dot{x}(t) &= A^c x(t) + B^c u(t) + E^c v(t), \\ z(t) &= Cx(t) + Hv(t), \end{aligned} \quad (1)$$

where $x(t) \in R^n$, $u(t) \in R^m$, $v(t) \in R^q$, and A^c, B^c, E^c, C, H are matrices of appropriate sizes and $v(t)$ is white noise with zero mean. The sampling period of the sensor is noted as T_s , and the sampling periods of controller and actuator are the same, noted as T_c . $T_c = T_s/N$ and N are a positive integer not less than 2. That is to say, the controller and actuator have a higher sampling frequency than the sensor. In order to facilitate the discussion, the delay of the system is considered to be a constant short delay, in this paper. The information transmission sequence of multirate NCSs is in Figure 1.

In convenience of investigation, we make the following rational assumptions.

- (A1) The sensor, the controller, and the actuator are all time-driven, sensor-to-controller delay is denoted by τ_{sc} , and the delay of controller-to-actuator is denoted by τ_{ca} . The time delay in the system is $\tau = \tau_{sc} + \tau_{ca} = hT_c$, $h \leq N$, and h is a positive integer.
- (A2) The number of successive packet dropouts is upper bounded, and the bound is denoted a known constant d .
- (A3) The system adopts the Zero Order Hold (ZOH) strategy.

In the multirate networked control systems, the inputs of sampling interval are different from sampling interval to interval. The model of multirate NCSs is described as follows.

Case $S_i^{(0)}$. There is no packet dropout which occurs in the current sampling interval. Such as in the interval $[(k+5)T_s, (k+6)T_s]$,

$$\begin{aligned}
x[(k+1)T_s] &= Ax(kT_s) \\
&+ \left(\int_{kT_s}^{kT_s+hT_c} e^{A^c[(k+1)T_s-\eta]} B^c d\eta \right) \\
&\times u[(k-1)T_s] \\
&+ \left(\int_{kT_s+hT_c}^{(k+1)T_s} e^{A^c[(k+1)T_s-\eta]} B^c d\eta \right) u(kT_s) \\
&+ E^c v(kT_s) \\
&= Ax(kT_s) + \left(\int_0^{(N-h)T_c} e^{A^c\eta_1} B^c d\eta_1 \right) u(kT_s) \\
&+ \left(\int_{(N-h)T_c}^{NT_c} e^{A^c\eta_1} B^c d\eta_1 \right) u[(k-1)T_s] \\
&+ Ev(kT_s) \\
&= Ax(kT_s) + (B_1 + B_2 + \dots + B_{N-h}) u(kT_s) \\
&+ (B_{N-h+1} + B_{N-h+2} + \dots + B_N) \\
&\times u[(k-1)T_s] + Ev(kT_s), \tag{2}
\end{aligned}$$

where

$$\begin{aligned}
A &= e^{A^c T_s}, \quad B_1 = \int_0^{T_c} e^{A^c\eta_1} B^c d\eta_1, \\
B_k &= D^{k-1} B_1, \quad D = \int_0^{T_c} e^{A^c\eta_1} d\eta_1, \quad 1 \leq k \leq N, \tag{3} \\
E &= \int_0^{T_s} e^{A^c\eta_1} E^c d\eta_1.
\end{aligned}$$

Case $S_i^{(1)}$. There are i successive packet dropouts in the current sampling interval. Such as in interval $[(k+2)T_s, (k+3)T_s]$ to interval $[(k+3)T_s, (k+4)T_s]$. The inputs of actuator in this period are the latest effective inputs,

$$\begin{aligned}
x[(k+1)T_s] &= Ax(kT_s) \\
&+ \left(\int_{kT_s}^{kT_s+T_s} e^{A^c[(k+1)T_s-\eta]} B^c d\eta \right) \\
&\times u[(k-i)T_s] + Ev(kT_s) \\
&= Ax(kT_s) + (B_1 + B_2 + \dots + B_N) \\
&\times u[(k-i)T_s] + Ev(kT_s). \tag{4a}
\end{aligned}$$

Case $S_i^{(2)}$. There is no packet dropout within the current sampling interval, but the last i times sampling intervals packet dropouts. Such as in the interval $[(k+3)T_s, (k+4)T_s]$

$$\begin{aligned}
x[(k+1)T_s] &= Ax(kT_s) \\
&+ \left(\int_0^{(N-h)T_c} e^{A^c\eta_1} B^c d\eta_1 \right) u(kT_s) \\
&+ \left(\int_{(N-h)T_c}^{NT_c} e^{A^c\eta_1} B^c d\eta_1 \right) u[(k-1)T_s] \\
&+ Ev(kT_s) \\
&= Ax(kT_s) + (B_1 + B_2 + \dots + B_{N-h}) u(kT_s) \\
&+ (B_{N-h+1} + B_{N-h+2} + \dots + B_N) \\
&\times u[(k-i-1)T_s] + Ev(kT_s). \tag{4b}
\end{aligned}$$

Definition 1. Let $\varsigma = \{i_1, i_2, \dots, i_k\}$ denote the point of each input signal arrived,

$$\xi_k = \{i_{k+1} - i_k\} \in \{1, 2, 3, \dots, d\}, \quad d = \max(i_{k+1} - i_k). \tag{5}$$

Definition 2. We assume the packet dropout progress on the basis of a discrete-time Markova chain process, the mode of transition probabilities:

$$P_{\xi_k} = \Pr(i_{k+1} = i + \xi_k \mid i_k = i) > 0, \quad i \in \varsigma, \tag{6}$$

where $\sum_{\xi_k=1}^d P_{\xi_k} = 1$.

The controlled process can be rewritten as

$$\begin{aligned}
x(i_{k+1}) &= A^{\xi_k} x(i_k) + \Gamma_0(\tau_k) u(i_k) \\
&+ \left[\Gamma_1(\tau_k) + \delta_{\xi_k} \left(\sum_0^{\xi_k} A^i \right) \Gamma_2(\tau_k) \right] u(i_k - \xi_{k-1}) \\
&+ Ev(i_k), \tag{7}
\end{aligned}$$

where $\delta_{\xi_k} = 1$ if $\xi_k > 1$, otherwise $\delta_{\xi_k} = 0$. $A^{\xi_k} = \underbrace{A \cdot A \cdot A \cdots A}_{\xi_k}$, $\Gamma_0(\tau_k) = \sum_{i=1}^{N-h} B_i$,

$$\Gamma_1(\tau_k) = \sum_{i=N-h+1}^N B_i, \quad \Gamma_2(\tau_k) = \sum_{i=1}^N B_i. \tag{8}$$

The state-based control scheme for the system (7) is described by

$$u(k) = Kx(k), \tag{9}$$

where $K \in R^{m \times n}$ is the controller gain. Substituting (9) into (7) results in the following system:

$$\begin{aligned} x(i_{k+1}) &= (A^{\xi_k} + \Gamma_0 K) x(i_k) \\ &+ \left(\Gamma_1(\tau_k) + \delta_{\xi_k} \left(\sum_0^{\xi_k} A^i \right) \Gamma_2 \right) K x(i_k - \xi_{k-1}) \\ &+ E v(i_k), \end{aligned} \quad (10)$$

where τ_k is omitted here.

3. Main Results and Proofs

Firstly, we introduce the following lemmas and definitions, which will be cited for the proofs in this section.

Definition 3. The closed-loop networked control systems (10) are stochastic mean-square stable if when $v(i_k) = 0$, $x_0 = x(0)$ such that

$$E \left(\sum_0^{\infty} \|x(i_k)\|^2 \right) < \infty. \quad (11)$$

Definition 4. Our object is to design a controller such that the closed loop networked system with both packet dropout and time delay is stochastic mean-square stable and satisfies H_{∞} performance constraint γ . That is to say (10) satisfies the following three conditions simultaneously.

(N1) The closed loop networked control systems (10) are stochastic mean-square stable.

(N2) For system (10), the defined cost function:

$$J = E \left\{ \sum_{k=0}^{\infty} x^T(i_k) S x(i_k) + u^T(i_k) R u(i_k) \right\} \quad (12)$$

satisfies $J \leq J^*$. J^* is a constant, where $S > 0$, $R > 0$.

(N3) Under the zero-initial condition, for all nonzero $v(i_k)$, the controlled output z_{i_k} satisfies

$$\sum_{k=0}^{\infty} E \left(z_{i_k}^T z_{i_k} \right) - \gamma^2 v_{i_k}^T v_{i_k} < 0. \quad (13)$$

Lemma 5 (Schur complement). For given a matrix $S = \begin{bmatrix} S_{11} & S_{12} \\ S_{12}^T & S_{22} \end{bmatrix}$, where S_{11} , S_{12} are square matrices, the following conditions are equivalent:

- (1) $S < 0$;
- (2) $S_{11} < 0$, $S_{22} - S_{12}^T S_{11}^{-1} S_{12} < 0$;
- (3) $S_{22} < 0$, $S_{11} - S_{12} S_{22}^{-1} S_{12}^T < 0$.

Theorem 6. For the system (10), if positive definite matrixes exist $P, Q > 0$, such that

- (1) $2G^T(P+Q)G - P + S + K^T R K < 0$,
- (2) $2H_{\xi_k}^T(P+Q)H_{\xi_k} - Q < 0$,

where $G = A^{\xi_k} + \Gamma_0 K$, $H_{\xi_k} = [\Gamma_1 + \delta_{\xi_k} (\sum_{i=0}^{\xi_k} A^i) \Gamma_2] K$. Then the system (10) with the controller (9) is stochastic mean-square stable and the cost function value is less than a bound. The corresponding cost function satisfies $J < x^T(i_0) P x(i_0) + x^T(i_{-1}) Q x(i_{-1})$.

Proof. Define a Lyapunov function as

$$\begin{aligned} V_1(i_k) &= x^T(i_k) P x(i_k), \\ V_2(i_k) &= \sum_{s=\xi_{k-1}}^{i_k-1} x^T(i_k - s) Q x(i_k - s), \\ V(i_k) &= \sum_{j=1}^2 V_j(i_k), \end{aligned} \quad (16)$$

where $P > 0$, $Q > 0$

$$\Delta V(i_k) = E[V(i_{k+1}) - V(i_k)] = \sum_{j=1}^2 E[\Delta V_j(i_k)]. \quad (17)$$

Along the solution of (9), $E(\Delta V_1(i_k))$, $E(\Delta V_2(i_k))$ takes the form of

$$\begin{aligned} E(\Delta V_1(i_k)) &= \sum_{\xi_k=1}^d p_{\xi_k} \left[G x(i_k) + H_{\xi_k} x(i_k - \xi_{k-1}) \right]^T P \\ &\quad \times \left[G x(i_k) + H_{\xi_k} x(i_k - \xi_{k-1}) \right] \\ &\quad - x^T(i_k) P x(i_k), \\ E(\Delta V_2(i_k)) &\leq \sum_{\xi_k=1}^d p_{\xi_k} \left[G x(i_k) + H_{\xi_k} x(i_k - \xi_{k-1}) \right]^T Q \\ &\quad \times \left[G x(i_k) + H_{\xi_k} x(i_k - \xi_{k-1}) \right] \\ &\quad - \sum_{\xi_k=1}^d p_{\xi_k} x^T(i_k) Q x(i_k). \end{aligned} \quad (18)$$

By (17) we can obtain

$$\begin{aligned} \Delta V(i_k) &\leq \sum_{\xi_k=1}^d p_{\xi_k} \left[G x(i_k) + H_{\xi_k} x(i_k - \xi_{k-1}) \right]^T (P+Q) \\ &\quad \times \left[G x(i_k) + H_{\xi_k} x(i_k - \xi_{k-1}) \right] \\ &\quad - x^T(i_k) P x(i_k) \\ &\quad - \sum_{\xi_k=1}^d p_{\xi_k} x^T(i_k - \xi_{k-1}) Q x(i_k - \xi_{k-1}). \end{aligned} \quad (19)$$

It is easy to obtain

$$\begin{aligned}
 & \sum_{\xi_k=1}^d p_{\xi_k} [Gx(i_k) + H_{\xi_k} x(i_k - \xi_{k-1})]^T (P + Q) \\
 & \quad \times [Gx(i_k) + H_{\xi_k} x(i_k - \xi_{k-1})] \\
 & = \sum_{\xi_k=1}^d p_{\xi_k} [x^T(i_k) G^T (P + Q) H_{\xi_k} x(i_k - \xi_{k-1})] \\
 & \quad + \sum_{\xi_k=1}^d p_{\xi_k} [x^T(i_k - \xi_{k-1}) H_{\xi_k}^T (P + Q) Gx(i_k)] \\
 & \quad + \sum_{\xi_k=1}^d p_{\xi_k} [x^T(i_k) G^T (P + Q) Gx(i_k)] \\
 & \quad + \sum_{\xi_k=1}^d p_{\xi_k} [x^T(i_k - \xi_{i_{k-1}}) H_{\xi_k}^T (P + Q) H_{\xi_k} x(i_k - \xi_{i_{k-1}})].
 \end{aligned} \tag{20}$$

By Lemma 5, $[Gx(i_k), H_{\xi_k} x(i_k - \xi_{k-1})]^T \begin{bmatrix} -P-Q & P+Q \\ P+Q & -P-Q \end{bmatrix} [Gx(i_k), H_{\xi_k} x(i_k - \xi_{k-1})]^T \leq 0$.
Therefore,

$$\begin{aligned}
 \Delta V(i_k) & \leq 2 \sum_{\xi_k=1}^d p_{\xi_k} [x^T(i_k) G^T (P + Q) Gx(i_k)] \\
 & \quad + 2 \sum_{\xi_k=1}^d p_{\xi_k} [x^T(i_k - \xi_{i_{k-1}}) H_{\xi_k}^T \\
 & \quad \quad \times (P + Q) H_{\xi_k} x(i_k - \xi_{i_{k-1}})].
 \end{aligned} \tag{21}$$

Corresponding to (20),

$$\begin{aligned}
 \Delta V(i_k) & \leq \sum_{\xi_k=1}^d p_{\xi_k} [x^T(i_k) [2G^T (P + Q) G - P] x(i_k)] \\
 & \quad + \sum_{\xi_k=1}^d [p_{\xi_k} x^T(i_k - \xi_{k-1}) [2H_{\xi_k}^T (P + Q) H_{\xi_k} - Q] \\
 & \quad \quad \times x(i_k - \xi_{k-1})].
 \end{aligned} \tag{22}$$

Denote $\Phi_i = 2G^T(P + Q)G - P + S + K^T R K$.

It is apparently $\Delta V(i_k) \leq 0$, when (1) $\Phi_i < 0$, (2) $2H_{\xi_k}^T(P + Q)H_{\xi_k} - Q < 0$.

Therefore, $E(V(i_k)) \leq -\min\{\lambda_{\min}(-\Phi_i)\} \|x(k)\|^2$. Denote $\mu = \min\{\lambda_{\min}(-\Phi_i)\}$

$$\Xi \left(\sum_{k=0}^{\infty} \|x(i_k)\|^2 \right) \leq \frac{1}{\mu} \Xi(V(x(0), \xi_0)) < \infty. \tag{23}$$

Then, the networked control systems (10) are stochastic mean-square stable.

Due to (22),

$$\begin{aligned}
 & \sum_{k=0}^{\infty} E(V(i_{k+1}) - V(i_k)) \leq -J \\
 & \implies J \leq V(i_0) - V(i_{\infty}) < x^T(i_0) P x(i_0) \\
 & \quad + x^T(i_{-1}) Q x(i_{-1}).
 \end{aligned} \tag{24}$$

□

Theorem 7. For given matrices R, S if there exist matrix M and positive definite matrices $X = P^{-1}, Y = Q^{-1}$ such that

$$(1) \begin{bmatrix} \Xi_1 & \Xi_2 \\ * & \Xi_3 \end{bmatrix} < 0; \quad (2) \begin{bmatrix} -\frac{1}{2}Y & * & * \\ \Gamma_1 M + \bar{H}M & -X & 0 \\ \Gamma_1 M + \bar{H}M & 0 & -Y \end{bmatrix} < 0. \tag{25}$$

Then $K = MX^{-1}$ is a guaranteed cost controller gain for the system (10) with disturbance $v_{i_k} = 0$ and the corresponding closed loop cost function satisfies

$$J < \lambda_{\max}(U^T P U) + \lambda_{\max}(U^T Q U), \tag{26}$$

where

$$\begin{aligned}
 \Xi_1 & = \begin{bmatrix} -X & * & * \\ A^{\xi_k} X + \Gamma_0 M & -\frac{1}{2}X & 0 \\ A^{\xi_k} X + \Gamma_0 M & 0 & -\frac{1}{2}Y \end{bmatrix}, \\
 \Xi_2 & = \begin{bmatrix} M^T & 0 \\ 0 & 0 \\ 0 & 0 \end{bmatrix}, \quad \Xi_3 = \begin{bmatrix} -R^{-1} & 0 \\ * & -S^{-1} \end{bmatrix},
 \end{aligned} \tag{27}$$

$$\bar{H} = \delta_{\xi_k} \left(\sum_{i=0}^{\xi_k} A^i \right) \Gamma_2.$$

Proof. By Lemma 5, (15) \Leftrightarrow (28),

$$(1) \begin{bmatrix} \Xi'_1 & \Xi'_2 \\ * & \Xi'_3 \end{bmatrix} < 0; \quad (2) \begin{bmatrix} -\frac{1}{2}Q & H_{\xi_{i_k}}^T & H_{\xi_{i_k}}^T \\ * & -P^{-1} & 0 \\ * & * & -Q^{-1} \end{bmatrix} < 0, \tag{28}$$

where

$$\Xi'_1 = \begin{bmatrix} -P & G^T & G^T \\ * & -\frac{1}{2}P^{-1} & 0 \\ * & * & -\frac{1}{2}Q^{-1} \end{bmatrix}, \quad \Xi'_2 = \begin{bmatrix} K^T & 0 \\ 0 & 0 \\ 0 & 0 \end{bmatrix}. \tag{29}$$

Pre- and postmultiplying (28)(1) by $\text{diag}(P^{-1}, I, I, I, I, I)$, Pre- and postmultiplying (28)(2) by $\text{diag}(Q^{-1}, I, I)$. Define $X = P^{-1}, Y = Q^{-1}$; we obtain (25).

The initial state of system is unknown; we suppose the initial state of the system (10) is arbitrary and belongs to the set $S = \{x(-i_k) \in R^n : x(-i_k) = UV(i_k), V^T(i_k)V(i_k) < 1, k = 0, 1\}$, where U is a given matrix. Then, the cost bound $J < x^T(i_0)Px(i_0) + x^T(i_{-1})Qx(i_{-1})$ leads to (26). \square

Remark 8. Denote the upper bound of the cost function J as J^* and $J^* = \theta_1 + \theta_2$ depends on matrices X, Y . The optimal guaranteed cost control gain of NCSs (10) can be solved by existing LMI that

$$\begin{aligned} & \text{Minimize } \theta_1 + \theta_2 \\ & \text{s.t.} \quad (1) \begin{bmatrix} -\theta_1 I & U^T \\ U & -X \end{bmatrix} \leq 0 \\ & \quad (2) \begin{bmatrix} -\theta_2 I & U^T \\ U & -Y \end{bmatrix} \leq 0. \end{aligned} \quad (30)$$

Theorem 9. Take given scalar $\gamma > 0$, and matrices R, S , if there exist matrix M and positive definite matrices $X = P^{-1}, Y = Q^{-1}$ such that

$$\begin{aligned} (1) \quad & \begin{bmatrix} \Xi_1 & \Xi_2 & \Xi_4 \\ * & \Xi_3 & 0 \\ * & * & \Xi_5 \end{bmatrix} < 0, \\ (2) \quad & \begin{bmatrix} -\frac{1}{2}Y & * & * \\ \Gamma_1 M + \bar{H}M & -X & 0 \\ \Gamma_1 M + \bar{H}M & 0 & -Y \end{bmatrix} < 0, \end{aligned} \quad (31)$$

where $\Xi_4 = \begin{bmatrix} XC^T H & (CX)^T \\ 0 & 0 \end{bmatrix}$, $\Xi_5 = \text{diag}(H^T H - \gamma^2 I, -I)$, and $\bar{H} = \delta_{\xi_k} (\sum_{i=0}^{\xi_k} A^i) \Gamma_2$.

Then $K = MX^{-1}$ is a guaranteed cost controller gain for the system (10) with H_∞ performance constraint (13) is achieved for all nonzero $v(k)$ and the cost function value is less than a bound:

$$J < \lambda_{\max}(U^T P U) + \lambda_{\max}(U^T Q U). \quad (32)$$

Proof. Consider

$$\begin{aligned} \sum_{k=0}^{\infty} E(z_k^T z_k) - \gamma^2 v_k^T v_k &= \sum_{k=0}^{\infty} E(z_k^T z_k) - \gamma^2 v_k^T v_k \\ &+ \Delta V(k) - V_\infty + V_0, \end{aligned} \quad (33)$$

$V_0 = 0, V_\infty > 0$ can be obtained from the zero initial conditions. Therefore,

$$\begin{aligned} & \sum_{k=0}^{\infty} E(z_k^T z_k) - \gamma^2 v_k^T v_k \\ & \leq \sum_{k=0}^{\infty} E(z_k^T z_k) - \gamma^2 v_k^T v_k + \Delta V(i_k) \end{aligned}$$

$$\begin{aligned} & z_{i_k}^T z_{i_k} - \gamma^2 v_{i_k}^T v_{i_k} + \Delta V(i_k) \\ & \leq \sum_{\xi_k=1}^d p_{\xi_k} \left[x^T(i_k) \left[2G^T(P+Q)G - P + S \right. \right. \\ & \quad \left. \left. + K^T R K + C^T C \right] x(i_k) \right] \\ & - x^T(i_k) \left[S + K^T R K \right] x(i_k) \\ & + p_{\xi_k} \sum_{\xi_k=1}^d \left[x^T(i_k) C^T H v^T(i_k) + v^T(i_k) H^T C x^T(i_k) \right. \\ & \quad \left. + v^T(i_k) H^T H v^T(i_k) \right] \\ & + p_{\xi_k} \sum_{\xi_k=1}^d \left[x^T(i_k - \xi_{k-1}) \left[3H_{\xi_k}^T (P+Q) H_{\xi_k} - Q \right] \right. \\ & \quad \left. \times x(i_k - \xi_{k-1}) \right]. \end{aligned} \quad (34)$$

By the Schur complement (34) is equivalent to

$$(1) \begin{bmatrix} \Xi'_1 & \Xi'_2 & \Xi'_4 \\ * & \Xi'_3 & 0 \\ * & * & \Xi'_5 \end{bmatrix} < 0; \quad (2) \begin{bmatrix} -\frac{1}{2}Q & H_{\xi_k}^T & H_{\xi_k}^T \\ * & -P^{-1} & 0 \\ * & * & -Q^{-1} \end{bmatrix} < 0. \quad (35)$$

Therefore, we can derive $z_{i_k}^T z_{i_k} - \gamma^2 v_{i_k}^T v_{i_k} + \Delta V(i_k) < 0$. Similar to Theorem 6, the networked system (10) is stochastic mean-square stable. Pre- and postmultiplying (35)(1) by $\text{diag}(P^{-1}, I, I, I, I, I, I)$, pre- and postmultiplying (35)(2) by $\text{diag}(Q^{-1}, I, I)$, and define $X = P^{-1}, Y = Q^{-1}$ we obtain (31).

Similar to Theorem 7, $J < \lambda_{\max}(U^T P U) + \lambda_{\max}(U^T Q U)$. \square

Remark 10. The optimal guaranteed cost control gain ($J^* = \theta_1 + \theta_2$) in Theorem 9 can be solved by existing LMI that

$$\begin{aligned} & \text{Minimize } \theta_1 + \theta_2 \\ & \text{s.t.} \quad (1) \begin{bmatrix} -\theta_1 I & U^T \\ U & -X \end{bmatrix} \leq 0 \\ & \quad (2) \begin{bmatrix} -\theta_2 I & U^T \\ U & -Y \end{bmatrix} \leq 0. \end{aligned} \quad (36)$$

4. Numerical Examples

Example 1. Consider the following system:

$$\dot{x} = \begin{bmatrix} -0.3 & -1 \\ 0 & -0.1 \end{bmatrix} x(t) + \begin{bmatrix} 0.01 \\ -0.01 \end{bmatrix} u(t). \quad (37)$$

The sampling period of controller is $T_c = 0.01$ s, and the sampling period of sensor is $T_s = 0.15$ s. And the packet loss upper bounds $d = 2$, and the time delay $\tau = 0.03$ s. Choose $U = \begin{bmatrix} 2.366 & 1.6282 \\ 1.3025 & -1.624 \end{bmatrix}$, $S = \begin{bmatrix} 1 & 0 \\ 0 & 1.1 \end{bmatrix}$, $R = 10$.

By solving the LMIs given in Theorem 7, we can obtain

$$X = \begin{bmatrix} 0.1978 & 0.0595 \\ 0.0595 & 0.1236 \end{bmatrix}, \quad M = 1.0e^{-10} \begin{bmatrix} 0.6131 & -0.9766 \end{bmatrix}. \quad (38)$$

Therefore, $K = MX^{-1} = 1.0e^{-008} \begin{bmatrix} 0.0640 & -0.1098 \end{bmatrix}$.

The state responses of closed loop system are shown in Figure 2, where the initial condition is $x(0) = (1, -1)^T$. Solving the LMIs given in Remark 8, $J^* = 51.9179$. The simulation results show that the proposed method is effective.

Example 2. Consider the following system:

$$\begin{aligned} \dot{x} &= \begin{bmatrix} -0.3 & -1 \\ 0 & -0.1 \end{bmatrix} x(t) + \begin{bmatrix} 0.01 \\ -0.01 \end{bmatrix} u(t) + \begin{bmatrix} 0.1 \\ -0.1 \end{bmatrix} v(t), \\ z(t) &= \begin{bmatrix} 1 & 0 \end{bmatrix} x(t) + 0.091v(t), \\ v(t) &= \begin{cases} 0.1 \sin(t), & 90 \leq t \leq 105, \\ 0, & \text{otherwise.} \end{cases} \end{aligned} \quad (39)$$

The other parameters are the same with Example 1. Solving the LMIs given in Theorem 9,

$$X = \begin{bmatrix} 3.9836 & 0.8675 \\ 0.8675 & 3.9836 \end{bmatrix}, \quad (40)$$

$$M = 1.0e^{-009} \begin{bmatrix} 0.5063 & -0.4462 \end{bmatrix}.$$

And we can obtain $K = MX^{-1} = 1.0e^{-009} \begin{bmatrix} 0.1353 & -0.0375 \end{bmatrix}$. Solving the LMIs given in Remark 10, $J^* = 63.3589$. The state responses of closed loop system are shown in Figure 3, where the initial condition is $x(0) = (1, -1)^T$.

Example 3. To illustrate the proposed method's effectiveness, which is obtained in this issue, we consider the following system in [7, 14]:

$$\begin{aligned} \dot{x} &= \begin{bmatrix} -1.84 & -0.33 \\ 7.18 & -1.14 \end{bmatrix} x(t) + \begin{bmatrix} 2.43 \\ -0.42 \end{bmatrix} u(t) + \begin{bmatrix} 1.86 \\ -0.76 \end{bmatrix} v(t), \\ z(t) &= \begin{bmatrix} 0.57 & 0.78 \end{bmatrix} x(t) - 0.56v(t). \end{aligned} \quad (41)$$

We can see, [7, 14] supposed that the sampling period of controller is $T_c = 0.01$ s, the sampling period of sensor is $T_s = 0.1$ s. And the packet loss upper bounds $d = 1$, and the time delay $\tau = 0.01$ s. Solving the LMIs given in Theorem 9, $K = [0.040, -0.051]$. We can obtain the H_∞ bounds from different methods in Table 1. Figure 4 illustrates the merits of the proposed multirate control system both with time delay and packet dropout.

5. Conclusions

For multirate NCSs, we mean that the sampling periods of the nodes in the system are not the same. In this paper, the guaranteed cost control for multirate networked control

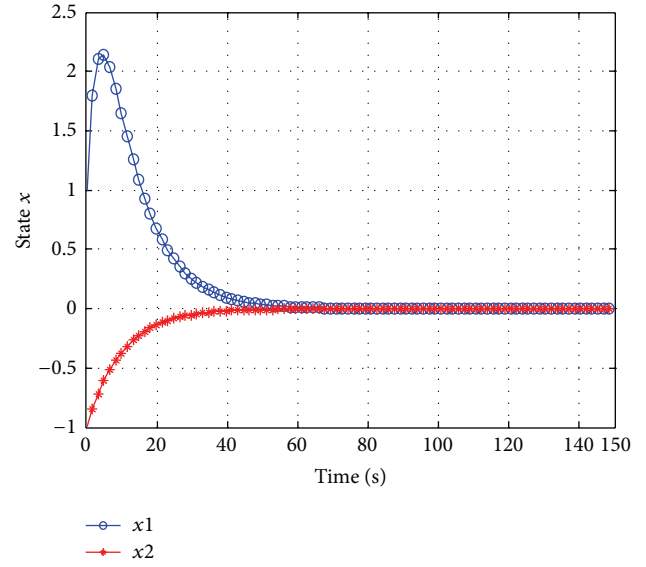


FIGURE 2: The state response of multirate NCSs.

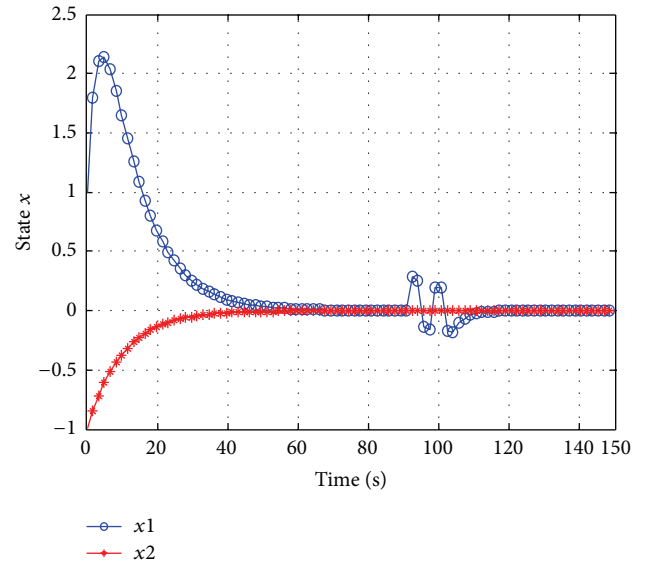


FIGURE 3: The state response of multirate NCSs with noise.

system with both time delay and packet dropout of multi-rates networked control is discussed. A multirate NCS with simultaneous consideration time delay and packet dropout is modeled as a time-varying sampling system with time delay, in which the newest control inputs are adopted and the Lyapunov function decreasing at each input signal updating point. Numerical examples are given to demonstrate the effectiveness of the proposed method.

The proposed problems in this paper for the nonlinear networked control systems [40, 41] have not fully been investigated. The method of fuzzy control [42, 43] will be adopted in the future work.

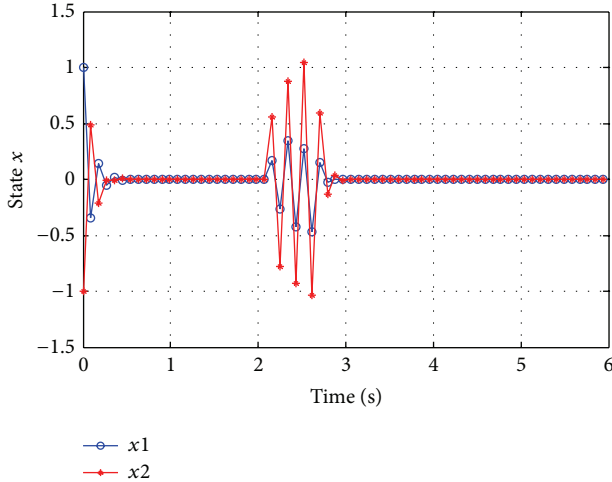


FIGURE 4: The state response of closed loop systems.

TABLE 1: H_∞ bounds.

Method	Theorem 6 [14]	Corollary 1 [7]	Theorem 9
γ	2.4966	4.4967	3.8705

Conflict of Interests

The authors declare that there is no conflict of interests regarding the publication of this paper.

Acknowledgments

This work was partly supported by National Nature Science Foundation of China (51375323, 61164014) and Science and Technology Support Project Plan of Jiangxi Province, China (2010BGB00607).

References

- [1] J. Nilsson, *Real-time control systems with delays [Ph.D. thesis]*, Department of Automatic Control, Lund Institute of Technology, Lund, Sweden, 1998.
- [2] Q. X. Zhu and S. S. Hu, "Stochastic optimal control and analysis of stability of networked control systems with long delay," *Automatica*, vol. 39, no. 11, pp. 1877–1884, 2003.
- [3] H. Lin, G. Zhai, and P. J. Antsaklis, "Robust stability and disturbance attenuation analysis of a class of networked control systems," in *Proceedings of the 42nd IEEE Conference on Decision and Control*, pp. 1182–1187, December 2003.
- [4] W. P. M. H. Heemels, A. R. Teel, N. Van De Wouw, and D. Nešić, "Networked control systems with communication constraints: tradeoffs between transmission intervals, delays and performance," *IEEE Transactions on Automatic Control*, vol. 55, no. 8, pp. 1781–1796, 2010.
- [5] A. V. Savkin and T. M. Cheng, "Detectability and output feedback stabilizability of nonlinear networked control systems," *IEEE Transactions on Automatic Control*, vol. 52, no. 4, pp. 730–735, 2007.
- [6] L. Q. Zhang, Y. Shi, T. W. Chen, and B. Huang, "A new method for stabilization of networked control systems with random delays," *IEEE Transactions on Automatic Control*, vol. 50, no. 8, pp. 1177–1181, 2005.
- [7] Y.-L. Wang and G.-H. Yang, "Multiple communication channels-based packet dropout compensation for networked control systems," *IET Control Theory and Applications*, vol. 2, no. 8, pp. 717–727, 2008.
- [8] M. Yu, L. Wang, G. M. Xie, and T. G. Chu, "Stabilization of networked control systems with data packet dropout via switched system approach," in *Proceedings of the IEEE International Symposium on Computer Aided Control System Design*, pp. 362–367, September 2004.
- [9] W. Zhang, M. S. Branicky, and S. M. Phillips, "Stability of networked control systems," *IEEE Control Systems Magazine*, vol. 21, no. 1, pp. 84–97, 2001.
- [10] A. S. Matveev and A. V. Savkin, "Almost sure nonobservability and unstabilizability of unstable noisy linear plants via communication channels with packet losses," in *Proceedings of the 44th IEEE Conference on Decision and Control, and the European Control Conference (CDC-ECC '05)*, pp. 7338–7341, December 2005.
- [11] Y. Liang, T. Chen, and Q. Pan, "Optimal linear state estimator with multiple packet dropouts," *IEEE Transactions on Automatic Control*, vol. 55, no. 6, pp. 1428–1433, 2010.
- [12] T. Liu, H. Zhang, and Q. J. Chen, "Control for networked control systems with communication constraints," *Control and Decision*, vol. 28, no. 4, pp. 537–546, 2013.
- [13] P. Shi, Y. Q. Xia, G. P. Liu, and D. Rees, "On designing of sliding-mode control for stochastic jump systems," *IEEE Transactions on Automatic Control*, vol. 51, no. 1, pp. 97–103, 2006.
- [14] Y.-L. Wang and G.-H. Yang, " H_∞ control of networked control systems with delay and packet disordering via predictive method," in *Proceedings of the American Control Conference (ACC '07)*, pp. 1021–1026, July 2007.
- [15] W.-A. Zhang and L. Yu, "Modelling and control of networked control systems with both network-induced delay and packet-dropout," *Automatica*, vol. 44, no. 12, pp. 3206–3210, 2008.
- [16] J. Wu and T. W. Chen, "Design of networked control systems with packet dropouts," *IEEE Transactions on Automatic Control*, vol. 52, no. 7, pp. 1314–1319, 2007.
- [17] M. Yu, L. Wang, T. G. Chu, and F. Hao, "Stabilization of networked control systems with data packet dropout and transmission delays: continuous-time case," *European Journal of Control*, vol. 11, no. 1, pp. 40–49, 2005.
- [18] X. He, Z. Wang, and D. H. Zhou, "Robust fault detection for networked systems with communication delay and data missing," *Automatica*, vol. 45, no. 11, pp. 2634–2639, 2009.
- [19] S. S. L. Chang and T. K. C. Peng, "Adaptive guaranteed cost control of systems with uncertain parameters," *IEEE Transactions on Automatic Control*, vol. 17, no. 4, pp. 474–483, 1972.
- [20] G.-R. Matías and B. Antonio, "Analysis of networked control systems with drops and variable delays," *Automatica*, vol. 43, no. 12, pp. 2054–2059, 2007.
- [21] I. R. Petersen and D. C. McFarlane, "Optimal guaranteed cost control and filtering for uncertain linear systems," *IEEE Transactions on Automatic Control*, vol. 39, no. 9, pp. 1971–1977, 1994.
- [22] L. Yu and J. Chu, "LMI approach to guaranteed cost control of linear uncertain time-delay systems," *Automatica*, vol. 35, no. 6, pp. 1155–1159, 1999.
- [23] B. Chen and X. Liu, "Fuzzy guaranteed cost control for nonlinear systems with time-varying delay," *IEEE Transactions on Fuzzy Systems*, vol. 13, no. 2, pp. 238–249, 2005.

- [24] H. G. Zhang, D. D. Yang, and T. Y. Chai, "Guaranteed cost networked control for T-S fuzzy systems with time delays," *IEEE Transactions on Systems, Man and Cybernetics Part C*, vol. 37, no. 2, pp. 160–172, 2007.
- [25] J. H. Park and H. Y. Jung, "On the design of nonfragile guaranteed cost controller for a class of uncertain dynamic systems with state delays," *Applied Mathematics and Computation*, vol. 150, no. 1, pp. 245–257, 2004.
- [26] H. Lin and P. J. Antsaklis, "Stability and persistent disturbance attenuation properties for a class of networked control systems: switched system approach," *International Journal of Control*, vol. 78, no. 18, pp. 1447–1458, 2005.
- [27] Q. X. Zhu, H. L. Liu, and S. S. Hu, "Uniformed model of networked control systems with long time delay," *Journal of Systems Engineering and Electronics*, vol. 19, no. 2, pp. 385–390, 2008.
- [28] L. Y. Xiang and G. Guo, "Model-based networked control system with multi-rate sampling," *Information and Control*, vol. 34, no. 3, pp. 373–378, 2005 (Chinese).
- [29] D. M. Tilbury and D. Georgiev, "Packet-based control: the H_2 -optimal solution," *Automatica*, vol. 42, no. 1, pp. 137–144, 2006.
- [30] V. H. Nguyen and Y. S. Suh, "A modified multirate controller for networked systems with a send-on-delta transmission method," in *Proceedings of the 3rd International Conference on Intelligent Computing*, pp. 304–315, 2007.
- [31] J. Jin, W. Zhiwen, and L. Dongsong, "Model-based control scheme for networked multi-rate sampling systems," in *Proceedings of the International Conference on Measuring Technology and Mechatronics Automation (ICMTMA '09)*, pp. 812–815, April 2009.
- [32] Z. H. Guan, C. -X. Yang, and J. Huang, "Stabilization of networked control systems with random delays: a new multirate method," in *Proceedings of the 17th World Congress of IFAC*, pp. 4204–4209, Seoul, Korea, July 2008.
- [33] Y. Liang, T. Chen, and Q. Pan, "Optimal linear state estimator with multiple packet dropouts," *IEEE Transactions on Automatic Control*, vol. 55, no. 6, pp. 1428–1433, 2010.
- [34] D. X. Wu, J. Wu, S. Chen, and J. Chu, "Optimal linear state estimator with multiple packet dropouts," *IEEE Transactions on Automatic Control*, vol. 55, no. 5, pp. 1202–1208, 2010.
- [35] Q. X. Zhu, "Controllability of multi-rate networked control systems with short time delay," *Advanced Materials Research*, vol. 219–220, pp. 855–859, 2011.
- [36] Q. X. Zhu, "Observability of multi-rate networked control systems with short time delay," *Communications in Computer and Information Science*, vol. 144, no. 2, pp. 396–401, 2011.
- [37] S. Yin, S. Ding, and H. Luo, "Real-time implementation of fault tolerant control system with performance optimization," *IEEE Transactions on Industrial Electronics*, vol. 61, no. 5, pp. 2402–2411, 2013.
- [38] S. Yin, S. Ding, A. Haghani, and H. Hao, "Data-driven monitoring for stochastic systems and its application on batch process," *International Journal of Systems Science*, vol. 44, no. 7, pp. 1366–1376, 2013.
- [39] S. Yin, S. Ding, A. Haghani, H. Hao, and P. Zhang, "A comparison study of basic data driven fault diagnosis and process monitoring methods on the benchmark Tennessee Eastman process," *Journal of Process Control*, vol. 22, no. 9, pp. 1567–1581, 2012.
- [40] H. J. Gao, T. W. Chen, and J. Lam, "A new delay system approach to network-based control," *Automatica*, vol. 44, no. 1, pp. 39–52, 2008.
- [41] H. J. Gao and T. W. Chen, "New results on stability of discrete-time systems with time-varying state delay," *IEEE Transactions on Automatic Control*, vol. 52, no. 2, pp. 328–334, 2007.
- [42] H. J. Li, H. H. Liu, H. J. Gao, and P. Shi, "Reliable fuzzy control for active suspension systems with actuator delay and fault," *IEEE Transactions on Fuzzy Systems*, vol. 20, no. 2, pp. 342–357, 2012.
- [43] H. Y. Li, J. Y. Yu, C. Hilton, and H. H. Liu, "Adaptive sliding-mode control for nonlinear active suspension vehicle systems using T-S fuzzy approach," *IEEE Transactions on Industrial Electronics*, vol. 60, no. 8, pp. 3328–3338, 2013.

Research Article

The Research on Modeling and Simulation of TFE Polymerization Process

Jing Gao Sun^{1,2} and Qin Cao^{1,2}

¹ Key Laboratory of Advanced Control and Optimization for Chemical Processes of Ministry of Education, Shanghai 200237, China

² School of Information Science and Engineering, East China University of Science and Technology, Shanghai 200237, China

Correspondence should be addressed to Jing Gao Sun; sunjinggao@126.com

Received 5 January 2014; Revised 10 March 2014; Accepted 13 March 2014; Published 16 April 2014

Academic Editor: Huaicheng Yan

Copyright © 2014 J. G. Sun and Q. Cao. This is an open access article distributed under the Creative Commons Attribution License, which permits unrestricted use, distribution, and reproduction in any medium, provided the original work is properly cited.

PTFE (polytetrafluoroethylene) is the fluorinated straight-chain polymer, made by the polymerization of tetrafluoroethylene monomer; it is used widely because of its excellent performance and can be obtained by the polymerization of body, solutions, suspensions, and emulsions. But only the last two are the main ways. This research paper makes simulation based on Polymer Plus. It uses the emulsion polymerization method at background to carry out a semibatch reactor system. Upon the actual production conditions, simulation process under the steady state conditions is used to analyze the effects of the changes on operating conditions; the corresponding dynamic model is created to analyze the impact of the changes of conditions on the entire system. Moreover, the amount of APS which plays an important part in this reaction is discussed for getting the most suitable amount of initiator. Because of less research work on this job, it is so difficult to find the related data from the literature. Therefore, this research will have a great significance for the process of the tetrafluoroethylene emulsion polymerization in the future.

1. Introduction

Polytetrafluoroethylene is the most important species in the fluorine-containing polymer and it is applied in many industrial areas, such as aerospace and medical areas. In China, PTFE is mainly obtained from suspension polymerization, but the PTFE from dispersion polymerization [1–3] which contains superior performance and is used to apply in the preparation of expanded porous products and hydraulic hose products is so less. There is a great gap in the performance of the dispersion resin compared with the foreign countries.

With the rapid development of industry, the size of the PTFE's demand has become a national economic indicator, so dealing with the control system of the production process of PTFE not only can improve the quality of the product and reduce energy consumption during the reaction, but also can provide guidance and advise to the scene of the process operation. The PTFE emulsion obtained from TFE dispersion polymerization has been applied in many important areas; foreign researchers have done a lot of work in the synthesis of fluorinated polymer emulsion and made good results in the application of research [4–8]. Some patents

about it are implied in the industrial area successfully. The countries in which science and technology are relatively developed have their own polymerization system. They have a very detailed presentation and research on the performance and application. However, they keep the process conditions and the recipe confidential; only a few patents involved are about this; most of the articles are the analysis of the synthesized product. Therefore, this paper about dispersion polymerization of TFE has a practical significance for the industrial craft process in domestic.

2. Process Background of TFE Dispersion Polymerization

The main object of this study is the polymerization process of tetrafluoroethylene which is commonly used in industry. It mainly uses the emulsion polymerization and semicontinuous feeding methods [9, 10], making ammonium persulfate as initiator and water as solvent. Because the initiator was decomposed under the acid condition, we add some glacial acetic acid to balance the liquid acid. Besides, we also should

TABLE I: The components involved in the reaction.

Name	Type	Code name	Molecular formula
Tetrafluoroethylene	Conventional	TFE	C_2F_4
Polytetrafluoroethylene	Polymer	PTFE	$(C_2F_4)_n$
Water	Conventional	H_2O	H_2O
Ammonium persulphate	Conventional	APS	$(NH_4)_2S_2O_8$
TFE chain segments	Segment	CF_2-R	CF_2-R
Glacial acetic acid	Conventional	CH_3COOH	CH_3COOH
Dodecyl mercaptan	Conventional	DDM	$C_{12}H_{26}S$

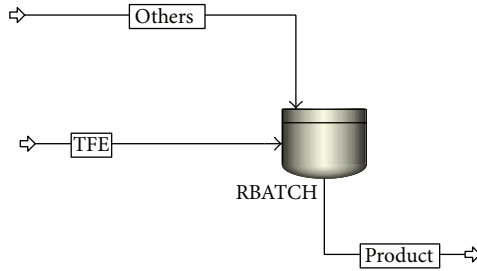


FIGURE 1: Process of the polymerization.

add stabilizer paraffin and chain transfer agent DDM; the main process can be summarized as follows: adding the deionized water and accessory ingredient (including initiators, stabilizers, modifiers, and chain transfer agent) which compounded well in advance (see Section 3.2); deflating and heating the reactor to make the temperature up to $70^\circ C$ with stirring; after the detection of oxygen amount, adding TFE monomer and making the temperature and pressure to the specified value; and adding the monomer to keep the pressure at a certain value and, after some minutes, adding the perfluorooctanoic acid. After that we stop stirring and cooling the reactor. During the total process, the temperature should be kept between 80 and $105^\circ C$; the pressure should be kept between 15 and 17 atm. The static simulation process is shown in Figure 1.

3. Steady-State Process Simulation and Analysis

3.1. Polymerization Reaction Components. The chemical substances were divided into conventional, segment, oligomer, and polymer in polymer plus. They have the properties data like the boiling and melting point, the molecular structure, and molecular weight. Segment mainly includes repetitive unit, endpoint, and grafting site. The properties of the polymer are mainly dependent on the polymer segment type, quantity, and composition forms. The reaction components in this paper are shown in Table 1.

In this process, APS is 5 g, CH_3COOH is 250 mL, DDM is 100 g, and water is 400 kg. And the feed temperature of TFE is $35^\circ C$. Polymerization reactor is the main place of reaction, so its parameter setting is the most critical and important; in this paper, volume is set to 1.2 cum, the temperature is

controlled between $80^\circ C$ and $105^\circ C$, and the pressure is controlled between 15 atm and 17 atm. Since this reaction is a semicontinuous process, we make the reaction stop when PTFE yields reach to 150 kg.

3.2. Polymerization Kinetics. The polymerization of tetrafluoroethylene is radical polymerization [11–13]; the reaction kinetics [14] mainly include four elementary reactions: chain initiator, chain growth [15], chain transfer, and chain termination [16]. The kinetic equation is expressed as follows:

- (1) chain initiator: $Aps \rightarrow e.n.R^* + a.A + b.B; Tfe + R^* \rightarrow P_1[TFe]$;
- (2) chain growth: $P_n[TFe] + Tfe \rightarrow P_{n+1}[TFe]$;
- (3) chain transfer:
 - transfer to monomer: $P_n[TFe] + Tfe \rightarrow D_n + P_1[TFe]$;
 - transfer to the regulator: $P_n[TFe] + CH_3COOH \rightarrow D_n + R^*$;
 - transfer to chain transfer agent: $P_n[TFe] + DDM \rightarrow D_n + R^*$;
- (4) chain termination: $P_n[TFe] + P_m[TFe] \rightarrow D_{n+m}$;

The first step includes two parts: initiator decomposing to radical ion, combining with monomer to be monomer radical. The second step is the process of chain transfer and the third step is the process of transferring to monomer, chain transfer agent, and regulator. The end step is the process of coupling termination. N is the number of the primary radical decomposition, R^* is the primary radicals, and P_1 represents that the polymerization degree of the living polymer is one. P_n and P_m are the polymeric chain of which unit length are n and m . D_n and D_{n+m} are the die polymers of which length is n and m , respectively.

Due to the diversity of PTFE process, polymerization kinetics data is also different; moreover, the confidentiality of technology makes it difficult to get the complete kinetic parameters. This paper combines the relative literature data and the correction in the actual simulation we have done, so it gets a better simulation effect. The polymerization of TFE is free radical polymerization, although Polymer Plus provides relevant radical polymerization model, but the kinetics parameters of different reactions are different and because of the diversity of PTFE process; kinetics parameters debugging is very difficult and time consuming. This paper combines literature data and the results of the simulation

TABLE 2: Reaction rate and preexponential factor setting.

Type	Component 1	Component 2	Pre-Exp (1/sec)	Act-energy (J/kmol)
INIT-DEC	APS		$1.13E + 16$	137000000
CHAIN-INI	C2F4		$3.62E + 13$	119710000
PROPAGATION	C2F4	C2F4	12490000	17413760
CHAT-MON	C2F4	C2F4	3320000	53020000
CHAT-AGENT	C2F4	CH3COOH	1051	20000000
CHAT-AGENT	C2F4	DDM	1051	20000000
TERM-COMB	C2F4	C2F4	1380000	13604500

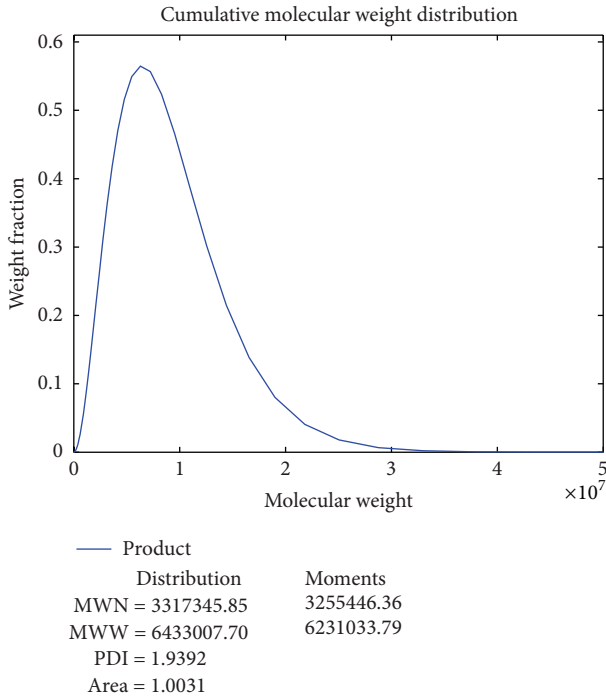


FIGURE 2: The MW distribution of polymer at $T = 82^{\circ}\text{C}$.

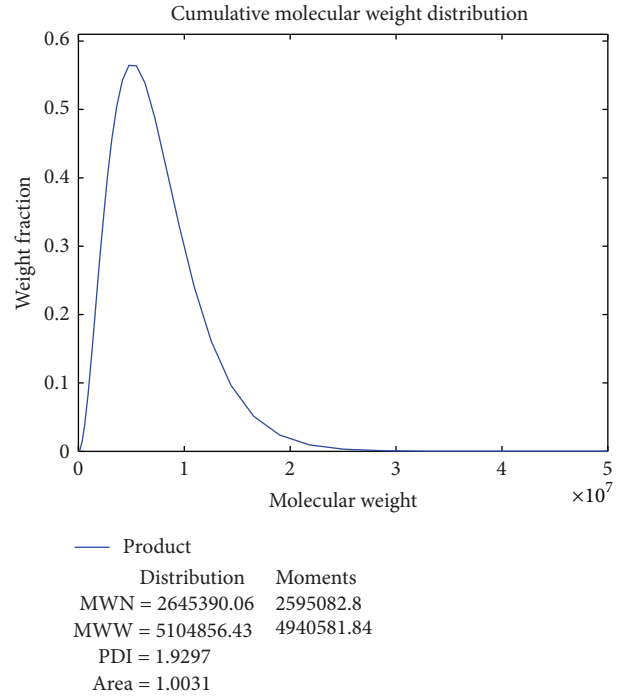


FIGURE 3: The MW distribution of polymer at $T = 85^{\circ}\text{C}$.

based on the actual correction data; therefore, it gets a better simulation results. Table 2 is the setting of the kinetic parameters.

3.3. The Analysis of the Steady State

3.3.1. The Effect of Reactor Temperature on the Product. For the polymerization reaction, the reaction temperature directly affects the polymerization degree which reflects the quality of the product. Too low temperature will lead to slow response and the product with low intensity. On the contrary, the reaction rate will be rapid and the reaction is difficult to control. Low temperature will get low monomer conversion rate, because low molecular motion is not conducive to the proliferation of free radicals and the collision between monomers and radical. With the rises of the temperature, the chain growth rate constant and the number of the growth active centers both increase and the probability of spreading and collision between monomer and active radicals

are elevated; meanwhile, the amount of PTFE increases leads to conversion rate of the monomer increasing. However, when the temperature reaches a certain stage, the curve of conversion rate will gradually tend to level because of the secondary reaction increasing, such as coupling termination and disproportionation termination. With the reaction proceeds continuing, the concentration of active centers is reduced, so the reaction rate is leveled off. The size of the molecular weight reaches unanimity basically as time increases. In order to investigate the impact of temperature on the molecular weight distribution of the polymer, the reactor temperature is set to 82°C , 85°C , and 88°C , respectively, observing the laws of the molecular weight distribution change with the different temperature; Figures 2, 3, and 4 show the change rules.

All the figures have shown the number-average molecular weight, weight-average molecular weight, and the dispersity of the polymer molecular weight in the relative temperature.

Figures 2 and 3 show that the number-average molecular weight of the product reduces to 2645390.8 from 3317345.81

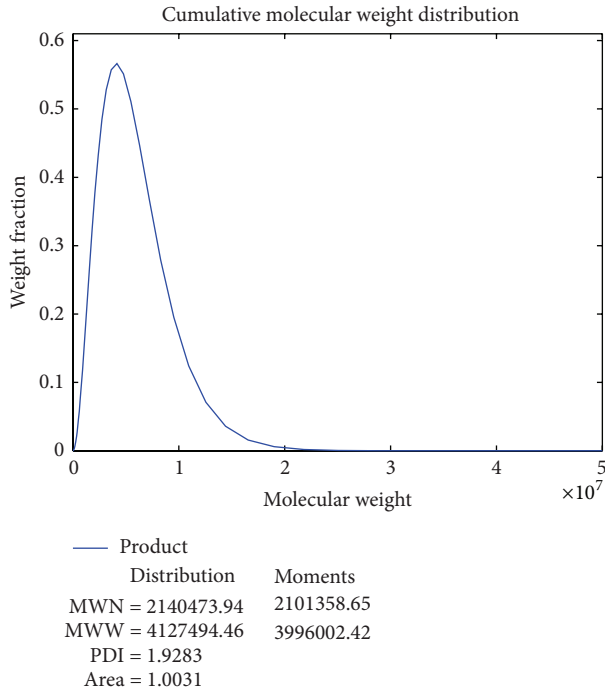


FIGURE 4: The MW distribution of polymer at $T = 88^\circ\text{C}$.

and weight-average molecular weight reduces to 5104856.48 from 6433007.62 when the temperature increases by 3 degree.

Figure 2, 3, and 4 show that the temperature changed the molecular weight and the overall curve move to the left when temperature increases; meanwhile, the curve is going to be narrow and steep. It is obvious that the increase of the temperature leads to the decrease of the molecular weight of polymer.

3.3.2. The Effect of the Initiator on the Product. Figure 5 shows the PTFE dispersion products molecular weight when APS is between 2 g and 8 g. Initiator is one of the most important part of emulsion formulations; it cannot be too much or too little. The reaction speed will be too fast if its usage is too much, on the contrary, too little will make it difficult to trigger the reaction and is not good for the polymer performance.

Product conversion rate will increase gradually when initiator increases, and the rise of the primary free radicals will increase the frequency of chain initiator and then lead to the rise of the monomers conversion as well as reaction rate. Meanwhile, in the chain termination and chain transfer stage, the rise of the active end of the initiation phase accelerates the collision probability between primary radicals and active chain. Therefore, the length of the molecular chain becomes short; it means that PDI reduces gradually. However, too much initiator will be treated as the electrolyte and reduce the stability of the emulsion polymerization process.

3.3.3. The Effect of the Regulator Feed on the Product. Since the initiator agent decomposed under the acidic conditions, its half-life will be shortened when PH value reduces. Hence

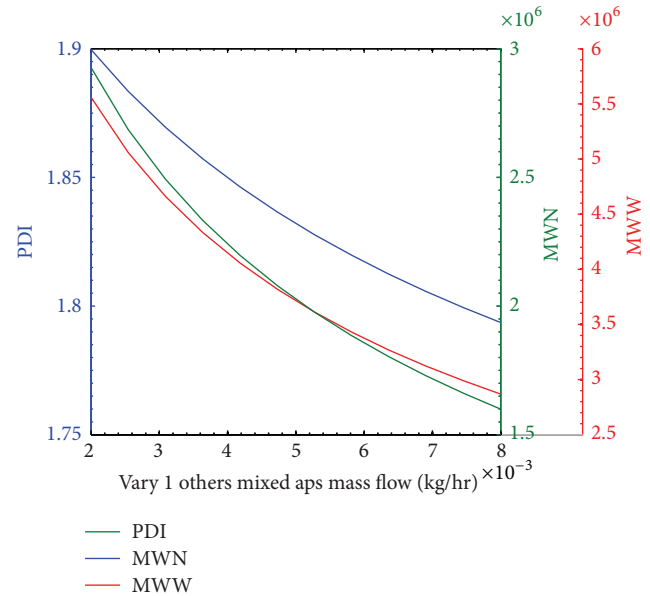


FIGURE 5: Effects of initiator flow on PDI.

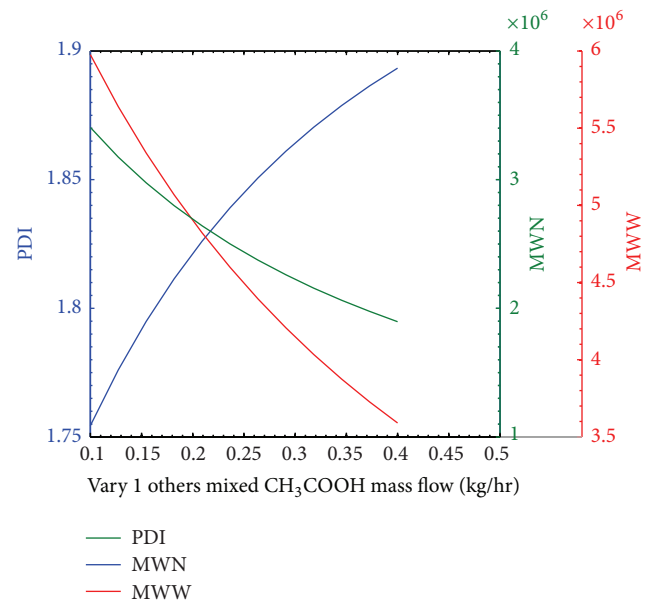


FIGURE 6: Effects of modifier flow on PDI.

we add the right amount of glacial acetic acid in the reactor to adjust the acidity of the liquid.

Figure 6 shows that PDI increases and the monomer conversion reduces as CH_3COOH increases; this is because CH_3COOH has a great effect on the polymerization reaction, especially in the liquid phase; it will be the chain transfer agent in the chain-transfer reaction. It is easy to react with growing macromolecular radicals and terminate the active chain, and the decrease of chain growth monomer will lead to the conversion rate reducing. Many active chains can't get enough chain length and the value of PDI will increase, This is because the product with low molecular weight increases.

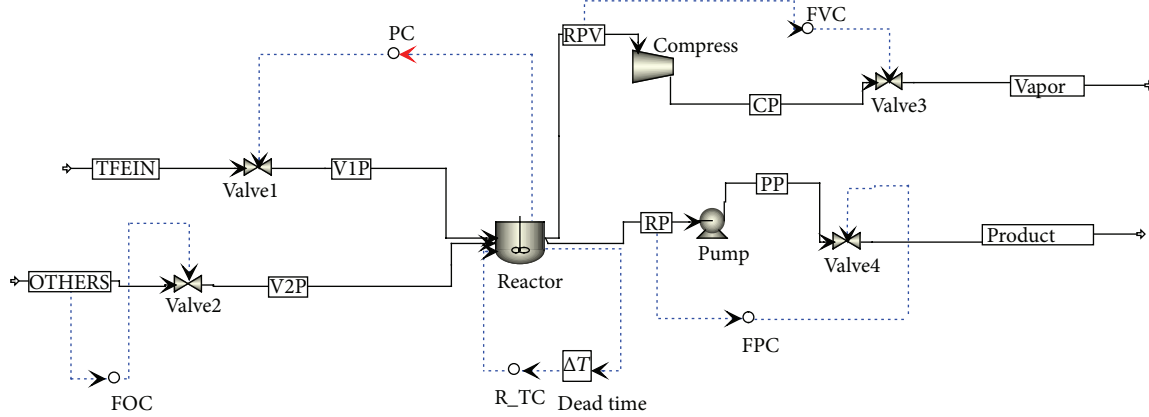


FIGURE 7: Process simulation of polymerization for TFE.

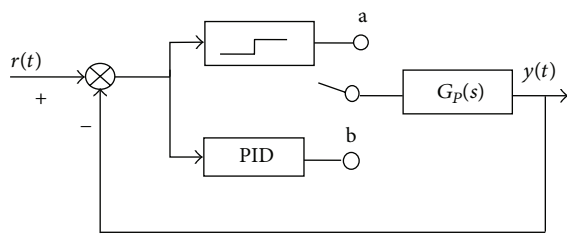


FIGURE 8: Relay feedback based parameter identification.

4. Dynamic Modeling and Analysis

4.1. *The Establishment of Dynamic.* Figure 7 is the dynamic process simulation; the pump and the compressor are mainly used to pump the air and discharge the liquid in the reactor. The valves are used to control the flow rate of each stream; OTHERS in Figure 7 represents water and accessory ingredient.

Pressure controller PC is used to control the opening degree of monomer valves through the reactor pressure and control the feeding amount indirectly. The temperature controller R_TC is mainly used to control the reactor temperature. The target value of reactor temperature is achieved by controlling the heat transfer.

4.2. *The Setting of PID Controller Parameters.* With the development of computer networks [17, 18], the control method is diverse. This paper introduces the autotuning PID controller based on relay feedback, shown in Figure 8, to control the process. There are test status and control status in the control system. In the former status, oscillation frequency and amplitude of the test system can be obtained from the relay link tested, and then the frequency domain information can be got in this case and it combines the control strategy to obtain the PID parameters. In the latter status, the system can be run through the PID parameters. In the process of the relay feedback control, the system can generate critical oscillation to obtain critical information as long as the controlled object has at least $-\pi$ phase lag. Setting the controller parameter

based on Ziegler-Nichols tuning formula. The main steps can be summarized as follows: the system enters the steady state through manual control; making the soft switch to connect point a in Figure 8 to make the system generate constant amplitude oscillation to obtain amplitude and frequency, calculating the controller parameter based on the tuning method, adjusting parameters and entering the closed-loop control.

This method is widely applied because of its many advantages, the main advantages include that oscillations generated by the system are entirely the internal characteristics of nonlinear systems; the system will not only be disturbed and cannot be operated normally in the closed loop, but it also can overcome the impact of the PID parameter tuning from nonlinear system; it requires little prior knowledge.

The flow controllers (FVC, FOC, and FPC) in Figure 7 are used to control the valve opening to determine the material flow in and out. According to the conventional flow controller setting, these controllers are set as $P = 0.5$, $I = 0.3$, and they are added by 0.1 min filter time. Valves3 and Valve4 are used at the beginning of the reactor process simulation to evacuate the air and discharge the residuum. The setting of the pressure controller is not complex as temperature control. It needs PI control alone. From the experience value and relevant documentation records [19, 20], it can be set as $P = 2$, $I = 10$. After many repeated analysis of the simulation, the results prove that this parameter can get a good control effect.

The adjustment process of temperature is very complex. Temperature plays an important role on the product quality and safety of the entire polymerization process. It is difficult to achieve the desired effect with PI control only, so PID control should be used. In the setting of the parameter, the relay feedback based parameter identification method is used and a dead time between 30 s and 60 s is added. This dead time is also often discussed in network control [21–23]. Considering that the dynamic temperature lag [24, 25] and the target value of the temperature setting cannot be reached immediately [26, 27], before the tuning of PID parameters, the hysteresis which equals to 1 minute needs to be added in the analog interface which includes the closed-loop temperature controller.

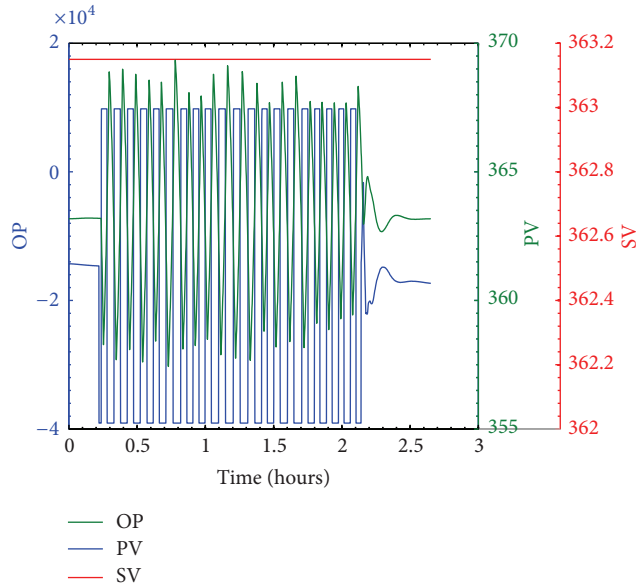


FIGURE 9: Relay-feedback test dynamic.

Figure 9 shows the process of autotuning based on relay feedback identification. Firstly, setting the target value of temperature to 363.15 K and using the relay feedback to acquire the amplitude and frequency of the system; secondly, Ziegler-Nichols rule was combined to it to get the PID parameter as $P = 0.6187$, $I = 2.82$ min, $D = 0.705$ min. In order to get better result, the target value of temperature is set to 366.15 K. Observing the result of this controller and modifying the parameter based on the former result to get the optimal parameter according to the overshoot and system response time. After many cycle tests, the best parameters can be acquired as $P = 0.535137$, $I = 3.27$ min, and $D = 0.8175$ min.

4.3. The Analysis of the Dynamic Simulation Process. The overall process of TFE polymerization reaction can be briefly summarized in the following steps: cleaning the reactor → adding the deionized water and accessory ingredient → evacuating the reactor → adding the monomer → elevating temperature and pressure to a predetermined value → stirring → stopping the stirring when the product reaches the target value → cooling the reactor and recycling monomer.

4.3.1. Pressure and Monomer Feed Changes with Time. The first five hours are the reactor cleaning and solvent injecting. After that, the TFE is added to the reactor. Figure 10 shows that the pressure in the reactor increases gradually from vacuum state along with TFE feeding. Because the target of the pressure is set to 15 atm, therefore, when the pressure exceeds this value, the opening degree of the valve becomes smaller and feeding amount is also reduced. Besides, the feed input can be controlled by pressure controller very well in this picture. When the amount of the product meets its requirement, the feeding valve is closed. The gas in the reactor is consumed gradually; the pressure begins to drop.

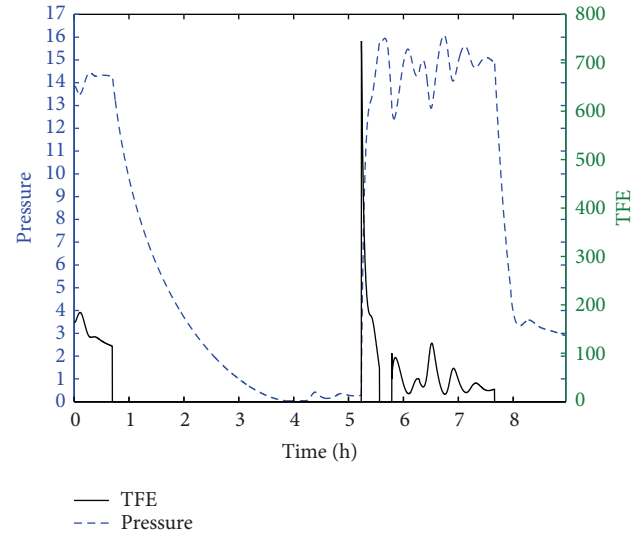


FIGURE 10: The change of the monomer feed and pressure.

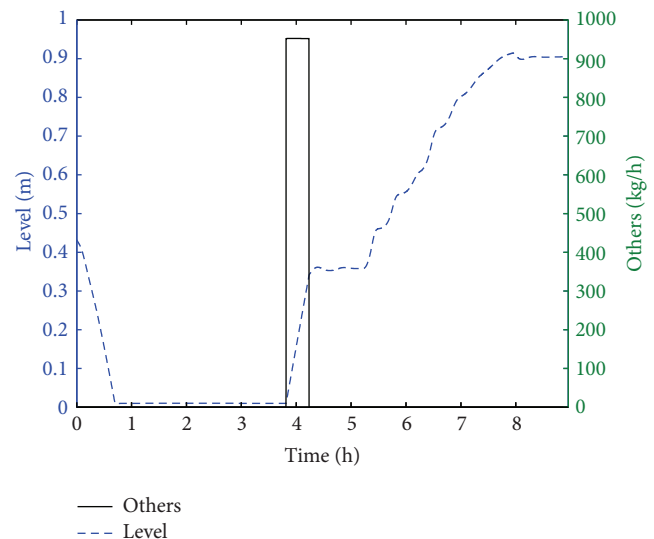


FIGURE 11: The changes of level and other additives.

4.3.2. The Liquid Level and Accessory Ingredient Changes with Time. Reactor cleaning contains two steps: the liquid was discharged via a pump; the compressor evacuates the gas from the reactor. When the level reaches 0 and pressure is lower than vacuum state, injecting deionized water and accessory ingredient to the reactor with constant speed, the level rises to 0.4 m from the start level rapidly. When the water content reaches 400 kg, valve2 is closed and the reactor is heated to 70°C. Figure 11 shows that the level rises when the monomer is injected to the reactor and PTFE is generated. When PTFE reaches the required yield, TFE feed valve is closed. The pressure in the reactor decreases to some degree gradually and the reactor is cooling. The liquid level reaches a certain height and remains unchanged with the reaction stopping.

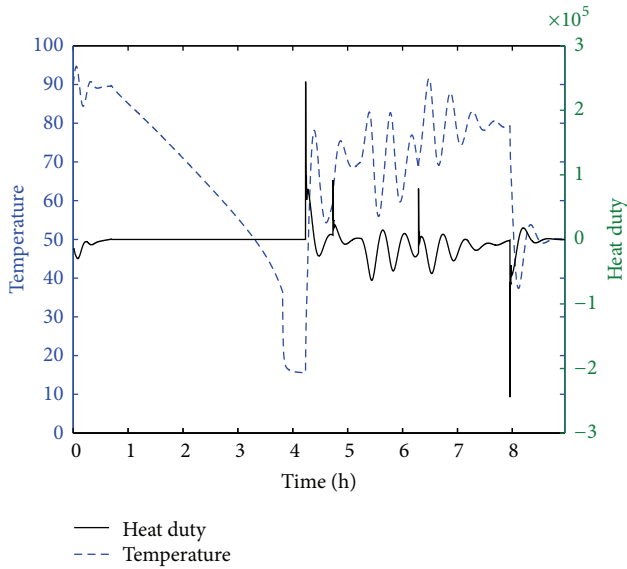


FIGURE 12: The change of the temperature and heat-duty.

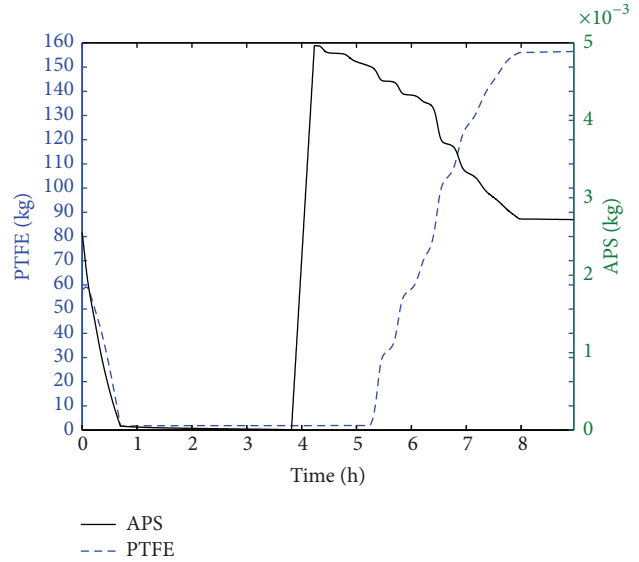


FIGURE 13: The change of PTFE and APS.

4.3.3. *Temperature and Heat Load Changes with Time.* The dynamic reaction is directly converted from the static simulation and the temperature in the beginning of the dynamic process stayed in the static setting temperature. The temperature is not controlled by the controller during the process of clearing reactor. Discharging the substance from the reactor and evacuating the gas make the reactor temperature decline rapidly from the steady-state temperature at 95°C soon.

Figure 12 shows that the heat duty is in a constant state in the first 4 hours, after adding deionized water and accessory ingredient to the reactor, the reactor is heated to 75°C. Then the monomer is injected and the reaction starts. This reaction is exothermic and the feed amount of the monomer is controlled by pressure, so the temperature changes constantly. The temperature is controlled by the transfer of the heat duty, so the size of the heat load will respond to the changes of the temperature. After the process is finished, the reactor is cooled when PTFE reaches the required yield.

4.3.4. *The Amount of APS and PTFE Changes with Time.* After injecting the solvents and accessory ingredient and heating the reactor, the initiator begins to decompose. The curve shows that PTFE is generated at five when temperature increases, meanwhile, APS decreases gradually and the decompose rate of APS in proportion to the temperature. Steady state is reached at the eighth hour; reactants and products are kept in a constant value. The changes of PTFE and APS are shown as in Figure 13.

5. Analysis of the Initiator Dosage

In general, APS begins to decompose when the temperature reaches 80°C. The decomposition rate is in proportion to the temperature. The usage of initiator should be controlled within a certain range; too much initiator will lead to the reaction speed too fast and also the reaction will be difficult

to be controlled well. Besides, polymerization degree of the product will be small and intensity will be low. Too little initiator will lead to the activity of initiator disappearing in the middle of the reaction; this will cause the reaction to not go on well. However, in the actual process, based on the premise of sufficient polymerization rate, the usage of the initiator should be minimum, because the residual initiator is not good for the product quality and the cost of initiator recycling is very high.

There are six dynamic simulations with different usage of APS which feed amount is from 2g to 7g. For each simulation, the time required for the whole process is recorded. Meanwhile, APS's consumption and APS's residual amount should also be recorded in the end of each simulation. Then calculate the residual rate of APS. The final result is shown in Table 3.

Table 3 shows that the required reaction time increases first and then decreases, and the residual rate is converse; the reason is that the increase of the dose at the beginning results in the increase of residual. When the amount of initiator exceeds a certain amount, the reaction rate increases and temperature rises sharply; meanwhile, the decomposition rate of APS accelerates and leads to the decrease of the reaction half-life. According to the optimal choice of law, when the content of APS equals to 3g and 2g, respectively, the total time required is close to or even more than 10 hours; it is a little long compared to other cases with different amounts of APS. When the amount of APS is equal to 7g, the quantity of the initiator is too much and this leads to the increase of the reaction rate; meanwhile, reaction heat cannot be removed in time to make temperature rise rapidly. Decomposition rate accelerates and retention rate is very low, but the total required time is 11 hours. This is because the initiator decomposes quickly and the reaction rate is very high; therefore, fewer initiators in later period make the reaction rate low. From the analysis above, we know that the amount of APS equaling to 2g, 3g, and 7g is not the optimal

TABLE 3: The effect of different contents of APS.

Feed amount of APS (g)	Consume amount of APS (g)	Required reaction time (h)	Residue amount of APS (g)	Residual rate of APS
2	1.23	10.698	0.77	0.385
3	1.672	9.792	1.328	0.443
4	2.047	9.28	1.953	0.488
5	2.49	8.956	2.51	0.507
6	2.9	8.598	3.1	0.517
7	6.77	11.644	0.23	0.033

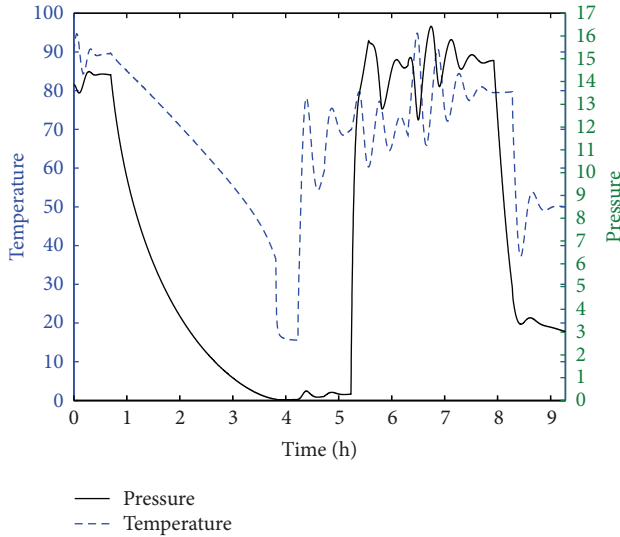


FIGURE 14: The effect on the reaction when APS = 4 g.

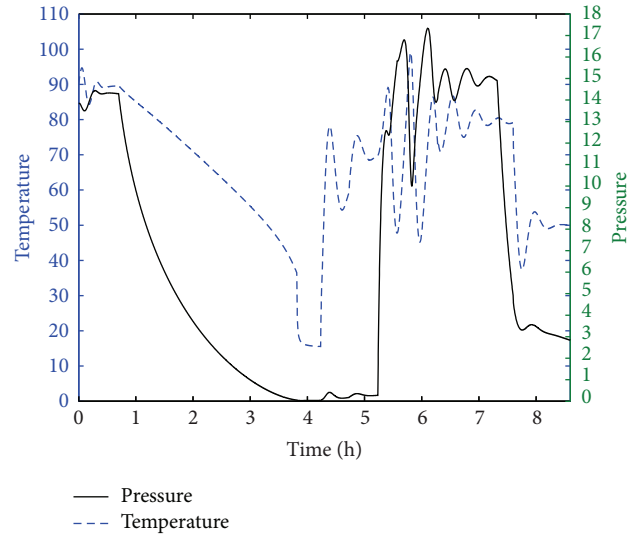


FIGURE 16: The effect on the reaction when APS = 6 g.

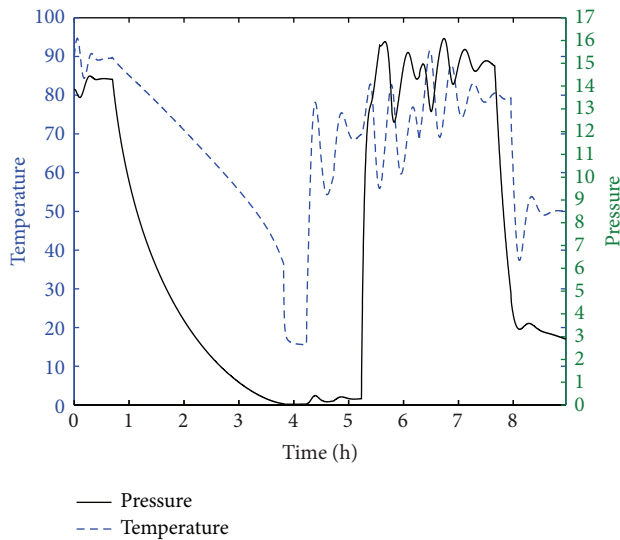


FIGURE 15: The effect on the reaction when APS = 5 g.

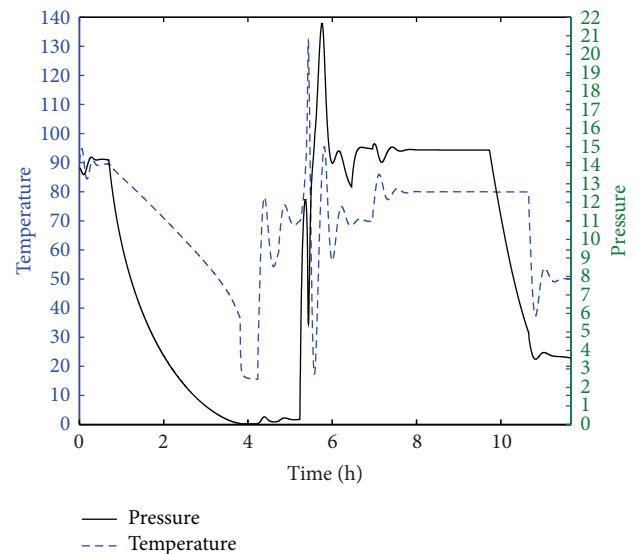


FIGURE 17: The effect on the reaction when APS = 7 g.

content for this reaction. Figures 14, 15, 16, and 17 show the the temperature and pressure of the reactor changes with time under the different amount of APS.

Figures 14, 15, 16, and 17 show that when the content of APS is 7 g, temperature reaches 130°C and the pressure

reaches 22 atm. The high content of APS leads to the rapid reaction rate in this process, and it also causes the temperature and pressure is difficult to be controlled well. When the content of APS is 6 g, the temperature rises suddenly

and reaches 100°C after adding TFE; meanwhile, the pressure exceeds 17 atm. When the content of APS is 4 g or 5 g, the temperature and pressure are in the controllable range, but relatively speaking, when the content of APS is 5 g, the temperature and pressure are controlled better. Table 1 also shows that productivity is higher and time consuming is less when APS is 5 g.

6. Conclusion

This paper has established the steady state and dynamic simulation of TFE polymerization and analyzed the changes in reactants and products with increasing time, meanwhile combining the method of relay feedback identification and Ziegler-Nichols rule to set and adjust controller parameters to keep the variables in the reaction process controlled well. The dynamic simulation records the entire polymerization reaction from beginning to the end. And it also can record each stage of the reaction process well; from the curve, we know that the temperature includes heating, balance, and cooling stages and the monomer feeding amount that is controlled by pressure controller is also ups and downs due to the pressure inside the reactor. PTFE and initiators increase and decrease gradually along with the reaction process. For APS part, we examine the influence on the reaction mainly through the total reaction time, the residual amount and the ease of control. The results show that when the content of APS is equal to 5 g, the reaction can not only be controlled well, but also guarantees a good rate of polymerization.

Conflict of Interests

The authors declare that there is no conflict of interests regarding the publication of this paper.

References

- [1] C. U. Kim, J. M. Lee, and S. K. Ihm, "Emulsion polymerization of tetrafluoroethylene: effects of reaction conditions on the polymerization rate and polymer molecular weight," *Journal of Applied Polymer Science*, vol. 73, no. 5, pp. 777–793, 1999.
- [2] C. U. Kim, J. M. Lee, and S. K. Ihm, "Emulsion polymerization of tetrafluoroethylene: effects of reaction conditions on particle formation," *Journal of Fluorine Chemistry*, vol. 96, no. 1, pp. 11–21, 1999.
- [3] J. Zeaiter, J. Romagnoli, and V. G. Gomes, "Reactor operating strategy and secondary nucleation in emulsion polymerization," *International Journal of Chemical Reactor Engineering*, vol. 2, no. 1, pp. 1–15, 2004.
- [4] C. U. Kim, J. M. Lee, and S. K. Ihm, "Emulsion polymerization of tetrafluoroethylene: effect of reaction conditions on the polymerization rate and polymer molecular weight," *Journal of Applied Polymer Science*, vol. 73, no. 5, pp. 789–792, 1999.
- [5] Y. Tabata, W. Ito, and K. Oshima, "Radiation-induced polymerization of tetrafluoroethylene," *Journal of Macromolecular Science A: Chemistry*, vol. 4, no. 4, pp. 789–799, 1970.
- [6] L. B. Zorina and V. P. Mel'nikov, "Polymerization of tetrafluoroethylene initiated by fluorinated petroleum coke," *Polymer Science A*, vol. 50, no. 9, pp. 942–947, 2008.
- [7] J. Ramos and J. Forcada, "Modeling the emulsion polymerization of amino-functionalized latex particles," *Polymer*, vol. 47, no. 4, pp. 1405–1413, 2006.
- [8] Y. Tabata, W. Ito, K. Oshima, and J. Takaci, "Radiation-induced polymerization of tetrafluoroethylene in solution," *Journal of Macromolecular Science*, vol. 4, no. 4, pp. 815–824, 1970.
- [9] X. Zhen and M. P. Duduković, "Modeling and simulation of semi-batch photo reactive distillation," *Chemical Engineering Science*, vol. 54, no. 10, pp. 1397–1403, 1999.
- [10] F. Dong, *Study on synthesis of ethylene glycol monoethers in semi-batch reactor [M.S. thesis]*, Ocean University of China, 2008.
- [11] N. Hamashima, "Monte Carlo simulation of size exclusion chromatography for branched polymers formed through free-radical polymerization with chain transfer to polymer," *Macromol Theory Simulation*, vol. 9, no. 8, pp. 453–462, 2000.
- [12] S. Thomas, A. Hamielec, and J. Soares, "Free radical polymerization—an elegant method of solving the population balance equations with chain transfer to polymer," *Polymer Reaction Engineering*, vol. 5, no. 4, pp. 183–203, 1997.
- [13] G. Moad and D. H. Solomon, *The Chemistry of Radical Polymerization*, Elsevier, 2006.
- [14] Y. J. Huang and L. J. Lee, "Kinetics of free radical polymerizations in reactive polymer processing," *American Institute of Chemical Engineers Journal*, vol. 31, no. 10, pp. 1585–1593, 1985.
- [15] O. F. Olaj, P. Vana, M. Zoder, A. Kornherr, and G. Zifferer, "Is the rate constant of chain propagation k_p in radical polymerization really chain-length independent?" *Macromolecular Rapid Communications*, vol. 21, no. 13, pp. 913–920, 2000.
- [16] I. N. Meshkova, V. I. Tsvetkova, and N. M. Chirkov, "Chain termination reactions in the polymerization of ethylene over $TiCl_4-AIR_2Cl$," *Bulletin of the Academy of Sciences of the USSR, Division of Chemical Science*, vol. 12, no. 5, pp. 732–737, 1963.
- [17] L. X. Zhang, H. J. Gao, and O. Kaynak, "Network-induced constraints in networked control systems—a survey," *IEEE Transactions on Industrial Informatics*, vol. 9, no. 1, pp. 403–416, 2013.
- [18] H. C. Yan, H. B. Shi, H. Zhang, and F. W. Yang, "Quantized H_∞ control for networked systems with communication constraints," *Asian Journal of Control*, vol. 15, no. 5, pp. 1468–1476, 2013.
- [19] W. L. Luyben, *Chemical Reactor Design and Control*, Wiley-Blackwell, 2007.
- [20] W. L. Luyben, *Distillation Design and Control Using Aspen Simulation*, American Institute of Chemical Engineers, 2006.
- [21] H. Zhang, H. C. Yan, F. W. Yang, and Q. J. Chen, "Quantized control design for impulsive fuzzy networked systems," *IEEE Transactions on Fuzzy Systems*, vol. 19, no. 6, pp. 1153–1162, 2011.
- [22] H. Zhang, H. C. Yan, F. W. Yang, and Q. J. Chen, "Distributed average filtering for sensor networks with sensor saturation," *IET Control Theory & Applications*, vol. 7, no. 6, pp. 887–893, 2013.
- [23] H. C. Yan, Z. Z. Su, H. Zhang, and F. W. Yang, "Observer-based H_∞ control for discrete-time stochastic systems with quantisation and random communication delays," *IET Control Theory & Applications*, vol. 7, no. 3, pp. 372–379, 2013.
- [24] H. J. Gao, T. W. Chen, and J. Lam, "A new delay system approach to network-based control," *Automatica*, vol. 44, no. 1, pp. 39–52, 2008.
- [25] H. Zhang, Z.-H. Guan, and G. Feng, "Reliable dissipative control for stochastic impulsive systems," *Automatica*, vol. 44, no. 4, pp. 1004–1010, 2008.

- [26] H. Zhang, Q. J. Chen, H. C. Yan, and J. H. Liu, "Robust H_∞ filtering for switched stochastic system with missing measurements," *IEEE Transactions on Signal Processing*, vol. 57, no. 9, pp. 3466–3474, 2009.
- [27] H. Zhang, H. C. Yan, T. Liu, and Q. J. Chen, "Fuzzy controller design for nonlinear impulsive fuzzy systems with time delay," *IEEE Transactions on Fuzzy Systems*, vol. 19, no. 5, pp. 844–856, 2011.

Research Article

Monitoring of Multimode Processes Based on Quality-Related Common Subspace Separation

Yunpeng Fan, Shipeng Li, and Yingwei Zhang

State Laboratory of Synthesis Automation of Process Industry, Northeastern University, Shenyang, Liaoning 110819, China

Correspondence should be addressed to Yingwei Zhang; zhangyingwei@mail.neu.edu.cn

Received 5 December 2013; Accepted 16 March 2014; Published 13 April 2014

Academic Editor: Lixian Zhang

Copyright © 2014 Yunpeng Fan et al. This is an open access article distributed under the Creative Commons Attribution License, which permits unrestricted use, distribution, and reproduction in any medium, provided the original work is properly cited.

A new monitoring approach for multimode processes based on quality-related common subspace separation is proposed. In the model, the data set forms a larger space when the correlation between process variables and quality variables is considered. And then the whole space is decomposed: quality-related common subspace, quality-related specific subspace, and the residual subspace. Monitoring method is performed in every subspace, respectively. The simulation results show the proposed method is effective.

1. Introduction

Multimode is one of the characteristics of the networked control systems. Adding product quality information into data set for complex process monitoring is a good approach in industrial process. It will be easier to monitor and forecast the product quality online if these data are utilized reasonably in process monitoring and fault diagnosis field. As we all know, in many production processes, the quality indexes of products are obtained by experimental analysis offline instead of being measured directly online owing to the limitations of existing technology [1–6]. However, data can be obtained online in some processes of chemical industry field, where we can get a mass of data directly and timely, and the quality information can also be contained there. To find the internal relations of the obtained data, thousands of domestic and foreign scholars have made a great effort, and many effective methods have been proposed to realize the quality monitoring and forecasting of products online [7].

Traditional quality monitoring and forecasting methods based on analytical model are highly dependent on the precise mathematical model of the object being diagnosed; thus its practical application is limited. Since multivariate statistical regression methods such as principal component regression (PCR) [8, 9] and partial least squares (PLS) [10] have overcome the deficiencies described above in recent

years, they are becoming the hotspot in quality monitoring and online forecasting field that the contemporary scholars at home and abroad focus on [11–16].

As a powerful multivariate statistical method, PLS can not only establish the relationship between quality data and process data accurately but also maintain good robustness with the assumption that the data obey a Gaussian distribution. It is an effective tool for monitoring the multivariable industrial process, which can be described by linear model. In the case of nonlinear data, traditional PLS may have a great error or even fail to establish the regression model. Despite all this, the PLS method can still be used to solve this problem if we do more preliminary work. Kim and Rosipal mapped the nonlinear data from the original space into a high-dimensional space, and they found the approximate linearity between these data in the new space and then utilized PLS. In this way, the regression problem for nonlinear data was resolved. In general, we call this preliminary work a kernel trick; the modified PLS is named KPLS which is short for kernel partial least squares. KPLS can also reduce the dimension of the sample space and eliminate the noise and correlation of data.

To solve the monitoring problems for multimode processes, various strategies have been proposed and put into process monitoring [17, 18]. Sub-PLS modeling algorithm has been developed to solve the multimode problem [19, 20]. In general, the monitoring programs will be adjusted according

to the different modes; that is, the monitoring program will be switched when the mode switches from one to another. Wang et al. studied the monitoring approach based on mode identification for multimode process with transitions [21]. However, the monitoring system often malfunctions in the transition processes. In this paper, considering that in the same system the common part exists in most modes, monitoring the common part and specific part, respectively, is a good way to reduce fault rate.

In this paper, a multimode process monitoring method based on quality-related common subspace separation is proposed. On the basis of the common subspace separation method, we consider the correlation between process variables and quality variables in model using KPLS, and then we separate the whole space into three parts: quality-related common subspace, quality-related specific subspace, and the residual subspace. At last, we monitor the fault in every subspace, respectively. Experiment results show the proposed method is effective. The advantages of this paper's methods are as follows. (1) The characteristic relationships between different modes are considered, and the complexity and fault rate of the monitoring program are reduced. (2) Fault can be detected accurately and timely in one of the three subspaces when it occurs. (3) Quality-related common subspace reflects local structural information of input data variables in each mode and has the strong ability to explain quality variables.

2. Quality-Related Common Subspace Separation

Suppose that the two industrial production patterns in the same production line are Modes A and B . X_A and X_B are the original process data sets of Modes A and B , where $X_A = [X_1^A, \dots, X_N^A]^T \in (N \times J)$, $X_B = [X_1^B, \dots, X_N^B]^T \in (N \times J)$, Y_A and Y_B are their quality data sets, where $Y_A = [Y_1^A, \dots, Y_N^A]^T \in (N \times J)$, $Y_B = [Y_1^B, \dots, Y_N^B]^T \in (N \times J)$. In addition, J and N are the variable number and sampling points, respectively. The extraction steps of the quality-related common subspace are as follows.

(1) Map the original process data and quality data from the original space to the feature space as $X_A \rightarrow \Phi(X_A)$, $X_B \rightarrow \Phi(X_B)$, $Y_A \rightarrow \Phi(Y_A)$, $Y_B \rightarrow \Phi(Y_B)$.

(2) Find the relationship between quality variables and process variables to get the quality-related process data: $\Phi(X_A) + \Phi(Y_A) \rightarrow \widehat{\Phi}(X_A)$, $\Phi(X_B) + \Phi(Y_B) \rightarrow \widehat{\Phi}(X_B)$.

(3) Put $\widehat{\Phi}(X_A)$ and $\widehat{\Phi}(X_B)$ together as the new data sets: $\widehat{\Phi}(X) = \widehat{\Phi}(X_A) + \widehat{\Phi}(X_B)$.

(4) Extract the quality-related common subspace: $\widehat{\Phi}(X) \rightarrow \widehat{\Phi}(X^C)$.

Important symbols and their meanings are listed in the abbreviation section.

In the second step, the interrelation of quality variables and process variables is established as follows:

$$\begin{aligned} \max \quad & w_A^T \Phi(X_A)^T \Phi(Y_A) c_A \\ \text{s.t.} \quad & \|w_A\|^2 = \|c_A\|^2 = 1, \\ \max \quad & w_B^T \Phi(X_B)^T \Phi(Y_B) c_B \\ \text{s.t.} \quad & \|w_B\|^2 = \|c_B\|^2 = 1. \end{aligned} \quad (1)$$

In the formulas (1), w_A and c_A are scores of the process variables and the quality variables of Mode A , respectively, and w_B and c_B are scores of the process variables and the quality variables of Mode B , respectively. Using the formulas above, we can get quality-related process data $\widehat{\Phi}(X_A)$ and $\widehat{\Phi}(X_B)$.

For every data point of the feature space $\widehat{\Phi}(X_i) \in \widehat{\Phi}(X)$, find the k nearest neighbors in $\chi_i = \{\widehat{\Phi}(X_{i_j})\}_{j=1}^k$. In addition, $\chi_i = \{\widehat{\Phi}(X_{i_j})\}_{j=1}^k$ are centered nonlinear mappings of the input variables.

Project k data points in χ_i into the tangent space at $\widehat{\Phi}(X_i)$, and linearly align the local coordinates into a single global coordinate system in R^d . Consider

$$\widehat{\Phi}(X_{i_j}^c) \approx \mathbf{L}_i \mathbf{Q}_i^T (\widehat{\Phi}(X_{i_j}) - \mathbf{C}_i) + \mathbf{b}_i, \quad j = 1, 2, \dots, k, \quad (2)$$

where $\mathbf{t}_j^{(i)} = \mathbf{Q}_i^T (\widehat{\Phi}(X_{i_j}) - \mathbf{C}_i)$, $j = 1, 2, \dots, k$ is named a local coordinate of $\widehat{\Phi}(X_{i_j})$, $\mathbf{C}_i = (1/k) \sum_{j=1}^k \widehat{\Phi}(X_{i_j})$ is the mean vector, and \mathbf{Q}_i is a tangent space projection matrix. \mathbf{Q}_i can be estimated by performing the optimal rank- d approximation of the centered data matrix. $\mathbf{L}_i \in R^{(d \times d)}$ is an affine transformation matrix and $\mathbf{b}_i \in R^d$ is a translation vector.

Consider $\mathbf{Q}_i \mathbf{L}_i^T$ in (2) as a transformation matrix; a linear transformation can be obtained as follows:

$$\widehat{\Phi}(X_{i_j}^C) \approx \mathbf{W}_i^T (\widehat{\Phi}(X_{i_j}) - \mathbf{C}_i) + \mathbf{b}_i, \quad j = 1, 2, \dots, k, \quad (3)$$

where $\mathbf{W}_i = \mathbf{Q}_i \mathbf{L}_i^T$, $\|\mathbf{W}_i\|_2 = 1$.

Solve \mathbf{W}_i and \mathbf{b}_i under the least-square regression. Obviously, the result is expected that each $\widehat{\Phi}(X_{i_j})$ can be directly mapped as $\widehat{\Phi}(X_{i_j}^C)$. Consider

$$\widehat{\Phi}(X_{i_j}^C) \approx g_i(\widehat{\Phi}(X_{i_j})), \quad (4)$$

where $g_i(x)$ is a function to make the measurement data approximate the common subspace data point $\widehat{\Phi}(X_{i_j}^C)$.

The least-square regression problem is given as follows:

$$\min \sum_{j=1}^k \left\| \widehat{\Phi}(X_{i_j}^C) - g(\widehat{\Phi}(X_{i_j})) \right\|_2^2 + \lambda \|\mathbf{W}_i\|_2^2, \quad (5)$$

where λ is a positive parameter.

According to (5), the object function $G(\mathbf{W}_i, \mathbf{b}_i)$ is as follows:

$$\begin{aligned} G(\mathbf{W}_i, \mathbf{b}_i) &= \min \sum_{j=1}^k \left\| \mathbf{W}_i^T \left(\widehat{\Phi}(\mathbf{X}_{i_j}) - \mathbf{C}_i \right) + \mathbf{b}_i - g\left(\widehat{\Phi}(\mathbf{X}_{i_j})\right) \right\|_2^2 \\ &\quad + \lambda \|\mathbf{W}_i\|_2^2. \end{aligned} \quad (6)$$

Let the replacing matrix $\widehat{\Phi}(\mathbf{X}_i^C) = [g(\widehat{\Phi}(\mathbf{X}_{i_1})) - \mathbf{C}_i, g(\widehat{\Phi}(\mathbf{X}_{i_2})) - \mathbf{C}_i, \dots, g(\widehat{\Phi}(\mathbf{X}_{i_k})) - \mathbf{C}_i]$ be the centralized data matrix and let $\widehat{\Phi}(\mathbf{X}_i^C) = [\widehat{\Phi}(\mathbf{X}_{i_1}^C), \widehat{\Phi}(\mathbf{X}_{i_2}^C), \dots, \widehat{\Phi}(\mathbf{X}_{i_k}^C)]$ collect the k data points.

The optimization \mathbf{W}_i and \mathbf{b}_i should meet the following conditions:

$$\begin{aligned} \frac{\partial G(\mathbf{W}_i, \mathbf{b}_i)}{\partial \mathbf{W}_i} &= \mathbf{0}, \\ \frac{\partial G(\mathbf{W}_i, \mathbf{b}_i)}{\partial \mathbf{b}_i} &= \mathbf{0}. \end{aligned} \quad (7)$$

Then

$$\begin{aligned} \frac{\partial G(\mathbf{W}_i, \mathbf{b}_i)}{\partial \mathbf{W}_i} &= \mathbf{0} \\ \implies 2\lambda \mathbf{W}_i + 2\widehat{\Phi}(\mathbf{X}_i^C) & \\ \times \left(\widehat{\Phi}(\mathbf{X}_i^C)^T \mathbf{W}_i + \mathbf{e}_k \mathbf{b}_i^T - \widehat{\Phi}(\mathbf{X}_i^C)^T \right) &= \mathbf{0} \\ \implies \left(\widehat{\Phi}(\mathbf{X}_i^C) \widehat{\Phi}(\mathbf{X}_i^C)^T + \lambda \mathbf{I}_m \right) \mathbf{W}_i & \\ = \widehat{\Phi}(\mathbf{X}_i^C) \left(\widehat{\Phi}(\mathbf{X}_i^C)^T - \mathbf{e}_k \mathbf{b}_i^T \right) & \\ \implies \mathbf{W}_i = \left(\widehat{\Phi}(\mathbf{X}_i^C) \widehat{\Phi}(\mathbf{X}_i^C)^T + \lambda \mathbf{I}_m \right)^{-1} & \\ \times \widehat{\Phi}(\mathbf{X}_i^C) \widehat{\Phi}(\mathbf{X}_i^C)^T, & \end{aligned}$$

$$\begin{aligned} \frac{\partial G(\mathbf{W}_i, \mathbf{b}_i)}{\partial \mathbf{b}_i} &= \mathbf{0} \\ \implies 2 \left(\mathbf{W}_i^T \widehat{\Phi}(\mathbf{X}_i^C) \mathbf{e}_k + \mathbf{b}_i \mathbf{e}_k^T \mathbf{e}_k - \widehat{\Phi}(\mathbf{X}_i^C) \mathbf{e}_k \right) & \\ = \mathbf{0} & \\ \implies k \mathbf{b}_i = \widehat{\Phi}(\mathbf{X}_i^C) \mathbf{e}_k - \mathbf{W}_i^T \widehat{\Phi}(\mathbf{X}_i^C) \mathbf{e}_k & \\ \implies \mathbf{b}_i = \frac{1}{k} \left(\widehat{\Phi}(\mathbf{X}_i^C) \mathbf{e}_k - \mathbf{W}_i^T \widehat{\Phi}(\mathbf{X}_i^C) \mathbf{e}_k \right) & \\ = \frac{1}{k} \widehat{\Phi}(\mathbf{X}_i^C) \mathbf{e}_k. & \end{aligned} \quad (8)$$

Here, the last equality holds because $\widehat{\Phi}(\mathbf{X}_i^C) \mathbf{e}_k = \mathbf{0}$. Thus, the optimal \mathbf{W}_i and \mathbf{b}_i can be obtained as follows:

$$\begin{aligned} \mathbf{W}_i &= \left(\widehat{\Phi}(\mathbf{X}_i^C) \widehat{\Phi}(\mathbf{X}_i^C)^T + \lambda \mathbf{I}_m \right)^{-1} \widehat{\Phi}(\mathbf{X}_i^C) \widehat{\Phi}(\mathbf{X}_i^C)^T, \\ \mathbf{b}_i &= \frac{1}{k} \widehat{\Phi}(\mathbf{X}_i^C) \mathbf{e}_k. \end{aligned} \quad (9)$$

After the optimal \mathbf{W}_i and \mathbf{b}_i are estimated, the sum of squared errors can be evaluated as follows:

$$\varepsilon_i = \sum_{j=1}^k \left\| \widehat{\Phi}(\mathbf{X}_{i_j}^C) - \left(\mathbf{W}_i^T \left(\widehat{\Phi}(\mathbf{X}_{i_j}) - \mathbf{C}_i \right) + \mathbf{b}_i \right) \right\|. \quad (10)$$

So we can get (11) from (9) as follows:

$$\begin{aligned} \varepsilon_i &= \sum_{j=1}^k \left\| \widehat{\Phi}(\mathbf{X}_{i_j}^C) - \left(\mathbf{W}_i^T \left(\widehat{\Phi}(\mathbf{X}_{i_j}) - \mathbf{C}_i \right) + \mathbf{b}_i \right) \right\|_2^2 \\ &= \text{tr} \left(\left(\widehat{\Phi}(\mathbf{X}_i^C) - \mathbf{W}_i^T \widehat{\Phi}(\mathbf{X}_i^C) - \mathbf{b}_i \mathbf{e}_k^T \right) \right. \\ &\quad \left. \times \left(\widehat{\Phi}(\mathbf{X}_i^C) - \mathbf{W}_i^T \widehat{\Phi}(\mathbf{X}_i^C) - \mathbf{b}_i \mathbf{e}_k^T \right)^T \right). \end{aligned} \quad (11)$$

Let $\widehat{\Phi}(\mathbf{X}_i^C) = \widehat{\Phi}(\mathbf{X}_i^C) \mathbf{L}$ and symmetric matrix $\mathbf{L} = \mathbf{L}^T = \mathbf{L}^2$. Then, simplify the expression as follows:

$$\begin{aligned} \widehat{\Phi}(\mathbf{X}_i^C) - \mathbf{W}_i^T \widehat{\Phi}(\mathbf{X}_i^C) - \mathbf{b}_i \mathbf{e}_k^T & \\ = \widehat{\Phi}(\mathbf{X}_i^C) \mathbf{L} \left(\mathbf{I}_k - \widehat{\Phi}(\mathbf{X}_i^C)^T \right. & \\ \times \left(\widehat{\Phi}(\mathbf{X}_i^C) \widehat{\Phi}(\mathbf{X}_i^C)^T + \lambda \mathbf{I}_m \right)^{-1} & \\ \times \widehat{\Phi}(\mathbf{X}_i^C) \left. \right). & \end{aligned} \quad (12)$$

Let

$$\begin{aligned} \mathbf{G}_i &= \mathbf{I}_k - \widehat{\Phi}(\mathbf{X}_i^C)^T \left(\widehat{\Phi}(\mathbf{X}_i^C) \widehat{\Phi}(\mathbf{X}_i^C)^T + \lambda \mathbf{I}_m \right)^{-1} \\ &\quad \times \widehat{\Phi}(\mathbf{X}_i^C), \end{aligned} \quad (13)$$

where both \mathbf{I}_m and \mathbf{I}_k are identity matrices and \mathbf{G}_i is symmetrical. Thus,

$$\varepsilon_i = \text{tr} \left(\widehat{\Phi}(\mathbf{X}_i^C) \mathbf{L} \mathbf{G}_i \mathbf{L} \widehat{\Phi}(\mathbf{X}_i^C)^T \right). \quad (14)$$

When the sum of the squared errors in each neighborhood χ_i is determined, an objective function can be constructed to express the global embedding as follows:

$$\mathbf{E}(\mathbf{X}_i^C) = \sum_{i=1}^n \text{tr} \left(\widehat{\Phi}(\mathbf{X}_i^C) \mathbf{L} \mathbf{G}_i \mathbf{L} \widehat{\Phi}(\mathbf{X}_i^C)^T \right). \quad (15)$$

Solve the following problem, and obtain the embedding:

$$\begin{aligned} \min \quad & \text{tr} \left(\widehat{\Phi}(\mathbf{X}_i^C) \mathbf{L} \mathbf{G}_i \mathbf{L} \widehat{\Phi}(\mathbf{X}_i^C)^T \right) \\ \text{s.t.} \quad & \widehat{\Phi}(\mathbf{X}_i^C)^T \widehat{\Phi}(\mathbf{X}_i^C) = \mathbf{I}_d. \end{aligned} \quad (16)$$

From (16), $\widehat{\Phi}(\mathbf{X}_i^C)$ can be gotten corresponding once the minimum trace was determined. In consequence we can obtain the quality-related common subspace $\widehat{\Phi}(\mathbf{X}^C) = [\widehat{\Phi}(\mathbf{X}_1^C), \widehat{\Phi}(\mathbf{X}_2^C), \dots, \widehat{\Phi}(\mathbf{X}_n^C)]$.

After obtaining the quality-related common subspace, we can decompose the quality-related process data of Mode *A* and Mode *B* into two different parts: the quality-related common subspace and two quality-related specific subspaces are independent to each other. One has

$$\begin{aligned}\widehat{\Phi}(\mathbf{X}_A) &= \widehat{\Phi}(\mathbf{X}^C) + \widehat{\Phi}(\mathbf{X}_A^S), \\ \widehat{\Phi}(\mathbf{X}_B) &= \widehat{\Phi}(\mathbf{X}^C) + \widehat{\Phi}(\mathbf{X}_B^S).\end{aligned}\quad (17)$$

Next, we built the principal component models of the common subspace and two specific subspaces as follows:

$$\begin{aligned}\widehat{\Phi}(\mathbf{X}^C) &= \widetilde{\widehat{\Phi}}(\mathbf{X}^C) + \widehat{\mathbf{E}}, \\ \widetilde{\widehat{\Phi}}(\mathbf{X}^C) &= \widehat{\mathbf{T}}^C \widehat{\mathbf{P}}_g^T, \\ \widehat{\mathbf{E}} &= \widehat{\mathbf{T}}_e^C \widehat{\mathbf{P}}_e^T, \\ \widehat{\Phi}(\mathbf{X}_A^S) &= \widetilde{\widehat{\Phi}}(\mathbf{X}_A^S) + \widehat{\mathbf{E}}_A^S, \\ \widetilde{\widehat{\Phi}}(\mathbf{X}_A^S) &= \widehat{\mathbf{T}}_A^S \widehat{\mathbf{P}}_A^T, \\ \widehat{\mathbf{E}}_A^S &= \widehat{\mathbf{T}}_{e,A}^S \widehat{\mathbf{P}}_{e,A}^S, \\ \widehat{\Phi}(\mathbf{X}_B^S) &= \widetilde{\widehat{\Phi}}(\mathbf{X}_B^S) + \widehat{\mathbf{E}}_B^S, \\ \widetilde{\widehat{\Phi}}(\mathbf{X}_B^S) &= \widehat{\mathbf{T}}_B^S \widehat{\mathbf{P}}_B^T, \\ \widehat{\mathbf{E}}_B^S &= \widehat{\mathbf{T}}_{e,B}^S \widehat{\mathbf{P}}_{e,B}^S,\end{aligned}\quad (18)$$

where $\widehat{\mathbf{P}}_g(J \times R)$ is the common loading and R is the PC number. $\widehat{\mathbf{P}}_A(J \times R_A)$ and $\mathbf{T}_{S,B}^2 = (\mathbf{t}_{\text{new},B}^S)^T (\Lambda_B^S)^{-1} \mathbf{t}_{\text{new},B}^S$ are the loadings of two quality-related specific subspaces; R_A and R_B are the retained PC numbers in the two quality-related specific subspaces. $\widehat{\mathbf{E}}_A^S$ and $\widehat{\mathbf{E}}_B^S$ are the specific residual matrixes.

3. Monitoring of Multimode Processes

To verify the validity of the method, we can monitor the Hotelling- T^2 and SPE, respectively, in quality-related common subspace, quality-related specific subspaces, and residuals spaces.

Assume $\mathbf{x}_{\text{new}}(J \times 1)$ is the new observation vector, which has been normalized by the mean and variance in advance. To calculate the common score, we project it onto the unified common subspace. The common score and Hotelling- T^2 statistic are calculated as follows:

$$\begin{aligned}\widehat{\mathbf{t}}_{\text{new}}^C &= \widehat{\mathbf{P}}_g^T \Phi(\mathbf{x}_{\text{new}}), \\ \widehat{\mathbf{T}}_c^2 &= (\widehat{\mathbf{t}}_{\text{new}}^C)^T (\Lambda^C)^{-1} (\widehat{\mathbf{t}}_{\text{new}}^C),\end{aligned}\quad (19)$$

where Λ^C is the covariance matrix of the common subspace, which is also connected with the retained PCs.

Use the following formulas to calculate the corresponding specific score and the Hotelling- T^2 statistic in quality-related specific subspaces:

$$\begin{aligned}\widehat{\mathbf{t}}_{\text{new},A}^S &= \widehat{\mathbf{P}}_A^T \mathbf{x}_{\text{new}}, \\ \widehat{\mathbf{t}}_{\text{new},B}^S &= \widehat{\mathbf{P}}_B^T \mathbf{x}_{\text{new}}, \\ \widehat{\mathbf{T}}_{S,A}^2 &= (\widehat{\mathbf{t}}_{\text{new},A}^S)^T (\Lambda_A^S)^{-1} \widehat{\mathbf{t}}_{\text{new},A}^S, \\ \widehat{\mathbf{T}}_{S,B}^2 &= (\widehat{\mathbf{t}}_{\text{new},B}^S)^T (\Lambda_B^S)^{-1} \widehat{\mathbf{t}}_{\text{new},B}^S, \\ \widehat{\mathbf{x}}_{\text{new}}^C &= \widehat{\mathbf{P}}_g \widehat{\mathbf{t}}_{\text{new}}^C, \\ \widehat{\mathbf{x}}_{\text{new}}^S &= \mathbf{x}_{\text{new}} - \widehat{\mathbf{x}}_{\text{new}}^C, \\ \widehat{\mathbf{x}}_{\text{new},m}^S &= \widehat{\mathbf{P}}_m \widehat{\mathbf{t}}_{\text{new},m}^S, \quad m = A, B, \\ \widehat{\mathbf{e}}_{\text{new},m}^S &= \widehat{\mathbf{x}}_{\text{new}}^S - \widehat{\mathbf{x}}_{\text{new},m}^S, \\ \text{SPE}_{\text{new},m} &= (\widehat{\mathbf{e}}_{\text{new},m}^S)^T \widehat{\mathbf{e}}_{\text{new},m}^S.\end{aligned}\quad (20)$$

Use the Hotelling- T^2 to detect the faults of the common features. If the result shows there are no faults in the common features, the specific Hotelling- T^2 can reflect the faults in the specific features. Simultaneously, the value of SPE can be used to detect the process faults in residual space.

4. Experimental Results

We add the correlation between process variables and quality variables in model based on the traditional subspace separation method and then apply the new multimode monitoring method to the process of the electrical fused magnesium furnace (EFMF). Simulation experiment verifies the method above is feasible. Firstly, define the normal process and quality data of Mode *A* and Mode *B* as, \mathbf{X}_A , \mathbf{X}_B , \mathbf{Y}_A , and \mathbf{Y}_B , respectively. There are seven crucial variables in each column of the data sets, including the value of three-phase current, the value of three-phase voltage, and the relative position of the electrode. The furnace temperature is the only quality data. A normal batch run which belongs to Mode *A* contains 400 sampling points. It is used to verify the feasibility of the above-proposed method. The Hotelling- T^2 statistics values, which are dependent on the confidence region of the common subspace, have been shown in Figure 1(a). In the case of the different specific subspaces, as is shown in Figures 1(b) and 1(c), the Hotelling- T^2 statistics values depend on the confidence region in Mode *A* only. We will know the operating mode of the EFMF from Figure 1. Both Hotelling- T^2 and SPE statistical variables of Mode *A* can show there are no faults. In the specific space of Mode *B*, SPE shows normal, while Hotelling- T^2 detects the fault. From the test results we have reason to think that the test data are normal data belonging to Mode *A* rather than Mode *B*.

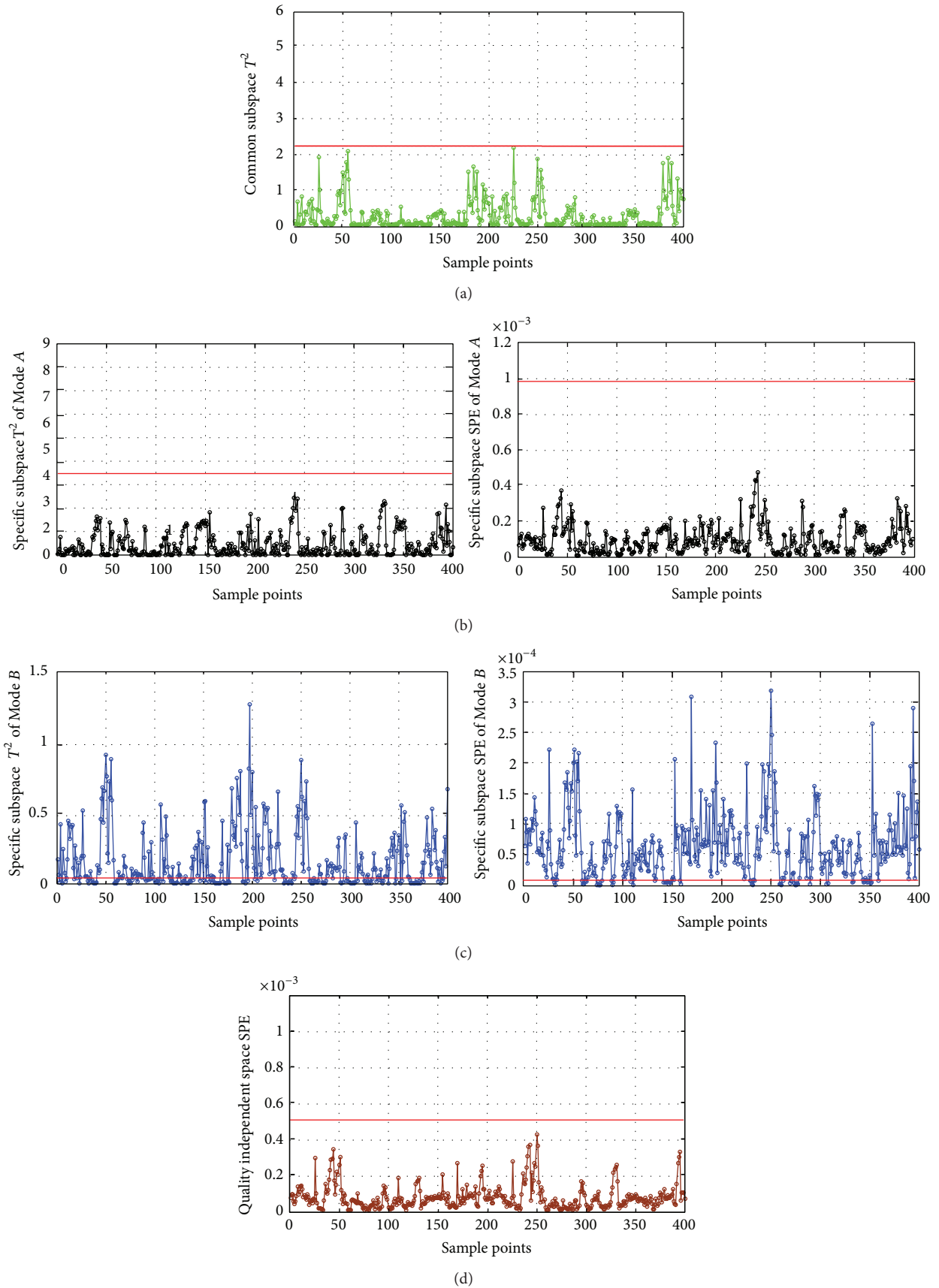


FIGURE 1: The proposed method monitoring results of the two different modes for (a) quality-related common part T^2 statistic, (b) quality-related specific part T^2 and SPE statistic of Mode A, and (c) quality-related specific part T^2 and SPE statistic of Mode B.

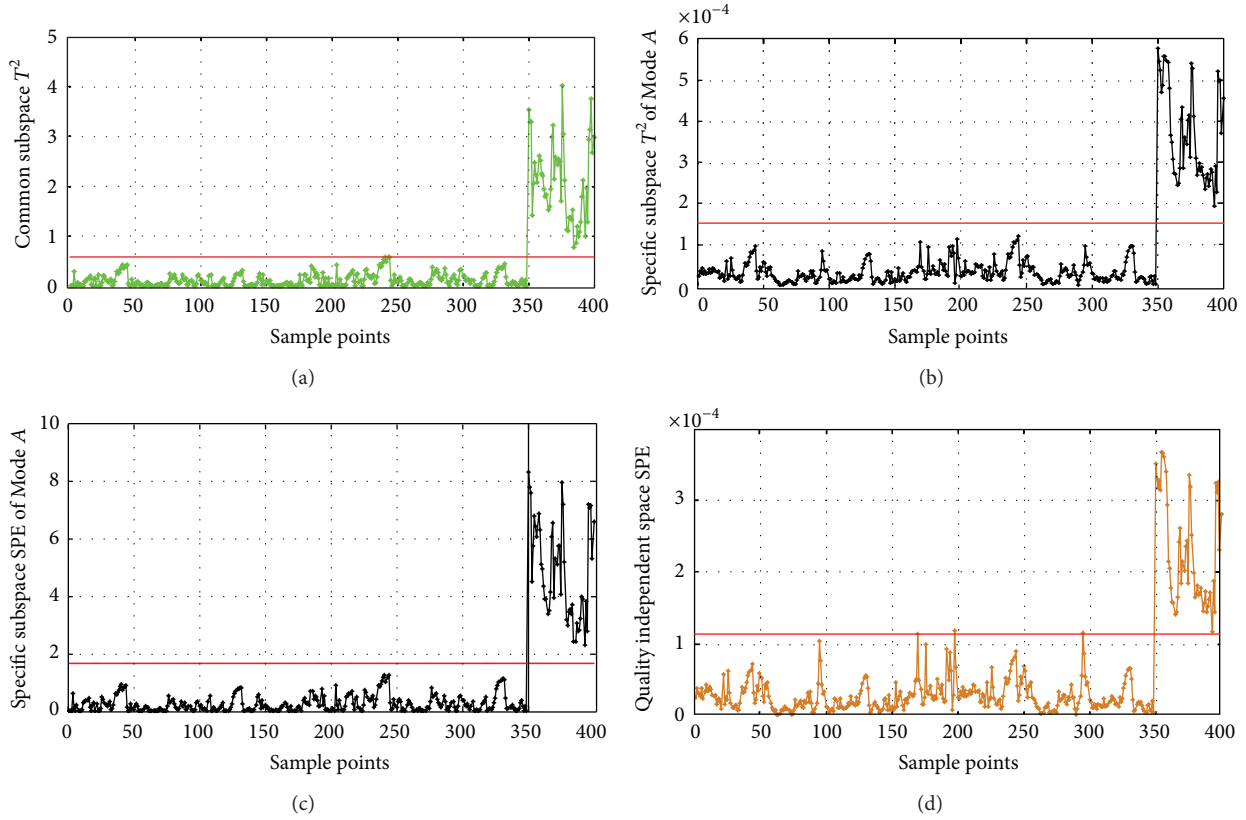


FIGURE 2: Monitoring results by Mode A for (a) quality-related common part T^2 statistic, (b) quality-related specific part T^2 statistic, (c) quality-related residual statistic, and (d) quality-unrelated residual statistic.

Next, we use the above-proposed method to monitor an abnormal batch run which belongs to Mode A. Previously, we introduced process faults from the 350th sample point. As shown in Figure 2, the proposed method can detect the fault effectively in quality-related common space, specific space, and residual space.

5. Conclusion

In this paper, the proposed approach, monitoring for multimode processes based on quality-related common subspace separation, is feasible. It makes the correlation between the quality-related common subspace and each mode data set and also reduces the complexity and fault rate of the monitoring program. Utilize the EFMF process as a backdrop; simulation experiment verifies the method above is effective. In the experiment we can see how the proposed method performs, which shows the desirable improvement in multimode processes. As application method, it should be applied in many similar multimode processes to help understanding and improving the monitoring model.

Abbreviations

X_A : Raw normal process data of Mode A
 X_B : Raw normal process data of Mode B

Y_A : Raw quality data of Mode A
 Y_B : Raw quality data of Mode B
 $\Phi(X_A)$: Process data mapped into high-dimensional space of Mode A
 $\Phi(X_B)$: Process data mapped into high-dimensional space of Mode B
 $\Phi(Y_A)$: Quality data mapped into high-dimensional space of Mode A
 $\Phi(Y_B)$: Quality data mapped into high-dimensional space of Mode B
 $\widehat{\Phi}(X_A)$: Quality-related process data mapped into high-dimensional space of Mode A
 $\widehat{\Phi}(X_B)$: Quality-related process data mapped into high-dimensional space of Mode B
 $\widehat{\Phi}(X^C)$: Component of quality common subspace
 $\widehat{\Phi}(X^C)$: Quality-related common subspace
 $\widehat{\Phi}(X_A^S)$: Quality-related specific subspace of Mode A
 $\widehat{\Phi}(X_B^S)$: Quality-related specific subspace of Mode B.

Conflict of Interests

The authors declare that there is no conflict of interests regarding the publication of this paper.

References

- [1] Z. Gao, X. Dai, T. Breikin, and H. Wang, "Novel parameter identification by using a high-gain observer with application to a gas turbine engine," *IEEE Transactions on Industrial Informatics*, vol. 4, no. 4, pp. 271–279, 2008.
- [2] Z. W. Gao, T. Breikin, and H. Wang, "High-gain estimator and fault-tolerant design with application to a gas turbine dynamic system," *IEEE Transactions on Control Systems Technology*, vol. 15, no. 4, pp. 740–753, 2007.
- [3] M. H. Kim, S. Lee, and K. C. Lee, "Kalman predictive redundancy system for fault tolerance of safety-critical systems," *IEEE Transactions on Industrial Informatics*, vol. 6, no. 1, pp. 46–53, 2010.
- [4] G. Gaderer, P. Loschmidt, and T. Sauter, "Improving fault tolerance in high-precision clock synchronization," *IEEE Transactions on Industrial Informatics*, vol. 6, no. 2, pp. 206–215, 2010.
- [5] T. J. Harris, C. T. Seppala, and L. D. Desborough, "A review of performance monitoring and assessment techniques for univariate and multivariate control systems," *Journal of Process Control*, vol. 9, no. 1, pp. 1–17, 1999.
- [6] V. Venkatasubramanian, R. Rengaswamy, K. Yin, and S. N. Kavuri, "A review of process fault detection and diagnosis part I: quantitative model-based methods," *Computers and Chemical Engineering*, vol. 27, no. 3, pp. 293–311, 2003.
- [7] P. Miller, R. E. Swanson, and C. E. Heckler, "Contribution plots: a missing link in multivariate quality control," *Applied Mathematics and Computer Science*, vol. 8, no. 4, pp. 775–792, 1998.
- [8] J. Chen and K. Liu, "On-line batch process monitoring using dynamic PCA and dynamic PLS models," *Chemical Engineering Science*, vol. 57, no. 1, pp. 63–75, 2002.
- [9] M. Misra, H. H. Yue, S. J. Qin, and C. Ling, "Multivariate process monitoring and fault diagnosis by multi-scale PCA," *Computers and Chemical Engineering*, vol. 26, no. 9, pp. 1281–1293, 2002.
- [10] S. W. Choi and I. Lee, "Multiblock PLS-based localized process diagnosis," *Journal of Process Control*, vol. 15, no. 3, pp. 295–306, 2005.
- [11] K. X. Peng, K. Zhang, and G. Li, "Total PLS based contribution plots for fault diagnosis," *Control Engineering Practice*, vol. 21, no. 4, pp. 360–369, 2012.
- [12] R. Boqué and A. K. Smilde, "Monitoring and diagnosing batch processes with multiway covariates regression models," *AIChE Journal*, vol. 45, no. 7, pp. 1504–1520, 1999.
- [13] Y. W. Zhang, L. J. Zhang, and H. L. Zhang, "Fault detection for industrial processes," *Mathematical Problems in Engineering*, vol. 2012, Article ID 757828, 18 pages, 2012.
- [14] J. Lee, C. Yoo, and I. Lee, "Statistical process monitoring with independent component analysis," *Journal of Process Control*, vol. 14, no. 5, pp. 467–485, 2004.
- [15] B. Dong, L. Zhang, Y. Wu, J. Feng, and T. Chai, "The fuzzy control research on electrodes of electrical-fused magnesia furnace," in *Proceedings of the Chinese Control and Decision Conference (CCDC '08)*, pp. 216–220, July 2008.
- [16] Y. W. Zhang, H. Zhou, S. J. Qin, and T. Chai, "Decentralized fault diagnosis of large-scale processes using multiblock kernel partial least squares," *IEEE Transactions on Industrial Informatics*, vol. 6, no. 1, pp. 3–10, 2010.
- [17] S. Reinikainen and A. Höskuldsson, "Multivariate statistical analysis of a multi-step industrial processes," *Analytica Chimica Acta*, vol. 595, no. 1-2, pp. 248–256, 2007.
- [18] H. H. Ma, Y. Hu, and H. B. Shi, "A novel local neighborhood standardization strategy and its application in fault detection of multimode processes," *Chemometrics and Intelligent Laboratory Systems*, vol. 118, pp. 287–300, 2012.
- [19] Y. Yang and F. Gao, "Adaptive control of the filling velocity of thermoplastics injection molding," *Control Engineering Practice*, vol. 8, no. 11, pp. 1285–1296, 2000.
- [20] J. Yu, "Localized Fisher discriminant analysis based complex chemical process monitoring," *AIChE Journal*, vol. 57, no. 7, pp. 1817–1828, 2011.
- [21] F. L. Wang, S. Tan, J. Peng, and Y. Chang, "Process monitoring based on mode identification for multi-mode process with transitions," *Chemometrics and Intelligent Laboratory Systems*, vol. 110, no. 1, pp. 144–155, 2012.

Research Article

H_∞ Control of Supply Chain Based on Switched Model of Stock Level

Junzhi Luo and Wanly Yang

School of Department of Fundamental Courses, Academy of Armored Force Engineering, Beijing 100072, China

Correspondence should be addressed to Junzhi Luo; zgyljz@126.com

Received 21 December 2013; Accepted 27 February 2014; Published 6 April 2014

Academic Editor: Huaicheng Yan

Copyright © 2014 J. Luo and W. Yang. This is an open access article distributed under the Creative Commons Attribution License, which permits unrestricted use, distribution, and reproduction in any medium, provided the original work is properly cited.

This paper is concerned with the problem of H_∞ control for a class of discrete supply chain systems. A new method based on network control technique is presented to address this issue. Supply chain systems are modeled as networked systems with stochastic time delay. Sufficient conditions for H_∞ controller design are given in terms of a set of linear matrix inequalities, based on which the mean-square asymptotic stability as well as H_∞ performance is satisfied for such systems. Simulation results are provided to demonstrate the effectiveness of the proposed method.

1. Introduction

A supply chain is a network of facilities and distribution entities (suppliers, manufacturers, distributors, and retailers) that manufactures raw materials into intermediate and finished products and distributes finished products to customers [1]. Nowadays, with the globalization of business, the phenomena of increasing competition among entities and more customer demanding lead to more complex dynamic behaviors of supply chain, such as demand fluctuation and lead-time delay. The static model is insufficient to model such systems with the dynamic characteristics; as a result, the dynamic analysis and control of supply chain systems have attracted more and more interests and attentions; see, for example, [2–13].

Various dynamic models have been employed for modeling and analyzing supply chain systems, which are mainly classified into continuous differential equations and discrete difference equations. For example, the piecewise-linear H_∞ controller was designed based on continuous differential equation for a production system in [5], the discrete difference models were provided to analyze system performance in [6–8, 10, 11], and the robust control strategy based on discrete models was given with uncertainty in [12, 13]. It should be noted that the information exchanging of production schedule, inventory positions, and procurement plan and customer demand, making decision, and implementing decision are

usually realized by network. In essence, supply chain systems are network control systems; the introduction of network facilitates the analysis and synthesis of supply chain systems.

As far as the network control systems (NCS) are concerned, they are spatially distributed systems in which the communication between sensors, actuators, and controllers occurs through a shared band-limited digital communication network. In the past decades, due to attractive features such as increased system flexibility, simple installation and maintenance, lower cost, and reduced weight and power, the study of NCSs has attracted considerable attention; see, for example, [14–18]. It is well recognized that the presence of network usually leads to the signal transmission delays. A common assumption in most of existing results on network-based control is that the network-induced delay has upper bounded or both lower and upper bounded. This assumption has been used in a great number of papers, such as [19, 20]. In fact, due to the unpredictability of the network environment, network-induced delay is random by nature. Furthermore, the disturbance of external factors or network congestion will make the induced delay become big, even bigger than upper bound of time delay. For these reasons, some researchers are devoted to the study of the problem of random delays in stochastic control systems [15, 21–25]. On the other hand, the switching among the different agents is the important feature of a supply chain system. It is essential

to consider the switching behavior when modeling a supply chain system. The great advance in the study of switched delay systems [26, 27] helps us to the modeling, analysis, and synthesis of a supply chain system. However, to the authors' best knowledge, the influence of the network factors and the switching behavior on supply chain systems is scarcely investigated in the existing literature. This motivates the present study.

In this paper, we are interested in the study of H_∞ control for a class of discrete supply chain systems. The following aspects are well addressed. Firstly, supply chain systems are modeled as switched network model with stochastic delay when considering the existence of switching and the random of network-induced delay. Discrete difference equations are utilized to describe the supply chain system, which is distinct from existed results that are concerned with the models of such systems. Secondly, sufficient conditions are obtained based on Lyapunov stability theory, which guarantee mean-square stability, and the bullwhip effect of supply chain system is studied in the sense of the stochastic H_∞ performance. Lastly, simulation results are provided to demonstrate the effectiveness of the proposed method.

The organization of this paper is as follows. In Section 2, the switched network model with stochastic delay is given to describe supply chain. In Section 3, the mean-square stability with H_∞ performance for supply chain systems is analyzed based on network model. Then, an example is provided to illustrate the effectiveness of the proposed method in Section 4. Finally, Section 5 concludes this paper.

Notations. In this paper, we use $P > 0$ ($\geq, <, \leq 0$) to denote a positive definite (semidefinite, negative definite, and seminegative definite) matrix P . "E" stands for mathematic expectation of random vector. The superscript "T" stands for matrix transpose and the symmetric terms in a matrix are denoted by "*"; " $\|\cdot\|$ " denotes the L_2 -norm which is given by $\|\omega(k)\| = (\sum_{k=0}^{\infty} \omega^T(k)\omega(k))^{1/2}$.

2. Problem Formulating

Consider the following supply chain system described by

$$\begin{aligned} x(k+1) &= \sum_{i=1}^3 \sigma_i(k) A_i x(k) + \sum_{i=1}^3 \sigma_i(k) B_i u(k) \\ &\quad + \sum_{i=1}^3 \sigma_i(k) F_i d(k), \\ z(k) &= \sum_{i=1}^3 \sigma_i(k) C_i x(k) + \sum_{i=1}^3 \sigma_i(k) D_i u(k), \end{aligned} \quad (1)$$

where $x(k) \in \mathbb{R}$, $u(k) \in \mathbb{R}$, and $d(k) \in \mathbb{R}$ denote the stock level, manufactured level, and customers demand, respectively. From the point view of control system, they are state variable, control input, and exogenous disturbance. $z(k) \in \mathbb{R}$ is output. $\sigma_i(k)$ is a switching signal which takes its value in the finite set $M = \{1, 2, 3\}$. Moreover, $\sigma_i(k) = i$ denotes that the i th subsystem is activated.

Before giving the switching rules, we define the switching function

$$\text{switch}(s) = \begin{cases} 1 & s > 0 \\ 0 & s \leq 0. \end{cases} \quad (2)$$

Now, the switched systems are given as follows.

- (i) If $\text{switch}[x(k) - L] = 1$, where L is a positive scalar, that is, the stock level is more than the value L of warning, some of the produced parts are being stored, the first subsystem is active.
- (ii) If $\text{switch}[x(k)(L - x(k))] = 1$, that is, the stock level is between 0 and the value L of warning, the second subsystem is active; otherwise, the third subsystem is active if $\text{switch}[-x(k)] = 1$.

In this paper, state feedback H_∞ controller based on networked control will be designed to stabilize the system (1), which takes the following form:

$$u(k) = K_\sigma x(k - d_k), \quad (3)$$

where d_k is network-induced delay.

Substituting the controllers (3) with system (1), the augmented system (1) with delays gives rise to the following system:

$$\begin{aligned} x(k+1) &= \sum_{i=1}^3 \sigma_i(k) A_i x(k) + \sum_{i=1}^3 \sigma_i(k) B_i K_i x(k - d_k) \\ &\quad + \sum_{i=1}^3 \sigma_i(k) F_i d(k), \\ z(k) &= \sum_{i=1}^3 \sigma_i(k) C_i x(k) + \sum_{i=1}^3 \sigma_i(k) D_i K_i x(k - d_k). \end{aligned} \quad (4)$$

Here, we assume that the network-induced delay d_k takes values in a finite set, that is, $d_k \in \{\tau_1, \tau_2, \dots, \tau_q\}$, and the occurrence probability of the delays τ_i is α_j , that is, $\text{Prob}\{d_k = \tau_j\} = \alpha_j$, where α_j is a positive scalar and $\sum_{j=1}^q \alpha_j = 1$.

Due to the random of d_k , the random vector $\Pi_{d_k=\tau_j}$ is defined as follows:

$$\Pi_{d_k=\tau_j} = \begin{cases} 1 & d_k = \tau_j \\ 0 & d_k \neq \tau_j. \end{cases} \quad (5)$$

Then, it is easy to get

$$E\{\Pi_{d_k=\tau_j}\} = \text{Prob}\{d_k = \tau_j\} = \alpha_j, \quad j = 1, 2, \dots, q. \quad (6)$$

By introducing random delay parameters, the supply chain system is transformed into a multiple delay system. The closed-loop supply chain system (1) can be rewritten as

$$\begin{aligned}
 x(k+1) &= \sum_{i=1}^3 \sigma_i(k) A_i x(k) \\
 &+ \sum_{i=1}^3 \sigma_i(k) \sum_{j=1}^q \Pi_{d_k=\tau_j} B_i K_i x(k-\tau_j) \\
 &+ \sum_{i=1}^3 \sigma_i(k) F_i d(k), \quad (7) \\
 z(k) &= \sum_{i=1}^3 \sigma_i(k) C_i x(k) \\
 &+ \sum_{i=1}^3 \sigma_i(k) \sum_{j=1}^q \Pi_{d_k=\tau_j} D_i K_i x(k-\tau_j).
 \end{aligned}$$

Before proceeding further, some definitions are given in the following.

Definition 1. The closed-loop supply chain system (7) with $d(k) = 0$ is said to be mean-square stable if, for any $\epsilon > 0$, there is $\delta(\epsilon) > 0$, such that $E\{\|x(k)\|^2\} < \epsilon$, $k > 0$ when $E\{\|x(0)\|^2\} < \delta(\epsilon)$.

In addition, if

$$\lim_{k \rightarrow \infty} E\{\|x(k)\|^2\} = 0 \quad (8)$$

for any initial conditions, the closed-loop system (7) is said to be globally mean-square asymptotically stable (GMSAS).

Definition 2. The closed-loop supply chain system (7) is said to satisfy the H_∞ performance, if

- (1) the augmented closed-loop system (7) is mean-square asymptotically stable with $d(k) = 0$,
- (2) the closed-loop system (7) satisfies $E\{\|z(k)\|^2\} \leq \gamma^2 \|d(k)\|^2$ for all nonzero $d(k) \neq 0$ under the zero initial condition.

Definition 3. The bullwhip effect is the amplification phenomenon which is described by the sum of the ratio of $z(k)$ to the customer's demand fluctuation $d(k)$; that is,

$$\gamma^2 = \sum_k \frac{\|z(k)\|^2}{\|d(k)\|^2}, \quad (9)$$

where $z(k)$ refers to production and inventory vector, $d(k)$ refers to demand fluctuation vector, time serial is $k = 1, 2, \dots, N$, and γ refers to the bullwhip effect.

Remark 4. For the existence of $d(k)$, the effect of $d(k)$ to $z(k)$ is also transformed into the problem of H_∞ performance analysis for the closed-loop supply chain systems; that is, the effect of bullwhip can be studied by the problem of H_∞ performance analysis.

Our purpose is to design a controller (3) such that the effect of $d(k)$ to the output $z(k)$ is under a desired level in the H_∞ performance.

3. Analysis on H_∞ Performance of Supply Chain

In this section, we will give the sufficient conditions such that the H_∞ performance can be guaranteed for system (7). The following theorem will play an important role in the controller design.

Theorem 5. For given scalars $\gamma > 0$, if there exist scholar $\mu > 1$ and symmetric positive definite matrices $P_i > 0$ ($i = 1, 2, 3$), $Q_j > 0$ ($j = 1, 2, \dots, q$), such that the following matrix inequalities simultaneously hold

$$\Omega_{ij} = \begin{bmatrix} \Xi_1 & \Xi_2 & \Xi_4 \\ * & \Xi_3 & 0 \\ * & * & \Xi_5 \end{bmatrix} < 0, \quad (10)$$

$$P_i \leq \mu P_l, \quad \forall (i, l) \in M \times M, \quad (11)$$

where

$$\begin{aligned}
 \Xi_1 &= \text{diag} \left\{ -P_i + \sum_{j=1}^q Q_j, -Q_1, -Q_2, \dots, -Q_q, -\gamma^2 I \right\}, \\
 \Xi_2 &= \begin{bmatrix} \sqrt{\alpha_1} A_i^T & \sqrt{\alpha_2} A_i^T & \cdots & \sqrt{\alpha_q} A_i^T & 0 \\ \sqrt{\alpha_1} K_i^T B_i^T & 0 & \cdots & 0 & 0 \\ * & \sqrt{\alpha_2} K_i^T B_i^T & \cdots & 0 & 0 \\ * & * & \ddots & \vdots & \vdots \\ * & * & * & \sqrt{\alpha_q} K_i^T B_i^T & 0 \\ * & * & * & * & F_i^T \end{bmatrix}, \quad (12) \\
 \Xi_3 &= \text{diag} \{-P_i^{-1}, -P_i^{-1}, \dots, -P_i^{-1}, -P_i^{-1}\}, \\
 \Xi_4 &= \begin{bmatrix} \sqrt{\alpha_1} C_i^T & \sqrt{\alpha_2} C_i^T & \cdots & \sqrt{\alpha_q} C_i^T \\ \sqrt{\alpha_1} K_i^T D_i^T & 0 & \cdots & 0 \\ * & \sqrt{\alpha_2} K_i^T D_i^T & \cdots & 0 \\ * & * & \ddots & \vdots \\ * & * & * & \sqrt{\alpha_q} K_i^T D_i^T \end{bmatrix}, \\
 \Xi_5 &= \text{diag} \{-I, -I, \dots, -I\},
 \end{aligned}$$

then system (7) is mean-square stable and satisfies H_∞ performance.

Proof. First, we consider system (7) with $d(k) = 0$.

Construct a Lyapunov function in the form of

$$V_{\sigma_i(k)}(x_k) = V_1(x_k) + V_2(x_k), \quad (13)$$

in which

$$\begin{aligned} V_1(x_k) &= x^T(k) P_\sigma x(k), \\ V_2(x_k) &= \sum_{j=1}^q \sum_{l=k-\tau_j}^{k-1} x^T(l) Q_j x(l). \end{aligned} \quad (14)$$

It is easy to see that

$$\begin{aligned} E(\Delta V_1 | x_k) &= E\{x^T(k+1) P_i x(k+1)\} - x^T(k) P_i x(k) \\ &= x^T(k) (A_i^T P_i A_i - P_i) x(k) \\ &\quad + 2 \sum_{j=1}^q \alpha_j x^T(k) A_i^T P_i K_i x(k - \tau_j) \\ &\quad + \sum_{j=1}^q \alpha_j x^T(k - \tau_j) K_i^T B_i^T P_i B_i K_i x(k - \tau_j), \\ E(\Delta V_2 | x_k) &= \sum_{j=1}^q [x^T(k) Q_j x(k) - x^T(k - \tau_j) Q_j x(k - \tau_j)] \\ E(\Delta V | x_k) &= x^T(k) \left(A_i^T P_i A_i - P_i + \sum_{j=1}^q Q_j \right) x(k) \\ &\quad + 2 \sum_{j=1}^q \alpha_j x^T(k) A_i^T P_i K_i x(k - \tau_j) \\ &\quad + \sum_{j=1}^q \alpha_j x^T(k - \tau_j) K_i^T B_i^T P_i B_i K_i x(k - \tau_j) \\ &\quad - \sum_{j=1}^q x^T(k - \tau_j) Q_j x(k - \tau_j) \\ &= \eta^T(k) \Gamma_{ij} \eta(k), \end{aligned} \quad (15)$$

where

$$\begin{aligned} \eta(k) &= [x^T(k) \quad x^T(k - \tau_1) \quad x^T(k - \tau_2) \quad \cdots \quad x^T(k - \tau_q)]^T, \\ \Gamma_{ij} &= \begin{bmatrix} \Gamma_{ij}^{11} & \Gamma_{ij}^{12} & \Gamma_{ij}^{13} & \cdots & \Gamma_{ij}^{15} \\ * & \Gamma_{ij}^{22} & \Gamma_{ij}^{23} & \cdots & \Gamma_{ij}^{25} \\ * & * & \Gamma_{ij}^{33} & \cdots & \Gamma_{ij}^{35} \\ * & * & * & \ddots & \vdots \\ * & * & * & \cdots & \Gamma_{ij}^{55} \end{bmatrix}, \\ \Gamma_{ij}^{11} &= A_i^T P_i A_i - P_i + \sum_{j=1}^q Q_j, \end{aligned}$$

$$\begin{aligned} \Gamma_{ij}^{12} &= \alpha_1 K_i^T P_i B_i K_i, \\ \Gamma_{ij}^{13} &= \alpha_2 K_i^T P_i B_i K_i, \\ \Gamma_{ij}^{15} &= \alpha_q K_i^T P_i B_i K_i, \\ \Gamma_{ij}^{22} &= \alpha_1 K_i^T B_i^T P_i B_i K_i - Q_1, \\ \Gamma_{ij}^{23} &= 0, \\ \Gamma_{ij}^{25} &= 0, \\ \Gamma_{ij}^{33} &= \alpha_2 K_i^T B_i^T P_i B_i K_i - Q_2, \\ \Gamma_{ij}^{35} &= 0, \\ \Gamma_{ij}^{55} &= \alpha_q K_i^T B_i^T P_i B_i K_i - Q_q. \end{aligned} \quad (16)$$

According to Schur complement, we can derive that $\Gamma_{ij} < 0$ which is equivalent to $\Lambda_{ij} < 0$, where

$$\begin{aligned} \Lambda_{ij} &= \begin{bmatrix} \bar{\Xi}_1 & \bar{\Xi}_2 \\ * & \bar{\Xi}_3 \end{bmatrix} < 0, \\ \bar{\Xi}_1 &= \text{diag} \left\{ -P_i + \sum_{j=1}^q Q_j, -Q_1, -Q_2, \dots, -Q_q \right\}, \\ \bar{\Xi}_2 &= \begin{bmatrix} \sqrt{\alpha_1} A_i^T & \sqrt{\alpha_2} A_i^T & \cdots & \sqrt{\alpha_q} A_i^T \\ \sqrt{\alpha_1} K_i^T B_i^T & 0 & \cdots & 0 \\ * & \sqrt{\alpha_2} K_i^T B_i^T & \cdots & 0 \\ * & * & \ddots & \vdots \\ * & * & * & \sqrt{\alpha_q} K_i^T B_i^T \end{bmatrix}, \\ \bar{\Xi}_3 &= \text{diag} \{-P_i^{-1}, -P_i^{-1}, \dots, -P_i^{-1}\}. \end{aligned} \quad (17)$$

At the same time, we can know $\Lambda_{ij} < 0$ if $\Omega_{ij} < 0$. \square

Let $0 = k_0 < k_1 < \cdots < k_l < \cdots < +\infty$, k_i ($i = 0, 1, 2, \dots, l$) be switching times over the interval $[0, k]$, $N_\sigma(s, t)$ be the switching numbers of switching signal $\sigma_i(k)$ over the interval $[s, t]$.

If $E[\Delta V | k] < 0$, there exists $0 < \alpha < 1$, such that the following inequality holds:

$$E(V_{\sigma_i(k+1)}(x_{k+1}) | x_k) \leq \alpha V_{\sigma_i(k)}(x_k), \quad \forall k \in [k_i, k_{i+1}). \quad (18)$$

Then

$$\begin{aligned} E(V_{\sigma_i(k)}(x_k)) &\leq \alpha^{k-k_i} V_{\sigma_i(k_i)}(x_{k_i}) \\ &\leq \alpha^{k-k_i} \mu V_{\sigma_i(k_{i-1})}(x_{k_i}) \\ &\leq \alpha^{k-k_i} \mu \alpha^{(k_i-k_{i-1})} V_{\sigma_i(k_{i-1})}(x_{k_{i-1}}) \\ &\leq \cdots \end{aligned}$$

$$\begin{aligned}
 &\leq \alpha^{k-k_0} \mu^i V_{\sigma_i(k_0)}(x_{k_0}) \\
 &= \alpha^k \mu^{N_{\sigma}(0,k)} V_{\sigma_i(0)}(x_0), \\
 E \left(\sum_{k=0}^N V_{\sigma_i(k)}(x_k) \right) \\
 &\leq V_{\sigma_i(0)}(x_0) + \alpha \mu^{N_{\sigma}(0,1)} V_{\sigma_i(0)}(x_0) \\
 &\quad + \alpha^2 \mu^{N_{\sigma}(0,2)} V_{\sigma_i(0)}(x_0) + \dots + \alpha^N \mu^{N_{\sigma}(0,N)} V_{\sigma_i(0)}(x_0) \\
 &\leq \mu^{T_{\max}} (1 + \alpha + \alpha^2 + \dots + \alpha^N) V_{\sigma_i(0)}(x_0) \\
 &\leq \mu^{T_{\max}} \frac{1 - \alpha^{N+1}}{1 - \alpha} V_{\sigma_i(0)}(x_0),
 \end{aligned} \tag{19}$$

where $T_{\max} = N_{\sigma}(0, N)$. Since $Q_j > 0$, $P_i > 0$, it can be given that

$$\begin{aligned}
 &\lim_{k \rightarrow \infty} E \left\{ \sum_{k=0}^N x(k)^T x(k) \mid x_0 \right\} \\
 &\leq \mu^{T_{\max}} \frac{1}{(1 - \alpha) \lambda_{\min}(P_0)} V_{\sigma_i(0)}(x_0).
 \end{aligned} \tag{20}$$

Furthermore, we can get

$$\lim_{k \rightarrow \infty} E \{ \|x(k)\|^2 \} = 0. \tag{21}$$

Based on Definition 1, we can derive that system (7) is mean-square asymptotically stable.

Second, we consider system (7) with $d(k) \neq 0$:

$$\begin{aligned}
 &E [z(k)^T z(k)] - \gamma^2 d(k)^T d(k) + E [\Delta V(k)] \\
 &= E \left[C_i x(k) + \sum_{j=1}^q \Pi_{d_k=\tau_j} D_i K_i x(k - \tau_j) \right]^T \\
 &\quad \times \left[C_i x(k) + \sum_{j=1}^q \Pi_{d_k=\tau_j} D_i K_i x(k - \tau_j) \right] \\
 &\quad + x(k)^T A_i^T P_i F_i d(k) - \gamma^2 d(k)^T d(k) \\
 &\quad + d(k)^T F_i^T P_i F_i d(k) \\
 &\quad + x^T(k) \left[A_i^T P_i A_i - P_i + \sum_{j=1}^q Q_j \right] x(k) \\
 &\quad + 2 \sum_{j=1}^q \alpha_j x^T(k) A_i^T P_i K_i x(k - \tau_j) \\
 &\quad + \sum_{j=1}^q \alpha_j x^T(k - \tau_j) K_i^T B_i^T P_i B_i K_i x(k - \tau_j) \\
 &\quad + \sum_{j=1}^q \alpha_j x^T(k - \tau_j) K_i^T B_i^T P_i F_i d(k)
 \end{aligned}$$

$$\begin{aligned}
 &- \sum_{j=1}^q x^T(k - \tau_j) Q_j x(k - \tau_j) \\
 &= \bar{\eta}^T(k) \Delta_{ij} \bar{\eta}(k),
 \end{aligned} \tag{22}$$

where

$$\begin{aligned}
 &\bar{\eta}(k) \\
 &= [x^T(k) \ x^T(k - \tau_1) \ x^T(k - \tau_2) \ \dots \ x^T(k - \tau_q) \ d(k)]^T,
 \end{aligned}$$

$$\Delta_{ij} = \begin{bmatrix} \Delta_{ij}^{11} & \Delta_{ij}^{12} & \Delta_{ij}^{13} & \dots & \Delta_{ij}^{15} & \Delta_{ij}^{16} \\ * & \Delta_{ij}^{22} & \Delta_{ij}^{23} & \dots & \Delta_{ij}^{25} & \Delta_{ij}^{26} \\ * & * & \Delta_{ij}^{33} & \dots & \Delta_{ij}^{35} & \Delta_{ij}^{36} \\ * & * & * & \ddots & \vdots & \vdots \\ * & * & * & * & \Delta_{ij}^{55} & \Delta_{ij}^{56} \\ * & * & * & * & * & \Delta_{ij}^{66} \end{bmatrix},$$

$$\Delta_{ij}^{11} = -P_i + \sum_{j=1}^q Q_j + A_i^T P_i A_i + C_i^T C_i,$$

$$\Delta_{ij}^{12} = \alpha_1 A_i^T P_i B_i K_i + \alpha_1 C_i^T D_i K_i,$$

$$\Delta_{ij}^{13} = \alpha_2 A_i^T P_i B_i K_i + \alpha_2 C_i^T D_i K_i,$$

$$\Delta_{ij}^{15} = \alpha_q A_i^T P_i B_i K_i + \alpha_q C_i^T D_i K_i,$$

$$\Delta_{ij}^{16} = A_i^T P_i F_i,$$

$$\Delta_{ij}^{22} = \alpha_1 K_i^T B_i^T P_i B_i K_i - Q_1 + \alpha_1 K_i^T D_i^T D_i K_i,$$

$$\Delta_{ij}^{23} = \alpha_1 \alpha_2 K_i^T B_i^T P_i B_i K_i + \alpha_1 \alpha_2 K_i^T D_i^T D_i K_i,$$

$$\Delta_{ij}^{25} = \alpha_1 \alpha_q K_i^T B_i^T P_i B_i K_i + \alpha_1 \alpha_q K_i^T D_i^T D_i K_i,$$

$$\Delta_{ij}^{26} = \alpha_1 K_i^T B_i^T P_i F_i,$$

$$\Delta_{ij}^{33} = \alpha_2 K_i^T B_i^T P_i B_i K_i - Q_2 + \alpha_2 K_i^T D_i^T D_i K_i,$$

$$\Delta_{ij}^{35} = \alpha_2 \alpha_q K_i^T B_i^T P_i B_i K_i + \alpha_2 \alpha_q K_i^T D_i^T D_i K_i,$$

$$\Delta_{ij}^{36} = \alpha_q K_i^T B_i^T P_i F_i,$$

$$\Delta_{ij}^{55} = \alpha_q K_i^T B_i^T P_i B_i K_i - Q_q + \alpha_q K_i^T D_i^T D_i K_i,$$

$$\Delta_{ij}^{56} = \alpha_q K_i^T B_i^T P_i F_i,$$

$$\Delta_{ij}^{66} = F_i^T P_i F_i - \gamma^2 I.$$

(23)

By Schur complement, we can obtain

$$\Delta_{ij} < 0 \tag{24}$$

which is equivalent to

$$\Omega_{ij} < 0. \quad (25)$$

Let $x(0) = 0$, for $E[\Delta V(k)] < 0$; then we have

$$E \left\{ \sum_{k=1}^{\infty} z(k)^T z(k) \right\} \leq \sum_{k=1}^{\infty} \gamma^2 d(k) d(k); \quad (26)$$

that is,

$$E \{ \|z(k)\|^2 \} \leq \gamma^2 \|d(k)\|^2. \quad (27)$$

According to the definition of H_{∞} performance, we can know that system (7) with $d(k) \neq 0$ satisfies H_{∞} performance.

It is important to note that the conditions of Theorem 5 are not linear matrix inequalities; the following Theorem 6 will give another equivalent condition.

Theorem 6. For given scalars $\gamma > 0$, if there exist scholar $\mu > 1$ and symmetric positive definite matrices $X_i > 0$, $Z_{ij} > 0$, $i = 1, 2, 3$, $j = 1, 2, \dots, q$, such that the following linear matrix inequalities simultaneously hold

$$\Pi_{ij} = \begin{bmatrix} \Lambda_1 & \Lambda_2 & \Lambda_4 \\ * & \Lambda_3 & 0 \\ * & * & \Lambda_5 \end{bmatrix} < 0, \quad (28)$$

$$X_l \leq \mu X_i, \quad \forall (i, l) \in M \times M, \quad (29)$$

where

$$\Lambda_1 = \text{diag} \left\{ -X_i + \sum_{i=1}^q Z_{ij}, -Z_{i1}, -Z_{i2}, \dots, -Z_{iq}, -\gamma^2 I \right\},$$

$$\Lambda_2 = \begin{bmatrix} \sqrt{\alpha_1} X_i A_i^T & \sqrt{\alpha_2} X_i A_i^T & \cdots & \sqrt{\alpha_q} X_i A_i^T & 0 \\ \sqrt{\alpha_1} Y_i^T B_i^T & 0 & \cdots & 0 & 0 \\ * & \sqrt{\alpha_2} Y_i^T B_i^T & \cdots & 0 & 0 \\ * & * & \ddots & 0 & 0 \\ * & * & * & \sqrt{\alpha_q} Y_i^T B_i^T & 0 \\ * & * & * & * & Y_i^T F_i^T \end{bmatrix},$$

$$\Lambda_3 = \text{diag} \{-X_i, -X_i, \dots, -X_i, -X_i\},$$

$$\Lambda_4 = \begin{bmatrix} \sqrt{\alpha_1} X_i C_i^T & \sqrt{\alpha_2} X_i C_i^T & \cdots & \sqrt{\alpha_q} X_i C_i^T \\ \sqrt{\alpha_1} Y_i^T D_i^T & 0 & \cdots & 0 \\ * & \sqrt{\alpha_2} Y_i^T D_i^T & \cdots & 0 \\ * & * & \ddots & 0 \\ * & * & * & \sqrt{\alpha_q} Y_i^T D_i^T \end{bmatrix},$$

$$\Lambda_5 = \text{diag} \{-I, -I, \dots, -I\}, \quad (30)$$

then, system (7) satisfies H_{∞} performance. Furthermore, the gain of controller can be given by $K_i = Y_i^T X_i^{-1}$.

Proof. Left and right multiplying (10) by the following matrix

$$\text{diag} \{-P_i^{-1}, -P_i^{-1}, \dots, -P_i^{-1}, -P_i^{-1}, I, I, \dots, I, I, \dots, I\} \quad (31)$$

and letting

$$X_i = P_i^{-1}, \quad Y_i = P_i^{-1} K_i^T, \quad Z_{ij} = P_i^{-1} Q_j^T P_i^{-1}, \quad (32)$$

we have

$$\Pi_{ij} < 0. \quad (33)$$

Meanwhile, left and right multiplying (11) by P_i^{-1} and P_i^{-1} gives rise to $X_l \leq \mu X_i$. According to condition (28) and (29) of Theorem 6, it is obvious that system (7) maintains H_{∞} performance. The proof is completed. \square

Remark 7. Let $q = 1$; the stochastic model of system (7) can be transformed into deterministic model. The stochastic model of system (7) is more universal than deterministic model. Moreover, the conditions of Theorems 5 and 6 have more applications than the one given based on the deterministic model.

4. Numerical Example

In this section, we will give a numerical example to demonstrate the effectiveness of the provided method for supply chain system modeled as network control system.

Example 8. We take the coefficient matrixes of system as follows:

$$\begin{aligned} A_1 &= [0.8], & A_2 &= [0.9], & A_3 &= [0]; \\ B_1 &= [0], & B_2 &= [0.1], & B_3 &= [0.1]; \\ C_1 &= [-0.05], & C_2 &= [-0.05], & C_3 &= [0]; \\ D_1 &= [0], & D_2 &= [-0.25], & D_3 &= [-0.32]; \\ F_1 &= [-1], & F_2 &= [-1], & F_3 &= [-1]. \end{aligned} \quad (34)$$

Let $\tau_1 = 1$, $\tau_2 = 2$, and $\tau_3 = 3$; $\alpha_1 = 0.1$, $\alpha_2 = 0.8$, and $\alpha_3 = 0.1$; and $\gamma = 1$. Solving the LMIs (28) with the help of the Matlab LMI Toolbox, we can obtain

$$\begin{aligned} X_1 &= [18.7701], & X_2 &= [20.1826], \\ X_3 &= [21.2242]; \\ Z_{11} &= Z_{12} = Z_{13} = [1.5447], \\ Z_{21} &= Z_{22} = Z_{23} = [0.6837], \\ Z_{31} &= Z_{32} = Z_{33} = [5.7842]; \\ Y_1 &= [13.002]; & Y_2 &= [14.0007]; \\ Y_3 &= [14.9991]. \end{aligned} \quad (35)$$

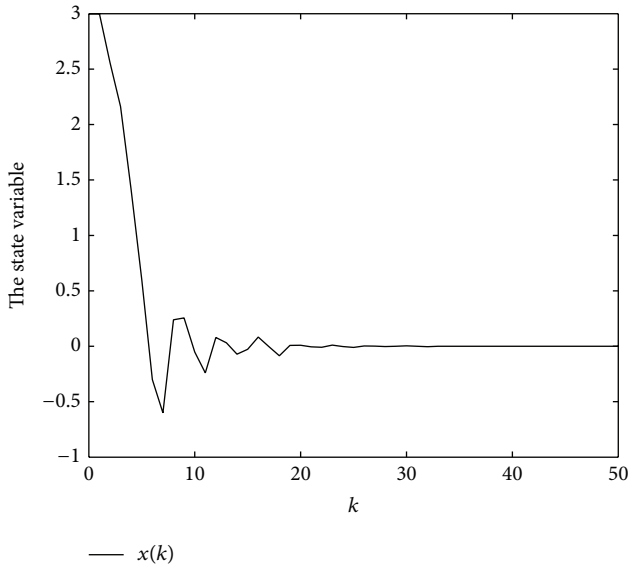


FIGURE 1: The state variable of system (7).

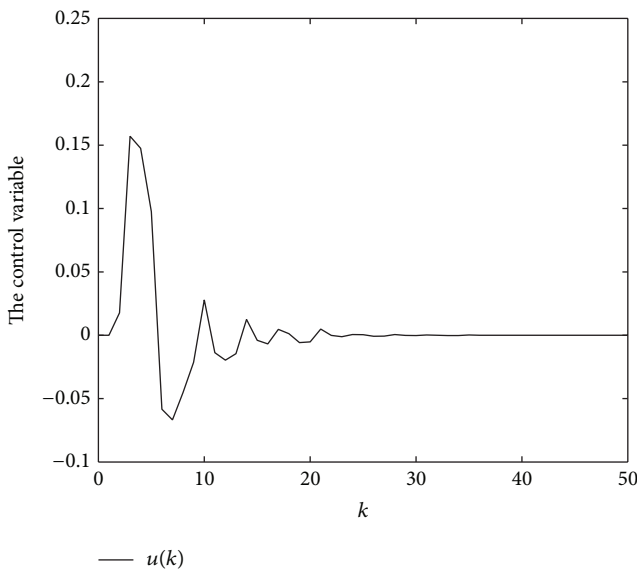


FIGURE 2: The control variable of system (7).

By further calculating, we obtain the following gain matrices for the H_∞ controller (3):

$$K_1 = [0.6926]; \quad K_2 = [0.6937]; \quad K_3 = [0.7067]. \tag{36}$$

Choosing the initial state as $x(0) = 3$ and the customer demand disturbance with $d(k) = \sin k$, the state response and the control input are illustrated in Figures 1 and 2. We find that the state is maintained at zero when the time is trending to infinity from Figure 1. That is to say, the stock level of supply chain can be maintained at the state of equilibrium and the

bullwhip effect is limited by scholar $\gamma = 1$; that is, the effect of $d(k)$ on $z(k)$ is limited by scholar $\gamma = 1$.

5. Conclusion

The problem of H_∞ control for a class of discrete supply chain systems is addressed in this paper. With the help of network control technique, supply chain systems are modeled as network control systems with stochastic time delay. The mean-square stability and H_∞ performance are studied based on the theory of switched and network control system. Sufficient conditions for the H_∞ controllers design are given in terms of a set of linear matrix inequalities. Finally, simulation examples are provided to illustrate the effectiveness of the developed results. If network-induced delay is random with probability distribution function, the problem of analysis and synthesis of such system will be considered in future work.

Conflict of Interests

The authors declare that there is no conflict of interests regarding the publication of this paper.

References

- [1] H. Sarimveis, P. Patrinos, C. D. Tarantilis, and C. T. Kiranoudis, "Dynamic modeling and control of supply chain systems: a review," *Computers and Operations Research*, vol. 35, no. 11, pp. 3530–3561, 2008.
- [2] B. M. Beamon, "Supply chain design and analysis: models and methods," *International Journal of Production Economics*, vol. 55, no. 3, pp. 281–294, 1998.
- [3] M. Boccadoro, F. Martinelli, and P. Valigi, "Supply chain management by H_∞ control," *IEEE Transactions on Automation Science and Engineering*, vol. 5, no. 4, pp. 703–707, 2008.
- [4] C. E. Riddalls and S. Bennett, "Production-inventory system controller design and supply chain dynamics," *International Journal of Systems Science*, vol. 33, no. 3, pp. 181–195, 2002.
- [5] L. Rodrigues and E. K. Boukas, "Piecewise-linear H_∞ controller synthesis with applications to inventory control of switched production systems," *Automatica*, vol. 42, no. 8, pp. 1245–1254, 2006.
- [6] X. Y. Huang, N. N. Yan, and H. F. Guo, "An H_∞ control method of the bullwhip effect for a class of supply chain system," *International Journal of Production Research*, vol. 45, no. 1, pp. 207–226, 2007.
- [7] X. Y. Huang, N. N. Yan, and R. Z. Qiu, "Dynamic models of closed-loop supply chain and robust H_∞ control strategies," *International Journal of Production Research*, vol. 47, no. 9, pp. 2279–2300, 2009.
- [8] M. Boccadoro, F. Martinelli, and P. Valigi, " H_∞ control of a supply chain model," in *Proceedings of the 45th IEEE Conference on Decision and Control (CDC '06)*, pp. 4387–4392, San Diego, Calif, USA, December 2006.
- [9] S. Srivathsan and M. Kamath, "An analytical performance modeling approach for supply chain networks," *IEEE Transactions on Automation Science and Engineering*, vol. 9, no. 2, pp. 265–275, 2012.
- [10] H. F. Guo, Y. L. Zhu, C. G. Chang, and X. M. Zhou, " H_∞ control of bullwhip effects in closed-loop supply chain networks

- with two chains cooperation,” in *Proceedings of the 7th World Congress on Intelligent Control and Automation (WCICA '08)*, pp. 2206–2211, Chong Qing, China, June 2008.
- [11] R. Z. Qiu and X. Y. Huang, “Two-stage supply chain dynamic model and robust H_∞ control,” *Control Engineering of China*, vol. 15, no. 1, pp. 9–12, 2008.
 - [12] R. G. Ge and X. Y. Huang, “Uncertain supply chain model based on switched inventory and robust H_∞ control,” *Systems Engineering*, vol. 27, no. 3, pp. 119–122, 2009.
 - [13] R. G. Ge and X. Huang, “Closed-loop supply chain switching model with outsourcing selection and its robust control,” *Computer Integrated Manufacturing Systems*, vol. 15, no. 10, pp. 2012–2016, 2009.
 - [14] L. Zhang, H. Gao, and O. Kaynak, “Network-induced constraints in networked control systems—a survey,” *IEEE Transactions on Industrial Informatics*, vol. 9, no. 1, pp. 403–416, 2013.
 - [15] H. J. Gao, T. W. Chen, and J. Lam, “A new delay system approach to network-based control,” *Automatica*, vol. 44, no. 1, pp. 39–52, 2008.
 - [16] H. Zhang, H. C. Yan, F. W. Yang, and Q. J. Chen, “Distributed average filtering for sensor networks with sensor saturation,” *IET Control Theory and Applications*, vol. 7, no. 6, pp. 887–893, 2013.
 - [17] X. M. Sun, G. P. Liu, W. Wang, and D. Rees, “ L_2 -gain of systems with input delays and controller temporary failure: zero-order hold model,” *IEEE Transactions on Control Systems Technology*, vol. 19, no. 3, pp. 699–706, 2011.
 - [18] H. C. Yan, H. B. Shi, H. Zhang, and F. W. Yang, “Quantized H_∞ control for networked systems with communication constraints,” *Asian Journal of Control*, vol. 15, no. 5, pp. 1468–1476, 2013.
 - [19] D. Yue, Q. L. Han, and J. Lam, “Network-based robust H_∞ control of systems with uncertainty,” *Automatica*, vol. 41, no. 6, pp. 999–1007, 2005.
 - [20] W. Zhang, M. S. Branicky, and S. M. Phillips, “Stability of networked control systems,” *IEEE Control Systems Magazine*, vol. 21, no. 1, pp. 84–99, 2001.
 - [21] L. Schenato, “Kalman filtering for networked control systems with random delay and packet loss,” in *Proceedings of the 17th International Symposium of Mathematical Theory of Networks and Systems*, Kyoto, Japan, 2006.
 - [22] H. J. Gao and T. W. Chen, “New results on stability of discrete-time systems with time-varying state delay,” *IEEE Transactions on Automatic Control*, vol. 52, no. 2, pp. 328–334, 2007.
 - [23] H. C. Yan, Z. Z. Su, H. Zhang, and F. W. Yang, “Observer-based H_∞ control for discrete-time stochastic systems with quantisation and random communication delays,” *IET Control Theory and Applications*, vol. 7, no. 3, pp. 372–379, 2013.
 - [24] H. Zhang, Q. J. Chen, H. C. Yan, and J. H. Liu, “Robust H_∞ filtering for switched stochastic system with missing measurements,” *IEEE Transactions on Signal Processing*, vol. 57, no. 9, pp. 3466–3474, 2009.
 - [25] H. Zhang, Z. H. Guan, and G. Feng, “Reliable dissipative control for stochastic impulsive systems,” *Automatica*, vol. 44, no. 4, pp. 1004–1010, 2008.
 - [26] Q. K. Li, J. Zhao, X. J. Liu, and G. M. Dimirovski, “Observer-based tracking control for switched linear systems with time-varying delay,” *International Journal of Robust and Nonlinear Control*, vol. 21, no. 3, pp. 309–327, 2011.
 - [27] X. M. Sun, J. Zhao, and D. J. Hill, “Stability and L_2 -gain analysis for switched delay systems: a delay-dependent method,” *Automatica*, vol. 42, no. 10, pp. 1769–1774, 2006.

Research Article

Information Exchange rather than Topology Awareness: Cooperation between P2P Overlay and Traffic Engineering

Jia Zhao,¹ Jianfeng Guan,² Changqiao Xu,² Wei Su,¹ and Hongke Zhang¹

¹ National Engineering Laboratory for Next Generation Internet Interconnection Devices, Beijing Jiaotong University, Beijing 100044, China

² State Key Laboratory of Networking and Switching Technology, Beijing University of Posts and Telecommunications, Beijing, China

Correspondence should be addressed to Jia Zhao; 11111004@bjtu.edu.cn

Received 3 November 2013; Revised 26 February 2014; Accepted 13 March 2014; Published 3 April 2014

Academic Editor: Yang Shi

Copyright © 2014 Jia Zhao et al. This is an open access article distributed under the Creative Commons Attribution License, which permits unrestricted use, distribution, and reproduction in any medium, provided the original work is properly cited.

Solutions to the routing strategic conflict between noncooperative P2P overlay and ISP underlay go separate ways: hyperselfishness and cooperation. Unpredictable (possibly adverse) impact of the hyperselfish topology awareness, which is adopted in both overlay routing and traffic engineering, has not been sufficiently studied in the literature. Topology-related information exchange in a cooperatively efficient way should be highlighted to alleviate the cross-layer conflict. In this paper, we first illustrate the hyperselfish weakness with two dynamic noncooperative game models in which hyperselfish overlay or underlay has to accept a suboptimal profit. Then we build a synergistic cost-saving (SC) game model to reduce the negative effects of noncooperation. In the SC model, through information exchange, that is, the classified path-delay metrics for P2P overlay and peer locations for underlay, P2P overlay selects proximity as well as saving traffic transit cost for underlay, and ISP underlay adjusts routing to optimize network cost as well as indicating short delay paths for P2P. Simulations based on the real and generated topologies validate cost improvement by SC model and find a proper remote threshold value to limit P2P traffic from remote area, cross-AS, or cross-ISP.

1. Introduction

P2P overlay systems impose tremendous traffic load on the Internet. Traffic engineering (TE) has been employed by Internet service providers (ISPs) to improve traffic transit cost on physical networks. Although P2P system and TE independently decide their own routing in different layers, they impact on each other, because routing strategic conflict exists between them. As shown in Figure 1, P2P overlay generates traffic with a profit objective to minimize all end-to-end delays, while underlay TE adjusts its routing strategy to minimize network cost. Both peers j and k in overlay have the content that peer i wants. Selfishly, peer i chooses k . Unfortunately, underlay uses physical path *CEFA* to transit traffic t_{ki} and cost (hops) two times more than path *BA* from j to i . Even if i chose j , considering the background traffic in link *BA*, too much traffic volume from j to a greedy peer i would be a congestion risk for underlay network. Such cross-layer conflict has been analyzed in the literature [1–6].

Negative impacts on both overlay and underlay, resulted from noncooperation, can be summarized in three aspects. (i) Different profit objectives lead to selfish routing and may increase cost of each other, for example, increasing delay for P2P and maximum link utilization (MLU) for ISP. (ii) Underlay always has slow reaction to overlay traffic change, while overlay is prone to inaccurate proximity discovery. (iii) Every time when routing changes in overlay/underlay, it takes the two-layer system a period of time to readjust and converge to a new stable equilibrium, before which the system performs unstable oscillation.

Solutions for the noncooperative interaction above go separate ways as below.

- (i) Hyperselfishness: more selfish than the noncooperation, self-improvement of underlay/overlay by detecting and benefiting from topology-related information of overlay/underlay without support of each other and regardless of possible profit damage to each other.

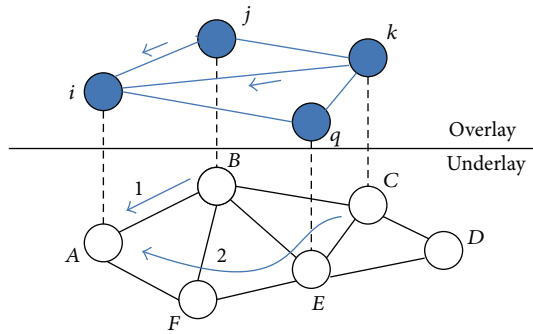


FIGURE 1: Overlay and underlay routing.

- (ii) Cooperation: topology information exchange between cooperative overlay and underlay.

On the involvement of hyperselfishness, P2P overlays deploy network-aware function to make proximity selection [7–9], while ISPs upgrade traffic monitors and evolve multi-protocol label switching- (MPLS-) based TE or IP-based TE like equal-cost multipath (ECMP) [10–13]. On the involvement of cooperation, topology-related information services, such as Oracle and P4P, have been proposed and implemented [14–17]. Comparing the two ways, an inevitable problem for hyperselfish topology-awareness is the unpredictable (possibly adverse) impact on the topology-transparent one (i.e., underlay/overlay whose topology-related information is detected and known to overlay/underlay). Network-aware overlay may disarrange underlying global traffic optimization and peer-location-aware underlay may intercept and restrain underlying content-sharing flexibility. Accordingly, we have two goals in this paper: (i) to illustrate weakness of hyperselfish behaviors and (ii) to utilize cooperation control to improve the three negative results from noncooperation.

ISPs and P2P content providers (CPs) always try self-improvement unilaterally. In many practical scenarios, CP and ISP regard each other as opponent and rely much on their own technology to obtain opponent information (topology) for their selfish profit optimization. This hyperselfishness may intensify the “arm race” between CP and ISP [18]. Additionally, negative impact and inefficiency of hyperselfish topology-awareness has not been sufficiently studied in the literature. Hence, avoiding hyperselfish weakness will help CP and ISP to converge to cooperation of their own accord.

P2P overlays desire end-to-end path information to find proximity and minimize delay. ISPs pursue peer locations in P2P to adjust routing and save traffic transit cost. Therefore, it is reasonable for a P2P system and an ISP to cooperate to exchange information and embody a common goal in their respective profit functions. In contrast to selfish profit loss, the common goal to reciprocate each other is a way to a win-win situation [18].

In this paper, our main contributions include the following. (1) We illustrate hyperselfish weakness with two dynamic noncooperative game models. In the dynamic games, overlay/underlay initiates hyperselfish topology-awareness, and then topology-transparent underlay/overlay uses a reacting

strategy as self-protection or punishment to the hyperselfish one. We explain why hyperselfish initiator, though having opponent information may not benefit more and have to bow to a suboptimal profit. (2) We build a synergistic cost-saving (SC) game model based on topology-related information exchange between underlay and overlay. On one hand, ISPs indicate a classified path metric (e.g., delay, distance, or other link cost metrics) for P2P to select proximity and generate traffic demand rationally. A remote threshold (RT) is also used to limit P2P traffic from remote area, cross-AS, or cross-ISP. On the other hand, underlay obtains peer-location information from CPs and chooses physical paths to split traffic for optimal network cost, for example, minimum MLU. Due to the cooperation above, the overlay chooses proximity as well as saving transit cost for the underlay, while the underlay decides routing to optimize network cost as well as indicating short delay path for the overlay. Simulation results validate the cost improvement by SC model and the importance of proper RT selection.

The remainder of the paper is organized as follows. Section 2 introduces related work. In Section 3, we use two dynamic game models to illustrate hyperselfish weakness. In Section 4, we propose the SC model and detail the mechanisms of path classes and RT selection. Simulations are shown in Section 5. Section 6 concludes the paper.

2. Related Work

Cross-layer conflict and negative results from noncooperation have been researched in the literature. Liu et al. first model the interaction between overlay routing and TE with a noncooperative game [1]. They consider delay as cost for both the layers and show that selfish overlay routing may cause huge cost and oscillations to the two-layer system. In the paper [3], the authors model the dynamic games in which the leader layer has preemptive strategy to restrain routing readjustment of the follower layer so as to overcome negative impact of the performance oscillations. Wang et al. study the noncooperation between P2P overlay and TE and propose that the interaction impacts the two layers and causes a nonoptimal performance of both layers [4].

Solutions to the conflict are also proposed in related work. DiPalantino and Johari use the congestion signal, matched to TE objective, to obtain efficient equilibrium in the game between TE and content distribution [2]. With regard to cooperation in papers [14, 15], physical path distances are provided for P2P overlay to select closer peers and save network cost. Jiang et al. propose a game with sharing control to save costs for cooperative CPs and ISPs [16]. For P2P traffic management, bilateral cooperation between network operator and peers of P2P systems is proposed in [17]. In the paper [18], authors analyze the cross-layer interaction pattern and give an overview of information that can be exchanged between cooperative P2P systems and ISPs.

One main difference between our work and the related work above lies in that we use two dynamic game models to analyze the hyperselfish behaviors of overlay/underlay who unilaterally tries topology-awareness to profit from topology

information of the other one, regardless of possible damage to each other. With emergence of more and more unilateral improvement such as evolving TE or network-aware P2P systems, it is necessary to prompt ISPs and P2P systems to avoid such possibly adverse topology-awareness and use cooperation to solve cross-layer conflict. Our work also differs from [2, 16] in that the cooperation way we use is the exchanged information including peer-locations and path-delay metrics. Additionally, differing from [14, 15, 17], our paper proposes path classes and remote threshold with which ISPs and P2P systems can achieve cost improvement with a common goal to limit traffic from remote areas.

3. Weakness of Hyperselfishness

Diversity of topology-aware mechanisms has been used as solution to the cross-layer conflict between P2P overlay routing and ISP's traffic engineering. These mechanisms are hyperselfish because either overlay or underlay only consider its own optimal routing and accordingly cannot deal with the possible adverse effect which causes damages to both layers. In this section, we build two dynamic game models to demonstrate the weakness of hyperselfish topology-awareness, and we use these models to explain the limitation of self-improvement from either layer.

3.1. Negative Impacts of Noncooperation. Both P2P overlay and ISP underlay have their own routing strategies and utility objectives. Peers in a P2P system demand contents from closer peers to obtain QoS, for example, fast file-download and fluent video playback [19, 20]. The utility of P2P overlay is to minimize total end-to-end delays. Underlay use TE and selects paths to transit traffic. The utility of the underlay is to optimize the overall network cost.

Overlay and underlay independently decide their strategy, but the strategy they choose will influence the utility of each other. Accordingly, a noncooperative game model can be built for interaction between overlay and underlay [21]. In a network $G = (V, E)$ and its overlay node set N and given the notations and descriptions in Notations, we model the noncooperative game as follows.

Underlay chooses the routing strategy $R = \{r_{ij}^k(e) \cdot f_{ij}^k\}$ by solving the problem as follows:

$$\min G(R, M_T) = \sum_{e \in E} \sum_{i, j \in N} \sum_{k \in S_{ij}} g_e(t_{ij}, r_{ij}^k(e) \cdot f_{ij}^k) \quad (1)$$

subject to $\sum_k f_{ij}^k = 1$, for all $e \in E$, $S_{ij} = \{1, \dots, |p_{ij}|\}$, $p_{ij} = \{p_{ij}^k\}$, $t_e^b + \sum_k \sum_{i, j} t_{ij} \cdot r_{ij}^k(e) \cdot f_{ij}^k \leq c_e$.

Overlay decides the overlay traffic matrix $M_T = \{t_{ij}\}$ by solving the problem as follows:

$$\min H(M_T, R) = \sum_{e \in E} \sum_{i, j \in N} h_{ij}(t_{ij}, P(p_{ij})) \quad (2)$$

subject to $t_e^b + \sum_{i, j \in N} \sum_{k \in S_{ij}} t_{ij} \cdot r_{ij}^k(e) \cdot f_{ij}^k \leq c_e$, $\sum_{i \in N} t_{ij} = T_j$.

Function $g_e(\cdot)$ represents the transit cost function of link e , $G(R, M_T)$ is underlay's total cost function whose value is

decided by R and M_T , function $h_{ij}(\cdot)$ represents the delay from overlay node i to j , $H(M_T, R)$ is overlay's total cost function whose value is decided by R and M_T , $|p_{ij}|$ denotes number of elements in physical path set p_{ij} for ij , and $P(p_{ij})$ denotes the underlay routing policy for logical link ij .

From this basic model, we draw three negative results from the cross-layer conflict.

3.1.1. Selfish Routing Conflict. Different utilities may lead to conflicting routing strategies. P2P system select closer peers to minimize delay. When the physical path under the logical link between two peers is overloaded, this shortest-delay choice of overlay may be a congestion risk to underlay links. On the other side, because underlay uses TE to optimize global traffic transit regardless of QoS of P2P overlay, TE routing adjustment may map overlay logical link between geographically nearby peers into a long-delay physical path.

3.1.2. Inefficiently Detecting Each Other. ISPs always deploy infrastructures to monitor traffic and update a traffic matrix periodically, so as to make optimal routing selection. Yet, overlay is always active and the traffic changes frequently. So, underlay routing is not instantly adjusted and subject to time lag. Besides, inefficient network-aware machinery of P2P overlay may cause inaccurate proximity selection.

3.1.3. Slow Convergence and Oscillation. Although it can be proved that strategy equilibrium exists in the game, the actual converging process will experience several rounds of adjustments from both overlay and underlay. During these rounds, selfish and rational overlay/underlay will react to the other by changing routing to obtain optimal utility again and again. Frequent readjustment (oscillation) and longtime of equilibrium convergence will bring systematic instability.

3.2. Hyperselfish Weakness of Overlay. We regard overlay and underlay as two players in the dynamic game. Unlike simultaneous strategy decision of noncooperative game in Section 3.1, one player in the dynamic game decides his strategy before the other one decides his, and the later player has the information of the first's choice [22]. Hyperselfish overlay as the later player tries to use network-awareness to obtain underlay routing information and make selfish profit optimization regardless of possible profit damage to underlay. As the first player, underlay has the advantage of knowing overlay's strategic rule which underlay can use to decide an optimal reacting strategy to restrain overlay profit to be suboptimal. To analyze weakness of overlay hyperselfish behavior, we model the dynamic game as follows.

According to the detected underlay strategy R , overlay chooses optimal traffic matrix as follows:

$$M_T^*(R) = \arg \min H(M_T, R). \quad (3)$$

Underlay punishes the hyperselfish behavior $M_T^*(R)$ with an optimal reacting routing strategy as follows:

$$R^* = \arg \min G(M_T^*(R), R) \quad (4)$$

subject to $\sum_k f_{ij}^{k*} = 1$, $S_{ij}^* = \{1, \dots, |P_{ij}^*|\}$, $p_{ij}^* = \{p_{ij}^{k*}\}$, for all $e \in E$, $t_e^b + \sum_{i,j \in N} \sum_{k \in S_{ij}^*} t_{ij}^{k*} \cdot r_{ij}^{k*}(e) \cdot f_{ij}^{k*} \leq c_e$, $\sum_{i \in N} t_{ij}^* = T_j$, $i, j \in N$.

In this game, hyperselfish overlay obeys the strategic rule $M_T^*(R)$ to generate as much as possible traffic M_T^* via the detected short-delay paths from network-awareness result R . This behavior is a congestion risk and disarranges underlying global traffic optimization. To restrain this hyperselfishness, underlay can use (4) to first choose action R^* as self-protection before overlay's possible adverse action $M_T^*(R)$.

Proposition 1. *A subgame perfect information Nash Equilibrium solution exists in the dynamic game about overlay hyperselfish behavior, if link cost function g_e and overly delay cost function h_{ij} are all continuous.*

Proof. On any link e , overlay traffic is subject to $t_{\text{over}}^e \leq c_e$. There are strategic constrains of $\sum_k f_{ij}^k = 1$ and $\sum_{i \in N} t_{ij} = T_j$. So, solution set $S = \{(M_T, R)\}$ is a closed space. Because g_e and h_{ij} are continuous, continuous function gets minimal value at the solution R^* , and H gets the minimal value at M_T^* . We have the inequalities as $G(M_T^*, R^*) \leq G(M_T^*, R)$ and $H(M_T^*, R^*) \leq H(M_T^*, R)$. When overlay decides the policy M_T^* and underlay decides the policy R^* , they will not deviate from this equilibrium solution, because they cannot gain more profit with other policies. Therefore, (M_T^*, R^*) is a subgame perfect information Nash Equilibrium. \square

Proposition 2. *Overlay's hyperselfish behavior and underlay's reaction can be modeled as the Stackelberg competition.*

Stackelberg's leadership model [23] is a game between two players; one of which is the leader and decides his strategy first and the other one is the follower and decides his strategy after the leader's decision. In the competition between overlay and underlay, underlay is the leader who first deploys traffic engineering in its networks to limit the traffic from selfish overlay routing.

Proposition 3. *Overlay hyperselfish behavior can just obtain a suboptimal profit when underlay decides an optimal reacting strategy to restrain the overlay.*

Proof. Underlay takes the leadership to control the traffic through its networks. The control strategies are decided to limit some unfriendly traffic that cause high transit cost and to ensure QoS of ISP-friendly traffic. P2P traffic and background traffic (from ISP-friendly applications) will compete for network bandwidth. The dynamic game can be formatted as follows:

$$t_{ij}^*(P(p_{ij})) = \arg \max_{P(p_{ij})} \sum t_{ij}, \quad (5)$$

$$P^*(p_{ij}) = \arg \min_{P(p_{ij})} \sum_{e \in E} \sum_{i,j \in N} \sum_{k \in S} w_e \cdot t_{ij}^*(P(p_{ij})) \cdot t_{ij}^k(e) \cdot f_{ij}^k. \quad (6)$$

Hyperselfish P2P overlay obeys the rule $t_{ij}^*(P(p_{ij}))$ to generate as much as possible traffic on its detected short-delay

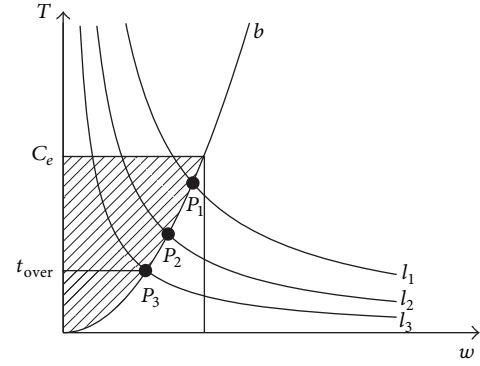


FIGURE 2: Suboptimal profit for hyperselfish overlay.

path p_{ij} . Underlay uses $P^*(p_{ij})$ as a congestion-proof strategy to reserve some bandwidth, leave enough bandwidth for ISP-friendly traffic, and leave the limited bandwidth for P2P traffic on the path p_{ij} .

Considering each single link, we have the link cost $l = t_e \cdot w_e$. As shown in Figure 2, l_1 , l_2 , and l_3 are three different equal-cost curves. Vertical axis indicates traffic amounts t_e . Horizontal axis indicates w_e , that is, link cost per traffic unit. Suppose that the link capacity is C_e . Curve b represents P2P traffic up-bound limited by ISP at each link (across horizontal W -axis). Curve b is an increasing function because we want $t_{\text{under}} = C_e - b(w_e)$ to be the bandwidth for ISP-friendly traffic. The cheaper (e.g., shorter delay or lower congestion) the link is, the more ISP-friendly traffic the link has, so that it ensures QoS of ISP-friendly traffic. According to (6), the underlay's strategy is to obtain the minimum link cost $l = t_e \cdot w_e$. From the three equal cost curves, underlay will choose l_3 . According to (5), overlay will choose t_{over} from the three points P_1 , P_2 , and P_3 on curve b because they are the maximum traffic volumes the overlay can generate. According to Proposition 2, underlay is the leader in this game and first chooses l_3 . Then overlay follows underlay's decision to choose the value t_{over} in Figure 2. Hence, cross-point P_3 is the equilibrium point of overlay and underlay. Compared with P_1 and P_2 , P2P overlay traffic t_{over} at equilibrium point P_3 is a suboptimal traffic. \square

For example in Figure 1, peer i chooses peer j rather than peer k to generate traffic demand, because overlay detects that underlay uses shorter (one hop) path 1 to transit traffic from j to i . If ISP limits P2P traffic on path BA , the low available bandwidth for P2P traffic on this path may also cause long time overlay delay. In this case, P2P's network-aware machinery is of no avail.

Take the interaction between MPLS-TE and network-aware P2P as an example. Suppose that a P2P system deploys the topology-aware algorithm and accordingly find the shortest delay path from requester to responder. The requesting peer decides to demand traffic via this detected-best-path and desires download speed as fast as possible. So, profit utility of the requester is to maximize his available download link bandwidth. What the P2P overlay does above is hyperselfish. This unilateral behavior may cause troubles (e.g., congestion

or bandwidth shortage) for the underlay ISPs when other background traffic also request bandwidth resource. Once the ISP discovers this hyperselfish intention, MPLS-TE can be used as self-adjustment for underlay and punishment to overlay. MPLS-TE enables ISP to map different services to multiple label switched paths (LSPs). Assisted by resource reservation protocol (RSVP), MPLS will provide background traffic (other ISP-friendly applications) with reserved path bandwidth firstly and optimally. Then, even if a short-delay end-to-end is detected by P2P, much bandwidth resource on this detected path has been reserved by ISP for transit cost-saving, leaving limited available bandwidth for P2P. This limitation by underlay will impact the QoS for overlay peers, but overlay cannot change this suboptimal profit by itself.

3.3. Hyperselfish Weakness of Underlay. Hyperselfish underlay regards P2P overlay as opponent and detects P2P traffic volume through physical network. As the first player, knowing underlay's strategic rule, overlay can firstly choose an optimal reacting strategy before underlay's action. The dynamic game is formatted as follows,

According to detected overlay traffic matrix M_T , underlay chooses optimal routing strategy as follows:

$$R^*(M_T) = \arg \min G(M_T, R). \quad (7)$$

Overlay reacts to the hyperselfish behavior $R^*(M_T)$ with an optimal traffic decision as follows:

$$M_T^* = \arg \min H(M_T, R^*(M_T)) \quad (8)$$

subject to $\sum_k f_{ij}^{k*} = 1$, $S_{ij}^* = \{1, \dots, |P_{ij}^*|\}$, $p_{ij}^* = \{p_{ij}^{k*}\}$, for all $e \in E$, $t_e^b + \sum_{i,j \in N} \sum_{k \in S_{ij}^*} t_{ij}^{k*} \cdot r_{ij}^{k*}(e) \cdot f_{ij}^{k*} \leq c_e$, $\sum_{i \in N} t_{ij}^* = T_j$, $i, j \in N$.

Proposition 4. *A subgame perfect information Nash Equilibrium solution exists in the dynamic game about underlay hyperselfish behavior, if link cost function g_e and path delay cost function h_{ij} are all continuous.*

This dynamic game model is applicable to many practical scenarios, where ISPs depend on traffic monitors to obtain traffic statistics of P2P or other applications. The statistics are used for bandwidth demand prediction or traffic routing adjustment in TE. Take bandwidth prediction as an example. ISPs always depend on current traffic state to predict bandwidth demand in future. ISP's TE wants to reserve optimal bandwidth for other ISP-friendly application traffic. So, TE control the underlay-friendly traffic t_u^e on each link e , while P2P overlay control the P2P traffic t_o^e on each link. Then underlay traffic and P2P traffic will compete for surplus bandwidth. The bandwidth competition game can be expressed as follows.

To find the optimal strategy t_u^e , underlay solves the following problem:

$$\max \frac{(\sum_e c_e - \sum_e t_u^e - \sum_e t_o^e) \cdot (\sum_e t_u^e)}{T}. \quad (9)$$

To find the optimal strategy t_o^e , overlay solves the following problem:

$$\max \frac{(\sum_e c_e - \sum_e t_u^e - \sum_e t_o^e) \cdot (\sum_e t_o^e)}{T} \quad (10)$$

subject to $t_u^e + t_o^e \leq c_e$, $\sum_e t_u^e + \sum_e t_o^e \leq T$.

c_e denotes the capacity of link e . Constant T is the limited total traffic volume. TE controls the incremental ISP-friendly traffic to take up the surplus bandwidth, which is matched with the current proportion of t_u^e to the total traffic amount T . P2P overlay also wants its incremental bandwidth matched with the current P2P traffic proportion $(\sum_e t_o^e)/T$. If TE tries to decide t_u^e according to t_o^e which is detected by the ISP traffic monitor, overlay can first decide a strategy t_o^{e*} as self-protection according to underlay's strategic rule $t_u^{e*}(t_o^e)$.

Proposition 5. *Hyperselfish underlay has a suboptimal result in the bandwidth competition with P2P overlay.*

Proof. Considering each link, underlay decides t_u^e and overlay decides t_o^e . We compare the two games: noncooperation and hyperselfishness. The former is a Cournot model [24] and can be expressed as follows,

Underlay solves the problem: $\max(c_e - t_u^e - t_o^e) \cdot t_u^e/T$.
Overlay solves the problem: $\max(c_e - t_u^e - t_o^e) \cdot t_o^e/T$.

Solutions are $t_u^{e*} = t_o^{e*} = c_e/3$. Both underlay's and overlay's bandwidth profit equal $c_e^2/9T$.

The dynamic game of hyperselfishness is a Stackelberg model [23] as follows:

$$\begin{aligned} t_u^{e*}(t_o^e) &= \arg \max (c_e - t_u^e - t_o^e) \cdot \frac{t_u^e}{T} = \frac{(c_e - t_o^e)}{2}, \\ t_o^{e*} &= \arg \max (c_e - t_u^{e*}(t_o^e) - t_o^e) \cdot \frac{t_o^e}{T} = \frac{c_e}{2}. \end{aligned} \quad (11)$$

Underlay profit equals $c_e^2/16T$, and overlay profit equals $c_e^2/8T$.

Comparing the results in the two cases above, optimal bandwidth profit in hyperselfish case is inferior to optimal result in noncooperative case. So, hyperselfish underlay profit is suboptimal. \square

Besides, hyperselfish weakness of underlay can also be ascribed to the routing change with P2P traffic state. ISPs rely too much on traffic monitoring infrastructures and distribute traffic engineering protocols (e.g., MPLS, ECMP) in many network nodes. So, it takes a relatively long time to update traffic statistics and to converge distributed TE to a stable equilibrium every time when overlay traffic change happens. Such hypersensitivity but slow reaction of the underlay fails to control the frequently changing P2P traffic.

3.4. From Hyperselfishness to Cooperation. Self-improvement by either CPs or ISPs may not achieve efficiency, though much effort has been made to evolve machinery for either traffic control or network-awareness. On the one hand, ISPs are committed to upgrade TE and enhance traffic control. MPLS-based TE can label different protocol packets and

establish tunnels for differentiated traffic. Changeable IGP link weights or BGP routing attributes are deployed for intra- or interdomain TE, for example, SculptTE [12]. Due to efficient traffic monitoring technologies [10], virtual network topology based TE systems, such as AMPLE, are proposed to split traffic and balance load [25]. By central routing control for software defined network (SDN), MPLS-TE on OpenFlow platform is implemented [11]. Yet, evolving TE will still encounter routing conflict with overlay because P2P traffic changes are random. On the other hand, P2P systems keep on improving proximity discovery or network-aware mechanism (e.g., TopBT, CLOSER, and NAPA-WINE) and overlay structure (e.g., tree, mesh, and DHT) to select short-delay paths and satisfy traffic demand among peers efficiently [7–9]. Nevertheless, inaccurate and unreliable delay measurement and poor topology-aware performance will still be the bottleneck in overlay utility optimization.

In many scenarios, without cooperation, no matter how much effort ISPs or CPs make, there is just a suboptimal profit for them. Hyperselfish topology-awareness does not solve the cross-layer routing problem because the path information which either layer gets by topology-awareness is not accurate or in real time. Such topology-awareness may cause damage to both layers. Hence, it is reasonable for both layers to cooperate by a deliberate mechanism of information exchange.

4. A Synergistic Cost-Saving Game

In contrast with noncooperation and hyperselfishness, cooperation enables underlay and overlay to optimize selfish profit without damaging each other. We highlight a common goal in cost functions of both underlay and overlay. Advantage of the common goal is due to reciprocity, that is, self-optimization as well as considering and supporting profit goal of the other. Topology-related information can be exchanged between cooperative underlay and overlay to achieve the common goal. With peer locations, for example, IP addresses, from overlay, underlay can indicate path delay between overlay peers. With path information, for example, delay metric such as IGP weight, from underlay, overlay can select closer peers to avoid generating traffic from remote area, cross AS, or cross ISPs.

According to Propositions 1 and 4, the link cost function g_e and the overly delay cost function h_{ij} should be continuous. Let $g_e(x) = u_{ij}^e \cdot x$ and let $h_{ij}(x) = v_{ij} \cdot x$ be two linear functions. These continuous and convex functions on the strategy set ensure the existence of the Nash Equilibrium solution. Our synergistic cost-saving game is modeled as follows.

Underlay chooses $R = \{r_{ij}^k(e) \cdot f_{ij}^k\}$ by solving the problem:

$$\min \sum_{i,j \in N} \sum_{e \in E} \sum_{k \in S} u_{ij}^e \cdot (t_{ij}^k \cdot f_{ij}^k \cdot r_{ij}^k(e) + t_b^e). \quad (12)$$

Overlay decides $M_T = \{t_{ij}\}$ by solving the problem:

$$\min \sum_{i,j \in N} v_{ij} \cdot t_{ij} \quad (13)$$

subject to $\sum_k \sum_{i,j} t_{ij} \cdot f_{ij}^k \cdot r_{ij}^k(e) + t_b^e \leq c_e$, $\sum_k f_{ij}^k = 1$, $\sum_i t_{ij} = T_j$.

v_{ij} refers to logical path-delay metric from i to j and is given by underlay. u_{ij}^e refers to link cost to transit per unit traffic on physical link e if e is on logical path ij . Path metric set $\{v_{ij}, \forall i, j \in N, i \neq j\}$ for all logical peer connections are classified into numbers of path classes according to the path metric value. For example in Figure 1, we take hop-count as the path-delay metric. Underlay maps logical path ij into physical path AB (1 hop), jk into BC (1 hop), qk into EC (1 hop), ik into ABC (2 hops), qi into EFA (2 hops), and ki into $CEFA$ (3 hops). These paths can be classified into three classes as $\{ij, jk, qk\}$, $\{ik, qi\}$, and $\{ki\}$.

Proposition 6. *A Nash Equilibrium solution exists in the synergistic cost-saving game.*

Proof. Link cost function in formula (12) and path-delay cost function in formula (13) are both continuous functions. Because of the constraints of $t_{\text{over}}^e \leq c_e$, $\sum_k f_{ij}^k = 1$, and $\sum_{i \in N} t_{ij} = T_j$, solution set $S = \{(M_T, R)\}$ is a closed space. So, both underlay and overlay can get minimal costs at the solution $S^* = \{(M_T^*, R^*)\}$, which satisfies $\sum_{i,j \in N} \sum_{e \in E} \sum_{k \in S} u_{ij}^e \cdot (t_{ij}^* \cdot f_{ij}^{k*} \cdot r_{ij}^{k*}(e) + t_b^e) \leq \sum_{i,j \in N} \sum_{e \in E} \sum_{k \in S} u_{ij}^e \cdot (t_{ij}^* \cdot f_{ij}^k \cdot r_{ij}^k(e) + t_b^e)$ and $\sum_{i,j \in N} v_{ij}^* \cdot t_{ij}^* \leq \sum_{i,j \in N} v_{ij} \cdot t_{ij}$. Underlay and overlay will not deviate from the solution $S^* = \{(M_T^*, R^*)\}$, because they cannot gain more profit with other policies. So, $S^* = \{(M_T^*, R^*)\}$ is a Nash Equilibrium solution. \square

In this synergistic game model, mechanisms of path information, path classes, and remote threshold are detailed as follows.

4.1. Path Information. Because each link has a weight to indicate delay or other cost metrics, each underlying physical path, consisting of one or multiple links, can get an accumulated weight, which is sum of link weights on the path. For logical path ij in overlay, underlay can split traffic into multiple physical paths. So, we use the average weight w_{ij} of k paths to express the path weight for ij as follows:

$$w_{ij} = \sum_k w_{ij}^k \cdot f_{ij}^k. \quad (14)$$

The path metric v_{ij} equals to or positively correlate to the path weight w_{ij} . According to the value of v_{ij} , path ij will be classified into a path class and the class number x_{ij} will be given to overlay. Because v_{ij} is given by underlay, overlay has the accurate path-delay for proximity selection.

Obtaining the peer locations from P2P overlay, for each logical path between peers, ISP underlay can provide the path information which includes the following.

- (i) Path class number x_{ij} : indicating the path class which ij belongs to.
- (ii) Remote threshold (RT) value k : a selected class number, used to distinct between near and remote path classes.
- (iii) Limited traffic volumes T_{ij} : T_{ij} is given only when $x_{ij} > k$ (to limit traffic from remote candidate peer i to requesting peer j).

- (iv) Path-delay metric v_{ij} : v_{ij} is given only when $x_{ij} \leq k$. By solving formula (13), overlay can decide optimal traffic from i to j .

For large-scale P2P overlays, it is difficult for ISP underlay to select a remote threshold from numerous logical paths, yet due to path classes, a proper class number can be selected as RT to limit traffic from remote areas and significantly improve cost for both overlay and underlay.

4.2. Remote Threshold. Remote threshold can be used to divide paths into the near and the remote. Suppose there are total n path-classes in the network. Path metric values increase with order of class numbers. x_{ij} is the class number of the logical path i to j . The threshold value is set to be k . When underlay gets the peer couple of i and j , it will calculate the path weight w_{ij} . Path ij can be classified into one of the n path classes. If the class number x_{ij} which ij belongs to is greater than k , distance between i and j is regarded as the remote, and the traffic from i to j is limited. If $x_{ij} > k$, path metric v_{ij} is not shown to overlay and only a limited value of traffic volume is included in path information for overlay. If $x_{ij} \leq k$, v_{ij} will be given to overlay, and overlay will use proximity optimal algorithm to generate traffic from the closer peers. This threshold mechanism helps overlay quickly exclude remote peers or generate traffic less than the limitation from remote peers.

ISPs do not want to transit cross-AS or cross-ISP traffic, because interdomain links cost much more than intradomain. In this scenario, RT can be used as a threshold for binary value classes, for example, "0" represents intradomain and "1" represents interdomain. When path class number $x = 1$, traffic on this path is limited. Through this way, underlay can guide overlay peers to generate traffic within the AS or the ISP.

4.3. Proximity Selection Process of Overlay. Only if two peers are close enough, that is, path class number not greater than RT, overlay can use the proximity selection algorithm to decide traffic between the two peers. Before making optimal traffic decision, overlay depends on the path information to delete remote candidate peers or know the traffic limitation from those peers.

Overlay solves the formula (13) to obtain optimal traffic demand. Before using the path metric v_{ij} , overlay has to consider path congestion risk and multiply v_{ij} by a weight. The weight is related to traffic demand t_{ij} , because t_{ij} affects the link delay. If link e is on the path ij , link delay is expressed as

$$D_e = \frac{1}{c_e - t_{ij}^e - t_b^e}. \quad (15)$$

Too much traffic into link e will cause long time delay. This part of delay cost should be included in the path weight.

For example in Figure 1, underlay uses path BA to transit t_{ji} , path $CEFA$ to transit t_{ki} , and path EFA to transit t_{qi} . Assume that total traffic demanded by i is a constant t . We use hop-count to weight each path. So $v_{ji} = 1$, $v_{qi} = 2$, and

```
// Impartial Service (IS) Algorithm:
for Round  $i = 1; i < n; i++$  do
  Receive locations of peer couple  $(i, j)$  from Overlay;
  Give  $(i, j)$  locations to Underlay and query path delay;
  Receive path-delay metric  $v_{ij}$  from Underlay;
  Classify all paths and get the path-class number  $x_{ij}$ ;
  Set RT to be  $k$ ;
  if  $x_{ij} \geq k$  then
    Set traffic up-bound  $T_{x_{ij}}$  and give it to Overlay;
  else
    Give Overlay the information including:  $x_{ij}, k, v_{ij}$ ;
  end if
end for

// Overlay Algorithm:
for Round  $i = 1; i < n; i++$  do
  for each  $x_{ij}$  do
    if  $x_{ij} > k$  then
      generate  $t_{ij} \leq T_{x_{ij}}$ ;
    else
      solve formula (13) to obtain optimal  $t_{ij}$ ;
    end if
  end for
  Report the updated peer locations to IS;
end for

// Underlay Algorithm:
for Round  $i = 1; i < n; i++$  do
  Receive  $(i, j)$  locations and detect  $t_{ij}$ ;
  Solve (12) to decide  $R = \{r_{ij}^k(e) \cdot f_{ij}^k\}$  in this round;
  Indicate path metric  $v_{ij}$  to IS;
end for
```

ALGORITHM 1: Synergistic cost-saving process.

$v_{ki} = 3$. The remote threshold is set to be 2. So, the overlay path ki is deleted by i . Assume that the links of the underlay have the same capacity 1. Multiplying the path weight by the delay factors, we get the new path weights as $v_{ji} = 1/(1 - t_{ji})$ and $v_{qi} = 2/(1 - t_{qi})$. With these new path weights, we solve the formula (13) as follows:

$$\min \frac{t_{ji}}{1 - t_{ji}} + \frac{2t_{qi}}{1 - t_{qi}} \quad (16)$$

subject to $t_{ji} + t_{qi} = t$, $t_{ji} \geq 0$, $t_{qi} \geq 0$. So, peer i can demand optimal traffic from j and q .

4.4. Algorithm. Information can be directly exchanged between P2P system and ISP or through an impartial service between overlay and underlay. SC optimization is shown as Algorithm 1.

5. Performance Evaluation

In this section, based on simulation in both real and generated topologies, we validate that SC model improves the negative impacts of noncooperation and a proper remote threshold should be selected for cost improvement.

5.1. Simulation Setup. To demonstrate the improvement for noncooperative negative impacts which have been summarized in Section 3, we use real network topology of Abilene [26] for analysis. Also, we use GT-ITM [27] to generate three network topologies for proper remote threshold selection. The backbone topology of Abilene has 11 point-of-presence nodes and its actual link capacities. End-to-end latency-based IGP link weights in [28] can be used to calculate the path metric v_{ij} in our SC model. We set the background traffic by referring to traffic statistical analysis of Abilene [29]. We refer to [30] and generate overlay traffic on several logical overlay paths. GT-ITM can generate transit-stub style topologies which can simulate ISP networks. We generate three topologies, each of which consists of 5 transit nodes and 2 stub domains connected to each transit node. Every stub domain has 3 nodes on average. Totally, in each topology, we get 35 underlay nodes and set the link capacity between each two nodes to be 10 Mbps. In each topology, 10 underlay nodes are mapped into a fully connected 10-node overlay. Each overlay node has its own constant traffic demand from other overlay nodes. We use hop-count as the path metric v_{ij} for overlay peering pairs. Then SC algorithm can be deployed for cost optimization. To select a proper RT from path classes for the three topologies, we use one topology for analytical selection and use the other two for validating rationality of the selected threshold. Besides, we add the delay factor as format of (15) to the path weights which are used in overlay proximity selection.

5.2. Improvement by SC. We use SC model with path classes to improve the negative impacts of noncooperation. In the game-theoretic optimization, underlay and overlay take several rounds to converge to a strategic equilibrium, that is, optimal traffic demand between peers for overlay and optimal physical path selection and traffic splits for underlay. In each round, according to the strategic decision of underlay/overlay, overlay/underlay will react and adjust with an optimal strategy by executing SC Algorithm. We study the case that each node in overlay has a constant total traffic demand from other nodes and decides fraction of traffic demand from every other node. This optimization takes several rounds because overlay needs to react to routing change of underlay in each round. On the other hand, underlay will react to traffic change between overlay peers in each round and make an optimal routing adjustment. Noncooperative game takes many rounds to converge to equilibrium and makes the two-layer system in unstable oscillation. In addition to slow convergence, suboptimal cost for both overlay and underlay leave margin for improvement. In contrast with noncooperation, our SC model uses topology-related information exchange to help both overlay and underlay to improve their suboptimal costs and shorten the convergence duration. We also investigate whether path-class mechanism helps SC go further to save costs.

Overlay traffic is set to 50 percents of the total traffic volume with the network utilization of 0.4 in the Abilene topology. We compare three cases: noncooperation, SC with path class mechanism in optimal algorithm and SC without

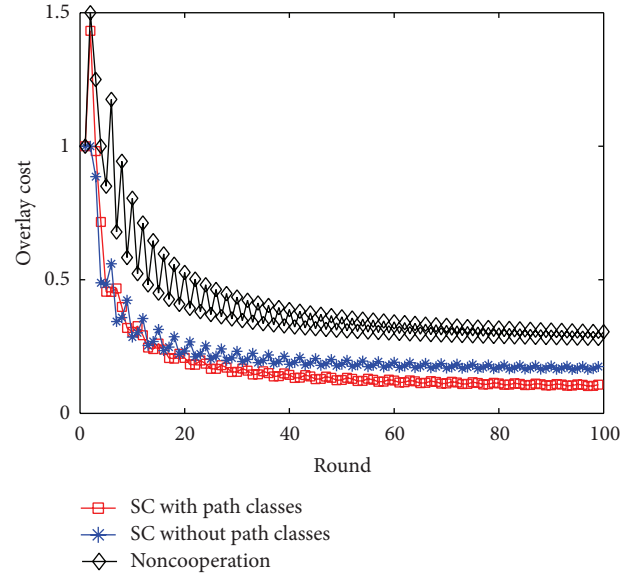


FIGURE 3: Overlay cost improvement.

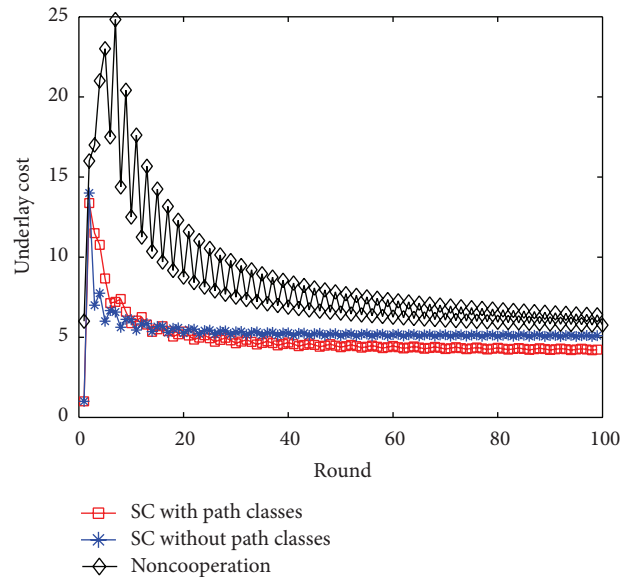


FIGURE 4: Underlay cost improvement.

path classes. Figures 3 and 4, respectively, show overlay cost (normalized average delay relative to the initial value 1) and underlay cost (normalized MLU relative to the initial value 1) in 100 rounds. We can see that two types of SC have a faster converging speed to equilibrium than noncooperation. Although the costs flap with independently reacting decisions of the two layers in different rounds, yet due to information exchange between cooperative overlay and underlay, SC shows far slighter oscillation than noncooperation case and obtains systematical stability. Comparing stable costs of SC with noncooperation, SC saves about 30% cost in overlay and about 20% cost in underlay.

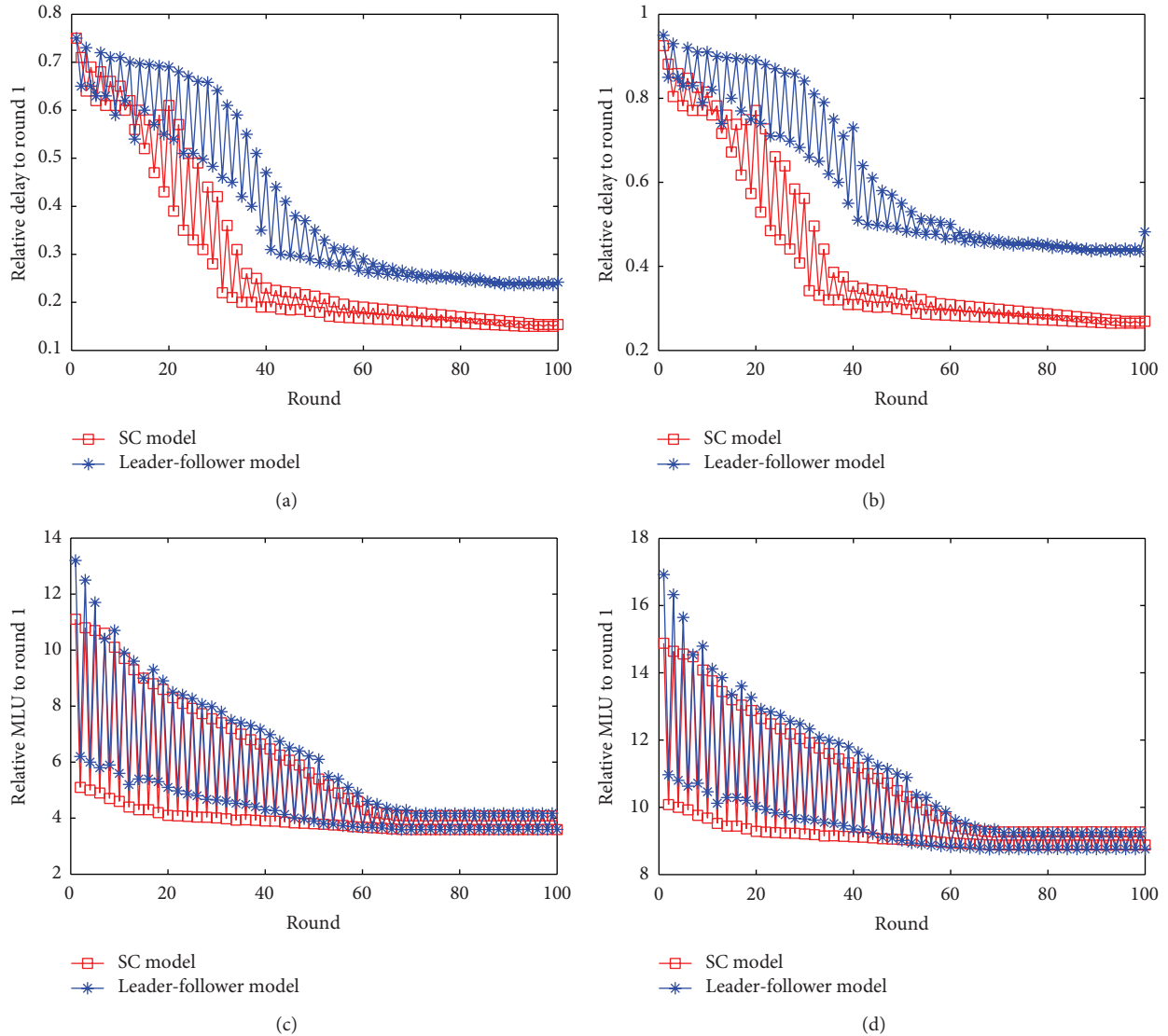


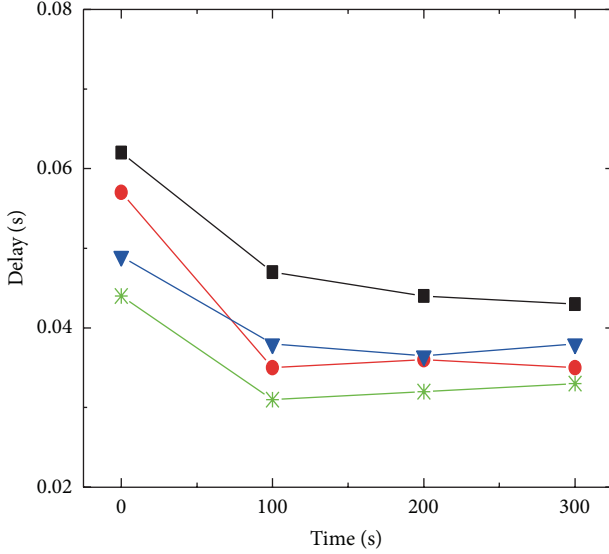
FIGURE 5: Comparison of two models at the overlay traffic proportion ρ : (a) $\rho = 30\%$, (b) $\rho = 60\%$, (c) $\rho = 30\%$, and (d) $\rho = 60\%$.

It is also remarkable that SC with path classes outperforms SC without path classes. That is because classified path can help overlay node quickly delete remote candidate peers in order to minimize average end-to-end delay. Hence, both overlay and underlay take advantage of the common goal to limit traffic from remote areas. We also compare SC model with the leader-follower model [3] at different proportions of overlay traffic. As shown in Figure 5, though two models perform nearly the same in the underlay cost Figures 5(c) and 5(d), SC model performs much better than the other for saving overlay cost at the relatively high load of overlay traffic.

5.3. Proper RT Selection. We use a topology generated by GT-ITM to explore the existence of a proper remote threshold of path classes. Hop account on physical path is used as path metric v_{ij} for overlay. We simulate performance of the two-layer system in 300 seconds and use cost results at four observation time points for analysis. In Figures 6(a) and

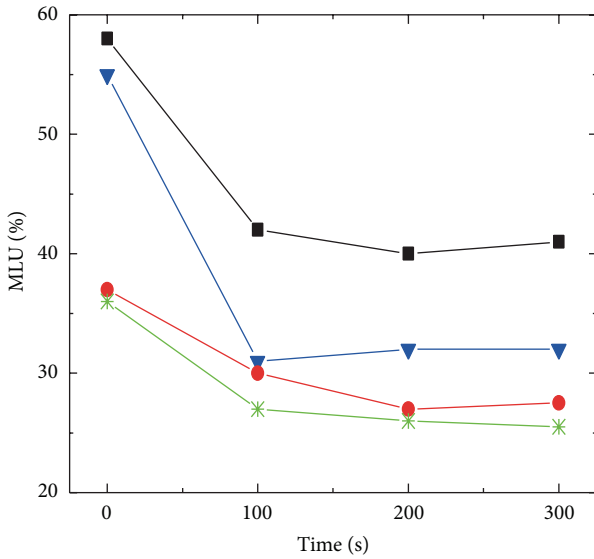
6(b), when remote threshold $k \leq 3$, the system shows lower and closer costs (delay and MLU) in stable state than $k = 4$ case. Results demonstrate that if underlay does not limit traffic on the path whose class is larger than 3, overlay and underlay costs will increase significantly. So, a proper threshold can distinct between near and remote so as to leave closer candidate peers for an overlay node to generate traffic demand optimally.

5.4. Rationality of Selected RT. We use the other two topologies generated by GT-ITM to validate rationality of the threshold selection. For each topology we set threshold k to be 3 and simulate system performance 25 times. Convergence duration means how long time it takes to arrive at the state of cost equilibria (i.e., stable delay, and stable MLU). Totally, we get 50 experimental points from the two topologies. Results are shown in Figure 7. Most (about 80%) of the points are around the point (13, 31, 0.042) which is approximate to the



■ $k = 4$ ● $k = 2$
 ▼ $k = 3$ * $k = 1$

(a)



■ $k = 4$ ● $k = 2$
 ▼ $k = 3$ * $k = 1$

(b)

FIGURE 6: (a) Delay of overlay at four RT values. (b) MLU of underlay at four RT values.

average experimental result in Section 5.3. So, the threshold value we selected is applicable to the same size networks (transit-stub topology with 35 underlay nodes and 10 overlay nodes). Corresponding to a topology with SC solution, a proper remote threshold exists and should be selected for cost improvement. Accordingly, it is efficient and convenient for ISPs to select a proper RT for one network and apply the RT to other same scale networks.

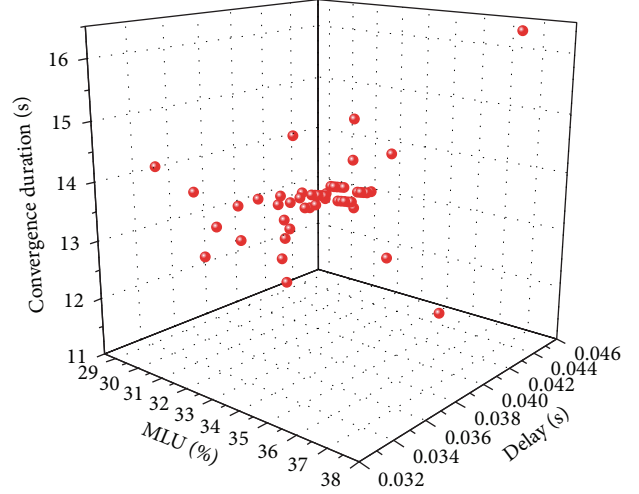


FIGURE 7: 50 times of test results when RT is equal to 3.

Path classes and RT are even more important for large-scale ISP topologies. One of the main goals of ISP underlay in this cost-saving cooperation is to divide paths into near and remote and to limit traffic from remote areas. Path classes are helpful for this coarse-grained division because ISP can choose a proper RT from limited numbers of classes rather than find threshold value from all of the numerous paths. Mechanism of path class enables ISPs to select proper RT quickly and efficiently for saving cost of traffic transit.

6. Conclusion

In this paper we investigate cross-layer conflict between P2P overlay and ISP underlay and highlight solutions to use cooperation rather than hyperselfish topology-awareness. Two dynamic game models are built to illustrate suboptimal profit of hyperselfish initiator. We build a topology-information-exchange-based game model to improve negative impact of noncooperation. Simulation results validate that SC model with path classes can improve costs for both layers and decrease the time consumption to arrive at the stable equilibrium. The proper remote threshold selection is also proved essential for cost improvement of the two-layer system. With popularity of P2P streaming and content oriented networks, our future work will pertain to ISP traffic management through cooperation with P2P streaming systems and cross-ISP content distribution between cooperative ISPs.

Notations

V : Node set of ISP's underlay network
 E : Set of links, $e \in E$, e connects two underlay nodes
 N : Overlay node set, $i, j \in N$
 ij : Overlay logical link from i to j
 p_{ij}^k : The k th underlay routing path for logical path ij
 t_{ij} : Traffic amount from i to j
 c_e : Capacity of link e
 t_e^b : Background traffic on link e

- T_j : Total traffic demanded by overlay node j
 f_{ij}^k : Fraction of t_{ij} on path p_{ij}^k
 $r_{ij}^k(e)$: Value 1 if link e on path p_{ij}^k , and 0 otherwise
 v_{ij} : Metric of logical path delay from i to j
 w_e : Cost of per traffic unit transit on link e .

Conflict of Interests

The authors declare that there is no conflict of interests regarding the publication of this paper.

Acknowledgments

This work is supported by the National Basic Research Program of China (973 Program) under Grant no. 2013CB329101 and by the 863 Program under Grant no. 2011AA010701 and by the National Natural Science Foundation of China (NSFC) under Grant nos. 61372112 and 61232017 and by the Beijing Natural Science Foundation (4142037).

References

- [1] Y. Liu, H. Zhang, W. Gongt, and D. Towsley, "On the interaction between overlay routing and underlay routing," in *Proceedings of the 24th Annual Joint Conference of the IEEE Computer and Communications Societies (INFOCOM '05)*, pp. 2543–2553, Miami, Fla, USA, March 2005.
- [2] D. DiPalantino and R. Johari, "Traffic engineering vs. content distribution: a game theoretic perspective," in *Proceedings of the 28th IEEE International Conference on Computer Communications (INFOCOM '09)*, pp. 540–548, Rio de Janeiro, Brazil, April 2009.
- [3] S. Seetharaman, V. Hilt, M. Hofmann, and M. Ammar, "Resolving cross-layer conflict between overlay routing and traffic engineering," *IEEE/ACM Transactions on Networking*, vol. 17, no. 6, pp. 1964–1977, 2009.
- [4] C. Wang, N. Wang, M. Howarth, and G. Pavlou, "On the interactions between non-cooperative P2P overlay and traffic engineering behaviors," in *Proceedings of the 53rd IEEE Global Communications Conference (GLOBECOM '10)*, Miami, Fla, USA, December 2010.
- [5] J. Kurian and K. Sarac, "A survey on the design, applications, and enhancements of application-layer overlay networks," *ACM Computing Surveys*, vol. 43, no. 1, article 5, 34 pages, 2010.
- [6] J. Dai, F. Liu, and B. Li, "The disparity between P2P overlays and ISP underlays: issues, existing solutions, and challenges," *IEEE Network*, vol. 24, no. 6, pp. 36–41, 2010.
- [7] R. Birke, E. Leonardi, M. Mellia et al., "Architecture of a network-aware P2P-TV application: the NAPA-WINE approach," *IEEE Communications Magazine*, vol. 49, no. 6, pp. 154–163, 2011.
- [8] M. P. Manzillo, L. Ciminiera, G. Marchetto, and F. Risso, "CLOSER: a collaborative locality-aware overlay SERVICE," *IEEE Transactions on Parallel and Distributed Systems*, vol. 23, no. 6, pp. 1030–1037, 2012.
- [9] S. Ren, E. Tan, T. Luo, S. Chen, L. Guo, and X. Zhang, "TopBT: a topology-aware and infrastructure-independent BitTorrent client," in *Proceedings of the 29th IEEE International Conference on Computer Communications (INFOCOM '10)*, San Diego, Calif, USA, March 2010.
- [10] S. Raza, G. Huang, C. N. Chuah, S. Seetharaman, and J. P. Singh, "MeasuRouting: a framework for routing assisted traffic monitoring," *IEEE/ACM Transactions on Networking*, vol. 20, no. 1, pp. 45–56, 2012.
- [11] A. R. Sharafat, S. Das, G. Parulkar, and N. McKeown, "MPLS-TE and MPLS VPNs with OpenFlow," in *Proceedings of the ACM SIGCOMM 2011 Conference*, pp. 452–453, Ontario, Canada, August 2011.
- [12] S. Sundaresan, C. Lumezanu, N. Feamster, and P. Francois, "Autonomous traffic engineering with self-configuring topologies," in *Proceedings of the 7th International Conference on Autonomic Computing (SIGCOMM '10)*, pp. 417–418, New Delhi, India, September 2010.
- [13] N. Wang, K. H. Ho, G. Pavlou, and M. Howarth, "An overview of routing optimization for internet traffic engineering," *IEEE Communications Surveys and Tutorials*, vol. 10, no. 1, pp. 36–56, 2008.
- [14] V. Aggarwal, A. Feldmann, and C. Scheidele, "Can ISPs and P2P users cooperate for improved performance?" *ACM Computer Communication Review*, vol. 37, no. 3, pp. 29–40, 2007.
- [15] H. Xie, Y. R. Yang, A. Krishnamurthy, Y. G. Liu, and A. Silberschatz, "P4p: provider portal for applications," in *Proceedings of the ACM SIGCOMM 2008 Conference on Data Communication*, pp. 351–362, Seattle, Wash, USA, August 2008.
- [16] W. Jiang, Z. S. Rui, J. Rexford, and M. Chiang, "Cooperative content distribution and traffic engineering in an ISP network," in *Proceedings of the 11th International Joint Conference on Measurement and Modeling of Computer Systems (SIGMETRICS '09)*, pp. 239–250, Seattle, Wash, USA, June 2009.
- [17] H. Lee, A. Nakao, and J. Kim, "BiCo: network operator-friendly P2P traffic control through bilateral cooperation with peers," *Computer Networks*, vol. 55, no. 9, pp. 2023–2034, 2011.
- [18] G. Dán, T. Hoßfeld, S. Oechsner et al., "Interaction patterns between P2P content distribution systems and ISPs," *IEEE Communications Magazine*, vol. 49, no. 5, pp. 222–230, 2011.
- [19] C. Xu, T. Liu, J. Guan, H. Zhang, and G. M. Muntean, "CMT-QA: quality-aware adaptive concurrent multipath data transfer in heterogeneous wireless networks," *IEEE Transactions on Mobile Computing*, vol. 12, no. 11, pp. 2193–2205, 2013.
- [20] C. Xu, F. Zhao, J. Guan, H. Zhang, and G. M. Muntean, "QoE-Driven user-Centric VoD services in urban multihomed P2P-based vehicular networks," *IEEE Transactions on Vehicular Technology*, vol. 62, no. 5, pp. 2273–2289, 2013.
- [21] J. F. Nash, "Non-cooperative games," *Annals of Mathematics*, vol. 54, pp. 286–295, 1951.
- [22] R. Selten, "Reexamination of the perfectness concept for equilibrium points in extensive games," *International Journal of Game Theory*, vol. 4, no. 1-2, pp. 25–55, 1975.
- [23] H. Van Stackelberg, D. Bazin, R. Hill, and L. Urch, *Market Structure and Equilibrium*, Springer, 2011.
- [24] M. J. Osborne, *An Introduction to Game Theory*, Oxford University Press, 2004.
- [25] N. Wang, K. H. Ho, and G. Pavlou, "AMPLE: an adaptive traffic engineering system based on virtual routing topologies," *IEEE Communications Magazine*, vol. 50, no. 3, pp. 185–191, 2012.
- [26] Abilene, <http://www.internet2.edu>.
- [27] GT-ITM's Web Site, <http://www.cc.gatech.edu/projects/gtitm/>.
- [28] H. Zheng, E. K. Lua, M. Pias, and T. G. Griffin, "Internet routing policies and round-trip-times," *Passive and Active Network Measurement*, vol. 3431, pp. 236–250, 2005.

- [29] Y. Zhang, "Abilene traffic matrix," <http://www.cs.utexas.edu/~yzhang/research/AbileneTM/>.
- [30] J. S. Otto, M. A. Sánchez, D. R. Choffnes, F. E. Bustamante, and G. Siganos, "On blind mice and the elephant: understanding the network impact of a large distributed system," in *Proceedings of the ACM SIGCOMM 2011 Conference*, pp. 110–121, Ontario, Canada, August 2011.

Review Article

An Overview of Networked Control of Complex Dynamic Systems

Huaicheng Yan,^{1,2} Sheng Yan,^{1,2} Hao Zhang,³ and Xudong Zhao^{4,5}

¹ Key Laboratory of Advanced Control and Optimization for Chemical Processes of Ministry of Education, Shanghai 200237, China

² School of Information Science and Engineering, East China University of Science and Technology, Shanghai 200237, China

³ Department of Control Science and Engineering, Tongji University, Shanghai 200092, China

⁴ College of Information Science and Technology, Bohai University, Jinzhou 121013, China

⁵ College of Information and Control Engineering, China University of Petroleum, Qingdao 266555, China

Correspondence should be addressed to Huaicheng Yan; hcyan@ecust.edu.cn

Received 6 January 2014; Accepted 31 March 2014; Published 3 April 2014

Academic Editor: Lixian Zhang

Copyright © 2014 Huaicheng Yan et al. This is an open access article distributed under the Creative Commons Attribution License, which permits unrestricted use, distribution, and reproduction in any medium, provided the original work is properly cited.

Networked control systems (NCSs) are spatially distributed systems for which communication between sensors, actuators, and controllers is supported by a shared communication network. In recent years, NCSs have brought many innovative impacts to control systems. However, grate challenges are also met due to the network-induced imperfection. In this paper, we particularly discuss various typical networked induced issues; namely, time delays, packet losses, disorder, time-varying transmission intervals, competition of multiple nodes accessing networks, and data quantization as well as event-triggered data transmission strategy are surveyed; at the same time, some research topics are also discussed. The common goal of discussion on these topics is to reveal the effect of the communication network on the operation of the networked systems.

1. Introduction

When a traditional feedback control system is closed via a certain digital communication network, then the control system is classified as networked control systems (NCSs). The network can be either the control networks that have been around for a considerable amount of time for specialized real-time purposes such as control area network (CAN), building automation control (BAC) net, Fieldbus, or, more recently, the wireline or wireless Ethernet, even Internet, for general purpose data communication tasks. Figure 1 typically illustrates the framework and information flow of network-based control systems. In the broadest terms, these systems are composed of actuators, sensors, controllers, and filters as nodes, and serial communication networks are employed to exchange information between spatially distributed system components.

Control loops that are closed over a communication network have become more and more common as the hardware devices for networks and network nodes have become

cheaper. Due to the introduction of communication networks to the systems, some significant advantages can be easily achieved compared with traditional point-to-point systems, such as low cost, reduced weight and power requirements, simple installation, and maintenance [1–4]. Such benefits have given a great impetus to extensive applications of NCSs in mobile sensor networks, electric factories, manufacture automation factories, advanced aircraft, and so on [5, 6]. However, the incorporation of a network in the feedback loop makes the analysis and design of NCSs complex since in most problems, estimation or control interacts with communication in various ways. This has drawn increasing attention from various research communities.

In recent years, to ease the practical application of NCSs, considerable efforts have been spent and some progress has been made in topics such as the modeling of NCSs, stability and performance analysis, networked controllers and filters design, network-based fault detection and tolerance, and identification via networks. Compared with traditional control systems, in NCSs, the communication architecture

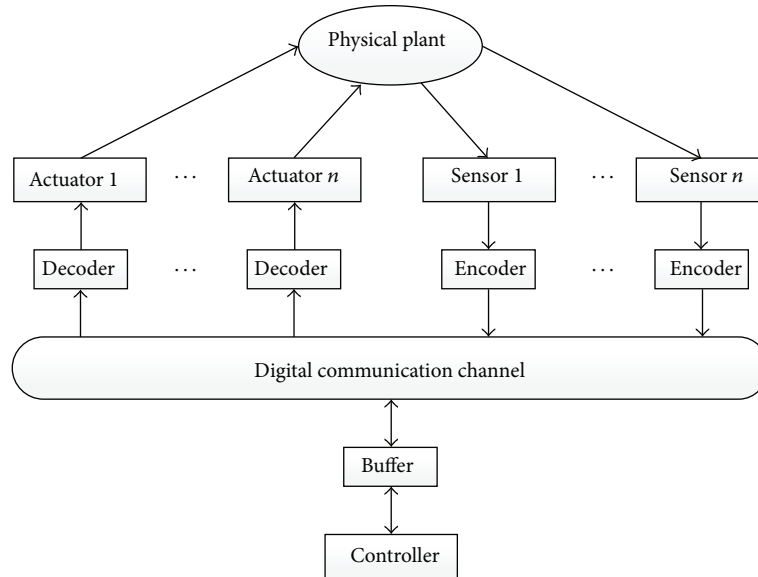


FIGURE 1: A typical structure of network-based control system.

changes from point-to-point to common network. This change may cause a series of problems that will deteriorate the system performance or even destabilize the system. Different levels of network-induced imperfections include the following:

- (1) time delays;
- (2) time-varying packet transmission/sampling intervals;
- (3) data packet dropouts and disorder;
- (4) data quantization;
- (5) the triggered strategy of nodes in the network;
- (6) medium access constraint.

NCSs lie at the intersection of control and communication theories. Traditionally, control theory focuses on the study of interconnected dynamical systems linked through “ideal channels,” whereas communication theory studies the transmission of information over “imperfect channels.” A combination of these two frameworks is needed to model NCSs. In this paper, we will focus on network imperfections and review the related studies, paying special attention to those carried out since the publishing dates of the surveys referred to. Some future research is also proposed in the paper. The main objective of the paper is to provide readers with an overview of the NCSs, and a vision for future development. The other objective is to provide a tutorial on NCSs. This paper is organized as follows. Section 2 talks about various NCSs classifications in brief and presents the main survey of the methodologies in the analysis and design of NCSs. Section 3 presents the conclusion and possible future research directions in NCSs.

2. Main Survey on Networked Control of Complex Dynamic Systems

The insertion of the communication network in the control loop makes the analysis and design of network-based control systems more complex. To fully deal with these difficulties, we should have an overview of the issues encountered in the systems.

In this section, the methodologies used for the handling of the common constraints introduced in NCSs will be surveyed. In what follows, some typical issues of communication constraints will be introduced one by one, and some other research topics will be discussed. In discussions for each constraint, we will first review the references focusing on it and then those references that simultaneously address it and some of the other constraints.

2.1. Time Delays. To transmit a continuous time signal over a network, the signal must be sampled, encoded in a digital format, and transmitted over the network and finally the data must be decoded at the receiver side. The overall delay in a NCS is composed of the computational delays in each component of the system, the network access delay, and the transmission delay through the network medium. With the rapid development in electronics, cheap and fast digital processors have become widely available, and the computational delay in a digital controller is negligible compared with the other two classes of delays that are commonly called the network-induced delays [3]. Network-induced delays are modeled and analyzed in various ways. They can be modeled as a constant delay (timed buffer), an independent random delay, and a delay with known probability distribution governed by the Markov chain model [7]. Different delays, together with specific plants, call for different control strategies in NCSs. In 1988, Sato et al. [8] explores some techniques which play

important roles in the development of the future universal transport network. In the network, the information can be efficiently integrated and transported by making the most of the burstiness of the information flows and by exploiting the store-and-forward process at the transport nodes. Tipsuwan and Chow [9] summarize the typical methodologies used in the literature up to 2003 in modeling, analysis, and synthesis of NCSs involved with delays, including the linear quadratic Gaussian (LQG) approach, the hybrid system approach, and the perturbation approach Gao et al. [10] that deal with the network based control for NCSs by a new delay system approach. Wu et al. [11] model and analyze the stability of NCSs with long random delay. They present a model for such systems and discuss the systems stability. Kamrani and Mehraban [12] propose a novel approach for modeling the end-to-end time-delay dynamics of the Internet using system identification and apply it to control real-time telerobotic operations via Internet with specific Quality of Service (QoS) offerings. Hespanha et al. [13] focus on the advances made from 2003 to 2007, such as the approach of modeling NCSs by delayed differential equations (DDEs) and the switched systems approach. Yang [14] reviews additional approaches for the delay issue, including the two Markov chains modeling approach by Zhang et al. [15] for both feedback and forward channels, and so forth. In [16], Liu et al. discusses the design of NCSs with a networked predictive controller in the presence of constant and random network delay in the forward and feedback channels, respectively. Zhang et al. [17] represents nonlinear NCSs by a Takagi-Sugeno (T-S) fuzzy model and addresses network delay as well as packet drop issues using robust H_∞ control. Li et al. [18] proposes a novel discrete-model switch system for NCSs with time delay and packet drop. Lai et al. [19] integrate Ethernet and CAN with the TCP/IP communication gateway. The developed system has been applied to a remote control system for an AC 400 W servomotor to verify the proposed adaptive Smith predictor control method with the time-delay estimation algorithm. Liu [20] studies the robustness of networked predictive control systems (NPCS) with uncertainties. A networked predictive control strategy is introduced to cope with time-varying network delay and data dropout. Yan and Liu [21] develop a new adaptive fuzzy sliding mode control (AFSMC) strategy. The adaptive fuzzy control algorithm based on the output of the sliding mode controller to decrease the influence of the network undetermined delay in the NCSs regulates the control law of the adaptive fuzzy sliding mode controller. In [22], a real-time nonlinear control system approach that checks a proposed network configuration to determine the time delay which the control data packets will encounter and determine the minimum acceptable sampled data rate that is presented. Taylor and Ibrahim [22] address the problem of time-varying network induced delay in industrial applications. A control design methodology that can assure the closed-loop performances of the industrial application while compensating the time-varying delays introduced by the communication network is proposed. In [23], NCSs model which network-induced delays, data packet dropout, and disordering are captured by time-varying delays in wide-area measurement systems, is

constructed for wide-area closed-loop power systems. Based on this model, a controller is designed for better power system performance using wide-area information as feedback signals.

2.2. Data Packet Dropouts and Disorder. The references for packet dropouts problems are classified according to whether the methodology is dependent on packet dropouts information on line or not. Packet dropouts can be modeled either as stochastic or deterministic phenomena. The simplest stochastic model assumes that dropouts are realizations of a Bernoulli process [24, 25]. Finite-state Markov chains can be used to model correlated dropouts [26] and Poisson processes can be used to model stochastic dropouts in continuous time. Deterministic models for dropouts have also been proposed, either specified in terms of time averages [3] or in terms of worst case bounds on the number of consecutive dropouts [27, 28]. In [24], the packet dropouts are modeled as a linear function of a stochastic variable satisfying Bernoulli random binary distribution. In the approach, the stability of the corresponding closed-loop system is described in a stochastic sense. Specifically, consider the discrete-time NCS

$$x(k+1) = Ax(k) + Bu(k); \quad (1)$$

the packet dropouts in both feedback channel and forward channel can be modeled via a stochastic process; that is

$$u_{ck} = \alpha(k)Kx_k, \quad u_k = \beta(k)u_{ck}, \quad (2)$$

where $\{\alpha(k)\}$ and $\{\beta(k)\}$ are independent Bernoulli processes. The process models the packet dropout phenomenon for the feedback channel and for the forward channel. Also, $\{\alpha(k) = 1\}$ and $\{\alpha(k) = 0\}$ denote the success and failure in the packet transmission, respectively, which also holds for $\{\beta(k)\}$. It is assumed that $\{\alpha(k)\}$ and $\{\beta(k)\}$ obey the following probability distribution:

$$\begin{aligned} \text{Prob}\{\alpha(k) = 1\} &= E\{\alpha(k)\} = \bar{\alpha}, \\ \text{Prob}\{\alpha(k) = 0\} &= 1 - \bar{\alpha}, \\ \text{Prob}\{\beta(k) = 1\} &= E\{\beta(k)\} = \bar{\beta}, \\ \text{Prob}\{\beta(k) = 0\} &= 1 - \bar{\beta}. \end{aligned} \quad (3)$$

Thus, we have $u_{ck} = \alpha(k)\beta(k)Kx(k)$. Furthermore, introduce another Bernoulli process $\{e(k)\}$ with $e(k) := \alpha(k)\beta(k)$. Then, we have $e(k) = 1$ only when $\alpha(k) = 1$ and $\beta(k) = 1$, and $e(k) = 0$ otherwise. Therefore

$$\begin{aligned} \text{Pr}\{e(k) = 1\} &= E\{e(k)\} = \bar{e}, \\ \text{Pr}\{e(k) = 0\} &= 1 - \bar{e}, \end{aligned} \quad (4)$$

the closed-loop system is given by

$$x(k+1) = (A + e(k)BK)x(k). \quad (5)$$

The control design is then carried out by using the expectation of the stochastic variable. In [4], taking a probability

approach to model packet dropouts can also be seen in an earlier work [29], where the transmission rate is proposed to regard the network with packet dropouts as a switch that closes at a certain rate. A further example is [30], where the controller design tolerates a large drop probability to ensure the system stability in the mean-square sense. In the approach, the running mode at receivers should be clock driven, and the plant output is assumed to be zero [31] or held at the previous value [3] during the periods of packet dropouts. There generally exists a tradeoff between maximizing the number of consecutive packet dropouts, maximizing the allowable probability of packet losses, or lowering the transmission rate and increasing the stability margins and system performance. Zhang et al. [32] studies the robust stability of a NCS via a fuzzy estimator (FE), where the controlled plant is a class of nonlinear systems with external disturbances. Both network-induced delay and packet dropout are concerned. The sufficient condition for the robust stability with H_∞ performance of the closed-loop system is obtained. Dang and Zhang [33] deal with the exponential stability of singular NCSs with time-delay and packet dropout. Two new control methods of dynamical state feedback control and dynamical state feedback proportional-integral (PI) control for the singular NCSs are addressed. Niu et al. [34] transfer the continuous-time control model to a digital form based on network QoS, such as network-induced delay and packet dropout; the stability of the control system under the nonideal condition is discussed based on LMIs. Finally, the authors propose a codesign method of control and scheduling to guarantee both networked control performance and network QoS. Pin and Parisini [35] address the robust state feedback stabilization of uncertain discrete-time constrained nonlinear systems in which the loop is closed through a packet-based communication network. Time-varying transmission delays, packet dropouts, and a robust control scheme combining model predictive control with a network delay compensation strategy are proposed in the context of nonacknowledged UDP-like networks. Wang et al. [36] study the problem of network induced delay and packet dropout compensation for continuous time NCSs. New model for NCSs with packet dropout and network-induced long delay is presented by proposing the one step prediction-based packet dropout compensation method. Then, a packet dropout compensation threshold time based Lyapunov functional is proposed, and H_∞ controller design method is presented. In [23], the authors propose the codesign approach of both the communication protocols and the interacting controlled system. In the approach, network issues such as bandwidth, quantization, survivability, reliability, and message delay will be considered simultaneously with controlled system issues such as stability, performance, fault tolerance, and adaptability. In [37], the predictive control scheme and the associated stability issue are investigated for the constrained nonlinear NCSs, where both the sensor-to-controller packet dropout and the controller-to-actuator packet dropout are considered simultaneously. The model predictive control based framework is proposed to compensate for the two-channel packet dropouts.

2.3. Time-Varying Sampling Intervals. As NCSs belong to the spectrum of digital control, the analog signals of plant outputs need to be sampled at sensor nodes before they are encoded into digital signals and packaged into the packets transmitted over networks. In classical sampled-data control systems, the time-varying sampling problem has been a major topic of study for a few decades. In recent years, the interest in this topic has grown, motivated by the increasing use of NCSs, where the sampled plant outputs are transmitted at instants that may vary significantly due to contention of multiple packets. Here, we will first review some results on time-varying sampling problem in classical digital control systems, then those that consider the problem in NCSs environment, and finally the works that simultaneously address other types of network-induced constraints. Motivations to study time-varying sampling intervals in digital feedback control can be found in [38–40]. In [38], a digital feedback control system with time-varying sampling periods consisting of an interconnection of a continuous-time nonlinear plant, a nonlinear digital controller, and appropriate interface elements between the plant and controller (A/D and D/A converters) is considered. Fridman et al. [40] introduce a new approach to robust sampled-data control. The system is modelled as a continuous-time one, where the control input has a piecewise-continuous delay. Sufficient LMIs conditions for sampled-data state-feedback stabilization of such systems are derived via descriptor approach to time-delay systems. The only restriction on the sampling is that the distance between the sequel sampling times is not greater than some prechosen $h > 0$ for which the LMIs are feasible. For $h \rightarrow 0$ the conditions coincide with the necessary and sufficient conditions for continuous-time state-feedback stabilization. Suh [41] is concerned with nonuniform sampling systems, where the sampling interval is time-varying within a certain known bound. The system is transformed into a time-varying discrete time system, where time-varying parts due to the sampling interval variation are treated as norm bounded uncertainties using robust control techniques.

2.4. Data Quantization. Data quantization is a common phenomenon in all digital control systems and thus has been a classical topic in conventional digital control theory even before the popularity of NCSs. In NCSs, both the control input and measurement output signals should be quantized before being transferred to next nodes, especially when concerning the limited bandwidth; then both the input and output quantization are absolutely necessary [42, 43]. Related studies of quantized control can be traced back to [44–48]. Wong and Brockett [49, 50] consider the issues of coding, communication protocols, and delays explicitly. A model with a memoryless and time-invariant coder-controller, stop-and-wait communication scheme, and impulsive control actuation is considered. The notion of containability is introduced as the appropriate notion of stability. Both necessary and sufficient conditions for containing ability are given in the form of bounds on the system data-rate. [44, 51] show a typical way to deal with the problem of quantization that is to design appropriate often complex controllers so

that the effects of the quantization can be minimized. Elia and Mitter [52] seek to quantize the state of the system as coarsely as possible while maintaining the stability of the system. In this paper, it is shown that the coarsest quantizer that quadratically stabilizes a single input linear discrete-time invariant system is logarithmic and can be computed by solving a special linear quadratic regulator problem. Fu and Xie [53] study a number of quantized feedback design problems for linear systems. The case where quantizers are static is considered. The problem of quadratic stabilization for the following system in [53] considers the simplest and most fundamental case:

$$x(k+1) = Ax(k) + Bu(k), \quad (6)$$

where $A \in \mathbb{R}^{n \times n}$, $B \in \mathbb{R}^{n \times 1}$, x is the state and u is the control input. A is unstable and (A, B) is stabilizable and quantized state feedback is considered in the following form:

$$\begin{aligned} u(k) &= f(v(k)), \\ v(k) &= g(x(k)), \end{aligned} \quad (7)$$

where $g(\cdot)$ is the unquantized feedback law and $f(\cdot)$ is a quantizer which is assumed to be symmetric.

The associated logarithmic quantizer is defined as follows:

$$f(v) = \begin{cases} u_i & \frac{1}{1+\delta}u_i < v \leq \frac{1}{1-\delta}u_i, v > 0 \\ 0 & v = 0 \\ -f(-v) & v < 0, \end{cases} \quad (8)$$

where

$$\delta = \frac{1-\rho}{1+\rho}. \quad (9)$$

u_i is the quantization level corresponds to a segment; ρ is the quantization density. The logarithmic quantizer is illustrated in Figure 2.

In [54], the authors study robust control problems for linear uncertain systems under the setting of quantized feedback considering both the static and dynamic logarithmic quantizers. Coutinho et al. [43] investigate the case of simultaneous input and output quantization for single input single output (SISO) linear output feedback systems. In [55], the authors present a new approach to the stability analysis of quantized feedback control systems. The method is based on Tsytkin-type Lyapunov functions that have been widely used in absolute stability analysis problems. The results are expressed in LMIs and are valid for both single-input and multiple-input discrete-time linear systems with a logarithmic quantizer.

In [56], the hybrid control problem for linear systems with output quantization is investigated. It is shown that if a linear system can be stabilized by a linear feedback law, then it can also be globally asymptotically stabilized by a hybrid quantized feedback control law. Liberzon and Nešić [57] consider the problem of achieving input-to-state stability (ISS) with respect to external disturbances for control systems

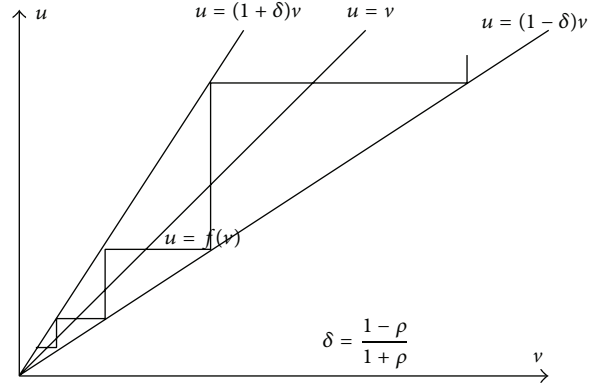


FIGURE 2: Logarithmic quantizer.

with linear dynamics and quantized state measurements. Quantizers considered in their paper take finitely many values and have an adjustable “zoom” parameter. In [58], a general case of finite-dimensional linear systems with process and observation noise is considered.

The stabilizability of uncertain stochastic systems in the presence of finite capacity feedback is studied in [59], where a variable rate digital link between the plant and the controller is considered. The authors also derive necessary and sufficient conditions for internal and external stabilizability of the feedback loop. The authors in [60] investigate the minimum data rate for mean square stabilization of discrete linear time-invariant systems over a lossy channel which is modeled as an independent and identically distributed stochastic process, and a necessary and sufficient condition for the single input system to be asymptotically stabilizable in the mean square sense is also given in terms of unstable eigenvalues of the open loop matrix and the packet dropouts rate. Trivellato and Benvenuto [61] solve the problem of optimum control around a target state for a stable system in case of both packet drops and signal quantization. Zhang et al. [62] investigate a continuous-time T-S fuzzy system with impulsive effects that are controlled through network. Network signal-transmission delays and signal-quantization effects are simultaneously considered. Zhang et al. [63] investigate the controller design for a class of linear network-based systems with communication constraints on both uplink and downlink channels, where the network-induced transmission time delay, packet dropouts, and signal quantization are considered simultaneously. A novel approach which converts the quantized state and control signal into a kind of actuator saturation with bounded disturbances is adopted to deal with the phenomenon of quantization. In [64], the synthesis approach of model predictive control (MPC) for the constrained linear systems under networked environment where both data quantization and packet dropout may occur is addressed. Based on a previous approach which considers packet dropout only, the authors propose an extended approach which incorporates data quantization effect.

2.5. The Triggered Strategy of Nodes in the Network. Sampled-data systems are such systems that sample continuous signals and making control decisions based on the sampled data. Traditionally, the control task is executed periodically; this allows the closed-loop system to be analyzed and the controller to be designed using the well-developed theory on sampled-data systems. However, the control strategy obtained based on this approach is conservative in the sense that resource usage is more frequent than necessary to ensure a specified performance level. To overcome this drawback, sporadic task models have been considered for real-time control, a hardware realization of such models is called event-triggering. In [65], the triggering mechanism is referred to Lebesgue sampling and event based sampling. A self-triggered task model is introduced by Velasco et al. [66] in which a heuristic rule is used to adjust task periods. Further work is done by Lemmon et al. [67] in which preliminary results supporting conjecture for a self-triggered real-time system implementing full-information H_∞ controllers are presented. In [68], adjustable deadbands are explored as a solution to reduce network traffic in NCSs. A method to determine the size of the deadbands is presented that relies on a performance metric that takes into account system response as well as network traffic. Kofman and Braslavsky [69] introduce a novel event-driven sampled-data feedback scheme where the plant output samples are triggered by the crossings with hysteresis of the signal through its quantization levels. The plant and controller communicate over binary channels that operate asynchronously and are assumed to be error- and delay-free. In [70], the author explores event bases sampling, and the architecture of a general structure for event based control is presented. Tabuada [71] revisits the problem of scheduling stabilizing control tasks on embedded processors. The author investigates a simple event-triggered scheduler based on the feedback paradigm that a real-time scheduler could be regarded as a feedback controller that decides which task is executed at any given instant and shows how it leads to guaranteed performance thus relaxing the more traditional periodic execution requirements. In all cases, the control signal is kept constant until violation of a triggering condition on certain signals of the plant triggers recomputation of the control signals.

In [72], the authors study self-triggering in sampled-data systems, where the next task release time and finishing time are predicted based on the sampled states. Yue et al. [73] investigate the event-triggered H_∞ control design for networked control systems with uncertainties and transmission delays. They consider the following system with parameter uncertainties and external disturbance:

$$\begin{aligned} \dot{x}(t) &= Ax(t) + Bu(t) + B_\omega \omega(t) \\ z(t) &= Cx(t) + Du(t). \end{aligned} \quad (10)$$

A mechanism, called event generator, is constructed between the sensor and the controller which is used to determine

whether the newly sampled state will be sent out to the controller by using the following judgment algorithm; that is,

$$\begin{aligned} & [x((k+j)h) - x(kh)]^\top \Omega [x((k+j)h) - x(kh)] \\ & \leq \sigma x^\top((k+j)h) \Omega x((k+j)h), \end{aligned} \quad (11)$$

where Ω is a positive matrix, $\sigma \in [0, 1)$.

Considering the effect of the transmission delay, a delay system model for the analysis is firstly constructed. Then, based on the model and Lyapunov functional method, criteria for the stability with an H_∞ norm bound and criteria for the codesign of both the feedback gain and the trigger parameters are derived. Hu and Yue [74] are concerned with the problem of event-based H_∞ filtering for networked systems with communication delay. In [75], the control design problem of event-triggered networked systems with both state and control input quantizations is concerned. An innovative delay system model is proposed that describes the network conditions, state and control input quantizations, and event-triggering mechanism in a unified framework. Peng and Yang [76] study an event-triggered communication scheme and an H_∞ control codesign method for NCSs with communication delay and packet dropout. Yu and Antsaklis [77] introduce a framework for output feedback based event-triggered NCSs. The triggering condition is derived based on passivity theory which allows us to characterize a large class of output feedback stabilizing controllers. They also take quantization of the transmitted signals in the communication network into consideration and we show that finite-gain L_2 stability can be achieved in the presence of time-varying network induced delays with bounded jitters, without requiring that the network induced delays be upper bounded by the interevent time.

2.6. Network-Based Systems with Medium Access Constraints.

In the previous subsections, the related works on control and estimation under communication constraints are reviewed with the simplest topology; that is, there exists only one sensor-controller and/or controller-actuator channel. However, many industrial systems are implemented in a distributed fashion and contain a great number of sensors, controllers, filters, and actuators communicating over a serial network with a complex topology [78]. Without any scheduling policy, the resulting network congestion, which essentially leads to those unanticipated phenomena such as network accessing delays and packet losses may be very serious. Recently, much research effort has been devoted to this issue, and a great number of related results are reported in the existing literature.

In most industrial applications where the CANs are used, the access of the nodes to the communication network is predetermined before the runtime, which is called static scheduling. In this case, [79] guarantees the stability of the closed-loop systems by an appropriate choice of a communication sequence. Hristu [80] aimed at exploring the interaction of communication and control in systems whose sensors and actuators are distributed across a shared network. The authors seek a stabilizing static output feedback controller

whose communication with the underlying plant follows a given periodic pattern. Lu et al. [81] discusses the optimal H_∞ control problem for networked systems with limited communication constraint. The limited communication constraint in control networks is taken into consideration in controller design by employing the notion of communication sequence. The objective is to find an optimal communication sequence and the corresponding optimal controller for the given plant and communication resource under the H_∞ performance index. Zhang and Hristu-Varsakelis [31] discuss the stabilization of NCSs in which sensors and actuators of a plant exchange information with a remote controller via a shared communication medium. Access to that medium is governed by a pair of periodic communication sequences. A method for exponentially stabilizing a NCS is proposed by first identifying a pair of communication sequences that preserve reachability and observability and then designing an observer-based feedback controller based on those sequences. Imer and Başar [82] consider a linear discrete-time optimal control problem where the controller has to choose between measurement and control. The controller is restricted in such a way that at a given time instance, it may either send a control packet to the actuator, or it can request a measurement packet from the sensor. Under a quadratic cost structure that does not penalize the control directly, the optimal control is a linear threshold policy, where the controller decides to measure or control by comparing its last measurement of the plant state against a predetermined threshold. In [83], a dynamic scheduling named maximum-error-first with try-once-discard is proposed, where each node will estimate how important the local data is, and the one with the greatest weighted error wins the right to transmit.

2.7. Fault-Tolerant Control in Network-Based Complex Systems. Built-in redundancy improves failure rates, while fault tolerance is implemented to prevent faults from propagating through the system; both are essential elements of a safety critical NCS. In [84], scheduling and control codesign for the robust fault-tolerant control of NCS is studied based on robust H_∞ fault-tolerant control idea. Parametric expression of controller is given based on feasible solution of LMIs. Patankar [85] presents a model for a fault-tolerant NCS using TTP/C communication. Appropriate features of TTP/C are incorporated in the model. Mendes et al. [86] propose a new multiagent platform for fault tolerant control (FTC) systems. The FTC platform uses simple and verifiable principles, allowing the use of agents with well-established FTC methodologies or new ones developed taking into account the NCSs specificities. Fang et al. [87] study the fault diagnosis and FTC theory for NCSs. It summarizes the authors' main ideas and results on fault diagnosis of NCSs, including the fundamentals of fault diagnosis for NCSs with information-scheduling, fault diagnosis approaches based on the simplified time-delay system models, and the quasi-T-S fuzzy model and fault diagnosis for linear and nonlinear NCS with long delay. In [88], a FTC method is presented for a class of the nonlinear NCSs with communication constraints.

Ding et al. [89] develop a design framework of fault-tolerant wireless NCSs for industrial automation applications. The main objective is to achieve an integrated parameterization and design of the communication protocols, the control, and fault diagnosis algorithms aiming at meeting high real-time requirements in industrial applications.

3. Conclusion and Future Works

In this paper, the studies seen in the literature on some types of network-induced constraints and several research topics are mainly surveyed, including time delays, time-varying packet transmission/sampling intervals, packet dropouts and disorder, data quantization, the triggered strategy of nodes in the network, medium access constraint, and FTC in NCSs. Section 2 provides an overview of the source of each network-induced constraints, their negative impacts, and the corresponding research lines in handling them.

Although networked control of complex dynamic systems has been a very promising research topic for decades, there are challenging problems and unsolved problems to be considered for future research. We highlight some of them as follows.

- (1) Control or estimation utilizing dynamic quantizers: it can be observed that the type of quantizers used in most works in this paper is static; that is, the parameters of quantizers do not change after being designed, which are much easier to implement in practice. However, in this case, the interval to be quantized also does not increase or decrease according to the dynamics of systems, which would lead to undesirable quantization error. To alleviate the effect of quantization errors as much as possible, the number of bits should be large enough to represent quantization levels. In contrast with static quantizers, dynamic ones could adjust the range of the quantized interval according to the dynamic of systems. With dynamic quantizers asymptotic stability of the closed-loop control system can be expected. Therefore, the control and estimation problems covered in this paper can be further studied by utilizing dynamic quantizers.
- (2) Scheduling for optimal control or estimation under medium access constraints: the H_∞ control problem for nonlinear network-based system with medium access constraint has been investigated in some existing bodies of literature, where one of measurement nodes and one of actuator nodes are stochastically chosen for communication according to the predetermined probability. However, one natural question then arises; that is, how to determine the transmission probability for each node. In other words, how can we schedule the communication sequence of these nodes to expect a better performance of closed loop systems? Although some algorithms have been proposed for communication scheduling in existing works, such as, exhausting search method in [90], and the heuristic search method in [81, 91], either it is time-consuming,

or optimal communication sequence cannot be guaranteed. Thus, the codesign of optimal control or estimation and scheduling deserves further investigation.

Due to the vast amount of citations in the NCSs and the limited pages of this paper, some other issues, for example, state estimation in NCS and network security in NCSs, and so on, are not surveyed in this paper; the authors apologize for not being able to list all the related citations in this paper.

Conflict of Interests

The authors declare that there is no conflict of interests regarding the publication of this paper.

Acknowledgments

This work is supported by the National Natural Science Foundation of China (61004028, 61272064, and 61273026), the Innovation Program of Shanghai Municipal Education Commission (12zz052), and the Fundamental Research Funds for the Central Universities.

References

- [1] H. Shousong and Z. Qixin, "Stochastic optimal control and analysis of stability of networked control systems with long delay," *Automatica*, vol. 39, no. 11, pp. 1877–1884, 2003.
- [2] H. Lin, G. Zhai, and P. J. Antsaklis, "Asymptotic stability and disturbance attenuation properties for a class of networked control systems," *Journal of Control Theory and Applications*, vol. 4, no. 1, pp. 76–85, 2006.
- [3] W. Zhang, M. S. Branicky, and S. M. Phillips, "Stability of networked control systems," *IEEE Control Systems Magazine*, vol. 21, no. 1, pp. 84–97, 2001.
- [4] Z. Wang, F. Yang, D. W. C. Ho, and X. Liu, "Robust H_∞ control for networked systems with random packet losses," *IEEE Transactions on Systems, Man, and Cybernetics B: Cybernetics*, vol. 37, no. 4, pp. 916–924, 2007.
- [5] P. Ögren, E. Fiorelli, and N. E. Leonard, "Cooperative control of mobile sensor networks: adaptive gradient climbing in a distributed environment," *IEEE Transactions on Automatic Control*, vol. 49, no. 8, pp. 1292–1302, 2004.
- [6] Y. Ge, Q. Chen, M. Jiang, and Z.-A. Liu, "Stability analysis of networked control systems with data dropout and transmission delays," in *Proceedings of the 7th World Congress on Intelligent Control and Automation (WCICA '08)*, pp. 7986–7991, Chongqing, China, June 2008.
- [7] F.-C. Liu and Y. Yao, "Modeling and analysis of networked control systems using hidden Markov models," in *Proceedings of the International Conference on Machine Learning and Cybernetics (ICMLC '05)*, vol. 2, pp. 928–931, Guangzhou, China, August 2005.
- [8] K. Sato, H. Nakada, and Y. Sato, "Variable rate speech coding and network delay analysis for universal transport network," in *Proceedings of the 7th Annual Joint Conference of the IEEE Computer and Communications Societies. Networks: Evolution or Revolution (INFOCOM '88)*, pp. 771–780, New Orleans, La, USA, March 1988.
- [9] Y. Tipsuwan and M.-Y. Chow, "Control methodologies in networked control systems," *Control Engineering Practice*, vol. 11, no. 10, pp. 1099–1111, 2003.
- [10] H. Gao, T. Chen, and J. Lam, "A new delay system approach to network-based control," *Automatica*, vol. 44, no. 1, pp. 39–52, 2008.
- [11] J. Wu, F.-Q. Deng, and J.-G. Gao, "Modeling and stability of long random delay networked control systems," in *Proceedings of the International Conference on Machine Learning and Cybernetics (ICMLC '05)*, vol. 2, pp. 947–952, Guangzhou, China, August 2005.
- [12] E. Kamrani and M. H. Mehraban, "Modeling internet delay dynamics using system identification," in *Proceedings of the IEEE International Conference on Industrial Technology (ICIT '06)*, pp. 716–721, Mumbai, India, December 2006.
- [13] J. P. Hespanha, P. Naghshtabrizi, and Y. Xu, "A survey of recent results in networked control systems," *Proceedings of the IEEE*, vol. 95, no. 1, pp. 138–162, 2007.
- [14] T.-C. Yang, "Networked control system: a brief survey," *IEE Proceedings: Control Theory and Applications*, vol. 153, no. 4, pp. 403–412, 2006.
- [15] L. Zhang, Y. Shi, T. Chen, and B. Huang, "A new method for stabilization of networked control systems with random delays," *IEEE Transactions on Automatic Control*, vol. 50, no. 8, pp. 1177–1181, 2005.
- [16] G.-P. Liu, Y. Xia, J. Chen, D. Rees, and W. Hu, "Networked predictive control of systems with random network delays in both forward and feedback channels," *IEEE Transactions on Industrial Electronics*, vol. 54, no. 3, pp. 1282–1297, 2007.
- [17] H. Zhang, J. Yang, and C.-Y. Su, "T-S fuzzy-model-based robust H_∞ design for networked control systems with uncertainties," *IEEE Transactions on Industrial Informatics*, vol. 3, no. 4, pp. 289–301, 2007.
- [18] H. Li, Z. Sun, M.-Y. Chow, and B. Chen, "State feedback controller design of networked control systems with time delay and packet dropout," in *Proceedings of the 17th World Congress, International Federation of Automatic Control (IFAC '08)*, pp. 6626–6631, Seoul, Republic of Korea, July 2008.
- [19] C.-L. Lai, P.-L. Hsu, and B.-C. Wang, "Design of the adaptive Smith Predictor for the time-varying network control system," in *Proceedings of the SICE Annual Conference, International Conference on Instrumentation, Control and Information Technology*, pp. 2933–2938, Tokyo, Japan, August 2008.
- [20] G.-P. Liu, "Analysis of networked predictive control systems with uncertainties," in *Proceedings of the IEEE International Conference on Systems, Man and Cybernetics (SMC '09)*, pp. 4819–4824, San Antonio, Tex, USA, October 2009.
- [21] X. Yan and J. Liu, "A novel sliding mode control for BLDC motor network control system," in *Proceedings of the 3rd International Conference on Advanced Computer Theory and Engineering (ICACTE '10)*, vol. 2, pp. V2-289–V2-293, Chengdu, China, August 2010.
- [22] J. H. Taylor and H. M. S. Ibrahim, "A new, practical approach to maintaining an efficient yet acceptably-performing wireless networked control system," in *Proceedings of the International Conference on System Science and Engineering (ICSSE '10)*, pp. 269–274, Taipei, Taiwan, July 2010.
- [23] S. Wang, X. Meng, and T. Chen, "Wide-area control of power systems through delayed network communication," *IEEE Transactions on Control Systems Technology*, vol. 20, no. 2, pp. 495–503, 2012.

- [24] B. Sinopoli, L. Schenato, M. Franceschetti, K. Poolla, M. I. Jordan, and S. S. Sastry, "Kalman filtering with intermittent observations," *IEEE Transactions on Automatic Control*, vol. 49, no. 9, pp. 1453–1464, 2004.
- [25] S. Tatikonda and S. Mitter, "Control under communication constraints," *IEEE Transactions on Automatic Control*, vol. 49, no. 7, pp. 1056–1068, 2004.
- [26] S. C. Smith and P. Seiler, "Estimation with lossy measurements: jump estimators for jump systems," *IEEE Transactions on Automatic Control*, vol. 48, no. 12, pp. 2163–2171, 2003.
- [27] P. Naghshtabrizi and J. P. Hespanha, "Designing an observer-based controller for a network control system," in *Proceedings of the 44th IEEE Conference on Decision and Control, and the European Control Conference (CDC-ECC '05)*, pp. 848–853, December 2005.
- [28] D. Yue, Q.-L. Han, and C. Peng, "State feedback controller design of networked control systems," *IEEE Transactions on Circuits and Systems II: Express Briefs*, vol. 51, no. 11, pp. 640–644, 2004.
- [29] L. X. Zhang, H. J. Gao, and O. Kaynak, "Network-induced constraints in networked control systems—a survey," *IEEE Transactions on Industrial Informatics*, vol. 9, no. 1, pp. 403–416, 2013.
- [30] N. Elia and J. N. Eisenbeis, "Limitations of linear control over packet drop networks," *IEEE Transactions on Automatic Control*, vol. 56, no. 4, pp. 826–841, 2011.
- [31] L. Zhang and D. Hristu-Varsakelis, "Communication and control co-design for networked control systems," *Automatica*, vol. 42, no. 6, pp. 953–958, 2006.
- [32] H. Zhang, M. Li, J. Yang, and D. Yang, "Fuzzy model-based robust networked control for a class of nonlinear systems," *IEEE Transactions on Systems, Man, and Cybernetics A: Systems and Humans*, vol. 39, no. 2, pp. 437–447, 2009.
- [33] X. Dang and Q. Zhang, "Stability for singular networked control system with dynamical state feedback," in *Proceedings of the 8th IEEE International Conference on Control and Automation (ICCA '10)*, pp. 785–789, Xiamen, China, June 2010.
- [34] Y. Niu, X. Wu, J. Kang, and J. He, "Method of control performance and network QoS co-design of networked control systems," in *Proceedings of the Chinese Control and Decision Conference (CCDC '10)*, pp. 108–113, Xuzhou, China, May 2010.
- [35] G. Pin and T. Parisini, "Networked predictive control of uncertain constrained nonlinear systems: recursive feasibility and input-to-state stability analysis," *IEEE Transactions on Automatic Control*, vol. 56, no. 1, pp. 72–87, 2011.
- [36] Y.-L. Wang, Q.-L. Han, and X. Yu, "One step prediction-based packet dropout compensation for networked control systems," in *Proceedings of the American Control Conference (ACC '11)*, pp. 2849–2854, San Francisco, Calif, USA, July 2011.
- [37] H. Li and Y. Shi, "Network-based predictive control for constrained nonlinear systems with twochannel packet dropouts," *IEEE Transactions on Industrial Electronics*, vol. 61, no. 3, pp. 1574–1582, 2014.
- [38] B. Hu and A. N. Michel, "Stability analysis of digital feedback control systems with time-varying sampling periods," *Automatica*, vol. 36, no. 6, pp. 897–905, 2000.
- [39] B. Wittenmark, J. Nilsson, and M. Torngren, "Timing problems in real-time control systems," in *Proceedings of the American Control Conference*, vol. 3, pp. 2000–2004, Seattle, Wash, USA, June 1995.
- [40] E. Fridman, A. Seuret, and J.-P. Richard, "Robust sampled-data stabilization of linear systems: an input delay approach," *Automatica*, vol. 40, no. 8, pp. 1441–1446, 2004.
- [41] Y. S. Suh, "Stability and stabilization of nonuniform sampling systems," *Automatica*, vol. 44, no. 12, pp. 3222–3226, 2008.
- [42] B. Picasso and A. Bicchi, "On the stabilization of linear systems under assigned I/O quantization," *IEEE Transactions on Automatic Control*, vol. 52, no. 10, pp. 1994–2000, 2007.
- [43] D. Coutinho, M. Fu, and C. E. de Souza, "Output feedback control of linear systems with input and output quantization," in *Proceedings of the 47th IEEE Conference on Decision and Control (CDC '08)*, pp. 4706–4711, Cancún, Mexico, December 2008.
- [44] D. F. Delchamps, "Stabilizing a linear system with quantized state feedback," *IEEE Transactions on Automatic Control*, vol. 35, no. 8, pp. 916–924, 1990.
- [45] P. Moroney, *Issues in the Implementation of Digital Compensators*, MIT Press, Cambridge, UK, 1983.
- [46] D. P. Bertsekas and I. B. Rhodes, "Recursive state estimation for a set-membership description of uncertainty," *IEEE Transactions on Automatic Control*, vol. 16, no. 2, pp. 117–128, 1971.
- [47] R. E. Curry, *Estimation and Control with Quantized Measurements*, MIT Press, Cambridge, UK, 1970.
- [48] F. Schweppe, "Recursive state estimation: unknown but bounded errors and system inputs," *IEEE Transactions on Automatic Control*, vol. 13, no. 1, pp. 22–28, 1968.
- [49] W. S. Wong and R. W. Brockett, "Systems with finite communication bandwidth constraints—part I: state estimation problems," *IEEE Transactions on Automatic Control*, vol. 42, no. 9, pp. 1294–1299, 1997.
- [50] W. S. Wong and R. W. Brockett, "Systems with finite communication bandwidth constraints—part I: stabilization with limited information feedback," *IEEE Transactions on Automatic Control*, vol. 44, no. 5, pp. 1049–1053, 1999.
- [51] R. K. Miller, A. N. Michel, and J. A. Farrell, "Quantizer effects on steady-state error specifications of digital feedback control systems," *IEEE Transactions on Automatic Control*, vol. 34, no. 6, pp. 651–654, 1989.
- [52] N. Elia and S. K. Mitter, "Stabilization of linear systems with limited information," *IEEE Transactions on Automatic Control*, vol. 46, no. 9, pp. 1384–1400, 2001.
- [53] M. Fu and L. Xie, "The sector bound approach to quantized feedback control," *IEEE Transactions on Automatic Control*, vol. 50, no. 11, pp. 1698–1711, 2005.
- [54] M. Fu and L. Xie, "Quantized feedback control for linear uncertain systems," *International Journal of Robust and Nonlinear Control*, vol. 20, no. 8, pp. 843–857, 2010.
- [55] B. Zhou, G.-R. Duan, and J. Lam, "On the absolute stability approach to quantized feedback control," *Automatica*, vol. 46, no. 2, pp. 337–346, 2010.
- [56] R. W. Brockett and D. Liberzon, "Quantized feedback stabilization of linear systems," *IEEE Transactions on Automatic Control*, vol. 45, no. 7, pp. 1279–1289, 2000.
- [57] D. Liberzon and D. Nešić, "Input-to-state stabilization of linear systems with quantized state measurements," *IEEE Transactions on Automatic Control*, vol. 52, no. 5, pp. 767–781, 2007.
- [58] G. N. Nair and R. J. Evans, "Stabilizability of stochastic linear systems with finite feedback data rates," *SIAM Journal on Control and Optimization*, vol. 43, no. 2, pp. 413–436, 2004.
- [59] N. C. Martins, M. A. Dahleh, and N. Elia, "Feedback stabilization of uncertain systems in the presence of a direct link," *IEEE*

- Transactions on Automatic Control*, vol. 51, no. 3, pp. 438–447, 2006.
- [60] K. You and L. Xie, “Minimum data rate for mean square stabilization of discrete LTI systems over lossy channels,” *IEEE Transactions on Automatic Control*, vol. 55, no. 10, pp. 2373–2378, 2010.
- [61] M. Trivellato and N. Benvenuto, “State control in networked control systems under packet drops and limited transmission bandwidth,” *IEEE Transactions on Communications*, vol. 58, no. 2, pp. 611–622, 2010.
- [62] H. Zhang, H. Yan, F. Yang, and Q. Chen, “Quantized control design for impulsive fuzzy networked systems,” *IEEE Transactions on Fuzzy Systems*, vol. 19, no. 6, pp. 1153–1162, 2011.
- [63] C. Zhang, G. Feng, J. Qiu, and Y. Shen, “Control synthesis for a class of linear network-based systems with communication constraints,” *IEEE Transactions on Industrial Electronics*, vol. 60, no. 8, pp. 3339–3348, 2013.
- [64] X. Tang and B. Ding, “Model predictive control of linear systems over networks with data quantizations and packet losses,” *Automatica*, vol. 49, no. 5, pp. 1333–1339, 2013.
- [65] K. J. Åström and B. M. Bernhardsson, “Comparison of Riemann and Lebesgue sampling for first order stochastic systems,” in *Proceedings of the 41st IEEE Conference on Decision and Control*, vol. 2, pp. 2011–2016, December 2002.
- [66] M. Velasco, P. Marti, and J. Fuertes, “The self triggered task model for real-time control systems,” in *Proceedings of the 24th IEEE Real-Time Systems Symposium Work-in-Progress (RTS '03)*, pp. 67–70, 2003.
- [67] M. Lemmon, T. Chantem, X. S. Hu, and M. Zyskowski, “On self-triggered full-information H_∞ -infinity controllers,” in *Hybrid Systems: Computation and Control*, vol. 4416 of *Lecture Notes in Computer Science*, pp. 371–384, Springer, Berlin, Germany, 2007.
- [68] P. G. Otanez, J. R. Moyne, and D. M. Tilbury, “Using deadbands to reduce communication in networked control systems,” in *Proceedings of the American Control Conference*, vol. 4, pp. 3015–3020, May 2002.
- [69] E. Kofman and J. H. Braslavsky, “Level crossing sampling in feedback stabilization under data-rate constraints,” in *Proceedings of the 45th IEEE Conference on Decision and Control (CDC '06)*, pp. 4423–4428, San Diego, Calif, USA, December 2006.
- [70] K. J. Åström, “Event based control,” in *Analysis and Design of Nonlinear Control Systems*, pp. 127–147, Springer, Berlin, Germany, 2008.
- [71] P. Tabuada, “Event-triggered real-time scheduling of stabilizing control tasks,” *IEEE Transactions on Automatic Control*, vol. 52, no. 9, pp. 1680–1685, 2007.
- [72] X. Wang and M. D. Lemmon, “Self-triggered feedback systems with state-independent disturbances,” in *Proceedings of the American Control Conference (ACC '09)*, pp. 3842–3847, St. Louis, Mo, USA, June 2009.
- [73] D. Yue, E. Tian, and Q. L. Han, “A delay system method to design of event-triggered control of networked control systems,” in *Proceedings of the 50th IEEE Conference on Decision and Control and European Control Conference (CDC-ECC '11)*, pp. 1668–1673, Orlando, Fla, USA, December 2011.
- [74] S. Hu and D. Yue, “Event-based H_∞ filtering for networked system with communication delay,” *Signal Processing*, vol. 92, no. 9, pp. 2029–2039, 2012.
- [75] S. Hu and D. Yue, “Event-triggered control design of linear networked systems with quantizations,” *ISA Transactions*, vol. 51, no. 1, pp. 153–162, 2012.
- [76] C. Peng and T. C. Yang, “Event-triggered communication and H_∞ control co-design for networked control systems,” *Automatica*, vol. 49, no. 5, pp. 1326–1332, 2013.
- [77] H. Yu and P. J. Antsaklis, “Event-triggered output feedback control for networked control systems using passivity: achieving L_2 stability in the presence of communication delays and signal quantization,” *Automatica*, vol. 49, no. 1, pp. 30–38, 2013.
- [78] A. S. Matveev and A. V. Savkin, “Decentralized stabilization of linear systems via limited capacity communication networks,” in *Proceedings of the 44th IEEE Conference on Decision and Control and the European Control Conference (CDC-ECC '05)*, pp. 1155–1161, December 2005.
- [79] R. Brockett, “Stabilization of motor networks,” in *Proceedings of the 34th IEEE Conference on Decision and Control*, vol. 2, pp. 1484–1488, December 1995.
- [80] D. Hristu, “Stabilization of LTI systems with communication constraints,” in *Proceedings of the American Control Conference*, vol. 4, pp. 2342–2346, June 2000.
- [81] L. Lu, L. Xie, and M. Fu, “Optimal control of networked systems with limited communication: a combined heuristic and convex optimization approach,” in *Proceedings of the 42nd IEEE Conference on Decision and Control*, vol. 2, pp. 1194–1199, December 2003.
- [82] O. C. Imer and T. Başar, “To measure or to control: optimal control with scheduled measurements and controls,” in *2006 American Control Conference*, pp. 1003–1008, Minneapolis, Minn, USA, June 2006.
- [83] G. C. Walsh and H. Ye, “Scheduling of networked control systems,” *IEEE Control Systems Magazine*, vol. 21, no. 1, pp. 57–65, 2001.
- [84] Z. Huo, H. Fang, and G. Yan, “Co-design for NCS robust fault-tolerant control,” in *Proceedings of the IEEE International Conference on Industrial Technology (ICIT '05)*, pp. 119–124, December 2005.
- [85] R. P. Patankar, “A model for fault-tolerant networked control system using TTP/C communication,” *IEEE Transactions on Vehicular Technology*, vol. 53, no. 5, pp. 1461–1467, 2004.
- [86] M. J. G. C. Mendes, B. M. S. Santos, and J. S. D. Costa, “Multi-agent platform for fault tolerant control systems,” in *Proceedings of the IEEE International Conference on Systems, Man, and Cybernetics (SMC '07)*, pp. 1321–1326, Montreal, Canada, October 2007.
- [87] H. Fang, H. Ye, and M. Zhong, “Fault diagnosis of networked control systems,” *Annual Reviews in Control*, vol. 31, no. 1, pp. 55–68, 2007.
- [88] Y. Wang, B. Jiang, and Z. Mao, “Fault-tolerant control design for a kind of nonlinear networked control system with communication constraints,” in *Proceedings of the Chinese Control and Decision Conference (CCDC '09)*, pp. 896–901, Guilin, China, June 2009.
- [89] S. Ding, P. Zhang, S. Yin, and E. Ding, “An integrated design framework of fault tolerant wireless networked control systems for industrial automatic control applications,” *IEEE Transactions on Industrial Informatics*, vol. 9, no. 1, pp. 462–471, 2013.
- [90] H. Ishii, “ H_∞ control with limited communication and message losses,” *Systems & Control Letters*, vol. 57, no. 4, pp. 322–331, 2008.
- [91] M. E. M. Ben Gaid and A. Çela, “Trading quantization precision for update rates for systems with limited communication in the uplink channel,” *Automatica*, vol. 46, no. 7, pp. 1210–1214, 2010.

Research Article

Design and Stability Analysis of Uncertain Networked Predictive Control Systems with Multiple Forward Channels

Hongbo Song

College of Information, Zhejiang University of Finance and Economics, Hangzhou 310018, China

Correspondence should be addressed to Hongbo Song; di7ganshb@163.com

Received 2 January 2014; Accepted 24 February 2014; Published 2 April 2014

Academic Editor: Huaicheng Yan

Copyright © 2014 Hongbo Song. This is an open access article distributed under the Creative Commons Attribution License, which permits unrestricted use, distribution, and reproduction in any medium, provided the original work is properly cited.

This paper is concerned with the design and stability of networked predictive control for uncertain systems with multiple forward channels. The delays and packet dropouts are distributed such that the classic networked predictive control (NPC) needs modifications to be implemented. An improved control signal selection scheme with distributed prediction length is proposed to increase the prediction accuracy and hence achieve better control performance. Moreover, stability analysis results are obtained for both constant and random cases. Interestingly, it is shown that the stability of the closed-loop NPC system is not related to the distributed delays when they are constant and the system model is accurate. Finally, a two-axis milling machine example is given to illustrate the effectiveness of the proposed method.

1. Introduction

As modern control systems become more and more complex, traditional point-to-point control architecture is no longer suitable under certain circumstances. Meanwhile, the technology of computer network improved significantly in the past decades and a new networked architecture emerges and attracts increasing attention. This kind of control systems are called networked control systems (NCSs), in which the control loops are closed via a network, for example, Field bus, Ethernet, and Internet [1–3]. Major advantages of NCSs include reduced cost, easy installation and maintenance, and high efficiency. However, the insertion of a network into the control loops introduces some challenging problems for NCSs such as network-induced delay, packet dropout, and quantization [4–7]. Moreover, beside the control problem for NCSs, state estimation or filtering for NCSs also attracts much attention [8–10]. Thus, NCSs have become a hot research area in the control and signal processing communities.

Among these problems, network-induced delay and packet dropout are two major issues that degrade the system performance or even cause instability [1]. Up to date, both network-induced delay and packet dropout issues have received extensive research attention and fruitful results were obtained. To name a few, time delay method [11, 12], stochastic

system method [13], switched system method [14], and robust control method [15] were proposed to deal with the delay. Switched system method [16] and stochastic system method [17] were presented to handle the packet dropout. These methods commonly model the delay or/and packet dropout into the closed-loop NCS and the corresponding controller were then designed based on conditions that make the closed-loop NCS stable. Most of the conditions are only sufficient and thus the design is conservative. Moreover, essentially, they all passively compensate for the negative effects of the delay and packet dropout after accepting them. Alternatively, a novel actively compensating method called networked predictive control (NPC) was presented in [18, 19]. In NPC, future control sequences are generated and transmitted in a packet through the network. At the plant side, appropriate control signals from the sequences are selected to control the plant based on delay measurements.

With accurate system model and delay measurements, NPC was shown to have the ability to achieve desired control performance and the stability of the closed-loop NPC system is not related to the delay and packet dropout in the constant case [20]. In [21], an event driven NPC was presented to avoid the practical problem that delay measurements are inaccurate. In [22], a switched controller structure was proposed and the controllers were designed

according to the delay based on switched system method. For more research results on NPC, see [23–28] and the references therein. However, two issues of NPC are not fully considered in the existing literature, which are the model uncertainty and multiple communication channels. The NPC for uncertain system with multiple distributed delays and packet dropouts in the feedback channels was studied in [29]. In [30], stability analysis was carried out for NPC systems with model uncertainty. In [31], a data reconstruction method was presented for NPC system with distributed delays in the feedback channels.

For a practical system, it is very difficult to obtain an accurate model. A nonlinear system is always linearized to be simplified. Thus, model uncertainty is an important issue to be investigated. On the other hand, when the plant to be controlled is spatially distributed, the corresponding NCSs have to be multiple communication channels. Obviously, for a NPC system with model uncertainty, larger input delay results in longer prediction length and thus leads to larger prediction error. Hence, the control performance becomes worse. In the case of multiple communication channels, delays and packet dropouts are distributed, which means that delays and packet dropout process may be different for each channel, while such case was not taken into account in classic NPC such as [18–20]. Introducing the queuing method in [32] can make the input delays the same for each channel, which makes the classic NPC applicable for the case without modification. However, input delays are actually enlarged in this way and the control performance will hence be degraded. Thus, this paper presents a modified control signal selection scheme such that the control signals which are predicted with distributed prediction length can be applied to control the plant. Such treatment essentially uses the most recent data and hence reduces the prediction length and improves the system performance. Only multiple forward channels are considered since the compensation scheme in the forward channels is different from the one in the feedback channels.

2. Design of NPC for Systems with Multiple Forward Channels

2.1. Structure of the NPC System. The structure of NPC systems with multiple forward channels is shown in Figure 1. The feedback channels are assumed to be ideal such that the plant outputs are transmitted to the predictive controller (PC) side without any delays or packet dropouts. The task of PC is to generate future control prediction sequences and transmit them to the control signal selector (CSS). The sequences are subjected to distributed delays and packet dropouts effects since the system has multiple forward channels. CSS receives the distributed prediction sequences and select proper control signal from them according to the measured input delays. The selected control signal is then used to control the plant.

The control performance of NPC systems highly depends on the prediction accuracy, which is related to both the discrepancy between the adopted model and real system dynamic and the prediction length. On the other hand, larger input delay results in longer prediction length. Based on the

NPC in [19, 30], it is known that larger modeling error and larger delay lead to larger prediction errors and hence degrade the control performance. Thus, intuitively, it can be inferred that two ways to improve the control performance of NPC systems are to reduce the modeling error and to make the prediction length shorter.

For the NPC systems with multiple forward channels, the delays and packet dropouts process are distributed. If we use the classic NPC, which assumes single communication channel, the input delays of all the channels should be the same and equal to a value which is the largest one of the distributed input delays. This can be done by the queuing method. However, with this treatment it can be seen that the prediction length is enlarged for the channels except the one with largest input delays. Based on the thought that shorter prediction length leads to better prediction accuracy, another way is to use an improved CSS with distributed prediction length, which makes the prediction length shorter than using classic NPC. This is the main idea of the paper.

The plant is represented by the following uncertain linear discrete-time state space system model:

$$\begin{aligned} x(k+1) &= (A + \Delta A)x(k) + (B + \Delta B)u(k), \\ y(k) &= Cx(k), \end{aligned} \quad (1)$$

where $x \in R^n$, $u \in R^m$, and $y \in R^p$ are the state, input, and output vectors of the plant, respectively, and A , B , and C are the nominal system matrices with compatible dimensions. ΔA and ΔB represent the system uncertainties and it is assumed that ΔA and ΔB satisfy the following structure:

$$[\Delta A \quad \Delta B] = EF(k)[G_1 \quad G_2], \quad (2)$$

where $F(k)^T F(k) \leq I$, and E , G_1 and G_2 are matrices with compatible dimensions.

The prediction sequences are designed based on the following standard state observer:

$$\begin{aligned} \hat{x}(k+1 | k) \\ = A\hat{x}(k | k-1) + Bu(k) + L(y(k) - C\hat{x}(k | k-1)), \end{aligned} \quad (3)$$

where $\hat{x}(k | k-1)$ is the state of the observer, and L is the observer gain matrix which can be designed by standard methods such as pole placement. The state feedback controller is as follows:

$$u(k) = -K\hat{x}(k | k-1), \quad (4)$$

where K is the controller gain matrix which can be designed by Lyapunov method and so on.

2.2. Assumptions and Notations. Before proceeding further, we need to introduce some reasonable assumptions and some notations.

- (1) Without loss of generality, it is assumed that there are m forward channels in the system and they are denoted by channel 1 to channel m , respectively. u_j are transmitted through channel j , $j \in M = \{1, 2, \dots, m\}$, respectively.

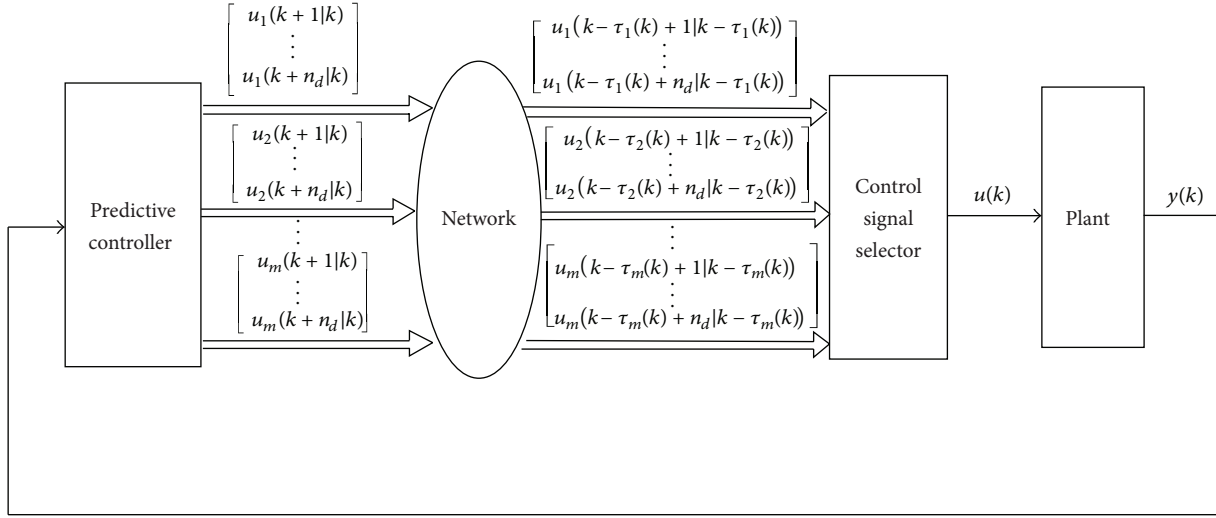


FIGURE 1: Structure of NPC systems with multiple forward channels.

- (2) The distributed delays are bounded. The upper bound for the delays is denoted by n_d and the lower bound is assumed to be 1 step without loss of generality.
- (3) The number of consecutive packet dropouts for channels 1 to m is bounded and the upper bound is denoted by n_p . The lower bound is assumed to be 0 steps, which means no packet dropout.
- (4) The transmitted packets are time-stamped and the clocks of the receiving sides and the transmitting sides are synchronized such that the input delays can be calculated.

At any time instant, it is probable that more than one packet are received or no packet is received because of packet dropouts or packet disorder. In both cases, the data in the most recent packet will be used. The input delays then can always be calculated by the time stamp.

Since the case random delays and packet dropouts are considered, the input delay for channel i at instant k is denoted by $\tau_i(k)$ and it is clear that the lower and upper bound for the input delays are 1 and n_f , respectively, where $n_f = n_d + n_p$. It can be seen that input delays may be of the same value for certain channels. That is to say, $\tau_i(k) = \tau_j(k)$, $i, j \in M$. Thus, we denote the number of different values for the input delays as $d(k)$. The corresponding values for the input delays are denoted by $\rho_1(k), \rho_2(k), \dots, \rho_{d(k)}(k)$, respectively, where $\rho_i(k) < \rho_j(k)$ for any $i < j$, $i, j \in M$. The set of the indexes of the channels in which $\rho_i(k) = \tau_j(k)$ is denoted by $Q_i(k)$. Introduce selection matrices $\Pi_j, \forall j \in M$, which is defined by

$$\Pi_j = \text{diag}\{\delta(j-1), \delta(j-2), \dots, \delta(j-m)\}, \quad (5)$$

where $\text{diag}\{\bullet\}$ represents a diagonal matrix and $\delta(j) = \begin{cases} 1, & j=0 \\ 0, & j \neq 0. \end{cases}$

An example is given to make these notations clear. Assume that the system has 3 forward channels, which means $m = 3$. At instant k , it is measured that $\tau_1(k) = 3$ and $\tau_2(k) = \tau_3(k) = 2$. Then, it can be seen that there are two

different values for the distributed delays; that is, $d(k) = 2$ and $\rho_1(k) = 2, \rho_2(k) = 3$. Furthermore, we have $Q_1(k) = \{2, 3\}$ and $Q_2(k) = \{1\}$, respectively.

For the constant delays case, the notations can be simply used by removing the index k of the ones for the random delays and packet dropouts case.

2.3. Predictive Controller. At the PC side, the state of the observer $\hat{x}(k+1|k)$ is obtained at instant k according to (3). Since future system outputs $y(k+i)$ and $i = 1, 2, \dots, n_f - 1$ are not available at instant k , the prediction sequences are generated as follows:

$$\hat{x}(k+2|k) = A\hat{x}(k+1|k) + Bu(k+1|k)$$

$$\hat{x}(k+3|k) = A\hat{x}(k+2|k) + Bu(k+2|k)$$

$$\vdots$$

$$\hat{x}(k+n_f|k) = A\hat{x}(k+n_f-1|k) + Bu(k+n_f-1|k). \quad (6)$$

The prediction is up to n_f steps to meet the worst case of delays and packet dropouts, that is, n_d steps delays and n_p consecutive packet dropouts. For the prediction procedure (6), it can be seen that the prediction accuracy at each instant depends on two factors. The first is how accurate (A, B, C) represents the system dynamic. The second is how close $u(k+i|k)$ to $u(k+i)$, $\forall i \in N = \{1, 2, \dots, n_f\}$. It is interesting to see that $u(k+i|k)$ are fundamentally different for the random and constant cases.

For the constant delays case, even though the future control input $u(k+i)$ is not applied, it can be inferred what control signal will be applied at instant $k+i$ and the control signal is already available at the PC side. That is to say, PC can use $u(k+i)$ instead of $u(k+i|k)$ in (6). For the random case, PC cannot determine what control signal will be used at

instant $k + i$, $\forall i \in N$. Thus, $u(k + i | k)$ can be approximated by (4) such that

$$u(k + i | k) = -K\hat{x}(k + i | k). \quad (7)$$

This will also lead to different techniques used for the stability analysis of random and constant cases.

In classic NPC, the future control sequence is transmitted in a packet to the CSS as follows:

$$\begin{bmatrix} u(k + 1 | k) \\ u(k + 2 | k) \\ \vdots \\ u(k + n_f | k) \end{bmatrix}. \quad (8)$$

However, this paper considers the multiple forward channels case and thus the packet that contains $u(k + i | k)$, $\forall i \in N$, is transmitted separately via m channels. The packets transmitted through channel i contains the following information, respectively. Consider

$$\begin{bmatrix} u_1(k + 1 | k) \\ u_1(k + 2 | k) \\ \vdots \\ u_1(k + n_f | k) \end{bmatrix}, \quad (9)$$

$$\begin{bmatrix} u_2(k + 1 | k) \\ u_2(k + 2 | k) \\ \vdots \\ u_2(k + n_f | k) \end{bmatrix}, \dots, \begin{bmatrix} u_m(k + 1 | k) \\ u_m(k + 2 | k) \\ \vdots \\ u_m(k + n_f | k) \end{bmatrix}.$$

2.4. Control Signal Selector. Subjected to the distributed delays and packet dropouts effects, the packets are received by the CSS in a distributed delayed manner. Specifically, the following data are received by CSS at instant k :

$$\begin{bmatrix} u_i(k - \tau_i(k) + 1 | k - \tau_i(k)) \\ u_i(k - \tau_i(k) + 2 | k - \tau_i(k)) \\ \vdots \\ u_i(k - \tau_i(k) + n_f | k - \tau_i(k)) \end{bmatrix}, \quad \forall i \in M. \quad (10)$$

As mentioned, classic NPC with using queuing method can be used and in this case the selected control signal is

$$u(k) = u(k | k - \bar{\tau}(k)), \quad (11)$$

where $\bar{\tau}(k) = \max_{i \in M} \tau_i(k)$.

Alternatively, a modified CSS scheme is presented here. We can see that for channel i , $\forall i \in M$, the predicted control signal with minimal prediction length is

$$u_i(k) = u_i(k | k - \tau_i(k)). \quad (12)$$

Then, it follows by using the notations in the second subsection of this section that

$$u_i(k) = \sum_{j \in Q_i(k)} \Pi_j u(k | k - \rho_i(k)). \quad (13)$$

It can be seen that the modified CSS selects control signal with distributed prediction length. Then, we can see that the following control signal to control the plant:

$$u(k) = - \sum_{i=1}^{d(k)} \sum_{j \in Q_i(k)} \Pi_j K \hat{x}(k | k - \rho_i(k)). \quad (14)$$

As a special case, if $\rho_i(k) = \rho_j(k)$, $\forall i \in M$, $j \in M/\{i\}$, which means that the length of the delays are all the same for each channel, then it can be seen that the control input (14) equals the control input (11).

3. Stability Analysis of the Closed-Loop NPC System

The last section designed a modified NPC strategy to control uncertain systems with multiple forward channels. Since stability is crucial for a control system, the stability of the closed-loop NPC system is studied in this section. Two cases are considered, which are the random distributed delays and packet dropouts case and the constant distributed delays case. As mentioned in the above section, the analysis techniques are different for the two cases.

3.1. Model of the Closed-Loop NPC System: Random Case. By (6) and (7), it follows that

$$\hat{x}(k + i | k) = (A - BK)^{i-1} \hat{x}(k + 1 | k). \quad (15)$$

Then, by (14) and (15) we have

$$u(k) = - \sum_{i=1}^{d(k)} \sum_{j \in Q_i(k)} \Pi_j K (A - BK)^{\rho_i(k)-1} \cdot \hat{x}(k - \rho_i(k) + 1 | k - \rho_i(k)). \quad (16)$$

Define an augmented vector to be

$$\xi(k) = \begin{bmatrix} x(k) \\ x(k | k - 1) \\ x(k - 1 | k - 2) \\ \vdots \\ x(k - n_f + 1 | k - n_f) \end{bmatrix}, \quad (17)$$

then the closed-loop NPC systems with random distributed delays and packet dropouts can be obtained by (1), (3), and (16) as follows:

$$\xi(k + 1) = (\Omega(k) + \Delta\Omega(k)) \xi(k), \quad (18)$$

where

$$\Omega(k) = \begin{bmatrix} \Omega_{11} & B\Omega_{12}(k) \\ \Omega_{21} & \Omega_{22} \end{bmatrix},$$

$$\Omega_{11} = \begin{bmatrix} A \\ LC \end{bmatrix},$$

$$\Omega_{21} = \begin{bmatrix} 0_{(n_f-2) \times n} \end{bmatrix},$$

$$\Omega_{22} = \begin{bmatrix} I_{(n_f-2) \times (n_f-2)} & 0_{(n_f-2) \times n} \end{bmatrix},$$

$$\begin{aligned}
\Omega_{12}(k) &= \Omega_{121} + \Omega_{122}(k), \\
\Omega_{121} &= \begin{bmatrix} 0_{n \times n} & 0_{n \times n} & 0_{n \times n} & \cdots & 0_{n \times n} \\ A - LC & 0_{n \times n} & 0_{n \times n} & \cdots & 0_{n \times n} \end{bmatrix}, \\
\Omega_{122}(k) &= \begin{bmatrix} \Omega_{1221}(k) & \Omega_{1222}(k) & \cdots & \Omega_{122d(k)}(k) & 0_{n \times (n_f - d(k))n} \\ \Omega_{1221}(k) & \Omega_{1222}(k) & \cdots & \Omega_{122d(k)}(k) & 0_{n \times (n_f - d(k))n} \end{bmatrix}, \\
\Omega_{1221}(k) &= [0_{(\rho_1(k)-1)n \times (\rho_1(k)-1)n} \quad \Omega_{12212}(k)], \\
\Omega_{1222}(k) &= [0_{(\rho_2(k)-1)n \times (\rho_2(k)-1)n} \quad \Omega_{12222}(k)], \\
&\vdots \\
\Omega_{122d(k)}(k) &= [0_{(\rho_{d(k)}(k)-1)n \times (\rho_{d(k)}(k)-1)n} \quad \Omega_{122d(k)2}(k)], \\
\Omega_{12212}(k) &= \sum_{j \in Q_1(k)} \Pi_j K(A - BK)^{\rho_1(k)-1}, \\
\Omega_{12222}(k) &= \sum_{j \in Q_2(k)} \Pi_j K(A - BK)^{\rho_2(k)-1}, \\
&\vdots \\
\Omega_{122d(k)2}(k) &= \sum_{j \in Q_{d(k)}(k)} \Pi_j K(A - BK)^{\rho_{d(k)}(k)-1}, \\
\Delta\Omega(k) &= \begin{bmatrix} \Delta A & \Delta B \Delta \Omega_{12}(k) \\ 0_{n_f n \times n} & 0_{n_f n \times n_f n} \end{bmatrix}, \\
\Delta\Omega_{12} &= \begin{bmatrix} I_{n \times n} & 0_{n \times n} \\ 0_{n \times n} & 0_{n \times n} \end{bmatrix} * \Omega_{122}(k).
\end{aligned} \tag{19}$$

Note that the dynamics of the closed-loop NPC system (18) is related to the input delays vector $\vec{\rho}(d(k), k) = [\rho_1(k) \ \rho_2(k) \ \cdots \ \rho_{d(k)}(k)]$; denote the set of all the possible values of $\vec{\rho}(d(k), k)$ as V . When $\vec{\rho}(d(k), k)$ takes a value in V , system (18) resides in the corresponding subsystem, which means that system (18) is a switched system. For simplicity of notation, introduce a one-to-one mapping that maps the set of $\vec{\rho}(d(k), k)$ to a set with numbers. For example, $[1, 1, \dots, 1]$ is mapped to 1, $[1, 1, \dots, 2]$ is mapped to 2, and so on. Denote the set of the numbers by C . Moreover, the system has model uncertainties. Thus, system (18) can be transformed into the following uncertain switched system:

$$\xi(k+1) = (\Phi_s + \Delta\Phi_s) \xi(k), \quad s \in C, \tag{20}$$

where

$$\begin{aligned}
\Phi_s &= \begin{bmatrix} \Omega_{11} & \Phi_{12s} \\ \Omega_{21} & \Omega_{22} \end{bmatrix}, \\
\Delta\Phi_s &= \begin{bmatrix} \Delta A & \Delta\Phi_{12s} \\ 0_{n_f n \times n} & 0_{n_f n \times n} \end{bmatrix},
\end{aligned} \tag{21}$$

and Φ_{12s} and $\Delta\Phi_{12s}$ are $B\Omega_{12}(k)$ and $\Delta B \Delta \Omega_{12}(k)$ with $\vec{\rho}(d(k), k)$ is mapped by $s, \forall s \in C$.

3.2. Stability Results: Random Case. The closed-loop NPC system with random distributed delays and packet dropouts in the multiple forward channels is modeled as the switched uncertain system (20). A sufficient condition for the stability of the closed-loop NPC system (20) is presented in this subsection. A lemma is first given as follows.

Lemma 1. For given appropriate matrices $\Upsilon_1, \Upsilon_2,$ and $\Upsilon_3,$ with $\Upsilon_1^T = \Upsilon_1,$

$$\Upsilon_1 + \Upsilon_2 F(k) \Upsilon_3 + \Upsilon_3^T F^T(k) \Upsilon_2^T < 0 \tag{22}$$

holds for all $F^T(k)F(k) \leq I$ if and only if there exists a scalar $\beta > 0$ such that

$$\Upsilon_1 + \beta \Upsilon_2 \Upsilon_2^T + \beta^{-1} \Upsilon_3^T \Upsilon_3 < 0. \tag{23}$$

Theorem 2. For the NPC system (20) with random distributed delays and packet dropouts, given all possible values of $\vec{\rho}(d(k), k)$, and controller gain matrix K and observer gain matrix L , if there exists a matrix X and a scalar $\beta > 0$ such that the following matrix inequalities

$$\begin{bmatrix} -X & X\Phi_s^T & X\bar{G}_s^T \\ \Phi_s X & -X + \beta \bar{E}\bar{E}^T & 0 \\ \bar{G}_s X & 0 & -\beta I \end{bmatrix} < 0, \quad \forall s \in C \tag{24}$$

hold, then the closed-loop NPC system (20) is stable.

Proof. It can be obtained by (2) that $\Delta\Omega_s$ has the structure $\Delta\Phi_s = \bar{E}F(k)\bar{G}_s$, where

$$\bar{E} = \begin{bmatrix} E \\ 0_{n_f n \times n} \end{bmatrix}, \quad \bar{G}_s = [G_1 \ G_2 \Phi_{12s}]. \tag{25}$$

By the stability result of switched system with arbitrary switching in [10], if there exists a matrix $P > 0$ such that the following

$$(\Phi_s + \Delta\Phi_s)^T P (\Phi_s + \Delta\Phi_s) - P < 0 \tag{26}$$

holds, then the closed-loop NPC system (20) is stable. Then, by Schur complement and some matrix operations, we have

$$\begin{bmatrix} -P & \Phi_s^T \\ \Phi_s & -P^{-1} \end{bmatrix} + \begin{bmatrix} 0 \\ \bar{E} \end{bmatrix} F [\bar{G}_s \ 0] + \begin{bmatrix} \bar{G}_s^T \\ 0 \end{bmatrix} F^T \begin{bmatrix} 0 & \bar{E}^T \end{bmatrix} < 0. \tag{27}$$

Then, by Lemma 1 it can be obtained that

$$\begin{bmatrix} -P & \Phi_s^T & \bar{G}_s^T \\ \Phi_s & -P^{-1} + \beta \bar{E}\bar{E}^T & 0 \\ \bar{G}_s & 0 & -\beta I \end{bmatrix} < 0. \tag{28}$$

Pre- and postmultiplying of (28) by $[P^{-1} \ I \ I]$ and letting $X = P^{-1}$ lead to (24). The proof is completed. \square

It should be pointed out that (24) is linear in matrix X and scalar β and thus can be conveniently solved by LMI toolbox in Matlab for example. This means that the stability of the closed-loop NPC system with random distributed delays and packet dropouts can be readily checked. However, a common Lyapunov function is used in the proof, which leads to some conservatism. One possible way to reduce conservatism is to use multiple Lyapunov function method.

3.3. Stability Results: Constant Case. In this section, the constant case is considered. Different from the random case, a necessary and sufficient condition is obtained. Define the state error as

$$e(k) = x(k) - \hat{x}(k | k-1). \quad (29)$$

Subtracting (3) from (1) leads to the following state error equation:

$$e(k+1) = (A - LC)e(k) + \Delta Ax(k) + \Delta Bu(k). \quad (30)$$

For an integer $\tau \geq 2$, it can be seen by (6) that the following two equalities hold:

$$\begin{aligned} \hat{x}(k | k-\tau) &= A^{\tau-1} \hat{x}(k-\tau+1 | k-\tau) \\ &\quad + \sum_{i=1}^{\tau-1} A^i Bu(k-i), \end{aligned} \quad (31)$$

$$\begin{aligned} \hat{x}(k | k-\tau+1) &= A^{\tau-2} \hat{x}(k-\tau+2 | k-\tau+1) \\ &\quad + \sum_{i=1}^{\tau-2} A^i Bu(k-i). \end{aligned} \quad (32)$$

By shifting (3) backward for τ steps, it can be obtained that

$$\begin{aligned} \hat{x}(k-\tau+2 | k-\tau+1) \\ &= A \hat{x}(k-\tau+1 | k-\tau) \\ &\quad + Bu(k-\tau+1) + LCe(k-\tau+1). \end{aligned} \quad (33)$$

Then, by (33) and subtracting (31) from (32) we have the following:

$$\hat{x}(k | k-\tau+1) - \hat{x}(k | k-\tau) = A^{\tau-2} LCe(k-\tau+1). \quad (34)$$

Applying (34) recursively results in the following equation that holds for any integer $\tau \geq 2$:

$$x(k | k-1) = x(k | k-\tau) + \sum_{i=1}^{\tau-1} A^{i-1} LCe(k-i). \quad (35)$$

We now have by (14) and (35)

$$\begin{aligned} u(k) &= -K \hat{x}(k | k-1) \\ &\quad + \sum_{i=1}^d \sum_{j \in Q_i} \Pi_j K \sum_{l=1}^{\rho_i-1} A^{l-1} LCe(k-l). \end{aligned} \quad (36)$$

For convenience of the representation of the closed-loop NPC system, $u(k)$ is transformed as follows:

$$\begin{aligned} u(k) &= -K \hat{x}(k | k-1) + \sum_{l=1}^{\rho_1-1} A^{l-1} LCe(k-l) \\ &\quad + \sum_{i=1}^{d-1} \sum_{j \in W_i} \Pi_j K \sum_{l=\rho_i}^{\rho_{i+1}-1} A^{l-1} LCe(k-l), \end{aligned} \quad (37)$$

where $W_i = Q_{i+1} \cup Q_{i+2} \cup \dots \cup Q_d$, $i = 1, 2, \dots, d$. Substituting $u(k)$ in (1) and (30), respectively, by (26) yields

$$\begin{aligned} x(k+1) &= (A - BK + \Delta A - \Delta BK)x(k) + (B + \Delta BK)e(k) \\ &\quad + \sum_{l=1}^{\rho_1-1} (B + \Delta B)KA^{l-1}LCe(k-l) \\ &\quad + \sum_{i=1}^{d-1} \sum_{j \in W_i} B \Pi_j K \sum_{l=\rho_i}^{\rho_{i+1}-1} A^{l-1} LCe(k-l) \\ &\quad + \sum_{i=1}^{d-1} \sum_{j \in W_i} \Delta B \Pi_j K \sum_{l=\rho_i}^{\rho_{i+1}-1} A^{l-1} LCe(k-l), \end{aligned} \quad (38)$$

$$\begin{aligned} e(k+1) &= (A - LC)e(k) + (\Delta A - \Delta BK)x(k) - \Delta BKe(k) \\ &\quad + \sum_{l=1}^{\rho_1-1} \Delta BKA^{l-1}LCe(k-l) \\ &\quad + \sum_{i=1}^{d-1} \sum_{j \in W_i} \Delta B \Pi_j K \sum_{l=\rho_i}^{\rho_{i+1}-1} A^{l-1} LCe(k-l). \end{aligned}$$

Define an augmented vector as

$$\begin{aligned} \eta(k) &= [x^T(k) \quad e^T(k) \quad \eta_1^T(k) \quad \eta_2^T(k) \quad \dots \quad \eta_d^T(k)]^T, \\ \eta_1(k) &= \begin{bmatrix} e(k-1) \\ e(k-2) \\ \vdots \\ e(k-\rho_1+1) \end{bmatrix}, \\ \eta_i(k) &= \begin{bmatrix} e(k-\rho_{i-1}) \\ e(k-\rho_{i-1}-1) \\ \vdots \\ e(k-\rho_i+1) \end{bmatrix}, \quad i = 2, 3, \dots, d. \end{aligned} \quad (39)$$

Then, the closed-loop NPC system with constant distributed delays is as follows:

$$\eta(k+1) = (\Gamma + \Delta \Gamma) \eta(k), \quad (40)$$

where

$$\begin{aligned} \Gamma &= \begin{bmatrix} \Gamma_{11} & B \Gamma_{12} \\ \Gamma_{21} & \Gamma_{22} \end{bmatrix}, \\ \Gamma_{11} &= \Omega_{11}, \quad \Gamma_{21} = \begin{bmatrix} 0_{n \times n} & I_{n \times n} \\ 0_{(d-2)n \times n} & 0_{(d-2)n \times n} \end{bmatrix}, \\ \Gamma_{22} &= \begin{bmatrix} 0_{n \times (d-2)n} & 0_{n \times n} \\ I_{(d-2)n \times (d-2)n} & 0_{(d-2)n \times n} \end{bmatrix}, \end{aligned}$$

$$\Gamma_{12} = \begin{bmatrix} \Gamma_{121} & \Gamma_{122} & \cdots & \Gamma_{12d} \\ 0_{n \times n} & 0_{n \times n} & \cdots & 0_{n \times n} \end{bmatrix},$$

$$\Gamma_{121} = [KLC \quad KALC \quad \cdots \quad KA^{\rho_1-2}LC],$$

$$\Gamma_{12i} = [\Gamma_{12i1} \quad \Gamma_{12i2} \quad \cdots \quad \Gamma_{12i(\rho_i-1)}] \\ i = 2, 3, \dots, d,$$

$$\Gamma_{12i1} = \sum_{j \in W_i} \Pi_j KA^{\rho_i-1} LC,$$

$$\Gamma_{12i2} = \sum_{j \in W_i} \Pi_j KA^{\rho_i-1} LC,$$

$$\vdots$$

$$\Gamma_{12i(\rho_i-1)} = \sum_{j \in W_i} \Pi_j KA^{\rho_i-2} LC,$$

$$\Delta\Gamma = \begin{bmatrix} \Delta\Gamma_{11} & \Delta B\Gamma_{12} \\ 0_{(d-1)n \times 2n} & 0_{(d-1)n \times (d-1)n} \end{bmatrix},$$

$$\Delta\Gamma_{11} = \Delta\Omega_{11}.$$

(41)

It is clear that system (40) is a standard uncertain system and the stability result is as follows.

Theorem 3. For the NPC system (40) with constant distributed delays, given $\rho_i, i \in D$, and controller K and observer L , if and only if there exists a matrix Y and a scalar $\gamma > 0$ such that the following matrix inequality

$$\begin{bmatrix} -Y & Y\Gamma^T & YH^T \\ \Gamma Y & -Y + J J^T & 0 \\ HY & 0 & -\gamma I \end{bmatrix} < 0 \quad (42)$$

holds, then the closed-loop NPC system (40) is stable, where

$$J = \begin{bmatrix} E & \\ E & \\ 0_{(n_f-1) \times n} & \end{bmatrix}, \quad (43)$$

$$H = [G_1 - G_2K \quad G_2K \quad G_2\Gamma_{12}].$$

Proof. It can be obtained by (2) that $\Delta\Gamma$ has the structure $\Delta\Gamma = JF(k)H$. Following the robust control system results such as [33], it can be obtained that system (40) is stable if and only if there exists a matrix P such that the following inequality holds:

$$(\Gamma + \Delta\Gamma)^T P (\Gamma + \Delta\Gamma) - P < 0. \quad (44)$$

Then, similar to the procedure in Theorem 2, the stability result can be obtained readily. The rest of the proof is thus omitted.

Assume that there are no model uncertainties; that is, $\Delta A = 0$ and $\Delta B = 0$, and then closed-loop NPC system (40) with constant distributed delays can be represented in a more concise form as follows:

$$\eta(k+1) = \Lambda\eta(k), \quad (45)$$

where

$$\Lambda = \begin{bmatrix} A - BK & \Lambda_{12} \\ 0 & \Lambda_{22} \end{bmatrix},$$

$$\Lambda_{12} = B\Gamma_{12}, \quad (46)$$

$$\Lambda_{22} = \text{diag}\{A - LC, A - LC, \dots, A - LC\}.$$

Clearly, a necessary and sufficient condition for the stability of the system (45) is the eigenvalues of $A - BK$ and $A - LC$ that are within the unit circle, which means that the stability of the closed-loop NPC system (45) is not related to the distributed delays. This extends the results in [20] to the multiple forward channels case. \square

4. Illustrative Example

To illustrate the effectiveness of the modified NPC with multiple forward channels, we consider the two-axis example of a three-axis milling machine. More details about the example can be referred to [34]. The parameters of the nominal model and the uncertain parts for the system are chosen as follows:

$$A = \begin{bmatrix} 1.0000 & 0.0461 & 0 & 0 \\ 0 & 0.1624 & 0 & 0 \\ 0 & 0 & 1.0000 & 0.0466 \\ 0 & 0 & 0 & 0.1676 \end{bmatrix},$$

$$B = \begin{bmatrix} 1.5287 & 0 \\ 23.7463 & 0 \\ 0 & 1.5458 \\ 0 & 24.0982 \end{bmatrix}, \quad C = \begin{bmatrix} 1 & 0 & 0 & 0 \\ 0 & 0 & 1 & 0 \end{bmatrix}, \quad (47)$$

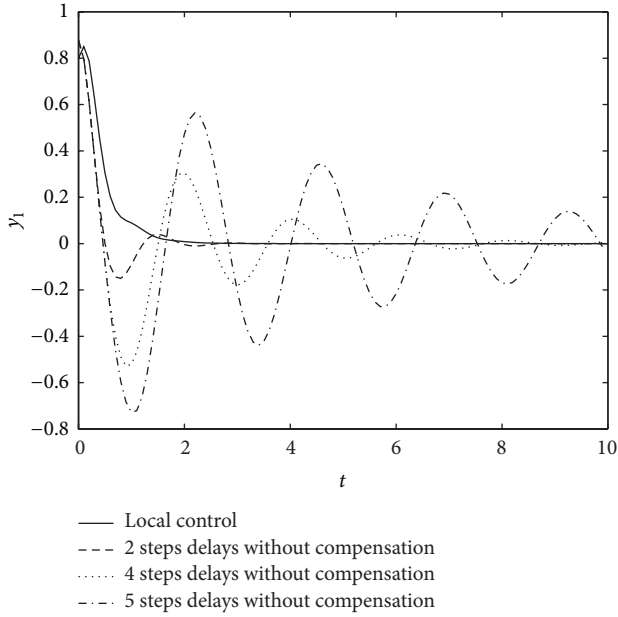
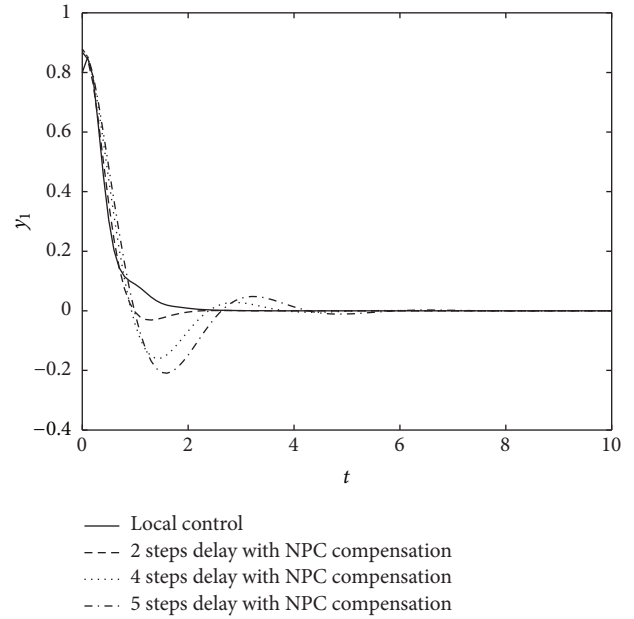
$$E = \begin{bmatrix} h_1 & 0 \\ h_2 & 0 \\ 0 & h_3 \\ 0 & h_4 \end{bmatrix}, \quad F(k) = \begin{bmatrix} \sin k & 0 \\ 0 & \sin k \end{bmatrix},$$

$$G_1 = \begin{bmatrix} 0 & g_1 & 0 & 0 \\ 0 & 0 & 0 & g_2 \end{bmatrix}, \quad G_2 = \begin{bmatrix} g_3 & 0 \\ 0 & g_4 \end{bmatrix},$$

where $h_1 = h_3 = 0.05$, $h_2 = h_4 = 0.3$, $g_1 = g_2 = 1$, and $g_3 = g_4 = 40$. The sampling period is chosen as 0.1 s. Clearly, $F^T(k)F(k) \leq I$. The observer gain matrix L and state feedback control gain matrix K are calculated by pole placement method and Lyapunov method, respectively. They are given as follows:

$$L = \begin{bmatrix} 0.4715 & 5.1526 & 0.1413 & -0.4592 \\ -0.0093 & -1.3443 & 0.4585 & 5.0377 \end{bmatrix}^T, \quad (48)$$

$$K = \begin{bmatrix} 0.0401 & 0.0083 & 0 & 0 \\ 0 & 0 & 0.0395 & 0.0084 \end{bmatrix}.$$

FIGURE 2: Trajectory of y_1 without NPC compensation.FIGURE 3: Trajectory of y_1 with NPC compensation.

In the simulation, the system model for the plant and the initial condition are chosen to be

$$A + \Delta A = \begin{bmatrix} 1.0000 & 0.0627 & 0 & 0 \\ 0 & 0.3613 & 0 & 0 \\ 0 & 0 & 1.0000 & 0.0636 \\ 0 & 0 & 0 & 0.3731 \end{bmatrix},$$

$$B + \Delta B = \begin{bmatrix} 2.1060 & 0 \\ 33.0988 & 0 \\ 0 & 2.1313 \\ 0 & 36.6922 \end{bmatrix}, \quad (49)$$

$$x(0) = [0.8 \ 0.8 \ 1 \ 1].$$

We can see from the structure of the system matrices that y_1 and y_2 are independent of each other. It is assumed that there are 2 forward channels for the system and that y_1 and y_2 are transmitted via channels 1 and 2, respectively.

First, the effects of NPC for uncertain NCSs with delays in the forward channels are considered. Let the delays in both channel 1 and channel 2 be equal and constant and see the system performance. Take y_1 for example, as shown in Figure 2; the system performance becomes worse with larger delay and the system is unstable with more than 6 steps delays. The trajectory of y_1 with NPC is shown in Figure 3, from which we can see that the delays are effectively compensated. By applying Theorem 3, the closed-loop NPC system is still stable with 10 steps delay.

Then, we consider the effectiveness of the modified NPC with distributed delays and packet dropouts. In this simulation of constant case, the delays in channel 1 and channel 2 are chosen to be 4 steps and 3 steps, respectively. By Theorem 3 it can be obtained that the corresponding closed-loop system is stable. From the analysis, it can be inferred that the trajectory of y_1 will be the same by using modified and

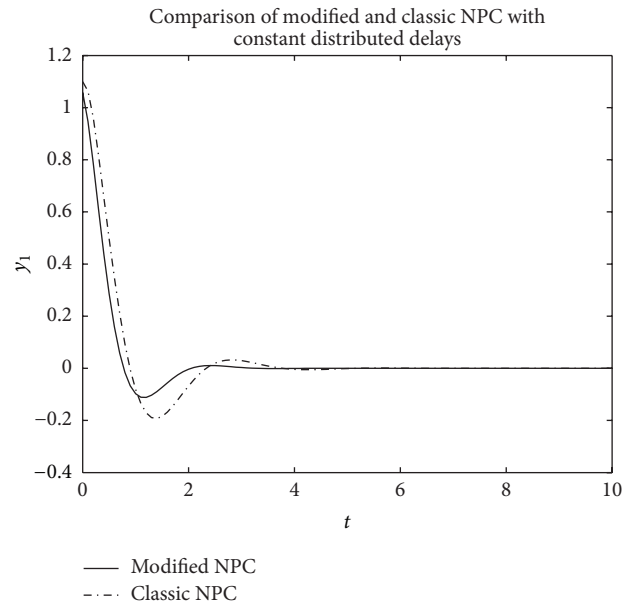


FIGURE 4: Comparison of modified and classic NPC with distributed constant delays.

classic NPC since the delay in channel 1 is always the largest. While the performance of y_2 will be better by using modified NPC than classic one. Figure 4 show the trajectory of y_2 with modified and classic NPC, supporting the theory.

Finally, the case of random distributed delays and packet dropouts is simulated. n_d and n_p are chosen to be 4 and 2, respectively. That is to say, the delays in channels 1 and 2 are both random between 1 step and 4 steps, and the number of consecutive packet dropouts in both channels is up to 2 steps. By Theorem 2, it follows that the closed-loop system is

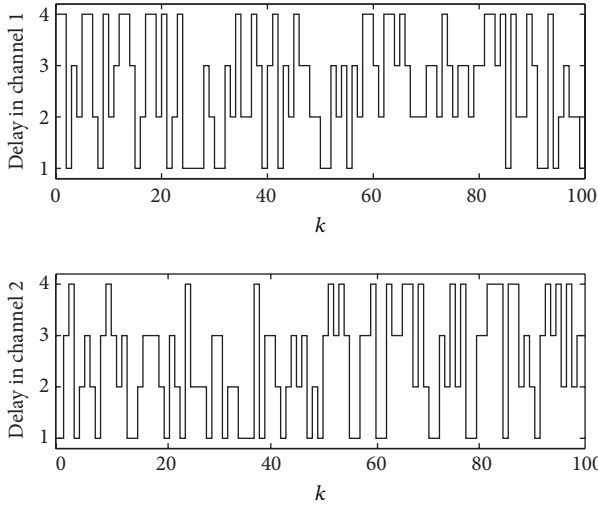


FIGURE 5: Random distributed delays.

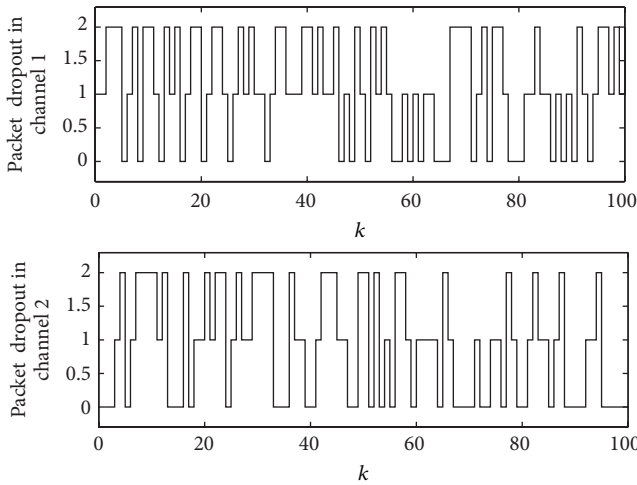


FIGURE 6: Random distributed packet dropouts process.

stable. The simulated distributed random delays and packet dropouts process are shown in Figures 5 and 6, respectively. The corresponding trajectories of y_1 and y_2 are shown in Figures 7 and 8, respectively. Clearly, we can see that the modified NPC achieves better performance than classic NPC method for this example.

5. Conclusions

This paper studied the design and stability analysis of uncertain networked predictive control systems with distributed delays and packet dropouts in the forward channels. A modified NPC was proposed, in which the key point is an improved control signal selection scheme. The CSS with distributed prediction length uses the most recent data and hence can make modified NPC achieve better control performance. Stability analysis results are obtained for both constant and random cases. They are formulated as linear matrix inequalities and can be readily checked. Moreover, it is shown

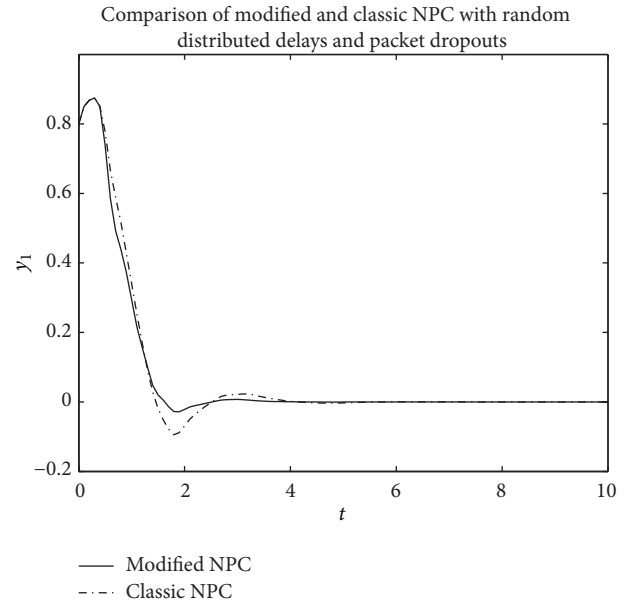


FIGURE 7: Trajectory of y_1 with modified and classic NPC with distributed random delays and packet dropouts.

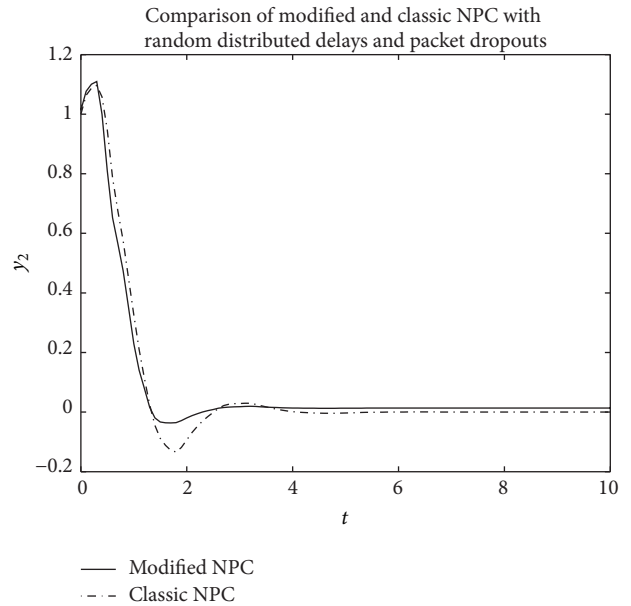


FIGURE 8: Trajectory of y_2 of modified and classic NPC with distributed random delays and packet dropouts.

that the stability of the closed-loop NPC system is not related to the distributed delays when they are constant and system model is accurate. An example was given to show that the modified NPC method achieves better performance than classic NPC in the case of distributed delays and packet dropouts in the forward channels.

Conflict of Interests

The author declares that there is no conflict of interests regarding the publication of this paper.

Acknowledgments

This research work was supported by the National Nature Science Foundation of China (Grant no. 61304040) and the Nature Science Foundation of Zhejiang Province (Grant no. LQ13F030005).

References

- [1] W. Zhang, M. S. Branicky, and S. M. Philips, "Stability of networked control systems," *IEEE Control Systems Magazine*, vol. 21, no. 1, pp. 84–99, 2001.
- [2] L. X. Zhang, H. J. Gao, and O. Kaynak, "Network-induced constraints in networked control systems—a survey," *IEEE Transactions on Industrial Informatics*, vol. 9, no. 1, pp. 403–416, 2013.
- [3] H. Gao, T. Chen, and J. Lam, "A new delay system approach to network-based control," *Automatica*, vol. 44, no. 1, pp. 39–52, 2008.
- [4] H. Yan, H. Shi, H. Zhang, and F. Yang, "Quantized H_∞ control for networked systems with communication constraints," *Asian Journal of Control*, vol. 15, no. 5, pp. 1468–1476, 2013.
- [5] J. P. Hespanha, P. Naghshabrizi, and Y. Xu, "A survey of recent results in networked control systems," *Proceedings of the IEEE*, vol. 95, no. 1, pp. 138–172, 2007.
- [6] Y.-G. Sun and Q.-Z. Gao, "Stability and stabilization of networked control system with forward and backward random time delays," *Mathematical Problems in Engineering*, vol. 2012, Article ID 834643, 15 pages, 2012.
- [7] H. Zhang, H. Yan, F. Yang, and Q. Chen, "Quantized control design for impulsive fuzzy networked systems," *IEEE Transactions on Fuzzy Systems*, vol. 19, no. 6, pp. 1153–1162, 2011.
- [8] D. Zhang, Q. G. Wang, L. Yu, and Q. K. Shao, " H_∞ filtering for networked systems with multiple time-varying transmissions and random packet dropouts," *IEEE Transactions on Industrial Informatics*, vol. 9, no. 3, pp. 1705–1716, 2013.
- [9] B. Chen, L. Yu, and W.-A. Zhang, "Robust Kalman filtering for uncertain state delay systems with random observation delays and missing measurements," *IET Control Theory & Applications*, vol. 5, no. 17, pp. 1945–1954, 2011.
- [10] H. Zhang, Q. Chen, H. Yan, and J. Liu, "Robust H_∞ filtering for switched stochastic system with missing measurements," *IEEE Transactions on Signal Processing*, vol. 57, no. 9, pp. 3466–3474, 2009.
- [11] D. Yue, E. Tian, and Q.-L. Han, "A delay system method for designing event-triggered controllers of networked control systems," *IEEE Transactions on Automatic Control*, vol. 58, no. 2, pp. 475–481, 2013.
- [12] H. Yan, Z. Su, H. Zhang, and F. Yang, "Observer-based H_∞ control for discrete-time stochastic systems with quantisation and random communication delays," *IET Control Theory & Applications*, vol. 7, no. 3, pp. 372–379, 2013.
- [13] L. Zhang, Y. Shi, T. Chen, and B. Huang, "A new method for stabilization of networked control systems with random delays," *IEEE Transactions on Automatic Control*, vol. 50, no. 8, pp. 1177–1181, 2005.
- [14] M. C. F. Donkers, W. P. M. H. Heemels, N. van de Wouw, and L. Hetel, "Stability analysis of networked control systems using a switched linear systems approach," *IEEE Transactions on Automatic Control*, vol. 56, no. 9, pp. 2101–2115, 2011.
- [15] W.-A. Zhang and L. Yu, "A robust control approach to stabilization of networked control systems with time-varying delays," *Automatica*, vol. 45, no. 10, pp. 2440–2445, 2009.
- [16] M. Yu, L. Wang, T. Chu, and G. Xie, "Stabilization of networked control systems with data packet dropout and network delays via switching system approach," in *Proceedings of the 43rd IEEE Conference on Decision and Control (CDC '04)*, pp. 3539–3544, Paradise Island, Bahamas, December 2004.
- [17] P. Seiler and R. Sengupta, "An H_∞ approach to networked control," *IEEE Transactions on Automatic Control*, vol. 50, no. 3, pp. 356–364, 2005.
- [18] G. P. Liu, J. X. Mu, D. Rees, and S. C. Chai, "Design and stability analysis of networked control systems with random communication time delay using the modified MPC," *International Journal of Control*, vol. 79, no. 4, pp. 288–297, 2006.
- [19] G.-P. Liu, Y. Xia, J. Chen, D. Rees, and W. Hu, "Networked predictive control of systems with random network delays in both forward and feedback channels," *IEEE Transactions on Industrial Electronics*, vol. 54, no. 3, pp. 1282–1297, 2007.
- [20] G. P. Liu, "Predictive controller design of networked systems with communication delays and data loss," *IEEE Transactions on Circuits and Systems II: Express Briefs*, vol. 57, no. 6, pp. 481–485, 2010.
- [21] W. Hu, G. Liu, and D. Rees, "Event-driven networked predictive control," *IEEE Transactions on Industrial Electronics*, vol. 54, no. 3, pp. 1603–1613, 2007.
- [22] R. Wang, G.-P. Liu, W. Wang, D. Rees, and Y.-B. Zhao, " H_∞ control for networked predictive control systems based on the switched Lyapunov function method," *IEEE Transactions on Industrial Electronics*, vol. 57, no. 10, pp. 3565–3571, 2010.
- [23] J. H. Zhang, Y. Q. Xia, and P. Shi, "Design and stability analysis of networked predictive control systems," *IEEE Transactions on Control Systems and Technology*, vol. 21, no. 4, pp. 1495–1501, 2013.
- [24] Y. Xia, W. Xie, B. Liu, and X. Wang, "Data-driven predictive control for networked control systems," *Information Sciences*, vol. 235, pp. 45–54, 2013.
- [25] G. Pin and T. Parisini, "Networked predictive control of uncertain constrained nonlinear systems: recursive feasibility and input-to-state stability analysis," *IEEE Transactions on Automatic Control*, vol. 56, no. 1, pp. 72–87, 2011.
- [26] A. Onat, T. Naskali, E. Parlakay, and O. Mutluer, "Control over imperfect networks: model-based predictive networked control systems," *IEEE Transactions on Industrial Electronics*, vol. 58, no. 3, pp. 905–913, 2011.
- [27] Y.-B. Zhao, J. Kim, and G.-P. Liu, "Error bounded sensing for packet-based networked control systems," *IEEE Transactions on Industrial Electronics*, vol. 58, no. 5, pp. 1980–1989, 2011.
- [28] Y.-B. Zhao, J. Kim, X.-M. Sun, and G.-P. Liu, "On the delay effects of different channels in Internet-based networked control systems," *International Journal of Systems Science*, vol. 44, no. 11, pp. 2119–2129, 2013.
- [29] H. B. Song, G. P. Liu, and L. Yu, "Networked predictive control of uncertain systems with multiple feedback channels," *IEEE Transactions on Industrial Electronics*, vol. 60, no. 11, pp. 5228–5238, 2013.

- [30] G.-P. Liu, "Analysis of networked predictive control systems with uncertainties," in *Proceedings of the IEEE International Conference on Systems, Man and Cybernetics (SMC '09)*, pp. 4819–4824, San Antonio, Tex, USA, October 2009.
- [31] Y. B. Zhao, J. Kim, G. H. Yang, and G. P. Liu, "Model-based compensation for multi-packet transmission in networked control systems," in *Proceedings of the 50th IEEE Conference on Decision and Control and European Control Conference*, pp. 3136–3141, Orlando, Fla, USA, December 2011.
- [32] R. Luck and A. Ray, "An observer-based compensator for distributed delays," *Automatica*, vol. 26, no. 5, pp. 903–908, 1990.
- [33] S. Boyd, L. El Ghaoui, E. Feron, and V. Balakrishnan, *Linear Matrix Inequalities in System and Control Theory*, vol. 15 of *SIAM Studies in Applied Mathematics*, SIAM, Philadelphia, Pa, USA, 1994.
- [34] F.-L. Lian, J. Moyne, and D. Tilbury, "Modelling and optimal controller design of networked control systems with multiple delays," *International Journal of Control*, vol. 76, no. 6, pp. 591–606, 2003.

Research Article

Fault Detection for Network Control Systems with Multiple Communication Delays and Stochastic Missing Measurements

Jie Zhang,¹ Ming Lyu,² Hamid Reza Karimi,³ Jian Zuo,¹ and Yuming Bo¹

¹ School of Automation, Nanjing University of Science & Technology, Nanjing 210094, China

² Information Overall Department, North Information Control Group Co., Ltd., Nanjing 211153, China

³ Department of Engineering, Faculty of Engineering and Science, University of Agder, 4898 Grimstad, Norway

Correspondence should be addressed to Jie Zhang; zhangjie.njust@gmail.com

Received 2 January 2014; Accepted 3 March 2014; Published 1 April 2014

Academic Editor: Xudong Zhao

Copyright © 2014 Jie Zhang et al. This is an open access article distributed under the Creative Commons Attribution License, which permits unrestricted use, distribution, and reproduction in any medium, provided the original work is properly cited.

This paper is concerned with fault detection problem for a class of network control systems (NCSs) with multiple communication delays and stochastic missing measurements. The missing measurement phenomenon occurs in a random way and the occurrence probability for each measurement output is governed by an individual random variable. Besides, the multiple communication delay phenomenon reflects that networked control systems have different communication delays when the signals are transferred via different channels. We aim to design a fault detection filter so that the overall fault detection dynamics is exponentially stable in the mean square. By constructing proper Lyapunov-Krasovskii functional, we acquire sufficient conditions to guarantee the stability of the fault detection filter for the discrete systems, and the filter parameters are also derived by solving linear matrix inequality. Finally, an illustrative example is provided to show the usefulness and effectiveness of the proposed design method.

1. Introduction

Over the past few decades, the fault detection problem has been attracting extensive research attention from scholars [1–6]. In a fault detection progress, we aim to construct a residual signal and compute a residual evaluation function which can then be compared with a predefined threshold; if the residual exceeds the threshold we set, then the fault is detected and an alarm of fault is generated. In many industrial applications, various filter schemes have been proposed recently for systems which assume that the measurements always contain a true signal. However, systems may exhibit process and measurement noise inputs. One approach to this problem is \mathcal{H}_∞ filtering, and the advantage of this approach is that the noise signals in the \mathcal{H}_∞ filtering setting are arbitrary signals with bounded energy, and no exact statistics are required to be known. So, \mathcal{H}_∞ filter has been widely applied to many actual systems due to its high accuracy and robustness [7–13].

Considering the fault detection problem in a class of networked control systems, some new problems have merged

out [14–16]. Communication delays and missing measurements are important issues in NCSs. Some existing literatures assume that measurement signal is completely lost. In fact, there often may be a part of the measurement information loss, and each individual sensor may also have different data loss probability [17–24]. For example, in [21], a model of multiple missing measurements has been presented by using a diagonal matrix to account for the different missing probability for individual sensors. The finite-horizon robust filtering problem has been considered in [22] for discrete-time stochastic systems with probabilistic missing measurements subject to norm-bounded parameter uncertainties. A Markovian jumping process has been employed in [23] to reflect the measurement missing problem. Moreover, the optimal filter design problem has been tackled in [24] for systems with multiple packet dropouts by solving a recursive difference equation (RDE). In addition, the presence of communication delays not only reduces relative stability and robustness but also degrades the performance. So far, many researchers have studied the stability and controller design

problems for networked systems in the presence of communication delays [25–33].

Summarizing the above discussion, in this paper, we are motivated to study the fault detection problem for a class of network control systems with multiple communication delays and stochastic missing measurements. A fault detection filter is constructed through the establishment of the existing model; then the addressed fault detection problem is converted into an auxiliary \mathcal{H}_∞ filtering problem. Sufficient conditions are established for the existence of the fault detection filter, and then the corresponding solvability conditions for the desired filter gains are established. In the end, a practical simulation example is given to show the effectiveness of the proposed method. The main contributions of this paper can be listed as follows. (1) A model is proposed to describe multiple communication delays, and randomly occurring packet dropout phenomenon is also considered. (2) The \mathcal{H}_∞ performance requirement and the fault detection specification can be obtained by employing stochastic analysis technique. (3) Sufficient conditions are established under which the augmented system is exponentially mean-square stable and satisfies the performance constraint for all nonzero exogenous disturbances under zero-initial condition.

Notation. The notation used in the paper is fairly standard. \mathbb{R}^n , $\mathbb{R}^{n \times m}$, and \mathbb{Z} (\mathbb{Z}^+ , \mathbb{Z}^-) denote, respectively, the n -dimensional Euclidean space, the set of all $n \times m$ real matrices, and the set of integers (nonnegative integers, negative integers). The notation $\|A\|$ refers to the norm of a matrix A defined by $\|A\| = \sqrt{\text{tr}(A^T A)}$. 0 represents zero matrix of compatible dimensions. The n -dimensional identity matrix is denoted as I_n or simply I , if no confusion is caused. The notation $P > 0$ means that P is real symmetric and positive definite. M^T represents the transpose of the matrix M . $\text{diag}\{\dots\}$ stands for a block-diagonal matrix. $\mathbb{E}\{x\}$ and $\mathbb{E}\{x | y\}$ will, respectively, mean expectation of the stochastic variable x and expectation of x conditional on y . $*$ is used as an ellipsis for terms induced by symmetry in symmetric block matrices. Matrices, if their dimensions are not explicitly stated, are assumed to be compatible for algebraic operations.

2. Problem Formulation

In this paper, we consider the fault detection problem for a class of network control systems with multiple communication delays and stochastic missing measurements; then a NCS model can be represented by the following dynamic model:

$$\begin{aligned} x(k+1) &= (A + \Delta A)x(k) \\ &+ \sum_{m=1}^N (A_d + \Delta A_d)x(k-m) \\ &+ D_1\omega(k) + E_f f(k), \\ \bar{y}(k) &= Cx(k) + D_2\omega(k), \\ x(k) &= \psi(k) \quad \forall k \in \mathbb{Z}^-, \end{aligned} \quad (1)$$

where $x(k) \in \mathbb{R}^{n_x}$ represents the state vector, $x(k-m) \in \mathbb{R}^{n_x}$ denotes the state delay of the system, and $\omega(k) \in \mathbb{R}^{n_\omega}$ denotes the unknown disturbance, while $f(k) \in \mathbb{R}^{n_f}$ is the fault of the system. $\bar{y}(k) \in \mathbb{R}^{n_y}$ denotes the system progress output. $\psi(k)$ ($k \in \mathbb{Z}^-$) is given random initial conditions satisfying $\sup_{k \in \mathbb{Z}^-} \mathbb{E}\{\|\psi(k)\|^2\} < \infty$. ΔA and ΔA_d are internal perturbation arising from uncertain factors A and A_d . A , A_d , D_1 , E_f , C , and D_2 are known real matrices with appropriate dimensions. Besides, the real-valued matrices ΔA and ΔA_d represent the norm-bounded parameter uncertainties of the following structure:

$$[\Delta A \quad \Delta A_d] = H_a F(k) [E_a \quad E_d], \quad (2)$$

where H_a , E_a , and E_d are known constant matrices with appropriate dimensions, and $F(k)$ is an unknown matrix function satisfying

$$F^T(k) F(k) \leq I. \quad (3)$$

Then, we model the missing measurements via a diagonal matrix consisting of a series of mutually independent random variables satisfying certain probabilistic distributions on the interval $[0 \ 1]$. So, the multiple missing measurements are described by

$$\begin{aligned} y(k) &= \Xi Cx(k) + D_2\omega(k) \\ &= \sum_{j=1}^r \beta_j C_j x(k) + D_2\omega(k), \end{aligned} \quad (4)$$

where $y(k) \in \mathbb{R}^{n_y}$ is the actual measurement signal output, and $\Xi = \text{diag}\{\beta_1, \dots, \beta_r\}$, β_j ($j = 1, \dots, r$) are a series of mutually independent random variables; it is assumed that β_j has the probabilistic density function $q_j(S)$ ($j = 1, \dots, r$) on the interval $[0 \ 1]$ with mathematical expectation u_j and variance σ_j^2 . C_j is defined by

$$C_j = \text{diag} \left\{ \underbrace{0, \dots, 0}_{j-1}, 1, \underbrace{0, \dots, 0}_{r-j} \right\} C. \quad (5)$$

For presentation convenience, we denote

$$\bar{\Xi} = \mathbb{E}\{\Xi\}, \quad \tilde{\Xi} = \Xi - \bar{\Xi}. \quad (6)$$

Remark 1. Because missing measurements in system occur in a stochastic way, β_j is the probabilistic missing statue of the j th sensor and can take value on the interval $[0 \ 1]$. In addition, for every sensor, their probability to take different values may differ from each other, which reflects stochastic character of the multiple missing measurements in system model.

Then, we can easily describe a NCS model with multiple communication delays and stochastic missing measurements as

$$\begin{aligned} x(k+1) &= (A + \Delta A)x(k) \\ &+ \sum_{m=1}^N (A_d + \Delta A_d)x(k-m) \\ &+ D_1\omega(k) + E_f f(k), \\ y(k) &= \Xi Cx(k) + D_2\omega(k), \\ x(k) &= \psi(k) \quad \forall k \in Z^-. \end{aligned} \quad (7)$$

The key step of fault detection schemes is the construction of a dynamic system called a fault detection observer or filter, in which the residual signal is generated in order to decide whether a fault has occurred or not. In this paper, according to the above formula, we build a fault detection filter whose model can be described as follows:

$$\begin{aligned} \hat{x}(k+1) &= A_f \hat{x}(k) + B_f y(k), \\ r(k) &= C_f \hat{x}(k) + D_f y(k), \end{aligned} \quad (8)$$

where $\hat{x}(k) \in \mathbb{R}^{n_x}$ represents the filter state vector, $r(k) \in \mathbb{R}^{n_r}$ is the so-called residual that is compatible with the fault vector $f(k)$, and A_f , B_f , C_f , and D_f are appropriately dimensioned filter matrices to be determined. We set the following variables:

$$\begin{aligned} e(k) &= r(k) - f(k), \\ \eta(k) &= [x^T(k) \quad \hat{x}^T(k)]^T, \\ \nu(k) &= [\omega^T(k) \quad f^T(k)]^T. \end{aligned} \quad (9)$$

Then, we can get the overall fault detection dynamics governed by the following system:

$$\eta(k+1) = (\bar{A} + \hat{A})\eta(k) + \sum_{m=1}^N \bar{A}_d \eta(k-m) + \bar{B}\nu(k), \quad (10)$$

$$e(k) = r(k) - f(k) = (\bar{C} + \hat{C})\eta(k) + \bar{D}\nu(k),$$

where

$$\begin{aligned} \bar{A} &= \begin{bmatrix} A + \Delta A & 0 \\ B_f \Xi C & A_f \end{bmatrix}, & \hat{A} &= \begin{bmatrix} 0 & 0 \\ B_f \Xi C & 0 \end{bmatrix}, \\ \bar{A}_d &= \text{diag}\{A_d + \Delta A_d, 0\}, \\ \bar{B} &= \begin{bmatrix} D_1 & E_f \\ B_f D_2 & 0 \end{bmatrix}, & \bar{C} &= [D_f \Xi C \quad C_f], \\ \hat{C} &= [D_f \Xi C \quad 0], & \bar{D} &= [D_f D_2 \quad -I]. \end{aligned} \quad (11)$$

Remark 2. There is a big probability of the existence of errors between theoretical and practical systems due to unexpected

factors in NCSs. In order to overcome this phenomenon, it is natural to assume system uncertainties. In this paper, we assume that the uncertainties occur on not only regular item of the system but also time-delay item. Therefore, this is a more general description for the NCSs.

The main purpose of this paper is to design a fault detection filter such that the overall fault detection dynamics is exponentially stable in the mean square and, at the same time, the error between the residual signal and the fault signal is made as small as possible. Until now, the fault detection problem to be addressed in this paper can be described by the following two steps.

Step 1. For system (7), we construct a fault detection filter as the model of (8); then we can obtain the residual signal $r(k)$. Furthermore, the filter is designed so that the overall fault detection system (10) is exponentially mean-square stable with the following \mathcal{H}_∞ performance constraint under zero-initial condition:

$$\sum_{k=0}^{\infty} \mathbb{E} \{\|e(k)\|^2\} \leq \gamma^2 \sum_{k=0}^{\infty} \|v(k)\|^2, \quad (12)$$

where $v(k) \neq 0$, and $\gamma > 0$ is made as small as possible.

Step 2. We set up a fault detection measure to judge whether a fault occurs. In this paper, we adopt two variables: an evaluation function $J(k)$ and a threshold J_{th} . The faults can be detected by comparing these two variables:

$$J(k) = \left\{ \sum_{k=s-\mathcal{L}}^{k=s} r^T(k) r(k) \right\}^{1/2}, \quad J_{\text{th}} = \sup_{w \in \mathcal{L}_2, f=0} \mathbb{E} \{J(k)\}, \quad (13)$$

where \mathcal{L} denotes the length of the finite evaluating time horizon. Based on (13), the occurrence of faults can be detected by comparing $J(k)$ with J_{th} according to the following rule:

$$\begin{aligned} J(k) > J_{\text{th}} &\implies \text{with faults} \implies \text{alarm}, \\ J(k) \leq J_{\text{th}} &\implies \text{no faults}. \end{aligned} \quad (14)$$

3. Main Results

First of all, let us introduce the following lemmas which will be used in deriving our main results.

Lemma 3 (Schur complement). *Given constant matrices S_1 , S_2 , S_3 , where $S_1 = S_1^T$ and $0 < S_2 = S_2^T$, then $S_1 + S_3^T S_2^{-1} S_3 < 0$ if and only if*

$$\begin{bmatrix} S_1 & S_3^T \\ S_3 & -S_2 \end{bmatrix} < 0 \quad \text{or} \quad \begin{bmatrix} -S_2 & S_3 \\ S_3^T & S_1 \end{bmatrix} < 0. \quad (15)$$

Lemma 4 (S-procedure). *Let $N = N^T$, H and E be real matrices with appropriate dimensions, and let $F^T(k)F(k) \leq I$. Then, the inequality $N + HFE + (HFE)^T < 0$ if and only if there*

exists a positive scalar ε such that $N + \varepsilon HH^T + \varepsilon^{-1} E^T E < 0$ or, equivalently,

$$\begin{bmatrix} N & \varepsilon H & E^T \\ \varepsilon H^T & -\varepsilon I & 0 \\ E & 0 & -\varepsilon I \end{bmatrix} < 0. \quad (16)$$

For convenience of presentation, we first discuss the nominal system without parameter uncertainties ΔA and ΔA_d in Theorems 5 and 6 and will eventually extend our main results to the general case in Theorem 7. Therefore, in Theorems 5 and 6, we redefine \bar{A} and \bar{A}_d as

$$\bar{A} = \begin{bmatrix} A & 0 \\ B_f \bar{E} C & A_f \end{bmatrix}, \quad \bar{A}_d = \text{diag}\{A_d, 0\}. \quad (17)$$

Theorem 5. Consider the nominal system model (10) and suppose that the filter parameters are given. The nominal fault detection filter (8) is exponentially mean-square stable with a disturbance attenuation level $\gamma > 0$, if there exist matrices $P > 0$, $Q_k > 0$ ($k = 1, 2, \dots, N$) satisfying

$$\Psi^T \check{P} \Psi + \widehat{\Psi}^T \check{P} \widehat{\Psi} + \bar{P} < 0, \quad (18)$$

where

$$\begin{aligned} \bar{Z} &= \underbrace{[\bar{A}_d \ \cdots \ \bar{A}_d]}_N, & \widehat{C}_j &= [D_f C_j \ 0], \\ \bar{\mathcal{A}} &= [\bar{A} \ \bar{Z} \ \bar{B}], & \mathcal{E}_m &= [\bar{C} \ 0 \ \bar{D}], \\ \Psi &= [\bar{\mathcal{A}}^T \ \mathcal{E}_m^T]^T, & \check{\mathcal{A}} &= \left[\sum_{j=1}^m \sigma_j \widehat{A}_j \ 0 \ 0 \right], \\ \check{\mathcal{E}} &= \left[\sum_{j=1}^m \sigma_j \widehat{C}_j \ 0 \ 0 \right], & \widehat{\Psi} &= [\check{\mathcal{A}}^T \ \check{\mathcal{E}}^T]^T, \\ \check{P} &= \text{diag}\{P, I\}, & \mathcal{F} &= \text{diag}\{-Q_1, \dots, -Q_N\}, \\ \bar{Q}_k &= \sum_{k=1}^N Q_k - P, & \widehat{P} &= \text{diag}\{\bar{Q}_k, \mathcal{F}\}, \\ \bar{P} &= \text{diag}\{\widehat{P}, -\gamma^2 I\}. \end{aligned} \quad (19)$$

Proof. Choose a Lyapunov functional for system (10):

$$V(k) = V_1(k) + V_2(k), \quad (20)$$

where

$$\begin{aligned} V_1(k) &= \eta^T(k) P \eta(k), \\ V_2(k) &= \sum_{m=1}^N \sum_{i=k-m}^{k-1} \eta^T(i) Q_m \eta(i). \end{aligned} \quad (21)$$

Then, along the trajectory of augmented system (10) with $\nu(k) = 0$, we have

$$\begin{aligned} &\mathbb{E}\{\Delta V_1(k)\} \\ &= \mathbb{E}\left\{ \left[(\bar{A} + \widehat{A}) \eta(k) + \sum_{m=1}^N \bar{A}_d \eta(k-m) + \bar{B} \nu(k) \right]^T P \right. \\ &\quad \times \left[(\bar{A} + \widehat{A}) \eta(k) + \sum_{m=1}^N \bar{A}_d \eta(k-m) + \bar{B} \nu(k) \right] \\ &\quad \left. - \eta(k)^T P \eta(k) \right\}, \\ &\mathbb{E}\{\Delta V_2(k)\} \\ &= \mathbb{E}\left\{ \sum_{m=1}^N \left[\eta^T(k) Q_m \eta(k) - \eta^T(k-m) Q_m \eta(k-m) \right] \right\}. \end{aligned} \quad (22)$$

For notational convenience, we denote

$$\begin{aligned} \eta(k-\tau) &= [\eta^T(k-1) \ \cdots \ \eta^T(k-N)]^T, \\ \widehat{\xi}(k) &= [\eta^T(k) \ \eta^T(k-\tau)]^T, \quad \xi(k) = [\widehat{\xi}^T(k) \ \nu^T(k)]^T, \\ \mathcal{A} &= [\bar{A} \ \bar{Z}], \quad \widehat{\mathcal{A}} = \left[\sum_{j=1}^m \sigma_j \widehat{A}_j \ 0 \right], \quad \widehat{A}_j = \begin{bmatrix} 0 & 0 \\ B_f C_j & 0 \end{bmatrix}. \end{aligned} \quad (23)$$

In the following, we first prove the exponential stability of the fault detection dynamics system (10) with $\nu(k) = 0$. Therefore, we can easily have

$$\mathbb{E}\{\Delta V(k)\} \leq \mathbb{E}\left\{ \widehat{\xi}^T(k) \left(\mathcal{A}^T P \mathcal{A} + \widehat{\mathcal{A}}^T P \widehat{\mathcal{A}} + \widehat{P} \right) \widehat{\xi}(k) \right\}. \quad (24)$$

By utilizing Schur complement Lemma 3, we know that $\mathbb{E}\{\Delta V(k)\} < 0$ if (18) is true. Furthermore, along the same line of the proof for Theorem 1 in [34], it can be concluded that the discrete-time nominal system of (10) with $\nu(k) = 0$ is exponentially mean-square stable.

Now, we are in a position to deal with the \mathcal{H}_∞ performance of the nominal system of (10). Under zero-initial condition, $J(n)$ can be described as the following forms:

$$\begin{aligned} J(n) &= \mathbb{E} \sum_{k=0}^n \left[e^T(k) e(k) - \gamma^2 \nu^T(k) \nu(k) \right] \\ &\leq \mathbb{E} \sum_{k=0}^n \left[e^T(k) e(k) - \gamma^2 \nu^T(k) \nu(k) + \Delta V(k) \right]. \end{aligned} \quad (25)$$

Then we have

$$J(n) \leq \mathbb{E} \left\{ \sum_{k=0}^n \xi^T(k) \left(\Psi^T \check{P} \Psi + \widehat{\Psi}^T \check{P} \widehat{\Psi} + \bar{P} \right) \xi(k) \right\}. \quad (26)$$

If there exist $P > 0, Q_k > 0$ ($k = 1, 2, \dots, N$) satisfying

$$\Psi^T \check{P} \Psi + \widehat{\Psi}^T \check{P} \widehat{\Psi} + \bar{P} < 0, \quad (27)$$

then we will have $J(n) < 0$ by considering Theorem 5.

Letting $n \rightarrow \infty$, we can obtain

$$\sum_{k=0}^{\infty} \mathbb{E} \{ \|e(k)\|^2 \} \leq \gamma^2 \sum_{k=0}^{\infty} \|v(k)\|^2 \quad (28)$$

which is equivalent to the inequality in (12). To this end, the proof of Theorem 5 is complete. \square

According to the analysis results established, we will deal with the fault detection filter design problem.

Theorem 6. Consider the nominal system model (10), and let $\gamma > 0$ be a given constant scalar which represents \mathcal{H}_∞ noise attenuation level bound. The desired full-order fault detection filter of form (8) exists if there exist matrices $P > 0, Q_k > 0$, ($k = 1, 2, \dots, N$), X , and K satisfying

$$\Omega = \begin{bmatrix} \bar{P} & * \\ \Gamma & -\check{\mathcal{P}} \end{bmatrix} < 0, \quad (29)$$

where

$$\begin{aligned} \Gamma_{11} &= \begin{bmatrix} P\widehat{A}_0 + X\widehat{R}_1 & P\bar{Z} \\ K\widehat{R}_1 & 0 \end{bmatrix}, & \Gamma_{12} &= \begin{bmatrix} P\bar{B}_0 + X\widehat{R}_2 \\ \widehat{E}_0 + K\widehat{R}_2 \end{bmatrix}, \\ \Gamma_{21} &= \begin{bmatrix} X\widehat{R}_4 & 0 \\ K\widehat{R}_4 & 0 \end{bmatrix}, & \widehat{R}_1 &= \begin{bmatrix} 0 & I \\ \bar{\bar{E}}C & 0 \end{bmatrix}, \\ \Gamma &= \begin{bmatrix} \Gamma_{11} & \Gamma_{12} \\ \Gamma_{21} & 0 \end{bmatrix}, & \widehat{A}_0 &= \begin{bmatrix} A & 0 \\ 0 & 0 \end{bmatrix}, \\ \bar{B}_0 &= \begin{bmatrix} D_1 & E_f \\ 0 & 0 \end{bmatrix}, & \widehat{R}_2 &= \begin{bmatrix} 0 & 0 \\ D_2 & 0 \end{bmatrix}, \\ \widehat{R}_4 &= \begin{bmatrix} 0 & 0 \\ \sum_{j=1}^m \sigma_j C_j & 0 \end{bmatrix}, & \widehat{E}_0 &= [0 \quad -I], \\ \widehat{E} &= [0 \quad I]^T, & \check{\mathcal{P}} &= I_2 \otimes \check{P}, \end{aligned} \quad (30)$$

and \bar{P} and \check{P} are defined in Theorem 5. Furthermore, if there exist $P > 0, Q_k > 0$, ($k = 1, 2, \dots, N$), X , and K satisfying (29), then the fault detection filter parameters in the form of (8) are given as follows:

$$[A_f \quad B_f] = (\widehat{E}^T P \widehat{E})^{-1} \widehat{E}^T X, \quad [C_f \quad D_f] = K. \quad (31)$$

Proof. First, let us rewrite the parameters in Theorem 5 in the following form:

$$\begin{aligned} \bar{A} &= \widehat{A}_0 + \widehat{E}L\widehat{R}_1, & \sum_{j=1}^m \sigma_j \widehat{A}_j &= \widehat{E}L\widehat{R}_4, \\ \bar{B} &= \bar{B}_0 + \widehat{E}L\widehat{R}_2, \\ \bar{C} &= K\widehat{R}_1, & \sum_{j=1}^m \sigma_j \widehat{C}_j &= K\widehat{R}_4, \\ \bar{D} &= \widehat{E}_0 + K\widehat{R}_2, & L &= [A_f \quad B_f]. \end{aligned} \quad (32)$$

Now, we can rewrite (18) by using Lemma 3 (Schur complement lemma) as follows:

$$\begin{bmatrix} \bar{P} & * \\ \widehat{\Gamma} & -\check{\mathcal{P}}^{-1} \end{bmatrix} < 0, \quad (33)$$

where

$$\begin{aligned} \widehat{\Gamma} &= \begin{bmatrix} \widehat{\Gamma}_{11} & \widehat{\Gamma}_{12} \\ \widehat{\Gamma}_{21} & 0 \end{bmatrix}, & \widehat{\Gamma}_{11} &= \begin{bmatrix} \widehat{A}_0 + \widehat{E}L\widehat{R}_1 & \bar{Z} \\ K\widehat{R}_1 & 0 \end{bmatrix}, \\ \widehat{\Gamma}_{12} &= \begin{bmatrix} \bar{B}_0 + \widehat{E}L\widehat{R}_2 \\ \widehat{E}_0 + K\widehat{R}_2 \end{bmatrix}, & \widehat{\Gamma}_{21} &= \begin{bmatrix} \widehat{E}L\widehat{R}_4 & 0 \\ K\widehat{R}_4 & 0 \end{bmatrix}. \end{aligned} \quad (34)$$

Pre- and postmultiplying inequalities (33) by $\text{diag}\{I, \check{\mathcal{P}}\}$ and letting $X = P\widehat{E}L$, then we can obtain (29) readily. The proof of this theorem is complete. \square

Now, according to previous Theorems 5 and 6, we can do further research about the system with uncertainties described in (7).

Theorem 7. Consider the uncertain fault detection system (10) with parameter uncertainties ΔA and ΔA_d , and let $\gamma > 0$ be a given constant scalar which represents \mathcal{H}_∞ noise attenuation level bound. The desired full-order fault detection filter of form (8) exists if there exist matrices $P > 0, Q_k > 0$, ($k = 1, 2, \dots, N$), X, K , and positive $\varepsilon > 0$ satisfying

$$\begin{bmatrix} \Omega & * & * \\ \bar{H}_a^T & -\varepsilon I & * \\ \varepsilon \bar{E}_a & 0 & -\varepsilon I \end{bmatrix} < 0, \quad (35)$$

where

$$\begin{aligned} \bar{H}_a &= [0 \quad 0 \quad 0 \mid 0 \quad \widehat{H}_a^T \quad 0 \mid 0 \quad 0]^T, \\ \bar{E}_a &= [\widehat{E}_a \quad \widehat{E}_d \quad 0 \mid 0 \quad 0 \mid 0 \quad 0], \\ \widehat{H}_a &= [H_a^T \quad 0]^T, & \widehat{E}_a &= [E_a \quad 0], \\ \widehat{E}_d &= \underbrace{[E_d \quad 0 \quad \dots \quad E_d \quad 0]}_N. \end{aligned} \quad (36)$$

Furthermore, if there exist appropriate matrices $P > 0, Q_k > 0$ ($k = 1, 2, \dots, N$), X , and K satisfying (35), then the fault

detection filter parameters in the form of (8) are given as follows:

$$[A_f \ B_f] = (\widehat{E}^T P \widehat{E})^{-1} \widehat{E}^T X, \quad [C_f \ D_f] = K. \quad (37)$$

Proof. According to result (29) in Theorem 6, we can replace A and A_d in (29) with $A + H_a F(k) E_a$ and $A_d + H_a F(k) E_d$; then we can obtain the following form:

$$\Omega + \overline{H}_a F(k) \overline{E}_a + \overline{E}_a^T F^T(k) \overline{H}_a^T < 0, \quad (38)$$

where the corresponding parameters have been defined in (36). According to Lemma 4, we can easily obtain (35), and the proof is then complete. \square

Remark 8. From Theorem 7, we can know that the fault detection filter is designed such that the overall fault detection dynamics is exponentially stable in the mean square and, at the same time, the error between the residual signal and the fault signal is made as small as possible.

Remark 9. The main results in Theorems 5–7 can be applied to a wide class of network control systems that involve uncertainties, multiple communication delays, and stochastic missing measurements that result typically from networked environments. Sufficient conditions are established for the existence of the desired fault detection filters. The corresponding solvability conditions for the desired filter gains are established, and the explicit expression of such filter matrices is characterized in terms of the solution to a LMI that can be effectively solved.

4. Numerical Example

In this section, we present an illustrative example to demonstrate the effectiveness of the proposed algorithm. Consider the following networked system with multiple communication delays and stochastic missing measurements:

$$\begin{aligned} x(k+1) &= (A + \Delta A) x(k) \\ &+ \sum_{m=1}^N (A_d + \Delta A_d) x(k-m) \\ &+ D_1 \omega(k) + E_f f(k), \\ y(k) &= \Xi C x(k) + D_2 \omega(k), \\ x(k) &= \psi(k) \quad k \in Z^-. \end{aligned} \quad (39)$$

The model parameters are given as follows:

$$\begin{aligned} A &= \begin{bmatrix} 0.6 & 0.2 \\ 0 & 0.7 \end{bmatrix}, & A_d &= \begin{bmatrix} 0.03 & 0 \\ 0.02 & 0.03 \end{bmatrix}, \\ D_1 &= \begin{bmatrix} 0.8 \\ 0.3 \end{bmatrix}, & E_f &= \begin{bmatrix} -1 \\ 0.6 \end{bmatrix}, & H_a &= \begin{bmatrix} 0.2 \\ 0.01 \end{bmatrix}, \end{aligned}$$

$$\begin{aligned} C &= \begin{bmatrix} 0.2 & -0.1 \\ 0.3 & -0.2 \end{bmatrix}, & D_2 &= \begin{bmatrix} 0.6 \\ 0.7 \end{bmatrix}, & \Xi &= \begin{bmatrix} \beta_1 & 0 \\ 0 & \beta_2 \end{bmatrix}, \\ E_a &= [0 \ 2], & E_d &= [0.1 \ 2], & F(k) &= \sin(k); \end{aligned} \quad (40)$$

β_1 and β_2 are independent random variables whose probability density functions $q(\beta_1)$ and $q(\beta_2)$ satisfy

$$q(\beta_1) = \begin{cases} 0 & \beta_1 = 0 \\ 0.1 & \beta_1 = 0.5 \\ 0.9 & \beta_1 = 1, \end{cases} \quad q(\beta_2) = \begin{cases} 0 & \beta_2 = 0 \\ 0.2 & \beta_2 = 0.5 \\ 0.8 & \beta_2 = 1. \end{cases} \quad (41)$$

We can easily get the mathematical expectation and variance of β_1 and β_2 : $u_1 = 0.95$, $u_2 = 0.9$, $\sigma_1 = 0.15$, and $\sigma_2 = 0.2$.

By applying Theorem 7, we can obtain the desired \mathcal{H}_∞ filter parameters as follows:

$$\begin{aligned} A_f &= \begin{bmatrix} -0.2854 & -0.2854 \\ -0.2854 & -0.2854 \end{bmatrix}, & B_f &= \begin{bmatrix} -0.4828 & -0.1696 \\ -0.4828 & -0.1696 \end{bmatrix}, \\ C_f &= [5.2489 \ 5.2489], & D_f &= [-18.6850 \ 4.9809] \end{aligned} \quad (42)$$

with the optimized performance index $\gamma^* = 16.61$.

To further illustrate the effectiveness of the designed fault detection filter, we give a fault signal; for $k = 0, 1, \dots, 150$, let the fault signal $f(k)$ be given as

$$f(k) = \begin{cases} 1, & 50 \leq k \leq 100 \\ 0, & \text{else.} \end{cases} \quad (44)$$

First, we assume our initial conditions as $x(0) = [\pi/8 \ 0]^T$, $\hat{x}(0) = [0 \ 0]^T$, and the external disturbance is $w(k) = 0$. The residual signal $r(k)$ and evolution of residual evaluation function $J(k)$ are shown in Figures 1 and 2, respectively, which indicate that the designed filter can detect the fault effectively when it occurs.

Next, we consider that the disturbance is given by

$$w(k) = \begin{cases} 0.5 \times \text{rand}[0 \ 1], & 30 \leq k \leq 130 \\ 0, & \text{else,} \end{cases} \quad (45)$$

where the rand function generates arrays of random numbers whose elements are uniformly distributed in the interval $[0 \ 1]$. Then, the residual signal $r(k)$ and evolution of residual evaluation function $J(k)$ are shown in Figures 3 and 4. Respectively, it can be seen that the residual can not only reflect the fault in time but also detect the fault without confusing it with the disturbance $w(k)$.

Selecting a threshold as $J_{\text{th}} = \sup_{f(k)=0} \mathbb{E}\{\sum_{k=0}^{200} r^T(k)r(k)\}^{1/2}$ and accordingly obtaining that $J_{\text{th}} = 36.9234$ in Figure 4 represented the Dotted curve after 200 Monte Carlo simulations with no faults. Solid curve represents the residual evaluation of the system. From Figure 4, it can be seen that $36.6700 = J(76) < J_{\text{th}} < J(77) = 37.1069$, which means that the fault can be detected in 27 time steps after its occurrence. From simulation results, it can be clearly observed that the smaller the threshold we obtain, the faster the fault detection will take.

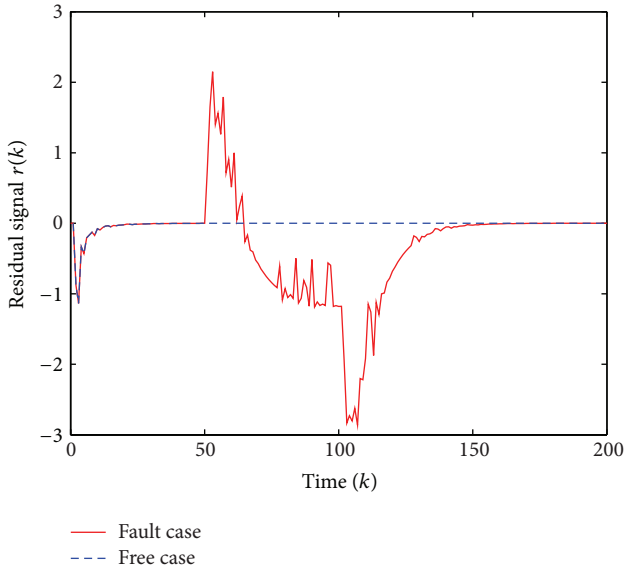


FIGURE 1: Residual signal $r(k)$ without $w(k)$.

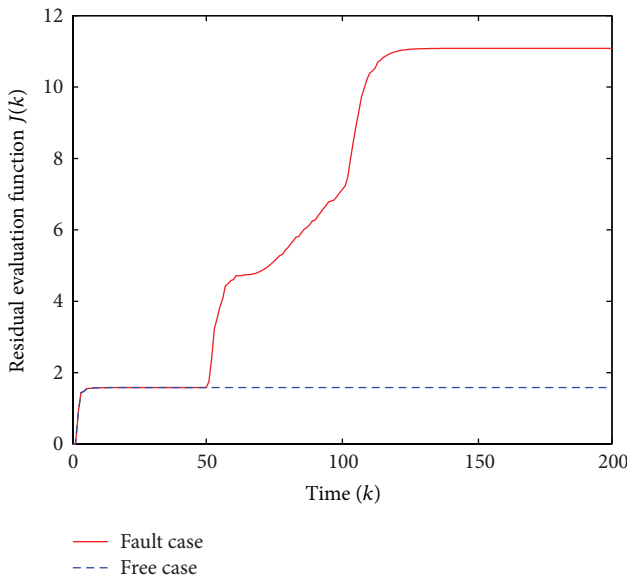


FIGURE 2: Evolution of residual evaluation function $J(k)$ without $w(k)$.

5. Conclusions

In this paper, we have addressed the fault detection problem for a class of network control systems comprising multiple communication delays and stochastic missing measurements. Our purpose is to build up a fault detection filter through an existing model of NCSs such that the overall fault detection dynamics is exponentially stable while preserving a guaranteed performance; at the same time, the error between the residual signal and the fault signal is made as small as possible. At the end, an illustrative simulation example has been given to demonstrate the effectiveness of the fault detection techniques presented in this paper.

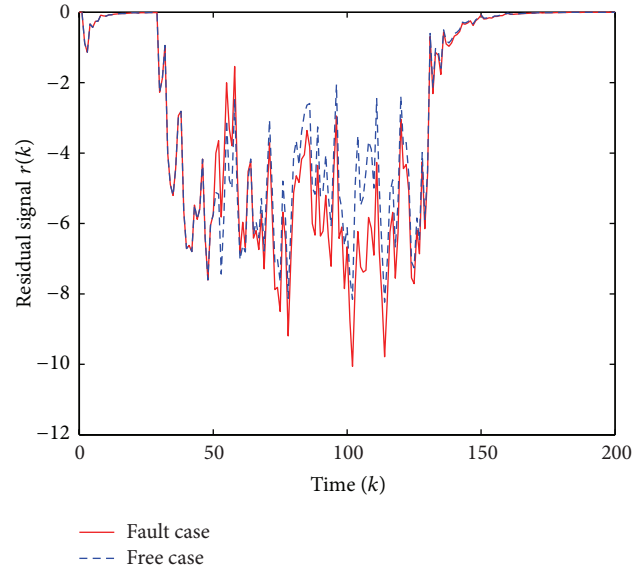


FIGURE 3: Residual signal $r(k)$ with $w(k) = 0.5 \times \text{rand}[0, 1], 30 \leq k \leq 130$.

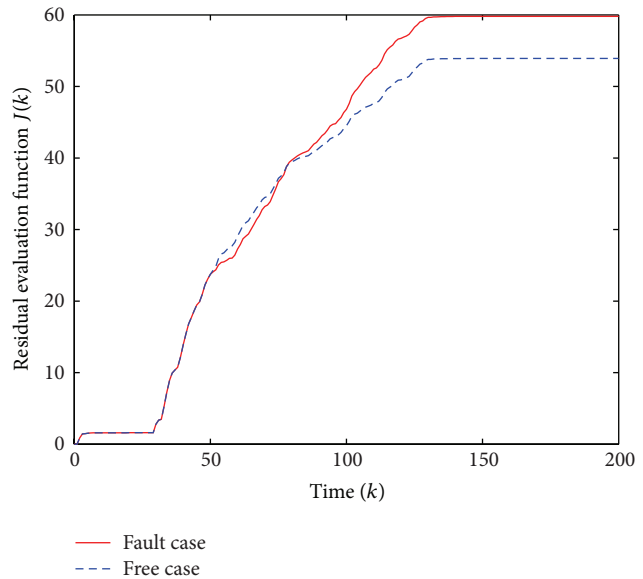


FIGURE 4: Evolution of residual evaluation function $J(k)$ with $w(k) = 0.5 \times \text{rand}[0, 1], 30 \leq k \leq 130$.

Conflict of Interests

The authors declare that there is no conflict of interests regarding the publication of this paper.

Acknowledgments

This work has been supported by the National Natural Science Foundation of China (Grant no. 61104109), the Natural Science Foundation of Jiangsu Province of China (Grant no. BK2011703), the Support of Science and Technology and Independent Innovation Foundation of Jiangsu Province of

China (Grant no. BE2012178), the NUST Outstanding Scholar Supporting Program, and the Doctoral Fund of the Ministry of Education of China (Grant no. 20113219110027).

References

- [1] L. Wu and D. W. C. Ho, "Fuzzy filter design for Itô stochastic systems with application to sensor fault detection," *IEEE Transactions on Fuzzy Systems*, vol. 17, no. 1, pp. 233–242, 2009.
- [2] P. Zhang, S. X. Ding, G. Z. Wang, and D. H. Zhou, "A frequency domain approach to fault detection in sampled-data systems," *Automatica*, vol. 39, no. 7, pp. 1303–1307, 2003.
- [3] Y. Wang, S. X. Ding, H. Ye, and G. Wang, "A new fault detection scheme for networked control systems subject to uncertain time-varying delay," *IEEE Transactions on Signal Processing*, vol. 56, no. 10, pp. 5258–5268, 2008.
- [4] L. Wu, X. Yao, and W. X. Zheng, "Generalized H_2 fault detection for two-dimensional Markovian jump systems," *Automatica*, vol. 48, no. 8, pp. 1741–1750, 2012.
- [5] X. Yao, L. Wu, and W. X. Zheng, "Fault detection filter design for Markovian jump singular systems with intermittent measurements," *IEEE Transactions on Signal Processing*, vol. 59, no. 7, pp. 3099–3109, 2011.
- [6] H. Dong, Z. Wang, J. Lam, and H. Gao, "Fuzzy-model-based robust fault detection with stochastic mixed time delays and successive packet dropouts," *IEEE Transactions on Systems, Man, and Cybernetics B: Cybernetics*, vol. 42, no. 2, pp. 365–376, 2012.
- [7] Q. Ding and M. Zhong, "On designing \mathcal{H}_∞ fault detection filter for Markovian jump linear systems with polytopic uncertainties," *International Journal of Innovative Computing, Information and Control*, vol. 6, no. 3, pp. 995–1004, 2010.
- [8] M. Liu, J. You, and X. Ma, " \mathcal{H}_∞ filtering for sampled-data stochastic systems with limited capacity channel," *Signal Process*, vol. 91, no. 8, pp. 1826–1837, 2011.
- [9] H. Gao and T. Chen, " \mathcal{H}_∞ estimation for uncertain systems with limited communication capacity," *IEEE Transactions on Automatic Control*, vol. 52, no. 11, pp. 2070–2084, 2007.
- [10] M. J. Khosrowjerdi, R. Nikoukhah, and N. Safari-Shad, "A mixed $\mathcal{H}_2/\mathcal{H}_\infty$ approach to simultaneous fault detection and control," *Automatica*, vol. 40, no. 2, pp. 261–267, 2004.
- [11] M. D. S. Aliyu and E. K. Boukas, "Mixed $\mathcal{H}_2/\mathcal{H}_\infty$ nonlinear filtering," *International Journal of Robust and Nonlinear Control*, vol. 19, no. 4, pp. 394–417, 2009.
- [12] Z. Wang, F. Yang, D. W. C. Ho, and X. Liu, "Robust filtering for stochastic time-delay systems with missing measurements," *IEEE Transactions on Signal Processing*, vol. 54, no. 7, pp. 2579–2587, 2006.
- [13] L. Wu, X. Su, and P. Shi, "Mixed $\mathcal{H}_2/\mathcal{H}_\infty$ approach to fault detection of discrete linear repetitive processes," *Journal of the Franklin Institute: Engineering and Applied Mathematics*, vol. 348, no. 2, pp. 393–414, 2011.
- [14] G. Wei, Z. Wang, and H. Shu, "Robust filtering with stochastic nonlinearities and multiple missing measurements," *Automatica*, vol. 45, no. 3, pp. 836–841, 2009.
- [15] F. Yang, Z. Wang, Y. S. Hung, and M. Gani, " \mathcal{H}_∞ control for networked systems with random communication delays," *IEEE Transactions on Automatic Control*, vol. 51, no. 3, pp. 511–518, 2006.
- [16] G.-H. Yang and D. Ye, "Adaptive reliable filtering against sensor failures," *IEEE Transactions on Signal Processing*, vol. 55, no. 7, pp. 3161–3171, 2007.
- [17] G. Chen, "A simple treatment for suboptimal Kalman filtering in case of measurement data missing," *IEEE Transactions on Aerospace and Electronic Systems*, vol. 26, no. 2, pp. 413–415, 1990.
- [18] S. Sun, L. Xie, W. Xiao, and Y. C. Soh, "Optimal linear estimation for systems with multiple packet dropouts," *Automatica*, vol. 44, no. 5, pp. 1333–1342, 2008.
- [19] H. Dong, Z. Wang, and H. Gao, "Distributed filtering for a class of time-varying systems over sensor networks with quantization errors and successive packet dropouts," *IEEE Transactions on Signal Processing*, vol. 60, no. 6, pp. 3164–3173, 2012.
- [20] Z. Wang, H. Dong, B. Shen, and H. Gao, "Finite-horizon H_∞ filtering with missing measurements and quantization effects," *IEEE Transactions on Automatic Control*, vol. 58, no. 7, pp. 1707–1718, 2013.
- [21] G. Wei, Z. Wang, and H. Shu, "Robust filtering with stochastic nonlinearities and multiple missing measurements," *Automatica*, vol. 45, no. 3, pp. 836–841, 2009.
- [22] Z. Wang, F. Yang, D. W. C. Ho, and X. Liu, "Robust finite-horizon filtering for stochastic systems with missing measurements," *IEEE Transactions on Signal Processing*, vol. 12, no. 6, pp. 137–144, 2005.
- [23] P. Shi, M. Mahmoud, S. K. Nguang, and A. Ismail, "Robust filtering for jumping systems with modedependent delays," *Signal Processing*, vol. 86, no. 1, pp. 140–152, 2006.
- [24] S. Sun, L. Xie, and W. Xiao, "Optimal full-order and reduced-order estimators for discrete-time systems with multiple packet dropouts," *IEEE Transactions on Signal Processing*, vol. 56, no. 8, pp. 4031–4038, 2008.
- [25] Y. Wang, S. X. Ding, H. Ye, and G. Wang, "A new fault detection scheme for networked control systems subject to uncertain time-varying delay," *IEEE Transactions on Signal Processing*, vol. 56, no. 10, pp. 5258–5268, 2008.
- [26] X. He, Z. Wang, and D. H. Zhou, "Robust fault detection for networked systems with communication delay and data missing," *Automatica*, vol. 45, no. 11, pp. 2634–2639, 2009.
- [27] Y. Liu, Z. Wang, and W. Wang, "Reliable \mathcal{H}_∞ filtering for discrete time-delay systems with randomly occurred nonlinearities via delay-partitioning method," *Signal Process*, vol. 91, no. 4, pp. 713–727, 2011.
- [28] R. Lu, Y. Xu, and A. Xue, " \mathcal{H}_∞ filtering for singular systems with communication delays," *Signal Process*, vol. 90, no. 4, pp. 1240–1248, 2010.
- [29] X. He, Z. Wang, and D. Zhou, "Robust \mathcal{H}_∞ filtering for networked systems with multiple state delays," *International Journal of Control*, vol. 80, no. 8, pp. 1217–1232, 2007.
- [30] P. Shi, "Robust filtering for uncertain delay systems under sampled measurements," *Signal Process*, vol. 58, no. 2, pp. 131–151, 1997.
- [31] F. O. Hounkpevi and E. E. Yaz, "Minimum variance generalized state estimators for multiple sensors with different delay rates," *Signal Process*, vol. 87, no. 4, pp. 602–613, 2007.
- [32] H. Dong, Z. Wang, and H. Gao, "Distributed H_∞ filtering for a class of Markovian jump nonlinear time-delay systems over lossy sensor networks," *IEEE Transactions on Industrial Electronics*, vol. 60, no. 10, pp. 4665–4672, 2013.

- [33] L. Wu, Z. Feng, and J. Lam, "Stability and synchronization of discrete-time neural networks with switching parameters and time-varying delays," *IEEE Transactions on Neural Networks and Learning Systems*, vol. 24, no. 12, pp. 1957–1972, 2013.
- [34] Z. Wang, D. W. C. Ho, Y. Liu, and X. Liu, "Robust H_∞ control for a class of nonlinear discrete time-delay stochastic systems with missing measurements," *Automatica*, vol. 45, no. 3, pp. 684–691, 2009.

Research Article

Impact of Social Network and Business Model on Innovation Diffusion of Electric Vehicles in China

D. Y. Kong¹ and X. H. Bi²

¹ School of Automotive Studies, Tongji University, Shanghai 201804, China

² School of Economics and Management, Tongji University, Room 262, Building 13, Caoan Road 4800, Jiading District, Shanghai 201804, China

Correspondence should be addressed to X. H. Bi; bixiaohang@sina.com

Received 24 December 2013; Accepted 19 February 2014; Published 26 March 2014

Academic Editor: Huaicheng Yan

Copyright © 2014 D. Y. Kong and X. H. Bi. This is an open access article distributed under the Creative Commons Attribution License, which permits unrestricted use, distribution, and reproduction in any medium, provided the original work is properly cited.

The diffusion of electric vehicles (EVs) involves not only the technological development but also the construction of complex social networks. This paper uses the theory of network control to analyze the influence of network forms on EV diffusion in China, especially focusing on the building of EV business models (BMs) and the resulting effects and control on the diffusion of EVs. The Bass model is adopted to forecast the diffusion process of EVs and genetic algorithm is used to estimate the parameters based on the diffusion data of Hybrid Electric Vehicle (HEV) in the United States and Japan. Two different social network forms and BMs are selected, that is, battery leasing model and vehicle purchasing model, to analyze how different network forms may influence the innovation coefficient and imitation coefficient in the Bass model, which will in turn result in different diffusion results. Thereby, we can find the appropriate network forms and BMs for EVs which is suitable to the local market conditions.

1. Introduction

As a technical innovation, EV has experienced a fluctuating popularity up and down over the last 100 years [1]. In the past 20 years, EVs again began to attract people's attention because of global climate change and increasing shortage of the world's oil resources. Generally speaking, technical innovation is the driving force to industry change but not the only one [2]. It can trigger the change but may not be sufficient to overwhelm the industry's dominant logic [3].

Under the background of industry change, constructing the social network is vital for the success diffusion of innovations [4, 5]. As to the automobile industry, the introduction of EVs is characterized by complex network. The successful diffusion of EVs relies on the integration of multiagent system to form the whole network [6]. The network of multiagent contains charging station operators, car manufacturers, consumers, parts providers, maintenance providers, government, and other organizations. These actors interact with each other and are interdependent, which makes the process and results of diffusion complicated and uncertain.

BM innovation which takes the construction of social network or value network as its core component is the key to break the existing technological lock-in [3]. Different BM may result in different forms of network and generate different economic value. That is to say, constructing social network through BM innovation can achieve the inherent economic value of an innovation [7–9]. A critical prerequisite of a sustainable BM of EV is that each agent in the network can gain benefit. Further, the ability of each agent, such as the fueling infrastructure operators, to benefit from the BM largely depends on the diffusion rate and scale of the EVs. Therefore, study on the relationship between social network, BM innovation, and market diffusion of EVs is critical to the search for the suitable EV BM and promoting innovation diffusion and marketization of EVs.

It is well known that the structure of a social network can favor or impede the diffusion of innovations in the network [10, 11]. Bass model, which is one of the most used diffusion models, describes the process of how new products get adopted in a social network [12, 13]. However, with

TABLE 1: Cumulative sales of HEVs in US.

Year	2000	2001	2002	2003	2004	2005	2006	2007	2008	2009	2010	2011
Sales	9350	20282	36035	47600	84199	209711	252636	352274	312386	290271	274210	268755

Data source: [15].

TABLE 2: Cumulative sales of HEVs in Japan.

Year	1997	1998	1999	2000	2001	2002	2003	2004	2005	2006
Sales	10000	22500	37400	50400	74600	91200	132500	196800	256600	346900

Data source: [16].

the difficulty to access relevant data, existing research on forecasting EV market diffusion is limited [14]. Existing research mostly concentrates on the influence on EV market diffusion by external factors such as price and infrastructure. Taking these factors into consideration, a market forecast model is established based on Bass diffusion model in this paper, analyzing influence by different forms of social networks in different BMs on the coefficient of Bass diffusion model and verifying the accuracy of the forecast model with the case study of Shenzhen.

2. Methodology

Bass model is established mainly on the basis of Rogers' innovation diffusion theory (1962), which defines the innovation diffusion as the process by which an innovation is communicated through certain channels over time among the members of a social system [17]. Communication channels are divided into two categories, public media and word of mouth. Rogers suggests that the adoption of an innovation follows an S curve when plotted over a length of time and adopters can be divided into five categories: innovators, early adopters, early majority, late majority, and laggards. Adoption choices and the time of adoption of the latter 4 categories are all influenced by the internal pressure of the social system, by which the pressure increases with the increase of adopters. Bass classified the latter 4 categories as imitators and established a model on the basis of Rogers' innovation theory, which is the Bass diffusion model. The model is shown as follows [12]:

$$\frac{f(T)}{1-F(T)} = p + \frac{q}{m}Y(T) = p + qF(T), \quad (1)$$

where $f(T)$ is the possibility of adoption choice made by adopters or the proportion rate of adoption in the time T .

$F(T) = \int_0^T f(t)dt$, $F(0) = 0$, and $F(T)$ is the cumulative proportion of adopters in the time between 0 and T ; p is the coefficient of innovation; q is the coefficient of imitation; m is the whole potential adopters of the innovative product; $Y(T)$ is the cumulative number of adopters in the time between 0 and T ; $S(T)$ is the number of adopters at the time of T :

$$Y(T) = \int_0^T S(t) dt = m \int_0^T f(t) dt = mF(T), \quad (2)$$

$$S(T) = mf(T).$$

The following result could be calculated from Formulation (1):

$$S(T) = \frac{m((p+q)^2/p)e^{-(p+q)T}}{(1+(q/p)e^{-(p+q)T})^2}. \quad (3)$$

Existing research on forecasting EV diffusion based on Bass model is limited. One of the important reasons is the difficulty to access relevant data. According to relevant research, forecast on coefficient could be based on the method of judgment, analogy, and so forth [18–22]. The method of judgment is to use external information to estimate parameters, such as information from experts. The method of analogy is to simulate according to diffusion data of analogous products. Besides, some optimization algorithms, such as genetic algorithms and ant colony algorithm, are increasingly applied in the innovation diffusion. Venkatesan and Kumar [23] believe that the parameter estimation result of genetic algorithm is better than that of other algorithms.

3. Diffusion Results of EVs in China under Different Business Models

According to Bass model, different p , q , m values will affect the diffusion rate and scale of an innovation product. EV BMs would have an impact on the innovation coefficient p and imitation coefficient q , thus affecting the market diffusion of EVs. According to Rogers, innovations could be classified along five dimensions, which are relative advantages, value compatibility, complexity, trialability, and the observability [17]. The BM, which can make early adopters' perception of EVs matching these five dimensions to the greatest degree, would have a higher innovation coefficient. Imitation coefficient q describes the process of communication and diffusion among imitators. The BM which is more suitable for word of mouth and has more possibilities to activate the choices of imitators would have a higher imitation coefficient.

3.1. Parameter Estimation. Considering that EV is still in the early stage of introduction and lack of available historical data for simulation, so we adopt the sales data of HEV as basis [14]. Since the time for HEV in Chinese market is short, we adopt the sales of HEVs in US and Japan and genetic algorithm to estimate the relevant parameters. The data and estimation results are shown in Tables 1, 2, and 3.

TABLE 3: Model estimation result.

Parameter	R^2	SSE * 10^7	m	p	q
Estimated value (US)	0.90	1911	2360513	0.0148	0.5676
Estimated value (Japan)	0.95	63	1020338	0.0032	0.4189

Determination coefficient R^2 is 0.90 in US and 0.95 in Japan, showing a good fit, particularly in Japan. Meanwhile, the innovation coefficient p is significantly smaller than the imitation coefficient q both in US and Japan, which is consistent with the general situation of innovation diffusion. This means that the diffusion of EVs would be relatively slow at the beginning and would be affected by the imitation coefficient to have an increasingly higher diffusion rate among consumers. In addition, Mahajan et al. [24] made a statistical summary of estimated value of p , q in a general condition as follows. According to this statistical summary, we can see that estimated result of data in Japan fits the statistical law better:

$$0.3 < p + q < 0.7, \quad p < 0.01, \quad 0.3 < q < 0.5. \quad (4)$$

Figure 1 shows the comparison of HEV sales in actual condition and estimated value. It can be seen that the actual value of HEV sales fits well with the estimated value in both countries.

3.2. Parameter Adjustment. Before using the above-mentioned parameters to forecast the EV diffusion in Chinese market, we need to adjust them according to the development of Chinese EV market so as to fit with the actual condition better.

3.2.1. Adjustment to the Value of m . The development of EVs in China is still in its infancy and is heavily influenced by policies, so the potential of Chinese EV market has a strong variability, which imposes uncertainty on the estimate of market potential [25, 26]. Taking all these factors into consideration, we choose the year of 2020 as the estimation time point of EV market’s potential and assume that this potential is stable.

According to estimate of HIS company, the ownership of light-duty vehicles would achieve 0.15 billion by 2020 [15]. And some experts predict that EV sales in China would reach a 5% penetration in 2020 (data source: <http://news.hexun.com/2009-10-24/121455528.html>, accessed on December 4, 2013). So this paper assumes that market potential m in China would be 7.5 million by 2020. It is worth mentioning that the estimation value of m is based on the current development trend of EVs in Chinese market and only represents the volume that EV ownership would reach by 2020, not the whole market potential of future EV market.

3.2.2. Adjustment to the Value of p and q . In Bass model, innovators’ purchasing decisions would not be affected by external pressure and p stands for the characteristic of the innovation [14], which varies not much among different countries. The differences between HEVs and ICEs are more

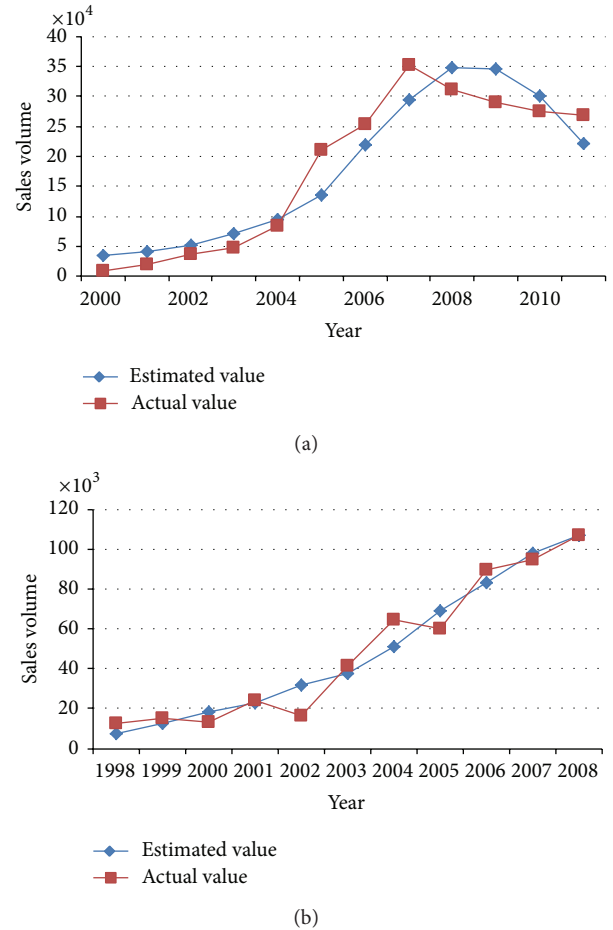


FIGURE 1: (a) Annual HEV sales in US. (b) Annual HEV sales in Japan.

evident, because HEVs and EVs both require a higher risk spirit for innovators. So, we choose the smaller value of p in the estimation of US and Japan. As to q , it mainly describes the impact of countries’ economy, culture, politics, and population on innovation diffusion [27–29]. So we would need to adjust the value of q so as to make it more suitable for consumers in Chinese market.

According to the report *Accenture End-Consumer Survey on the Electrification of Private Transport* by Accenture in 2011, the proportion of positive choice made by Chinese consumers to the question “Whether consider purchasing EV as the second car” is much higher than US and Japan [30]. The survey results are listed in Table 4. We can also see that the acceptance ratio in US is higher than Japan, which is consistent with the estimation results of parameter q . Moreover, a survey from Deloitte also shows the same

TABLE 4: Acceptance ratio of EV from consumers of different nations.

China	Italy	Korea	Canada	US	Germany	Japan	Sweden	UK	France
95%	73%	70%	58%	57%	57%	53%	53%	51%	42%

TABLE 5: Comparison of q in US, Japan, and Taiwan.

Durable consumer goods	Monochrome TV	Washing machine	AC	Car
US	0.39	0.13	0.39	0.29
Japan	0.59	0.19	0.47	0.39
Taiwan	0.75	0.36	0.65	0.45

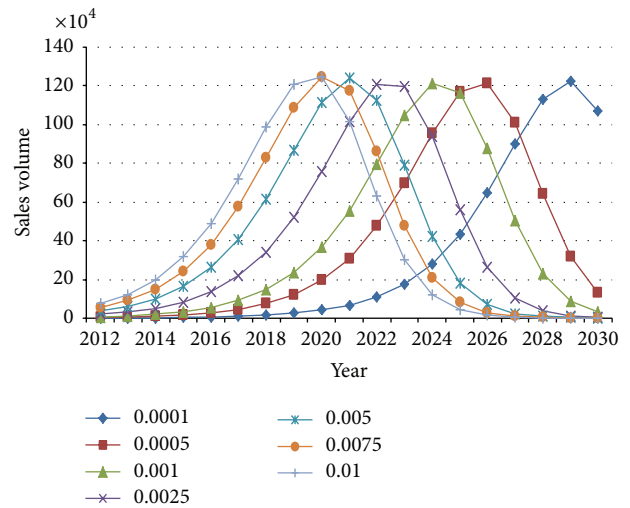
conclusion (data source: http://auto.sina.com.cn/news/2011-10-12/1947852631_6.shtml, accessed on December 4, 2013). Based on the comparison between China, US, and Japan, adjusting the estimated parameter q to be higher would be appropriate.

To further determine the exact adjustment figure of q , this paper adopts the study results by Takada [27], who compared the imitation coefficient q among three Pacific Rim countries and regions. Table 5 shows the comparison results and we can see that four kinds of imitation coefficient q in Taiwan are much higher than those in US and Japan. Moreover, in automotive industry, the coefficient in Taiwan is about 15% higher than that in US and Japan. Taking the condition in Taiwan into consideration, we adjust the above-mentioned parameter q into 0.6527.

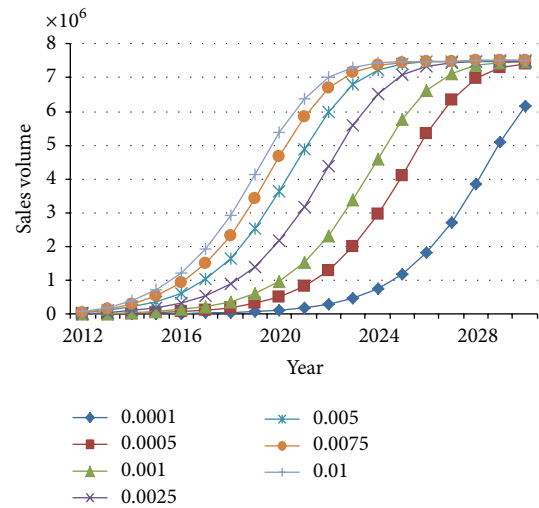
3.3. Diffusion Result of EV Market under Different BM. Since the values of p and q are not directly obtained on Chinese EV data, it would be more analyzable to forecast EV diffusion in China based on the different values of p and q rather than on using constant parameters. So this paper conducts a sensitivity analysis over p and q .

3.3.1. Sensitivity Analysis over Innovation Coefficient p . EV BMs in China could be categorized as two basic types: vehicle purchasing and battery leasing. Vehicle purchasing is more alike the traditional automotive BM, of which the value compatibility, complexity, and observability of innovations show more possibilities to improve early innovators' perception level of EVs, so the parameter p under the BM of vehicle purchasing should be higher than that under battery leasing BM. The results are shown in Figure 2.

Figure 2(a) shows the annual sales of EVs in China with different values of p and Figure 2(b) shows the cumulative sales with different values of p . We can see that the change of p affects slightly the sales of EV. However, the change of p affects directly the time required in the diffusion of EV reaching the critical mass, which is the key factor influencing the success diffusion of new products. When the threshold of new product diffusion is reached, the subsequent diffusion would no longer need to rely on the external variables, and the cumulative amount of the product itself can generate continuous growth momentum, attracting a sufficient number of



(a)



(b)

FIGURE 2: (a) Sales volume of EVs by p . (b) Cumulative sales volume of EVs by p .

potential consumers, thus completing the diffusion process of new products.

3.3.2. Sensitivity Analysis over Imitation Coefficient. The battery leasing business model could reduce the price of EVs

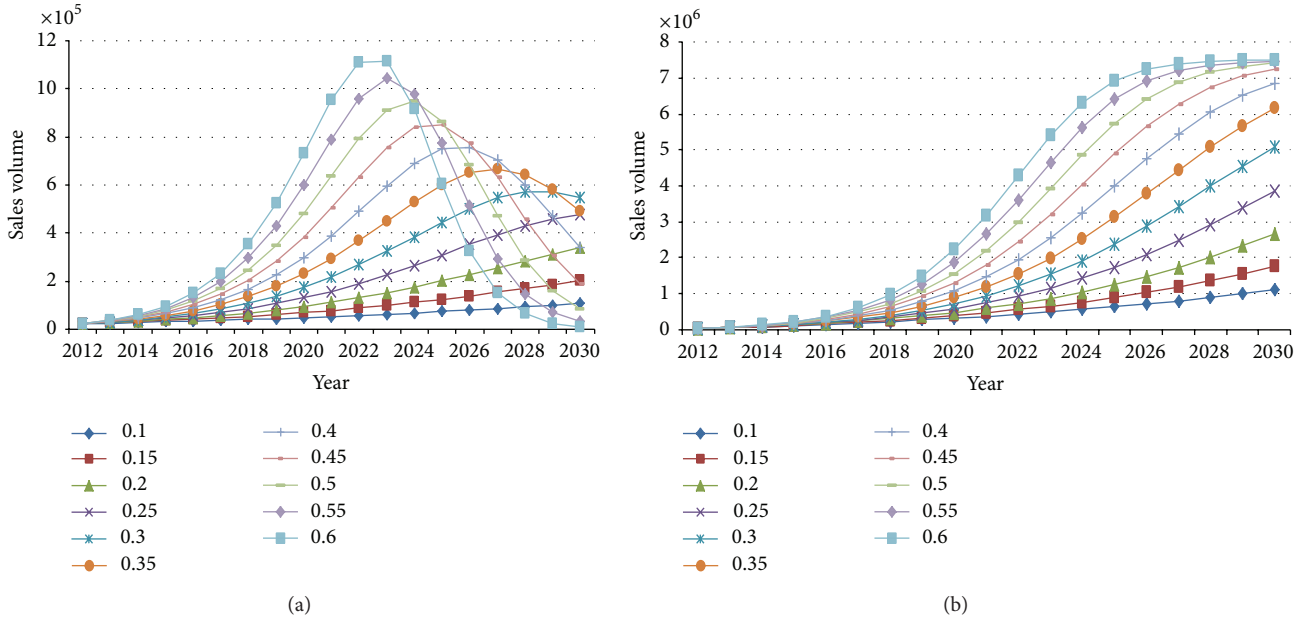


FIGURE 3: (a) Sales volume of EVs by q . (b) Cumulative sales volume of EVs by q .

and improve the convenience of battery charging and vehicle daily use, thus affecting more imitation coefficient q . That is to say, once the battery leasing model breaks the critical value of the initial stage of development, its diffusion rate would be higher than the vehicle purchasing model, which means that the imitation coefficient q under battery leasing model is higher than that under vehicle purchasing model.

In this paper, we could analyze the impact from different BMs on the sales of EV in China by giving different values to parameter q , of which the results are shown in Figures 3(a) and 3(b). Figure 3(a) shows the annual sales number of EV in China from 2012 to 2030 with different values of parameter p and Figure 2(b) shows the cumulative result with different values of parameter p .

Figure 3 shows that the change of parameter q affects slightly the time required for the sales of EV in China to reach the critical mass but affects significantly the maximum annual sales of EV in China. When the imitation coefficient increases from 0.1 to 0.55, the minimum annual sale increases from 0.2 million to 1.11 million, which is a big variation.

Figure 3 also shows that the slope of the diffusion curves with different imitation coefficients had a significant change after the diffusion of EV market reaches the critical value, which means the change of imitation coefficient directly affects the time required in EV market to reach the saturation. For example, when the imitation coefficient varies from 0.1 to 0.55, the time required for the EV market to reach saturation extends from the year of 2013 to 2047.

3.3.3. Economic Analysis of the BM. Based on the study of EV innovation diffusion, it would be possible to analyze the economy of EV BM. This paper adopts the EV BM in Shenzhen as an example because it is representative in China. Sosna et al. argue that a single case would be appropriate

if the case is extreme, unique, or revelatory [31]. Chinese government launched a demonstration program Ten Cities, Ten Thousand Vehicles in 2009, and 13 cities (Batch I) were approved to carry out the demonstration, which was followed by 7 additional pilot cities (Batch II) and five more cities (Batch III). One aim of this program is to explore appropriate BMs for EVs through testing and implementing new BMs in the 25 demonstration cities. Among the 25 cities, Shenzhen is one of the “dual-pilot cities:” EV demonstration pilots and pilots of subsidizing private EV buyers. During 2009–2012, SZ has established two different BM models in taxi and bus sectors. The BMs are very representative in China and Shenzhen achieved large-scale commercial operation for the first time in electric buses and electric taxis areas. By June 2012, there are 3147 EVs out on the road in Shenzhen, which is the highest nationwide. So, we select SZ to conduct a case study.

The business model of EVs in Shenzhen can be categorized into the model of vehicle purchasing and it takes three years for Shenzhen to achieve the social network of EVs. This business model or social network is mainly made up of six groups, which are government, grid operators, infrastructure operators, auto manufacturers, taxi companies or bus companies, and consumers. In this social network, the government of Shenzhen is mainly responsible for policy development and financial subsidy. The government grants financial subsidy to the auto manufactures so that the manufacturers can sell the EVs at a relative lower price. In Shenzhen, one of the major EV manufactures is BYD. It sells EVs to taxi companies and consumers. China Southern Power Grid (CSPG) in Shenzhen is responsible for electricity supply and is one of the two infrastructure operators. The other infrastructure operator is China Potevio. The taxi company purchases EV taxi from BYD and the EV taxi is charged in

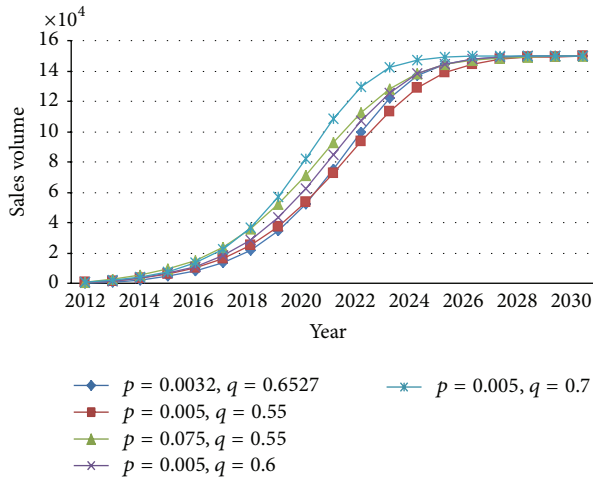


FIGURE 4: Different scenarios of EV diffusion in Shenzhen.

the charging stations run by CSPG and China Potevio. To sustain this social network, it is necessary for any of the agents such as infrastructure operators and EV manufacturers in this social network to get profit. The diffusion number of EVs in Shenzhen is one critical factor to determine the profitability for these companies.

According to the national and Shenzhen regional civilian and private car ownership statistics in 2009 and 2010, both civilian and private car ownerships in Shenzhen account for about 2% of the whole country [32, 33], so we assume that the proportion of EV sales in Shenzhen is also about 2% of the whole country. By setting five different groups of p and q , we can get the diffusion results of EVs in Shenzhen from 2012 to 2030 as shown in Figure 4.

Figure 4 shows that total ownership of EVs in Shenzhen varies from 4000 to 7000 based on different scenarios. According to [34], to achieve sustainable BM, EV charging stations in Shenzhen would need to serve 2,301 EVs every day to achieve breakeven under existing technical constraints. Currently there are four charging stations and this figure would reach 150 by 2015 according to the report *Electric Vehicle Charging Facilities Planning 2010–2015* released by Shenzhen government. Considering the competition, it would be difficult for each station to achieve the breakeven point. So, keeping the number of charging stations in a reasonable level is critical in maintaining the profitability of charging stations in the early stage of EV diffusion.

4. Discussion

This paper analyzes how different social networks would affect the EV diffusion results by the terms of different BMs. By affecting the innovation and imitation coefficients, different social networks would lead to different diffusion effects. Vehicle purchasing model has a higher innovation coefficient, which is conducive to promoting EV market to reach a critical value earlier. The other battery leasing model has a higher imitation coefficient, which would increase the maximum annual sales of EVs and shorten the time required

for EV to reach saturation. This would further affect the time amount for different commercial agents to achieve profit in the networks. Estimation results indicate that innovation coefficient in China is not very high, while the imitation coefficient is much higher. It means once EVs are purchased by some innovators, it would diffuse quickly among the potential consumers, but it also means that if innovators were not satisfied with EVs, the negative opinions would also diffuse quickly in potential consumers and affect their choices and may lead to the failure of EVs. So we suggest that EVs should be positioned in a niche market precisely in the early stage and should not be marketed too rapidly. Meanwhile, early purchasers' needs should be met through a variety of tools and policies so that they can give positive word of mouth which can greatly influence the potential consumers in the network.

Conflict of Interests

The authors declare that there is no conflict of interests regarding the publication of this paper.

Acknowledgment

The authors would like to acknowledge the support from The National Key Technology R&D Program of the Ministry of Science and Technology of China (Grant no. 2013BAG06B04).

References

- [1] C. C. Chan, "The state of the art of electric, hybrid, and fuel cell vehicles," *Proceedings of the IEEE*, vol. 95, no. 4, pp. 704–718, 2007.
- [2] F. T. Rothaermel and C. W. L. Hill, "Technological discontinuities and complementary assets: a longitudinal study of industry and firm performance," *Organization Science*, vol. 16, no. 1, pp. 52–70, 2005.
- [3] V. Sabatier, A. Craig-Kennard, and V. Mangematin, "When technological discontinuities and disruptive business models challenge dominant industry logics: insights from the drugs industry," *Technological Forecasting & Social Change*, vol. 79, no. 5, pp. 949–962, 2012.
- [4] L. Orsenigo, F. Pammolli, and M. Riccaboni, "Technological change and network dynamics: lessons from the pharmaceutical industry," *Research Policy*, vol. 30, no. 3, pp. 485–508, 2001.
- [5] L. X. Zhang, H. J. Gao, and O. Kaynak, "Network-induced constraints in networked control systems—a survey," *IEEE Transactions on Industrial Informatics*, vol. 9, no. 1, pp. 403–416, 2013.
- [6] G. O. Collantes, "Incorporating stakeholders' perspectives into models of new technology diffusion: the case of fuel-cell vehicles," *Technological Forecasting & Social Change*, vol. 74, no. 3, pp. 267–280, 2007.
- [7] H. Chesbrough and R. S. Rosenbloom, "The role of the business model in capturing value from innovation: evidence from Xerox corporation's technology spin-off companies," *Industrial and Corporate Change*, vol. 11, no. 3, pp. 529–555, 2002.
- [8] H. Zhang, H. Yan, F. Yang, and Q. Chen, "Quantized control design for impulsive fuzzy networked systems," *IEEE Transactions on Fuzzy Systems*, vol. 19, no. 6, pp. 1153–1162, 2011.

- [9] H. C. Yan, H. B. Shi, H. Zhang, and F. W. Yang, "Quantized H-infinity control for networked delayed systems with communication constraints," *Asian Journal of Control*, vol. 15, no. 5, pp. 1468–1476, 2013.
- [10] F. Deroian, "Formation of social networks and diffusion of innovations," *Research Policy*, vol. 31, no. 5, pp. 835–846, 2002.
- [11] H. C. Yan, Z. Z. Su, H. Zhang, and F. W. Yang, "Observer-based H-infinity control for discrete-time stochastic systems with quantization and random communication delays," *IET Control Theory and Applications*, vol. 7, no. 3, pp. 372–379, 2013.
- [12] F. M. Bass, "A new product growth for model consumer durables," *Management Science*, vol. 50, no. 12, pp. 1825–1832, 2004.
- [13] N. Meade and T. Islam, "Modelling and forecasting the diffusion of innovation—a 25-year review," *International Journal of Forecasting*, vol. 22, no. 3, pp. 519–545, 2006.
- [14] S. Y. Park, J. W. Kim, and D. H. Lee, "Development of a market penetration forecasting model for Hydrogen Fuel Cell Vehicles considering infrastructure and cost reduction effects," *Energy Policy*, vol. 39, no. 6, pp. 3307–3315, 2011.
- [15] B. Ren, L. N. Shao, and J. X. You, "Development of a generalized bass model for Chinese electric vehicles based on innovation diffusion theory," *Soft Science*, vol. 27, no. 4, pp. 17–22, 2013.
- [16] JAMA, *The Motor Industry of Japan*, Japan Automobile Manufacturers Association Inc., 2009.
- [17] E. M. Rogers, *Diffusion of Innovations*, Free Press, New York, NY, USA, 1962.
- [18] V. Mahajan and S. Sharma, "A simple algebraic estimation procedure for innovation diffusion models of new product acceptance," *Technological Forecasting & Social Change*, vol. 30, no. 4, pp. 331–345, 1986.
- [19] H. Gatignon, J. Eliashberg, and T. S. Robertson, "Modeling multinational diffusion patterns: an efficient methodology," *Marketing Science*, vol. 8, no. 3, pp. 231–247, 1989.
- [20] H. Gao, T. Chen, and J. Lam, "A new delay system approach to network-based control," *Automatica*, vol. 44, no. 1, pp. 39–52, 2008.
- [21] B. L. Bayus, "High-definition television. Assessing demand forecasts for a next generation consumer durable," *Management Science*, vol. 39, no. 11, pp. 1319–1333, 1993.
- [22] B. L. Bayus and C. C. Carlstrom, "Grouping durable goods," *Applied Economics*, vol. 22, no. 6, pp. 759–774, 1990.
- [23] R. Venkatesan and V. Kumar, "A genetic algorithms approach to growth phase forecasting of wireless subscribers," *International Journal of Forecasting*, vol. 18, no. 4, pp. 625–646, 2002.
- [24] V. Mahajan, E. Muller, and F. M. Bass, "Diffusion of new products: empirical generalizations and managerial uses," *Marketing Science*, vol. 14, no. 3, pp. 79–88, 1995.
- [25] H. Zhang, H. C. Yan, F. W. Yang, and Q. J. Chen, "Distributed average filtering for sensor networks with sensor saturation," *IET Control Theory and Applications*, vol. 7, no. 6, pp. 887–893, 2013.
- [26] H. Zhang, H. Yan, T. Liu, and Q. Chen, "Fuzzy controller design for nonlinear impulsive fuzzy systems with time delay," *IEEE Transactions on Fuzzy Systems*, vol. 19, no. 5, pp. 844–856, 2011.
- [27] J. Takada, "Cross-national analysis of diffusion of consumer durable goods in Pacific Rim countries," *Journal of Marketing*, vol. 55, pp. 48–54, 1991.
- [28] H. Zhang, Q. Chen, H. Yan, and J. Liu, "Robust H_∞ filtering for switched stochastic system with missing measurements," *IEEE Transactions on Signal Processing*, vol. 57, no. 9, pp. 3466–3474, 2009.
- [29] H. Zhang, Z.-H. Guan, and G. Feng, "Reliable dissipative control for stochastic impulsive systems," *Automatica*, vol. 44, no. 4, pp. 1004–1010, 2008.
- [30] Accenture, "Changing perceptions, hedging bets: accenture end-consumer survey on the electrification of private transport," 2011, <http://www.accenture.com/microsites/accenture-smartsolutions-electricvehicles/Pages/index.aspx>.
- [31] M. Sosna, R. N. Trevinyo-Rodríguez, and S. R. Velamuri, "Business model innovation through trial-and-error learning: the naturhouse case," *Long Range Planning*, vol. 43, no. 2-3, pp. 383–407, 2010.
- [32] National Bureau of Statistics of China, *China Statistical Yearbook 2010*, China Statistic Press, Beijing, China, 2011.
- [33] Bureau of Statistics of Shenzhen City, *Shenzhen Statistical Yearbook 2010*, China Statistic Press, Beijing, China, 2011.
- [34] Y. X. Xue, Y. Chen, and D. Y. Kong, "Business model innovations for electric vehicles from the perspective of value network," *Science of Science and Management of S&T*, vol. 35, no. 3, pp. 49–57, 2014.

Research Article

A Novel Mathematical Formula for Retrieval Algorithm

Yuping Qin,¹ Hamid Reza Karimi,² Aihua Zhang,¹ and Qiangkui Leng³

¹ College of Engineering, Bohai University, Jinzhou 121013, China

² Department of Engineering, Faculty of Engineering and Science, The University of Agder, 4898 Grimstad, Norway

³ College of Computer Science, Beijing University of Technology, Beijing 100124, China

Correspondence should be addressed to Yuping Qin; qlq888888@sina.com

Received 6 January 2014; Accepted 23 January 2014; Published 26 March 2014

Academic Editor: Xudong Zhao

Copyright © 2014 Yuping Qin et al. This is an open access article distributed under the Creative Commons Attribution License, which permits unrestricted use, distribution, and reproduction in any medium, provided the original work is properly cited.

A method is proposed to retrieve mathematical formula in LaTeX documents. Firstly, we represent the retrieved mathematical formula by binary tree according to its LaTeX description, normalize the structure of the binary tree, and obtain the structure code and then search the mathematical formula table that is named by the structure code and the formula elements of the first two levels of the binary tree in the mathematical formula database. If the table exists, then we search the normalizing variable name preorder traversing sequence of the binary tree in the table and display the document information that contain the mathematical formula. The experimental results show that the algorithm realizes the retrieval of mathematical formula in LaTeX documents and has higher retrieval precision and faster retrieval speed.

1. Introduction

With the rapid development of the internet and digital libraries, more and more documents that contain mathematical formulas are stored on the computer. In order to share and communicate these documents quickly, online retrieval for mathematical formulas has attracted much attention and has become an important research area.

The retrieval technology for text already is relatively mature [1–7]. However, how to effectively retrieve mathematical formulas in documents is still an ongoing research issue [8]. And some control ideas, such as data driven [9–13] and system switch [14–17], have also been employed for this. Lee and Wang [18] presented a system of mathematical formula reorganization, but this system cannot handle multiline mathematical formulas, as well as more complex single-line ones. Fateman et al. [19] designed a system of mathematical formula reorganization, but the system can only reorganize integral tables with fixed format. Zanibbi et al. [20–22] proposed methods that can achieve good results for scanned images of the formulas and support automatic evaluation of recognition performance. Nonetheless, the methods cannot analyze the expression with two or more modifiers. MatheReader [23] can recognize more kinds of

mathematical expressions; however, it still does not reach the degree of practical application.

The description methods of mathematical formulas mainly include MathML, LaTeX, and image. Among them, LaTeX has been widely used to edit scientific papers, books, files, dissertations, manuscripts, personal letters, and a variety of complex symbolic formulas. In addition, other format documents can be easily converted to LaTeX format. Therefore, a method is proposed to retrieve mathematical formula in LaTeX documents.

The rest of the paper is organized as follows. Section 2 gives the binary tree description of mathematical formula. Section 3 introduces the design of database. Section 4 describes our mathematical formula retrieval method in detail. Experimental results are presented in Section 5. Conclusion is outlined in Section 6.

2. Binary Tree Representation of Mathematical Formula

2.1. Construction of Binary Tree. Due to the noticeable structural feature, a complicated mathematical formula in LaTeX form can be divided into multiple subexpressions and then

TABLE 1: Data structure of a binary tree.

Field	Data type	Meaning
Formula element	String	Operator, variable, or constant
Category	String	OPS (satisfying the commutative law), VAR (variable), OPU (not satisfying the commutative law), and CON (constant)
Priority	Integer	Operator priority (the larger the value is, the higher the priority is; maximum machine number if priority is for variables and constants)
Combination	String	LR (left-right), UD (up-down), and SG (single)
Node height	Integer	The height of the binary tree that regards current node as root
Structure code	String	Structure code of current node = structure code of its left child + node height + its structure code of right child

each subexpression can be divided into much smaller ones. We repeat the procedure until no collapsible component is left. The final subexpressions are called formula elements.

The operator has three operands, such as “ \sum ,” which has a close relationship with its top region, bottom region, and right region. We combine it with the right subexpression by adding an operator “link.”

We traverse the formula element string with “link” from left to right to generate the priority list of formula elements and then the binary tree representation of a mathematical formula can be obtained according to its structural feature and the priority list. The data structure of the binary tree is given in Table 1.

We use recursion approach to get the binary tree representation of a formula element. Root, the lowest priority element, is first created and then we create the left subtree according to the elements before the root element in the formula element string. Accordingly, the right subtree can be created by the elements after the root element in the formula element string.

For each node, its element category and combination can be determined by the formula element. The height of each node can be calculated by the following:

$$H(\text{node}) = H_r > H_l? \quad H_r : H_l + 1, \quad (1)$$

where $H(\text{node})$ is the height of node, H_l is the height of left child of node, and H_r is the height of right child of node.

For example, for mathematical formula $(\sum_{i=1}^{10} a^i + x \times y \times z) \times (x \times y + y \times z)$, its LaTeX form is $(\sum_{i=1}^{10} a^i + x \times y \times z) \times (x \times y + y \times z)$. The corresponding binary tree representation is given in Figure 1.

2.2. Normalization Processing. Due to the fact that some operators satisfy the commutative law, that is, for these operands, one can exchange them randomly for constituting different mathematical expressions; the meanings of these

expressions are identical. But it is worth noting that the structures of the corresponding binary trees are likely to be different. Hence, the normalization must be done for differently structural but identically meaningful binary trees. We traverse the binary tree in preorder, if the category of the formula element is OPS and the height of left child is higher than that of right child, then exchanging the left subtree and right subtree of the node. Figure 2 shows the normalized binary tree corresponding to Figure 1.

After normalizing the binary tree, the structure code of every node can be generated by traversing the binary tree in postorder. The structure code of node “node” can be obtained according to the following:

$$C(\text{node}) = \begin{cases} C_l(\text{code}) + H(\text{code}) + C_r(\text{code}) & \text{nonleft node} \\ 1 & \text{left node,} \end{cases} \quad (2)$$

where $C_l(\text{node})$ is the structure code of left child of node and $C_r(\text{node})$ is the structure code of right child of node.

Note that variable names of mathematical expression are independent of the formula meaning. For a given structure binary tree, we can get its corresponding sequence of the formula elements according to given traversal order. To make the sequence unique, we still need to normalize all the variable names in the sequence. The normalization approach is to use a fixed set of variable names to successively replace each formula element labeled “VAR” in the formula element sequence.

3. Database Designing

Retrieval database of mathematical formulas contains two kinds of tables: one is document information table and the other is formula information table. Their structures are given in Tables 2 and 3. Naming rule for the formula information table is described as follows:

$$C(\text{root}) + E(\text{root}) + E(\text{left child of root}) + E(\text{right child of root}), \quad (3)$$

where $E(\text{root})$ is the formula element of root, $E(\text{left child of root})$ is the formula element of left child of root, and $E(\text{right child of root})$ is the formula element of right child of root.

Mathematical formulas with the same information, including structure code, formula element of root, formula element of the left child, and element of the right child, are stored in a table.

4. Retrieval Algorithm

For the retrieved mathematical formula, we create the corresponding binary tree representation by its LaTeX format, obtain the structure code after normalizing the structure of binary trees, and then search the formula information table

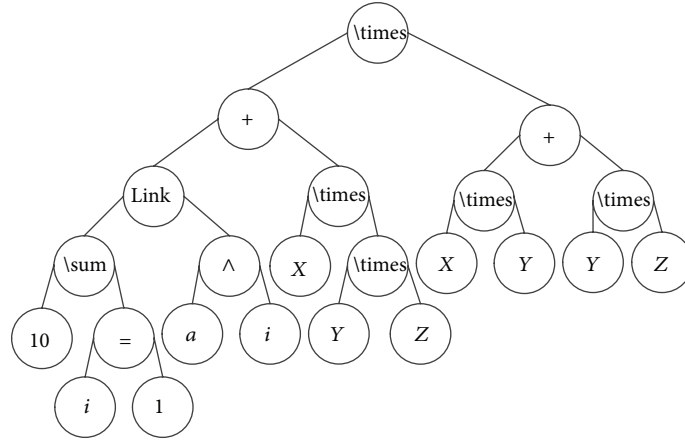


FIGURE 1: Binary tree representation of a mathematical formula.

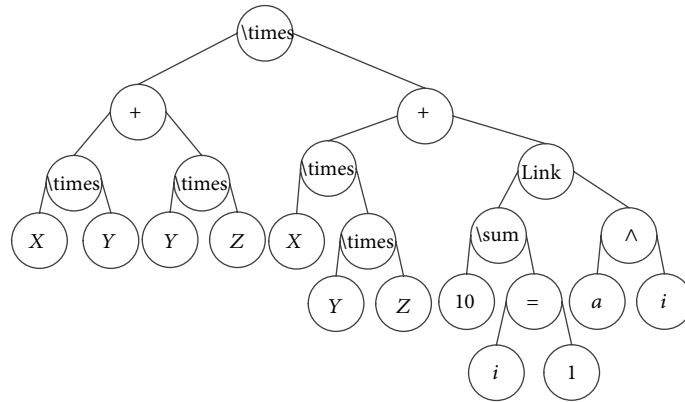


FIGURE 2: Normalized binary tree.

TABLE 2: Structure of document information table.

Field name	Type	Content
PAPER.ID	Text	Document code
PAPER.NAME	Text	Document name
PAPER.INFO	Text	Document information

TABLE 3: Structure of formula information table.

Field name	Type	Content
FORMULA.ID	Text	Formula code
PAPER.ID	Text	Document code
NORMALIZED	Text	Normalized formula element sequence

named by structure code and the formula elements of the first two layers of the binary tree in the formula database. If the table exists, we find the preorder traversing sequence of the binary tree in the table. The retrieval algorithm is described in detail as follows.

Step 1. For a candidate testing LaTeX document, extract all mathematical formulas to get a retrieved formula set $Formula = \{f_1, f_2, \dots, f_n\}$ and go to Step 2.

Step 2. If $Formula$ is nonempty, then take out a formula f_i from $Formula$, create its binary tree representation, and normalize structure of the binary tree to get binary tree T_i . Traverse T_i in preorder and normalize variable names to get traversing sequence L_1 and go to Step 3; else, go to Step 8.

Step 3. Calculate the structure code of root according to (2). Let T_name be $C(\text{root}) + E(\text{root}) + E(\text{left child of root}) + E(\text{right child of root})$; go to Step 4.

Step 4. Search the data table named T_name in the formula database. If the table exists, go to Step 5; else, go to Step 7.

Step 5. $L = \{L_1\}$. For each nonleft node, if its element category is OPS and the heights of left child and right child are identical, exchange its left and right subtrees. Traverse the tree in preorder and normalize variable names to get the corresponding traversal sequence. If the sequence is not existing in L , then add the sequence to L . Finally, get formula element sequence set $L = \{L_1, L_2, \dots, L_m\}$ and go to Step 6.

Step 6. Search the formula element sequence that is the same as L_i ($i = 1, 2, \dots, m$) in the table. If it exists, output the document information containing formula f_i ; else, go to Step 7.

TABLE 4: The way of modifying mathematical formula.

1	2	3	4
Not modifying	Modifying variable name	Exchanging operands that the operator satisfies commutative law	Modifying variable name and exchanging operands that the operator satisfies commutative law

Step 7. If the element category of the root is OPS and heights of its left child and right child are identical, exchange $E(\text{left child of root})$ and $E(\text{right child of root})$ in T_name and go to Step 3; else, go to Step 2.

Step 8. End.

5. Experimental Results

To verify the effectiveness of the proposed method on different types of mathematical formulas, we collect 1138 different mathematical formulas from 500 pressed research papers written in English and Chinese. We represent every mathematical formula by binary tree according to its LaTeX description, normalize the structure of the binary tree, and obtain the structure code. We save the preorder traversing sequence of normalizing variable name to the formula information table that is named by the structure code and the formula elements of the first two levels of the binary tree. We Save these documents information to the document information table at the same time.

The computational experiments were done on a Pentium 2.0 G with 2.0 MB memory, Windows XP SP3, and ACCESS 2007. The precision, recall, and F_1 values are used to evaluate the retrieval performance of the algorithm:

$$\begin{aligned}
 P &= \frac{A}{A + C}, \\
 R &= \frac{A}{A + B}, \\
 F_1 &= \frac{P \times R \times 2}{P + R},
 \end{aligned} \tag{4}$$

where A is the number of mathematical formulas retrieved correctly in retrieval results, B is the number of mathematical formulas that should be retrieved but do not appear in retrieval results, and C is the number of mathematical formulas that should not be retrieved but appear in retrieval results.

To verify the performance of the proposed method, some mathematical formulas are modified according to Table 4.

In experiments, retrievals are done 2016 times; the average precision is 96.35%, the average recall is 95.38%, the average F_1 value is 96.86%, and the retrieval time is 378 ms.

The experimental results show that the proposed method obtains high retrieval accuracy. The key reasons are that the method realized semantic retrieval. If the semantic of retrieved mathematical formula is the same as the destination mathematical formula, then the corresponding structure of

binary tree is uniform after normalizing the structure of the binary tree. Even if the destination mathematical formula exists in more than one binary tree representation, after normalizing variable names, at least one preorder traversing sequence of binary tree is the same as retrieved mathematical formula. The retrieval speed of the proposed approach is fast. The key reasons are that the method searches the table named by the structure code and the formula elements of the first two levels of the binary tree. If the table exists in the mathematical formula database, then to search the preorder traversing sequence of the retrieved mathematical formula in the table.

6. Conclusion

Based on the binary tree representation of mathematical formula, a mathematical formula retrieval method for LaTeX documents is introduced in this paper. Experimental results show that the algorithm not only realizes semantic retrieval of mathematical formula but also has higher retrieval precision and faster retrieval speed. The results achieved in the offline retrieval promise the proposed method will work in the online case as well. The disadvantage of the existing retrieval system is that it cannot retrieve mathematical formula in LaTeX documents when it is solved. How to retrieve mathematical formula in PDF documents and WORD documents would be our research work in future.

Conflict of Interests

The authors declare that there is no conflict of interests regarding the publication of this paper.

Acknowledgments

This study is partly supported by the National Natural Science Foundation of China (no. 61304149), the Polish-Norwegian Research Programme (Project no. Pol-Nor/200957/47/2013), the Natural Science Foundation of Liaoning Province in China (no. 201202003), and the Program for New Century Excellent Talents in University (no. NCET-11-1005).

References

- [1] T. C. Hoard and J. Zobel, "Methods for identifying versioned and plagiarized documents," *Journal of the American Society for Information Science and Technology*, vol. 54, no. 3, pp. 203–215, 2003.
- [2] A. Chowdhury, O. Frieder, D. Grossman, and M. C. McCabe, "Collection statistics for fast duplicate document detection," *ACM Transactions on Information Systems*, vol. 20, no. 2, pp. 171–191, 2002.
- [3] J. Zobel and A. Moffat, "Exploring the similarity space," *ACM SIGIR Forum*, vol. 32, no. 1, pp. 18–34, 1998.
- [4] A. Si, H. V. Leong, and R. W. Lau, "CHECK: a document plagiarism detection system," in *Proceedings of the ACM Symposium on Applied Computing*, pp. 70–77, 1997.

- [5] J.-P. Bao, J.-Y. Shen, X.-D. Liu, and Q.-B. Song, "Survey on natural language text copy detection," *Journal of Software*, vol. 14, no. 10, pp. 1753–1760, 2003.
- [6] J.-J. Zhao and X.-G. Hu, "A way to judge plagiarism in academic papers based on word-frequency statistics of paragraphs," *Computer Technology and Development*, vol. 19, pp. 231–233, 2009.
- [7] N. Kang, A. Gelbukh, and S. Han, "PPChecker: plagiarism pattern checker in document copy detection," in *Text, Speech and Dialogue*, vol. 4188 of *Lecture Notes in Computer Science*, pp. 661–667, 2006.
- [8] Y.-S. Guo, L. Huang, C.-P. Liu, and X. Jiang, "An automatic mathematical expression understanding system," in *Proceedings of the 9th International Conference on Document Analysis and Recognition (ICDAR '07)*, pp. 719–723, Parana, Brazil, September 2007.
- [9] S. Yin, S. X. Ding, A. H. A. Sari, and H. Hao, "Data-driven monitoring for stochastic systems and its application on batch process," *International Journal of Systems Science*, vol. 44, no. 7, pp. 1366–1376, 2013.
- [10] S. Yin, S. X. Ding, A. Haghani, H. Hao, and P. Zhang, "A comparison study of basic data-driven fault diagnosis and process monitoring methods on the benchmark Tennessee Eastman process," *Journal of Process Control*, vol. 22, no. 9, pp. 1567–1581, 2012.
- [11] S. Yin, H. Luo, and S. Ding, "Real-time implementation of fault-tolerant control systems with performance optimization," *IEEE Transactions on Industrial Electronics*, vol. 61, no. 5, pp. 2402–2411, 2013.
- [12] S. Yin, G. Wang, and H. R. Karimi, "Data-driven design of robust fault detection system for wind turbines," *Mechatronics*, 2013.
- [13] S. Yin, X. Yang, and H. R. Karimi, "Data-driven adaptive observer for fault diagnosis," *Mathematical Problems in Engineering*, vol. 2012, Article ID 832836, 21 pages, 2012.
- [14] X. Zhao, X. Liu, S. Yin, and H. Li, "Improved results on stability of continuous-time switched positive linear systems," *Automatica*, 2013.
- [15] X. Zhao, P. Shi, and L. Zhang, "Asynchronously switched control of a class of slowly switched linear systems," *Systems and Control Letters*, vol. 61, no. 12, pp. 1151–1156, 2012.
- [16] X. Zhao, L. Zhang, and P. Shi, "Stability of a class of switched positive linear time-delay systems," *International Journal of Robust and Nonlinear Control*, vol. 23, no. 5, pp. 578–589, 2013.
- [17] X. Zhao, L. Zhang, P. Shi, and H. Karimi, "Robust control of continuous-time systems with state-dependent uncertainties and its application to electronic circuits," *IEEE Transactions on Industrial Electronics*, 2013.
- [18] H.-J. Lee and J.-S. Wang, "Design of a mathematical expression recognition system," in *Proceedings of the 3rd International Conference on Document Analysis and Recognition*, vol. 2, pp. 1084–1087, Montreal, Canada, August 1995.
- [19] R. J. Fateman, T. Tokuyasu, B. P. Berman, and N. Mitchell, "Optical character recognition and parsing of typeset mathematics," *Journal of Visual Communication and Image Representation*, vol. 7, no. 1, pp. 2–15, 1996.
- [20] R. Zanibbi, D. Blostein, and J. R. Cordy, "Recognizing mathematical expressions using tree transformation," *IEEE Transactions on Pattern Analysis and Machine Intelligence*, vol. 24, no. 11, pp. 1455–1467, 2002.
- [21] D. Martín-Albo, V. Romero, and E. Vidal, "An experimental study of pruning techniques in handwritten text recognition systems," in *Pattern Recognition and Image Analysis*, pp. 559–566, Springer, New York, NY, USA, 2013.
- [22] H. M. Twaakyondo and M. Okamoto, "Structure analysis and recognition of mathematical expressions," in *Proceedings of the 3rd International Conference on Document Analysis and Recognition*, vol. 1, pp. 430–437, Montreal, Canada, August 1995.
- [23] J. M. Jin, H. Y. Jiang, and Q. R. Wang, "Mathematical expression recognition system: MatheReader," *Chinese Journal of Computers*, vol. 29, no. 11, pp. 2018–2026, 2006.

Research Article

Coarse-Grain QoS-Aware Dynamic Instance Provisioning for Interactive Workload in the Cloud

Jianxiong Wan, Limin Liu, Jie Lv, and Zhiwei Xu

School of Information Engineering, Inner Mongolia University of Technology, Hohhot 010080, China

Correspondence should be addressed to Jianxiong Wan; jxwan@csnet1.cs.tsinghua.edu.cn

Received 22 November 2013; Revised 22 January 2014; Accepted 23 January 2014; Published 25 March 2014

Academic Editor: Huiping Li

Copyright © 2014 Jianxiong Wan et al. This is an open access article distributed under the Creative Commons Attribution License, which permits unrestricted use, distribution, and reproduction in any medium, provided the original work is properly cited.

Cloud computing paradigm renders the Internet service providers (ISPs) with a new approach to deliver their service with less cost. ISPs can rent virtual machines from the Infrastructure-as-a-Service (IaaS) provided by the cloud rather than purchasing them. In addition, commercial cloud providers (CPs) offer diverse VM instance rental services in various time granularities, which provide another opportunity for ISPs to reduce cost. We investigate a Coarse-grain QoS-aware Dynamic Instance Provisioning (CDIP) problem for interactive workload in the cloud from the perspective of ISPs. We formulate the CDIP problem as an optimization problem where the objective is to minimize the VM instance rental cost and the constraint is the percentile delay bound. Since the Internet traffic shows a strong self-similar property, it is hard to get an analytical form of the percentile delay constraint. To address this issue, we propose a lookup table structure together with a learning algorithm to estimate the performance of the instance provisioning policy. This approach is further extended with two function approximations to enhance the scalability of the learning algorithm. We also present an efficient dynamic instance provisioning algorithm, which takes full advantage of the rental service diversity, to determine the instance rental policy. Extensive simulations are conducted to validate the effectiveness of the proposed algorithms.

1. Introduction

Before the advent of cloud computing, Internet service providers (ISPs) used to reserve mass amount of resources in order to deal with the peak workload; otherwise the service response time may increase to an intolerable degree while facing the flash crowd and greatly degrade the user experience. However, this approach is energy-ineffective since peak resource utilization is often three times larger than the average utilization for a typical ISP. Things get even worse in systems that provide interactive service where the average utilization is only around 10% of the total capacity provisioned for the peak load [1]. The cloud computing technology provides a novel service paradigm called Infrastructure-as-a-Service (IaaS) to reduce the hardware cost and maintenance cost. In the IaaS, the ISPs only need to rent resource (e.g., virtual servers and network bandwidths) from the cloud providers (CPs) instead of purchasing a vast number of physical servers themselves. The IaaS service enables a more flexible and effective approach for resource provisioning. For

example, users in the Amazon EC2 system can rent resource for a small period of time to cope with the flash traffic.

This paper studies a Coarse-grain Dynamic Virtual Machine (VM) Instance Provisioning (CDIP) problem for interactive workload subjected to a percentile delay constraint in the cloud from the perspective of ISPs. More specifically, this problem is related to the dynamic VM rental policy for the ISPs to minimize the resource rental cost while satisfying QoS constraints. A fine-grain (in the orders of seconds or minutes) resource provisioning policy may be more effective in increasing resource utilization and reducing cost, but it is more complex and hard to implement. For example, the startup phase of a VM instance in EC2 which “typically takes less than 10 minutes [2] (observed on November 2nd, 2013)” is not sufficient to support the fine-grain control policy. Further, the fine-grain policy can induce fluctuation and undermine the system stability. CPs like Amazon EC2 nowadays do provide a coarse-grain IaaS service instead of the fine-grain one. For example, the EC2 system offers IaaS service at 2 time scales. At a higher level,

TABLE 1: The pricing structure for Amazon EC2.

Notation	C_L	C_S
Cost (\$/hr)	0.448	0.680

there is a VM rental service for 1 or 3 years (denoted as *Reserved Instance Service*, RIS); at a lower level, VM instances can also be acquired on an hourly bases (denoted as *Marginal Instance Service*, MIS) to absorb the instant flash traffic. Generally speaking, the cost for using MIS instances is much higher than using RIS instances (refer to Table 1 for a detailed pricing structure in Amazon's EC2 platform). How to properly use these two services is one of the most important problems faced by ISPs to minimize cost.

Beside the VM instance rental cost, ISPs also care about the Quality-of-Service (QoS) issue for their end users. For interactive workload, traditional QoS is expressed by the mean queueing delay which is easy to analyze using classic queueing theory. However, the self-similar nature revealed in the Internet traffic [3] failed queueing-based analysis. In addition, the fact that interactive workload can tolerate some QoS violations drives researchers to propose an alternative form of QoS specification

$$\Pr(d \geq D_{th}) \leq x, \quad (1)$$

where d is the system response delay, D_{th} and x are the desired threshold value determined by Service Level Agreement (SLA). Unfortunately, there is no analytical form of (1) for the self-similar traffic.

In this paper, we formulate the CDIP problem as an optimization problem where the QoS constraints cannot be precisely determined. We develop efficient algorithms to solve the CDIP problem and conduct numerical analysis to evaluate the proposed algorithms. Our contributions are that

- (i) we design a resource prediction algorithm to estimate the performance of resource provisioning policy in the self-similar traffic,
- (ii) we extend the resource prediction algorithm with function approximations to enhance the scalability of the algorithm,
- (iii) we present a VM instance provisioning algorithm for ISPs to determine the optimal number of RIS and MIS VM instance, which minimizes the VM instance rental cost.

This paper proceeds as follows. Section 2 discusses the related works; Section 3 shows the opportunity for reducing rental cost using hybrid RIS/MIS; Section 4 presents a general optimization framework for the CDIP problem as well as the solution algorithms; Section 5 extends the algorithms with function approximations to address the scalability issue; Section 6 evaluates the proposed algorithms in various settings, followed with conclusions in Section 7.

2. Related Works

To make resource provisioning in the cloud computing environment, the first issue that must be addressed is to

predict the future resource demand accurately. There are many researches dedicated to this area. Chen et al. [4] used a multiplicative Seasonal Autoregressive Moving Average (S-ARMA) approach to predict the mean and standard deviation of interarrival times and used a simple decomposed model as well as Winter's smoothing method to predict the mean and standard deviation of file size. Gmach et al. [5] developed a pattern prediction method for cyclic workload through a workload periodogram function and an autocorrelation function. Caron and Desprez [6] used pattern matching to forecast the resource demand in the cloud. Niu et al. [7] proposed a channel interleaving scheme which can predict demand for new videos that lack historical demand data.

There are a number of works to lower the operational cost for the cloud providers (CPs). Ahmad and Vijaykumar [8] proposed a PowerTrade method to lower the total energy consumption of active servers, standby servers, and cooling facilities. They also developed a SurgeGuard method to maintain an extra number of servers at two time granularities to absorb flash crowd. Meisner et al. [1] developed a PowerNap mechanism which includes a sleep-active state scheduling component and a network interface card (NIC) supported by Wake-on-LAN functionality. The system is put into the sleep mode when there are no workloads. The NIC can wake the system up within 1 ms as long as there are packet arrivals from the networks. Leverich and Kozyrakis [9] integrated Hadoop system with an energy controller which recasts the data layout and task distribution to enable significant portions of a cluster to be shut down. Our work, on the other hand, studies how to reduce the cost from the perspective of Internet service providers (ISPs).

There are some recent researches close to our works. In [10], the author formulated the resource leasing problem as an Integer Programming Problem (IPP) and developed CoH, a family of heuristic policy to solve the problem. However, [10] treated batch jobs only and had little SLA considerations. Reference [11] also studied the instance provisioning problem and purposed a dynamic instance purchasing scheme based on the Central Limit Theorem to minimize the cost. The SLA constraint they considered is the overload probability which is not suitable for delay-sensitive interactive workload. The works [12, 13] make resource provisioning decision based on the Autoregressive Integrated Moving Average (ARIMA) prediction method; they still did not consider delay constraint. In contrast, [14] explicitly incorporated the delay into the objective function of the optimization problem. However, the delay was derived based on Markovian queueing theory which is not the case in today's Internet dominated by self-similar traffic.

3. Problem Statement

The structure of a data center in a cloud computing system is shown in Figure 1. Inside the data center, there are a number of physical servers. A physical server hosts one or more Virtual Machine (VM) according to its resource capacity. Note that we only present the VM instead of the physical server in the figure. An ISP rents VMs from the cloud

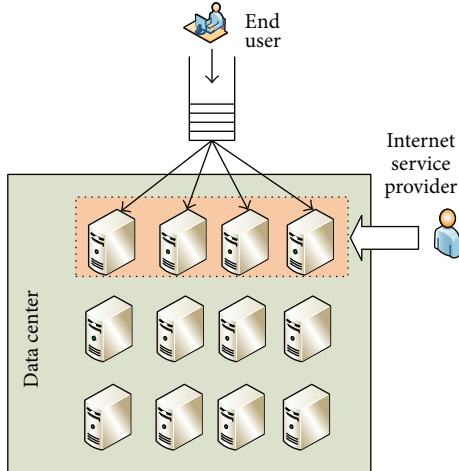


FIGURE 1: A data center in the cloud computing system.

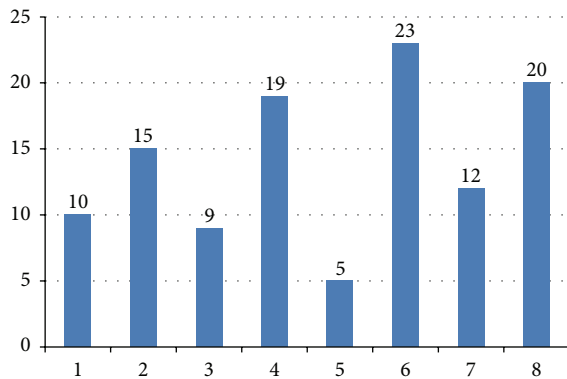


FIGURE 2: An example of VM instance demand in different hours of a day.

provider serve to its end users. To reduce the request response time, the data center often employs a shared queue structure.

The arrival rate of end user varies over time, which induces a time-changing VM instance demand. Figure 2 presents an example which divides a day into 8 phases (3 hr/phase) and the y -axis shows the VM instance demand to ensure the QoS requirement in each phase. The marginal rental cost in Amazon EC2 is given in Table 1. From Figure 2, we can see that there is a big gap between the maximum and the minimum instance demand. If the ISP only uses RIS instance, he must acquire 23 instances in order to satisfy the peak workload appeared in the 6th phase, which wastes a lot of resource and rises the daily instance rental cost to 247.96\$ (the rental cost for using only RIS instance can be computed as $23 \times 0.448 \times 24 = 247.96$ \$ (the product of the number of instance, the marginal cost, and total 24 hours)). In contrast, if the ISP only adopts MIS instance, he will obtain the highest resource utilization, and there is an opportunity to reduce the daily rental cost to 230.52\$ (from Figure 2, the total number of MIS instances is $10 + 15 + 9 + 19 + 5 + 23 + 12 + 20 = 113$. Since a phase contains 3 hours, the rental cost for using only MIS instance can be computed as $113 \times 3 \times 0.680 = 230.52$ \$).

If the ISP uses a hybrid approach which includes both RIS and MIS, on the other hand, the daily instance rental cost can be remarkably reduced. To see that, consider a resource provisioning policy which rents 10 RIS VM instances and acquires extra MIS instances if RIS instances are insufficient. The number of MIS instance can be formally written as $[K_i - 10]^+$ where K_i denotes the number of VM instance demand in phase i . The daily rental cost for this hybrid approach is 187.08\$, (the rental cost for RIS instance is $10 \times 0.448 \times 24 = 107.52$ \$. The total number of MIS instances is $5 + 0 + 9 + 13 + 2 + 10 = 39$; therefore the rental cost for MIS instance is $39 \times 0.680 \times 3 = 79.56$ \$. Thus, the total cost is $107.52 + 79.56 = 187.08$ \$.), which saves 24.3% and 18.8% compared with using purely RIS and MIS instance, respectively.

The above analysis suggests 2 assumptions. First, the QoS performance in terms of percentile delay can be precisely predicted; second, the number of RIS and MIS instances can be determined to minimize the VM instance rental cost. The following sections explain these two assumptions in detail.

4. A General Optimization Framework for the CDIP Problem

The notations used in this paper are shown in Notations section. The CDIP problem can be formulated as

$$\min_{k_i, i \in \{0, \dots, N\}} k_0 \times N \times C_L + C_S \times \sum_{i=1}^N k_i \quad (2)$$

subject to

$$\Pr(d_i \geq D) \leq x, \quad \forall i \in \{1, \dots, N\}, \quad (3)$$

where k_0 is the number of RIS instance and $k_i, i > 0$, is the number of MIS instance in phase i .

Note that, in the CDIP problem, the distribution of d_i is determined by the characteristics of exogenous interactive workload arrivals and the number of active VM instance k_i . As stated in Section 1, this problem is hard to solve, since we can hardly derive an explicit form of constraint (3). In this section, we will show how to approximately characterize constraint (3) and obtain the optimal solution.

4.1. A Learning Algorithm to Characterize the Percentile QoS Constraint in Self-Similar Traffic. Algorithm 1 learns the performance of various instance provisioning policies in the form of percentile delay via the stochastic gradient method. The algorithm first creates a data structure called VP_table (Violation Probability Table), in which each item $VP_table[i][k]$ estimates the delay violation probability given the number of instance being k in phase i . The algorithm runs for several iterations to obtain unbiased delay violation probability samples $p[i][k]$ for each phase i . These samples, which can be generated via real system running or simulation, are further smoothed into $VP_table[i][k]$. Therefore, $VP_table[i][k]$ is an unbiased estimation of delay violation probability with k VM instances in phase i . Variables η , i , and k are iteration counter, decision point counter, and instance number counter, respectively. Algorithm 1 has the following property.

Proposition 1. *Algorithm 1 converges to the unbiased estimation of percentile QoS performance of using k VM instances in phase i .*

Proof. The right-hand side of line 11 in Algorithm 1 can be rewritten as

$$E[i][k] = \frac{(\eta - 1) \times \text{VP_table}[i][k] + p[i][k]}{\eta}. \quad (4)$$

Since $p[i][k]$ is an unbiased sample of percentile QoS performance metric, $E[i][k]$ is the mean value of all samples up to iteration η . As long as the end user request arrival process and service process are stationary stochastic processes in phase i with k VM instances, $E[i][k]$ must be an unbiased estimation of percentile QoS performance as $\eta \rightarrow \infty$. \square

In practice, it is impossible to let $\eta \rightarrow \infty$. In fact, Algorithm 1 converges very fast in our numerical analysis (it converges within tens of iterations). Alternatively, we can also use the following equation as the stop criterion:

$$|\text{VP_table}[i][k]_{\eta} - \text{VP_table}[i][k]_{\eta-1}| \leq T, \quad \forall i, k, \quad (5)$$

where T is a threshold value to get a desired precision.

4.2. The Instance Provisioning Algorithm. Based on the VP_table, we can obtain the minimum number of VM instances needed to meet the QoS constraints in phase i , that is, K_i . To find the number of RIS instances k_0 is equal to solve the following optimization problem

$$\min_{k_0} N \times C_L \times k_0 + \sum_{i=1}^N [K_i - k_0]^+ \times C_S \quad (6)$$

subject to

$$\Pr(d_i(k_i) \geq D_{\text{th}}) \leq x, \quad (7)$$

where delay is considered as a function of the number of VM instances.

Problems (6)-(7) are an integer piece-wise function of k_0 where the optimal solution must appear in the boundary points. Algorithm 2 provides the solution method for problem (6). It can be divided into three parts as follows.

- (i) The first part (lines 1-8) uses exhaustive search to obtain the minimum number of VM instance required to satisfy QoS constraints. The result is stored in vector $K_i, i \in \{1, \dots, N\}$.
- (ii) The second part (lines 9-17) solves problems (6)-(7), and the result is k_0 , the optimal number of RIS instances, and the corresponding value of object function m .
- (iii) The third part (lines 18-20) computes the number of MIS instances based on K_i and k_0 .

The worst time complexity of Algorithm 2 is $\mathcal{O}(N \times (\text{MAX_NUM} - \text{MIN_NUM} + 2))$.

5. Extensions

Algorithms 1 and 2 can effectively predict the number of instances needed for satisfying QoS constraints and reducing total rental cost for the ISPs. However, the scalability of these two algorithms is questionable: in order to obtain a precise estimation of the violation probability in VP_table, we must visit all possible instance provisioning policies and get sufficient violation probability samples. This section starts from the point of simplifying VP_table by function approximation techniques to enhance the scalability of Algorithms 1 and 2.

The idea of function approximation is to use a function $x = f_i(K_i)$ to approximate the mapping between the number of instances and the violation probability in phase i . In this paper, we use two forms of approximation:

- (i) a linear approximation given by

$$x = a_i + b_i K_i, \quad b_i < 0, \quad x > 0, \quad (8)$$

- (ii) a nonlinear approximation given by

$$x = a_i \times K_i^{b_i}, \quad b_i < 0. \quad (9)$$

Note that function $f_i(K_i)$ is related to a certain phase i ; therefore the parameters a and b have a subscript i . We have further remarks for these function approximations as follows.

- (1) Intuitively, the QoS violation probability decreases as there are more VM instances; that is, f_i is a decreasing function with respect to K_i ; therefore b_i must be negative in the nonlinear case.
- (2) The value of f_i will all be 0 when K_i exceeds a certain threshold, since no QoS violations occur if there is sufficient number of VM instances. When using linear approximation, we should filter out the case $f_i(K_i) = 0$; otherwise the estimation precision will be remarkably undermined for cases where $f_i(K_i) > 0$.

We use the least square approach to obtain parameters a_i and b_i in the approximate function f_i . Formally, the least square approach is given by

$$\min_{a_i, b_i} F(a_i, b_i) = \frac{1}{2} \sum_{j=1}^n (\hat{x}_i^j - f_i(K_i^j))^2, \quad (10)$$

where n is the amount of samples and \hat{x}_i^j is the j th unbiased sample for violation probability x .

For the linear approximation, the optimal solution should satisfy

$$\frac{\partial F}{\partial a_i} = - \sum_{j=1}^n (\hat{x}_i^j - (a_i + b_i K_i^j)) = 0, \quad (11)$$

$$\frac{\partial F}{\partial b_i} = - \sum_{j=1}^n (\hat{x}_i^j - (a_i + b_i K_i^j)) K_i^j = 0.$$

Input: ITE , N , and SLA specification D_{th} ; { ITE is the number of iterations and N is the number of decision points in a day.}

Output: VP_table;

- (1) Create VP_table and initialize each item in VP_table to 0;
- (2) Create $p[i][k]$ and *counter*; { $p[i][k]$ is a sample of QoS violation ratio of using k VM instances in phase i , and *counter* logs the number of delay violations in a phase.}
- (3) **for** $\eta = 1$ to ITE **do**
- (4) **for** $i = 1$ to N **do**
- (5) **for** $k = \text{MIN_NUM}$ to MAX_NUM **do**
- (6) Log response time d_i for each incoming request;
- (7) **if** $d_i > D_{th}$ **then**
- (8) *counter* + +;
- (9) **end if**
- (10) Calculate an unbiased sample of delay violation probability $p[i][k] = \text{counter}/n_i^\eta$, where n_i^η is the total number of requests arrived in phase i , iteration η ;
- (11) VP_table[i][k] $\leftarrow (\eta - 1)/\eta \times \text{VP_table}[i][k] + (1/\eta) p[i][k]$;
- (12) **end for** {Loop k ;}
- (13) **end for** {Loop i ;}
- (14) **end for** {Loop η ;}

ALGORITHM 1: The learning Algorithm to characterize the Percentile QoS Constraint.

Input: VP_table;

Output: $k_i, i \in \{0, \dots, N\}$; { k_0 is the number of RIS instance, and $k_i, i \neq 0$ is the number of MIS instance in phase i .}

- (1) **for** $i = 1$ to N **do**
- (2) **for** $j = \text{MIN_NUM}$ to MAX_NUM **do**
- (3) **if** VP_table[i][j] $\leq x$ and VP_table[i][$j + 1$] $\geq x$ **then**
- (4) $K_i = j + 1$;
- (5) **break**;
- (6) **end if**
- (7) **end for**
- (8) **end for**
- (9) $k_0 = 0$;
- (10) $m = N \times C_L \times k_0 + \sum_{i=1}^N [K_i - k_0]^+ \times C_S$;
- (11) **for** $i = 1$ to N **do**
- (12) $j = K_i$;
- (13) temp = $N \times C_L \times j + \sum_{i=1}^N [K_i - j]^+ \times C_S$;
- (14) **if** temp < m **then**
- (15) $k_0 = j$;
- (16) **end if**
- (17) **end for**
- (18) **for** $i = 1$ to N **do**
- (19) $k_i = K_i - k_0$;
- (20) **end for**

ALGORITHM 2: The instance provisioning algorithm.

Rearranging these two equations, we have

$$na_i + b_i \sum_{j=1}^n K_i^j = \sum_{j=1}^n \hat{x}_i^j, \quad (12)$$

$$a_i \sum_{j=1}^n K_i^j + b_i \sum_{j=1}^n (K_i^j)^2 = \sum_{j=1}^n K_i^j \hat{x}_i^j.$$

The above analysis suggests

$$b_i = \frac{\sum_{j=1}^n K_i^j \times \sum_{j=1}^n \hat{x}_i^j - n \sum_{j=1}^n K_i^j \hat{x}_i^j}{\left(\sum_{i=1}^n K_i^j\right)^2 - n \sum_{j=1}^n (K_i^j)^2}, \quad (13)$$

$$a_i = \frac{\sum_{j=1}^n \hat{x}_i^j - b_i \sum_{j=1}^n K_i^j}{n}.$$

```

(1) for  $i = 1$  to  $L$  do
(2)   Measure  $\lambda_i$ ;  $\{\lambda_i$  is the number of request arrivals in time window  $i\}$ 
(3)    $t_i = 1/\lambda_i$ ;  $\{\text{Estimate the average inter-arrival time in time window } i.\}$ 
(4)    $A \leftarrow A + \lambda_i$ ;  $\{A$  logs the accumulative total number of request in this time slot. $\}$ 
(5) end for
(6)  $t_a = L/A$ ;  $\{\text{Estimate the average inter-arrival times in the time slot.}\}$ 
(7)  $\sigma = \sqrt{\sum_{i=1}^L \lambda_i (t_i - t_a)^2}$ ;  $\{\text{Estimate the standard deviation of inter-arrival time.}\}$ 
(8)  $C_A = \sigma/t_a$ ;

```

ALGORITHM 3: Online estimation of C_A .

For the nonlinear approximation, let $\chi = \ln x$, $\kappa_i = \ln K_i$, $A_i = \ln a_i$, and $B_i = \ln b_i$, and take “ln” in both sides of (9), which transforms the nonlinear approximation into a linear approximation

$$\chi = A_i + B_i \kappa_i. \quad (14)$$

Following the idea of the linear approximation, we can obtain the solution for the nonlinear approximation as

$$b_i = \frac{\sum_{j=1}^n \ln K_i^j \times \sum_{j=1}^n \ln \hat{x}_i^j - n \sum_{j=1}^n \ln K_i^j \ln \hat{x}_i^j}{\left(\sum_{i=1}^n \ln K_i^j\right)^2 - n \sum_{j=1}^n \left(\ln K_i^j\right)^2}, \quad (15)$$

$$a_i = \exp \left\{ \frac{\sum_{j=1}^n \ln \hat{x}_i^j - b_i \sum_{j=1}^n \ln K_i^j}{n} \right\}.$$

We integrate the function approximations into Algorithms 1 and 2 where VP_table is replaced by an array func_app[N]. Each item in func_app[N] contains 2 elements, that is, a and b . With function approximations, some revisions are needed for Algorithms 1 and 2, which are shown in Table 5.

6. Evaluations

6.1. Simulation Setup. Internet traffic shows a strong self-similar property [3, 15]. We use the Multiscale Markov-Modulated Poisson Processes (MMPP) model to generate a self-similar like traffic. This approach has been proved effective in previous researches [16–18] and was successfully applied in the literatures like [19–22]. We use the approach the same as in [22], that is, a three-dimension Markov on-off modulated Poisson process, to generate the interactive workload arrivals. Consider the following.

- (i) The first dimension is the workload burst in the order of 1 second. We assume that the peak workload arrives at the middle of the day, that is, the 43200th second; therefore the arrival rate as a function of time can be given by

$$\lambda(t) = \begin{cases} \frac{5t}{216 + 1000}, & \text{if } 0 \leq t \leq 43200 \\ \frac{-5t}{216 + 3000}, & \text{if } 43200 < t \leq 86400. \end{cases} \quad (16)$$

- (ii) The second dimension of workload burst is 2000 requests per 5 second.
- (iii) The last dimension of workload burst is 5000 requests per 10 second.

6.2. Estimation of the Response Time. In a production cloud system, it is impossible to log the response time for each incoming request to calculate the delay violation probability. A more practical way is to measure the mean response delay \bar{d} in a small time slot and view \bar{d} as the response delay for all requests arrived in this time slot. This approximation of response delay will be more accurate as the length of the time slot decreases. For example, in [23], the length of the time slot is set to 10 minutes. In our work, we set it to 10 seconds since we need to measure delay violation probability in a higher precision.

To estimate the mean response time in a time slot, we employ the Allen-Cunneen approximation formula [24, 25] for the $G/G/m$ queueing system:

$$R = \frac{1}{\mu} + \frac{P_m}{\mu(1-\rho)} \times \frac{C_A^2 + C_S^2}{2m}, \quad (17)$$

where R is the average response time, μ is the average service rate, λ is the average arrival rate, $\rho = \lambda/\mu m$ is the average utilization of a server, m is the number of servers. P_m takes value from the following formula:

$$P_m = \begin{cases} \rho^{(m+1)/2}, & \text{if } \rho \leq 0.7 \\ \frac{\rho^m + \rho}{2}, & \text{if } \rho > 0.7, \end{cases} \quad (18)$$

C_A and C_S are the coefficients of variation of request interarrival times and service times, respectively.

In this paper, we assume a Poisson service process with $\mu = 100$ requests per second; therefore $C_S = 1$. In order to online estimate C_A , we further divide a time slot into L time windows (see Figure 3). The algorithm to estimate C_A is shown in Algorithm 3.

6.3. Result Analysis

6.3.1. Cost of Various Instance Provisioning Policies. In this experiment, the length of a phase is set to 1hr. From

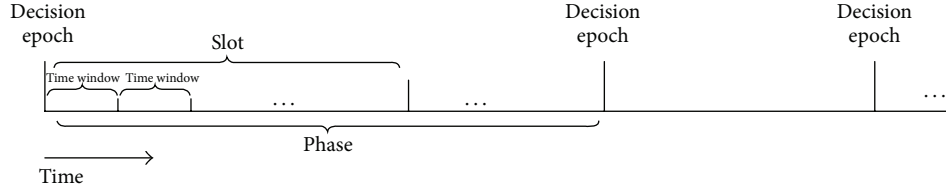


FIGURE 3: The time structure for simulation. A day is divided into several *phases*. The delay violation probability is evaluated in each phase. A phase is divided into several *slots*. The response delay for each request arrived within a slot is approximated by the mean response delay in this slot. To estimate the mean response delay using the Allen-Cunneen formula, a slot is further divided into several time windows to measure the coefficient of variation of inter-arrival time.

Algorithms 1 and 2, we can obtain that the optimal number of RIS instances is 29. Figure 4 shows the cost of three instance provisioning policies. Consider the following.

- (i) In the RIS mode, the ISP should rent 37 instances in all hours of a day since the system must satisfy the peak workload demand. This policy yields 408.576\$ per day.
- (ii) In the MIS mode, the ISP makes instances provisioning decision in each hour according to the predicted demand; therefore the resource utilization is the highest. Unfortunately, the total daily cost (514.08\$) is even higher than the one in the RIS mode.
- (iii) In the hybrid mode, the optimal number of RIS instances is 29. Although, in some cases, this is a little waste of resource, the daily cost of this policy is the lowest (360.768\$).

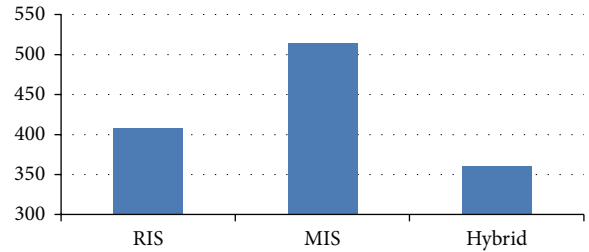


FIGURE 4: Cost of three instance provisioning policies.

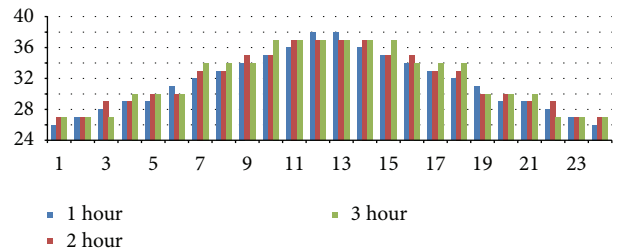


FIGURE 5: The optimal number of reserved VM instances for various rental granularities.

6.3.2. *Effects of the Rental Granularity.* The length of the phase (or interdecision time) in the Amazon EC2 is 1 hour. Here, we vary the length to 2 and 3 hours to study its impact on the daily cost. Figure 5 plots the optimal number of reserved instances in each hour. It goes “smoother” as the length of the interdecision time becomes longer. For example, the numbers of reserved instances for the three rental granularities in time interval [10, 15] are {35, 36, 38, 38, 36, 35}, {35, 37, 37, 37, 37, 35}, and {37, 37, 37, 37, 37, 37}. The mean numbers in time interval [4, 6] and [7, 9] in the 3 hr granularity are 30 and 34, and the counterparts in the 1 hr granularity are 29.67 and 33. This implies that the instance provisioning policy could be more flexible as the interdecision time goes small.

Figure 6 presents the total cost for three rental granularities. It is obvious that the total cost is an increasing function of the length of the interdecision time. However, we can also see that this function is not linear; that is, the marginal cost is shrinking as the length of the interdecision time goes smaller. In production systems, a small interdecision time may induce additional system overhead; therefore there should be a tradeoff between the rental cost and system overhead.

Figure 7 describes the impacts of rental granularity to the delay violation probability. Using instance provisioning policies generated by Algorithms 1 and 2, the target SLA specification is satisfied in all three rental granularities. A

TABLE 2: Means and standard deviations for various rental granularities.

Rental granularity	1 hour	2hours	3hours
Mean	0.041215	0.041218	0.040743
standard deviation	0.002773	0.003848	0.006968

more detailed comparison is provided in Table 2. The means of delay violation probability in 1 hr granularity and 2 hr granularity are very close to each other, and the one in 3 hr granularity is relatively small, implying that more resources are reserved. On the other hand, the standard deviation of the delay violation probability decreases as the length of interdecision time goes smaller. Since a small standard deviation implies a more stable response delay, we propose to use 1 hr granularity rental policy in delay- and jitter-sensitive applications such as VoIP and video streaming.

6.3.3. *Effects of Function Approximations.* Here, we evaluate the effectiveness of two function approximation approaches with 1 hr rental granularity. We can obtain parameters *a* and

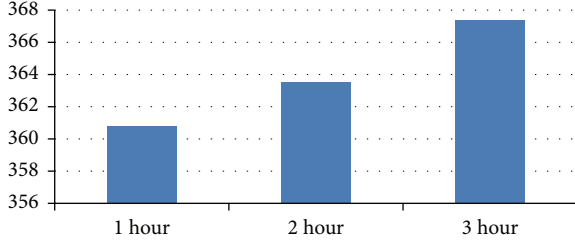


FIGURE 6: Cost for various rental granularities.

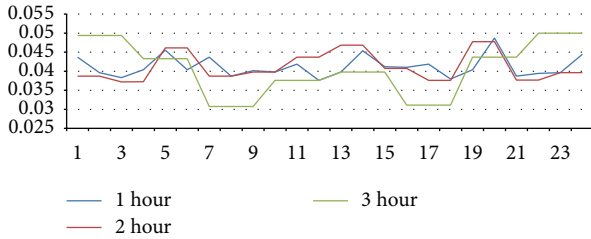


FIGURE 7: Impacts of rental granularity on the delay violation probability.

b using (13) and (15) for all phases, which are shown in Table 3. Specifically, the results in the first hour are plotted in Figure 8, where we can see that the nonlinear approximation is more accurate than the linear approximation. Figure 9 shows the estimation of VM instance demands. The linear approximation tends to overestimate the demand by 2–4, and the nonlinear approximation underestimates the demand by 0–1. Figure 10 shows the delay violation probability. By using VP_table structure, the delay violation probability is around 4%. The linear approximation approach reduces the delay violation probability to about 1% since it reserves more instances. By contrast, the delay violation probabilities in 13 phases (out of total 24 phases) exceed the target 5% objective. The delay violation probabilities even exceed 9% in the 10th and 16th phases.

The basic instance provisioning algorithm makes the best resource-SLA tradeoff but suffers from the scalability problem. The two function approximation approaches only need to estimate two parameters in each phase. They visit fewer instance provisioning policies and evade the lookup table structure (VP_table); thus the scalability of Algorithms 1 and 2 is enhanced. The effectiveness, however, lies in how well the function approximates the behavior of VP_table. A poor approximation may severely deviate from VP_table and generate a wrong instance provisioning policy which either damages the performance or increases the rental cost. Figures 11 and 12 present the number of RIS instances and total daily rental cost. We can see that the number of RIS instances in the VP_table approach is the same as in the one in the nonlinear approximation approach (29 VMs). The linear approximation approach, although achieves a lower delay violation probability, overestimates the VM instance demand too much (33 VMs).

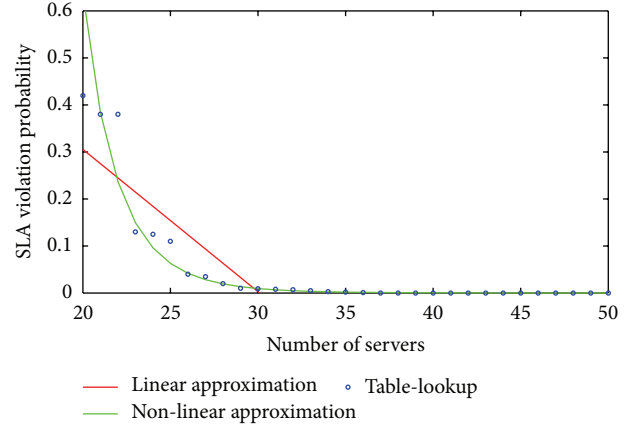


FIGURE 8: Function approximations for VP_table.

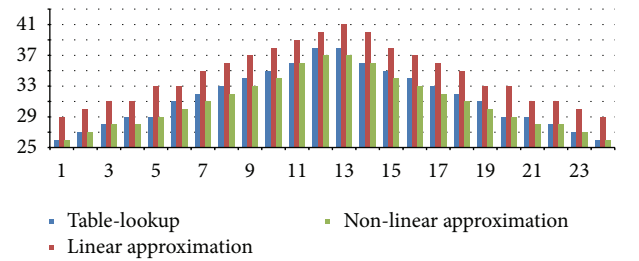


FIGURE 9: Impacts of function approximation on the instance demand estimation.

In order to further evaluate the two function approximation approaches, define the instance deviation D_m and the violation probability deviation D_s as

$$D_m = \sum_{i=1}^{24} |K_i^f - K_i|, \quad (19)$$

$$D_s = \sum_{i=1}^{24} |s_i^f - s_i|,$$

where K_i^f and s_i^f denote the number of rented instances (including both RIS and MIS instances) and the violation probability using function approximations and K_i and s_i denote the same parameters but using the VP_table structure. Clearly, smaller D_m and D_s indicate a more accurate approximation. The results are shown in Table 4. The linear approximation achieves a lower violation probability at the expense of a much higher number of instances. In addition, nonlinear approximation has a lower violation probability deviation. Therefore, we purpose to use nonlinear approximation in Algorithms 1 and 2.

7. Conclusions

Dynamic instance provisioning is a key issue for Internet service providers in the cloud computing environment. In this paper, we investigate the coarse-grain (in the order of hours) QoS-aware dynamic instance provisioning problem

TABLE 3: Parameters for two function approximation approaches.

Decision epoch	Linear approximation		Nonlinear approximation	
	a	b	a	b
1	0.910558	-0.03026	$1.96E + 13$	-10.3672
2	1.17268	-0.03832	$3.42E + 13$	-10.4338
3	1.31243	-0.04182	$6.23E + 13$	-10.5444
4	1.50093	-0.04697	$4.04E + 13$	-10.3147
5	1.46158	-0.04394	$1.62E + 13$	-9.97221
6	1.59491	-0.04727	$3.68E + 12$	-9.43435
7	1.49158	-0.04142	$5.56E + 11$	-8.76771
8	1.57272	-0.043	$2.35E + 11$	-8.44603
9	1.63012	-0.04319	$1.16E + 11$	-8.13732
10	1.6601	-0.04237	$5.02E + 10$	-7.84783
11	1.75972	-0.04396	$1.81E + 10$	-7.47832
12	1.81333	-0.04415	$6.70E + 09$	-7.12764
13	1.81285	-0.04386	$8.02E + 09$	-7.17651
14	1.75933	-0.0437	$1.76E + 10$	-7.4644
15	1.7186	-0.04436	$4.01E + 10$	-7.77709
16	1.63952	-0.04352	$6.46E + 10$	-7.9815
17	1.58403	-0.04322	$1.83E + 11$	-8.36223
18	1.55035	-0.04373	$1.20E + 12$	-9.01639
19	1.54785	-0.0454	$3.54E + 12$	-9.41871
20	1.38708	-0.04119	$5.03E + 12$	-9.60535
21	1.50875	-0.04732	$8.56E + 13$	-10.5575
22	1.31375	-0.04188	$2.37E + 13$	-10.2367
23	1.16168	-0.03787	$3.70E + 13$	-10.4633
24	0.866371	-0.02836	$1.52E + 13$	-10.2863

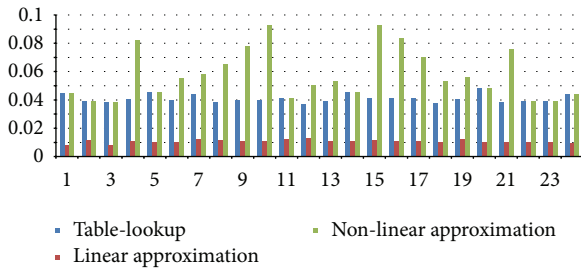


FIGURE 10: Impacts of function approximation on the delay violation probability.

for interactive workload. The optimization problem in our consideration (see (2)-(3)) is not a traditional optimization problem since the QoS constraint (3) has no analytical form for the self-similar Internet traffic; therefore it cannot be solved using classic methods. We use various approaches, for example, a lookup table and two function approximations to characterize constraint (3). The lookup table approach suffers from the scalability issue, because, in order to obtain a precise estimation of the violation probability in the table, we must visit all possible instance provisioning policies and get sufficient violation probability samples. In contrast, function approximations can predict the performance using a small set of samples. Function approximations (especially

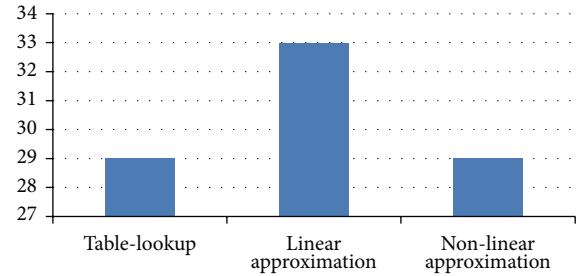


FIGURE 11: The optimal number of RIS instances.

TABLE 4: The instance deviation and the violation probability deviation for two function approximation approaches.

Metric	Approximations	
	Linear	Nonlinear
D_m	70	14
D_s	0.730222	0.407333

nonlinear approximation) address the scalability problem at the expense of a little sacrifice of prediction precision. We conduct extensive simulations to evaluate the effectiveness of the proposed dynamic instance provisioning policy.

TABLE 5: Revisions for Algorithms 1 and 2 with function approximations.

Revisions for Algorithm 1	Revisions for Algorithm 2
<p>(i) In line 5, there is no need to test each instance provisioning policy in [MIN_NUM, MAX_NUM]. Instead, we can use either approach listed as follows.</p> <p>(1) Define a positive integer variable <i>stepsize</i> which is greater than 1, and increase <i>k</i> by <i>stepsize</i> rather than 1.</p> <p>(2) Pick a small set of <i>k</i> randomly from [MIN_NUM, MAX_NUM].</p> <p>(ii) Compute a_i and b_i using (13) and (15) after line 19.</p> <p>(iii) The output of the algorithm is $\text{func_app}[N]$.</p>	<p>(i) The input of the algorithm is $\text{func_app}[N]$.</p> <p>(ii) The exhausted search approach (lines 2–7) is replaced by the inverse functions of (8) and (9) as follows.</p> <p>(1) For linear approximation case,</p> $K_i = \left\lceil \frac{x - \text{func_app}[i] \cdot a}{\text{func_app}[i] \cdot b} \right\rceil.$ <p>(2) For nonlinear approximation case,</p> $K_i = \left\lceil \frac{\text{func_app}[i] \cdot b}{\sqrt{\text{func_app}[i] \cdot a}} \right\rceil,$ <p>where $\lceil x \rceil$ is the smallest integer no less than x.</p>

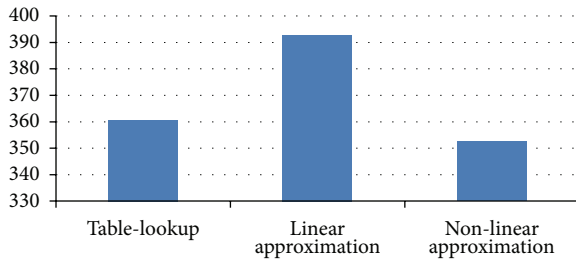


FIGURE 12: The daily rental cost.

Notations

- N : The number of phases in a day to make instance provisioning decisions, that is, the number of decision points
- K_i : The number of instances needed in phase i to meet the QoS requirement
- C_L : The marginal rental cost for a RIS instance
- C_S : The marginal rental cost for a MIS instance
- d_i : The delay in phase i
- D_{th} : The threshold delay set by the SLA
- x : The threshold violation probability set by the SLA.

Conflict of Interests

The authors declare that there is no conflict of interests regarding the publication of this paper.

Acknowledgments

The work is funded in part by the National Natural Science Foundation of China (NSFC) under Grant no. 61363052, the Inner Mongolia Provincial Natural Science Foundation under Grant nos. 2010MS0913 and 2013MS0920, and the Science Research Project for Inner Mongolia College under Grant nos. NJZY14064 and NJZY13120.

References

- [1] D. Meisner, B. T. Gold, and T. F. Wenisch, "PowerNap: Eliminating server idle power," in *Proceedings of the 14th International Conference on Architectural Support for Programming Languages and Operating Systems (ASPLOS '09)*, pp. 205–216, Washington, DC, USA, March 2009.
- [2] "A. E. instance launch time," <http://aws.amazon.com/ec2/faqs/#Howquicklywillsystemsberunning>.
- [3] W. E. Leland, M. S. Taqqu, W. Willinger, and D. V. Wilson, "On the self-similar nature of Ethernet traffic (extended version)," *IEEE/ACM Transactions on Networking*, vol. 2, no. 1, pp. 1–15, 1994.
- [4] Y. Chen, A. Das, W. Qin, A. Sivasubramaniam, Q. Wang, and N. Gautam, "Managing server energy and operational costs in hosting centers," in *Proceedings of the ACM International Conference on Measurement and Modeling of Computer Systems (SIGMETRICS)*, Banff, Canada, 2005.
- [5] D. Gmach, J. Rolia, L. Cherkasova, and A. Kemper, "Workload analysis and demand prediction of enterprise data center applications," in *proceedings of the IEEE 10th International Symposium on Workload Characterization (IISWC '07)*, Boston, Mass, USA, 2007.
- [6] E. Caron and F. Desprez, "Forecasting for grid and cloud computing ondemand resources based on pattern matching," in *Proceedings of the 2nd IEEE International Conference on Cloud Computing Technology and Science (CloudCom '10)*, pp. 456–463, Indianapolis, Ind, USA, 2010.
- [7] D. Niu, H. Xu, B. Li, and S. Zhao, "Quality-assured cloud bandwidth auto-scaling for video-on-demand applications," in *Proceedings of the IEEE INFOCOM*, pp. 460–468, Orlando, Fla, USA, 2012.
- [8] F. Ahmad and T. N. Vijaykumar, "Joint optimization of idle and cooling power in data centers while maintaining response time," in *Proceedings of the 15th International Conference on Architectural Support for Programming Languages and Operating Systems (ASPLOS '10)*, pp. 243–256, March 2010.
- [9] J. Leverich and C. Kozyrakis, "On the energy (in)efficiency of hadoop clusters," *ACM SIGOPS Operating Systems Review*, vol. 44, no. 1, pp. 61–65.
- [10] S. Shen, K. Deng, A. Iosup, and D. Epema, "Scheduling jobs in the cloud using on-demand and reserved instances," in *Euro-Par 2013 Parallel Processing*, vol. 8097 of *Lecture Notes in Computer Science*, pp. 242–254, Springer, Berlin, Germany, 2013.
- [11] W. Ming, Y. Jian, and R. Yongyi, "Dynamic instance provisioning strategy in an iaas cloud," in *Proceedings of the 32nd*

- Chinese Control Conference (CCC '13)*, pp. 6670–6675, Xi'an, China, 2013.
- [12] D. Deng, Z. Lu, W. Fang, and J. Wu, "Cloudstreammedia: a cloud assistant global video on demand leasing scheme," in *Proceedings of the IEEE 10th International Conference on Services Computing (SCC '13)*, pp. 486–493, Washington, DC, USA, 2013.
- [13] W. Fang, Z. Lu, J. Wu, and Z. Cao, "Rpps: a novel resource prediction and provisioning scheme in cloud data center," in *IEEE Ninth International Conference on Services Computing (SCC '12)*, pp. 609–616, Honolulu, Hawaii, USA, 2012.
- [14] J. Jiang, J. Lu, G. Zhang, and G. Long, "Optimal cloud resource auto-scaling for web applications," in *Proceedings of the 13th IEEE/ACM International Symposium on Cluster, Cloud and Grid Computing (CCGrid)*, pp. 58–65, Delft, The Netherlands, 2013.
- [15] M. E. Crovella and A. Bestavros, "Self-similarity in world wide web traffic: evidence and possible causes," *IEEE/ACM Transactions on Networking*, vol. 5, no. 6, pp. 835–846, 1997.
- [16] T. Yoshihara, S. Kasahara, and Y. Takahashi, "Practical time-scale fitting of self-similar traffic with markov-modulated poisson process," *Telecommunication Systems*, vol. 17, no. 1-2, pp. 185–211, 2001.
- [17] P. Salvador, R. Valadas, and A. Pacheco, "Multiscale Fitting Procedure Using Markov Modulated Poisson Processes," *Telecommunication Systems*, vol. 23, no. 1-2, pp. 123–148, 2003.
- [18] A. T. Andersen and B. F. Nielsen, "A Markovian approach for modeling packet traffic with long-range dependence," *IEEE Journal on Selected Areas in Communications*, vol. 16, no. 5, pp. 719–732, 1998.
- [19] M. Guazzone, C. Anglano, and M. Canonico, "Exploiting VM migration for the automated power and performance management of green cloud computing systems," in *Energy Efficient Data Centers*, vol. 7396 of *Lecture Notes in Computer Science*, pp. 81–92, Springer, Berlin, Germany, 2012.
- [20] D. Bruneo, "A stochastic model to investigate data center performance and qos in iaas cloud computing systems," *IEEE Transactions on Parallel and Distributed Systems*, vol. 25, no. 3, pp. 560–569, 2013.
- [21] T. H. Szymanski, "Low latency energy efficient communications in global-scale cloud computing systems," in *Proceedings of the ACM Workshop on Energy Efficient High Performance Parallel and Distributed Computing (EEHDPC '13)*, pp. 13–22, 2013.
- [22] J. Tai, J. Zhang, J. Li, W. Meleis, and N. Mi, "Ara: Adaptive resource allocation for cloud computing environments under bursty workloads," in *Proceedings of the IEEE 30th International Performance Computing and Communications Conference (IPCCC '11)*, pp. 1–8, 2011.
- [23] Y. J. Hong, J. Xue, and M. Thottethodi, "Selective commitment and selective margin: techniques to minimize cost in an iaas cloud," in *Proceedings of the IEEE International Symposium on Performance Analysis of Systems and Software (ISPASS '12)*, pp. 99–109, 2012.
- [24] A. O. Allen, *Probability, Statistics, and Queueing Theory with Computer Science Applications*, Academic Press, Boston, Mass, USA, 1990.
- [25] G. Bolch, S. Greiner, H. de Meer, and K. S. Trivedi, *Queueing Networks and Markov Chains*, Wiley-Interscience, New York, NY, USA, 1998.

Research Article

A Bayesian Network Method for Quantitative Evaluation of Defects in Multilayered Structures from Eddy Current NDT Signals

Bo Ye,¹ Hongchun Shu,¹ Min Cao,² Fang Zeng,¹ Gefei Qiu,¹ Jun Dong,¹
Wenyong Zhang,¹ and Jieshan Shan¹

¹Engineering Research Center of Smart Grid, Faculty of Electric Power Engineering, Kunming University of Science and Technology, Kunming, Yunnan 650500, China

²Oxbridge College, Kunming University of Science and Technology, Kunming 650106, China

Correspondence should be addressed to Bo Ye; yeripple@hotmail.com

Received 12 December 2013; Accepted 19 February 2014; Published 25 March 2014

Academic Editor: Huaicheng Yan

Copyright © 2014 Bo Ye et al. This is an open access article distributed under the Creative Commons Attribution License, which permits unrestricted use, distribution, and reproduction in any medium, provided the original work is properly cited.

Accurate evaluation and characterization of defects in multilayered structures from eddy current nondestructive testing (NDT) signals are a difficult inverse problem. There is scope for improving the current methods used for solving the inverse problem by incorporating information of uncertainty in the inspection process. Here, we propose to evaluate defects quantitatively from eddy current NDT signals using Bayesian networks (BNs). BNs are a useful method in handling uncertainty in the inspection process, eventually leading to the more accurate results. The domain knowledge and the experimental data are used to generate the BN models. The models are applied to predict the signals corresponding to different defect characteristic parameters or to estimate defect characteristic parameters from eddy current signals in real time. Finally, the estimation results are analyzed. Compared to the least squares regression method, BNs are more robust with higher accuracy and have the advantage of being a bidirectional inferential mechanism. This approach allows results to be obtained in the form of full marginal conditional probability distributions, providing more information on the defect. The feasibility of BNs presented and discussed in this paper has been validated.

1. Introduction

Detection and quantitative evaluation of internal defects in multilayered structures are an essential task in a range of technological applications, such as maintaining the integrity of structures, enhancing the safety of aging aircraft, and assuring the quality of products [1–3]. Defects are generally formed in multilayered structures by residual stress or physical or metallurgical processes, and they can increase in both number and size with time, due to fatigue and corrosion, causing damage and sometimes sudden structural failure. Quantitative evaluation of defect characteristics, such as size, shape, and orientation, is highly desirable and is an emergent technique [4]. Experimental measurement should take advantage of advanced nondestructive testing (NDT) technologies, and it will be extremely valuable if early and

accurate detection of defects is possible, especially where defects are related to internal damage.

Over the last several years, a number of NDT techniques have been developed for the detection and characterization of defects in multilayered structures. They are based on eddy current (EC) [5], ultrasonic [6], terahertz ray [7], thermal [8], acoustic emission [9], and X-ray [10] measurements of the various structures tested. In the inspection of multilayered metallic structures, radiographic inspection has problems associated with radiation protection, ultrasound methods suffer from the high attenuation and the low reliability, and in thermographic inspection there is a problem with measurement precision. It would appear that these techniques have certain limitations in inspecting defects in multilayered structures where it is only possible to obtain access to one side of the sample. In contrast, eddy current nondestructive

testing (ECNDT) is relatively rapid and has the advantages of having high sensitivity, being noncontact, of low cost, and easily implemented for automated, online testing and is one of the rigorous, physics-based approaches for identifying micro hidden defects [11, 12].

Characterizing defects from measurements of the change in the eddy current is generally considered as the inverse problem [13–15]. Thus, the results of the quantitative evaluation of defects are retrieved by inversion of the measured data representing the change in impedance of a coil as it scans the specimen [16, 17]. Since the physical model of ECNDT is often complicated and nonlinear, the inversion process is often ill posed [18]. The methods based on solving Maxwell equations of electromagnetic field using numerical analysis, such as finite element method (FEM), boundary element method (BEM), and volume integral method (VIM), have been successfully developed to simulate the response of the measurement system to different thickness aluminum alloy planar structures and, to some extent, more realistic defects with complex profiles [19]. Nevertheless, the inverse problems are not yet fully resolved, for even the quantitative evaluation of simple shaped defects from ECNDT signals [20].

More recently, quantitative evaluation of defects has been implemented by using many sophisticated algorithms. The template matching method is firstly advocated [21]. Measurements are recorded on calibration samples and specific defect signals are stored as a standard template such as EC signals shape, peak voltage, phase data, smoothness, convexity, unimodality, or existence of derivatives. The evaluation results are obtained from the comparison of the currently collected signals with each calibration defect. In this type of method, the features used to characterize the probe response are not sufficient for inspection and can easily become ineffective owing to noise, interference, and lift-off variation, leading to inaccurate results. Then, some researchers present model-based approaches to evaluate defects from EC signals [22]. These methods iteratively solve the forward model to simulate the inspection process and predict the probe response. The inverse problem of quantitative evaluation of defects is formulated as an optimization problem, which seeks a set of defect characteristic parameters by minimizing an objective function, representing the difference between the model predicted signals and the measured signals. Such approaches usually involve significant computational effort, since the physical model needs to be solved repeatedly. Afterwards, methods based on neural networks and the least squares (LS) regression have been used to establish the relationship between the defect characteristic parameters and the observed data [23, 24]. These methods usually require a large volume of prior knowledge, space limitations, and database of signals from defects for training. However, the training samples are often difficult to obtain for real industrial applications and there are obvious errors when a sample has never been contained in training set. Recently, there has been much interest in use of probability density function estimation and Bayesian estimation methods for quantitative evaluation of defects [25–27]. These methods employ sampling techniques such as Markov Chain Monte Carlo (MCMC) and Bootstrap methods, for probability density function estimation of defect

characteristic parameters to obtain not only the quantity but also the uncertainty characterization of the measurand. The main problem with these methods is that sampling techniques require a significant amount of time. Therefore, a general framework for quantitative evaluation of defects from EC signals is very desirable, which can rapidly and accurately give the evaluation of defect characteristics.

In this paper, we propose the use of Bayesian networks (BNs) [28] to evaluate defects quantitatively from EC inspection signals. In ECNDT, the output signals may be corrupted by noise and other anomalous signals, arising from lift-off, edge effects, high frequency, probe angle variations, and so forth. This will result in unreliable detection and inaccurate characterization of defect. Although some of noise may be eliminated or decreased by a number of preprocessing algorithms, the inherent uncertainty and stochastic nature of inspection still need to be dealt with. BNs are a useful method for EC inversion modeling, because of their capability of handling uncertainty and incorporating prior information, providing more accurate evaluation results. They offer a natural and compact tool for dealing with two problems that occur throughout EC inversion modeling, uncertainty and complexity, and also a basis for efficient probabilistic inference [29]. In ECNDT, BNs generalize not only the forward model but also the inverse model by using bidirectional probability inference. This is an important advantage compared with traditional methods (e.g., LS regression method) that encode only the values of the dependent variables, given the input variables. In this paper, BNs are applied to quantitatively evaluate the realistic multidimensional characteristic parameters of defects by probability inference. We mainly discuss how to construct BNs from the domain knowledge and the real research data and how to perform probability inference in BNs. The proposed BNs allow us to obtain the full probability distributions of the needed evaluation characteristic parameters of defects, which give the accurate evaluation of defects and quantify its uncertainty characterization. Experimental results show that the proposed method maintains higher estimation accuracy than the previous methods.

The remainder of the paper is organized as follows. Section 2 gives the general formulation of quantitative evaluation of defects in multilayered structures using BNs. Section 3 reviews the principle of BNs which are applied to evaluate defect characteristics. Section 4 presents experiments and results. Finally, Section 5 contains conclusions.

2. Problem Description

The eddy current problem can be described mathematically by partial differential equations in terms of the magnetic vector potential:

$$\nabla^2 \mathbf{A} + k^2 \mathbf{A} = -\mu \mathbf{J}_s, \quad (1)$$

where \mathbf{A} represents the magnetic vector potential, $k^2 = -j\omega\mu(\sigma + j\omega\epsilon)$, j is imaginary unit, ω is the angular frequency of the excitation current, μ is the magnetic permeability of the media involved (H/m), σ is the electrical conductivity (S/m),

ε is the dielectric constant (F/m), and \mathbf{J}_s is the excitation current density (Amp/m²).

The forward problem under consideration is the calculation of the field perturbation due to a volumetric defect assuming time harmonic operations and linear and nonmagnetic conductors [30]. The main goal of solving the forward problem is to predict the probe response signals, given the defect parameters. On the contrary, the inverse problem is described as the task of quantitative evaluation of defect characteristics from the measured EC signals [31].

In this paper, EC inspection is treated as a static, stochastic process. The defect characteristic parameters and the observed signals are regarded as continuous random variables. Initially, the probability distributions of all variables are assumed as multivariate Gaussian, with unknown means and variances (classical assumptions). We construct a multivariate Gaussian model for the process of ECNDT, represented as a simple graphical model within the BNs which provide a modeling language and associated inference algorithm for stochastic domains. Then, the following work is to obtain the posterior probability distributions of all unknown variables, using Bayesian inference. Bayesian inference is based on Bayes Theorem as [32]

$$p(\mathbf{X} | \mathbf{D}) = \frac{p(\mathbf{X}) p(\mathbf{D} | \mathbf{X})}{p(\mathbf{D})} = \frac{p(\mathbf{X}) p(\mathbf{D} | \mathbf{X})}{\int_{\mathbf{X}} p(\mathbf{X}) p(\mathbf{D} | \mathbf{X}) d\mathbf{X}}, \quad (2)$$

where \mathbf{D} is the observed data set, \mathbf{X} is the unknown variables needing estimation, $p(\mathbf{X})$ is the prior probability of \mathbf{X} , $p(\mathbf{D} | \mathbf{X})$ is the likelihood function, which incorporates the statistical relationships in addition to the mechanistic relationships among \mathbf{D} and \mathbf{X} , and $p(\mathbf{X} | \mathbf{D})$ is the posterior probability of \mathbf{X} . Using BNs, we calculate the posterior distributions of \mathbf{X} , when the known data arrive. However, normally one is interested in giving point predictions and/or probability intervals for predictions. We may use the means of distributions of \mathbf{X} as predictions and variances for probability intervals.

A complete diagram of the quantitative evaluation of defects is shown in Figure 1. The quantitative evaluation procedure is summarized as follows. The domain knowledge about ECNDT is used to formulate the structure of BNs representing the inspection models. Then, it is trained using real research labeled data, consisting of the EC signals and the corresponding defect characteristic parameters. After training, the results produce a generative model, suitable for use in ECNDT systems, which is able to predict the signals corresponding to different defect characteristic parameters or estimate defect characteristic parameters from the EC signals in real time.

3. Bayesian Networks

BNs were initially developed in the late 1970s. Over the last decade, BNs have become an established framework for representing and reasoning with uncertain knowledge [33]. More recently, researchers have developed methods using BNs to analyze measured data. These techniques that have been developed are new and still evolving, but they

have been shown to be remarkably effective for many real-life inversion problems such as diagnosis of space shuttle propulsion systems, situation assessment for nuclear power plant, and information retrieval [34].

3.1. Bayesian Networks Models. BNs are mathematical models, combining graphics and probabilities to express mutual relationships between variables [35]. Let $\mathbf{V} = \{\mathbf{V}_1, \mathbf{V}_2, \dots, \mathbf{V}_N\}$ be a set of random variables, with each variable \mathbf{V}_i taking values in some finite domain $\text{Dom}\{\mathbf{V}_i\}$. BNs over \mathbf{V} is a pair (\mathbf{G}, θ) that represents a set of distributions over the joint space of \mathbf{V} . \mathbf{G} is a set of directed acyclic graphs (DAGs), whose nodes correspond to the random variables in \mathbf{V} , and whose structure encodes conditional independence properties about the joint distributions. Each node \mathbf{V}_i directly depends on its parents $\text{Par}(\mathbf{V}_i)$. θ is a set of parameters which quantify the network by specifying the conditional probability distributions (CPDs) $P(\mathbf{V}_i | \text{Par}(\mathbf{V}_i))$. Given $\text{Par}(\mathbf{V}_i) \subseteq \{\mathbf{V}_1, \mathbf{V}_2, \dots, \mathbf{V}_{i-1}\}$ is a set of variables that renders \mathbf{V}_i and $\{\mathbf{V}_1, \mathbf{V}_2, \dots, \mathbf{V}_{i-1}\}$ independent, we can decompose a joint probability density $P(\mathbf{V})$ using the chain rule of probability

$$P(\mathbf{V}) = \prod_{i=1}^N P(\mathbf{V}_i | \text{Par}(\mathbf{V}_i)). \quad (3)$$

Note that $\text{Par}(\mathbf{V}_i)$ does not need to include all elements of $\{\mathbf{V}_1, \mathbf{V}_2, \dots, \mathbf{V}_{i-1}\}$ which indicate conditional independence between those variables not included in $\text{Par}(\mathbf{V}_i)$ and \mathbf{V}_i , given that the variables in $\text{Par}(\mathbf{V}_i)$ are known.

In this paper, we use these ideas in context with continuous variables and dependencies, where the probability distributions of all continuous variables are multivariate Gaussian distributions. Each variable \mathbf{V}_i is a multivariate Gaussian distribution $N(\boldsymbol{\mu}_i, \boldsymbol{\Sigma}_i)$, and its probability density function is

$$P(\mathbf{V}_i) = (2\pi)^{-n/2} |\boldsymbol{\Sigma}_i|^{-1/2} \cdot \exp \left\{ -\frac{1}{2(\mathbf{V}_i - \boldsymbol{\mu}_i)^T \boldsymbol{\Sigma}_i^{-1} (\mathbf{V}_i - \boldsymbol{\mu}_i)} \right\}, \quad (4)$$

where $\boldsymbol{\mu}_i$ is the n -dimensional mean vector, $\boldsymbol{\Sigma}_i$ is the $n \times n$ variance matrix, $|\boldsymbol{\Sigma}_i|$ is the determinant of $\boldsymbol{\Sigma}_i$, and $(\mathbf{V}_i - \boldsymbol{\mu}_i)^T$ denotes the transpose of $(\mathbf{V}_i - \boldsymbol{\mu}_i)$. Then, the CPDs can be represented in BNs by using linear Gaussian conditional densities. Given its parents are known, in this representation, the conditional density of \mathbf{V}_i is

$$P(\mathbf{V}_i | \text{Par}(\mathbf{V}_i)) \sim N(\boldsymbol{\phi}_i, \boldsymbol{\tau}_i^2), \quad (5)$$

where $\boldsymbol{\phi}_i = \boldsymbol{\mu}_i + \sum_{j=1}^{i-1} \beta_{ij}(\mathbf{V}_j - \boldsymbol{\mu}_j)$, β_{ij} is the regression coefficient of \mathbf{V}_j in the regression of \mathbf{V}_i on the parents of \mathbf{V}_i , $\text{Par}(\mathbf{V}_i)$, and $\boldsymbol{\tau}_i^2 = \boldsymbol{\Sigma}_i - \boldsymbol{\Sigma}_{i\text{Par}(\mathbf{V}_i)} \boldsymbol{\Sigma}_{\text{Par}(\mathbf{V}_i)}^{-1} \boldsymbol{\Sigma}_{i\text{Par}(\mathbf{V}_i)}^T$ is the conditional variance of \mathbf{V}_i , given $\text{Par}(\mathbf{V}_i)$, where $\boldsymbol{\Sigma}_i$ is the unconditional variance of \mathbf{V}_i , $\boldsymbol{\Sigma}_{i\text{Par}(\mathbf{V}_i)}$ is the matrix of covariance between \mathbf{V}_i and the variables in $\text{Par}(\mathbf{V}_i)$, and $\boldsymbol{\Sigma}_{\text{Par}(\mathbf{V}_i)}$ is the covariance matrix of $\text{Par}(\mathbf{V}_i)$ [36].

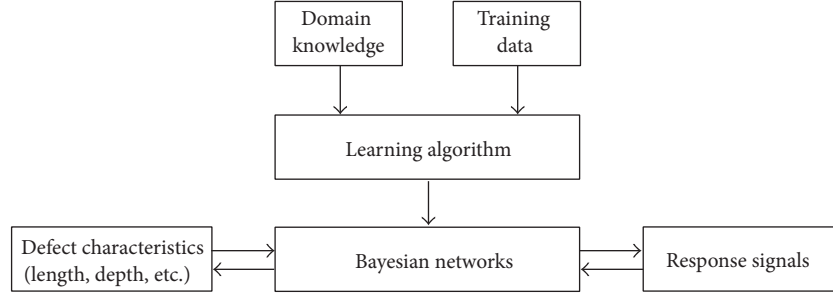


FIGURE 1: The flowchart of quantitative evaluation of defects using BNs.

3.2. Learning Bayesian Networks. Learning generally refers to learning the graphical structure or the parameters (CPDs) for that structure or both [37, 38]. The learning results are a set of techniques for data analysis that combines prior knowledge with real data to produce improved knowledge. In a real application, the domain knowledge is based on a special set of rules, which can be used to create BNs structures on a case-by-case basis. It is clear that the models created in this way are strictly based on the special physical process, since the structure of the graph is automatically generated, given the rules and the background facts. During the quantitative evaluation of defects from ECNDT signals, the BNs structures can be constructed using the knowledge about ECNDT and defect characteristics. The structure construction approaches will be described in Section 4 in detail. In this section, we consider only the problem of using data to determine the probabilities of a given structure.

The problem of learning BNs in this case can be stated as follows. Given a training set $\mathbf{D} = \{\mathbf{D}_1, \mathbf{D}_2, \dots, \mathbf{D}_M\}$ of independent instances, find the θ of BNs that best matches \mathbf{D} . The assumption of the linear Gaussian conditional distributions of all variables in the BNs would be considered. The task of unknown parameters θ estimation is to find the maximum likelihood estimation (MLE) of mean and variance vectors [39]. The MLE method is versatile and easy implementation and can be applied to most models and different types of data. If Gaussian prior distributions are assumed over the parameters, the MLE coincides with the most probable values thereof. The normalized log-likelihood of the training set \mathbf{D} is a sum of terms:

$$\begin{aligned}
 L(\theta) &= \ln \prod_{m=1}^M P(\mathbf{D}_m | \theta) \\
 &= \sum_{i=1}^N \sum_{m=1}^M \ln P(\mathbf{V}_i | \text{Par}(\mathbf{V}_i), \mathbf{D}_m).
 \end{aligned} \tag{6}$$

The MLE method maximizes $L(\theta)$ by finding the value of $\hat{\theta}$:

$$\hat{\theta} = \arg \max_{\theta} L(\theta). \tag{7}$$

The log-likelihood function decomposes according to the structure of the graph, and hence the contribution to the log-likelihood of each node can be maximized independently.

For the multivariate Gaussian CPDs, the log-likelihood function is given by

$$\begin{aligned}
 L(\theta) &= \ln \prod_{m=1}^M P(\mathbf{D}_m | \theta) \\
 &= -\frac{1}{2} \ln [(2\pi)^{-n} |\boldsymbol{\tau}|] - \frac{1}{2} \sum_{m=1}^M (\mathbf{D}_m - \boldsymbol{\phi})^T \boldsymbol{\tau}^{-1} (\mathbf{D}_m - \boldsymbol{\phi}).
 \end{aligned} \tag{8}$$

The family of distributions has two parameters: $\theta = (\boldsymbol{\phi}, \boldsymbol{\tau}^2)$. Therefore, we maximize the likelihood over both parameters simultaneously, or if possible individually. Taking the partial derivatives of $L(\theta)$, with respect to each one of the parameters and setting it equal to zero yields

$$\begin{aligned}
 \frac{\partial}{\partial \boldsymbol{\phi}} \left\{ -\frac{1}{2} \ln [(2\pi)^{-n} |\boldsymbol{\tau}|] \right. \\
 \left. - \frac{1}{2} \sum_{m=1}^M (\mathbf{D}_m - \boldsymbol{\phi})^T \boldsymbol{\tau}^{-1} (\mathbf{D}_m - \boldsymbol{\phi}) \right\} &= 0, \\
 \frac{\partial}{\partial \boldsymbol{\tau}} \left\{ -\frac{1}{2} \ln [(2\pi)^{-n} |\boldsymbol{\tau}|] \right. \\
 \left. - \frac{1}{2} \sum_{m=1}^M (\mathbf{D}_m - \boldsymbol{\phi})^T \boldsymbol{\tau}^{-1} (\mathbf{D}_m - \boldsymbol{\phi}) \right\} &= 0.
 \end{aligned} \tag{9}$$

Solving (9) simultaneously yields

$$\begin{aligned}
 \hat{\boldsymbol{\phi}} &= \frac{1}{M} \sum_{m=1}^M \mathbf{D}_m, \\
 \hat{\boldsymbol{\tau}} &= \frac{1}{M} \sum_{m=1}^M (\mathbf{D}_m - \hat{\boldsymbol{\phi}}) (\mathbf{D}_m - \hat{\boldsymbol{\phi}})^T.
 \end{aligned} \tag{10}$$

Formally, we say that the maximum likelihood estimator for $\theta = (\boldsymbol{\phi}, \boldsymbol{\tau}^2)$ is $\hat{\theta} = (\hat{\boldsymbol{\phi}}, \hat{\boldsymbol{\tau}}^2)$.

3.3. Inference in Bayesian Networks. In general, the computation of marginal CPDs of interest is known as probabilistic inference [40, 41]. The main goal of inference is to estimate the values and their probabilities of the unknown nodes, given

the values of the observed nodes. When observations are given, this knowledge is integrated into the network and all the probabilities are updated accordingly. If we observe the “leaves” of a generative model and try to infer the values of the causes, this is called diagnosis or bottom-up reasoning. If we observe the “roots” of a generative model and try to predict the effects, this is called prediction or top-down reasoning. BNs can be used for both of these tasks and others. In ECNDT, bidirectional probability inference permits BNs to respond to both predictive inference and diagnostic inference. Thus, BNs will have the utmost flexibility for predicting the signals corresponding to different defect characteristic parameters or for estimating defect characteristic parameters from the EC signals in real time.

The junction tree method is a new iterative algorithm that efficiently combines dynamic discretization with robust propagation algorithms to perform inference in BNs [42]. A junction tree representing BNs (\mathbf{G}, θ) is constructed by moralization and triangulation of \mathbf{G} ; that is, it connects together all parents who share a common child, then drops the directionality of the arcs, and selectively adds arcs to the moral graph to form a triangulated graph. In a junction tree, the basic nodes are represented as cliques which are maximal complete subgraphs of the triangulated graph. The separator $\mathbf{S} = \mathbf{C}_i \cap \mathbf{C}_j$ is a path between two cliques \mathbf{C}_i and \mathbf{C}_j and the subset of \mathbf{C}_i and \mathbf{C}_j [43].

After building a junction tree “shell,” we define potentials over cliques and separators. A potential is a nonnegative function of its arguments, which can be interpreted as the probabilities over cliques and separators. We denote these potentials as $\psi(\mathbf{C})$ and $\psi(\mathbf{S})$. Every CPD of the original BNs $P(\mathbf{V}_i \mid \text{Par}(\mathbf{V}_i))$ is associated with a clique, such that the domain of the distributions is the subset of the clique domain. The notation $\text{Dom}(\psi)$ represents the domain of a potential ψ . A Gaussian clique potential can be represented in either moment form

$$\begin{aligned} \psi(\mathbf{C}) &= P(\mathbf{C}; \boldsymbol{\mu}, \boldsymbol{\Sigma}) \\ &= (2\pi)^{-n/2} |\boldsymbol{\Sigma}|^{-1/2} \exp \left[-\frac{1}{2} (\mathbf{C} - \boldsymbol{\mu})^T \boldsymbol{\Sigma}^{-1} (\mathbf{C} - \boldsymbol{\mu}) \right] \end{aligned} \quad (11)$$

or canonical form

$$\psi(\mathbf{C}) = P(\mathbf{C}; \mathbf{g}, \mathbf{h}, \mathbf{K}) = \exp \left(\mathbf{g} + \mathbf{C}^T \mathbf{h} - \frac{1}{2} \mathbf{C}^T \mathbf{K} \mathbf{C} \right), \quad (12)$$

where $\boldsymbol{\mu}$ is the mean vector, $\boldsymbol{\Sigma}$ is the variance matrix, $\mathbf{K} = \boldsymbol{\Sigma}^{-1}$, $\mathbf{h} = \boldsymbol{\Sigma}^{-1} \boldsymbol{\mu}$, and $\mathbf{g} = \ln[(2\pi)^{-n/2} |\boldsymbol{\Sigma}|^{-1/2}] - (1/2) \boldsymbol{\mu}^T \mathbf{K} \boldsymbol{\mu}$. Thus, we must represent the initial potentials in canonical form, because they may represent conditional likelihoods, rather than probability distributions, whereas, one can convert to the moment form at the end of the calculation. Then, the belief potentials encode the joint distribution $P(\mathbf{V})$ of the BNs according to

$$P(\mathbf{V}) = \frac{\prod_i \psi(\mathbf{C}_i)}{\prod_j \psi(\mathbf{S}_j)}, \quad (13)$$

where $\psi(\mathbf{C}_i)$ is the clique potentials and $\psi(\mathbf{S}_j)$ is separator potentials.

Inference in junction tree based architectures is performed by passing messages between the adjacent cliques. At the beginning of message passing, each separator is initially empty. During inference, each separator is updated to hold each of the potentials passed over the separator. The clique potentials are, on the other hand, left unchanged. When evidence is absorbed from \mathbf{C}_j to \mathbf{C}_i , the potential $\psi^*(\mathbf{S})$ passed over the separator \mathbf{S} connecting \mathbf{C}_i and \mathbf{C}_j is calculated as

$$\psi^*(\mathbf{S}) = \sum_{\mathbf{C}_j \setminus \mathbf{S}} \psi(\mathbf{C}_j) \prod_{\mathbf{S}' \in \text{ne}(\mathbf{C}_j) \setminus \{\mathbf{S}\}} \psi(\mathbf{S}'), \quad (14)$$

where $\text{ne}(\mathbf{C}_j)$ is the set of neighboring separators of a clique \mathbf{C}_j .

After a full round of message passing, the joint probability distributions of any clique \mathbf{C}_i in the junction tree can be computed as the combination of the potentials of \mathbf{C}_i and all the received potentials associated with neighboring separators:

$$\psi^*(\mathbf{C}_i) = \psi(\mathbf{C}_i) \prod_{\mathbf{S} \in \text{ne}(\mathbf{C}_i)} \psi(\mathbf{S}). \quad (15)$$

From a consistent junction tree, the posterior marginal CPDs of a variable \mathbf{X} and the evidence \mathbf{E} can be computed from any clique or separator potential ψ containing \mathbf{X} by eliminating all variables in $\text{Dom}(\psi)$ except \mathbf{X} :

$$P(\mathbf{X}, \mathbf{E}) = \sum_{\mathbf{Y} \in \text{Dom}(\psi) \setminus \{\mathbf{X}\}} \psi. \quad (16)$$

4. Experiments and Results

4.1. Measurement System Configuration. The automatic system based on ECNDT for quantitative evaluation of defects in multilayered structures is obtained by integrating the test device with a computer. A schematic diagram of the system is shown in Figure 2. The computer based system can thus increase the reliability of the detection. It provides fast and robust database methods for retrieving old inspection data, which is important in monitoring defect initiation and growth. In the system, reference structures and a reference probe have been used. By comparing the signals from the reference structures with those from the monitored special structures, the system can easily make a decision on material condition and usage state.

The system is readily decomposed into a few main components: an AC excitation generator, two eddy current probes (an inspecting probe and a reference probe), a demodulation module, a low pass filter, a data acquisition interface (A/D converter), a coordinate measuring machine (CMM), and a computer. A sinusoidal current source provides a current through coils with amplitude 1 A at a frequency 200 Hz. In the system, the right-cylindrical air-cored coil probe has been used. The coil parameters are inner radius $r_1 = 3.0$ mm, outer radius $r_2 = 5.11$ mm, length $l = 20.7$ mm, and lift-off 0.5 mm. Consisting of exciting coils and pick-up coils, the probes scan over the surface of the specimen by using a CMM. A computer program is used to set the scan area and velocity. During

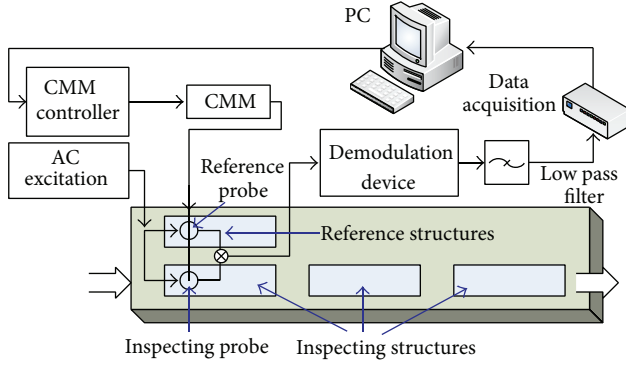


FIGURE 2: Schematic view of an automatic online ECNDT system.

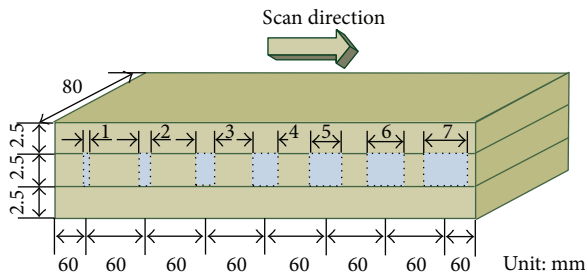


FIGURE 3: The sketch of defects with varying diameter in multilayered structures (specimen number 1).

measurements, the sensor's output signals are amplified by a low cost, high accuracy instrumentation amplifier AD620. Then, the amplified signals are sent to a phase sensitive detector using X-R orthogonal decomposition techniques to directly compute the horizontal components (real part, in-phase components) and the vertical components (imaginary part, quadrature components) of impedance signals. These two components are filtered by a second-order low-pass filter with a cutoff frequency of 20 Hz. A data acquisition program written in Labview collects data from the output of the filter via a National Instruments DAQPad 6016 16 × 6 bit analog-to-digital converter. The computer is controlling the whole system and it is performing such tasks as automating the process of inspection, data acquisition and displaying, and applying some signal processing techniques to automate the process of defect detection and quantification.

4.2. Two Groups of Experiments and Results. To verify the feasibility of the proposed method for quantitative evaluation of defects in multilayered structures from ECNDT signals, comparative experiments are carried out. Multilayered samples resembling a part of the wing splice of the aircraft are analyzed. In particular, corrosion is a critical problem for in-service aircraft structures which may lead to a degradation of structure integrity and fatigue resistance, directly affect the durability of structure, and even result in loss of function. So detection of deeply buried defects in multilayered airframe joints is widely recognized as the urgent and difficult NDT problem. We assume that the shape and position of defects

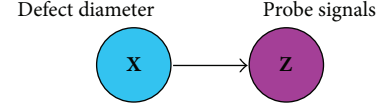


FIGURE 4: The BN used in example 1 (specimen number 1).

are known in advance. This paper mainly discusses the defect evaluation problem concerning estimation of defect dimensions in multilayered structures in order to simulate inspection of the internal corrosion and local interlayer air gaps in real structures.

Firstly, we considered a simple problem where only one parameter of defects in multilayered structures needs to be determined. The first experimental specimen (specimen number 1) is shown schematically in Figure 3. It is composed of three layers of aluminum with a total thickness of 7.5 mm. Each plate has electrical conductivity $\sigma = 18.5 \text{ MS/m}$, magnetic permeability $\mu = \mu_0 = 4\pi \times 10^{-7} \text{ H/m}$, length 480 mm, width 80.0 mm, and thickness 2.5 mm. There are 7 holes with different diameters in the center of the middle plate. The parameters of holes are electrical conductivity $\sigma = 0 \text{ S/m}$, magnetic permeability $\mu = \mu_0 = 4\pi \times 10^{-7} \text{ H/m}$, diameter 1, 2, 3, 4, 5, 6, and 7 mm, and depth 2.5 mm, respectively. A major goal is to utilize BNs for the defect diameter estimation. The skin depth $\delta = 1/\sqrt{\pi f \mu \sigma}$ is about 8.28 mm and indicates promising robustness for the inspection of inner defects in the multilayered structures.

In this experiment, the random variables are the defect diameter \mathbf{X} and the probe response signals \mathbf{Z} . We assume that the other factor's influence is very small. From a general knowledge of ECNDT, the probe response signals vary due to the difference of the defect diameter. It is clear that the link between \mathbf{X} and \mathbf{Z} will lead to a BN given in Figure 4. It is a basic BN which contains two nodes. For the root node \mathbf{X} , the CPDs only contain the priori probability of each state. The CPDs of \mathbf{Z} are then defined by the conditional probabilities $P(\mathbf{Z} | \mathbf{X})$ over each \mathbf{Z} state. As mentioned above, the distributions of \mathbf{X} and \mathbf{Z} are initially assumed as multivariate Gaussian with unknown means and variances.

Then, we train this model using real research data and the results would be a generative model suitable for use in defect diameter estimation. A total of 210 complex valued EC data vectors containing signals corresponding to seven types of defects are available for the experiment (each type having 30 records). The data set is denoised by the wavelet packet analysis method with Shannon entropy. Then, the resulting signals and corresponding defect diameters constitute the labeled data which are sent to train the BN.

After the aforementioned operations, a new trained BN and inference engine are obtained. One thing we can do to verify that the model is reasonable is to draw samples from it and visually compare with the simulated data [44]. Once built, the model could be used to estimate defect diameters when the inspection signals are available. The main step is to enter each of inspection signals as evidence and calculate the posterior marginal CPDs of the node \mathbf{X} . We use the means of the node \mathbf{X} as prediction and the marginal CPDs for

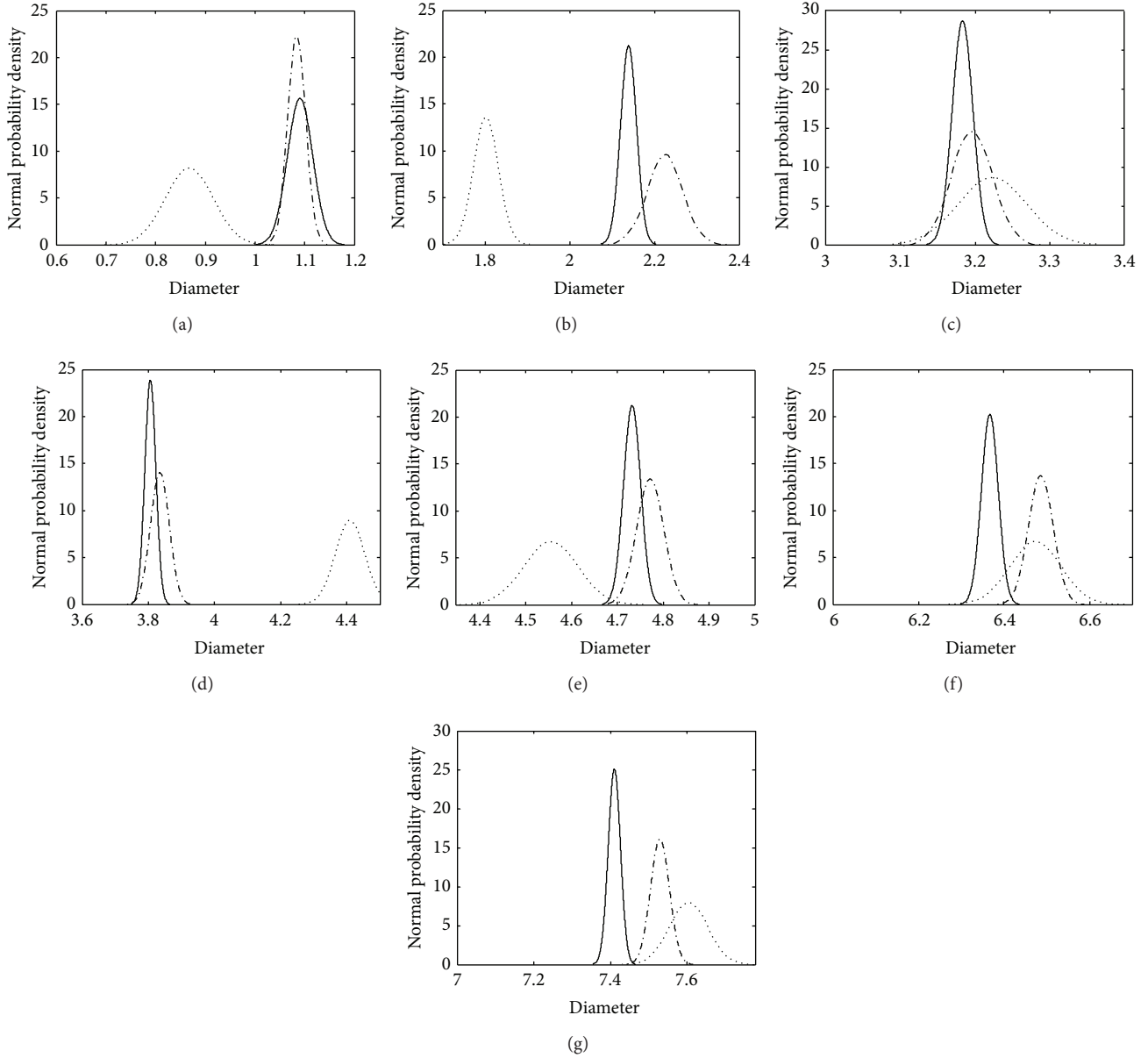


FIGURE 5: The estimated results (diameter) obtained from signals injected in three different levels of artificial random noise using BN method: noise-free (—), 10% noise (---), and 20% noise (.....) (specimen number 1).

probability intervals. The BN method is also tested on signals containing artificial injected random noise. Real inspection signals are modified to contain additional 10% and 20% random noise and are used to evaluate the performance of the BN method in response to measurement noise. The performance of estimation is evaluated with the bootstrap cross-validation method [45]. The results obtained from signals containing three different levels of artificial random noise (noise-free, 10%, and 20% noise) using the BN method are shown in Figure 5. Furthermore, we compare the estimated results obtained from the BN method with those from the LS regression method which is very simple and usually used as a benchmark for all the other quantitative evaluation

methods [24]. Figure 6 and Table 1 show the comparison results obtained from signals containing three different levels of artificial random noise (noise-free, 10%, and 20% noise) using the BN and LS regression methods, respectively.

Secondly, a more complex example is studied, where the signals are collected from a multilayer sample with defects varying diameter and depth. Figure 7 illustrates the second experimental specimen (specimen number 2). The specimen consists of three layers of aluminum with a total thickness of 10 mm (2.5, 5, 2.5 mm), electrical conductivity $\sigma = 18.5 \text{ MS/m}$, magnetic permeability $\mu = \mu_0 = 4\pi \times 10^{-7} \text{ H/m}$, length 420 mm, and width 80 mm. There are 5 holes with different diameters and depths in the center of

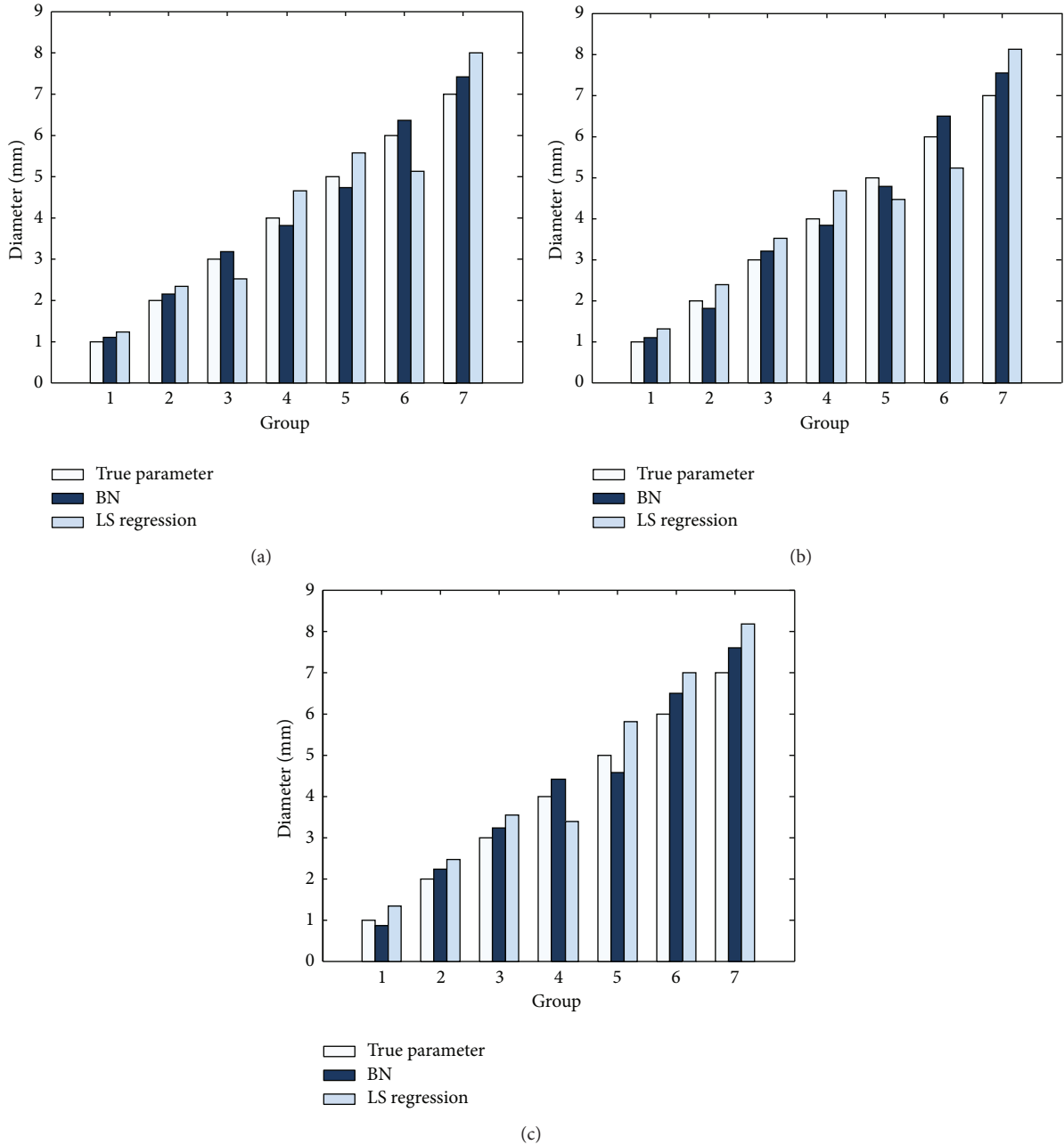


FIGURE 6: The comparison of three sets of results (diameter) obtained from signals injected in three different levels of artificial random noise using BN and LS regression methods, respectively, (a) noise-free, (b) 10% noise, and (c) 20% noise (specimen number 1).

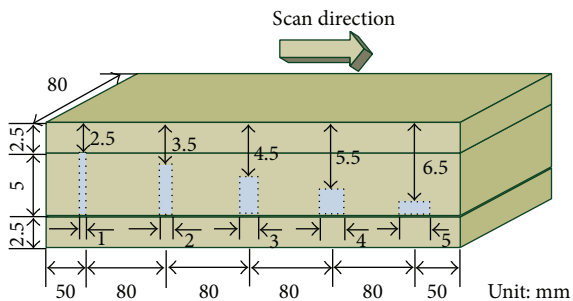


FIGURE 7: The sketch of defects with varying diameter and depth in multilayered structures (specimen number 2).

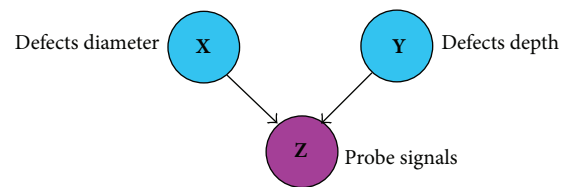


FIGURE 8: The BN used in example 2 (specimen number 2).

the middle plate. The holes parameters $\sigma = 0$ S/m, $\mu = \mu_0 = 4\pi \times 10^{-7}$ H/m, diameter, and depth are (1, 2.5), (2, 3.5), (3, 4.5), (4, 5.5), and (5, 6.5) mm, respectively.

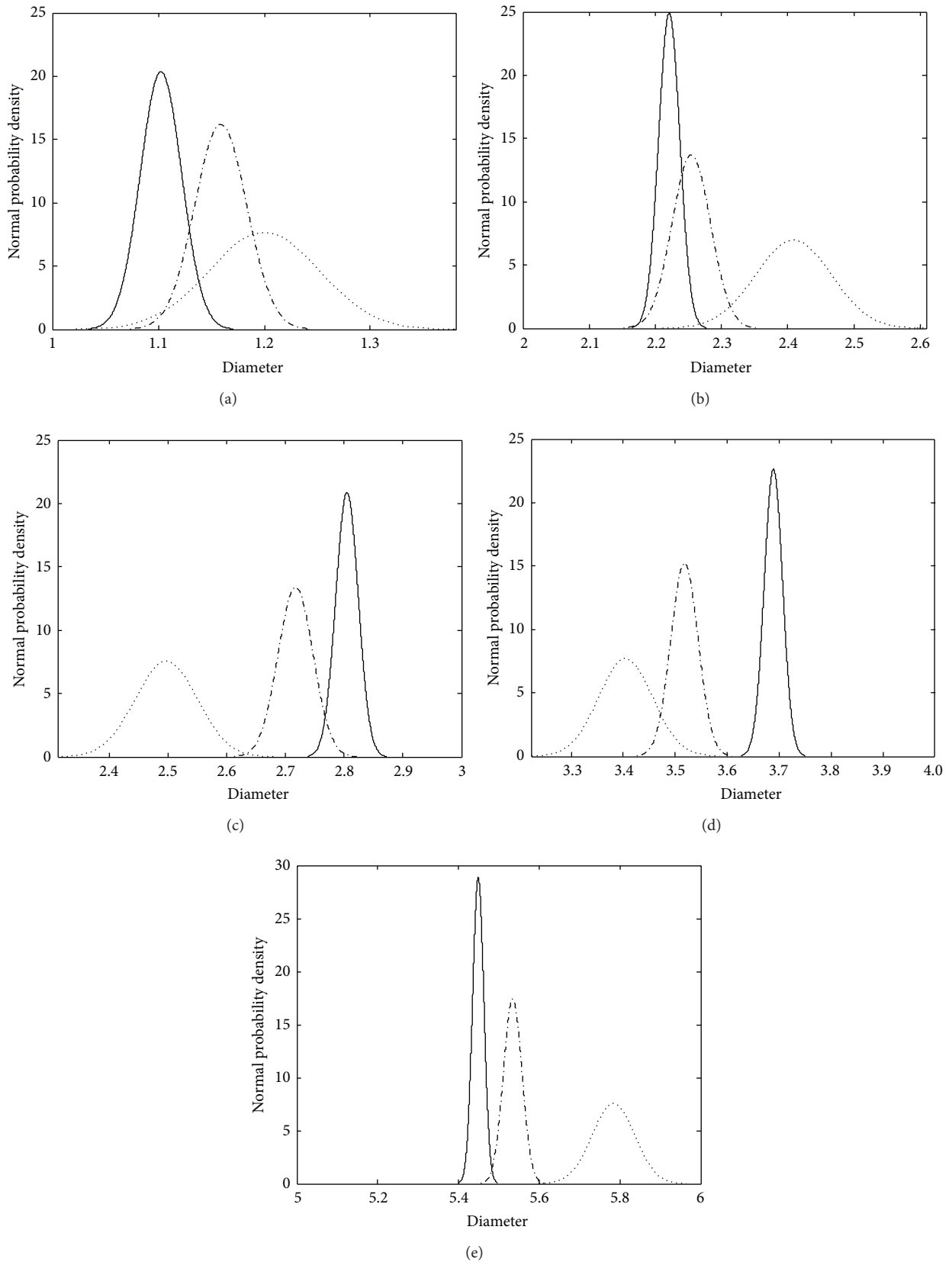


FIGURE 9: The estimated results (diameter) obtained from signals injected in three different levels of artificial random noise using BN method: noise-free (—), 10% noise (---), and 20% noise (.....) (specimen number 2).

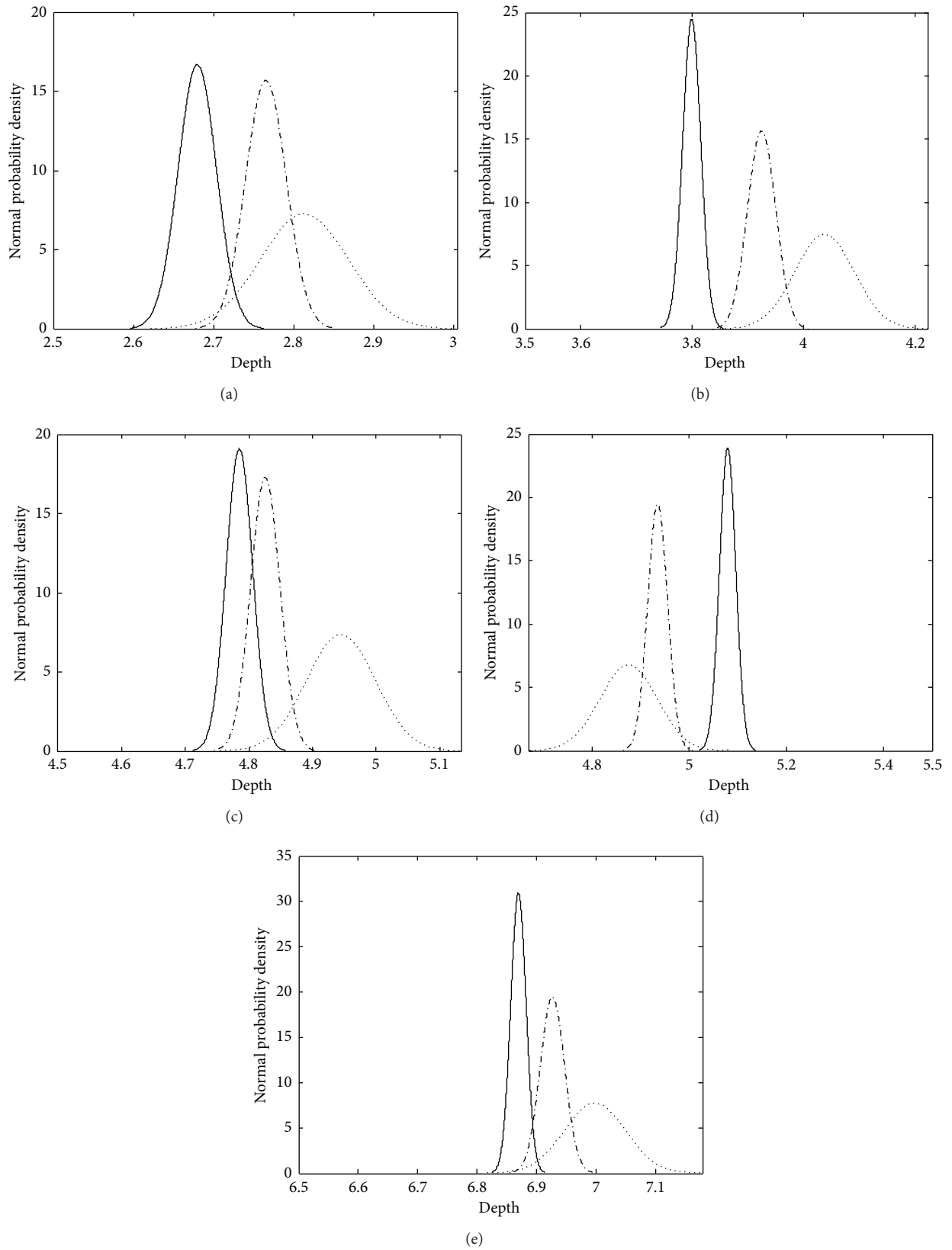


FIGURE 10: The estimated results (depth) obtained from signals injected in three different levels of artificial random noise using BN method: noise-free (—), 10% noise (---), and 20% noise (.....) (specimen number 2).

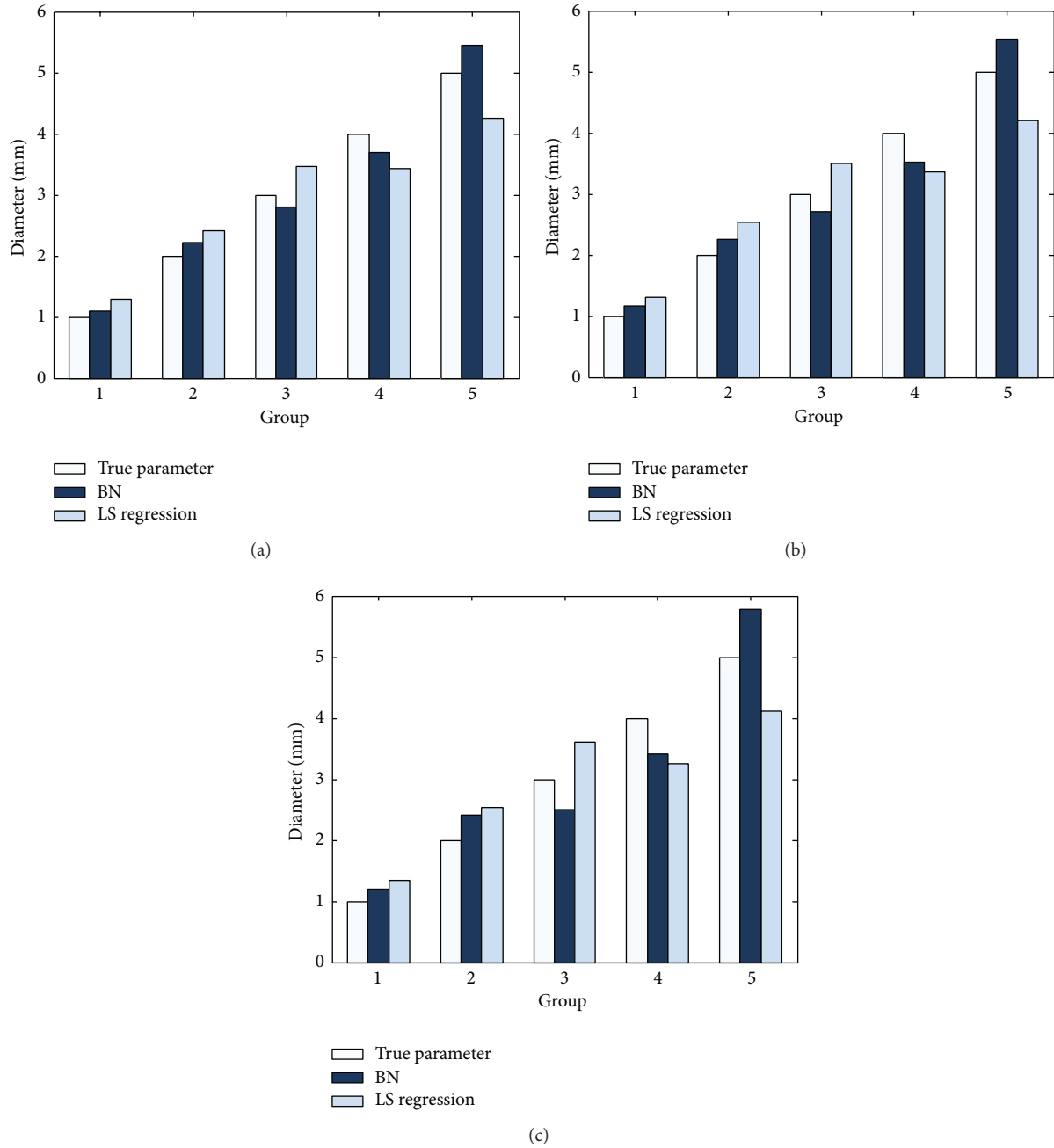


FIGURE 11: The comparison of three sets of results (diameter) obtained from signals injected in three different levels of artificial random noise using BN and LS regression methods, respectively, (a) noise-free, (b) 10% noise, and (c) 20% noise (specimen number 2).

In this example, the random variables are the defect diameter X , defect depth Y , and the probe response signals Z . The defect diameter and depth are two independent influencing factors of the probe signals. Using this special relationship, we can obtain the BN structure given in Figure 8. Node X and node Y are linked to node Z by an arc, respectively. Like the first example, the distributions of X , Y , and Z are also assumed as multivariate Gaussian with unknown means and variances.

In the experiment, a dataset with 150 records is acquired during scanning. The dataset contains EC signals from 5 types

of defects (each type having 30 records). As described in the previous experiments, the same procedures are carried out. The diameter and depth estimation results obtained from signals containing three different levels of artificial random noise (noise-free, 10%, and 20% noise) using the BN method are shown in Figures 9 and 10, respectively. The comparison results of the estimated diameter and depth obtained from signals containing three different levels of artificial random noise (noise-free, 10%, and 20% noise) using the BN and LS regression methods are shown in Figures 11 and 12 and Table 2, respectively.

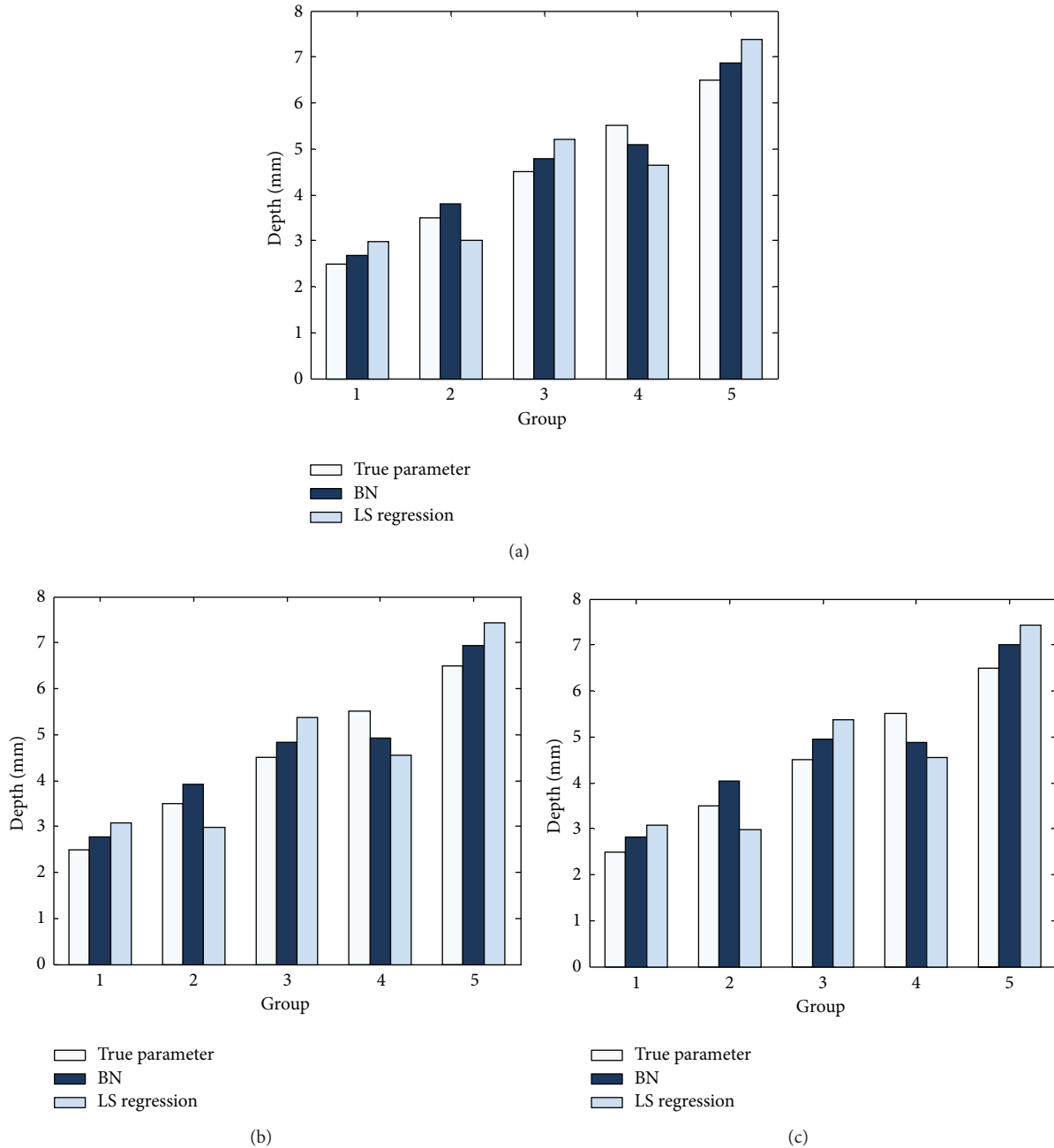


FIGURE 12: The comparison of three sets of results (depth) obtained from signals injected in three different levels of artificial random noise using BN and LS regression methods, respectively, (a) noise-free, (b) 10% noise, and (c) 20% noise (specimen number 2).

Tables 1 and 2 show quantitatively the estimation error and the corresponding methods. It can be seen that the BN method has a higher precision than the LS regression method. The LS regression method has difficulty performing more accurate estimation and the satisfactory solution becomes unlikely in the case of signals containing high-level noise.

In contrast, the BN method can achieve greater accuracy and robustness, even in the case of signals containing high-level noise. It provides not only the accurate estimation of defect characteristic parameters, but also the probability distributions of these values. With increasing noise level,

the estimated variances also increase, whereas the estimated means deviations from their actual values increase very limitedly. This demonstrates that although the variances growth means increasing the uncertainty of the results, the estimated error of BNs increases only slightly with the increasing noise level. It shows that BNs are effective in the quantitative evaluation of defects, due to their remarkable characteristics such as the combination of the domain knowledge and the reasoning under uncertainty in AI. This eventually results in better generalization performance in the BN method than the LS regression method. In brief, the BN method is able to

TABLE 1: Defect parameter estimation errors obtained by the BN method and the LS method (specimen number 1).

	Signals	LS	BN
Diameter error (RMSE)	Noise-free	0.6465	0.2597
	10% noise	0.6761	0.3119
	20% noise	0.7556	0.3915

TABLE 2: Defect parameter estimation errors obtained by the BN method and the LS method (specimen number 2).

	Signals	LS	BN
Diameter error (RMSE)	Noise-free	0.6596	0.2813
	10% noise	0.6918	0.3709
	20% noise	0.7271	0.4464
Depth error (RMSE)	Noise-free	0.7050	0.3213
	10% noise	0.7942	0.4140
	20% noise	0.8893	0.4944

successfully cope with highly complex and ill-posed ECNDE inverse problems, where each defect is hidden deeply in a multilayered structure.

5. Conclusions

A new approach for quantitative evaluation of defects in multilayered structures from ECNDT signals using BNs has been proposed and investigated. BNs discussed in this paper are simple and powerful, and their structures and parameters are easily learned from the domain knowledge of ECNDT and experimental data. The generative model can predict the probe response signals given the defect characteristic parameters or estimate the defect characteristic parameters from the inspection signals by using probability inference. In this paper, we mainly describe how the problem of defect characteristic parameter estimation from ECNDT signals can be modeled using BNs, in which the general model accommodates the uncertainties of the EC inspection. Two experiments have been carried out. Compared with the LS regression method, BNs have the advantage of being a bidirectional inferential mechanism and higher accuracy and robustness. They allow results to be obtained in the form of full CPDs, accounting for all the information available (evidences). It can be seen that the estimation results are probabilities rather than a single value. More information about the estimated parameters can be deduced from their probabilities, such as the means and variances, which describe the value itself and the degree of uncertainty respectively. The experimental results demonstrate the feasibility and effectiveness of the BN method proposed in this paper. This also encourages the attempts to tackle the other evaluation problems.

In this paper, the multivariate Gaussian assumption of all variables has been taken. Nevertheless, in real problems where the distributions are nonuniform, a non-Gaussian assumption also could be more suitable. In fact, the validity of BNs is not restricted to the particular case of multivariate Gaussian distributions but to more general distributions

(Gamma, Poisson, etc.). BNs can handle the problem where each conditional distribution of each variable can be any distributions. However, these possibilities are out of the scope of this paper and are the topic of current and future work of the authors. It will be helpful to analyze the EC signals more accurately in detail and lead to more precise predictions.

In addition, it is necessary to note that, in this paper, the problem under investigation is simple. However, in most ECNDT problems, the more complex configuration (interacting defects, partially conducting defects, defects with nonregular shape as corruptions, real defects, etc.) is to be handled. Future work, hopefully, will be done to extend the proposed BN method to the more complex ECNDT problems where the more unknown parameters of defects need to be estimated. We consider that the independence of causal influence can be exploited in Bayesian networks to reduce both the time and space cost of inference. The increase of the computational costs with the increase of the unknown parameters is the computation of the decomposed additional local joint probability density inference.

Conflict of Interests

The authors declare that there is no conflict of interests regarding the publication of this paper.

Acknowledgment

This work is supported by the National Natural Science Foundation of China Grant nos. 51105183 and 51307172, the Research Fund for the Doctoral Program of Higher Education of China Grant no. 20115314120003, the Applied Basic Research Programs of Science and Technology Commission Foundation of Yunnan Province of China Grant no. 2010ZC050, the Foundation of Yunnan Educational Committee Grant no. 2013Z121, the National College Student Innovation Training Program Funded Projects Grant no. 201210674014, and the Science and Technology Project of Yunnan Power Grid Corporation Grant no. K-YN2013-110.

References

- [1] B. A. Auld and J. C. Moulder, "Review of advances in quantitative eddy current nondestructive evaluation," *Journal of Nondestructive Evaluation*, vol. 18, no. 1, pp. 3–36, 1999.
- [2] H. Zhang, H. C. Yan, F. W. Yang, and Q. J. Chen, "Quantized control design for impulsive fuzzy networked systems," *IEEE Transactions on Fuzzy Systems*, vol. 19, no. 6, pp. 1153–1162, 2011.
- [3] N. Meyendorf and A. Berthold, "New trends in NDE and health monitoring," in *Advanced Sensor Technologies for Nondestructive Evaluation and Structural Health Monitoring II*, vol. 6179 of *Proceedings of SPIE*, pp. 617901–617910, San Diego, Calif, USA, March 2006.
- [4] F. Kojima and T. Fujioka, "Quantitative evaluation of material degradation parameters using nonlinear magnetic inverse problems," *International Journal of Applied Electromagnetics and Mechanics*, vol. 25, no. 1–4, pp. 157–163, 2007.
- [5] K. Chomsuwan, S. Yamada, and M. Iwahara, "Improvement on defect detection performance of PCB inspection based on ECT

- technique with multi-SV-GMR sensor," *IEEE Transactions on Magnetics*, vol. 43, no. 6, pp. 2394–2396, 2007.
- [6] J. H. Cantrell and W. T. Yost, "Nonlinear ultrasonic characterization of fatigue microstructures," *International Journal of Fatigue*, vol. 23, supplement 1, pp. S487–S490, 2001.
- [7] H. Němec, P. Kužel, F. Garet, and L. DuVillaret, "Time-domain terahertz study of defect formation in one-dimensional photonic crystals," *Applied Optics*, vol. 43, no. 9, pp. 1965–1970, 2004.
- [8] M. R. Clark, D. M. McCann, and M. C. Forde, "Application of infrared thermography to the non-destructive testing of concrete and masonry bridges," *NDT and E International*, vol. 36, no. 4, pp. 265–275, 2003.
- [9] T. Toutountzakis and D. Mba, "Observations of acoustic emission activity during gear defect diagnosis," *NDT and E International*, vol. 36, no. 7, pp. 471–477, 2003.
- [10] H. Elaqla, N. Godin, G. Peix, M. R'Mili, and G. Fantozzi, "Damage evolution analysis in mortar, during compressive loading using acoustic emission and X-ray tomography: effects of the sand/cement ratio," *Cement and Concrete Research*, vol. 37, no. 5, pp. 703–713, 2007.
- [11] Y. Bar-Cohen, "Emerging NDT technologies and challenges at the beginning of the third millennium, part 1," *Materials Evaluation*, vol. 58, no. 1, pp. 17–30, 2000.
- [12] Y. Bar-Cohen, "Emerging NDT technologies and challenges at the beginning of the third millennium, part 2," *Materials Evaluation*, vol. 58, no. 2, pp. 141–150, 2000.
- [13] S. J. Norton and J. R. Bowler, "Theory of eddy current inversion," *Journal of Applied Physics*, vol. 73, no. 2, pp. 501–512, 1993.
- [14] H. J. Gao, T. W. Chen, and J. Lam, "A new delay system approach to network-based control," *Automatica*, vol. 44, no. 1, pp. 39–52, 2008.
- [15] J. Pávó, "Approximate methods for the calculation of the ECT signal of a crack in a plate coated by conducting deposit," *IEEE Transactions on Magnetics*, vol. 40, no. 2, pp. 659–662, 2004.
- [16] A. Sophian, G. Y. Tian, D. Taylor, and J. Rudlin, "Electromagnetic and eddy current NDT: a review," *Insight: Non-Destructive Testing and Condition Monitoring*, vol. 43, no. 5, pp. 302–306, 2001.
- [17] H. Zhang, H. C. Yan, F. W. Yang, and Q. J. Chen, "Distributed average filtering for sensor networks with sensor saturation," *IET Control Theory & Applications*, vol. 7, no. 6, pp. 887–893, 2013.
- [18] O. Bottauscio, M. Chiampì, and A. Manzin, "Eddy current problems in nonlinear media by the element-free Galerkin method," *Journal of Magnetism and Magnetic Materials*, vol. 304, no. 2, pp. e823–e825, 2006.
- [19] T. Dogaru, C. H. Smith, R. W. Schneider, and S. T. Smith, "Deep crack detection around fastener holes in airplane multi-layered structures using GMR-based eddy current probes," in *Quantitative Nondestructive Evaluation*, vol. 23 of *AIP Conference Proceedings*, pp. 398–405, Green Bay, Wis, USA, July–August 2004.
- [20] E. Cardelli, A. Faba, R. Specogna, A. Tamburrino, F. Trevisan, and S. Ventre, "Analysis methodologies and experimental benchmarks for eddy current testing," *IEEE Transactions on Magnetics*, vol. 41, no. 5, pp. 1380–1383, 2005.
- [21] P. G. Kaup, F. Santosa, and M. Vogelius, "Method for imaging corrosion damage in thin plates from electrostatic data," *Inverse Problems*, vol. 12, no. 3, pp. 279–293, 1996.
- [22] B. Ye, G. Zhang, P. Huang, M. Fan, S. Zheng, and Z. Zhou, "Quantifying geometry parameters of defect in multi-layered structures from eddy current nondestructive evaluation signals by using genetic algorithm," in *Proceedings of the 6th World Congress on Intelligent Control and Automation*, vol. 2, pp. 5358–5362, Dalian, China, June 2006.
- [23] I. T. Rekanos, T. P. Theodoulidis, S. M. Panas, and T. D. Tsiboukis, "Impedance inversion in eddy current testing of layered planar structures via neural networks," *NDT and E International*, vol. 30, no. 2, pp. 69–74, 1997.
- [24] H. C. Yan, Z. Z. Su, H. Zhang, and F. W. Yang, "Observer-based H_∞ control for discrete-time stochastic systems with quantisation and random communication delays," *IET Control Theory & Applications*, vol. 7, no. 3, pp. 372–379, 2013.
- [25] J. I. de la Rosa, G. A. Fleury, S. E. Osuna, and M. E. Davoust, "Markov chain Monte Carlo posterior density approximation for a groove-dimensioning purpose," *IEEE Transactions on Instrumentation and Measurement*, vol. 55, no. 1, pp. 112–122, 2006.
- [26] H. C. Yan, H. B. Shi, H. Zhang, and F. W. Yang, "Quantized H_∞ control for networked systems with communication constraints," *Asian Journal of Control*, vol. 15, no. 5, pp. 1468–1476, 2013.
- [27] T. Khan and P. Ramuhalli, "A recursive bayesian estimation method for solving electromagnetic nondestructive evaluation inverse problems," *IEEE Transactions on Magnetics*, vol. 44, no. 7, pp. 1845–1855, 2008.
- [28] J. Pearl, *Probabilistic Reasoning in Intelligent Systems: Networks of Plausible Inference*, The Morgan Kaufmann Series in Representation and Reasoning, Morgan Kaufmann, San Mateo, Calif, USA, 1988.
- [29] D. Heckerman, "A tutorial on learning Bayesian networks," Tech. Rep. MSR-TR-95-06, Microsoft Research, 1995.
- [30] A. Kameari, "Three dimensional eddy current calculation using finite element method with A-V in conductor and in vacuum," *IEEE Transactions on Magnetics*, vol. 24, no. 1, pp. 118–121, 1987.
- [31] S. J. Norton and J. R. Bowler, "Theory of ECT inversion," *Journal of Applied Physics*, vol. 73, no. 2, pp. 501–512, 1993.
- [32] J. Gill, *Bayesian Methods: A Social and Behavioral Sciences Approach*, Chapman & Hall/CRC, Boca Raton, Fla, USA, 2002.
- [33] E. Castillo, J. M. Gutiérrez, and A. S. Hadi, *Expert Systems and Probabilistic Network Models*, Springer, New York, NY, USA, 1997.
- [34] H. Zhang, H. C. Yan, T. Liu, and Q. J. Chen, "Fuzzy controller design for nonlinear impulsive fuzzy systems with time delay," *IEEE Transactions on Fuzzy Systems*, vol. 19, no. 5, pp. 844–856, 2011.
- [35] F. V. Jensen, *Bayesian Networks and Decision Graphs*, Statistics for Engineering and Information Science, Springer, New York, NY, USA, 2001.
- [36] C. R. Kenley, *Influence diagram models with continuous variables [Ph.D. thesis]*, Stanford University, Stanford, Calif, USA, 1986.
- [37] D. Heckerman, D. Geiger, and D. M. Chickering, "Learning Bayesian networks: the combination of knowledge and statistical data," *Machine Learning*, vol. 20, no. 3, pp. 197–243, 1995.
- [38] H. Zhang, Q. J. Chen, H. C. Yan, and J. H. Liu, "Robust H_∞ filtering for switched stochastic system with missing measurements," *IEEE Transactions on Signal Processing*, vol. 57, no. 9, pp. 3466–3474, 2009.
- [39] I. Cohen, N. Sebe, F. G. Gozman, M. C. Cirelo, and T. S. Huang, "Learning Bayesian network classifiers for facial expression recognition both labeled and unlabeled data," in *Proceedings of the IEEE Computer Society Conference on Computer Vision and Pattern Recognition*, vol. 1, pp. I-595–I-601, June 2003.

- [40] C. Meek, "Causal inference and causal explanation with background knowledge," in *Proceedings of the 11th Annual Conference on Uncertainty in Artificial Intelligence (UAI '95)*, pp. 403–410, 1995.
- [41] H. Zhang, Z. H. Guan, and G. Feng, "Reliable dissipative control for stochastic impulsive systems," *Automatica*, vol. 44, no. 4, pp. 1004–1010, 2008.
- [42] L. X. Zhang, H. J. Gao, and O. Kaynak, "Network-induced constraints in networked control systems—a survey," *IEEE Transactions on Industrial Informatics*, vol. 9, no. 1, pp. 403–416, 2013.
- [43] C. Huang and A. Darwiche, "Inference in belief networks: a procedural guide," *International Journal of Approximate Reasoning*, vol. 15, no. 3, pp. 225–263, 1996.
- [44] P. Huang, G. Zhang, Z. Wu, J. Cai, and Z. Zhou, "Inspection of defects in conductive multi-layered structures by an eddy current scanning technique: simulation and experiments," *NDT and E International*, vol. 39, no. 7, pp. 578–584, 2006.
- [45] R. O. Duda, P. E. Hart, and D. G. Stork, *Pattern Classification*, John Wiley & Sons, New York, NY, USA, 2nd edition, 2001.

Research Article

Multiagent and Particle Swarm Optimization for Ship Integrated Power System Network Reconfiguration

Zheng Wang,^{1,2} Li Xia,² Yongji Wang,¹ and Lei Liu¹

¹ School of Automation, Huazhong University of Science and Technology, Wuhan 430074, China

² School of Electrical Engineering, Naval University of Engineering, Wuhan 430033, China

Correspondence should be addressed to Yongji Wang; wangyjch@mail.hust.edu.cn

Received 11 December 2013; Accepted 2 February 2014; Published 25 March 2014

Academic Editor: Huaicheng Yan

Copyright © 2014 Zheng Wang et al. This is an open access article distributed under the Creative Commons Attribution License, which permits unrestricted use, distribution, and reproduction in any medium, provided the original work is properly cited.

Ship integrated power system adopts electric power propulsion. Power network and electric power network are integrated into complicated one. Network reconfiguration of ship integrated power system is a typical nonlinear optimization that is multitarget and multiconstraint. According to the characteristics of ship integrated power system, simplified network model and reconfiguration mathematical model are established. A multiagent and particle swarm optimization is presented to solve network reconfiguration problem. The results of simulation show that multiagent and particle swarm optimization can reconfigure ship integrated power system efficiently.

1. Introduction

Ship integrated power system (SIPS) adopts electric power propulsion. Power network and electric power network are integrated into complicated one. Integrated power system is the trend of ship power system. Due to the application of high power density-integrated generating system, DC medium voltage transmission, zonal distribution system, power conversion device and high power electric propulsion system, and the generation capacity and scale of SIPS keep on enlarging. The way the system works and its protection become more complex. It is important to reconfigure the system as fast as possible when faults occur. Because of many differences between the ship and the land power system, the network reconfiguration of land power system which is based on how to lower the network loss of system does not work well on the ship [1–5]. Network reconfiguration of SIPS is to be researched.

Network reconfiguration of SIPS is a nonlinear combinatorial optimization problem. Srivastava et al. used improved algorithm for reconfiguration, but it cannot restore the loads as much as possible [6]; Nagata used multiagent technique for reconfiguration, but it also cannot make the result most optimal [7].

Based on analyzing many methods in existence and according to the characteristics of ship integrated power system, a multiagent and particle swarm optimization (MAPSO) is presented to solve the power system network reconfiguration problem. Theoretical analysis and simulation results show that MAPSO can reconfigure the network of ship integrated power system better.

2. Simplified Network Model and Reconfiguration Mathematical Model of SIPS

2.1. Simplified Network Model of SIPS. A typical SIPS is made up of 4 power stations. There are 2 generators in each station. Power stations connect with each other by jumper wires. Generators generate DC 4000 V power, which is converted to DC 700 V power by converters and access to DC zonal distribution switchboards and then to AC 400 V by inverters or DC 230 V by choppers. Loads in SIPS include propulsion loads, important loads, and common loads. According to the importance, the loads can be graded into three ranks, of which Rank 1 and Rank 2 loads usually have two power supply routes, the normal one and the alternative. When

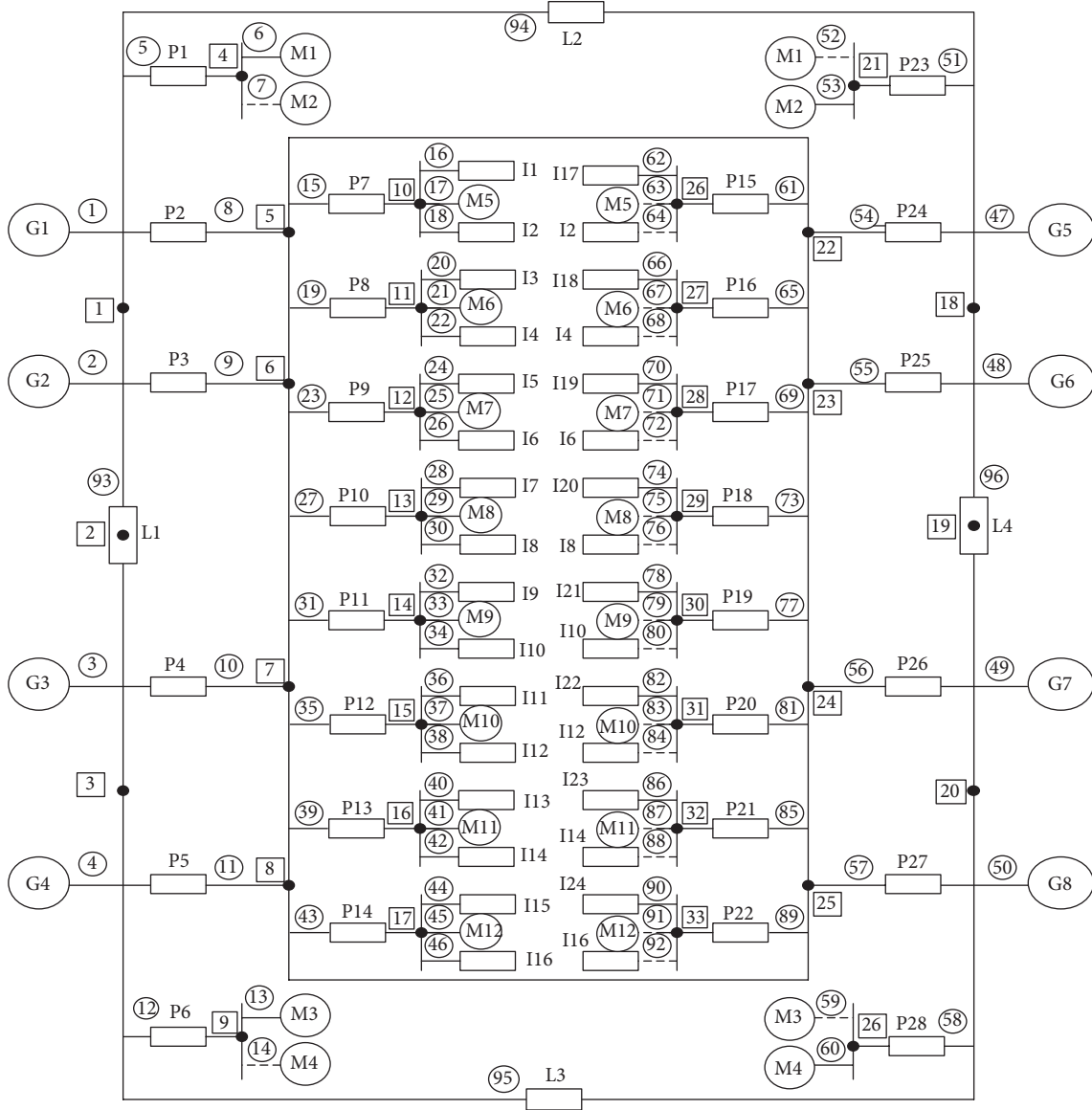


FIGURE 1: The simplified network model of SIPS.

the SIPS goes wrong, the circuit breaker or other protective devices isolate the failure load or generator, by changing the state of the switch to ensure that the important load can get maximum degree of power restoration under the system constraints, and unimportant loads are removed if necessary.

According to the graph theory [8–10], the electrical devices (including feeders and jumper wires connected with the device) in SIPS are abstracted to be branches, while the connection points between the devices are abstracted to be nodes. Then, we can establish a node-branch topology mode. Depth-first search and breadth-first search are adopted to number the branches and nodes. First, we should number generators branches by breadth-first search. Then, we number distribution branches also by breadth-first search. If we meet feeder branches, we adopt depth-first search for numbering, until we meet load branches. After that, we number the jumper wires.

The simplified network model of SIPS is shown in Figure 1. ①–⑨⑥ represents branches, 1–33 represent nodes, G1–G8 are generators, M1–M4 are propulsion loads, M5–M12 are motor loads, I represents static loads, P1–P28 are power electronic equipment, and L1–L4 are jumper wires. The alternative routes of propulsion and important loads are connected by dashed lines.

2.2. Network Reconfiguration Mathematical Model. SIPS requires the maximum loads to restore and supply power for important loads (Rank 1 and Rank 2) in priority after network reconfiguration and make the operation times of switches as few as possible [11]. So the object function can be expressed as follows:

$$\max F(X) = \sum_{i=1}^{n_1} \lambda_1 L_{g1i} + \sum_{i=1}^{n_2} \lambda_2 L_{g2i} + \sum_{i=1}^{n_3} \lambda_3 L_{g3i} - \eta S_x, \quad (1)$$

where $F(X)$ is the total power restored; L_{g1i} , L_{g2i} , and L_{g3i} are the 3 grade loads, n_1 , n_2 , and n_3 are the total number of each grade loads, λ_1 , λ_2 , and λ_3 are the weight coefficients of each grade loads, S_x is the total operation times of switches, and η is the punitive weight coefficient. We can get the maximum important load restored and the least operation times of switches by choosing the proper weight coefficients. For example, $\lambda_1 = 1$ for Rank 1 loads, $\lambda_2 = 0.1$ for Rank 2 loads, and $\lambda_3 = 0.01$ for Rank 3 loads.

The network reconfiguration of SIPS should be constrained as follows.

- (1) Power flow constraint: $AP = D$, where A is the node-branch incidence matrix, P is the feeder current vector, and D is the load demand vector.
- (2) Capacity constraint: $P_i \leq P_i^{\max}$.
- (3) Voltage constraint: $V_{i\min} \leq V \leq V_{i\max}$.
- (4) Radiation constraint: there is only one route connected with the load restored, normal one or alternative.
- (5) Priority constraint: priority of power supply is based on the ranks of loads.

3. Multiagent and Particle Swarm Optimization

3.1. Application of Multiagent in Network Reconfiguration of SIPS. Generally, agent is an entity with active behavioral capacity in any environment, such as organism, software system or controller in control system. Multiagent system (MAS) is a loose coupling network formed by several agents. Physically or logically the agents are scattered, and their behaviors are self-governed. That is to say, their targets and behaviors would not be restricted by any other agents. To achieve the same task or the same goal, all the agents link with each other under some kind of protocol. They can solve problems beyond single agent's capability by communication and cooperation [12–14].

Considering regional autonomy of multiagent, the set of nonswitch devices controlled by switch devices on the same regional feeder (including generators, loads, jumper wires, switches, etc.) can be regarded as one agent. Therefore, the SIPS network may be divided into some separate power supply agents.

The SIPS network shown in Figure 1 can be divided into several feeder units. Each one is abstracted as a regional feeder agent. A regional feeder multiagent network model is proposed, as shown in Figure 2.

The regional feeder agents are intelligent; they can judge and make decision autonomous. According to the operation condition of SIPS, the regional feeder agents can communicate electric parameters, such as power, current, and voltage, with adjacent agents so as to guarantee stable operation of SIPS.

3.2. Particle Swarm Optimization. In 1995, the American social psychologist James Kennedy and electrical engineers

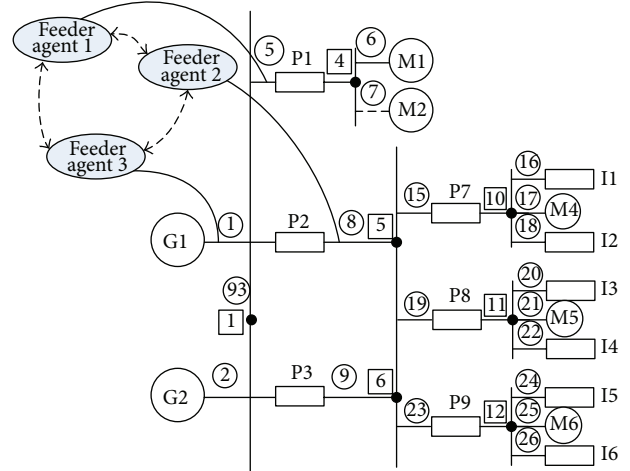


FIGURE 2: Regional feeder multiagent network model of SIPS.

Russell Eberhart proposed the particle swarm algorithm [15]. The positions of particles are used to solve the optimization problem. In the algorithm, a velocity vector of a particle determines the flight direction and speed. Located in an M -dimensional search space, the location of particle i can be expressed as $X_i = (x_{i1}, x_{i2}, \dots, x_{iD})^T$, and speed can be expressed as $V_i = (v_{i1}, v_{i2}, \dots, v_{iD})^T$. The best position of the particle is $X_i^{pb} = (X_{i1}^{pb}, X_{i2}^{pb}, \dots, X_{iD}^{pb})^T$, while the best position of the whole swarm is $X^{gb} = (X_1^{gb}, X_2^{gb}, \dots, X_D^{gb})^T$. In the process of swarm initialization, the particles are distributed in the whole solution space randomly, to obtain the optimal solution through iteration gradually. Each particle tracks X^{pb} and X^{gb} to determine their movement [16–22]:

$$V_{id}^{t+1} = \omega V_{id}^t + c_1 R (X_{id}^{pb} - X_{id}^t) + c_2 R (X_d^{gb} - X_{id}^t), \quad (2)$$

$$X_{id}^{t+1} = X_{id}^t + V_{id}^{t+1},$$

where $d = 1, 2, \dots, D$, D is the particle dimension and t is iterations. ω is inertia weight, c_1 and c_2 are the cognitive and social parameters, and R is a random number between 0 and 1. In addition, the velocity of particles V_{id} is limited by a maximum speed $V_{\max, d}$.

Consider that the position of the particles in each dimension and the best place of individual particle are 0 or 1. Then, only the particle speed is considered, and introduce the speed formula, that is, sigmoid function as follows:

$$\text{Sigmoid}(x) = \frac{1}{1 + e^{-x}}. \quad (3)$$

The bigger the speed value of particle is, the closer the sigmoid function value is to 1. However, the smaller the speed value is, the closer the sigmoid function is to 0. So the value of sigmoid function can be considered as the probability of the particle position, that is, 0 or 1.

Meanwhile, considering the sigmoid function is not saturated, it is to make the following adjustment:

$$\text{Sigmoid}(x) = \begin{cases} 0.98, & x > 4 \\ \frac{1}{1 + e^{-x}}, & -4 \leq x \leq 4 \\ 0.02, & x < 4. \end{cases} \quad (4)$$

In the iterative process, the calculation formula of X_{id}^{t+1} is

$$X_{id}^{t+1} = \begin{cases} 0, & \text{rand} \geq \text{Sigmoid}(V_{id}^{t+1}) \\ 1, & \text{rand} < \text{Sigmoid}(V_{id}^{t+1}), \end{cases} \quad (5)$$

where rand is the random number in the interval [0, 1].

3.3. Multiagent and Particle Swarm Optimization. MAPSO is an intelligent algorithm based on PSO and multiagent with autonomous learning, competition, and collaboration. Regional feeder agents are defined by the SIPS network model. The agents learn evolutionary mechanism of PSO by self-learning and communication with adjacent agents and update the particle swarm according to some rules, so as to make the swarm converge to the global optimal solution faster and more accurate.

In MAPSO, a regional feeder agent is equal to a particle in the particle swarm, so that the topology of the particle swarm is determined by the SIPS network reconfiguration model. By agents' self-updating and cooperation with adjacent agents, MAPSO can present a solution for the SIPS network reconfiguration. Multiagent can get the optimal objective function value in PSO. The flow chart of SIPS network reconfiguration based on MAPSO is shown in Figure 3.

4. Simulation Results

For the SIPS network model in Figure 1, according to the different complexity degrees of faults, there are two cases of reconfiguration using MAPSO.

The data sources of samples are based on the simplified network model of SIPS in Figure 1. Power of devices is changed into standard per unit, as shown in Table 1.

In the simulation, particles of swarm represent the states of branches in the power system, 0 for circuit open and 1 for circuit closed.

Example 1. Assuming that a fault occurs in regional feeder agent 17, MAPSO is used to carry out network reconfiguration, and simulation results are as follows.

Regional feeder agent 63: the initial value is 0; the ultimate value is 1.

Fitness value is 5.63305 and switch operation times (SOT) is 1.

The changes of fitness and SOT are shown in Figure 4. Simulation results show that regional feeder agent 17 communicates with adjacent agent when fault occurs, and then

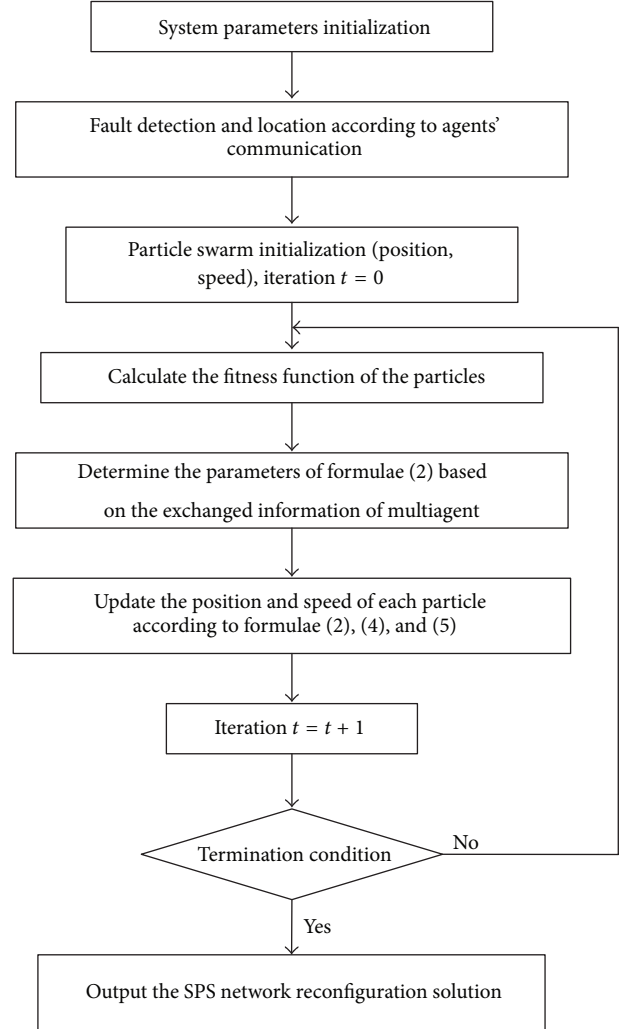


FIGURE 3: The flow chart of SIPS network reconfiguration based on MAPSO.

chooses the alternative route (regional feeder agent 63) for power supply. MAPSO gets the best fitness value 5.63305 from the 16th iteration, but only until the 18th iteration it gets the minimum SOT: 1. So we get the best network reconfiguration solution from the 18th iteration.

Example 2. Assuming that faults occur in regional feeder agents 3, 31, 93, and 95, MAPSO is used to carry out network reconfiguration, and simulation results are as follows.

Regional feeder agent 79: the initial value is 0; the ultimate value is 1.

Regional feeder agent 80: the initial value is 0; the ultimate value is 1.

Regional feeder agent 84: the initial value is 0; the ultimate value is 1.

Fitness value is 5.60925; SOT is 3.

TABLE 1: Device parameters of the SIPS.

Number	Device	Power	Rank
1	G1	21	0
2	G2	3.75	0
3	G3	3.75	0
4	G4	21	0
5	P1	0.005	0
6	M1	20	1
7	M2	20	1
8	P2	0.005	0
9	P3	0.005	0
10	P4	0.005	0
11	P5	0.005	0
12	P6	0.005	0
13	M3	20	1
14	M4	20	1
15	P7	0.005	0
16	I1	0.05	3
17	M5	1.2705	2
18	I2	1.1024	2
19	P10	0.005	0
20	I3	0.05	3
21	M6	0.8976	2
22	I4	1.4937	2
23	P9	0.005	0
24	I5	0.05	3
25	M7	1.2705	2
26	I6	0.7692	2
27	P10	0.005	0
28	I7	0.05	3
29	M8	1.2705	2
30	I8	3.0	2
31	P11	0.005	0
32	I9	0.05	3
33	M9	1.2705	2
34	I10	1.4937	2
35	P12	0.005	0
36	I11	0.005	3
37	M10	0.7295	2
38	I12	1.2705	2
39	P13	0.005	0
40	I13	0.05	3
41	M11	1.2705	2
42	I14	1.392	2
43	P14	0.005	0
44	I15	0.005	3
45	M12	0.7692	2
46	I16	1.2308	2
47	G5	21	0
48	G6	3.75	0
49	G7	3.75	0

TABLE 1: Continued.

Number	Device	Power	Rank
50	G8	21	0
51	P23	0.005	0
52	M1	20	1
53	M2	20	1
54	P24	0.005	0
55	P25	0.005	0
56	P26	0.005	0
57	P27	0.005	0
58	P28	0.005	0
59	M3	20	1
60	M4	20	1
61	P15	0.005	0
62	I17	0.05	3
63	M5	1.2705	2
64	I2	1.1024	2
65	P15	0.005	0
66	I18	0.05	3
67	M6	0.8976	2
68	I4	1.4937	2
69	P17	0.005	0
70	I19	0.05	3
71	M7	1.2705	2
72	I6	0.7692	2
73	P18	0.005	0
74	I20	0.05	3
75	M8	1.2705	2
76	I8	3.0	2
77	P19	0.005	0
78	I21	0.05	3
79	M9	1.2705	2
80	I10	1.4937	2
81	P20	0.005	0
82	I22	0.005	3
83	M10	0.7295	2
84	I12	1.2705	2
85	P21	0.005	0
86	I23	0.05	3
87	M11	1.2705	2
88	I14	1.392	2
89	P22	0.005	0
90	I24	0.005	3
91	M12	0.7692	2
92	I16	1.2308	2
93	L1	0.005	0
94	L2	0.005	0
95	L3	0.005	0
96	L4	0.005	0

TABLE 2: Simulation results of Example 1 compared with traditional PSO.

Algorithm type	Fitness			SOT			Best iteration
	MAX	MIN	AVG	MAX	MIN	AVG	
Traditional PSO	5.63215	5.50513	5.58676	25	1	5.6	27
MAPSO	5.63305	5.50642	5.62084	22	1	3.8	18

TABLE 3: Simulation results of Example 2 compared with traditional PSO.

Algorithm type	Fitness			SOT			Best iteration
	MAX	MIN	AVG	MAX	MIN	AVG	
Traditional PSO	5.60115	5.50582	5.54486	24	7	8.9	36
MAPSO	5.60925	5.55364	5.59183	18	3	5.3	27

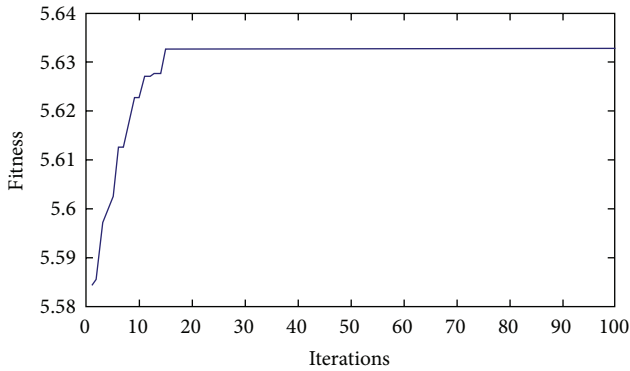


FIGURE 4: The changes of fitness and SOT of Example 1.

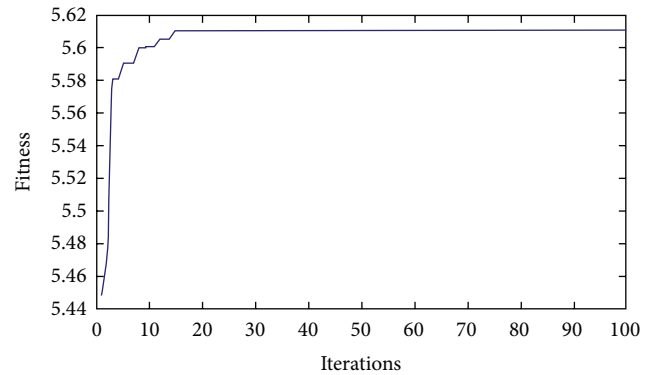


FIGURE 5: The changes of fitness and SOT of Example 2.

The changes of fitness and SOT are shown in Figure 5. When faults occur, the regional feeder agents with faults communicate with adjacent agents. The adjacent agents would firstly estimate self-capacity. If all the constraint conditions are satisfied, they would supply power to the fault agents by alternative routes. MAPSO gets the best fitness value 5.60925 from the 15th iteration, but only until the 27th iteration it gets the minimum SOT: 3. So we get the best network reconfiguration solution from the 27th iteration.

5. Comparison with Traditional PSO

In order to verify the validity of MAPSO, the simulation results of two examples are compared with traditional PSO, as shown in Tables 2 and 3.

Tables 2 and 3 show that the application of multi-agent could significantly enhance the effect of intelligent network reconfiguration. It can accelerate convergence and optimization of intelligent algorithm. In Example 1, multi-agent speeds up convergence and optimization of traditional PSO. In Example 2, based on the information exchange between agents, MAPSO change the network topology in the minimum scope for reconfiguration. It gets a better reconfiguration solution.

6. Conclusions

The simplified network model and reconfiguration mathematical model of SIPS are established. PSO and multiagent technology are analyzed. Regional feeder agents are defined. Combining PSO with multiagent, MAPSO is presented. In

this algorithm, regional feeder agents communicate with adjacent agents to accomplish SIPS network reconfiguration. Simulation and comparison results show that MAPSO can reconfigure SIPS network more efficient.

Conflict of Interests

The authors declare that there is no conflict of interests regarding the publication of this paper.

Acknowledgment

This work is supported by National Natural Science Foundation of China under Grant no. 51177168.

References

- [1] J. Huang, X. Zhang, Y. Chen, L. Fu, and Z. Ye, "Multiobjective optimal model of service restoration for integrated ship power system and its application," *Transactions of China Electrotechnical Society*, vol. 25, no. 3, pp. 130–137, 2010.
- [2] F. He and X. Cai, "Based on improved genetic algorithm for ship power system reconfiguration," *Electrotechnical Society*, vol. 21, pp. 25–30, 2006.
- [3] Q. Liu, L.-B. Shi, Y.-X. Ni, and Z.-Y. Dong, "Intelligent optimization strategy of the power grid reconfiguration during power system restoration," *Proceedings of the Chinese Society of Electrical Engineering*, vol. 29, no. 13, pp. 8–15, 2009.
- [4] H. Zhang, H. Yan, T. Liu, and Q. Chen, "Fuzzy controller design for nonlinear impulsive fuzzy systems with time delay," *IEEE Transactions on Fuzzy Systems*, vol. 19, no. 5, pp. 844–856, 2011.
- [5] H. Zhang, H. Yan, F. Yang, and Q. Chen, "Quantized control design for impulsive fuzzy networked systems," *IEEE Transactions on Fuzzy Systems*, vol. 19, no. 6, pp. 1153–1162, 2011.
- [6] S. K. Srivastava, K. L. Butler-Purpy, and N. D. R. Sarma, "Shipboard power restored for active duty," *IEEE Computer Applications in Power*, vol. 15, no. 3, pp. 16–23, 2002.
- [7] T. Nagata and H. Sasaki, "A multi-agent approach to power system restoration," *IEEE Transactions on Power Systems*, vol. 17, no. 2, pp. 457–462, 2002.
- [8] H. C. Yan, Z. Z. Su, H. Zhang, and F. W. Yang, "Observer-based H_∞ control for discrete-time stochastic systems with quantisation and random communication delays," *IET Control Theory & Applications*, vol. 7, no. 3, pp. 372–379, 2013.
- [9] H. Yan, H. Shi, H. Zhang, and F. Yang, "Quantized H_∞ control for networked systems with communication constraints," *Asian Journal of Control*, vol. 15, no. 5, pp. 1468–1476, 2013.
- [10] H. Zhang, H. Yan, F. Yang, and Q. Chen, "Distributed average filtering for sensor networks with sensor saturation," *IET Control Theory & Applications*, vol. 7, no. 6, pp. 887–893, 2013.
- [11] W. Zheng, X. Li, and W. Yongji, "Application of multi-agent and genetic algorithm in network reconfiguration of ship power system," *Electronics & Electrical Engineering*, vol. 18, no. 9, pp. 7–10, 2012.
- [12] F. Yushun and C. Junwei, *Multi-Agent Systems: Theory, Method and Applications*, Springer Press, 2005.
- [13] Z. Hongxia and Y. Quan, "Application of multi-agent technology in power system," *Journal of Chongqing University*, vol. 29, no. 11, pp. 53–57, 2006.
- [14] H.-C. Shu, L. Tang, and J. Dong, "A survey on application of multi-agent system in power system," *Power System Technology*, vol. 29, no. 6, pp. 27–31, 2005.
- [15] X.-F. Xie, W.-J. Zhang, and Z.-L. Yang, "Overview of particle swarm optimization," *Control and Decision*, vol. 18, no. 2, pp. 129–134, 2003.
- [16] Z. Wang, D. Zhao, Y. Wang, and D. Liu, "Reconfiguration of shipboard power system using discrete particle swarm optimisation," *International Journal of Modelling, Identification and Control*, vol. 15, no. 4, pp. 277–283, 2012.
- [17] J. Lu, H. Yang, and J. Du, "Improved strategy of particle swarm optimization algorithm for reactive power optimization," *International Journal of Bio-Inspired Computation*, vol. 2, no. 1, pp. 27–33, 2010.
- [18] X. Zhang and H. Qiu, "Hybrid particle swarm optimization with k-centres method and dynamic velocity range setting for travelling salesman problems," *International Journal of Bio-Inspired Computation*, vol. 2, no. 1, pp. 34–41, 2010.
- [19] J. Kennedy and R. C. Eberhart, "A discrete binary version of the particle swarm algorithm," in *Proceedings of the IEEE International Conference on Systems, Man, and Cybernetics*, pp. 4104–4108, IEEE Press, Piscataway, NJ, USA, October 1997.
- [20] C. K. Mohan and B. Al-kazemi, "Discrete particle swarm optimization," in *Proceedings of the Workshop on Particle Swarm Optimization*, Purdue School of Engineering and Technology, Indianapolis, Indiana, 2001.
- [21] R. Yang, H. Gao, and W. Pang, "Based on discrete particle swarm optimization algorithm for multi-user detector," *Harbin Institute of Technology*, vol. 37, no. 9, pp. 1303–1306, 2005.
- [22] X. Wang, J. Li, and J. Xiao, "Solving the network reconfiguration of the shipboard power system DPSO greedy algorithm," *Control and Decision*, vol. 23, pp. 157–161, 2008.

Research Article

Output-Feedback Controller Design of a Wireless Networked Control System with Packet Loss and Time Delay

Zhen Hong,¹ JinFeng Gao,¹ and Ning Wang²

¹ Faculty of Mechanical Engineering & Automation, Zhejiang Sci-Tech University, Hangzhou 310018, China

² College of Business Administration, Zhejiang University of Finance & Economics, Hangzhou 310018, China

Correspondence should be addressed to Zhen Hong; zhong@zstu.edu.cn

Received 6 December 2013; Revised 20 February 2014; Accepted 20 February 2014; Published 25 March 2014

Academic Editor: Xudong Zhao

Copyright © 2014 Zhen Hong et al. This is an open access article distributed under the Creative Commons Attribution License, which permits unrestricted use, distribution, and reproduction in any medium, provided the original work is properly cited.

This paper investigates the problem of modeling and stabilization of a wireless network control system (NCS) with both time-varying delay and packet-dropout. And the time-varying delay can be more or less than one sampling period. The wireless NCS is modeled as an asynchronous dynamic system (ADS) with three subsystems. Sufficient condition of the closed-loop NCS to be stable is obtained by using the ADS approach. A numerical example is presented to demonstrate the effectiveness of the proposed result.

1. Introduction

In modern control systems, the sensors, controllers, and controlled process are often connected by a real-time network medium. Such systems are called network control systems (NCSs) [1]. In the last decade, the general theory for NCSs has been widely investigated. It is widely used at almost all levels of operation and information processing in various areas, including manufacturing plants, automobiles, aircraft, remote operation, and teleautonomy [2–8]. As an alternative item for the wired network, wireless NCSs are becoming fundamental components of modern control systems due to their flexibility, ease of deployment, and low cost [9–12]. Thus, wireless NCS is considered in this paper.

One of the main issues in the NCS is the effect of network-induced delay that occurs when sensors, actuators, and controllers exchange data across the shared network. Without considering the delay, it not only degrades the performance of the control system but also even destabilizes the system. On the other hand, packet-dropout results from the network traffic congestion and the limited network reliability. When a data packet is dropped, the complete information of the NCS becomes unavailable. In this case, the controller or actuator has to decide what control signal is output with incomplete information.

Recently, many researchers have tried to solve the above problems with network-induced delay and packet-dropout in wireless NCS. For the problem with delay, for example, Hu and Yuan [2] introduce a finite sum equality based on quadratic terms to H_∞ output-feedback control for switched linear discrete-time systems. Together with a Lyapunov sequence, a novel delay-dependent condition is implemented for H_∞ without ignoring the useful terms. It can obtain the suboptimal H_∞ static and dynamic output-feedback controllers at last, when a procedure involving a modified iterative algorithm is performed. For the problems with packet-dropout, for instance, the sufficient conditions for the exponential stability of the closed-loop NCSs using the average dwell time method are proposed in [5]. Furthermore, the relation between the packet-dropout rate and the stability of the closed-loop NCSs is also explicitly established in order to prove the effectiveness.

Unlike separately considered these two issues of the delay and the packet-dropout, this paper intends to deal with the modelling, analysis, and synthesis for the wireless NCS with both delay and packet-dropout as shown in Figure 1. An asynchronous dynamic system (ADS) approach is presented to stabilize the wireless NCS. Firstly, a switched system with time-varying delay model is presented to describe the wireless NCS. In [4], a new switched linear system model is proposed to describe NCS while the delay is assumed

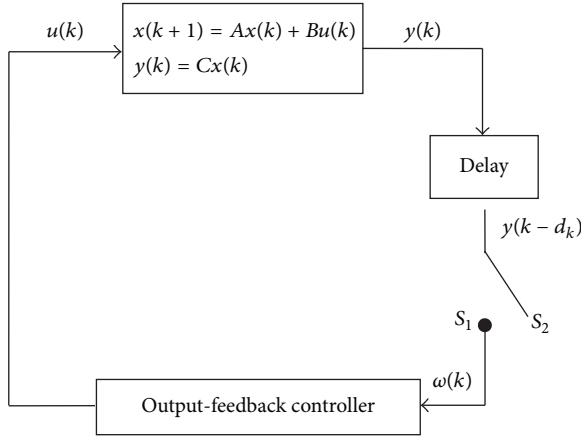


FIGURE 1: Diagram of network control system with network-induced delay and packet-dropout.

to be less than one sampling period with the state feedback controller. And stochastic optimal control method is used by an adaptive estimator (AE) and ideas from Q-learning to solve the infinite horizon optimal regulation of unknown wireless NCS with time-varying system matrices in [13]. Nevertheless, the computational complexity of the controller will increase when the delay bound is increased in NCS in [13]. Furthermore, the network system identification problem and estimation problem are also studied in [14, 15] based on the Matlab/Simulink simulator TrueTime and orthogonal projection principle, respectively, which aim at identifying mathematical models required in network control/estimation/filtering systems while stabilization is not considered. Similarly, we can also get the new ideas and future applications from the related papers [16, 17], respectively.

Summarizing the aforementioned discussion, in this paper, we aim to investigate the problem of modeling and stabilization of a wireless NCS with both time-varying delay and packet-dropout, where the wireless NCS is modeled as an ADS with three subsystems, and sufficient condition of the closed-loop NCS is obtained to be stable using this ADS method. The main contribution of this paper is highlighted as follows: to obtain the observer-based output-feedback controller, particularly, when the output of the sensor is dropped and delay appeared to the controller input, the ADS approach is presented to stabilize the considered wireless NCS with delay and packet-dropout.

Notations. Throughout this paper, R denotes the set of real numbers, R^n denotes the n -dimensional Euclidean space, and $R^{n \times m}$ refers to the set of all $n \times m$ real matrices. A^T represents the transpose of the matrix A , while A^{-1} denotes the inverse of A . For real symmetric matrices, X and Y , the notation $X \geq Y$ (resp., $X > Y$) means that the matrix $X - Y$ is positive semidefinite (resp., positive-definite). I is the identity matrix with appropriate dimensions. $\|x\|$ refers to the Euclidean norm of the vector x ; that is, $\|x\| = \sqrt{x^T x}$. For a symmetric matrix, $*$ denotes the matrix entries implied by symmetry.

2. Problem Formulation and NCS Modeling

The NCS with packet-dropout and possible delay is illustrated in Figure 1, where the plant is described by the following model denoted by Ω :

$$\begin{aligned} x(k+1) &= Ax(k) + Bu(k), \\ y(k) &= Cx(k), \end{aligned} \quad (1)$$

where $x(k) \in R^n$ is the system state, $u(k) \in R^m$ is the control input, and $y(k) \in R^r$ is the measured output. And the model of an observer-based output-feedback controller is described as follows:

$$\begin{aligned} \hat{x}(k+1) &= A\hat{x}(k) + Bu(k) + L[\omega(k) - \hat{y}(k)], \\ \hat{y}(k) &= C\hat{x}(k), \\ u(k) &= K\hat{x}(k), \end{aligned} \quad (2)$$

where $\hat{x}(k) \in R^n$ is the estimated state of the system (1) and $\hat{y}(k) \in R^r$ is the estimated output. $L \in R^{n \times r}$ and $K \in R^{m \times n}$ are the observer and controller gain, respectively. It is also assumed that the pairs (A, B) are controllable and (C, A) are observable. In Figure 1, we can use a switch to denote the packet loss of the states in the network channel. If the switch is closed, the data packet is successfully transmitted. And we have $\omega(k) = y(k)$ without network delay or $\omega(k) = y(k - d_k)$ with network delay. When the switch is open, the previous value of the switch output will be used in the controller (2) and a packet is dropped. Then we have $\omega(k) = \omega(k-1)$ in this case.

Under consideration for the NCS, without loss of generality, we give the following assumptions, which will be useful in our main results.

Assumption 1. (1) The sensors and controllers are all time-driven and synchronized.

(2) Time-stamping of measurements is necessary to reorder data packet at the observer side since they can arrive out of order. And the controller can get the delay of each data packet.

(3) The maximum delay in the network is d_M that is a known integer.

Define the estimation error by $e(k) = x(k) - \hat{x}(k)$ and let

$$z(k) = [x^T(k) \quad e^T(k) \quad w^T(k-1)]^T. \quad (3)$$

Then the dynamics of the closed-loop system can be described by the following three subsystems.

(S1) There is packet loss and the corresponding controller gain is K_1 . Then the closed-loop NCS is described as

$$\begin{aligned} \Omega_1 : z(k+1) &= A_1 z(k), \\ A_1 &= \begin{bmatrix} A + BK_1 & -BK_1 & 0 \\ LC & A - LC & -L \\ 0 & 0 & I \end{bmatrix}. \end{aligned} \quad (4)$$

(S2) The data packet is transmitted successfully without network delay and the corresponding controller gain is K_2 in this case. Then the closed-loop NCS can be described as

$$\Omega_2 : z(k+1) = A_2 z(k),$$

$$A_2 = \begin{bmatrix} A + BK_2 & -BK_2 & 0 \\ 0 & A - LC & 0 \\ C & 0 & 0 \end{bmatrix}. \quad (5)$$

(S3) The data packet is transmitted successfully with network delay d_k and the corresponding controller gain becomes K_{3,d_k} here. Then the closed-loop NCS is as follows:

$$\Omega_3 : z(k+1) = A_3 z(k) + A_{d3} z(k - d_k),$$

$$A_3 = \begin{bmatrix} A + BK_{3,d_k} & -BK_{3,d_k} & 0 \\ LC & A - LC & 0 \\ 0 & 0 & 0 \end{bmatrix}, \quad (6)$$

$$A_{d3} = \begin{bmatrix} 0 & 0 & 0 \\ -LC & 0 & 0 \\ C & 0 & 0 \end{bmatrix}.$$

From the above analysis, we can conclude that there are three different cases which may appear during every sampling period. So the closed-loop NCS can be described as a discrete-time switched system within three subsystems Ω_1 to Ω_3 . In subsystem Ω_3 , when $d_k = 0$, Ω_3 turns to Ω_2 . And the system matrices Ω_1 and Ω_2 are similar. So subsystem Ω_3 in case 3 includes cases 1 and 2 by appropriately choosing the value of the matrices. Then the wireless NCS can be represented by the following switched system with time-varying delay:

$$z(k+1) = A_i z(k) + A_{di} z(k - d_k), \quad i = 1, 2, 3, \quad (7)$$

where $A_{d1} = 0$, $A_{d2} = 0$, and $d_k = 1, 2, \dots, d_M$.

To end this section, the following definition and lemma are introduced to obtain our main results.

Definition 2. For any given initial conditions $(k_0, \phi) \in \mathfrak{R}^+ \times C^n$, (7) is globally exponentially stable if the solutions of (10) satisfy

$$\|x(k)\| \leq a \lambda^{-(k-k_0)} \|x(k_0)\|, \quad \forall k \geq k_0, \quad (8)$$

where $a > 0$ is a constant and $\lambda > 1$ is the decay rate.

Lemma 3 (see [2]). For any appropriately dimensional matrices $R = R^T > 0$, N , X , $\eta(l) \triangleq x(l+1) - x(l)$ and two positive integer time-varying $d(k_1)$, $d(k_2)$ satisfying $d(k_1)+1 \leq d(k_2) \leq d_M$, the following equality holds:

$$- \sum_{l=k-d(k_2)}^{k-d(k_1)-1} \eta^T(l) R \eta(l)$$

$$= 2\xi^T(k) N [x(k-d(k_1)) - x(k-d(k_2))]$$

$$+ (d(k_2) - d(k_1)) \xi^T(k) X \xi(k)$$

$$- \sum_{l=k-d(k_2)}^{k-d(k_1)-1} \begin{bmatrix} \xi(k) \\ \eta(l) \end{bmatrix}^T \begin{bmatrix} X & N \\ * & R \end{bmatrix} \begin{bmatrix} \xi(k) \\ \eta(l) \end{bmatrix}. \quad (9)$$

3. Stability Analysis of the Wireless NCS

More generally, we consider the following discrete-time switched system with time-varying delay:

$$z(k+1) = A_i z(k) + A_{di} z(k - d_k), \quad i = 1, 2, \dots, N, \quad (10)$$

$$d_k = 1, 2, \dots, d_M,$$

where N is the number of the subsystems. Suppose that the event rates of the described subsystems S_i are defined as r_1, r_2, \dots, r_N . The time interval $[0, kT]$ will be simplified $[0, k]$ in the following text. Let n_i , $i = 1, 2, \dots, N$ denote the times in which the subsystems S_i are activated on the interval $[0, k]$. Then we can obtain

$$k = \sum_{i=1}^N n_i; \quad r_i = \frac{n_i}{k}, \quad i = 1, 2, \dots, N; \quad \sum_{i=1}^N r_i = 1. \quad (11)$$

The following theorem gives a criterion to guarantee that the Lyapunov function $V(k)$ exponentially decays along state trajectory of system (10).

Theorem 4. Given scalar $\lambda > 0$ and any delay satisfying $0 \leq d_k \leq d_M$, if there exist appropriate dimensional symmetric positive-definite matrices P , Q_1 , Q_2 , R , symmetric matrix $X = \begin{bmatrix} X_1 & X_2 \\ * & X_3 \end{bmatrix} \geq 0$, and matrices $G, N = \begin{bmatrix} N_1^T & N_2^T \end{bmatrix}^T$ and $M = \begin{bmatrix} M_1^T & M_2^T \end{bmatrix}^T$, such that the following matrix inequalities hold:

$$\Phi(d_k) = \begin{bmatrix} \Phi_{11} & \Phi_{12} & -N_1 & P + (\widehat{A}_i^T - I)G^T - G \\ * & \Phi_{22} & -N_2 & \widehat{A}_{di}^T G^T \\ * & * & -Q_2 & 0 \\ * & * & * & P + d_M R - G - G^T \end{bmatrix} < 0, \quad (12)$$

$$\begin{bmatrix} X & N \\ * & R \end{bmatrix} > 0, \quad \begin{bmatrix} X & M \\ * & R \end{bmatrix} > 0, \quad (13)$$

where $d_k = 0, \dots, d_M$, $\widehat{A}_i = \lambda A_i$, $\widehat{A}_{di} = \lambda^{1+d_k} A_{di}$, and

$$\Phi_{11} = d_M Q_1 + Q_2 + d_M X_1 + \text{Sym}(M_1 + G(\widehat{A}_i - I)),$$

$$\Phi_{12} = d_M X_2 + N_1 - M_1 + M_2^T + G \widehat{A}_{di}, \quad (14)$$

$$\Phi_{22} = d_M X_3 - Q_1 + \text{Sym}(N_2 - M_2),$$

then

$$V(k) < \lambda^{-2(k-k_0)} V(k_0). \quad (15)$$

Proof. The following expression of $V(k)$ is the Lyapunov function of system (10):

$$\begin{aligned}
V_1(k) &= z^T(k) P z(k), \\
V_2(k) &= \sum_{l=k-d_k}^{k-1} \lambda^{2(l-k)} z^T(l) Q_1 z(l) \\
&\quad + \sum_{m=-d_M+2}^0 \sum_{l=k+m-1}^{k-1} \lambda^{2(l-k)} z^T(l) Q_1 z(l), \\
V_3(k) &= \sum_{l=k-d_M}^{k-1} \lambda^{2(l-k)} z^T(l) Q_2 z(l), \\
V_4(k) &= \sum_{m=-d_M}^{-1} \sum_{l=k+m}^{k-1} \lambda^{2(l-k)} (\lambda z(l+1) - z(l))^T \\
&\quad \times R (\lambda z(l+1) - z(l)).
\end{aligned} \tag{16}$$

And defining $\xi(k) = \lambda^{k-k_0} z(k)$, $\lambda > 0$, $\widehat{A}_i = \lambda A_i$, $\widehat{A}_{di} = \lambda^{1+d_k} A_{di}$, combined with (10), we have

$$\begin{aligned}
\xi(k+1) &= \widehat{A}_i \xi(k) + \widehat{A}_{di} \xi(k-d_k), \\
i &= 1, 2, \dots, N, \quad d_k = 1, 2, \dots, d_M.
\end{aligned} \tag{17}$$

Choose the following Lyapunov function of system (17):

$$\begin{aligned}
W(k) &= \xi^T(k) P \xi(k) + \sum_{l=k-d_k}^{k-1} \xi^T(l) Q_1 \xi(l) \\
&\quad + \sum_{m=-d_M+2}^0 \sum_{l=k+m-1}^{k-1} \xi^T(l) Q_1 \xi(l) \\
&\quad + \sum_{l=k-d_M}^{k-1} \xi^T(l) Q_2 \xi(l) \\
&\quad + \sum_{m=-d_M}^{-1} \sum_{l=k+m}^{k-1} \delta^T(l) R \delta(l),
\end{aligned} \tag{18}$$

where $\delta(l) = \xi(l+1) - \xi(l)$. Then the forward difference for $W(k)$ along any trajectory of system (17) is given by

$$\begin{aligned}
\Delta W(k) &= W(k+1) - W(k) \\
&= \xi^T(k+1) P \xi(k+1) - \xi^T(k) P \xi(k) \\
&\quad + d_M \xi^T(k) Q_1 \xi(k) + \sum_{l=k+1-d_{k+1}}^{k-1} \xi^T(l) Q_1 \xi(l) \\
&\quad - \sum_{l=k-d_M+1}^{k-1} \xi^T(l) Q_1 \xi(l) - \sum_{l=k-d_k}^{k-1} \xi^T(l) Q_1 \xi(l) \\
&\quad + \xi^T(k) Q_2 \xi(k) - \xi^T(k-d_M) Q_2 \xi(k-d_M) \\
&\quad + d_M \delta^T(k) R \delta(k)
\end{aligned}$$

$$\begin{aligned}
&\quad + d_M \begin{bmatrix} \xi(k) \\ \xi(k-d_k) \end{bmatrix}^T X \begin{bmatrix} \xi(k) \\ \xi(k-d_k) \end{bmatrix} \\
&\quad + 2 \begin{bmatrix} \xi(k) \\ \xi(k-d_k) \end{bmatrix}^T \begin{bmatrix} N_1 \\ N_2 \end{bmatrix} \\
&\quad \times (\xi(k-d_k) - \xi(k-d_M)) \\
&\quad + 2 \begin{bmatrix} \xi(k) \\ \xi(k-d_k) \end{bmatrix}^T \begin{bmatrix} M_1 \\ M_2 \end{bmatrix} (\xi(k) - \xi(k-d_k)) \\
&\quad - \sum_{l=k-d_M}^{k-d_k-1} \begin{bmatrix} \xi(k) \\ \xi(k-d_k) \\ \delta(l) \end{bmatrix}^T \begin{bmatrix} X & N \\ * & R \end{bmatrix} \begin{bmatrix} \xi(k) \\ \xi(k-d_k) \\ \delta(l) \end{bmatrix} \\
&\quad - \sum_{l=k-d_k}^{k-1} \begin{bmatrix} \xi(k) \\ \xi(k-d_k) \\ \delta(l) \end{bmatrix}^T \begin{bmatrix} X & M \\ * & R \end{bmatrix} \begin{bmatrix} \xi(k) \\ \xi(k-d_k) \\ \delta(l) \end{bmatrix} \\
&\quad + 2 (\xi^T(k) + \delta^T(k)) G \\
&\quad \times [(A_i - I) \xi^T(k) + A_{di} \xi^T(k-d_k) - \delta(k)] \\
&\quad < \theta^T(k) \Phi \theta(k) < 0,
\end{aligned} \tag{19}$$

where $\theta^T(k) = [\xi^T(k) \ \xi^T(k-d_k) \ \xi^T(k-d_M) \ \delta^T(k)]$, which means that $W(k) < W(k_0)$ for any $k \geq k_0$. Furthermore,

$$\begin{aligned}
V_1(k) &= z^T(k) P z(k) = \lambda^{-2(k-k_0)} \xi^T(k) P \xi(k) \\
V_2(k) &= \sum_{l=k-d_k}^{k-1} \lambda^{2(l-k)} \lambda^{-2(l-k_0)} \xi^T(l) Q_1 \xi(l) \\
&\quad + \sum_{m=-d_M+2}^0 \sum_{l=k+m-1}^{k-1} \lambda^{2(l-k)} \lambda^{-2(l-k_0)} \xi^T(l) Q_1 \xi(l) \\
V_3(k) &= \sum_{l=k-d_M}^{k-1} \lambda^{2(l-k)} \lambda^{-2(l-k_0)} \xi^T(l) Q_2 \xi(l) \\
V_4(k) &= \sum_{m=-d_M}^{-1} \sum_{l=k+m}^{k-1} \lambda^{2(l-k)} \lambda^{-2(l-k_0)} \delta^T(l) R \delta(l) \\
V(k) &= V_1(k) + V_2(k) + V_3(k) + V_4(k) = \lambda^{-2(k-k_0)} W(k).
\end{aligned} \tag{20}$$

As $W(k_0) = V(k_0)$, it is easy to verify that $V(k) < \lambda^{-2(k-k_0)} V(k_0)$. This completes the proof. \square

The following theorem gives a sufficient condition for the closed-loop NCS (10) to be exponentially stable.

Theorem 5. *The discrete-time switched system (10) is stable if there exist Lyapunov function $V(k)$, r_i defined in (11), and some*

positive scalars μ_i , $i = 1, 2, \dots, N$ which correspond to each subsystem such that the following inequalities hold:

$$V(k) < \mu_i^{-2(k-k_0)} V(k_0),$$

$$\prod_{i=1}^N \mu_i^{r_i} < 1. \quad (21)$$

Proof. Defining the transition time of the subsystems to be $t_1 = 0, t_2, \dots, t_k = k$, then

$$V(k) < \mu_k^{t_k - t_{k-1}} V(t_{k-1}) < \mu_k^{t_k - t_{k-1}} \mu_{k-1}^{t_{k-1} - t_{k-2}} V(t_{k-2})$$

$$< \dots < \prod_{i=1}^N \mu_i^{n_i} V(0) = \left(\prod_{i=1}^N \mu_i^{r_i} \right)^k V(0). \quad (22)$$

So the system is stable if $\prod_{i=1}^N \mu_i^{r_i} < 1$. This completes the proof. \square

4. Output-Feedback Controller Design

An algorithm to design the observer-based output-feedback controller of the wireless NCS is presented in this section. Since the data packets are time-stamped, the packet loss rate and time delay are known to the controller, which is designed to depend on both the packet loss rate and time delay. Firstly, A_i can be rewritten as $A_i = A_{0i} + B_{00} D_i C_{0i}$, $i = 1, 2, 3$, where

$$A_{01} = \begin{bmatrix} A & 0 & 0 \\ 0 & A & 0 \\ 0 & 0 & I \end{bmatrix}, \quad B_{00} = \begin{bmatrix} B & 0 \\ 0 & I \\ 0 & 0 \end{bmatrix},$$

$$D_i = \begin{bmatrix} K_i & 0 \\ 0 & L \end{bmatrix}, \quad C_{01} = \begin{bmatrix} I & -I & 0 \\ C & -C & -I \end{bmatrix}$$

$$A_{02} = \begin{bmatrix} A & 0 & 0 \\ 0 & A & 0 \\ C & 0 & 0 \end{bmatrix}, \quad C_{02} = \begin{bmatrix} I & -I & 0 \\ 0 & C & 0 \end{bmatrix} \quad (23)$$

$$A_{03} = \begin{bmatrix} A & 0 & 0 \\ 0 & A & 0 \\ 0 & 0 & 0 \end{bmatrix}, \quad C_{03} = \begin{bmatrix} I & -I & 0 \\ C & -C & 0 \end{bmatrix}$$

Theorem 6. *The system (7) is stable if there exist positive scalars μ_i , $i = 1, 2, 3$ satisfying $\prod_{i=1}^3 \mu_i^{r_i} < 1$ and appropriate dimensional matrices P, Q_1, Q_2, R, X_1, X_3 , matrices M_1, M_2, N_1, N_2, X_2 and matrices G_1, G_2, G_3 , and matrices K_1, K_2, K_{3,d_k} such that the following matrix inequality holds:*

$$\Phi_0 + \Phi_1 < 0,$$

$$\Phi_0 + \Phi_2 < 0,$$

$$\Phi_0 + \Phi_3(d_k) < 0, \quad d_k = 1, 2, \dots, d_M, \quad (24)$$

$$\begin{bmatrix} X & N \\ * & R \end{bmatrix} > 0, \quad \begin{bmatrix} X & M \\ * & R \end{bmatrix} > 0,$$

where

$$\Phi_0 = \begin{bmatrix} \Sigma_{11} & \Sigma_{12} & -N_1 & P - G^T - G \\ * & \Sigma_{22} & -N_2 & 0 \\ * & * & -Q_2 & 0 \\ * & * & * & P + d_M R - G - G^T \end{bmatrix},$$

$$\Sigma_{11} = d_M Q_1 + Q_2 + d_M X_1 + \text{Sym}(M_1 - G),$$

$$\Sigma_{12} = d_M X_2 + N_1 - M_1 + M_2^T,$$

$$\Sigma_{22} = d_M X_3 - Q_1 + \text{Sym}(N_2 - M_2),$$

$$G = \begin{bmatrix} G_1 & 0 & 0 \\ 0 & G_2 & 0 \\ 0 & 0 & G_3 \end{bmatrix}, \quad \Phi_1 = \begin{bmatrix} \bar{\phi}_{11} & 0 & 0 & \bar{\phi}_{14} \\ * & 0 & 0 & 0 \\ * & * & 0 & 0 \\ * & * & * & 0 \end{bmatrix},$$

$$\bar{\phi}_{11} = \begin{bmatrix} \bar{\psi}_{11} & \bar{\psi}_{12} & 0 \\ * & \bar{\psi}_{22} & -\mu_1 G_2 L \\ * & * & \mu_1 G_3 + \mu_1 G_3^T \end{bmatrix},$$

$$\bar{\psi}_{11} = \text{Sym}(\mu_1 G_1 A + \mu_1 G_1 B K_1),$$

$$\bar{\psi}_{12} = -\mu_1 G_1 B K_1 + \mu_1 C^T L^T G_2^T,$$

$$\bar{\psi}_{22} = \text{Sym}(\mu_1 G_2 A - \mu_1 G_2 L C),$$

$$\bar{\phi}_{14} = \begin{bmatrix} \bar{\varphi}_{11} & -\mu_1 C^T L^T G_2^T & 0 \\ -\mu_1 K_1^T B^T G_1^T & \bar{\varphi}_{22} & 0 \\ 0 & -\mu_1 L^T G_2^T & \mu_1 G_3^T \end{bmatrix},$$

$$\bar{\varphi}_{11} = \mu_1 A^T G_1^T + \mu_1 K_1^T B^T G_1^T,$$

$$\bar{\varphi}_{22} = \mu_1 A^T G_2^T - \mu_1 C^T L^T G_2^T,$$

$$\Phi_2 = \begin{bmatrix} \hat{\phi}_{11} & 0 & 0 & \hat{\phi}_{14} \\ * & 0 & 0 & 0 \\ * & * & 0 & 0 \\ * & * & * & 0 \end{bmatrix},$$

$$\hat{\phi}_{11} = \begin{bmatrix} \hat{\psi}_{11} & \hat{\psi}_{12} & 0 \\ * & \hat{\psi}_{22} & 0 \\ * & * & 0 \end{bmatrix},$$

$$\hat{\psi}_{11} = \text{Sym}(\mu_2 G_1 A + \mu_2 G_1 B K_2),$$

$$\hat{\psi}_{12} = -\mu_2 G_1 B K_2,$$

$$\hat{\psi}_{22} = \text{Sym}(\mu_2 G_2 A - \mu_2 G_2 L C),$$

$$\hat{\phi}_{14} = \begin{bmatrix} \hat{\varphi}_{11} & 0 & \mu_2 C^T G_3^T \\ -\mu_2 K_2^T B^T G_1^T & \hat{\varphi}_{22} & 0 \\ 0 & 0 & 0 \end{bmatrix},$$

$$\hat{\varphi}_{11} = \mu_2 A^T G_1^T + \mu_2 K_2^T B^T G_1^T,$$

$$\hat{\varphi}_{22} = \mu_2 A^T G_2^T - \mu_2 C^T L^T G_2^T,$$

$$\begin{aligned}
\Phi_3 &= \begin{bmatrix} \tilde{\phi}_{11} & \tilde{\phi}_{12} & 0 & \tilde{\phi}_{14} \\ * & 0 & 0 & \tilde{\phi}_{24} \\ * & * & 0 & 0 \\ * & * & * & 0 \end{bmatrix}, \\
\tilde{\phi}_{11} &= \begin{bmatrix} \tilde{\psi}_{11} & \tilde{\psi}_{12} & 0 \\ * & \tilde{\psi}_{22} & 0 \\ * & * & 0 \end{bmatrix}, \\
\tilde{\psi}_{11} &= \text{Sym}(\mu_3 G_1 A + \mu_3 G_1 B K_{3,d_k}), \\
\tilde{\psi}_{12} &= -\mu_3 (G_1 B K_{3,d_k} + C^T L^T G_2^T), \\
\tilde{\psi}_{22} &= \text{Sym}(\mu_3 G_2 A - \mu_3 G_2 L C), \\
\tilde{\phi}_{12} &= \begin{bmatrix} 0 & 0 & 0 \\ -\mu^{1+d_k} G_2 L C & 0 & 0 \\ 0 & 0 & 0 \end{bmatrix}, \quad \tilde{\phi}_{24} = \tilde{\phi}_{12}^T, \\
\tilde{\phi}_{14} &= \begin{bmatrix} \tilde{\phi}_{11} & \mu_3 C^T L^T G_2^T & 0 \\ -\mu_3 K_{3,d_k}^T B^T G_1^T & \tilde{\phi}_{22} & 0 \\ 0 & 0 & 0 \end{bmatrix}, \\
\tilde{\phi}_{11} &= \mu_3 A^T G_1^T + \mu_3 K_{3,d_k}^T B^T G_1^T, \\
\tilde{\phi}_{22} &= \mu_3 A^T G_2^T - \mu_3 C^T L^T G_2^T.
\end{aligned} \tag{25}$$

Replacing the system matrices of (12) by (7), it is easy to obtain the above results according to Theorems 4 and 5. Furthermore, let $G_2 L = \bar{L}$, $G_1 B K_i = \bar{K}_i$, $i = 1, 2$, $G_1 B K_3 = \bar{K}_{3,d_k}$, and the controllers gain matrices K_i , L can be gained by solving the corresponding linear matrix inequalities.

5. Simulation Results

A numerical example of output-feedback stabilization of wireless NCS is evaluated in this section.

Consider the following discrete-time system:

$$\begin{aligned}
A &= \begin{bmatrix} 0.6852 & 0.3358 & 0.5832 \\ 0.8098 & 0.7896 & 0.4389 \\ 0.2065 & 0.6633 & 0.8528 \end{bmatrix}, \\
B &= \begin{bmatrix} 0 \\ 1 \\ 1 \end{bmatrix}, \quad C = \begin{bmatrix} 1 \\ 1 \\ 0 \end{bmatrix}^T.
\end{aligned} \tag{26}$$

The eigenvalues of A are 1.7183 and $0.3142 \pm 0.2595i$ and the system is unstable without control. Let the event rates of the packet loss and time delay be $r_1 = 0.5$ and $r_3 = 0.2$, respectively, and let the maximum delay be $d_M = 3$. Choose $\mu_1 = 1.8$, $\mu_2 = 0.5$, and $\mu_3 = 0.6$. So

$$\mu_1^{r_1} \mu_2^{r_2} \mu_3^{r_3} = 1.8^{0.5} \times 0.5^{0.3} \times 0.6^{0.2} = 0.9839 < 1. \tag{27}$$

By using Theorem 6, a suitable controller gain matrix can be obtained. The simulation result is shown in Figure 2. The above subgraph depicts the packet loss and the time delay

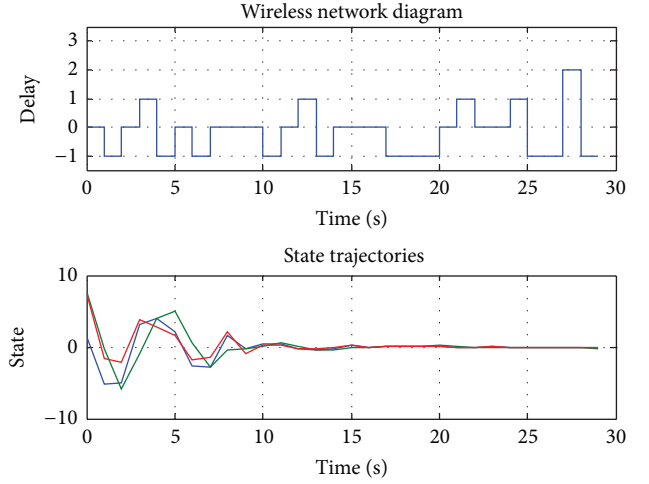


FIGURE 2: State trajectories of NCS with delay and packet loss.

of the wireless NCS in Figure 2. When the delay value is -1 , it means that this packet is lost. And the below graph is to describe the state trajectories of closed-loop wireless NCS. From Figure 2, the states of the system diverge at the case when the data packets are dropped, but they converge to zero finally. Therefore, the example illustrates the effectiveness of the proposed method.

6. Conclusions

The problem of modeling and stabilization of wireless NCS with both packet loss and time-varying delay is discussed in this paper. The output-feedback controller based on state observer is designed to stabilize the closed-loop wireless NCS by using ADS approach. And the numerical example is presented to demonstrate the effectiveness of the proposed result.

Conflict of Interests

The authors declare that there is no conflict of interests regarding the publication of this paper.

Acknowledgments

This work was supported by the National Natural Science Foundation of China under Grant nos. 61304256 and 61374083, Zhejiang Provincial Natural Science Foundation of China (LQ13F030013), Project of the Education Department of Zhejiang Province (Y201327006), and Science Foundation of Zhejiang Sci-Tech University (1202815-Y).

References

- [1] L. Zhang, Y. Shi, T. Chen, and B. Huang, "A new method for stabilization of networked control systems with random delays," *IEEE Transactions on Automatic Control*, vol. 50, no. 8, pp. 1177–1181, 2005.

- [2] K. Hu and J. Yuan, "Finite sum equality approach to H_∞ output-feedback control for switched linear discrete-time systems with time-varying delay," *IET Control Theory & Applications*, vol. 3, no. 8, pp. 1006–1016, 2009.
- [3] W. Zhang, M. S. Branicky, and S. M. Phillips, "Stability of networked control systems," *IEEE Control Systems Magazine*, vol. 21, no. 1, pp. 84–97, 2001.
- [4] W.-A. Zhang and L. Yu, "Modelling and control of networked control systems with both network-induced delay and packet-dropout," *Automatica*, vol. 44, no. 12, pp. 3206–3210, 2008.
- [5] Y. Sun and S. Qin, "Stability of networked control systems with packet dropout: an average dwell time approach," *IET Control Theory & Applications*, vol. 5, no. 1, pp. 47–53, 2011.
- [6] G. C. Walsh, "Asymptotic behavior of networked control systems," in *Proceedings of the IEEE International Conference on Control Applications (CCA '99)*, vol. 2, pp. 1448–1453, August 1999.
- [7] D. Nešić and A. R. Teel, "Input-output stability properties of networked control systems," *IEEE Transactions on Automatic Control*, vol. 49, no. 10, pp. 1650–1667, 2004.
- [8] L. A. Montestruque and P. J. Antsaklis, "On the model-based control of networked systems," *Automatica*, vol. 39, no. 10, pp. 1837–1843, 2003.
- [9] Y. Tipsuwan and M.-Y. Chow, "Control methodologies in networked control systems," *Control Engineering Practice*, vol. 11, no. 10, pp. 1099–1111, 2003.
- [10] G. C. Walsh, H. Ye, and L. G. Bushnell, "Stability analysis of networked control systems," *IEEE Transactions on Control Systems Technology*, vol. 10, no. 3, pp. 438–446, 2002.
- [11] L. Schenato and F. Fiorentin, "Average TimeSynch: a consensus-based protocol for clock synchronization in wireless sensor networks," *Automatica*, vol. 47, no. 9, pp. 1878–1886, 2011.
- [12] D. Bernardini and A. Bemporad, "Energy-aware robust model predictive control based on noisy wireless sensors," *Automatica*, vol. 48, no. 1, pp. 36–44, 2012.
- [13] H. Xu, S. Jagannathan, and F. L. Lewis, "Stochastic optimal control of unknown linear networked control system in the presence of random delays and packet losses," *Automatica*, vol. 48, no. 6, pp. 1017–1030, 2012.
- [14] J. Wang, W. X. Zheng, and T. Chen, "Identification of linear dynamic systems operating in a networked environment," *Automatica*, vol. 45, no. 12, pp. 2763–2772, 2009.
- [15] W.-A. Zhang, L. Yu, and G. Feng, "Optimal linear estimation for networked systems with communication constraints," *Automatica*, vol. 47, no. 9, pp. 1992–2000, 2011.
- [16] H. Dong, Z. Wang, and H. Gao, "Distributed H_∞ filtering for a class of markovian jump nonlinear time-delay system over lossy sensor networks," *IEEE Transactions on Industrial Electronics*, vol. 60, no. 10, pp. 4665–4672, 2013.
- [17] X. Xie, S. Yin, H. Gao, and O. Kaynak, "Asymptotic stability and stabilisation of uncertain delta operator systems with time-varying delays," *IET Control Theory & Applications*, vol. 7, no. 8, pp. 1071–1078, 2013.

Research Article

Phoenix: A Collaborative Location-Based Notification System for Mobile Networks

Yongping Xiong,¹ Yubo Deng,² Wendong Wang,¹ and Jian Ma¹

¹ State Key Lab. of Networking and Switching Tech., Beijing University of Posts and Telecom., Beijing 100876, China

² Institute of Sensing Technology and Business, Beijing University of Posts and Telecom., Beijing 100876, China

Correspondence should be addressed to Yongping Xiong; ypxiong@bupt.edu.cn

Received 28 November 2013; Revised 29 January 2014; Accepted 18 February 2014; Published 24 March 2014

Academic Editor: Yang Shi

Copyright © 2014 Yongping Xiong et al. This is an open access article distributed under the Creative Commons Attribution License, which permits unrestricted use, distribution, and reproduction in any medium, provided the original work is properly cited.

Location-based notification (LBN) aims to alert the users in a target area to their interested information. With a wide range of applications, LBN has been gaining more and more attraction among wireless users and service providers. The mainstream centralized solution based on cellular networks may incur high service cost. In this paper, we present an innovative scheme called Phoenix, which does not rely on any infrastructure, to implement location-based notification service. In our design, devices (users) across the target area form a dynamic peer-to-peer network, where a user can be a message source, a message carrier, or a message subscriber. When a user meets the message carrier, he will get a copy of the message. Phoenix keeps messages of interest being circulated in the target area; hence users are being notified. To achieve desired notification performance, Phoenix adaptively controls when a user should take the carrier role and help disseminating a message in order to keep the message “alive,” given the fact that message carriers may leave the target area and drop the message. Extensive simulations have been conducted to show the efficacy of Phoenix notification system.

1. Introduction

In recent years, we have seen rapid growth in the area of location-based services (LBS). Different from LBS based on pull model requiring users to send request to a server, location-based notification (LBN) [1], say LBS based push model, actively alerts users with their interested information when they are in a specific geographical area. This model facilitates retrieving information for mobile users and brings a better user experience. It has been gaining more and more attraction among wireless users and service providers.

LBN has a wide range of applications in automatic parking places searching, traffic jam warning, electronic advertising, and so on. A typical scenario is proximity-based electronic advertisement which is shown in Figure 1, where a shopping mall (or the source) is publishing messages about the time-limited sales promotion and desires to notify all the potential clients in the certain proximity (e.g., 1 km) of the store before the sales activity ends.

The mainstream LBN solution relies on the infrastructure networks (such as cellular networks). In the solution,

the position of a user determined by his mobile device with the GPS module or by the mobile network infrastructure is published continuously to a central tracking server. Then the servers push the matched information to the user according to his registered interests when they enter the specific destination area. However, the centralized solution has a significant limitation; say the service cost is expensive because users' positions need to be published continuously to the server which consumes large amounts of bandwidth. Meanwhile, the available bandwidth per user in a crowded area would be severely limited [2] for cellular technology like UMTS. Thus, the solution in an ad hoc manner may avoid the above drawback and act as a beneficial supplement of the centralized solution to provide LBN services.

In this paper, we develop a system called *Phoenix* to provide the location-based notification service to push information to subscribers. In Phoenix, mobile users across the target area form a mobile peer-to-peer network, where a user may take three possible roles for each message: *source*, *carrier*, and *subscriber*. The source generates the original notification messages with the propagation parameters such

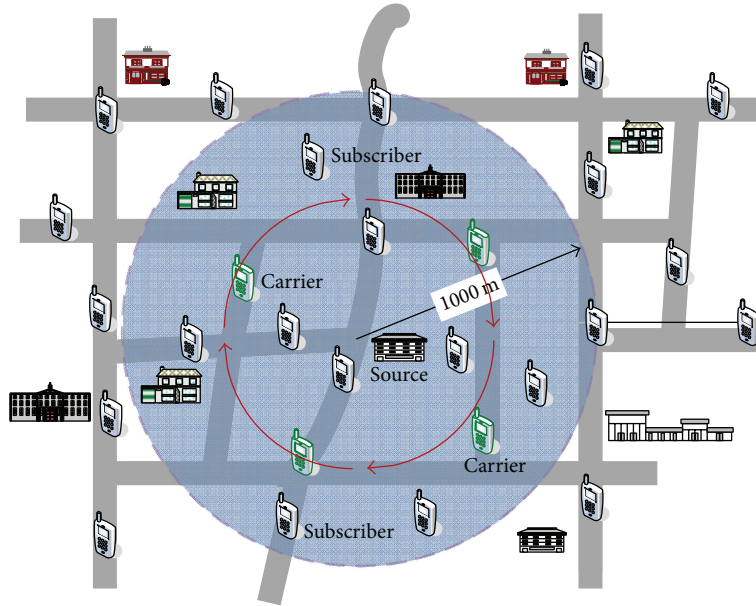


FIGURE 1: Location-based electronic ad application.

as destination propagation region. It initializes the message dissemination procedure by sending it to those who move into the communication range of the source. Those receivers willing to carry and disseminate the message replicas are called carriers. With the movement of message carriers through the area, the message replicas are transmitted to the encountered users according to certain rules, which produce new carriers. When leaving the specified target area, carriers delete the corresponding messages and stop taking the carrier role for those. Based on the above procedure, Phoenix keeps the messages “immortal” over the target area through the peer-to-peer opportunistic message swapping. The users interested in a message are subscribers which specify their interests in the local devices. When a subscriber meets any of the message carriers, it downloads the interested message from the carrier. The source and subscriber roles are predetermined, and carrier role is determined dynamically by Phoenix.

A critical performance metric of a location-based notification service is *notification ratio* which denotes the percentage of subscribers who receive the messages when passing through the area. Additionally, due to the constrained resources in mobile devices, *message overhead* is another important design concern. In this paper, the design goal of Phoenix is to satisfy the user-specified notification ratio while minimizing the transmission overhead of the system. To achieve this goal, we derive the analytic expression of notification ratio of Phoenix and observe that the notification ratio relies on two parameters: the percentage of carriers and the number of mobile users in the destination zone. Then we propose an adaptive message propagation scheme which computes periodically the desired percentage of carriers according to the estimated number of mobile users in the area and then adjusts the message propagation procedure to achieve that percentage.

In this paper, we carried out simulations with the mobility model capturing the realistic characteristics of human mobility and real-world city map to evaluate the system performance. The results show that Phoenix achieves the desired notification ratio with the low message overhead. Moreover, Phoenix is robust to tolerate a nontrivial percentage (20%) of selfish users in the network.

The main advantages of Phoenix include the following: (1) the service cost is very low because the users collaborate to implement the location-based notification and it does not rely on any infrastructure; (2) it is flexible because the notification system is tunable to achieve the tradeoff between the user-specified notification ratio and system overhead.

The rest of this paper is organized as follows. Section 2 reviews the related work. Section 3 describes the system architecture of Phoenix. Section 4 presents the design of the core component in Phoenix. Section 5 discusses the design considerations of Phoenix. Section 6 presents the evaluation results and Section 7 concludes the paper.

2. Related Work

There are plenty of works related to location-based system in the mobile networks. Thus, only the most relevant works are discussed due to the space limit in this paper.

2.1. Location Dependent Data Service in Mobile Networks. A lot of researchers study the location-based services in mobile networks. Chen et al. [3] proposed a method to provide information relevant to location and users subscription using a centralized architecture which works in cellular networks. The centralized solution is far from our work. STEAM [4], LPS [5], and L-ToPSS [6] are the location-based publish/subscribe systems in wireless ad hoc network.

These systems deliver messages only to the interested users which are inside a destination region exactly at publishing time. Autonomous gossiping [7] spreads messages selectively based on vulnerability of nodes instead of flooding the network. By specifying the nodes' profile, it can be used to provide location-based services. Leontiadis and Mascolo [8] presented an opportunistic spatiotemporal dissemination system for vehicular networks. It generates the message replicas dynamically according to the collected subscriptions. However, all of these efforts fail to consider keeping the message circulated in the destination region to notify all interested users across the area.

To the best of our knowledge, the most related work is [9] in terms of maintaining a message over a geographical area to notify the interested users. In order to implement the persistent dissemination, it employs three methods including fixed infostation, ad hoc dissemination, and opportunistic dissemination. However, it did not consider satisfying the expected notification performance.

2.2. Location Aware Routing/Casting in Ad Hoc Networks. This type of research tries to deliver the message to those destination nodes identified/limited by their location in the ad hoc networks. Geocast is the earliest concept to deliver the message to the set of nodes within the specified geographical area in the mobile ad hoc networks (MANET). As a more relevant work, Abiding Geocast [10] aims to deliver time-stable message in a geographical area. It employs periodic epidemic spreading to disseminate the message to a group of users in an area. Comparing with Phoenix, its overhead of route establishment and maintenance caused by the continuous changes in network topology is very expensive. Several researches [11–13] aim to deliver messages to multiple target users in the specific area. Their basic idea is to utilize the variant of constrained epidemic protocols to constrain the propagation of a message within the given area specified by the source. By contrast, researchers [14–16] define the notion of “relevance” to enable the routing layer to self-identify the geographical areas in which the messages should be delivered. In contrast to these works, Phoenix offers much richer semantics in which publishers and subscribers are decoupled as the former define the notification area while the latter express their interests.

3. System Architecture

The proposed system architecture of Phoenix is shown in Figure 2, which consists of four components described as follows.

Application Interface. Application interface provides application developers with two classes of uniform interfaces. Users may exploit *subscribe/unsubscribe* primitive to register/unregister their interested information. All interests are stored in the local repository and not required to pass to other users or central servers. Besides, source users may use *notify* primitive to publish messages. The operation takes four parameters as follows. *MsgArea* is the destination

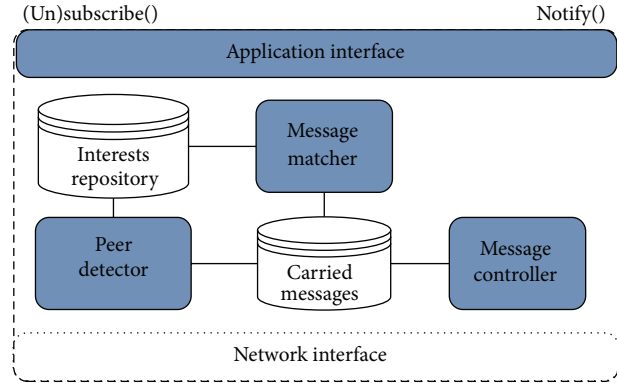


FIGURE 2: The architecture of Phoenix.

geographical area that a message should reach. Typically, the circular destination area in the aforementioned e-ad example may be denoted as a triple $\langle x, y, r \rangle$ where (x, y) and r are, respectively, the coordinate of the circle center and the radius of the circle. Note that the area may be independent of the current position of the message source. $MsgNR \in (0, 1]$ is the desired notification ratio of the message. This makes Phoenix flexible to support the multiple applications with different notification service requirements. A message is deleted from the current carrier when it lives longer than *MsgDuration*. Here, the absolute time is unnecessary to avoid the strict time synchronization. *MsgBody* means the message content being propagated.

Peer Detector. Peer detector is responsible for discovering neighboring users in the mutual radio range and executing the handshaking process. After identifying the new neighbor peer by receiving the periodic beacon message, it exchanges further the control information including the list of local interests and the IDs of all carried messages. The information is used by the following message matcher and message controller.

Message Matcher. Message matcher controls which messages should be filtered out and which messages should be transmitted to the encountered users according to their interests. In Phoenix, the content of a message (*MsgBody*) is expressed as a collection of attribute values. For example, a sales message may be represented as $\langle \text{type} = \text{"sales push"}, \text{brand} = \text{"NIKE"}, \text{discount} = \text{"20\%"}, \text{location} = \text{"X Market"}, \text{data} = \text{description of the shoes} \rangle$. The data item can be text or multimedia such as pictures and videos. The interest is expressed as a combination of these attributes pattern, for example, $\langle \text{type} = \text{"..."}, \text{brand} = \text{"..."} \rangle$. When a carried message has the corresponding attribute conditions stated in an interest, a match occurs and the message is transmitted to the peer.

Message Controller. Message controller manages the message propagation to adjust the system performance. Individual message carriers decide whether a carried message should be deleted or copied to the encountered peer which does not hold the corresponding replica. If the message is epidemically

sent to all encountered users, the system achieves the highest notification ratio. However, such system suffers from the high message overhead and the waste of resources and vice versa. Considering its key impact on the system performance, we focus on the design of message controller, in which two main design issues of message controller include the following.

- (i) How to satisfy the notification performance requirements specified by the message?
- (ii) How can we control the message overhead to improve the scalability?

Bearing the design issues in mind, we propose the algorithm of the Message Controller detailed in the next section.

4. Design of Message Controller

In this section, we firstly model the notification ratio and analyze several main impact parameters, then develop an adaptive message propagation algorithm to achieve the design goal.

4.1. Notification Ratio. As stated in Section 3, a subscriber will be notified successfully if it encounters any message carrier. Thus, the notification ratio P is the probability of meeting at least one carrier when a subscriber moves through the target area. Supposing that the message carriers are always distributed uniformly in the zone, the probability that an encountered user is a carrier at a time equals the percentage of carriers to all users in the area. Then the notification ratio is computed as

$$P = 1 - (1 - \rho)^{\beta \times n \times t_s}, \quad (1)$$

where ρ is the percentage of carriers (carrier percentage for short), n is the number of mobile users in the area, t_s is the average time spent staying in the area, and β is the pairwise meeting rate (meeting times in a time unit) between two users. It is shown [17] to follow nearly an exponential distribution under common mobility models (such as the random waypoint or random direction). Also, β can be estimated approximately as follows:

$$\beta = \frac{2wdE[V^*]}{A}, \quad (2)$$

where w is a constant specific to the mobility model (the details can be referred to [17]), d is the transmission range, $E[V^*]$ is the average relative speed between two users, and A is the area of the target region.

4.1.1. Correlation between n and ρ . For most realistic applications, it is reasonable to assume that users' moving speed and transmission range keep constant, while they stay in the area. Thus, we focus on exploring the other two main parameters affecting notification ratio: number of users in the area n and carrier percentage ρ .

n is time varying and not controllable because users autonomously enter and exit the target area continuously.

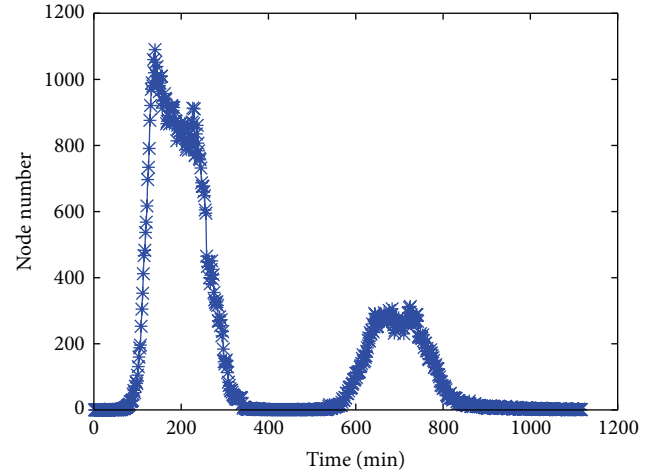


FIGURE 3: Variation of the number of mobile users in a realistic area.

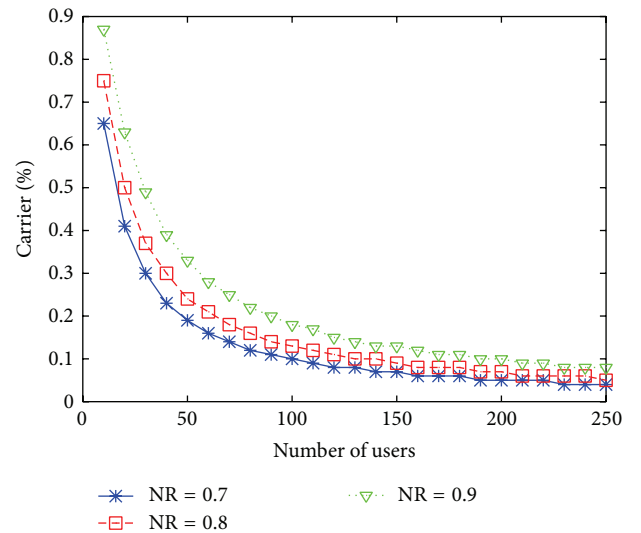


FIGURE 4: Number of users versus carrier percentage.

However, the statistics of a realistic mobility traces exhibit interesting characteristic that n keeps roughly stable during the peak traffic time. These traces are obtained from a multiagent microscopic traffic simulator (MMTS) which is capable of simulating public and private traffic over real regional road maps of Switzerland with a high level of realism [18]. Figure 3 shows the number of mobile users in around 18 hours of a day in a 3000 m \times 3000 m central region of the Zurich city. During around 3 hours in two peak hours, the number of users varies in a small range (800–1000 users and 220–300 users for the morning and evening peak time, resp.).

We study the correlation between n and ρ under the given notification ratio in a typical scenario, where users with transmission range of 50 m move at the speed of 1 m/s in the circular area with 1 km radius. The parameter w for random waypoint is set to 1.37 according to [17]. Figure 4 depicts their correlation when the desired notification ratios are 0.7, 0.8, and 0.9, respectively. It can be seen that ρ is less sensitive to n

as n increases and exceeds a certain value. For example, ρ may be around 0.13 for the notification ratio of 0.9 when n varies from 150 to 200. From the view point of applications, LBN service is meaningful and commercially feasible only when there are enough users in the destination region. It means that rough estimation of n is enough to determine the value of ρ in order to achieve the desired notification ratio.

4.2. Adaptive Message Propagation Algorithm. The basic idea of our message propagation algorithm is to adjust the carrier percentage according to current number of users in the area to achieve the desired notification ratio. Specifically, the adaptive algorithm takes the following three steps. (1) Estimate continually the number of mobile users in the target area. We assume that the communication range and moving speed of all nodes keep roughly constant. When a user receives a message and becomes its carrier, it uses the target area indicated in the message to compute the pairwise meeting rate β according to (2). Each user keeps a variable x to record the number of the encountered users in a time unit. We have $x = \beta \times n$ according to the definition of β in Section 4.1, so n can be figured out directly. (2) Compute the carrier percentage ρ corresponding to the specified notification ratio (*MsgNR*) in a message according to (1). (3) Adjust the message propagation procedure and drive the system to reach a steady state with the calculated ρ for a message to achieve the desired notification ratio. We introduce a key algorithm parameter \mathcal{M} to control the message propagation procedure, which will be elaborated in the following.

Achieving the desired carrier percentage ρ in a dynamic peer-to-peer network is not trivial. Suppose that the carrier percentage equals ρ at current moment; it will fall down since new users enter and existing carriers leave the area from time to time. In order to keep dynamically the desired ρ , we propose a message propagation procedure which produces new message carriers at the same rate as the leaving rate of existing carriers. Without loss of generality, suppose that current carrier is denoted as i . It runs procedure (see Algorithm 1) while meeting user j , where \mathcal{D} represents the set of the messages carried by i in line 1. When leaving the destination region, the corresponding messages are deleted from the carrier in lines 2–5. In lines 6–15, i keeps a variable C_m for a carried message m , which denotes the number of consecutive noncarriers for message m of i met. When carrier i meets \mathcal{M} noncarrier users consecutively, the carrier generates a message replica for the \mathcal{M} th users and assign it as a new carrier.

\mathcal{M} controls the carrier generation rate. The larger its value is, the more slowly the message carrier is generated. When \mathcal{M} is set to 1, the algorithm produces the message copies at the maximum rate, which is equivalent to the epidemic spreading. Therefore, the key issue is transformed to select the appropriate \mathcal{M} to achieve the desired ρ .

4.3. Parameter Selecting. Next, we will derive the value of \mathcal{M} . Let us assume that the target area of message m is a circular area with the radius r , so its area $A = \pi r^2$. n users reside in

Require: receive the carried message identifiers from j

```

(1) for all  $m \in \mathcal{D}$  do
(2)   if  $i$  leave the target area of  $m$  then
(3)      $\mathcal{D} \leftarrow \mathcal{D} - m$ 
(4)   else if  $j$  carries  $m$  then
(5)      $C_m \leftarrow 0$ 
(6)   else
(7)     if  $C_m = \mathcal{M} - 1$  then
(8)       Generating and transferring a new copy of
          $m$  to  $j$  and making  $j$  a carrier
(9)        $C_m \leftarrow 0$ 
(10)    else
(11)       $C_m \leftarrow C_m + 1$ 
(12)    end if
(13)  end if
(14) end for

```

ALGORITHM 1: Message propagation procedure.

TABLE 1: Summary of major notations.

r	Radius of target area
A	Area of target area
n	Number of users in the target area
v	Average moving speed
C_m	Variable maintained for message m
d	Transmission range
w	Mobility model parameter
β	Pairwise meeting rate
θ	Movement direction angle to leave the area
ρ	Desired carrier percentage
λ	Rate of users leaving target area
r_p	Rate of producing message copies
r_d	Rate of carrier leaving target area
P_s	Expected notification ratio

the area and move according to an (*iid*) model at the average speed v . These assumptions are used to derive the theoretical results, but our solution does not rely on them, which will be verified in the evaluation results. Nodal transmission range is denoted by d . The symbols and notations used in the model are summarized in Table 1.

4.3.1. Carrier Leaving Rate. We first compute the rate at which users leave the target area. As shown in Figure 5, the users which will leave probably the area at the next moment must be those located in the shaded annular area defined by a radius $r - v$ and a radius r at the current moment. Any user u located in the shaded area at the current moment will leave the target area at the next moment only if it chooses the movement

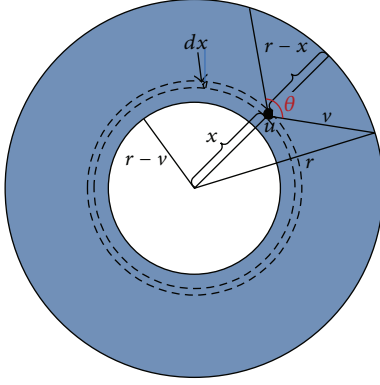


FIGURE 5: The calculation of users leaving rate.

direction within the angle θ . Under uniform mobility model, users' leaving rate is calculated by

$$\begin{aligned} \lambda &= \int_{r-v}^r \frac{n}{A} 2\pi x dx \frac{\theta}{2\pi} \\ &= \frac{2n}{A} \int_{r-v}^r \left(\pi - a \cos \left(\frac{v^2 + x^2 - r^2}{2vx} \right) \right) x dx. \end{aligned} \quad (3)$$

A portion of users in the area are carriers, so the carrier leaving rate is calculated by

$$r_d = \lambda \rho = \frac{2n\rho}{A} \int_{r-v}^r \left(\pi - a \cos \left(\frac{v^2 + x^2 - r^2}{2vx} \right) \right) x dx. \quad (4)$$

4.3.2. Carrier Generating Rate. We use variable C_m to track the number of consecutive noncarriers the carrier has met. Upon meeting \mathcal{M} consecutive noncarriers, the carrier generates a message replica and then resets C_m to 0. Thus, the variable can take any value from 0 to $\mathcal{M} - 1$. It can be represented in a Markov process illustrated in Figure 6. For any contact at steady state, the probability of meeting a noncarrier and increasing C_m is $1 - \rho$. The probability of meeting a carrier and resetting C_m is ρ .

Thus, the transit probability matrix of the Markov process is represented by

$$\mathbf{P} = \begin{pmatrix} \rho & 1-\rho & 0 & \dots & 0 \\ \rho & 0 & 1-\rho & \dots & 0 \\ \rho & 0 & 0 & 1-\rho & \dots \\ \vdots & \vdots & \vdots & \ddots & \vdots \\ 1 & 0 & 0 & \dots & 0 \end{pmatrix}. \quad (5)$$

The matrix is ergodic and has a steady distribution $\alpha = \alpha P$. Thus, α is an eigenvector of P with eigenvalue of exactly 1. Here we are interested in the probability of residing the $\mathcal{M} - 1$ state, which equals

$$\alpha_{\mathcal{M}-1} = \frac{\rho(1-\rho)^{\mathcal{M}-1}}{1 - (1-\rho)^{\mathcal{M}}}. \quad (6)$$

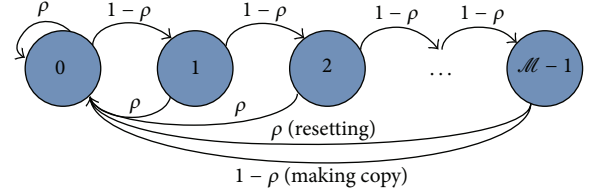


FIGURE 6: Markov process for message production.

Therefore, the expected rate at which the message carriers are generated is

$$r_p = (\rho n) n\beta (1-\rho) \alpha_{\mathcal{M}-1}, \quad (7)$$

where β is the pairwise meeting rate.

4.3.3. Computation of \mathcal{M} . Let the carrier generating rate equal the carrier leaving rate; say $r_p = r_d$ and then substitute (6); we obtain the close-form solution of \mathcal{M} :

$$\begin{aligned} &(\rho n) n\beta (1-\rho) \alpha_{\mathcal{M}-1} \\ &= \frac{2n\rho}{A} \int_{r-v}^r \left(\pi - a \cos \left(\frac{v^2 + x^2 - r^2}{2vx} \right) \right) x dx \implies \mathcal{M} \\ &= -\log_{1-\rho} \\ &\quad \times \left(1 + \rho \frac{nA\beta}{2 \int_{r-v}^r (\pi - a \cos((v^2 + x^2 - r^2)/2vx)) x dx} \right). \end{aligned} \quad (8)$$

We carry out a simulation to evaluate the accuracy of this model. In the designed scenario with the same network parameters in the Section 4, all users' mobility follows random waypoint model. We firstly compute the \mathcal{M} corresponding to the desired ρ according to (8). Then we run a simulation program to measure the realistic carrier percentage when parameter \mathcal{M} varies. As shown in Figure 7, the closeness between the theoretical and measured results verifies the accuracy of the model. Besides, it shows further that smaller \mathcal{M} should be set to achieve the higher carrier percentage.

4.4. Message Overhead Analysis. Message overhead is caused mainly by exchanging the information messages (messages for short) and control messages including the interest list and the carried message list. In most applications, the size of control messages is much smaller than the information messages, so the overhead analysis focuses on the latter, that is, the overhead caused by maintaining the desired carrier percentage. According to our algorithm, the message replica should be generated continuously to make new carriers in order to achieve the expected notification performance. Specifically, each carrier produces and transmits a message replica only when it meets \mathcal{M} noncarrier users consecutively. Thus, the transmission overhead in a time unit equals $(\rho n) n\beta (1-\rho) \alpha_{\mathcal{M}-1} \times s_m$ where s_m is the size of the information message.

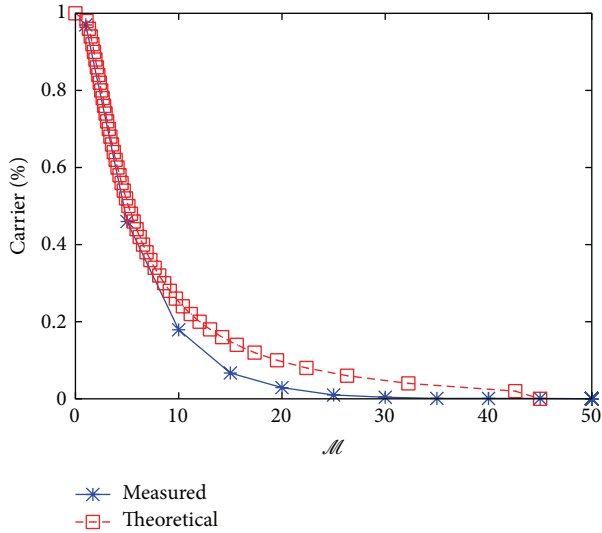


FIGURE 7: Comparison between theoretical and measured results.

5. Discussions

5.1. System Feasibility. The theoretical analysis of our paper assumes that all users are willing to be message carriers. In reality, users may be selfish or not collaborative. The following strategies will make our system feasible in real applications. First, we use an incentive scheme based on economic model or game theory [19, 20]. Let us take the electronic ads as an example. An available business solution is to let the mall advertisers add a certain amount of money-saving e-coupon messages to the normal ads messages in order to attract volunteer users. Second, the service is almost free of charge except the low battery and storage resources consumption which are verified in the following evaluation. Third, the feasibility is further improved due to its robustness to tolerate a percentage of selfish users, which will be illustrated in the next section.

5.2. Distributed Design. In our design, the message notification system does not rely on the centralized server to exchange information. All users are autonomous and able to control their own data and mobility. The proposed self-controlled and adaptive approach to determine the carriers makes the system flexible and scalable. However, the performance of the fully distributed system degrades probably at several extreme situations, for example, if the number of users in the target area is so small that existing carriers have no opportunities to send a message replica to the encountered users before they leave the area. The message probably disappears in the area and the future entering subscribers fail to be notified. Thus, in the real applications, the user may place at least a fixed message source in the target area in order to guarantee the performance when the number of users is too small.

5.3. Optimization. In current solution, subscribers receive the message of interest only from the encountered carriers.

The performance can be further optimized if subscribers that have received the message are permitted to act as additional *carriers* for the message in the circulation. In addition, when a carrier is transmitting a message replica to another user and assign it as a new carrier, other users in the transmission range can receive the message and store it locally. The two types of users do not need to behave like the real carriers to exchange information to keep the dynamic percentage. In contrast, they play a role of the moving message cache to help in delivering messages to the encountered subscribers, which improve the notification performance. If no subscriber is encountered, the optimization methods do not cause additional network overhead.

6. Performance Evaluation

In this section, we evaluate the performance of Phoenix through simulation in the realistic city map as well as the power-law mobility model. We first study the spatial distribution of the carrier users and carrier percentage distribution, and then we explore the impact of users' number on notification performance. Finally, we also examine the effect of selfish users on system performance.

6.1. Simulation Setup. We implemented Phoenix in the opportunistic network environment (ONE) [21] simulator. To simulate the realistic scenarios, we need large scale data. However, the large scale realistic mobility trace based on absolute position is not available. To the best of our knowledge, the publicly available large scale human trace is the Dartmouth College trace collected through the Wi-Fi access points covering the entire campus. It includes the mobility traces of 6300 users for a long period. However, the movement of all users is only limited on the campus and the position of each user is fairly coarse because the trace of each user is represented by a series of the location of access points associated with the user. Besides, an access point covers several hundred meters distance and users are not always connected to the closest access point. Thus, the trace is not suitable to study the performance of location-based notification systems. In the evaluation, we make use of a realistic city map in which the users move along roads and walkways. Meanwhile, their movement follows a power-law mobility model which is elaborated below.

The realistic city area that we selected is 8500 m \times 7500 m Helsinki city's central area which is illustrated in Figure 8. Two hundred points of interests (POIs) are deployed randomly on the map to model popular locations, for example, shops, restaurants, and tourist attractions. We use the similar algorithm proposed in the literature [22] to generate the mobility trace. The experiment results from [22] have shown that the generated mobility trace contains those similar statistical features including the truncated power-law flights, pause time, and intercontact time, which are observed in the real gathered human mobility trace over various scales of time and space.

In this mobility model, each user is deployed randomly at a POI. For a user located at the current POI i ,

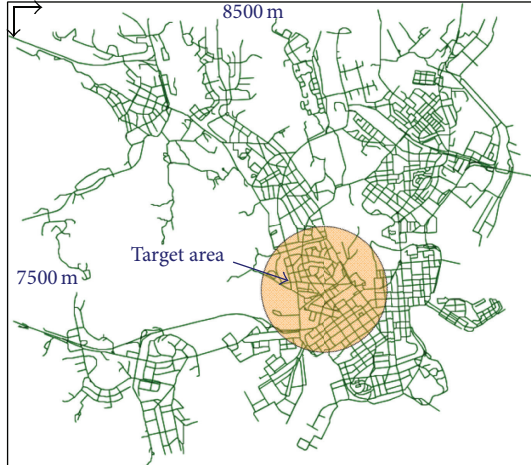


FIGURE 8: The target area on the Helsinki city's central area.

the probability that a next POI j is chosen is computed as $(1/d_{ij}^\phi)/(\sum_{k \in V-V'} 1/d_{ik}^\phi)$ where d_{ij} is the Euclidean distance from i to j , ϕ is a fixed constant within 0 to infinity, and V and V' are, respectively, the set of all the POIs and visited POIs so far. Based on this probability, the next POI is chosen from unvisited POIs. Specifically, if ϕ is infinite, a user always chooses the nearest unvisited POI and if it is zero, a user randomly chooses the destination point. Then the user calculates the shortest path to the next POI using Dijkstra's algorithm and moves to the destination following the calculated path. Then we use a truncated power-law pause time distribution with parameter φ to decide the amount time to stay at each POI. The selected target area is located in the downtown area of Helsinki with a radius of 1 km, as shown in Figure 8. The message source is fixed in the center point of the area with coordinates (5200, 5000). The source generates 10 kinds of information messages to notify the interested users passing through the area. There are different proportions of users subscribing to these information messages. The information message packet size is 1024 bytes and has the same lower bound of notification ratio 80%. The simulation lasts for 5 hours (18000 seconds), and results are averaged over the achieved notification performance of all messages. Unless otherwise stated, we use the default simulation parameters listed in Table 2.

6.2. Spatial Distribution of Carriers. The design of Phoenix relies on the premise that the probability of a user encountering a message carrier is equal to the global carrier percentage. Its validity depends on whether the carrier users distribute uniformly throughout the network. Thus, we firstly explore whether the condition is met under the power-law mobility model. Figure 9 illustrates the spatial distribution of carrier users in the target area through the entire simulation. The red users are carrier users; the gray users are noncarriers. As expected, the message carriers are nearly uniformly distributed throughout the target area for the most of the simulation duration.

TABLE 2: Default simulation parameters.

Parameter	Value
Size of network area	$8500 \times 7500 \text{ m}^2$
Radius of target area	1000 m
Number of POIs	200
Transmission range	150 m
Total number of users	1000
Control message size	80 bytes
Information message size	1024 bytes
Average nodal speed	1 m/s
Lower bound of notification ratio	80%
Parameter ϕ	1.5
Power exponent for pause time φ	1

6.3. Time Stability of Carrier Percentage. After the system reaches the steady state, we need to maintain the carrier percentage around an expected level in order to achieve the desired notification performance. Figure 10 depicts the variation of carrier percentage with time in the scenario with different number of users when $\mathcal{M} = 2$ and $\mathcal{M} = 5$, respectively.

It can be observed that the carrier percentage keep nearly stable after a short initialization phase. As expected, different carrier percentage levels are achieved for the different \mathcal{M} . Besides, the higher the number of users is, the more stable the kept carrier percentage is. It is because the number of users residing in the target area is little and considerably fluctuates in the low density scenario. Thus, the generating and leaving of carriers result in the drastic change of carrier percentage.

6.4. The Achieved Notification Ratio and Message Overhead. We also compare the notification performance in terms of achieved notification ratio and message overhead between Phoenix and Epidemic which is a simple version of our algorithm where $\mathcal{M} = 1$ all the time. The expected lower bound of notification ratio is set to 80%. The number of mobile users in the scenario varies from 500 to 2500 at a step of 250, and our adaptive message propagation algorithm recomputes the desired carrier percentage according to (1) and then adjusts the parameter \mathcal{M} . We measure the realistic notification ratios for each user density. Besides, we also use the total number of the messages transmitted to keep the desired carrier percentage by all carriers as the message overhead.

Figure 11(a) compares the achieved notification ratio between Phoenix and Epidemic. When the number of users is less than 1000, they have the same performance because our adaptive algorithm chooses $\mathcal{M} = 1$ for low density users. In this cast, they cannot satisfy the expected lower bound 80% of the notification ratio. It is because notification ratio relies on both carrier percentage and other factors such as user number and transmission range. In the highly sparse network, subscribers can probably not be notified because of failing to meet any message carrier although the carrier percentage is 100%. Therefore, the enough user density is necessary to ensure the desired performance. When

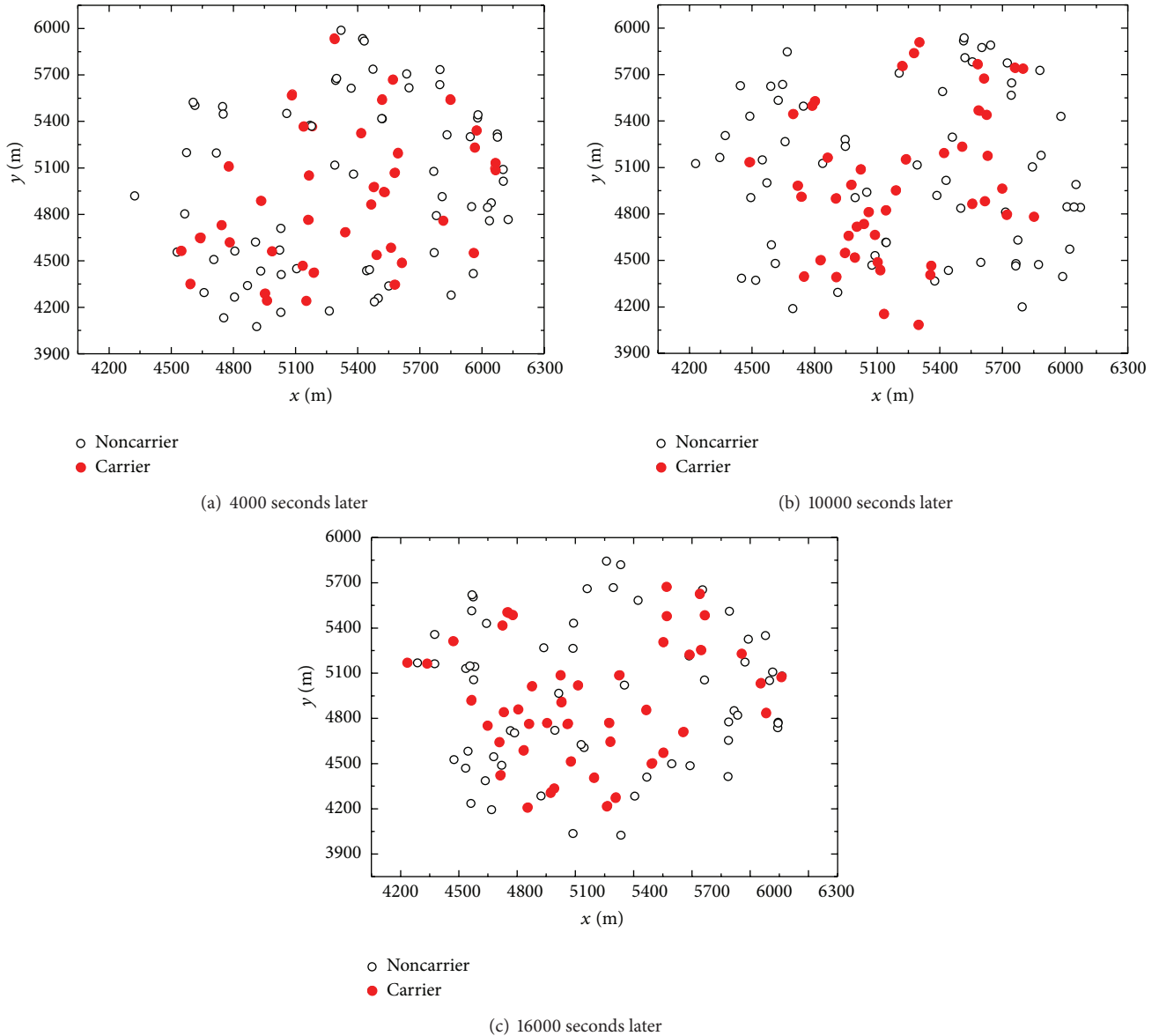


FIGURE 9: Spatial distribution of message carriers.

there are over 1000 users in the area, Phoenix achieves the better agreement with the desired performance requirement than Epidemic because of its adaptive message propagation scheme.

As demonstrated in Figure 11(b), our algorithm brings much lower message overhead than Epidemic scheme. Moreover, the more the number of users is, the better our algorithm performs. It can be explained below. In our algorithm, the rate of message generation is adjusted adaptively to the optimal level by observing the variation of the user density in the area, which means more stable transmission overhead and better scalability. In contrast, Epidemic makes a message replica for each encountered user, resulting in that the message overhead increases rapidly as the user density rises. When the number of mobile users in the area becomes large enough, Epidemic might even fail to work because of the transmission collision.

6.5. Against Selfish Users. We evaluate the robustness of the system against selfish users, which only receive the messages and refuse to spread the received messages. The proportion of selfish users varies from 10% to 50% in two scenarios with 1000 and 2000 users, respectively. We record the achieved notification ratios of 10 runs with different random seeds.

As shown in Figure 12, it is observed that the achieved notification ratio falls with the increase of the selfish users. When the proportion of selfish users is smaller than 20%, it hardly has the obvious effect on the success ratio, it hardly place the obvious impact on the success ratio which always stay around the expected 80%. However, the notification performance decreases significantly when the selfish user proportion reaches 40% and basically fails to satisfy the desired performance. It is because the number of the encountered users by the subscribers passing through the target

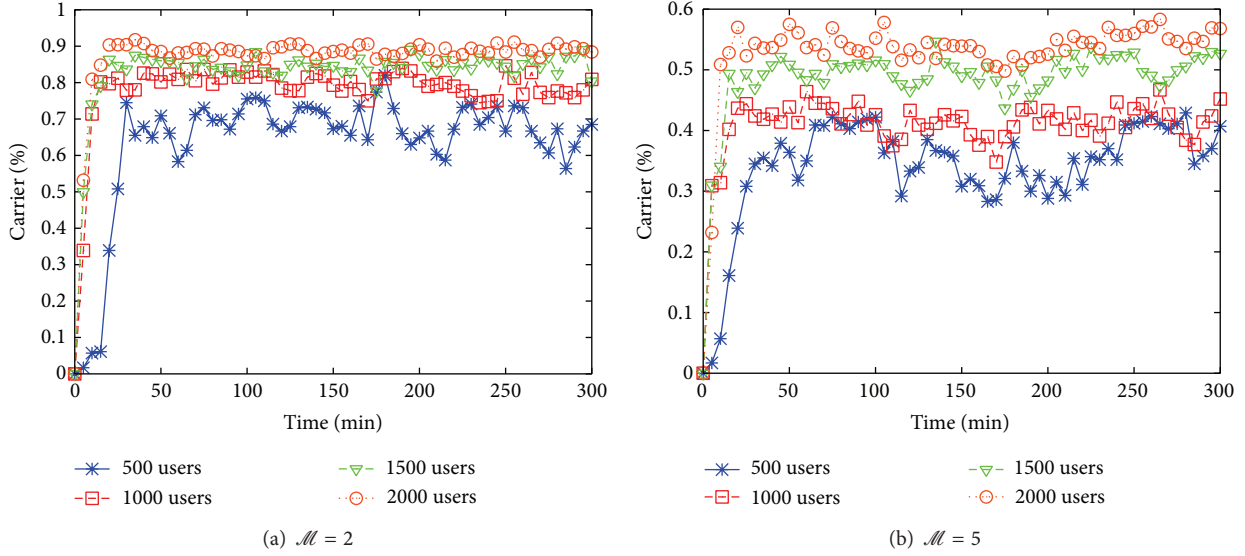


FIGURE 10: Variation of carrier percentage for the desired notification ratio 80%.

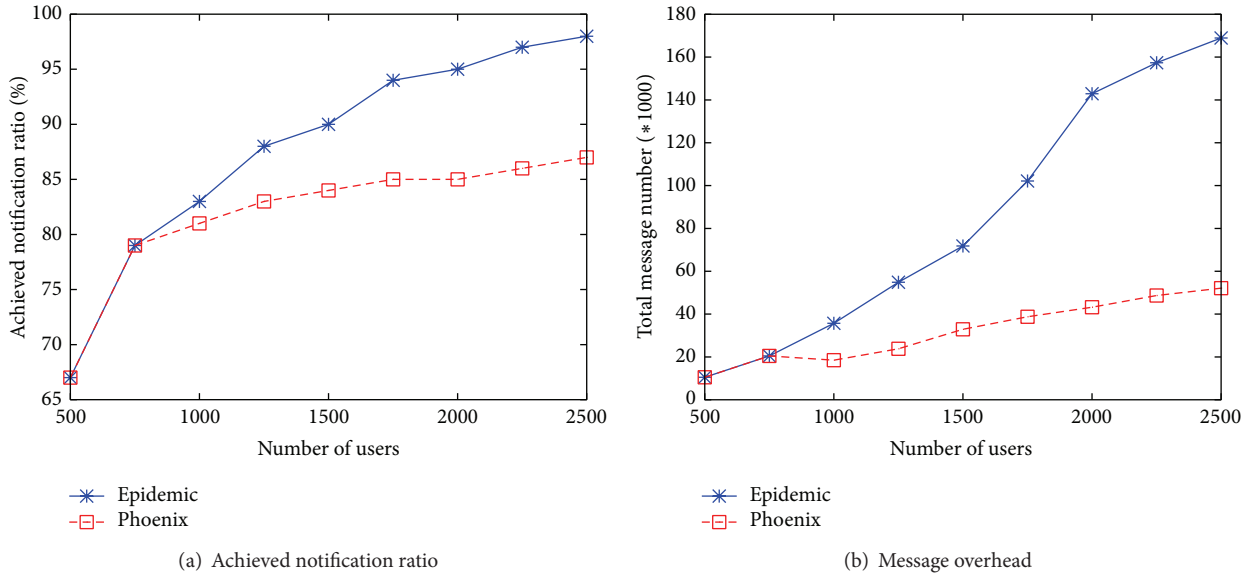


FIGURE 11: Phoenix versus Epidemic.

area is approximately constant in a given network. The more the selfish users are, the lower the probability of meeting a carrier for a subscriber accordingly is. The results illustrate that Phoenix is robust to the certain proportion of selfish users.

7. Conclusion

In this paper, we design a peer-to-peer location-based notification system, Phoenix. We focus on the design of the key component message controller. Message controller aims to satisfy the expected lower bound of notification ratio

while minimizing the transmission overhead. For this target, we firstly model the notification ratio and then propose an adaptive algorithm which adjusts the message propagation procedure to achieve the desired notification performance by observing the number of mobile users in the destination region. We also discuss some other design problems such as the system feasibility, distributed design, and performance optimization. Finally, we evaluate the system performance in the simulation with a realistic city map and power-law movement model. The results show that Phoenix can satisfy the user-specified notification performance with the low transmission overhead. Moreover, Phoenix is robust to the certain proportion of selfish users in the network.

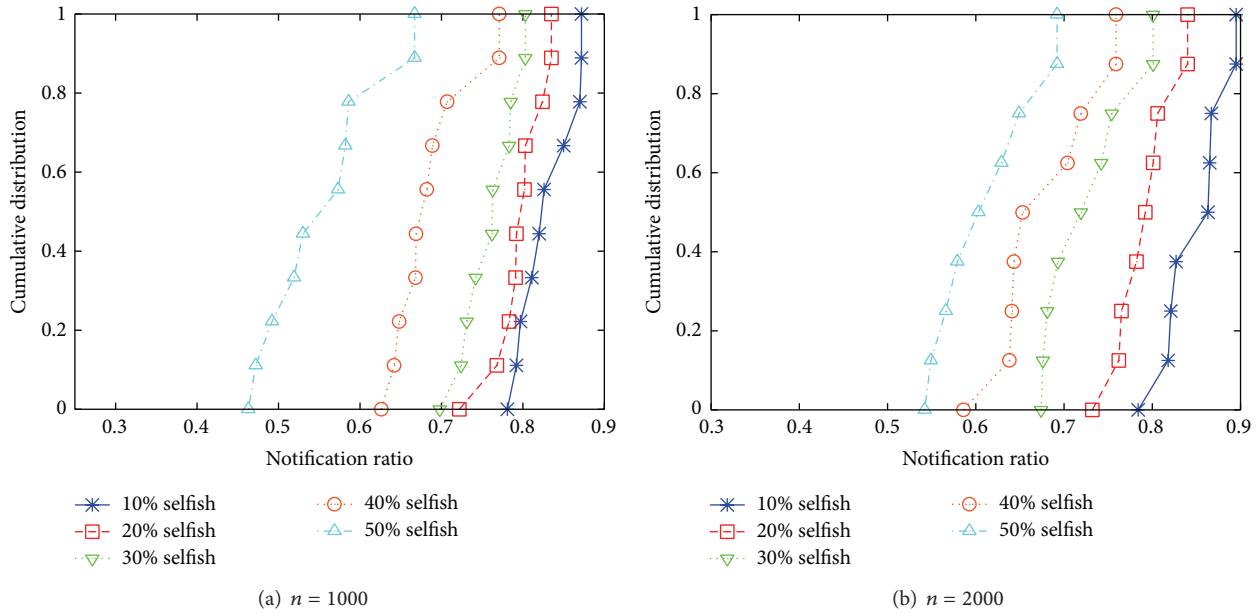


FIGURE 12: Impact of selfish users when the user specified is 80%.

Conflict of Interests

The authors declare that there is no conflict of interests regarding the publication of this paper.

Acknowledgments

This work was supported in part by the National Natural Science Foundation of China (Grant no. 61202436 and Grant no. 61271041) and State Key Development Program for Basic Research of China (Grant no. 2011CB302902).

References

- [1] J. P. Munson and V. K. Gupta, "Location-based notification as a general-purpose service," in *Proceedings of the 2nd International Workshop on Mobile Commerce (WMC '02)*, pp. 40–44, September 2002.
- [2] A. Chief, "Operators aren't prepared for onslaught of data traffic," 2009, <http://tinyurl.com/at-t-chief>.
- [3] X. Chen, Y. Chen, and F. Rao, "An efficient spatial publish/subscribe system for intelligent location-based services," in *Proceedings of the 2nd International Workshop on Distributed Event-Based Systems*, pp. 1–6, September 2003.
- [4] R. Meier and V. Cahill, "STEAM: event-based middleware for wireless ad hoc networks," in *Proceedings of the 22nd International Conference on Distributed Computing Systems Workshops*, pp. 639–644, July 2002.
- [5] P. T. Eugster, B. Garbinato, and A. Holzer, "Location-based publish/subscribe," in *Proceedings of the 4th IEEE International Symposium on Network Computing and Applications (NCA '05)*, pp. 279–282, Cambridge, Mass, USA, July 2005.
- [6] I. Burcea and H. Jacobsen, "L-ToPSS-push-oriented location-based services," in *Proceedings of the 4th VLDB Workshop on Technologies for E-Services (TES '03)*, 2003.
- [7] A. Datta, S. Quarteroni, and K. Aberer, "Autonomous gossiping: a self-organizing epidemic algorithm for selective information dissemination in wireless mobile ad-hoc networks," in *Semantics of a Networked World. Semantics for Grid Databases*, Lecture Notes in Computer Science, pp. 126–143, Springer, Berlin, Germany, 2004.
- [8] I. Leontiadis and C. Mascolo, "Opportunistic spatio-temporal dissemination system for vehicular networks," in *Proceedings of the 1st International MobiSys Workshop on Mobile Opportunistic Networking*, pp. 39–46, July 2007.
- [9] I. Leontiadis, P. Costa, and C. Mascolo, "Persistent content-based information dissemination in hybrid vehicular networks," in *Proceedings of the IEEE International Conference on Pervasive Computing and Communications (PerCom '09)*, pp. 1–10, Galveston, Tex, USA, March 2009.
- [10] C. Maihöfer, T. Leinmüller, and E. Schoch, "Abiding geocast: time-stable geocast for ad hoc networks," in *Proceedings of the 2nd ACM International Workshop on Vehicular Ad Hoc Networks*, pp. 20–29, April 2005.
- [11] S. Eichler, C. Schroth, T. Kosch, and M. Strassberger, "Strategies for context-adaptive message dissemination in vehicular ad hoc networks," in *Proceedings of the 3rd Annual International Conference on Mobile and Ubiquitous Systems*, pp. 1–9, San Jose, Calif, USA, July 2006.
- [12] P. Costa, D. Frey, M. Migliavacca, and L. Mottola, "Towards lightweight information dissemination in inter-vehicular networks," in *Proceedings of the 3rd ACM International Workshop on Vehicular Ad Hoc Networks (VANET '06)*, pp. 20–29, April 2006.
- [13] G. Korkmaz, F. Özgüner, E. Ekici, and Ü. Özgüner, "Urban multi-hop broadcast protocol for inter-vehicle communication systems," in *Proceedings of the 1st ACM International Workshop on Vehicular Ad Hoc Networks (VANET '04)*, pp. 76–85, Philadelphia, Pa, USA, October 2004.
- [14] C. Adler, R. Eigner, C. Schroth, and M. Strassberger, "Context-adaptive information dissemination in vanets—maximizing the global benefit," in *Proceedings of the 5th IASTED International*

- Conference on Communication Systems and Networks (CSN '06)*, pp. 7–12, Palma de Mallorca, Spain, August 2006.
- [15] M. Caliskan, D. Graupner, and M. Mauve, “Decentralized discovery of free parking places,” in *Proceedings of the 3rd International Workshop on Vehicular Ad Hoc Networks (VANET '06)*, pp. 30–39, September 2006.
- [16] T. Kosch, C. Schwingenschlogl, and L. Ai, “Information dissemination in multihop inter-vehicle networks,” in *Proceedings of the IEEE 5th International Conference on Intelligent Transportation Systems*, pp. 685–690, August 2002.
- [17] R. Groenevelt, P. Nain, and G. Koole, “The message delay in mobile ad hoc networks,” *Performance Evaluation*, vol. 62, no. 1–4, pp. 210–228, 2005.
- [18] V. Naumov, R. Baumann, and T. Gross, “An evaluation of inter-vehicle ad hoc networks based on realistic vehicular traces,” in *Proceedings of the 7th ACM International Symposium on Mobile Ad Hoc Networking and Computing (MOBIHOC '06)*, pp. 22–25, May 2006.
- [19] L. Buttyán and J.-P. Hubaux, “Stimulating cooperation in self-organizing mobile ad hoc networks,” *Mobile Networks and Applications*, vol. 8, no. 5, pp. 579–592, 2003.
- [20] P. Antoniadis, C. Courcoubetis, and R. Mason, “Comparing economic incentives in peer-to-peer networks,” *Computer Networks*, vol. 46, no. 1, pp. 133–146, 2004.
- [21] A. Keranen, J. Ott, and T. Karkkainen, “The ONE simulator for DTN protocol evaluation,” in *Proceedings of the 2nd International Conference on Simulation Tools and Techniques*, pp. 1–10, April 2009.
- [22] K. Lee, S. Hong, S. J. Kim, I. Rhee, and S. Chong, “SLAW: a mobility model for human walks,” in *Proceedings of the 28th Annual Joint Conference of the IEEE Computer and Communications Societies (INFOCOM '09)*, pp. 855–863, Rio de Janeiro, Brazil, April 2009.

Research Article

Group Synchronization of Nonlinear Complex Dynamics Networks with Sampled Data

Man Li,¹ Bo Liu,² Yuqing Zhu,¹ Lijun Wang,³ and Mei Zhou²

¹ *Mathematics and Physics, Nanyang Institute of Technology, Nanyang, Henan 473004, China*

² *College of Science, North China University of Technology, Beijing 100144, China*

³ *School of Economics and Management, Beijing University of Technology, Beijing 100022, China*

Correspondence should be addressed to Bo Liu; boliu@ncut.edu.cn

Received 6 December 2013; Accepted 5 February 2014; Published 24 March 2014

Academic Editor: Huaicheng Yan

Copyright © 2014 Man Li et al. This is an open access article distributed under the Creative Commons Attribution License, which permits unrestricted use, distribution, and reproduction in any medium, provided the original work is properly cited.

Based on a nonlinear consensus protocol, this paper considers the group synchronization of complex dynamical networks with sampled data. Using the Lyapunov method, the group synchronization of the nonlinear complex networks is analyzed. All the nodes in each group can converge to their own synchronous state asymptotically, if the sampled period satisfies some matrix inequality conditions. Furthermore, the theoretical results are verified by some simulations.

1. Introduction

Because of the wide application of the complex dynamical networks [1–26], the synchronization problem of the complex networks has become a hot topic recently. A lot of researches concentrate on the continuous information transmission; that is, every node can receive or detect neighbor information of the network all the time [1–3, 5–7, 10]. In [1], the authors considered the group synchronization of the nonlinear complex dynamical network via pinning control. A new criterion for the cluster synchronization of coupling networks with time-varying delays was established in continuous time in [2]. Moreover, Liu et al. [3] considered the adaptive synchronization of complex dynamical networks with switching topology by local Lipschitz nonlinearity. In [5], group consensus of multiagent systems with switching topologies and communication delays was studied in the continuous-time case.

However, in many engineering practices, the information communication between nodes could be interrupted at any time due to some factors, such as the unreliability of communication channels and the limitations of the node detection ability. Hence, it is necessary to consider the information transmission under the discrete state [9, 13–16, 18–21, 23, 26].

Information data on the discrete time can also be regarded as sampled data [11, 25]. In [11], the group consensus of linear multiagent systems with sampled-data was considered. Xiao and Wang further considered a discrete-time model with time delays in [13] and analyzed a consensus problem in the existence of the time delay when agents exchanged information between each other. Gao and Wang [16] studied the continuous-time consensus of multiagent systems with sampled data by time-varying topology. In [18], consensus of multiple dynamic agents with sampled information was considered. In [20], average consensus control of networks with sampled data and measurement noises was studied on continuous time. In this paper, we consider the group synchronization of nonlinear complex dynamical network with sampled data.

The rest of this paper is organized as follows. In Section 2, we consider the group synchronization of a complex dynamical network with sampled data and give some assumptions and lemmas. In Section 3, we analyze group synchronization of the proposed network and give the synchronization condition based on linear matrix inequality (LMI). In Section 4, we give the synchronization condition for a special case. In Section 5, the simulations verify the theoretical results. Conclusion is finally summarized in Section 6.

2. Preliminaries and Problem Statement

Consider a complex dynamical network of $n + m$ nodes with sampled data as follows:

$$\dot{x}_i(t) = u_i(t), \quad (1)$$

with

$$u_i(t) = \begin{cases} f(x_i(t_k)) + c \sum_{j \in N_{1,i}} a_{ij} \Gamma(x_j(t_k) - x_i(t_k)) \\ \quad + c \sum_{j \in N_{2,i}} b_{ij} \Gamma x_j(t_k) + \mu_i(t_k) \\ \quad \forall i \in \ell_1, \quad \forall t \in [t_k, t_{k+1}]; \\ f(x_i(t_k)) + c \sum_{j \in N_{2,i}} a_{ij} \Gamma(x_j(t_k) - x_i(t_k)) \\ \quad + c \sum_{j \in N_{1,i}} b_{ij} \Gamma x_j(t_k) + \mu_i(t_k) \\ \quad \forall i \in \ell_2, \quad \forall t \in [t_k, t_{k+1}], \end{cases} \quad (2)$$

where $x_i = (x_i^1(t), x_i^2(t), \dots, x_i^n(t))^T \in R^n$ represents the state vectors of the node i at time t , $f(\cdot) \in R^n$ is continuously differentiable, c is coupling strength, and $\Gamma = \text{diag}(\gamma_1, \gamma_2, \dots, \gamma_n) \in R^{n \times n}$ is an inner-coupling matrix, if the node links through its i th state with its neighbors $\gamma_i > 0$; otherwise $\gamma_i = 0$. In this protocol, let $X_1 = \{x_1, x_2, \dots, x_n\}$, and let $X_2 = \{x_{n+1}, x_{n+2}, \dots, x_{n+m}\}$, where $X = X_1 \cup X_2$. $\ell_1 = 1, 2, \dots, n$, $\ell_2 = n + 1, n + 2, \dots, n + m$, with $\ell = \ell_1 \cup \ell_2$. N_i is the neighbors of the node i , $N_i \in N_{1i} \cup N_{2i}$, where $N_{1i} = \{x_j \in X_1 : a_{ij} > 0, i, j \in \ell_1\}$, $N_{2i} = \{x_j \in X_2 : a_{ij} > 0, i, j \in \ell_2\}$.

In protocol (2), $\mu_i(t)$ is the control input:

$$\mu_i(t) = \begin{cases} -ch_i \Gamma(x_i(t_k) - \bar{x}_1(t_k)), & i \in \ell_1 \\ -ch_i \Gamma(x_i(t_k) - \bar{x}_2(t_k)), & i \in \ell_2, \end{cases} \quad (3)$$

where h_i is an on-off control; if the system is sampling the data, then $h_i = 1$; otherwise $h_i = 0$. If node i can get information from node j in the same group, then $a_{ij} > 0$; otherwise $a_{ij} = 0$; if node i can get information from node j between different groups, then $b_{ij} \neq 0$; otherwise $b_{ij} = 0$. Thus the coupling configuration matrix $A \in R^{(n+m) \times (n+m)}$ can be written as

$$A = \begin{bmatrix} cA_{11}^{n \times n} & cB_{12}^{n \times m} \\ cB_{21}^{m \times n} & cA_{22}^{m \times m} \end{bmatrix}, \quad (4)$$

where

$$ca_{ii} = - \sum_{j=1, j \neq i}^n ca_{ij}, \quad i = 1, 2, \dots, n, \quad (5)$$

$$ca_{ii} = - \sum_{j=n+1, j \neq i}^{n+m} ca_{ij}, \quad i = n + 1, n + 2, \dots, n + m.$$

$cA_{11} = ca_{ij} \in R^{n \times n}$ and $cA_{22} = ca_{ij} \in R^{m \times m}$ represent the coupling configuration of the subgroups, respectively.

Network (1) is said to group synchronization if

$$\lim_{t \rightarrow \infty} \|(x_i(t) - x_j(t))\| = 0, \quad \forall i, j \in \ell_1, \quad (6)$$

$$\lim_{t \rightarrow \infty} \|(x_i(t) - x_j(t))\| = 0, \quad \forall i, j \in \ell_2,$$

where the nonlinear function satisfies

$$f(\bar{x}_1(t), t) = \dot{\bar{x}}_1(t), \quad (7)$$

$$f(\bar{x}_2(t), t) = \dot{\bar{x}}_2(t),$$

and $\bar{x}_1(t), \bar{x}_2(t) \in R^n$ are the synchronous states.

Given a positive real number α and a sampled period T , we suppose that

$$t_{i+1} - t_i = \alpha T_i, \quad \forall i = 0, 1, 2, \dots, \quad (8)$$

where $t_0 < t_1 < \dots$ shows the discrete time that the node j can obtain information from its neighbors and positive integer T_i is a sampled time about the i th time ($\forall i = 0, 1, 2, \dots$), and it satisfies $T_i \leq T$. Under this condition, a linear consensus protocol based on a linear estimation-based sampling period is designed as follows [11]:

$$u_i(t_k + \alpha) = u_i(t_k) - \frac{1}{T} u_i(t_k) = \left(1 - \frac{1}{T}\right) u_i(t_k),$$

$$u_i(t_k + 2\alpha) = u_i(t_k + \alpha) + (u_i(t_k + \alpha) - u_i(t_k))$$

$$= \left(1 - \frac{2}{T}\right) u_i(t_k),$$

\vdots

$$u_i(t_{k+1} - \alpha) = u_i(t_{k+1} - 2\alpha) + (u_i(t_k - 2\alpha) - u_i(t_{k+1} - 3\alpha))$$

$$= \left(1 - \frac{t_{k+1} - t_k - 1}{T}\right) u_i(t_k)$$

$$= \left(1 - \frac{T_k - 1}{T}\right) u_i(t_k). \quad (9)$$

Thus, we have

$$u_i(t) = \begin{cases} \left(1 - \frac{T_k - 1}{T}\right) \\ \times \left[f(x_i(t_k)) + c \sum_{j \in N_{1,i}} a_{ij} \Gamma(x_j(t_k) - x_i(t_k)) \right. \\ \left. + c \sum_{j \in N_{2,i}} b_{ij} \Gamma x_j(t_k) + \mu_i(t_k) \right] \\ \forall i \in \ell_1, \quad \forall t \in [t_k, t_{k+1}]; \\ \left(1 - \frac{T_k - 1}{T}\right) \\ \times \left[f(x_i(t_k)) + c \sum_{j \in N_{2,i}} a_{ij} \Gamma(x_j(t_k) - x_i(t_k)) \right. \\ \left. + c \sum_{j \in N_{1,i}} b_{ij} \Gamma x_j(t_k) + \mu_i(t_k) \right] \\ \forall i \in \ell_2, \quad \forall t \in [t_k, t_{k+1}]. \end{cases} \quad (10)$$

Then the complex dynamical network (1) in every sampled period becomes

$$\dot{x}_i(t) = u_i(t), \quad (11)$$

with

$$u_i(t) = \begin{cases} \left(1 - \frac{h}{T}\right) \\ \times \left[f(x_i(t_k)) + c \sum_{j \in N_{1,i}} a_{ij} \Gamma(x_j(t_k) - x_i(t_k)) \right. \\ \left. + c \sum_{j \in N_{2,i}} b_{ij} \Gamma x_j(t_k) + \mu_i(t_k) \right] \\ \forall i \in \ell_1, \quad \forall t \in [t_k + h\alpha, t_k + (h+1)\alpha], \\ \quad \quad \quad h = 0, 1, \dots, T_k - 1; \\ \left(1 - \frac{h}{T}\right) \\ \times \left[f(x_i(t_k)) + c \sum_{j \in N_{2,i}} a_{ij} \Gamma(x_j(t_k) - x_i(t_k)) \right. \\ \left. + c \sum_{j \in N_{1,i}} b_{ij} \Gamma x_j(t_k) + \mu_i(t_k) \right] \\ \forall i \in \ell_2, \quad \forall t \in [t_k + h\alpha, t_k + (h+1)\alpha], \\ \quad \quad \quad h = 0, 1, \dots, T_k - 1. \end{cases} \quad (12)$$

Some assumptions and lemmas are needed.

Assumption 1 (see [3]). If each f_i of the nonlinear function $f(x_i(t)) = (f_1(x_i(t)), f_2(x_i(t)), \dots, f_n(x_i(t)))^T$ in network (1)

satisfies the local Lipschitz condition, for any compact set $S \in \mathbb{R}^m$, there exists a positive constant matrix $\eta(S)$, such that

$$(x - y)^T [f(x) - f(y)] \leq (x - y)^T K \Gamma (x - y) \leq \eta(s) (x - y)^T \Gamma (x - y), \quad (13) \\ \forall x, y \in S, \quad \eta(s) = \|K\|_1.$$

Assumption 2 (see [1]). Assume that protocol (1) satisfies the balance of effectiveness between the subgroups

$$\sum_{j=n+1}^{n+m} b_{ij} = 0, \quad i \in \ell_1, \\ \sum_{j=1}^n b_{ij} = 0, \quad i \in \ell_2. \quad (14)$$

Lemma 3 (see [1]). Define $d_0 = (1/2) \sum_{i=1}^N (x_i(0) - x_0)^2$, and construct a closed space

$$B(\sigma d_0, x_0) = \left\{ x \in \mathbb{R}^{Nn} \mid \frac{1}{2} \sum_{i=1}^N \|x_i(0) - x_0\|^2 \leq \sigma d_0 \right\}, \quad (15)$$

where $x = (x_1^T, x_2^T, \dots, x_N^T)^T$ and $\sigma > 1$ is a constant. For $\forall x \in B(\sigma d_0, x_0)$, there exists a constant $\eta(\sigma, x_0)$ such that

$$\sum_{i=1}^N (x_i - x_0) (f(x_i) - f(x_0)) \leq \eta(\sigma, x_0) \|x_i - x_0\|^2. \quad (16)$$

Lemma 4 (see [1]). Suppose that $a \in \mathbb{R}^n$ and $b \in \mathbb{R}^m$ are vectors, and in matrix M , the following inequality holds:

$$2x^T y \leq x^T M x + y^T M^{-1} y. \quad (17)$$

In this paper, $A > 0 (\geq, <, \leq)$ means that A is a positive (or semipositive, negative, or seminegative) definite matrix; $\|A\|_1 = \max_{1 \leq j \leq n} \sum_{i=1}^n |a_{ij}|$, $\|A\|_\infty = \max_{1 < i < n} \sum_{j=1}^n |a_{ij}|$.

3. Group Synchronization Analysis in Complex Network with Sampled Data

In this section, we consider group synchronization problem of the complex networks with sampled data. We have the following theorem.

Theorem 5. For network (1) with protocol (12) of $n + m$ nodes, under Assumptions 1-2 and Lemmas 3-4, if h, T satisfy

$$\frac{h}{1 - T} \left\{ [\eta(\sigma, \bar{x}_1) I_n + c(A_{11} - H_1)] \otimes \Gamma \right. \\ \left. + \frac{c}{2} (\|B_{12}\|_1 I_n + \|B_{21}\|_\infty I_n) \otimes \Gamma \right\} < 0, \\ h = 0, 1, \dots, T_k - 1;$$

$$\begin{aligned} & \frac{h}{1-T} \left\{ [\eta(\sigma, \bar{x}_2) I_m + c(A_{22} - H_2)] \otimes \Gamma \right. \\ & \quad \left. + \frac{c}{2} (\|B_{21}\|_1 I_m + \|B_{12}\|_\infty I_m) \otimes \Gamma \right\} < 0, \\ & \quad h = 0, 1, \dots, T_k - 1, \end{aligned} \quad (18)$$

then all the nodes in each group can converge to their own synchronous state asymptotically, where

$$\begin{aligned} H_1 &= \text{diag} \{h_1, h_2, \dots, h_p, 0, \dots, 0\}, \\ H_2 &= \text{diag} \{h_{n+1}, h_{n+2}, \dots, h_{n+l}, 0, \dots, 0\}. \end{aligned} \quad (19)$$

Proof. Construct a Lyapunov function as follows:

$$V(t_k) = V_1(t_k) + V_2(t_k), \quad (20)$$

where

$$V_1(t_k) = \frac{1}{2} \sum_{i=1}^n (x_i(t_k) - \bar{x}_1(t_k))^T (x_i(t_k) - \bar{x}_1(t_k)), \quad (21)$$

$$V_2(t_k) = \frac{1}{2} \sum_{i=n+1}^{n+m} (x_i(t_k) - \bar{x}_2(t_k))^T (x_i(t_k) - \bar{x}_2(t_k)).$$

Define

$$\begin{aligned} e_{i,1}(t_k) &= x_i(t_k) - \bar{x}_1(t_k), \quad i = 1, 2, \dots, n, \\ e_{i,2}(t_k) &= x_i(t_k) - \bar{x}_2(t_k), \quad i = n+1, n+2, \dots, n+m, \\ e_1(t_k) &= (e_{1,1}(t_k), e_{2,1}(t_k), \dots, e_{n,1}(t_k))^T, \\ e_2(t_k) &= (e_{n+1,2}(t_k), e_{n+2,2}(t_k), \dots, e_{n+m,2}(t_k))^T. \end{aligned} \quad (22)$$

Then,

$$\begin{aligned} V_1(t_k) &= \frac{1}{2} \sum_{i=1}^n e_{i,1}(t_k)^T e_{i,1}(t_k), \\ V_2(t_k) &= \frac{1}{2} \sum_{i=n+1}^{n+m} e_{i,2}(t_k)^T e_{i,2}(t_k). \end{aligned} \quad (23)$$

Under Assumption 2, we can know

$$\begin{aligned} \dot{V}_1(t_k) &= \frac{h}{1-T} \\ & \times \sum_{i=1}^n (x_i(t_k) - \bar{x}_1(t_k))^T \\ & \times \left[f(x_i(t_k)) - f(\bar{x}_1(t_k)) \right. \end{aligned}$$

$$\begin{aligned} & \left. + c \sum_{j \in N_{1,i}} a_{ij} \Gamma \left((x_j(t_k) - \bar{x}_1(t_k)) \right. \right. \\ & \quad \left. \left. - (x_i(t_k) - \bar{x}_1(t_k)) \right) \right) \\ & + c \sum_{j \in N_{2,i}} b_{ij} \Gamma (x_j(t_k) - \bar{x}_2(t_k)) \\ & + c \sum_{j \in N_{2,i}} b_{ij} \bar{x}_2(t_k) - ch_i \Gamma (x_i(t_k) - \bar{x}_1(t_k)) \left. \right] \\ & = \frac{h}{1-T} \sum_{i=1}^n e_{i,1}^T(t_k) \\ & \times \left[f(x_i(t_k)) - f(\bar{x}_1(t_k)) \right. \\ & \quad + c \sum_{j \in N_{1,i}} a_{ij} \Gamma (e_{j,1}(t_k) - e_{i,1}(t_k)) \\ & \quad + c \sum_{j \in N_{2,i}} b_{ij} \Gamma e_{j,2}(t_k) - ch_i \Gamma e_{i,1}(t_k) \left. \right]. \end{aligned} \quad (24)$$

Under Assumption 1 and Lemma 3, we can have

$$\begin{aligned} \dot{V}_1(t_k) &\leq \frac{h}{1-T} \\ & \times \sum_{i=1}^n e_{i,1}^T(t_k) \left[\eta(\sigma, \bar{x}_1) \Gamma e_{i,1}(t_k) \right. \\ & \quad + c \sum_{j \in N_{1,i}} a_{ij} \Gamma (e_{j,1}(t_k) - e_{i,1}(t_k)) \\ & \quad \left. + c \sum_{j \in N_{2,i}} b_{ij} \Gamma e_{j,2}(t_k) - ch_i \Gamma e_{i,1}(t_k) \right] \\ & = \frac{h}{1-T} \left[e_1^T(t_k) (\eta(\sigma, \bar{x}_1) I_n \otimes \Gamma) e_1(t_k) \right. \\ & \quad + e_1^T(t_k) (c(A_{11} - H_1) \otimes \Gamma) e_1(t_k) \\ & \quad \left. + c \sum_{i=1}^n e_{i,1}^T(t_k) \sum_{j \in N_{2,i}} b_{ij} \Gamma e_{j,2}(t_k) \right]. \end{aligned} \quad (25)$$

Then, we can get

$$\begin{aligned} \dot{V}_2(t_k) &\leq \frac{h}{1-T} \\ & \times \sum_{i=n+1}^{n+m} e_{i,2}^T(t_k) \left[\eta(\sigma, \bar{x}_2) \Gamma e_{i,2}(t_k) \right. \end{aligned}$$

$$\begin{aligned}
 & + c \sum_{j \in N_{2,i}} a_{ij} \Gamma (e_{j,2}(t_k) - e_{i,2}(t_k)) \\
 & + c \sum_{j \in N_{1,i}} b_{ij} \Gamma e_{j,1}(t_k) - ch_i \Gamma e_{i,2}(t_k) \Big] \\
 = & \frac{h}{1-T} \left[e_2^T(t_k) (\eta(\sigma, \bar{x}_2) I_m \otimes \Gamma) e_2(t_k) \right. \\
 & + e_2^T(t_k) (c(A_{22} - H_2) \otimes \Gamma) e_2(t_k) \\
 & \left. + c \sum_{i=n+1}^{n+m} e_{i,2}^T(t_k) \sum_{j \in N_{1,i}} b_{ij} \Gamma e_{j,1}(t_k) \right]. \quad (26)
 \end{aligned}$$

Using Lemma 4, we can have

$$\begin{aligned}
 & c \sum_{i=1}^n e_{i,1}^T(t_k) \sum_{j \in N_{2,i}} b_{ij} \Gamma e_{j,2}(t_k) \\
 & \leq \frac{c}{2} \sum_{i=1}^n \sum_{j \in N_{2,i}} b_{ij} (e_{i,1}^T(t_k) \Gamma e_{i,1}(t_k) + e_{j,2}^T(t_k) \Gamma e_{j,2}(t_k)) \\
 & \leq \frac{c}{2} \|B_{12}\|_1 \sum_{i=1}^n e_{i,1}^T(t_k) \Gamma e_{i,1}(t_k) \\
 & \quad + \frac{c}{2} \|B_{12}\|_\infty \sum_{j \in N_{2,i}} e_{j,2}^T(t_k) \Gamma e_{j,2}(t_k) \\
 & = e_{i,1}^T(t_k) \left[\frac{c}{2} \|B_{12}\|_1 I_n \otimes \Gamma \right] e_{i,1}(t_k) \\
 & \quad + e_{i,2}^T(t_k) \left[\frac{c}{2} \|B_{12}\|_\infty I_m \otimes \Gamma \right] e_{i,2}(t_k), \\
 & c \sum_{i=n+1}^{n+m} e_{i,2}^T(t_k) \sum_{j \in N_{1,i}} b_{ij} \Gamma e_{j,1}(t_k) \\
 & \leq \frac{c}{2} \sum_{i=n+1}^{n+m} \sum_{j \in N_{1,i}} b_{ij} (e_{i,2}^T(t_k) \Gamma e_{i,2}(t_k) + e_{j,1}^T(t_k) \Gamma e_{j,1}(t_k)) \\
 & \leq \frac{c}{2} \|B_{21}\|_1 \sum_{i=n+1}^{n+m} e_{i,2}^T(t_k) \Gamma e_{i,2}(t_k) \\
 & \quad + \frac{c}{2} \|B_{21}\|_\infty \sum_{j \in N_{1,i}} e_{j,1}^T(t_k) \Gamma e_{j,1}(t_k) \\
 & = e_{i,2}^T(t_k) \left[\frac{c}{2} \|B_{21}\|_1 I_m \otimes \Gamma \right] e_{i,2}(t_k) \\
 & \quad + e_{i,1}^T(t_k) \left[\frac{c}{2} \|B_{21}\|_\infty I_n \otimes \Gamma \right] e_{i,1}(t_k). \quad (27)
 \end{aligned}$$

Thus, we can obtain

$$\begin{aligned}
 \dot{V}(t_k) & = \dot{V}_1(t_k) + \dot{V}_2(t_k) \\
 & \leq \frac{h}{1-T} \left\{ e_1^T(t_k) (\eta(\sigma, \bar{x}_1) I_n \otimes \Gamma) e_1(t_k) \right. \\
 & \quad + e_1^T(t_k) (c(A_{11} - H_1) \otimes \Gamma) e_1(t_k) \\
 & \quad + e_2^T(t_k) (\eta(\sigma, \bar{x}_2) I_m \otimes \Gamma) e_2(t_k) \\
 & \quad + e_2^T(t_k) (c(A_{22} - H_2) \otimes \Gamma) e_2(t_k) \\
 & \quad + e_{i,1}^T(t_k) \left[\frac{c}{2} \|B_{12}\|_1 I_n \otimes \Gamma \right] e_{i,1}(t_k) \\
 & \quad + e_{i,2}^T(t_k) \left[\frac{c}{2} \|B_{12}\|_\infty I_m \otimes \Gamma \right] e_{i,2}(t_k) \\
 & \quad + e_{i,2}^T(t_k) \left[\frac{c}{2} \|B_{21}\|_1 I_m \otimes \Gamma \right] e_{i,2}(t_k) \\
 & \quad \left. + e_{i,1}^T(t_k) \left[\frac{c}{2} \|B_{21}\|_\infty I_n \otimes \Gamma \right] e_{i,1}(t_k) \right\} \\
 & = e_1^T(t_k) \left\{ \frac{h}{1-T} [\eta(\sigma, \bar{x}_1) I_n + c(A_{11} - H_1)] \otimes \Gamma \right. \\
 & \quad \left. + \frac{c}{2} (\|B_{12}\|_1 I_n + \|B_{21}\|_\infty I_n) \otimes \Gamma \right\} e_1(t_k) \\
 & \quad + e_2^T(t_k) \left\{ \frac{h}{1-T} [\eta(\sigma, \bar{x}_2) I_m + c(A_{22} - H_2)] \otimes \Gamma \right. \\
 & \quad \left. + \frac{c}{2} (\|B_{21}\|_1 I_m + \|B_{12}\|_\infty I_m) \otimes \Gamma \right\} e_2(t_k). \quad (28)
 \end{aligned}$$

If

$$\begin{aligned}
 & \frac{h}{1-T} \left\{ [\eta(\sigma, \bar{x}_1) I_n + c(A_{11} - H_1)] \otimes \Gamma \right. \\
 & \quad \left. + \frac{c}{2} (\|B_{12}\|_1 I_n + \|B_{21}\|_\infty I_n) \otimes \Gamma \right\} < 0, \\
 & \frac{h}{1-T} \left\{ [\eta(\sigma, \bar{x}_2) I_m + c(A_{22} - H_2)] \otimes \Gamma \right. \\
 & \quad \left. + \frac{c}{2} (\|B_{21}\|_1 I_m + \|B_{12}\|_\infty I_m) \otimes \Gamma \right\} < 0, \quad (29)
 \end{aligned}$$

then

$$\dot{V}(t_k) < 0. \quad (30)$$

Therefore, $V(t_k)$ decreases on an interval $\forall t \in [t_k + h\alpha, t_k + (h+1)\alpha]$, $h = 0, 1, \dots, T_k - 1$, and $V(t_k) \leq V(t_0)$. From the above discussion, we have

$$\begin{aligned}
 \lim_{t \rightarrow \infty} \| (x_i(t) - x_j(t)) \| & = 0, \quad \forall i, j \in \ell_1, \\
 \lim_{t \rightarrow \infty} \| (x_i(t) - x_j(t)) \| & = 0, \quad \forall i, j \in \ell_2. \quad (31)
 \end{aligned}$$

Then, network (1) with sampled data is group-synchronized under protocol (12). \square

4. A Special Case

In this section, we consider a special case about network (1). For convenience, we let $\bar{A}_{11} = A_{11} - H_1$ and $\bar{A}_{22} = A_{22} - H_2$.

Lemma 6 (see [1]). *If $A = (a_{ij}) \in R^{N \times N}$ is a symmetric irreducible matrix with $a_{ii} = -\sum_{j=1, j \neq i}^N a_{ij}$ and $a_{ij} = a_{ji} \geq 0 (i \neq j)$, then for any matrix $E = \text{diag}(e, 0, \dots, 0)$ with $e \geq 0$ all eigenvalues of the matrix $(A - E)$ are negative.*

In networks, when the information transmission is the same between the nodes i and j , the coupling configuration matrix A is symmetric. From Lemma 6, when A is symmetric, \bar{A}_{11} and \bar{A}_{22} are negative. Hence, all of their eigenvalues are strictly negative; one denotes them as

$$\begin{aligned} \lambda_n(\bar{A}_{11}) \leq \dots \leq \lambda_2(\bar{A}_{11}) \leq \lambda_1(\bar{A}_{11}) < 0, \\ \lambda_m(\bar{A}_{22}) \leq \dots \leq \lambda_2(\bar{A}_{22}) \leq \lambda_1(\bar{A}_{22}) < 0. \end{aligned} \quad (32)$$

Then, using Lemma 6, we can obtain the following result when the coupling configuration matrix is symmetric.

Theorem 7. *For network (1) with protocol (12) of $n + m$ nodes, when the coupling configuration matrix is symmetric, under Assumptions 1-2 and Lemmas 3-6, if h, T satisfy*

$$\begin{aligned} \frac{h}{1-T} \left\{ \left[\eta(\sigma, \bar{x}_1) I_n + c \lambda_1(\bar{A}_{11}) \right] \otimes \Gamma \right. \\ \left. + \frac{c}{2} (\|B_{12}\|_1 I_n + \|B_{21}\|_{\infty} I_n) \otimes \Gamma \right\} < 0, \\ h = 0, 1, \dots, T_k - 1; \\ \frac{h}{1-T} \left\{ \left[\eta(\sigma, \bar{x}_2) I_m + c \lambda_1(\bar{A}_{22}) \right] \otimes \Gamma \right. \\ \left. + \frac{c}{2} (\|B_{21}\|_1 I_m + \|B_{12}\|_{\infty} I_m) \otimes \Gamma \right\} < 0, \\ h = 0, 1, \dots, T_k - 1, \end{aligned} \quad (33)$$

then all the nodes in each group can converge to their own synchronous state asymptotically, where $\bar{A}_{11} = A_{11} - H_1$ and $\bar{A}_{22} = A_{22} - H_2$.

The proof of Theorem 7 is similar to that of Theorem 5 and here is omitted.

5. Simulations

In this section, we give some simulation results of the above discussions. For convenience, let $n = 5, m = 4, c = 12, a_{ij} \neq a_{ji}$ for all i, j , and $H_1 = \text{diag}\{0, 1, 1, 1, 0\}$, $H_2 = \text{diag}\{0, 0, 0, 1\}$. We consider group synchronization of complex dynamical network with sampled data in the time interval $[0, 6]$. The curves in the graphs are the locations of $5 + 4$ nodes and the synchronous targets in the network.

From Figures 1, 2, and 3, the synchronous states are $\bar{x}_1(0) = [0, -3.4 + 80 \cos x]$, $\bar{x}_2(0) = [2, 30 + 20 \cos(20x)]$. From these figures, we can see that all the nodes in each subgroup can converge to their own synchronous targets. But,

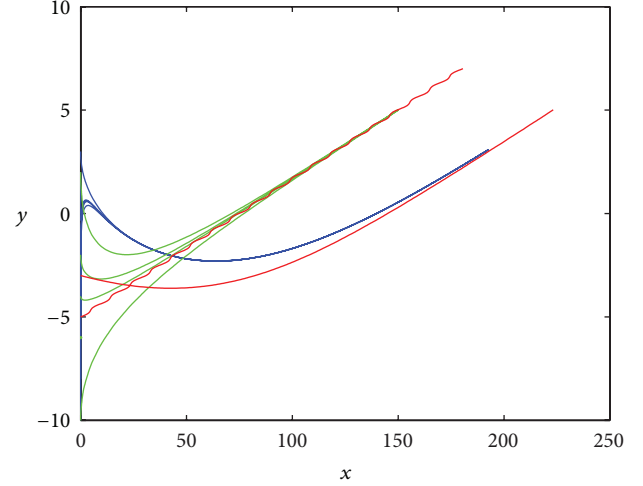


FIGURE 1: The positions of the nodes of network (1) on interval $t \in [0, 6]$.

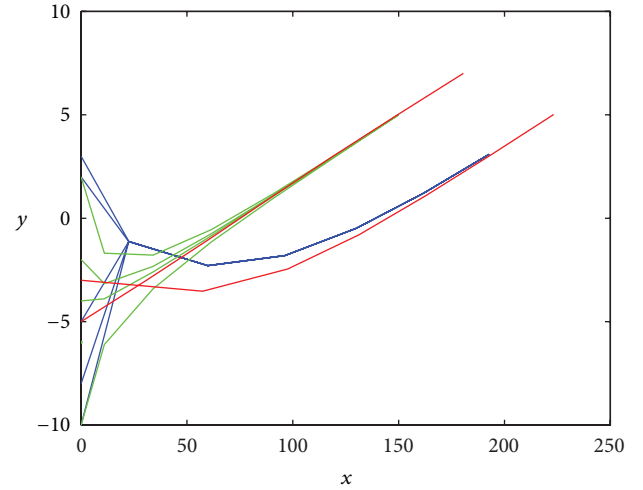


FIGURE 2: The positions of the nodes of network (1) on interval $t \in [0, 6]$, sampled period $T = 1$.

in Figures 4, 5, and 6, all of the nodes can asymptotically converge to a synchronous state, when the synchronous state is the only one $\bar{x}_1(0) = \bar{x}_2(0) = [0, 30 + 20 \cos(20x)]$.

In Figures 1 and 4, we simulate synchronization of the network including two subgroups without sampled data. In Figures 2 and 5, we chose $T = 1$ as the sampled period. That is, the complex network is sampling at the moment $t = k$, for $k = 0, 1, \dots$. In Figures 3 and 6, we chose $T = 2.5$ as the sampled period; that is, the complex network is sampling at the moment $t = 2.5k$, for $k = 0, 1, \dots$.

In these simulation results, we can find that the nodes of the system keep their state value in the first nT time until before the moment $(n + 1)T$, keeping their state value in $(n + 1)T$ time until the moment $(n + 2)T$ and so on. By comparing, when choosing the sampled data on every period, the rate of convergence of the nodes in the complex dynamics network is slow. Moreover, the bigger the sampled period is,

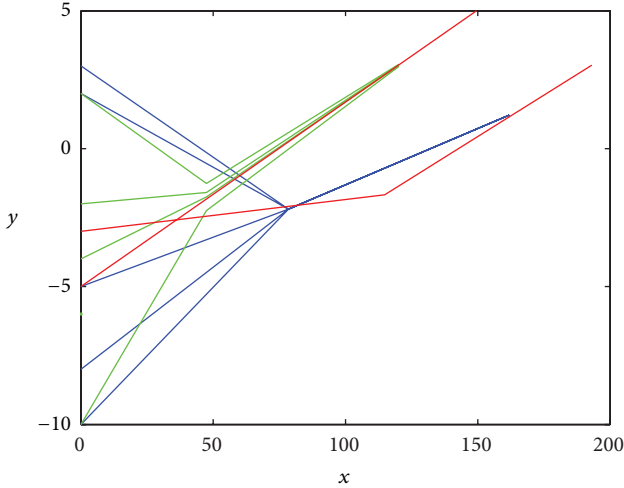


FIGURE 3: The positions of the nodes of network (1) on interval $t \in [0, 6]$, sampled period $T = 2.5$.

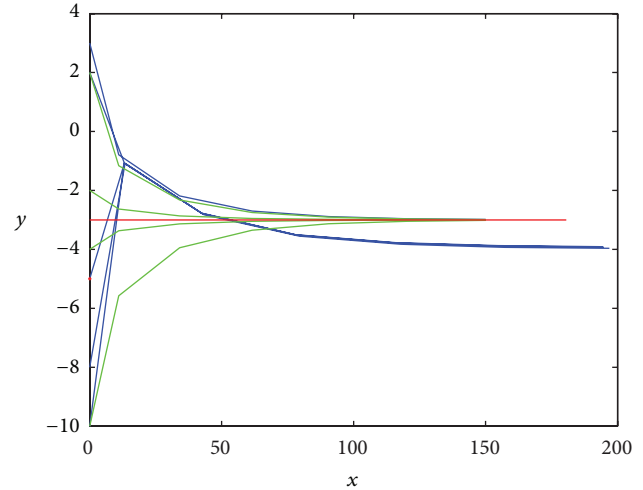


FIGURE 5: The nodes of network (1) on interval $t \in [0, 6]$ converge to the same target, sampled period $T = 1$.

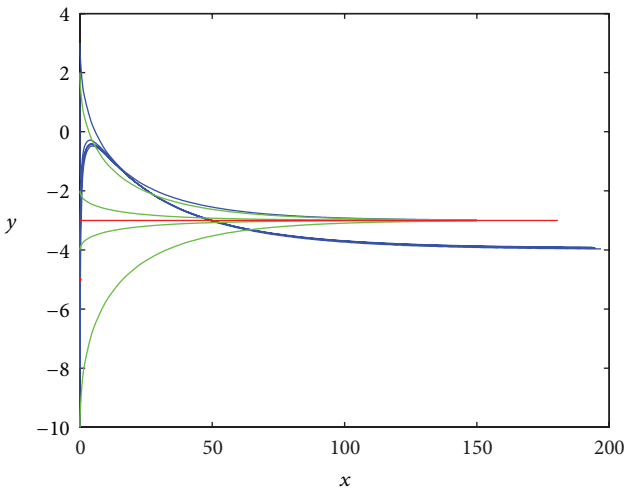


FIGURE 4: The nodes of network (1) on interval $t \in [0, 6]$ converge to the same target.

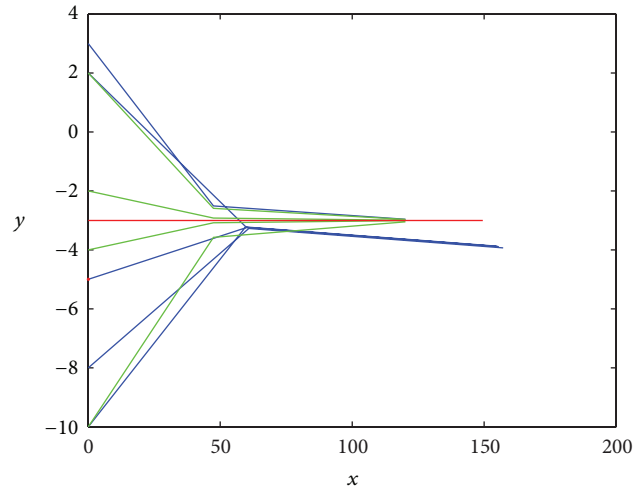


FIGURE 6: The nodes of network (1) on interval $t \in [0, 6]$ converge to the same target, sampled period $T = 2.5$.

the slower the rate of convergence of the nodes in the complex dynamics network is.

6. Conclusion

In this paper, we have investigated the group synchronization problem of a complex dynamical network with sampled data. We prove that the nodes of the network arrive at synchronization in two subgroups if the sampling period satisfies the condition based on the linear matrix inequality (LMI). In addition, we have given some simulation results about the proposed complex network.

Conflict of Interests

The authors declare that there is no conflict of interests regarding the publication of this paper.

Acknowledgments

This work was supported by the National Natural Science Foundation of China under Grant no. 61304049, Funding Project for Academic Human Resources Development in Institutions of Higher Learning under the Jurisdiction of Beijing Municipality (PHR201108055), and Science and Technology Development Plan Project of Beijing Education Commission (nos. KM201310009011 and KM201310009013).

References

- [1] B. Liu, P. F. Wei, X. F. Wang et al., “Group synchronization of complex networks with nonlinear dynamics via pinning control,” in *Proceeding of the 32nd Chinese Control Conference*, pp. 235–240, 2013.
- [2] S. Wang, H. Yao, S. Zheng, and Y. Xie, “A novel criterion for cluster synchronization of complex dynamical networks with

- coupling time-varying delays," *Communications in Nonlinear Science and Numerical Simulation*, vol. 17, no. 7, pp. 2997–3004, 2012.
- [3] B. Liu, X. L. Wang, Y. P. Gao, G. M. Xie, and H. S. Su, "Adaptive synchronization of complex dynamical networks governed by local lipschitz nonlinearity on switching topology," *Journal of Applied Mathematics*, vol. 2013, Article ID 818242, 7 pages, 2013.
- [4] H. Zhang, H. Yan, F. Yang, and Q. Chen, "Quantized control design for impulsive fuzzy networked systems," *IEEE Transactions on Fuzzy Systems*, vol. 19, no. 6, pp. 1153–1162, 2011.
- [5] L. Wang, X.-J. Kong, H. Shi, H.-P. Dai, and Y.-X. Sun, "LMI-based criteria for synchronization of complex dynamical networks," *Journal of Physics A*, vol. 41, no. 28, Article ID 285102, pp. 1751–8113, 2008.
- [6] H. Su, X. Wang, and Z. Lin, "Flocking of multi-agents with a virtual leader," *IEEE Transactions on Automatic Control*, vol. 54, no. 2, pp. 293–307, 2009.
- [7] J. Yu and L. Wang, "Group consensus in multi-agent systems with switching topologies and communication delays," *Systems and Control Letters*, vol. 59, no. 6, pp. 340–348, 2010.
- [8] H. Zhang, H. C. Yan, F. W. Yang, and Q. J. Chen, "Distributed average filtering for sensor networks with sensor saturation," *IET Control Theory and Applications*, vol. 7, no. 6, pp. 887–893, 2013.
- [9] H. C. Yan, Z. Z. Su, H. Zhang, and F. W. Yang, "Observer-based H_∞ control for discrete-time stochastic systems with quantization and random communication delays," *IET Control Theory and Applications*, vol. 7, no. 3, pp. 372–379, 2013.
- [10] J. Yu and L. Wang, "Group consensus of multi-agent systems with directed information exchange," *International Journal of Systems Science*, vol. 2, no. 2, pp. 334–348, 2012.
- [11] Y. J. Yu, M. Yu, J. P. Hu, and B. Liu, "Group consensus of multi-agent systems with sampled data," in *Proceeding of the 32nd Chinese Control Conference*, pp. 7168–7172, 2013.
- [12] H. C. Yan, H. B. Shi, H. Zhang, and F. W. Yang, "Quantized H_∞ control for networked delayed systems with communication constraints," *Asian Journal of Control*, vol. 15, no. 5, pp. 1468–1476, 2013.
- [13] F. Xiao and L. Wang, "Consensus protocols for discrete-time multi-agent systems with time-varying delays," *Automatica*, vol. 44, no. 10, pp. 2577–2582, 2008.
- [14] J. Yu and L. Wang, "Group consensus of multi-agent systems with directed information exchange," *International Journal of Systems Science*, vol. 43, no. 2, pp. 334–348, 2012.
- [15] H. Su, X. Wang, and G. Chen, "A connectivity-preserving flocking algorithm for multi-agent systems based only on position measurements," *International Journal of Control*, vol. 82, no. 7, pp. 1334–1343, 2009.
- [16] Y. Gao and L. Wang, "Sampled-data based consensus of continuous-time multi-agent systems with time-varying topology," *IEEE Transactions on Automatic Control*, vol. 56, no. 5, pp. 1226–1231, 2011.
- [17] H. Zhang, H. Yan, T. Liu, and Q. Chen, "Fuzzy controller design for nonlinear impulsive fuzzy systems with time delay," *IEEE Transactions on Fuzzy Systems*, vol. 19, no. 5, pp. 844–856, 2011.
- [18] Y. Gao and L. Wang, "Consensus of multiple dynamic agents with sampled information," *IET Control Theory and Applications*, vol. 4, no. 6, pp. 945–956, 2010.
- [19] H. C. Yan, H. Zhang, M. Q. Meng, and H. Shi, "Delay-range-dependent robust H_∞ filtering for uncertain systems with interval time-varying delays," *Asian Journal of Control*, vol. 13, no. 2, pp. 356–360, 2011.
- [20] T. Li and J. Zhang, "Sampled-data based average consensus control for networks of continuous-time integrator agents with measurement noises," in *Proceedings of the 26th Chinese Control Conference (CCC '07)*, pp. 716–720, July 2007.
- [21] H. Su, X. Wang, and Z. Lin, "Synchronization of coupled harmonic oscillators in a dynamic proximity network," *Automatica*, vol. 45, no. 10, pp. 2286–2291, 2009.
- [22] H. Zhang, Q. Chen, H. Yan, and J. Liu, "Robust H_∞ filtering for switched stochastic system with missing measurements," *IEEE Transactions on Signal Processing*, vol. 57, no. 9, pp. 3466–3474, 2009.
- [23] H. Su, G. Chen, X. Wang, and Z. Lin, "Adaptive second-order consensus of networked mobile agents with nonlinear dynamics," *Automatica*, vol. 47, no. 2, pp. 368–375, 2011.
- [24] L. X. Zhang, H. J. Gao, and O. Kaynak, "Network-induced constraints in networked control systems—a survey," *IEEE Transactions on Industrial Informatics*, vol. 9, no. 1, pp. 403–416, 2013.
- [25] H. Liu, G. Xie, and L. Wang, "Necessary and sufficient conditions for solving consensus problems of double-integrator dynamics via sampled control," *International Journal of Robust and Nonlinear Control*, vol. 20, no. 15, pp. 1706–1722, 2010.
- [26] H. Su, X. Wang, and G. Chen, "Rendezvous of multiple mobile agents with preserved network connectivity," *Systems and Control Letters*, vol. 59, no. 5, pp. 313–322, 2010.

Research Article

An Improved Car-Following Model in Vehicle Networking Based on Network Control

D. Y. Kong¹ and H. Y. Xu²

¹ School of Automotive Studies, Tongji University, Shanghai 201804, China

² Sino-German College, Tongji University, Shanghai 201804, China

Correspondence should be addressed to H. Y. Xu; xuhaiyang630@163.com

Received 24 December 2013; Accepted 19 February 2014; Published 24 March 2014

Academic Editor: Huaicheng Yan

Copyright © 2014 D. Y. Kong and H. Y. Xu. This is an open access article distributed under the Creative Commons Attribution License, which permits unrestricted use, distribution, and reproduction in any medium, provided the original work is properly cited.

Vehicle networking is a system to realize information interoperability between vehicles and people, vehicles and roads, vehicles and vehicles, and cars and transport facilities, through the network information exchange, in order to achieve the effective monitoring of the vehicle and traffic flow. Realizing information interoperability between vehicles and vehicles, which can affect the traffic flow, is an important application of network control system (NCS). In this paper, a car-following model using vehicle networking theory is established, based on network control principle. The car-following model, which is an improvement of the traditional traffic model, describes the traffic in vehicle networking condition. The impact that vehicle networking has on the traffic flow is quantitatively assessed in a particular scene of one-way, no lane changing highway. The examples show that the capacity of the road is effectively enhanced by using vehicle networking.

1. Introduction

Network control system (NCS) is a closed-loop feedback control system through real-time network control [1–3]. NCS simplifies cabling system structure and improves the reliability of the system. It has successfully been applied in remote robot, which attracted the attention of many experts. Meanwhile, NCS has become a hotspot of international academic research and obtained a profound impact on the deep-sea robot operation, automobile manufacturing, automotive networking, aerospace industry, and so forth [4–7]. Vehicle networking is a system to realize information interoperability between vehicles and people, vehicles and roads, vehicles and vehicles, and cars and transport facilities, through the network information exchange, in order to achieve the effective monitoring of the vehicle and traffic flow. Realizing information interoperability between vehicles and vehicles, which can improve road capacity effectively and affect the traffic flow, is an important application of NCS.

In the domestic auto market, the Telematics system has been used in many commercial areas, such as Onstar from GM, Gbook from Toyota, InkaNet from SAIC Motor [8].

These systems may not be perfect, but they basically have the following features: voice navigation system of whole journey, safety services, security services, remote diagnostics, information services, and multimedia entertainment services [9]. These systems play an important role in the emergency information announcement, real-time traffic monitoring, avoidance of traffic accidents, and other aspects [10]. These vehicle systems focus primarily on the information exchange between the car and the call center and have not realized the real-time interoperability communication between vehicles and vehicles, vehicles and road, and vehicles and infrastructure; therefore they are not in the true sense of vehicle networking. The essence of vehicle networking is actually to improve traffic efficiency and avoid accidents through aided driving, automatic collaboration driving, traffic information collection, and so forth [10]. In addition, vehicle networking can also save fuel and reduce carbon dioxide emissions, because there would be no need for drivers to wait for the traffic light under vehicle networking [11]. However, the related researches on vehicle networking are only in its infancy in China, staying in the small-scale closed-loop system. Although some achievements have been achieved,

there are many thorny issues still need to be resolved to reach the target of establishing a large-scale open-loop cross domain application system [12].

As the core technology of vehicle networking, VANET provides an efficient platform for information sharing and technical support and guarantees for the intelligent transportation systems and the large-scale implementation of vehicle networking [13]. With the development of communication technology in recent years, the research about VANET has also been deepening. But few quantitative studies have been done regarding the impact of vehicle networking on traffic capacity. Moreover, the applications of vehicle networking will significantly change the traffic situation and result in the inapplicability of the traditional car-following model.

In this paper, recent developments of network communication and control technology in the vehicle networking field are summarized, the car-following model based on network control is established, and the impact of vehicle networking on traffic capacity is assessed by quantitative study.

2. Network Communication and Control Technology in the Vehicle Networking Field

In recent years, communications protocols, control mechanisms, algorithms, and dynamic VANET technology have obtained certain research results in network communications of vehicle networking [14–17]. The application of the advanced communications technology will make the traffic environment safer, more efficient, and more intelligent.

In standards development and system testing platform fields, IEEE 802.11p promulgated in July 2010 formally formed the basic framework of the vehicle wireless communication protocols. IEEE 802.11p protocol is the promotion and expansion of IEEE 802.11 in the vehicle networking field and uses IEEE1609 series of protocols as the upper layer protocol. It mainly stipulates the standard of media access control layer (MAC) and physical layer (PHY) in IEEE 802.11p [12]. During that period, more than one test platform was built to validate and test the relative theory, such as Wireless MESH Network Test of the University of Illinois Urbana Champaign Bench, System Test Platform of UCLA, and WAVE System Channel Test Platform of the University of Michigan [18–20].

At the present stage, the research hotspot of VANET is centralized in the following parts based on WAVE protocol (IEEE 802.11p): the application of multichannel coordination in vehicle communication; multicast routing management; and the switching of fixed relay technology and the resource scheduling based on WiMAX protocol (IEEE 802.16). The application of WiMAX technology in vehicle communication networking, which means provide vehicle-mounted broadband wireless access for vehicle and the users inside by using technology based on WiMAX, can overcome some certain weakness of 802.11 protocol, such as small scale coverage, switching the roadside units frequently during the movement of the vehicle, the weakness of quality of service (QOS) support [21, 22]. So the IEEE 802.16 standards development groups want to use the vehicle-mounted MRS site which

provides broadband wireless access service for user terminal groups in the car [23].

To ensure the safety application of QOS (Quality of Service), [24] proposes that multichannel media access control (MAC) mechanism can be used, which means the communication can be achieved using different channels between nodes, so as to get better network throughput volume and delay characteristics than single channel. Location-based multicast routing will also appear, because the original agreement of routing mechanism in WAVE protocol is not entirely suitable to dynamic changing topology of vehicle-mounted communication network. In these routing protocols, the delay correspondingly increases with the increasing in the number of communication hops and speed of vehicle speed [25, 26]. In [27], to improve multicast routing mechanism, vehicle networking is organized into multiple peer units (cluster), thereby improving scalability mobile environment.

The information communication, that is between vehicles and infrastructure when in high-speed, is becoming another research hotspot. The scheduling mechanism based on two-stage fixed relay can improve system throughput, reduce packet loss rate, and reduce delay time [28]. Besides, some scholars proposed the multihop cellular relay auxiliary switching technology and the group switching technology based on MRS, to guarantee channel QoS indicators and to reduce switching blocking rate and switching delay [29–31]. These theories provide solutions to information exchange process with road side infrastructure for vehicles traveling at high speed.

Currently, there are some research findings on dynamic self-organization, most of which centralize in self-organizing network routing algorithm technology. But the limitation is that most of them remain in the small-scale closed-loop system and do not consider building demand networking with the change of demand and environmental resiliency under the large-scale network environment, which can meet the current task demand [12].

Reference [32], based on the characteristics and research status of VANET analysis, proposes the multidimensional theoretical models and network architecture of VANET; discusses the focal and difficult points of physical layer and related standards, MAC layer and network layer protocol design; explains the broadcast protocol design ideas. Reference [33] proposes a new dynamic distribution perceptual data dissemination system based on Publish-Subscribe for VANET and proposes Notify the Token Mechanism based on the mobility of vehicles. Only token holders can broadcast information to around subscribers. In addition, other scholars have proposed a variety of algorithms to achieve the effective operation of VANET, such as the structure of the basic topology of distributed algorithms, cluster-based routing algorithm method, content-based routing, and dissemination of technology new network architecture [34–36]. Reference [37] suggests that percolation theory can be used to analyze the VANET connection. The study found that there is a quantitative relationship between the vehicle density and transmission distance in the network connection. When the vehicle density or transmission range is large enough, there is a jump of a network connection. This result has

important implications for the development of real-world VANET: this theorem can be used to calculate the minimum transmission range of a reliable network connection to the certain density of vehicles given the vehicle density. Reference [38] constructs a dynamic traffic information system by using a variety of algorithms, such as traffic information collection and traffic incident detection synergy algorithm based on VANET, distributed organization and real-time processing methods of large-scale mass traffic information, location-based traffic information distribution protocol, and so forth, which can realize the improvement of event detection accuracy and instantaneity in traffic information system and promotion large-scale real-time traffic information processing. Reference [39] introduces the history, characteristics, and application areas of VANET, discusses the advantages and disadvantages of various wireless communication technologies for VANET using analysis and comparison methods. Reference [40] summarizes the current model of simulating vehicle networking simulation including Flow Model of Motorway (FMM), Manhattan Flow Model (MMM), and the random waypoint mobility model and builds a random waypoint model and evaluates its effectiveness through software. Reference [41] classifies the existing VANET simulator and describes and compares several typical emulators.

3. Establishment of Vehicle Networking Car-Following Model

In the circumstance that the vehicle networking has been built perfectly, that is, VANET has been completed constructed, real-time communication between vehicles and vehicles can be achieved. In the transportation system, one car can transmit driving parameter packages to the surrounding vehicles at high frequency. The surrounding vehicles can receive the data packages at a high reception rate and low delay time and then get the driving state of the car, so that the surrounding vehicles can take appropriate measures. Through the above steps, it is possible to drive unmanned, thus effectively reducing distance between vehicles, reducing traffic accidents, and improving transportation efficiency.

In the context, the traditional classical transport theory will not be all applicable to vehicle networking system as the applicable conditions change. The classical car-following model needs to be improved so as to describe the transportation state based on vehicle networking.

3.1. Basic Assumption. In the model, the following basic assumptions are made.

- (1) *Vehicle automatic mode.* In the fleet, all vehicles take autopilot mode. That is, when the information is received from the leading vehicle, following vehicles can automatically take appropriate measures. Thus, the reaction time of human can be ignored. This is easy to achieve in the background of vehicle networking.
- (2) *Information transmission without delay.* When the leading vehicle takes appropriate measures, it can

simultaneously transmit information to surrounding vehicles, and then other vehicles can receive information and immediately take appropriate measures. When the transmission frequency and the reception frequency are sufficiently high and the delay time is short enough, we can assume the delay time can be negligible in the model. In addition, in a small-scale fleet, that is to say there are a small number of vehicles, the time lag that the last car and the leading car take corresponding measures is less enough.

- (3) *Acceleration consistency.* All vehicles in fleet have the same maximum acceleration in braking and driving process.

3.2. Analysis about Driving Characteristics. In the vehicle networking, when vehicles have been compiled as fleet, vehicles are still in the nonfree-running state, but driving characteristics differ from the traditional classical theories. The driving characteristics of a car-following model in vehicle networking are as follows.

- (1) *Restriction.* In fleet, back cars closely follow the front cars, meeting “immediately followed” requirement. Meanwhile, the speed of back cars cannot be greater than the cars in front, only swing near the front cars in fleet. As the automotive control is electronic and accurate, swing amplitude is minimal and difference in speed is negligible, so the speed is quite suitable. This is the “speed conditions.” “Immediately followed” requirement, the equal speed and small distance constitute the restriction of the car-following model in vehicle networking.
- (2) *Without hysteretic.* The restriction characteristic above shows that the changes of driving condition of front vehicle lead to the changes of back vehicle. In vehicle networking condition, based on the assumption that vehicles take autopilot mode and no delay in information transmission, the driving condition of front and back vehicles changes to the same extent simultaneously, which means no reaction time.
- (3) *Transitivity.* Similar to the traditional model, the condition of the entire fleet will change when the driving condition of the leading car changes. The driving condition of 1st vehicle restricts the 2nd one; the 2nd one restricts the 3rd one and so on. Because there is no delay of delivery, the information is passed back along the fleet smoothly.

3.3. Description and Derivation. In vehicle networking, assuming the distance between leading vehicle and following vehicle in the car-following model is $s(t)$, the information delay time is T . Delay time T is calculated from the moment leading car brake to the moment following car taking brake measure. The speed of following car stays invariability in T . The relative position of two vehicles at the moment of t is shown in Figure 1. In Figure 1, n represents the leading car, and $n + 1$ represents the following car. At the moment of t ,

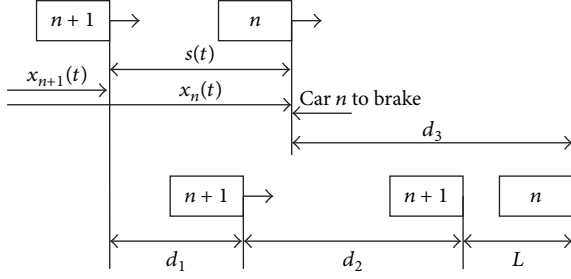


FIGURE 1: The relative position of two adjacent vehicles.

the leading car starts to brake; the relative position of the two vehicles at some time is shown in the lower half of Figure 1.

In this figure,

- L is the distance between head of two vehicles;
- d_1 is the distance vehicle $n+1$ traveled by the reaction time Δt ;
- d_2 is the distance vehicle $n+1$ traveled from brake;
- d_3 is the distance vehicle n traveled from brake.

Thus, at time t , the required distance of the front vehicle that suddenly stops without collision is

$$s(t) = x_n(t) - x_{n+1}(t) = d_1 + d_2 + L - d_3. \quad (1)$$

The speed of the vehicle is

$$v(t) = \frac{dx(t)}{dt} = \dot{x}(t). \quad (2)$$

The acceleration is

$$a(t) = \frac{d^2x(t)}{dt^2} = \ddot{x}(t). \quad (3)$$

Since $\dot{x}(t)$ is a finite and under the assumption that T approaches 0 then $d_1 \approx 0$:

$$s(t) = \frac{\dot{x}_{n+1}^2(t)}{2\ddot{x}_{n+1}(t)} + L - \frac{\dot{x}_n^2(t)}{2\ddot{x}_n(t)}. \quad (4)$$

As vehicles of the fleet have taken autopilot mode, the speed of each vehicle is same. The back vehicle will take brake with the same acceleration, when receiving the brake signal from front vehicle. Then

$$\dot{x}_{n+1}(t) = \dot{x}_n(t) \quad \ddot{x}_{n+1}(t) = \ddot{x}_n(t). \quad (5)$$

So

$$s(t) = L. \quad (6)$$

From the above calculation, we can see that the distance between front and back vehicles remain unchanged during the braking; that is, the distance is the same in travelling and after braking. Therefore, in the vehicle networking context, if all vehicles have the capabilities of communicating with others, the distance between leading and following vehicles can be infinitely small in car-following process.

TABLE 1: The main variables for the model application.

Variable	Meaning
v_{f1}	Ideal free flow speed in traditional conditions
v_{f2}	Ideal free flow speed in vehicle networking conditions
Q_{m2}	Road capacity in vehicle networking conditions
D_1	Average distance between vehicles in single lane, in traditional conditions, when reaching the blocking density. Unit: m
D_2	Average distance between vehicles in single lane, in vehicle networking conditions, when reaching the blocking density. Preceding analysis shows $D_2 \approx 0$
L	Average length of car (m)
K_{j1}	Traffic density maximum in traditional conditions, blocking density
K_{j2}	Maximum density in vehicle networking conditions, blocking density
Q_{m1}	Road capacity in traditional conditions

4. Model Application

This improved car-following model can be used to calculate the typical traffic scene road traffic capacity, thus assessing the influence of the vehicle networking to the traffic capacity in quantitative assessment.

Assuming that the vehicle fleet forms one-way traffic on a flat straight highway without considering overtaking, lane change, toll stations, and so forth, this paper uses traditional and improved linear car-following models, respectively, and analyzes two different scene traffic capacities. The main parameters are shown in Table 1.

4.1. In Traditional Conditions. In traditional situation, the equation to describe the relationship between traffic flow and density is as follows:

$$Q = v_f \left(K - \frac{K^2}{K_j} \right). \quad (7)$$

So, when $dQ/dK = 0$, Q gets the maximum, we can get

$$Q_m = \frac{1}{4} v_f K_j. \quad (8)$$

As we know $K_{j1} = 1000/(L + D_1)$.

So the road capacity can be describe as

$$Q_{m1} = \frac{250}{L + D_1} v_{f1}. \quad (9)$$

4.2. In Vehicle Networking Conditions. In vehicle networking conditions $Q = Kv$.

K and v have no necessary connection, so

$$Q_{m2} = v_{f2} K_{j2} \quad (10)$$

because of

$$K_{j2} = \frac{1000}{L + D_2} \approx \frac{1000}{L}. \quad (11)$$

So we can get

$$Q_{m2} = \frac{1000}{L} v_{f2}. \quad (12)$$

4.3. *Impact Assessment.* In conclusion, the effect of car networking on traffic capacity is

$$K = \frac{Q_{m2}}{Q_{m1}} = 4 \frac{L + D_1}{L} \cdot \frac{v_{f2}}{v_{f1}}. \quad (13)$$

On account of $v_{f2} \geq v_{f1}$, there is

$$K \geq 4 \cdot \frac{L + D_1}{L}. \quad (14)$$

From the analysis above, we can see that in the ideal state of no lane change highway, the role of vehicle networking will make the traffic capacity of roads improve $4 \cdot ((L + D_1)/L)$ times compared to the original.

On the highway, it is assumed that the distance between the high-speed cars is not less than 100 m, and the average car length is about 5 m. In an ideal condition, compared with the traditional conditions, vehicle networking will increase the maximum traffic flow of highway by more than 84 times and correspondingly improve the traffic capacity of road greatly.

This situation is mainly thanks to the following two reasons.

- (a) *Shortening of vehicle distance.* In vehicle networking condition, vehicles can establish a real-time communication and exchange information instantaneously. That allows vehicles to take the same measures almost at the same time without reaction time. The distance between vehicles can be shortened without loss in safety.
- (b) *No direct relevance between speed and density.* In the traditional conditions, velocity decreases with the increase of density. But in vehicle networking conditions, speed and density have no direct relationship. When the density is very high, the fleet can still run at the speed of free stream.

5. Conclusion

The core technology in realizing the information exchange of vehicle networking is the communication technology represented by network control technology. The development level of communication technology affects VANET application directly. A car-following model using vehicle networking theory is established, describing the traffic condition in vehicle networking condition. The impact that vehicle networking has on the traffic flow is quantitatively assessed in the particular scene of one-way, no lane changing highway. The examples show that the capacity of the road is effectively enhanced by using vehicle networking.

This paper provides a method to assess the impact of vehicle networking on the traffic flow quantitatively. But the amendment of the model in complex conditions, such as lane changing and steering, remains to be further studied.

Conflict of Interests

The authors declare that there is no conflict of interests regarding the publication of this paper.

Acknowledgment

The authors would like to acknowledge the support from The National Key Technology R&D Program of the Ministry of Science and Technology of China (Grant no. 2013BAG06B04).

References

- [1] W. Zhang, M. S. Branicky, and S. M. Phillips, "Stability of networked control systems," *IEEE Control Systems Magazine*, vol. 21, no. 1, pp. 84–97, 2001.
- [2] G. C. Walsh, H. Ye, and L. Bushnell, "Stability analysis of networked control systems," in *Proceedings of the American Control Conference (ACC '99)*, pp. 2876–2880, Institute of Electrical and Electronics Engineers Inc, San Diego, Calif, USA, June 1999.
- [3] G. C. Walsh and H. Ye, "Scheduling of networked control systems," *IEEE Control Systems Magazine*, vol. 21, no. 1, pp. 57–65, 2001.
- [4] C. Rhodes, M. Morari, L. S. Tsimring, and N. F. Rulkov, "Data-based control trajectory planning for nonlinear systems," *Physical Review E*, vol. 56, no. 3, pp. 2398–2406, 1997.
- [5] H. Zhang, H. Yan, F. Yang, and Q. Chen, "Quantized control design for impulsive fuzzy networked systems," *IEEE Transactions on Fuzzy Systems*, vol. 19, no. 6, pp. 1153–1162, 2011.
- [6] M. Arif, T. Ishihara, and H. Inooka, "Incorporation of experience in iterative learning controllers using locally weighted learning," *Automatica*, vol. 37, no. 6, pp. 881–888, 2001.
- [7] L. X. Zhang, H. J. Gao, and O. Kaynak, "Network-induced constraints in networked control systems—a survey," *IEEE Transactions on Industrial Informatics*, vol. 9, no. 1, pp. 403–416, 2013.
- [8] W. W. Hu, "The internet revolution of vehicles," *Business Value*, 2013.
- [9] J. Deng, L. P. Xia, L. H. Lu, and Z. W. Zhang, "Technical feasibility analysis of vehicle network in independent brand automobile," *Automobile Parts*, no. 2, pp. 56–58, 2012.
- [10] G. Cheng and D. Guo, "The current status and development of vehicle networking," *Mobile Communications*, no. 17, pp. 23–26, 2011.
- [11] T. Tielert, M. Killat, H. Hartenstein, R. Luz, S. Hausberger, and T. Benz, "The impact of traffic-light-to-vehicle communication on fuel consumption and emissions," in *Proceedings of the 2nd International Internet of Things Conference (IOT '10)*, December 2010.
- [12] J. J. Cheng and M. C. Zhou, "The third important information space: vehicle networking technology and application analysis," *Overseas Scholars*, 2012.
- [13] C. Chen, *Research on key issues VANET system security [Ph.D. thesis]*, Fudan University, 2011.
- [14] H. Gao, T. Chen, and J. Lam, "A new delay system approach to network-based control," *Automatica*, vol. 44, no. 1, pp. 39–52, 2008.
- [15] H. Yan, H. Shi, H. Zhang, and F. Yang, "Quantized H_∞ control for networked systems with communication constraints," *Asian Journal of Control*, vol. 15, no. 5, pp. 1468–1476, 2013.

- [16] H. Zhang, H. Yan, T. Liu, and Q. Chen, "Fuzzy controller design for nonlinear impulsive fuzzy systems with time delay," *IEEE Transactions on Fuzzy Systems*, vol. 19, no. 5, pp. 844–856, 2011.
- [17] H. Zhang, Q. Chen, H. Yan, and J. Liu, "Robust H_∞ filtering for switched stochastic system with missing measurements," *IEEE Transactions on Signal Processing*, vol. 57, no. 9, pp. 3466–3474, 2009.
- [18] T. Shen, *Experiments on a multichannel multi-interface wireless mesh network [M.S. thesis]*, University of Illinois at Urbana-Champaign, 2008.
- [19] G. Pau and A. Rowstron, *PVRP: Efficient Disruption Tolerant Discovery in Vehicular Ad Hoc Networks*, ACM MobiComm, 2009.
- [20] F. Q. Liu and L. H. Shan, "Vehicular heterogeneous networks architecture and key technologies," *ZTE Communications*, vol. 16, no. 3, pp. 47–51, 2010.
- [21] K. Yang, S. Ou, H.-H. Chen, and J. He, "A multihop peer-communication protocol with fairness guarantee for IEEE 802.16-based vehicular networks," *IEEE Transactions on Vehicular Technology*, vol. 56, no. 6, pp. 3358–3370, 2007.
- [22] L. Shan, F. Liu, and K. Yang, "Performance analysis of group handover scheme for IEEE 802.16j-enabled vehicular networks," in *Proceedings of the Joint International Conferences on Asia-Pacific Web Conference and Web-Age Information Management*, 2009.
- [23] IEEE C802.16j-D5, "Draft amendment for local and metropolitan area networks, Part 16: air interface for mobile broadband wireless systems multihop relay specification," 2008.
- [24] J. Crichigno, M.-Y. Wu, and W. Shu, "Protocols and architectures for channel assignment in wireless mesh networks," *Ad Hoc Networks*, vol. 6, no. 7, pp. 1051–1077, 2008.
- [25] C. Lochert, H. Hartenstein, J. Tian, H. Fussler, D. Hermann, and M. Mauve, "A routing strategy for vehicular ad hoc networks in city environments," in *Proceedings of the IEEE Intelligent Vehicles Symposium*, 2003.
- [26] G. Korkmaz, F. Özgüner, E. Ekici, and Ü. Özgüner, "Urban multi-hop broadcast protocol for inter-vehicle communication systems," in *Proceedings of the 1st ACM International Workshop on Vehicular Ad Hoc Networks (VANET '04)*, pp. 76–85, October 2004.
- [27] F. Li and Y. Wang, "Routing in vehicular ad hoc networks: a survey," *IEEE Vehicular Technology Magazine*, vol. 2, no. 2, pp. 12–22, 2007.
- [28] L. Wang, Y. Ji, and F. Liu, "Adaptive subframe partitioning and efficient packet scheduling in OFDMA cellular system with fixed decode-and-forward relays," *IEICE Transactions on Communications*, vol. E92-B, no. 3, pp. 755–765, 2009.
- [29] S. Jeon and S. Lee, "A relay-assisted handover technique with network coding over multihop cellular networks," *IEEE Communications Letters*, vol. 11, no. 3, pp. 252–254, 2007.
- [30] H. Yan, Z. Su, H. Zhang, and F. Yang, "Observer-based H_∞ control for discrete-time stochastic systems with quantisation and random communication delays," *IET Control Theory & Applications*, vol. 7, no. 3, pp. 372–379, 2013.
- [31] L. Shan, F. Liu, L. Wang, and Y. Ji, "Predictive group handover scheme with channel borrowing for mobile relay systems," in *Proceedings of the IEEE International Wireless Communications and Mobile Computing Conference (IWCMC '08)*, pp. 153–158, August 2008.
- [32] M. O. Cherif, S. M. Senouci, and B. Ducourthial, "Vehicular network self-organizing architectures," in *Proceedings of the 5th IEEE GCC Conference and Exhibition (GCC '09)*, March 2009.
- [33] L. Wu, M. Liu, X. Wang, and H. Gong, "Dynamic distribution-aware data dissemination for vehicular ad hoc networks," in *Proceedings of the 2nd International Conference on Future Computer and Communication (ICFCC '10)*, pp. V2353–V2360, May 2010.
- [34] A. Yair and M. Segal, "Near-optimal, reliable and self-organizing hierarchical topology in VANET," in *Proceedings of the 8th ACM International Workshop on Vehicular Inter-Networking*, September 2011.
- [35] D. Rajini Girinath and S. Selvan, "A novel cluster based routing algorithm for hybrid mobility model in VANET," *International Journal of Computer Applications*, vol. 1, no. 15, 2010.
- [36] G. Arnould, D. Khadraoui, and Z. Habbas, "A self-organizing content centric network model for hybrid vehicular Ad-Hoc networks," in *Proceedings of the 1st ACM International Symposium on Design and Analysis of Intelligent Vehicular Networks and Applications (DIVANet '11)*, pp. 15–22, November 2011.
- [37] X. Jin, W. Su, and Y. Wei, "A study of the VANET connectivity by percolation theory," in *Proceedings of the IEEE Consumer Communications and Networking Conference (CCNC '11)*, pp. 85–89, January 2011.
- [38] Y. Xiang, "Dynamic traffic data mining based on vehicular ad hoc networking," *ZTE Technology Journal*, vol. 17, no. 3, pp. 29–34, 2011.
- [39] C.-Y. Chang, Y. Xiang, and M.-L. Shi, "Development and status of vehicular ad hoc networks," *Journal on Communications*, vol. 28, no. 11, pp. 116–126, 2007.
- [40] V. D. Khairnar and S. N. Pradhan, "Mobility models for Vehicular Ad-hoc Network simulation," in *Proceedings of the IEEE Symposium on Computers and Informatics (ISCI '11)*, pp. 460–465, March 2011.
- [41] L. Xiao, R.-F. Li, and J. Luo, "Simulation of vehicular ad hoc networks: a survey," *Journal of System Simulation*, vol. 21, no. 17, pp. 5330–5356, 2009.

Research Article

Optimal Placement of Actors in WSNs Based on Imposed Delay Constraints

Chunxi Yang,¹ Xinyu Wu,¹ Jian Huang,² and Lingyun Huang³

¹ Faculty of Chemical Engineering, Kunming University of Science and Technology, Kunming 650500, China

² Department of Control Science and Engineering, Huazhong University of Science and Technology, Wuhan 430074, China

³ Faculty of Land Resource Engineering, Kunming University of Science and Technology, Kunming 650500, China

Correspondence should be addressed to Lingyun Huang; hly0510@126.com

Received 20 November 2013; Accepted 2 February 2014; Published 23 March 2014

Academic Editor: Huaicheng Yan

Copyright © 2014 Chunxi Yang et al. This is an open access article distributed under the Creative Commons Attribution License, which permits unrestricted use, distribution, and reproduction in any medium, provided the original work is properly cited.

Wireless Sensor and Actor Networks (WSANs) refer to a group of sensors and actors linked by wireless medium to probe environment and perform specific actions. Such certain actions should always be taken before a deadline when an event of interest is detected. In order to provide such services, the whole monitor area is divided into several virtual areas and nodes in the same area form a cluster. Clustering of the WSNs is often pursued to give that each actor acts as a cluster-head. The number of actors is related to the size and the deployment of WSNs cluster. In this paper, we find a method to determine the accurate number of actors which enables them to receive data and take actions in an imposed time-delay. The k -MinTE and the k -MaxTE clustering algorithm are proposed to form the minimum and maximum size of cluster, respectively. In those clustering algorithms, actors are deployed in such a way that sensors could route data to actors within k hops. Then, clusters are arranged by the regular hexagon. At last, we evaluate the placement of actors and results show that our approach is effective.

1. Introduction

Networked control systems (NCSs) have attracted a lot of interest for its low cost, reduced system wiring, simple system diagnosis, and maintenance [1–3]. As special NCSs, Wireless Sensor and Actor Networks (WSANs) [4] have started to attract growing interest from the research and engineering communities in recent years. WSNs can increase the effectiveness of numerous applications such as home automation, infrastructure health monitoring, intelligent buildings, and sewer management [5, 6]. Such networks employ a large quantity of miniaturized sensor nodes and a few number of actor nodes [7]. Sensor nodes are small and inexpensive, usually with limited power and limited data processing capabilities, while actor nodes are more capable nodes with relatively more onboard energy supply and richer computation and communication resources. Sensors probe their surroundings and report their detective parameters to the actor nodes, which process the collected sensor's reports and respond to emerging events of interest, shown in Figure 1.

Real-time requirement is one of the most important design goals in time critical applications. Certain actions should be taken quickly enough after sensors detect an event. However, a minimal transmission delay may not guarantee a valid data that meets certain applications' requirements. Some applications may impose a time deadline on sensed data to be delivered to an actor for timely acting [8]. For example in forest monitoring applications, actors such as robots need to be engaged in a short interval to control a fire accident and prevent it from spreading.

In order to fulfill the real-time requirement, the whole monitor area is divided into several virtual areas and nodes in the same area form a cluster [9]. Clustering of the WSNs is often pursued to give that each actor act as a cluster-head and takes certain actions based on the received information from the sensors within its cluster [3, 10]. The larger areas a cluster of WSNs covers, the more hops that sensed data need to pass through correspondingly. In the case of that, the end-to-end delay and action time would be extended.

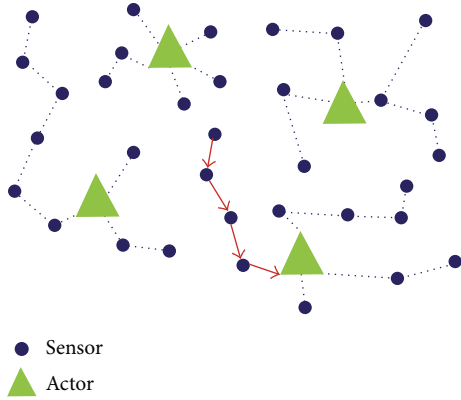


FIGURE 1: A wireless sensor and actor network.

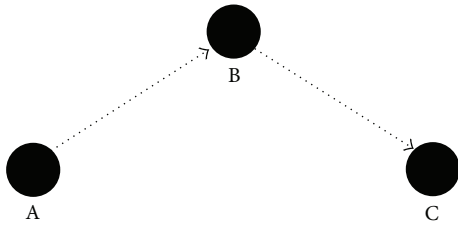


FIGURE 2: MTE routing path.

In this paper, we find a method to determine the accurate number of actors needed to cover the monitoring area where they receive data and take actions in an imposed time-delay. The number of actors is related to the size and the deployment of WSANs clusters. Different clustering algorithms lead to the different clusters' size. Based on the classical MTE routing protocol [11], we propose a k -MinTE clustering algorithm to minimize the size of cluster, while a k -MaxTE clustering algorithm is presented to maximize the size of clusters in WSANs. By statistical analysis of simulation experiments, we determine both maximum and minimum size of WSANs clustered by both clustering algorithms. According to the size of WSANs clusters, the minimal number of actors needed in both algorithms can be determined.

This paper is organized as follows. Section 2 summarizes the related work and distinguishes our work from the previous studies. In Section 3 we provide system modeling and problem description. Section 4 presents the details of k -MinTE and k -MaxTE clustering algorithm. The simulation of the approach is in Section 5. Section 6 concludes the paper with a summary.

2. Related Work

2.1. Maximum Allowable Response Time. In [12], it revealed the relationship between the maximum acceptable response time for actors and the number of hops that collected data

passed through. The maximum acceptable response time R_{\max} can be described by

$$R_{\max} = \sum_{i=1}^{N_h} T_{i,i+1} + T_h \times (N_h + 1) + T_a, \quad (1)$$

where $T_{i,i+1}$ is the time cost in transmitting or receiving data by any corresponding couple of hops i and $i + 1$. T_h is the time spent in each node for data process and congestion, including actor node. N_h is the number of hops from the source sensor to the destination actor. T_a is the time to initiate the first action by the destination actor. It is assumed that each cluster's coverage is equal in our context; we regard T_a as the maximum acting time from center to the edge.

In the application of WSANs, it is usually given an imposed delay which could be regarded as the maximum acceptable response time. Thus, according to (1), the maximum hops between sensor and actor in a cluster could be determined. Therefore, information delivered to an actor could be guaranteed to meet the delay constraints.

2.2. Regular Hexagonal Node Coverage Model. Recently, there has been a lot of works to improve the coverage of WSANs through intelligent actor deployment. The main idea in [10] is to apply repelling forces among neighboring actors, similar to molecular particles in Physics. Their actor deployment algorithm is based on triangular grid, which means that uncovered areas still exist.

The work in [13] presented a Distributed Actor Deployment Algorithm for Maximum Coverage (DA²MC), which divides the monitored area into several virtual regular hexagon areas and nodes in each regular hexagon area form a cluster. Actors are also selected as cluster-heads. They proved that regular hexagonal node coverage model can reach maximum coverage without uncovered areas. Because the overlaps between clusters are minimum, DA²MC covers the area with the least actors deployed. However, they regarded actor's radio range as the radius of circle. Actors may not be guaranteed to take actions in an imposed deadline, since the action range (cluster's size) is always smaller than radio range.

Considering these situations, we focus on determining the cluster's size in WSANs which could guarantee the end-to-end delay within an acceptable span (Figure 11).

2.3. MTE Routing Protocol. The main idea of minimum transmission energy (MTE) protocol is to minimize the transmit amplifier energy. Routes from each sensor to the actors are chosen such that each sensor's next-hop neighbor is the closest node that is in the direction of the actors [11]. In this case, node A would transmit a message through node B to node C, shown in Figure 2.

Since each sensor chooses the closest node to route data, the size of cluster formed by MTE protocol is minimum. However, since the MTE protocol could not guarantee to meet delay requirement, we present a k -MinTE clustering algorithm which minimizes the size of WSANs cluster and enables data route to actors within k hops to meet the delay constraints at the same time. Corresponding to the k -MinTE

***k*-MinTE clustering algorithm**

```

// for each actor I perform the following
(1) Broadcast message ("cluster-head I", "location  $I(x, y)$ ") within its cluster

// for each sensor j in the cluster I perform the following
(2) Receive message from cluster-head I
(3) Calculate the distance to the cluster-head  $D-I-j$ 
(4) Broadcast message ("sensor j", "distance  $D-I-j$ ", "hops  $H-j$ ") within the cluster I
(5) Receive message from neighbors
(6) Generate a maximum acceptable hop k
(7) while  $D-I-j <$  sensor's radio range R
(8)   then connect to the actor I directly
(9)     hops  $H-j = H-j + 1$ 
(10) while  $D-I-j \geq$  sensor's radio range R
(11)   then find a minimum distance  $D-j-z$  to sensor z
(12)     if  $D-j-z < R$  and  $H-z > 0$  and  $H-z < k$ 
(13)       then connect to the sensor z

```

ALGORITHM 1: The *k*-MinTE clustering algorithm pseudocode.***k*-MaxTE clustering algorithm**

```

// for each actor I perform the following
(1) Broadcast message ("cluster-head I", "location  $I(x, y)$ ") within its cluster

// for each sensor j in the cluster I perform the following
(2) Receive message from cluster-head I
(3) Calculate the distance to the cluster-head  $D-I-j$ 
(4) Broadcast message ("sensor j", "distance  $D-I-j$ ", "hops  $H-j$ ") within the cluster I
(5) Receive message from neighbors
(6) Generate a maximum acceptable hop k
(7) while  $D-I-j <$  sensor's radio range R
(8)   then connect to the actor I directly
(9)     hops  $H-j = H-j + 1$ 
(10) while  $D-I-j \geq$  sensor's radio range R
(11)   then find a maximum distance  $D-j-z$  to sensor z
(12)     if  $D-j-z < R$  and  $H-z > 0$  and  $H-z < k$ 
(13)       then connect to the sensor z

```

ALGORITHM 2: The *k*-MaxTE clustering algorithm pseudocode.

algorithm, a *k*-MaxTE clustering algorithm is presented to maximize the size of WSANs clusters.

3. System Modeling and Problem Description

3.1. Network Initialization. We assume that a set of sensors are spread randomly throughout a field of interest. All the sensor nodes are homogeneous and stationary, which is typical for WSANs.

The actors will be placed in the same area to collect information from sensors and take necessary actions based on received information. It is assumed that actors cannot sense information and can only take actions based on sensors' information. We also divide the monitored area into several virtual regular hexagon areas and nodes in each regular hexagon area form a cluster. The range of a cluster is a limited circle circumscribed about the regular hexagon and assumed to be equal. Finally we assume that both the sensors and

actors know their locations through mechanisms like GPS or other means.

3.2. Problem Description. We define the problem as follows. "Given a set of abundant sensors initially deployed randomly in an area of interest and an unknown number of actors, we are interested in determining the minimum number of actor nodes and the maximum cluster size of WSANs such that transformed time delay could be limited in an imposed period and actors can cover the whole area without uncovered areas."

4. *K*-MinTE and *k*-MaxTE Clustering Algorithm

4.1. Description of *k*-MinTE Clustering Algorithm. We also divide the monitored area into several virtual regular hexagon

areas and actors are placed in the center of each regular hexagon as cluster-heads.

Based on the MTE routing protocol, we present a k -MinTE clustering algorithm. Here, the parameter k shows the number of hops for a sensor to reach its dominator and thus its cluster-head. If k is infinity, the k -MinTE becomes classic MTE algorithm. While k is a certain positive integer, the cluster will be formed such that a sensor reaches its actor within k hops routes. The main idea is that each sensor connects its closest next-hop neighbor, while the route from sensors to the actor is guaranteed within k hops. The completing k -MinTE clustering algorithm pseudocode is given in Algorithm 1.

As shown in line 1, each actor in the area broadcast a CLUSTER-HEAD and LOCATION message within its action range. Then sensors wait to receive the message from cluster-head within its cluster at line 2. In lines 3–5, sensors would calculate the distance away from cluster-head and transmit the message to neighbors. Based on the information of sensors, the nodes begin to connect with each other.

Lines 6–16 are the procedure for a sensor to choose a route. A sensor would choose its closest neighbor and route its data to the actor within k hops. If the route is more than k hops, the sensor would choose another neighbor until fulfilling the requirement.

4.2. Description of k -MaxTE Clustering Algorithm. Differed from the k -MinTE algorithm, a k -MaxTE clustering algorithm is presented to maximize the size of cluster. Here, the parameter k is also the number of hops for a sensor to reach its cluster-head. The main idea is that each sensor connects its next-hop neighbor within its communication span which has the shortest path to actor node, while the route from sensors to the actor is guaranteed within k hops. The complete k -MaxTE clustering algorithm pseudocode is given in Algorithm 2.

Remark 1. In k -MaxTE algorithm, if we adopt that each sensor connects with its farthest next-hop neighbor, the phenomenon that some nodes connect with its farthest next-hop node instead of connecting to actor directly happened. As a result, the given hop k with largest communication radius cannot be found.

Remark 2. k -MinTE algorithm and k -MaxTE algorithm have the minimum radius and the maximum radius of cluster unit, respectively, in all clustering algorithms. Consequently, these two radiuses can be looked as boundary conditions in clustering algorithms design.

5. Experimental Evaluation

5.1. Determination of the Cluster's Size. Since the sizes of all the clusters are equal, we only need to determine one cluster's size so that it could be applied to other clusters. We would determine a cluster's size by the following steps.

- (1) Deploy a number of sensors in a big enough circle area and put an actor which acts as cluster-head in the

TABLE 1: The relative parameters.

Maximum acceptable response time R_{\max}	10 s
Action time T_a	5 s
Receiving and transmitting time T_h	1 s
Computation time $T_{i,i+1}$	1 s

center of the circle. Then, cluster nodes naturally by running k -MinTE and k -MaxTE algorithms, respectively, in which k is set to be large enough. This step is to form a big cluster with enough hops.

- (2) Record the distribution of each hop's range with radius in the cluster.
- (3) Set k to a certain positive integer and run both clustering algorithms in a circle with the radius of k hops nodes. Sensors would be isolated if they cannot reach actors within k hops. This step is to form a k -hop cluster.
- (4) Deduce the cluster's range gradually and search a radius in which sensors of certain hop could be sufficiently included.
- (5) Simulate the deployment of WSNs cluster with the radius founded and thus determine the number of actors.

5.2. Simulation Results. According to (1) and the assumed values listed in Table 1, we have

$$10 = \sum_{i=1}^{N_h} 1 + 1 \times (N_h + 1) + 5. \quad (2)$$

The number of hops is $N_h = 2$. We take the clusters run by 2-MinTE and 2-MaxTE algorithm as an example to determine its size. Both clustering algorithms are realized under a visualized emulator wrote by MATLAB.

At first, 500 sensors nodes are placed randomly in a big circle area where radius is 50 meters and an actor is placed in the center. It is set that the communication range of sensors is 10 m. The nodes form a cluster naturally by running the k -MinTE and k -MaxTE clustering algorithm, respectively, in which k is set to be large enough in this case, as shown in Figures 3 and 4.

Remark 3. It can be seen from Figures 3 and 4 that nodes choose the nearest neighbor to cluster in k -MinTE algorithm, while nodes link next-hop neighbor which is as far as possible in k -MaxTE algorithm. Therefore, the number of hops from the same source sensor to cluster-head using k -MaxTE algorithm is much less than that of using k -MinTE algorithm.

Remark 4. If we define a side where a sensor is connected with its neighbor as degree 1, then the number of sensors with bigger degree using k -MaxTE algorithm is much more than those of k -MinTE algorithm. As a result, the life-time of WSNs created by k -MaxTE algorithm becomes much shorter than that of using k -MinTE algorithm.

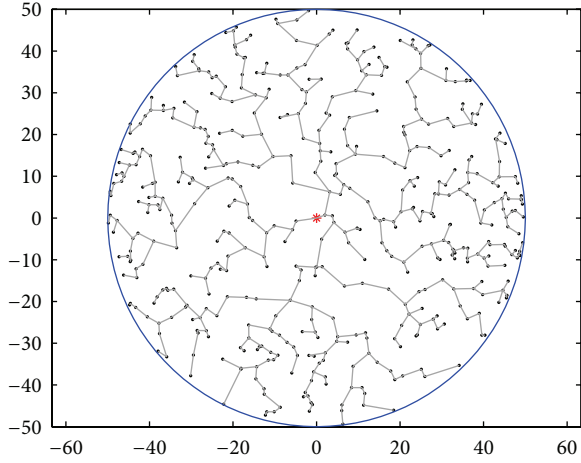


FIGURE 3: A cluster formed by running the k -MinTE algorithm.

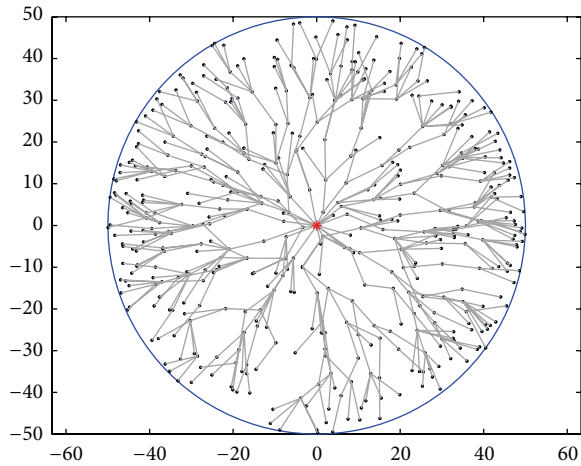


FIGURE 4: A cluster formed by running the k -MaxTE algorithm.

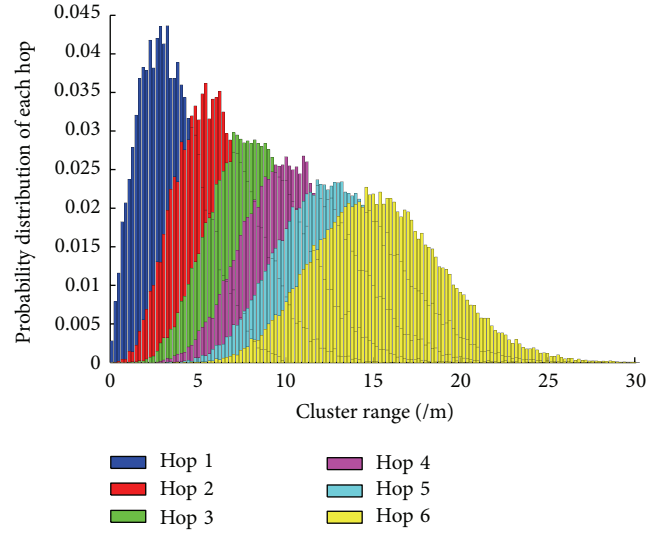


FIGURE 5: The hop's range distribution in k -MinTE algorithm.

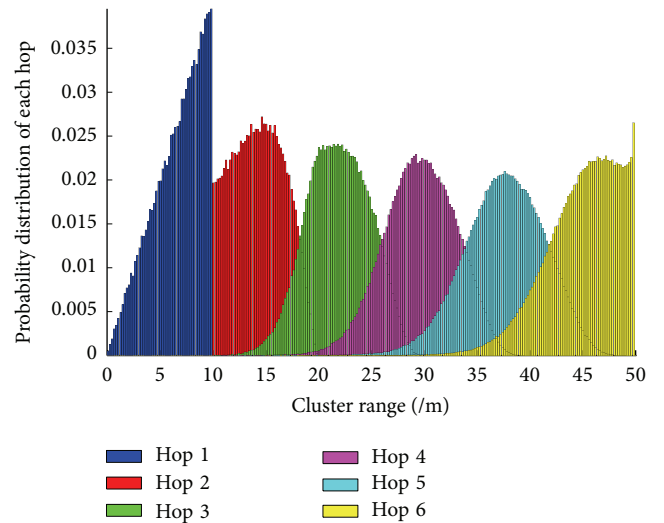


FIGURE 6: The hop's range distribution in k -MaxTE algorithm.

We record each hop's range distribution in the cluster with radius in Figures 5 and 6. Different color stands for different number of hops. From the bar chart Figure 5, it could be seen that the radius of hop 2 range approximately from 0.4 m to 15 m in k -MinTE algorithm. And in Figure 6, it shows that the radius of hop 2 in k -MaxTE algorithm ranges from about 10 m to 20 m.

The range of cluster is searched that 2-hop sensors could be sufficiently included. Figure 7 shows the distribution of the sensors with 2-hop in k -MinTE and k -MaxTE clustering algorithm. It can be seen that, with radius increased in both algorithms, the number of 2-hop sensors is decreasing. 90% of sensors in 2-hop clustered by k -MinTE are deployed within an approximate range of 4 m, while less than 10% deploy within 10 m. And in k -MaxTE clustering algorithm, the percentage of sensors is decreasing from nearly 90% in

15 m to 0% in 20 m. We would have searched the accurate clusters' radius in the dramatically changed ranges that the 2-hop sensors could be sufficiently included.

The radius is reduced gradually to determine this accurate range by running 2-MinTE and 2-MaxTE algorithm. Some sensors would be isolated if they cannot reach actors within 2 hops. We observe that nearly 97% of 2-MinTE clustered sensors clustered in the radius of nearly 5 m and 99% of sensors were included in 4 m as seen in Figure 8. In Figure 9, it can be seen that about 97% of 2-MaxTE clustered sensors clustered in the radius of nearly 16 m and more than 95% of sensors deployed in 16.5 m.

Finally, we simulate the placement of WSANs with the clusters' radius where 97% of sensors can be included in. In the experiment of 2-MinTE clustering algorithm, the area of

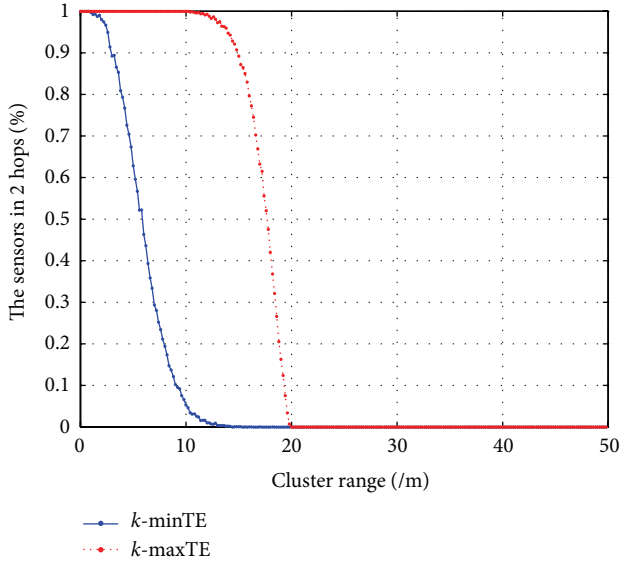


FIGURE 7: The distribution of sensors in 2 Hops.

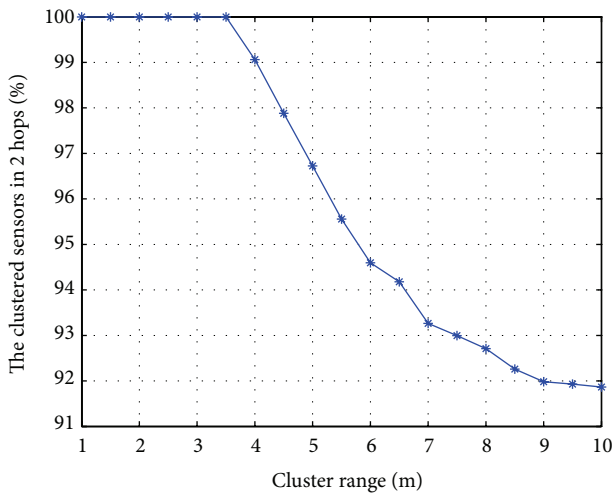


FIGURE 8: The distribution of sensors in 2 hops by 2-MinTE.

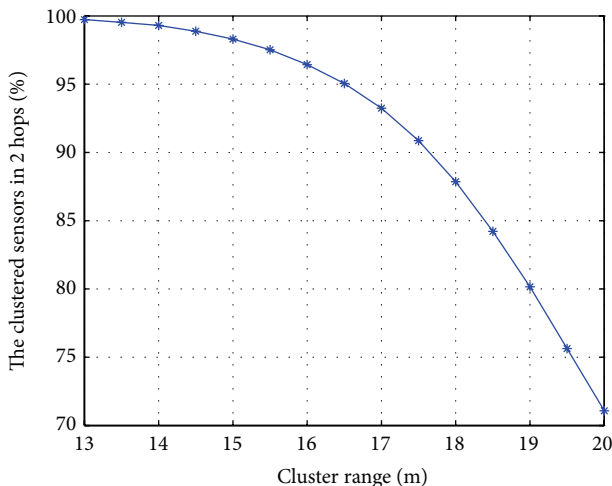


FIGURE 9: The distribution of sensors in 2 hops by 2-MaxTE.

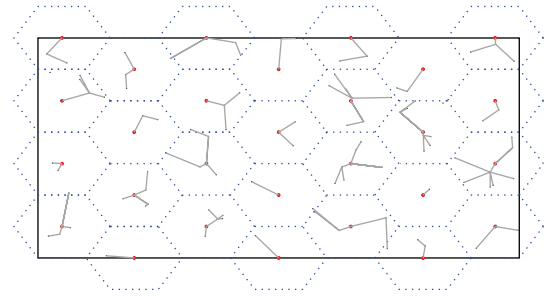


FIGURE 10: WSANs clustered by 2-MinTE.

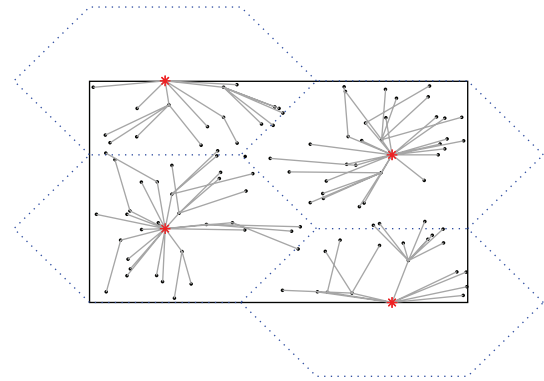


FIGURE 11: WSANs clustered by 2-MaxTE.

a rectangle is $50 \times 30 \text{ m}^2$, and 95 nodes of the same density as before are randomly deployed. Since the radius range of the WSANs cluster determined above is 5 m, the whole area is divided into 28 regular six hexagons correspondingly and thus 28 actors are deployed shown in Figure 10. The result shows that above 97.8% of sensors are clustered, which means more than 97.8% of sensors could reach actors in 2 hops. In the simulation of 2-MaxTE clustering algorithm, the area is $40 \times 41.5 \text{ m}^2$, and 105 nodes of the same density as before are randomly deployed. The cluster's radius is 16 m determined above and thus the whole area is divided into 4 six hexagons. The simulation result shows that about 99.05% of sensors are clustered.

Tables 2 and 3 show the relationship between the minimal number of actors needed and the density of sensors clustered by 2-MinTE and 2-MaxTE clustering algorithms. Table 2 illustrates the minimal number of actors needed to cover the $50 \times 30 \text{ m}^2$ area in different density of sensors clustered by 2-MinTE algorithm. It can be clearly seen that more actors are needed when the density of sensors is increasing, while Table 3 presents that less actors are needed in 2-MaxTE algorithm when the density of sensors is increasing in the area of $135 \times 110 \text{ m}^2$.

6. Conclusion

WSANs are gaining more and more interests in numerous fields. Actors need to collect sensor's data and take certain actions in an imposed deadline to perform tasks. According

TABLE 2: The minimal number of actors in different density in 2-MinTE.

The density of sensors in 2-MinTE algorithm (/m ²)	The minimal number of actors
0.05	21
0.10	45
0.15	55
0.20	78
0.25	91
0.30	97
0.35	105
0.40	136
0.45	161
0.50	180

TABLE 3: The minimal number of actors in different density in 2-MaxTE.

The density of sensors in 2-MaxTE algorithm (/m ²)	The minimal number of actors
0.025	35
0.050	30
0.075	27
0.100	27
0.125	24
0.150	24

to the relationship of maximum imposed response time and the number of hops between the source sensor and the destination actor, we turn to search the maximum size of WSANs cluster with certain hops. Based on the size of WSANs cluster determined by k -MaxTE and k -MinTE algorithm, the minimum number of actors could be determined. At last, the simulation results prove that our approach is effective.

Conflict of Interests

The authors declare that there is no conflict of interests regarding the publication of this paper.

Acknowledgments

This work is supported by National Natural Science Foundation (NNSF) of China under Grants 61004033 and 61364002 and 2012 Jin Chuan school-enterprise cooperation.

References

- [1] W. Zhang, M. S. Branicky, and S. M. Phillips, "Stability of networked control systems," *IEEE Control Systems Magazine*, vol. 21, no. 1, pp. 84–97, 2001.
- [2] L. X. Zhang, H. J. Gao, and O. Kaynak, "Network-induced constraints in networked control systems—a survey," *IEEE Transactions on Industrial Informatics*, vol. 9, no. 1, pp. 403–416, 2013.
- [3] H. Zhang, H. C. Yan, F. W. Yang, and Q. J. Chen, "Quantized control design for impulsive fuzzy networked systems," *IEEE Transactions on Fuzzy Systems*, vol. 19, no. 6, pp. 1153–1162, 2011.
- [4] I. F. Akyildiz and I. H. Kasimoglu, "Wireless sensor and actor networks: research challenges," *Ad Hoc Networks*, vol. 2, no. 4, pp. 351–367, 2004.
- [5] H. Salarian, K. Chin, and F. Naghdy, "Coordination in wireless sensor-actuator networks: a survey," *Journal of Parallel and Distributed Computing*, vol. 72, pp. 856–867, 2012.
- [6] I. F. Akyildiz, W. Su, Y. Sankarasubramaniam, and E. Cayirci, "A survey on sensor networks," *IEEE Communications Magazine*, vol. 40, no. 8, pp. 102–114, 2002.
- [7] C. Yang, X. Wu, C. Li, and J. Huang, "Dynamic characters of a distributed fusion algorithm in wireless sensor and actor networks," in *Proceedings of the 31st Chinese Control Conference*, pp. 26–28, Hefei, China, 2012.
- [8] K. Akkaya, F. Senel, and B. McLaughlan, "Clustering of wireless sensor and actor networks based on sensor distribution and connectivity," *Journal of Parallel and Distributed Computing*, vol. 69, no. 6, pp. 573–587, 2009.
- [9] X. Ren and Z. Cai, "A distributed actor deployment algorithm for maximum connected coverage in WSAN," in *Proceedings of the 5th International Conference on Natural Computation (ICNC '09)*, pp. 283–287, Tianjin, China, 2009.
- [10] K. Akkaya and S. Janapala, "Maximizing connected coverage via controlled actor relocation in wireless sensor and actor networks," *Computer Networks*, vol. 52, no. 14, pp. 2779–2796, 2008.
- [11] W. R. Heinzelman, A. Chandrakasan, and H. Balakrishnan, "Energy-efficient communication protocol for wireless microsensor networks," in *Proceedings of the 33rd Annual Hawaii International Conference on System Sciences (HICSS '33)*, Honolulu, Hawaii, USA, 2000.
- [12] M. H. Alaiwy, F. H. Alaiwy, and S. Habib, "Optimization of actors placement within wireless sensor-actor networks," in *Proceedings of the 12th IEEE International Symposium on Computers and Communications (ISCC '07)*, pp. 179–184, Aveiro, Portugal, 2007.
- [13] K. Akkaya and M. Younis, "Coverage and delay aware actor placement mechanisms for wireless sensor and actor networks," *International Journal of Sensor Networks*, vol. 3, pp. 152–164, 2008.

Research Article

Design of Attitude Control System for UAV Based on Feedback Linearization and Adaptive Control

Wenya Zhou,^{1,2} Kuilong Yin,² Rui Wang,^{1,2} and Yue-E Wang³

¹ State Key Laboratory of Structural Analysis for Industrial Equipment, Dalian University of Technology, Dalian 116023, China

² School of Aeronautics and Astronautics, Dalian University of Technology, Dalian 116023, China

³ College of Mathematics and Information Science, Shanxi Normal University, Xi'an 710062, China

Correspondence should be addressed to Wenya Zhou; zwy@dlut.edu.cn

Received 6 January 2014; Accepted 9 February 2014; Published 20 March 2014

Academic Editor: Huaicheng Yan

Copyright © 2014 Wenya Zhou et al. This is an open access article distributed under the Creative Commons Attribution License, which permits unrestricted use, distribution, and reproduction in any medium, provided the original work is properly cited.

Attitude dynamic model of unmanned aerial vehicles (UAVs) is multi-input multioutput (MIMO), strong coupling, and nonlinear. Model uncertainties and external gust disturbances should be considered during designing the attitude control system for UAVs. In this paper, feedback linearization and model reference adaptive control (MRAC) are integrated to design the attitude control system for a fixed wing UAV. First of all, the complicated attitude dynamic model is decoupled into three single-input single-output (SISO) channels by input-output feedback linearization. Secondly, the reference models are determined, respectively, according to the performance indexes of each channel. Subsequently, the adaptive control law is obtained using MRAC theory. In order to demonstrate the performance of attitude control system, the adaptive control law and the proportional-integral-derivative (PID) control law are, respectively, used in the coupling nonlinear simulation model. Simulation results indicate that the system performance indexes including maximum overshoot, settling time (2% error range), and rise time obtained by MRAC are better than those by PID. Moreover, MRAC system has stronger robustness with respect to the model uncertainties and gust disturbance.

1. Introduction

The applications of unmanned aerial vehicles (UAVs) have dramatically extended in both military and civilian fields around the world in the last twenty years. UAVs are used currently in all branches of military ranging from investigation, monitoring, intelligence gathering, and battlefield damage assessment to force support. Civilian applications include remote sensing, transport, exploration, and scientific research. Because of the diversified mission in the aviation field, UAVs play a more and more important role.

The attitude dynamic model of UAVs is nonlinear and three attitude channels are coupled. Nonlinearity and coupling dynamic characteristics will become more disturbing under flight condition with big angle of attack so that more obstacles will be brought during the design of attitude control system for UAVs.

In recent years, some advanced control theories are gradually introduced into the design of attitude control system

for UAVs with the development of computer technology [1–17]. In [1], the output feedback control method was used to design the attitude control system for UAV. An observer was designed to estimate the states online. In [2], in order to provide a basis for comparison with more sophisticated nonlinear designs, a PID controller with feedforward gravity compensation was derived using a small helicopter model and tested experimentally. In [3], a roll-channel fractional order proportional integral (PI^λ) flight controller for a small fixed-wing UAV was designed and time domain system identification methods are used to obtain the roll-channel model. In [4], a second-order sliding structure with a second-order sliding mode including a high-order sliding mode observer for the estimation of the uncertain sliding surfaces was selected to develop an integrated guidance and autopilot scheme. In [5], the fuzzy sliding mode control based on the multiobjective genetic algorithm was proposed to design the altitude autopilot of UAV. In [6], the attitude tracking system was designed for a small quad rotor UAV through model

reference adaptive control method. In [7], to control the position of UAV in three dimensions, altitude and longitude-latitude location, an adaptive neurofuzzy inference system was developed by adjusting the pitch angle, the roll angle, and the throttle position. In [8], an L_1 adaptive controller as autopilot inner loop controller candidate was designed and tested based on piecewise constant adaptive laws. Navigation outer loop parameters are regulated via PID control. The main contribution of this study is to demonstrate that the proposed control design can stabilize the nonlinear system. In [9], an altitude hold mode autopilot for UAV which is nonminimum phase was designed by combination of classic controller as the principal section of autopilot and the fuzzy logic controller to increase the robustness. The multiobjective genetic algorithm is used to mechanize the optimal determination of fuzzy logic controller parameters based on an efficient cost function that comprises undershoot, overshoot, rise time, settling time, steady state error, and stability. In [10, 11], a novel intelligent control strategy based on a brain emotional learning (BEL) algorithm was investigated in the application of attitude control of UAV. Time-delay phenomenon and sensor saturation are very common in practical engineering control and is frequently a source of instability and performance deterioration [18–20]. Taking time delay into consideration, the influence of time delay on the stability of the low-altitude and low-speed small Unmanned Aircraft Systems (UAS) flight control system had been analyzed [21]. There are still some other methods [22, 23]; no details will be listed here.

The design method based on characteristic points can obtain multiple control gains. To realize the gain scheduling, look-up table is one common way applied in practice. Actually, the gains between characteristic points do not exist but can be obtained only by interpolation method. It is hard to ensure the control satisfaction between characteristic points [24]. As for sliding control method, it is difficult to select the intermediate control variables for partial derivatives of a sliding surface. As for the intelligent control method, though the stability of control system can be verified, the algorithm is too complicated and it is unable to guarantee the control timeliness in application. In a word, the attitude control system design of UAVs is an annoying task. Multi-input multioutput (MIMO), nonlinearity, and coupling dynamic characteristics will cause more difficulties during the design of attitude control system. In addition, model uncertainties and external disturbances should be taken into account also.

Feedback linearization method can be used to realize linearization and decoupling of a complicated model. Model reference adaptive control (MRAC) system can suppress model uncertainties and has stronger robustness with respect to gust disturbances. With these considerations, feedback linearization method and MRAC method are integrated to design the attitude control system for a fixed wing UAV. As far as we know, there is only few research in which the above two methods are integrated. Moreover, this design principle is simple and the control performance is superior. The maximum overshoot, settling time, and rise time of the system can satisfy the desired indexes, and the system has strong robustness with respect to the

uncertainties of aerodynamic parameters variation and gust disturbance.

This paper is organized as follows. firstly, the complicated attitude dynamic model is decoupled into three independent channels by feedback linearization method; secondly, according to the control performance indexes of each attitude channel, such as maximum overshoot, settling time, and rise time, reference model is established and MRAC is used to design the adaptive control law; thirdly, the control performance comparison between MRAC and PID control is given; finally, conclusions are presented.

2. Attitude Dynamic Model of UAV

The origin O of UAV body coordinate system $Ox_b y_b z_b$ is located at mass center. Axis x_b coincides with aircraft longitudinal axis and points to the nose. Axis y_b is perpendicular to aircraft longitudinal symmetric plane and points to the right side. Axis z_b is defined following the right-hand rule. The dynamic models of three attitude channels including roll, pitch, and yaw are given as follows:

$$\dot{\phi} = p + \tan \theta (r \cos \phi + q \sin \phi), \quad (1)$$

$$\dot{\theta} = q \cos \phi - r \sin \phi, \quad (2)$$

$$\dot{\psi} = \frac{r \cos \phi + q \sin \phi}{\cos \theta}, \quad (3)$$

$$\dot{p} = [I_z L + I_{xz} (N + (I_x + I_z - I_y) pq) - qr (I_z^2 + I_{xz}^2 - I_y I_z)] \times (I_x I_z - I_{xz}^2)^{-1}, \quad (4)$$

$$\dot{q} = \frac{M - pr (I_x - I_z) - I_{xz} (p^2 - r^2)}{I_y}, \quad (5)$$

$$\dot{r} = \frac{[I_{xz} L + I_x N + pq (I_x^2 + I_{xz}^2 - I_y I_x) + qr I_{xz} (I_y - I_x - I_z)]}{(I_x I_z - I_{xz}^2)}. \quad (6)$$

The models describe the behavior of aircraft following control input, where ϕ , θ , and ψ represent roll angle, pitch angle, and yaw angle, respectively; p , q , and r represent the angle velocity components on body axis x_b , y_b , and z_b ; I_x , I_y , and I_z represent the inertia moment of body axis; I_{xz} denotes the inertia product against axis Ox_b and Oz_b ; L , M , and N represent the resultant moment components on body axis x_b , y_b , and z_b , and

$$L = \frac{1}{2} \rho V^2 S_w b (C_{l\beta} \beta + C_{l\dot{\beta}} \dot{\beta} + C_{l\delta a} \delta_a + C_{l\delta r} \delta_r + C_{l_r} r + C_{l_p} p),$$

$$M = \frac{1}{2} \rho V^2 S_w c (C_{m0} + C_{m\alpha} \alpha + C_{m\delta e} \delta_e + C \dot{\alpha} + C_{mq} q),$$

$$N = \frac{1}{2}\rho V^2 S_w b \left(C_{n\beta}\beta + C_{n\dot{\beta}}\dot{\beta} + C_{n\delta a}\delta a + C_{n\delta r}\delta r + C_{nr}r + C_{np}p \right), \quad (7)$$

where ρ is the atmosphere density relative to height; V is airspeed of UAV; S_w , b , and c represent wing area, span, and mean aerodynamic chord, respectively; β and α represent sideslip angle and attack angle, respectively. δa , δe , and δr represent the deflection angle of aileron, elevator, and rudder, respectively; C represents the aerodynamic moment coefficient and its subscript is composed of corresponding moments and variables, where C_{m0} represents the aerodynamic moment coefficient at 0° attack angle.

It is obvious that attitude dynamic model of UAV is nonlinear and there are strong coupling among three channels. Substitute the aerodynamic moment equations (7) into attitude dynamic model equations (4)~(6) and rewrite them as follows:

$$\begin{aligned} \dot{\mathbf{x}} &= \mathbf{f}(\mathbf{x}) + \mathbf{g}\mathbf{u}, \\ \mathbf{y} &= \mathbf{h}(\mathbf{x}), \end{aligned} \quad (8)$$

where

$$\mathbf{x} = [p \ q \ r \ \phi \ \theta \ \psi]^T,$$

$$\mathbf{u} = [\delta a \ \delta e \ \delta r]^T,$$

$$\mathbf{h}(\mathbf{x}) = [\phi \ \theta \ \psi]^T,$$

$$\mathbf{f}(\mathbf{x}) = [f_1 \ f_2 \ f_3 \ f_4 \ f_5 \ f_6]^T,$$

$$\begin{aligned} f_1 &= [2pqI_{zx}(I_z + I_x - I_y) + 2qr(I_y I_z - I_z^2 - I_{zx}^2) \\ &\quad + I_z \rho V^2 S_w b (C_{l\beta}\beta + C_{l\dot{\beta}}\dot{\beta} + C_{lr}r + C_{lp}p) \\ &\quad + I_{zx} \rho V^2 S_w b (C_{n\beta}\beta + C_{n\dot{\beta}}\dot{\beta} + C_{nr}r + C_{np}p)] \\ &\quad \times (2I_x I_z - 2I_{zx}^2)^{-1}, \end{aligned}$$

$$\begin{aligned} f_2 &= [-2pr(I_x - I_z) - 2(p^2 - r^2)I_{zx} \\ &\quad + \rho V^2 S_w c (C_{m0} + C_{m\alpha}\alpha + C_{m\dot{\alpha}}\dot{\alpha} + C_{mq}q)] \times (2I_y)^{-1}, \end{aligned}$$

$$\begin{aligned} f_3 &= [2pq(I_{zx}^2 + I_x^2 - I_y I_x) + 2qr(I_y - I_z - I_x) \\ &\quad + I_{zx} \rho V^2 S_w b (C_{l\beta}\beta + C_{l\dot{\beta}}\dot{\beta} + C_{lr}r + C_{lp}p) \\ &\quad + I_x \rho V^2 S_w b (C_{n\beta}\beta + C_{n\dot{\beta}}\dot{\beta} + C_{nr}r + C_{np}p)] \\ &\quad \times (2I_x I_z - 2I_{zx}^2)^{-1}, \end{aligned}$$

$$f_4 = p + q \sin \phi \tan \theta + r \cos \phi \tan \theta,$$

$$f_5 = q \cos \phi - r \sin \phi,$$

$$f_6 = q \sin \phi \sec \theta + r \cos \phi \sec \theta,$$

$$\mathbf{g} = \frac{\rho V^2 S_w}{2I_y (I_x I_z - I_{zx}^2)} \begin{bmatrix} g_{11} & 0 & g_{13} \\ 0 & g_{22} & 0 \\ g_{31} & 0 & g_{33} \\ 0 & 0 & 0 \\ 0 & 0 & 0 \\ 0 & 0 & 0 \end{bmatrix},$$

$$g_{11} = I_y b (I_z C_{l\delta a} + I_{zx} C_{n\delta a}),$$

$$g_{13} = I_y b (I_z C_{l\delta r} + I_{zx} C_{n\delta r}),$$

$$g_{22} = C_{m\delta e} (I_x I_z - I_{zx}),$$

$$g_{31} = I_y b (I_{zx} C_{l\delta a} + I_x C_{n\delta a}),$$

$$g_{33} = I_y b (I_{zx} C_{l\delta r} + I_x C_{n\delta r}). \quad (9)$$

3. Linearization and Decoupling of Model

In order to obtain the SISO form of the three attitude channels, feedback linearization method is used in this paper. As for nonlinear equations (8), we can obtain the following equation according to Lie derivative:

$$\mathbf{u} = \frac{1}{L_g L_f^n \mathbf{h}} (-L_f^n \mathbf{h} + \mathbf{v}), \quad (10)$$

where $L_f \mathbf{h}$ and $L_g L_f \mathbf{h}$ represent Lie derivative of \mathbf{h} with respect to \mathbf{f} and \mathbf{g} . Superscript n represents the derivative order. The new input \mathbf{v} is $\mathbf{v} = [v_1 \ v_2 \ v_3]^T$.

Let

$$\mathbf{Q} = L_g L_f^n \mathbf{h} = [Q_1 \ Q_2 \ Q_3]^T, \quad (11)$$

$$\mathbf{P} = L_f^n \mathbf{h} = [P_1 \ P_2 \ P_3]^T.$$

We can get

$$\begin{aligned} \mathbf{Q}_1^T &= \frac{1}{2} \rho V^2 S_w b \\ &\times \left[\frac{\cos \phi \tan \theta (I_{xz} C_{l\delta a} + I_x C_{n\delta a}) + I_z C_{l\delta a} + I_{xz} C_{n\delta a}}{I_x I_z - I_{zx}^2} \right. \\ &\quad \left. \frac{c \sin \phi \tan \theta C_{m\delta e}}{b I_y} \right], \end{aligned}$$

$$\mathbf{Q}_2^T = \frac{1}{2} \rho V^2 S_w b \left[\frac{\cos \phi \tan \theta (I_{xz} C_{l\delta r} + I_x C_{n\delta r}) + I_z C_{l\delta r} + I_{xz} C_{n\delta r}}{I_x I_z - I_{zx}^2} \right],$$

$$\mathbf{Q}_3^T = \frac{1}{2} \rho V^2 S_w b \left[\frac{\sin \phi (I_{xz} C_{l\delta a} + I_x C_{n\delta a})}{I_x I_z - I_{zx}^2} \right. \\ \left. \frac{c \cos \phi C_{m\delta e}}{b I_y} \right. \\ \left. \frac{\sin \phi (I_{xz} C_{l\delta r} + I_x C_{n\delta r})}{I_x I_z - I_{zx}^2} \right],$$

$$\mathbf{Q}_3^T = \frac{1}{2} \rho V^2 S_w b \begin{bmatrix} \frac{\cos \phi (I_{xz} C_{l\delta a} + I_x C_{n\delta a})}{\cos \theta (I_x I_z - I_{xz}^2)} \\ \frac{c \sin \phi C_{m\delta e}}{b \cos \theta I_y} \\ \frac{\cos \phi (I_{xz} C_{l\delta r} + I_x C_{n\delta r})}{\cos \theta (I_x I_z - I_{xz}^2)} \end{bmatrix}. \quad (12)$$

Expressions of P_1 , P_2 , and P_3 are more complicated and can be obtained by referring to the literature [17].

The system relative order is $n_1 + n_2 + n_3 = 6$ according to Lie derivative. The input and output linearization of MIMO nonlinear system is realized by the above derivation. There is no internal dynamic state in new system that asymptotic stability and tracking control can be realized. The feedback linearization diagram is shown as Figure 1.

It is visible that the nonlinear dynamic model is transformed into one equivalent linear model with state variables as follows:

$$\bar{\mathbf{x}} = [\phi \ \dot{\phi} \ \theta \ \dot{\theta} \ \psi \ \dot{\psi}]^T. \quad (13)$$

State equations are rewritten in matrix form:

$$\begin{bmatrix} \dot{\phi} \\ \ddot{\phi} \\ \dot{\theta} \\ \ddot{\theta} \\ \dot{\psi} \\ \ddot{\psi} \end{bmatrix} = \begin{bmatrix} 0 & 1 & 0 & 0 & 0 & 0 \\ 0 & 0 & 0 & 0 & 0 & 0 \\ 0 & 0 & 0 & 1 & 0 & 0 \\ 0 & 0 & 0 & 0 & 0 & 0 \\ 0 & 0 & 0 & 0 & 0 & 1 \\ 0 & 0 & 0 & 0 & 0 & 0 \end{bmatrix} \begin{bmatrix} \phi \\ \dot{\phi} \\ \theta \\ \dot{\theta} \\ \psi \\ \dot{\psi} \end{bmatrix} + \begin{bmatrix} 0 & 0 & 0 \\ 1 & 0 & 0 \\ 0 & 0 & 0 \\ 0 & 1 & 0 \\ 0 & 0 & 0 \\ 0 & 0 & 1 \end{bmatrix} \times \begin{bmatrix} v_1 \\ v_2 \\ v_3 \end{bmatrix}. \quad (14)$$

Remark 1. Although new errors are not produced in the process of decoupling the dynamic equations by feedback linearization, it is impossible to describe all dynamic characteristics of attitude moment precisely, the reason for this is modeling errors and model uncertainties cannot be eliminated in dynamic model.

4. Control Laws Design

Aiming at the above three independent two-order systems and according to the performance indexes of attitude response, MRAC is used in this paper to design the attitude control law.

4.1. MRAC Law Design. The differential equation for each channel in (14) can be written as

$$\ddot{y}_p = \bar{u}_1. \quad (15)$$

The adaptive control law is designed by taking the pitch channel as an example. Suppose the form of control law is

$$\bar{u}_1 = kr + f_0 y_p + f_1 \dot{y}_p, \quad (16)$$

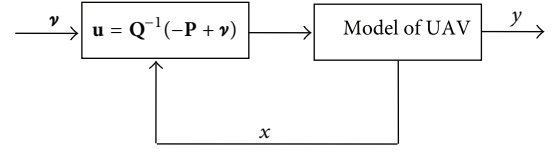


FIGURE 1: Feedback linearization diagram.

where k is the feedforward gain, r is the reference input, f_0 and f_1 are feedback gains. The approach of MRAC is to adjust parameters k , f_0 , and f_1 so that the system output can track the output of the reference model.

Select the same order of reference model as that of pitch channel model and the differential equation is

$$\ddot{y}_m + a_1 \dot{y}_m + a_0 y_m = br. \quad (17)$$

Coefficients a_0 , a_1 , and b should be determined according to control performance indexes of pitch channel.

Consider the standard form of two-order system:

$$\phi(s) = \frac{\omega_n^2}{s^2 + 2\xi\omega_n s + \omega_n^2}. \quad (18)$$

We can get

$$\begin{aligned} t_s &= \frac{3.5}{\xi\omega_n}, \\ \sigma\% &= \frac{e^{-\pi\xi}}{\sqrt{1-\xi^2}} \times 100\%, \\ t_r &= \frac{\pi - \beta}{\omega_d}, \\ \omega_d &= \omega_n \sqrt{1 - \xi^2}, \\ \xi &= \cos \beta, \end{aligned} \quad (19)$$

where ξ denote damping ratio; ω_n and ω_d denote natural oscillation angular frequency and damping oscillation angular frequency, respectively; t_s and t_r denote settling time and rise time, respectively; $\sigma\%$ denotes overshoot; set $t_p = 5$ s, $\sigma = 2\%$; it is easy to get $\xi = 0.7797$, $\omega_n = 1.0035$ rad/s.

Substitute (16) into (15); the adjustable differential equation can be obtained:

$$\ddot{y}_p - f_1 \dot{y}_p - f_0 y_p = kr. \quad (20)$$

Define $e = y_m - y_p$ as the generalized error and according to (17) and (20), the generalized error equation is

$$\begin{aligned} \ddot{e} + a_1 \dot{e} + a_0 e &= -(a_1 + f_1) \dot{y}_p \\ &\quad - (a_0 + f_0) y_p + (b - k) r. \end{aligned} \quad (21)$$

Let

$$\delta_1 = -a_1 - f_1, \quad \delta_0 = -a_0 - f_0, \quad \sigma = b - k. \quad (22)$$

Equation (21) can be rewritten as

$$\ddot{e} + a_1 \dot{e} + a_0 e = \delta_1 \dot{y}_p + \delta_0 y_p + \sigma r. \quad (23)$$

Define parameter error vector θ and generalized error vector ϵ , respectively, as

$$\theta = [\delta_0 \quad \delta_1 \quad \sigma]^T, \quad \epsilon = [e \quad \dot{e}]^T. \quad (24)$$

Then error expression equation (23) can be written in matrix-vector form:

$$\dot{\epsilon} = \mathbf{A}\epsilon + \Delta_a + \Delta_b, \quad (25)$$

where

$$\mathbf{A} = \begin{bmatrix} 0 & 1 \\ -a_0 & -a_1 \end{bmatrix}, \quad \Delta_a = \begin{bmatrix} 0 \\ \delta_0 y_p + \delta_1 \dot{y}_p \end{bmatrix}, \quad (26)$$

$$\Delta_b = \begin{bmatrix} 0 \\ \sigma r \end{bmatrix}.$$

Select the Lyapunov function:

$$\bar{V} = \frac{1}{2} (\epsilon^T \mathbf{P} \epsilon + \theta^T \mathbf{\Gamma} \theta), \quad (27)$$

where \mathbf{P} is 2×2 positive definite symmetric matrix, $\mathbf{\Gamma}$ is 3-dimensional positive definite diagonal matrix:

$$\mathbf{\Gamma} = \text{diag}(\lambda_0 \quad \lambda_1 \quad \mu). \quad (28)$$

Let $\mathbf{P} = \begin{bmatrix} p_{11} & p_{12} \\ p_{21} & p_{22} \end{bmatrix}$ and $p_{12} = p_{21}$; we can get the derivative of \bar{V} with respect to time:

$$\begin{aligned} \dot{\bar{V}} &= \frac{1}{2} \epsilon^T (\mathbf{P}\mathbf{A} + \mathbf{A}^T \mathbf{P}) \epsilon + \delta_0 [\lambda_0 \dot{\delta}_0 + (ep_{12} + \dot{e}p_{22}) y_p] \\ &\quad + \delta_1 [\lambda_1 \dot{\delta}_1 + (ep_{12} + \dot{e}p_{22}) \dot{y}_p] \\ &\quad + \sigma [\mu \dot{\sigma} + (ep_{12} + \dot{e}p_{22}) r]. \end{aligned} \quad (29)$$

Select positive definite symmetric matrix \mathbf{Q} and make

$$\mathbf{P}\mathbf{A} + \mathbf{A}^T \mathbf{P} = -\mathbf{Q}. \quad (30)$$

Select the adaptive laws:

$$\begin{aligned} \dot{\delta}_0 &= -\frac{(ep_{12} + \dot{e}p_{22}) y_p}{\lambda_0}, \\ \dot{\delta}_1 &= -\frac{(ep_{12} + \dot{e}p_{22}) \dot{y}_p}{\lambda_1}, \\ \dot{\sigma} &= -\frac{(ep_{12} + \dot{e}p_{22}) r}{\mu}. \end{aligned} \quad (31)$$

Obviously, $\dot{\bar{V}}$ is negative definite; therefore the closed-loop system is asymptotically stable. Calculate the derivative of each equation in (24) with respect to time with considering

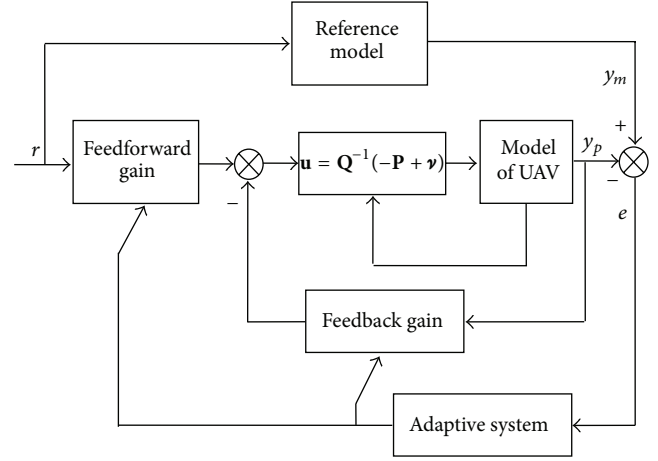


FIGURE 2: MRAC system diagram.

(31), the adaptive laws of feedback gains f_0 , f_1 and feedforward gain k can be obtained:

$$\begin{aligned} f_0 &= \int_0^t \frac{(ep_{12} + \dot{e}p_{22}) y_p}{\lambda_0} d\tau + f_0(0), \\ f_1 &= \int_0^t \frac{(ep_{12} + \dot{e}p_{22}) \dot{y}_p}{\lambda_1} d\tau + f_1(0), \\ k &= \int_0^t \frac{(ep_{12} + \dot{e}p_{22}) r}{\mu} d\tau + k(0). \end{aligned} \quad (32)$$

The MRAC laws of roll and yaw channels can be designed in the same way. However, different reference model for each channel is selected based on the performance index of respective channel. The MRAC system diagram of attitude control system is shown as Figure 2.

Remark 2. The control performance indexes of each channel determine the form of the reference model. Although model uncertainties and gust disturbances exist in the actual system, only if the output of system can track the output of reference model, the performance can be guaranteed. Therefore, MRAC system has strong robustness with respect to the model uncertainties and external disturbances.

4.2. PID Control Law Design. For the simplified model of pitch channel, PID control law can be obtained. The expression of control law is

$$\bar{u}_2 = k_1 \bar{e} + k_2 \int_0^t \bar{e} dt + k_3 \dot{\bar{e}}, \quad (33)$$

where \bar{e} is the error between reference input and system output; Gains k_1 , k_2 , and k_3 can be determined by root locus according to the control performance indexes of pitch channel.

In the same way, the control laws of roll and yaw channels can be designed by PID method and the control diagram of attitude control system for UAV is shown as Figure 3.

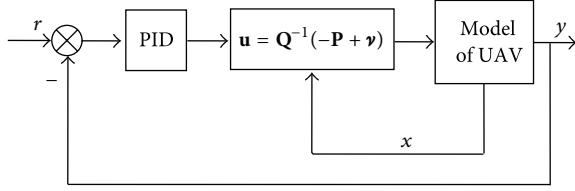


FIGURE 3: PID control system diagram.

5. Mathematics Simulations

In order to verify the performance of attitude control system for UAV, the PID control law and the MRAC law are applied to the coupling and nonlinear attitude dynamic model of UAV, respectively.

The reference motion states are as follows:

$$V = 1360 \text{ m/s}, \quad H = 30 \text{ Km}. \quad (34)$$

The initial conditions of simulation are

$$\phi = \theta = \psi = 0^\circ, \quad p = q = r = 0 \text{ rad/s}. \quad (35)$$

The allowed maximum deflection angles of three actuators in simulation are:

$$\begin{aligned} -5^\circ \leq \delta_a \leq 5^\circ, \quad -15^\circ \leq \delta_e \leq 15^\circ, \\ -10^\circ \leq \delta_r \leq 10^\circ. \end{aligned} \quad (36)$$

The reference inputs of three attitude channels are 10° step signals. The control performance of attitude control system will be verified through below three cases: Case 1, there is no uncertainty in the system; Case 2, aerodynamic parameters vary within the range of 0~30%; Case 3, gust disturbance is considered as the external disturbance.

Figures 4, 5, and 6 show the output responses of roll, pitch, and yaw channels for the above three cases, respectively, where solid line represents the attitude angle under MRAC law and dashed line represents the attitude angle under PID control law.

The performance indexes of attitude control system under all cases are listed in Table 1.

We can see from above that there is almost no difference for attitude angle response under MRAC laws for all cases shown in Figures 4 to 6. In other words, the control performance indexes still can be satisfied even with parameter perturbation and external disturbance. Adjust PID control law parameters and make the control performance under Case 1 to satisfy the design index. However, the maximum overshoot and settling time of output response will increase while the same PID parameters are applied to Case 2 and Case 3. The control performance becomes worse.

6. Conclusions

The design of attitude control system for UAV is presented by integrating feedback linearization and MRAC methods. The complicated coupling nonlinear dynamic model was

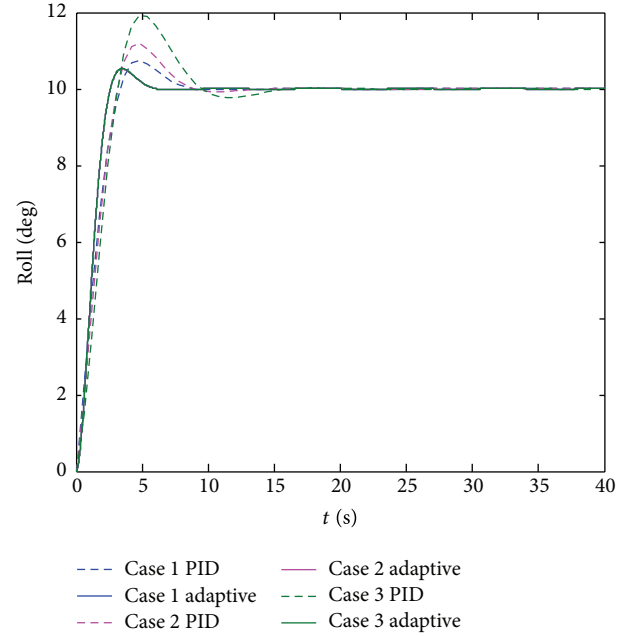


FIGURE 4: Output response of roll channel.

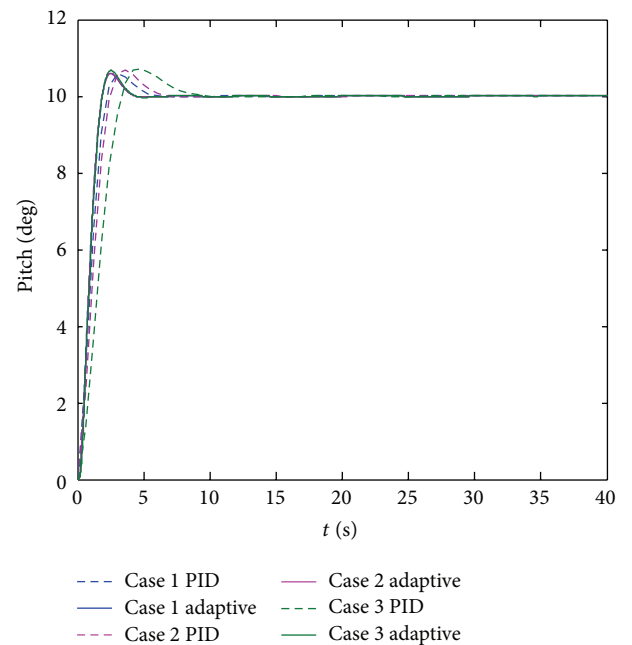


FIGURE 5: Output response of pitch channel.

decoupled into three independent SISO systems by feedback linearization. Then, the control law of each channel was designed using MRAC method and PID method, respectively. The mathematics simulation results indicate that the attitude control system can achieve better control performance including maximum overshoot, settling time, and rise time under MRAC law than that under PID control law. In addition, a stronger robustness with respect to aerodynamic parameter perturbation and gust disturbance has been obtained in MRAC system.

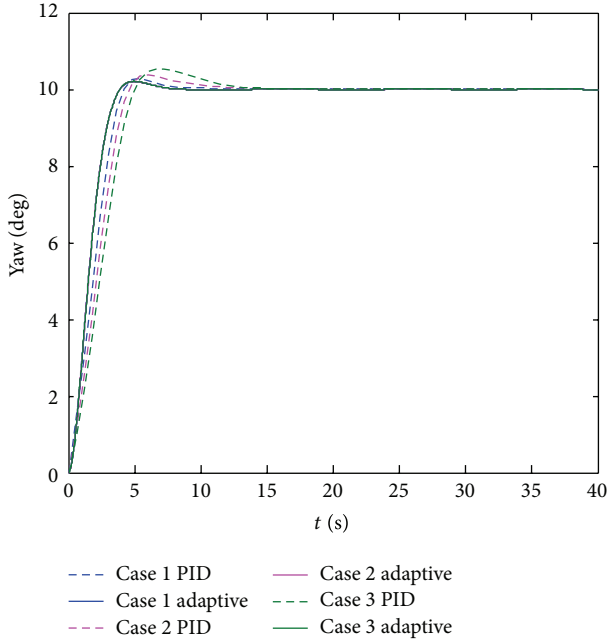


FIGURE 6: Output response of yaw channel.

TABLE 1: Comparison of control performance indexes between MRAC and PID control.

	Indexes	Case 1	Case 2	Case 3
Roll channel				
PID	δ_{max}	7.4%	11.8%	19.2%
	t_s (s)	7.21	7.77	12.71
	t_r (s)	3.13	3.14	3.34
Adaptive	δ_{max}	5.2%	5.3%	5.3%
	t_s (s)	4.86	4.87	4.88
	t_r (s)	2.58	2.58	2.59
Pitch channel				
PID	δ_{max}	5.9%	7.0%	7.2%
	t_s (s)	4.62	5.35	7.46
	t_r (s)	2.27	2.45	3.33
Adaptive	δ_{max}	5.9%	6.0%	6.7%
	t_s (s)	3.57	3.58	3.66
	t_r (s)	1.85	1.85	1.87
Yaw channel				
PID	δ_{max}	2.8%	3.7%	5.4%
	t_s (s)	6.26	8.18	10.74
	t_r (s)	4.17	4.61	5.04
Adaptive	δ_{max}	2.1%	2.1%	2.1%
	t_s (s)	5.27	5.32	5.35
	t_r (s)	3.90	3.89	3.88

Conflict of Interests

The authors declare that there is no conflict of interests regarding the publication of this paper.

References

- [1] M. Lorenzo, N. Roberto, and I. Alberto, “High-gain output feedback for a miniature UAV,” *Journal of Robust and Nonlinear Control*, 2013.
- [2] B. Godbolt, N. I. Vitzilaios, and A. F. Lynch, “Experimental validation of a helicopter autopilot design using model-based PID control,” *Journal of Intelligent and Robotic Systems*, vol. 70, pp. 385–399, 2013.
- [3] H. Chao, Y. Luo, L. Di, and Y. Q. Chen, “Roll-channel fractional order controller design for a small fixed-wing unmanned aerial vehicle,” *Control Engineering Practice*, vol. 18, no. 7, pp. 761–772, 2010.
- [4] T. Yamasaki, S. N. Balakrishnan, and H. Takano, “Integrated guidance and autopilot design for a chasing UAV via high-order sliding modes,” *Journal of the Franklin Institute*, vol. 349, no. 2, pp. 531–558, 2012.
- [5] A. R. Babaei, M. Mortazavi, and M. H. Moradi, “Classical and fuzzy-genetic autopilot design for unmanned aerial vehicles,” *Applied Soft Computing Journal*, vol. 11, no. 1, pp. 365–372, 2011.
- [6] B. T. Whitehead and S. R. Bieniawski, “Model reference adaptive control of a quadrotor UAV,” in *Proceedings of the AIAA Guidance, Navigation, and Control Conference*, Toronto, Canada, 2010.
- [7] S. Kurnaz, O. Cetin, and O. Kaynak, “Adaptive neuro-fuzzy inference system based autonomous flight control of unmanned air vehicles,” *Expert Systems with Applications*, vol. 37, no. 2, pp. 1229–1234, 2010.
- [8] E. Capello, G. Guglieri, F. Quagliotti, and D. Sartori, “Design and validation of an L1 adaptive controller for mini-UAV autopilot,” *Journal of Intelligent and Robotic Systems*, vol. 69, pp. 109–118, 2013.
- [9] A. R. Babaei, M. Mortazavi, and M. H. Moradi, “Fuzzy sliding mode autopilot design for nonminimum phase and nonlinear UAV,” *Journal of Intelligent and Fuzzy Systems*, vol. 24, pp. 499–509, 2013.
- [10] H. Pu, Z. Zhen, and D. Wang, “Modified shuffled frog leaping algorithm for optimization of UAV flight controller,” *International Journal of Intelligent Computing and Cybernetics*, vol. 4, no. 1, pp. 25–39, 2011.
- [11] H. Z. Pu, Z. Y. Zhen, J. Jiang, and D. B. Wang, “UAV flight control system based on an intelligent BEL algorithm,” *Journal of Advanced Robotic Systems*, vol. 10, no. 121, pp. 1–8, 2013.
- [12] C. X. Lu and Q. Huang, “Design of the platform for a UAV flight control system based on STM32,” *Journal of Digital Content Technology and Its Applications*, vol. 7, no. 5, pp. 1033–1041, 2013.
- [13] I. Yavrucuk and V. Kargin, “Autolanding controller strategies for a fixed wing UAV in adverse atmospheric conditions,” in *Proceedings of the AIAA Guidance, Navigation and Control Conference and Exhibit*, Portland, Ore, USA, August 2008.
- [14] Y. C. Paw and G. J. Balas, “Development and application of an integrated framework for small UAV flight control development,” *Mechatronics*, vol. 21, no. 5, pp. 789–802, 2011.
- [15] A. B. Milhim and Y. M. Zhang, “Quad-rotor UAV: high-fidelity modeling and nonlinear PID control,” in *Proceedings of the AIAA Modeling and Simulation Technologies Conference*, Toronto, 2010.
- [16] M. Lungu and R. Lungu, “Adaptive backstepping flight control for a mini-UAV,” *International Journal of Adaptive Control and Signal Processing*, vol. 27, no. 8, pp. 635–650, 2013.

- [17] J. Shin, H. Jin Kim, and Y. Kim, "Adaptive support vector regression for UAV flight control," *Neural Networks*, vol. 24, no. 1, pp. 109–120, 2011.
- [18] H. Gao, T. Chen, and J. Lam, "A new delay system approach to network-based control," *Automatica*, vol. 44, no. 1, pp. 39–52, 2008.
- [19] H. Yan, Z. Su, H. Zhang, and F. Yang, "Observer-based H_∞ control for discrete-time stochastic systems with quantisation and random communication delays," *IET Control Theory & Applications*, vol. 7, no. 3, pp. 372–379, 2013.
- [20] H. Zhang, H. Yan, F. Yang, and Q. Chen, "Distributed average filtering for sensor networks with sensor saturation," *IET Control Theory & Applications*, vol. 7, no. 6, pp. 887–893, 2013.
- [21] S. Y. Yang, S. J. Tang, C. Liu, and J. Guo, "Design and verification the simulation system of UAS flight control considering the effects of time delay," *Applied Mechanics and Materials*, vol. 278–280, pp. 1746–1753, 2013.
- [22] H. Zhang, H. Yan, F. Yang, and Q. Chen, "Quantized control design for impulsive fuzzy networked systems," *IEEE Transactions on Fuzzy Systems*, vol. 19, no. 6, pp. 1153–1162, 2011.
- [23] L. X. Zhang, H. J. Gao, and O. Kaynak, "Network-induced constraints in networked control systems-a survey," *IEEE Transactions on Industrial Informatics*, vol. 9, no. 1, pp. 403–416, 2013.
- [24] J.-P. Gao and Z.-J. Chen, "Study on gain-scheduling problem in flight control," *Chinese Journal of Aeronautics*, vol. 12, no. 4, pp. 217–221, 1999.

Research Article

Nonlinear Disturbance Observer Based Robust Tracking Control of Pneumatic Muscle

Youssif Mohamed Toum Elobaid,^{1,2} Jain Huang,¹ and Yongji Wang¹

¹ School of Automation, Huazhong University of Science and Technology, No. 1037 Luoyu Road, Hongshan District, Wuhan, Hubei 430074, China

² Department of Control Engineering, University of Alneelain, Gamhoria Street, 11121 Khartoum, Sudan

Correspondence should be addressed to Jain Huang; huang.jan@mail.hust.edu.cn

Received 4 December 2013; Accepted 9 February 2014; Published 20 March 2014

Academic Editor: Huaicheng Yan

Copyright © 2014 Youssif Mohamed Toum Elobaid et al. This is an open access article distributed under the Creative Commons Attribution License, which permits unrestricted use, distribution, and reproduction in any medium, provided the original work is properly cited.

Presently pneumatic muscles (PMs) are used in various applications due to their simple construction, lightweight, and high force-to-weight ratio. However, pneumatic muscles are facing various problems due to their nonlinear characteristics and various uncertainties in real applications. To cope with the uncertainties and strong nonlinearity of a PM model, a nonlinear disturbance observer (NDO) is designed to estimate the lumped disturbance. Based on the disturbance observer, the tracking control of PM is studied. Stability analysis based on Lyapunov method with respect to our proposed control law is discussed. The simulation results show the validity, effectiveness, and enhancing robustness of the proposed methods.

1. Introduction

Designing a robot arm that performs tasks in anthropic environments in a fashion similar to a human arm is the goal of many ongoing research projects. Task-oriented rehabilitation therapy is becoming exciting as an important issue and needs to be addressed in a sufficient way. In particular, safe and not inducing further injury or pain during motor function training need to be carefully investigated since they are the main challenges in such kind of task [1, 2]. Owing to the absence of compliance in robot, pneumatic muscle actuators (PMAs) are considered to be basic actuators and offer the advantage of intrinsic elasticity to achieve joint compliance [3]. A PMA is an interesting actuator, which is very similar to animal skeletal muscle action in size, weight, and power output. It works in a similar manner to human or animal muscles. There are several advantages of PMA, such as lower cost, light weight, compliance, and very high power/weight and power/volume ratios. These ratios are about five times higher in comparison to an electric motor or a hydraulic actuator [4].

However, all that glitter is not gold. The slower response in force-generation and nonlinear parameters depending on

the load, position, and speed of PMAs compared to electric motors is the main problem making pneumatic actuators inaccurate and difficult to control [4, 5]. To overcome this complexity and hindrance, in recent years a great effort in human-friendly robotic systems has focused on the development of actuation systems that can provide robots with the characteristics of safety, accuracy, ease to control, and high performance. So far, the researchers presented a number of novel approaches to alleviate the design of controller in practical applications of PMA. Repperger et al. modelled the PMA as a stiffness-visco model consisting of a spring element and damping element arranged in parallel [6]. Reynolds et al. proposed and constructed an improved new phenomenological model, which is consisting of a contractile element, a spring element, and a damping element based on Repperger's model [7]. With a progress in the area of networked robotic systems interact closely with humans [8]; researchers have investigated nonlinear control methods, with attention to safety requirements as well as the traditional metrics of performance. Accordingly, there are an abundance of researches on safe robots and new results on stability and H_∞ performance have been developed to help humans [9, 10].

Xing et al. presented a wearable exoskeletal robot for upper extremity stroke rehabilitation called “RUPERT” which has four actuated degrees of freedom driven by compliant and safe pneumatic muscles (PMs) on the shoulder, elbow, and wrist [9]. A nonlinear control strategy as a cascaded tracking control concept for pneumatic muscle actuators is presented in [11]. The main objective is to control a trolley, which is driven by an artificial muscle to follow a reference path.

To improve the control performance of the PM, Xing et al. have driven a new type of actuator, which comprises a pneumatic muscle (PM) and a torsion spring; in this study, the sliding mode approach is applied to the tracking control problem of a planar arm manipulator system [12, 13].

In [14–16] a fuzzy logic control has been used to overcome poor models, the approach is not mathematical and mimics how a person would make decisions. Emanuel Todorov et al. have worked with pneumatically actuated robots and reported results on modeling and control of a 2-DOF robot, as well as preliminary results on a state-of-the-art 38-DOF humanoid [17]. Varga and Moučka have presented results gained in research experiments with an artificial muscle; the realized experiments were focused on finding the exact mechanical features of artificial muscle, which will be used for development of a theoretical model. This model can be later used for direct control of the muscle [18].

It is found that using a disturbance observer can further improve the robustness of nonlinear control system. Recently, some works have been presented about the observer design for nonlinear systems [1, 12, 19–21].

This study proposes a Nonlinear Disturbance Observer Based Control (NDOBC) approach for the PM system. A major advantage and novelty of our framework is that it allows us to develop in a separate way the control law from the observer design provided that each part satisfies some stability properties. In general, the main objective of the use of a disturbance observer is to deduce the external unknown or uncertain disturbance without the use of an additional sensor. Friction is a very common phenomenon in mechanical systems and plays an important role in system performance. Many friction models and compensation methods have been proposed, one of the most promising methods is Nonlinear Disturbance Observer Based Control (NDOBC) where a NDO is used to estimate the friction.

To cope with the uncertainties and strong nonlinearity of the pneumatic muscle a nonlinear disturbance observer (NDO) is presented in this paper. Lyapunov concepts are the fundamental tools invoked to analyze the closed-loop PM behavior which leads, by carefully selecting the observer gain function, to the stability and utilization of asymptotic position tracking performance. Stabilization controller is designed by using Lyapunov theory on the pneumatic muscle system, and then the observer design theory is used for interference suppression under the condition of existing model error and external disturbance. The scheme enhances the robustness of the position tracking and improves the tracking accuracy.

PID controllers are one of the most used types of controllers in practice. They are easy to realize and can stabilize

a system even without knowing the model. However, in spite of the simplicity and the small number of parameters that have to be adjusted, it is hard to analyze the stability and tune the parameters when using PID controllers. Therefore, the major significance of the proposed Nonlinear Disturbance Observer Based Control (NDOBC) controller lies in its high robustness against disturbance and superior performance over the conventional PID controller (see Figure 10). Moreover, NDOBC’s engineering implementation is also easy, which explores a convenient engineering method to improve the performance of the PM control system.

The layout of this paper is as follows. In Section 2, we derive the model of the PM system. Section 3 concerns with Nonlinear Disturbance Observer Based Control design. Section 4 discusses the stability analysis. Simulation results are presented and discussed in Section 5. We finally end by the conclusion in Section 6.

2. System Model

PMAs are assumed as actuators in many applications, where their static and dynamic characteristics play an important role in the overall behavior of the control system. Therefore, improving the dynamic behavior of the pneumatic muscle actuator is of prime interest to control system designers.

Two main categories for the mathematical models of a pneumatic muscle actuator are prevalent: the theoretical and the phenomenological models. The theoretical models, which are derived from the law of energy conservation, describe PMA behavior based on quasistatic states without inclusion of explicitly temporal information. However, this approach limits its application for real-time control because not only it is too complex in structure, but also it requires too many parameters that are difficult to obtain during experimentation [1, 22, 23].

In this paper, we adopt the phenomenological model as a combination of effects from nonlinear friction, spring, and contraction components to describe the dynamic behavior of a pneumatic muscle (PM) pulling a mass against gravity as in Figure 1(b).

The coefficients related to these three elements depend on the input pressure of the PM [1]. The equations describing approximately the dynamics of a PM are given by

$$M\ddot{x} + B(P)\dot{x} + K(P)x = F(P) - Mg, \quad (1)$$

$$K(P) = K_0 + K_1P, \quad (2)$$

$$B(P) = B_{0i} + B_{1i}P \quad (\text{inflation}), \quad (3)$$

$$B(P) = B_{0d} + B_{1d}P \quad (\text{deflation}), \quad (4)$$

$$F(P) = F_0 + F_1P, \quad (5)$$

where M is the mass, g is the acceleration of gravity, $\Delta x = 0$ corresponds to the fully deflated position (see Figure 1(a)), and P is the input pressure. The coefficients $K(P)$ and $B(P)$ are pressure dependent for the spring and the damping, respectively. The contractile element presented the effective

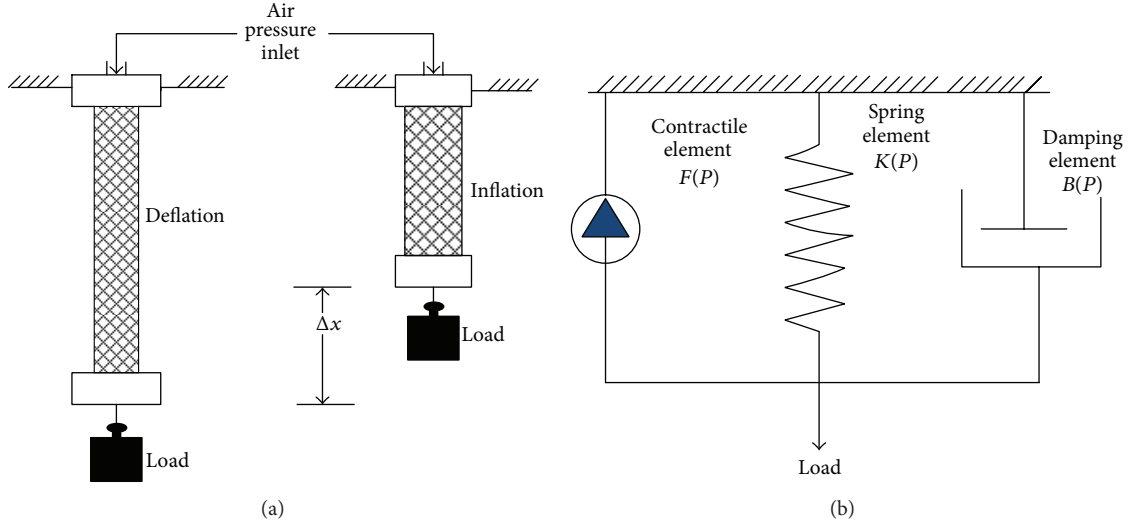


FIGURE 1: (a) The operational principle of a PM; (b) the three-element model of PM.

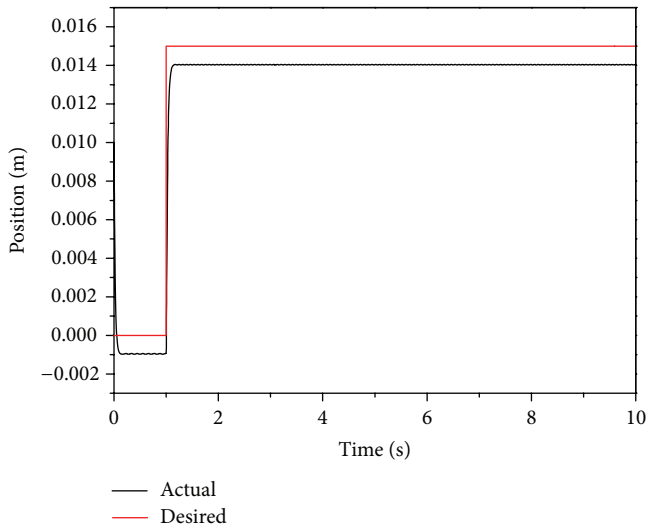


FIGURE 2: Step-trajectory tracking result without NDO.

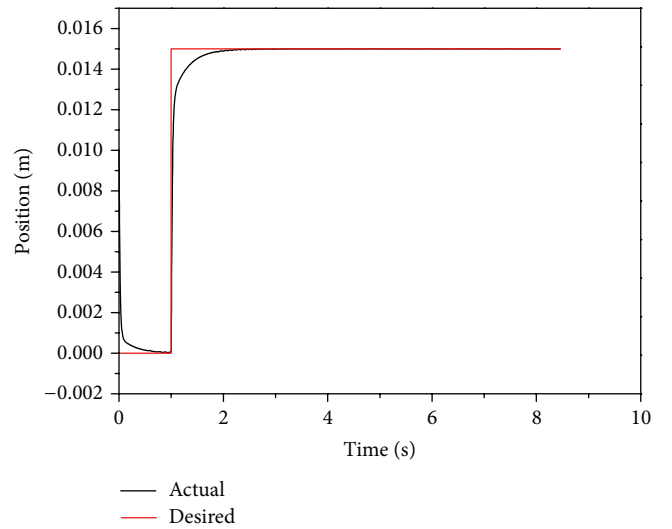


FIGURE 3: Step-trajectory tracking result with NDO.

force $F(P)$. The damping coefficient depends on whether the PM is inflated and deflated. From the dynamic equations (1)–(5), we can write for the PM the following state model:

$$\dot{q}_1 = q_2,$$

$$\dot{q}_2 = \frac{1}{M} [(F_0 - Mg - B_0 q_2 - K_0 q_1) + (F_1 - B_1 q_2 - K_1 q_1) P], \quad (6)$$

with state variable $[q_1, q_2]^T = [x, \dot{x}]^T$. In summary, the dynamics model of PM can be concretely represented as

$$M\ddot{x} + B_0\dot{x} + K_0x + (Mg - F_0) = (F_1 - B_1\dot{x} - k_1x) P. \quad (7)$$

Let us define $e = x - x_r$, $\dot{e} = \dot{x} - \dot{x}_r$, and $\ddot{e} = \ddot{x} - \ddot{x}_r$ where e , \dot{e} and \ddot{e} are the position, speed, and acceleration tracking

error, respectively. Substituting these errors in (7) then we have error-differential equation satisfying the following:

$$\begin{aligned} M\ddot{e} + M\ddot{x}_r + B_0\dot{e} + B_0\dot{x}_r + K_0e + K_0x_r + (Mg - F_0) \\ = (F_1 - B_1\dot{e} - B_1\dot{x}_r - K_1e - K_1x_r) P. \end{aligned} \quad (8)$$

Let us introduce an additional control component ν satisfying

$$\begin{aligned} (F_1 - B_1\dot{e} - B_1\dot{x}_r - K_1e - K_1x_r) P \\ = M\ddot{x}_r + B_0\dot{x}_r + K_0x_r + (Mg - F_0) - K_P e + \nu, \end{aligned} \quad (9)$$

$$\nu = M\ddot{e} + B_0\dot{e} + (K_0 + K_P)e = M\ddot{e} + B_0\dot{e} + \beta e, \quad (10)$$

where $\beta = K_0 + K_P$ is a constant.

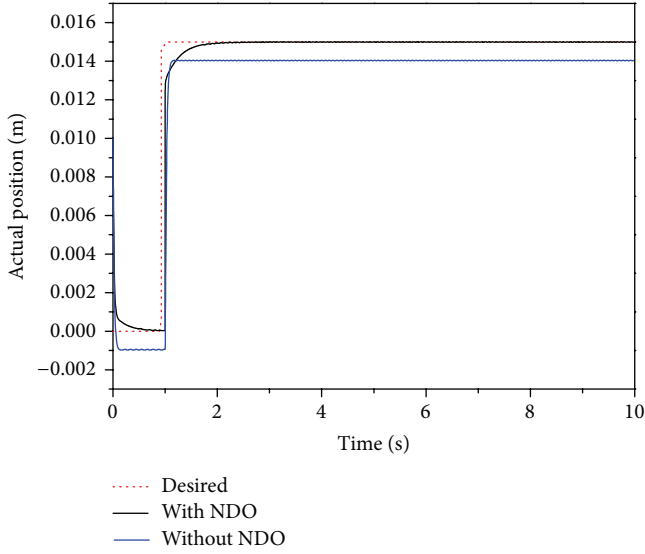


FIGURE 4: Step-trajectory comparison for position tracking with/without NDO.

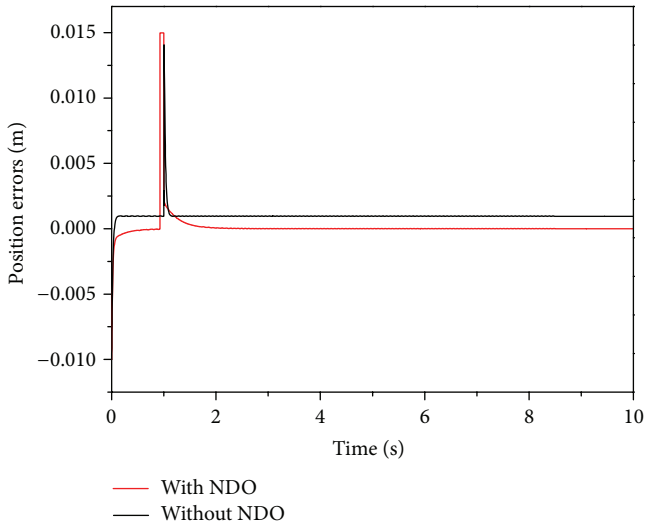


FIGURE 5: Step-input tracking control error (amplitude = 15 mm).

Let us define another state variable satisfying $[x_1, x_2]^T = [e, \dot{e} + e]^T$. Then the error dynamic model in (10) can be translated into the following equation of state:

$$\begin{aligned} \dot{x}_1 &= -x_1 + x_2, \\ \dot{x}_2 &= \frac{1}{M} ((B_0 - K_0 - K_P - M)x_1 - (B_0 - M)x_2 - H_0) \\ &\quad + \frac{H_1}{M} P, \end{aligned} \quad (11)$$

where $H_0 = M\dot{x}_r + B_0\dot{x}_r + K_0x_r + (Mg - F_0) - K_P e$ and $H_1 = F_1 - B_1\dot{e} - B_1\dot{x}_r - K_1e - K_1x_r$.

3. Nonlinear Disturbance Observer (NDO) Based Control Design

In this section, we discuss the Nonlinear Disturbance Observer Based Robust Control (NDOBRC) approach for PM-tracking control. Estimation of nonlinear uncertainty can be pursued through generating the uncertainties as the output of some exogenous system, allowing estimation and compensation under certain conditions. It is a matter of fact that a model of the exosystems must be included into the controller to reach the design goals. Owing to this, a composite controller must be built consisting of two parts: a controller without or having poor disturbance attenuation ability and a disturbance observer.

As the dynamics of a PM is nonlinear and hard to model precisely, the design of the model-based control algorithm is more cumbersome. Besides the modeling uncertainties, external disturbances are inevitable in real environments which degrade the control performance. Therefore, the controller should have a robust capability to achieve the desired objective. Since the PM model shows highly nonlinear behavior, it is difficult to estimate the proper norm bound and, thus, the usual robust control method for PM control often results in a conservative design. Therefore, the use of a disturbance observer resolves these difficulties.

Considering the external disturbances ω and the model error in (11) the general PM model with interference is given by

$$\dot{X} = f(X) + g_1(X)P + g_2(X)\omega, \quad (12)$$

where

$$\dot{X} = [\dot{x}_1 \quad \dot{x}_2]^T, \quad g_1(X) = \begin{bmatrix} 0 & \frac{H_1}{M} \end{bmatrix}^T,$$

$$g_2(X) = \begin{bmatrix} 0 & \frac{1}{M} \end{bmatrix}^T,$$

$f(X)$

$$= \begin{bmatrix} -x_1 + x_2 & \frac{1}{M} ((B_0 - K_0 - K_P - M)x_1 - (B_0 - M)x_2 - H_0) \end{bmatrix}^T. \quad (13)$$

To estimate the disturbance ω a nonlinear disturbance observer is proposed as

$$\dot{\hat{\omega}} = \alpha (\dot{X} - f(X) - g_1(X)P - g_2(X)\hat{\omega}) \quad (14)$$

with $\alpha = [c_1 \quad c_2]$ where $c_1 > 0$ and $c_2 > 0$.

Let us define observer residuals as $\tilde{\omega} = \omega - \hat{\omega}$; then the observer in (14) can be given by

$$\begin{aligned} \dot{\hat{\omega}} &= \alpha (\dot{X} - f(X) - g_1(X)P - g_2(X)\hat{\omega}) \\ &= \alpha \cdot g_2(X) (\omega - \hat{\omega}) = [c_1 \quad c_2] g_2(X) \tilde{\omega}. \end{aligned} \quad (15)$$

Since $g_2(X) = [0 \quad 1/M]^T$ then we have $\hat{\omega} = c_2 \tilde{\omega}/M$.

Define an auxiliary vector $z = \hat{\omega} - \rho(X)$ where $z \in R^2$, $\rho(X)$ is a nonlinear function to be designed, and the nonlinear

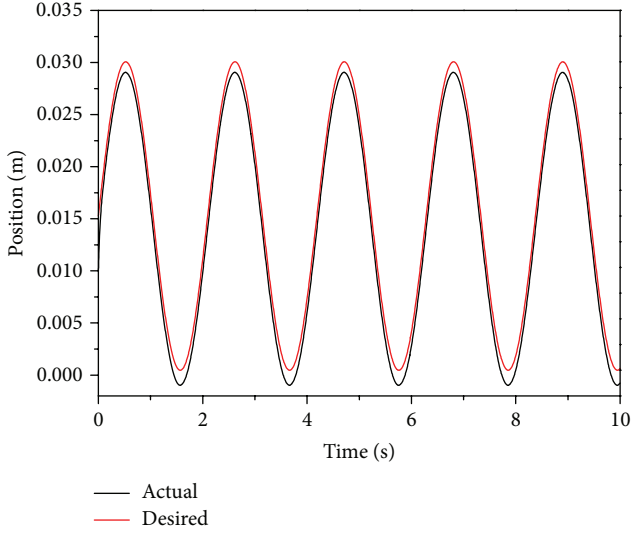


FIGURE 6: Sinusoidal-trajectory tracking result without NDO.

observer gain α is defined as $\alpha = \partial\rho(X)/\partial X$. Taking the time derivative of z and substituting (14) give us

$$\dot{z} = -\alpha (f(X) + g_1(X)P + g_2(X)(z + \rho(X))). \quad (16)$$

Substituting α in (16) the disturbance observer can be deduced as

$$\begin{aligned} \hat{\omega} &= z + \rho(X), \\ \dot{z} &= -c_1(-x_1 + x_2) - \frac{c_2}{M} \\ &\quad \times ((B_0 - K_0 - K_P - M)x_1 - (B_0 - M)x_2 - H_0 + H_1P) \\ &\quad - \frac{c_2}{M}(z + c_1x_1 + c_2x_2), \end{aligned} \quad (17)$$

where $\rho(X) = c_1x_1 + c_2x_2$.

Considering (9) and (12), the Nonlinear Disturbance Observer Based Robust Control (NDOBRC) law can be given by

$$P = \frac{M\ddot{x}_r + B_0\dot{x}_r + K_0x_r + (Mg - F_0) - K_P e + \nu - \hat{\omega}}{F_1 - B_1\dot{e} - B_1\dot{x}_r - K_1e - K_1x_r}. \quad (18)$$

4. Stability Analysis

The main focus will be on control design based on the state-space model for a given PM. There is typically some freedom in the choice of Lyapunov function for the control design; we call V a Lyapunov function if, in a certain neighborhood of the equilibrium point, V is positive definite and its derivative along the system trajectories is negative semidefinite. The main Lyapunov stability results for PM control systems can be summarized by the following lemma and theorem.

Lemma 1 (see [24]). *If, in a ball B_{R_0} around the equilibrium point 0, there exists a scalar function $V(x, t)$ with continuous partial derivatives such that*

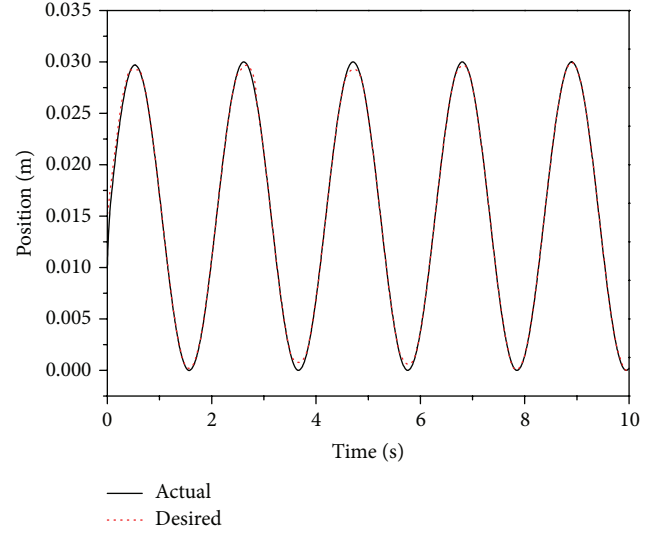


FIGURE 7: Sinusoidal-trajectory tracking result with NDO.

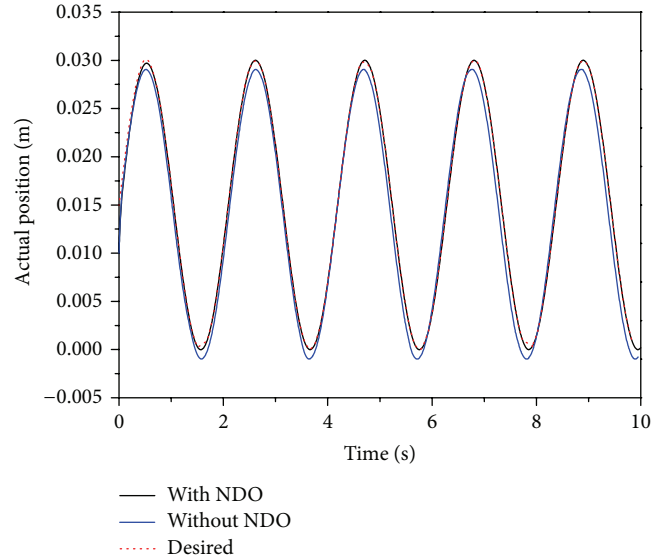


FIGURE 8: Sinusoidal-trajectory comparison for position tracking with/without NDO.

- (a) V is positive definite
- (b) \dot{V} is negative semidefinite

then the equilibrium point 0 is stable in the sense of Lyapunov. If, furthermore,

- (c) V is decrescent

then the origin is uniformly stable. If condition (b) is strengthened by requiring that V be negative definite, then the equilibrium point is uniformly asymptotically stable.

If the ball B_R is replaced by the whole state space, and condition (a), the strengthened condition (b), condition (c), and the condition

- (d) $V(x, 0)$ is radially unbounded

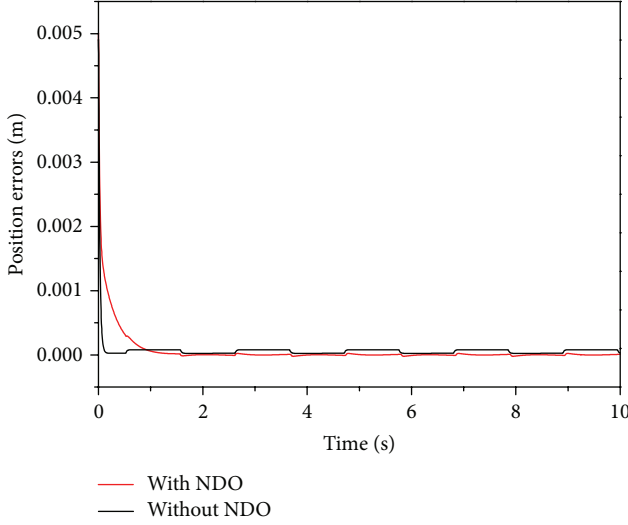


FIGURE 9: Sinusoidal-input tracking control error.

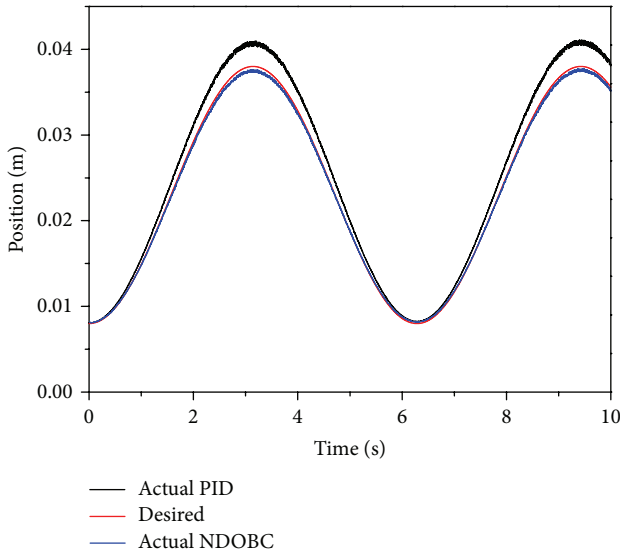


FIGURE 10: A comparison between NDOBC and conventional PID controller.

are all satisfied, then the equilibrium point at 0 is globally uniformly asymptotically stable.

Generally in $\tilde{\omega} = \omega - \hat{\omega}$, there is no prior information about the derivative of the disturbance ω . When the disturbance varies slowly relative to the observer dynamics, it is reasonable to suppose that $\dot{\omega} = 0$, and then we have $\tilde{\dot{\omega}} = -\hat{\dot{\omega}}$.

Theorem 2. Consider the pneumatic muscle system (1) with a NDOBC controller (18). Assume that the disturbance ω varies slowly relative to the observer dynamics. Then, the trajectory of system (1) can be driven asymptotically onto the desired trajectory.

Proof. Consider a positive-definite Lyapunov function $V(t)$ of the form

$$V = \frac{1}{2} \dot{e}^T M \dot{e} + \frac{1}{2} e^T \beta e + \frac{1}{2} \tilde{\omega}^2. \quad (19)$$

By differentiating both sides of (19) we have

$$\dot{V} = \dot{e}^T M \ddot{e} + e^T \beta \dot{e} + \tilde{\omega} \dot{\tilde{\omega}}. \quad (20)$$

From (10) we can write

$$M \ddot{e} = \nu - B_0 \dot{e} - \beta e. \quad (21)$$

Substituting (21) in (20) \dot{V} can be deduced as

$$\begin{aligned} \dot{V} &= \dot{e}^T (\nu - B_0 \dot{e} - \beta e) + e^T \beta \dot{e} + \tilde{\omega} \dot{\tilde{\omega}} \\ &= \dot{e}^T \nu - \dot{e}^T B_0 \dot{e} + \tilde{\omega} \dot{\tilde{\omega}} \leq \dot{e}^T \nu + \tilde{\omega} \dot{\tilde{\omega}}. \end{aligned} \quad (22)$$

Using $\tilde{\dot{\omega}} = -\hat{\dot{\omega}} = -c_2 \tilde{\omega} / M$ in (22) we get

$$\dot{V} \leq \dot{e}^T \nu + \tilde{\omega} \dot{\tilde{\omega}} = \dot{e}^T \nu - \frac{c_2 \tilde{\omega}^2}{M}, \quad (23)$$

$$\dot{V} \leq \dot{e}^T \nu.$$

Consider Lemma 1 and the simple control law for the additional control component ν with a real and positive constant K satisfying the condition $\nu = -K\dot{e}$ with $K > 0$. The Lyapunov function is decreasing. This completes the proof. \square

Considering (18) with $\nu = -K\dot{e}$, our Lyapunov control law-based disturbance observer can be deduced as

$$P = \frac{M \ddot{x}_r + B_0 \dot{x}_r + K_0 x_r + (Mg - F_0) - K_p e - K \dot{e} - \hat{\omega}}{F_1 - B_1 \dot{e} - B_1 \dot{x}_r - K_1 e - K_1 x_r}. \quad (24)$$

Substituting (24) in (17) and using $x_1 = e$, $x_2 = \dot{e} + e$ the nonlinear disturbance observer can be deduced as

$$\hat{\omega} = z + \rho(X),$$

$$\begin{aligned} \dot{z} &= - \left[c_1 \dot{e} + \frac{c_2}{M} (-\beta e - (B_0 + K - M) \dot{e}) \right] \\ &= \left(\frac{c_2}{M} (B_0 + K - M) - c_1 \right) \dot{e} + \frac{c_2 \cdot \beta}{M} e \\ &= \alpha_1 \cdot \dot{e} + \alpha_2 \cdot e, \end{aligned} \quad (25)$$

where $\beta = K_0 + K_p$, $\alpha_1 = (c_2/M)(B_0 + K - M) - c_1$, and $\alpha_2 = (c_2 \cdot \beta)/M$.

5. Simulation Results and Discussion

The simulation has been undertaken in MATLAB/SIMULINK. The simulation objective is to reveal the strength of the proposed controller. In our simulation, we let the load $M = 0.829$ kg; the parameters K and K_p have been selected as 700 and 500, respectively. The PM coefficients used for the simulation are shown in Table 1.

TABLE 1: PM coefficient sets used for the simulation.

Coefficient	C (Evaluation)	C_1 ($0.9 \times C$)	C_2 ($1.1 \times C$)
F_0 ($\times 10^2$)	-1.0336	-0.9302	-1.137
F_1 ($\times 10^{-6}$)	719.75	647.78	791.73
K_0 ($\times 10^4$)	1.5010	1.351	1.651
K_1 ($\times 10^{-2}$)	-5.703	-5.133	-6.2733
B_0	52.08	46.87	57.29
B_1 ($\times 10^{-6}$)	-124.5	-112.1	-137.0

The parameters $F(P)$, $K(P)$, and $B(P)$ of columns C_1 and C_2 are chosen assuming $\pm 10\%$ error in the evaluation values (C); the simulation interval time was selected as 10 ms.

The exogenous disturbance in our simulation system was considered as Coulomb and viscous friction. When we use our proposed Nonlinear Disturbance Observer based Robust Control (NDOBC), the external nonlinear disturbance can be approximately estimated by this nonlinear disturbance observer (NDO). The performance of the proposed controller was assessed by setting a step and a sinusoidal-trajectory tracking problem.

Using amplitude of 0.015 m of step response, in Figure 2 we show the representations of the position with respect to time without integrating the nonlinear disturbance observer (NDO) in the controller. As we can see from the figure, the curves obtained from the proposed controller tend to the desired position after small number of fluctuations. This is due to the fact that the system needs time before reaching the stability point.

When using our proposed NDOBC method, the influence of disturbances is estimated by a disturbance observer and then compensated for the controller. Therefore, the effects of disturbances and uncertainties are reduced significantly, as depicted in Figure 3. As we can see in this figure, a more satisfactory tracking performance can be achieved.

Figure 4 shows a comparison of control efforts with/without the NDO, as we can see in this figure, the maximum effort was made near the peaks. This is an expected result due to the high rate of change in the peak which makes the disturbance effect of the system stronger. Also the figure indicates that the controller with NDO leads to more accurate tracking performance compared to the controller without NDO.

In Figure 5, we further show the tracking error with respect to the time for the step input. From the figure we can observe that the tracking error tends to zero after the transient phase, which confirms again the accuracy and robustness of our controller.

The next simulation shows the ability to follow a slow changing reference value represented by a sinusoidal input. For this purpose and for evaluating the performance of the proposed controller, a sinusoidal trajectory-tracking problem was studied. The desired trajectory is given by $0.015 \sin(3t) + 0.015$, and the simulation interval time was selected as 0.01s. Furthermore a nonlinear disturbance observer is presented to estimate the unknown exogenous disturbances. The simulation results for evaluation of the tracking performance with/without NDO are depicted in Figures 6 and 7, respectively.

From Figure 6, it is obvious that the tracking performance of the system using only the proposed controller without integrating the nonlinear disturbance observer (NDO) is not satisfactory when there are modeling uncertainties and perturbations. On the other hand, as shown in Figure 7, the deviation between the actual and the desired trajectory is significantly reduced, when we integrate the NDO in the simulation system. The difference between the actual and the desired trajectory applying or not applying the nonlinear disturbance observer is highlighted by a comparison as depicted in Figure 8.

In Figure 9 a tracking error comparison between the desired and actual trajectory is illustrated. We can see that the tracking error with NDO tends asymptotically, with very small overshoot at the initial transients caused by the disturbances, to the zero. While the tracking error without NDO shows a number of fluctuations above the zero, this ensures again that the tracking performance or regulation obtained from the proposed controller (NDOBC) behaves better than the system without NDO.

As addressed earlier, it is hard to analyze the stability and tune the controller parameters when using PID controllers, in spite of the simplicity and the small number of parameters that they have to be adjusted. Therefore, a comparison has been conducted between NDOBC and conventional PID controller in Figure 10 to illustrate the advantage of our proposed Nonlinear Disturbance Observer Based Control (NDOBC) and its superior performance over the conventional PID controller.

6. Conclusion

The proposed Nonlinear Disturbance Observer Based Control law (NDOBC) provides a relatively new thread for the control of PMA. The advantage of this method not only is reflected in its high accuracy, but also manifests itself in convenience. The proposed approach represents a simple, yet robust, mechanism for guaranteeing finite time performance of zero error condition. The results of simulations demonstrate the validity of the proposed controller and show its superiority in tracking performance. In particular, the rapid response to parameter's changes and following of the desired trajectory are the deciding features. Based on the obtained results it is possible to realize the trajectory tracking control of pneumatic muscle (PM) pulling a mass against gravity practically.

Conflict of Interests

The authors declare that there is no conflict of interests regarding the publication of this paper.

Acknowledgments

This work was supported by the Natural Science Foundation of China under Grant 61075095, the International Science and Technology Cooperation Program of China "Precision Manufacturing Technology and Equipment for Metal Parts" under

Grant no. 2012DFG70640, and the International Science and Technology Cooperation Program of Hubei Province “Joint Research on Green Smart Walking Assistance Rehabilitant Robot” under Grant no. 2012IHA00601.

References

- [1] K. Xing, J. Huang, Y. Wang, J. Wu, Q. Xu, and J. He, “Tracking control of pneumatic artificial muscle actuators based on sliding mode and non-linear disturbance observer,” *IET Control Theory and Applications*, vol. 4, no. 10, pp. 2058–2070, 2010.
- [2] Y. M. Elobaid, J. Huang, Y. Wang, and J. Wu, “Tracking control of pneumatic muscle using Lyapunov based control method,” in *Proceedings of the International Conference on Modelling, Identification and Control (ICMIC '12)*, pp. 223–227, 2012.
- [3] T.-Y. Choi and J.-J. Lee, “Control of manipulator using pneumatic muscles for enhanced safety,” *IEEE Transactions on Industrial Electronics*, vol. 57, no. 8, pp. 2815–2825, 2010.
- [4] D. G. Caldwell, G. A. Medrano-Cerda, and M. Goodwin, “Control of pneumatic muscle actuators,” *IEEE Control Systems Magazine*, vol. 15, no. 1, pp. 40–48, 1995.
- [5] D. G. Caldwell, N. Tsagarakis, and G. A. Medrano-Cerda, “Bio-mimetic actuators: polymeric pseudo muscular actuators and pneumatic muscle actuators for biological emulation,” *Mechatronics*, vol. 10, no. 4-5, pp. 499–530, 2000.
- [6] D. W. Repperger, K. R. Johnson, and C. A. Phillips, “Nonlinear feedback controller design of a pneumatic muscle actuator system,” in *Proceedings of the American Control Conference (ACC '99)*, pp. 1525–1529, San Diego, Calif, USA, June 1999.
- [7] D. B. Reynolds, D. W. Repperger, C. A. Phillips, and G. Bandry, “Modeling the dynamic characteristics of pneumatic muscle,” *Annals of Biomedical Engineering*, vol. 31, no. 3, pp. 310–317, 2003.
- [8] L. Zhang, H. Gao, and O. Kaynak, “Network-induced constraints in networked control systems—a survey,” *IEEE Transactions on Industrial Informatics*, vol. 9, pp. 403–416, 2013.
- [9] K. Xing, Q. Xu, J. He, Y. Wang, Z. Liu, and X. Huang, “A wearable device for repetitive hand therapy,” in *Proceedings of the 2nd Biennial IEEE/RAS-EMBS International Conference on Biomedical Robotics and Biomechanics (BioRob '08)*, pp. 919–923, October 2008.
- [10] H. Gao, T. Chen, and J. Lam, “A new delay system approach to network-based control,” *Automatica*, vol. 44, no. 1, pp. 39–52, 2008.
- [11] A. Hildebrandt, O. Sawodny, R. Neumann, and A. Hartmann, “A cascaded tracking control concept for pneumatic muscle actuators,” in *Proceedings of the European Control Conference*, pp. 345–350, 2003.
- [12] K. Xing, J. Huang, J. He, Y. Wang, Q. Xu, and J. Wu, “Sliding mode tracking for actuators comprising pneumatic muscle and torsion spring,” *Transactions of the Institute of Measurement and Control*, vol. 34, no. 2-3, pp. 255–277, 2012.
- [13] J. Huang, Z.-H. Guan, T. Matsuno, T. Fukuda, and K. Sekiyama, “Sliding-mode velocity control of mobile-wheeled inverted-pendulum systems,” *IEEE Transactions on Robotics*, vol. 26, no. 4, pp. 750–758, 2010.
- [14] H. Zhang, H. Yan, F. Yang, and Q. Chen, “Quantized control design for impulsive fuzzy networked systems,” *IEEE Transactions on Fuzzy Systems*, vol. 19, no. 6, pp. 1153–1162, 2011.
- [15] Y. Manai and M. Benrejeb, “Robust stabilization for continuous Takagi-Sugeno fuzzy system based on observer design,” *Mathematical Problems in Engineering*, vol. 2012, Article ID 836814, 18 pages, 2012.
- [16] H. Zhang, H. Yan, T. Liu, and Q. Chen, “Fuzzy controller design for nonlinear impulsive fuzzy systems with time delay,” *IEEE Transactions on Fuzzy Systems*, vol. 19, no. 5, pp. 844–856, 2011.
- [17] E. Todorov, C. Hu, A. Simpkins, and J. Movellan, “Identification and control of a pneumatic robot,” in *Proceedings of the 3rd IEEE RAS and EMBS International Conference on Biomedical Robotics and Biomechanics (BioRob '10)*, pp. 373–380, September 2010.
- [18] Z. Varga and M. Moučka, “Mechanics of pneumatic artificial muscle,” *Journal of Applied Science in the Thermodynamics and Fluid Mechanics*, vol. 3, no. 2, p. 6, 2009.
- [19] J. S. R. Jang, C. T. Sun, and E. Mizutani, “Neuro-fuzzy and soft computing—a computational approach to learning and machine intelligence,” *IEEE Transactions on Automatic Control*, vol. 42, pp. 1482–1484, 1997.
- [20] Z. Z. S. H. C. Yan, H. Zhang, and F. W. Yang, “Observer-based H-infinity control for discrete-time stochastic systems with quantization and random communication delays,” *IET Control Theory and Applications*, vol. 7, pp. 372–379, 2013.
- [21] H. Zhang, Q. Chen, H. Yan, and J. Liu, “Robust H_∞ filtering for switched stochastic system with missing measurements,” *IEEE Transactions on Signal Processing*, vol. 57, no. 9, pp. 3466–3474, 2009.
- [22] H. Schulte, “The characteristics of the McKibben artificial muscle, appendix H,” in *The Application of External Power in Prosthetics and Orthotics*, National Academy of Sciences, National Research Council, Washington, DC, USA, 1961.
- [23] G. K. Klute and B. Hannaford, “Accounting for elastic energy storage in McKibben artificial muscle actuators,” *Journal of Dynamic Systems, Measurement and Control*, vol. 122, no. 2, pp. 386–388, 2000.
- [24] J. J. E. Slotine and W. Li, *Applied Nonlinear Control*, vol. 199, Prentice-Hall, Englewood Cliffs, NJ, USA, 1991.

Research Article

Fast Consensus Tracking of Multiagent Systems with Diverse Communication Delays and Input Delays

Chun-xi Yang,¹ Wei-xing Hong,¹ Ling-yun Huang,² and Hua Wang³

¹ Faculty of Chemical Engineering, Ministry of Education and Faculty of Metallurgical and Energy Engineering, Kunming University of Science and Technology, Kunming 650500, China

² Faculty of Land Resource Engineering, Ministry of Education and Faculty of Metallurgical and Energy Engineering, Kunming University of Science and Technology, Kunming 650500, China

³ Engineering Research Center of Metallurgical Energy Conservation & Emission Reduction, Ministry of Education and Faculty of Metallurgical and Energy Engineering, Kunming University of Science and Technology, Kunming 650500, China

Correspondence should be addressed to Ling-yun Huang; hly0510@126.com

Received 20 November 2013; Accepted 6 February 2014; Published 19 March 2014

Academic Editor: Huaicheng Yan

Copyright © 2014 Chun-xi Yang et al. This is an open access article distributed under the Creative Commons Attribution License, which permits unrestricted use, distribution, and reproduction in any medium, provided the original work is properly cited.

The consensus tracking problem for discrete-time multiagent systems with input and communication delays is studied. A sufficient condition is obtained over a directed graph based on the frequency-domain analysis. Furthermore, a fast decentralized consensus tracking conditions based on increment *PID* algorithm are discussed for improving convergence speed of the multiagent systems. Based on this result, genetic algorithm is introduced to construct increment *PID* based on genetic algorithm for obtaining optimization consensus tracking performance. Finally, a numerable example is given to compare convergence speed of three tracking algorithms in the same condition. Simulation results show the effectiveness of the proposed algorithm.

1. Introduction

As an effective method to solve decentralized multiagent cooperative control which is widely applied into many fields such as flocking [1, 2], formation control [3, 4], and unmanned air vehicles [5], consensus algorithms designing of multiagent systems has attracted great attention in recent years. A key task for consensus algorithms is to achieve a global common behavior through designing a distributed protocol based on local information. Reference [6] proposed a simple model for phase transition of self-driven of the model. A simple consensus protocol to solve the average consensus problem was discussed in [7]. Furthermore, two survey papers which introduce the basic concepts of consensus of multiagent systems, the methods of convergence, and performance analysis for the protocols and recent development can be seen in [8, 9]. In real applications, when local information data travel along channels in a multiagent network, a communication delay exists due to the physical

characteristics of the medium transmitting the information. And at the same time, each agent also needs computing time to process its information. As a result, time-delay problem including communication delays and computing delays (also called input delays) is not avoided in designing consensus algorithms. Reference [10] discusses the consensus problem for multiagent systems with input and communication delays based on the frequency-domain in discrete-time formulation and a conclusion where the consensus condition is dependent on input delays but independent of communication delays is obtained.

Convergence rate or speed is an important performance index in the analysis of consensus problems. For example, sensors need to reach fast consensus on the estimates between sensor observing intervals in distributed estimation problem. In this field, main research works focus on fast consensus [11–13] and finite-time consensus [14–16]. Reference [11] proposes a new consensus protocol which considers the average

information of the agents' states in a certain time interval and increases consensus speed of multiagent systems through determining suitable upper limit of time interval based on the frequently domain analysis and matrix theory. Reference [12] proposes a class of pinning predictive controllers for consensus networks to substantially increase their convergence speed towards consensus. In [13], an optimal synchronization protocol was designed for the fastest convergence speed when the protocol is perturbed by an additive measurement and process noise. As to finite-time consensus algorithms design, [14] designed continuous distributed control algorithms for double integrators leaderless and leader-follower multiagent systems with external disturbances based on the finite-time control technique. Based on positive or negative values of errors between their neighbor's values and their own state values in multiagent systems, a simple distributed continuous-time protocol is introduced by [15] that guarantees finite-time consensus in networks of autonomous agents when the network has directed switching network topologies and time-delayed communications.

Although fast or finite-time consensus without a virtual leader is interesting, it is sometimes more meaningful and interesting to study consensus tracking problem when the virtual leader's state (also called reference) may represent the state of interest for these systems. In [17], a coordinated tracking algorithm with a time-varying leader for first-order dynamics is proposed and bounded control and directed switching interaction topologies are considered when a time-varying consensus reference state is available to only a subset of a team. However, this algorithm requires the estimates of the neighbors' velocities. In [18], distributed coordinated tracking algorithms are studied when only partial measurements of the states of the virtual leader and the followers are available. Reference [19] studies the issues associated with distributed coordinated tracking for multiple networked Euler-Lagrange systems where only a subset of the followers has access to the leader. As to discrete-time formulation, [20] considers consensus tracking problem when location information of the active leader is completely known but the acceleration information may not be measured; a neighbor-based pinning control law and a neighbor-based state estimation rule are proposed. Although consensus tracking problem is discussed widely, few works focus on fast consensus tracking with time-delays in discrete-time formulation.

Motivated by these topics, fast consensus tracking problem of discrete-time multiagent systems with communication delays and input delays is discussed in this paper. The main contribution of this paper is to establish a simple protocol in order to guarantee consensus tracking convergence in general directed network topology based on the frequency-domain analysis. Then, an increment *PID* algorithm is introduced to improve the convergent speed and an inequity condition which can describe relations of controller gain, input delays, communications delays and topology structure is obtained. Furthermore, genetic algorithm [21] is introduced to construct increment *PID* based on genetic algorithm for obtaining optimization consensus tracking performance. This makes the proposed protocol more practical for application to real-time applications.

This paper is organized as follows. In the next section, preliminary notions and multiagent systems model are provided. A conventional *P*-like discrete-time consensus tracking algorithm for a single-integrator systems is stated in Section 3 and a fast discrete-time consensus tracking algorithm based on increment *PID* is established in Section 4. By applying to genetic algorithms, the fast consensus tracking algorithm mentioned above is optimized in order to obtain an optimal cost in Section 5. Simulation example is shown in Section 6. Finally, concluding remarks are stated in Section 7.

2. Preliminaries and Multiagent Systems Modeling

2.1. Graph Theory Notions

Notations. The notation used in this paper for graph theory is quite standard. For a system with N agents, the communication graph among these agents is modeled by a directed weighted graph $G = (V, W, A)$, where $V = \{v_1, v_2, \dots, v_n\}$, $W \subseteq V^2$, and $A = \{a_{ij}\} \in \mathfrak{R}^{n \times n}$ represent the set of agents, the edge set, and the weighted adjacency matrix, respectively. The agent indexes belong to a finite index set $\Phi = \{1, 2, \dots, N\}$. An edge denoted as (v_i, v_j) means that the v_j th agent can access the information of the v_i th agent. We assume that the adjacency elements associated with the edges of the digraph are positive. That means $a_{ij} > 0$, if agent i receives information from agent j otherwise $a_{ij} = 0$. Moreover, we assume feedback gain $a_{ii} > 0$ for all $i \in \Phi$, if i th agent has feedback control loop and $a_{ii} = 0$ otherwise. Define the set of neighbors of agent v_i as $N_i = \{v_j \in V : (v_i, v_j) \in W\}$. For the directed digraph the outdegree of agent i is defined as $\text{deg}_{\text{out}}(v_i) = \sum_{j=1}^n a_{ij}$. Let D be the degree matrix of G , which is defined as a diagonal matrix with the degree of each agent along its diagonal. The Laplacian matrix of the weighted digraph is defined as $L = D - A$ satisfying zero-row sum.

In multiagent systems, each agent can be considered as a node in a digraph, and the information flow between two agents can be regarded as a directed path between the nodes. Thus, a directed graph has a directed spanning tree if there exists at least one agent called a globally reachable agent that has a directed path to all other agents.

2.2. Multiagent System Modeling. Consider agents with a single-integrator kinematics in discrete-time formulation given by

$$x_i(k+1) = x_i(k) + u_i(k), \quad i \in \Phi, \quad (1)$$

where $x_i \in \mathfrak{R}$ and $u_i \in \mathfrak{R}$ denote the state and the control input of agent i , respectively. The following consensus tracking protocol for the multiagent systems (1) is a classical formulation mentioned by literature [10] which can be described by

$$u_i(k) = -g_{i(0)} a_{ii} (x_i(k) - \zeta^r(k)) + \sum_{v_j \in N_i} a_{ij} (x_j(k) - x_i(k)), \quad (2)$$

where $\zeta^r(k)$ is a time-varying reference state or a virtual leader with the states, named agent 0 and the other agents indexed by $1, 2, \dots, N$ are referred to as followers without loss of generality. (Especially, if $\zeta^r(k) = \zeta^r$, this reference state can be simplified to a constant one). $g_{i(0)}$ is 1 if agent i has access to $\zeta^r(k)$ and 0 otherwise. N_i denotes the neighbors of agent i and $a_{ij} > 0$ is the adjacency element of A in the directed digraph $G = (V, W, A)$. $a_{ii} > 0$ denotes the feedback control gain of agent i and $a_{ii} = 0$ otherwise.

When agent i is subjected to a time-varying input delay $T_{ii}(t)$, system (1) can be rewritten as follows:

$$x_i(k+1) = x_i(k) + u_i(k - T_{ii}(t)), \quad i \in \Phi. \quad (3)$$

Consider the total delay where an agent receives data from its neighbors is sum of time-varying input delay and time-varying diverse communication delay, so the consensus tracking protocol becomes

$$\begin{aligned} u_i(k - T_{ii}(t)) &= -g_{i(0)}a_{ii}(x_i(k - T_{ii}(t)) - \zeta^r(k)) \\ &\quad + \sum_{v_j \in N_i} a_{ij}(x_j(k - T_{jj}(t) - T_{ij}(t)) - x_i(k - T_{ii}(t))), \end{aligned} \quad (4)$$

where $T_{ii}(t), T_{jj}(t)$ denotes time-varying input delays of agent i, j and $T_{ij}(t)$ denotes time-varying communication delay from agent j to agent i , respectively. It is assumed that each agent has similar computer capacity, so the time-varying input delay of each agent can be treated with the same time-delay value; that is, $T_{ii}(t) = T_{jj}(t)$. To simplify the complexity of calculation, we assume that agent i needs to possess memory capability such that $x_i(k - T_{ii}(t) - T_{ij}(t))$ can be used in the consensus tracking protocol. Substitute state $x_i(k - T_{ii}(t))$ in coupling terms of (4) for $x_i(k - T_{ii}(t) - T_{ij}(t))$ and let the total delay $\hat{T}_{ij}(t) = T_{ii}(t) + T_{ij}(t)$ which satisfies $T_{ii}(t) \leq \hat{T}_{ij}(t)$. As a result, (4) can be rewritten as

$$\begin{aligned} u_i(k - T_{ii}(t)) &= -g_{i(0)}K_i(x_i(k - T_{ii}(t)) - \zeta^r(k)) \\ &\quad + \sum_{v_j \in N_i} a_{ij}(x_j(k - \hat{T}_{ij}(t)) - x_i(k - \hat{T}_{ij}(t))). \end{aligned} \quad (5)$$

Moreover, these two classes of delays can be approximated by $T_{ii}(t) = (m_i - 1)T + \varepsilon_i$ and $\hat{T}_{ij}(t) = (n_{ij} - 1)T + \varepsilon_{ij}$, respectively. Where $T_{ii}(t), \hat{T}_{ij}(t) \geq 0$, T denotes sample period of this discrete-time system, m_i, n_{ij} are all nonnegative integers and $\varepsilon_i, \varepsilon_{ij}$ are unknown-but-bounded variables which belong to interval $(0, T)$. So it is reasonable that $T_{ii}(t)$ and $\hat{T}_{ij}(t)$ are approximated by m_i and n_{ij} although some artificial delays are included. In the end, (4) can be rewritten as

$$\begin{aligned} u_i(k - m_i) &= -g_{i(0)}K_i(x_i(k - m_i) - \zeta^r(k)) \\ &\quad + \sum_{v_j \in N_i} a_{ij}(x_j(k - n_{ij}) - x_i(k - n_{ij})). \end{aligned} \quad (6)$$

Substituting protocol (6) to the system (3), we have

$$\begin{aligned} x_i(k+1) &= x_i(k) - g_{i(0)}K_i[x_i(k - m_i) - \zeta^r(k)] \\ &\quad + \sum_{v_j \in N_i} a_{ij}[x_j(k - n_{ij}) - x_i(k - n_{ij})], \quad i \in \Phi. \end{aligned} \quad (7)$$

Using algorithm (6), each agent essentially updates its next state based on its past state with limited time delay and its neighbors' current as well as the reference's current if the reference is a neighbor of the agent. As a result, (6) can be easily implemented in practice.

3. P-Like Discrete-Time Consensus Tracking with Input Delays and Communication Delays

In this section we consider consensus tracking problem of multiagent systems with both communication delays and input delays. Firstly, two lemmas related to this topic need to be introduced. Then, a sufficient consensus tracking condition of multiagent systems (7) with conventional P-like algorithm is proposed based on the frequency-domain analysis and matrix theory.

Lemma 1 (Gershgorin's disk theorem). *Let $\Lambda = (a_{ij})$ be a $N \times N$ complex matrix; then all eigenvalues of matrix Λ belong to the union set of N circular disc on the complex plane; that is,*

$$D_i(\Lambda) = \{z \mid |z - a_{ii}| \leq R_i, \quad (i = 1, 2, \dots, N)\}, \quad (8)$$

where $R_i = |a_{i1}| + |a_{i2}| + \dots + |a_{i,i-1}| + |a_{i,i+1}| + \dots + |a_{iN}|$.

Lemma 2 (see [10]). *The following inequality:*

$$\frac{\sin(((2D+1)/2)\omega)}{\sin(\omega/2)} \leq 2D+1 \quad (9)$$

holds for all nonnegative integers D and all $\omega \in [-\pi, \pi]$.

In the following, we apply Lemmas 1 and 2 to derive our main result.

Theorem 3. *Consider multiagent systems (3) with algorithm (6). Assume that the interconnection topology digraph $G = (V, W, A)$ of the system has no less than a globally reachable agent and at least one globally reachable agent can receive reference information. Then the system achieves a consensus tracking asymptotically if*

$$K_{ii}(2m_i + 1) + K_{ij}(2n_{ij} + 1) < 1, \quad (10)$$

where $K_{ii} = g_{i(0)}K_i$ denotes the feedback control gain of agent i , $K_{ij} = \sum_{v_j \in N_i} a_{ij}$ denotes outdegree of agent i .

Proof. The multiagent systems of (3) with (6) are given by (7). Taking the z -transformation of the system (7), we get

$$\begin{aligned} zX_i(z) &= X_i(z) - g_{i(0)}K_i[z^{-m_i}X_i(z) - \zeta^r(z)] \\ &\quad + \sum_{v_j \in N_i} a_{ij}[z^{-n_{ij}}X_j(z) - z^{-n_{ij}}X_i(z)], \end{aligned} \quad (11)$$

where $X_i(z)$ and $\zeta^r(z)$ are the z -transformation of $x_i(k)$ and $\zeta^r(k)$, respectively. Define a $N \times N$ matrix $\tilde{L}(z) = \{\tilde{L}_{ij}(z)\}$ as follows:

$$\tilde{L}_{ij}(z) = \begin{cases} -a_{ij}z^{-n_{ij}}, & v_j \in N_i, \\ g_{i(0)}K_i z^{-m_i} + \sum_{v_j \in N_i} a_{ij}z^{-n_{ij}}, & i = j, \\ 0, & \text{otherwise,} \end{cases} \quad (12)$$

and $X(z) = [X_1(z), \dots, X_N(z)]^T$, $Q = \text{diag}(g_{1(0)}K_1, \dots, g_{N(0)}K_N)$, and then (11) becomes

$$zX(z) = X(z) + Q(1 \otimes \zeta^r(z)) - \tilde{L}(z)X(z). \quad (13)$$

Let $\zeta^r(z)$ denote input signal and let $X(z)$ denote output signal; then the transform function is denoted by

$$G(z) = \frac{X(z)}{\zeta^r(z)} = \frac{Q}{(z-1)I + \tilde{L}(z)}, \quad (14)$$

and correspondent characteristic equation of multiagent system (13) is $p(z) = \det[I + (1/(z-1))\tilde{L}(z)]$. Then, we will prove that all the zeros of $p(z)$ have modulus less than unity in the following.

Based on the general Nyquist stability criterion, the modulus of all roots satisfying $p(z) = 0$ should be less than unity, if all poles $\lambda((1/(e^{j\omega} - 1))\tilde{L}(e^{j\omega}))$ of $(1/(e^{j\omega} - 1))\tilde{L}(e^{j\omega})$ do not enclose the point $(-1, j0)$ for $\omega \in [-\pi, \pi]$. By Lemma 1, all poles $\lambda((1/(e^{j\omega} - 1))\tilde{L}(e^{j\omega}))$ belong to the union set of N circular disks; that is,

$$D_i = \left\{ \left| \xi - \frac{g_{i(0)}K_i e^{-j\omega m_i} + \sum_{v_j \in N_i} a_{ij} e^{-j\omega n_{ij}}}{e^{j\omega} - 1} \right| \leq \sum_{v_j \in N_i} \left| \frac{a_{ij} e^{-j\omega n_{ij}}}{e^{j\omega} - 1} \right| \right\}. \quad (15)$$

To simplify, we define $K_{ii} = g_{i(0)}K_i$, $K_{ij} = \sum_{v_j \in N_i} a_{ij}$ and let

$$G_i(\omega) = \frac{K_{ii}e^{-j\omega m_i} + K_{ij}e^{-j\omega n_{ij}}}{e^{j\omega} - 1}. \quad (16)$$

It is easy to see that $G_i(\omega)$ is the center of the disc D_i . Thus, the point $(-1, j0)$ does not enclose in disc D_i for all $\omega \in [-\pi, \pi]$ as long as the point $(-a, j0)$ with $a \geq 1$. As a result, when $\omega \in [-\pi, \pi]$, $a \geq 1$, we have

$$\left| -a + j0 - \frac{K_{ii}e^{-j\omega m_i} + K_{ij}e^{-j\omega n_{ij}}}{e^{j\omega} - 1} \right| > \left| \frac{K_{ii}e^{-j\omega m_i} + K_{ij}e^{-j\omega n_{ij}}}{e^{j\omega} - 1} \right|. \quad (17)$$

Then this inequality can be rewritten as

$$\begin{aligned} & \left| -a + j0 - \frac{K_{ii}e^{-j\omega m_i} + K_{ij}e^{-j\omega n_{ij}}}{e^{j\omega} - 1} \right|^2 - \left| \frac{K_{ii}e^{-j\omega m_i} + K_{ij}e^{-j\omega n_{ij}}}{e^{j\omega} - 1} \right|^2 \\ &= a \left(a - \frac{K_{ii} \sin(((2m_i + 1)/2)\omega) + K_{ij} \sin(((2n_{ij} + 1)/2)\omega)}{\sin(\omega/2)} \right) \\ &> 0. \end{aligned} \quad (18)$$

According to Lemma 2, we have $\sin(((2m_i + 1)/2)\omega)/\sin(\omega/2) \leq 2m_i + 1$, $\sin(((2n_{ij} + 1)/2)\omega)/\sin(\omega/2) \leq 2n_{ij} + 1$ for $\omega \in [-\pi, \pi]$. Then the following inequality is obtained by

$$\begin{aligned} & \frac{K_{ii} \sin(((2m_i + 1)/2)\omega) + K_{ij} \sin(((2n_{ij} + 1)/2)\omega)}{\sin(\omega/2)} \\ & \leq K_{ii}(2m_i + 1) + K_{ij}(2n_{ij} + 1) < a. \end{aligned} \quad (19)$$

Let $a = 1$; then all disc D_i do not enclose the point $(-1, j0)$. As a result, multiagent systems (7) can achieve a consensus tracking asymptotically. That is end of this proof. \square

Remark 4. If we rewrite (19) as $(K_{ii} + K_{ij})(2m_i + 1) + 2K_{ij}(n_{ij} - m_i) < 1$, it is easy to know that consensus tracking problem of multiagent systems is more sensitive to input delays than communication delays. Moreover, Theorem 3 is also suitable for the case when it only has input delays if we let $m_i = n_{ij}$.

4. Fast Discrete-Time Consensus Tracking Algorithm Based on Increment PID

Considering feedback control gains K_i , $i = 1, 2, \dots, n$ is the similar with conventional P -like controllers, an increment PID algorithm is proposed consequently to accelerate the convergence speed of multiagent systems (7). Discrete PID algorithm is described by

$$h_i(k) = K_p \left[e_i(k) + \frac{T}{T_i} \sum_{j=0}^k e_i(j) + T_d \frac{e_i(k) - e_i(k-1)}{T} \right], \quad (20)$$

where $h_i(k)$ is feedback control signal of agent i at time interval k . $e_i(k)$ denotes the error of current state between agent i and current reference state and $e_i(k-1)$ denotes the error of the value between agent i and reference state at time interval $k-1$, respectively. K_p denotes proportional coefficient, T_i denotes integral time, T_d denotes derivative time, and sampling period is described by T .

Through $h_i(k) - h_i(k-1)$, we obtain increment PID algorithm as

$$\begin{aligned} \Delta h_i(k) &= h_i(k) - h_i(k-1) \\ &= \bar{A}e_i(k) - \bar{B}e_i(k-1) + \bar{C}e_i(k-2), \end{aligned} \quad (21)$$

where $\bar{A} = K_p(1 + T/T_i + T_d/T)$, $\bar{B} = K_p(1 + 2(T_d/T))$, and $\bar{C} = K_p(T_d/T)$.

Remark 5. From (21) we know that if sampling period T and coefficient A, B, C are chosen, control signal $\Delta h_i(k)$ will be obtained by only using three adjacent deviation values. Because this algorithm is easily realized in the agent with limited computing capacity, it is very suitable for multiagent system.

Let $e_i(k - m_i) = x_i(k - m_i) - \zeta^r(k)$ in (7) and substitute feedback control gains K_i into increment *PID* algorithm as (21); (7) can be rewritten by

$$\begin{aligned} x_i(k+1) &= x_i(k) \\ &\quad - g_{i(0)} \left[\bar{A}e_i(k - m_i) \right. \\ &\quad \quad \left. - \bar{B}e_i(k - m_i - 1) + \bar{C}e_i(k - m_i - 2) \right] \\ &\quad + \sum_{v_j \in N_i} a_{ij} \left[x_j(k - n_{ij}) - x_i(k - n_{ij}) \right], \quad i, j \in \Phi. \end{aligned} \quad (22)$$

Then, we obtain sufficient fast consensus tracking condition of multiagent system (22) based on increment *PID* algorithm as follows.

Theorem 6. Consider multiagent systems (3) with algorithm (5). Assume that the interconnection topology digraph $G = (V, W, A)$ of the system has no less than a globally reachable agent and at least one globally reachable agent can receive reference information. Then the system achieves a fast consensus tracking asymptotically if

$$\begin{aligned} A(2m_i + 1) + B(2m_i + 3) + C(2m_i + 5) \\ + K_{ij}(2n_{ij} + 1) \leq 1, \quad i, j \in \Phi, \end{aligned} \quad (23)$$

where $A = g_{i(0)}K_p(1 + T/T_i + T_d/T)$, $B = g_{i(0)}K_p(1 + 2(T_d/T))$, and $C = g_{i(0)}K_p(T_d/T)$ and $K_{ij} = \sum_{v_j \in N_i} a_{ij}$ denotes outdegree of agent i .

Proof. The multiagent systems of (3) with (5) and (21) are given by (22). Taking the z -transformation of the system (22), we get

$$\begin{aligned} zX_i(z) &= X_i(z) - (Az^{-m_i} + Bz^{-m_i-1} + Cz^{-m_i-2})X_i(z) \\ &\quad + (A + Bz^{-1} + Cz^{-2})\zeta^r(z) \\ &\quad + \sum_{v_j \in N_i} a_{ij}z^{-n_{ij}} [X_j(z) - X_i(z)], \end{aligned} \quad (24)$$

where $X_i(z)$ and $\zeta^r(z)$ are the z -transformation of $x_i(k)$ and $\zeta^r(k)$, respectively. Define a $N \times N$ matrix $\tilde{L}(z) = \{\tilde{l}_{ij}(z)\}$ as follows:

$$\tilde{l}_{ij}(z) = \begin{cases} -a_{ij}z^{-n}, & v_j \in N_i \\ Az^{-m_i} + Bz^{-m_i-1} + Cz^{-m_i-2} + \sum_{v_j \in N_i} a_{ij}z^{-n_{ij}}, & j = i \\ 0, & \text{otherwise} \end{cases} \quad (25)$$

and $X(z) = [X_1(z), \dots, X_N(z)]^T$, $Q = A + Bz^{-1} + Cz^{-2}$; then (24) becomes

$$zX(z) = X(z) + Q\zeta^r(z)1_N - \tilde{L}(z)X(z). \quad (26)$$

Let $\zeta^r(z)$ denote input and let $X(z)$ denote output and 1_N as unit column vector with $N \times 1$ dimensions; then the characteristic equation of system (26) becomes $p(z) = \det[I + (1/(z-1))\tilde{L}(z)]$. In consequence, we will prove the all roots of $p(z) = 0$ whose module is less than unity.

According to general Nyquist stability criterion, modulus of all roots satisfied $p(z) = 0$ should be less than unity, if all poles $\lambda((1/(e^{j\omega} - 1))\tilde{L}(e^{j\omega}))$ of $(1/(e^{j\omega} - 1))\tilde{L}(e^{j\omega})$ do not enclose the point $(-1, j0)$ for $\omega \in [-\pi, \pi]$. By Lemma 1, all poles $\lambda((1/(e^{j\omega} - 1))\tilde{L}(e^{j\omega}))$ belong to the union set of N circular disks; that is,

$$\begin{aligned} D_i &= \left\{ \left| \xi - \frac{Ae^{-j\omega m_i} + Be^{-j\omega(m_i+1)} + Ce^{-j\omega(m_i+2)} + \sum_{v_j \in N_i} a_{ij}e^{-j\omega n_{ij}}}{e^{j\omega} - 1} \right| \right. \\ &\quad \left. \leq \sum_{v_j \in N_i} \left| \frac{a_{ij}e^{-j\omega n_{ij}}}{e^{j\omega} - 1} \right| \right\}. \end{aligned} \quad (27)$$

Moreover, we have

$$\begin{aligned} D_i &= \left\{ \left| \xi - \frac{Ae^{-j\omega m_i} + Be^{-j\omega(m_i+1)} + Ce^{-j\omega(m_i+2)} + K_{ij}e^{-j\omega n_{ij}}}{e^{j\omega} - 1} \right| \right. \\ &\quad \left. < \left| \frac{Ae^{-j\omega m_i} + Be^{-j\omega(m_i+1)} + Ce^{-j\omega(m_i+2)} + K_{ij}e^{-j\omega n_{ij}}}{e^{j\omega} - 1} \right| \right\}, \end{aligned} \quad (28)$$

where $K_{ij} = \sum_{v_j \in N_i} a_{ij}$.

Define $G_i(\omega) = (Ae^{-j\omega m_i} + Be^{-j\omega(m_i+1)} + Ce^{-j\omega(m_i+2)} + K_{ij}e^{-j\omega n_{ij}})/(e^{j\omega} - 1)$; it is easy to see that $G_i(\omega)$ is center of disc D_i . Then, the point $(-1, j0)$ does not enclose in disc D_i for all $\omega \in [-\pi, \pi]$ as long as the point $(-a, j0)$ with $a \geq 1$. As a result, when $\omega \in [-\pi, \pi]$, we have

$$\begin{aligned} &\left| -a + j0 - \frac{Ae^{-j\omega m_i} + Be^{-j\omega(m_i+1)} + Ce^{-j\omega(m_i+2)} + K_{ij}e^{-j\omega n_{ij}}}{e^{j\omega} - 1} \right| \\ &> \left| \frac{Ae^{-j\omega m_i} + Be^{-j\omega(m_i+1)} + Ce^{-j\omega(m_i+2)} + K_{ij}e^{-j\omega n_{ij}}}{e^{j\omega} - 1} \right|. \end{aligned} \quad (29)$$

Through several trivial transform, we have

$$\begin{aligned} & \left| -a + j0 - \frac{Ae^{-j\omega m_i} + Be^{-j\omega(m_i+1)} + Ce^{-j\omega(m_i+2)} + K_{ij}e^{-j\omega n_{ij}}}{e^{j\omega} - 1} \right|^2 - \left| \frac{Ae^{-j\omega m_i} + Be^{-j\omega(m_i+1)} + Ce^{-j\omega(m_i+2)} + K_{ij}e^{-j\omega n_{ij}}}{e^{j\omega} - 1} \right|^2 \\ & = a \left(-\frac{A \sin(((2m_i + 1)/2)\omega) + B \sin(((2m_i + 3)/2)\omega)}{2 \sin(\omega/2)} - \frac{C \sin(((2m_i + 5)/2)\omega) + K_{ij} \sin(((2n_{ij} + 1)/2)\omega)}{2 \sin(\omega/2)} \right) > 0. \end{aligned} \quad (30)$$

As for Lemma 2, we have $\sin(((2m_i + 1)/2)\omega)/\sin(\omega/2) \leq 2m_i + 1$, $\sin(((2m_i + 3)/2)\omega)/\sin(\omega/2) \leq 2m_i + 3$, \sin

$\sin(((2m_i + 5)/2)\omega)/\sin(\omega/2) \leq 2m_i + 5$, and $\sin(((2n_{ij} + 1)/2)\omega)/\sin(\omega/2) \leq 2n_{ij} + 1$. Then the following inequality is obtained by

$$\begin{aligned} & \frac{A \sin(((2m_i + 1)/2)\omega) + B \sin(((2m_i + 3)/2)\omega) + C \sin(((2m_i + 5)/2)\omega) + K_{ij} \sin(((2n_{ij} + 1)/2)\omega)}{2 \sin(\omega/2)} \\ & \leq A(2m_i + 1) + B(2m_i + 3) + C(2m_i + 5) + K_{ij}(2n_{ij} + 1) < a. \end{aligned} \quad (31)$$

Similar to (19), this inequality holds under the conditions of $\omega \in [-\pi, \pi]$ and $a = 1$. That is end of this proof. \square

Remark 7. Because an inequality is used in (28), the result of Theorem 6 is considerable conservatism. If $A = K_{ij}$, $B, C = 0$, we can obtain Theorem 3. That is to say, this conservatism can be ignored if B, C are very small.

Remark 8. By using increment *PID* algorithm, the maximum allowable time delay of consensus tracking of multiagents system become larger; even input delays m_i and communication delay n_{ij} in Theorem 6 are chosen to disobey the inequality; this multiagent systems is still converged to its reference in many cases.

5. Optimization Consensus Tracking *PID* Algorithm Based on Genetic Algorithm

The main result in Section 4 gives a consensus tracking range whose multiagent systems can converge to reference. However, our interesting is how fast these multiagent systems can converge to reference or are there optimal *PID* parameters which make these systems track reference with optimal performances? Here, a new optimization increment *PID* algorithm based on genetic algorithm (*GA-PID*) is proposed for optimization cost including rise time, output energy of controllers, and tracking error.

Here, the fast consensus tracking problem of multiagent system is described as follows: finding the optimal *PID*

parameters K_p, T_i, T_d of Theorem 6 which can make the system achieve faster consensus tracking. It is well known that the genetic algorithm is an effective method that can find the global optimal solution, so we improve the conventional genetic algorithm in order to solve this optimization tracking problem. The basic design steps of self-adjusting *PID* controller based on the genetic algorithm are as follows.

- (1) To ascertain parameters. To ascertain the values of *PID* parameters according to the mathematic model of the system so as to narrow the searching scope and improve the efficiency of optimization, here, let $K_p, T_i, T_d \leq 1$.
- (2) To select the initial population. Here, 50 initial populations are chosen at random, so populations size M is equal to 50.
- (3) To ascertain the adaptation parameter. Combing three control performances stability, *raPIDity*, and accuracy, the target functions shown as below can be used as the optimal index for the selection of parameters:

$$\begin{aligned} J_s &= \sum J_i, \\ J_i &= \int_0^\infty (\omega_1 |e_i(k)| + \omega_2 u_i^2(k)) dt + \omega_3 k_u^i, \quad i \in \Phi, \end{aligned} \quad (32)$$

where J_s is the global optimal index, J_i is the local optimal index of agent i for tracking reference. $e_i(k)$, $u_i(k)$, and k_u^i are the error, controller input, and rising time

TABLE 1: Comparison of convergence time among three algorithms in different topologies ($m = 1, n = 3$).

Agents received constant reference	P -like algorithm $P = 0.1$	Increment PID algorithm $P = 0.1, I = 2, D = 0.1$	Increment PID algorithm based on GA
All	84	45	24
Agent 6	155	87	60
Agent 2	179	76	56
Agent 3	123	78	56
Agents (1, 4, 5, and 6)	153	87	76
Agents (1, 4, 5, and 3)	119	78	64
Agents (1, 4, 5, and 2)	175	70	56
Agents (2, 6)	89	45	32
Agents (2, 3)	85	41	43
Agents (3, 6)	91	47	68
Agents (2, 3, and 6)	84	41	33

of agent i , respectively. $\omega_1, \omega_2, \omega_3$ denotes weighted values of these three parameters.

In order to avoid overshooting, a punishment mechanism is introduced. That is, if the overshooting happened, this overshoot should become a term of local optimal index of agent i . As a result, the local optimal index becomes

If $e_i(k) < 0$,

$$\text{then } J_i = \int_0^{\infty} (\omega_1 |e_i(k)| + \omega_2 u_i^2(k) + \omega_4 |e_i(k)|) dt \quad (33)$$

$$+ \omega_3 k_u^i,$$

where ω_4 is a weighted value satisfying $\omega_4 \gg \omega_1$. Here related weighted values are $\omega_1 = 0.999$, $\omega_2 = 0.001$, and $\omega_3 = 2.0$. The weighted value of punishment mechanism is $\omega_4 = 100$. The fitness function is $F = 1/J_s$.

- (4) Design of genetic operator. Designing genetic operator is a basic operation of genetic algorithm to populations including selection operator, crossover operator, and mutation operator. Selection operator is determined by its selection probability described by $p_i = F_i / \sum_1^M F_i$, where F_i is fitness of agent i . Crossover operator is determined by crossover probability P_c . Mutation operator is determined by mutation probability P_m .
- (5) To ascertain evolution parameters. Here, let initial population $M = 50$, end-up generation $G = 100$, crossover probability $P_c = 0.9$, and initial mutation probability $P_m = 0.1$.

6. Simulation Example

Example 9. Consider the multiagent systems which are composed of one virtue leader and 6 following agents with an interconnection digraph shown by Figure 1. The weights of the directed paths are $a_{12} = 0.1$, $a_{16} = 0.05$, $a_{23} =$

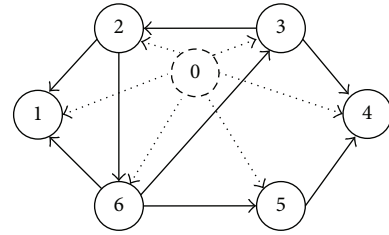


FIGURE 1: Digraph of a group of seven agents.

0.15 , $a_{36} = 0.1$, $a_{43} = 0.05$, $a_{45} = 0.1$, and $a_{56} = 0.15$, $a_{62} = 0.15$. Agent "0" is consensus tracking reference $\zeta^r(k)$ and interconnection with dotted line denotes a communication existing between reference agent and neighbors of this reference agent. Without loss of generality, the virtual leader 0 can also be known only for part of agents and differences topologies could be seen in Table 1. Initial state of all agents is $x(0) = (8, 6, 5, 3, 0, -2)^T$ and sample period of these systems is $T = 1$ second. For simplify, here let $m_i = m, n_{ij} = n, i, j \in (1, 2, \dots, 6)$.

It is easy to see that there exist three globally reachable agents named agent 2, agent 3, and agent 6 in this directed graph. Firstly, all agents which can receive reference are considered when this reference is constant ($\zeta^r(k) = 4$) or time varying ($\zeta^r(k) = \sin(0.15k) + 4$), respectively, and consensus tracking responds could be seen in Figures 2, 3, 4, 5, and 6 under the condition of $m = 1, n = 3$. From Figures 2–4, we can see that the multiagent systems can converge to the constant reference when P -like ($K_{ii} = K_1 = K_2 = \dots = K_6 = 0.1$), Increment PID ($K_p = 0.1, T_i = 0.5, T_d = 0.1$), and GA- PID ($K_p = 0.5122, T_i = 2.4149, T_d = 0.0515$) and GA- PID algorithm has faster convergent speed than that of the two. If we compare maximum allowable time delay, GA- PID has the largest consensus tracking allowable time delays known as $m = 1, n = 21$ in contrast to $m = 1, n = 5$ as to conventional P -like algorithm and $m = 1, n = 12$ as to increment PID algorithm. Figure 5 show the optimization process of Best J based on genetic algorithm.

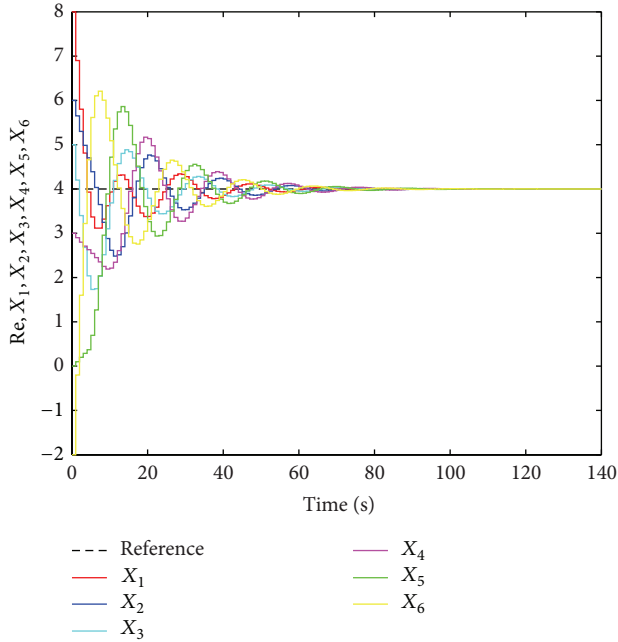


FIGURE 2: States trajectory achieving consensus by P -like algorithm.

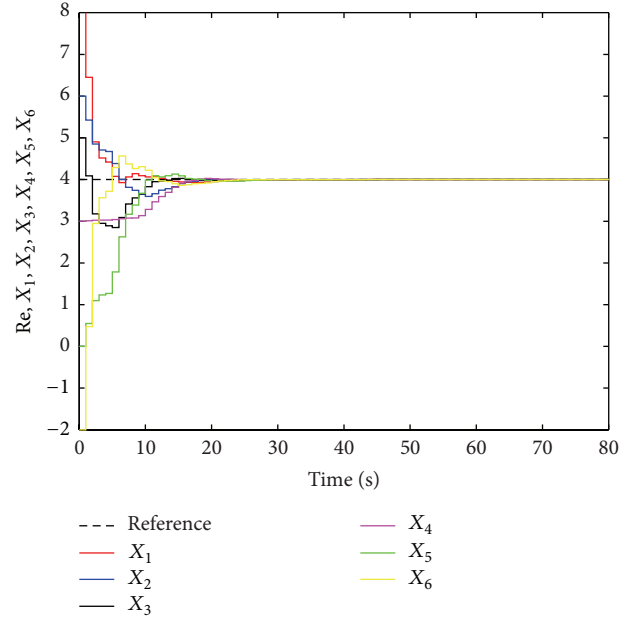


FIGURE 4: States trajectory achieving consensus by GA- PID algorithm.

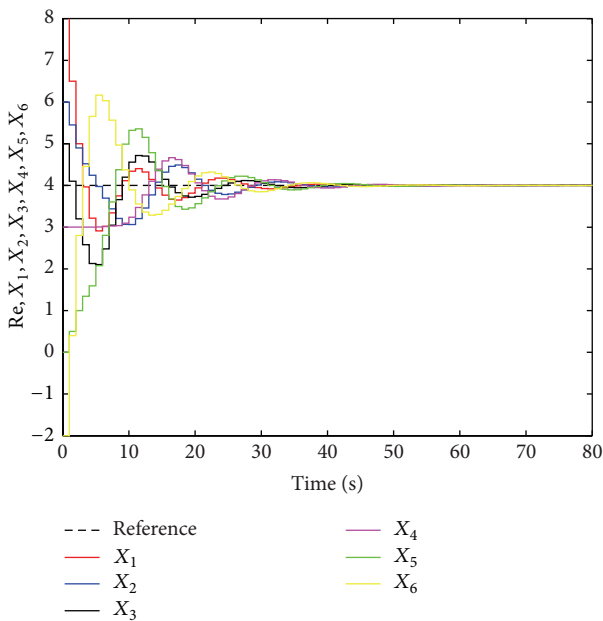


FIGURE 3: States trajectory achieving consensus by increment PID algorithm.

In fact, the multiagent systems can converge to the reference on the condition that at least one globally reachable agent can receive the constant reference. Similar results can also be obtained in different topologies. Details could be seen in Table 1. Comparing these three algorithms we can see that P -like algorithm has slowest convergence speed, increment PID algorithm has strongest robustness performance, and increment PID based on GA has fastest convergence speed in almost all cases. What is more, a very interesting thing

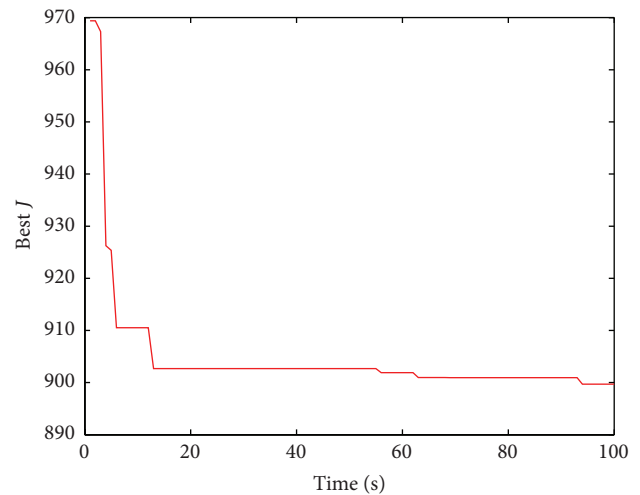


FIGURE 5: Best J for GA- PID algorithm.

is also deduced from Table 1. That is, convergence speed is similar between all agents receiving the reference and only globally reachable agents receiving the reference. This means that only globally reachable agents instead of all agents receive reference and a similar convergence speed can also be obtained.

From [9] we know that conventional P -like algorithm is not sufficient for consensus tracking when all agents receive a time-varying consensus reference. However, if our increment PID algorithm is adopted, consensus tracking can be achieved through choosing suitable PID parameters. Comparing Figure 6 with Figure 7 we can see that suitable PID parameters not only decrease errors between reference and current states of agents, but also increase the convergence

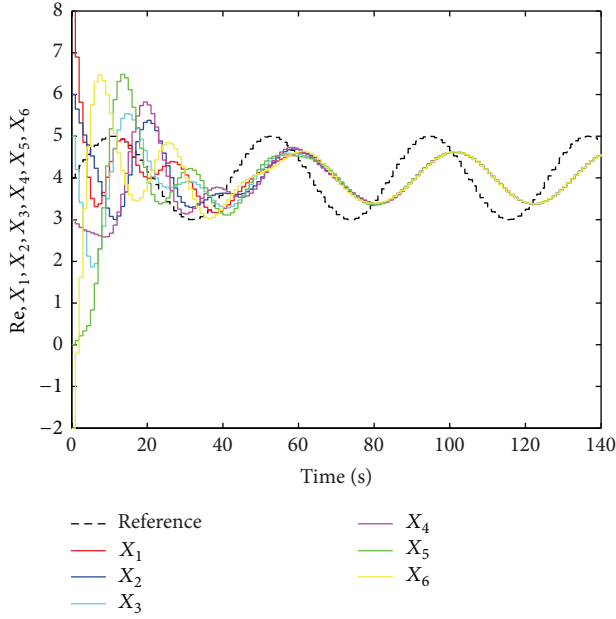


FIGURE 6: States trajectory with time-varying reference by P -like algorithm when $P = 0.1$.

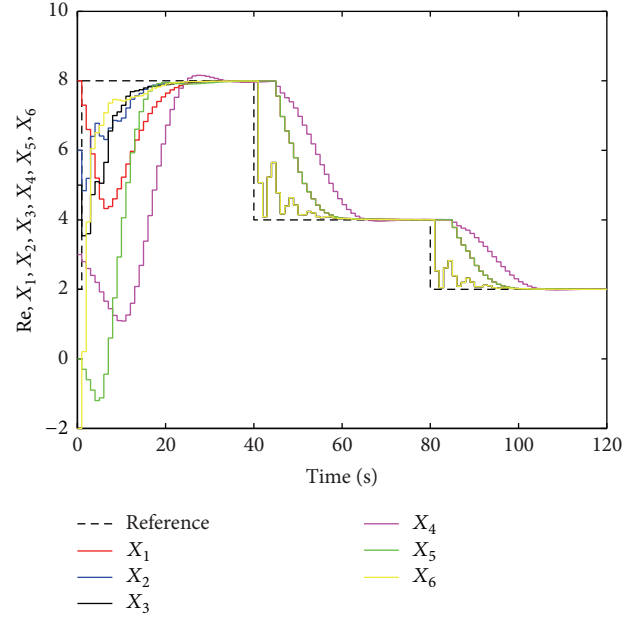


FIGURE 8: Consensus tracking in piecewise constant by GA-PID algorithm only (2, 3, 6) receiving reference.

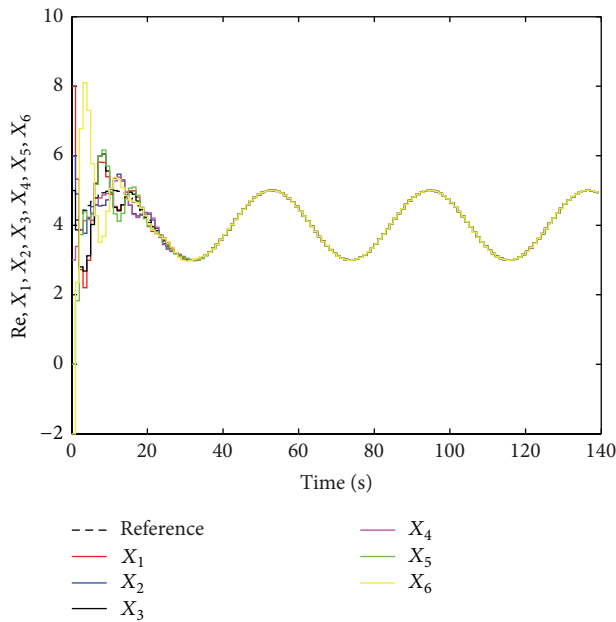


FIGURE 7: States trajectory achieving consensus with time-varying reference by increment PID algorithm when $P = 0.2$, $I = 2.56$, and $D = 0.125$.

speed. Regrettably, these three algorithms cannot be used to track a time-varying reference, that is, available to only a subset of the team members for only receiving time-varying reference state. If time-varying reference changes in a piecewise constant case, increment PID algorithm based on genetic algorithm can track this time-varying reference whether the reference is available to all team members or to a subset of the team member. From Figure 8 we can see that

the multiagent systems can converge to a piecewise constant reference within about 40 seconds when only agents (2, 3, 6) receive this time-varying reference. This characteristic can be applied to many fields such as synchronizing a network of clocks [13].

7. Conclusions

In this paper, three consensus tracking algorithms named P -like algorithm, increment PID algorithm, and increment PID algorithm based on genetic algorithm, respectively, for discrete-time multiagent systems with time-varying input delays and communication delays are proposed based on the frequency-domain analysis. Firstly, a consensus tracking sufficient condition of conventional P -like algorithm is obtained. Secondly, a new increment PID algorithm based on similar frequency-domain method is designed for improving consensus convergence speed and an inequality condition is also deduced. Finally, considering three control performances stability, rapidity, and accuracy, an increment PID algorithm based on genetic algorithm is designed to find optimal PID parameters within an inequality allowable span for achieving optimization cost. These three algorithms can solve tracking problem of multiagent systems with a constant reference effectively when reference state is available to all the team members. If the reference state might only be available to a portion of the agents in the team, the convergence speed may increase in the same condition. As for a time-varying reference case, if the reference state has a directed path to all team agents, increment PID algorithm and increment PID algorithm based on genetic algorithm can realize consensus tracking through choosing suitable PID parameters while conventional P -like algorithm fails to track the reference.

However, these three algorithms cannot be used to track a time-varying reference state when the reference is available to only a subset of team members. In the future research, we will focus on more complex issues in the controller design such as actuator delay and fault, H_∞ controller design with control delay, quantized control, and global consensus problem with saturated control [22–29].

Conflict of Interests

The authors declare that there is no conflict of interests regarding the publication of this paper.

Acknowledgments

This research was supported by the National Natural Science Foundation of China under Grant nos. 61004033 and 61364002, Foundation of 2012 Jinchuan School-Enterprise Cooperation, and the Yunnan Natural Science Foundation of Yunnan Province, China, under Grant no. 2010ZC035.

References

- [1] X. Luo, D. Liu, X. Guan, and S. Li, "Flocking in target pursuit for multi-agent systems with partial informed agents," *IET Control Theory and Applications*, vol. 6, no. 4, pp. 560–569, 2012.
- [2] H. Su, X. Wang, and Z. Lin, "Flocking of multi-agents with a virtual leader," *IEEE Transactions on Automatic Control*, vol. 54, no. 2, pp. 293–307, 2009.
- [3] R. Sepulchre, D. A. Paley, and N. E. Leonard, "Stabilization of planar collective motion with limited communication," *IEEE Transactions on Automatic Control*, vol. 53, no. 3, pp. 706–719, 2008.
- [4] J. A. Fax and R. M. Murray, "Information flow and cooperative control of vehicle formations," *IEEE Transactions on Automatic Control*, vol. 49, no. 9, pp. 1465–1476, 2004.
- [5] R. W. Beard, T. W. McLain, M. A. Goodrich, and E. P. Anderson, "Coordinated target assignment and intercept for unmanned air vehicles," *IEEE Transactions on Robotics and Automation*, vol. 18, no. 6, pp. 911–922, 2002.
- [6] T. Vicsek, A. Czirak, E. Ben-Jacob, I. Cohen, and O. Shochet, "Novel type of phase transition in a system of self-driven particles," *Physical Review Letters*, vol. 75, no. 6, pp. 1226–1229, 1995.
- [7] R. Olfati-Saber and R. M. Murray, "Consensus problems in networks of agents with switching topology and time-delays," *IEEE Transactions on Automatic Control*, vol. 49, no. 9, pp. 1520–1533, 2004.
- [8] R. M. Murray, "Recent research in cooperative control of multi-vehicle systems," *Journal of Dynamic Systems, Measurement, and Control*, vol. 129, no. 5, pp. 571–583, 2007.
- [9] W. Ren and R. W. Beard, *Distributed Consensus in Multi-Vehicle Cooperative Control: Theory and Applications*, Communications and Control Engineering, Springer, 2008.
- [10] Y.-P. Tian and C.-L. Liu, "Consensus of multi-agent systems with diverse input and communication delays," *IEEE Transactions on Automatic Control*, vol. 53, no. 9, pp. 2122–2128, 2008.
- [11] Y. She and H. Fang, "Fast distributed consensus control for second-order multi-agent systems," in *Proceedings of the Chinese Control and Decision (CCDC '10)*, pp. 87–92, Xuzhou, China, May 2010.
- [12] H.-T. Zhang, M. Z. Q. Chen, and G.-B. Stan, "Fast consensus via predictive pinning control," *IEEE Transactions on Circuits and Systems I*, vol. 58, no. 9, pp. 2247–2258, 2011.
- [13] R. Carli, A. Chiuso, L. Schenato, and S. Zampieri, "Optimal synchronization for networks of noisy double integrators," *IEEE Transactions on Automatic Control*, vol. 56, no. 5, pp. 1146–1152, 2011.
- [14] S. Li, H. Du, and X. Lin, "Finite-time consensus algorithm for multi-agent systems with double-integrator dynamics," *Automatica*, vol. 47, no. 8, pp. 1706–1712, 2011.
- [15] H. Sayyaadi and M. R. Doostmohammadian, "Finite-time consensus in directed switching network topologies and time-delayed communications," *Scientia Iranica*, vol. 18, no. 1 B, pp. 21–34, 2011.
- [16] Y. Zheng and L. Wang, "Finite-time consensus of heterogeneous multi-agent systems with and without velocity measurements," *Systems & Control Letters*, vol. 61, pp. 871–878, 2012.
- [17] W. Ren, "Consensus tracking under directed interaction topologies: algorithms and experiments," *IEEE Transactions on Control Systems Technology*, vol. 18, no. 1, pp. 230–237, 2010.
- [18] Y. Cao and W. Ren, "Distributed coordinated tracking with reduced interaction via a variable structure approach," *IEEE Transactions on Automatic Control*, vol. 57, no. 1, pp. 33–48, 2012.
- [19] J. Mei, W. Ren, and G. Ma, "Distributed coordinated tracking with a dynamic leader for multiple euler-lagrange systems," *IEEE Transactions on Automatic Control*, vol. 56, no. 6, pp. 1415–1421, 2011.
- [20] Z. Chen, L. Xiang, and Z. Yuan, "A tracking control scheme for leader based multi-agent consensus for discrete-time case," in *Proceedings of the 27th Chinese Control Conference (CCC '08)*, pp. 494–498, Kunming, China, July 2008.
- [21] D. Whitley, "A genetic algorithm tutorial," *Statistics and Computing*, vol. 4, no. 2, pp. 65–85, 1994.
- [22] H. Li, H. Liu, H. Gao, and P. Shi, "Reliable fuzzy control for active suspension systems with actuator delay and fault," *IEEE Transactions on Fuzzy Systems*, vol. 20, no. 2, pp. 342–357, 2012.
- [23] H. Li, X. Jing, and H. R. Karimi, "Output-feedback based H-infinity control for active suspension systems with control delay," *IEEE Transactions on Industrial Electronics*, vol. 61, no. 1, pp. 436–446, 2014.
- [24] Z. Su, H. Zhang, and F. W. Yang, "Observer-based H-infinity control for discrete-time stochastic systems with quantization and random communication delays," *IET Control Theory and Applications*, vol. 7, no. 3, pp. 372–379, 2013.
- [25] H. Zhang, Q. Chen, H. Yan, and J. Liu, "Robust H ∞ filtering for switched stochastic system with missing measurements," *IEEE Transactions on Signal Processing*, vol. 57, no. 9, pp. 3466–3474, 2009.
- [26] Q. Wang and H. Gao, "Global consensus of multiple integrator agents via saturated controls," *Journal of the Franklin Institute*, vol. 350, no. 8, pp. 2261–2276, 2013.
- [27] H. Zhang, H. Yan, F. Yang, and Q. Chen, "Quantized control design for impulsive fuzzy networked systems," *IEEE Transactions on Fuzzy Systems*, vol. 19, no. 6, pp. 1153–1162, 2011.
- [28] Q. Wang, C. Yu, and H. Gao, "Semiglobal synchronization of multiple generic linear agents with input saturation," *International Journal of Robust and Nonlinear Control*, 2013.
- [29] Q. Wang, C. Yu, and H. Gao, "Semiglobal synchronization of multiple generic linear agents with input saturation," *International Journal of Robust and Nonlinear Control*, 2013.

Research Article

Robust Decentralized Adaptive Neural Control for a Class of Nonaffine Nonlinear Large-Scale Systems with Unknown Dead Zones

Huanqing Wang,¹ Qi Zhou,² Xuebo Yang,³ and Hamid Reza Karimi⁴

¹ School of Mathematics and Physics, Bohai University, Liaoning, Jinzhou 121000, China

² College of Information Science and Technology, Bohai University, Liaoning, Jinzhou 121000, China

³ College of Engineering, Bohai University, Liaoning, Jinzhou 121000, China

⁴ Department of Engineering, Faculty of Engineering and Science, University of Agder, 4898 Grimstad, Norway

Correspondence should be addressed to Huanqing Wang; ndwhq@163.com

Received 6 January 2014; Accepted 11 February 2014; Published 19 March 2014

Academic Editor: Huaicheng Yan

Copyright © 2014 Huanqing Wang et al. This is an open access article distributed under the Creative Commons Attribution License, which permits unrestricted use, distribution, and reproduction in any medium, provided the original work is properly cited.

The problem of robust decentralized adaptive neural stabilization control is investigated for a class of nonaffine nonlinear interconnected large-scale systems with unknown dead zones. In the controller design procedure, radical basis function (RBF) neural networks are applied to approximate packaged unknown nonlinearities and then an adaptive neural decentralized controller is systematically derived without requiring any information on the boundedness of dead zone parameters (slopes and break points). It is proven that the developed control scheme can ensure that all the signals in the closed-loop system are semiglobally uniformly ultimately bounded in the sense of mean square. Simulation study is provided to further demonstrate the effectiveness of the developed control scheme.

1. Introduction

During the past several decades, a large number of research results have been obtained on the problems of stability analysis and control design for nonlinear systems because of the extensive existence of nonlinearity in the practical systems. So far, there are many control methods proposed to control design of nonlinear systems, such as adaptive backstepping control [1–4], fault-tolerant control [5–9], H_∞ control [10–16], and fuzzy control [17–21]. In the control of uncertain complex nonlinear systems, backstepping-based neural networks or fuzzy adaptive control technique is an efficient and practical strategy, and many interesting results have been obtained for a class of uncertain nonlinear strict-feedback systems; for example, see [22–37]. In addition, adaptive neural or fuzzy backstepping control approach can also be extended to control a class of nonaffine pure-feedback nonlinear systems representing a class of more general lower triangular systems, in which no affine appearance of the state variables can be used as virtual control signals. This

makes it quite difficult and more meaningful to control the pure-feedback systems. By using small-gain theorem, in [38], an adaptive neural control scheme is presented for a class of completely nonaffine pure-feedback systems. Afterwards, some researchers further consider other types of pure-feedback nonlinear systems, such as pure-feedback systems with time-delay [39] and with dead-zone [40].

Large-scale system is considered as a dynamical system which is composed of some lower-order subsystems with interconnections and often exists in many practical applications such as electric power systems, computer network systems, and aerospace systems. Decentralized adaptive control of unknown nonlinear interconnected systems has attracted much research attention because this problem is important both theoretically and practically. Up to now, many interesting adaptive decentralized control approaches for large-scale nonlinear systems have been proposed in [41, 42] and the references therein. By combining backstepping technique together with adaptive neural or fuzzy control, many research papers have been published in [28–32] for

affine nonlinear large-scale interconnected systems and in [43, 44] for nonaffine nonlinear large-scale systems. However, these researches have not considered the effect of the system input signal with dead zone. The existence of dead zone input nonlinearity severely degrades system performance. So, dead zone nonlinearity has to be considered when controller is designed in many industrial processes, such as valves, DC servo motors, and other devices. In [45], an adaptive robust control scheme is proposed for a class of nonlinear systems, in which the dead zone nonlinearity is expressed by a combination of a line and a disturbance-like term and its parameters are tuned by using adaptive technique. Then, some backstepping-based adaptive control schemes are developed for nonlinear systems with unknown dead zone input [46–50].

Based on the above observations, this paper focuses on the problem of adaptive neural decentralized control for a class of nonaffine large-scale nonlinear systems with unknown dead zones. The proposed adaptive neural controller guarantees that all the signals in the closed-loop systems remain semiglobally uniformly ultimately bounded in the sense of mean square, and the error signals eventually converge to small neighborhood around the origin. The main advantages of this research lie in that (i) the dead-zone inverse as well as the prior knowledge of bounds of dead-zone parameters (slopes and break-points) is not required; (ii) only one adaptive parameter is involved in the developed controller for each subsystem. As a result, the computational burden is significantly alleviated. In this way, the proposed control law could be easily implemented in practical applications. Simulation results are provided to further illustrate the effectiveness of the proposed control approach.

The paper is organized as follows. Section 2 provides the problem formulation and preliminaries. The control design and analysis of state feedback controller are given in Section 3, following a simulation example in Section 4. Section 5 concludes this paper.

2. Problem Formulation and Preliminaries

Consider a class of pure-feedback nonlinear interconnected large-scale systems with dead zones and N subsystems, and the i th ($i = 1, 2, \dots, N$) subsystem is in the following form:

$$\begin{aligned}\dot{x}_{i,j} &= f_{i,j}(\bar{x}_{i,j}, x_{i,j+1}) + \varphi_{i,j}(\bar{y}), \quad 1 \leq j \leq n_i - 1, \\ \dot{x}_{i,n_i} &= f_{i,n_i}(\bar{x}_{i,n_i}, u_i) + \varphi_{i,n_i}(\bar{y}), \\ y_i &= x_{i,1},\end{aligned}\quad (1)$$

where $\bar{x}_{i,j} = [x_{i,1}, x_{i,2}, \dots, x_{i,j}]^T$ and $\bar{y} = [y_1, y_2, \dots, y_N]^T$. $x_i = [x_{i,1}, x_{i,2}, \dots, x_{i,n_i}]^T \in R^{n_i}$ and $y_i \in R$ are the state variables and the output of the i th subsystem, respectively. $f_{i,j}(\cdot) : R^{j+1} \rightarrow R$, ($j = 1, 2, \dots, n_i$) are unknown smooth nonlinear functions; $\varphi_{i,j}(\cdot) : R^N \rightarrow R$ ($j = 1, 2, \dots, n_i$) are unknown interconnections between the i th subsystem and

other subsystems, with $f_{i,j}(0) = \varphi_{i,j}(0) = 0$; $u_i \in R$ is the output of an unknown dead zone and defined as

$$u_i = D(v_i) = \begin{cases} g_{ir}(v_i), & v_i \geq b_{ir}, \\ 0, & b_{il} < v_i < b_{ir}, \\ g_{il}(v_i), & v_i \leq b_{il}, \end{cases}\quad (2)$$

where $b_{il} < 0$ and $b_{ir} > 0$ are the unknown parameters and $v_i(t) \in R$ is the input of the dead zone.

For the unknown dead zone input, the following assumption is required.

Assumption 1 (see [40]). The functions, $g_{il}(v_i)$ and $g_{ir}(v_i)$, are smooth and there exist unknown positive constants, $k_{il0}, k_{il1}, k_{ir0}$, and k_{ir1} , such that

$$\begin{aligned}0 < k_{il0} \leq g'_{il}(v_i) \leq k_{il1}, \quad \forall v_i \in (-\infty, b_{il}], \\ 0 < k_{ir0} \leq g'_{ir}(v_i) \leq k_{ir1}, \quad \forall v_i \in [b_{ir}, +\infty),\end{aligned}\quad (3)$$

and $\beta_{i0} \leq \min\{k_{il0}, k_{ir0}\}$ is an unknown positive constant, where $g'_{il}(v_i) = (dg_{il}(z)/dz)|_{z=v_i}$ and $g'_{ir}(v_i) = (dg_{ir}(z)/dz)|_{z=v_i}$.

Remark 2. Assumption 1 is similar to the assumption in [40] where β_{i0} is a known constant. However, Assumption 1 does not require it to be known. So, Assumption 1 relaxes the limitation in [40].

Based on Assumption 1, the dead zone (2) can be rewritten as [40]

$$u_i = D(v_i) = K_i^T(t) \Phi_i(t) v_i + d_i(v_i), \quad (4)$$

where

$$\begin{aligned}\Phi_i(t) &= [\varphi_{ir}(t), \varphi_{il}(t)]^T, \\ \varphi_{ir}(t) &= \begin{cases} 1, & v_i(t) > b_{il}, \\ 0, & v_i(t) \leq b_{il}, \end{cases} \\ \varphi_{il}(t) &= \begin{cases} 1, & v_i(t) < b_{ir}, \\ 0, & v_i(t) \geq b_{ir}, \end{cases}\end{aligned}$$

$$K_i(t) = [K_{ir}(v_i(t)), K_{il}(v_i(t))]^T,$$

$$K_{ir}(v_i(t)) = \begin{cases} 0, & v_i(t) \leq b_{il}, \\ g'_{ir}(\xi_{ir}(v_i(t))), & b_{il} < v_i(t) < +\infty, \end{cases}$$

$$K_{il}(v_i(t)) = \begin{cases} g'_{il}(\xi_{il}(v_i(t))), & -\infty < v_i(t) < b_{ir}, \\ 0, & v_i(t) \geq b_{ir}, \end{cases}$$

$$d_i(v_i) = \begin{cases} -g'_{ir}(\xi_{ir}(v_i)) b_{ir}, & v_i \geq b_{ir}, \\ -[g'_{il}(\xi_{il}(v_i)) + g'_{ir}(\xi_{ir}(v_i))] v_i, & b_{il} < v_i < b_{ir}, \\ -g'_{il}(\xi_{il}(v_i)) b_{il}, & v_i \leq b_{il}, \end{cases}\quad (5)$$

where $\xi_{il}(v_i) \in (v_i, b_{il})$, if $v_i < b_{il}$; $\xi_{il}(v_i) \in (b_{il}, v_i)$, if $b_{il} \leq v_i < b_{ir}$; $\xi_{ir}(v_i) \in (b_{ir}, v_i)$, if $b_{ir} < v_i$; $\xi_{ir}(v_i) \in (v_i, b_{ir})$, and if $b_{il} < v_i \leq b_{ir}$, and $|d_i(v_i)| \leq p_i^*$, p_i^* is an unknown positive constant with $p_i^* = (k_{ir1} + k_{il1}) \max\{b_{ir}, -b_{il}\}$.

Remark 3. As shown in [40], there exist some other expressions for the case of linear dead zone outside the deadband, but (4) includes the most actual cases and $K_i^T(t)\Phi_i(t) \in [\beta_{i0}, k_{i1l} + k_{i1r}] \subset (0, +\infty)$.

Based on mean value theorem [51], $f_{i,j}(\cdot)$ in (1) can be described as

$$\begin{aligned} f_{i,j}(\bar{x}_{i,j}, x_{i,j+1}) &= f_{i,j}(\bar{x}_{i,j}, x_{i,j+1}^0) + h_{\mu_{i,j}}(x_{i,j+1} - x_{i,j+1}^0), \\ f_{i,n_i}(\bar{x}_{i,n_i}, u_i) &= f_{i,n_i}(\bar{x}_{i,n_i}, u_i^0) + h_{\mu_{i,n_i}}(u_i - u_i^0), \end{aligned} \quad (6)$$

where smooth function $f_{i,j}(\cdot)$ is explicitly analyzed between $f_{i,j}(\bar{x}_{i,j}, x_{i,j+1})$ and $f_{i,j}(\bar{x}_{i,j}, x_{i,j+1}^0)$, $h_{\mu_{i,j}} := h_{i,j}(\bar{x}_{i,j}, x_{\mu_{i,j}}) = (\partial f_{i,j}(\bar{x}_{i,j}, x_{i,j+1}) / \partial x_{i,j+1})|_{x_{i,j+1}=x_{\mu_{i,j}}}$, $x_{i,n_i+1} = u_i$, $x_{\mu_{i,j}} = \mu_{i,j}x_{i,j+1} + (1 - \mu_{i,j})x_{i,j+1}^0$, $0 < \mu_{i,j} < 1$, $i = 1, 2, \dots, N$, $j = 1, 2, \dots, n_i$.

Next, by substituting (6) and (4) into (1), and choosing $x_{i,j+1}^0 = 0$, $u_i^0 = 0$, we obtain

$$\begin{aligned} \dot{x}_{i,j} &= h_{\mu_{i,j}}x_{i,j+1} + f_{i,j}(\bar{x}_{i,j}, 0) + \varphi_{i,j}(\bar{y}), \quad 1 \leq j \leq n_i - 1, \\ \dot{x}_{i,n_i} &= h_{\mu_{i,n_i}}K_i^T(t)\Phi_i(t)v_i + h_{\mu_{i,n_i}}d_i(v_i) + f_{i,n_i}(\bar{x}_{i,n_i}, 0) \\ &\quad + \varphi_{i,n_i}(\bar{y}), \\ y_i &= x_{i,1}. \end{aligned} \quad (7)$$

Assumption 4 (see [40]). The signs of $h_{\mu_{i,j}}$, $1 \leq i \leq N$, $1 \leq j \leq n_i$, do not change, and there exist unknown constants b_m and c such that

$$0 < b_m \leq |h_{\mu_{i,j}}| \leq c < \infty. \quad (8)$$

Remark 5. Assumption 4 means that $h_{\mu_{i,j}}$ are strictly either positive or negative. Without loss of generality, it is assumed that $0 < b_m \leq h_{\mu_{i,j}}$. In addition, by means of Assumptions 1 and 4, it can be further supposed that

$$\begin{aligned} 0 < b \leq h_{\mu_{i,j}}, \quad 1 \leq i \leq N, \quad 1 \leq j \leq n_i - 1, \\ 0 < b \leq h_{\mu_{i,n_i}}K_i^T(t)\Phi_i(t), \end{aligned} \quad (9)$$

where $b = \min\{b_m, b_m\beta_{i0}\}$ is an unknown constant.

Assumption 6 (see [31]). For uncertain nonlinear functions $\varphi_{i,j}(\bar{y})$ in (1), there exist unknown smooth functions $\varphi_{i,j,l}(y_l)$ such that for $1 \leq i \leq N$, $1 \leq j \leq n_i$,

$$|\varphi_{i,j}(\bar{y})|^2 \leq \sum_{l=1}^N \varphi_{i,j,l}^2(y_l), \quad (10)$$

where $\varphi_{i,j,l}(0) = 0$, $l = 1, 2, \dots, N$.

Noting that $\varphi_{i,j,l}(y_l)$ in (10) is smooth function with $\varphi_{i,j,l}(0) = 0$, so there exist unknown smooth functions $\bar{\varphi}_{i,j,l}(y_l)$ such that

$$|\varphi_{i,j}(\bar{y})|^2 \leq \sum_{l=1}^N y_l^2 \bar{\varphi}_{i,j,l}^2(y_l). \quad (11)$$

In what follows, RBF neural networks are applied to approximate any continuous function $f(X) : R^n \rightarrow R$,

$$f_m(X) = W^T \phi(X), \quad (12)$$

where $X \in \Omega_Z \subset R^q$ is the input vector with q being the neural networks input dimension, weight vector $W = [w_1, w_2, \dots, w_l]^T \in R^l$, $l > 1$ is the neural networks node number, and $\phi(X) = [\phi_1(X), \phi_2(X), \dots, \phi_l(X)]^T$ means the basis function vector with $\phi_i(X)$ being chosen as the commonly used Gaussian function of the form

$$\phi_i(X) = \exp\left[-\frac{(X - \mu_i)^T(X - \mu_i)}{\eta_i^2}\right], \quad i = 1, 2, \dots, l, \quad (13)$$

where $\mu_i = [\mu_{i1}, \mu_{i2}, \dots, \mu_{iq}]^T$ is the center of the receptive field and η_i is the width of the Gaussian function. In [52], it has been indicated that with sufficiently large node number l , the RBF neural networks (12) can approximate any continuous function $f(X)$ over a compact set $\Omega_Z \subset R^q$ to arbitrary any accuracy $\varepsilon > 0$ as

$$f(X) = W^{*T} \phi(X) + \delta(X), \quad \forall z \in \Omega_Z \in R^q, \quad (14)$$

where W^* is the ideal constant weight vector and defined as

$$W^* := \arg \min_{W \in \bar{R}^l} \left\{ \sup_{Z \in \Omega_Z} |f(X) - W^T \phi(X)| \right\}, \quad (15)$$

and $\delta(X)$ denotes the approximation error and satisfies $|\delta(X)| \leq \varepsilon$.

Lemma 7 (see [53]). *Consider the Gaussian RBF networks (12) and (2). Let $\rho := (1/2)\min_{i \neq j} \|\mu_i - \mu_j\|$; then an upper bound of $\|\phi(X)\|$ is taken as*

$$\|\phi(X)\| \leq \sum_{k=0}^{\infty} 3q(k+2)^{q-1} e^{-2\rho^2 k^2 / \eta^2} := s. \quad (16)$$

It has been shown in [38] that the constant s in Lemma 7 has a limited value and is independent of the variable X and the dimension of neural weights l .

3. Adaptive Neural Control Design

In this section, an adaptive neural backstepping control scheme will be developed. During the controller design, for the i th subsystem, RBF neural network $W_{i,j}^T \phi(X_{i,j})$ will be utilized to approximate the packaged unknown function $F_{i,j}(X_{i,j})$ at step j . Both the virtual control signals $\alpha_{i,j}(X_{i,j})$

and adaption laws $\dot{\hat{\theta}}_i$ will be constructed in the following forms:

$$\alpha_{i,j}(X_{i,j}) = -k_{i,j}z_{i,j} - \frac{1}{2a_{i,j}^2}z_{i,j}\hat{\theta}_i\phi_{i,j}^T(X_{i,j})\phi_{i,j}(X_{i,j}), \quad (17)$$

$$\dot{\hat{\theta}}_i = \sum_{j=1}^{n_i} \frac{\lambda_i}{2a_{i,j}^2}z_{i,j}^2\phi_{i,j}^T(X_{i,j})\phi_{i,j}(X_{i,j}) - \gamma_i\hat{\theta}_i, \quad (18)$$

where $i = 1, 2, \dots, N$, $j = 1, 2, \dots, n_i$, $k_{i,j}$, $a_{i,j}$, λ_i , and γ_i are positive design parameters, $X_{i,1} = x_{i,1}$, $X_{i,j} = [\bar{x}_{i,j}^T, \hat{\theta}_i]^T$, ($j = 2, \dots, n_i$) with $\bar{x}_{i,j} = [x_{i,1}, x_{i,2}, \dots, x_{i,j}]^T$, and $z_{i,j}$ satisfy the following coordinate transformation:

$$z_{i,j} = x_{i,j} - \alpha_{i,j-1} \quad (19)$$

with $\alpha_{i,0} = 0$. $\hat{\theta}_i$ is used to estimate an unknown constant θ_i which will be defined as

$$\theta_i = \max \left\{ \frac{1}{b} \|W_{i,j}\|^2; j = 1, 2, \dots, n_i \right\}, \quad (20)$$

where b is specified in Remark 5, and $\|W_{i,j}\|$ will be defined at the j th step. Specially, α_{i,n_i} is the actual control input signal u_i .

For simplicity, in the following, the time variable t and the state vector $\bar{x}_{i,j}$ will be omitted from the corresponding functions and let $\phi_{i,j}(X_{i,j}) = \phi_{i,j}$.

Step 1. Based on $z_{i,1} = x_{i,1}$, $z_{i,2} = x_{i,2} - \alpha_{i,1}$, the error dynamic $z_{i,1}$ satisfies

$$\dot{z}_{i,1} = h_{\mu_{i,1}}z_{i,2} + h_{\mu_{i,1}}\alpha_{i,1} + f_{i,j}(\bar{x}_{i,j}, 0) + \varphi_{i,1}(\bar{y}). \quad (21)$$

Consider a Lyapunov function candidate as $V_{i,1} = (1/2)z_{i,1}^2 = (1/2)y_i^2$. Then, the time derivative of $V_{i,1}$ along (21) satisfies

$$\dot{V}_{i,1} = y_i(h_{\mu_{i,1}}z_{i,2} + h_{\mu_{i,1}}\alpha_{i,1} + f_{i,1}(\bar{x}_{i,1}, 0) + \varphi_{i,1}(\bar{y})). \quad (22)$$

By using (11) and the completion of squares, we get

$$y_i\varphi_{i,1}(\bar{y}) \leq \frac{1}{2}y_i^2 + \frac{1}{2}\sum_{l=1}^N y_l^2\bar{\varphi}_{i,1,l}^2(y_l). \quad (23)$$

Further, (22) can be rewritten as

$$\begin{aligned} \dot{V}_{i,1} &= y_i \left(h_{\mu_{i,1}}z_{i,2} + h_{\mu_{i,1}}\alpha_{i,1} + f_{i,1}(\bar{x}_{i,1}, 0) + \frac{1}{2}y_i \right) \\ &\quad + \frac{1}{2}\sum_{l=1}^N y_l^2\bar{\varphi}_{i,1,l}^2(y_l). \end{aligned} \quad (24)$$

Step j ($2 \leq j \leq n_i - 1$). According to (19), one has

$$\dot{z}_{i,j} = h_{\mu_{i,j}}z_{i,j+1} + h_{\mu_{i,j}}\alpha_{i,j} + f_{i,j}(\bar{x}_{i,j}, 0) + \varphi_{i,j}(\bar{y}) - \dot{\alpha}_{i,j-1}, \quad (25)$$

where

$$\dot{\alpha}_{i,j-1} = \sum_{k=1}^{j-1} \frac{\partial \alpha_{i,j-1}}{\partial x_{i,k}} (f_{i,k}(\bar{x}_{i,k+1}) + \varphi_{i,k}(\bar{y})) + \frac{\partial \alpha_{i,j-1}}{\partial \hat{\theta}_i} \dot{\hat{\theta}}_i. \quad (26)$$

Take Lyapunov function $V_{i,j} = (1/2)z_{i,j}^2$; then we have

$$\begin{aligned} \dot{V}_{i,j} &= z_{i,j} \left(g_{\mu_{i,j}}z_{i,j+1} + g_{\mu_{i,j}}\alpha_{i,j} + f_{i,j}(\bar{x}_{i,j}, 0) + \varphi_{i,j}(\bar{y}) \right. \\ &\quad \left. - \sum_{k=1}^{j-1} \frac{\partial \alpha_{i,j-1}}{\partial x_{i,k}} (f_{i,k}(\bar{x}_{i,k+1}) + \varphi_{i,k}(\bar{y})) - \frac{\partial \alpha_{i,j-1}}{\partial \hat{\theta}_i} \dot{\hat{\theta}}_i \right). \end{aligned} \quad (27)$$

Following the same line as the procedures used in (23), one has

$$-z_{i,j} \sum_{k=1}^{j-1} \frac{\partial \alpha_{i,j-1}}{\partial x_{i,k}} \varphi_{i,k}(\bar{y}) \quad (28)$$

$$\leq \frac{1}{2}z_{i,j}^2 \sum_{k=1}^{j-1} \left(\frac{\partial \alpha_{i,j-1}}{\partial x_{i,k}} \right)^2 + \frac{1}{2} \sum_{k=1}^N \sum_{l=1}^N y_l^2 \bar{\varphi}_{i,k,l}^2(y_l),$$

$$z_{i,j}\varphi_{i,j}(\bar{y}) \leq \frac{1}{2}z_{i,j}^2 + \frac{1}{2} \sum_{l=1}^N y_l^2 \bar{\varphi}_{i,j,l}^2(y_l). \quad (29)$$

It can be easily verified from (27) to (29) that

$$\begin{aligned} \dot{V}_{i,j} &\leq z_{i,j} \left(h_{\mu_{i,j}}z_{i,j+1} + h_{\mu_{i,j}}\alpha_{i,j} + f_{i,j}(\bar{x}_{i,j}, 0) \right. \\ &\quad \left. - \sum_{k=1}^{j-1} \frac{\partial \alpha_{i,j-1}}{\partial x_{i,k}} f_{i,k}(\bar{x}_{i,k+1}) + \frac{1}{2}z_{i,j} \right. \\ &\quad \left. + \frac{1}{2}z_{i,j} \sum_{k=1}^{j-1} \left(\frac{\partial \alpha_{i,j-1}}{\partial x_{i,k}} \right)^2 - \frac{\partial \alpha_{i,j-1}}{\partial \hat{\theta}_i} \dot{\hat{\theta}}_i \right) \\ &\quad + \frac{1}{2} \sum_{k=1}^j \sum_{l=1}^N y_l^2 \bar{\varphi}_{i,k,l}^2(y_l). \end{aligned} \quad (30)$$

Step n_i . Similar to (25), the following equation can be obtained:

$$\begin{aligned} \dot{z}_{i,n_i} &= h_{\mu_{i,n_i}}K_i^T(t)\Phi_i(t)v_i + h_{\mu_{i,n_i}}d_i(v_i) + f_{i,n_i}(\bar{x}_{i,n_i}, 0) \\ &\quad + \varphi_{i,n_i}(\bar{y}) - \dot{\alpha}_{i,n_i-1}, \end{aligned} \quad (31)$$

where $\dot{\alpha}_{i,n_i-1}$ is shown in (26) with $j = n_i$. Choose a Lyapunov function as

$$V_{i,n_i} = \frac{1}{2}z_{i,n_i}^2 + \frac{b}{2\lambda_i}\bar{\theta}_i^2, \quad (32)$$

where $\bar{\theta}_i = \theta_i - \hat{\theta}_i$ is the parameter error and $\lambda_i > 0$ is a design parameter.

Then, the following result holds.

$$\begin{aligned} \dot{V}_{i,n_i} = & z_{i,n_i} \left(h_{\mu_i,n_i} K_i^T(t) \Phi_i(t) v_i + h_{\mu_i,n_i} d_i(v_i) \right. \\ & + f_{i,n_i}(\bar{x}_{i,n_i}, 0) + \varphi_{i,n_i}(\bar{y}) - \frac{\partial \alpha_{i,n_i-1}}{\partial \hat{\theta}_i} \dot{\hat{\theta}}_i \\ & \left. - \sum_{k=1}^{n_i-1} \frac{\partial \alpha_{i,n_i-1}}{\partial x_{i,k}} (f_{i,k}(\bar{x}_{i,k+1}) + \varphi_{i,k}(\bar{y})) \right) \\ & - \frac{b}{\lambda_i} \tilde{\theta}_i \dot{\hat{\theta}}_i. \end{aligned} \quad (33)$$

Repeating the same derivations as (28)–(30) produces

$$\begin{aligned} \dot{V}_{i,n_i} \leq & z_{i,n_i} \left(h_{\mu_i,n_i} K_i^T(t) \Phi_i(t) v_i + h_{\mu_i,n_i} d_i(v_i) \right. \\ & + f_{i,n_i}(\bar{x}_{i,n_i}, 0) - \sum_{k=1}^{n_i-1} \frac{\partial \alpha_{i,n_i-1}}{\partial x_{i,k}} f_{i,k}(\bar{x}_{i,k+1}) \\ & + \frac{1}{2} z_{i,n_i} \sum_{k=1}^{n_i-1} \left(\frac{\partial \alpha_{i,n_i-1}}{\partial x_{i,k}} \right)^2 + \frac{1}{2} z_{i,n_i} - \frac{\partial \alpha_{i,n_i-1}}{\partial \hat{\theta}_i} \dot{\hat{\theta}}_i \left. \right) \\ & + \frac{1}{2} \sum_{k=1}^{n_i} \sum_{l=1}^N \gamma_l^2 \bar{\varphi}_{i,k,l}^2(\gamma_l) - \frac{b}{\lambda_i} \tilde{\theta}_i \dot{\hat{\theta}}_i. \end{aligned} \quad (34)$$

Now, consider a Lyapunov function for the whole system as

$$V = \sum_{i=1}^N \sum_{j=1}^{n_i} V_{i,j} = \sum_{i=1}^N \left(\frac{1}{2} \gamma_i^2 + \sum_{j=2}^{n_i} \frac{1}{2} z_{i,j}^2 + \frac{b}{2\lambda_i} \tilde{\theta}_i^2 \right). \quad (35)$$

Then, combining (24) together with (30) and (34), one has

$$\begin{aligned} \dot{V} \leq & \sum_{i=1}^N \gamma_i \left\{ h_{\mu_i,1} \alpha_{i,1} + f_{i,1}(\bar{x}_{i,1}, 0) + \frac{1}{2} \gamma_i \right. \\ & \left. + \frac{1}{2} \gamma_i \sum_{l=1}^N \sum_{s=1}^{n_i} \sum_{k=1}^s \bar{\varphi}_{i,k,l}^2(\gamma_l) \right\} \\ & + \sum_{i=1}^N \sum_{j=2}^{n_i-1} z_{i,j} \left\{ h_{\mu_i,j} \alpha_{i,j} + h_{\mu_i,j} z_{i,j-1} \right. \\ & + f_{i,j}(\bar{x}_{i,j}, 0) - \sum_{k=1}^{j-1} \frac{\partial \alpha_{i,j-1}}{\partial x_{i,k}} f_{i,k}(\bar{x}_{i,k+1}) \\ & \left. + \frac{1}{2} z_{i,j} + \frac{1}{2} z_{i,j} \sum_{k=1}^{j-1} \left(\frac{\partial \alpha_{i,j-1}}{\partial x_{i,k}} \right)^2 \right\} \end{aligned}$$

$$\begin{aligned} & + \sum_{i=1}^N z_{i,n_i} \left\{ h_{\mu_i,n_i} K_i^T(t) \Phi_i(t) v_i + h_{\mu_i,n_i} d_i(v_i) \right. \\ & + f_{i,n_i}(\bar{x}_{i,n_i}, 0) - \sum_{k=1}^{n_i-1} \frac{\partial \alpha_{i,n_i-1}}{\partial x_{i,k}} f_{i,k}(\bar{x}_{i,k+1}) \\ & \left. + \frac{1}{2} z_{i,n_i} \sum_{k=1}^{n_i-1} \left(\frac{\partial \alpha_{i,n_i-1}}{\partial x_{i,k}} \right)^2 + \frac{1}{2} z_{i,n_i} \right\} \\ & - \sum_{i=1}^N \sum_{j=2}^{n_i} z_{i,j} \frac{\partial \alpha_{i,j-1}}{\partial \hat{\theta}_i} \dot{\hat{\theta}}_i - \sum_{i=1}^N \frac{b}{\lambda_i} \tilde{\theta}_i \dot{\hat{\theta}}_i, \end{aligned} \quad (36)$$

where the fact of

$$\begin{aligned} & \frac{1}{2} \sum_{i=1}^N \sum_{s=1}^{n_i} \sum_{k=1}^s \sum_{l=1}^N \gamma_l^2 \bar{\varphi}_{i,k,l}^2(\gamma_l) \\ & = \frac{1}{2} \sum_{i=1}^N \sum_{l=1}^N \sum_{s=1}^{n_i} \sum_{k=1}^s \gamma_l^2 \bar{\varphi}_{l,k,i}^2(\gamma_l) \end{aligned} \quad (37)$$

has been used in above inequality.

By using adaptive laws defined in (18) and rearranging sequence, we can obtain

$$\begin{aligned} & - \sum_{i=1}^N \sum_{j=2}^{n_i} z_{i,j} \frac{\partial \alpha_{i,j-1}}{\partial \hat{\theta}_i} \dot{\hat{\theta}}_i \\ & = - \sum_{i=1}^N \sum_{j=2}^{n_i} z_{i,j} \frac{\partial \alpha_{i,j-1}}{\partial \hat{\theta}_i} \left(\sum_{k=1}^{n_i} \frac{\lambda_i}{2a_{i,k}^2} z_{i,k}^2 \phi_{i,k}^T \phi_{i,k} - \gamma_i \hat{\theta}_i \right) \\ & = \sum_{i=1}^N \sum_{j=2}^{n_i} z_{i,j} \frac{\partial \alpha_{i,j-1}}{\partial \hat{\theta}_i} \gamma_i \hat{\theta}_i \\ & \quad - \sum_{i=1}^N \sum_{j=2}^{n_i} z_{i,j} \frac{\partial \alpha_{i,j-1}}{\partial \hat{\theta}_i} \sum_{k=1}^{j-1} \frac{\lambda_i}{2a_{i,k}^2} z_{i,k}^2 \phi_{i,k}^T \phi_{i,k} \\ & \quad - \sum_{i=1}^N \sum_{j=2}^{n_i} z_{i,j} \frac{\partial \alpha_{i,j-1}}{\partial \hat{\theta}_i} \sum_{k=j}^{n_i} \frac{\lambda_i}{2a_{i,k}^2} z_{i,k}^2 \phi_{i,k}^T \phi_{i,k} \\ & \leq \sum_{i=1}^N \sum_{j=2}^{n_i} z_{i,j} \frac{\partial \alpha_{i,j-1}}{\partial \hat{\theta}_i} \gamma_i \hat{\theta}_i \\ & \quad - \sum_{i=1}^N \sum_{j=2}^{n_i} z_{i,j} \frac{\partial \alpha_{i,j-1}}{\partial \hat{\theta}_i} \sum_{k=1}^{j-1} \frac{\lambda_i}{2a_{i,k}^2} z_{i,k}^2 \phi_{i,k}^T \phi_{i,k} \\ & \quad + \sum_{i=1}^N \sum_{j=2}^{n_i} \frac{\lambda_i}{2a_{i,j}^2} z_{i,j}^2 \left(\sum_{k=2}^j \left| z_{i,k} \frac{\partial \alpha_{i,k-1}}{\partial \hat{\theta}_i} \right| \right). \end{aligned} \quad (38)$$

Taking $|d_i(v_i)| \leq p_i^*$ into account, one has

$$z_{i,n_i} h_{\mu_i,n_i} d_i(v_i) \leq \frac{1}{2} z_{i,n_i}^2 h_{\mu_i,n_i}^2 + \frac{1}{2} p_i^{*2}. \quad (39)$$

By substituting (38) and (39) into (36), it follows

$$\begin{aligned} \dot{V} \leq & \sum_{i=1}^N y_i \left(h_{\mu_{i,1}} \alpha_{i,1} + F_{i,1}(X_{i,1}) \right) \\ & + \sum_{i=1}^N \sum_{j=2}^{n_i-1} z_{i,j} \left(h_{\mu_{i,j}} \alpha_{i,j} + F_{i,j}(X_{i,j}) \right) \\ & + \sum_{i=1}^N z_{i,n_i} \left(h_{\mu_{i,n_i}} K_i^T(t) \Phi_i(t) v_i + F_{i,n_i}(X_{i,n_i}) \right) \\ & + \frac{1}{2} \sum_{i=1}^N p_i^* - \frac{1}{2} \sum_{i=1}^N \sum_{j=1}^{n_i} z_{i,j}^2 - \sum_{i=1}^N \frac{b}{\lambda_i} \tilde{\theta}_i \dot{\hat{\theta}}_i, \end{aligned} \quad (40)$$

where the packaged functions $F_{i,j}(X_{i,j})$, $i = 1, 2, \dots, N$, are specified as

$$\begin{aligned} F_{i,1}(X_{i,1}) &= f_{i,1}(\bar{x}_{i,1}, 0) + y_i + \frac{1}{2} y_i \sum_{l=1}^N \sum_{s=1}^{n_l} \sum_{k=1}^s \bar{\varphi}_{l,k,i}^2(y_i), \\ F_{i,j}(X_{i,j}) &= h_{\mu_{i,j}} z_{i,j-1} + f_{i,j}(\bar{x}_{i,j}, 0) - \sum_{k=1}^{j-1} \frac{\partial \alpha_{i,j-1}}{\partial x_{i,k}} f_{i,k}(\bar{x}_{i,k+1}) \\ &+ z_{i,j} + \frac{1}{2} z_{i,j} \sum_{k=1}^{j-1} \left(\frac{\partial \alpha_{i,j-1}}{\partial x_{i,k}} \right)^2 + \frac{\partial \alpha_{i,j-1}}{\partial \hat{\theta}_i} \gamma_i \hat{\theta}_i \\ &- \frac{\partial \alpha_{i,j-1}}{\partial \hat{\theta}_i} \sum_{k=1}^{j-1} \frac{\lambda_i}{2a_{i,k}^2} z_{i,k}^2 \phi_{i,k}^T \phi_{i,k} \\ &+ \frac{\lambda_i}{2a_{i,j}^2} z_{i,j} \left(\sum_{k=2}^j \left| z_{i,k} \frac{\partial \alpha_{i,k-1}}{\partial \hat{\theta}_i} \right| \right), \\ & \quad j = 2, \dots, n_i - 1, \\ F_{i,n_i}(X_{i,n_i}) &= f_{i,n_i}(\bar{x}_{i,n_i}, 0) - \sum_{k=1}^{n_i-1} \frac{\partial \alpha_{i,n_i-1}}{\partial x_{i,k}} f_{i,k}(\bar{x}_{i,k+1}) \\ &+ \frac{1}{2} z_{i,n_i} \sum_{k=1}^{n_i-1} \left(\frac{\partial \alpha_{i,n_i-1}}{\partial x_{i,k}} \right)^2 + \frac{1}{2} z_{i,n_i} h_{\mu_{i,n_i}}^2 + z_{i,n_i} \\ &+ \frac{\partial \alpha_{i,n_i-1}}{\partial \hat{\theta}_i} \gamma_i \hat{\theta}_i - \frac{\partial \alpha_{i,n_i-1}}{\partial \hat{\theta}_i} \sum_{k=1}^{n_i-1} \frac{\lambda_i}{2a_{i,k}^2} z_{i,k}^2 \phi_{i,k}^T \phi_{i,k} \\ &+ \frac{\lambda_i}{2a_{i,n_i}^2} z_{i,n_i} \left(\sum_{k=2}^{n_i} \left| z_{i,k} \frac{\partial \alpha_{i,k-1}}{\partial \hat{\theta}_i} \right| \right). \end{aligned} \quad (41)$$

Because $f_{i,j}$, $h_{\mu_{i,j}}$, and $\bar{\varphi}_{l,k,i}$ are unknown smooth functions, $F_{i,j}(X_{i,j})$, $i = 1, 2, \dots, N$, $j = 1, 2, \dots, n_i$ cannot be used to define the virtual control input $\alpha_{i,j}$ and the real controller u_i . Then, RBF neural network $W_{i,j}^T \phi_{i,j}(X_{i,j})$ is utilized to model $F_{i,j}(X_{i,j})$, such that for a given positive constant $\varepsilon_{i,j}$,

$$F_{i,j}(X_{i,j}) = W_{i,j}^T \phi_{i,j}(X_{i,j}) + \delta_{i,j}(X_{i,j}), \quad (42)$$

where $\delta_{i,j}(X_{i,j})$ is approximation error and satisfies $|\delta_{i,j}(X_{i,j})| < \varepsilon_{i,j}$. Subsequently, by Young's inequality, one has

$$\begin{aligned} z_{i,j} F_{i,j}(X_{i,j}) &= z_{i,j} \frac{W_{i,j}^T}{\|W_{i,j}\|} \phi_{i,j} \|W_{i,j}\| + z_{i,j} \delta_{i,j}(X_{i,j}) \\ &\leq \frac{b}{2a_{i,j}^2} z_{i,j}^2 \theta_i \phi_{i,j}^T \phi_{i,j} + \frac{1}{2} a_{i,j}^2 + \frac{1}{2} z_{i,j}^2 + \frac{1}{2} \varepsilon_{i,j}^2, \end{aligned} \quad (43)$$

where $i = 1, 2, \dots, N$, $j = 1, 2, \dots, n_i$ and the unknown constant $\theta_i = \max\{(1/b)\|W_{i,j}\|^2; j = 1, 2, \dots, n_i\}$.

Substituting (42) into (40) and using (43) produces

$$\begin{aligned} \dot{V} \leq & \sum_{i=1}^N z_{i,1} \left(h_{\mu_{i,1}} \alpha_{i,1} + \frac{b}{2a_{i,1}^2} z_{i,1} \theta_i \phi_{i,1}^T \phi_{i,1} \right) \\ & + \sum_{i=1}^N \sum_{j=2}^{n_i-1} z_{i,j} \left(h_{\mu_{i,j}} \alpha_{i,j} + \frac{b}{2a_{i,j}^2} z_{i,j} \theta_i \phi_{i,j}^T \phi_{i,j} \right) \\ & + \sum_{i=1}^N z_{i,n_i} \left(h_{\mu_{i,n_i}} K_i^T(t) \Phi_i(t) v_i + \frac{b}{2a_{i,n_i}^2} z_{i,n_i} \theta_i \phi_{i,n_i}^T \phi_{i,n_i} \right) \\ & + \frac{1}{2} \sum_{i=1}^N p_i^* + \sum_{i=1}^N \sum_{j=1}^{n_i} \left(\frac{1}{2} a_{i,j}^2 + \frac{1}{2} \varepsilon_{i,j}^2 \right) - \sum_{i=1}^N \frac{b}{\lambda_i} \tilde{\theta}_i \dot{\hat{\theta}}_i. \end{aligned} \quad (44)$$

Now, construct the virtual control signals $\alpha_{i,j} = -k_{i,j} z_{i,j} - (1/2a_{i,j}^2) z_{i,j} \hat{\theta}_i \phi_{i,j}^T \phi_{i,j}$, where $i = 1, 2, \dots, N$, $j = 1, 2, \dots, n_i$, and $\alpha_{i,n_i} = u_i$. Then, by using (9), we can obtain

$$\begin{aligned} z_{i,j} h_{\mu_{i,j}} \alpha_{i,j} &\leq -k_{i,j} b z_{i,j}^2 - \frac{b}{2a_{i,j}^2} z_{i,j}^2 \hat{\theta}_i \phi_{i,j}^T \phi_{i,j}, \\ & \quad j = 1, \dots, n_i - 1, \end{aligned}$$

$$z_{i,n_i} h_{\mu_{i,n_i}} K_i^T(t) \Phi_i(t) v_i \leq -k_{i,n_i} b z_{i,n_i}^2 - \frac{b}{2a_{i,n_i}^2} z_{i,n_i}^2 \hat{\theta}_i \phi_{i,n_i}^T \phi_{i,n_i}, \quad (45)$$

where $i = 1, 2, \dots, N$.

Substituting (45) into (44) and using adaptive laws $\dot{\hat{\theta}}_i$ in (18) result in

$$\begin{aligned} \dot{V} \leq & \sum_{i=1}^N \sum_{j=1}^{n_i} z_{i,j} \left(-k_{i,j} b z_{i,j} + \frac{b}{2a_{i,j}^2} z_{i,j} \tilde{\theta}_i \phi_{i,j}^T \phi_{i,j} \right) \\ & + \sum_{i=1}^N \sum_{j=1}^{n_i} \left(\frac{1}{2} a_{i,j}^2 + \frac{1}{2} \varepsilon_{i,j}^2 \right) + \frac{1}{2} \sum_{i=1}^N p_i^* \\ & - \sum_{i=1}^N \frac{b}{\lambda_i} \tilde{\theta}_i \left(\sum_{j=1}^{n_i} \frac{\lambda_i}{2a_{i,j}^2} z_{i,j}^2 \phi_{i,j}^T \phi_{i,j} - \gamma_i \hat{\theta}_i \right) \end{aligned}$$

$$\begin{aligned}
 &\leq -\sum_{i=1}^N \sum_{j=1}^{n_i} k_{i,j} b z_{i,j}^2 + \sum_{i=1}^N \frac{\gamma_i b}{\lambda_i} \tilde{\theta}_i \hat{\theta}_i \\
 &\quad + \sum_{i=1}^N \sum_{j=1}^{n_i} \left(\frac{1}{2} a_{i,j}^2 + \frac{1}{2} \varepsilon_{i,j}^2 \right) + \frac{1}{2} \sum_{i=1}^N p_i^{*2} \\
 &\leq -\sum_{i=1}^N \left(\sum_{j=1}^{n_i} k_{i,j} b z_{i,j}^2 + \frac{\gamma_i b}{2\lambda_i} \tilde{\theta}_i^2 \right) \\
 &\quad + \sum_{i=1}^N \sum_{j=1}^{n_i} \left(\frac{1}{2} a_{i,j}^2 + \frac{1}{2} \varepsilon_{i,j}^2 + \frac{\gamma_i b}{2\lambda_i} \theta_i^2 \right) + \frac{1}{2} \sum_{i=1}^N p_i^{*2},
 \end{aligned} \tag{46}$$

where $\tilde{\theta}_i \hat{\theta}_i \leq -(1/2)\tilde{\theta}_i^2 + (1/2)\theta_i^2$ has been used in the above inequality.

Define

$$\begin{aligned}
 a_0 &= \min \{ 2k_{i,j} b, \gamma_i, i = 1, 2, \dots, N, j = 1, 2, \dots, n_i \}; \\
 b_0 &= \sum_{i=1}^N \sum_{j=1}^{n_i} \left(\frac{1}{2} a_{i,j}^2 + \frac{1}{2} \varepsilon_{i,j}^2 + \frac{\gamma_i b}{2\lambda_i} \theta_i^2 \right) + \frac{1}{2} \sum_{i=1}^N p_i^{*2},
 \end{aligned} \tag{47}$$

we have

$$\dot{V} \leq -a_0 V + b_0, \quad t \geq 0. \tag{48}$$

Furthermore, multiplying (48) by $e^{a_0 t}$ yields

$$\frac{d}{dt} (V e^{a_0 t}) \leq b_0 e^{a_0 t}. \tag{49}$$

Integrating (49) over $[0, t]$ gives

$$0 \leq V(t) \leq \frac{b_0}{a_0} + \left(V(0) - \frac{b_0}{a_0} \right) e^{-a_0 t}, \tag{50}$$

which implies that

$$V(t) \leq V(0) + \frac{b_0}{a_0}, \quad \forall t > 0, \tag{51}$$

which means that all the signals in the closed-loop system are semiglobally uniformly ultimately bounded.

Furthermore, it is easily obtained that

$$V(t) \leq \frac{b_0}{a_0}, \quad t \rightarrow +\infty. \tag{52}$$

Therefore, based on the definition of V in (50), the error signals $z_{i,j}$ and $\tilde{\theta}_i$ eventually converge to the compact set Ω_s , which is specified as

$$\begin{aligned}
 \Omega_s &= \left\{ z_{i,j}, \tilde{\theta}_i \mid |z_{i,j}| \leq \sqrt{\frac{2b_0}{a_0}}, |\tilde{\theta}_i| \leq \sqrt{\frac{2\lambda_i b_0}{b a_0}}, \right. \\
 &\quad \left. 1 \leq i \leq N, 1 \leq j \leq n_i \right\}.
 \end{aligned} \tag{53}$$

At the present stage, adaptive decentralized control procedure has been completed via backstepping technique. The above design procedures and stable analysis are summarized in the following theorem.

Theorem 8. Under Assumptions 1–6, consider the closed-loop nonlinear system consisted of (1), unknown dead zone nonlinearities (2), controller (17), and adaptive law (18). Under the action of controller (17), for any initial conditions $[z_i^T(0), \hat{\theta}_i(0)]^T \in \Omega_0$ (where Ω_0 is an appropriately chosen compact set), all the signals in the closed-loop system are semiglobally uniformly ultimately bounded in the sense of mean square, and the error signals $z_{i,j}$ and $\tilde{\theta}_i$ eventually converge to the compact set Ω_s in (53).

4. Simulation Example

In this section, in order to illustrate the effectiveness of the proposed control scheme, consider the nonaffine interconnected nonlinear system with dead zones as

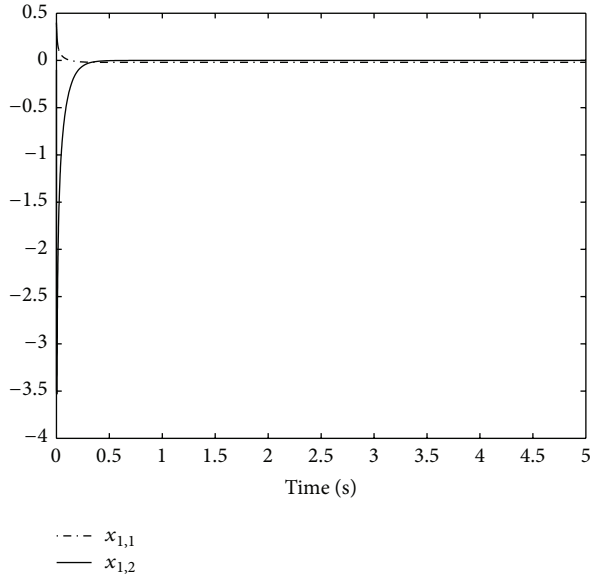
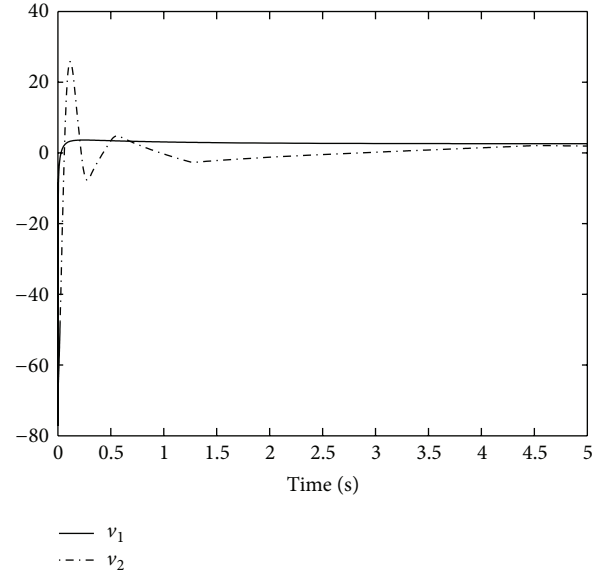
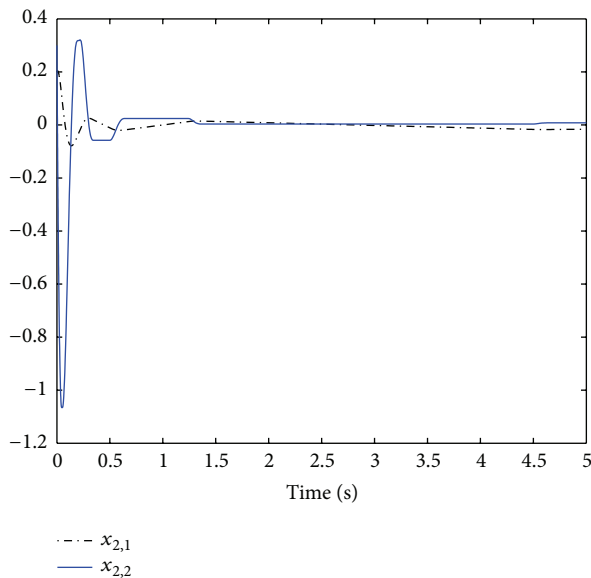
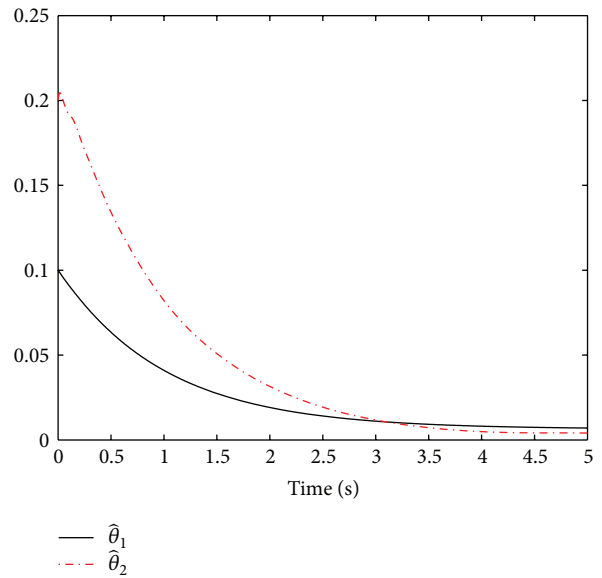
$$\begin{aligned}
 \dot{x}_{1,1} &= (1 + x_{1,1}^2) x_{1,2} + x_{1,2}^3 + y_2 \ln(1 + y_1^2), \\
 \dot{x}_{1,2} &= (5 + \sin(x_{1,1} x_{1,2})) u_1 + 0.2 u_1^5 + \sin(y_1^2) y_2, \\
 y_1 &= x_{1,1}, \\
 \dot{x}_{2,1} &= (3 + \sin(x_{2,1})) x_{2,2} + 0.3 x_{2,2}^5 + y_1 \cos(y_2^2), \\
 \dot{x}_{2,2} &= (2 + x_{2,1}^2) u_2 + \frac{1}{5} \sin(u_2) + y_2^3 y_1, \\
 y_2 &= x_{2,1},
 \end{aligned} \tag{54}$$

where $u_i = D(v_i)$ is defined as

$$\begin{aligned}
 u_1 = D(v_1) &= \begin{cases} 1.5(v_1 - 2.5), & v_1 \geq 2.5, \\ 0, & -1 < v_1 < 2.5, \\ 0.5(v_1 + 1), & v_1 \leq -1, \end{cases} \\
 u_2 = D(v_2) &= \begin{cases} 0.8(v_2 - 2), & v_2 \geq 2, \\ 0, & -1.8 < v_2 < 2, \\ 1.2(v_2 + 1.8), & v_2 \leq -1.8, \end{cases}
 \end{aligned} \tag{55}$$

where $x_{1,1}$, $x_{1,2}$, $x_{2,1}$, and $x_{2,2}$ are the state variables and y_i is the system output. u_i and v_i are the output and input of the dead zone nonlinearity, respectively. It is obvious that the system is of nonaffine structure and satisfies Assumptions 1, 4, and 6. By using Theorem 8, the virtual control law, the actual controller, and the adaptive laws are constructed as

$$\begin{aligned}
 \alpha_{i,1} &= -k_{i,1} z_{i,1} - \frac{1}{2a_{i,1}^2} z_{i,1} \hat{\theta}_i \phi_{i,1}^T \phi_{i,1}, \\
 u_i &= -k_{i,2} z_{i,2} - \frac{1}{2a_{i,2}^2} z_{i,2} \hat{\theta}_i \phi_{i,2}^T \phi_{i,2}, \\
 \dot{\hat{\theta}}_i &= \sum_{j=1}^2 \frac{\lambda_i}{2a_{i,j}^2} z_{i,j}^2 \phi_{i,j}^T \phi_{i,j} - \gamma_i \hat{\theta}_i,
 \end{aligned} \tag{56}$$

FIGURE 1: State variables $x_{1,1}$ and $x_{1,2}$.FIGURE 3: The control signals v_1 and v_2 .FIGURE 2: State variables $x_{2,1}$ and $x_{2,2}$.FIGURE 4: Adaptive laws $\hat{\theta}_1$ and $\hat{\theta}_2$.

where $z_{i,1} = x_{i,1}$, $z_{i,2} = x_{i,2} - \alpha_{i,1}$, and $i = 1, 2$. The simulation is run under the initial conditions $[x_{1,1}(0), x_{1,2}(0), x_{2,1}(0), x_{2,2}(0)]^T = [0.4, -0.1, 0.2, 0.3]^T$, and $[\hat{\theta}_1(0), \hat{\theta}_2(0)]^T = [0.1, 0.2]^T$. In the simulation, design parameters are taken as follows: $k_{1,1} = k_{1,2} = k_{2,1} = k_{2,2} = 11$, $a_{1,1} = a_{1,2} = a_{2,1} = a_{2,2} = 3$, $\gamma_1 = \gamma_2 = 1$, and $\lambda_1 = \lambda_2 = 2$.

The simulation results are indicated by Figures 1–4. Figure 1 shows the state variables $x_{1,1}$ and $x_{1,2}$ of the first subsystems. Figure 2 shows the second subsystems state variables $x_{2,1}$ and $x_{2,2}$. Figure 3 displays the control signals v_1 and v_2 , and Figure 4 shows the response curve of the adaptive parameters $\hat{\theta}_1$ and $\hat{\theta}_2$. Apparently, simulation results show

that good convergence performances are achieved and all the signals in the closed-loop system are bounded.

5. Conclusion

In this paper, a robust decentralized adaptive neural control approach has been developed for a class of large-scale nonaffine nonlinear systems with dead zones. The proposed decentralized controller can guarantee that all the signals in the closed-loop systems are semiglobally uniformly ultimately bounded in the sense of mean square, and the error signals eventually converge to small neighborhood around the origin. The main advantage of the proposed controller

is that the prior knowledge of bounds of dead zone slopes is not required. In addition, only one adaptive parameter needs to be updated online for each n -order subsystem. In this way, the computational burden is significantly alleviated. Simulation results have been provided to further illustrate the effectiveness of our results.

There are some problems remaining to be considered, for example, how to generalize the result in this paper to stochastic pure-feedback nonlinear systems with dead zones and how to design an output-feedback adaptive neural controller for original system (1).

Conflict of Interests

The authors declare that there is no conflict of interests regarding the publication of this paper.

Acknowledgments

This work is partially supported by the Natural Science Foundation of China (61304002 and 61304003), the Program for New Century Excellent Talents in University (NECT-13-0696), the Program for Liaoning Innovative Research Team in University under Grant LT2013023, the Program for Liaoning Excellent Talents in University under Grant LR2013053, the Polish-Norwegian Research Programme operated by the National Centre for Research and 24 Development under the Norwegian Financial Mechanism 2009–2014 in the frame of Project Contract no. Pol-Nor/200957/47/2013, and the Education Department of Liaoning Province under the General Project Research Grant no. L2013424.

References

- [1] M. Krstić, I. Kanellakopoulos, and P. V. Kokotovic, *Nonlinear and Adaptive Control Design*, Wiley, New York, NY, USA, 1995.
- [2] Z. Wu, M. Cui, P. Shi, and H. R. Karimi, "Stability of stochastic nonlinear systems with state-dependent switching," *IEEE Transactions on Automatic Control*, vol. 58, no. 8, pp. 1904–1918, 2013.
- [3] L. Liu and X.-J. Xie, "Output-feedback stabilization for stochastic high-order nonlinear systems with time-varying delay," *Automatica*, vol. 47, no. 12, pp. 2772–2779, 2011.
- [4] L. Liu, N. Duan, and X.-J. Xie, "Output-feedback stabilization for stochastic high-order nonlinear systems with a ratio of odd integers power," *Acta Automatica Sinica*, vol. 36, no. 6, pp. 858–864, 2010.
- [5] S. Yin, S. Ding, and H. Luo, "Real-time implementation of fault tolerant control system with performance optimization," *IEEE Transactions on Industrial Electronics*, vol. 61, no. 5, pp. 2402–2411, 2014.
- [6] S. Yin, S. Ding, A. Haghani, H. Hao, and P. Zhang, "A comparison study of basic data-driven fault diagnosis and process monitoring methods on the benchmark Tennessee Eastman process," *Journal of Process Control*, vol. 22, no. 9, pp. 1567–1581, 2012.
- [7] M. Liu, X. Cao, and P. Shi, "Fault estimation and tolerant control for fuzzy stochastic systems," *IEEE Transactions on Fuzzy Systems*, vol. 21, no. 2, pp. 221–229, 2013.
- [8] M. Liu, X. Cao, and P. Shi, "Fuzzy-model-based fault tolerant design for nonlinear stochastic systems against simultaneous sensor and actuator faults," *IEEE Transactions on Fuzzy Systems*, vol. 21, no. 5, pp. 789–799, 2013.
- [9] X. D. Zhao, L. X. Zhang, P. Shi, and H. R. Karimi, "Robust control of continuous-time systems with state-dependent uncertainties and its application to electronic circuits," *IEEE Transactions on Industrial Electronics*, vol. 61, no. 8, pp. 4161–4170, 2014.
- [10] H. R. Karimi, "Robust delay-dependent H_∞ control of uncertain time-delay systems with mixed neutral, discrete, and distributed time-delays and Markovian switching parameters," *IEEE Transactions on Circuits and Systems*, vol. 58, no. 8, pp. 1910–1923, 2011.
- [11] H. Y. Li, X. J. Jing, and H. R. Karimi, "Output-feedback based H-infinity control for active suspension systems with control delay," *IEEE Transactions on Industrial Electronics*, vol. 61, no. 1, pp. 436–446, 2014.
- [12] H. Gao, T. Chen, and J. Lam, "A new delay system approach to network-based control," *Automatica*, vol. 44, no. 1, pp. 39–52, 2008.
- [13] L. X. Zhang, H. J. Gao, and O. Kaynak, "Network-induced constraints in networked control systems—a survey," *IEEE Transactions on Industrial Informatics*, vol. 9, no. 1, pp. 403–416, 2013.
- [14] H. Yan, Z. Su, H. Zhang, and F. Yang, "Observer-based H_∞ control for discrete-time stochastic systems with quantisation and random communication delays," *IET Control Theory & Applications*, vol. 7, no. 3, pp. 372–379, 2013.
- [15] H. Yan, H. Shi, H. Zhang, and F. Yang, "Quantized H_∞ control for networked systems with communication constraints," *Asian Journal of Control*, vol. 15, no. 5, pp. 1468–1476, 2013.
- [16] H. Zhang, Q. Chen, H. Yan, and J. Liu, "Robust H_∞ filtering for switched stochastic system with missing measurements," *IEEE Transactions on Signal Processing*, vol. 57, no. 9, pp. 3466–3474, 2009.
- [17] H. Zhang, H. Yan, T. Liu, and Q. Chen, "Fuzzy controller design for nonlinear impulsive fuzzy systems with time delay," *IEEE Transactions on Fuzzy Systems*, vol. 19, no. 5, pp. 844–856, 2011.
- [18] H. Zhang, H. Yan, F. Yang, and Q. Chen, "Quantized control design for impulsive fuzzy networked systems," *IEEE Transactions on Fuzzy Systems*, vol. 19, no. 6, pp. 1153–1162, 2011.
- [19] H. Y. Li, J. Y. Yu, C. Hilton, and H. H. Liu, "Adaptive sliding mode control for nonlinear active suspension vehicle systems using T-S fuzzy approach," *IEEE Transactions on Industrial Electronics*, vol. 60, no. 8, pp. 3328–3338, 2013.
- [20] X. D. Zhao, L. X. Zhang, P. Shi, and H. R. Karimi, "Novel stability criteria for T-S fuzzy systems," *IEEE Transactions on Fuzzy Systems*, vol. 21, no. 6, pp. 1–11, 2013.
- [21] X. Su, P. Shi, L. Wu, and Y. Song, "A novel approach to filter design for T-S fuzzy discretetime systems with time-varying delay," *IEEE Transactions on Fuzzy Systems*, vol. 20, no. 6, pp. 1114–1129, 2012.
- [22] H. Q. Wang, B. Chen, X. P. Liu, K. F. Liu, and C. Lin, "Robust adaptive fuzzy tracking control for pure-feedback stochastic nonlinear systems with input constraints," *IEEE Transaction on Cybernetics*, vol. 43, no. 6, pp. 2093–2104, 2013.
- [23] S. Bououden, M. Chadli, F. Allouani, and S. Filali, "A new approach for fuzzy predictive adaptive controller design using particle swarm optimization algorithm," *International Journal of Innovative Computing, Information and Control*, vol. 9, no. 9, pp. 3741–3758, 2013.

- [24] S. Sefriti, J. Boumhidi, M. Benyakhlef, and I. Boumhidi, "Adaptive decentralized sliding mode neural network control of a class of nonlinear interconnected systems," *International Journal of Innovative Computing, Information and Control*, vol. 9, no. 7, pp. 2941–2947, 2013.
- [25] Y.-J. Liu, W. Wang, S.-C. Tong, and Y.-S. Liu, "Robust adaptive tracking control for nonlinear systems based on bounds of fuzzy approximation parameters," *IEEE Transactions on Systems, Man, and Cybernetics A*, vol. 40, no. 1, pp. 170–184, 2010.
- [26] H. Q. Wang, B. Chen, and C. Lin, "Approximation-based adaptive fuzzy control for a class of non-strict-feedback stochastic nonlinear systems," *Science China Information Sciences*, 2013.
- [27] T. Shaocheng, C. Bin, and W. Yongfu, "Fuzzy adaptive output feedback control for MIMO nonlinear systems," *Fuzzy Sets and Systems*, vol. 156, no. 2, pp. 285–299, 2005.
- [28] W. Chen and J. Li, "Decentralized output-feedback neural control for systems with unknown interconnections," *IEEE Transactions on Systems, Man, and Cybernetics B*, vol. 38, no. 1, pp. 258–266, 2008.
- [29] S. Tong, C. Liu, and Y. Li, "Fuzzy-adaptive decentralized output-feedback control for large-scale nonlinear systems with dynamical uncertainties," *IEEE Transactions on Fuzzy Systems*, vol. 18, no. 5, pp. 845–861, 2010.
- [30] S. C. Tong, Y. M. Li, and H.-G. Zhang, "Adaptive neural network decentralized backstepping output-feedback control for nonlinear large-scale systems with time delays," *IEEE Transactions on Neural Networks*, vol. 22, no. 7, pp. 1073–1086, 2011.
- [31] J. Li, W. Chen, and J.-M. Li, "Adaptive NN output-feedback decentralized stabilization for a class of large-scale stochastic nonlinear strict-feedback systems," *International Journal of Robust and Nonlinear Control*, vol. 21, no. 4, pp. 452–472, 2011.
- [32] H. Q. Wang, B. Chen, and C. Lin, "Adaptive fuzzy decentralized control for a class of large-scale stochastic nonlinear strict-feedback systems," *Neurocomputing*, vol. 103, pp. 155–163, 2013.
- [33] H. Q. Wang, B. Chen, K. F. Liu, X. P. Liu, and C. Lin, "Adaptive neural tracking control for a class of non-strict-feedback stochastic nonlinear systems with unknown backlashlike hysteresis," *IEEE Transactions on Neural Networks and Learning Systems*, 2013.
- [34] H. Y. Li, X. J. Jing, H. K. Lam, and P. Shi, "Fuzzy sampled-data control for uncertain vehicle suspension systems," *IEEE Transactions on Cybernetics*, 2013.
- [35] T.-S. Li, D. Wang, G. Feng, and S.-C. Tong, "A DSC approach to robust adaptive nn tracking control for strict-feedback nonlinear systems," *IEEE Transactions on Systems, Man, and Cybernetics B*, vol. 40, no. 3, pp. 915–927, 2010.
- [36] M. Chen, S. S. Ge, and B. V. E. How, "Robust adaptive neural network control for a class of uncertain MIMO nonlinear systems with input nonlinearities," *IEEE Transactions on Neural Networks*, vol. 21, no. 5, pp. 796–812, 2010.
- [37] B. Chen, X. Liu, K. Liu, and C. Lin, "Direct adaptive fuzzy control of nonlinear strict-feedback systems," *Automatica*, vol. 45, no. 6, pp. 1530–1535, 2009.
- [38] C. Wang, D. J. Hill, S. S. Ge, and G. Chen, "An ISS-modular approach for adaptive neural control of pure-feedback systems," *Automatica*, vol. 42, no. 5, pp. 723–731, 2006.
- [39] M. Wang, S. S. Ge, and K.-S. Hong, "Approximation-based adaptive tracking control of pure-feedback nonlinear systems with multiple unknown time-varying delays," *IEEE Transactions on Neural Networks*, vol. 21, no. 11, pp. 1804–1816, 2010.
- [40] T. P. Zhang and S. S. Ge, "Adaptive dynamic surface control of nonlinear systems with unknown dead zone in pure feedback form," *Automatica*, vol. 44, no. 7, pp. 1895–1903, 2008.
- [41] Z. Huaguang and L. Cai, "Decentralized nonlinear adaptive control of an HVAC system," *IEEE Transactions on Systems, Man and Cybernetics C*, vol. 32, no. 4, pp. 493–498, 2002.
- [42] J. Zhou and C. Wen, "Decentralized backstepping adaptive output tracking of interconnected nonlinear systems," *IEEE Transactions on Automatic Control*, vol. 53, no. 10, pp. 2378–2384, 2008.
- [43] B. Karimi and M. B. Menhaj, "Non-affine nonlinear adaptive control of decentralized large-scale systems using neural networks," *Information Sciences*, vol. 180, no. 17, pp. 3335–3347, 2010.
- [44] Z.-Z. Mao and X.-S. Xiao, "Decentralized adaptive tracking control of nonaffine nonlinear large-scale systems with time delays," *Information Sciences*, vol. 181, no. 23, pp. 5291–5303, 2011.
- [45] X.-S. Wang, C.-Y. Su, and H. Hong, "Robust adaptive control of a class of nonlinear systems with unknown dead-zone," *Automatica*, vol. 40, no. 3, pp. 407–413, 2004.
- [46] J. Zhou, C. Wen, and Y. Zhang, "Adaptive output control of nonlinear systems with uncertain dead-zone nonlinearity," *IEEE Transactions on Automatic Control*, vol. 51, no. 3, pp. 504–511, 2006.
- [47] S. Tong and Y. Li, "Adaptive fuzzy output feedback tracking backstepping control of strict-feedback nonlinear systems with unknown dead zones," *IEEE Transactions on Fuzzy Systems*, vol. 20, no. 1, pp. 168–180, 2012.
- [48] H. Wang, B. Chen, and C. Lin, "Direct adaptive neural tracking control for a class of stochastic pure-feedback nonlinear systems with unknown dead-zone," *International Journal of Adaptive Control and Signal Processing*, vol. 27, no. 4, pp. 302–322, 2013.
- [49] H. Q. Wang, B. Chen, and C. Lin, "Adaptive neural tracking control for a class of stochastic nonlinear systems with unknown dead-zone," *International Journal of Innovative Computing, Information and Control*, vol. 9, no. 8, pp. 3257–3270, 2013.
- [50] Y. M. Li and S. C. Tong, "Adaptive fuzzy output-feedback control of pure-feedback uncertain nonlinear systems with unknown dead-zone," *IEEE Transactions on Fuzzy Systems*, 2013.
- [51] T. M. Apostol, *Mathematical Analysis*, Addison-Wesley, Reading, Mass, USA, 1963.
- [52] R. M. Sanner and J.-J. E. Slotine, "Gaussian networks for direct adaptive control," *IEEE Transactions on Neural Networks*, vol. 3, no. 6, pp. 837–863, 1992.
- [53] A. J. Kurdila, F. J. Narcowich, and J. D. Ward, "Persistency of excitation in identification using radial basis function approximations," *SIAM Journal on Control and Optimization*, vol. 33, no. 2, pp. 625–642, 1995.

Review Article

Fundamental Issues and Prospective Directions in Networked Multirate Control Systems

Wang Zhiwen^{1,2} and Guo Ge²

¹ College of Electrical and Information Engineering, Lanzhou University of Technology, Lanzhou 730050, China

² School of Control Science and Engineering, Dalian University of Technology, Dalian 116026, China

Correspondence should be addressed to Wang Zhiwen; wwwangzhiwen@163.com

Received 4 December 2013; Revised 15 February 2014; Accepted 16 February 2014; Published 19 March 2014

Academic Editor: Hak-Keung Lam

Copyright © 2014 W. Zhiwen and G. Ge. This is an open access article distributed under the Creative Commons Attribution License, which permits unrestricted use, distribution, and reproduction in any medium, provided the original work is properly cited.

In view of the synchronized uniform equidistant sampling method that is widely used in network control systems (NCSs), multirate sampling control for NCSs is presented by considering the natural characteristics of NCSs. Two kinds of typical structures of network multirate control systems (NMCSs) are presented and the multirate sampling mechanisms are formulated. Then, fundamental issues and prospective directions in NMCSs are preliminarily discussed. The contents involve modeling, sampling pattern selection, control strategies, scheduling algorithms, and codesign of NMCSs. The purpose of this paper is to arouse more attention of researchers in related subjects, so that a complete theory for NCSs can be established.

1. Introduction

In the past decade, we were faced with the significant advances of computer science and communication technology. The unprecedented interactions and penetrations between developments in computer, communication, and control have accelerated the progress of the networked control. Motivations for using the networked framework in control systems come from lower cost, ease of maintenance, great flexibility, and sharing of information resources, which make networked control systems (NCSs) more and more popular. NCSs are comprised of the plant to be controlled and some components (sensors, controller, actuators, etc.) whose operation is coordinated through a real-time communication network. The nature characteristic of NCSs is that information, such as reference input, plant output, and control signals, is exchanged among control system by communication network and multisubsystem sharing this information to accomplish their respective control tasks. These features make NCSs as the preferred architecture in modern large-scale complex system. Examples comprise spatially distributed resource allocation networks, supervisory control of continuous plants, intelligent vehicle highway systems,

power generation and distribution networks, mobile sensor networks, remote surgery, and many others. Consequently, considerable attention has been directed to the study of NCSs; see, for example, the survey papers [1–3], the recent special issues [4, 5], and the references therein.

NCSs are typical multivariable and multiloop computer control systems with both continuous-time analog and discrete-time digital signals inside. In the course of system modeling, analysis, and design, the problems of signal sampling and holding will be involved inevitably. The existing achievements of NCSs were almost employing the fundamental assumption about sampler and holder of traditional control theory; that is, the sampling rate of each node in NCSs is identical and synchronous. Such uniformly spaced samples may result in easier reconstruction algorithms and bring more convenience for the theoretical research of NCSs. However, in view of the essential features such as large-scale, complicated framework and high distribution level, it is unrealistic for NCSs to acquire all nodes' information by adopting the traditional sampling manner in practical. Therefore, the previous theoretical achievements based on synchronous uniformly spaced sampling are questionable and should be reconsidered.

Multirate sampling control is motivated by practical implementation of aerospace system originally [6] and is of prominent interest in current control research. Further utility of multirate sampling in control applications can be found for highly distributed systems, such as communication networks and power generation and distribution networks. These examples can be regarded to some extent as the preliminary applications of multirate sampling in NCSs. But, to the best of the author's knowledge, lesser attention has been directed to multirate sampling theory of NCSs and few literatures address the related issues deeply till now. In [7], modeling problem of NCSs is discussed by taking not only network-induced time delay, but also asynchronous multirate sampling into account. Optimal multirate control of the NCSs is investigated in [8]. By using lifting technology, linear periodic time-invariant model of NCSs with multirate sampling is established. Then, controllability and observability are analyzed and optimal state and output feedback control are given. In [9], model-based control scheme of NCSs with multirate input sampling is studied. State feedback and output feedback control are discussed, respectively. Necessary and sufficient conditions for system to be globally exponentially stable are derived. In [10], the stabilization of multirate networked control systems is investigated. The key idea is to use the channel resource allocation to stabilize the system. Conclusions show that a multirate networked control system could be stabilized by state feedback under an appropriate resource allocation. The result can also be applied to multirate quantized networked control systems. In [11], model predictive control (MPC) for NMCSs with the output sampling period several times larger than the input updating period is investigated. Sufficient stability conditions are established via a switched Lyapunov function approach and a controller design method for stabilising NMCSs is proposed. In [12], a multirate method was proposed to formulate NCSs with network-induced time delays as jump linear systems and the sufficient conditions of stability were established. In [13], the NCSs problem was formulated as a dual-rate control problem: low transmission rate for data over the network and high updating rate for actuator commands. In [14], an adaptive sampling rate scheduling methodology is proposed to maintain the transmitted measurement signals' fidelity and conserve available bandwidth in order to help supervisory control system under normal and abnormal operating conditions. As a complement, adaptive multiple sampling rate scheduling algorithm is presented in [15] to dynamically adjust sampling rates and allocate available bandwidths to transmit measurements from the remote plants to the supervisors.

The above-mentioned works can be divided into two categories. One mainly discusses the basic problems of NCSs with multirate sampling, such as modeling, controllability and observability, stabilization and stability analysis. The other focuses on the problems of scheduling scheme, data rate control, and bandwidth allocation, which are closely related to system sampling period and expected to achieve by means of variable sampling or multirate sampling. These works are worthy of recognition for their contributions; meanwhile, we have to realize that great efforts must be made for further

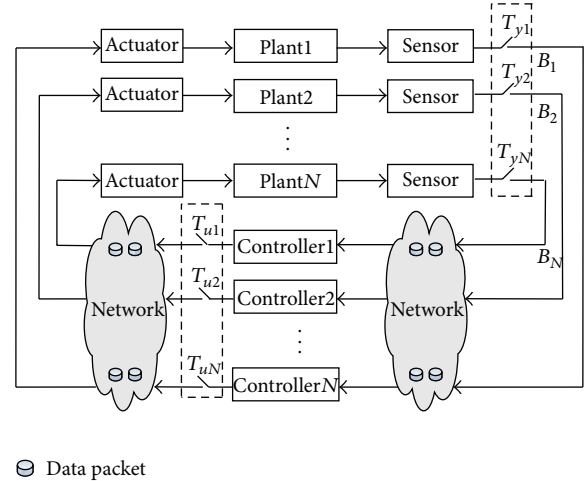


FIGURE 1: GM-NCSs in the direct structure.

pursuit and understanding of the basic theory of NCSs with multirate sampling. Inspired by this, this paper discusses the fundamental issues of networked multirate control systems (NMCSs) tentatively.

The remainder of this paper is organized as follows. In Section 2, two kinds of typical structures of NMCSs are presented and the mechanisms of multirate sampling are described. In Section 3, fundamental issues and prospective directions are discussed tentatively in time domain. Section 4 summarizes the paper and puts forward the future works.

2. System Descriptions

There are two general NCSs configurations termed as direct structure and hierarchical structure [1]. The direct structure is the most common NCSs structure where the controller and the plant are physically located at different locations and are directly linked by a data network in order to perform remote closed-loop control as illustrated in Figure 1. The hierarchical structure NCSs is also called networked supervisory control system. It consists of a main controller and remote closed-loop subsystems as depicted in Figure 2. The main controller computes and sends the reference signal in a frame or a packet via a network to the remote system. The remote system then processes the reference signal to perform local closed-loop control and returns to the sensor measurement to the main controller for networked closed-loop control.

Generally speaking, according to the relationship between each sampling period, multirate sampling system can be divided into the following three categories: multirate input control system (MRICS), multirate output control system (MROCS), and generalized multirate control system (GMCS). MRICS and MROCS can be seen as the special case of GMCS. In MRICS, the sampling rate of the input channel is higher than that of output channel. Namely, in a certain time interval, one time samples the output and several times the input. Therefore, MRICS is also known as fast-slow sampling system. On the contrary, the sampling rate of the output channel is higher than that of input channel in

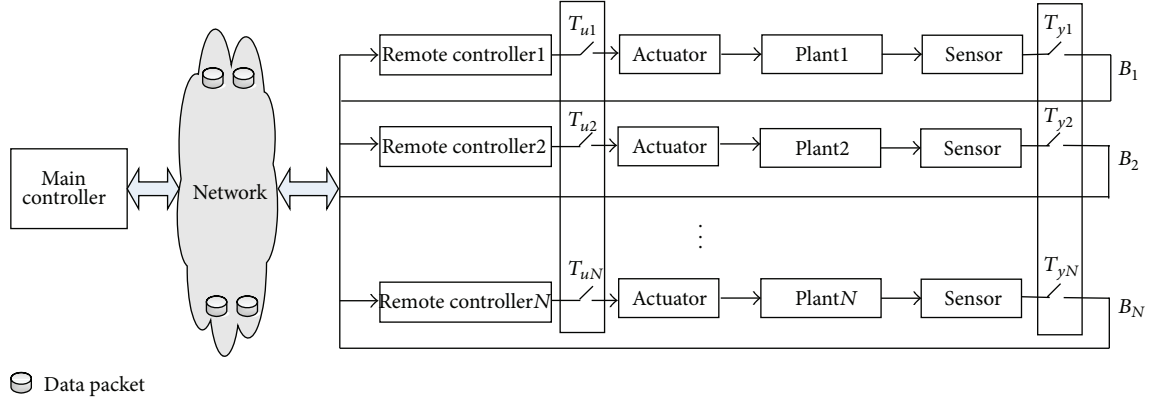


FIGURE 2: GM-NCSs in the hierarchical structure.

MROCS, and it is referred to as slow-fast sampling system. Based on the above principle, we can classify NMCSs as MRI-NCSs, MRO-NCSs, and GM-NCSs. Figures 1 and 2 show two typical structures of GM-NCSs.

Consider the GM-NCSs consisting of a collection of continuous time LTI plants, as illustrated in Figures 1 and 2, where the i th plant is given by

$$\begin{aligned} \dot{x}_i(t) &= A_i x_i(t) + B_i u_i(t), \\ y_i(t) &= C_i x_i(t), \end{aligned} \quad (1)$$

where $x_i \in \mathfrak{R}^{n_i}$, $u_i \in \mathfrak{R}^{m_i}$, and $y_i \in \mathfrak{R}^{p_i}$ are the system state, the control input, and the output, respectively, and $i = 1, 2, \dots, N$ denotes the loop number. A_i , B_i and C_i are the real matrices with appropriate dimensions.

For convenience of investigation, reasonable assumptions are made that all sensors, controllers, and actuators are driven by synchronized clock. Then, the multirate sampling process can be summarized as follows. In MRI-NCSs, the plant outputs are sampled with the same sampling period T_0 and the plant input of different loop is sampled with different period T_{ui} , where T_0 is the cyclic period of the whole system and known as the frame period. Namely, in a frame period T_0 , one time samples the output and several times the input. Similarly, in MRO-NCSs, the plant inputs are sampled with the same sampling period T_0 and the plant output of different loop is sampled with different period T_{yi} . In GM-NCSs, the inputs and outputs are sampled with T_{ui} and T_{yi} in a frame period, respectively.

3. Fundamental Issues and Prospective Directions of NMCSs

The research of multirate sampling has experienced two stages: frequency domain and time domain. Time-domain method was initiated by Kalman and Bertram [16] in 1959 and is the dominating method for its power and flexibility in characterizing many types of sampled data control systems till now. To further understand the interaction between control and communication in NMCSs, fundamental issues, such as modeling and controller design, will be discussed tentatively

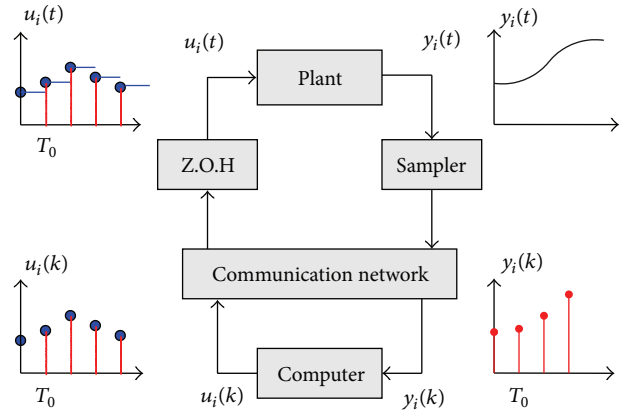


FIGURE 3: Schematic diagram of single-rate sampled-data system.

in time domain in the following, and it is an important initial step toward some larger goals.

3.1. Modeling of NMCSs. In conventional single-rate sampled-data systems, the controller switch at the sampling instant and the control action is held at the same time, as shown in Figure 3. Sampling (1) with period T_0 , the discrete-time model of the whole system can be described by

$$\begin{aligned} x_i(k+1) &= \Phi_i x_i(k) + \Gamma_i u_i(k), \\ y_i(k) &= C_i x_i(k), \end{aligned} \quad (2)$$

where $\Phi_i = e^{A_i T_0}$, $\Gamma_i = \int_0^{T_0} e^{A_i t} B_i dt$ and $k \in \mathbb{Z}_0^+$ (nonnegative integers) is the time index.

Different from single-rate sampled-data systems, modeling of NMCSs is more complicated since both the inherent characteristics of communication network and the particularity of multirate sampling will impact the mathematical model dramatically.

One main issue in communication network is the presence of network-induced delays stemming from the fact of utilizing a common communication channel for closing the loop as well as additional functionality required for physical signal coding and communication processing. According

to the direction of data transfers, network-induced delay can be categorized as the sensor-to-controller delay τ^{sc} and controller-to-actuator delay τ^{ca} . It is clear that network-induced delays result in the disorder and missynchronization of the sampled sequence inevitably and may introduce vacant sampling and message rejection, as shown in Figure 4.

The occurrence of network-induced delay not only impacts the dynamics of both plant and controller but also degrades control performance and introduces potential instability. In [17], the effects of the network-induced delays, that is, data latency, message rejection, and vacant sampling, on the system dynamic performance are systematically considered. In [18], discrete-time modeling approaches for four significant classes of NCSs were presented. In [19], modeling and control of NCSs with different loop topology structures are considered and the uniform discrete state-space model is established by introducing state augmentation for both short- and long-time delays. In summary, modeling of NCSs with network-induced delay has received considerable attentions and some preferable results were obtained.

Modeling of multirate sampling system is always a difficult problem since the distinction of sampling periods between input and output channel and the missynchronization of the sampled sequence. For the sake of simplicity, assumptions are always made that the sampling period of input channel is operated at a rate some integer ratio higher or lower than that of the output channel. Figure 5 shows the schematic diagram of MRI-NCSs with $T_0 = 2T_{ui}$ and MRO-NCSs with $T_0 = 3T_{yi}$, respectively.

For example, in MRI-NCSs, the relationship between T_0 and T_{ui} fulfills $T_0 = N_i T_{ui}$, where $N_i \in \mathbb{Z}^+$ (positive integers). Let $N_0 = \text{LCM}(N_1, \dots, N_N)$, where $\text{LCM}(\cdot)$ is the least common multiple. The basic sampling period of MRI-NCSs can be defined as $T = T_0/N_0$. In view of the characteristic of the multirate input sampling, using the ‘‘lifting’’ technique and defining the augmented input vectors as follows:

$$u_e(kT_0) = \begin{bmatrix} u_{e1}(kT_0) \\ u_{e2}(kT_0) \\ \vdots \\ u_{eN}(kT_0) \end{bmatrix}, \quad (3)$$

where

$$u_{ei}(kT_0) = \begin{bmatrix} u_i(kT_0) \\ u_i(kT_0 + T_{ui}) \\ \vdots \\ u_i(kT_0 + (N_i - 1)T_{ui}) \end{bmatrix}, \quad i = 1, 2, \dots, N. \quad (4)$$

Then, for periodic sampling with constant period T_0 , the linear time invariant state space model of the whole system can be established [20].

Remark 1. It can be seen from Figures 4 and 5, to eliminate vacant sampling and message rejection in NMCSs, the following conditions must be held: (1) $\tau < T_{ui}$ for MRI-NCSs; (2) $\tau < T_{yi}$ for MRO-NCSs; (3) $\tau < \min(T_{ui}, T_{yi})$ for GM-NCSs, where $\tau = \{\tau^{sc}, \tau^{ca}\}$.

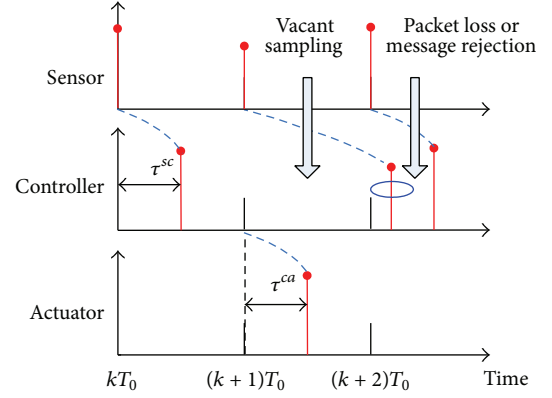


FIGURE 4: Timing diagram of NCSs.

From the above analysis we can draw a conclusion that both the adverse factors caused by network-induced delay and the missynchronization of the sampled sequence introduced by multirate sampling pattern should be taken into account in the course of NMCSs modeling. But, to the author’s knowledge, few literatures considered these issues comprehensively. In [7], under the assumption of delay bounded by sampling period, modeling problem of NCSs is discussed by introducing the definition of discrete lifting. Modeling of MRO-NCSs and MRI-NCSs are established, respectively, but no hints on GM-NCSs and the case of long-time delay. In [21], the models of multirate networked control systems with no network-induced delay and long-time delay are proposed, respectively. It is stated that the multirate networked control systems with long-time delay can be formulated as a discrete-time switched stochastic system.

Remark 2. In the previous, we have made the assumption that all sensors, controllers, and actuators in NMCSs are driven by synchronized clock. That is to say, all these components work with their own period. Time-driven manner can avoid the disorder of the sampled sequence on the one hand but will introduce additional time delay, which degrades control performance, on the other hand.

Remark 3. Network-induced delay is originated in the very fact of utilizing the shared communication network with limited capacity and data rate. It is impracticable to eliminate network-induced delay since it is the intrinsic property of communication network. So, the emphasis should be put on the minimization of the delay rather than elimination. Fortunately, this objective is expected to achieve by means of multirate sampling and/or variable sampling which will be discussed in what follows.

Remark 4. The introduction of the augmented vectors leads to the high dimensionality of the system model and makes the analysis and design of the system complicated. So, the reduction of unnecessary augmented vectors and dimensions of the state space model are key issues worthy of considering.

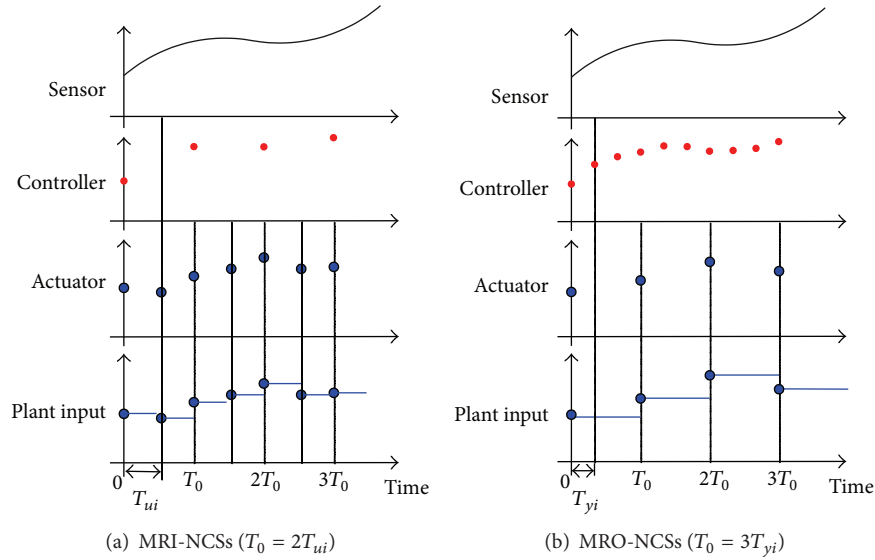


FIGURE 5: Schematic diagram of multirate sampling system.

3.2. Sampling Guaranteeing Controllability and Observability. Controllability and observability are of the two basic concepts to describe the internal structure characteristics of the control systems. They appear as necessary and sometimes as sufficient conditions for the existence of a solution to most control problems and play a central role in modern control theory.

In NMCSs, the plant inputs (and/or outputs) are sampled with different sampling periods in one frame period. Compared with equidistant periodic sampling pattern, the acceleration of sampling frequency in one frame period in multirate sampling can acquire more information about the system and will improve the controllability and observability to some extent. But, on the other hand, when a continuous-time system is converted into discrete-time form by means of a sample and hold operation, the improper selection of the sampling periods will cause the change of the system controllability and observability.

In a general way, a condition on the sampling period T , which is sufficient (and in many cases also necessary) to rule out pathological situations, is that

$$T \neq \frac{2l\pi}{\text{Im}(\lambda_i - \lambda_j)}, \quad l = \pm 1, \pm 2, \dots, \quad (5)$$

where λ_i, λ_j are of different eigenvalues of the continuous-time system. Based on the above condition, controllability and observability of multirate sampling control system are discussed and the conditions for system to be controllable and observable are presented in [20]. A nonequidistant periodic sampling pattern, which has the property to guarantee the controllability and observability during discretization, is proposed in [22] and is further discussed in [23], but no hints on the selection of the sampling rates. To the author's knowledge, besides some empirical formulae and conventions, there is hardly any literature discussing the topic of sampling period

selection in multirate control system. These backgrounds strongly motivate the interest in pursuing for the sampling patterns and the selection of sampling rate in NMCSs.

3.3. Multirate Sampling Control Strategies of NCSs. The introduction of multirate sampling in NCSs makes the analysis and design of the system more complex. Meanwhile, it is possible for NCSs to achieve some unexpected control objectives since the periodic time-varying controller of multirate sampling can increase the degrees of freedom in controller design and improve the control performance to some extent. In [24], pole placement for multirate sampled linear systems by output feedback is studied. The presented approach allows for simultaneous selection of the sampling regime and the closed-loop poles. Also, pole-placement problem is solved by resorting to a controller composed by a periodic state observer and a non-dynamic control law in [25]. In [26, 27], optimal control for multirate systems is discussed and stability robustness issues in periodic and multirate systems are analyzed. In [28], the strong and simultaneous stabilization problems for discrete-time linear time-invariant systems are completely solved by periodic time-varying controllers. In [29], a decentralized control approach to multirate sampled-data systems based on lifting technique is considered and a reliable decentralized multirate controller design is presented. Robust performance and robust stability of the decentralized multirate systems can be achieved by using the design method proposed. In [30], the authors study the use of generalized sampled-data hold functions (GSHF) in the problem of simultaneous controller design for linear time-invariant plants. In [31], solutions to the simultaneous regulation problem of multirate systems are presented. In [32], the problem of pole assignment of decentralized multirate sampling system is discussed. It can be seen that the periodic time-varying controllers of multirate system may achieve some special functions which cannot

be realized by conventional linear time-invariant controller. Some of these functions, such as robust control, simultaneous stabilization, and decentralized control, are the desired control objectives in NCSs design.

In MRICS, the sampling rate of the input channel is higher than that of output channel. The acceleration of the input sampling rate is equivalent to the increase of the effective input. From the point of view of the continuous time, feedback control is performed in both the sample instant and the intersample, which will strengthen the control ability to the plant of the controller. In MROCS, the plant outputs are measured several times in a frame period and more information about the plant is obtained. The extension of effective output of the system corresponds to the increase of the controller's input, which will strengthen the control ability of the controller, especially the output feedback controller. So, how to make full use of the above characteristics of MRI and MRO to design the periodic time-varying control strategies is a major concern and worthy of further considering.

3.4. Scheduling of NCSs Based on Multirate Sampling and Variable Sampling. NCSs include control and network; the performance of control loops depends not only on the design of the control strategies but also on the scheduling of the shared network resources. Sampling period plays an important role between control system and communication network in NCSs. A larger sampling period means lower data transmission rate, which can help to reduce the network-induced time delay and information conflict in a communication network. However, it will lead to the sacrifice of control performance and the reduction of the network utilization, which affects the overall performance of NCSs. On the contrary, smaller sampling period makes the best use of the network utilization and will improve the control performance consequently but aggravates the network congestion and may result in delays and packet dropouts, which will also affect NCSs performance.

Constant sampling is the simplest and most traditional sampling methods in NCSs. It refers to the sampling period in the process of system operation remains the same. It is worth noting that, if constant sampling period is adopted, it should be large enough to avoid network congestion when the network is occupied by the most users. Clearly, the constant sample period results in network resource waste and may obtain the conservative results for the NCSs. Motivations for using variable sampling and multirate sampling in NCSs come from the full use of the limited network resource and the reduction of network-induced delays and its effects on system.

RM (rate monotonic) and EDF (earliest deadline first) [33] are traditional real-time scheduling algorithms and theoretically applicable to control network scheduling. RM algorithm is a kind of statistic scheduling methods. The priority of each task is determined before being executed and not changed along with time. Moreover, RM algorithm is a preemptive algorithm; that is, the currently executing task is preempted by a newly arrived task with shorter period. In [34], an improved RM algorithm is put forward and sufficient

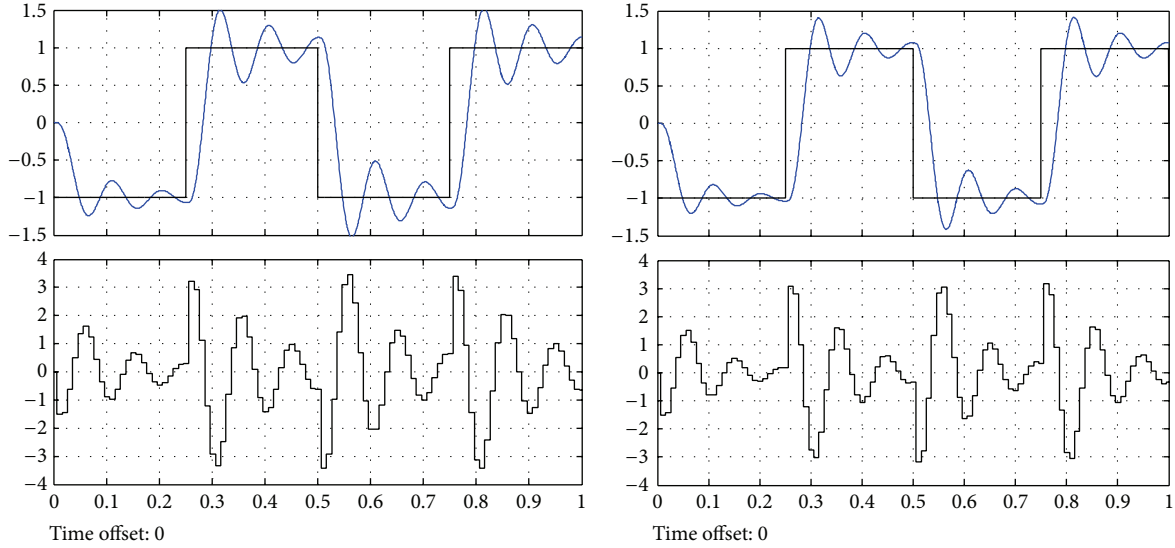
condition for the network to be schedulable is given. EDF algorithm is a kind of dynamic scheduling algorithms. The priority of each task is determined according to the time vary to the deadline of each task; the smaller the time varying, the higher the task priority. Task priority is not fixed but changes along with the time. RM and EDF algorithms are all "open loop" scheduling algorithms. Once the scheduling mechanisms are created, they cannot adjust themselves with the changing of the system. They can perform well in predictable environments in which the network loads can be accurately modeled but poorly in unpredictable environments.

In view of the disadvantages of traditional scheduling algorithms, scheduling algorithms based on the adjustment of sampling period dynamically are emerged. In [35], the influence of sampling period on the performance of NCSs is analyzed systematically and the guidelines for obtaining the optimal working range of sampling times are provided. By analyzing the influence of sampling period, the performance of control systems is studied in [36, 37]. In [38], a scheduling algorithm which could allocate the bandwidth and determine the sampling periods of sensors under constraint that the networked-induced delays were less than the sampling periods is presented. Concerned with different types of data, a scheduling method for NCSs was proposed in [39] under the assumption that the other control loops' sampling period was the integral multiples of the basic sampling period. In [40], a time window algorithm to determine the sampling period to reduce the effect of delay is proposed. In addition, a calculational method to show the relationship between networked-induced delay and the sampling period was proposed in [41], but how to optimize the sampling period is not considered. In [42–44], multiloop sampling period optimization problems are analyzed with nonlinear programming and Kuhn-Tucker theory. In [45], an adaptive sampling rate scheduling method is proposed to allocate the limited network resource based on the requirement of QoP and QoS. The closed-loop system is modeled as a discrete switched system, and then the stability condition and switched feedback controller design method are given based on switched theory.

In our previous works [46–48], variable sampling and multirate sampling scheduling algorithms are put forward by online supervision of the control performance and the available bandwidth. We considered the networked DC-Motor with transfer function $G(s) = 1000/(s^2 + s)$. The parameters of P - D control algorithm can be described by

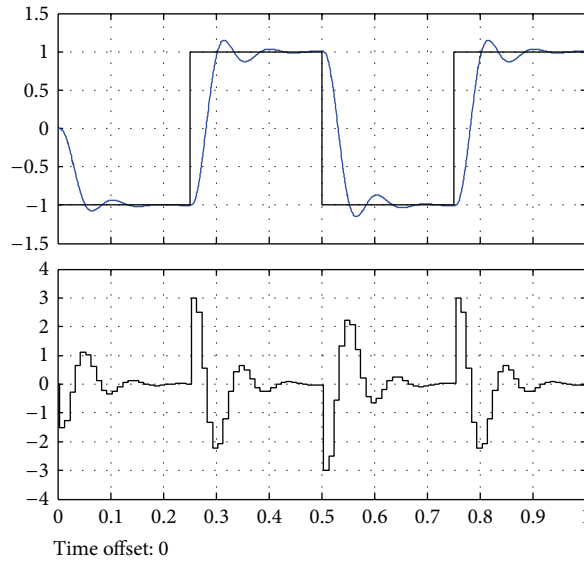
$$\begin{aligned} P(k) &= K(r(k) - y(k)), \\ D(k) &= a_d D(k-1) + b_d (y(k-1) - y(k)), \\ u(k) &= P(k) + D(k), \end{aligned} \quad (6)$$

where $a_d = T_d/(Nh+T_d)$, $b_d = NKT_d/(Nh+T_d)$, $N = 100000$, $T_d = 0.05$, $K = 0.6$, and $h = 0.0075$. The performance of the proposed algorithms is compared with RM and EDF scheduling algorithms in TrueTime toolbox under Matlab environment, as shown in Figure 6. It is clear that the variable sampling algorithm shows a good performance in overshoot, stability, and the suppression on the influence of time delay than that of RM and EDF algorithm.



(a) RM algorithm

(b) EDF algorithm



(c) Variable sampling algorithm

FIGURE 6: Control performance of different scheduling algorithms.

3.5. *Codesign of NMCS.* There have reached a consensus that the whole performance of NCSs correlated with not only the control algorithms but also the network resource allocation. Namely, a successful NCSs design should consider the quality of performance (QoP) of the control system and the quality of service (QoS) of the communication network simultaneously. Hence, the thought of control and scheduling codesign is put forward in [49] in order to resolve the problems caused by QoP and QoS which influence and restrict each other mutually.

Denote B_g as the available global bandwidth of communication network and B_i as the necessary bandwidth for loop i to accomplish its control task, as shown in Figures 1 and 2. With traditional constant sampling manner in NCSs, all subsystems will transfer data synchronously and occupy

the bandwidth averagely. That is, $B_1 = B_2 = \dots = B_N$ and $\sum_{i=1}^N B_i = B_g$. Such bandwidth allocation mechanism is obviously the most simple manner and ease of realizing, on one hand, but, on the other hand, it will cause the waste of network bandwidth resources, the aggravation of network-induced delay, and the decline in overall quality of the system, even worse.

Multirate sampling, considering either the physical properties of the controlled plants or the limitations of the communication network, is an inevitable choice of NCSs. In NMCSs, different control loop is sampled with different sampling period, which can realize the reasonable allocation of the bandwidth resources and guarantee the QoS of the communication network. The distribution principle is that the higher the sampling rate is, the bigger the bandwidth would

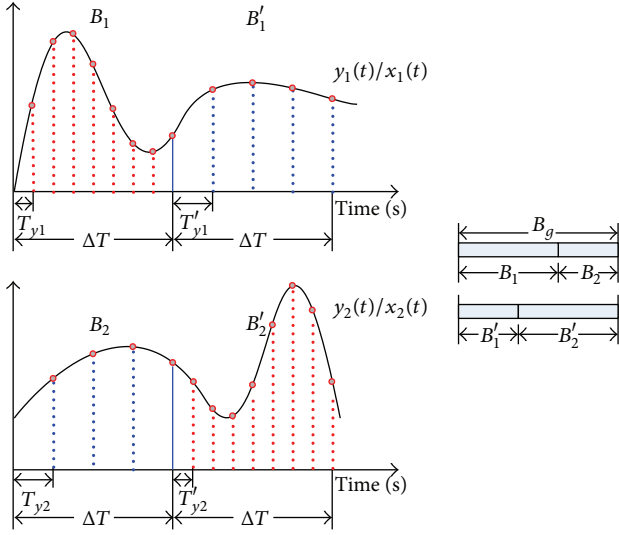


FIGURE 7: Schematic diagram of dynamic bandwidth allocation.

be. For example, in MRO-NCSs, suppose that the sampling periods of the N output channels are $T_{y1}, T_{y2}, \dots, T_{yN}$ and $T_{yi} \leq T_{y(i+1)}$. Then, the bandwidth assigned to the i th subsystem can be calculated by solving the optimization problem

$$\begin{aligned}
 \min \quad & r_i \\
 \text{s.t.} \quad & B_i \geq B_{i+1}, \quad \sum_{i=1}^N B_i < B_g \\
 & r_i \geq r_{\min} \\
 & T_{yi} \leq T_{y(i+1)}, \quad \tau < T_{yi}, \quad \forall i = 1, 2, \dots, N,
 \end{aligned} \tag{7}$$

where r_{\min} denotes the minimum transmission rate that guarantees that no packet dropout occurs in the course of data transmission and r_i denotes the actual transmission rate of the i th output channel.

Meanwhile, different channel (input and output) is sampled with different sampling period making the dynamic bandwidth allocation possible since the synchronous data transmission is avoided in NMCSs. In time-driven manner, a subsystem with no data transmission currently can release its own bandwidth to others till the next transmission starts. These extra bandwidths can be assigned to other subsystems to accomplish data transmission faster. Such dynamic bandwidth allocation strategy, on one hand, reduces the network load and induced delays to some extent, on the other hand, guarantees the QoP of the all subsystems.

For example, in a MRO-NCS with two dependent subsystems, the outputs are sampled with periods T_{y1}, T_{y2} , respectively, and $T_{y1} < T_{y2}$. According to the aforementioned bandwidth allocation principle, the bandwidths assigned to the two subsystems are B_1 and B_2 . Clear, $B_1 > B_2$ and this guarantees sufficient transmission rate of both two channels. In a certain time interval ΔT , by monitoring and evaluating the real-time performance of the whole system online, the sampling periods of the two channels are adjusted to T_{y1}' and

T_{y2}' since the outputs response is changed observably. Then, the bandwidths of the two subsystems are B_1', B_2' and $B_1' > B_2'$. The overall process can be illustrated in Figure 7.

Generally speaking, the distinction of sampling period in NMCSs and the fast-slow and slow-fast characteristics of multirate sampling provide the possibility and methodology to achieve the dynamic bandwidth scheduling. The above-mentioned control and scheduling codesign method can guarantee both the QoP of the control system and QoS of the communication network simultaneously by comprehensively considering the unique characteristics of multirate sampling.

4. Conclusions and Future Works

This survey paper has introduced and reviewed the fundamental issues and prospective directions for NMCSs. One can draw the conclusions that the introduction of multirate sampling in NCSs, on the one hand, will make the modeling, analysis, and synthesis of NCSs more complicated and challenge the achieved theoretical results, and, on the other hand, it will bring opportunities toward some higher goals for NCSs. Problems should be considered in the near future highlight as follows.

- (1) Much effort has been directed to NCSs with variable sampling rate, but most results investigate the stability for a given worst-case interval between consecutive sampling times. This generally leads to conservative results that could be improved by taking into account a stochastic characterization for the intersampling times.
- (2) A combination of multirate sampling and variable sampling in NCSs design may realize the allocation of network bandwidth and reduction of network-induced delays preferably. Namely, multirate sampling implements on subsystems and variable sampling implements within each closed loop.
- (3) Some other basic properties of control system such as controllability and observability should be reconsidered before they can be applied to networked setting.

From the point of view of the development of the control theory, multirate sampling complies with the trends of large-scale, high distribution level and networked framework of computer control system and the research of NMCSs will be bound to further promote the development of the relevant theory and applications of NCSs.

Conflict of Interests

The authors declare that there is no conflict of interests regarding the publication of this paper.

Acknowledgments

This work was supported by the Natural Science Foundation (61263003), Fundamental Research Funds for the Central Universities (2009JC11 and 2009QN120) of China,

and Fundamental Research Funds for Universities of Gansu Province. Also, it was partially supported by Doctor Foundation (BS03200901) and Excellent Young Teachers Foundation (Q201012) of Lanzhou University of Technology.

References

- [1] Y. Tipsuwan and M.-Y. Chow, "Control methodologies in networked control systems," *Control Engineering Practice*, vol. 11, no. 10, pp. 1099–1111, 2003.
- [2] T. C. Yang, "Networked control system: a brief survey," *Institution of Electrical Engineers Proceedings: Control Theory and Applications*, vol. 153, no. 4, pp. 403–412, 2006.
- [3] J. P. Hespanha, P. Naghshtabrizi, and Y. Xu, "A survey of recent results in networked control systems," *Proceedings of the IEEE*, vol. 95, no. 1, pp. 138–172, 2007.
- [4] J. Baillieul, "Special issue on networked control systems," *IEEE Transactions on Automatic Control*, vol. 49, no. 9, pp. 1421–1423, 2004.
- [5] P. Antsaklis and J. Baillieul, "Special issue on technology of networked control systems," *Proceedings of the IEEE*, vol. 95, no. 1, pp. 5–8, 2007.
- [6] D. P. Glasson, "Development and applications of multirate digital control," *IEEE Control Systems Magazine*, vol. 3, no. 4, pp. 2–8, 1983.
- [7] Z. Xia, Z. Wei, Z. Hao, and C. Qijun, "Modeling of multirate input and output networked control system," in *Proceedings of the Global Congress on Intelligent Systems (GCIS '09)*, pp. 258–263, May 2009.
- [8] X. Zhang and J. Xiao, "On the optimal multirate control of networked control systems," *WSEAS Transactions on Systems*, vol. 7, no. 7, pp. 721–731, 2008.
- [9] Z.-W. Wang and G. Guo, "On model-based networked control system with multi-rate input sampling," *International Journal of Modelling, Identification and Control*, vol. 10, no. 1-2, pp. 160–166, 2010.
- [10] W. Chen and L. Qiu, "Stabilization of multirate networked control systems," in *Proceedings of the 50th IEEE Conference on Decision and Control and European Control Conference (CDC-ECC '11)*, pp. 5274–5280, Orlando, Fla, USA, December 2011.
- [11] Y. Zou, T. Chen, and S. Li, "Network-based predictive control of multirate systems," *IET Control Theory and Applications*, vol. 4, no. 7, pp. 1145–1156, 2010.
- [12] Z. H. Guan, C. X. Yang, and J. Huang, "Stabilization of networked control systems with random delays: a new multirate method," in *Proceedings of the 17th World Congress of the International Federation of Automatic Control*, pp. 4204–4209, Seoul, Republic of Korea, 2008.
- [13] Y. S. Suh, H. H. Lee, Y. S. Ro, and M. J. Yi, "Networked control systems using H_2 multirate control," in *Proceedings of the IEEE International Workshop on Factory Communication Systems (WFCS '04)*, pp. 403–406, Vienna, Austria, September 2004.
- [14] Z. Li and M.-Y. Chow, "Adaptive multiple sampling rate scheduling of real-time networked supervisory control system—part I," in *Proceedings of the 32nd Annual Conference on IEEE Industrial Electronics (IECON '06)*, pp. 4604–4609, November 2006.
- [15] Z. Li and M.-Y. Chow, "Adaptive multiple sampling rate scheduling of real-time networked supervisory control system—part II," in *Proceedings of the 32nd Annual Conference on IEEE Industrial Electronics (IECON '06)*, pp. 4610–4615, November 2006.
- [16] R. E. Kalman and J. E. Bertram, "A unified approach to the theory of sampling systems," *Journal of the Franklin Institute*, vol. 267, no. 5, pp. 405–436, 1959.
- [17] A. Ray and Y. Halevi, "Integrated communication and control systems—part II: design considerations," *Journal of Dynamic Systems, Measurement and Control, Transactions of the ASME*, vol. 110, no. 4, pp. 374–381, 1988.
- [18] L. Dritsas, G. Nikolakopoulos, and A. Tzes, "On the modeling of networked controlled systems," in *Proceedings of the Mediterranean Conference on Control and Automation (MED '07)*, Athens, Greece, July 2007.
- [19] Z. Wang, Z. Li, and D. Luo, "Modeling and control of networked systems with different loop topologies," in *Proceedings of the International Conference on Advanced in Control Engineering and Information Science (CEIS '11)*, pp. 594–600, August 2011.
- [20] J. Xiao, *Multi-Rare Digital Control Systems*, Science Publishing House, Beijing, China, 2003.
- [21] Q. Zhu and G. Xie, "Analysis and modeling of multi-rate networked control systems with long time delay," in *Proceedings of the 24th Chinese Control and Decision Conference (CCDC '12)*, pp. 2978–2983, 2012.
- [22] G. Kreisselmeier, "On sampling without loss of observability/controllability," *IEEE Transactions on Automatic Control*, vol. 44, no. 5, pp. 1021–1025, 1999.
- [23] G. Guo, "Systems with nonequidistant sampling: controllable? Observable? Stable?" *Asian Journal of Control*, vol. 7, no. 4, pp. 455–461, 2005.
- [24] L. F. Godbout Jr., D. Jordan, and M. E. Striefler, "Pole placement algorithms for multirate-sampled linear systems," *Automatica*, vol. 30, no. 4, pp. 723–727, 1994.
- [25] P. Colaneri, R. Scattolini, and N. Schiavoni, "Stabilization of multirate sampled-data linear systems," *Automatica*, vol. 26, no. 2, pp. 377–380, 1990.
- [26] P. G. Voulgaris, M. A. Dahleh, and L. S. Valavani, " H_∞ and H_2 optimal controllers for periodic and multirate systems," *Automatica*, vol. 30, no. 2, pp. 251–263, 1994.
- [27] P. G. Voulgaris and B. Bamieh, "Optimal H_∞ and H_2 control of hybrid multirate systems," *Systems and Control Letters*, vol. 20, no. 4, pp. 249–261, 1993.
- [28] P. P. Khargonekar, K. Poolla, and A. Tannenbaum, "Robust control of linear time invariant plants using periodic compensation," *IEEE Transactions on Automatic Control*, vol. 30, no. 11, pp. 1088–1096, 1985.
- [29] M. E. Sezer and D. D. Siljak, "Decentralized multirate control," *IEEE Transactions on Automatic Control*, vol. 35, no. 1, pp. 60–65, 1990.
- [30] P. T. Kabamba and Y. Chang, "Simultaneous controller design for linear time-invariant systems," *IEEE Transactions on Automatic Control*, vol. 36, no. 1, pp. 106–111, 1991.
- [31] A. Locatelli and N. Schiavoni, "Simultaneous regulation of multirate sampled-data systems," in *Proceedings of the American Control Conference*, pp. 1503–1507, Seattle, Wash, USA, June 1995.
- [32] J. Xiao and L. Tang, "Pole assignment of multirate digital control systems with decentralized structure," in *Proceedings of the International Workshop on Autonomous Decentralized System*, pp. 216–219, 2000.
- [33] C. L. Liu and J. W. Layland, "Scheduling algorithms for multiprogramming in a hard real-time environment," *The Journal of the Association for Computing Machinery*, vol. 20, no. 1, pp. 46–61, 1973.
- [34] M. S. Branicky, S. M. Phillips, and W. Zhang, "Scheduling and feedback co-design for networked control systems," in

- Proceedings of the 41st IEEE Conference on Decision and Control*, pp. 1211–1217, December 2002.
- [35] F.-L. Lian, J. Moyne, and D. Tilbury, “Network design consideration for distributed control systems,” *IEEE Transactions on Control Systems Technology*, vol. 10, no. 2, pp. 297–307, 2002.
- [36] J. Q. He and H. C. Zhang, “Optimal sampling period selection method for network control system,” *Journal of Jilin University*, vol. 34, no. 3, pp. 479–482, 2004.
- [37] J.-Q. He, H.-C. Zhang, and Y.-Z. Jing, “Study on feedback scheduling for NCS with packet losses,” *Journal of the University of Electronic Science and Technology of China*, vol. 35, no. 5, pp. 791–822, 2006.
- [38] S. H. Hong, “Scheduling algorithm of data sampling times in the integrated communication and control systems,” *IEEE Transactions on Control System Technology*, vol. 3, pp. 225–231, 1995.
- [39] H. S. Park, Y. H. Kim, S. Kimd, and W. H. Kwon, “A scheduling method for network based control systems,” *IEEE Transactions on Control System Technology*, vol. 10, pp. 318–330, 2002.
- [40] S. H. Hong, “Scheduling algorithm of data sampling times in the integrated communication and control systems,” *IEEE Transactions on Control Systems Technology*, vol. 3, no. 2, pp. 225–230, 1995.
- [41] D. Yue, Q.-L. Han, and C. Peng, “State feedback controller design of networked control systems,” *IEEE Transactions on Circuits and Systems II: Express Briefs*, vol. 51, no. 11, pp. 640–644, 2004.
- [42] K. Peng, X.-F. Li, L. Chen, and J.-D. Chen, “Determination of optimal sampling frequencies in multi-loop networked control system,” *Control and Decision*, vol. 19, no. 10, pp. 1151–1154, 2004.
- [43] C. Peng, D. Yue, Z. Gu, and F. Xia, “Sampling period scheduling of networked control systems with multiple-control loops,” *Mathematics and Computers in Simulation*, vol. 79, no. 5, pp. 1502–1511, 2009.
- [44] C. Peng, D. Yue, and Z. Gu, “Multiple sampling periods scheduling of networked control systems,” in *Proceedings of the 27th Chinese Control Conference (CCC '08)*, pp. 447–451, Yunnan, China, July 2008.
- [45] W. Yan and J. Zhicheng, “Switched feedback control for wireless networked control system with adaptive sampling rate,” in *Proceedings of the 31st Chinese Control Conference*, July 2012.
- [46] Z. W. Wang and H. T. Sun, “Bandwidth scheduling of networked control system based on time varying sampling period,” in *Proceedings of the 32nd Chinese Control Conference*, July 2013.
- [47] Z. W. Wang and H. T. Sun, “Bandwidth allocation strategy of networked control system based on multirate sampling method,” *International Journal of Digital Content Technology and Its Applications*, vol. 6, no. 23, pp. 651–659, 2012.
- [48] Z. W. Wang and S. H. Han, “Dynamic scheduling of networked control systems based on variable-sampling,” Submit to the 25th Chinese Process Control Conference.
- [49] D. Steo, J. Lehoczky, P. L. Sha, and K. G. Shin, “On task schedulability in real-time control systems,” in *Proceeding of the IEEE Conference on Decision and Control*, vol. 4, pp. 865–870, Piscataway, NJ, USA, 2000.

Research Article

Fault Diagnosis System Based on Multiagent Technique for Ship Power System

Zheng Wang,^{1,2} Li Xia,² Yongji Wang,¹ and Lei Liu¹

¹ School of Automation, Huazhong University of Science and Technology, Wuhan 430074, China

² School of Electrical Engineering, Naval University of Engineering, Wuhan 430033, China

Correspondence should be addressed to Yongji Wang; wangyjch@mail.hust.edu.cn

Received 11 December 2013; Accepted 9 February 2014; Published 19 March 2014

Academic Editor: Huaicheng Yan

Copyright © 2014 Zheng Wang et al. This is an open access article distributed under the Creative Commons Attribution License, which permits unrestricted use, distribution, and reproduction in any medium, provided the original work is properly cited.

Fault diagnosis system of ship power system can assist the crew to deal with faults, shorten the processing time, and prevent faults expanding. Multiagent technique is adopted for the fault diagnosis system. Ship power system is divided into several feeder units. Each one is abstracted as a regional feeder agent (FED-Agent). A multiagent fault diagnosis system is established with FED-Agent and other functional agents. Considering of the characteristics of agent, the multiagent system processes both autonomy and interactivity. It can solve fault diagnosis problem of ship power system effectively.

1. Introduction

Modern ship power systems become larger and more complex, and once faults occur, there will be a great deal of alarm information. Although most ship power monitoring systems at present have some simple fault diagnosis functions, but when some failures occur, they just provide numerous pieces of alarm information to the crew unselectively. That is very difficult for the crew to determine fault quickly and accurately. So the research on fault diagnosis techniques for ship power system is an interesting topic. It can assist the crew to deal with power system faults, shorten the processing time, and prevent faults expanding. Fault diagnosis system plays an important role for ensuring safe and stable operation of ship power systems [1–3].

Currently, researchers have proposed many kinds of fault diagnosis methods, such as diagnosis method based on expert system, neural network, and information fusion. Simulation results show methods that can effectively improve the rapidity of ship power system fault diagnosis [4–15]. However, by the above methods, diagnosis information is required to converge to the centralized control center for analysis and processing, which requires that all pieces of information must be totally correct. Once there is incomplete information,

false information, or conflicting information, the accuracy of fault diagnosis is hard to be guaranteed. This is the defect of “centralized” fault diagnosis techniques. To solve this problem, multiagent techniques can be used.

2. Multiagent System and Its Application in Ship Power System

2.1. Simplified Network Model of Ship Power System. Large ship power system is usually made up of several power stations; every station is composed of several generators. A ring or ladder power system is built by loop switches among buses and main switchboards, and the loads get power from buses or distribution switchboards [16].

The research of this paper is based on the typical three-power-station ladder shipboard power system [17]; its simplified network model is given in Figure 1.

The system is made up of 6 generators G, 18 loads (including static loads I and motors M), 10 feeders F, and 6 jumper wires L. The switchboards and jumper wires divide the whole system into three power stations. The alternative routes of important loads are connected by dashed lines.

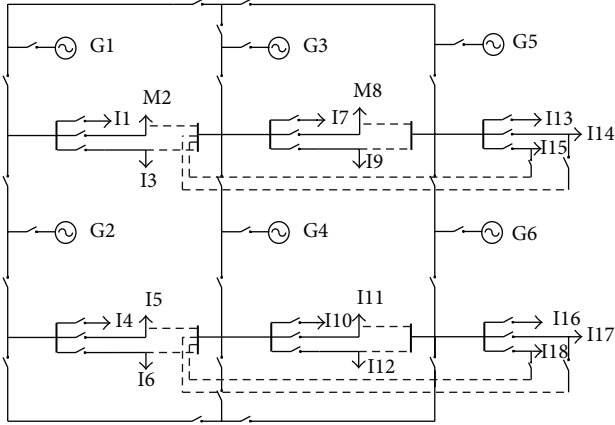


FIGURE 1: Simplified network model of SPS.

According to the graph theory, in Figure 1, the electrical devices and wires (including generators, loads, jumper wires, and switches) are abstracted to be branches, while the connection points between the devices are to be nodes, and then get a node-branch topology, as shown in Figure 2. There are totally 15 nodes and 51 branches in the whole system.

In Figure 2, nodes and branches get their number according to depth-first search and breadth-first search of graph theory; that is, 0~51 in the circle represents branches and 0~15 in the square represents nodes.

2.2. Multiagent System for Fault Diagnosis. Agent and Multiagent System (MAS) originate in the field of artificial intelligence. Because of its advantages, MAS is now one of main research domains of distributed artificial intelligence. Generally, agent is an entity with active behavioral capacity in any environment, such as organism, software system, or controller in control system. MAS is a loose coupling network formed by several agents. Physically or logically the agents are scattered, and their behaviors are self-governing. That is to say, their targets and behaviors would not be restricted by any other agents. To achieve the same task or the same goal, all agents link with each other under some kind of protocol. They can solve problems beyond single agent's capability by communication and cooperation [18–20].

Considering of distributed characteristics of multiagent, the set of nonswitch devices controlled by switch devices on the same regional feeder can be regarded as one agent. Therefore, the ship power system can be divided into several feeder units. Each one is abstracted as a regional feeder agent (FED-Agent). A regional feeder multiagent network model is proposed, as shown in Figure 3.

In its precinct, a FED-Agent can collect and analyze relevant information for fault diagnosis, so as to find faults in real time accurately, and forward fault information to other agents and upper centralized control unit. By communication and cooperation with each other, MAS can implement distributed system-level fault diagnosis.

3. Research on Multiagent Fault Diagnosis System

3.1. Structure of Multiagent Fault Diagnosis System. According to the characteristics of ship power system, a distributed multiagent fault diagnosis system is established in Figure 4.

In this system, there are distributed parallel architecture FED-Agent (regional feeder agent) at the bottom, SCM-Agent (subcommunication manage agent) in the middle layer, and FDI-Agent (fault diagnosis and infusion agent), PDB-Agent (primary data base agent), BDB-Agent (backup data base agent), and OPC-Agent (OPC communication agent) in the upper layer.

FED-Agent implements fault diagnosis in its precinct by fuzzy cognitive map reasoning and fuzzy relational contract net collaboration. The information of fault diagnosis will communicate with other FED-Agent and upload to the FDI-Agent by way of SCM-Agent. By means of communication and cooperation of multiagent, fault diagnosis of ship power system is implemented.

3.2. Internal Logical Structure of Agent. The internal logical structure of FED-Agent is BDI (Belief-Desire-Intention) framework logical structure model based on decision making [21].

BDI framework structure is an important representative of the deliberative type agent. It imitates the process of a series of actions to achieve certain goals that people have taken. It is composed of three basic concepts, which are belief, desire, and intention. Belief reflects the cognitive characteristics of agent, desire reflects the preference feelings of agent, and intention reflects the goal of agent.

Define the agent structure based on BDI framework as follows:

$$\text{Agent} = \{A, E, B, D, I, A, \text{see}, \text{bmp}, \text{opt}, \text{filter}, \text{exe}\}. \quad (1)$$

In which, A represents the set of agents. E represents the basic set of event types. Define Bel as a set of agent's all possible beliefs, so $B \in \gamma(\text{Bel})$ represents one certain set of beliefs; define Des as a set of agent's all possible desires, so $D \in \gamma(\text{Des})$ represents one certain set of desires; define Int as a set of agent's all possible intentions, so $I \in \gamma(\text{Int})$ represents one certain set of intentions. According to the definitions above, the internal behavior of agent can be represented as follows:

$\text{see}: S \rightarrow P$ represents the process of belief determining;

$\text{bmp}: \gamma(\text{Bel}) \times P \rightarrow \gamma(\text{Bel})$ represents the process of belief revision;

$\text{opt}: r(\text{Bel}) \times r(\text{Int}) \rightarrow r(\text{Des})$ represents the process of desire determining;

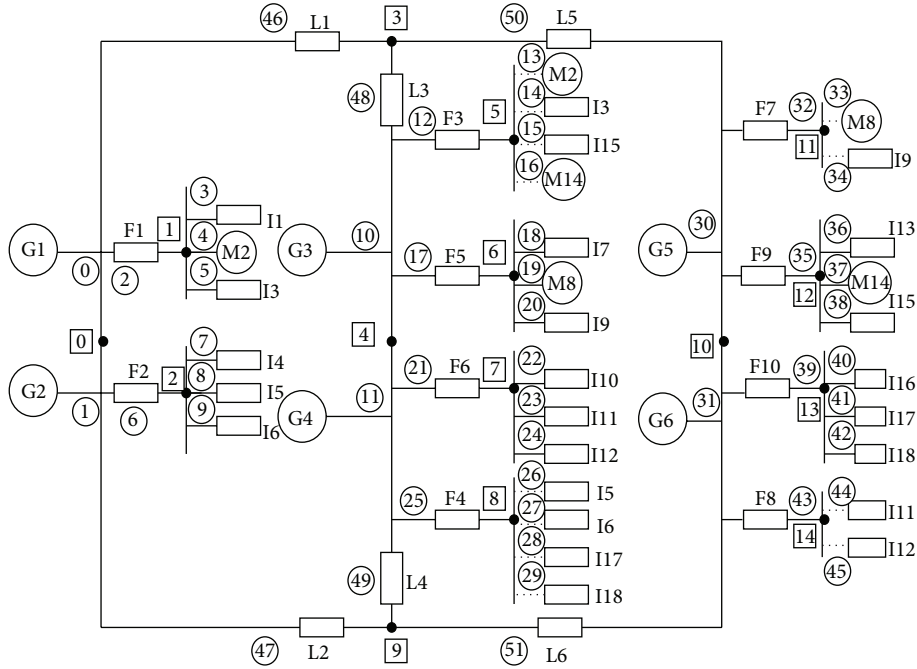


FIGURE 2: Ladder ship power system.

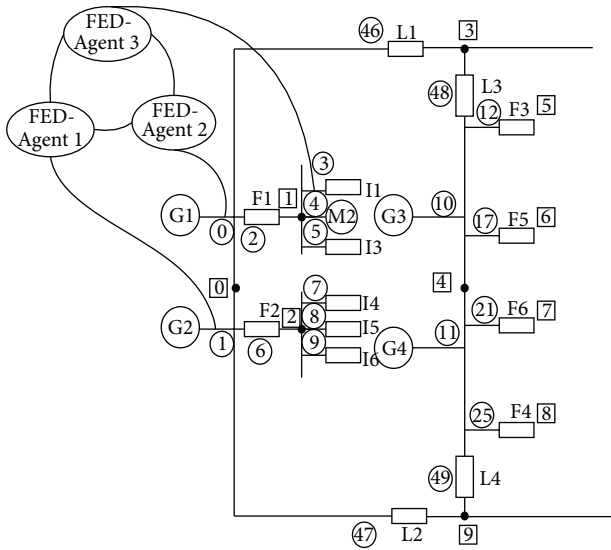


FIGURE 3: Regional feeder multiagent network model of ship power system.

filter: $\gamma(\text{Bel}) \times \gamma(\text{Des}) \times \gamma(\text{Int}) \rightarrow \gamma(\text{Int})$ represents the process of intention determining;

exe: $\gamma(\text{Int}) \rightarrow A$ represents specific behavior for a certain intention.

(2)

The agent structure based on BDI framework is shown in Figure 5.

Since the BDI framework is based on the theory of practical reasoning, it has a profound basis of cognitive psychology and philosophy, so agent's structure established is conformed to the trend of artificial intelligence. Meanwhile, it is difficult to express the concepts of belief, desire, and intention and complete the appropriate reasoning conversion in the actual structure of agent. To establish mature agent model based on BDI framework, an accurate description of the appropriate methods for agent knowledge reasoning process and communication with the environment is needed.

3.3. Main Functions of Multiagent Fault Diagnosis System.

The aim of multiagent fault diagnosis system is to find out the faults in ship power system in real time and isolate and exclude the faults. To guarantee stable operation of SPS, the following functions of the fault diagnosis system are needed:

- (1) monitoring and fault detection: each FED-Agent collects fault diagnosis information in its precinct and communicates with other FED-Agents to diagnose regional faults collaboratively. By cooperating with SCM-Agent and FDI-Agent, system-level faults can be diagnosed.
- (2) Fault notification in real time (warning): simple fault information is delivered to SCM-Agent in real time, and complex fault diagnosis is implemented by FDI-Agent. Alarms are displayed immediately on the GUI to the maintenance staff to ensure that fault is processed timely.
- (3) Alarm status settings and active alarm list: setting alarm status of the corresponding device after alarm and maintaining active alarm list for finding out

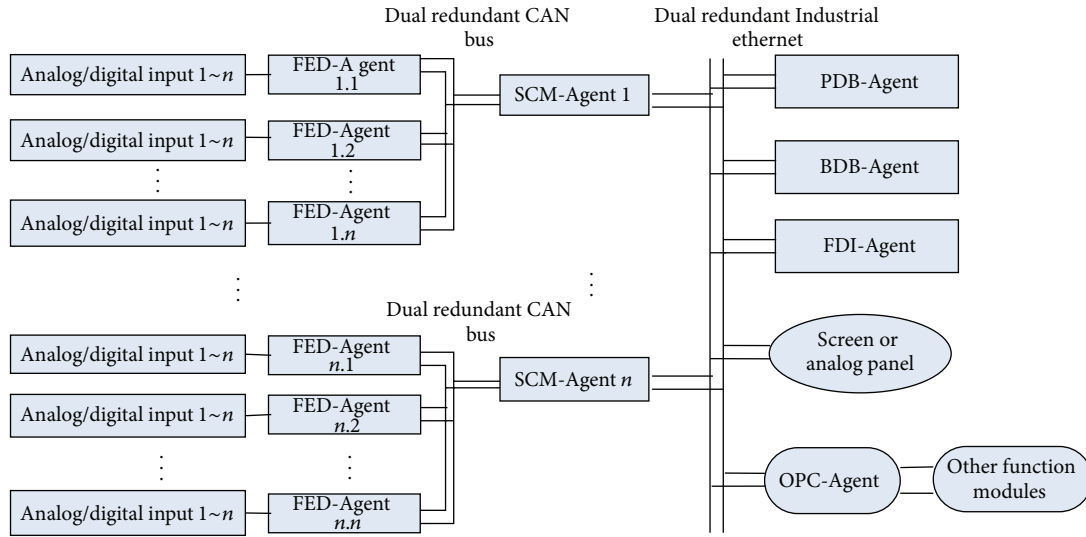


FIGURE 4: Multiagent fault diagnosis system for ship power system.

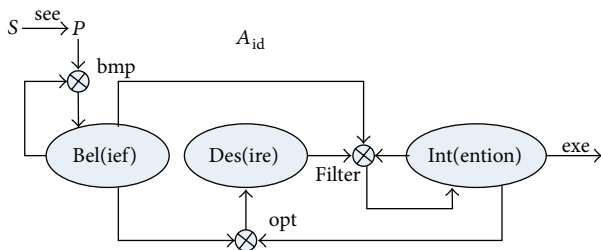


FIGURE 5: Agent structure based on BDI framework.

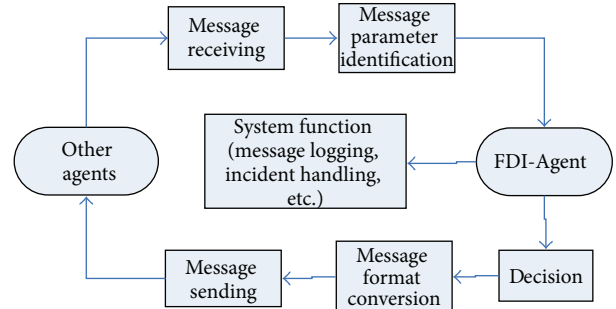


FIGURE 6: Message communication schematic diagram of multiagent fault diagnosis system.

the current alarm status and detailed active alarm information.

- (4) Alarm clear: clearing the corresponding alarm status and active alarm information of the fault device after excluding faults; automatic clearing and artificial clearing are both supported.
- (5) Alarm filtration: setting alarm filtering conditions for selective alarm.
- (6) Fault isolation: stopping the faulty pieces of equipment.
- (7) Failure analysis: analyzing the causes of faults and restoring the device to work properly.
- (8) Alarm history data saving: collecting and saving the alarm information for future alarm analysis.

3.4. Management and Cooperation of Multiagent. To ensure effective cooperation among multiagents, fuzzy contract net model is adopted. In this model, agents can take advantage of master-slave relationship with each other, so that information resources can be fully utilized to implement fault diagnosis [22–25].

Message communication mode is adopted among FED-Agents and between FED-Agent and SCM-Agent. This communication mode is also adopted between SCM-Agent and FDI-Agent. Message communication is simple; three conditions are needed to meet: first, there should be a communication protocol. Second, common communication language among multiagents is needed. Third, common understanding for the language is required.

From the perspective of system implementation, agent is just like object; the interface independent of its internal data structure and message-based is needed to be provided. In the object-oriented field, communication is called by method; the meaning of message is different for each object. But in the agent-oriented software engineering, common language is used by message, regardless of agent's semantics.

The message communication schematic diagram of multiagent fault diagnosis system is shown in Figure 6.

Because of message communication adopted, there are some characteristics of communication in multiagent fault diagnosis system as following: communication data is less, which will shorten network transmission time, reduce time delay, and improve real time of the system. The collaborative

behavior described in message belongs to senior semantic information, so that there are low degrees of coupling and high heterogeneity among cooperative application programs. That is beneficial to build distributed and heterogeneous system. A hierarchical communication structure is designed, the communication protocol specification is presented, and the appropriate communication language and the message-based communication mode are adopted in the paper. So the agents of multiagent fault diagnosis system can communicate and cooperate effectively, and implement distributed fault diagnosis.

3.5. Database Agent. Database agents provide data support for detailed design, programming, and testing of multiagent fault diagnosis system. There are PDB-Agent and BDB-Agent, and both of them have almost the same structure.

We select Oracle Company's database product, because it has perfect functions and high reliability and is easy to operate and maintain easy access to technical support. SCM-Agent is implemented by calling OCI (Oracle Call Interface), which is provided by ORACAL database. FDI-Agent has access to ODBC (Open Database Connectivity) by calling ADO (ActiveX Data Objects), which is provided by Microsoft, so as to access to ORACAL database.

4. Algorithm and Simulation

4.1. Aim Function of Multiagent Fault Diagnosis System. There are many problems in fault diagnosis models in existence. For example, the fault diagnosis model shown as Formula (3) has multiple solutions [26]. We analyze the cause of multiple solutions; the improved fault diagnosis model considering the influence of each protection and the joint influence between the main and back-up protections is presented, shown as Formula (4)

$$E(X) = \sum |r_{km} - r_{km}^*| + \sum |r_{kp} - r_{kp}^*| + \sum |r_{ks} - r_{ks}^*| + \sum |C_i - C_i^*|, \quad (3)$$

$$E(X) = \sum |r_{km} - r_{km}^*| \left| 1 - r_{kp} r_{kp}^* - \sum r_{ks} r_{ks}^* \right| + \sum |r_{kp} - r_{kp}^*| \left| 1 - \sum r_{ks} r_{ks}^* \right| + \sum |r_{ks} - r_{ks}^*| + \sum |r_{jmal} - r_{jmal}^*| + \sum |C_i - C_i^*| \left| 1 - r_{imal} r_{imal}^* \right|. \quad (4)$$

In the Formulas (3) and (4), the continuous-or-operation is represented to be \sum , the main protection of certain element real and anticipant estate is represented to be r_{km} and r_{km}^* , the near backup protection of certain element real and anticipant estate is represented to be r_{kp} and r_{kp}^* , the remote backup protection of certain element real and anticipant estate is represented to be r_{ks} and r_{ks}^* , the breaker's real and anticipant estate is represented to be C_i and C_i^* , and breaker failure

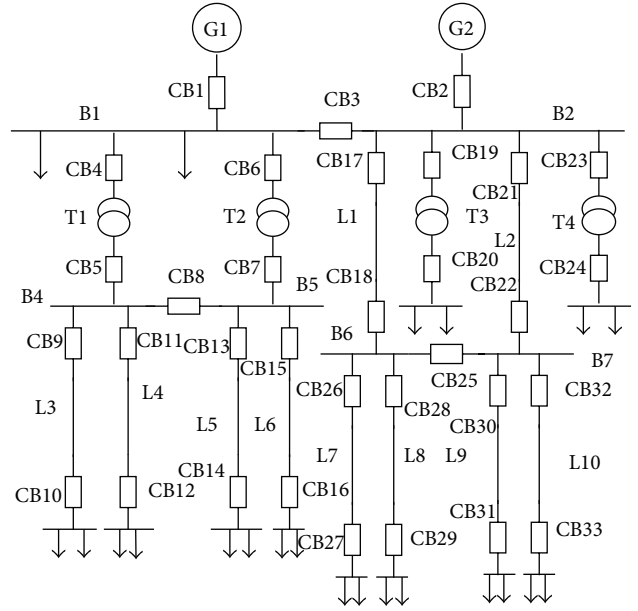


FIGURE 7: Power station 1st of ship power system.

protection's real and anticipant estate is represented to be r_{jmal} and r_{jmal}^* .

In ship power system, the elements which are linked with the load directly only have the main protection and near backup protection. The remote backup protection is only provided by the element which is near to the source. So we can get the aim function of multiagent fault diagnosis system for ship power system as Formula (5)

$$E(X) = \sum |r_{km} - r_{km}^*| \left| 1 - r_{kp} r_{kp}^* - r_{ks} r_{ks}^* \right| + \sum |r_{kp} - r_{kp}^*| \left| 1 - r_{ks} r_{ks}^* \right| + \sum |r_{ks} - r_{ks}^*| + \sum |C_i - C_i^*|. \quad (5)$$

4.2. Example. Power station 1st of ship power system in Figure 2 is taken as example object, shown in Figure 7.

This system has 20 elements, 33 breakers, and 50 protections. ($S_1 \sim S_{20}$) are represented by 20 elements: B1, ..., B6; T1, ..., T4; L1, ..., L10; ($C_1 \sim C_{33}$) are represented by 33 breakers: CB1, CB2, ..., CB33; ($r_1 \sim r_{20}$) are represented by 20 main protections: B1m, ..., B6m; T1m, ..., T4m; L1m, ..., L10m; ($r_{21} \sim r_{40}$) are represented by 20 near backup protections: B1p, ..., B6p; T1p, ..., T4p; L1p, ..., L10p; ($r_{41} \sim r_{50}$) are represented by 10 remote backup protections: B1s, ..., B6s; T1s, T2s; L1s, L2s.

If there are faults that occur in the system, we get the warning signal: the protections of T1p, B1s, T2m, and L5p and the breakers of CB5, CB3, CB1, CB6, CB7, and CB13 act. The elements in the power cut area are B1, B3, B4, T1, T2, L3, L4, L5, and L6 by the network topology analysis.

TABLE 1: Protections anticipant estates.

$r_1^* = s_1$	$r_2^* = s_1(1 - r_1)$	$r_3^* = 1 - [1 - s_4(1 - c_3)][1 - s_5(1 - c_5)]$
$r_4^* = s_2$	$r_5^* = s_2(1 - r_4)$	$r_6^* = 1 - [1 - s_6(1 - c_7)][1 - s_7(1 - c_9)]$
$r_7^* = s_3$	$r_8^* = s_3(1 - r_7)$	$r_9^* = 1 - [1 - s_8(1 - c_{11})][1 - s_9(1 - c_{13})]$
$r_{10}^* = s_4$	$r_{11}^* = s_4(1 - r_{10})$	$r_{12}^* = 1 - [1 - s_2(1 - c_4)]$
$r_{13}^* = s_5$	$r_{14}^* = s_5(1 - r_{13})$	$r_{15}^* = 1 - [1 - s_3(1 - c_6)]$
	$r_{16}^* = s_6$	$r_{17}^* = s_6(1 - r_{16})$
	$r_{18}^* = s_7$	$r_{19}^* = s_7(1 - r_{18})$
	$r_{20}^* = s_8$	$r_{21}^* = s_8(1 - r_{20})$
	$r_{22}^* = s_9$	$r_{23}^* = s_9(1 - r_{22})$

TABLE 2: Breakers anticipant estates.

$c_1^* = \max\{r_1^* r_1, r_2^* r_2, r_3^* r_3\}$	$c_8^* = \max\{r_{16}^* r_{16}, r_{17}^* r_{17}\}$
$c_2^* = \max\{r_1^* r_1, r_2^* r_2, r_3^* r_3\}$	$c_9^* = \max\{r_4^* r_4, r_5^* r_5, r_6^* r_6, r_{18}^* r_{18}, r_{19}^* r_{19}\}$
$c_3^* = \max\{r_1^* r_1, r_2^* r_2, r_3^* r_3, r_{10}^* r_{10}, r_{11}^* r_{11}, r_{12}^* r_{12}\}$	$c_{10}^* = \max\{r_{18}^* r_{18}, r_{19}^* r_{19}\}$
$c_4^* = \max\{r_4^* r_4, r_5^* r_5, r_6^* r_6, r_{10}^* r_{10}, r_{11}^* r_{11}, r_{12}^* r_{12}\}$	$c_{11}^* = \max\{r_7^* r_7, r_8^* r_8, r_9^* r_9, r_{20}^* r_{20}, r_{21}^* r_{21}\}$
$c_5^* = \max\{r_1^* r_1, r_2^* r_2, r_3^* r_3, r_{13}^* r_{13}, r_{14}^* r_{14}, r_{15}^* r_{15}\}$	$c_{12}^* = \max\{r_{20}^* r_{20}, r_{21}^* r_{21}\}$
$c_6^* = \max\{r_7^* r_7, r_8^* r_8, r_9^* r_9, r_{13}^* r_{13}, r_{14}^* r_{14}, r_{15}^* r_{15}\}$	$c_{13}^* = \max\{r_7^* r_7, r_8^* r_8, r_9^* r_9, r_{22}^* r_{22}, r_{23}^* r_{23}\}$
$c_7^* = \max\{r_4^* r_4, r_5^* r_5, r_6^* r_6, r_{16}^* r_{16}, r_{17}^* r_{17}\}$	$c_{14}^* = \max\{r_{22}^* r_{22}, r_{23}^* r_{23}\}$

Corresponding elements estate vector is $S = [s_1, s_2, \dots, s_9]$, the breakers real estate vector is

$$C = [c_1, c_2, c_3, c_4, c_5, c_6, c_7, c_8, c_9, c_{10}, c_{11}, c_{12}, c_{13}, c_{14}] \quad (6)$$

$$= [1, 1, 0, 1, 1, 1, 0, 0, 0, 0, 1, 0, 0, 0].$$

Corresponding breakers are CB1, CB3, CB4, CB5, CB6, CB7, CB9, CB10, CB11, CB12, CB13, CB14, CB15, and CB16. The protections real estate vector is

$$R = [r_1, r_2, \dots, r_{23}]$$

$$= [0, 0, 1, 0, 0, 0, 0, 0, 0, 0, 1, 0, 0, 0, 0, 0, 0, 0, 0, 0, 0, 0, 0, 1, 0, 0]. \quad (7)$$

Corresponding protections are B1m, B1p, B1s, B3m, B3p, B3s, B4m, B4p, B4s, T1m, T1p, T1s, T2m, T2p, T2s, L3m, L3p, L4m, L4p, L5m, L5p, L6m, and L6p. The protections and breakers anticipant estates are shown in Tables 1 and 2.

According to Formula (5), we can get the example's aim function, shown as Formula (8):

$$E(S) = 10 + (2s_1 + 4)(1 - s_4) + 2s_2 + 2s_3 - s_4 - s_5 + 2s_6 + 3s_7 - s_8 + 3s_9 - \max\{s_4, s_5\}. \quad (8)$$

By means of calculation and communication among multiagents, we can get the result of this fault diagnosis model as follows: the failure elements are transformers T1 and T2 and line L5. From the results and analysis, we know that the main protection of transformer T1 refuses to act; breaker CB4 refuses to act; the main protection of line L5 refuses to act; the information of CB14 is missing.

5. Conclusions

Considering of the characteristics of agent, multiagent technique is suitable to be applied in fault diagnosis system for

ship power system. Each agent can independently complete some simple tasks and accomplish complex tasks by communicating with other agents. Agents in the fault diagnosis system have clear division of functions; they can cooperate effectively to solve fault diagnosis problem for ship power system. The multiagent fault diagnosis system has both autonomy and interactivity; it is a new effective way for ship power system fault diagnosis.

Conflict of Interests

The authors declare that there is no conflict of interests regarding the publication of this paper.

Acknowledgment

This work is supported by National Natural Science Foundation of China under Grant no. 51177168.

References

- [1] S. D. J. McArthur, E. M. Davidson, J. A. Hossack et al., "Automating power system fault diagnosis through multi-agent system," in *Proceedings of the 37th Annual Hawaii International Conference on System Sciences*, pp. 947–954, Big Island, Hawaii, USA, 2004.
- [2] Z. Haiyan and X. Fei, "A survey of marine power system fault diagnosis," *Ship Science and Technology*, vol. 32, no. 4, pp. 134–137, 2010.
- [3] J. Chen, J.-H. Wang, B. Zhang, and Z.-Y. Zhu, "Data fusion algorithm for ship power station fault diagnosis system," *Electric Power Automation Equipment*, vol. 26, no. 3, pp. 28–30, 2006.
- [4] G. Cardoso, J. G. Rolim, and H. H. Zurn, "Application of neural-network modules to electric power system fault section

- estimation," *IEEE Transactions on Power Delivery*, vol. 19, no. 3, pp. 1034–1041, 2004.
- [5] C. Liu, Z.-Y. He, and J.-W. Yang, "A quantum neural network based fault diagnosis algorithm for power grid," *Power System Technology*, vol. 32, no. 9, pp. 57–60, 2008.
- [6] Y. Xu, Z. Lu, and Z. Guo, "Layered information fault diagnosis based on genetic algorithm," *Power System Protection and Control*, vol. 28, no. 10, pp. 15–18, 2000.
- [7] J. Sun, S. Qin, and Y. Song, "Fault diagnosis method for power systems based on petri nets and probability information," *Automation of Electric Power Systems*, vol. 27, no. 13, pp. 10–14, 2003.
- [8] Z. Zhang, R. Yuan, T. Yang, and M. Liu, "Rule extraction for power system fault diagnosis based on the combination of rough sets and niche genetic algorithm," *Transactions of China Electrotechnical Society*, vol. 24, no. 1, pp. 158–163, 2009.
- [9] Y. Sun and Z. Liao, "Assessment of data mining model based on the different combination rough set with neural network for fault section diagnosis of distribution networks," *Automation of Electric Power Systems*, vol. 27, no. 6, pp. 31–35, 2003.
- [10] H. Zhang, H. C. Yan, F. W. Yang, and Q. J. Chen, "Quantized control design for impulsive fuzzy networked systems," *IEEE Transactions on Fuzzy Systems*, vol. 19, no. 6, pp. 1153–1162, 2011.
- [11] H. C. Yan, Z. Z. Su, H. Zhang, and F. W. Yang, "Observer-based H_∞ control for discrete-time stochastic systems with quantization and random communication delays," *IET Control Theory and Applications*, vol. 7, no. 3, pp. 372–379, 2013.
- [12] H. Zhang, H. C. Yan, F. W. Yang, and Q. J. Chen, "Distributed average filtering for sensor networks with sensor saturation," *IET Control Theory and Applications*, vol. 7, no. 6, pp. 887–893, 2013.
- [13] H. C. Yan, H. B. Shi, H. Zhang, and F. W. Yang, "Quantized H_∞ control for networked delayed systems with communication constraints," *Asian Journal of Control*, vol. 15, no. 5, pp. 1468–1476, 2013.
- [14] H. J. Gao, T. W. Chen, and J. Lam, "A new delay system approach to network-based control," *Automatica*, vol. 44, no. 1, pp. 39–52, 2008.
- [15] H. Zhang, Q. J. Chen, H. C. Yan, and J. H. Liu, "Robust H_∞ filtering for switched stochastic system with missing measurements," *IEEE Transactions on Signal Processing*, vol. 57, no. 9, pp. 3466–3474, 2009.
- [16] Z. Wang, L. Xia, and Y. Wang, "Application of multi-agent and genetic algorithm in network reconfiguration of ship power system," *Elektronika ir Elektrotechnika*, vol. 18, no. 9, pp. 7–10, 2012.
- [17] Z. Wang, D. Zhao, Y. Wang, and D. Liu, "Reconfiguration of shipboard power system using discrete particle swarm optimisation," *International Journal of Modelling, Identification and Control*, vol. 15, no. 4, pp. 277–283, 2012.
- [18] T. Nagata and H. Sasaki, "A multi-agent approach to power system restoration," *IEEE Transactions on Power Systems*, vol. 17, no. 2, pp. 457–462, 2002.
- [19] H. Zhan and Q. Yan, "Application of multi-agent technology in power system," *Journal of Chongqing University (Natural Science Edition)*, vol. 29, no. 11, pp. 53–57, 2006.
- [20] H.-C. Shu, L. Tang, and J. Dong, "A survey on application of multi-agent system in power system," *Power System Technology*, vol. 29, no. 6, pp. 27–31, 2005.
- [21] Y. Fan and J. Cao, *Multi-Agent System Theory, Methods and Applications*, Springer, Berlin, Germany, 2005.
- [22] R. Khosla and Q. Li, "Multi-layered multi-agent architecture with fuzzy application in electrical power systems," in *Proceedings of the IEEE International Conference on Fuzzy Systems*, vol. 1, pp. 209–214, Honolulu, Hawaii, USA, May 2002.
- [23] H. Zhang, H. C. Yan, T. Liu, and Q. J. Chen, "Fuzzy controller design for nonlinear impulsive fuzzy systems with time delay," *IEEE Transactions on Fuzzy Systems*, vol. 19, no. 5, pp. 844–856, 2011.
- [24] H. Zhang, Z. H. Guan, and G. Feng, "Reliable dissipative control for stochastic impulsive systems," *Automatica*, vol. 44, no. 4, pp. 1004–1010, 2008.
- [25] L. X. Zhang, H. J. Gao, and O. Kaynak, "Network-induced constraints in networked control systems—a survey," *IEEE Transactions on Industrial Informatics*, vol. 9, no. 1, pp. 403–416, 2013.
- [26] H. Weng, P. Mao, and X. Lin, "An improved model for optimizing power system fault diagnosis," *Automation of Electric Power Systems*, vol. 31, no. 7, pp. 66–70, 2007.

Research Article

Robust H_∞ Filtering for Networked Control Systems with Random Sensor Delay

Shenping Xiao, Liyan Wang, Hongbing Zeng, Lingshuang Kong, and Bin Qin

School of Electrical and Information Engineering, Hunan University of Technology, Zhuzhou 412007, China

Correspondence should be addressed to Shenping Xiao; xsph_519@163.com

Received 4 December 2013; Accepted 2 February 2014; Published 19 March 2014

Academic Editor: Huaicheng Yan

Copyright © 2014 Shenping Xiao et al. This is an open access article distributed under the Creative Commons Attribution License, which permits unrestricted use, distribution, and reproduction in any medium, provided the original work is properly cited.

The robust H_∞ filtering problem for a class of network-based systems with random sensor delay is investigated. The sensor delay is supposed to be a stochastic variable satisfying Bernoulli binary distribution. Using the Lyapunov function and Wirtinger's inequality approach, the sufficient conditions are derived to ensure that the filtering error systems are exponentially stable with a prescribed H_∞ disturbance attenuation level and the filter design method is proposed in terms of linear matrix inequalities. The effectiveness of the proposed method is illustrated by a numerical example.

1. Introduction

Networked control systems (NCSs) which are new control systems where sensor-controller and controller-actuator signal link is through a real time network [1]. Because of the advantages, such as convenient fault diagnosis, low cost, and simplicity, the NCSs have been widely applied in many application areas such as industrial automation, remote process, and manufacturing plants. However, the insertion of the communication network may cause time delay, so the signal transferred in NCSs loses the stationary, integrity, and determinacy, which makes the analysis of NCSs become complicate. Therefore, increasing attention has been paid to the study of networked control systems (see, e.g., [2–6] and references therein).

On the other hand, the filtering problem for NCSs has attracted constant research [7–11] since it is important in control engineering and signal processing. In [7], the H_∞ filtering for NCSs with multiple packet dropouts is considered. The problem of designing H_∞ filter design for a class of discrete nonlinear NCSs with stochastic time-varying delays and missing measurements is addressed in [9], where sector nonlinearities and parameter uncertainties are also studied. In [10], by using a stochastic sampled-data approach, the problem of distributed H_∞ filtering in sensor networks is considered. And distributed average filtering for sensor

networks with sensor saturation is designed by averagely fusing the information of each local node in [11]. However, there are few literatures to analyze the problem of H_∞ filtering for continuous-time NCSs with random sensor delay, which motivates the present study.

In this paper, a delay-dependent H_∞ performance analysis result is derived for the filtering error system and a new random sensor delay model with stochastic parameter matrix is proposed. Combining the reciprocally convex combination technique in [12] and employing Wirtinger's inequality approach, new criteria are derived for H_∞ performance analysis, which reduces the conservatism. Based on the derived criteria for H_∞ performance analysis, the novel H_∞ filter criteria are obtained in terms of LMIs. Finally, a numerical example is presented to show the effectiveness of the proposed approach.

2. Problem Description

Consider the following networked control systems:

$$\begin{aligned}\dot{x}(t) &= Ax(t) + Bw(t), \\ y(t) &= Cx(t), \\ z(t) &= Lx(t),\end{aligned}\tag{1}$$

where $x(t) \in R^n$ and $y(t) \in R^m$ are the state and measurable output vector, respectively. $z(t) \in R^q$ is the signal to be estimated and $w(t) \in R^p$ is the external disturbance signal belonging to $L_2[0, \infty]$. A, B, C , and L are known matrices with appropriate dimensions.

Consider the following filter for the estimation of $z(t)$:

$$\begin{aligned}\dot{x}_f(t) &= A_f x_f(t) + B_f \tilde{y}(t), \\ z_f(t) &= L_f x_f(t),\end{aligned}\quad (2)$$

where $x_f(t) \in R^n$ and $\tilde{y}(t) \in R^m$ are the filter's state and input vector, respectively. $z_f(t) \in R^q$ is the estimated output. A_f, B_f , and L_f are the filter matrices to be designed.

In the actual networked control systems, the measured output $\tilde{y}(t) \in R^m$ may or may not experience sensor delay, which can be described by two random events:

- Event 1: $y(t)$ does not experience sensor delay, (3)
Event 2: $y(t)$ experiences sensor delay.

Assume that the occurrences probability of the above given event can be described as the following formula:

$$\begin{aligned}P\{\text{Event 1}\} &= v_0, \\ P\{\text{Event 2}\} &= 1 - v_0.\end{aligned}\quad (4)$$

Define a stochastic variable $v(t)$:

$$v(t) = \begin{cases} 1, & \text{if Event 1 occurs,} \\ 0, & \text{if Event 2 occurs.} \end{cases}\quad (5)$$

By using Bernoulli distributed sequence, the variable $v(t)$ can be assumed to follow an exponential distribution of switching, which satisfies

$$\begin{aligned}P\{v(t) = 1\} &= E\{v(t)\} = v_0, \\ P\{v(t) = 0\} &= E\{1 - v(t)\} = 1 - v_0,\end{aligned}\quad (6)$$

where v_0 is a known constant on $[0, 1]$. Considering the random sensor delay, we suppose that the corresponding measurement is defined as

$$\tilde{y}(t) = v_0 y(t) + (1 - v_0) y(t - \tau(t)),\quad (7)$$

where $\tau(t)$ stands for time-varying delay which satisfies $\tau_m \leq \tau(t) \leq \tau_M$.

Define $\xi(t) = [x^T(t) \ x_f^T(t)]^T$ and $e(t) = z(t) - z_f(t)$; then the filtering error system can be described as follows:

$$\begin{aligned}\dot{\xi}(t) &= \tilde{A}\xi(t) + v_0 \tilde{B}_d \xi(t) + (1 - v_0) \tilde{A}_d E \xi(t - \tau(t)) \\ &\quad + \tilde{B}w(t), \\ e(t) &= \tilde{L}\xi(t),\end{aligned}\quad (8)$$

where

$$\begin{aligned}\tilde{A} &= \begin{bmatrix} A & 0 \\ 0 & A_f \end{bmatrix}, & \tilde{B}_d &= \begin{bmatrix} 0 & 0 \\ B_f C & 0 \end{bmatrix}, \\ \tilde{B} &= \begin{bmatrix} B \\ 0 \end{bmatrix}, & E &= [I \ 0], \\ \tilde{A}_d &= \begin{bmatrix} 0 \\ B_f C \end{bmatrix}, & \tilde{L} &= [L \ L_f].\end{aligned}\quad (9)$$

Our aim in this paper is to design a robust H_∞ filter in the form of (8) such that

- (1) system (1) is robustly exponentially stable, subject to $w(t) = 0$,
- (2) under zero initial condition and for the disturbance attenuation level γ , the controlled output $e(t)$ satisfies $\|e(t)\|_2 \leq r \|w(t)\|_2$ for $w(t) \in L_2[0, \infty]$, $w(t) \neq 0$.

Throughout this paper, we use the following lemmas.

Lemma 1 (see [13]). *For any positive matrix R , and for differentiable signal x in $[\alpha, \beta] \rightarrow R^n$, the following inequality holds:*

$$\int_\alpha^\beta \dot{x}^T(u) R \dot{x}(u) du \geq \frac{1}{\beta - \alpha} \begin{bmatrix} x(\beta) \\ x(\alpha) \\ \chi \end{bmatrix}^T W(R) \begin{bmatrix} x(\beta) \\ x(\alpha) \\ \chi \end{bmatrix},\quad (10)$$

where

$$\begin{aligned}\chi &= \frac{1}{\beta - \alpha} \int_\alpha^\beta w(u) du, \\ W(R) &= \begin{bmatrix} R & -R & 0 \\ * & R & 0 \\ * & * & 0 \end{bmatrix} + \frac{\pi^2}{4} \begin{bmatrix} R & R & -2R \\ * & R & -2R \\ * & * & 4R \end{bmatrix}.\end{aligned}\quad (12)$$

Lemma 2 (see [14]). *For any positive matrix $M > 0$, scalar $r > 0$, and a vector function $w : [0, r] \rightarrow R^n$ such that the integration $\int_0^r w(s)^T M w(s) ds$ is well defined, then*

$$r \left(\int_0^r w(s)^T M w(s) ds \right) \geq \left(\int_0^r w(s) ds \right)^T M \left(\int_0^r w(s) ds \right).\quad (13)$$

Lemma 3 (see [12]). *Let $F_1, F_2, F_3, \dots, F_N : R^m \mapsto R$ have positive values for arbitrary value of independent variable in an open subset W of R^m . The reciprocally convex combination of F_i ($i = 1, 2, \dots, N$) in W satisfies*

$$\begin{aligned}\min & \sum_{i=1}^l \frac{1}{\eta_i} F_i(t) = \sum_{i=1}^l F_i(t) + \max \sum_{i=1}^l \sum_{j=1, j \neq i}^l W_{i,j}(t) \\ \text{subject to} & \left\{ \eta_i > 0, \sum_{i=1}^N \eta_i = 1, W_{i,j}(t) : R^m \mapsto R, \right. \\ & \left. W_{j,i}(t) = W_{i,j}(t), \begin{bmatrix} F_i(t) & W_{i,j}(t) \\ * & F_j(t) \end{bmatrix} \geq 0 \right\}.\end{aligned}\quad (14)$$

3. Main Results

In this section, a H_∞ performance condition for the filtering error system (8) and the robust H_∞ filter design for the system (1) are presented, respectively.

3.1. Performance Analysis of H_∞ Filter

Theorem 4. Defining $\tau_1 = \tau_m$, $\tau_2 = (\tau_m + \tau_M)/2$, $\tau_3 = \tau_M$, and $\delta = \tau_M - \tau_m$, for given positive scalars $0 \leq \tau_m < \tau_M$, the filtering error system (8) is robustly exponentially stable with a H_∞ norm bound γ if there exist positive matrices $P = \begin{bmatrix} P_1 & P_2 \\ P_2^T & P_3 \end{bmatrix} > 0$,

$R = \begin{bmatrix} R_{11} & R_{12} \\ R_{12}^T & R_{22} \end{bmatrix} > 0$, $Q_i > 0$ ($i = 1, 2, 3$), $S_j > 0$ ($j = 1, 2$), and proper dimensions Z_{12} such that

$$\Omega = \begin{bmatrix} \Omega_1 & \tau_2 \Psi^T S_1 & \delta \Psi^T S_2 & \Theta^T \\ * & -S_1 & 0 & 0 \\ * & * & -S_2 & 0 \\ * & * & * & -I \end{bmatrix} < 0, \quad (15)$$

$$\begin{bmatrix} S_2 & Z_{12} \\ * & S_2 \end{bmatrix} > 0,$$

with

$$\Omega_1 = \begin{bmatrix} \Omega_{11} & \Omega_{12} & \Omega_{13} & \Omega_{14} & (1-v_0)P_2 B_f C & 0 & 0 & \Omega_{18} \\ * & \Omega_{22} & 0 & 0 & (1-v_0)P_3 B_f C & 0 & 0 & P_2^T B \\ * & * & \Omega_{33} & \Omega_{34} & 0 & 0 & 0 & 0 \\ * & * & * & -\frac{\pi^2}{\tau_2^2} S_1 & 0 & 0 & 0 & R_{12}^T B \\ * & * & * & * & \Omega_{55} & \Omega_{56} & \Omega_{57} & 0 \\ * & * & * & * & * & \Omega_{66} & Z_{12} & 0 \\ * & * & * & * & * & * & \Omega_{77} & 0 \\ * & * & * & * & * & * & * & -\gamma^2 I \end{bmatrix}, \quad (16)$$

where

$$\begin{aligned} \Omega_{11} &= A^T P_1 + P_1 A + A^T R_{11} + R_{11} A + R_{12} + R_{12}^T \\ &+ Q_1 - S_1 - \frac{\pi^2}{4} S_1 + v_0 P_2 B_f C + v_0 C^T B_f^T P_2, \\ \Omega_{12} &= A^T P_2 + P_2 A_f + v_0 C^T B_f^T P_3, \\ \Omega_{13} &= -R_{12} + S_1 - \frac{\pi^2}{4} S_1, \\ \Omega_{14} &= A^T R_{12} + R_{22} + \frac{\pi^2}{2\tau_2} S_1, \\ \Omega_{18} &= P_1 B + R_{11}^T B, \\ \Omega_{22} &= P_3 A_f + A_f^T P_3, \\ \Omega_{33} &= Q_3 - Q_2 - S_1 - \frac{\pi^2}{4} S_1, \\ \Omega_{34} &= -R_{22} + \frac{\pi^2}{2\tau_2} S_1, \\ \Omega_{55} &= -S_2 - S_2^T + Z_{12} + Z_{12}^T, \\ \Omega_{56} &= S_2 - Z_{12}, \\ \Omega_{57} &= S_2 - Z_{12}^T, \\ \Omega_{66} &= -Q_1 + Q_2 - S_2, \\ \Omega_{77} &= -Q_3 - S_2, \end{aligned}$$

$$\Theta = [L \quad -L_f \quad 0 \quad 0 \quad 0 \quad 0 \quad 0 \quad 0],$$

$$\Psi = [A \quad 0 \quad 0 \quad 0 \quad 0 \quad 0 \quad 0 \quad B].$$

(17)

Proof. Consider the Lyapunov-Krasovskii functional candidate as

$$\begin{aligned} V(x_t) &= \xi^T(t) P \xi(t) + \int_{t-\tau_1}^t x^T(s) Q_1 x(s) ds \\ &+ \left[\int_{t-\tau_2}^t x(s) ds \right]^T R \left[\int_{t-\tau_2}^t x(s) ds \right] \\ &+ \int_{t-\tau_2}^{t-\tau_1} x^T(s) Q_2 x(s) ds \\ &+ \int_{t-\tau_3}^{t-\tau_2} x^T(s) Q_3 x(s) ds \\ &+ \tau_2 \int_{t-\tau_2}^t \int_s^t \dot{x}^T(v) S_1 \dot{x}(v) dv ds \\ &+ \delta \int_{t-\tau_3}^{t-\tau_1} \int_s^t \dot{x}^T(v) S_2 \dot{x}(v) dv ds. \end{aligned} \quad (18)$$

Calculating the time derivative of $V(x_t)$ along the trajectory of (8) yields

$$\begin{aligned} \dot{V}(x_t) &= 2\xi^T(t) P \dot{\xi}(t) + x^T(t) Q_1 x(t) \\ &- x^T(t - \tau_1) Q_1 x(t - \tau_1) \end{aligned}$$

$$\begin{aligned}
& + 2 \begin{bmatrix} \dot{x}(t) \\ x(t) - x(t - \tau_2) \end{bmatrix}^T R \begin{bmatrix} x(t) \\ \int_{t-\tau_2}^t x(s) ds \end{bmatrix} \\
& + x^T(t - \tau_1) Q_2 x(t - \tau_1) \\
& - x^T(t - \tau_2) Q_2 x(t - \tau_2) \\
& + x^T(t - \tau_2) Q_3 x(t - \tau_2) \\
& - x^T(t - \tau_3) Q_3 x(t - \tau_3) \\
& + \tau_2^2 \dot{x}^T(t) S_1 \dot{x}(t) + \delta^2 \dot{x}^T(t) S_2 \dot{x}(t) \\
& - \tau_2 \int_{t-\tau_2}^t \dot{x}^T(s) S_1 \dot{x}(s) ds \\
& - \delta \int_{t-\tau_3}^{t-\tau_1} \dot{x}^T(s) S_2 \dot{x}(s) ds.
\end{aligned} \tag{19}$$

By utilizing Lemma 1, the integral term $-\tau_2 \int_{t-\tau_2}^t \dot{x}^T(s) S_1 \dot{x}(s) ds$ can be estimated as

$$\begin{aligned}
& -\tau_2 \int_{t-\tau_2}^t \dot{x}^T(s) S_1 \dot{x}(s) ds \\
& \leq \begin{bmatrix} x(t) \\ x(t - \tau_2) \\ \frac{1}{\tau_2} \int_{t-\tau_2}^t x(s) ds \end{bmatrix}^T W(S_1) \begin{bmatrix} x(t) \\ x(t - \tau_2) \\ \frac{1}{\tau_2} \int_{t-\tau_2}^t x(s) ds \end{bmatrix}, \tag{20}
\end{aligned}$$

where

$$W(S_1) = - \begin{bmatrix} S_1 & -S_1 & 0 \\ * & S_1 & 0 \\ * & * & 0 \end{bmatrix} - \frac{\pi^2}{4} \begin{bmatrix} S_1 & S_1 & -2S_1 \\ * & S_1 & -2S_1 \\ * & * & 4S_1 \end{bmatrix}. \tag{21}$$

On the other hand, defining $\alpha = (\tau(t) - \tau_1)/\delta$ and $\beta = (\tau_3 - \tau(t))/\delta$, by the reciprocally convex combination in Lemma 3, the following inequality holds:

$$\begin{aligned}
& - \begin{bmatrix} \sqrt{\frac{\beta}{\alpha}} (x(t - \tau_1) - x(t - \tau(t))) \\ -\sqrt{\frac{\alpha}{\beta}} (x(t - \tau(t)) - x(t - \tau_3)) \end{bmatrix}^T \begin{bmatrix} S_2 & Z_{12} \\ * & S_2 \end{bmatrix} \\
& \times \begin{bmatrix} \sqrt{\frac{\beta}{\alpha}} (x(t - \tau_1) - x(t - \tau(t))) \\ -\sqrt{\frac{\alpha}{\beta}} (x(t - \tau(t)) - x(t - \tau_3)) \end{bmatrix} < 0.
\end{aligned} \tag{22}$$

Note that due to $\tau_1 \leq \tau(t) \leq \tau_3$, according to Lemma 2 and inequalities (22), we have

$$\begin{aligned}
& -\delta \int_{t-\tau_3}^{t-\tau_1} \dot{x}^T(s) S_2 \dot{x}(s) ds \\
& = -\delta \int_{t-\tau(t)}^{t-\tau_1} \dot{x}^T(s) S_2 \dot{x}(s) ds \\
& \quad - \delta \int_{t-\tau_3}^{t-\tau(t)} \dot{x}^T(s) S_2 \dot{x}(s) ds \\
& \leq -\frac{\delta}{\tau(t) - \tau_1} \begin{bmatrix} x(t - \tau_1) \\ x(t - \tau(t)) \end{bmatrix}^T \begin{bmatrix} S_2 & -S_2 \\ * & S_2 \end{bmatrix} \\
& \quad \times \begin{bmatrix} x(t - \tau_1) \\ x(t - \tau(t)) \end{bmatrix} - \frac{\delta}{\tau_3 - \tau(t)} \begin{bmatrix} x(t - \tau(t)) \\ x(t - \tau_3) \end{bmatrix}^T \\
& \quad \times \begin{bmatrix} Z_2 & -Z_2 \\ * & Z_2 \end{bmatrix} \begin{bmatrix} x(t - \tau(t)) \\ x(t - \tau_3) \end{bmatrix} \\
& \leq - \begin{bmatrix} x(t - \tau_1) - x(t - \tau(t)) \\ x(t - \tau(t)) - x(t - \tau_3) \end{bmatrix}^T \begin{bmatrix} S_2 & Z_{12} \\ * & S_2 \end{bmatrix} \\
& \quad \times \begin{bmatrix} x(t - \tau_1) - x(t - \tau(t)) \\ x(t - \tau(t)) - x(t - \tau_3) \end{bmatrix} \\
& = \eta^T(t) \begin{bmatrix} -2S_2 + Z_{12} + Z_{12}^T & S_2 - Z_{12} & S_2 - Z_{12}^T \\ * & -S_2 & Z_{12} \\ * & * & -S_2 \end{bmatrix} \eta(t), \tag{23}
\end{aligned}$$

where

$$\eta^T(t) = [x^T(t - \tau(t)) \quad x^T(t - \tau_1) \quad x^T(t - \tau_3)]. \tag{24}$$

Substituting (20)–(23) into (19) and then applying the Schur complement, it can be concluded that

$$\begin{aligned}
& \dot{V}(x_t) + e^T(t) e(t) - \gamma^2 w^T(t) w(t) \\
& \leq \zeta^T(t) (\Omega_1 + \delta^2 \Psi^T S_1 \Psi + \tau_2^2 \Psi^T S_1 \Psi + \Theta^T \Theta) \zeta(t), \tag{25}
\end{aligned}$$

where

$$\begin{aligned}
& \zeta^T(t) = \begin{bmatrix} x^T(t) & x_f^T(t) & x^T(t - \tau_2) & \int_{t-\tau_2}^t x(s) ds \\ x^T(t - \tau) & x^T(t - \tau_1) & x^T(t - \tau_3) & w^T(t) \end{bmatrix}. \tag{26}
\end{aligned}$$

If (25) holds, we have

$$\dot{V}(x_t) + e^T(t) e(t) - \gamma^2 w^T(t) w(t) < 0. \tag{27}$$

Carrying out integral manipulations on (27) from 0 to ∞ and noting that $V(x_t)|_{t=0} = 0$ under zero initial conditions, we obtain

$$\begin{aligned}
& \int_0^\infty e^T(s) e(s) ds - \int_0^\infty \gamma^2 w^T(s) w(s) ds \\
& < V(x_t)|_{t \rightarrow 0} - V(x_t)|_{t \rightarrow \infty} < 0.
\end{aligned} \tag{28}$$

That is, $\|e(t)\|_2 \leq \gamma \|w(t)\|_2$, so the filtering error system has an H_∞ disturbance attenuation level γ under zero initial conditions.

Second, we also can prove that the filtering error system with $w(t) = 0$ is robustly exponentially stable under the condition of Theorem 4. This completes the proof. \square

Remark 5. Similar to [15], we divide the delay interval into two subintervals uniformly. However, the new Lyapunov-Krasovskii functional in our paper which not only divides the delay interval into two subintervals but also makes use of the information of $\int_{t-\tau_2}^t x(s)ds$ is proposed. The results will be less conservative.

3.2. Design of H_∞ Filter

Theorem 6. Defining $\tau_1 = \tau_m$, $\tau_2 = ((\tau_m + \tau_M)/2)$, $\tau_3 = \tau_M$, and $\delta = \tau_M - \tau_m$, for some given constants $0 \leq \tau_m < \tau_M$, v_0 , and γ , the filtering error system (8) is robustly exponentially stable with a H_∞ norm bound γ if there exist positive matrices $P_1 > 0$, $X > 0$, $R = \begin{bmatrix} R_{11} & R_{12} \\ R_{12}^T & R_{22} \end{bmatrix} > 0$, $Q_i > 0$ ($i = 1, 2, 3$) and $S_j > 0$ ($j = 1, 2$) and matrices \bar{A}_f , \bar{B}_f , \bar{L}_f , and Z_{12} of appropriate dimensions such that the following LMIs are satisfied:

$$\tilde{\Omega} = \begin{bmatrix} \tilde{\Omega}_1 & \tau_2 \Psi^T S_1 & \delta \Psi^T S_2 & \tilde{\Theta}^T \\ * & -S_1 & 0 & 0 \\ * & * & -S_2 & 0 \\ * & * & * & -I \end{bmatrix} < 0, \quad (29)$$

$$\begin{bmatrix} S_2 & Z_{12} \\ * & S_2 \end{bmatrix} > 0,$$

$$X - P_1 < 0,$$

with

$$\tilde{\Omega}_1 = \begin{bmatrix} \tilde{\Omega}_{11} & \tilde{\Omega}_{12} & \Omega_{13} & \Omega_{14} & (1-v_0)\bar{B}_f C & 0 & 0 & \Omega_{18} \\ * & \tilde{\Omega}_{22} & 0 & 0 & (1-v_0)\bar{B}_f C & 0 & 0 & XB \\ * & * & \Omega_{33} & \Omega_{34} & 0 & 0 & 0 & 0 \\ * & * & * & -\frac{\pi^2}{\tau_2^2} S_1 & 0 & 0 & 0 & R_{12}^T B \\ * & * & * & * & \Omega_{55} & \Omega_{56} & \Omega_{57} & 0 \\ * & * & * & * & * & \Omega_{66} & Z_{12} & 0 \\ * & * & * & * & * & * & \Omega_{77} & 0 \\ * & * & * & * & * & * & * & -\gamma^2 I \end{bmatrix}, \quad (30)$$

where

$$\begin{aligned} \tilde{\Omega}_{11} &= A^T P_1 + P_1 A + A^T R_{11} + R_{11} A + R_{12} + R_{12}^T \\ &+ Q_1 - S_1 - \frac{\pi^2}{4} S_1 + v_0 \bar{B}_f C + v_0 C^T \bar{B}_f^T, \\ \tilde{\Omega}_{12} &= A^T X + \bar{A}_f + v_0 C^T \bar{B}_f^T, \\ \tilde{\Omega}_{22} &= \bar{A}_f + \bar{A}_f^T, \\ \tilde{\Theta} &= [L \quad -\bar{L}_f \quad 0 \quad 0 \quad 0 \quad 0 \quad 0 \quad 0]. \end{aligned} \quad (31)$$

Then, the H_∞ filtering problem is solvable. Moreover, the parameter matrices of the filter are given by

$$A_f = \bar{A}_f X^{-1}, \quad B_f = \bar{B}_f, \quad L_f = \bar{L}_f X^{-1}. \quad (32)$$

Proof. Defining

$$P = \begin{bmatrix} P_1 & P_2 \\ P_2^T & P_3 \end{bmatrix}, \quad X = P_2 P_3^{-1} P_2^T, \quad (33)$$

$$J = \text{diag} \{I, P_2 P_3^{-1}, I, I, \dots, I\}.$$

Applying the Schur complement, it can be concluded that $P > 0$ is equivalent to

$$P_1 - P_2 P_3^{-1} P_2^T = P_1 - X > 0. \quad (34)$$

Set $\bar{A}_f = P_2 A_f P_3^{-1} P_2^T$, $\bar{B}_f = P_2 B_f$, and $\bar{L}_f = L_f P_3^{-1} P_2^T$. Pre- and postmultiplying (15) by J^T and J give

$$J^T \Omega_1 J = \tilde{\Omega}_1. \quad (35)$$

Thus we can conclude that the filtering error system is robustly exponentially stable with a H_∞ norm bound γ . The transfer function of the filter is defined as

$$T = L_f (sI - A_f)^{-1} B_f. \quad (36)$$

According to (32), we can get

$$\begin{aligned} T &= L_f (sI - A_f)^{-1} B_f \\ &= \bar{L}_f P_2^{-T} P_3 (sI - P_2^{-1} \bar{A}_f P_2^{-T} P)^{-1} P_2^{-1} \bar{B}_f \\ &= \bar{L}_f (sX - \bar{A}_f)^{-1} \bar{B}_f \\ &= \bar{L}_f (sI - X^{-1} \bar{A}_f)^{-1} X^{-1} \bar{B}_f \\ &= \bar{L}_f X^{-1} (sI - \bar{A}_f X^{-1})^{-1} \bar{B}_f. \end{aligned} \quad (37)$$

Therefore, the parameter matrices of the filter can be chosen as in (32). This completes the proof. \square

Remark 7. According to LMIs (29), we can find that the variable numbers are fewer than Theorem 2 in [16]; therefore, the filter design method provides a more simple form.

4. Simulation Example

Example 1. Consider the system described by (1) with the following parameters in [16]:

$$A = \begin{bmatrix} 0.5 & 3 \\ -2 & -5 \end{bmatrix}, \quad B = \begin{bmatrix} -0.5 \\ 0.9 \end{bmatrix}, \quad (38)$$

$$C = [0 \quad 1], \quad L = [1 \quad 1].$$

Assume that $\tau(t)$ satisfies $0.01 \leq \tau(t) < 0.2$, $w(t) = 0.2 \sin e^{-0.2t}$, and the measured output experiences sensor

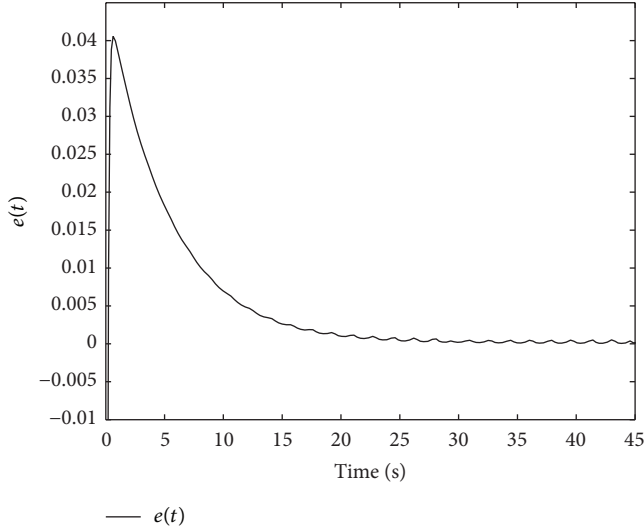


FIGURE 1: The error response $e(t) = z(t) - z_f(t)$.

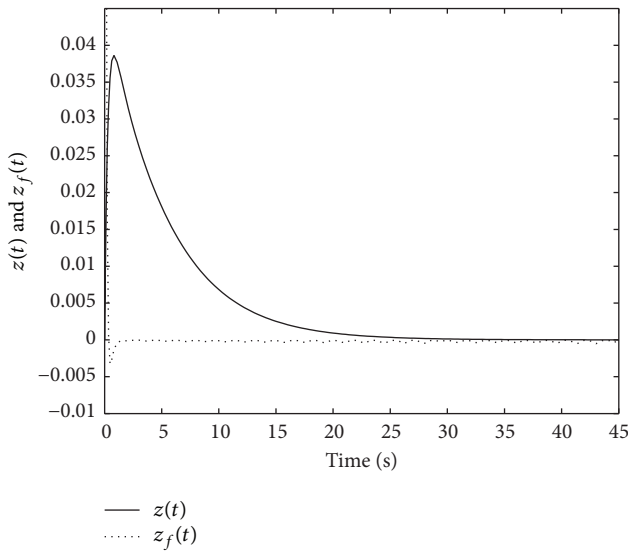


FIGURE 2: The output response of $z(t)$ and $z_f(t)$.

delay, that is, the sensor delay occurrences probability, $v_0 = 0.5$. The initial conditions $x(t)$ and $x_f(t)$ are $[0.2 \ -0.2]^T$ and $[0.03 \ -0.05]^T$, respectively. According to Theorem 6 with the help from Matlab LMI toolbox, it can be solved that the desired H_∞ filter parameters are as follows with the performance level $\gamma = 0.2143$:

$$\begin{aligned} A_f &= \begin{bmatrix} -4.5071 & -3.8049 \\ -0.7971 & -9.9490 \end{bmatrix}, \\ B_f &= \begin{bmatrix} -0.0002 \\ -0.0078 \end{bmatrix}, \\ C_f &= [-1.7957 \ -8.2983]. \end{aligned} \quad (39)$$

The simulation results are shown in Figures 1 and 2. Figure 1 shows the error response $e(t) = z(t) - z_f(t)$. The output $z(t)$ and $z_f(t)$ are depicted in Figure 2. All the simulations have confirmed that the designed H_∞ filter can stabilize the system (1) with random sensor delay.

5. Conclusion

In this paper, we have studied the network-based robust H_∞ filtering problem for continuous-time systems with random sensor delay. A novel Lyapunov-Krasovskii functional has been constructed to design a filter by means of LMIs, which guarantees a prescribed H_∞ disturbance rejection attenuation level for the filter error system. A numerical example has been provided to show the effectiveness of the proposed filter design method and the input or state delays in the systems should be further considered in the future work.

Conflict of Interests

The authors declare that there is no conflict of interests regarding the publication of this paper.

Acknowledgments

This work was supported by the National Nature Science Foundation of China (61203136, 61304064, and 61074067); this work was supported by Natural Science Foundation of Hunan Province of China (11JJ2038); this work was supported by the Construct Program for the Key Discipline of electrical engineering in Hunan province.

References

- [1] G. C. Walsh, H. Ye, and L. G. Bushnell, "Stability analysis of networked control systems," *IEEE Transactions on Control Systems Technology*, vol. 10, no. 3, pp. 438–446, 2002.
- [2] H. C. Yan, H. B. Shi, H. Zhang, and F. W. Yang, "Quantized H_∞ control for networked systems with communication constraints," *Asian Journal of Control*, vol. 15, no. 5, pp. 1468–1476, 2013.
- [3] C. Lin, Z. D. Wang, and F. W. Yang, "Observer-based networked control for continuous-time systems with random sensor delays," *Automatica*, vol. 45, no. 2, pp. 578–584, 2009.
- [4] H. Zhang, H. C. Yan, F. W. Yang, and Q. J. Chen, "Quantized control design for impulsive fuzzy networked systems," *IEEE Transactions on Fuzzy Systems*, vol. 19, no. 6, pp. 1153–1162, 2011.
- [5] Y. He, G. P. Liu, D. Rees, and M. Wu, "Improved stabilisation method for networked control systems," *IET Control Theory and Applications*, vol. 1, no. 6, pp. 1580–1585, 2007.
- [6] H. C. Yan, Z. Z. Su, H. Zhang, and F. W. Yang, "Observer-based H_∞ control for discrete-time stochastic systems with quantisation and random communication delays," *IET Control Theory & Applications*, vol. 7, no. 3, pp. 372–379, 2013.
- [7] T. C. M. Sahebsara, T. Chen, and S. L. Shah, "Optimal H_∞ filtering in networked control systems with multiple packet dropouts," *Systems & Control Letters*, vol. 57, no. 9, pp. 696–702, 2008.

- [8] X.-M. Zhang and Q.-L. Han, "Network-based H_∞ filtering for discrete-time systems," *IEEE Transactions on Signal Processing*, vol. 60, no. 2, pp. 956–961, 2012.
- [9] H. L. Dong, Z. D. Wang, and H. J. Gao, "Robust H_∞ filtering for a class of nonlinear networked systems with multiple stochastic communication delays and packet dropouts," *IEEE Transactions on Signal Processing*, vol. 58, no. 4, pp. 1957–1966, 2010.
- [10] B. Shen, Z. D. Wang, and X. H. Liu, "A stochastic sampled-data approach to distributed H_∞ filtering in sensor networks," *IEEE Transactions on Circuits and Systems*, vol. 58, no. 9, pp. 2237–2246, 2011.
- [11] H. Zhang, H. C. Yan, F. W. Yang, and Q. J. Chen, "Distributed average filtering for sensor networks with sensor saturation," *IET Control Theory & Applications*, vol. 7, no. 6, pp. 887–893, 2013.
- [12] P. Park, J. W. Ko, and C. Jeong, "Reciprocally convex approach to stability of systems with time-varying delays," *Automatica*, vol. 47, no. 1, pp. 235–238, 2011.
- [13] A. Seuret and F. Gouaisbaut, "On the use of Wirtinger's inequalities for time-delay systems," in *Proceedings of the the 10th IFAC Workshop on Time Delay Systems (IFAC TDS '12)*, Boston, Mass, USA, 2012.
- [14] K. Gu, "An integral inequality in the stability problem of time-delay systems," in *Proceedings of the 39th IEEE Conference on Decision and Control*, pp. 2805–2810, December 2000.
- [15] X.-M. Zhang and Q.-L. Han, "A less conservative method for designing H_∞ filters for linear time-delay systems," *International Journal of Robust and Nonlinear Control*, vol. 19, no. 12, pp. 1376–1396, 2009.
- [16] L. L. Du, Z. Gu, and J. L. Liu, "Network-based reliable H_∞ filter designing for the systems with sensor failures," in *Proceedings of the International Conference on Modelling, Identification and Control (ICMIC '10)*, pp. 797–800, Okayama, Japan, July 2010.

Research Article

Steady Modeling for an Ammonia Synthesis Reactor Based on a Novel CDEAS-LS-SVM Model

Zhuoqian Liu,¹ Lingbo Zhang,¹ Wei Xu,² and Xingsheng Gu¹

¹ Key Laboratory of Advanced Control and Optimization for Chemical Process, Ministry of Education, Shanghai 200237, China

² Shanghai Electric Group Co. Ltd., Central Academe, Shanghai 200070, China

Correspondence should be addressed to Xingsheng Gu; xsgu@ecust.edu.cn

Received 6 December 2013; Accepted 5 February 2014; Published 18 March 2014

Academic Editor: Huaicheng Yan

Copyright © 2014 Zhuoqian Liu et al. This is an open access article distributed under the Creative Commons Attribution License, which permits unrestricted use, distribution, and reproduction in any medium, provided the original work is properly cited.

A steady-state mathematical model is built in order to represent plant behavior under stationary operating conditions. A novel modeling using LS-SVR based on Cultural Differential Evolution with Ant Search is proposed. LS-SVM is adopted to establish the model of the net value of ammonia. The modeling method has fast convergence speed and good global adaptability for identification of the ammonia synthesis process. The LS-SVR model was established using the above-mentioned method. Simulation results verify the validity of the method.

1. Introduction

Ammonia is one of the important chemicals that has innumerable uses in a wide range of areas, that is, explosive materials, pharmaceuticals, polymers, acids and coolers, particularly in synthetic fertilizers. It is produced worldwide on a large scale with capacities extending to about 159 million tons at 2010. Generally, the average energy consumption of ammonia production per ton is 1900 KG of standard coal in China, which is much higher than the advanced standard of 1570 KG around the world. At the same time, the haze and particulate matter 2.5 has been serious exceeded in big cities in China at recent years, and one of the important reasons is the emission of coal chemical factories. Thus, an economic potential exists in energy consumption of the ammonia synthesis as prices of energy rise and reduce the ammonia synthesis pollution to protect the environment. Ammonia synthesis process has the characteristics of nonlinearity, strong coupling, large time-delay and great inertia load, and so forth. Steady-state operation-optimization can be a reliable technique for output improvement and energy reduction without changing any devices.

The optimization of ammonia synthesis process highly relies on the accurate system model. To establish an appropriate mathematical model of ammonia synthesis process is a

principal problem of operation optimization. It has received considerable attention since last century. Heterogeneous simulation models imitating different types of ammonia synthesis reactors have been developed for design, optimization and control [1]. Elnashaie et al. [2] studied the optimization of an ammonia synthesis reactor which has three adiabatic beds. The optimal temperature profile was obtained using the orthogonal collocation method in the paper. Pedemera et al. [3] studied the steady state analysis and optimization of a radial-flow ammonia synthesis reactor.

The above study indicated that both the productive capacity and the stability of the ammonia reactor are influenced by the cold quench and the feed temperature significantly. Babu and Angira [4] described the simulation and optimization design of an auto-thermal ammonia synthesis reactor using Quasi-Newton and NAG subroutine method. The optimal temperature trajectory along the reactor and optimal flows throughput 3.3% additional ammonia production. Sadeghi and Kavianiboroujeni [1] evaluated the process behavior of an industrial ammonia synthesis reactor by one-dimensional model and two-dimensional model; genetic algorithm (GA) was applied to optimize the reactor performance in varying its quench flows. From the above literatures we can find that most models are built based on thermodynamic, kinetic and mass equilibria calculations. It is very difficult to simulate the

specific internal mechanism because a lot of parameters are unknown in real industrial process.

In order to achieve the required accuracy of the model, some researches focus on the novel modeling methods combining some heuristic methods such as ANN (Artificial Neural Network), LS-SVM (Least Squares Support Vector Machine) with Evolutionary Algorithm, for example, genetic algorithm, ant colony optimization (ACO), particle swarm optimization (PSO), differential evolution (DE), and so forth. DE is one of the most popular algorithms for this problem and has been applied in many fields. Sacco and Henderson [5] introduced a variant of the differential evolution algorithm with a new mutation operator based on a topographical heuristic, and used it to solve the nuclear reactor core design optimization problem. Rout et al. [6] proposed a simple but promising hybrid prediction model by suitably combining an adaptive autoregressive moving average architecture and differential evolution for forecasting of exchange rates. Ozcan et al. [7] carried out the cost optimization of an air cooling system by using Lagrange multipliers method, differential evolution algorithm and particle swarm optimization for various temperatures and mass flow rates. The results showed that the method gives high accuracy results within a short time interval. Zhang et al. [8] proposed a hybrid differential evolution algorithm for the job shop scheduling problem with random processing times under the objective of minimizing the expected total tardiness. Arya and Choubé [9] described a methodology for allocating repair time and failure rates to segments of a meshed distribution system using differential evolution technique. Xu et al. [10] proposed a model of ammonia conversion rate by LS-SVM and a hybrid algorithm of PSO and DE is described to identify the hyper-parameters of LS-SVM.

To describe the relationship between net value of ammonia in ammonia synthesis reactor and the key operational parameters, least squares support vector machine is employed to build the structure of the relationship model, in which a novel algorithm called CDEAS is proposed to identify the parameters. The experiment results showed that the proposed CDEAS-LS-SVM optimizing model is very effective of being used to obtain the optimal operational parameters of ammonia synthesis converter.

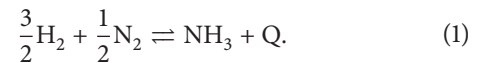
The remaining of the paper is organized as follows. Section 2 describes the ammonia synthesis production process. Section 3 proposes a novel Cultural Differential Evolution with Ant Colony Search (CDEAS) algorithm. Section 4 constructs a model using LS-SVM based on the proposed CDEAS algorithm. Section 5 presents the experiments and computational results and discussion. Finally, Section 6 summarizes the above results and presents several problems which remain to be solved.

2. Ammonia Synthesis Production Process

A normal ammonia production flow chart includes the synthesis gas production, purification, gas compression, and ammonia synthesis. Ammonia synthesis loop is one of the most critical units in the entire process. The system has

been realized by LuHua Inc., a medium fertilizers factory of YanKuang Group, China.

Figure 1 represents a flow sheet for the ammonia synthesis process. The ammonia synthesis reactor is a one-axial flow and two-radial flow three-bed quench-type unit [11]. Hydrogen-nitrogen mixture is reacted in the catalyst bed under high temperature and pressure. The temperature in the reactor is sustained by the heat of reaction because the reaction is exothermic [1]. The reaction of ammonia synthesis process contains



The reaction is limited by the unfavorable position of the chemical equilibrium and by the low activity of the promoted iron catalysts with high pressure and temperature [12]. In general, no more than 20% of the synthesis gas is converted into ammonia per pass even at high pressure of 30 MPa [12]. As the ammonia reaction is exothermic, it is necessary for removing the heat generated in the catalyst bed by the progress of the reaction to obtain a reasonable overall conversion rate as same as to protect the life of the catalyst [13]. The mixture gas from the condenser is divided into two parts Q1 and Q2 to go to the converter. The first cold shot Q1 is recirculated to the annular space between the outer shell reactor and catalyst bed from the top to the bottom to refrigerate the shell and remove the heat released by the reaction. Then the gas Q1 from the bottom of reactor goes through the preheater and is heated by the counter-current flowing reacted gas from waste heat boiler. Q1 gas is divided into 4 cold quench gas (q1, q2, q3, and q4) and Q2 gas for mixing with the gas between consecutive catalyst beds to quench the hot spots before entry to the subsequent catalyst beds. The hot spot temperatures (TIRA705, TIRA712N, and TIRA714) represent the highest reaction temperatures at each stage of the catalyst bed.

Figure 2 represents the ammonia synthesis unit. The reacted gas including N_2 , H_2 , NH_3 , and inert gas after reactor passes through the waste heat boiler. Then it goes through the preheater and the water cooler to be further cooled. Part of the ammonia is condensed and separated by ammonia separator I. Inert gas from the ammonia synthesis loop are ejected by purge gas from separator to prevent accumulation of inert gas in the system. The fresh feed gas is produced by the Texaco coal gasification air separation section, a process that converts the Coal Water Slurry into synthesis gas for ammonia. The fresh gas consists of hydrogen and nitrogen in stoichiometric proportions of 3:1 approximately and mixes with small amounts of argon and methane. The fresh gas which passes compressor is compounded with the recycle gas which comes from the circulator, and then the mixture goes through oil separator and condenser. Mixture gas is further cooled by liquid ammonia and goes through ammonia separator II to separate the partial liquid ammonia, and then it goes out with very few ammonia. The liquid ammonia from ammonia separator I and separator II flows to the liquid ammonia jar. Mixture is heated in ammonia condenser to about 25°C and flows to the reactor and the whole cycle starts again.

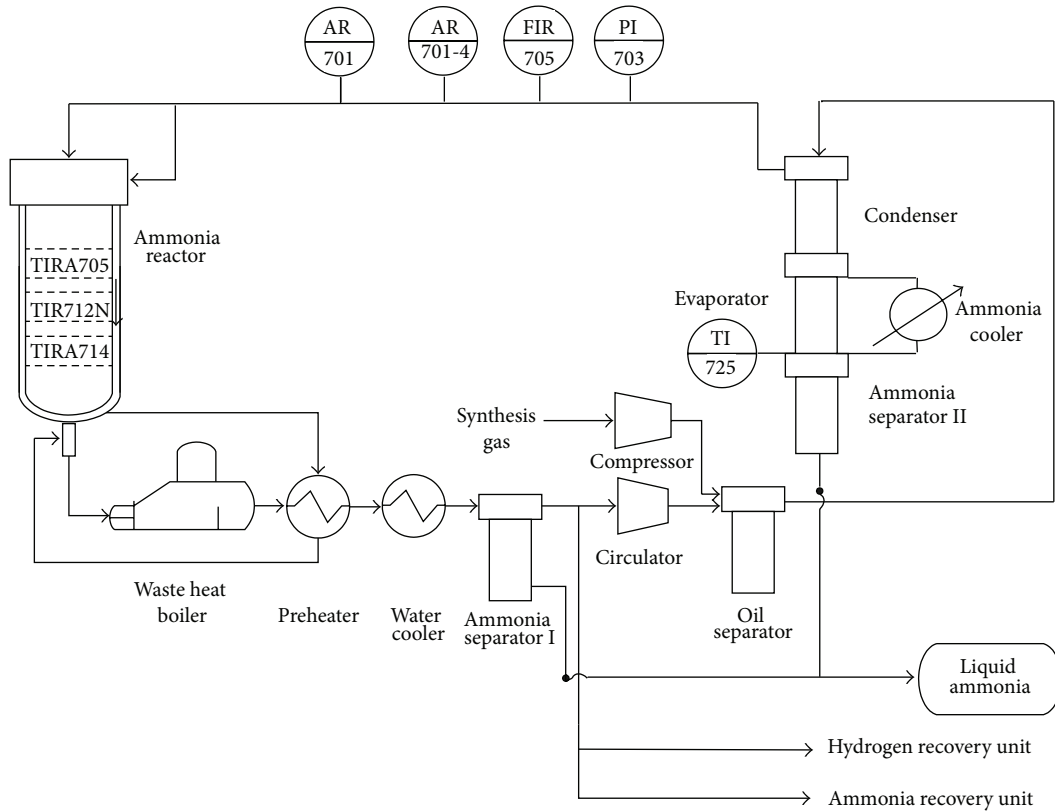


FIGURE 1: Ammonia synthesis system.

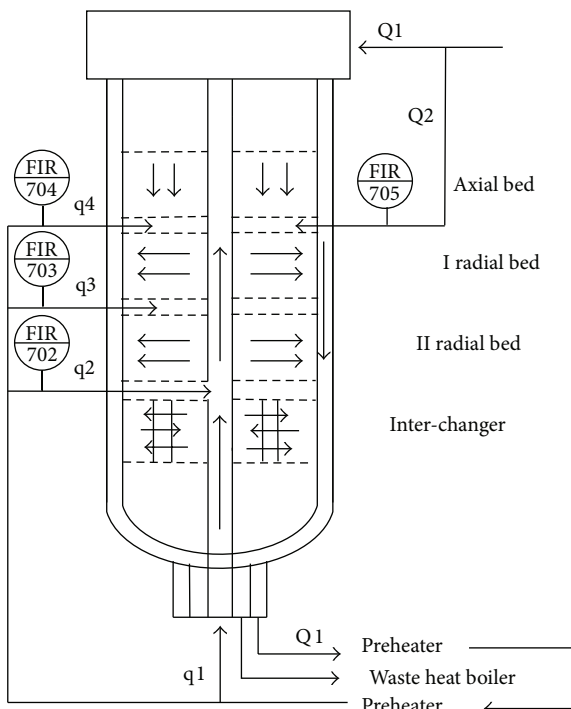


FIGURE 2: The ammonia synthesis unit.

3. Proposed Cultural Differential Evolution with Ant Search Algorithm

3.1. *Differential Evolution Algorithm.* Evolutionary Algorithms, which are inspired by the evolution of species, have been adopted to solve a wide range of optimization problems successfully in different fields. The primary advantage of Evolutionary Algorithms is that they just require the objective function values, while properties such as differentiability and continuity are not necessary [14].

Differential evolution, proposed by Storn and Price, is a fast and simple population based stochastic search technique [15]. DE employs mutation, crossover, and selection operations. It focuses on differential vectors of individuals with the characteristics of simple structure and rapid convergence. The detailed procedure of DE is presented below.

(1) *Initialization.* In a D -dimension space, NP parameter vectors so-called individuals cover the entire search space by uniformly randomizing the initial individuals within the search space constrained by the minimum and maximum parameter bounds X_{\min} and X_{\max} :

$$x_{i,d}^0 = x_{\min,d}^0 + \text{rand}(0, 1) (x_{\max,d}^0 - x_{\min,d}^0) \quad j = 1, 2, \dots, D. \quad (2)$$

(2) *Mutation*. DE employs the mutation operation to produce a mutant vector u_{id}^t called target vector corresponding to each individual x_{id}^t after initialization. In iteration t , the mutant vector u_{id}^t of individual x_{id}^t can be generated according to certain mutation strategies. Equations (3)–(7) indicate the most frequent mutation strategies version, respectively:

$$\text{DE/rand/1} \quad u_{id}^t = X_{r1^i,d}^t + F \left(X_{r2^i,d}^t - X_{r3^i,d}^t \right), \quad (3)$$

$$\text{DE/rand/2} \quad u_{id}^t = X_{r1^i,d}^t + F \left(X_{r2^i,d}^t - X_{r3^i,d}^t \right) \\ + F \left(X_{r4^i,d}^t - X_{r5^i,d}^t \right), \quad (4)$$

$$\text{DE/best/1} \quad u_{id}^t = X_{\text{best},d}^t + F \left(X_{r1^i,d}^t - X_{r2^i,d}^t \right), \quad (5)$$

$$\text{DE/best/2} \quad u_{id}^t = X_{\text{best},d}^t + F \left(X_{r1^i,d}^t - X_{r2^i,d}^t \right) \\ + F \left(X_{r3^i,d}^t - X_{r4^i,d}^t \right), \quad (6)$$

$$\text{DE/rand-to-best/1} \quad u_{id}^t = X_{i,d}^t + F \left(X_{\text{best},d}^t - X_{i,d}^t \right) \\ + F \left(X_{r1^i,d}^t - X_{r2^i,d}^t \right), \quad (7)$$

where $r1^i, r2^i, r3^i, r4^i$, and $r5^i$ are mutually exclusive integers randomly generated within the range $[1, \text{NP}]$ which should not be i . F is the mutation factor for scaling the difference vector, usually bounded in $[0, 2]$. X_{best}^t is the best individual with the best fitness value at generation t in the population.

(3) *Crossover*. The individual X_i^t and mutant vector u_i^t are hybridized to compose the trial vector y_i^t after mutation operation. The binomial crossover is adopted by the DE in the paper, which is defined as

$$y_{id}^t = \begin{cases} u_{id}^t & \text{if rand} \leq C_R \text{ or } i = i_{\text{rand}} \\ X_{i,d}^t & \text{otherwise,} \end{cases} \quad (8)$$

where rand is a random number between in 0 and 1 distributed uniformly. The crossover factor C_R is a probability rate within the range 0 and 1, which influences the tradeoff between the ability of exploration and exploitation. i_{rand} is an integer chosen randomly in $[1, D]$. To ensure that the trial vector (y_i^t) differs from its corresponding individual (X_i^t) by at least one dimension, $i = i_{\text{rand}}$ is recommended.

(4) *Selection*. When a newly generated trial vector exceeds its corresponding upper and lower bounds, it is reinitialized within the presetting range uniformly and randomly. Then the trial individual y_i^t is compared with the individual X_i^t , and the one with better fitness is selected as the new individual in the next iteration:

$$X_{id}^{t+1} = \begin{cases} y_{id}^t & \text{if } f(y_{id}^t) \leq f(X_{i,d}^t) \\ X_{i,d}^t & \text{otherwise.} \end{cases} \quad (9)$$

(5) *Termination*. All above three evolutionary operations continue until termination criterion is achieved, such as the evolution reaching the maximum/minimum of function evaluations.

As an effective and powerful random optimization method, DE has been successfully used to solve real world problems in diverse fields both unconstrained and constrained optimization problems.

3.2. *Cultural Differential Evolution with Ant Search*. As we mentioned in Section 3.1, mutation factor F , mutation strategies, and crossover factor C_R have great influence on the balance of DE's exploration and exploitation ability. F decides the amplification of differential variation; C_R is used to control the possibility of the crossover operation; mutation strategies have great influence on the results of mutation operation. In some literatures F , C_R , and mutation strategies are defined in advance or varied by some specific regulations. But the factors F , C_R , and strategies are very difficult to choose since the prior knowledge is absent. Therefore, Ant Colony Search is used to search the suitable combination of F , C_R , and mutation strategies adaptively to accelerate the global search. Some researchers have found an inevitable relationship between the parameters (F , C_R , and mutation strategies) and the optimization results of DE [16–18]. However, the approaches above are not applying the most suitable F , C_R , and mutation strategies simultaneously.

In this paper, based on the theory of Cultural Algorithm and Ant Colony Optimization (ACO), an improved Cultural Differential Algorithm incorporation with Ant Colony Search is presented. In order to accelerate searching out the global solution, the Ant Colony Search is used to search the optimal combination of F and C_R in subpopulation 1 as well as mutation strategy in subpopulation 2. The framework of Cultural Differential Evolution with Ant Search is briefly described in Figure 3.

3.2.1. *Population Space*. The population space is divided into two parts: subpopulation 1 and subpopulation 2. The two subpopulations contain equal number of the individuals.

In subpopulation 1, the individual is set as ant at each generation. F and C_R are defined to be the values between $[0, 1]$, $F \in \{0.1 \times i\}$, $i = 1, 2, \dots, 10$ and $C_R \in \{0.1 \times i\}$, $i = 1, 2, \dots, 10$. Each of the ants chooses a combination of F and C_R according to the information which is calculated by the fitness function of ants. During search process, the information gathered by the ants is preserved in the pheromone trails τ . By exchanging information according to pheromone, the ants cooperate with each other to choose appropriate combination of F and C_R . Then ant colony renews the pheromone trails of all ants.

Then, the pheromone trail τ_{mn} is updated in the following equation:

$$\tau_{mn}(t+1) = (1 - \rho_1) \tau_{mn}(t) + \sum_{i=1}^{\text{subpopulation1}} \Delta \tau_{mn}^i(t), \quad (10)$$

where $0 \leq \rho_1 < 1$ means the pheromone trail evaporation rate, $n = 1, 2, \dots, 10$, $m = 1, 2$; 1st parameter represents F and

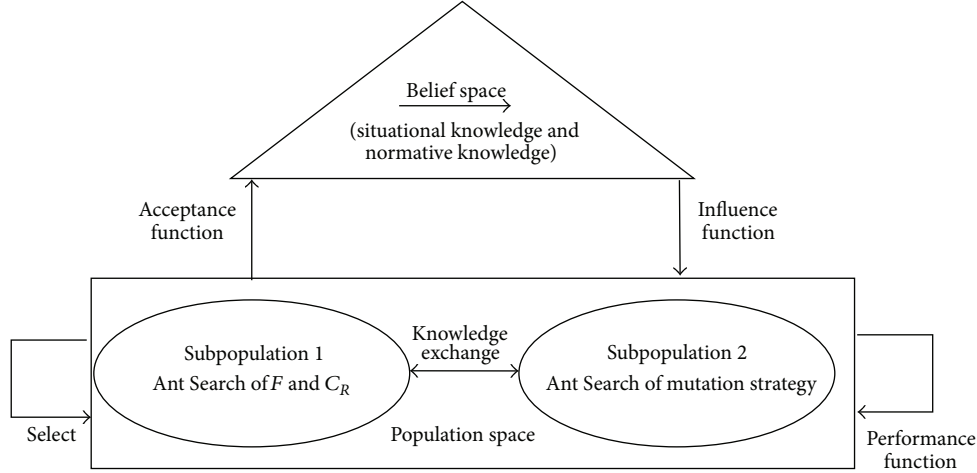


FIGURE 3: The framework of CDEAS algorithm.

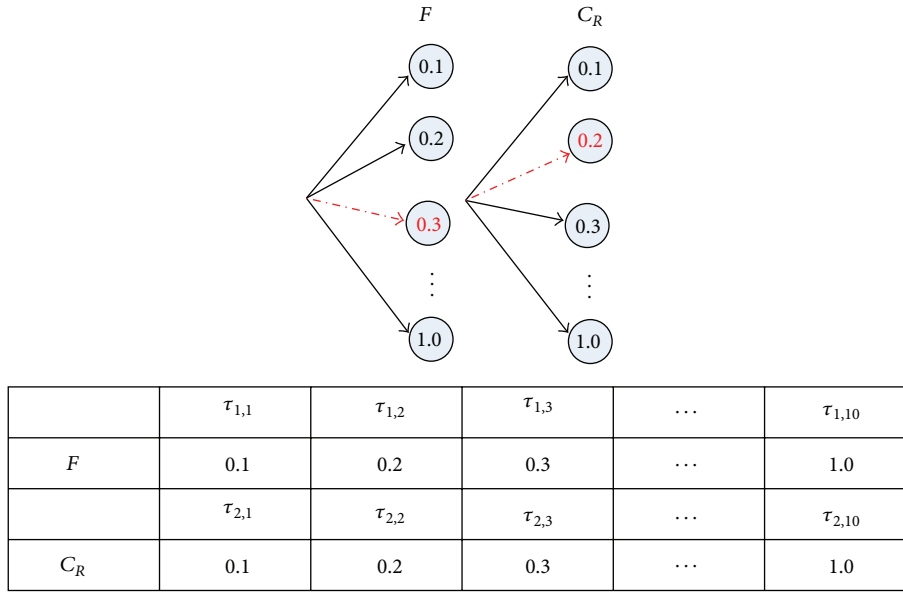


FIGURE 4: Relationship between pheromone and ant paths of F, C_R .

2nd parameter represents C_R ; $\Delta\tau_{mn}^i(t)$ is the quantity of the pheromone trail of ant i ,

$$\Delta\tau_{mn}^i(t) = \begin{cases} 1 & \text{if } i \in X_{mn} \text{ and fitness } (y_i^t) < \text{fitness } (x_{best}^t), \\ 0.5 & \text{if } i \in X_{mn} \text{ and fitness } (x_{best}^t) < \text{fitness } (y_i^t) \\ & \text{and fitness } (y_i^t) < \text{fitness } (x_i^t), \\ 0 & \text{otherwise,} \end{cases} \quad (11)$$

where X_{mn} is the ant group that chooses n th value as the selection of m th parameter; x_{best}^t denotes the best individual of ant colony till t th generation.

In order to prevent the ants from being limited to one ant path and improve the possibility of choosing other paths

considerably, the probability of each ant chooses n th value of m th parameter (F and C_R) in Figure 4 is set by

$$p_{mn}(t) = \begin{cases} \frac{\tau_{mn}^i(t)}{\sum_n \tau_{mn}(t)} & \text{if } \text{rand}_1 < P_s \\ \text{rand}_2 & \text{otherwise.} \end{cases} \quad (12)$$

Figure 4 illustrates the relationship between pheromone matrix and ant path of F and C_R , where P_s is a constant which is defined as selection parameter and rand_1 and rand_2 are two random values which are uniformly distributed in $[0, 1]$. Selection of the values of F and C_R depends on the performance of all the individuals, the individual is chosen by the most appropriate combination of F and C_R in each generation.

In subpopulation 2, the individual is set as ant at each generation. Mutation strategies which are listed at (3)–(7) are

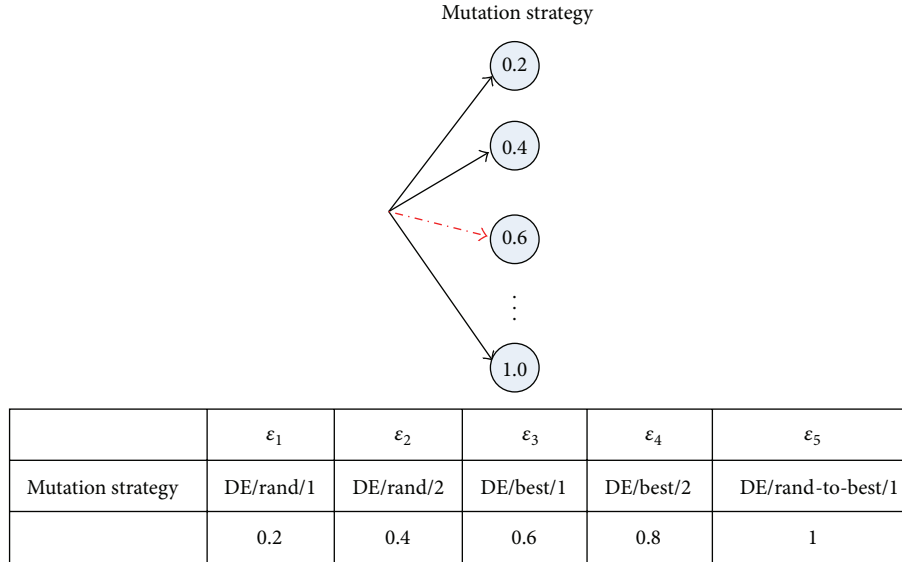


FIGURE 5: Relationship between and ant paths of mutation strategy.

defined to be of the values $\{0.2, 0.4, 0.6, 0.8, 1.0\}$, respectively. For example, 0.2 means the first mutation strategy equation (3) is selected. Each of the ants chooses a mutation strategy according to the information which is calculated by the fitness function of ants. During search process, the information gathered by the ants is preserved in the pheromone trails ε . By exchanging information according to pheromone, the ants cooperate with each other to choose appropriate mutation strategy. Then ant colony renews the pheromone trails of all ants.

Then, the pheromone trail ε is updated in the following equation:

$$\varepsilon_k(t+1) = (1 - \rho_2) \varepsilon_k(t) + \sum_{i=1}^{\text{subpopulation2}} \Delta \varepsilon_k^i(t), \quad (13)$$

where $0 \leq \rho_2 < 1$ means the pheromone trail evaporation rate and $\Delta \varepsilon_k^i(t)$ is the quantity of the pheromone trail of ant i ,

$$\varepsilon_k^i(t) = \begin{cases} 1 & \text{if } i \in X_k \text{ and fitness } (y_i^t) < \text{fitness } (x_{\text{best}}^t), \\ 0.5 & \text{if } i \in X_k \text{ and fitness } (x_{\text{best}}^t) < \text{fitness } (y_i^t) \\ & \text{and fitness } (y_i^t) < \text{fitness } (x_i^t), \\ 0 & \text{otherwise,} \end{cases} \quad (14)$$

where X_k is the ant group that chooses k th value as the selection of parameter; x_{best}^t denotes the best individual of ant colony till t th generation.

In order to prevent the ants from being limited to one ant path and improve the possibility of choosing other paths

considerably, the probability of each ant choosing n th value of m th parameter (mutation strategies) is set by

$$p_k(t) = \begin{cases} \frac{\varepsilon_k^i(t)}{\sum_n \varepsilon_k(t)} & \text{if } \text{rand}_3 < P'_s \\ \text{rand}_4 & \text{otherwise,} \end{cases} \quad (15)$$

where P'_s is a constant which is defined as selection parameter and rand_3 and rand_4 are two random values which are uniformly distributed in $[0, 1]$. Selection of the values of mutation strategies depends on the pheromone of each path. According to the performance of all the individuals, the individual is chosen by the most appropriate combination of mutation strategies in each generation.

Figure 5 illustrates the relationship between pheromone matrix and ant path of mutation strategies.

3.2.2. Belief Space. In our approach, the belief space is divided into two knowledge sources, situational knowledge and normative knowledge.

Situational knowledge consists of the global best exemplar E which is found along the searching process and provides guidance for individuals of population space. The update of the situational knowledge is done if the best individual found in the current populations space is better than E .

The normative knowledge contains the intervals that decide the individuals of population space where to move. l_i and u_i are the lower and upper bounds of the search range in population space. L_i and U_i are the value of the fitness function associated with that bound. If the l_i and u_i are updated, the L_i and U_i must be updated too.

l_i and u_i are set by

$$\begin{aligned} l_i &= \begin{cases} x_{i,\min}, & \text{if } x_{i,\min} < l_i \text{ or } f(x_{i,\min}) < L_i \\ l_i & \text{otherwise,} \end{cases} \\ u_i &= \begin{cases} x_{i,\max}, & \text{if } x_{i,\max} > u_i \text{ or } f(x_{i,\max}) > U_i \\ u_i & \text{otherwise.} \end{cases} \end{aligned} \quad (16)$$

3.2.3. Acceptance Function. Acceptance function controls the amount of good individuals which impact on the update of belief space [19]. In this paper, 30% of the individuals in the belief space are replaced by the good ones in population space.

3.2.4. Influence Function. In the CDEAS, situational knowledge and normative knowledge are involved to influence each individual in the population space, and then population space is updated.

The individuals in population space are updated in the following equation:

$$\begin{aligned} x_{i,d}^{t+1} &= \begin{cases} x_{i,d}^t + |N(0.5, 0.3) * (X_{r2^i,d}^t - X_{r3^i,d}^t)| \times \text{rand}, & \text{if } x_{i,d}^t \leq E_j, x_{i,d}^t \geq u_i, \\ x_{i,d}^t - |N(0.5, 0.3) * (X_{r2^i,d}^t - X_{r3^i,d}^t)| \times \text{rand}, & \text{if } x_{i,d}^t > E_j, x_{i,d}^t < u_i, \\ X_{r1^i,d}^t + |N(0.5, 0.3) * (u_i - X_{r3^i,d}^t)| \times \text{rand}, & \text{if } x_{i,d}^t \leq E_j, x_{i,d}^t \geq l_i, \\ X_{r1^i,d}^t - |N(0.5, 0.3) * (l_i - X_{r3^i,d}^t)| \times \text{rand}, & \text{if } x_{i,d}^t > E_j, x_{i,d}^t < l_i, \end{cases} \\ x_{i,d}^{t+1} &= \begin{cases} X_{r1^i,d}^t + F * (u_i - X_{r1^i,d}^t) \times \text{rand}, & \text{if } x_{i,d} > l_i \\ X_{r1^i,d}^t - F * (X_{r1^i,d}^t - l_i) \times \text{rand}, & \text{if } x_{i,d} < u_i \\ X_{r1^i,d}^t + F * (u_i - l_i) \times \text{rand}, & \text{if } l_i < x_{i,d} < u_i, \end{cases} \end{aligned} \quad (17)$$

where F is a constant of 0.2.

3.2.5. Knowledge Exchange. After t steps, the F and C_R of subpopulation 2 are replaced by the suitable F and C_R calculated by subpopulation 1 and the mutation strategy of subpopulation 1 is displaced by the suitable mutation strategy calculated by subpopulation 2 simultaneously. So the F and C_R and mutation strategy are varying in the two subpopulations to enable the individuals to converge globally and fast.

3.2.6. Procedure of CDEAS. The procedure of CDEAS is proposed as follows.

Step 1. Initialize the population spaces and the belief spaces; the population space is divided into subpopulation 1 and subpopulation 2.

Step 2. Evaluate each individual's fitness.

Step 3. To find the proper F , C_R , and mutation strategy, the Ant Colony Search strategy is used in subpopulation 1 and subpopulation 2, respectively.

Step 4. According to acceptance function, choose good individuals from subpopulation 1 and subpopulation 2, and then update the normative knowledge and situational knowledge.

Step 5. Adopt the normative knowledge and situational knowledge to influence each individual in population space through the influence functions, and generate two corresponding subpopulations.

Step 6. Select individuals from subpopulation 1 and subpopulation 2, and update the belief spaces including the two knowledge sources for the next generation.

Step 7. If the algorithm reaches the given times, exchange the knowledge of F , C_R , and mutation strategy between subpopulation 1 and subpopulation 2; otherwise, go to Step 8.

Step 8. If the stop criteria are achieved, terminate the iteration; otherwise, go back to Step 2.

3.3. Simulation Results of CDEAS. The proposed CDEAS algorithm is compared with original DE algorithm. To get the average performance of the CDEAS algorithm 30 runs on each problem instance were performed and the solution quality was averaged. The parameters of CDEAS and original DE algorithm are set as follows: the maximum evolution generation is 2000; the size of the population is 50; for original DE algorithm $F = 0.3$ and $C_R = 0.5$; for CDEAS, the size of both two subpopulations is 25; the initial F and C_R are randomly selected in $(0, 1)$ and the initial mutation strategy is DE/rand/1; the interval information exchanges between the two subpopulations t is 50 generations; the thresholds $P_s = P'_s = 0.5$ and $\rho_1 = \rho_2 = 0.1$.

To illustrate the effectiveness and performance of CDEAS algorithm for optimization problems, a set of 18 representative benchmark functions which were listed in the appendix were employed to evaluate them in comparison with original DE. The test problems are heterogeneous, nonlinear, and numerical benchmark functions and the global optimum for $f_2, f_4, f_7, f_9, f_{11}, f_{13}$, and f_{15} is shifted. Functions $f_1 \sim f_7$ are unimodal and functions $f_8 \sim f_{18}$ are multimodal. The detailed principle of functions is presented in [11]. The comparisons results of CDEAS and original DE algorithm are shown in Table 4 of the appendix. The experimental results of original DE and CDEAS algorithm on each function are listed in Table 1. Mean, best, worst, std., success rate, time represent the mean minimum, best minimum, worst minimum, the standard deviation of minimum, the success rate, and the average computing time in 30 trials, respectively.

From simulation results of Table 1 we can obtain that CDEAS reached the global optimum of f_2 and f_7 in all trials, and the success rate reached 100% of functions $f_1, f_2, f_3, f_4, f_6, f_7$, and f_{18} . For most of the test functions, the success

TABLE 1: The comparison results of the CDEAS algorithm and original DE algorithm.

	Original DE	CDEAS
Sphere function f_1		
Best	1.1746×10^{-65}	5.0147×10^{-79}
Worst	1.0815×10^{-23}	9.3244×10^{-75}
Mean	3.6052×10^{-25}	1.6390×10^{-75}
Std.	1.9746×10^{-24}	2.2315×10^{-75}
Success rate (%)	100	100
Times (s)	1.8803	14.6017
Shifted sphere function f_2		
Best	0	0
Worst	8.0779×10^{-28}	0
Mean	3.3658×10^{-29}	0
Std.	1.5078×10^{-28}	0
Success rate (%)	100	100
Times (s)	2.1788	18.1117
Schwefel's Problem 1.2 f_3		
Best	2.4386×10^{-65}	3.0368×10^{-78}
Worst	2.4820×10^{-22}	9.2902×10^{-73}
Mean	8.2736×10^{-24}	7.2341×10^{-74}
Std.	4.5316×10^{-23}	2.0187×10^{-73}
Success rate (%)	100	100
Times (s)	3.1647	24.1178
Shifted Schwefel's Problem 1.2 f_4		
Best	0	0
Worst	5.6545×10^{-27}	3.4331×10^{-27}
Mean	2.0868×10^{-28}	1.8848×10^{-28}
Std.	1.0323×10^{-27}	7.9813×10^{-28}
Success rate (%)	100	100
Times (s)	3.3956	27.7058
Rosenbrock's function f_5		
Best	13.0060	5.2659
Worst	166.1159	139.1358
Mean	70.9399	39.4936
Std.	40.0052	31.2897
Success rate (%)	86.67	96.67
Times (s)	1.9594	16.7233
Schwefel's Problem 1.2 with noise in fitness f_6		
Best	3.1344×10^{-39}	3.98838×10^{-49}
Worst	3.61389×10^{-36}	1.6124×10^{-43}
Mean	5.7744×10^{-37}	7.4656×10^{-45}
Std.	9.5348×10^{-37}	2.9722×10^{-44}
Success rate (%)	100	100
Times (s)	3.2141	24.2426
Shifted Schwefel's Problem 1.2 with noise in fitness f_7		
Best	0	0
Worst	0	0
Mean	0	0

TABLE 1: Continued.

	Original DE	CDEAS
Std.	0	0
Success rate (%)	100	100
Times (s)	3.3374	28.5638
Ackley's function f_8		
Best	7.1054×10^{-15}	3.5527×10^{-15}
Worst	4.8999×10^{-7}	1.3404
Mean	1.6332×10^{-8}	0.1763
Std.	8.9457×10^{-8}	0.4068
Success rate (%)	100	83.33
Times (s)	2.4820	20.9353
Shifted Ackley's function f_9		
Best	7.1054×10^{-15}	3.5527×10^{-15}
Worst	0.9313	0.9313
Mean	0.0310	0.0620
Std.	0.1700	0.2362
Success rate (%)	96.67	93.33
Times (s)	2.7337	21.6841
Griewank's function f_{10}		
Best	0	0
Worst	0.0367	0.0270
Mean	0.0020	0.0054
Std.	0.0074	0.0076
Success rate (%)	90	56.67
Times (s)	2.535	20.7793
Shifted Griewank's function f_{11}		
Best	0	0
Worst	0.0319	0.0343
Mean	0.0056	0.0060
Std	0.0089	0.0088
Success rate (%)	80	76.67
Times (s)	2.7768	22.8541
Rastrigin's function f_{12}		
Best	8.1540	1.9899
Worst	35.5878	12.9344
Mean	20.3594	6.5003
Std.	6.3072	2.6612
Success rate (%)	3.33	90
Times (s)	2.7264	22.3237
Shifted Rastrigin's function f_{13}		
Best	5.9725	0.9949
Worst	36.9923	6.7657
Mean	19.4719	8.2581
Std.	8.9164	3.8680
Success rate (%)	16.67	76.67
Times (s)	2.9313	23.8838
Noncontiguous Rastrigin's function f_{14}		
Best	20.7617	3.9949
Worst	29.9112	11.9899
Mean	25.4556	8.1947

TABLE I: Continued.

	Original DE	CDEAS
Std.	2.9078	2.2473
Success rate (%)	0	86.67
Times (s)	3.1663	25.5374
Shifted noncontiguous Rastrigin's function f_{15}		
Best	0	0
Worst	16	6
Mean	6.7666	1.5333
Std.	3.4509	1.8519
Success rate (%)	40	96.67
Times (s)	3.3374	25.9430
Schwefel's function f_{16}		
Best	118.4387	236.8770
Worst	710.6303	1362.0521
Mean	357.61725	676.4166
Std.	144.41244	324.2317
Success rate (%)	90	40
Times (s)	2.5028	19.0009
Schwefel's Problem 2.21 f_{17}		
Best	0.1640	0.3254
Worst	4.5102	4.7086
Mean	1.1077	1.9849
Std.	0.8652	1.16418
Success rate (%)	53.33	23.33
Times (s)	2.3806	19.2505
Schwefel's Problem 2.22 f_{18}		
Best	1.2706×10^{-35}	8.5946×10^{-45}
Worst	1.6842×10^{-34}	1.8362×10^{-42}
Mean	6.1883×10^{-35}	2.6992×10^{-43}
Std.	3.4937×10^{-35}	4.6257×10^{-43}
Success rate (%)	100	100
Times (s)	2.6297	20.8573

rate of CDEAS is higher in comparison with original DE. Moreover, CDEAS gets very close to the global optimum in some other functions f_1 , f_3 , f_4 , f_6 , and f_{18} . It also presents that the mean minimum, best minimum, worst minimum, the standard deviation of minimum, and the success rate of CDEAS algorithm are clearly better than the original DE for functions f_1 , f_3 , f_4 , f_5 , f_6 , f_{12} , f_{13} , f_{14} , f_{15} , and f_{18} although the computing time of CDEAS is longer than that of original DE because of its complexity.

The convergence figures of CDEAS comparing with original DE for 18 instances are listed as Figure 6.

From Figure 6 one can observe that the convergence speed of CDEAS is faster than original DE for f_1 , f_2 , f_3 , f_4 , f_6 , f_7 , f_{11} , f_{12} , f_{13} , f_{14} , f_{15} , and f_{18} .

All these comparisons of CDEAS with original DE algorithm have shown that CDEAS is a competitive algorithm to solve all the unimodal function problems and most of the multimodal function optimization problems listed above. As shown in the descriptions and all the illustrations before, CDEAS is efficacious on those typical function optimizations.

4. Model of Net Value of Ammonia Using CDEAS-LS-SVM

4.1. Auxiliary Variables Selection of the Model. There are some process variables which have the greatest influence on the net value of ammonia, such as system pressure, recycle gas flow rate, feed composition (H/N ratio), ammonia and inert gas concentration in the gas of reactor inlet, hot spot temperatures, and so forth. The relations between the process variables are coupling and the operational variables interact with each other.

The inlet ammonia concentration is an important process variable which is beneficial to operation-optimization but the device of online catharometer is very expensive. According to the mechanism and soft sensor model, a IIO-BP model was built to get the more accurate value of the inlet ammonia concentration [20]

$$\Delta(\text{NH}_3) = A_{\text{NH}_3,\text{OUT}} - A_{\text{NH}_3,\text{IN}}. \quad (18)$$

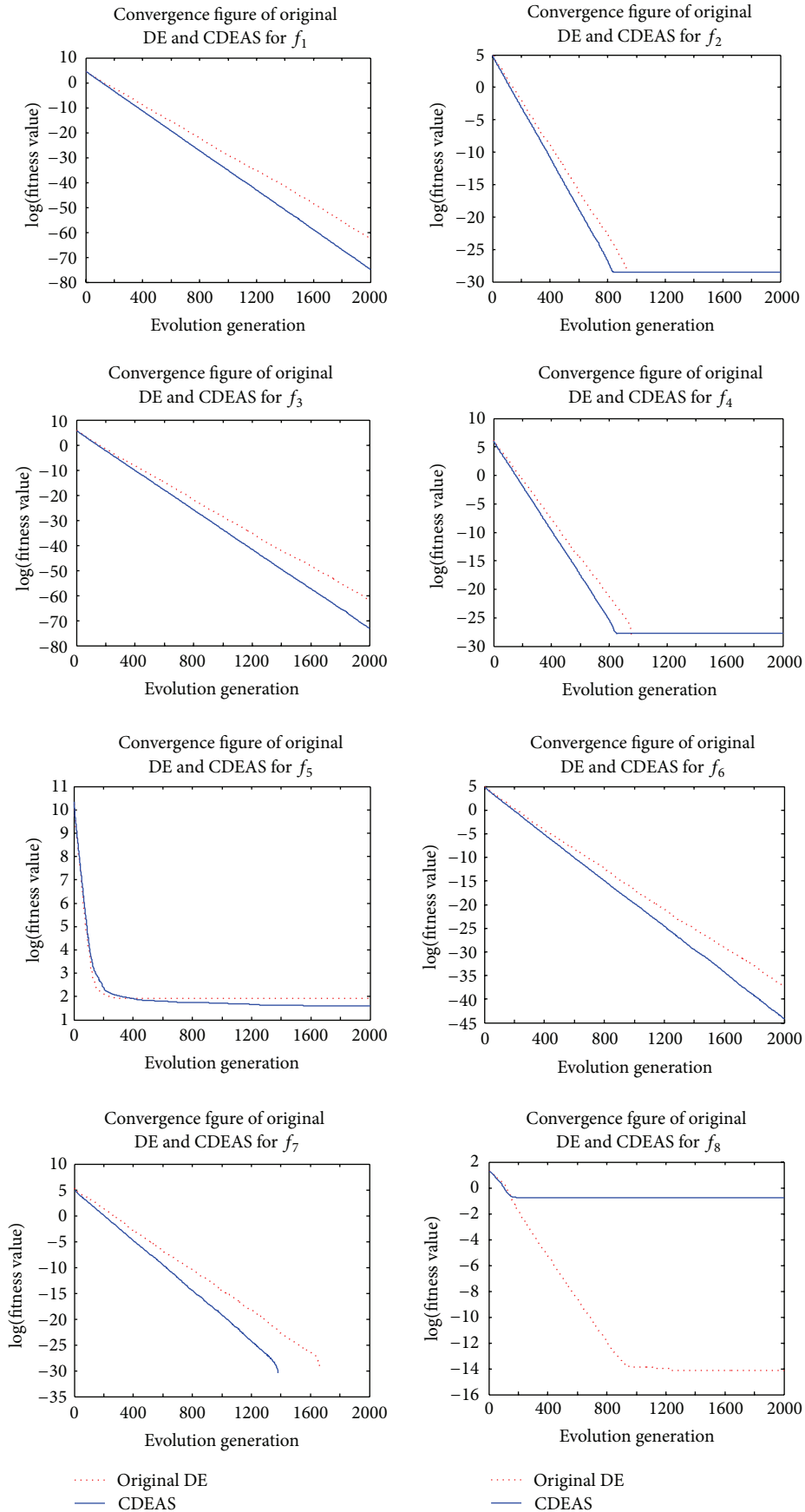


FIGURE 6: Continued.

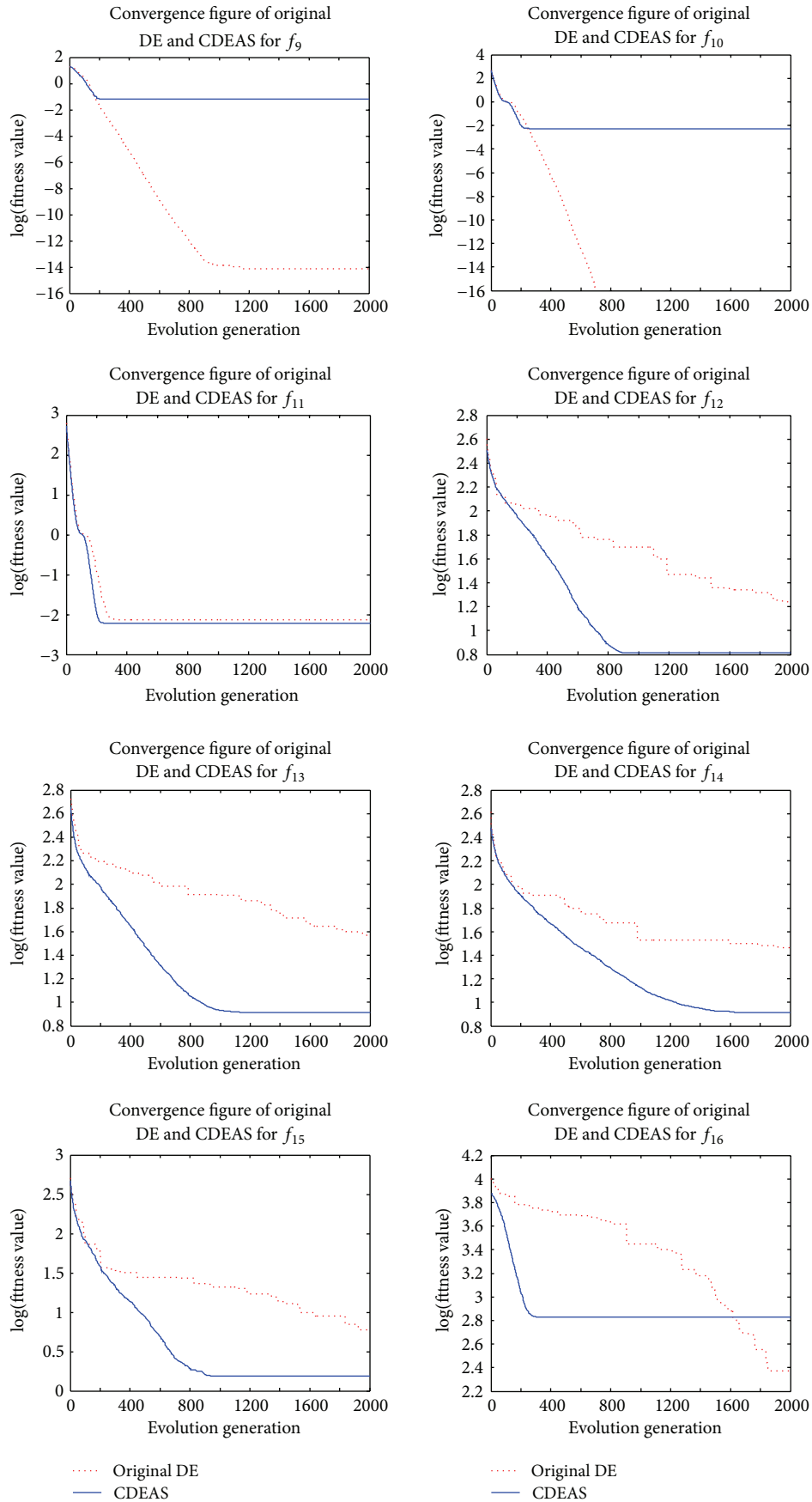


FIGURE 6: Continued.

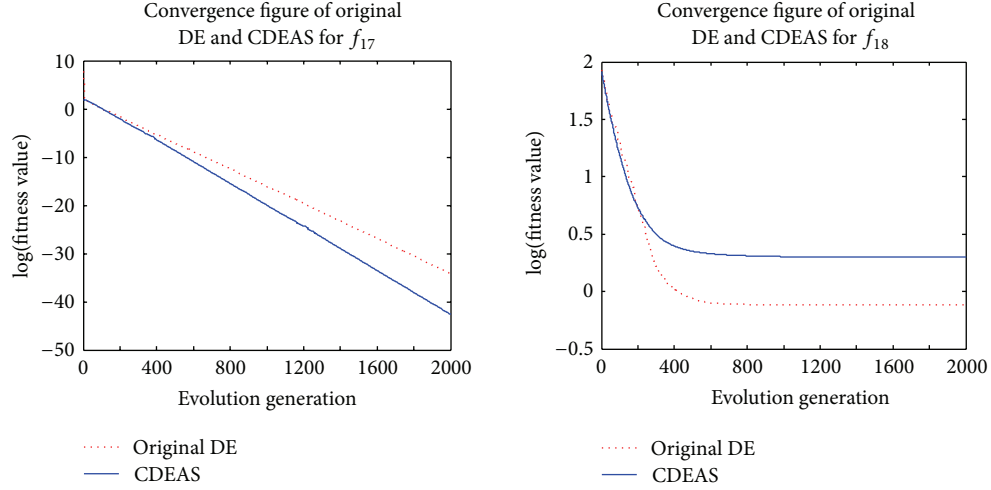

 FIGURE 6: Convergence figure of CDEAS comparing with original DE for $f_1 \sim f_{18}$.

TABLE 2: Auxiliary variables of model of net value of Ammonia.

List	Symbols	Name	Unit
1	$R_{H/N}$	H/N ratio	%
2	A_{CH_4}	Methane concentration in recycled synthesis gas at the reactor inlet	Mole ratio
3	A_{NH_3}	Ammonia concentration in recycled synthesis gas at the reactor inlet	Mole ratio
4	P_S	System pressure	Mpa
5	F_Q	Recycle gas flow rate	Nm^3/h
6	F_{Q1}	Quench gas flows of axial layer	Nm^3/h
7	F_{q2}	Cold quench gas flows of 1st radial layers	Nm^3/h
8	F_{q3}	Quench gas flows of 2nd radial layers	Nm^3/h
9	F_{q4}	Hot quench gas flows of 1st radial layers	Nm^3/h
10	T_A	Hot-spot temperatures of axial bed	$^{\circ}C$
11	T_{R1}	Hot-spot temperatures of radial bed I	$^{\circ}C$
12	T_{R2}	Hot-spot temperatures of radial bed II	$^{\circ}C$
13	T_{EO}	Outlet gas temperature of evaporator	$^{\circ}C$

From the analysis discussed above, some important variables have significant effects on the net value of ammonia. By discussion with experienced engineers and taking into consideration a priori knowledge about the process, the system pressure, recycle gas flow rate, the H/N ratio, hot-spot temperatures in the catalyst bed, and ammonia and methane concentration in the recycle gas are identified as the key auxiliary variables to model net value of ammonia which is listed in Table 2.

4.2. Modeling the Net Value of Ammonia Using CDEAS-LS-SVM. LS-SVM is an alternate formulation of SVM, which is proposed by Suykens. The e-insensitive loss function is replaced by a squared loss function, which constructs the Lagrange function by solving the problem linear Karush-Kuhn-Tucker (KKT)

$$\begin{bmatrix} 0 & I_n^T \\ I_n & K + \gamma^{-1}I \end{bmatrix} \begin{bmatrix} b_0 \\ b \end{bmatrix} = \begin{bmatrix} 0 \\ \gamma \end{bmatrix}, \quad (19)$$

where I_n is a $[n \times 1]$ vector of ones, T is the transpose of a matrix or vector, γ is a weight vector, b_0 means the model offset, and b is regression vector.

K is Mercer kernel matrix, which is defined as

$$K = \begin{pmatrix} k_{1,1} & \cdots & k_{1,n} \\ \vdots & \ddots & \vdots \\ k_{n,1} & \cdots & k_{n,n} \end{pmatrix}, \quad (20)$$

where $k_{i,j}$ is defined by kernel function.

There are several kinds of kernel functions, such as hyperbolic tangent, polynomial, and Gaussian radial basis function (RBF) which are commonly used. Literatures have proved that RBF kernel function has strong generalization, so in this study RBF kernel was used:

$$k_{i,j} = e^{-|x_i - x_j|^2 / 2\sigma^2}, \quad (21)$$

where x_i and x_j indicated different training samples, σ is the kernel width parameter.

TABLE 3: The comparisons of training error and testing error of LS-SVM.

Method	Type of error	RE*	MAE*	MSE*
BP-NN	Training error	9.4422×10^{-04}	1.0544×10^{-04}	1.3970×10^{-04}
	Testing error	0.008085	8.9666×10^{-04}	0.001188
LS-SVM	Training error	0.002231	2.4785×10^{-04}	4.1672×10^{-04}
	Testing error	0.005328	5.9038×10^{-04}	7.8169×10^{-04}
DE-LS-SVM	Training error	0.002739	3.04286×10^{-04}	4.08512×10^{-04}
	Testing error	0.005252	5.8241×10^{-04}	7.7032×10^{-04}
CDEAS-LS-SVM	Training error	0.002830	3.1415×10^{-04}	3.3131×10^{-04}
	Testing error	0.004661	5.1752×10^{-04}	6.8952×10^{-04}

*RE: relative error; MAE: mean absolute error; MSE: mean square error.

As we can see from (19)~(21), only two parameters (γ, σ) are needed for LS-SVM. It makes LS-SVM problem computationally easier than SVR problem.

Grid search is a commonly used method to select the parameters of LS-SVM, but it is time-consuming and inefficient. CDEAS algorithm has strong search capabilities, and the algorithm is simple and easy to implement. Therefore, this paper proposes the CDEAS algorithm to calculate the best parameters (γ, σ) of LS-SVM.

5. Results and Discussion

Operational parameters such as A_{H_2} , A_{CH_4} , and P_S were collected and acquired from plant DCS from the year 2011-2012. In addition, data on the inlet ammonia concentration of recycle gas A_{NH_3} were simulated by mechanism and soft sensor model [20].

The extreme values are eliminated from the data using the 3σ criterion. After the smoothing and normalization, each data group is divided into 2 parts: 223 groups of training samples which are used to train model while 90 groups of testing samples which are valuing the generalization of the model for identifying the parameters of the LS-SVM, the kernel width parameter, and the weight vector.

BP-NN, LS-SVM, and DE-LS-SVM are also used to model the net value of ammonia, respectively. BP-NN is a 13-15-1 three-layer network with back-propagation algorithm. LS-SVM gains the (γ, σ) with grid-search and cross-validation. The parameter settings of CDEAS-LS-SVM are the same as those in the benchmark tests. Each model is run 30 times and the best value is shown in Table 3. Descriptive statistics of training results and testing results of model include the relative error, absolute error, and mean square error. The performance of the four models is compared as shown in Table 3. The training and testing results of four models are illustrated in Figure 7.

Despite the fact that the training error using BP-NN is smaller than that using CDEAS-LS-SVM, which is because BP-NN is overfitting to the training data, the mean square error (MSE) on training data using CDEAS-LS-SVM is reduced by 25.6% and 23.2% compared with LS-SVM and DE-LS-SVM, respectively. In comparison with the other models (BP-NN, LS-SVM, and DE-LS-SVM), testing error using CDEAS-LS-SVM model is reduced by 14.1% and 11.2%,

respectively. The results indicate that the proposed CDEAS-LS-SVM model has a good tracking precision performance and guides production better.

6. Conclusion

In this paper, an optimizing model which describes the relationship between net value of ammonia and key operational parameters in ammonia synthesis has been proposed. Some representative benchmark functions were employed to evaluate the performance of a novel algorithm CDEAS. The obtained results show that CDEAS algorithm is efficacious for solving most of the optimization problems comparisons with original DE. Least squares support vector machine is used to build the model while CDEAS algorithm is employed to identify the parameters of LS-SVM. The simulation results indicated that CDEAS-LS-SVM is superior to other models (BP-NN, LS-SVM, and DE-LS-SVM) and meets the requirements of ammonia synthesis process. The CDEAS-LS-SVM optimizing model makes it a promising candidate for obtaining the optimal operational parameters of ammonia synthesis process and meets the maximum benefit of ammonia synthesis production.

Appendix

(1) Sphere function

$$f_1(x) = \sum_{i=1}^D x_i^2, \quad (A.1)$$

$o = [0, 0, \dots, 0]$: the global optimum.

(2) Shifted sphere function

$$f_2(x) = \sum_{i=1}^D z_i^2, \quad (A.2)$$

$$z = x - \theta,$$

$\theta = [\theta_1, \theta_2, \dots, \theta_D]$: the shifted global optimum.

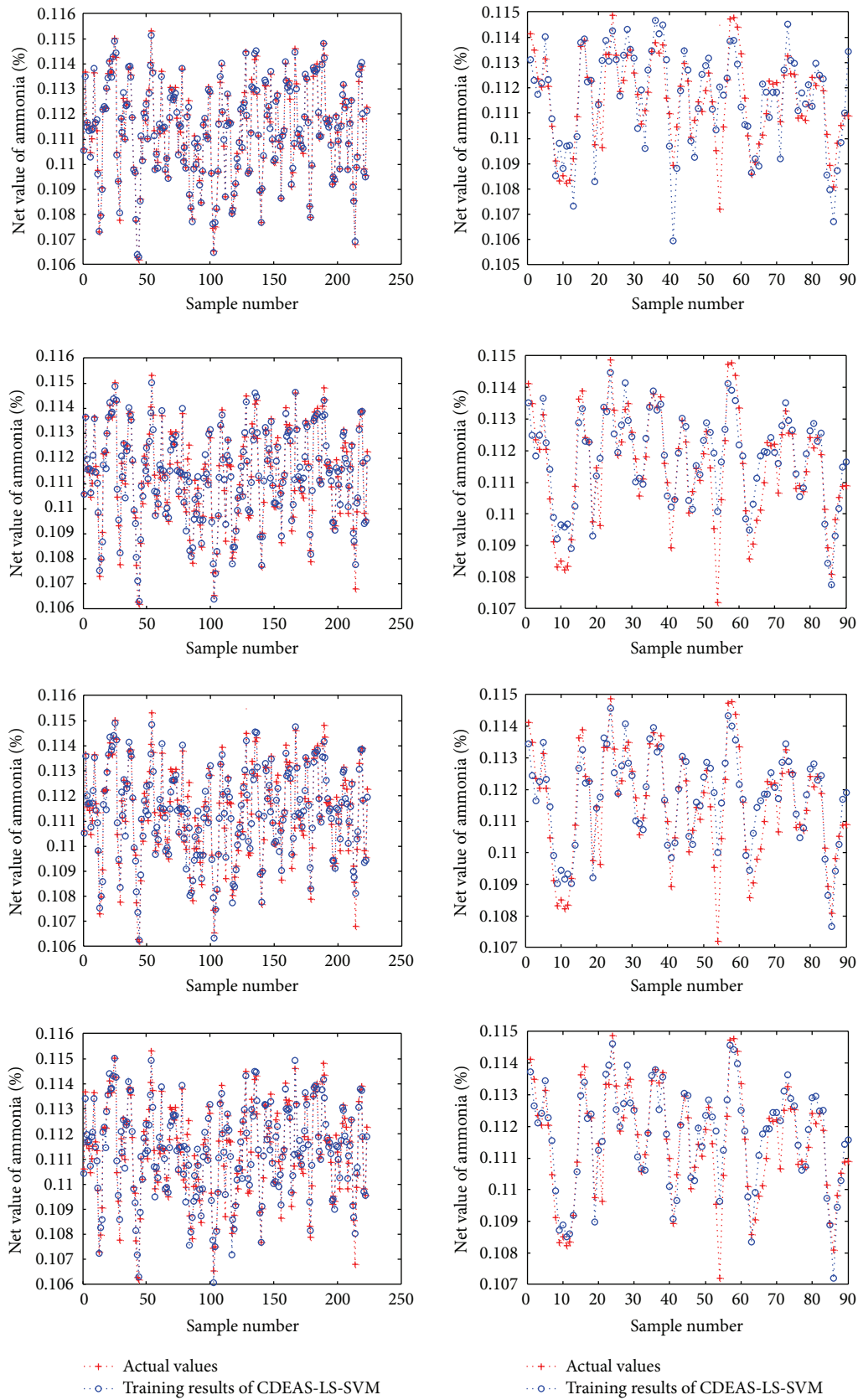


FIGURE 7: The analyzed results, training results, and testing results of BP-NN, LS-SVM, DE-LS-SVM, and CDEAS-LS-SVM.

TABLE 4: Global optimum, search ranges, and initialization ranges of the test functions.

f	Dimension	Global optimum \bar{x}	$f(\bar{x})$	Search range	Target
f_1		0	0	$[-100, 100]^D$	10^{-5}
f_2		θ	0	$[-100, 100]^D$	10^{-5}
f_3		0	0	$[-100, 100]^D$	10^{-5}
f_4		θ	0	$[-100, 100]^D$	10^{-5}
f_5		1	1	$[-100, 100]^D$	100
f_6		0	0	$[-32, 32]^D$	10^{-5}
f_7		θ	0	$[-32, 32]^D$	10^{-5}
f_8		0	0	$[-32, 32]^D$	10^{-5}
f_9	30	θ	0	$[-32, 32]^D$	0.1
f_{10}		0	0	$[0, 600]^D$	0.001
f_{11}		θ	0	$[-600, 600]^D$	0.01
f_{12}		0	0	$[-5, 5]^D$	10
f_{13}		θ	0	$[-5, 5]^D$	10
f_{14}		0	0	$[-5, 5]^D$	10
f_{15}		θ	0	$[-5, 5]^D$	5
f_{16}		418.9829	0	$[-500, 500]^D$	500
f_{17}		0	0	$[-100, 100]^D$	1
f_{18}		0	0	$[-10, 10]^D$	10^{-5}

θ is the shifted vector.

(3) Schwefel's Problem 1.2

$$f_3(x) = \sum_{i=1}^D \left(\sum_{j=1}^i x_j \right)^2, \quad (\text{A.3})$$

$o = [0, 0, \dots, 0]$: the global optimum.

(4) Shifted Schwefel's Problem 1.2

$$f_4(x) = \sum_{i=1}^D \left(\sum_{j=1}^i z_j \right)^2, \quad (\text{A.4})$$

$$z = x - \theta,$$

$\theta = [\theta_1, \theta_2, \dots, \theta_D]$: the shifted global optimum.

(5) Rosenbrock's function

$$f_5(x) = \sum_{i=1}^{D-1} \left(100(x_i^2 - x_{i+1}^2)^2 + (x_i - 1)^2 \right), \quad (\text{A.5})$$

$o = [1, 1, \dots, 1]$: the global optimum.

(6) Schwefel's Problem 1.2 with noise in fitness

$$f_6(x) = \left(\sum_{i=1}^D \left(\sum_{j=1}^i x_j \right)^2 \right) * (1 + 0.4|N(0, 1)|), \quad (\text{A.6})$$

$o = [0, 0, \dots, 0]$: the global optimum.

(7) Shifted Schwefel's Problem 1.2 with noise in fitness

$$f_7(x) = \left(\sum_{i=1}^D \left(\sum_{j=1}^i z_j \right)^2 \right) * (1 + 0.4|N(0, 1)|), \quad (\text{A.7})$$

$$z = x - \theta,$$

$\theta = [\theta_1, \theta_2, \dots, \theta_D]$: the shifted global optimum.

(8) Ackley's function

$$f_8(x) = -20 \exp \left(-0.2 \sqrt{\frac{1}{D} \sum_{i=1}^D x_i^2} \right) - \exp \left(\frac{1}{D} \sum_{i=1}^D \cos(2\pi x_i) \right) + 20 + e, \quad (\text{A.8})$$

$o = [0, 0, \dots, 0]$: the global optimum.

(9) Shifted Ackley's function

$$f_9(x) = -20 \exp \left(-0.2 \sqrt{\frac{1}{D} \sum_{i=1}^D z_i^2} \right) - \exp \left(\frac{1}{D} \sum_{i=1}^D \cos(2\pi z_i) \right) + 20 + e, \quad (\text{A.9})$$

$$z = x - \theta,$$

$\theta = [\theta_1, \theta_2, \dots, \theta_D]$: the shifted global optimum.

(10) Griewank's function

$$f_{10}(x) = \sum_{i=1}^D \frac{x_i^2}{4000} - \prod_{i=1}^D \cos \frac{x_i}{\sqrt{i}} + 1, \quad (\text{A.10})$$

$o = [0, 0, \dots, 0]$: the global optimum.

(11) Shifted Griewank's function

$$f_{11}(x) = \sum_{i=1}^D \frac{z_i^2}{4000} - \prod_{i=1}^D \cos \frac{z_i}{\sqrt{i}} + 1, \quad (\text{A.11})$$

$$z = x - \theta,$$

$\theta = [\theta_1, \theta_2, \dots, \theta_D]$: the shifted global optimum.

(12) Rastrigin's function

$$f_{12}(x) = \sum_{i=1}^D (x_i^2 - 10 \cos(2\pi x_i) + 10), \quad (\text{A.12})$$

$o = [0, 0, \dots, 0]$: the global optimum.

(13) Shifted Rastrigin's function

$$f_{13}(x) = \sum_{i=1}^D (z_i^2 - 10 \cos(2\pi z_i) + 10), \quad (\text{A.13})$$

$$z = x - \theta,$$

$\theta = [\theta_1, \theta_2, \dots, \theta_D]$: the shifted global optimum.

(14) Noncontiguous Rastrigin's function

$$f_{14}(x) = \sum_{i=1}^D (y_i^2 - 10 \cos(2\pi y_i) + 10),$$

$$y_i = \begin{cases} x_i & |x_i| < \frac{1}{2} \\ \frac{\text{round}(2x_i)}{2} & |x_i| \geq \frac{1}{2} \end{cases} \quad \text{for } i = 1, 2, \dots, D,$$

$$o = [0, 0, \dots, 0]: \text{ the global optimum.} \quad (\text{A.14})$$

(15) Shifted noncontiguous Rastrigin's function

$$f_{15}(x) = \sum_{i=1}^D (y_i^2 - 10 \cos(2\pi y_i) + 10),$$

$$y_i = \begin{cases} z_i & |z_i| < \frac{1}{2} \\ \frac{\text{round}(2z_i)}{2} & |z_i| \geq \frac{1}{2} \end{cases} \quad \text{for } i = 1, 2, \dots, D,$$

$$z = x - \theta,$$

$$\theta = [\theta_1, \theta_2, \dots, \theta_D]: \text{ the shifted global optimum.} \quad (\text{A.15})$$

(16) Schwefel's function

$$f_{16}(x) = 418.9829 \times D - \sum_{i=1}^D x_i \sin(|x_i|^{1/2}),$$

$o = [418.9829, 418.9829, \dots, 418.9829]$: the global optimum. (A.16)

(17) Schwefel's Problem 2.21

$$f_{18}(x) = \max\{|x_i|, 1 \leq i \leq D\}, \quad (\text{A.17})$$

$o = [0, 0, \dots, 0]$: the global optimum.

(18) Schwefel's Problem 2.22

$$f_{17}(x) = \sum_{i=1}^D |x_i| + \prod_{i=1}^D x_i, \quad (\text{A.18})$$

$o = [0, 0, \dots, 0]$: the global optimum.

Conflict of Interests

The authors declare that there is no conflict of interests regarding the publication of this paper.

Acknowledgments

The authors are grateful to the anonymous reviewers for giving us helpful suggestions. This work is supported by National Natural Science Foundation of China (Grant nos. 61174040 and 61104178) and Fundamental Research Funds for the Central Universities, Shanghai Commission of Science and Technology (Grant no. 12JC1403400).

References

- [1] M. T. Sadeghi and A. Kavianiboroujeni, "The optimization of an ammonia synthesis reactor using genetic algorithm," *International Journal of Chemical Reactor Engineering*, vol. 6, no. 1, article A113, 2009.
- [2] S. S. E. H. Elnashaie, A. T. Mahfouz, and S. S. Elshishini, "Digital simulation of an industrial ammonia reactor," *Chemical Engineering and Processing*, vol. 23, no. 3, pp. 165–177, 1988.
- [3] M. N. Pedemera, D. O. Borio, and N. S. Schbib, "Steady-State analysis and optimization of a radial-flow ammonia synthesis reactor," *Computers & Chemical Engineering*, vol. 23, no. 1, pp. S783–S786, 1999.
- [4] B. V. Babu and R. Angira, "Optimal design of an auto-thermal ammonia synthesis reactor," *Computers & Chemical Engineering*, vol. 29, no. 5, pp. 1041–1045, 2005.
- [5] W. F. Sacco and N. Hendersonb, "Differential evolution with topographical mutation applied to nuclear reactor core design," *Progress in Nuclear Energy*, vol. 70, pp. 140–148, 2014.
- [6] M. Rout, B. Majhi, R. Majhi, and G. Panda, "Forecasting of currency exchange rates using an adaptive ARMA model with differential evolution based training," *Journal of King Saud University*, vol. 26, no. 1, pp. 7–18, 2014.
- [7] H. Ozcan, K. Ozdemir, and H. Ciloglu, "Optimum cost of an air cooling system by using differential evolution and particle swarm algorithms," *Energy and Buildings*, vol. 65, pp. 93–100, 2013.

- [8] R. Zhang, S. Song, and C. Wu, "A hybrid differential evolution algorithm for job shop scheduling problems with expected total tardiness criterion," *Applied Soft Computing Journal*, vol. 13, no. 3, pp. 1448–1458, 2013.
- [9] R. Arya and S. C. Choube, "Differential evolution based technique for reliability design of meshed electrical distribution systems," *International Journal of Electrical Power & Energy Systems*, vol. 48, pp. 10–20, 2013.
- [10] W. Xu, L. Zhang, and X. Gu, "Soft sensor for ammonia concentration at the ammonia converter outlet based on an improved particle swarm optimization and BP neural network," *Chemical Engineering Research and Design*, vol. 89, no. 10, pp. 2102–2109, 2011.
- [11] M. R. Sawant, K. V. Patwardhan, A. W. Patwardhan, V. G. Gaikar, and M. Bhaskaran, "Optimization of primary enrichment section of mono-thermal ammonia-hydrogen chemical exchange process," *Chemical Engineering Journal*, vol. 142, no. 3, pp. 285–300, 2008.
- [12] Z. Kirova-Yordanova, "Exergy analysis of industrial ammonia synthesis," *Energy*, vol. 29, no. 12–15, pp. 2373–2384, 2004.
- [13] B. Månsson and B. Andresen, "Optimal temperature profile for an ammonia reactor," *Industrial & Engineering Chemistry Process Design and Development*, vol. 25, no. 1, pp. 59–65, 1986.
- [14] R. Mallipeddi, P. N. Suganthan, Q. K. Pan, and M. F. Tasgetiren, "Differential evolution algorithm with ensemble of parameters and mutation strategies," *Applied Soft Computing Journal*, vol. 11, no. 2, pp. 1679–1696, 2011.
- [15] R. Storn and K. Price, "Differential evolution—a simple and efficient heuristic for global optimization over continuous spaces," *Journal of Global Optimization*, vol. 11, no. 4, pp. 341–359, 1997.
- [16] C. Hu and X. Yan, "A hybrid differential evolution algorithm integrated with an ant system and its application," *Computers & Mathematics with Applications*, vol. 62, no. 1, pp. 32–43, 2011.
- [17] K. Vaisakh and L. R. Srinivas, "Genetic evolving ant direction HDE for OPF with non-smooth cost functions and statistical analysis," *Expert Systems with Applications*, vol. 38, no. 3, pp. 2046–2062, 2011.
- [18] R. Wang, J. Zhang, Y. Zhang, and X. Wang, "Assessment of human operator functional state using a novel differential evolution optimization based adaptive fuzzy model," *Biomedical Signal Processing and Control*, vol. 7, no. 5, pp. 490–498, 2012.
- [19] W. Xu, L. Zhang, and X. Gu, "A novel cultural algorithm and its application to the constrained optimization in ammonia synthesis," *Communications in Computer and Information Science*, vol. 98, no. 2, pp. 52–58, 2010.
- [20] Z. Liu and X. Gu, "Soft-sensor modelling of inlet ammonia content of synthetic tower based on integrated intelligent optimization," *Huagong Xuebao*, vol. 61, no. 8, pp. 2051–2055, 2010.

Research Article

Identification of LTI Time-Delay Systems with Missing Output Data Using GEM Algorithm

Xianqiang Yang¹ and Hamid Reza Karimi²

¹ *Research Institute of Intelligent Control and Systems, Harbin Institute of Technology, Harbin, Heilongjiang 150080, China*

² *Department of Engineering, Faculty of Engineering and Science, University of Agder, 4898 Grimstad, Norway*

Correspondence should be addressed to Xianqiang Yang; xianqiangyang@gmail.com

Received 28 December 2013; Accepted 13 February 2014; Published 17 March 2014

Academic Editor: Xudong Zhao

Copyright © 2014 X. Yang and H. R. Karimi. This is an open access article distributed under the Creative Commons Attribution License, which permits unrestricted use, distribution, and reproduction in any medium, provided the original work is properly cited.

This paper considers the parameter estimation for linear time-invariant (LTI) systems in an input-output setting with output error (OE) time-delay model structure. The problem of missing data is commonly experienced in industry due to irregular sampling, sensor failure, data deletion in data preprocessing, network transmission fault, and so forth; to deal with the identification of LTI systems with time-delay in incomplete-data problem, the generalized expectation-maximization (GEM) algorithm is adopted to estimate the model parameters and the time-delay simultaneously. Numerical examples are provided to demonstrate the effectiveness of the proposed method.

1. Introduction

The advanced process control theories have enjoyed rapid development in the past several decades to meet the growing demands of closed-loop system performances, such as improved process safety and efficiency of plant operation, consistent product quality, and economic optimization [1]. These control strategies have improved the process automation and stability through providing control solutions for the process operated under the abnormal working conditions, such as process fault [2–5], network transmission delay [6], data packet dropouts [7], and modeling error. Generally, the implementation of these control strategies relies on the understanding of the process dynamics and the availability of an accurate mathematical model of the process. In view of the difficulties and complexities imposed by modeling using first principle method, the data-driven modeling method, in which the process model is retrieved from the process data, has become a main modeling method.

Typically, the process data used in process modeling are generated by performing an identification experiment, in which a testing signal is designed and utilized to excite the process. Most of the conventional parameter estimation methods, such as prediction error method (PEM),

instrumental variable (IV) method, and subspace method, assume that the identification data are sampled regularly and recorded properly. However, this is not always true in practical industry. For example, in the development of an inferential model for the sulfur content in the gas oil product, the sulfur concentration cannot be measured directly and the lab analysis is required which takes a long time. The process variable can be sampled in every minute, but the sulfur concentration is only available in every twelve hours. Another example is the industrial process with data transmission through the network. The recorded process data are corrupted by many network-induced problems, such as transmission delay and packet dropout or missing. Therefore, parameter estimation with irregular data has not been extensively investigated in the literature.

Time-delays are commonly encountered in various engineering systems, such as chemical processes, mechanical systems, network control systems, transmission line, and economic systems [8]. Since the existence of time-delay usually causes performance degradation of the inferential model and is frequently a source of instability of the closed-loop system, it should be handled carefully in the modeling process. Common methods to estimate the time-delays are

nonparametric methods (e.g., step test or correlation analysis) and grid searching method. For example, Wang and Zhang [9] considered the robust identification problems of linear continuous time-delay systems from step responses. A linear regression equation was derived from the solution of the output time response and its various-order integrals and solved by using IV-least squares (LS) method. The parameters of the transfer function were then recovered from the LS solution. Weyer [10] considered to build a model for the open water channel. The model parameters were estimated using the grid searching method in which one model was established for each time-delay in a range. The final model was selected as the model which gave the best prediction performance for a validation data set. The time-delay estimation methods mentioned above are to estimate the time-delay and model parameters in a separate way.

Missing data problem is very common in process industry. A special example is the irregularly sampling system. Many critical parameters, such as the product concentration, steam quality, and 90% boiling point, cannot be measured directly by using the sensors. These parameters are measured through lab analysis, so only the slow rate data are available. However, the process variables, such as the temperature, pressure, and flow rate, can be measured on-line in fast rate by using the sensors. Therefore, we can treat the data samples between the slow rate data as missing data. Another example is the network control system in which data transmit via the wireless network or internet. Data missing occurs due to data packet dropout or missing. Other reasons for missing data are sensor fault, data recording system malfunction, and so forth. Several methods have been reported in the literature to handle missing data problem in system identification. For example, F. Ding and J. Ding [11] proposed an auxiliary model-based approach to cope with the problems of parameter estimation and output estimation with irregularly missing output data using the PEM method. The outputs of the auxiliary model were used in the identification process. Zhu et al. [12] considered the identification of systems with slowly and irregularly sampled output data. The output error method was employed to estimate the fast rate model based on the fast input and slow output data. However, the methods mentioned above just used part of the process data, which may lead to information missing. Moreover, the statistical properties of the model parameters and the process noise cannot be given in these methods.

The work introduced in this paper aims at handling the identification problem of the LTI systems with missing output data in the presence of time-delay. The identification problem is formulated under the scheme of the generalized expectation-maximization (GEM) algorithm and the time-delay and missing output data are handled simultaneously. The GEM algorithm consists of expectation step (E-step) and maximization step (M-step). In the M-step, the maximization problem is transformed into an equivalent minimization problem and this problem is solved by using a general numerical optimization algorithm.

The rest of this paper is organized as follows. The problem statement is presented in Section 2. A brief revisit of the GEM algorithm and the mathematical formulation of

the identification of LTI time-delay systems with incomplete data set are given in Section 3. Numerical examples are presented in Section 4 to show the effectiveness of the proposed method. The conclusions are given in Section 5.

2. Problem Statement

Consider the LTI system described by the following output error (OE) time-delay model:

$$y_t = G(z^{-1})u_{t-\tau} + e_t, \quad (1)$$

where τ is the time-delay which is assumed to be integer multiples of the sampling period, e_t is the Gaussian white noise with zero mean and variance σ^2 , and y_t and u_t are the output and input, respectively. The transfer function $G(z^{-1})$ has the following form:

$$G(z^{-1}) = \frac{\sum_{i=1}^{n_b} b_i z^{-i}}{1 + \sum_{i=1}^{n_a} a_i z^{-i}}. \quad (2)$$

Here, we assume that the model orders n_a and n_b are known a priori and the time-delay τ is uniformly distributed in a known range of $[d_1, d_2]$.

The identification data $\{y_t, u_t\}_{t=1,2,\dots,N}$ are collected. We denote $\{y_t\}_{t=1,2,\dots,N}$ as Y and $\{u_t\}_{t=1,2,\dots,N}$ as U . Since part of the output data are missing completely at random (MCAR), the output data set Y can be divided into $Y_{\text{obs}} = \{y_t\}_{t=t_1,\dots,t_\alpha}$ and $Y_{\text{mis}} = \{y_t\}_{t=m_1,\dots,m_\beta}$. Therefore, the identification problem is to estimate the parameters $\theta = \{a_1, \dots, a_{n_a}, b_1, \dots, b_{n_b}\}$, the noise variance σ^2 , and the time-delay τ based on the identification data Y_{obs} and U .

3. Parameter Estimation Using the GEM Algorithm

3.1. GEM Algorithm Revisit. The GEM algorithm is a general-purpose iterative optimization algorithm to derive the maximum likelihood (ML) estimate and it has attracted great attentions of the researcher due to its flexibility in handling the missing data or hidden state [13]. Denote the missing data set by C_{mis} and the observed data set by C_{obs} . The main idea of the GEM algorithm is that, instead of optimizing the likelihood of the observed Y_{obs} , the conditional expectation of the complete data likelihood function with respect to the missing data set is calculated in the E-step and the maximization problem is solved in the M-step. The procedures of the GEM algorithm to calculate the ML estimate can be described as follows [13]:

E-step: given the C_{obs} and the parameter estimate Θ^s in previous iteration, the Q-function can be calculated by

$$Q(\Theta | \Theta^s) = E_{C_{\text{mis}} | C_{\text{obs}}, \Theta^s} \{\log p(C_{\text{mis}}, C_{\text{obs}} | \Theta)\}, \quad (3)$$

M-step: find the Θ^{s+1} to increase $Q(\Theta | \Theta^s)$ over its value at Θ^s ; that is,

$$Q(\Theta^{s+1} | \Theta^s) \geq Q(\Theta^s | \Theta^s). \quad (4)$$

The E-step and M-step alternate until the relative change of the parameter estimate between neighboring iterations is smaller than a prespecified arbitrary small constant or the maximal iteration number is achieved.

3.2. LTI Time-Delay System Identification with Missing Output Using GEM Algorithm. Here, we treat the time-delay τ as a hidden state variable. The observed data set C_{obs} is constructed as $C_{\text{obs}} = \{Y_{\text{obs}}, U\}$ and the missing data set C_{mis} is constructed as $C_{\text{mis}} = \{Y_{\text{mis}}, \tau\}$. The parameter vector Θ is constructed as $\Theta = \{\theta, \sigma^2\}$.

Based on the Bayesian property, the likelihood function of the complete data set can be decomposed into

$$\begin{aligned} p(C_{\text{mis}}, C_{\text{obs}} | \Theta) &= p(Y, U, \tau | \Theta) \\ &= p(Y | U, \tau, \Theta) p(\tau | U, \Theta) p(U | \Theta). \end{aligned} \quad (5)$$

The term $p(Y | U, \tau, \Theta)$ can be further decomposed into

$$\begin{aligned} p(Y | U, \tau, \Theta) &= p(y_N, \dots, y_1 | u_N, \dots, u_1, \tau, \Theta) \\ &= p(y_N | y_{N-1}, \dots, y_1, u_N, \dots, u_1, \tau, \Theta) \\ &\quad \times p(y_{N-1}, \dots, y_1 | u_N, \dots, u_1, \tau, \Theta) \\ &= \prod_{t=1}^N p(y_t | y_{t-1}, \dots, y_1, u_N, \dots, u_1, \tau, \Theta). \end{aligned} \quad (6)$$

Based on (1) and (2), y_t depends only on the previous input sequence $u_{t-1:1} = \{u_{t-1}, \dots, u_1\}$, the time-delay τ , and the parameter vector Θ . Therefore, (6) can be rewritten as

$$p(Y | U, \tau, \Theta) = \prod_{t=1}^N p(y_t | u_{t-1:1}, \tau, \Theta). \quad (7)$$

Since the time-delay τ is uniformly distributed in the range $[d_1, d_2]$, the probability of τ taking any value in this range is a constant. Since the input U is measurable data and it is independent of the parameter vector Θ , the term $p(U | \Theta)$ is a constant. Therefore, the last two terms of (5) will not play a role in the following derivations. The complete data likelihood function can be further written as

$$p(Y, U, \tau | \Theta) = \prod_{t=1}^N p(y_t | u_{t-1:1}, \tau, \Theta) C_1, \quad (8)$$

where $C_1 = p(\tau | U, \Theta)p(U | \Theta)$.

Therefore, the conditional expectation of the log complete data density $Q(\Theta | \Theta^s)$ in (3) can be written as

$$\begin{aligned} Q(\Theta | \Theta^s) &= E_{Y_{\text{mis}}, \tau | C_{\text{obs}}, \Theta^s} \{ \log p(Y, U, \tau | \Theta) \} \\ &= E_{Y_{\text{mis}}, \tau | C_{\text{obs}}, \Theta^s} \left\{ \sum_{t=1}^N \log p(y_t | u_{t-1:1}, \tau, \Theta) + \log C_1 \right\} \\ &= E_{Y_{\text{mis}}, \tau | C_{\text{obs}}, \Theta^s} \left\{ \sum_{t=m_1}^{m_\beta} \log p(y_t | u_{t-1:1}, \tau, \Theta) \right. \\ &\quad \left. + \sum_{t=t_1}^{t_\alpha} \log p(y_t | u_{t-1:1}, \tau, \Theta) + \log C_1 \right\}. \end{aligned} \quad (9)$$

The expectation is firstly taken with respect to the discrete variable τ ; then we have

$$\begin{aligned} Q(\Theta | \Theta^s) &= E_{Y_{\text{mis}} | C_{\text{obs}}, \tau, \Theta^s} \left\{ \sum_{d=d_1}^{d_2} p(\tau = d | C_{\text{obs}}, \Theta^s) \right. \\ &\quad \times \sum_{t=m_1}^{m_\beta} \log p(y_t | u_{t-1:1}, \tau = d, \Theta) \\ &\quad \left. + \sum_{d=d_1}^{d_2} p(\tau = d | C_{\text{obs}}, \Theta^s) \right. \\ &\quad \times \sum_{t=t_1}^{t_\alpha} \log p(y_t | u_{t-1:1}, \tau = d, \Theta) \\ &\quad \left. + \log C_1 \right\}. \end{aligned} \quad (10)$$

The expectation is then taken with respect to the continuous variable Y_{miss} , so we have

$$\begin{aligned} Q(\Theta | \Theta^s) &= \sum_{d=d_1}^{d_2} p(\tau = d | C_{\text{obs}}, \Theta^s) \\ &\quad \times \sum_{t=m_1}^{m_\beta} \int p(y_t | C_{\text{obs}}, \tau = d, \Theta^s) \\ &\quad \times \log p(y_t | u_{t-1:1}, \tau = d, \Theta) dy_t \\ &\quad + \sum_{d=d_1}^{d_2} p(\tau = d | C_{\text{obs}}, \Theta^s) \\ &\quad \times \sum_{t=t_1}^{t_\alpha} \log p(y_t | u_{t-1:1}, \tau = d, \Theta) + \log C_1. \end{aligned} \quad (11)$$

In order to calculate $Q(\Theta | \Theta^s)$, the unknown terms should be calculated firstly. Consider

$$\begin{aligned}
p(\tau = d | C_{\text{obs}}, \Theta^s) &= p(\tau = d | Y_{\text{obs}}, U, \Theta^s) \\
&= \frac{p(Y_{\text{obs}} | U, \tau = d, \Theta^s) p(\tau = d | U, \Theta^s)}{\sum_{d=d_1}^{d_2} p(Y_{\text{obs}} | U, \tau = d, \Theta^s) p(\tau = d | U, \Theta^s)} \\
&= \frac{\prod_{t=t_1}^{t_\alpha} p(y_t | u_{t-1:1}, \tau = d, \Theta^s) p(\tau = d)}{\sum_{d=d_1}^{d_2} \prod_{t=t_1}^{t_\alpha} p(y_t | u_{t-1:1}, \tau = d, \Theta^s) p(\tau = d)} \\
&= \frac{\prod_{t=t_1}^{t_\alpha} p(y_t | u_{t-1:1}, \tau = d, \Theta^s)}{\sum_{d=d_1}^{d_2} \prod_{t=t_1}^{t_\alpha} p(y_t | u_{t-1:1}, \tau = d, \Theta^s)}, \\
\int p(y_t | C_{\text{obs}}, \tau = d, \Theta^s) \log p(y_t | u_{t-1:1}, \tau = d, \Theta) dy_t &= \int p(y_t | C_{\text{obs}}, \tau = d, \Theta^s) \log \frac{1}{\sqrt{2\pi\sigma^2}} \\
&\quad \times \exp \left\{ -\frac{(y_t - G(z^{-1})u_{t-d})^2}{2\sigma^2} \right\} dy_t \\
&= -\frac{1}{2} \log(2\pi\sigma^2) - \frac{1}{2\sigma^2} \int p(y_t | C_{\text{obs}}, \tau = d, \Theta^s) \\
&\quad \times (y_t - G(z^{-1})u_{t-d})^2 dy_t \\
&= -\frac{1}{2} \log(2\pi\sigma^2) - \frac{1}{2\sigma^2} \left((\sigma^s)^2 + (G^s(z^{-1})u_{t-d})^2 \right) \\
&\quad + \frac{1}{\sigma^2} (G(z^{-1})u_{t-d})(G^s(z^{-1})u_{t-d}) \\
&\quad - \frac{1}{2\sigma^2} (G(z^{-1})u_{t-d})^2 \\
&= -\frac{1}{2} \log(2\pi\sigma^2) \\
&\quad - \frac{1}{2\sigma^2} \left((\sigma^s)^2 + (G(z^{-1})u_{t-d} - G^s(z^{-1})u_{t-d})^2 \right), \\
p(y_t | u_{t-1:1}, \tau = d, \Theta) &= \frac{1}{\sqrt{2\pi\sigma^2}} \exp \left\{ -\frac{(y_t - G(z^{-1})u_{t-d})^2}{2\sigma^2} \right\}. \tag{12}
\end{aligned}$$

Therefore, the Q-function can be rewritten as

$$\begin{aligned}
Q(\Theta | \Theta^s) &= \sum_{d=d_1}^{d_2} p(\tau = d | C_{\text{obs}}, \Theta^s) \\
&\quad \times \sum_{t=m_1}^{m_\beta} \left\{ -\frac{1}{2} \log(2\pi\sigma^2) - \frac{1}{2\sigma^2} \right. \\
&\quad \times \left. \left((\sigma^s)^2 + (G(z^{-1})u_{t-d} - G^s(z^{-1})u_{t-d})^2 \right) \right\} \\
&\quad + \log C_1. \tag{13}
\end{aligned}$$

In the M-step of the GEM algorithm, the unknown parameters should be estimated to increase the Q-function by solving an optimization problem. Taking the gradient of the Q-function (13) with respect to the σ^2 and setting it to zeros, we have

$$\begin{aligned}
\hat{\sigma}^2 &= \frac{1}{N} \left\{ \sum_{d=d_1}^{d_2} p(\tau = d | C_{\text{obs}}, \Theta^s) \right. \\
&\quad \times \sum_{t=m_1}^{m_\beta} \left((G(z^{-1})u_{t-d} - G^s(z^{-1})u_{t-d})^2 + (\sigma^s)^2 \right) \\
&\quad + \sum_{d=d_1}^{d_2} p(\tau = d | C_{\text{obs}}, \Theta^s) \\
&\quad \times \left. \sum_{t=t_1}^{t_\alpha} (y_t - G(z^{-1})u_{t-d})^2 \right\}. \tag{14}
\end{aligned}$$

Substituting $\hat{\sigma}^2$ into the Q-function (13), we get

$$\begin{aligned}
Q(\Theta | \Theta^s) &= -\frac{N}{2} \log(2\pi) - \frac{N}{2} \\
&\quad - \frac{N}{2} \log \left\{ \frac{1}{N} \left[\sum_{d=d_1}^{d_2} p(\tau = d | C_{\text{obs}}, \Theta^s) \right. \right. \\
&\quad \times \left. \left(\sum_{t=m_1}^{m_\beta} \left((G(z^{-1})u_{t-d} - G^s(z^{-1})u_{t-d})^2 \right. \right. \right. \\
&\quad \left. \left. \left. + (\sigma^s)^2 \right) \right. \right. \\
&\quad \left. \left. + \sum_{t=t_1}^{t_\alpha} (y_t - G(z^{-1})u_{t-d})^2 \right) \right\}. \tag{15}
\end{aligned}$$

Based on the monotonicity of the log function, the problem is transformed into optimizing the following cost function:

$$\begin{aligned}
J(\theta | \theta^s) &= \frac{1}{N} \left[\sum_{d=d_1}^{d_2} p(\tau = d | C_{\text{obs}}, \Theta^s) \right. \\
&\quad \times \left(\sum_{t=m_1}^{m_\beta} \left((G(z^{-1})u_{t-d} - G^s(z^{-1})u_{t-d})^2 + (\sigma^s)^2 \right) \right. \\
&\quad \left. \left. + \sum_{t=t_1}^{t_\alpha} (y_t - G(z^{-1})u_{t-d})^2 \right) \right]. \tag{16}
\end{aligned}$$

Here, we introduce the variable x_t^τ denoting the noise-free output with time-delay τ . Based on (1) and (2), we have

$$x_t^\tau = \frac{\sum_{i=1}^{n_b} b_i z^{-i}}{1 + \sum_{i=1}^{n_a} a_i z^{-i}} u_{t-\tau} = (\phi_{t-\tau}^\tau)^T \theta, \tag{17}$$

where $\phi_{t-\tau}^\tau = [-x_{t-1}^\tau, \dots, -x_{t-n_a}^\tau, u_{t-\tau-1}, \dots, u_{t-\tau-n_b}]^T$. Therefore, the cost function can be rewritten as

$$\begin{aligned}
J(\theta | \theta^s) &= \frac{1}{N} \left[\sum_{d=d_1}^{d_2} p(\tau = d | C_{\text{obs}}, \Theta^s) \right. \\
&\quad \times \left(\sum_{t=m_1}^{m_\beta} \left(((\phi_{t-d}^d)^T \theta - (x_t^d)^s)^2 + (\sigma^s)^2 \right) \right. \\
&\quad \left. \left. + \sum_{t=t_1}^{t_\alpha} (y_t - (\phi_{t-d}^d)^T \theta)^2 \right) \right], \tag{18}
\end{aligned}$$

where $(x_t^d)^s = (\phi_{t-d}^d)^T \theta^s$. However, the cost function (18) cannot be optimized directly due to the unmeasurable $\{x_t^d\}_{t=1, \dots, N, d=d_1, \dots, d_2}$. Here, we adopt the auxiliary model principle and the auxiliary model can be constructed based on the estimates obtained in the previous iteration. That is,

$$\hat{x}_t^\tau = \frac{\sum_{i=1}^{n_b} \hat{b}_i z^{-i}}{1 + \sum_{i=1}^{n_a} \hat{a}_i z^{-i}} u_{t-\tau} = (\hat{\phi}_{t-\tau}^\tau)^T \hat{\theta}, \tag{19}$$

where $\hat{\phi}_{t-\tau}^\tau = [-\hat{x}_{t-1}^\tau, \dots, -\hat{x}_{t-n_a}^\tau, u_{t-\tau-1}, \dots, u_{t-\tau-n_b}]^T$. Therefore, the cost function (18) with $\phi_{t-\tau}^\tau$ substituted by $\hat{\phi}_{t-\tau}^\tau$ can be optimized by using the damped Newton algorithm,

$$\theta^{s+1} = \theta^s - [R^s]^{-1} J'(\theta^s | \theta^s), \tag{20}$$

where

$$\begin{aligned}
J'(\theta^s | \theta^s) &= \frac{2}{N} \left[\sum_{d=d_1}^{d_2} p(\tau = d | C_{\text{obs}}, \Theta^s) \right. \\
&\quad \times \left(\sum_{t=m_1}^{m_\beta} \hat{\phi}_{t-d}^d \left((\hat{\phi}_{t-d}^d)^T \theta^s - (x_t^d)^s \right) \right. \\
&\quad \left. \left. + \sum_{t=t_1}^{t_\alpha} \hat{\phi}_{t-d}^d \left((\hat{\phi}_{t-d}^d)^T \theta^s - y_t \right) \right) \right], \\
R^s &= \frac{2}{N} \left[\sum_{d=d_1}^{d_2} p(\tau = d | C_{\text{obs}}, \Theta^s) \sum_{t=1}^N \hat{\phi}_{t-d}^d (\hat{\phi}_{t-d}^d)^T \right] + \lambda I, \tag{21}
\end{aligned}$$

where λ is a constant.

The time-delay τ can be selected as the delay in the range with maximal posterior probability. That is,

$$\hat{\tau} = \underset{d}{\operatorname{argmax}} p(\tau = d | C_{\text{obs}}, \Theta^s). \tag{22}$$

The E-step and M-step alternate until the convergence condition of the GEM algorithm is met.

4. Simulation Examples

4.1. A Numerical Simulation Example. Consider the following LTI time-delay system described by the OE time-delay model:

$$y_t = \frac{0.3z^{-1}}{1 - 0.7z^{-1}} u_{t-3} + e_t. \tag{23}$$

The input data and output data are generated by simulation and the noise e_t with zero mean and variance 0.01 is added to the output. The input and output data are shown in Figure 1. In the simulation, 12.5% output data are randomly missing. The parameter range of the time-delay is set to [1, 5]. The method proposed in this paper is used to estimate the parameters and the time-delay. The parameter estimate trajectories of the model parameters and the noise variance are shown in Figures 2 and 3, respectively. The estimated time-delay is 3 which is consistent with the true time-delay. To further verify the effectiveness of the proposed method, the simulations are also performed with 25% output data missing and 50% output data missing. The estimated parameters after 13 iterations are summarized in Table 1. It can be seen from these figures and the table that the proposed GEM algorithm has a good identification performance.

4.2. The Continuous Stirred Tank Reactor. The Continuous Stirred Tank Reactor (CSTR) is a benchmark example used to test the performances of different modeling and control

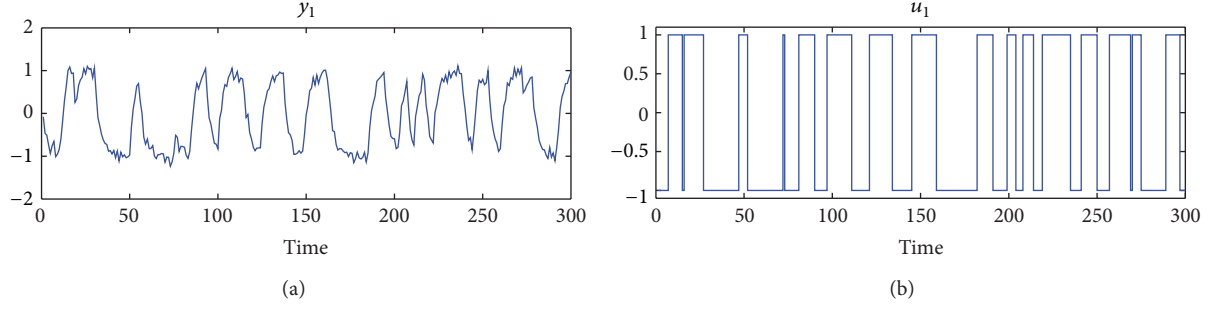


FIGURE 1: The input and output data.

TABLE 1: Estimated parameters after 13 iterations.

True value	$a = -0.7$	$b = 0.3$	$\tau = 3$	$\sigma^2 = 0.01$
Proportion of missing output	a	b	τ	σ^2
Full data set	-0.695	0.3026	3	0.0114
12.5%	-0.694	0.3042	3	0.0116
25%	-0.7012	0.2994	3	0.0121
50%	-0.6979	0.3017	3	0.0124

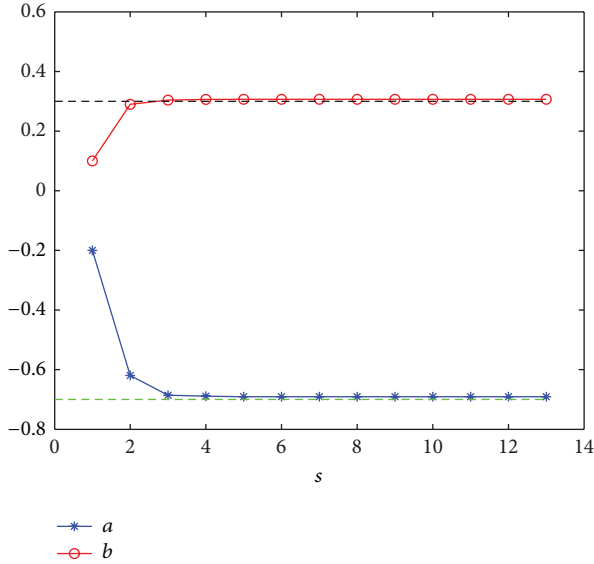


FIGURE 2: The estimated model parameters in each iteration.

algorithms and the first principle model of the CSTR is described as [14]

$$\begin{aligned}
 \frac{dC_A}{dt} &= \frac{q}{V} (C_{A0} - C_A) - k_0 C_A \exp\left(\frac{-E}{RT}\right), \\
 \frac{dT}{dt} &= \frac{q}{V} (T_0 - T) - \frac{(\Delta H) k_0 C_A}{\rho C_p} \exp\left(\frac{-E}{RT}\right) \\
 &\quad + \frac{\rho_c C_{pc}}{\rho C_p V} q_c \left\{ 1 - \exp\left(\frac{-hA}{q_c \rho C_p}\right) \right\} (T_{c0} - T),
 \end{aligned} \quad (24)$$

where the product concentration C_A and the temperature T are output variables and the coolant flow rate q_c is the input

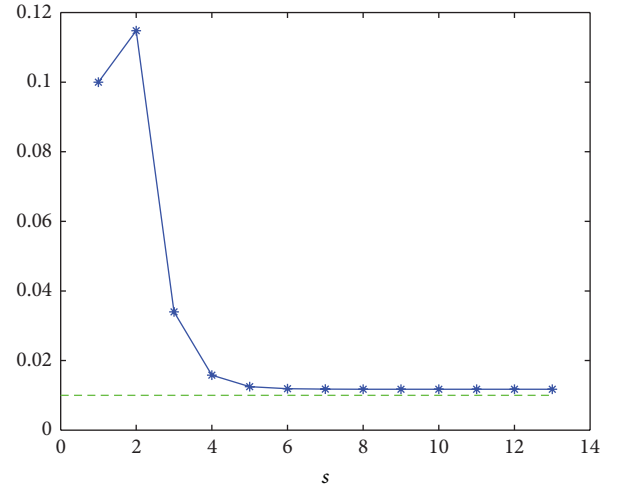


FIGURE 3: The estimated noise variance in each iteration.

variable. The steady state values of the process variables can be found in Gopaluni [14]. In this simulation, the CSTR is operated at a steady state working point which is at $q_c = 97$ L/min, $C_A = 0.0795$ mol/L, and $T = 443.4566$ K. The task here is to build a first-order model between C_A and q_c . The input and output data are generated through simulation and the noise with zero mean and variance 1×10^{-7} is added to the output data. Since time is needed to measure the concentration C_A , so the measurement delay with 1.5 minutes is also added to the output data. The input and output data is shown in Figure 4. In this simulation, 25% output data are randomly missing and the parameter range of the time-delay is set to $[0.9, 2.1]$. The proposed GEM algorithm is used to estimate the unknown parameters. The estimated parameters are $\hat{a} = -0.468$, $\hat{b} = 0.0015$, $\hat{\sigma}^2 = 1.5 \times 10^{-7}$, and $\hat{\tau} = 1.5$. The self-validation and the cross-validation results are shown in Figures 5 and 6. It can be seen from these results that the proposed method has a good identification performance and the estimated model can capture the dynamic behavior of the CSTR.

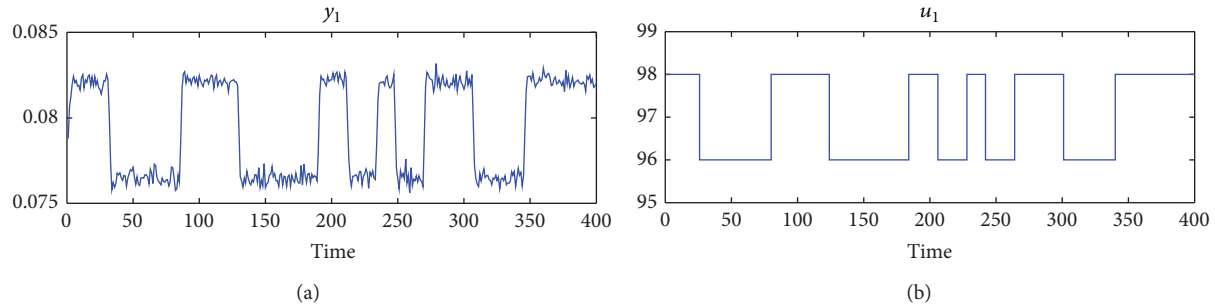


FIGURE 4: The input and output data.

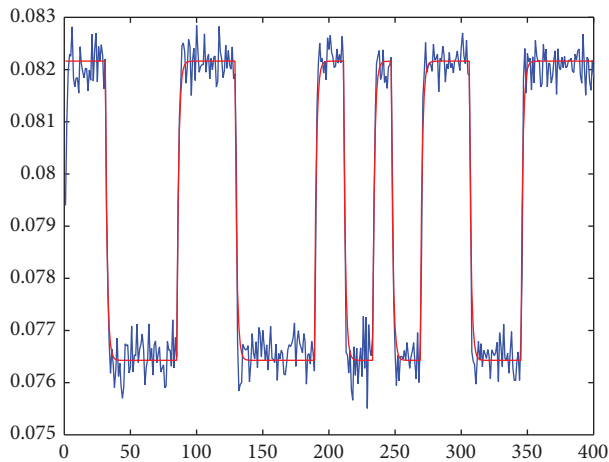


FIGURE 5: The self-validation results. The blue line is the real process data and the red line is the simulated output of the estimated model.

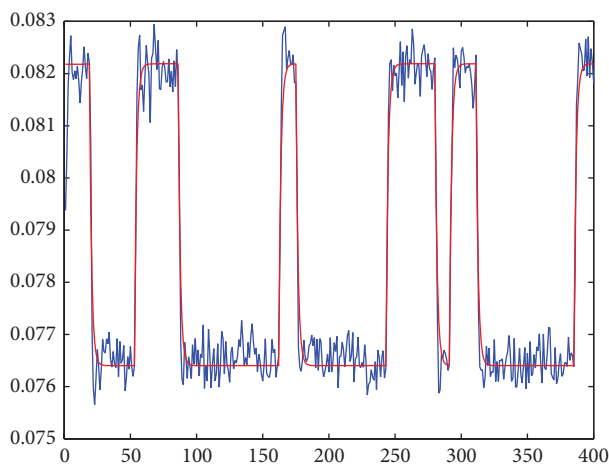


FIGURE 6: The cross-validation results. The blue line is the real process data and the red line is the simulated output of the estimated model.

5. Conclusion

This paper considers the identification problem of LTI systems with irregular data set. The time-delay and the missing

data are commonly encountered problems in process industry and the existence of these problems makes the process modeling a challenging task. The identification problem with incomplete data set in the presence of time-delay is formulated under the scheme of the GEM algorithm and the model parameters and the time-delay are estimated simultaneously in this algorithm. Numerical examples are presented to demonstrate the efficacy of the proposed method.

Conflict of Interests

The authors declare that there is no conflict of interests regarding the publication of this paper.

References

- [1] S. Yin, H. Luo, and S. X. Ding, "Real-Time implementation of fault-tolerant control systems with performance optimization," *IEEE Transactions on Industrial Electronics*, vol. 61, no. 5, pp. 2402–2411, 2014.
- [2] S. Yin, S. X. Ding, A. Haghani, and P. Zhang, "A comparison study of basic data-driven fault diagnosis and process monitoring methods on the benchmark Tennessee Eastman process," *Journal of Process Control*, vol. 22, no. 9, pp. 1567–1581, 2012.
- [3] S. Yin, X. Yang, and H. R. Karimi, "Data-driven adaptive observer for fault diagnosis," *Mathematical Problems in Engineering*, vol. 2012, Article ID 832836, 21 pages, 2012.
- [4] S. Yin, S. X. Ding, A. H. A. Sari, and H. Hao, "Data-driven monitoring for stochastic systems and its application on batch process," *International Journal of Systems Science*, vol. 44, no. 7, pp. 1366–1376, 2013.
- [5] S. Yin, G. Wang, and H. Karimi, "Data-driven design of robust fault detection system for wind turbines," *Mechatronics*, 2013.
- [6] H. Dong, Z. Wang, and H. Gao, "Distributed H_∞ filtering for a class of Markovian jump nonlinear time-delay systems over lossy sensor networks," *IEEE Transactions on Industrial Electronics*, vol. 60, no. 10, pp. 4665–4672, 2013.
- [7] H. Dong, Z. Wang, J. Lam, and H. Gao, "Fuzzy-model-based robust fault detection with stochastic mixed time delays and successive packet dropouts," *IEEE Transactions on Systems, Man, and Cybernetics B*, vol. 42, no. 2, pp. 365–376, 2012.
- [8] J. P. Richard, "Time-delay systems: an overview of some recent advances and open problems," *Automatica*, vol. 39, no. 10, pp. 1667–1694, 2003.

- [9] Q. G. Wang and Y. Zhang, "Robust identification of continuous systems with dead-time from step responses," *Automatica*, vol. 37, no. 3, pp. 377–390, 2001.
- [10] E. Weyer, "System identification of an open water channel," *Control Engineering Practice*, vol. 9, no. 12, pp. 1289–1299, 2001.
- [11] F. Ding and J. Ding, "Least-squares parameter estimation for systems with irregularly missing data," *International Journal of Adaptive Control and Signal Processing*, vol. 24, no. 7, pp. 540–553, 2010.
- [12] Y. C. Zhu, H. Telkamp, J. H. Wang, and Q. L. Fu, "System identification using slow and irregular output samples," *Journal of Process Control*, vol. 19, no. 1, pp. 58–67, 2009.
- [13] G. J. McLachlan and T. Krishnan, *The EM Algorithm and Extensions*, John Wiley & Sons, New York, NY, USA, 2007.
- [14] R. B. Gopaluni, "A particle filter approach to identification of nonlinear processes under missing observations," *The Canadian Journal of Chemical Engineering*, vol. 86, no. 6, pp. 1081–1092, 2008.

Research Article

Eddy Current Inversion Models for Estimating Dimensions of Defects in Multilayered Structures

Bo Ye,¹ Jun Dong,¹ Gefei Qiu,¹ Siqi Li,¹ Fang Zeng,¹ Tanghua Yang,²
Biao Bai,² and Zhangzhou He¹

¹ Faculty of Electric Power Engineering, Kunming University of Science and Technology, Kunming 650500, China

² Puer Power Supply Bureau, Yunnan Power Grid Corporation, Pu'er 665000, China

Correspondence should be addressed to Bo Ye; yripple@hotmail.com

Received 11 December 2013; Accepted 5 February 2014; Published 17 March 2014

Academic Editor: Huaicheng Yan

Copyright © 2014 Bo Ye et al. This is an open access article distributed under the Creative Commons Attribution License, which permits unrestricted use, distribution, and reproduction in any medium, provided the original work is properly cited.

In eddy current nondestructive evaluation, one of the principal challenges is to determine the dimensions of defects in multilayered structures from the measured signals. It is a typical inverse problem which is generally considered to be nonlinear and ill-posed. In the paper, two effective approaches have been proposed to estimate the defect dimensions. The first one is a partial least squares (PLS) regression method. The second one is a kernel partial least squares (KPLS) regression method. The experimental research is carried out. In experiments, the eddy current signals responding to magnetic field changes are detected by a giant magnetoresistive (GMR) sensor and preprocessed for noise elimination using a wavelet packet analysis (WPA) method. Then, the proposed two approaches are used to construct the inversion models of defect dimension estimation. Finally, the estimation results are analyzed. The performance comparison between the proposed two approaches and the artificial neural network (ANN) method is presented. The comparison results demonstrate the feasibility and validity of the proposed two methods. Between them, the KPLS regression method gives a better prediction performance than the PLS regression method at present.

1. Introduction

Estimating dimensions of defects occurring in multilayered structures is important not only for ensuring the safety of the structural system (e.g., aging nuclear structures, composite aircraft structures, and other civil engineering structures), but also for getting a huge economic benefit from the view of the possible extension of in-service inspection of period [1–3]. To ensure the highest possible operational safety along with economic efficiency, it is necessary to carry out experimental inspections with high sensitivity and reliability. One of the possible solutions of this problem is based on the measurement of magnetic field change generating eddy current (EC) in multilayered structures [4, 5].

Eddy current nondestructive evaluation (ECNDE) is a structure evaluation technique which allows for detecting and characterizing the defects affecting an object without damaging it or altering its functionality [6]. Pioneered by Friedrich Forster in the 1940s, ECNDE as currently practiced is used with electrically conducting materials for various types of

measurements. These mainly include measurement of the thickness of metallic plates or nonmetallic coatings on metal substrates, estimation of electrical conductivity or magnetic permeability distributions, and determination of surface and subsurface defect shape and size [7]. However, in point of safety and economic efficiency assessment, there is not too much interest in electrical conductivity and magnetic permeability distributions. The defect dimensions (depth, length, width, and so on) are the main concerns [8]. In ECNDE, the dimensions of defects will be retrieved by inversion of the measured signals [9]. Since the physical model of ECNDE is often complicated and nonlinear, as a result, the inversion model is often ill-posed [10]. In the traditional way, the defect dimensions would be estimated by the analyst visual perception of EC inspection signals [6]. This method usually requires highly trained personnel, and the results are always influenced by the analyst's subjectivity. Then, model-based approaches are used to estimate defect dimensions from EC signals [11]. These methods iteratively solve the forward model to simulate the inspection process and predict the

probe responses. The problem of defect dimension estimation is formulated as an optimization problem, which seeks a set of defect dimensions by minimizing an objective function, representing the difference between the model predicted signals and the measured signals. Such approaches usually involve significant computational efforts, since the physical model needs to be solved repeatedly. Due to their complexity and low speed, the model-based approaches seem not to be suitable for being used to estimate the defect dimensions directly from EC inspection signals. Some researchers begin to turn to the model-free approaches. Initially, the defect dimension estimation problem is treated as a complex statistical pattern recognition problem [12]. These methods usually extract the special properties of defect signals such as shape, phase, peak value, smoothness, convexity, unimodality, or existence of derivatives as the feature vectors. Corresponding defect dimensions are discretized into a set of class labels. The defect dimensions are obtained from the classification of the currently collected signals based on the extracted features. The classification methods yield discrete values instead of continuous values, which lead to insufficiently accurate results. Then, Popa and Miya [13] and Yusa et al. [14] present an artificial neural network (ANN) method to estimate crack depth and reconstruct crack depth profile from EC signals. Davoust et al. [15] propose to use the bilinear regression and ANN methods to estimate flaw size. Rosa et al. [16, 17] use the probability density function estimation methods for defect dimension estimation. They employed sample techniques such as Markov Chain Monte Carlo (MCMC) and Bootstrap methods for estimation of probability density function of defect dimensions to obtain not only the quantity but also the uncertainly characterization of the measurand. Krzywosz [18] applies a multivariate linear regression algorithm to establish the relationship between the inside diameter pit depth and three features (frequency, amplitude, and phase angle) of EC inspection signals. Bernieri et al. propose a model-free method for the reliable estimation of crack shape and dimensions based on the integration of an EC instrument and a support vector machine (SVM) processing algorithm [19]. Among these methods, ANN is an efficient nonlinear statistical data modeling tool, but it usually requires a number of prior knowledge, space limitations, and database of defect signals for neural network training. The multivariate linear regression method can establish a direct and compact model. However, such method often fails to arrive at a sufficient accurate estimation due to the natural nonlinearity of the magnetic field distribution in complex multilayered structures. The probability density function estimation methods have a great problem that sample techniques require much computational time. Although the results SVM method present are quite impressive, the main drawback of SVM is that solving the problem requires an optimization with a complexity that varies at least quadratically with the number of training examples, which becomes intractable in large scale problems. Therefore, a general framework for defect dimension estimation from EC signals is very desirable, which can not only rapidly but also accurately carry out the dimensions of defects in multilayered structures.

This paper presents a general robust procedure for estimating dimensions of defects in multilayered structures from EC signals. Here, a novel EC testing technique with a giant magnetoresistive (GMR) sensor is used to enhance the sensitivity and spatial resolution of the measurement [20]. Since electromagnetic sensor based on GMR effect is sensitive to the magnitude of the magnetic field, the GMR-based EC probe can perform better than the conventional probe for low-frequency applications, that is, when detecting defects deeply buried in multilayered structures. During scanning inspection, eddy currents are induced in multilayered structures as a result of the application of an alternating magnetic field. In the presence of defects, the output voltage variation of the sensor is usually detected as the magnitude perturbations of the magnetic field. This special property of the GMR sensor will lead to a simplified signal conditioning circuit. Theoretically, there is a relationship between defect dimensions and GMR sensor response. In practice, however, this relationship is influenced by noises and many other factors. Therefore, the original signals are preprocessed by wavelet packet analysis (WPA) for noise elimination [21]. Then, two approaches are proposed to find the relationship between defect dimensions and GMR sensor's output voltage, respectively. The first one is a partial least squares (PLS) regression method [22, 23]. The second approach consists in generalizing the kernel method into PLS (kernel partial least squares KPLS) regression [24, 25]. In the second method, the original inputs are mapped into a high-dimensional space using a kernel method. The PLS regression is calculated in the high-dimensional space. Then, we will obtain a nonlinear regression model in the original input space. Finally, the estimation results are given using two methods and compared with those of the ANN method, in terms of estimation accuracy, generalization capability, and robustness, respectively. The ANN approach is employed in ECNDE in order to perform a nonlinear statistical regression. It is very simple and used as a benchmark for the proposed two quantitative evaluation methods. Experimental results show that the proposed two methods present further advances including good generalization capability, robustness of the results, avoidance of overfitting, and low computational burden.

The remainder of the paper is organized as follows. Section 2 gives the general formulation of the problem of dimension estimation of defects in multilayered structures. Section 3 briefly surveys signal denoising technique using the wavelet packet analysis (WPA) method. Section 4 describes two approaches used to estimate the defect dimensions. Section 5 presents the measurement system configuration and the experimental results. Finally, Section 6 contains conclusions.

2. Problem Description

The EC inverse problem here can be described as the task of quantitative estimating dimensions of defects in multilayered structures, where the measured EC signals are given and the unknown dimensions of defects require estimation [26]. During the probe moving over the defect, the output signal of the GMR sensor is produced, which is proportional to the

magnitude perturbations of the magnetic field. The sensor's output signal is

$$\mathbf{X} = K\dot{B}, \quad (1)$$

where $\mathbf{X} = (x_1, x_2, \dots, x_N)$ is the sensor's output voltage, N is the number of sample points during the scanning inspection, K is the proportionality coefficient, and \dot{B} is magnetic induction intensity. The unknown defect dimensions $\mathbf{Y} = (y_1, y_2, \dots, y_M)$ have to be estimated from a set of observed signals \mathbf{X} . M is the number of dimension variables. The relationship between GMR sensor's output voltage and defect dimensions can be given by the classical regression model:

$$\mathbf{Y} = f(\mathbf{X}, \boldsymbol{\theta}) + \mathbf{E}, \quad (2)$$

where function $f(\cdot)$ describes the relationship between defect dimensions and GMR sensor's output voltage, $\boldsymbol{\theta}$ is the unknown parameter vector, and \mathbf{E} is an error term. The parameter estimation techniques are needed to learn the unknown parameter vector $\boldsymbol{\theta}$ from the real experimental data which contain observations for the calibrated defects (defects with known dimensions). Then, we can construct the relationship $f(\cdot)$ using these parameters. Thus, a general inversion model is obtained. We can use this model to predict the defect dimensions given the acquired EC inspection signals.

Finally, to compare the accuracy and efficiency of the inversion models, several measures of a model's ability to fit data and predictive power are introduced [27]. All of these measures provide an estimate of the average deviation of the model from the data. The root mean square error (RMSE) of the residuals is defined as

$$\text{RMSE} = \sqrt{\frac{\sum_{i=1}^n (\mathbf{Y}_i - \hat{\mathbf{Y}}_i)^2}{n}}, \quad (3)$$

where \mathbf{Y}_i is the actual value, $\hat{\mathbf{Y}}_i$ is the predicted value, and n is the total number of samples. The RMSE is termed the root mean square error in calibration (RMSEC) for the training (calibration) set and the root mean square error in prediction (RMSEP) for the testing set.

Another measure of the model fit to the training data is the coefficient of determination R^2 , defined as

$$R^2 = 1 - \frac{\text{RSS}}{\text{SS}}, \quad (4)$$

where RSS is the residual sum of squares and SS is the sum of squares of the response variable \mathbf{Y} corrected for the mean. The R^2 indicates the strength of statistical correlation between actual values and predicted values for the model. A model fits the data perfectly if a value of R^2 is higher than 0.9. R^2 between 0.8 and 0.9 indicates that the model fits the data well. R^2 between 0.6 and 0.8 is considered a useful representation of the data, whereas R^2 between 0.5 and 0.6 indicates a poor representation of the data.

The same test can be used for the values predicted from the testing set, Q^2 . Consider

$$Q^2 = 1 - \frac{\text{PRESS}}{\text{SS}}, \quad (5)$$

where PRESS is the prediction error sum of squares and SS is the sum of squares of the response variable \mathbf{Y} corrected for the mean. The Q^2 indicates how well the model predicts new data. Usually, R^2 for a training set is larger than Q^2 for a testing set, since calibration models can easily lead to overfitting of the data. A large Q^2 ($Q^2 > 0.5$) indicates the good predictive ability.

3. Signal Preprocessing

In the process of EC inspection, the GMR sensor's output signals may be corrupted by noises and other artificial signals, arising from lift-off, edge effects, high frequency, probe angle variations, and so forth, resulting in unreliable detection and inaccurate characterization of defect dimensions. In order to remove the influence of noise and extract the amplitude of the main components from the measurements, a number of preprocessing steps are required before the defect dimension estimation is possible [21].

WPA [28, 29] has proved its great capabilities in decomposing, denoising, and signal analysis, which makes the analysis of nonstationary signals achievable as well as detecting transient feature components, since wavelet can concurrently impart time and frequency structures. In wavelet packet framework, wavelet packets offer a more complex and flexible analysis, because, in WPA, the details as well as the approximations are split. Before denoising, the GMR sensor's output signals are processed by normalizing so that they have means of zero and standard deviations of 1. Then, the WPA denoising procedure is implemented as in the following four steps.

- (1) Decomposition: for a given wavelet, compute the wavelet packet decomposition of signal $f(t)$ at level m .
- (2) Computation of the best tree: for a given entropy, compute the optimal wavelet packet tree. Of course, this step is optional.
- (3) Threshold of wavelet packet coefficients: for each packet (except for the approximation), select a threshold and apply it to coefficients. In general, the threshold will be refined by trial and error so as to optimize the results to fit particular analysis and design criteria.
- (4) Reconstruction: compute wavelet packet reconstruction based on the original approximation coefficients at level m and the modified coefficients.

In this paper, the mother wavelet chosen for simplifying the implementation is the Daubechies 4 wavelet due to the nonsymmetric shape of its wavelet function, which is the best adjustable to the transient nature of EC inspection signals. Using the signal to noise ratio (SNR) and RMSE as a criterion, the WPA denoising effect comparison using a real signal from the scanning inspection of a subsurface rectangular defect (length 5 mm, width 1 mm, height 1 mm, and depth 4 mm) in an aluminum sample is shown in Table 1. The results show that the WPA method with Shannon entropy threshold is superior for EC signal denoising. Figure 1 shows the performance of the WPA denoising method with Shannon entropy threshold using the same signal and the comparison

TABLE 1: De-noising effect comparison of different WPA methods.

Threshold rules	Shannon	Norm	Energy	Thre
SNR (db)	52.822	49.211	49.985	47.938
RMSE	0.00203	0.00271	0.00253	0.00323

with that of the mean filtering algorithm. In mean filtering algorithm denoising, the SNR and RMSE of the same signal calculated are 32.676 db and 0.01167, respectively. The signal denoising effect using the WPA method is significantly better than the use of mean filtering algorithm.

4. Defect Dimension Estimation Approaches

4.1. Partial Least Squares Regression. PLS regression [22, 23] is a wide class of methods for modeling relationships between sets of observed variables by means of latent variables (components and score vectors). It was first introduced by the Herman Wold and gained popularity in chemometrics research and later industrial applications [30]. In ECNDE, the samples are often difficult to obtain for constructing the inversion model. PLS regression has the advantage of allowing more variables than samples in the data and dealing in a natural way with collinearity. In this case, the solution of the classical least squares method does not exist or is unstable and unreliable. Furthermore, PLS regression allows graphical display of the latent variable space in terms of plots and also interactive diagnostic exploration of the data. Unlike the principal component regression method, PLS regression chooses the latent variables in such a way as to provide maximum correlation with dependent variables. Thus, PLS model contains the smallest necessary number of latent variables. These special properties make the PLS approach more appropriate for modeling the ECNDE inverse problem [31].

In the estimation of defect dimensions, PLS regression is used to find the fundamental relationship between two matrices, \mathbf{X} and \mathbf{Y} . Denote by $\mathbf{X} \in \mathbb{R}^N$ an N -dimensional space of variables representing the GMR sensor's output voltage and similarly by $\mathbf{Y} \in \mathbb{R}^M$ an M -dimensional space representing the defect dimensions. After observing n samples from each block of variables, the PLS decomposes the $(n \times N)$ matrix of variables \mathbf{X} and the $(n \times M)$ matrix of variables \mathbf{Y} into the forms

$$\begin{aligned} \mathbf{X} &= \mathbf{U}\mathbf{P}^T + \mathbf{E}, \\ \mathbf{Y} &= \mathbf{V}\mathbf{Q}^T + \mathbf{F}, \end{aligned} \quad (6)$$

where \mathbf{U} and \mathbf{V} are $(n \times p)$ matrices of the p extracted latent vectors, the $(N \times p)$ matrix \mathbf{P} and the $(M \times p)$ matrix \mathbf{Q} represent matrices of loadings, the $(n \times N)$ matrix \mathbf{E} and the $(n \times M)$ matrix \mathbf{F} are the matrices of residuals, and the superscript T denotes the transpose of matrix. The nonlinear iterative PLS algorithm is implemented as follows [31].

Step 1. Randomly initialize \mathbf{v} as any column of \mathbf{Y} .

Step 2. Let $\mathbf{w} = \mathbf{X}^T \mathbf{v}$.

Step 3. Let $\mathbf{u} = \mathbf{X}\mathbf{w}$, $\mathbf{u} \leftarrow \mathbf{u}/\|\mathbf{u}\|$.

Step 4. Let $\mathbf{c} = \mathbf{Y}^T \mathbf{u}$.

Step 5. Let $\mathbf{v} = \mathbf{Y}\mathbf{c}$, $\mathbf{v} \leftarrow \mathbf{v}/\|\mathbf{v}\|$.

Step 6. Iterate Step 2~Step 5 until convergence or the maximum number of iterations is reached.

Step 7. Calculate the deflation of \mathbf{X} and \mathbf{Y} matrices: $\mathbf{X} \leftarrow \mathbf{X} - \mathbf{u}\mathbf{u}^T \mathbf{X}$, $\mathbf{Y} \leftarrow \mathbf{Y} - \mathbf{u}\mathbf{u}^T \mathbf{Y}$.

Step 8. Go to Step 1 to calculate the next latent variable.

Note that a minor difference of this algorithm from the classical PLS algorithm is that the modified PLS algorithm normalizes the latent vectors \mathbf{u} , \mathbf{v} rather than the weight vectors \mathbf{w} and \mathbf{c} . After the extraction of the p latent vectors, we can create the $(n \times p)$ matrices \mathbf{U} and \mathbf{V} , the $(N \times p)$ matrix \mathbf{W} , and the $(L \times p)$ matrix \mathbf{C} consisting of the columns created by the vectors $\{\mathbf{u}_i\}_{i=1}^p$, $\{\mathbf{v}_i\}_{i=1}^p$, $\{\mathbf{w}_i\}_{i=1}^p$ and $\{\mathbf{c}_i\}_{i=1}^p$, respectively, extracted during the individual iterations. The PLS regression model can be expressed with regression coefficient \mathbf{B} and residual matrix \mathbf{R} as follows:

$$\mathbf{Y} = \mathbf{X}\mathbf{B} + \mathbf{R}, \quad (7)$$

$$\mathbf{B} = \mathbf{X}^T \mathbf{V} (\mathbf{U}^T \mathbf{X} \mathbf{X}^T \mathbf{V})^{-1} \mathbf{U}^T \mathbf{Y}.$$

To avoid overfitting the training data and obtain a model with good predictive ability, in practice, the selection of the optimal number of PLS components is needed to be carried out. The optimum number of components is usually determined via cross-validation [32]. The cross-validation is often performed on the calibration samples, which has become the standard in PLS regression analysis. During the cross-validation, the model increases one PLS component until the prediction on the calibration samples shows that further PLS components do not improve predictive ability. In this work, the cross-validation is performed by leaving out one sample at a time. In leave-one-out cross-validation, the prediction error sum of squares (PRESS) and the residual sum of squares (SS) are computed and collected. The ratio $\text{PRESS}_h/\text{SS}_{h-1}$ is calculated after each component, and a component is judged to be significant if this ratio is smaller than around 0.95^2 . This is often reexpressed as $Q_h^2 = 1 - \text{PRESS}_h/\text{SS}_{h-1} \geq (1 - 0.95^2) = 0.0975$ for all \mathbf{Y} -variables. Here h is the number of components used in a PLS model.

4.2. Kernel Partial Least Squares Regression. Recently, Kernel methods have become an increasingly popular tool for machine learning tasks such as classification, regression, and novelty detection. The notion of kernels has drawn much interest as it allows one to obtain nonlinear algorithms from linear ones. The attractiveness of such algorithms stems from their efficiency in high-dimensional nonlinear problems and their easy implementation because there are few free parameters to adjust, and the architecture does not need to be found

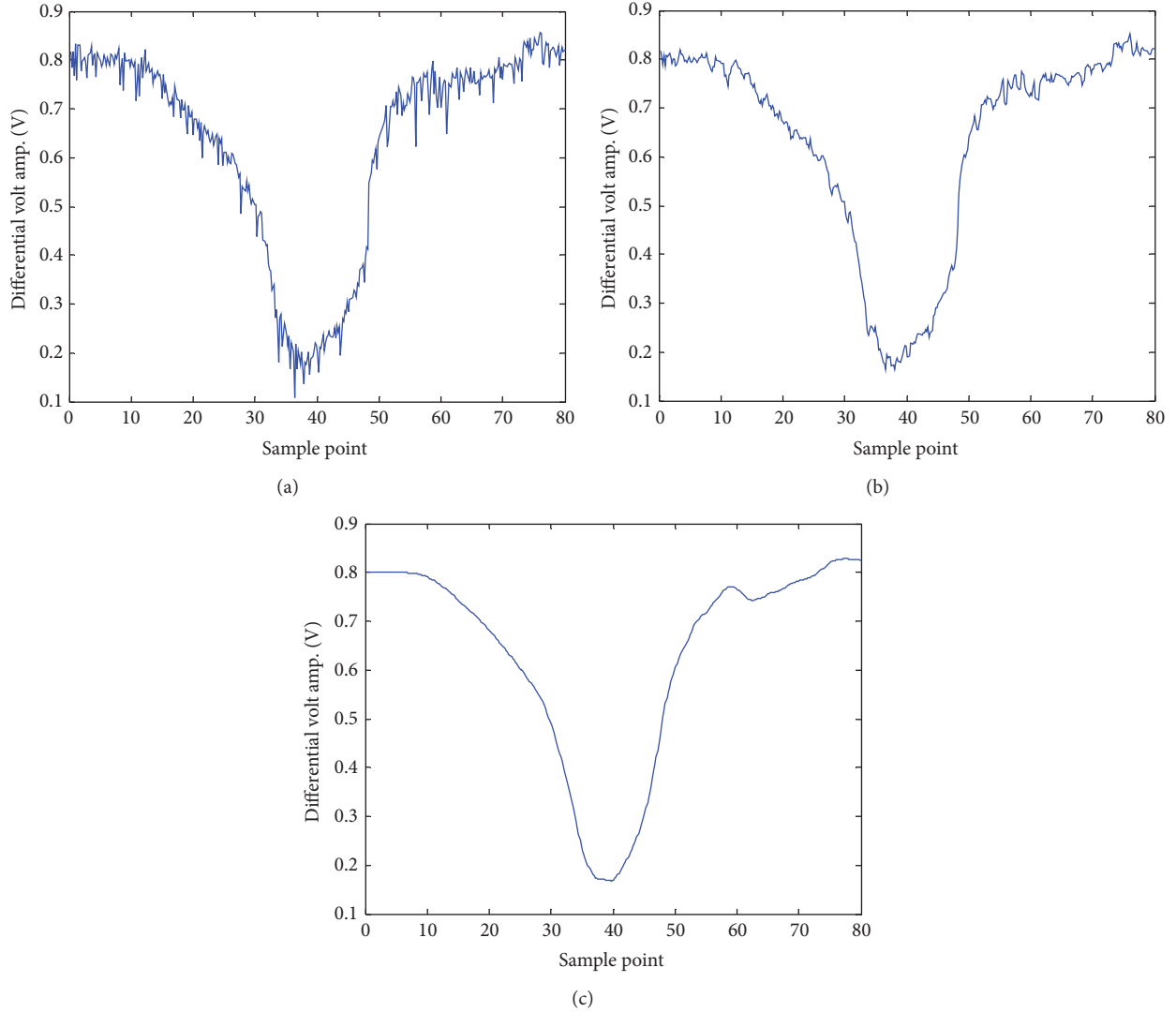


FIGURE 1: The comparison of denoising performance: (a) the original EC signal, (b) the output of denoising using the mean filtering algorithm, and (c) the output of denoising using the WPA method.

by experimentation [33]. It is well known that the estimation of defect dimensions from EC signals is an important aspect of the ECNDE inverse problem which is often nonlinear in realistic inspection. The defect dimension estimation procedures can benefit from a kernel perspective, making them more powerful and applicable to nonlinear processing.

KPLS regression [24, 25] is one type of nonlinear PLS regression developed by generalizing the kernel method into the PLS regression. It can be used to model nonlinear EC data relations. The KPLS regression is presented by Rosipal and Trejo [24]. Specifically, it firstly maps the original inputs into a high-dimensional feature space using the kernel method and then calculates the PLS regression in the high-dimensional feature space to find the fundamental relationships between two matrices (\mathbf{X} and \mathbf{Y}). Thus, it means that we can obtain a nonlinear regression model in the space of the original input variables [25].

Now, consider a nonlinear transformation of \mathbf{X} into a feature space F :

$$\mathbf{X} \in R^N \longrightarrow \phi(\mathbf{X}) \in F, \quad (8)$$

where $\phi(\cdot)$ is a nonlinear mapping function that projects the input vectors from the input space to F and $\sum_{i=1}^N \phi(x_i) = 0$. Denote by ϕ the $(n \times S)$ matrix whose i th row is the vector $\phi(\mathbf{X}_i)$ in an S -dimensional feature space F . The KPLS algorithm directly derived from the PLS algorithm is shown as follows.

Step 1. Randomly initialize \mathbf{v} as any column of \mathbf{Y} .

Step 2. Let $\mathbf{u} = \phi\phi^T \mathbf{v} = \mathbf{Kv}$, $\mathbf{u} \leftarrow \mathbf{u}/\|\mathbf{u}\|$.

Step 3. Let $\mathbf{c} = \mathbf{Y}^T \mathbf{u}$.

Step 4. Let $\mathbf{v} = \mathbf{Y}\mathbf{c}$, $\mathbf{v} \leftarrow \mathbf{v}/\|\mathbf{v}\|$.

Step 5. Iterate Step 2~Step 4 until convergence or the maximum number of iterations is reached.

Step 6. Calculate the deflation of \mathbf{K} and \mathbf{Y} matrices: $\mathbf{K} \leftarrow (\mathbf{I} - \mathbf{u}\mathbf{u}^T)\mathbf{K}(\mathbf{I} - \mathbf{u}\mathbf{u}^T)$, $\mathbf{Y} \leftarrow \mathbf{Y} - \mathbf{u}\mathbf{u}^T\mathbf{Y}$.

Step 7. Go to Step 1 to calculate the next latent variable.

Note that \mathbf{K} is the kernel matrix and $\phi\phi^T$ represents the $(n \times n)$ kernel matrix \mathbf{K} of the inner dot products between all mapped input data points $\phi(\mathbf{X}_i)$, $i = 1, \dots, n$. That is, $\mathbf{K}(\mathbf{X}_i, \mathbf{X}_j) = \phi(\mathbf{X}_i) \cdot \phi(\mathbf{X}_j)$. As the calculations of the dot product $\phi(\mathbf{X}_i) \cdot \phi(\mathbf{X}_j)$ are all replaced with the kernel function $\mathbf{K}(\mathbf{X}_i, \mathbf{X}_j)$, the mapping of $\phi(\mathbf{X}_i)$ from \mathbf{X}_i is implicit. The elegance of using \mathbf{K} is that one can deal with $\phi(\mathbf{X}_i)$ of arbitrary dimensionality without having to compute $\phi(\mathbf{X}_i)$ explicitly. The matrix of regression coefficient \mathbf{B} in the KPLS algorithm will have the form

$$\mathbf{B} = \phi^T \mathbf{V} (\mathbf{U}^T \mathbf{K} \mathbf{V})^{-1} \mathbf{U}^T \mathbf{Y}. \quad (9)$$

As a result, the predictions on training subset and testing subset can be made as follows, respectively:

$$\begin{aligned} \hat{\mathbf{Y}} &= \phi \mathbf{B} = \mathbf{K} \mathbf{V} (\mathbf{U}^T \mathbf{K} \mathbf{V})^{-1} \mathbf{U}^T \mathbf{Y}, \\ \hat{\mathbf{Y}}_t &= \phi_t \mathbf{B} = \mathbf{K}_t \mathbf{V} (\mathbf{U}^T \mathbf{K} \mathbf{V})^{-1} \mathbf{U}^T \mathbf{Y}, \end{aligned} \quad (10)$$

where ϕ_t is the mapped matrix of the testing subset and \mathbf{K}_t is the corresponding kernel matrix. Note that both \mathbf{K} and \mathbf{K}_t should also be mean-centered in feature space before applying (10).

In KPLS, just like other kernel methods, any function satisfying Mercer's condition can be used as the kernel function. Two typical kernel functions are listed below:

$$\begin{aligned} \text{Polynomial: } \mathbf{K}(\mathbf{X}_i, \mathbf{X}_j) &= (\mathbf{X}_i \cdot \mathbf{X}_j + 1)^d, \\ \text{Radial Basis Function: } \mathbf{K}(\mathbf{X}_i, \mathbf{X}_j) &= \exp\left(\frac{-\|\mathbf{X}_i - \mathbf{X}_j\|^2}{2\sigma^2}\right). \end{aligned} \quad (11)$$

Finally, the cross-validation technique is similarly applied to select the appropriate components which will help avoid overfitting caused by the use of too large dimensional models.

5. Experiments and Results

5.1. Measurement System Configuration. The automatic system based on ECNDE for estimating dimensions of defects in multilayered structures is obtained by integrating the test device with a computer. A block scheme of the system is shown in Figure 2. The system consists of a few main components: an AC excitation generator, two eddy current probes (an inspecting probe and a reference probe), a low pass filter, a data acquisition interface (A/D converter), a

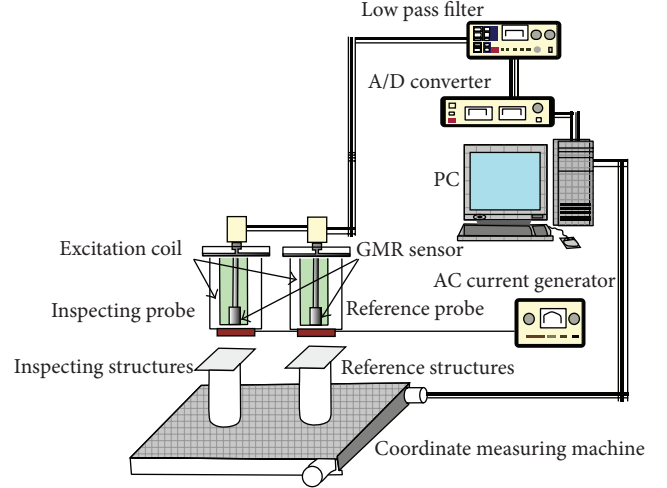


FIGURE 2: Schematic view of an automatic ECNDE system.

coordinate measuring machine (CMM), and a computer. The sinusoidal current source provides current through coils with amplitude 1 A at a frequency 200 Hz. In the system the right-cylindrical air-cored coil probe has been used. The coil parameters are inner radius $r_1 = 3$ mm, outer radius $r_2 = 4.5$ mm, length $l = 20$ mm, and lift-off = 0.5 mm. The probes consist of exciting coils and GMR sensors. The basic AA-Series GMR sensors from Nonvolatile Electronics, Inc. (NVE) are general-purpose magnetometers for use in a wide variety of ECNDE applications. In all subsequent experiments, the AA002-02 GMR sensor is used, due to its' excellent linearity, high sensitivity and resolution, stable and linear temperature characteristics, and a purely ratiometric output. The probes are scanned over the surface of the specimen by using a CMM. A computer program is used to set the scan area and velocity. During measurements, the sensing axis of the GMR sensor is directed orthogonally to the magnetic field generated by the coil. The GMR sensor's output signals are amplified by a low cost, high accuracy instrumentation amplifier AD620. Then, the amplified signals are filtered by a second-order low pass filter with a cutoff frequency of 20 Hz. A data acquisition program written in Labview collects the data from the output of the filter via a National Instrument DAQPad 6016 16×6 bit analog-to-digital converter. The computer is controlling the whole system and performing such tasks as automating the process of inspection, data acquisition and displaying, and applying some signal processing techniques to automate the process of defect detection and quantification. The computer-based system can thus increase the reliability of the detection and enhance the performance of EC inspection of complex engineering structures by avoiding errors related to human factors such as inexperience and inconsistency. It also offers fast and robust database methods for retrieving old inspection data, which is important in monitoring defect initiation and growth. In the system, reference structures and a reference probe have been used. By comparing the signals from the reference structures with those from the monitored special

structures, the system can easily make a decision on structure conditions and usage states.

5.2. Experimental Results. To verify the feasibility of the proposed EC inversion models for estimating dimensions of defects in multilayered structures, comparative experiments are carried out. Detection of deeply buried defects in multilayered airframe joints is widely recognized as an urgent and difficult NDE problem [34]. Multilayered samples resembling a part of the projected wing splice of the aircraft are analyzed. We assume that the shape and position of defects are known in advance. Therefore, this paper mainly discusses the inversion problem of estimating dimensions of defects in multilayered structures to simulate the quantification of internal cracks, corrosions, and local interlayer air gaps in real structures.

The experimental specimen is shown schematically in Figure 3. The specimen consists of three layers of aluminum with a total thickness of 10 mm (2.5, 5, 2.5 mm), electrical conductivity $\sigma = 18.5 \times 10^6$ S/m, magnetic permeability $\mu = \mu_0 = 4\pi \times 10^{-7}$ H/m, length $l = 200$ mm, and width $w = 120$ mm. The layers are bolted together with 5 mm diameter Titanium bolts, whose upper part is conically shaped having a diameter of 8 mm at the surface of the specimen. The second layer contains an exchangeable sheet, in which calibrated rectangular defects with different dimensions have been introduced in the center of the plate. The set of defects are of height 1 mm, five depth values varying from 2.5 mm to 6.5 mm, four length values varying from 1 mm to 4 mm, and four width values varying from 1 mm to 4 mm with step 1 mm. A dataset with 80 records is acquired during the scanning. Of the overall 80 samples, we randomly extract 50 samples and use them as the training (calibration) set. The remaining 30 samples are used as the validation set for testing the model. To ensure a fair comparison, the same calibration and validation sets are used for each model. The skin depth $\delta = (\sqrt{\pi f \mu \sigma})^{-1}$ is equal to about 8.28 mm and indicates promising robustness of inspection of all inner defects in the multilayered structures.

The data set is denoised by the WPA method. After the signals are denoised, all the data are mean-centered and scaled to unit variance before modeling. Then, the presented approaches are implemented to construct the inversion models for estimating dimensions of defects, respectively.

Firstly, the PLS regression method is used to construct the calibration model of defect dimension estimation. The PLS components are computed as certain linear combinations of the measured GMR sensor's output signals. The optimal number of PLS components is determined by implementing leave-one-out cross-validation. In cross-validation, the Q_h^2 of each component of the PLS regression calibration model is illustrated in Figure 4. It shows that the model has seven significant components. This gives a strong indication that seven PLS components are appropriate for modeling. Then, the corresponding defect dimensions are predicted linearly based on these extracted components. Thus, the final predictive function is also a linear combination of the measured GMR sensor's output signals. Figure 5 shows the model overview plot of the cumulative R^2 , the fraction of the variation of Y (all

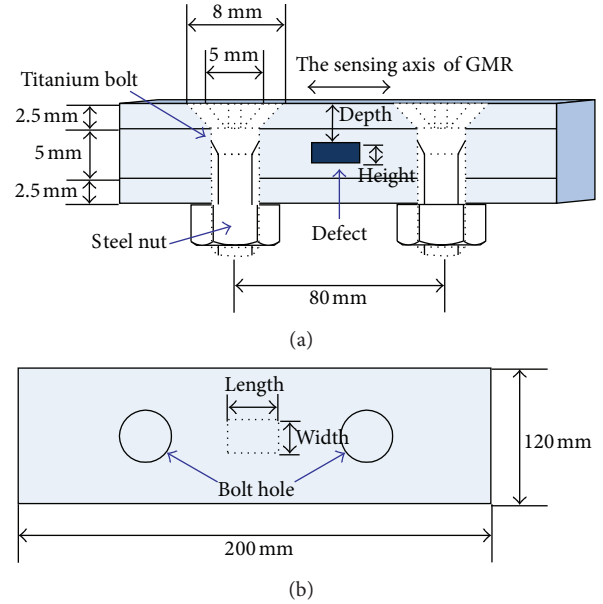


FIGURE 3: The sketch of an experimental aircraft multilayered structure: (a) cutaway view of the whole structure; (b) vertical view of the second layer.

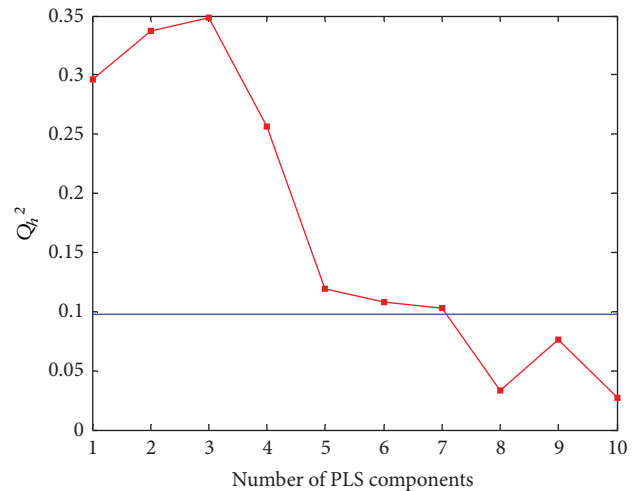


FIGURE 4: The Q_h^2 of each component of the PLS regression model.

the responses) explained by the model after each component from the training set, and the cumulative Q^2 , the fraction of the variation of Y (all the responses) that can be predicted by the model after each component from the testing set. Values of the cumulative R^2 and Q^2 are higher than 0.8, which indicates the model is appropriate.

Secondly, the KPLS regression method is used to construct the calibration model of defect dimension estimation. In KPLS regression, a radial basis kernel is employed as the kernel function. The same leave-one-out cross-validation procedure is implemented to choose the optimal number of KPLS components. Figure 6 shows the Q_h^2 of each component of the KPLS regression calibration model. From

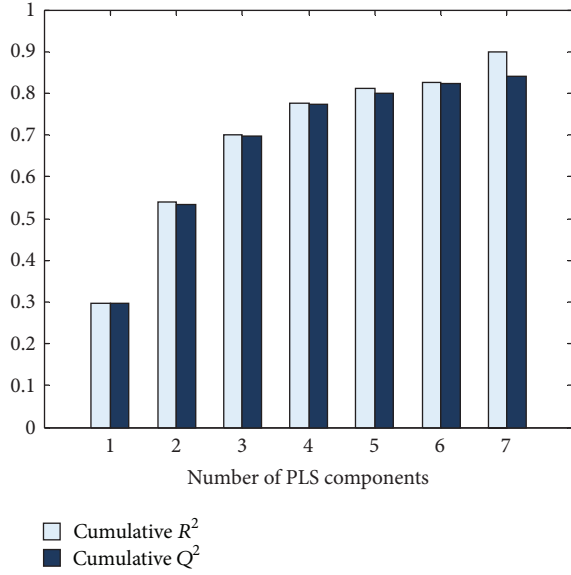
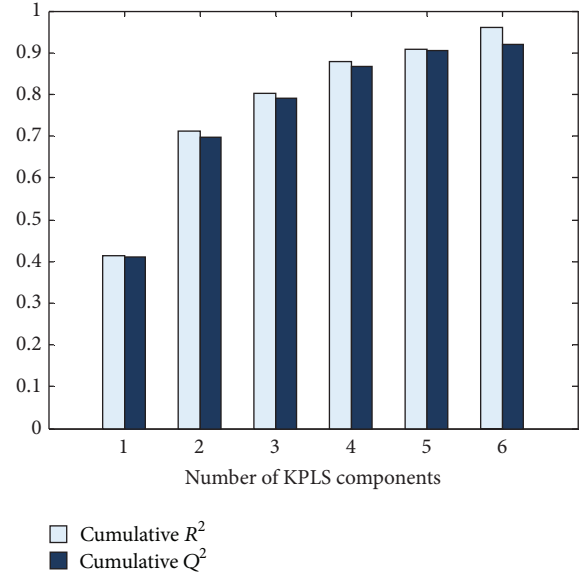
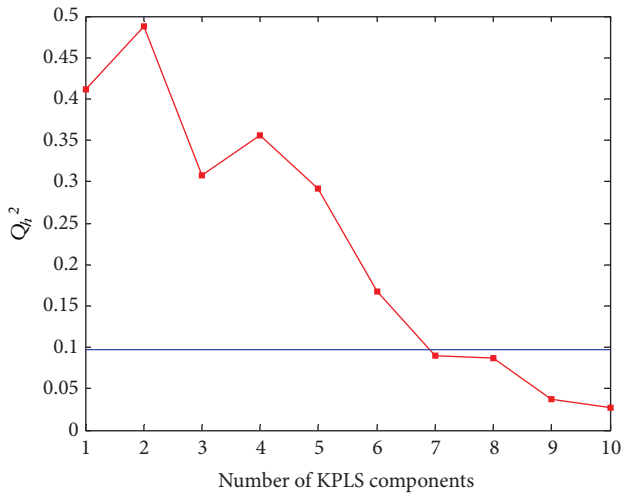
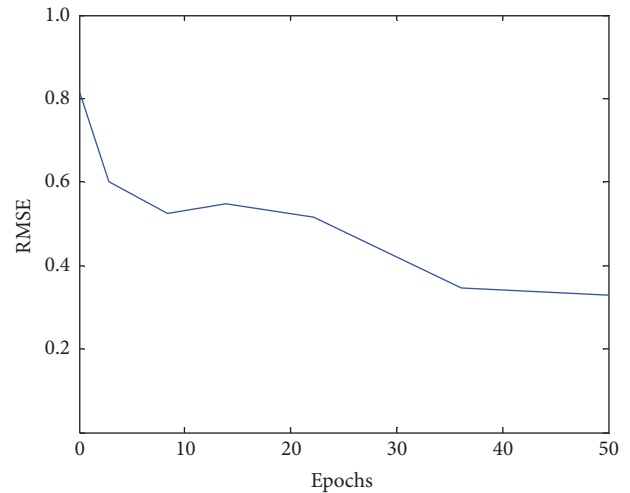
FIGURE 5: The cumulative R^2 and Q^2 of the PLS regression model.FIGURE 7: The cumulative R^2 and Q^2 of the KPLS regression model.FIGURE 6: The Q_h^2 of each component of the KPLS regression model.

FIGURE 8: The training curve of ANN.

Figure 6, we can see that the model only has six significant components. Figure 7 shows the model overview plot of the cumulative R^2 and Q^2 . Values of the cumulative R^2 and Q^2 are close to 1.0, which indicates that the model is an excellent model.

In addition, in the experiments' tests, a performance comparison between the proposed two methods and the ANN method is carried out. We use a feed-forward neural network with one hidden layer containing 12 neurons. The number of neurons of input layer and output layer is dependent upon the dimensions of X (GMR sensor's output voltage) and Y (defect dimensions), respectively. Then, the training data subset is used for updating the network weight and bias. During training, the error is evaluated in terms of RMSE. The training curve of ANN is shown in Figure 8. Error with respect to the testing data subset is not monitored during

training but is quantified to assess the final performance of the trained ANN model.

Finally, to compare the prediction qualities of the three approaches, Figure 9 plots the estimated values obtained from the three approaches against the actual values of defect dimensions of the testing set. The main results obtained from the three inversion models for the training set and the testing set are summarized in Table 2.

From Figure 9 and Table 2, it can be seen that the proposed two methods can gain a better prediction performance than the ANN method. The defect dimension estimation from the proposed two inversion models is more accurate and robust. Among three inversion models, the ANN model gives better prediction results for the training set than those for the testing set, indicating that the ANN model can easily lead to overfitting of the training data and will give

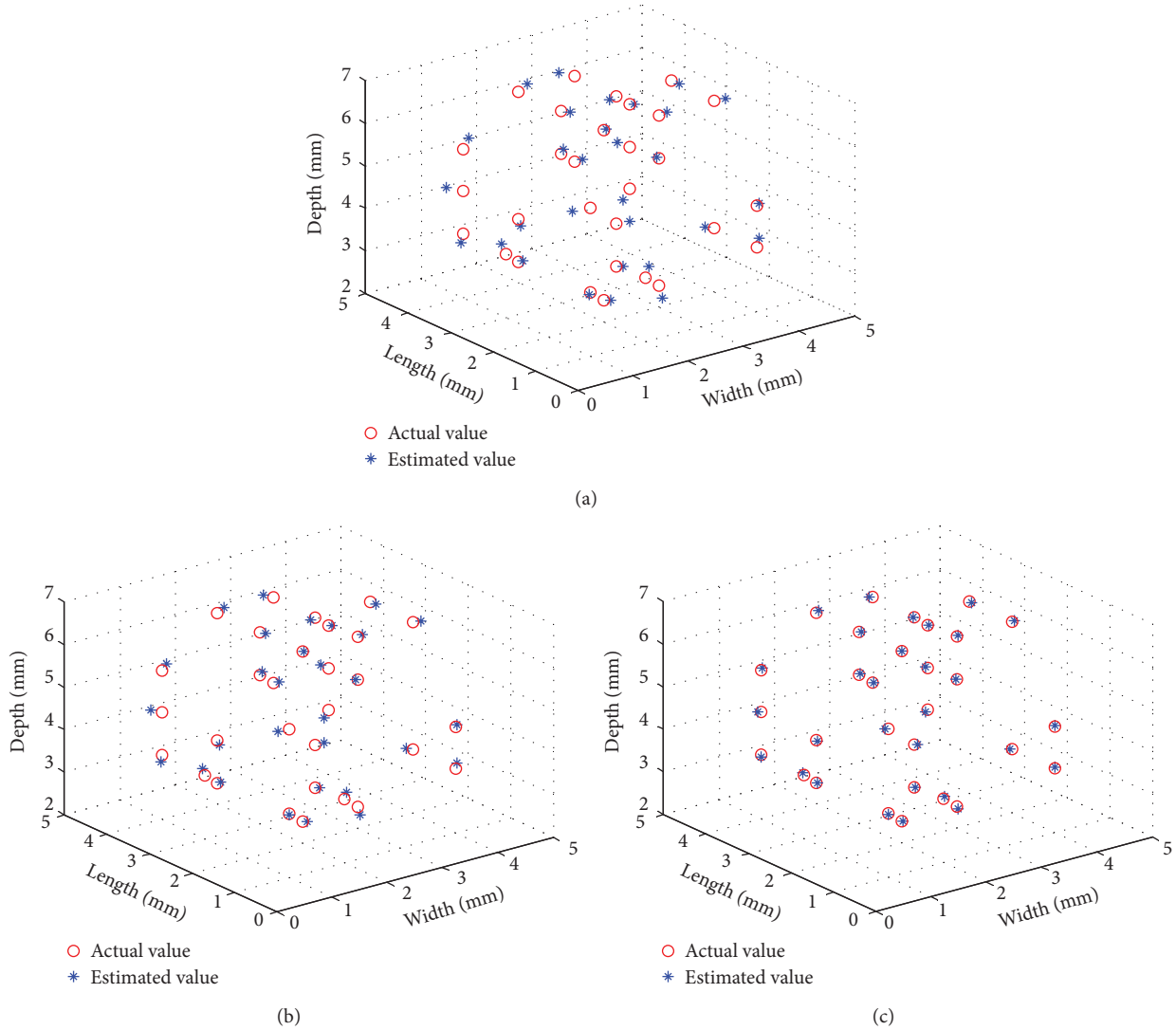


FIGURE 9: Scatter plots of the actual values versus the estimated values of defect dimensions of the testing set: (a) the ANN method, (b) the PLS regression method, and (c) the KPLS regression method.

obvious errors when the samples have never been contained in the training set. In the PLS regression model, the optimal number of PLS components selected by implementing the cross-validation procedure simplifies the PLS model and enhances the predictive ability of the model. Despite the fact that the PLS model shows a slightly lower fitting of the training data, it has a better prediction ability than the ANN model. Compared to the PLS regression model, the KPLS regression model needs less number of components selected to construct the calibration model, which make the complexity of the model further reduced. When the KPLS regression is used to approximate the model, R^2 and Q^2 are greatly increased, and RMSEC and RMSEP are reduced. The increased prediction performance of the KPLS regression model could be explained by the fact that the ECNDE is an inherently nonlinear process and the KPLS model could capture the nonlinearities in the original data space benefiting from the linear data structure in the feature space. This special

property of the KPLS regression may be considered as a more proper way to interpret the nonlinear and nonstationary ECNDE signals.

6. Conclusions

In this study, two EC inversion models for estimating dimensions of defects in multilayered structures are proposed and investigated. The WPA denoising method removes the influence of noise and information not correlated to the target parameter, which effectively improves the performance of the proposed approaches when using time-domain signals. Then, the PLS regression and KPLS regression inversion models are constructed to estimate defect dimensions, respectively. The PLS regression provides an approach to the quantitative modeling for estimating defect dimensions, where the correlation structure of the acquired EC inspection data is considered. The cross-validation is implemented to choose the optimal

TABLE 2: Main results obtained with the ANN, PLS regression and KPLS regression methods.

Data sets			ANN	PLS	KPLS
Training set	Length	R^2	0.915	0.911	0.986
		RMSEC	0.316	0.323	0.128
	Width	R^2	0.907	0.887	0.931
		RMSEC	0.338	0.372	0.291
	Depth	R^2	0.929	0.902	0.966
		RMSEC	0.381	0.448	0.264
Testing set	Length	Q^2	0.705	0.858	0.953
		RMSEP	0.598	0.412	0.235
	Width	Q^2	0.691	0.821	0.894
		RMSEP	0.611	0.471	0.358
	Depth	Q^2	0.712	0.841	0.916
		RMSEP	0.618	0.573	0.415

number of PLS components to obtain a model with the appropriate complexity and good predictive ability. The KPLS regression is one type of nonlinear PLS regression. Compared with other nonlinear methods, the KPLS regression has the advantage that it does not require a nonlinear optimization procedure. It involves calculations as simple as those used for the PLS regression. At the same time, in comparison to the PLS regression, the KPLS regression uses a smaller number of components.

To test the proposed two inversion models, a strict experiment has been carried out. Two approaches are compared with the ANN method in terms of model's ability to fit data, predictive accuracy, and robustness. Experimental results show that the proposed two approaches can provide better estimation performance than the conventional approaches (the ANN method) in aspects of estimation accuracy, generalization capability, robustness, and computational burden. The results demonstrate the feasibility and effectivity of the proposed two inversion models. They all give the accurate estimation of dimensions of defects in multilayered structures. Between them, the KPLS gives a better prediction performance. The algorithms' capability of quantitative evaluation of defects in multilayered structures is fairly general and fruitful, as this encourages the attempts to tackle the problem of other evaluation problems. In fact, it is necessary to note that, in this paper, we assume that the shape and position of defects are known in advance. However, in most real industrial environments, this hypothesis is not always met. We usually do not know the shape and position of defects in advance. Moreover, in the real ECNDE problems, defects to be detected are usually smaller than the ones considered in the experiments and the shape of defects is very abnormal. Future work, hopefully, will be done to extend the proposed methods to the more complex ECNDE problems where the kind of defect is more general and the smaller abnormal defects are considered.

Conflict of Interests

The authors declare that there is no conflict of interests regarding the publication of this paper.

Acknowledgments

This work is supported by the National Natural Science Foundation of China Grant nos. 51105183 and 51307172, the Research Fund for the Doctoral Program of Higher Education of China Grant no. 20115314120003, the Applied Basic Research Programs of Science and Technology Commission Foundation of Yunnan Province of China Grant no. 2010ZC050, the Foundation of Yunnan Educational Committee Grant no. 2013Z121, the National College Student Innovation Training Program Funded Projects Grant no. 201210674014, and the Science and Technology Project of Yunnan Power Grid Corporation Grant no. K-YN2013-110.

References

- [1] A. L. Jones and K. F. Pezdirtz, "Nondestructive eddy current testing," *IEEE Transactions on Instrumentation and Measurement*, vol. 21, no. 1, pp. 11–15, 1972.
- [2] H. Zhang, H. C. Yan, F. W. Yang, and Q. J. Chen, "Quantized control design for impulsive fuzzy networked systems," *IEEE Transactions on Fuzzy Systems*, vol. 19, no. 6, pp. 1153–1162, 2011.
- [3] H. Zhang, H. C. Yan, F. W. Yang, and Q. J. Chen, "Distributed average filtering for sensor networks with sensor saturation," *IET Control Theory & Applications*, vol. 7, no. 6, pp. 887–893, 2013.
- [4] B. A. Auld and J. C. Moulder, "Review of advances in quantitative eddy current nondestructive evaluation," *Journal of Nondestructive Evaluation*, vol. 18, no. 1, pp. 3–36, 1999.
- [5] H. C. Yan, Z. Z. Su, H. Zhang, and F. W. Yang, "Observer-based H-infinity control for discrete-time stochastic systems with quantization and random communication delays," *IET Control Theory & Applications*, vol. 7, no. 3, pp. 372–379, 2013.
- [6] H. L. Libby, *Introduction To Electromagnetic Nondestructive Test Methods*, John Wiley & Sons, New York, NY, USA, 1971.
- [7] A. M. Armour, "Eddy current and electrical methods of crack detection," *Journal of Scientific Instruments*, vol. 25, no. 6, pp. 209–210, 1948.
- [8] W. Cheng, S. Kanemoto, I. Komura, and M. Shiwa, "Depth sizing of partial-contact stress corrosion cracks from ECT signals," *NDT & E International*, vol. 39, no. 5, pp. 374–383, 2006.
- [9] J. R. Bowler, "Review of eddy current inversion with application to nondestructive evaluation," *International Journal of Applied Electromagnetics and Mechanics*, vol. 8, no. 1, pp. 3–16, 1997.
- [10] H. C. Yan, H. B. Shi, H. Zhang, and F. W. Yang, "Quantized H-infinity control for networked delayed systems with communication constraints," *Asian Journal of Control*, vol. 5, no. 5, pp. 1468–1476, 2013.
- [11] H. J. Gao, T. W. Chen, and J. Lam, "A new delay system approach to network-based control," *Automatica*, vol. 44, no. 1, pp. 39–52, 2008.
- [12] L. X. Zhang, H. J. Gao, and O. Kaynak, "Network-induced constraints in networked control systems—a survey," *IEEE Transactions on Industrial Informatics*, vol. 9, no. 1, pp. 403–416, 2013.

- [13] R. C. Popa and K. Miya, "Approximate inverse mapping in ECT, based on aperture shifting and neural network regression," *Journal of Nondestructive Evaluation*, vol. 17, no. 4, pp. 209–221, 1998.
- [14] N. Yusa, W. Cheng, Z. Chen, and K. Miya, "Generalized neural network approach to eddy current inversion for real cracks," *NDT & E International*, vol. 35, no. 8, pp. 609–614, 2002.
- [15] M. Davoust, L. L. Brusquet, and G. Fleury, "Robust estimation of flaw dimensions using remote field eddy current inspection," *Measurement Science and Technology*, vol. 17, no. 11, pp. 3006–3014, 2006.
- [16] J. Rosa, G. Fleury, E. O. Sonia, and M. Davoust, "Markov chain Monte Carlo posterior density approximation for a groove-dimensioning purpose," *IEEE Transactions on Instrumentation and Measurement*, vol. 55, no. 1, pp. 112–122, 2006.
- [17] J. Rosa and G. Fleury, "Bootstrap methods for a measurement estimation problem," *IEEE Transactions on Instrumentation and Measurement*, vol. 55, no. 3, pp. 820–827, 2006.
- [18] K. Krzywosz, "Enhanced Id pit sizing using multivariate regression algorithm," *Review of Progress in Quantitative Nondestructive Evaluation*, vol. 26, pp. 741–748, 2007.
- [19] A. Bernieri, L. Ferrigno, M. Laracca, and M. Molinara, "Crack shape reconstruction in eddy current testing using machine learning systems for regression," *IEEE Transactions on Instrumentation and Measurement*, vol. 57, no. 9, pp. 1958–1968, 2008.
- [20] T. Dogaru and S. T. Smith, "Giant magnetoresistance-based eddy-current sensor," *IEEE Transactions on Magnetics*, vol. 37, no. 5, pp. 3831–3838, 2001.
- [21] F. C. Morabito, "Wavelet tools for improving the accuracy of neural network solution of electromagnetic inverse problems," *IEEE Transactions on Magnetics*, vol. 34, no. 5, pp. 2964–2967, 1998.
- [22] H. Wold, "Path models with latent variables: the NIPALS approach," in *Quantitative Sociology: International Perspectives on Mathematical and Statistical Modeling*, pp. 307–357, Academic, New York, NY, USA, 1975.
- [23] S. Wold, M. Sjöström, and L. Eriksson, "PLS-regression: a basic tool of chemometrics," in *Chemometrics and Intelligent Laboratory Systems*, vol. 58, pp. 109–130, 2001.
- [24] R. J. Rosipal and L. Trejo, "Kernel partial least squares regression in reproducing kernel Hilbert space," *Journal of Machine Learning Research*, vol. 2, no. 6, pp. 97–123, 2001.
- [25] K. Kim, J. M. Lee, and I.-B. Lee, "A novel multivariate regression approach based on kernel partial least squares with orthogonal signal correction," *Chemometrics and Intelligent Laboratory Systems*, vol. 79, no. 1-2, pp. 22–30, 2005.
- [26] S. Norton and J. R. Bowler, "Theory of eddy current inversion," *Journal of Applied Physics*, vol. 73, no. 2, pp. 501–512, 1993.
- [27] M. H. Kutner, C. J. Nachtsheim, and J. Neter, *Application Linear Regression Models*, McGraw-Hill, 4th edition, 2004.
- [28] Y. J. Chen, Y. W. Shi, and Y. P. Lei, "Use of a wavelet analysis technique for the enhancement of signal-to-noise ratio in ultrasonic NDE," *Insight: Non-Destructive Testing and Condition Monitoring*, vol. 38, no. 11, pp. 800–803, 1996.
- [29] I. Daubechies, S. Mallat, and A. S. Willsky, "Introduction to the special issue on wavelet transforms and multiresolution signal analysis," *IEEE Transactions on Information Theory*, vol. 38, pp. 529–532, 1992.
- [30] S. Wold, "Discussion: PLS in chemical practice," *Technometrics*, vol. 35, pp. 136–139, 1993.
- [31] S. Rännar, F. Lindgren, P. Geladi, and S. Wold, "A PLS kernel algorithm for data sets with many variables and fewer objects—part I: theory and algorithm," *Journal of Chemometrics*, vol. 8, pp. 111–125, 1994.
- [32] I. N. Wakeling and J. J. Morris, "A test of significance for partial least squares regression," *Journal of Chemometrics*, vol. 7, no. 4, pp. 291–304, 1993.
- [33] F. Pérez-Cruz and O. Bousquet, "Kernel methods and their potential use in signal processing," *IEEE Signal Processing Magazine*, vol. 21, no. 3, pp. 57–65, 2004.
- [34] T. Dogaru, C. H. Smith, R. W. Schneider, and S. T. Smith, "Deep crack detection around fastener holes in airplane multi-layered structures using GMR-based eddy current probes," *Review of Progress in Quantitative Nondestructive Evaluation*, vol. 23, pp. 398–405, 2004.

Research Article

A Local and Global Search Combined Particle Swarm Optimization Algorithm and Its Convergence Analysis

Weitian Lin,¹ Zhigang Lian,² Xingsheng Gu,¹ and Bin Jiao²

¹ Key Laboratory of Advanced Control and Optimization for Chemical Process, Ministry of Education, Shanghai 200237, China

² Shanghai Dianji University, Shanghai 201306, China

Correspondence should be addressed to Xingsheng Gu; xsgu@ecust.edu.cn

Received 4 December 2013; Accepted 6 February 2014; Published 16 March 2014

Academic Editor: Huaicheng Yan

Copyright © 2014 Weitian Lin et al. This is an open access article distributed under the Creative Commons Attribution License, which permits unrestricted use, distribution, and reproduction in any medium, provided the original work is properly cited.

Particle swarm optimization algorithm (PSOA) is an advantage optimization tool. However, it has a tendency to get stuck in a near optimal solution especially for middle and large size problems and it is difficult to improve solution accuracy by fine-tuning parameters. According to the insufficiency, this paper researches the local and global search combine particle swarm algorithm (LGSCPSOA), and its convergence and obtains its convergence qualification. At the same time, it is tested with a set of 8 benchmark continuous functions and compared their optimization results with original particle swarm algorithm (OPSOA). Experimental results indicate that the LGSCPSOA improves the search performance especially on the middle and large size benchmark functions significantly.

1. Introduction

Swarm intelligence (SI) techniques, including particle swarm optimization (PSO) and ant colony optimization (ACO), use swarm behavior to solve the problem, and they use the concept of neighborhood intelligence along with individual intelligence. Particle swarm was originally formulated to study the interesting concept of a social behavior (bird flocking or fish schooling) in a simplified manner in simulation. However, very soon the potential of this technique was realized to develop into a powerful optimization tool which can be successfully applied in the fields of both continuous and discrete optimization problems such as function optimization, scheduling and hence received many attentions since it is originated.

The particle swarm concept originated as a simulation of simplified social system, and this technique has been developing rapidly. Eberhart and Kennedy in [1, 2] originally formulated particle swarm in 1995, and recently, several investigations have been undertaken to improve the performance of original PSO. There are many improved PSO algorithm such as Shi and Eberhart who introduced an inertia weight making the influence of the previous velocity on the

new velocity in [3–5] and Kennedy and Mendes use cluster analysis improving PSO's performance in [6]. Angeline presented the model of improved PSO algorithm called (HPSO) in [7] which uses selection operation of evolution computing. Literature [8] Suganthan sets up the model of PSO with adjacent filed operation. Jiao et al. present a dynamic inertia weight particle swarm optimization algorithm in paper [9] in which the dynamic inertia weight that decreases according to iterative generation increasing is used. Many experts also studied others properties of PSO such as Clerc and Kennedy in [10, 11] who have researched the particle swarm explosion stability and convergence in a multidimensional complex space. Eberhart and Shi have investigated PSO developments, applications, and resources in [12] and parameter selection in [13] and dimension selection methods in [13].

PSO has been successfully applied in many areas: function optimization, artificial neural network training, fuzzy system control, and other areas where GA can be applied. Parsopoulos and Vrahatis approach global optimization problems using PSO in [14, 15] and Abido uses PSO optimizing power flow in [16]. PSO technique have been used in assignment problem in [17], reactive power and voltage control considering voltage security assessment in [18], and so forth.

PSO algorithm is widely used, such as the paper [19, 20] that introduces a Hybrid Particle Swarm algorithm with artificial Immune Learning (HPSIL) for solving Fixed Charge Transportation Problem (FCTP). Hamta et al. in paper [21] presented a hybrid PSO algorithm for a multiobjective assembly line balancing problem with flexible operation times, sequence-dependent setup times, and learning effect. Chou [22] used a particle swarm optimization with cocktail decoding method for hybrid flow shop scheduling problems with multiprocessor tasks. This study searches for a number of solid decoding methods that can be incorporated into the cocktail decoding method. Then, it develops a particle swarm optimization (PSO) algorithm that can be combined with the cocktail decoding method. PSO has particularly gained prominence due to its relative ease of operation and capability to quickly arrive at an optimal/near-optimal solution. However it was pointed out in our studies that original PSO might frequently tend to get stuck in a near optimal solution in reaching optimum solutions especially for middle or large size function optimization problems. According to the shortcoming of original PSO, a local and global search combine particle swarm optimization algorithm is presented in this paper, and the simulation results show that it is efficacious. At the same time, this paper rigorously analyzes new PSO algorithm convergence and obtains its convergence qualification.

This work differs from the existing ones at least in four aspects: firstly, it proposes a local and global search combine particle swarm optimization (LGSCPSO) algorithm iterative formula, in which all particles share the best information of the local particles, global particles and neighborhood particles. Secondly, it finds the best combine parameters of LGSCPSO for different size optimization problems. Thirdly, it is to compare the original PSO with LGSCPSO and shows that the latter is more efficacious for optimization problems. Fourthly, it strictly analyzes the PSO algorithm's convergence and obtains its convergence qualification. The rest of the paper is organized as follows: The next section introduces the original PSO model. The iteration formulation of LGSCPSO algorithm is presented in Section 3. In Section 4, it analyzes the PSO algorithm's convergence and finds its convergence qualification. Then, it describes the test functions, experimental settings, and compares experimental results of original PSO with LGSCPSO algorithm. Finally, Section 5 summarizes the contribution of this paper and conclusions.

2. Original Particle Swarm Optimization Algorithm

2.1. Description of Original Particle Swarm Optimization Algorithm. Particle swarm optimization (PSO) is an evolutionary computation technique, and its concept originated as a simulation of a simplified social system. The major difference is that the evolution computing techniques use genetic operators whereas swarm intelligence techniques use the physical movements of the individuals in the swarm. PSO is distinctly different from other evolutionary-type methods

in a way that it does not need complex encoding and decoding processes and does not use the operation (such as crossover and/or mutation), and it takes real numbers as particles in the aspects of representation solution. From the procedure, one can learn that PSO shares many common points with GA; for example, they start with a neighborhood of a randomly generated population, evaluate the population with fitness values, update the population and search for the optimum with random techniques, and do not guarantee optimal. Similar to other population-based algorithms, PSO as an optimization tool can solve a variety of difficult optimization problems. Compared to GA, one of the important attractive factors of PSO is simple that there are very few parameters to adjust. It can achieve the optimal or near-optimal solutions in a rather short time without enormous iterative computations in digital implementation.

Swarm intelligence simulates a social behavior such as bird flocking to a promising position for certain objectives in a multidimensional space. It is initialized with a population of random solutions and searches for optima by updating generations. PSO system combines local search method (through self-experience) with global search methods (through neighboring experience), attempting to balance exploration. Like evolutionary algorithm, PSO search uses a population (called swarm) of individuals (called particles) that are updated from iteration to iteration. Each particle represents a candidate position (i.e., solution) to the problem at hand, resembling the chromosome of GA. A particle is treated as a point in an M -dimension space, and the status of a particle is characterized by its position and velocity. Initialized with a swarm of random particles, PSO is achieved through particle flying along the trajectory that will be adjusted based on the best experience or position of the one particle (called local best) and ever found by all particles (called global best). PSO updates a population of particles with the internal velocity and attempts to profit from the discoveries of themselves and previous experiences of all other companions.

2.2. The Model of Original Particle Swarm Optimization Algorithm. In every search iteration, each particle is updated by following two "best" values. The first one is the best solution (fitness) it has achieved so far, and this value is called $pBest$. Another "best" value obtained so far by any particle in the population, and this best value is a global best and called $gBest$. After finding the two best values, the particle updates its velocity and positions with following formulas (1) and (2):

$$v_{id}(k+1) = wv_{id}(k) + c_1r_1(p_{id}(k) - x_{id}(k)) + c_2r_2(p_{gd}(k) - x_{id}(k)), \quad (1)$$

$$x_{id}(k+1) = x_{id}(k) + v_{id}(k+1) \quad (i = 1, 2, \dots, m; d = 1, 2, \dots, D). \quad (2)$$

In (1), $P_i = (p_{i1}, p_{i2}, \dots, p_{iD})$ is the best previous position of the i th particle (also known as $pBest$). According to the different definitions, there are two different versions of PSO, with local version, and particles only have information of their own and their neighbors' bests, rather than that of

the entire neighborhood. If $P_g = (p_1, p_2, \dots, p_D)$ is the best position among all the particles in the swarm (also known as $gBest$), such a version is called the global version. If P_g is taken from some smaller number of adjacent particles of the population (also known as $lBest$), such a version is called the local version. In (1) and (2) k represents the iterative number and D is dimension of particles, and range of particles are all determined by the problem to be optimized. Variables c_1, c_2 are learning factors, usually $c_1 = c_2 = 2$, which represent the weighting of the stochastic acceleration terms that pull each particle towards $pBest$ and $gBest$ positions. Thus, adjustment of these constants changes the amount of “tension” in the system. $r_1 \sim U(0, 1)$, $r_2 \sim U(0, 1)$, and w are an inertia weight, which is initialized typically in the range of $[0, 1]$. Inertia weight controls the impact of previous historical values of particle velocity on its current one. A larger inertia weight pressures towards global exploration (searching new area), while a smaller inertia weight pressures toward fine-tuning the current search area. Particle’s velocities on each dimension are confined to a maximum velocity $V_{max} \sim x$ which is a parameter specified by the user. If the iteration formulas would cause the velocity on that dimension to exceed $V_{max} \sim x$, then the velocity on that dimension is limited to V_{max} . The termination criterion for the iterations is determined according to whether the max generation or a designated value of the fitness of P_g is reached.

The main disadvantage of the above original PSO is that it is difficult to keep the diversity of population and to balance local and global search and hence it may result in local optimal solutions. Besides, their search rates are commonly lower and sometimes need more computation when solving some difficult optimization problems. The original PSO frequently gets into the local solution, especially when the problem size is middle or large. In the following a local and global search combine particle swarm optimization algorithm is proposed to deal with the above disadvantages of original PSO in solving optimization problems.

3. A Local and Global Search Combined Particle Swarm Optimization Algorithm

3.1. The Model of a Local and Global Search Combined Particle Swarm Optimization Algorithm. Because both local and global version have their own advantages and disadvantage, respectively, one can use them both in the algorithm, while global version is used to get quick result and local version can refine the search space. In original PSO algorithm, the information of individual best and global best was shared by next generation particles, in which it tends to get stuck in a near optimal solution especially for middle and large size problems. A local and global combine particle swarm optimization (LGSCPSO) algorithm is presented in this paper, in which the particles of next generation share the best information of one particle itself, the best of particles in neighborhood population (local best particles), and the best of all particles in the swarm (global best particles). Among the neighborhood population, the particles are constituted by the best particles of every generation with different proportion,

which is called $lBest$. As the generation increases, neighborhood population diversity will grow larger and larger. LGSCPSO algorithm improves upon the original PSO variation to increase accuracy of solution without sacrificing the speed of solution significantly, and its detailed information will be given in following.

Suppose that the searching space is D -dimensional and m particles form the colony. The i th particle represents a D -dimensional vector $X_i = (x_{i1}, x_{i2}, \dots, x_{iD})$ ($i = 1, 2, \dots, m$). It means that the i th particle locates at X_i in the searching space and the position of each particle is a potential solution. We could calculate the particle’s fitness by putting its position into a designated objective function. When the fitness is lower, the corresponding X_i is “better.” The i th particle’s “flying” velocity is also a D -dimensional vector, denoted as $V_i = (v_{i1}, v_{i2}, \dots, v_{iD})$. Denote the best position of the i th particle as $P_i = (p_{i1}, p_{i2}, \dots, p_{iD})$, the best position of the local as $P_l = (p_{l1}, p_{l2}, \dots, p_{lD})$, and the best position of the global as $P_g = (p_1, p_2, \dots, p_D)$, respectively. After finding the three best values, the particle of LGSCPSO updates its velocity and positions with the following formulas:

$$v_{id}(k+1) = wv_{id}(k) + c_1r_1(\alpha * (p_{id}(k) - x_{id}(k)) + (1 - \alpha) * (p_{ld}(k) - x_{id}(k))) \quad (3)$$

$$+ c_2r_2(p_g(k) - x_{id}(k)),$$

$$x_{id}(k+1) = x_{id}(k) + v_{id}(k+1), \quad (4)$$

where w is an inertia weight, which is initialized typically in the range of $[0, 1]$. The neighborhood particles of k generation are composed by the best neighborhood particle (local the particle) of k generation. $\alpha \in [0, 1]$ is weight index that is chosen according to different optimization problem, which reflects relatively important degree of the best position of the i th particle and the best position of the k th generation neighborhood particle. The variables c_1, c_2 are acceleration constant, which control how far a particle will move in a single iteration, and others parameters are same as in (1) and (2).

The searching is a repeat process, and the stop criteria are that the maximum iteration number is reached or the minimum error condition is satisfied. The stop condition depends on the problem to be optimized. In LGSCPSO algorithm, each particle of the swarm shares mutual information globally and benefits from discoveries and previous experiences of all other colleagues during the search process.

3.2. Pseudocode of LGSCPSO (See Pseudocode 1). Because PSO has very deep intelligent background, it is suitable for science computation and engineering applications. A thorough mathematical foundation for the methodology was not developed so far with the step of the algorithm; however, it has been proven to be very effective for application.

3.3. Convergence Analysis of LGSCPSO. In this section the LGSCPSO algorithm’s convergence is studied.

Step 1. Let parameters; including swarm size PS , maximum of generation $endgen$ and others parameters will be used in LGSCPSO algorithm.

Step 2. Iteration process

- (i) Generate stochastically initialization population and velocity;
- (ii) Evaluate each particle's fitness;
- (iii) Initialize $gBest$ position with the lowest fitness particle in the whole swarm;
- (iv) Initialize $pBest$ position with a copy of particle itself;
- (v) Initialize $lBest$ position with the best particle of initializing population;
- (vi) $k := 0$;

While (the maximum $endgen$ of generation is not met)

{

- (i) $k := k + 1$;
- (ii) Generate next swarm by (3), (4);
- (iii) Evaluate swarm;
 - { (a) Compute each particle's fitness in the swarm;
 - (b) Find new P_g, P_i of the swarm and P_i of each particle by comparison, and update P_i and P_g ;
 - (c) Update P_i using the best particle of k generation colony;}

}

Step 3. Output optimization results.

PSEUDOCODE 1

Theorem 1. In LGSCPSO algorithm in which its recurrence equation is (3) and (4), when parameters relation $c_1 r_1 + c_2 r_2 \leq 1 + w - 2\sqrt{w}$ or $1 + w + 2\sqrt{w} \leq c_1 r_1 + c_2 r_2 < 2w + 2$ is satisfied, it is convergent.

Proof. Let $R_1 = c_1 r_1$ and $R_2 = c_2 r_2$; from (3) and (4) we have

$$\begin{aligned} x_{id}(k+1) &= (1 - R_1 - R_2) x_{id}(k) + w v_{id}(k) \\ &\quad + R_1 \alpha p_{id}(k) + R_1 (1 - \alpha) p_{ld}(k) \\ &\quad + R_2 p_{gd}(k). \end{aligned} \quad (5)$$

From (4) we can get $v_{id}(k) = x_{id}(k) - x_{id}(k-1)$, and combining (5) we have

$$\begin{aligned} x_{id}(k+1) - (1 + w - R_1 - R_2) x_{id}(k) + w x_{id}(k-1) \\ = R_1 \alpha p_{id}(k) + R_1 (1 - \alpha) p_{ld}(k) + R_2 p_{gd}(k). \end{aligned} \quad (6)$$

LGSCPSO algorithm's recurrence equation is linearity constant coefficient nonhomogeneous, and the secular equation of corresponding homogeneous recurrence equation is as follows:

$$x^2 - (1 + w - R_1 - R_2)x + w = 0. \quad (7)$$

Latent roots of above secular equation are as follows:

$$\begin{aligned} \mu_1 &= \frac{1 + w - R_1 - R_2 + \sqrt{(1 + w - R_1 - R_2)^2 - 4w}}{2}, \\ \mu_2 &= \frac{1 + w - R_1 - R_2 - \sqrt{(1 + w - R_1 - R_2)^2 - 4w}}{2}. \end{aligned} \quad (8)$$

According to the relations of recurrence equation and its special solution, let the special solution of LGSCPSO

algorithm's recurrence equation (6) $H^*(k) = S$ substitute into (6), and we can solve

$$S = \frac{R_1 \alpha p_{id}(k) + R_1 (1 - \alpha) p_{ld}(k) + R_2 p_{gd}(k)}{R_1 + R_2}. \quad (9)$$

According to the relations of recurrence equation's general solution, special solution, and its latent roots, we can obtain the general solution of LGSCPSO algorithm's recurrence equation (6) as follows:

$$x(k) = S + c_1'' \mu_1^k + c_2'' \mu_2^k. \quad (10)$$

The initial solution and velocity of LGSCPSO algorithm recurrence equation is stochastically generated; suppose first and second solution is $x_{id}(1)$ and $x_{id}(2)$, respectively, and according to (10), we can obtain that

$$\begin{aligned} c_1'' &= \frac{\mu_2 (S - x(1)) + x(2) - S}{\mu_1 (\mu_1 - \mu_2)}, \\ c_2'' &= \frac{\mu_1 (x(1) - S) - x(2) + S}{\mu_2 (\mu_1 - \mu_2)}. \end{aligned} \quad (11)$$

To use (11) substitution into (10) simplification, we can obtain the general solution of LGSCPSO recurrence equation (6) as follows:

$$\begin{aligned} x(k) &= S + \frac{\mu_2 (S - x(1)) + x(2) - S}{\mu_1 - \mu_2} * \mu_1^{k-1} \\ &\quad + \frac{\mu_1 (x(1) - S) - x(2) + S}{\mu_1 - \mu_2} * \mu_2^{k-1}. \end{aligned} \quad (12)$$

If the limit of above $x(k)$ exists when $k \rightarrow \infty$, the LGSCPSO algorithm is convergent.

Let

$$f(x) = x^2 - (1 + w - R_1 - R_2)x + w. \quad (13)$$

So the Δ of above function is as follows:

$$\Delta = (1 + w - R_1 - R_2)^2 - 4w. \quad (14)$$

Evidently, when

$$\begin{aligned} f(1) &> 0, \\ f(-1) &> 0, \\ \Delta &\geq 0 \end{aligned} \quad (15)$$

hold, we can obtain the function (13) latent roots $-1 < \mu_1, \mu_2 < 1$.

Namely, when $0 < c_1 r_1 + c_2 r_2 \leq 1 + w - 2\sqrt{w}$ or $1 + w + 2\sqrt{w} \leq c_1 r_1 + c_2 r_2 < 2w + 2$ is satisfy, we can obtain $-1 < \mu_1, \mu_2 < 1$.

From LGSCPSO algorithm theory, we obviously get that $p_{id}(k)$ and $p_{gd}(k)$ are descending with k increase, and S is also descending with k increase.

When $0 < c_1 r_1 + c_2 r_2 \leq 1 + w - 2\sqrt{w}$ or $1 + w + 2\sqrt{w} \leq c_1 r_1 + c_2 r_2 < 2w + 2$ is satisfied, namely, $-1 < \mu_1, \mu_2 < 1$ hold, we have

$$\begin{aligned} &\lim_{k \rightarrow \infty} x(k) \\ &= \lim_{k \rightarrow \infty} \left(S + \frac{\mu_2 (S - x(1)) + x(2) - S}{\mu_1 - \mu_2} * \mu_1^{k-1} \right. \\ &\quad \left. + \frac{\mu_1 (x(1) - S) - x(2) + S}{\mu_1 - \mu_2} \mu_2^{k-1} \right) \\ &= \lim_{k \rightarrow \infty} \frac{R_1 \alpha p_{id}(k) + R_1 (1 - \alpha) p_{ld}(k) + R_2 p_{gd}(k)}{R_1 + R_2}. \end{aligned} \quad (16)$$

Because $(R_1 \alpha p_{id}(k) + R_1 (1 - \alpha) p_{ld}(k) + R_2 p_{gd}(k)) / (R_1 + R_2)$ is monotone decreasing and have lower bound which is its optimum solution, $\lim_{k \rightarrow \infty} (R_1 \alpha p_{id}(k) + R_1 (1 - \alpha) p_{ld}(k) + R_2 p_{gd}(k)) / (R_1 + R_2)$ exist, namely, the endless particle sequence brought about by LGSCPSO algorithm's recurrence equation is limited. So we can obtain that the LGSCPSO algorithm is convergent when its parameters relations $0 < c_1 r_1 + c_2 r_2 \leq 1 + w - 2\sqrt{w}$ or $1 + w + 2\sqrt{w} \leq c_1 r_1 + c_2 r_2 < 2w + 2$ is satisfied. \square

4. Numerical Simulation

4.1. Test Functions. To illustrate the effectiveness and performance of LGSCPSO algorithm for optimization problems, a set of 8 representative benchmark functions with different dimensions were employed to evaluate it in comparison with

original PSO. Many authors tested algorithm using them widely.

Sphere Model. Consider $f_1(x) = \sum_{i=1}^n x_i^2$, where $x_i \in [-100, 100]$.

Schwefel's Problem 1.2. Consider $f_2(x) = \sum_{i=1}^n (\sum_{j=1}^i x_j)^2$, where $x_i \in [-100, 100]$.

Schwefel's Problem 2.21. Consider $f_3(x) = \max_i \{|x_i|, 1 \leq i \leq n\}$, where $x_i \in [-100, 100]$.

Generalized Rosenbrock's Function. Consider $f_4(x) = \sum_{i=1}^{n-1} (100(x_{i+1} - x_i^2)^2 + (x_i - 1)^2)$, where $x_i \in [-100, 100]$.

Ackley's Function. Consider $f_5(x) = -20 \exp(-0.2 \sqrt{(1/n) \sum_{i=1}^n x_i^2}) - \exp((1/n) \sum_{i=1}^n \cos 2\pi x_i) + 20 + e$, where $x_i \in [-32, 32]$.

Generalized Griewank Function. Consider $f_6(x) = (1/4000) \sum_{i=1}^n (x_i - 100)^2 - \prod_{i=1}^n \cos((x_i - 100)/\sqrt{i}) + 1$, where $x_i \in [-600, 600]$.

Generalized Penalized Functions. Consider

$$\begin{aligned} f_7(x) &= \frac{\pi}{n} \left\{ 10 \sin^2(\pi y_1) + \sum_{i=1}^{n-1} (y_i - 1)^2 \right. \\ &\quad \left. \times [1 + 10 \sin^2(\pi y_{i+1})] + (y_n - 1)^2 \right\} \\ &\quad + \sum_{i=1}^n u(x_i, 10, 100, 4), \\ f_8(x) &= 0.1 \left\{ \sin^2(\pi y_1) + \sum_{i=1}^{n-1} (y_i - 1)^2 \right. \\ &\quad \left. \times [1 + 10 \sin^2(\pi y_{i+1})] + (y_n - 1)^2 \right\} \\ &\quad + \sum_{i=1}^n u(x_i, 10, 100, 4), \end{aligned} \quad (17)$$

where

$$u(x_i, a, k, m) = \begin{cases} k(x_i - a)^m, & x_i > a \\ 0, & -a \leq x_i \leq a, \\ k(-x_i - a)^m, & x_i < -a \end{cases} \quad (18)$$

$$y_i = 1 + \left(\frac{1}{4}\right)(x_i + 1), \quad x_i \in [-50, 50].$$

They can be divided into unimodal (function f_1 - f_3) and multimodal functions (function f_4 - f_8), where the number of local minima increases exponentially with the problem dimension.

4.2. Experimental Results and Comparison. The experimental results of original PSO and LGSCPSO algorithm on

TABLE 1: The comparison results of the PSO algorithm and the LGSCPSO algorithm.

a	Min./Max./Average ($e \sim \pi$ represents $\times 10^7$)				
	0.1	0.2	0.3	0.4	0.5
LCG					
F_{un}					
f_1	7.9247/798.1366/119.2735	4.8684/788.0086/137.7727	3.4298/466.1351/29.4039	6.2134/108.3578/34.9678	202.8074/3.8168e + 3/899.1347
f_2	1.0216/328.5215/56.3621	0.2372/39.3515/29.25	0.2165/36.7093/9.1546	0.3367/29.7551/35.9433	25.8671/1.26.0089/74.3555
Dim	0.1788/3.6762/0.9580	0.0516/72.579/18.8086	0.0446/0.9215/0.3245	0.0931/2.9157/0.6956	2.0381/42.814/7.393
150,	0.0276/1.0302/0.1732	0.0024/16.9442/2.0285	0.0081/5.1882/0.6059	0.0255/12.8562/1.5062	0.2738/12.3747/2.6693
$Best$	0.0015/0.2004/0.0345	0.0011/6.0067/0.7585	0.0021/15.3744/3.103	0.0042/1.563/0.276	0.0354/0.9538/0.2124
0;	6.199e - 4/2.0.4397/2.1839	0.1109/326.9967/38.2332	9.091e - 4/50.1812/9.9065	0.0031/1.3039/0.2172	0.0088/0.3742/0.0659
PS	8.7194e - 4/32.076/3.5118	217.0564/2.5137e + 3/922.9063	0.1802/416.0314/88.5176	1.5877e - 4/2.5115/0.3145	0.0027/0.3203/0.0554
150,	0.0027/1.0443/0.3794	131.8696/1.0093e + 3/605.7608	22.3952/2.7571e + 3/760.49	4.9801e - 5/0.0052/8.8123e - 4*	0.0104/0.1721/0.0678
EG	0.0301/3.1973e + 5/5.7818e + 4	3.5023/3.5197e + 5/7.5222e + 4	3.3725/3.3151e + 5/3.3313e + 4	9.7207e - 5/390.2679/40.2488	0.5088/4.2984e + 5/2.6068e + 5
2500					
PSO	3.5545e + 5/4.2006e + 5/3.9996e + 5	3.6563e + 5/4.1904e + 5/3.9654e + 5	3.8295e + 5/4.1465e + 5/4.0243e + 5	0.5082/4.185e + 5/3.4273e + 5	3.834e + 5/4.2439e + 5/4.0552e + 5
LCG					
F_{un}					
f_1	1.5314e - 5/0.0012/2.3471e - 4	3.4819e - 8/9.7461e - 7/2.8081e - 7	1.6392e - 9/8.0260e - 8/2.4483e - 8	1.9438e - 8/4.5893e - 6/1.0199e - 6	0.0016/0.0746/0.0181
f_2 ,	7.544e - 6/4.1057e - 4/1.2064e - 4	3.6274e - 9/2.252e - 7/6.7068e - 8	4.3649e - 11/1.9808e - 8/3.0528e - 9	6.9751e - 9/4.4344e - 6/5.5416e - 7	4.1506e - 5/0.0025/1.297e - 4
Dim	3.3468e - 6/2.5205e - 4/8.7442e - 5	1.7849e - 10/6.8322e - 8/1.3459e - 8	4.3800e - 11/8.3452e - 9/2.3903e - 9	3.0993e - 10/2.9669e - 8/6.9531e - 9	1.3450e - 5/1.3095e - 4/6.5852e - 5
30,	2.2108e - 5/3.3094e - 4/9.2148e - 5	9.6468e - 11/1.3930e - 7/2.0447e - 8	2.9752e - 12/5.6342e - 10/1.6065e - 10*	5.1336e - 11/6.7099e - 8/9.4611e - 9	1.1121e - 6/2.0099e - 5/6.5348e - 6
$Best$	1.4607e - 5/3.3855e - 4/9.0081e - 5	7.8029e - 11/9.93e - 9/4.5009e - 9	7.1437e - 12/4.1282e - 9/8.6320e - 10	1.2011e - 10/6.3320e - 9/1.7701e - 9	1.5491e - 6/1.6945e - 5/6.7154e - 6
0;	1.4749e - 4/0.0097/0.0016	3.0876e - 9/4.2278e - 7/5.6384e - 8	2.0796e - 11/5.0013e - 9/1.0295e - 9	4.0553e - 10/3.5928e - 8/5.5263e - 9	3.3047e - 7/7.1073e - 5/2.0406e - 5
PS	2.2105e - 4/0.0705/0.0232	1.8076e - 7/1.0146e - 5/2.1222e - 6	1.1123e - 10/2.6655e - 8/8.6717e - 9	6.2429e - 9/6.8153e - 7/1.8691e - 7	2.4160e - 5/5.8853e - 4/1.5538e - 4
150,	0.0879/0.9873/0.4732	1.437e - 6/6.4389e - 4/2.8104e - 4	8.3474e - 8/7.0419e - 6/2.2156e - 6	9.0305e - 7/1.0765e - 4/1.9495e - 5	6.3392e - 4/0.0096/0.0042
EG	1.3288/15.724/5.0923	0.0042/0.1077/0.0241	7.8655e - 5/0.0055/0.002	2.6371e - 4/0.0057/0.0024	0.0595/1.9094/0.3682
2000					
PSO	364.253/2.493e + 4/1.0134e + 4	1.3765/4.6947e + 3/4.818464	0.0691/2.5876/0.7283	0.1723/3.9289/1.8005	17.3828/984.8965/188.1513
LCG					
F_{un}					
f_1 ,	2.3621e - 4/0.0013/7.311e - 4	1.3902e - 5/2.0080e - 4/8.8198e - 5	1.6884e - 5/3.3877e - 4/1.194e - 4	1.5547e - 5/6.6884e - 4/1.4984e - 4	0.001/0.0262/0.0055
f_2 ,	6.0977e - 5/4.2674e - 4/2.1957e - 4	1.1701e - 6/2.8489e - 5/8.0878e - 6	7.4212e - 7/4.1010e - 6/1.8869e - 6	3.5838e - 7/8.3143e - 6/4.7977e - 6	1.1206e - 5/5.1122e - 4/1.9353e - 4
Dim	5.5341e - 5/7.051e - 4/2.1313e - 4	3.8603e - 7/8.6707e - 6/1.7948e - 6	5.1647e - 8/1.5398e - 6/3.7869e - 7	3.9851e - 8/2.4747e - 6/7.3211e - 7	3.1555e - 6/3.1428e - 5/1.2056e - 5
30,	4.9251e - 5/3.4147e - 4/1.4638e - 4	1.4e - 7/5.6791e - 6/1.3055e - 6	1.5353e - 9/1.8722e - 7/6.9333e - 8*	3.4271e - 8/4.2062e - 7/1.0447e - 7	1.8188e - 7/1.3756e - 5/3.7208e - 6
$Best$	5.2814e - 5/0.0019/4.5195e - 4	1.6044e - 7/1.6259e - 6/5.7405e - 7	4.7963e - 9/3.1684e - 7/6.3918e - 8	6.6274e - 9/8.7745e - 7/1.4709e - 7	2.2951e - 7/1.1701e - 6/5.3581e - 7
0;	4.8841e - 4/0.0063/0.0029	1.7168e - 7/6.7027e - 6/2.6332e - 6	2.0730e - 9/6.1577e - 7/9.0325e - 8	2.0358e - 9/4.6960e - 8/1.9028e - 8	8.2804e - 8/2.1413e - 5/3.1923e - 6
PS	0.0046/0.0476/0.0191	9.6091e - 6/7.5094e - 5/2.8845e - 5	3.4465e - 8/7.9999e - 6/1.0596e - 6	3.9048e - 8/3.9274e - 7/1.5350e - 7	1.0194e - 6/1.0954e - 5/3.7688e - 6
150,	0.0569/0.5819/0.2266	8.2486e - 5/0.0012/3.9755e - 4	1.1441e - 6/1.3502e - 5/5.7652e - 6	7.5274e - 7/1.2135e - 5/3.6172e - 6	9.2958e - 6/1.813e - 4/1.0582e - 4
EG	0.4589/4.2785/1.3995	0.001/0.0436/0.0158	2.4963e - 5/0.0027/6.1308e - 4	4.4217e - 5/5.6209e - 4/1.7621e - 4	0.0016/0.031/0.0073
2000					
PSO	0.9442/7.2642/3.7178	0.1348/0.5193/0.2436	0.005/0.0675/0.0212	0.0084/0.043/0.03	0.2007/0.9216/0.4999

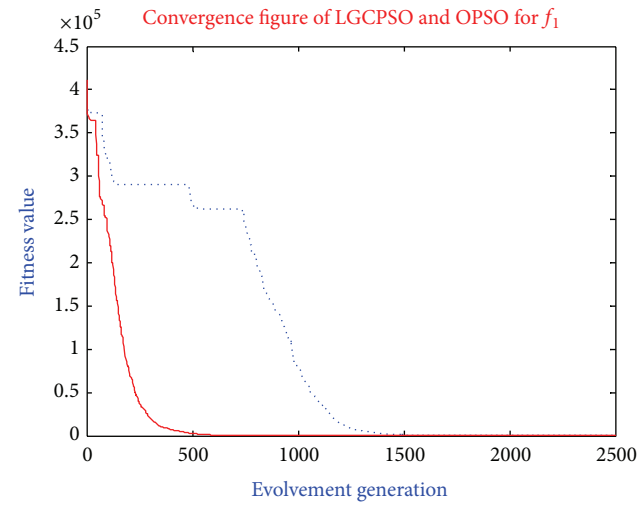
TABLE I: Continued.

a	Min./Max./Average ($e \sim n$ represents $\times 10^7$)			
	0.1	0.2	0.3	0.4
LCG				0.5
F_{un}				
f_6	1.8571/1.229e + 3/135.8807	6.2873/3.2863e + 3/709.8222	0.2013/2.85.8471/44.28	0.5944/144.3777/23.7188
f_5	0.1568/2.5441e + 3/388.2091	0.0113/789.7377/115.475	4.0693/4.9375e + 3/562.5381	1.8021/937.5994/153.7682
Dim	0.6066/799.8443/169.6422	2.3034/796.4533/123.7322	3.983e - 4/302.2135/32.9758	0.0455/207.5395/40.3132
25		9.6966e - 5/6.8529/2.0791*	0.2062/179.2151/21.4179	3.4459/962.925/115.1339
$Best$	0.2485/181.0596/25.4415	0.0069/23.873/4.9974	3.5267e - 4/3.8396/0.8494	0.0125 /423.4865/75.3354
0;	0.0237/40.8918/11.1441	2.547e - 4/9.0536/4.042	3.6341e - 4/6.6633/3.6567	0.1299/26.4581/10.2862
PS	0.2485/181.0596/25.4415	0.0702/14.2596/6.6687	0.0372/152.4195/22.0972	0.1671/672.3137/106.7018
150;	0.0916/228.4057/30.7965	0.0189/16.2452/9.9379	0.1941/238.9312/38.1225	0.6944/213.5931/30.5417
EG	0.4745/435.3273/56.9634	3.2415/638.6487/128.4819	0.7361/334.4369/49.1472	0.2055/11812e + 3/161.6274
2500	4.3957/341.7015/67.9295			
PSO	4.3221e + 4/5.1189e + 4/4.6655e + 4	3.9971e + 4/5.4303e + 4/4.6593e + 4	2.876e + 4/5.5191e + 4/4.7462e + 4	3.937e + 4/5.2589e + 4/4.6619e + 4
LCG				0.5
F_{un}				
f_6	7.9936e - 15/4.3521e - 14/2.256e - 14	7.9936e - 15/7.9936e - 15/7.9936e - 15	4.4409e - 15/7.9936e - 15/7.2831e - 15	7.9936e - 15/2.0851e - 10/7.4168e - 11
f_5	7.9936e - 15/7.9936e - 15/7.9936e - 15	4.4409e - 15/7.9936e - 15/5.1514e - 15	4.4409e - 15/7.9936e - 15/7.2831e - 15	1.8652e - 14/4.1656e - 13/9.1838e - 14
Dim	4.4409e - 15/7.9936e - 15/7.2831e - 15	4.4409e - 15/7.9936e - 15/5.0677e - 15*	4.4409e - 15/1.5017/0.1502	7.9936e - 15/1.5099e - 14/8.7041e - 15
30		4.4409e - 15/1.6462/0.2801	4.4409e - 15/2.0119/0.3167	4.4409e - 15/7.9936e - 15/5.862e - 15
$Best$	4.4409e - 15/7.9936e - 15/5.8620e - 15	4.4409e - 15/2.3162/0.5967	4.4409e - 15/1.6462/0.7128	4.4409e - 15/7.9936e - 15/5.862e - 15
0;	4.4409e - 15/2.3162/0.2316	4.4409e - 15/2.3162/1.0934	4.4409e - 15/3.6807/1.3585	4.4409e - 15/7.9936e - 15/6.9278e - 15
PS	4.4409e - 15/1.908e - 10	7.9936e - 15/2.8871/1.089	4.4409e - 15/2.4949/1.2564	4.4409e - 15/7.9936e - 15/7.6383e - 15
100;	6.9209e - 5/2.2201/0.7328	0.0021/3.0268/1.7571	7.9936e - 15/2.0133/1.2372	4.4409e - 15/7.9936e - 15/7.6383e - 15
EG	4.8998e - 5/1.6162/0.3991	0.0043/2.5791/1.7115	7.9936e - 15/2.6602/0.8856	7.9936e - 15/7.9936e - 15/7.9936e - 15
2000				
PSO	2.4655e - 5/2.2315/1.1133	1.6387e - 4/2.8859/0.7401	7.9936e - 15/2.4959/0.6931	7.9936e - 15/1.5099e - 14/1.2967e - 14
LCG				0.5
F_{un}				
f_6	0.9416/1.4223/1.1635	0.5782/1.4520/0.9452	0.3887/8.8918/1.7237	3.0738/12.5482/6.1513
f_5	0.2941/0.9446/0.4842	0.0804/2.7225/0.5028	0.0397/2.1197/0.4602	1.1998/2.6794/1.5013
Dim	0.0383/0.2488/0.0994	0.0036/0.8091/0.1571	0.0055/4.4603/0.5501	0.5451/2.0070/0.8291
150;	0.002/0.3372/0.0945	6.6171e - 4/1.0833/0.1775	8.199e - 4/0.4379/0.122	0.0217/6.2987/0.8092
$Best$	4.6926e - 4/0.2611/0.0958	8.1220e - 5/2.1079/0.4195	2.5102e - 4/0.5375/0.3158	0.0061/0.2465/0.0621
0;	3.7473e - 5/0.1647/0.0541	0.2266/6.0141/2.1203	0.0023/3.2548/0.7676	0.0015/0.3055/0.0567
PS	1.572e - 4/0.0664/0.0194	1.6879/24.0771/1.2293	0.2953/4.2413/1.1668	2.6726e - 4/0.1051/0.0241
150;	1.1609e - 4/0.2322/0.0541	1.9272/17.0006/712.86	1.3151/17.8887/9.7229	4.8173e - 4/0.0609/0.019
EG	0.0129/3.4498e + 3/668.9998	0.2582/3.767e + 3/668.9854	0.0979/12.3986/3.8033	0.0283/3.9697e + 3/2.3201e + 3
2500				
PSO	3.1058e + 3/3.9496e + 3/3.6383e + 3	2.766e + 3/3.952e + 3/3.5857e + 3	0.9187/3.9622e + 3/2.9803e + 3	3.5377e + 3/3.9083e + 3/3.7889e + 3

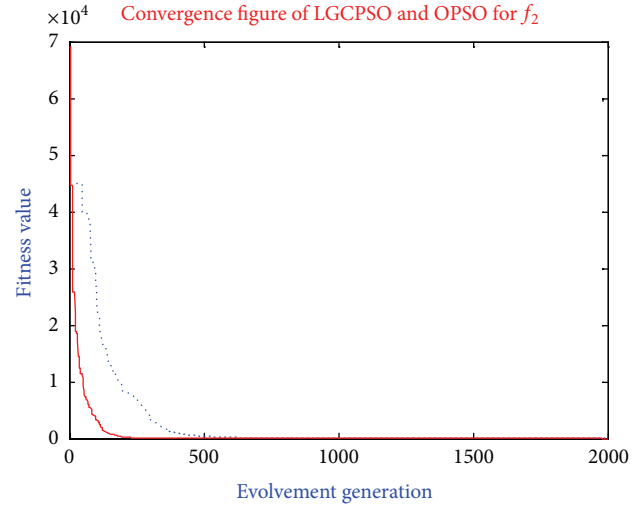
TABLE 1: Continued.

a	Min./Max./Average ($e \sim \pi$ represents $\times 10^{\pi}$)			
	0.1	0.2	0.3	0.4
<i>Fun</i>				
f_7	0.0014/0.1015/0.0268	2.1663e - 5/0.1245/0.0189	1.0775e - 5/0.1866/0.0314	3.9207e - 4/0.3284/0.0888
<i>Dim</i>	4.7654e - 5/0.031/0.0034	6.125e - 7/0.0622/0.0097	2.6987e - 7/0.1557/0.0249	3.7171e - 6/0.2498/0.0605
100	3.3537e - 5/0.0628/0.0165	7.1955e - 9/0.0311/0.0062	9.1232e - 9/0.1868/0.0374	3.4490e - 7/0.1244/0.0467
<i>Best</i>	5.8595e - 7/0.031/0.0036	4.1191e - 9/0.1555/0.0249	2.9509e - 9/0.1868/0.0467	3.8808e - 9/0.499/0.0872
0	8.2125e - 7/0.1685/0.0298	5.3424e - 8/0.3743/0.0717	5.224e - 7/0.6882/0.2318	4.4126e - 9/0.2497/0.0655
<i>PS</i>	5.8595e - 7/0.031/0.0036	4.1946e - 8/1.731/0.3794	5.6598e - 10/1.3103/0.2872	3.7644e - 9/0.2808/0.0779
150	0.0022/2.5577/0.8246	0.1557/2.8177/0.8995	4.3761e - 5/1.3392/0.4191	1.0263e - 10/0.2490/0.0498*
<i>EG</i>	30.7659/1.0297e + 9/3.6691e + 8	3.3049e - 4/2.7669e + 8/2.7669e + 7	1.3321e - 5/1.4361/0.5313	8.0965e - 6/0.2789/0.0448
2500		2.05e + 9/2.6638e + 9/2.3786e + 9	1.9676e + 9/2.8563e + 9/2.3233e + 9	1.8631e + 9/2.8019e + 9/2.2317e + 9
<i>Fun</i>				
f_8	0.0014/0.1008/0.0187	6.9482e - 5/0.1026/0.0114	1.9512e - 5/0.0023/7.8123e - 4	2.037e - 4/0.1195/0.0183
<i>Dim</i>	2.0521e - 4/0.0132/0.0039	8.9263e - 7/8.6653e - 5/2.0482e - 5	1.3466e - 6/0.2978/0.0307	6.6231e - 5/0.0019/5.873e - 4
100	9.8083e - 5/0.9506/0.1062	2.1132e - 7/4.1564e - 5/9.8935e - 6	2.7567e - 8/1.1156e - 4/2.2848e - 5	1.1378e - 6/0.0015/2.6495e - 4
<i>Best</i>	3.0775e - 7/0.0037/5.5843e - 4	1.8204e - 8/5.2730e - 5/1.0100e - 5	8.9066e - 10/1.4026e - 4/2.3733e - 5	1.8884e - 7/0.0905/0.0091
0	3.3459e - 6/4.3813e - 4/1.47e - 4	4.9008e - 8/6.3249e - 4/8.0700e - 5	1.4968e - 9/0.5878/0.0688	5.5391e - 10/8.5755e - 5/9.8527e - 6
<i>PS</i>	2.891e - 6/2.5064/0.497	1.649e - 7/1.8877/0.5009	4.0322e - 7/3.0954/0.8618	4.9993e - 10/7.1912e - 5/8.2796e - 6*
150	7.7979e - 4/9.103/2.623	2.1485e - 4/2.7725/0.8736	2.6562e - 6/6.9698/2.0345	3.5393e - 9/0.0011/1.6126e - 4
<i>EG</i>	2.0949e + 9/2.7924e + 9/2.4913e + 9	2.1328e + 2/8.009e + 9/2.5344e + 9	1.816e + 9/2.8674e + 9/2.4126e + 9	1.6523e - 7/2.1877/0.3866
2500		2.05e + 9/2.6165e + 9/2.2883e + 9	1.5174e + 9/2.7626e + 9/2.2677e + 9	1.8631e + 9/2.8019e + 9/2.2317e + 9

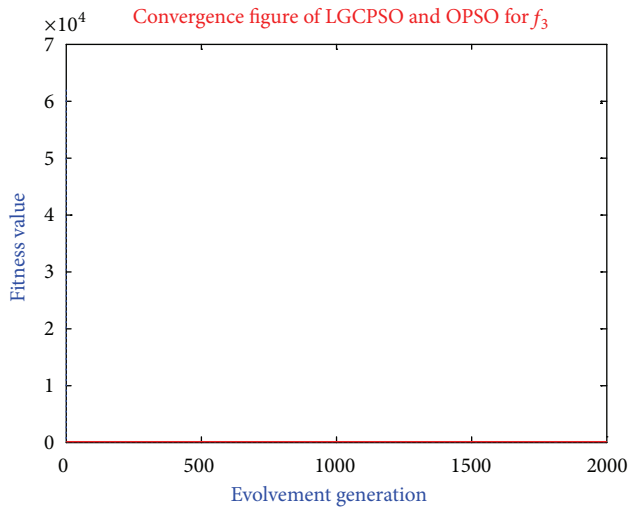
Remark : In Table 1, *Fun* and *Dim* denote function and its dimension, respectively; the *Best* is this function's optimum value; *PS* and *EG* indicate the population size and algorithm terminate generation. *PSO* and *LGC* denote the original *PSO* and *LGSCPSO* algorithm. The better solutions and the parameters found in *LGSCPSO* are illustrated with bold letters, and the best solutions are shown in data with asterisk.



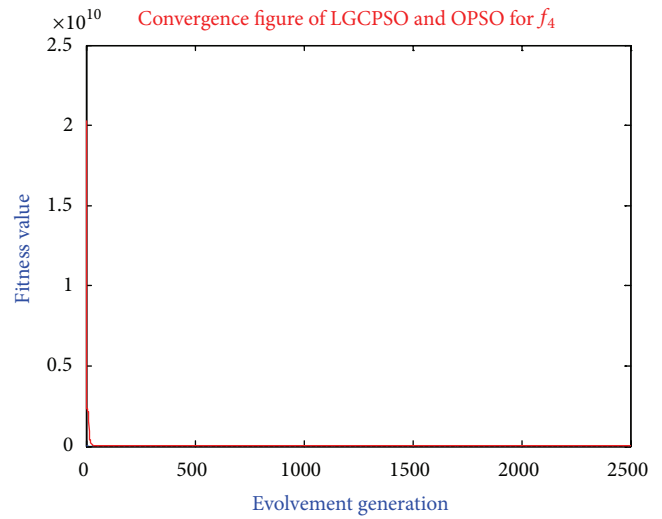
(a) Number 1



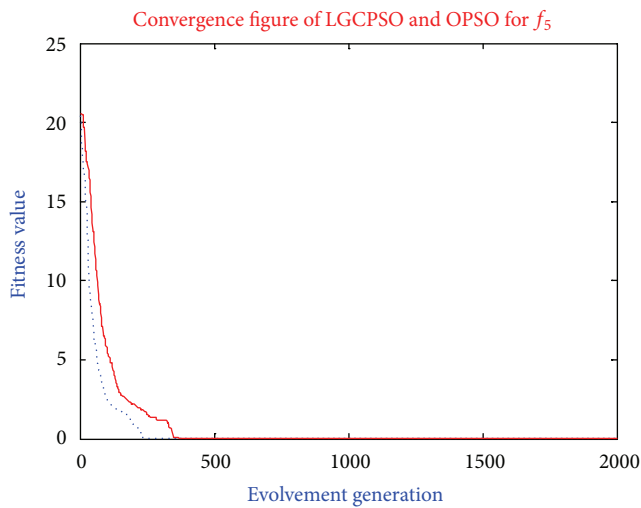
(b) Number 2



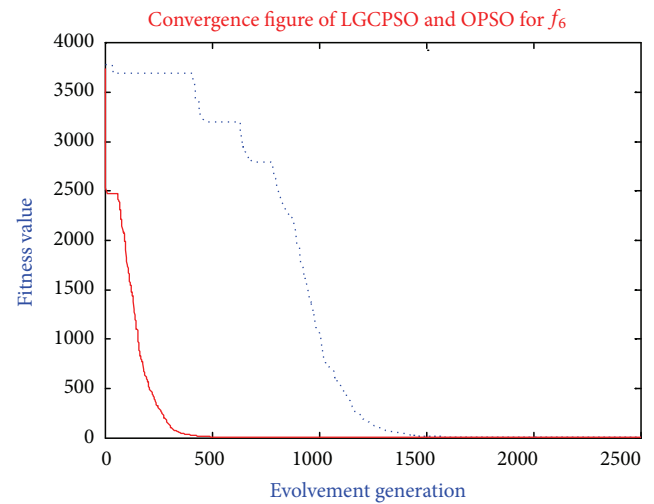
(c) Number 3



(d) Number 4



(e) Number 5



(f) Number 6

..... OPSO optimum
— LGCPSO optimum

..... OPSO optimum
— LGCPSO optimum

FIGURE 1: Continued.

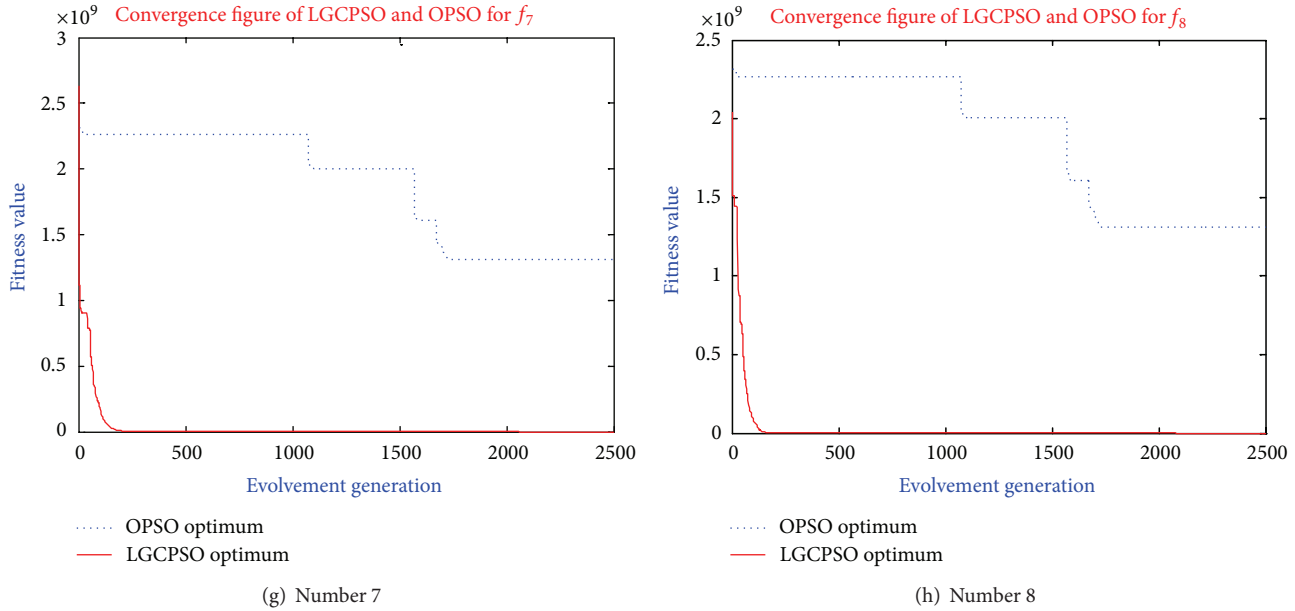


FIGURE 1: Convergence figure of LGSCPSO comparing with original OPPO for f_1-f_8 .

each test function are listed in Table 1. To get the average performance of the LGSCPSO algorithm ten runs on each problem instance were performed and the solution quality was averaged. The comparisons results of LGSCPSO and Original PSO algorithm are shown in Table 1 of the appendix.

From Table 1 one can observe that $w \in [0.2, 0.4]$ have the highest performance since using them has smaller minimum and smaller arithmetic mean in relation to the solutions obtained by the others, especially $w \approx 0.4$ has the better search efficiency. In LGSCPSO algorithm, various parameter α should be selected for optimizing different problems, as a whole, it is better when $\alpha \in [0.3, 0.9]$, especially $\alpha \approx 0.4$. From simulation results we can obtain that the LGSCPSO algorithm is clearly better than the original PSO for continuous nonlinear function optimization problem. The convergence figures of most effective LGSCPSO comparing with original PSO for 8 instances are as follows.

From Figure 1 we can discover that the convergence rate of LGSCPSO algorithm is clearly faster than the OPPO on every benchmark function, especially it is more efficacious than OPPO for middle and large size optimization problem. Accordingly, we can state that the LGSCPSO algorithm is more effective than OPPO algorithm. For test function 5, the search capability of LGSCPSO algorithm is worse than that of OPPO at the beginning of the iteration. However, seen from the enlarged figure, the search capability of LGSCPSO is markedly enhanced along with the iteration increasing. In addition we can find that the simulation data from test function 5 has a strong advantage.

5. Conclusions and Perspectives

According to the shortcoming of OPPO algorithm that it frequently gets the local solution especially solving the middle

or large size problem, a LGSCPSO algorithm is presented, and simulations show that it is efficacious. The performance of the new approach is evaluated in comparison to OPPO algorithm for eight representative instances with different dimensions and obtained results show that LGSCPSO algorithm is efficacious for solving optimization problems.

The proposed LGSCPSO algorithm approach in this paper can be considered as effective mechanisms from this point of view. There are a number of research directions that can be considered as useful extensions of this research. Although the proposed algorithm is tested with eight representative instances, a more comprehensive computational study should be made to test the efficiency of proposed solution technique. In the future it is maybe used for solving other discrete combinatorial optimization problems such as traveling salesman problem and scheduling.

Appendix

See Table 1.

Conflict of Interests

The authors declare that they have no conflict of interests to this paper.

Acknowledgments

The authors are grateful to the anonymous reviewers for giving us helpful suggestions. This work is supported by National Natural Science Foundation of China (Grant nos. 61174040 and 61104178), Fundamental Research Funds for the Central Universities, Shanghai Commission of Science and Technology (Grant no. 12JC1403400), and Shanghai Dianji

University Computer Application Technology Disciplines (Grant no. 13XKJ01).

References

- [1] R. Eberhart and J. Kennedy, "New optimizer using particle swarm theory," in *Proceedings of the 6th International Symposium on Micro Machine and Human Science*, pp. 39–43, Nagoya, Japan, October 1995.
- [2] J. Kennedy and R. Eberhart, "Particle swarm optimization," in *Proceedings of the IEEE International Conference on Neural Networks*, pp. 1942–1948, Perth, Australia, December 1995.
- [3] Y. Shi and R. C. Eberhart, "A modified particle swarms optimizer," in *Proceedings of the IEEE International Conference on Evolutionary Computation*, pp. 303–308, 1997.
- [4] Y. Shi and R. Eberhart, "Modified particle swarm optimizer," in *Proceedings of the IEEE International Conference on Evolutionary Computation (ICEC '98)*, pp. 69–73, May 1998.
- [5] H. Zhang, H. Yan, F. Yang, and Q. Chen, "Quantized control design for impulsive fuzzy networked systems," *IEEE Transactions on Fuzzy Systems*, vol. 19, no. 6, pp. 1153–1162, 2011.
- [6] J. Kennedy and R. Mendes, "Population structure and particle swarm performance," in *Proceedings of the Congress on Evolutionary Computation (CEC '02)*, pp. 1671–1676, IEEE Press, 2002.
- [7] P. J. Angeline, "Using selection to improve particle swarm optimization," in *Proceedings of the IEEE International Conference on Evolutionary Computation (ICEC '98)*, pp. 84–89, Anchorage, Alaska, May 1998.
- [8] M. Lovbjerg, T. K. Rasmussen, and T. Krink, "Hybrid particle swarm optimization with breeding and subpopulations," in *Proceedings of the IEEE International Conference on Evolutionary Computation*, pp. 1217–1222, San Diego, Calif, USA, 2000.
- [9] B. Jiao, Z. Lian, and X. Gu, "A dynamic inertia weight particle swarm optimization algorithm," *Chaos, Solitons and Fractals*, vol. 37, no. 3, pp. 698–705, 2008.
- [10] M. Clerc and J. Kennedy, "The particle swarm-explosion, stability, and convergence in a multidimensional complex space," *IEEE Transactions on Evolutionary Computation*, vol. 6, no. 1, pp. 58–73, 2002.
- [11] H. Zhang, H. Yan, F. Yang, and Q. Chen, "Distributed average filtering for sensor networks with sensor saturation," *IET Control Theory & Applications*, vol. 7, no. 6, pp. 887–893, 2013.
- [12] R. C. Eberhart and Y. Shi, "Particle swarm optimization: developments, applications and resources," in *Proceedings of IEEE International Conference on Evolutionary Computation*, pp. 81–86, May 2001.
- [13] Y. Shi and R. C. Eberhart, "Parameter selection in particle swarm optimization," in *Evolutionary Programming VII: Proceedings of the 7th Annual Conference on Evolutionary Programming*, pp. 591–600, Springer, New York, NY, USA, 1998.
- [14] F. van den Bergh and A. P. Engelbecht, "Cooperative learning in neural networks using particle swarm optimizers," *South African Computer Journal*, vol. 26, pp. 84–90, 2000.
- [15] H. C. Yan, Z. Z. Su, H. Zhang, and F. W. Yang, "Observer-based H_∞ control for discrete-time stochastic systems with quantisation and random communication delays," *IET Control Theory & Applications*, vol. 7, no. 3, pp. 372–379, 2013.
- [16] M. A. Abido, "Optimal power flow using particle swarm optimization," *International Journal of Electrical Power and Energy Systems*, vol. 24, no. 7, pp. 563–571, 2002.
- [17] A. Salman, I. Ahmad, and S. Al-Madani, "Particle swarm optimization for task assignment problem," *Microprocessors and Microsystems*, vol. 26, no. 8, pp. 363–371, 2002.
- [18] H. Yoshida, K. Kawata, Y. Fukuyama, S. Takayama, and Y. Nakanishi, "A Particle swarm optimization for reactive power and voltage control considering voltage security assessment," *IEEE Transactions on Power Systems*, vol. 15, no. 4, pp. 1232–1239, 2000.
- [19] M. M. El-Sherbiny and R. M. Alhamali, "A hybrid particle swarm algorithm with artificial immune learning for solving the fixed charge transportation problem," *Computers & Industrial Engineering*, vol. 64, pp. 610–620, 2013.
- [20] H. Zhang, H. Yan, T. Liu, and Q. Chen, "Fuzzy controller design for nonlinear impulsive fuzzy systems with time delay," *IEEE Transactions on Fuzzy Systems*, vol. 19, no. 5, pp. 844–856, 2011.
- [21] N. Hamta, S. M. T. Fatemi Ghomi, F. Jolai, and M. Akbarpour Shirazi, "A hybrid PSO algorithm for a multi-objective assembly line balancing problem with flexible operation times, sequence-dependent setup times and learning effect," *International Journal of Production Economics*, vol. 141, no. 1, pp. 99–111, 2012.
- [22] F. D. Chou, "Particle swarm optimization with cocktail decoding method for hybrid flow shop scheduling problems with multiprocessor tasks," *International Journal of Production Economics*, vol. 141, pp. 137–145, 2013.

Research Article

Cultural-Based Genetic Tabu Algorithm for Multiobjective Job Shop Scheduling

Yuzhen Yang and Xingsheng Gu

Key Laboratory of Advanced Control and Optimization for Chemical Processes, Ministry of Education, East China University of Science and Technology, Shanghai 200237, China

Correspondence should be addressed to Xingsheng Gu; xsgu@ecust.edu.cn

Received 5 December 2013; Accepted 6 February 2014; Published 13 March 2014

Academic Editor: Huaicheng Yan

Copyright © 2014 Y. Yang and X. Gu. This is an open access article distributed under the Creative Commons Attribution License, which permits unrestricted use, distribution, and reproduction in any medium, provided the original work is properly cited.

The job shop scheduling problem, which has been dealt with by various traditional optimization methods over the decades, has proved to be an NP-hard problem and difficult in solving, especially in the multiobjective field. In this paper, we have proposed a novel quadspace cultural genetic tabu algorithm (QSCGTA) to solve such problem. This algorithm provides a different structure from the original cultural algorithm in containing double brief spaces and population spaces. These spaces deal with different levels of populations globally and locally by applying genetic and tabu searches separately and exchange information regularly to make the process more effective towards promising areas, along with modified multiobjective domination and transform functions. Moreover, we have presented a bidirectional shifting for the decoding process of job shop scheduling. The computational results we presented significantly prove the effectiveness and efficiency of the cultural-based genetic tabu algorithm for the multiobjective job shop scheduling problem.

1. Introduction

The scheduling problem is one of the most important and hardest combinatorial optimization problems on account of its complexity and frequency in practical applications. The purpose of scheduling generally is to allocate a set of resources to tasks by the definition of Pinedo. Since the first appearance of the systematic method to scheduling problems was in the mid-1950s, thousands of articles on different scheduling problems have arisen in the literature, which can be categorized in accordance with shop environments, including single machine, parallel machines, flow shop, flexible flow shop, job shop, open shop, and others.

Job shop scheduling problem (JSSP) is one of the most difficult ones among all the scheduling problems. Literature [1] has summarized the approaches applied to JSSP. Gradually it has been handled using exact methods, branch and bound, and heuristic procedures based on priority rules and shifting bottleneck. However, it is a nonlinear control problem, just as other complex control systems [2]. Therefore, large-size problems are still considered to surpass the reach of exact methods. And then over the last decades, a growing

number of heuristics have been presented to solve these complex optimization problems: simulated annealing (SA), tabu search (TS), and evolutionary algorithms (EA), among others.

Among all these algorithms, the cultural algorithm has been paid attention to gradually and applied to solve scheduling problems. Similar to the development of evolutionary computation, Reynolds developed a model of the evolution of cultural systems and subsequently the cultural algorithms in 1994 [3]. The cultural algorithm proposed is a dual evolutionary system, which provides an interaction and cooperation between two different evolutions: brief and population spaces. And the acceptance and influence functions allow the dual inheritance to make interactions. After Reynolds proposed the cultural algorithm, he and his students applied the use of cultural algorithms to global optimization problems with better results [4]. They presented five knowledge sources [5–7] and proposed a full fuzzy cultural algorithm [8] and combined genetic algorithm. And incorporation of other evolutionary algorithms [9–11] with cultural algorithms has become a research focus. Cultural algorithm has been extensively and successfully applied to optimization problems

and has advantages in overcoming some weaknesses of conventional optimization methods, such as data mining, scheduling, and multiobjective optimization [12–14]. It is an intelligent technique that incorporates knowledge in the evolutionary process to make the process more effective and efficient.

It is common sense that practical scheduling problems are multiobjective by nature. And a number of solutions should be provided to decision makers to make a conclusion. Smith started the researches on multiobjective scheduling in 1956 by providing a Smith algorithm for some scheduling problems with weighted sum of completion time minimization, subject to all jobs being completed by their due dates [15]. Afterwards, plenty of scholars studied the multiobjective scheduling. However, the approaches they provided cannot be spread to a multiobjective context because they aim at a specific problem. Gradually research methods on multiobjective scheduling problem have converted from exact methods to the multiobjective decision-making theory [16, 17] and modern heuristic search methods such as GA [18, 19], particle swarm optimization (PSO) [20], simulated annealing (SA) [21, 22], and water drops algorithm [23]. Literature [24] proposed an interactive solution to $J|d_i|F_T(C_{\max}, \bar{C}, \bar{I}, T_{\max}, \bar{U})$, which is interactive with DM based on Tchebycheff-approximation in the first module and then using the greedy heuristic algorithm in the second module. But due to the disadvantages of heuristics, the genetic algorithm with its inherent global search advantage has been considered to be an efficient and effective means to solve JSSP with multiple criteria. Lei [25] put forward a simplified multiobjective genetic algorithm SMGA for stochastic job shop scheduling with makespan and total tardiness minimization. Literature [26] applied a hybrid genetic algorithm and tabu search for dynamic JSSP.

However, different from the research in the area of the single objective scheduling problem, researches that pay attention to multiple criteria have been scarce. The goal of multiobjective JSSP is to find as many different promising schedules as possible. In this work, we apply makespan and mean flow time as the objectives of our algorithm. After considering the advantage and disadvantage of the cultural algorithm, we modified the structure and strategies of the original one to coordinate with multiobjective JSSP.

In this paper, we present a novel quad-space cultural genetic tabu algorithm to solve the multiobjective scheduling problem, which consists of four spaces, including double brief spaces and double population spaces. The search process is divided into two parts, which have their own cultural structures while exchanging with each other at a predefined frequency, which is one of the novelties of our paper. The other novelty is to design two different brief spaces and their influence functions along with the multiobjective selection strategy. Last but not least, a bidirectional shifting is presented for decoding the presentation, which could help improve the solutions efficiently. The goals of this paper are twofold: first, to analyze the effects when changing the parameters of our algorithm and to verify the proposed cultural algorithm, second, use the algorithm to deal with the real multiobjective JSSP. To justify our approach, we compared our proposed

approach with other well established MOEAs- (NSGAI [27], SPEA2 [28]) and MPSO- [29] based approaches and found that the QSCGTA-based scheduling approach is able to outperform others in some fields.

The remainder of the paper is organized as follows. In Section 2, we explain the scheduling problem and multiobjective problem specifically as well as the concept and structure of both the original cultural algorithm and our novel cultural structure in Section 3. In Section 4, the four spaces cultured genetic tabu algorithm is developed to JSSP subsequently. Section 5 analyzes the performance results of QSCGTA when applied to solve common benchmarks in literature. At last, we come to our conclusion and some possible future directions.

2. Problems Formulation

JSSP is one of the most famous and hardest combinatorial optimization problems. During the past decades, a bunch of literature has been published, but no efficient algorithm has been presented yet for solving it to optimality in polynomial time.

Suppose we are given n jobs and m machines. Each machine can handle one job at most at a time. Each job consists of a sequence of operations and needs to be processed during an uninterrupted time period on a given machine. The purpose is to find a schedule, that is, the job sequence on the machines as to optimize one or more performance measurements, makespan, and mean flow time in our case. The traditional n jobs, m machines multiobjective JSSP can be described as follows:

$$\text{Minimize } \min_{X \in D} \{f_l(X)\}; \quad l = 1, \dots, k \quad (1)$$

$$f_1 = \max(T_{i,m}) \quad i = 1, \dots, n, \quad (2)$$

$$f_2 = \frac{1}{m} \sum_{i=1}^n T_{i,m}, \quad (2)$$

$$\text{Subject to: } T_{i,j} + \text{op}_{i,j} \leq T_{i,(j+1)} \quad i \in (1, n); \quad j \in (1, p_i), \quad (3)$$

$$\sum P_{(i,j),k} \leq 1 \quad (i, j) \in L(t); \quad k \in (1, m); \quad t \geq 0, \quad (4)$$

$$T_{i,j} \geq 0 \quad i \in (1, n); \quad j \in (1, p_i). \quad (5)$$

The indices and variables of the model are enumerated as follows: m : number of machines; n : number of jobs; i : job index; j : operation number index; p_i : number of operations of job i ; $T_{i,j}$: finish time of operation j th of job i ; $\text{op}_{i,j}$: processing time of operation j th of job i ; $L(t)$: set of operations being processed at time t .

Functions (1) and (2) infer the two objectives of JSSP. Constraints (3) ensure that the processing sequence of operations in each job is in accordance with the predetermined order. Constraints (4) demand that there is only one job on one machine at a time and (5) assures that the completion of all jobs should not be negative.

The conflicting character, where improving one objective may only be achieved when worsening another objective,

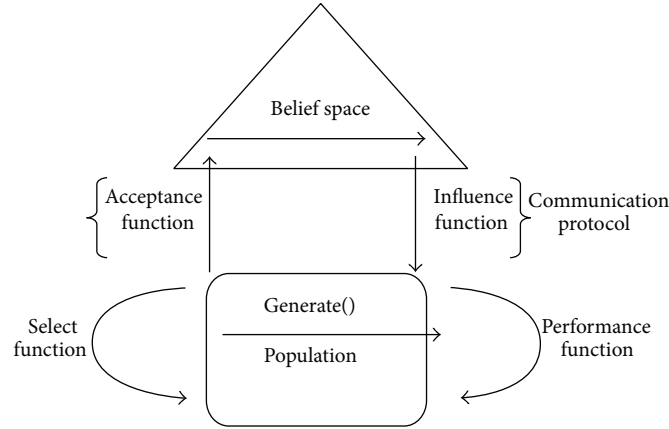


FIGURE 1: The cultural algorithm framework.

exists in objective functions generally. Therefore, obtaining an optimal scheduling solution that optimizes all the objectives is nearly impossible. However, there exists a set of equally efficient, nondominated, or noninferior solutions, known as the Pareto-optimal set. We recall the basic notion of efficient solution: a feasible solution X^* is Pareto optimal if there does not exist any other $X \in D$ such that $f_i(X) \leq f_i(X^*)$, for all i with at least one strict inequality. The set of all Pareto optima is called the Pareto optimal set and the set of all nondominant objective vectors is called Pareto front.

Many metaheuristic techniques have been proposed in the literature to search for near-optimal scheduling solutions. But the researches [30, 31] mainly focused on single machine or flow shop scheduling. Therefore, in this paper we deal with the multiobjective JSSP with makespan and mean flow time minimization.

3. A Novel Cultural Algorithm

The concept of culture can be defined in plenty of ways. Durham [32] described it as “a system of symbolically encoded conceptual phenomenon that are socially and historically transmitted within and between populations” in 1994. Therefore, culture can be taken as a vehicle for information storage. The information is accessible to all members of the society and can be useful in improving their problem solving activities. In other words, culture provides guidance and information to the new generation of a society. Without it, the only method for an individual to adapt to its environment is through plentiful trials and errors.

3.1. The Original Cultural Algorithm. Cultural algorithm is an evolution model through observing the cultural process in nature. It is a dual inheritance system that characterizes evolution at both the macroevolutionary level, which occurs at the belief space, and at the microevolutionary level, which takes place within the population space. These two spaces interface with each other through two functions: an acceptance function and an influence function. The cultural algorithm framework is shown in Figure 1.

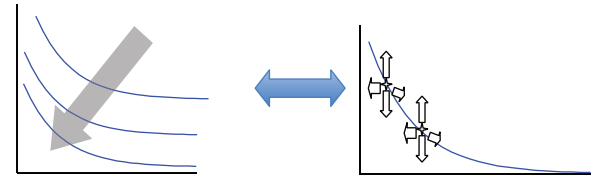


FIGURE 2: Overview of the exploration and exploitation processes.

As described in Figure 1, firstly the belief space and population space are initialized and the algorithm would repeat processing until a termination condition is met. The population space contains a set of possible solutions to the problem, and these individuals are evaluated by a performance function. Then an acceptance function decides which individuals in the current population should be selected and transformed to the current belief space. Those selected ones are adjusted with other individuals to update the belief space by an update function. Next, the updated knowledge in belief space is used to guide and influence the evolution in the population space through an influence function. Moreover, a selection function is used to select the population for the next generation. Most cultural-based algorithms applied the basic structure in Figure 1 while few modified it, such as literature [33], which designed a multilayer belief spaces structure.

3.2. The New Cultural Structure. It is well known that GA is not good at fine-tuning the solutions that are already close to the optimal solution, which means its local search ability is not as good as the global one. Hence, it is necessary to incorporate local search methods to find more effective optimal solutions, which is tabu search in this paper. We are not going to apply some local search after GA like many other researches do. The way we do it is to employ the two searching processes simultaneously with some interactions. The advantage of our approach is to gain more near-optimal solutions without suffering from premature convergence. The overview of the two processes is shown in Figure 2, in which the left one means exploration searching with genetic search and exploitation searching in the right one stands for TS.

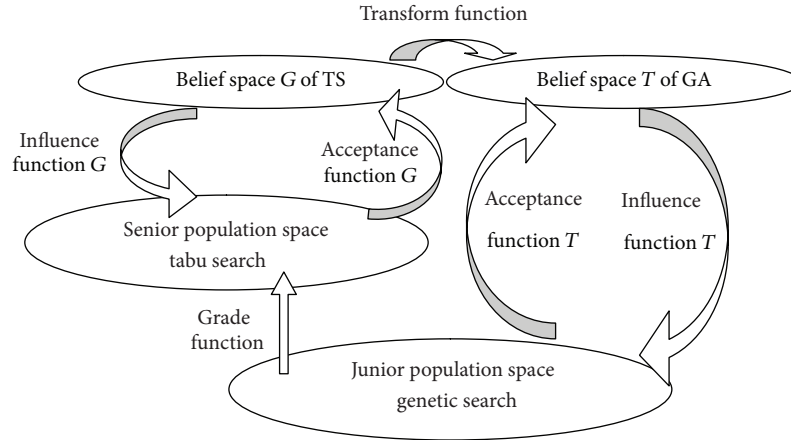


FIGURE 3: The framework of QSCGTA.

The proposed model, which consists of four spaces and dual evolution processes, takes advantage of a parallel and thorough search process compared to the original one. GA and TS are for the purpose of global and local search separately. The better individuals generated by genetic search in junior space are sent to the senior population space for further local search at regular or irregular intervals. The number and frequency of the individuals transmitted are determined by the grade function. Corresponding to the dual evolution process, there are two belief spaces guiding them separately toward the promising area through the influence functions and updated by the acceptance functions. And the best individuals in belief space of TS will be sent to the belief space of GA at predefined intervals by transform function. It is obvious that the advantage of the double search processes, besides the exploration and exploitation simultaneously, is that users can design different specific knowledge and influence functions for different goals. The flowchart of the advanced cultural algorithm is shown in Figure 3.

4. The Cultural-Based Genetic Tabu Algorithm for JSSP

Generally speaking, heuristic methods own advantages than exact methods in solving combinatorial optimization problems. Because it can provide more near-optimal solutions to decision makers. Therefore, we proposed the cultural genetic tabu algorithm to deal with the multiobjective JSSP.

4.1. The Representation and Schedule Builder

4.1.1. Representation. Chromosome representation is a key point in designing efficient evolutionary algorithms for constrained JSSPs. The reason is that different formulations in solutions correspond to different search spaces and different difficulties for further optimization operators. Although there have been all sorts of representation methods, generally speaking, these representations can be classified into the following two encoding approaches: direct approach and

indirect approach [34]. In direct approach, a schedule is encoded into a chromosome and algorithms are used to evolve those chromosomes to search for a better schedule. However, in the indirect approach, the chromosome is not a schedule, such as a sequence of dispatching rules for job assignment in priority rule-based representation. Algorithms then are used to find a better strategy to construct a schedule.

In our work, direct representation that belongs to operation-based representation with a schedule builder is used. This representation encodes a schedule as a sequence of operations and each gene represents one operation. To avoid the infeasibility raised by the precedence constraints, all operations for a job are named with the same symbol and interpreted by the order of occurrence in the given chromosome. This representation was employed by Bierwirth [35] and mathematically known as “permutation with repetition.” Considering a 3-job 3-machine problem, the chromosome contains $3 * 3$ genes, for example, given by

$$J_1 J_2 J_1 J_3 J_2 J_3 J_1 J_3 J_2 (1 \ 2 \ 1 \ 3 \ 2 \ 3 \ 1 \ 3 \ 2). \quad (6)$$

To obtain a feasible solution, the coding is interpreted as a task sequence

$$o_{11} o_{21} o_{12} o_{31} o_{22} o_{32} o_{13} o_{33} o_{23}. \quad (7)$$

By searching the permutation from left to right, a task o_{ij} of job J_i has to be scheduled on the determined machine by the technological order P_i . Therefore, one of the advantages of this representation is that any individual can be decoded to a feasible schedule. There does not exist the special case that processes the schedule operations whose technological predecessors have not been scheduled yet. Moreover, it shows another advantage in that the search template of the evolutionary search has no concern with details of particular scheduling problems. Last but not least, the decoding needed belongs to a simple mapping relation, which makes the decoding much easier.

The initial solutions are generated randomly with the length of $n * m$ in order to verify the robustness of our algorithm, which is one of the most important performances of algorithms [36].

```

Begin
for each  $o_{i,j}$ 
   $M = \text{findmachine}(o_{i,j});$     %find the corresponding machine
   $\text{count}_M = \text{count}_M + 1;$ 
   $\text{ldletime} = \text{scan}(M, T_{(i,j-1)});$  %scan the idle time on machine from the left to right
  if  $o_{P_{i,j}} < \text{ldletime}$ 
     $\text{LeftShift}(o_{i,j});$     %place the operation on that idle time
  else
     $\text{Place}(o_{i,j}, M, \text{count}_M);$  %place the operation at the end of the machine
  end
end
End %all the operations have been scheduled
For each  $o_{i,j}$  %in each machine from the right to left
   $\text{SL}(o_{i,j}) = \text{lastesttime}(o_{i,j});$  %calculate the last starting time of the operation
   $\text{idletime2} = \text{scanreverse}(M, T_{(i,j+1)});$  %scan the machine from the right to left
  if  $\text{SL}(o_{i,j}) < \max(\text{idletime2})$ 
     $\text{Place}(o_{i,j}, M, \text{idletime2});$ 
  else
     $\text{Place}(o_{i,j}, M, \text{SL}(o_{i,j}));$ 
  end
end
end
  modify the scheduling and output the results;
end

```

ALGORITHM 1: Illustration of the bidirectional decoding procedure.

4.1.2. Schedule Builder. After the representation, the chromosome must be transformed into a feasible schedule. And computational experiments performed in [37] showed that a powerful decoding strategy plays an important role in improving the final solutions in JSSP.

The schedule builder used in this paper is bidirectional decoding, which performs a kind of local search. The decoding allocates each operation on its assigned machine one by one in the order represented by the coding. When operation o_{ij} is scheduled on machine k , the idle time between operations that have already been processed on that machine is examined from left to right to find the earliest one that is not shorter than the process time of operation o_{ij} . If such an interval exists, it is allocated there, otherwise, it is allocated at the current end of machine j , which is called left shifting. After all the operations have been scheduled, we could obtain the latest starting time of each operation o_{ij} , represented by $\text{SL}(o_{ij})$ from right to left, which is the latest time at which operation o_{ij} can begin without delaying the makespan. Then the decoding allocates each operation with its latest starting time from right to left and shifting them orderly from right to left. This one is called right shifting. The left shifting has already proved to be effective in reducing the makespan. And right shifting procedure, which means reverse left shifting, can provide better performance along with left shifting.

The pseudocode of our proposed bidirectional shifting is as shown in Algorithm 1.

Through the bidirection shifting, the actual processing order of operations p and q may be opposite to the operation sequence vector. In order to allow offspring to inherit the information of their parents, the coding is reordered according to the operations' starting time in the decoded schedule.

4.2. Genetic Algorithm for Global Search. Genetic algorithms are stochastic search methods, containing complex interactions among parameters. The mechanics of the complex parameter interactions play an essential role in the performance of GA. Based on probability calculations and simulation results, Deb and Agrawal [38] observed that for simple problems, the mutation operator is the key search operator, while for complex problems, crossover operator plays an important role and performs well with an adequate population size. Based on these studies, it is recommended that the use of the crossover operator with an adequate population size is a reliable approach. Therefore, we prefer to apply the crossover with a large probability along with mutation with a small probability, as well as the analysis of population size with simulation results in the next section.

4.2.1. Crossover. Crossover is considered as the backbone of GA, which aims to inherit information of two parent solutions to offspring. Provided that the parents keep different aspects of better solutions, such as in multiobjective problems, crossover owns a good opportunity to find better offspring. Considering the repetition structure of the representation, crossover operators containing more genes should be applied instead of the one-point or two-point crossover.

In this paper, we applied two kinds of crossover and each applied with half possibility. Firstly the generalized order crossover [39] is used with a slight modification of getting two offspring in one crossover operation. We proposed a length of crossover-string between one-fourth and two-third of the total length of a chromosome. Secondly, the binary crossover, shown in Figure 4, is started by generating a binary string randomly, which consists by 0 and 1. The length of the string

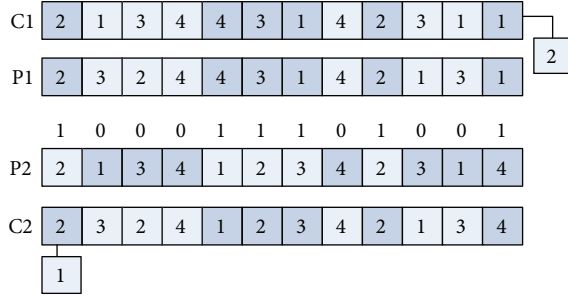


FIGURE 4: Illustration of the procedure of binary crossover.

is the same as the chromosomes. The offspring inherits the element of one parent at positions with bit 1 while inherits the element of the other one at positions with bit 0. And the redundant jobs would be replaced by the missing job sequencing. The other offspring is obtained likewise.

4.2.2. Mutation. Mutation is another important operator in GA and is usually performed after the crossover with a small probability. Considering the validation of the chromosome, we apply in this paper a swap mutation that needs no repair. Two different operations are picked randomly and then they exchange their positions.

The new individuals will be compared with the corresponding parent solutions by the following rules:

$$P_i^{t+1} = \begin{cases} P_i^t, & \text{if } \text{obj}(P_i^t) < \text{obj}(N_i) \\ N_i, & \text{otherwise,} \end{cases} \quad (8)$$

where obj is the objective functions, N_i is the i th new individual, and P_i^t is i th individual of the previous generation. And the rule of selecting individuals to perform crossover and mutation operators is 10-tournament selection to expand the selection of chromosomes, so that the ones with better performance have more chances to be chosen.

4.3. Tabu Algorithm for Further Local Search. Tabu search is one of the most efficient local search strategies for scheduling problems. It is obtained by transforming one solution to the next according to some neighborhood structures. The main elements of TS are the neighborhood structures, the tabu list length, and stopping rules. In our paper, because TS is a kind of point-search, the size should be much smaller than GA. It worked every ten iterations and shares the same stopping rules with global search. As for the neighborhood structure, we applied two kinds of neighborhood structures. Firstly, we chose the two-job exchange mutation as the neighborhood and an example of (1, 3) has been chosen as follows:

$$\begin{aligned} \text{Parent: } & 2 \underline{3} 2 4 4 \underline{3} 1 4 2 \underline{1} \underline{3} 1, \\ \text{Child: } & 2 \underline{1} 2 4 4 \underline{1} \underline{3} 4 2 \underline{3} \underline{1} 3. \end{aligned} \quad (9)$$

Secondly, the reversal of any two successive operations v and w on the critical path, where the two operations are not from the same job, was applied as another neighborhood structure. Because movements in the critical path

with certain constraints in multiobjective problems do not work remarkably as in single ones, movements between operations on different machines in the critical path have a certain possibility in improving the mean flow time while maintaining the same makespan. Last but not least, the tabu list length is decided by the experiments in Section 5.

4.4. Cultural Mechanism. The cultural mechanism in this paper plays a key role in guiding the evolution to promising areas, which consists of dual belief space, acceptance functions, influence functions, grade function, and transform function.

4.4.1. Grade Function and Transform Function. The grade function is proposed to decide how many and how frequent the individuals from GA should be sent to go through TS. Because of the single-point search nature of TS, we send a small population to TS compared to the population in GA. The number of grade population is self-adapted as shown in formula (10) and the frequency number is constant. And the transform function is to send one of the nondominated solutions to belief space of GA at a certain number of iterations

$$\begin{aligned} \text{mize} & \\ & = \begin{cases} \text{popsizeTS}, & \text{if } \text{exetime} = N \\ \text{popsizeTS} * A \\ * \exp\left(\frac{(1-g)}{(\text{max_iter} + 1 - g)}\right), & \text{if } \text{exetime} = n * N, \end{cases} \quad (10) \end{aligned}$$

where N means an interval the function works, A is constant coefficient, $n \in (1, \dots, (\text{max_iter}/N))$, max_iter infers the max generations, g is transforming times, and popsizeTS is the size of population for TS.

4.4.2. The Belief Space and Knowledge Structures. Generally speaking, the belief space of the cultural algorithm consists of several knowledge structures and is updated at a certain frequency. In our structure, there are two brief spaces that have different knowledge structures. Because our purpose is to enlarge the search space for GA in order to process global search while reduce the search space to guide the TS for local search, in brief space for GA, situational and topographical knowledge are adopted while situational and normative knowledge are applied for TS, while the history and domain knowledge are not applied for they are usually effective when the fitness landscape is dynamic.

The situational knowledge for GA consists of the best exemplars found along the evolution process. The structure is $[E_1, E_2, \dots, E_n]$. It records the nondominated set in GA. And the situational knowledge for TS is the same as the one for GA.

The normative knowledge represents the best district in the objective space and consists of two members (L_j^t, U_j^t) ,

which refers to lower and upper limits of a nondominated set of individuals. It means that

$$\begin{aligned} L_i^t &= \{\min \text{obj}_i(x^t), \forall x^t \in \text{NS}^t\} \quad i = 1, 2, \dots, N, \\ U_i^t &= \{\max \text{obj}_i(x^t), \forall x^t \in \text{NS}^t\} \quad i = 1, 2, \dots, N, \end{aligned} \quad (11)$$

where NS^t is the nondominated set, obj_i is the i th objective function, and N is the number of objectives.

The topographical knowledge is used to record the distribution of solutions to later help adapt the global acceleration. The space represented by normative knowledge is divided into grids of $s_1 \times s_2 \times \dots \times s_N$, where N is the number of objectives and s_i is the number of division in i th objective. Each cell will be represented by three elements $L_{\text{cell}} = [l_1, l_2, \dots, l_N]$, $U_{\text{cell}} = [u_1, u_2, \dots, u_N]$, and N_{cell} is the number of nondominated solutions in that cell. Consider

$$\begin{aligned} l_i^t &= L_i^t + p \times \frac{U_i^t - L_i^t}{s_i}, \quad i = 1, 2, \dots, N, \quad p = 0, 1, \dots, s_i - 1, \\ u_i^t &= l_i^t + \frac{U_i^t - L_i^t}{s_i}, \quad i = 1, 2, \dots, N. \end{aligned} \quad (12)$$

During each iteration, this knowledge will be updated to rebuild a new cell following the normative knowledge.

4.4.3. Acceptance Functions and Updating Brief Spaces and Knowledge. The knowledge of current belief space is updated by the individuals selected by acceptance function. The nondominated sets of populations are chosen to update the belief spaces.

The situational and normative knowledge are updated as follows:

$$\begin{aligned} E^{t+1} &= \begin{cases} E^t \cup x_i^t \setminus e, & \text{if } \exists e, \text{obj}(x_i^t) < \text{obj}(e) \\ E^t, & \text{if } \forall e, \text{obj}(e) < \text{obj}(x_i^t) \\ E^t \cup x_i^t, & \text{else,} \end{cases} \\ L_i^{t+1} &= \begin{cases} \text{obj}_i(x_k^t), & \text{if } \text{obj}_i(x_k^t) < L_i^t, x_k^t \in \text{NS}^t \\ L_i^t, & \text{otherwise} \end{cases} \\ U_i^{t+1} &= \begin{cases} \text{obj}_i(x_j^t), & \text{if } \text{obj}_i(x_j^t) > U_i^t, x_j^t \in \text{NS}^t \\ U_i^t, & \text{otherwise.} \end{cases} \end{aligned} \quad (13)$$

4.4.4. Influence Functions. Influence function is one of the key issues in cultural algorithms in guiding the evolutionary search. In this paper, we propose two totally different influence function structures for GA and TS.

The influence function applied on the genetic search consists of three parts. The first one is sending 10% individuals randomly to GA. This method will improve the quality of the population and then improve the evolution process.

The second one is applied to the mutation procedure. We apply the formula (14)~(15) to modify the mutation probability CM according to the topographical knowledge

$$\text{CM}^{t+1} = \begin{cases} \text{CM}^t + \frac{(N_{\text{best}}^t - N_{\text{best}}^{t+1})}{10}, & \text{if } N_{\text{best}}^t > N_{\text{best}}^{t+1} \\ \text{CM}^t - \frac{(N_{\text{best}}^{t+1} - N_{\text{best}}^t)}{10}, & \text{if } N_{\text{best}}^t < N_{\text{best}}^{t+1} \\ \text{CM}^t, & \text{otherwise,} \end{cases} \quad (14)$$

$$\text{CM}^{t+1} = \begin{cases} \text{CM}_{\text{max}}, & \text{if } \text{CM}^{t+1} > \text{CM}_{\text{max}} \\ \text{CM}_{\text{min}}, & \text{if } \text{CM}^{t+1} < \text{CM}_{\text{min}}, \end{cases} \quad (15)$$

where N_{best}^t is the number of nondominated ones in the cell where the best individual at t generation is located and N_{best}^{t+1} is the number of nondominated ones in the cell where the best individual at $t + 1$ generation is located. This formula implants a piecewise dynamic into the variation of the global acceleration. The values of N_{best}^t and N_{best}^{t+1} are stored in the topographical knowledge and CM should be limited in a range of $[\text{CM}_{\text{min}}, \text{CM}_{\text{max}}]$ according to formula (15).

And the last one is towards crossover. This is inspired by the phenomenon called Atavism, which is a theory in heredity holding that the reappearance of a characteristic in an organism after several generations of absence is usually caused by the chance recombination of genes. Therefore, we make the best individuals in situational knowledge crossover with the worst individuals in GA expecting that the offspring in several generations will inherit the good gene from the best individuals. We use the topographical knowledge stored in the belief space to select the best individual. Firstly, we use the roulette wheel selection to choose the least populated cell, and then randomly select a nondominated individual from that cell to be the best individual. Each cell is assigned a fitness of

$$\text{fitness}_{\text{cell}} = \frac{5}{N_{\text{cell}}}, \quad (16)$$

where N_{cell} is the number of nondominated ones located in that cell.

The influence function for TS consists of a combined effect by both situational knowledge and normative knowledge. Its strategy is, as formula (17) shows, towards tabu length L :

$$\begin{aligned} \text{Len}^{t+1} &= \begin{cases} \text{Len}^t + \Delta l, & \text{if } \text{obj}_i(x^t) < L_i^t \\ & \text{or } \text{obj}(x^t) > \text{obj}(e) \\ \text{Len}^t - \Delta l, & \text{if } \text{obj}(x^t) < \text{obj}(e) \\ \text{Len}^t, & \text{otherwise,} \end{cases} \\ \text{Len}^{t+1} &= \begin{cases} L_{\text{max}}, & \text{if } \text{Len}^{t+1} > L_{\text{max}} \\ L_{\text{min}}, & \text{if } \text{Len}^{t+1} < L_{\text{min}}. \end{cases} \end{aligned} \quad (17)$$

4.4.5. Global Archive. We design a limited archive to store the best solutions. And each new nondominated solution from

the two processes will be compared with members in the archive. If P_{new} dominates any member of the archive, P_{new} will replace the member in the archive. If P_{new} is dominated by any member of the archive, P_{new} will be disregarded. And if P_{new} neither dominates nor is dominated by the members of the archive, there will be two parts. If the archive is not full, P_{new} would be added to archive. However, if it is full, P_{new} would replace the one with the shortest distance between adjacent individuals. And the members in the archive take part in the selection process of GA along with the population.

To sum up, we proposed a novel hypergenetic algorithm incorporated with tabu search under the frame of cultural algorithm. The flowchart of our QSCGTA is shown in Figure 5.

5. Experimental Results and Discussion

5.1. The Testing Problem. Computational experiments are carried out to investigate the performance of our proposed cultural genetic tabu search. In order to evaluate the performance of our algorithm, we run the algorithm on a series of benchmark problems from the OR-Library (<http://people.brunel.ac.uk/~mastjib/jeb/info.html>), which is regarded as the standard testing problems in scheduling. The testing benchmark problems in this paper include MT problems, ABZ problems, and LA problems.

All the programs in the experiments were written in Matlab and all the experiments were running on platform using Intel Core 4 Quad 2.4 GHZ CPU with 2 GB RAM. First we applied orthogonal experiments to decide our parameter settings in the QSCGTA. And then we compared our algorithm with other well-known multiobjective evolutionary algorithms, which are NSGAI, SPEA2, and MPSO.

A set of solutions that are superior to the rest of the solutions exists in multiobjective optimization. Therefore, new approaches, which differ from the single objective, are required to compare the performance of the algorithms. The performance measures that are used are as follows.

- (1) Number of Pareto solution (NPS): this performance measurement is calculated by counting the number of nondominated solutions obtained. A larger number corresponds to better performance.
- (2) Hyperarea ratio (HR) [40]: this indicator shows the ratio between the area dominated by solutions and the entire solution area. A bigger ratio corresponds to a better solution. Given the difficulty in deciding the extent of the entire solution area, we used the rectangle constituted by the maximum and minimum of each objective as PF_{TRUE} :

$$HR = \frac{H_{PF_{\text{KNOWN}}}}{H_{PF_{\text{TRUE}}}}. \quad (18)$$

- (3) Spread of nondominance solutions (SNS): this criterion, which is known as an indicator of diversity, is calculated through the following formula. Larger

TABLE 1: Levels of the parameters.

Levels	PS (A)	CP (B)	MP (C)	TL (D)
1	50	0.6	0.1	5
2	100	0.7	0.2	10
3	150	0.8	0.3	15
4	200	0.9	0.4	20

values of this criterion correspond to higher quality solutions:

$$\begin{aligned} SNS &= \sqrt{\frac{\sum_{i=1}^n (\text{MID} - c_i)^2}{n-1}}, \\ \text{MID} &= \frac{\sum_{i=1}^n c_i}{n}, \\ c_i &= \sqrt{f_{1i}^2 + f_{2i}^2}, \end{aligned} \quad (19)$$

where n is the number of nondominated solutions and f_{1i} and f_{2i} are the values of the two objectives.

5.2. Computation Results

5.2.1. Parameters Selection through Orthogonal Experiment. The parameters, which can be uncertainty, had a great influence on the performance of the algorithm [41]. There have been several parameters that should be set properly in order to make the algorithm more effective, which are population size of genetic search (PS), the crossover possibility (CP), the mutation possibility (MP), and tabu list length (TL).

If the authors apply the factorial experiment to design the parameters, it requires $4^4 = 256$ experiments. It is a waste of time and resource. Therefore, the orthogonal experiment is carried out to tune the adjustable parameters of our algorithm, which just needs $4^2 = 16$ experiments.

The orthogonal experiment used here is to design experiments to investigate how different parameters affect the mean and variance of a process performance characteristic. The experiment design involves using orthogonal arrays to organize the parameters, which affect the process, and levels at which the parameters should be varies.

Generally first we considered the hyperarea ratio of problem MT10, LA25, LA28, LA36, and ABZ7 for ten times at 500 generations as the objective. Then we chose the four levels for population size of genetic search (PS), the crossover possibility (CP), the mutation possibility (MP), tabu list length (TL). The levels of all the parameters are listed in Table 1.

Here we chose the L16 orthogonal array and Table 2 shows the experiments results of MT10. The best HR of each column is shown in bold. Then after the range analysis, it is obvious that the major one is the size of population followed by mutation possibility and crossover possibility. And it also shows that the parameters PS = 150, CP = 0.8, MP = 0.4, and TL = 15 work better for MT10.

The parameter settings for the other four instances are applied the same way as MT10 and the results are shown in

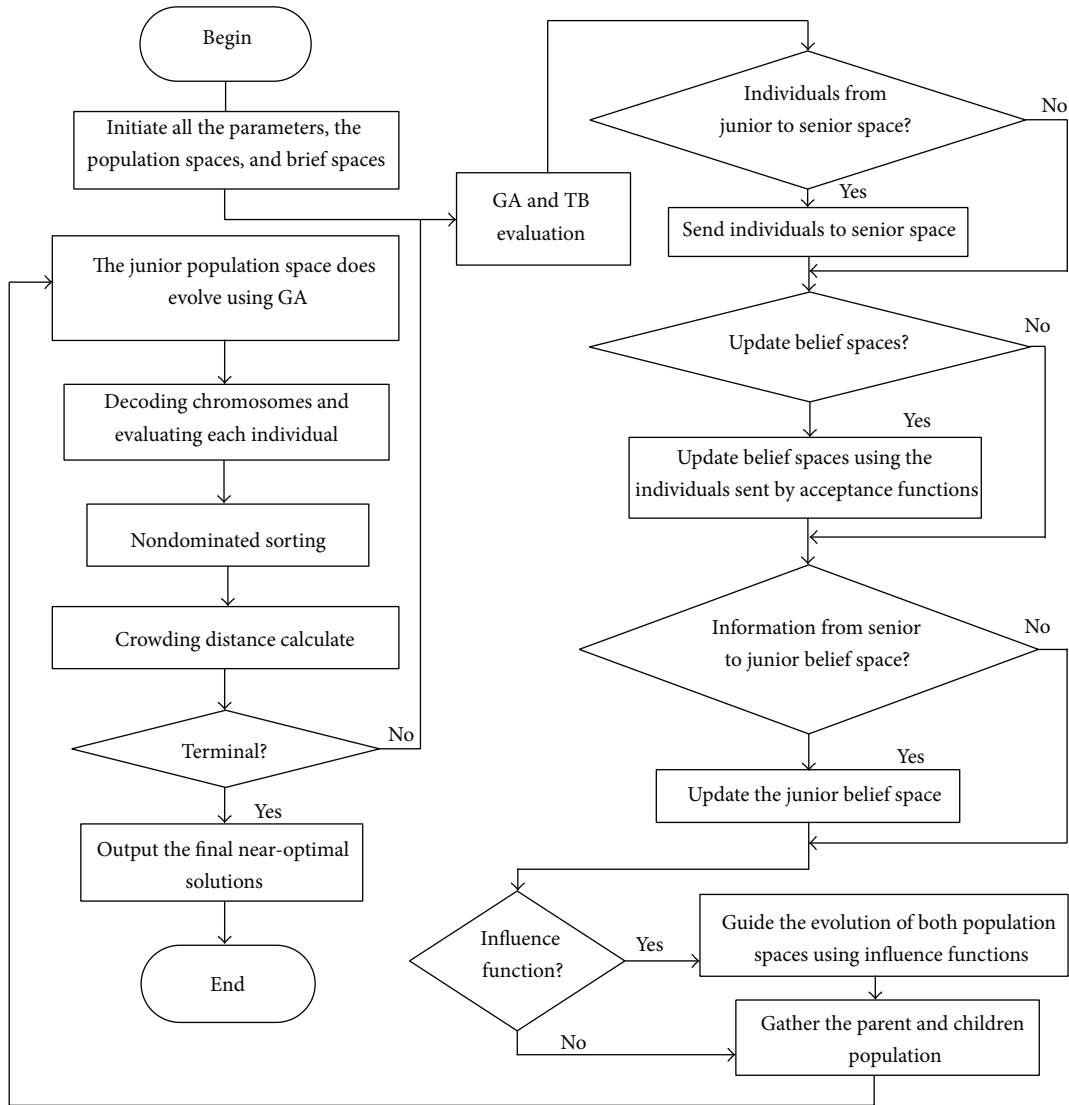


FIGURE 5: The flowchart of multiobjective QSCGTA.

Tables 3, 4, 5, and 6. The best HR of each column is shown in bold. Based on the data in tables, the best parameters settings are not completely consistent in all the problems. Concluding from all these tables, the authors set 150 for population, 0.4 for mutation possibility, 0.8 for crossover possibility, and 15 for tabu list length.

5.2.2. *Multiobjective Comparison.* Multiobjective optimization has two goals: one is to find a set of solutions as close as possible to the Pareto front, while the other is to find a set of solutions as diverse as possible.

The parameter settings of our algorithm are the same as above and the one for MPSO is the same as literature [29]. The parameters for NSGAI and SPEA2 are decided by the aforementioned orthogonal experiment and the settings are as follows.

- (1) The initial population is randomly generated and the number is set to 150.

- (2) Tournament selection is chosen.
- (3) The GOX and swap are used as crossover and mutation operators.
- (4) The ratios of GOX and swap are set to 0.8 and 0.4, respectively.
- (5) The size of archive is set to 40 and number of iteration is set to 500.

Each benchmark problem was tested for twenty times with different seeds. Then all the final generations were combined and the nondominated sorting was performed to constitute the final nondominated solutions.

The results in Table 7 showed that QSCGTA has the highest average hyperarea ratios in 14 of 18 instances, followed by PSO with 3 instances, SPEA2 with one instance, and NSGAI with none. With regard to number and spread of nondominance solutions, our approach found more near-optimal solutions with diversity than MPSO, SPEA2, and

TABLE 2: Range analysis of the orthogonal experiment for MT10.

	A	B	C	D	Empty	Results (HR)
	1	2	3	4	5	
1	1	1	1	1	1	0.0027
2	1	2	2	2	2	0.0635
3	1	3	3	3	3	0.5675
4	1	4	4	4	4	0.2822
5	2	1	2	3	4	0.4233
6	2	2	1	4	3	0.2439
7	2	3	4	1	2	0.5076
8	2	4	3	2	1	0.0566
9	3	1	3	4	2	0.5441
10	3	2	4	3	1	0.8328
11	3	3	1	2	4	0.6879
12	3	4	2	1	3	0.4633
13	4	1	4	2	3	0.9712
14	4	2	3	1	4	0.5825
15	4	3	2	4	1	0.4239
16	4	4	1	3	2	0.4315
k_1	0.2290	0.4853	0.3415	0.3890	0.3290	
k_2	0.3079	0.4307	0.3435	0.4448	0.3867	
k_3	0.6320	0.5465	0.4377	0.5638	0.5615	
k_4	0.6023	0.3084	0.6485	0.3735	0.4940	
Range	0.4030	0.2381	0.3070	0.1903	0.2325	
Order of test factors			A > C > B > D			
Optimal level	A3	B3	C4	D3		

TABLE 3: Results of parameter settings for LA25.

LA25	A	B	C	D
k	1	2	3	4
k_1	0.4387	0.4048	0.5426	0.3867
k_2	0.7944	0.5185	0.3827	0.4956
k_3	0.2409	0.5372	0.3646	0.5208
k_4	0.4611	0.4747	0.6453	0.5320
Range	0.5535	0.1324	0.2807	0.1453

TABLE 5: Results of parameter settings for LA36.

LA36	A	B	C	D
k	1	2	3	4
k_1	0.4552	0.3858	0.5321	0.4192
k_2	0.3872	0.3948	0.4202	0.3370
k_3	0.6345	0.6725	0.4628	0.4482
k_4	0.4889	0.5127	0.5507	0.4614
Range	0.2473	0.2866	0.1305	0.1112

TABLE 4: Results of parameter settings for LA28.

LA28	A	B	C	D
k	1	2	3	4
k_1	0.4724	0.3571	0.3343	0.3309
k_2	0.2277	0.6099	0.4581	0.4901
k_3	0.4347	0.4316	0.5659	0.3810
k_4	0.6196	0.3556	0.4961	0.3924
Range	0.3919	0.2543	0.2315	0.1592

TABLE 6: Results of parameter settings for ABZ7.

ABZ7	A	B	C	D
k	1	2	3	4
k_1	0.2854	0.3627	0.2734	0.3707
k_2	0.2108	0.2395	0.3141	0.3541
k_3	0.6236	0.1939	0.5829	0.3837
k_4	0.4304	0.5540	0.3798	0.2416
Range	0.2196	0.3601	0.2095	0.1422

NSGAI as well. Because the application of TS along with GA guides the search with more possibilities towards promising areas than traditional TS. Moreover it makes the search process converge more quickly than traditional GA. Besides, the cultural frame quickens the two searching processes.

To further test the stability of algorithms, we run the four algorithms twenty times independently, under the aforementioned environment, on randomly selected instances with different sizes, which are LA03, MT10, LA17, LA27, LA40, and ABZ7. The box plots of hyperarea ratio on these

TABLE 7: Results of algorithms on multiobjective JSSP.

	$N * M$	NSGAI			SPEA2			MPSO			QSCGTA		
		NPS	HR	SNS	NPS	HR	SNS	NPS	HR	SNS	NPS	HR	SNS
LA03	10 * 5	2	0.44	5.17	5	0.48	2.71	4	0.48	3.12	5	0.99	8.94
LA04	10 * 5	1	0.42	—	2	0.94	1.96	2	0.94	1.96	2	0.94	1.96
LA05	10 * 5	1	—	—	1	—	—	1	—	—	1	—	—
Mt10	10 * 10	3	0.53	1.11	1	0.69	—	3	0.93	2.13	4	0.94	12.00
LA16	10 * 10	2	0.45	5.19	5	0.62	4.85	3	0.60	21.56	6	0.86	10.41
LA17	10 * 10	1	0.39	—	7	0.60	14.17	6	0.75	12.87	7	0.89	18.06
LA18	10 * 10	3	0.42	7.70	3	0.52	1.75	5	0.79	2.81	5	0.78	9.70
LA22	15 * 10	4	0.32	9.31	6	0.69	18.23	3	0.73	3.15	2	0.99	23.54
LA23	15 * 10	3	0.51	5.25	1	0.43	—	1	0.69	—	7	0.79	22.00
LA25	15 * 10	2	0.54	9.42	7	0.86	1.68	10	0.77	9.36	5	0.95	6.07
LA27	20 * 10	2	0.44	4.10	3	0.59	5.86	2	0.70	6.07	5	0.83	4.62
LA28	20 * 10	3	0.52	6.38	3	0.54	3.42	3	0.71	8.88	5	0.82	9.67
LA29	20 * 10	1	0.29	—	2	0.81	5.28	4	0.64	7.33	2	0.67	7.22
LA36	15 * 15	3	0.38	9.15	6	0.52	3.89	3	0.63	3.92	8	0.93	14.71
LA38	15 * 15	1	0.30	—	2	0.75	14.25	2	0.79	12.23	4	0.95	7.35
LA40	15 * 15	4	0.37	7.69	1	0.61	—	3	0.96	1.19	5	0.81	7.73
ABZ7	20 * 15	3	0.43	2.51	5	0.52	4.03	3	0.63	0.79	4	0.95	11.77
ABZ8	20 * 15	1	0.37	—	2	0.78	0.21	1	0.52	—	5	0.87	5.77
ABZ9	20 * 15	3	0.52	9.95	6	0.70	1.79	3	0.77	26.84	2	0.73	13.32

TABLE 8: Performance of algorithms on instances generated randomly.

$N * M$	NSGAI		SPEA2		MPSO		QSCGTA	
	HR	SNS	HR	SNS	HR	SNS	HR	SNS
10 * 10	0.39	9.06	0.37	13.59	0.50	5.49	0.46	6.49
10 * 15	0.34	8.85	0.50	6.10	0.75	6.36	0.85	8.85
10 * 20	0.51	5.19	0.72	4.79	0.81	6.89	0.81	11.58
15 * 15	0.22	5.32	0.48	4.66	0.70	8.15	0.83	12.14
15 * 20	0.43	4.58	0.61	6.34	0.78	6.67	0.87	8.20
20 * 20	0.37	3.14	0.50	5.17	0.68	7.99	0.92	7.24

instances are shown in Figure 6. This figure clearly indicates that the QSCGTA outperforms the NSGAI and SPEA2 both in stability and distribution. With regard to MPSO, QSCGTA is with a less concentrated distribution, however, with better optimal and mean. Moreover, observing from the computation time comparison in Figure 7, QSCGTA requires about a quarter of time MPSO needed, half time of NSGAI, and slightly larger than SPEA2. In other words, QSCGTA owns advantages over the other three algorithms.

Moreover, to further verify the performance of our algorithm, the performance for HR is computed for each algorithm on randomly generated instances. Several problem scenarios were generated by varying one or more of the number of machines and number of jobs. For each scenario, 20 problems were randomly generated by setting operation processing times from a uniform distribution in the interval [5, 100], and the average values across these instances were recorded. All jobs had randomly assigned routing through the system. The results on instances generated randomly,

shown in Table 8, also validated the exploration and exploitation of our QSCGTA.

6. Conclusions

Multiobjective scheduling has become the main research field in scheduling problems because of the multiobjective character, by nature, of many real-world scheduling problems. Due to the complexity of the job shop scheduling problem, many researches have been focused on multiobjective single machine problems or flow shop problems. The researches on multiobjective job shop problems are very rare. Therefore, in this paper, we have proposed QSCGTA for solving the multiobjective JSSP. The GA and TS have been incorporated in the frame of a novel cultural algorithm to search for the Pareto-optimal schedules.

The experiments indicated that our approach is suitable for applied benchmark problems and obviously yielded better performance in terms of solutions, stability, and computation

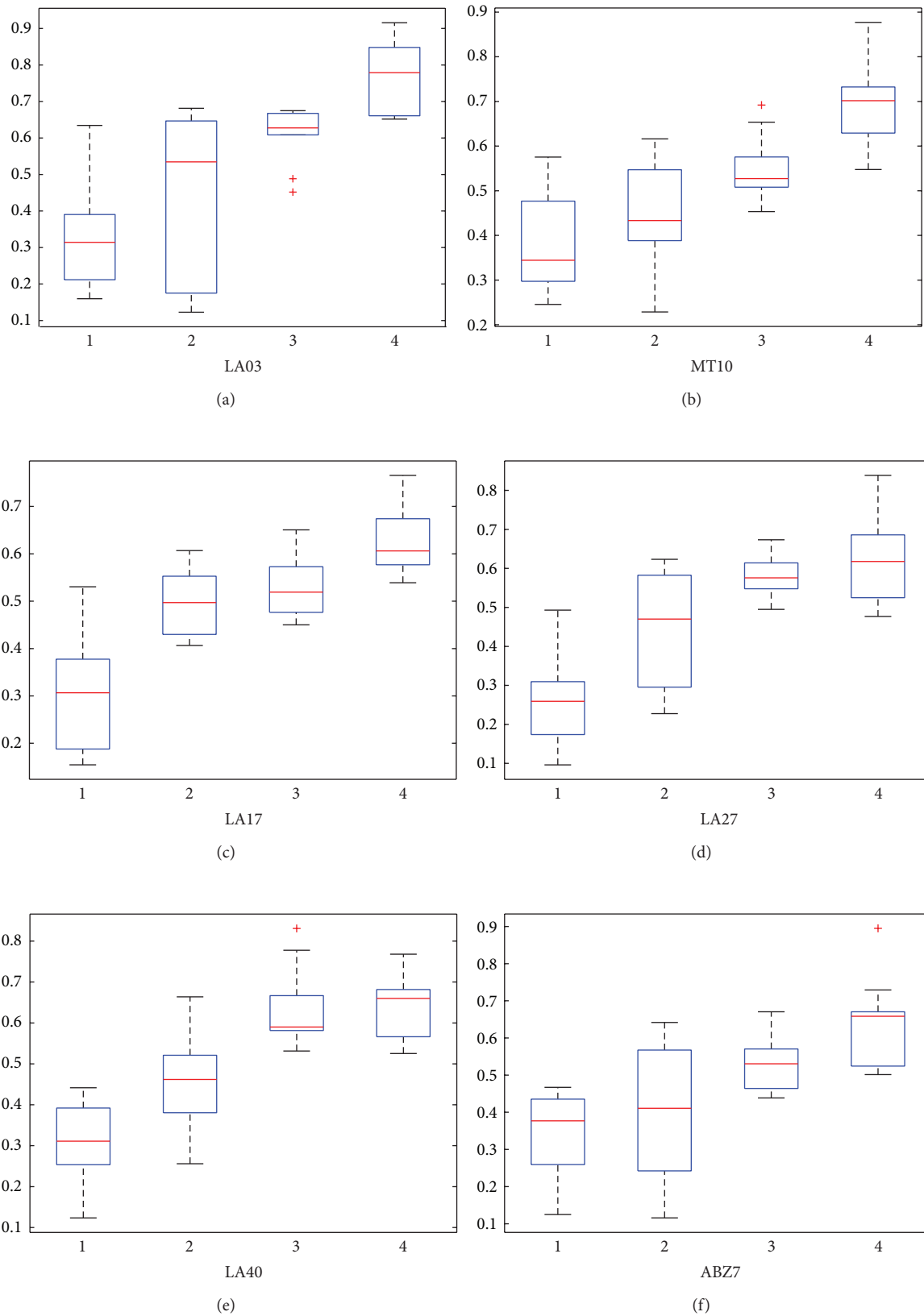


FIGURE 6: The box plots of hyperarea ratio for different problems. Column numbers refer to (1) NSGAI, (2) SPEA2, (3) MPSO, and (4) QSCGTA.

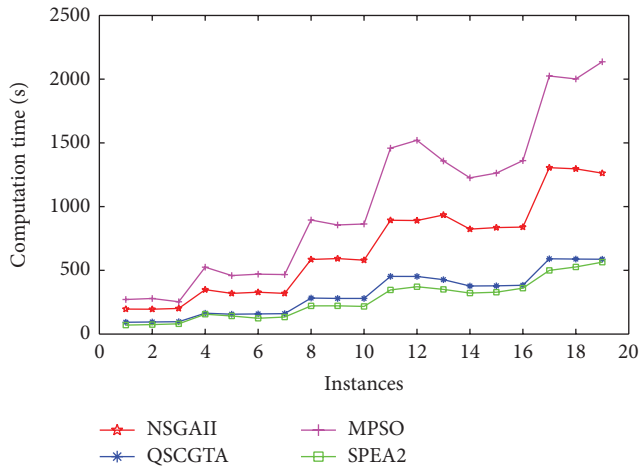


FIGURE 7: Computational time of four algorithms for different problems.

time compared with the other three algorithms. The main strength of our approach is in combination with global and local search under a novel cultural algorithm frame in order to produce diverse solutions while maintaining the convergence of the nondominated solutions. In each generation, only a predefined number of the best solutions of GA is selected for applying TS. It provides more diversity toward Pareto-optimal solutions. All in all, our proposed QSCGTA-based evolutionary scheduling approach accomplished the goals of multiobjective job shop scheduling problems both in convergence and diversity.

More comprehensive studies can be applied to extend the QSCGTA. Other possible criteria in multiobjective optimization will be considered. Furthermore, more local search methods will be analyzed to integrate to the QSCGTA algorithm.

Conflict of Interests

The authors declare that there is no conflict of interests regarding the publication of this paper.

Acknowledgments

The authors appreciate the support of National Natural Science Foundation of China (Grant nos. 61174040 and 61104178), Shanghai Commission of Science and Technology (Grant no. 12JC1403400), and Fundamental Research Funds for the Central Universities.

References

- [1] J. F. Gonçalves, J. J. M. Mendes, and M. G. C. Resende, "A hybrid genetic algorithm for the job shop scheduling problem," *European Journal of Operational Research*, vol. 167, no. 1, pp. 77–95, 2005.
- [2] H. Zhang, H. Yan, F. Yang, and Q. Chen, "Quantized control design for impulsive fuzzy networked systems," *IEEE Transactions on Fuzzy Systems*, vol. 19, no. 6, pp. 1153–1162, 2011.
- [3] R. G. Robert, "An introduction to cultural algorithms," in *Proceeding of the 3rd Annual Conference Evolution Programming*, pp. 131–136, Singapore, 1994.
- [4] C. Chung and R. G. Reynolds, "A testbed for solving optimization problems using cultural algorithms," in *Proceedings of the 5th Annual Conference on Evolutionary Programming*, pp. 225–236, Cambridge, Mass, USA, 1996.
- [5] R. G. Reynolds and X. Jin, "Using region-schema to solve non-linear constraint optimization problems: a culture algorithm approach," in *Proceedings of the Conference in honor of John H. Holland*, The Netherlands, 1999.
- [6] S. M. Saleem, *Knowledge-based solution to dynamic optimization problems using cultural algorithms [Ph.D. thesis]*, Wayne State University, Detroit, Mich, USA, 2001.
- [7] C. J. Chung, *Knowledge-based approaches to self-adaptation in cultural algorithms [Ph.D. thesis]*, Wayne State University, Detroit, Mich, USA, 1997.
- [8] S. Zhu and R. G. Reynolds, "Fuzzy cultural algorithms with evolutionary programming," *Evolutionary Programming VII*, vol. 1447, pp. 209–218, 1998.
- [9] A. V. Abs da Cruz, M. A. C. Pacheco, M. Vellasco, and C. R. H. Barbosa, "Cultural operators for a quantum-inspired evolutionary algorithm applied to numerical optimization problems," in *Artificial Intelligence and Knowledge Engineering Applications: A Bioinspired Approach*, vol. 3562, pp. 1–10, 2005.
- [10] M. Daneshyari and G. G. Yen, "Constrained multiple-swarm particle swarm optimization within a cultural framework," *IEEE Transactions on Systems, Man, and Cybernetics A*, vol. 42, no. 2, pp. 475–490, 2012.
- [11] Y. Sun, L. B. Zhang, and X. S. Gu, "A hybrid co-evolutionary cultural algorithm based on particle swarm optimization for solving global optimization problems," *Neurocomputing*, vol. 98, pp. 76–89, 2012.
- [12] X. D. Jin, *Solving constrained optimization problems using cultural algorithms and regional schemata [Ph.D. thesis]*, Wayne State University, Detroit, Mich, USA, 2001.
- [13] M. Daneshyari and G. G. Yen, "Cultural-based multiobjective particle swarm optimization," *IEEE Transactions on Systems, Man, and Cybernetics B*, vol. 41, no. 2, pp. 553–567, 2011.
- [14] H. F. Zhang, J. Z. Zhou, N. Fang et al., "Daily hydrothermal scheduling with economic emission using simulated annealing technique based multi-objective cultural differential evolution approach," *Energy*, vol. 50, pp. 24–37, 2013.
- [15] W. E. Smith, "Various optimizers for single-stage production," *Naval Research Logistics Quarterly*, vol. 3, pp. 59–66, 1956.
- [16] E. P. C. Kao, "A multiple objective decision theoretic approach to one-machine scheduling problems," *Computers and Operations Research*, vol. 7, no. 4, pp. 251–259, 1980.
- [17] R. L. Daniels, "Incorporating preference information into multi-objective scheduling," *European Journal of Operational Research*, vol. 77, no. 2, pp. 272–286, 1994.
- [18] A. H. Kashan, B. Karimi, and F. Jolai, "An effective hybrid multi-objective genetic algorithm for bi-criteria scheduling on a single batch processing machine with non-identical job sizes," *Engineering Applications of Artificial Intelligence*, vol. 23, no. 6, pp. 911–922, 2010.
- [19] P.-C. Chang and S.-H. Chen, "The development of a sub-population genetic algorithm II (SPGA II) for multi-objective

- combinatorial problems,” *Applied Soft Computing Journal*, vol. 9, no. 1, pp. 173–181, 2009.
- [20] G. Zhang, X. Shao, P. Li, and L. Gao, “An effective hybrid particle swarm optimization algorithm for multi-objective flexible job-shop scheduling problem,” *Computers and Industrial Engineering*, vol. 56, no. 4, pp. 1309–1318, 2009.
- [21] Y. Xu, R. Qu, and R. Li, “A simulated annealing based genetic local search algorithm for multi-objective multicast routing problems,” *Annals of Operations Research*, vol. 206, pp. 527–555, 2013.
- [22] T. Loukil, J. Teghem, and P. Fortemps, “A multi-objective production scheduling case study solved by simulated annealing,” *European Journal of Operational Research*, vol. 179, no. 3, pp. 709–722, 2007.
- [23] S. H. Niu, S. K. Ong, and A. Y. C. Nee, “An improved intelligent water drops algorithm for solving multi-objective job shop scheduling,” *Engineering Applications of Artificial Intelligence*, vol. 26, pp. 2431–2442, 2013.
- [24] K. Huckert, R. Rhode, O. Roglin, and R. Weber, “On the interactive solution to a multicriteria scheduling problem,” *Zeitschrift für Operations Research*, vol. 24, no. 1, pp. A47–A60, 1980.
- [25] D. Lei, “Simplified multi-objective genetic algorithms for stochastic job shop scheduling,” *Applied Soft Computing Journal*, vol. 11, no. 8, pp. 4991–4996, 2011.
- [26] L. P. Zhang, L. Gao, and X. Y. Li, “A hybrid genetic algorithm and tabu search for a multi-objective dynamic job shop scheduling problem,” *International Journal of Production Research*, vol. 51, no. 12, pp. 3516–3531, 2013.
- [27] K. Deb, A. Pratap, S. Agarwal, and T. Meyarivan, “A fast and elitist multiobjective genetic algorithm: NSGA-II,” *IEEE Transactions on Evolutionary Computation*, vol. 6, no. 2, pp. 182–197, 2002.
- [28] E. Zitzler, M. Laumanns, and L. Thiele, “SPEA2: improving the strength pareto evolution algorithm for multiobjective optimization,” in *Proceedings of the Evolutionary Methods for Design, Optimization and Control with Applications to Industrial Problems (EUROGEN '01)*, 2001.
- [29] R. Tavakkoli-Moghaddam, M. Azarkish, and A. Sadeghnejad-Barkousaraie, “A new hybrid multi-objective Pareto archive PSO algorithm for a bi-objective job shop scheduling problem,” *Expert Systems with Applications*, vol. 38, no. 9, pp. 10812–10821, 2011.
- [30] V. T'kindt, N. Monmarché, F. Tercinet, and D. Laügt, “An ant colony optimization algorithm to solve a 2-machine bicriteria flowshop scheduling problem,” *European Journal of Operational Research*, vol. 142, no. 2, pp. 250–257, 2002.
- [31] R. Qing-dao-er-ji and Y. Wang, “Inventory based bi-objective flow shop scheduling model and its hybrid genetic algorithm,” *Mathematical Problems in Engineering*, vol. 2013, Article ID 976065, 7 pages, 2013.
- [32] W. Durham, *Co-Evolution: Genes, Culture, and Human Diversity*, Stanford University, Stanford, Calif, USA, 1994.
- [33] H.-Y. Huang, X.-S. Gu, and M.-D. Liu, “Research on cultural algorithm for solving nonlinear constrained optimization,” *Acta Automatica Sinica*, vol. 33, no. 10, pp. 1115–1120, 2007.
- [34] R. Cheng, M. Gen, and Y. Tsujimura, “A tutorial survey of job-shop scheduling problems using genetic algorithms—I. Representation,” *Computers and Industrial Engineering*, vol. 30, no. 4, pp. 983–997, 1996.
- [35] C. Bierwirth, “A generalized permutation approach to job shop scheduling with genetic algorithms,” *OR Spektrum*, vol. 17, no. 2-3, pp. 87–92, 1995.
- [36] H. Yan, Z. Su, H. Zhang, and F. Yang, “Observer-based H_∞ control for discrete-time stochastic systems with quantisation and random communication delays,” *IET Control Theory & Applications*, vol. 7, no. 3, pp. 372–379, 2013.
- [37] T. Yamada, *Studies on meta heuristics for jobshop and flowshop scheduling problems [Ph.D. thesis]*, Kyoto University, Kyoto, Japan, 2003.
- [38] K. Deb and S. Agrawal, “Understanding interactions among genetic algorithm parameters,” in *Foundations of Genetic Algorithms V*, pp. 265–286, Morgan Kaufmann, San Mateo, Calif, USA, 1999.
- [39] C. Bierwirth, D. C. Matfield, and H. Kopfer, “On permutation representation for scheduling problems,” in *Parallel Problem Solving from Nature*, vol. 1141, pp. 310–318, 1996.
- [40] E. Zitzler, *Evolutionary algorithms for multiobjective optimization: methods and applications [Ph.D. thesis]*, Shaker Verlag, Aachen, Germany, 1999.
- [41] H. Zhang, Z.-H. Guan, and G. Feng, “Reliable dissipative control for stochastic impulsive systems,” *Automatica*, vol. 44, no. 4, pp. 1004–1010, 2008.

Research Article

Switched Quantization Level Control of Networked Control Systems with Packet Dropouts

Shuo Wang, Mei Yu, Hangfei Wang, and Wen Tan

School of Control and Computer Engineering, North China Electric Power University, Beijing 102206, China

Correspondence should be addressed to Mei Yu; meiyu@ncepu.edu.cn

Received 2 December 2013; Revised 28 January 2014; Accepted 30 January 2014; Published 12 March 2014

Academic Editor: Yang Shi

Copyright © 2014 Shuo Wang et al. This is an open access article distributed under the Creative Commons Attribution License, which permits unrestricted use, distribution, and reproduction in any medium, provided the original work is properly cited.

This paper investigates the relationship between the maximum allowable dropout bound and the quantization density. Networked Control System (NCS) is described as a time-delay switched system with constrained switching signals. A switched dynamic output feedback controller with prescribed disturbance attenuation level is designed via a cone complement linearization approach. A novel stability criterion is obtained by switched system theory. Furthermore, finding an appropriate quantization density used when packet dropout occurs is converted to an optimization problem.

1. Introduction

Networked Control System (NCS) has been widely used in industrial production such as aerospace engineering, robotic engineering, and power system. The control information is exchanged via communication networks in NCS. It has many attractive advantages, such as less wiring, low costs, ease of system diagnosis and maintenance, and increased flexibility. On the contrary, it may induce some problems such as quantization error and packet dropouts which deteriorate the performance of system or even cause instability [1].

Quantization effect cannot be avoided in the digital control process, and the stabilization problem by quantized feedback has been extensively studied in the last few years [2–5]. In [6], a sufficient condition is presented for filtering error system to be mean square exponentially stable with prescribed H_∞ performance by employing the multiple Lyapunov function method. The obtained condition depends on packet dropout rate of NCS. In [7], coarsest memoryless quantizer which can stabilize a single-input system with packet loss is proposed in the sense of stochastic quadratic stability. All of the aforementioned works use time-invariant signal quantization strategy and ignore network load condition. Actually, it is less conservative to switch quantization level according to network load condition. To achieve this, [8] proposes an adaptive quantization density method to reduce

network congestion. The quantization density is designed to be a function of the networked load modeled by a Markov process. However, no specific parameters reflecting network load has been introduced. The Markov chain may not be obtained easily and might vary under some unknown disturbance. Packet loss is an important indicator for load condition and it can be measured easily by adding a counter at controller node. Therefore, packet loss number is treated as switching signal of load condition in our paper. A large packet loss number means that the network load condition is worse. A coarser quantization density which implies transmitting less information can decrease the incidence rates of packet drop. So the quantization density should be increased as much as possible in order to exchange for better network performance when successive packet dropouts occur. Nevertheless, the quantization density cannot be increased indefinitely for a specified number of packet loss because this may cause oscillation in system [9–12]. Hence, it is essential to investigate the relationship between packet loss number and quantization level.

Many researchers have studied packet loss in NCS and lots of stability analysis results have been obtained [13–16]. For most of the aforementioned papers about packet loss problem, stochastic system approach is usually adopted to investigate the stability criterion of NCS. Generally, packet dropout process is modeled as an independent and identical

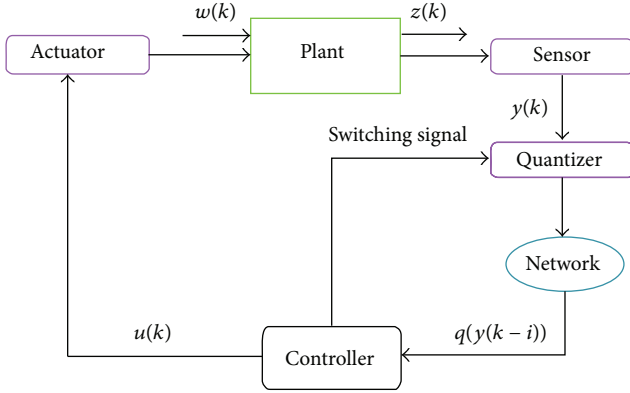


FIGURE 1: Structure of NCS.

distributed Bernoulli process [17–20]. It is easy to study the relationship between packet loss rate and quantization density by this method. However, this makes it difficult to add successive packet dropout number to the NCS model. The transition probability matrix or packet loss probability must be known beforehand by experimentation. The controller designed via stochastic system approach is constrained by packet loss probability. Once the probability changes, the controller should be redesigned, which reduces the flexibility. The quantitative relationship between packet dropouts number and quantization density has not been studied by switched system approach yet. Switched system approach is more flexible and independent of packet loss probability. This inspires us to try modeling the NCS as a switched linear discrete-time system.

In this paper, the switched quantization strategy is set as follows: if the successive packet drop number increases, coarser quantization densities will be used at the next sampling time to relieve network congestion; a fine quantization density is selected when the data is transmitted successfully. An algorithm of a dynamic output feedback controller synthesis is proposed. A stability criterion dependent on quantization density and successive packet dropout number is given. The relationship between number of packet dropouts and quantization density is established through switched system theory. The structure of NCS proposed in this paper is depicted in Figure 1.

The advantage of the method presented in this paper is that the probability of packet loss need not be prior informed. Less experiments about network load mean that the costs of test and lots of time can be saved. The load condition of network can be dynamically optimized by transmitting less information when packet dropout happens. Fewer inequalities need to be solved since the constrained switching signal approach [21] is used to model the packet dropout. This greatly reduces the computation.

Two assumptions are needed for designing the controller and quantization density as follows: (1) the network locates between the sensor and controller node; (2) if packet loss occurs, the actuator will use the last successful transmitted data.

This paper is organized as follows. Section 2 gives the system description, the form of dynamic output feedback controller, and quantization error model. Main results for controller synthesis and stability analysis are presented in Section 3. The validity of the approach is illustrated by a simulation example in Section 4. In Section 5, a summary for this paper is proposed.

2. System Modeling and Problem Formulation

Consider a discrete-time linear system model

$$x(k+1) = Ax(k) + B_1w(k) + B_2u(k),$$

$$z(k) = C_1x(k) + D_1w(k), \quad (1)$$

$$y(k) = C_2x(k),$$

where $x(k) \in \mathfrak{R}^n$, $u(k) \in \mathfrak{R}^m$, $z(k) \in \mathfrak{R}^{m_1}$, $y(k) \in \mathfrak{R}^{m_2}$ are the state vector, input, controlled output, and measured output. $w(k)$ is the disturbance which belongs to $l_2[0, \infty)$. $A, B_1, B_2, C_1, C_2, D_1$ are known matrices with appropriate dimensions.

When the number of packet dropouts increases, the quantization density should be switched to reduce the network congestion. The logarithmic quantizer is proposed as follows:

$$q(v, \sigma) = \begin{cases} \rho^h(\sigma) & \text{if } \frac{1}{1+\delta(\sigma)}\rho^h(\sigma) < v \\ & \leq \frac{1}{1-\delta(\sigma)}\rho^h(\sigma), \\ 0 & \text{if } v = 0, \\ -q(-v, \sigma) & \text{if } v < 0, \end{cases} \quad (2)$$

where v is the signal to be quantized and $q(v, \sigma)$ is the quantized signal. The introduction of variable σ aims to represent the switching signal of quantization density. $0 < \rho(\sigma) < 1$ is related to $\delta(\sigma)$ by

$$\delta(\sigma) = \frac{1-\rho(\sigma)}{1+\rho(\sigma)}. \quad (3)$$

The associated quantized set \mathcal{U} is given as

$$\mathcal{U} = \{\pm\rho^h(\sigma), h = 0, \pm 1, \pm 2, \dots\} \cup \{0\}. \quad (4)$$

The quantization error $e(k, \sigma)$ is proposed as follows:

$$e(k, \sigma) = q(v(k), \sigma) - v(k) = \Delta_q(\sigma)v(k),$$

$$\Delta_q(\sigma) \in [-\delta(\sigma), \delta(\sigma)], \quad (5)$$

$$\sigma \in \{0, 1, \dots, d\},$$

where d is the maximum number of packet loss. According to the definition of $\Delta_q(\sigma)$, it can be treated as norm-bounded time-varying uncertain parameter in NCS [22]. This means that

$$\Delta_q(\sigma) = HFE, \quad (6)$$

where

$$\begin{aligned} H &= 1, & E &= \delta(\sigma), \\ F^T F &\leq I. \end{aligned} \quad (7)$$

A switched dynamic output feedback (DOF) controller is used to compensate the packet dropouts as follows:

$$\begin{aligned} \hat{x}(k+1) &= A_c(i) \hat{x}(k) + B_c(i) q(y(k-i)), \\ u(k) &= C_c(i) \hat{x}(k). \end{aligned} \quad (8)$$

Remark 1. The variable i has two different meanings in the system. It stands for: (a) the switching signal of controller; (b) the successive dropout number of networked control system at instant $(k+1)T$. The switching signal of quantizer is a map, $\sigma: \mathbb{Z}^+ \mapsto \{0, 1, \dots, d\}$.

Remark 2. In this paper, the switching signal i is not arbitrary, but satisfies the following constraints. If the successive packet dropout number is $i-1$ ($i \in \{1, 2, \dots, d\}$) at the present time, the number of consecutive packet loss is equal to i or 0 at the next instant; if the packet drop number is d at this instant, the data must be transmitted successfully at next sampling time.

Now define a new state vector $\xi(k) = [x^T(k), \hat{x}^T(k)]^T$. From (1), (5), and (8), the closed-loop system is given as follows:

$$\begin{aligned} \xi(k+1) &= A_{cl}(i) \xi(k) + B_{cl}(i) (1 + \Delta_q(\sigma)) \bar{C}_2 \xi(k-i) \\ &\quad + \bar{B}_1 w(k), \\ z(k) &= \bar{C}_1 \xi(k) + D_1 w(k), \end{aligned} \quad (9)$$

where $A_{cl}(i) = \begin{bmatrix} A & B_c C_c(i) \\ 0 & A_c(i) \end{bmatrix}$, $B_{cl}(i) = \begin{bmatrix} 0 \\ B_c(i) \end{bmatrix}$, $\bar{B}_1 = \begin{bmatrix} B_1 \\ 0 \end{bmatrix}$, $\bar{C}_2 = [C_2 \ 0]$, $\bar{C}_1 = [C_1 \ 0]$.

The problem under investigation is formulated as follows.

(i) For a prescribed $\gamma > 0$ and quantization densities $\delta(\sigma)$, design a switched DOF controller of the form (8) such that:

- (1) the system (9) is asymptotically stable with $w(k) = 0$;
- (2) under the zero-initial condition, the controlled output $z(k)$ satisfies

$$\sum_{k=0}^{\infty} z^T(k) z(k) \leq \gamma^2 \sum_{k=0}^{\infty} w^T(k) w(k) \quad (10)$$

for all nonzero $w(k)$.

- (ii) For an H_∞ controller obtained by the method above, select a maximum $\delta(\sigma)$ in order to ease network congestion.

The following lemmas will play a key role in designing the DOF controller for NCS.

Lemma 3 (see [23]). Define two new vectors: $\tilde{\xi}(k) = \xi(k+1) - \xi(k)$, $\eta(k) = [\tilde{\xi}^T(k), \tilde{\xi}^T(k-i), w^T(k)]^T \in \mathfrak{R}^{4n+1}$; then for any matrices $R \in \mathfrak{R}^{2n \times 2n}$, $M \in \mathfrak{R}^{2n \times (4n+1)}$, and $Z \in \mathfrak{R}^{(4n+1) \times (4n+1)}$ satisfying

$$\begin{bmatrix} R & M \\ M^T & Z \end{bmatrix} \geq 0, \quad (11)$$

the following inequality holds

$$-\sum_{j=k-i}^{k-1} \tilde{\xi}^T(j) R \tilde{\xi}(j) \leq \eta^T(k) \{Y_1 + Y_1^T + iZ\} \eta(k), \quad (12)$$

where $Y_1 = M^T [I, -I, 0]$.

Lemma 4 (see [24]). Assume that H, F, E are real matrices with appropriate dimensions and $F^T F \leq I$. The inequality $Y + HFE + E^T F^T H^T < 0$ holds if there exists a scalar $\varepsilon > 0$ satisfying

$$Y + \varepsilon^{-1} E^T E + \varepsilon H H^T < 0. \quad (13)$$

3. Controller Synthesis and Stability Analysis

The following theorem provides a methodology of designing a switched output feedback controller.

Theorem 5. For a given scalar $\gamma > 0$ and quantization densities $\delta(\sigma)$, if there exist positive symmetric matrices $P(i) > 0$, $\mathcal{P}(i) > 0$, $P(0) > 0$, $\mathcal{P}(0) > 0$, matrices $R, R_1 \in \mathfrak{R}^{2n \times 2n}$, $M_1 \in \mathfrak{R}^{2n \times 2n}$, $M_2 \in \mathfrak{R}^{2n \times 2n}$, $M_3 \in \mathfrak{R}^{2n \times 1}$, $Z_{11} \in \mathfrak{R}^{2n \times 2n}$, $Z_{12} \in \mathfrak{R}^{2n \times 2n}$, $Z_{13} \in \mathfrak{R}^{2n \times 1}$, $Z_{22} \in \mathfrak{R}^{2n \times 2n}$, $Z_{23} \in \mathfrak{R}^{2n \times 1}$, $Z_{33} \in \mathfrak{R}^{1 \times 1}$, $A_c(0), B_c(0), C_c(0), A_c(i), B_c(i), C_c(i)$, scalar $\varepsilon > 0$ satisfying the following inequalities for all $i \in \{1, \dots, d\}$:

$$\begin{bmatrix} R_1 & M_1 & M_2 & M_3 \\ * & Z_{11} & Z_{12} & Z_{13} \\ * & * & Z_{22} & Z_{23} \\ * & * & * & Z_{33} \end{bmatrix} \geq 0, \quad (14)$$

$$\begin{bmatrix} \Phi(i-1) & * & * & * \\ \Gamma_1(i) & -\mathcal{P}(i) & * & * \\ i\Gamma_2(i) & 0 & -iR & * \\ 0 & \bar{C}_2^T B_{cl}^T(i) & i\bar{C}_2^T B_{cl}^T(i) & -\varepsilon^{-1}I \end{bmatrix} < 0, \quad (15)$$

$$\begin{bmatrix} \Lambda(i) & * & * \\ \Pi_1(0) & -\mathcal{P}(0) & * \\ 0 & \bar{C}_2^T B_{cl}^T(0) & -\varepsilon^{-1}I \end{bmatrix} < 0, \quad (16)$$

$$\begin{bmatrix} \Lambda(0) & * & * \\ \Pi_1(0) & -\mathcal{P}(0) & * \\ 0 & \bar{C}_2^T B_{cl}^T(0) & -\varepsilon^{-1}I \end{bmatrix} < 0, \quad (17)$$

where

$$\Phi(i-1) = \begin{bmatrix} -P(i-1) + \bar{C}_1^T \bar{C}_1 + M_1 + M_1^T + iZ_{11} & M_2 - M_1^T + iZ_{12} & \bar{C}_1^T D_1 + M_3 + iZ_{13} \\ * & \varepsilon^{-1} \delta^2 (d) I - M_2 - M_2^T + iZ_{22} & iZ_{23} - M_3 \\ * & * & D_1^T D_1 - \gamma^2 + iZ_{33} \end{bmatrix},$$

$$\Gamma_1(i) = [A_{cl}(i) \ B_{cl}(i) \ \bar{C}_2 \ \bar{B}_1],$$

$$\Gamma_2(i) = [A_{cl}(i) - I \ B_{cl}(i) \ \bar{C}_2 \ \bar{B}_1],$$

$$\Lambda(i) = \begin{bmatrix} -P(i) + \bar{C}_1^T \bar{C}_1 + \varepsilon^{-1} \delta^2 (i) I & \bar{C}_1^T D_1 \\ * & D_1^T D_1 - \gamma^2 \end{bmatrix},$$

$$\Pi_1(0) = [A_{cl}(0) + B_{cl}(0) \ \bar{C}_2 \ \bar{B}_1],$$

$$P(i) \mathcal{P}(i) = I, \quad P(0) \mathcal{P}(0) = I, \quad R_1 R = I,$$
(18)

then the closed-loop system is stable with the prescribed H_∞ performance.

Proof. Construct a switched Lyapunov function $V(k)$ for the closed-loop system as

$$V(k) = \xi^T(k) P(i-1) \xi(k) + \sum_{l=i}^{-1} \sum_{j=k+l}^{k-1} \tilde{\xi}^T(j) R_1 \tilde{\xi}(j). \quad (19)$$

Case 1. Assume that at times kT and $(k+1)T$, the numbers of packet loss are $i-1$ and i ($1 \leq i \leq d$); then the forward difference of $V(k)$ is given as follows:

$$\begin{aligned} \Delta V(k) &= \xi^T(k+1) P(i) \xi(k+1) - \xi^T(k) P(i-1) \xi(k) \\ &\quad + i \tilde{\xi}^T(k) R_1 \tilde{\xi}(k) - \sum_{j=k-i}^{k-1} \tilde{\xi}^T(j) R_1 \tilde{\xi}(j). \end{aligned} \quad (20)$$

Using Lemma 3, the following inequality can be obtained:

$$\begin{aligned} \Delta V(k) &= \eta^T(k) \bar{\Gamma}_1^T(i) P(i) \bar{\Gamma}_1(i) \eta(k) - \xi^T(k) P(i-1) \xi(k) \\ &\quad + i \eta^T(k) \bar{\Gamma}_2^T(i) R_1 \bar{\Gamma}_2(i) \eta(k) - \sum_{j=k-i}^{k-1} \tilde{\xi}^T(j) R_1 \tilde{\xi}(j) \\ &\leq \eta^T(k) \bar{\Gamma}_1^T(i) P(i) \bar{\Gamma}_1(i) \eta(k) - \xi^T(k) P(i-1) \xi(k) \\ &\quad + i \eta^T(k) \bar{\Gamma}_2^T(i) R_1 \bar{\Gamma}_2(i) \eta(k) \\ &\quad + \eta^T(k) (\Upsilon_1 + \Upsilon_1^T + iZ) \eta(k) \end{aligned}$$

$$\begin{aligned} &+ \eta^T(k) \Psi^T \Psi \eta(k) - \gamma^2 w^T(k) w(k) \\ &- z^T(k) z(k) + \gamma^2 w^T(k) w(k), \end{aligned} \quad (21)$$

where

$$\Upsilon_1 = M^T [I, -I, 0],$$

$$\bar{\Gamma}_1(i) = [A_{cl}(i), B_{cl}(i) (1 + \Delta_q(\sigma)) \bar{C}_2, \bar{B}_1], \quad (22)$$

$$\bar{\Gamma}_2(i) = [A_{cl}(i) - I, B_{cl}(i) (1 + \Delta_q(\sigma)) \bar{C}_2, \bar{B}_1],$$

$$\Psi = [\bar{C}_1, 0, D_1].$$

Partition matrices M and Z as $M = [M_1, M_2, M_3]$, $Z = \begin{bmatrix} Z_{11} & Z_{12} & Z_{13} \\ * & Z_{22} & Z_{23} \\ * & * & Z_{33} \end{bmatrix}$.

Applying Schur complement (see [25]) on (21), $\Delta V(k) \leq -z^T(k)z(k) + \gamma^2 w^T(k)w(k)$ is equivalent to the following matrix inequality:

$$\begin{bmatrix} \bar{\Phi}(i-1) & * & * \\ \bar{\Gamma}_1(i) & -P^{-1}(i) & * \\ i \bar{\Gamma}_2(i) & 0 & -i R_1^{-1} \end{bmatrix} < 0, \quad (23)$$

where

$$\tilde{\Phi}(i-1) = \begin{bmatrix} -P(i-1) + \bar{C}_1^T \bar{C}_1 + M_1 + M_1^T + iZ_{11} & * & * \\ -M_1 + M_2^T + iZ_{12} & -M_2 - M_2^T + iZ_{22} & * \\ D_1^T \bar{C}_1 + M_3^T + iZ_{13} & -M_3^T + iZ_{23} & D_1^T D_1 - \gamma^2 + iZ_{33} \end{bmatrix}. \quad (24)$$

From (6), we know that

$$B_{cl}(i) \Delta_q(\sigma) \bar{C}_2 = B_{cl}(i) F \delta(\sigma) \bar{C}_2. \quad (25)$$

Rewriting inequality (23), we can note that

$$\begin{bmatrix} \tilde{\Phi}(i-1) & * & * \\ \Gamma_1(i) & -P^{-1}(i) & * \\ i\Gamma_2(i) & 0 & -iR^{-1} \end{bmatrix} + \begin{bmatrix} 0 \\ \tilde{B}_{cl}(i) \\ i\tilde{B}_{cl}(i) \end{bmatrix} F [\delta(\sigma) \tilde{I} \ 0 \ 0] \\ + \begin{bmatrix} \delta(\sigma) \tilde{I}^T \\ 0 \\ 0 \end{bmatrix} F^T [0 \ \tilde{B}_{cl}^T(i) \ i\tilde{B}_{cl}^T(i)] < 0, \quad (26)$$

where

$$\tilde{I} = [0 \ I \ 0], \quad \tilde{B}_{cl}(i) = B_{cl}(i) \bar{C}_2. \quad (27)$$

Applying Lemma 4 and Schur complement on the inequality above, (15) is easy to be obtained according to $\Delta_q(\sigma) \leq \delta(\sigma) \leq \delta(d)$. This guarantees inequality (23). Adding $\Delta V(k)$ from 0 to ∞ , the following result can be derived owing to the zero-initial condition ($V(0) = 0$):

$$V(\infty) - V(0) \leq \sum_{k=0}^{\infty} -z^T(k) z(k) + \gamma^2 w^T(k) w(k). \quad (28)$$

This yields

$$\sum_{k=0}^{\infty} z^T(k) z(k) \leq \gamma^2 \sum_{k=0}^{\infty} w^T(k) w(k). \quad (29)$$

When $w(k) = 0$, it is obvious that $\Delta V(k) \leq 0$.

Case 2. At time kT , the packet dropout number is i or 0. At time $(k+1)T$, the packet is transmitted successfully. In this case, the second term of the Lyapunov functional becomes zero. Eliminate $\xi(k-i)$ in $\eta(k)$. Replacing $P(i)$ in (21) with $P(0)$ and $P(i-1)$, the proof is almost the same with that of Case 1. We can see that inequalities (16) and (17) guarantee the stabilization of NCS with prescribed H_∞ performance. \square

A switched controller can be obtained by solving the Bilinear Matrix Inequalities in Theorem 5. A cone complement approach shown as follows can be used to solve the problem [26]:

$$\begin{aligned} \min \quad & \text{Tr} \left(R_1 R + \sum_{i=0}^d P(i) \mathcal{P}(i) \right) \\ \text{subject to} \quad & (14), (15), (16), (17) \text{ and} \\ & \begin{bmatrix} P(i) & I \\ I & \mathcal{P}(i) \end{bmatrix} \geq 0 \quad (i \in \{0, 1, \dots, d\}), \\ & \begin{bmatrix} R_1 & I \\ I & R \end{bmatrix} \geq 0. \end{aligned} \quad (30)$$

For given controller matrices of system (9), a method of stability analysis is also needed in the sense of time-variant quantization density. Therefore, a novel stability criterion for system (9) with switched quantization level is proposed as follows. This method can also be used in choosing a suitable quantization density.

Theorem 6. For a prescribed scalar i ($i = 1, \dots, d$), $\gamma > 0$, controller matrices $A_c(0), B_c(0), C_c(0), A_c(i), B_c(i), C_c(i)$, and quantization densities $\delta(\sigma)$, if there exist sets of symmetric positive-definite matrices $P(i) > 0, P(0) > 0$, matrices $R_1, Z_{11}, Z_{12}, Z_{13}, Z_{22}, Z_{23}, Z_{33}, M_1, M_2, M_3$, scalar $\varepsilon > 0$ satisfy the following inequalities:

$$\begin{bmatrix} R_1 & M_1 & M_2 & M_3 \\ * & Z_{11} & Z_{12} & Z_{13} \\ * & * & Z_{22} & Z_{23} \\ * & * & * & Z_{33} \end{bmatrix} \geq 0, \quad (31)$$

$$\begin{bmatrix} \Theta_{11} & \Theta_{12} & \Theta_{13} \\ * & \Theta_{22} & \Theta_{23} \\ * & * & \Theta_{33} \end{bmatrix} < 0, \quad (32)$$

$$\begin{bmatrix} \Xi_{11} & \Xi_{12} \\ * & \Xi_{22} \end{bmatrix} < 0, \quad (33)$$

$$\begin{bmatrix} \tilde{\Xi}_{11} & \tilde{\Xi}_{12} \\ * & \tilde{\Xi}_{22} \end{bmatrix} < 0, \quad (34)$$

where

$$\begin{aligned}
\Theta_{11} &= \Phi(i-1), \\
\Theta_{12} &= \Gamma_1^T(i)P(i), \\
\Theta_{13} &= [i\Gamma_2^T(i)R_1 \ 0], \\
\Theta_{22} &= -P(i), \\
\Theta_{23} &= [0 \ P(i)B_{cl}(i)\bar{C}_2], \\
\Theta_{33} &= \begin{bmatrix} -iR_1 & iR_1B_{cl}(i)\bar{C}_2 \\ * & -\varepsilon^{-1}I \end{bmatrix}, \\
\Xi_{11} &= \Lambda(i), \\
\Xi_{12} &= [\Pi_1^T(0)P(0) \ 0], \\
\Xi_{22} &= \begin{bmatrix} -P(0) & P(0)B_{cl}(i)\bar{C}_2 \\ * & -\varepsilon^{-1}I \end{bmatrix}, \\
\tilde{\Xi}_{11} &= \Lambda(0),
\end{aligned} \tag{35}$$

the closed-loop system is asymptotically stable with the disturbance attenuation level γ .

Proof. Consider Case 1 in the proof of Theorem 5. Multiply (15) to the right by the matrix $\text{diag}\{I, P(i), R_1, I\}$ and the left by its transpose. By Schur complement, if the inequalities (31) and (32) hold, then the inequality (23) holds [27]. Thus the closed-loop system is asymptotically stable with the disturbance attenuation level γ .

Case 2: Pre- and postmultiply (16) and (17) by $\text{diag}\{I, P(0), I\}$; then if (33) and (34) hold, the closed-loop system is asymptotically stable with the disturbance attenuation level γ . The proof is similar to that of Case 1. \square

After designing a switched H_∞ controller, a $\delta(d)$ that is large enough should be selected to reduce the packet dropouts. This can be converted to a convex optimization problem as follows:

$$\begin{aligned}
&\max \quad \delta(d) \\
&\text{subject to} \quad \text{inequalities (31), (32), (33), (34) in Theorem 6.}
\end{aligned} \tag{36}$$

Remark 7. The quantization density for the worst packet loss case $\delta(d)$ can be increased until the LMIs are infeasible. The maximum $\delta(d)$ can be used to quantize the data transmitted to the controller when the load condition takes a turn for the worse. By the approach proposed in this paper, we not only design a less conservative controller by changing quantization level when network load is heavy but also search for an optimized quantization density.

4. Numerical Examples

In this section, the numerical simulation is given to illustrate the main results in this paper.

Consider the following example of a discrete-time LTI system (1), where

$$\begin{aligned}
A &= \begin{bmatrix} 0.08 & -0.025 & 0 & 1 \\ 1 & 0 & 0 & 0 \\ -0.8 & 0.5 & 0.002 & -0.03 \\ 0 & 0 & 0.0792 & 0 \end{bmatrix}, & B_1 &= \begin{bmatrix} 0 \\ 0.1 \\ 0 \\ 0.05 \end{bmatrix}, \\
B_2 &= \begin{bmatrix} 1 \\ 0 \\ 0 \\ 0 \end{bmatrix}, & C_1 &= [0 \ 0.1 \ 0 \ 0], \\
C_2 &= [4.5 \ -4.5 \ 0 \ 2], & D_1 &= 0.03.
\end{aligned} \tag{37}$$

The maximum number of packet loss is assumed to be 3. For the simplicity of presentation, the switched output feedback controller is designed to have two modes $\{0, 1\}$. 0 represents that there is no packet dropout at this time, whereas 1 means that packet loss happens. Set the initial value of quantization density as $\delta(0) = 0.02$, $\delta(1) = 0.04$. $\gamma = 0.95$ is chosen for the design of controller. Using the approach given in Theorem 5, the controller matrices are obtained as follows:

$$\begin{aligned}
A_c(0) &= \begin{bmatrix} -0.0304 & -0.1710 & -0.1544 & 0.0041 \\ 0.1589 & 0.1676 & 0.0222 & -0.1436 \\ -0.1773 & -0.0481 & 0.1254 & 0.1836 \\ 0.0730 & -0.1047 & -0.1861 & -0.0964 \end{bmatrix}, \\
B_c(0) &= \begin{bmatrix} 0.0059 \\ 0.0133 \\ 0.0085 \\ -0.0041 \end{bmatrix}, \\
C_c(0) &= [-0.1794 \ -0.1404 \ 0.0277 \ 0.1704], \\
A_c(1) &= \begin{bmatrix} 0.5117 & -0.0017 & -0.0517 & -0.0568 \\ -0.0068 & 0.5088 & 0.0601 & 0.0145 \\ -0.0419 & -0.0606 & 0.4383 & 0.0358 \\ 0.0615 & 0.0314 & -0.0276 & 0.4012 \end{bmatrix}, \\
B_c(1) &= \begin{bmatrix} -0.0035 \\ 0.0017 \\ 0.0053 \\ 0.0040 \end{bmatrix}, \\
C_c(1) &= [-0.0143 \ -0.0731 \ -0.0648 \ 0.0032].
\end{aligned} \tag{38}$$

After designing a switched output feedback controller, a suitable $\delta(\sigma)$ should be selected according to the method given above. Solving inequalities (31), (32), (33), and (34) in Theorem 6, we can find that the LMIs are still feasible when $\delta(1) = 0.07$ and $\gamma = 0.197$ which is smaller than the prescribed 0.95. This means that the quantization density can be switched to 0.07 when network load is heavy. The network congestion can be reduced. The states evolution of system is shown in Figures 2, 3, 4, and 5.

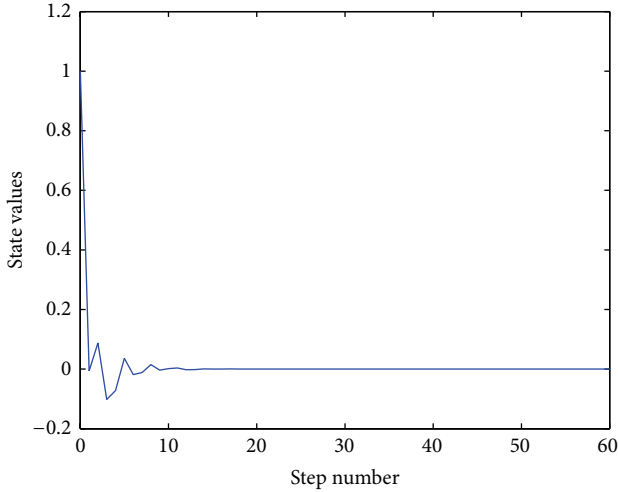


FIGURE 2: State X_1 .

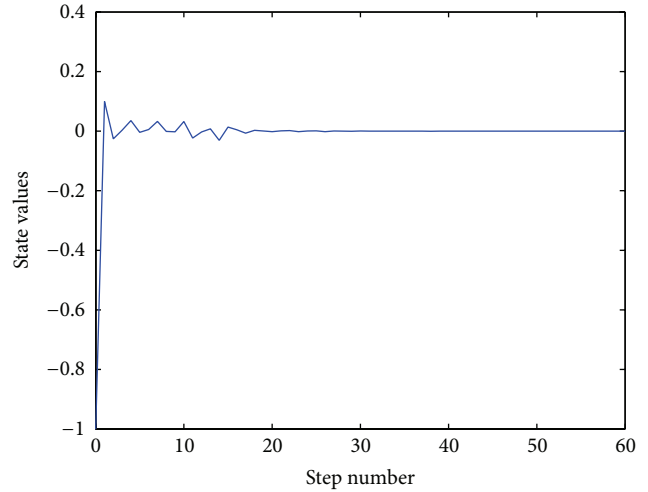


FIGURE 5: State X_4 .

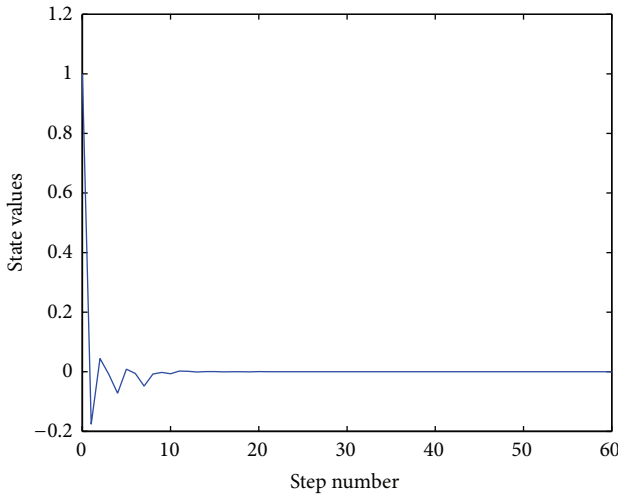


FIGURE 3: State X_2 .

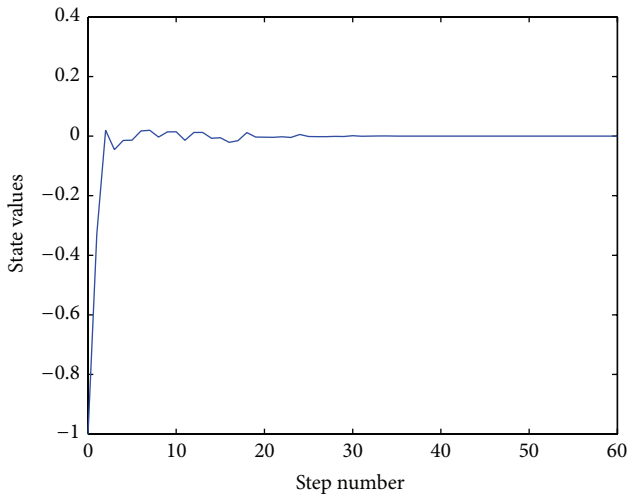


FIGURE 4: State X_3 .

To compare with the case of fixed quantization density, $\delta = 0.07$ which corresponds to heavy load is adopted for quantizing data. In this case, network load condition is ignored for design of the controller. A fixed quantization density implies that the load condition cannot be dynamically optimized and the control law can only be computed for the worst load condition. Using Theorem 5, no feasible solution can be found with this density. This indicates that the proposed approach is less conservative.

5. Conclusions

The quantitative relationship between quantization density and packet loss number has been studied by switched system approach in this paper. A robust H_∞ feedback control law has been derived in terms of bilinear matrix inequalities which can be solved by a cone complement algorithm. A new method for stability analysis of NCS with quantization error and packet drop has been given in the form of Linear Matrix inequalities. An approach to choose suitable quantization density $\delta(d)$ has been presented. The result is less conservative but more flexible since a switched controller and quantization level are used. The effectiveness of the method is illustrated by a simulation example.

Conflict of Interests

The authors declare that there is no conflict of interests regarding the publication of this paper.

Acknowledgments

This work is supported by Beijing Municipal Natural Science Foundation (4122075), the National Natural Science Foundation of China under Grants (no. 61004031, no. 61174096, and no. 61104141), and the Fundamental Research Funds for the Central Universities.

References

- [1] P. Antsaklis and J. Baillieul, "Special issue on technology of networked control systems," *Proceedings of the IEEE*, vol. 95, no. 1, pp. 5–8, 2007.
- [2] Y. Ishido, K. Takaba, and D. E. Quevedo, "Stability analysis of networked control systems subject to packet-dropouts and finite-level quantization," *Systems & Control Letters*, vol. 60, no. 5, pp. 325–332, 2011.
- [3] W. Yang, M. Liu, and P. Shi, " H_∞ filtering for nonlinear stochastic systems with sensor saturation, quantization and random packet losses," *Signal Processing*, vol. 92, no. 6, pp. 1387–1396, 2012.
- [4] C. Peng and Y.-C. Tian, "Networked H_∞ control of linear systems with state quantization," *Information Sciences*, vol. 177, no. 24, pp. 5763–5774, 2007.
- [5] M. Trivellato and N. Benvenuto, "State control in networked control systems under packet drops and limited transmission bandwidth," *IEEE Transactions on Communications*, vol. 58, no. 2, pp. 611–622, 2010.
- [6] H. Song, L. Yu, and W.-A. Zhang, "Networked H_∞ filtering for linear discrete-time systems," *Information Sciences*, vol. 181, no. 3, pp. 686–696, 2011.
- [7] K. Tsumura, H. Ishii, and H. Hoshina, "Tradeoffs between quantization and packet loss in networked control of linear systems," *Automatica*, vol. 45, no. 12, pp. 2963–2970, 2009.
- [8] F. Rasool, D. Huang, and S. K. Nguang, "Robust H_∞ output feedback control of discrete-time networked systems with limited information," *Systems & Control Letters*, vol. 60, no. 10, pp. 845–853, 2011.
- [9] D. Liberzon, "A note on stabilization of linear systems using coding and limited communication," in *Proceedings of the 41st IEEE Conference on Decision and Control*, vol. 1, pp. 836–841, Las Vegas, Nev, USA, 2002.
- [10] D. F. Delchamps, "Stabilizing a linear system with quantized state feedback," *IEEE Transactions on Automatic Control*, vol. 35, no. 8, pp. 916–924, 1990.
- [11] R. W. Brockett and D. Liberzon, "Quantized feedback stabilization of linear systems," *IEEE Transactions on Automatic Control*, vol. 45, no. 7, pp. 1279–1289, 2000.
- [12] Y. Zhang and Q. Meng, "Stability of networked control system with quantization," in *Proceedings of the Chinese Control and Decision Conference*, pp. 559–564, Guilin, China, 2009.
- [13] O. C. Imer, S. Yüksel, and T. Başar, "Optimal control of LTI systems over unreliable communication links," *Automatica*, vol. 42, no. 9, pp. 1429–1439, 2006.
- [14] N. Elia and J. N. Eisenbeis, "Limitations of linear remote control over packet drop networks," in *Proceedings of the 43rd IEEE International Conference on Decision and Control*, vol. 4, pp. 5152–5157, Paradise Island, Bahamas, 2004.
- [15] Y. Shi, J. Huang, and B. Yu, "Robust tracking control of networked control systems: application to a networked DC motor," *IEEE Transactions on Industrial Electronics*, vol. 60, no. 12, pp. 5864–5874, 2013.
- [16] H. Li and Y. Shi, "Network-based predictive control for constrained nonlinear systems with two-channel packet dropouts," *IEEE Transactions on Industrial Electronics*, vol. 61, no. 3, pp. 1574–1582, 2014.
- [17] L. Schenato, "Optimal estimation in networked control systems subject to random delay and packet drop," *IEEE Transactions on Automatic Control*, vol. 53, no. 5, pp. 1311–1317, 2008.
- [18] G. N. Nair and R. J. Evans, "Stabilizability of stochastic linear systems with finite feedback data rates," *SIAM Journal on Control and Optimization*, vol. 43, no. 2, pp. 413–436, 2004.
- [19] L. Schenato, B. Sinopoli, M. Franceschetti, K. Poolla, and S. S. Sastry, "Foundations of control and estimation over lossy networks," *Proceedings of the IEEE*, vol. 95, no. 1, pp. 163–187, 2007.
- [20] M. Huang and S. Dey, "Stability of Kalman filtering with Markovian packet losses," *Automatica*, vol. 43, no. 4, pp. 598–607, 2007.
- [21] Z. Sun, "Reachability analysis of constrained switched linear systems," *Automatica*, vol. 43, no. 1, pp. 164–167, 2007.
- [22] M. Fu and L. Xie, "The sector bound approach to quantized feedback control," *IEEE Transactions on Automatic Control*, vol. 50, no. 11, pp. 1698–1711, 2005.
- [23] S. Chae, F. Rasool, S. K. Nguang, and A. Swain, "Robust mode delay-dependent H_∞ control of discrete-time systems with random communication delays," *IET Control Theory & Applications*, vol. 4, no. 6, pp. 936–944, 2009.
- [24] H.-L. Zhang, Y.-W. Jing, and S.-Y. Zhang, "Parameter uncertainty-based controller design for networked control systems with active varying sampling period," in *Proceedings of the Chinese Control and Decision Conference*, pp. 80–85, Shandong, China, July 2008.
- [25] D. Xie and Y. Wu, "Stabilisation of time-delay switched systems with constrained switching signals and its applications in networked control systems," *IET Control Theory & Applications*, vol. 4, no. 10, pp. 2120–2128, 2010.
- [26] L. El Ghaoui, F. Oustry, and M. AitRami, "A cone complementarity linearization algorithm for static output-feedback and related problems," *IEEE Transactions on Automatic Control*, vol. 42, no. 8, pp. 1171–1176, 1997.
- [27] S. Boyd, L. El Ghaoui, E. Feron, and V. Balakrishnan, *Linear Matrix Inequalities in System and Control Theory*, vol. 15, SIAM, Philadelphia, Pa, USA, 1994.

Research Article

Event-Triggered H_∞ Control for Networked Control Systems with Time-Varying Delay

Huaicheng Yan,¹ Sheng Yan,¹ Hao Zhang,² and Hongbo Shi^{1,2}

¹ Key Laboratory of Advanced Control and Optimization for Chemical Processes of Ministry of Education and the School of Information Science and Engineering, East China University of Science and Technology, Shanghai 200237, China

² Department of Control Science and Engineering, Tongji University, Shanghai 200092, China

Correspondence should be addressed to Sheng Yan; yanyouth@126.com

Received 6 January 2014; Accepted 6 February 2014; Published 11 March 2014

Academic Editor: Xudong Zhao

Copyright © 2014 Huaicheng Yan et al. This is an open access article distributed under the Creative Commons Attribution License, which permits unrestricted use, distribution, and reproduction in any medium, provided the original work is properly cited.

This paper deals with H_∞ controller design problem for event-triggered networked control systems (NCSs), where the next task release time and finishing time are predicted based on the sampled states. A new model of NCSs that involves the network conditions, state, and event-triggered communication strategy is proposed. Based on this model, some novel criteria for the asymptotic stability analysis and H_∞ state feedback controller design of the event-triggered NCSs with timevarying delay are established to guarantee a prescribed H_∞ disturbance rejection attenuation level. Finally, a numerical example is provided to illustrate the effectiveness of the proposed method.

1. Introduction

NCSs are spatially distributed systems for which communication between sensors, actuators, and controllers is connected by a shared communication network. In recent years, NCSs have brought many innovative impacts on control systems. They are becoming increasingly important in industrial processes for many advantages, such as low installation and maintenance costs, high reliability, increased system flexibility, and decreased wiring and [1]. As such, network-based analysis and design have many industrial applications in, for example, aircrafts, manufacturing plants, robots, automobiles, and remote surgery [2–7]. However, great challenges are also met due to the network induced imperfection, namely, time delays, packet losses, disorder, time-varying transmission intervals, and competition of multiple nodes accessing networks as well as data quantization, which can deteriorate the performance of the NCSs and even destabilize the systems [3]. So far, much effort has been devoted to modeling, analysis, and design of NCSs in the presence of network-induced delays, packet dropouts, and disorder; see, for example, [8–14] and the references therein.

Notice that the network in NCSs is the shared band-limited digital communication network [3]. One common problem to be addressed when considering NCSs is whether there is sufficient communication bandwidth to feedback information to the controller and then send the control commands to the actuators and the plant. Traditionally, the control task is executed periodically; this allows the closed-loop system to be analyzed and the controller to be designed using the well-developed theory on sampled-data systems [15]. However, the control strategy obtained based on this approach is conservative in the sense that resource usage is more frequent than necessary to ensure a specified performance level, since stability is guaranteed in the worst case scenarios under sufficiently fast periodic execution of the control action. To overcome this drawback, several researchers suggested the idea of event-triggered control. Event-triggered communication scheme has been proved to be an efficient way to reduce the transmitted data in the networks, which can relieve the burden of network bandwidth occupation in comparison with a traditional periodic sampling method. In [16], started from the paradigm that a real-time scheduler could be regarded as a feedback controller that decides which task is executed at any given instant, a simple

event-triggered scheduler based on this feedback paradigm was investigated to guarantee performance thus relaxing the more traditional periodic execution requirements. In [17], a decentralized event-triggered implementation, over sensor/actuator networks, of centralized nonlinear controllers was presented. In [18], a new self-triggering scheme that ensures finite-gain L_2 stability of the resulting self-triggered feedback systems was proposed. This scheme relaxes the assumptions that the magnitude of the process noise is bounded by a linear function of the norm of the system state. In [19], a novel event-triggering scheme was presented to ensure exponential stability of the resulting sampled-data system. The scheme postpones the triggering of events over previously proposed methods and therefore enlarges the intersampling period. The control design problem of event-triggered networked systems with both state and control input quantizations was addressed in [20]. An innovative delay system model was proposed, and the criteria for the asymptotical stability analysis and control synthesis of event-triggered NCSs were established. Unfortunately, to the best of the authors' knowledge, up to now, the stabilization and H_∞ control problems for general NCSs with simultaneous consideration of the network-induced time-varying delays and event-triggered communication scheme have not been adequately addressed yet, which still remains an interesting research topic. This motivates the current research.

In this paper, the H_∞ state feedback controller design method for the event-triggered NCSs with time-varying delays is presented. Different from some existing ones, the feedback NCSs in this paper is modeled as a delay system considering the network-induced delays and event-triggering scheme. By using Lyapunov-Krasovskii function approach, some new sufficient conditions that guarantee the asymptotic stability of the closed-loop NCSs are established in terms of linear matrix inequities (LMIs). Moreover, the explicit expression of feedback gain is also derived with event-triggering and network-induced delays. Finally, a simulation example is given to illustrate the effectiveness of the proposed method.

Notation. \mathbb{R}^n and Z^+ denote the n -dimensional Euclidean space and positive integer set, respectively. $\mathbb{R}^{m \times n}$ is the set of $m \times n$ real matrices. $\text{Sym}\{X\}$ denotes the expression $X + X^\top$. I_n denotes the $n \times n$ identity matrix. The notation $X > 0$ (resp., $X \geq 0$) denotes a real symmetric positive definite (positive semidefinite). In symmetric block matrices, “*” is used as ellipsis for terms induced by symmetry; $\text{diag}\{\cdot\}$ denotes the block-diagonal matrix. Matrixes, if not explicitly stated, are assumed to have appropriate dimensions.

2. Problem Formulation

Consider the NCSs with event-triggering shown in Figure 1. The physical plant is given by

$$\begin{aligned} \dot{x}(t) &= Ax(t) + Bu(t) + B_\omega \omega(t), \\ z(t) &= Cx(t) + Du(t), \end{aligned} \quad (1)$$

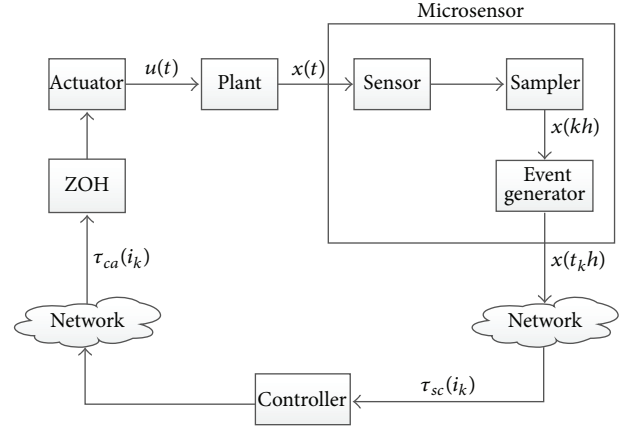


FIGURE 1: The structure of event-triggered NCSs with time-varying delay.

where $x(t) \in \mathbb{R}^n$ is the state vector, $u(t) \in \mathbb{R}^m$ is the control input vector, $\omega(t) \in L_2[0, \infty)$ is the disturbance input, and $z(t) \in \mathbb{R}^p$ is the control output vector, respectively. A , B , B_ω , C , and D are the parameter matrices with appropriate dimensions. The initial condition of the system (1) is given by $x(t_0) = x_0$. Throughout this paper, we assume that system (1) is controlled throughout a network with a networked state feedback controller, which is directly connected to the actuator through a zero-order holder (ZOH) [21].

The purpose of this paper is to design a linear controller $u(t) = Kx(t)$, where K is a matrix to be determined later, such that the resulting closed-loop system satisfies the required H_∞ performance.

To facilitate theoretical development, the following assumptions, which are common in NCSs research in open literature, are made in this paper.

Assumption 1. The sensors in the communication network are time-triggered with a constant sampling period h , while the controllers and actuators are event-triggered.

Assumption 2. The signal in a network is transmitted with a single packet, and the computational delay of the controller is negligible [22–25], and the data packet losses do not occur in transmission.

Assumption 3. The total network-induced delay τ_k ($k \in Z^+$) is bounded; that is, $0 < \tau_m \leq \tau_k \leq \tau_M$, where τ_m and τ_M denote the lower and upper delay bounds, respectively [15, 21].

As depicted in (1), considering the limited capacity of the communication channels and also for reducing the data transmission rate in the network, we show a framework of the proposed event-triggered communication scheme for the NCSs. The event-triggered communication scheme can be expressed as [20]

$$e_{\gamma_{k+j}h}^\top V e_{\gamma_{k+j}h} \geq \sigma x^\top(i_{k+j}h) V x(i_{k+j}h), \quad (2)$$

where $q_{\gamma_{k+j}h} = x(i_{k+j}h) - x(i_k h)$ is the error between the current sampling data $x(i_{k+j}h)$ and the latest transmitted sampling data $x(i_k h)$, V is a positive matrix, $j \in Z^+$, and $\sigma \in [0, 1]$.

Remark 4. The communication scheme (2) is characterized by the parameters σ , V , and h . Only the sampled state data $x(i_{k+j}h)$ that satisfy the quadratic condition will be transmitted to the controller. Obviously, this scheme will determine the load of the communication in the network. As a special case, if $\sigma = 0$ in (2), inequality (2) holds for all the sampled state data $x(i_{k+j}h)$; this scheme will reduce to a time-triggered communication scheme.

Under communication scheme (2), we assume that the release times are t_0h , t_1h , t_2h , \dots , where t_0h is the initial time; $\gamma_k h = t_{k+1}h - t_k h$ denotes the transmission period of the event generator. Take the network-induced time-varying delay τ_{i_k} into consideration; these release signals will arrive at the controller side at the instants $t_0h + \tau_0$, $t_1h + \tau_1$, $t_2h + \tau_2$, \dots , respectively.

Based on the above analysis, considering the effect of the time-varying delay in the communication network and the event-triggered communication scheme (2), for $t \in [t_k h + \tau_{i_k}, t_{k+1}h + \tau_{i_{k+1}})$, the system (1) under the control $u(t) = Kx(t)$ can be described as

$$\begin{aligned} \dot{x}(t) &= Ax(t) + Bu(t_k h) + B_\omega \omega(t), \\ z(t) &= Cx(t) + Du(t_k h), \end{aligned} \quad (3)$$

$$u(t_k h) = Kx(t_k h), \quad t \in [t_k h + \tau_{i_k}, t_{k+1}h + \tau_{i_{k+1}}).$$

Based on the above analysis, we consider the following intervals:

$$[t_k h + \tau_{i_k}, t_{k+1}h + \tau_{i_{k+1}}). \quad (4)$$

It is easy to make the conclusion that $\gamma_k h \geq h$.

(1) If $\gamma_k h \leq h + \tau_M - \tau_{i_{k+1}}$, we define

$$\tau(t) = t - t_k h, \quad t \in [t_k h + \tau_{i_k}, t_{k+1}h + \tau_{i_{k+1}}). \quad (5)$$

Furthermore, we define an error vector as

$$q_k(t) = 0. \quad (6)$$

(2) If $\gamma_k h > h + \tau_M - \tau_{i_{k+1}}$, it can be easily shown that $l \geq 1$ exists such that

$$lh + \tau_M - \tau_{i_{k+1}} < \gamma_k h \leq (l+1)h + \tau_M - \tau_{i_{k+1}}. \quad (7)$$

Then the range $[t_k h + \tau_{i_k}, t_{k+1}h + \tau_{i_{k+1}})$ can be divided into the following $l+1$ subranges:

$$\begin{aligned} & [t_k h + \tau_{i_k}, t_{k+1}h + \tau_{i_{k+1}}) \\ &= [t_k h + \tau_{i_k}, t_k h + h + \tau_M) \\ &\cup \left\{ \bigcup_{n=1}^{l-1} [t_k h + nh + \tau_M, t_k h + (n+1)h + \tau_M) \right\} \\ &\cup [t_k h + lh + \tau_M, t_{k+1}h + \tau_{i_{k+1}}). \end{aligned} \quad (8)$$

Define a function $\tau(t)$ as

$$\tau(t) = \begin{cases} t - t_k h & t \in [t_k h + \tau_{i_k}, t_k h + h + \tau_M), \\ t - t_k h - nh & t \in \bigcup_{n=1}^{l-1} [t_k h + nh + \tau_M, t_k h + (n+1)h + \tau_M), \\ t - t_k h - lh & t \in [t_k h + lh + \tau_M, t_{k+1}h + \tau_{i_{k+1}}). \end{cases} \quad (9)$$

It follows from (9) that

$$\tau_m \leq \tau(t) \leq h + \tau_M. \quad (10)$$

At this time, we define the error vector as

$$q_k(t) = \begin{cases} 0 & t \in [t_k h + \tau_{i_k}, t_k h + h + \tau_M), \\ x(t_k h + nh) - x(t_k h) & t \in \bigcup_{n=1}^{l-1} [t_k h + nh + \tau_M, t_k h + (n+1)h + \tau_M), \\ x(t_k h + lh) - x(t_k h) & t \in [t_k h + lh + \tau_M, t_{k+1}h + \tau_{i_{k+1}}). \end{cases} \quad (11)$$

Combining (6) and (11), it can be seen that

$$\begin{aligned} q_k^\top(t) V q_k(t) &< \sigma x^\top(t - \tau(t)) V x(t - \tau(t)), \\ &t \in [t_k h + \tau_{i_k}, t_{k+1}h + \tau_{i_{k+1}}). \end{aligned} \quad (12)$$

Combining (5), (6), (9), and (11) together with (3), define $h_1 = \tau_m$, $h_2 = \tau_M + h$; we can obtain the following closed-loop system as follows:

$$\begin{aligned} \dot{x}(t) &= Ax(t) + BKx(t - \tau(t)) - BKq_k(t) + B_\omega \omega(t), \\ &t \in [t_k h + \tau_{i_k}, t_{k+1}h + \tau_{i_{k+1}}), \\ z(t) &= Cx(t) + DKx(t - \tau(t)) - DKq_k(t), \\ x(t) &= \phi(t), \quad t \in [t_0 - h_2, t_0 - h_1), \end{aligned} \quad (13)$$

where we define $\phi(t)$ as the initial function of $x(t)$.

To make the theoretical development easier, the following definition will be used.

Definition 5. The closed-loop system (13) is said to be asymptotically stable with an H_∞ disturbance attenuation level γ ; that is, (1) system (13) is asymptotically stable with $\omega(t) \equiv 0$. (2) Under zero initial condition, $\|z(t)\|_2 < \gamma\|\omega(t)\|_2$, for any nonzero $\omega(t) \in L_2[0, \infty)$ and a prescribed $\gamma > 0$.

3. Main Results

Firstly, we develop a stability criterion for the system (13) with time-varying communication delay. Then, Theorem 7 is presented which lays the foundation for the H_∞ controller design.

Theorem 6. For some given parameters h_1, h_2, γ, σ , and feedback gain K , under the event-triggered communication scheme (2), the system (13) is asymptotically stable with an H_∞ performance index γ for the disturbance attention, if there exist real matrixes $P > 0, Q_i > 0, L_i > 0$ ($i = 1, 2$), $V > 0$, and G with appropriate dimensions such that the following LMIs hold:

$$\begin{bmatrix} \Sigma_{11} & * \\ \Sigma_{21} & \Sigma_{22} \end{bmatrix} < 0, \quad (14)$$

$$\begin{bmatrix} L_2 & * \\ G & L_2 \end{bmatrix} > 0, \quad (15)$$

where

$$\Sigma_{11} = \begin{bmatrix} \Phi_{11} & * & * & * & * & * \\ \Phi_{21} & \Phi_{22} & * & * & * & * \\ \Phi_{31} & \Phi_{32} & \Phi_{33} & * & * & * \\ 0 & \Phi_{42} & \Phi_{43} & \Phi_{44} & * & * \\ \Phi_{51} & 0 & 0 & 0 & \Phi_{55} & * \\ \Phi_{61} & 0 & 0 & 0 & 0 & \Phi_{66} \end{bmatrix},$$

$$\Sigma_{21} = [h_1 \xi_1^\top L_1^\top \quad h \xi_1^\top L_2^\top \quad \xi_2^\top]^\top,$$

$$\Sigma_{22} = \text{diag} \{-L_1 \quad -L_2 \quad -I\},$$

$$\Phi_{11} = PA + A^\top P + Q_1 + Q_2 - L_1, \quad \Phi_{21} = L_1,$$

$$\Phi_{22} = -Q_1 - L_2 - L_1, \quad \Phi_{31} = K^\top B^\top P,$$

$$\Phi_{32} = -G + L_2, \quad \Phi_{33} = \sigma V - 2L_2 + G + G^\top,$$

$$\Phi_{42} = G, \quad \Phi_{43} = -G + L_2, \quad \Phi_{44} = -Q_2 - L_2,$$

$$\Phi_{51} = -K^\top B^\top P, \quad \Phi_{55} = -V, \quad \Phi_{61} = B_\omega^\top P, \quad \Phi_{66} = -\gamma^2 I,$$

$$\xi_1 = [A \quad 0 \quad BK \quad 0 \quad -BK \quad B_\omega],$$

$$\xi_2 = [C \quad 0 \quad DK \quad 0 \quad -DK \quad 0],$$

$$h = h_2 - h_1.$$

(16)

Proof. Construct a Lyapunov-Krasovskii functional candidate as

$$\begin{aligned} V(t) &= x^\top(t) P x(t) + \int_{t-h_1}^t x^\top(s) Q_1 x(s) ds \\ &\quad + \int_{t-h_2}^t x^\top(s) Q_2 x(s) ds \end{aligned}$$

$$\begin{aligned} &+ h_1 \int_{-h_1}^0 \int_{t+s}^t \dot{x}^\top(v) L_1 \dot{x}(v) dv ds \\ &+ h \int_{-h_2}^{-h_1} \int_{t+s}^t \dot{x}^\top(v) L_2 \dot{x}(v) dv ds, \end{aligned} \quad (17)$$

where $P > 0, V > 0, Q_j > 0$, and $L_j > 0$ ($j = 1, 2$). Taking the derivation of $V(t)$ for $t \in [t_k h + \tau_k, t_{k+1} h + \tau_{k+1})$ and by adding and subtracting the term $\varrho_k^\top(t) V \varrho_k(t)$, we have

$$\begin{aligned} \dot{V}(t) &= 2x^\top(t) P \dot{x}(t) + x^\top(t) Q_1 x(t) \\ &\quad - x^\top(t-h_1) Q_1 x(t-h_1) + x^\top(t) Q_2 x(t) \\ &\quad - x^\top(t-h_2) Q_2 x(t-h_2) + h_1^2 \dot{x}^\top(t) L_1 \dot{x}(t) \\ &\quad - h_1 \int_{t-h_1}^t \dot{x}^\top(v) L_1 \dot{x}(v) dv + h^2 \dot{x}^\top(t) L_2 \dot{x}(t) \\ &\quad - h \int_{t-h_2}^{t-h_1} \dot{x}^\top(v) L_2 \dot{x}(v) dv + \varrho_k^\top(t) V \varrho_k(t) \\ &\quad - \varrho_k^\top(t) V \varrho_k(t) + z^\top(t) z(t) - z^\top(t) z(t). \end{aligned} \quad (18)$$

Applying Jensen's inequality [26] and convex reciprocally approach [27] to deal with the integral items in (18), noticing (15), we obtain

$$\begin{aligned} &-h_1 \int_{t-h_1}^t \dot{x}^\top(v) L_1 \dot{x}(v) dv \leq -\eta^\top(t) \Pi_1 \eta(t), \\ &-h \int_{t-h_2}^{t-h_1} \dot{x}^\top(v) L_2 \dot{x}(v) dv \\ &= -h \left[\int_{t-\tau(t)}^{t-h_1} \dot{x}^\top(v) L_2 \dot{x}(v) dv \right. \\ &\quad \left. + \int_{t-h_2}^{t-\tau(t)} \dot{x}^\top(v) L_2 \dot{x}(v) dv \right] \\ &\leq -\frac{h}{\tau(t) - h_1} [x^\top(t-h_1) L_2 x(t-h_1) \\ &\quad - x^\top(t-\tau(t)) L_2 x(t-\tau(t))] \\ &\quad - \frac{h}{h_2 - \tau(t)} [x^\top(t-\tau(t)) L_2 x(t-\tau(t)) \\ &\quad - x^\top(t-h_2) L_2 x(t-h_2)] \\ &\leq -\eta^\top(t) \Pi_2 \eta(t), \end{aligned} \quad (19)$$

with $\eta^\top(t) = [x^\top(t) \ x^\top(t - h_1) \ x^\top(t - \tau(t)) \ x^\top(t - h_2) \ \varrho_k^\top(t) \ \omega^\top(t)]$,

$$\Pi_1 = \begin{bmatrix} L_1 & * & 0 & 0 & 0 & 0 \\ -L_1 & L_1 & 0 & 0 & 0 & 0 \\ 0 & 0 & 0 & 0 & 0 & 0 \\ 0 & 0 & 0 & 0 & 0 & 0 \\ 0 & 0 & 0 & 0 & 0 & 0 \\ 0 & 0 & 0 & 0 & 0 & 0 \end{bmatrix}, \quad (20)$$

$$\Pi_2 = \begin{bmatrix} 0 & 0 & 0 & 0 & 0 & 0 \\ 0 & L_2 & * & * & 0 & 0 \\ 0 & G - L_2 & 2L_2 - G - G^\top & * & 0 & 0 \\ 0 & -G & G - L_2 & L_2 & 0 & 0 \\ 0 & 0 & 0 & 0 & 0 & 0 \\ 0 & 0 & 0 & 0 & 0 & 0 \end{bmatrix}.$$

Notice that $\Sigma_{21}^\top \Sigma_{22}^{-1} \Sigma_{21} = -[h_1^2 \xi_1^\top L_1 \xi_1 + h^2 \xi_1^\top L_2 \xi_1 + \xi_2^\top \xi_2]$, $\dot{x}(t) = \xi_1 \eta(t)$, and $z(t) = \xi_2 \eta(t)$; we have

$$\begin{aligned} & \eta^\top(t) [\Sigma_{21}^\top \Sigma_{22}^{-1} \Sigma_{21}] \eta(t) \\ &= -\eta^\top(t) [h_1^2 \xi_1^\top L_1 \xi_1 + h^2 \xi_1^\top L_2 \xi_1 + \xi_2^\top \xi_2] \eta^\top(t) \\ &= -h_1^2 \dot{x}^\top(t) L_1 \dot{x}(t) - h^2 \dot{x}^\top(t) L_2 \dot{x}(t) - z^\top(t) z(t). \end{aligned} \quad (21)$$

Combining (12), (17), (19), and (21), we obtain

$$\begin{aligned} \dot{V}(t) &\leq \eta^\top(t) (\Sigma_{11} - \Sigma_{21}^\top \Sigma_{22}^{-1} \Sigma_{21}) \eta(t) \\ &\quad - z^\top(t) z(t) + \gamma^2 \omega^\top(t) \omega(t), \end{aligned} \quad (22)$$

where Σ_{11} , Σ_{21} , and Σ_{22} are defined in (14).

By the Schur complements, the Lyapunov-Krasovskii function (14) guarantees that $\dot{V}(t) < 0$ in (17); we can derive that the system (13) with $\omega(t) \equiv 0$ is asymptotically stable and $\|z(t)\|_2 < \gamma \|\omega(t)\|_2$ under zero initial condition. This completes the proof. \square

Now we are in a position to design the state feedback H_∞ controller for the closed-loop system (13).

Theorem 7. For given parameters h_1 , h_2 , γ , and σ , under the event-triggered communication scheme (2), the system (13) is asymptotically stable with an H_∞ performance index γ for the disturbance attention, and the feedback gain $K = YX^{-1}$, if there exist real matrixes $X > 0$, $\bar{Q}_i > 0$, $\bar{L}_i > 0$ ($i = 1, 2$), $\bar{V} > 0$, and \bar{G} with appropriate dimensions such that the following matrix inequities hold:

$$\begin{bmatrix} \Sigma'_{11} & * \\ \Sigma'_{21} & \Sigma'_{22} \end{bmatrix} < 0, \quad (23)$$

$$\begin{bmatrix} \bar{L}_2 & * \\ \bar{G} & \bar{L}_2 \end{bmatrix} > 0, \quad (24)$$

where

$$\Sigma'_{11} = \begin{bmatrix} \bar{\Phi}_{11} & * & * & * & * & * \\ \bar{\Phi}_{21} & \bar{\Phi}_{22} & * & * & * & * \\ \bar{\Phi}_{31} & \bar{\Phi}_{32} & \bar{\Phi}_{33} & * & * & * \\ 0 & \bar{\Phi}_{42} & \bar{\Phi}_{43} & \bar{\Phi}_{44} & * & * \\ \bar{\Phi}_{51} & 0 & 0 & 0 & \bar{\Phi}_{55} & * \\ \bar{\Phi}_{61} & 0 & 0 & 0 & 0 & \bar{\Phi}_{66} \end{bmatrix},$$

$$\Sigma'_{21} = [h_1 \bar{\xi}_1^\top \quad h \bar{\xi}_1^\top \quad \bar{\xi}_2^\top]^\top,$$

$$\Sigma'_{22} = \text{diag} \{-X \bar{L}_1^{-1} X, -X \bar{L}_2^{-1} X, -I\},$$

$$\bar{\Phi}_{11} = XA + A^\top X + \bar{Q}_1 + \bar{Q}_2 - \bar{L}_1, \quad \bar{\Phi}_{21} = \bar{L}_1,$$

$$\bar{\Phi}_{22} = -\bar{Q}_1 - \bar{L}_2 - \bar{L}_1, \quad \bar{\Phi}_{31} = Y^\top B^\top, \quad \bar{\Phi}_{32} = -\bar{G} + \bar{L}_2,$$

$$\bar{\Phi}_{33} = \sigma \bar{V} - 2\bar{L}_2 + \bar{G} + \bar{G}^\top, \quad \bar{\Phi}_{42} = \bar{G},$$

$$\bar{\Phi}_{43} = -\bar{G} + \bar{L}_2, \quad \bar{\Phi}_{44} = -\bar{Q}_2 - \bar{L}_2, \quad \bar{\Phi}_{51} = -Y^\top B^\top,$$

$$\bar{\Phi}_{55} = -\bar{V}, \quad \bar{\Phi}_{61} = B_\omega^\top, \quad \bar{\Phi}_{66} = -\gamma^2 I,$$

$$\bar{\xi}_1 = [AX \ 0 \ BY \ 0 \ -BY \ B_\omega],$$

$$\bar{\xi}_2 = [CX \ 0 \ DY \ 0 \ -DY \ 0],$$

$$h = h_2 - h_1.$$

(25)

Proof. Define $X = P^{-1}$, $XQ_i X = \bar{Q}_i$, $XL_i X = \bar{L}_i$ ($i = 1, 2$), $XVX = \bar{V}$, $XGX = \bar{G}$, and $Y = KX$, and pre- and postmultiply (14), (15) with $\text{diag}\{X, X, X, X, X, I, L_1^{-1}, L_2^{-1}, I\}$, $\text{diag}\{X, X\}$, and their transposes, respectively. By Schur complement, we can obtain (23) and (24) from (14) and (15). Therefore, we can know from Theorem 6, (23), and (24) that the system (13) is asymptotically stable with an H_∞ performance index γ for the disturbance attention. \square

Remark 8. Theorem 7 provides a useful way of codesign for both the state feedback controller gain and the event-triggered parameter by solving a set of LMIs in (23). However, the derived matrix inequalities cannot be solved directly by making use of the MATLAB LMI control toolbox due to the nonlinear terms such as XVX in (23). To reduce the conservatism that may result from the driving LMIs based on (23), one can apply the cone complementarity linearization (CCL) algorithm [28]. The information of the transmission delay is also involved in (23). So our design method can be used to deal with the case with network transmission delay. For given condition on the time-varying delay, by solving (23), the state feedback gain matrix K and triggered constant V can be obtained, which can be used to guarantee the required H_∞ performance.

4. Illustrative Example

In this section, a numerical example is provided to validate the effectiveness of the theoretical results. The inverted

pendulum introduced by [18] is considered. The plant's state-space representation is given by

$$\dot{x}(t) = \begin{bmatrix} 0 & 1 & 0 & 0 \\ 0 & 0 & -\frac{mg}{M} & 0 \\ 0 & 0 & 0 & 1 \\ 0 & 0 & \frac{g}{l} & 0 \end{bmatrix} x(t) + \begin{bmatrix} 0 \\ \frac{1}{M} \\ 0 \\ -\frac{1}{Ml} \end{bmatrix} u(t). \quad (26)$$

We choose other parameter matrices as

$$C = [1 \ 1 \ 1 \ 1]^T, \quad D = 0.1, \quad B_\omega = C^T, \quad (27)$$

$$\omega(t) = \begin{cases} \text{sgn}(\sin t) & \text{if } t \in [0, 10] \\ 0 & \text{otherwise,} \end{cases}$$

where $M = 10$ is the cart mass and $m = 1$ is the mass of the pendulum bob, $l = 3$ is the length of the pendulum arm, and $g = 10$ is the gravitational acceleration. The initial state is chosen as $x_0 = [0.98, 0, 0.2, 0]^T$. As we can see, the eigenvalues of the system matrices are 0, 0, 1.8257, and -1.8257 ; thus the system is unstable without a controller. Applying Theorem 7 with $\sigma = 0.1$, $\gamma = 200$, $h_1 = 0.01$, and $h_2 = 0.11$, the corresponding feedback gain and the triggered matrix are obtained as

$$K = [-1.9739 \ -9.7238 \ 53.0167 \ 34.9453], \quad (28)$$

$$V = \begin{bmatrix} 70.8218 & 58.5581 & 23.0154 & 32.7182 \\ 58.5581 & 88.5920 & 8.3766 & 28.5856 \\ 23.0154 & 8.3766 & 171.6515 & 103.9430 \\ 32.7182 & 28.5856 & 103.9430 & 91.7903 \end{bmatrix}. \quad (29)$$

Taking the sampling period $h = 0.1$ s, the release instants and release intervals of system (26) are shown in Figure 2. The state response of system (26) with feedback controller gain (28) and event-triggered communication scheme (29) are depicted in Figure 3, respectively. Figure 3 shows that the system state converges to zero.

5. Conclusion

To reduce the communication load in the network, a novel event-triggered scheme has been proposed to determine when the sampling signal data will be transmitted. An event-triggered H_∞ control design method has been proposed for NCSs with time-varying delay. A delay system model has been used to describe the prosperities of the event trigger and effects of the transmission delay on the system. Based on this model, new criteria for stability with an H_∞ norm bound and H_∞ control design are developed. Since the relationship between the network-induced delay, the state feedback controller gain, and the trigger parameters are established, it can be used to schedule NCSs resources through adjusting one or more parameters for a better tradeoff between the control performance and the network conditions. The numerical example is given to demonstrate the effectiveness of the proposed algorithm.

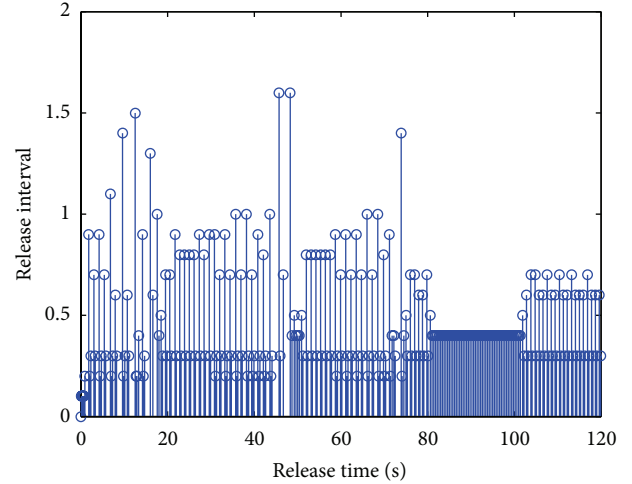


FIGURE 2: The release instants and release interval.

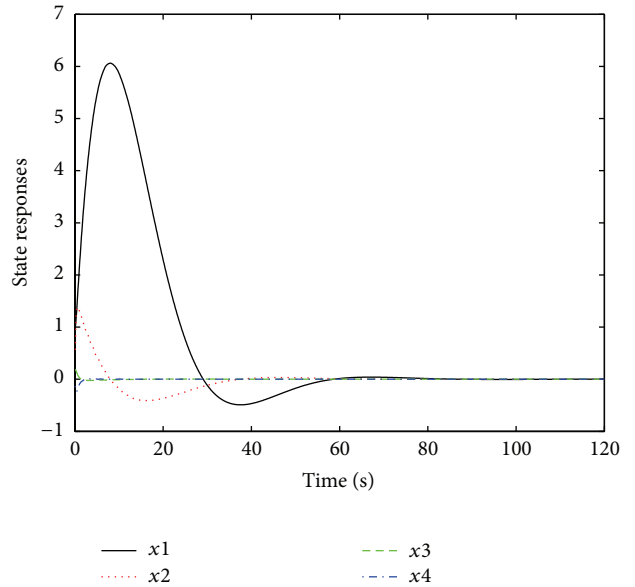


FIGURE 3: The state response of system.

Conflict of Interests

The authors declare that there is no conflict of interests regarding the publication of this paper.

Acknowledgment

This work is supported by the National Natural Science Foundation of China (61004028, 61272064, and 61273026), the Innovation Program of Shanghai Municipal Education Commission (12zz052), and the Fundamental Research Funds for the Central Universities.

References

- [1] L. G. Bushnell, "Networks and control," *IEEE Control Systems Magazine*, vol. 21, no. 1, pp. 22–23, 2001.
- [2] R. Gupta and M. Chow, "Networked control system: overview and research trends," *IEEE Transactions on Industrial Electronics*, vol. 57, no. 7, pp. 2527–2535, 2010.
- [3] J. P. Hespanha, P. Naghshtabrizi, and Y. Xu, "A survey of recent results in networked control systems," in *Proceedings of the 45th IEEE International Conference on Decision and Control*, pp. 138–162, 2007.
- [4] Y. Tipsuwan and M. Chow, "Control methodologies in networked control systems," *Control Engineering Practice*, vol. 11, no. 10, pp. 1099–1111, 2003.
- [5] C. Meng, T. Wang, W. Chou, S. Luan, Y. Zhang, and Z. Tian, "Remote surgery case: robot-assisted teleneurosurgery," *IEEE International Conference on Robotics and Automation*, vol. 1, pp. 819–823, 2004.
- [6] S. Yin, S. Ding, and H. Luo, "Real-time implementation of fault tolerant control system with performance optimization," *IEEE Transactions on Industrial Electronics*, vol. 61, no. 5, pp. 2402–2411, 2014.
- [7] H. Li, H. Gao, and P. Shi, "New passivity analysis for neural networks with discrete and distributed delays," *IEEE Transactions on Neural Networks*, vol. 21, no. 11, pp. 1842–1847, 2010.
- [8] L. X. Zhang, H. J. Gao, and O. Kaynak, "Network-induced constraints in networked control systems—a survey," *IEEE Transactions on Industrial Informatics*, vol. 9, no. 1, pp. 403–416, 2013.
- [9] H. J. Gao, T. W. Chen, and J. Lam, "A new delay system approach to network-based control," *Automatica*, vol. 44, no. 1, pp. 39–52, 2008.
- [10] H. Zhang, H. C. Yan, F. W. Yang, and Q. J. Chen, "Quantized control design for impulsive fuzzy networked systems," *IEEE Transactions on Fuzzy Systems*, vol. 19, no. 6, pp. 1153–1162, 2011.
- [11] H. C. Yan, Z. Z. Su, H. Zhang, and F. W. Yang, "Observer-based H_∞ control for discrete-time stochastic systems with quantisation and random communication delays," *IET Control Theory & Applications*, vol. 7, no. 3, pp. 372–379, 2013.
- [12] H. Zhang, H. C. Yan, T. Liu, and Q. J. Chen, "Fuzzy controller design for nonlinear impulsive fuzzy systems with time-delay," *IEEE Transactions on Fuzzy Systems*, vol. 19, no. 5, pp. 844–856, 2011.
- [13] K. Y. You and L. H. Xie, "Survey of recent progress in studying networked control systems," *Acta Automatica Sinica*, vol. 39, no. 2, pp. 101–117, 2013.
- [14] T. C. Yang, "Networked control system: a brief survey," *IET Control Theory and Applications*, vol. 153, no. 4, pp. 403–412, 2006.
- [15] D. Yue, Q.-L. Han, and J. Lam, "Network-based robust H_∞ control of systems with uncertainty," *Automatica*, vol. 41, no. 6, pp. 999–1007, 2005.
- [16] P. Tabuada, "Event-triggered real-time scheduling of stabilizing control tasks," *IEEE Transactions on Automatic Control*, vol. 52, no. 9, pp. 1680–1685, 2007.
- [17] M. Mazo, Jr. and P. Tabuada, "Decentralized event-triggered control over wireless sensor/actuator networks," *IEEE Transactions on Automatic Control*, vol. 56, no. 10, pp. 2456–2461, 2011.
- [18] X. F. Wang and M. D. Lemmon, "Self-triggered feedback control systems with finite-gain L_2 stability," *IEEE Transactions on Automatic Control*, vol. 54, no. 3, pp. 452–467, 2009.
- [19] X. F. Wang and M. D. Lemmon, "On event design in event-triggered feedback systems," *Automatica*, vol. 47, no. 10, pp. 2319–2322, 2011.
- [20] S. L. Hu and D. Yue, "Event-triggered control design of linear networked systems with quantizations," *ISA Transactions*, vol. 51, no. 1, pp. 153–162, 2012.
- [21] Y. Xu and J. P. Hespanha, "Optimal communication logics in networked control systems," in *Proceedings of the 43rd IEEE Conference on Decision and Control*, vol. 4, pp. 3527–3532, 2004.
- [22] D. Yue, E. Tian, and Q.-L. Han, "A delay system method for designing event-triggered controllers of networked control systems," *IEEE Transactions on Automatic Control*, vol. 58, no. 2, pp. 475–481, 2013.
- [23] X. Jia, D. Zhang, X. Hao, and N. Zheng, "Fuzzy H_∞ tracking control for nonlinear networked control systems in TS fuzzy model," *IEEE Transactions on Systems, Man, and Cybernetics B*, vol. 39, no. 4, pp. 1073–1079, 2009.
- [24] C. Peng and Y.-C. Tian, "Networked H_∞ control of linear systems with state quantization," *Information Sciences*, vol. 177, no. 24, pp. 5763–5774, 2007.
- [25] H. K. Lam and L. D. Seneviratne, "LMI-based stability design of fuzzy controller for nonlinear systems," *IET Control Theory & Applications*, vol. 1, no. 1, pp. 393–401, 2007.
- [26] K. Gu, J. Chen, and V. L. Kharitonov, *Stability of Time Delay Systems*, Springer, 2003.
- [27] P. Park, J. W. Ko, and C. Jeong, "Reciprocally convex approach to stability of systems with time-varying delays," *Automatica*, vol. 47, no. 1, pp. 235–238, 2011.
- [28] L. E. Ghaoui, F. Oustry, and M. AitRami, "A cone complementarity linearization algorithm for static output-feedback and related problems," *IEEE Transactions on Automatic Control*, vol. 42, no. 8, pp. 1171–1176, 1997.

Research Article

Optimal Distributed Controller Design for Nonlinear Coupled Dynamical Networks

Hao Zhang,¹ Huaicheng Yan,² and Qijun Chen¹

¹ Department of Control Science and Engineering, Tongji University, Shanghai 200092, China

² The Key Laboratory of Advanced Control and Optimization for Chemical Processes of Ministry of Education, School of Information Science and Engineering, East China University of Science and Technology, Shanghai 200237, China

Correspondence should be addressed to Huaicheng Yan; hcyan@ecust.edu.cn

Received 6 January 2014; Accepted 6 February 2014; Published 11 March 2014

Academic Editor: Xudong Zhao

Copyright © 2014 Hao Zhang et al. This is an open access article distributed under the Creative Commons Attribution License, which permits unrestricted use, distribution, and reproduction in any medium, provided the original work is properly cited.

This paper is concerned with the optimal distributed impulsive controller design for globally exponential synchronization of nonlinear dynamical networks with coupling delay. By the Lyapunov-Razumikhin method, a novel criterion is proposed to guarantee the global exponential synchronization of the coupled delayed network with distributed impulsive control in terms of matrix inequalities. The sum of coupling strengths of the distributed impulsive control is minimized to save the control effort. Finally, the effectiveness of the proposed method has been demonstrated by some simulations.

1. Introduction

During the last decade, a great amount of effort has been devoted to the study of synchronization of coupled networks due to their applications in many fields including secure communication, neural networks [1], and information science [2–10]. It is well known that there are three primary methods to be used to study the synchronization of the coupled network, that is, the Master Stability Function method, Lyapunov's direct method, and Connection Graph Stability method. Based on these methods, many research results have been reported on the synchronization from different points of view. Bounded H_∞ synchronization and state estimation for discrete time-varying stochastic complex networks over a finite horizon have been investigated in [2]. A time-varying complex dynamical network model and its controlled synchronization criteria have been considered in [5]. In [6], pinning synchronization of directed and undirected complex dynamical networks has been studied. An adaptive feedback controller has been proposed in [3] to synchronize a general complex dynamical network with delayed nodes.

In recent years, there are many control schemes that have been introduced to realize the network synchronization. For example, robust impulsive synchronization [11, 12], pinning

control [13], and adaptive control [14]. In impulsive control, the impulse signal is input into the nodes only at impulsive instance. The essential benefit of the impulsive control approach is derived from the fact that such control requires much less information, computational power, and bandwidth in sensing data communications in coupled networks and increases the robustness against the disturbance. Hence, the impulsive control is more effective compared with the control approaches using continuous measurement. In [13, 15–17], impulsive controllers for the stabilization or synchronization of complex dynamical networks are applied. Considering the impulsive effect as disturbance of the system, many researchers have done investigation to analyze the bound of the impulsive interval, parameter of the node, and topology of the network [11, 18–22]. In these references, the impulsive controller or disturbance only effect on the local sensor or node and the coupling of the impulsive effect has not been considered. However, in this paper, the distributed impulsive controller is designed to synchronize the coupled network not only based on its local measurement but also on its neighboring measurement according to the topology of distributed impulsive controller. Although the synchronization of coupled networks has been investigated intensively in recent years, however, to our best knowledge, the

distributed impulsive control for nonlinear coupled networks has received little attention, in particular the optimal of the coupling strength. This motivates the current study.

In this paper, we aim to deal with the synchronization of nonlinear coupled networks with time-varying delay via distributed impulsive control and specify the minimum coupling strengths of the corresponding links in the distributed controller topology. The rest of the paper is organized as follows. In Section 2, the problem we are considering is described and some useful lemmas and definitions are presented. Section 3 provides the main results of this paper. The distributed impulsive controller is designed to synchronize the coupled networks with time-varying delay and the sum of the coupling strength of the controller is minimum. An example is presented in Section 4 and some simulations are presented to illustrate the effectiveness of the proposed methods. Finally, the conclusions are given in Section 5.

Notations. For vector $x = \text{col}(x_1, \dots, x_n) \in \mathbb{R}^n$ and matrix $A = (a_{ij})_{n \times n} \in \mathbb{R}^{n \times n}$, $\|x\|$ and $\|A\|$ denote 2-norms of x and A , respectively. A real matrix $P > 0$ ($P < 0$) denotes P being a positive (negative) definite matrix, and $A > B$ means $A - B > 0$. M^T denotes the transpose of matrix M . The identity matrix of order m is denoted as I_m (or simply I if no confusion arises). Moreover, matrices are assumed to have compatible dimensions if not explicitly stated. $*$ denotes the symmetric block of a symmetric matrix, and $\text{diag}\{\cdot\}$ denotes the block diagonal matrix. $\lambda_{\max}(P)$ and $\lambda_{\min}(P)$ are used to denote the maximum and minimum eigenvalue of matrix P , respectively. \mathbb{N} is the set of all positive natural numbers.

2. Preliminaries and Problem Formulation

We consider a dynamical network consisting of N linearly coupled oscillators. Each node of the network is an n -dimensional dynamical system, which is described by

$$\begin{aligned} \dot{x}_i(t) &= f(x_i(t)) + \sum_{j=1}^N a_{ij} \Gamma x_j(t - \tau(t)) + u_i(t), \\ i &= 1, 2, \dots, N, \end{aligned} \quad (1)$$

where $x_i(t) = (x_{i1}(t), x_{i2}(t), \dots, x_{in}(t))^T \in \mathbb{R}^n$ is the state of the i th oscillator, $f(x_i(t)) \in \mathbb{R}^n \rightarrow \mathbb{R}^n$ is a continuous function, and there exists a unique continuous solution for any initial condition. Suppose that the uniform Lipschitz condition holds; that is, for any $x, y \in \mathbb{R}^n$. Then, there exists a positive constant $L > 0$ such that $\|f(x) - f(y)\| \leq L\|x - y\|$. $\Gamma \in \mathbb{R}^{n \times n}$ is the inner-coupling matrix, and a_{ij} is the coupling strength from the j th oscillator to the i th oscillator, where $a_{ij} > 0$ means that the i th oscillator is coupled with the j th oscillator directly and $a_{ij} = 0$ means that the i th oscillator is decoupled from the j th oscillator. Suppose that the communication topology is strongly connected [23]. $\tau(t)$ is the time delay between nodes which satisfies $\tau(t) \leq \tau$ [13, 24–26]. Moreover, $u_i(t) \in \mathbb{R}^n$ are the controllers designed for the network.

The topology of the coupled networks in (1) is described as a directed graph $\mathcal{G} = (\mathcal{V}, \mathcal{E})$ of order N with the set

of nodes $\mathcal{V} = \{1, 2, \dots, N\}$, and the elements in \mathcal{V} are the oscillator's indexes. \mathcal{E} is a set of directed link sets, and when oscillator i is coupled with oscillator j directly, there is a directed link $(i, j) \in \mathcal{E}$ from node j to node i ; that is, $\mathcal{E} = \{(i, j) \mid a_{ij} > 0, \forall i, j = 1, 2, \dots, N\}$. The set of neighbors of vertex i is denoted by $\mathcal{N}_i = \{j \in \mathcal{V} : (i, j) \in \mathcal{E}\}$. In the following, we introduce some definitions and lemma that are essential for the development of main results in this paper.

Definition 1. The coupled network (1) is said to be globally exponentially synchronous if there exist constants $\gamma > 0$ and $\mu > 0$, such that for any initial conditions the inequality

$$\|x_i(t) - x_j(t)\|^2 \leq \gamma e^{-\mu t} \quad (2)$$

holds for $t \geq 0$.

Definition 2. A coupling matrix \mathcal{A} is defined as

$$\begin{aligned} \mathcal{A} &= \begin{bmatrix} -\sum_{j=2}^N a_{1j} & a_{12} & \cdots & a_{1N} \\ a_{21} & -\sum_{j=1, j \neq 2}^N a_{2j} & \cdots & a_{2N} \\ \vdots & \ddots & \ddots & \ddots \\ a_{N1} & a_{N2} & \cdots & -\sum_{j=1}^{N-1} a_{Nj} \end{bmatrix} \\ &= \sum_{(i,j) \in \mathcal{E}} a_{ij} A_{ij}, \end{aligned} \quad (3)$$

where $A_{ij} \in \mathbb{R}^{N \times N}$ denotes the constant matrices corresponding to the directed links (i, j) and each A_{ij} only contains two nonzero entries, that is, -1 at the i th entry and 1 at the j th entry. From Definition 2, the coupled network (1) can be rewritten in a compact form:

$$\dot{\bar{x}}(t) = f(\bar{x}(t)) + \mathcal{A} \otimes \Gamma \bar{x}(t - \tau(t)) + u(t), \quad (4)$$

where $\bar{x}(t) = (x_1^T(t), x_2^T(t), \dots, x_N^T(t))^T$, $f(\bar{x}(t)) = (f(x_1^T(t)), f(x_2^T(t)), \dots, f(x_N^T(t)))^T$, and $u(t) = [u_1^T(t), u_2^T(t), \dots, u_N^T(t)]^T$. Define matrices G and W as

$$\begin{aligned} G &= \begin{bmatrix} 1 & -1 & 0 & \cdots & 0 \\ 0 & \ddots & \ddots & \ddots & 0 \\ \vdots & \ddots & 1 & -1 & \vdots \\ 0 & \cdots & 0 & 1 & -1 \end{bmatrix} \in \mathbb{R}^{N-1 \times N}, \\ W &= \begin{bmatrix} 1 & 1 & 1 & 1 \\ 0 & 1 & \cdots & 1 \\ 0 & 0 & \ddots & \vdots \\ 0 & 0 & \cdots & 1 \\ 0 & 0 & \cdots & 0 \end{bmatrix} \in \mathbb{R}^{N \times N-1}, \end{aligned} \quad (5)$$

which satisfies

$$GW = I_{N-1}, \quad \mathcal{A} = \mathcal{A}WG, \quad G \otimes I_m \begin{bmatrix} x_1 \\ \vdots \\ x_N \end{bmatrix} = \begin{bmatrix} e_1 \\ \vdots \\ e_{N-1} \end{bmatrix}, \quad (6)$$

where $e_i = x_i - x_{i+1}$, $i = 1, \dots, N-1$. By the multiplication of $G \otimes I_m$ on (4), one has

$$\dot{\bar{e}}(t) = F(\bar{x}(t)) + ((G\mathcal{A}W) \otimes \Gamma) \bar{e}(t - \tau(t)) + \bar{u}(t), \quad (7)$$

where

$$\begin{aligned} \bar{e}(t) &= \begin{bmatrix} \dot{e}_1(t) \\ \vdots \\ \dot{e}_{N-1}(t) \end{bmatrix}, \\ F(\bar{x}(t)) &= \begin{bmatrix} f(x_1) - f(x_2) \\ \vdots \\ f(x_{N-1}) - f(x_N) \end{bmatrix}, \\ \bar{e}(t - \tau(t)) &= \begin{bmatrix} e_1(t - \tau(t)) \\ \vdots \\ e_{N-1}(t - \tau(t)) \end{bmatrix}, \\ \bar{u}(t) &= \begin{bmatrix} u_1(t) - u_2(t) \\ \vdots \\ u_{N-1}(t) - u_N(t) \end{bmatrix}. \end{aligned} \quad (8)$$

In order to achieve synchronization of coupled network (1) and inspired by the controller proposed in [27], a distributed impulsive controller for the i th node is designed as

$$\begin{aligned} u_i(t) &= \sum_{k=1}^{\infty} \sum_{j \in \mathcal{N}_i} v_{ij} \Gamma (x_j(t) - x_i(t)) \delta(t - t_k), \\ i &= 1, 2, \dots, N, \end{aligned} \quad (9)$$

where v_{ij} denotes the coupling strength corresponding to the directed links (i, j) , which need to be designed. The impulsive instant sequence $\{t_k\}_0^{\infty}$ satisfies $0 \leq t_0 < t_1 < t_2 < \dots < t_k < \dots$, $\lim_{k \rightarrow \infty} t_k = \infty$. $\delta(\cdot)$ is the Dirac impulsive function; that is, $\delta(t) = 0$ for $t \neq 0$, and $\int_{-\infty}^{\infty} \delta(t) dt = 1$. In many applications, the Dirac delta function is usually used to model an impulse. Taking integral on both sides of (1) from $t_k - h$ to $t_k + h$, where $h \rightarrow 0^+$, one has

$$\Delta x_i(t_k) = \sum_{j \in \mathcal{N}_i} v_{ij} \Gamma (x_j(t_k) - x_i(t_k)), \quad (10)$$

where $\Delta x_i(t_k) = x_i(t_k^+) - x_i(t_k^-)$, $\lim_{h \rightarrow 0^+} x_i(t_k - h) = x_i(t_k^-)$, and $\lim_{h \rightarrow 0^+} x_i(t_k + h) = x_i(t_k^+)$, with discontinuity instants $0 \leq t_0 < t_1 < t_2 < \dots < t_k < \dots$. Without loss of generality, it is assumed that $x_i(t_k) = x_i(t_k^-) = \lim_{h \rightarrow 0^+} x_i(t_k - h)$; that is, $x_i(t)$ is left continuous at $t = t_k$. Equation (10) implies that the node i will suddenly update its state variables not only according to the state variables of itself but also its neighbors at instant t_k .

Since the distributed controller can use the original topology of the coupled network and will not cause additional effort in building new links, the topology of the distributed controller is designed as the same with the coupled network

(1). Hence, the coupling matrix of the distributed impulsive controller can be defined as

$$\begin{aligned} \mathcal{V} &= \begin{bmatrix} -\sum_{j=2}^N v_{1j} & v_{12} & \cdots & v_{1N} \\ v_{21} & -\sum_{j=1, j \neq 2}^N v_{2j} & \cdots & v_{2N} \\ \vdots & \ddots & \ddots & \vdots \\ v_{N1} & v_{N2} & \cdots & -\sum_{j=1}^{N-1} v_{Nj} \end{bmatrix} \\ &= \sum_{(i,j) \in \mathcal{E}} v_{ij} A_{ij}, \end{aligned} \quad (11)$$

where $A_{ij} \in \mathbb{R}^{N \times N}$ is defined in (3). Then, one can rewrite (10) into a compact form:

$$\Delta \bar{x}(t_k) = (\mathcal{V} \otimes \Gamma) \bar{x}(t_k), \quad (12)$$

where $\Delta \bar{x}^\top(t_k) = (\Delta x_1(t_k), \Delta x_2(t_k), \dots, \Delta x_N(t_k))^\top$, $\bar{x}^\top(t_k) = (x_1(t_k), x_2(t_k), \dots, x_N(t_k))^\top$. By the multiplication of $G \otimes I_m$ on (12), one has

$$\Delta \bar{e}(t_k) = ((G\mathcal{V}W) \otimes \Gamma) \bar{e}(t_k), \quad (13)$$

where $\Delta \bar{e}(t_k) = (\Delta e_1^\top(t_k), \Delta e_2^\top(t_k), \dots, \Delta e_{N-1}^\top(t_k))^\top$, $\bar{e}(t_k) = (e_1^\top(t_k), e_2^\top(t_k), \dots, e_{N-1}^\top(t_k))^\top$, $\Delta e_i(t_k) = \Delta x_i(t_k) - \Delta x_{i+1}(t_k)$, and $e_i(t_k) = x_i(t_k) - x_{i+1}(t_k)$, $i = 1, 2, \dots, N-1$.

From (7) and (13), the impulsively controlled error system can be described by the following impulsive differential equation:

$$\begin{aligned} \dot{\bar{e}}(t) &= F(\bar{x}(t)) + ((G\mathcal{A}W) \otimes \Gamma) \bar{e}(t - \tau(t)), \quad t \neq t_k, \\ \Delta \bar{e}(t_k) &= ((G\mathcal{V}W) \otimes \Gamma) \bar{e}(t_k), \end{aligned} \quad (14)$$

$$\bar{e}(t_0 + \theta) = \phi(\theta), \quad -\tau \leq \theta \leq 0,$$

where $\phi \in \mathcal{C}([-\tau, 0], \mathbb{R}^n)$.

Lemma 3 (see [28]). *For matrices A, B, C , and D with appropriate dimensions, one has*

$$\begin{aligned} (A \otimes B)^\top &= A^\top \otimes B^\top, \\ A \otimes (B + C) &= A \otimes B + A \otimes C, \\ (A \otimes B)(C \otimes D) &= AC \otimes BD, \\ (A \otimes B)^{-1} &= A^{-1} \otimes B^{-1}. \end{aligned} \quad (15)$$

In the following section, the exponential synchronization of coupled networks with distributed impulsive control is investigated based on this model.

3. Main Results

In this section, a novel contradiction method is proposed to analyze the global exponential synchronization of system (1) to obtain an optimal distributed impulsive control law.

Theorem 4. Let $\rho = \sup_{k \in \mathbb{N}} \{t_k - t_{k-1}\} < \infty$, given positive scalars α , and $0 < \gamma < 1$, if there exists matrix $P > 0$, matrix \mathcal{V} , and positive scalar ε , such that the following inequalities

$$\begin{bmatrix} \varepsilon \bar{L} + \left(\frac{\alpha}{\gamma} + \frac{\ln \gamma}{\rho} \right) P & P((G\mathcal{A}W) \otimes \Gamma) & P \\ * & -\alpha P & 0 \\ * & * & -\varepsilon I \end{bmatrix} < 0, \quad (16)$$

$$\begin{bmatrix} -\gamma P & (I + (G\mathcal{Z}W) \otimes \Gamma)^T P \\ * & -P \end{bmatrix} < 0, \quad (17)$$

hold; then the coupled network (1) can achieve global exponential synchronization.

Proof. In the following, for convenience, we assume $t_0 = 0$. For $\phi \in \mathcal{C}([-\tau, 0], \mathbb{R}^n)$, we denote the solution $\bar{e}(t, t_0, \phi)$ of (14) by $\bar{e}(t)$. Consider a Lyapunov function candidate for the error dynamic system (14) as

$$V(t) = \bar{e}^T(t) P \bar{e}(t), \quad (18)$$

where $P > 0$. Calculating the Dini derivative of $V(t)$ along the solution of the system (14) for $t \in (t_{k-1}, t_k], k \in \mathbb{N}$, one has

$$\begin{aligned} DV(t) &= 2\bar{e}^T(t) P (F(\bar{x}(t)) + ((G\mathcal{A}W) \otimes \Gamma) \bar{e}(t - \tau(t))) \\ &\leq \bar{e}^T(t) \left(\frac{1}{\varepsilon} P^2 + \varepsilon \bar{L} \right) \bar{e}(t) \\ &\quad + 2\bar{e}^T(t) P ((G\mathcal{A}W) \otimes \Gamma) \bar{e}(t - \tau(t)), \end{aligned} \quad (19)$$

where $\bar{L} = I_{N-1} \otimes L^2$. Noting that $0 < \gamma < 1$ and inequality (16), there exist positive scalars h, μ , and ε , where $h + \gamma < 1$, such that the following linear matrix inequality is satisfied:

$$\begin{bmatrix} \varepsilon \bar{L} + \left(\frac{\alpha}{\gamma} + \frac{\ln(\gamma + h)}{\rho} + \mu \right) P & P((G\mathcal{A}W) \otimes \Gamma) & P \\ * & -\alpha e^{-\mu\tau} P & 0 \\ * & * & -\varepsilon I \end{bmatrix} < 0. \quad (20)$$

From (17), one has

$$(I + (G\mathcal{Z}W) \otimes \Gamma)^T P (I + (G\mathcal{Z}W) \otimes \Gamma) - \gamma P < 0. \quad (21)$$

Hence,

$$\begin{aligned} V(t_k^+) &= \bar{e}^T(t_k^+) P \bar{e}(t_k^+) \\ &= \bar{e}^T(t_k) (I + (G\mathcal{Z}W) \otimes \Gamma)^T \\ &\quad \times P (I + (G\mathcal{Z}W) \otimes \Gamma) \bar{e}(t_k) \\ &\leq \gamma \bar{e}^T(t_k) P \bar{e}(t_k) = \gamma V(t_k). \end{aligned} \quad (22)$$

Let $\mathcal{W}(t) = e^{\mu t} V(t)$; then

$$\dot{\mathcal{W}}(t) = \mu e^{\mu t} V(t) + e^{\mu t} \dot{V}(t), \quad t \in [t_{k-1}, t_k], k \in \mathbb{N}. \quad (23)$$

Let $\nu > \lambda_{\max}(P)/\gamma\lambda_{\min}(P)$ be a fixed number. In the following, we will prove that $\mathcal{W}(t) < \lambda_{\min}(P)\nu\|\phi\|^2, t \geq t_0 - \tau$. Note that

$$\begin{aligned} \mathcal{W}(t_0 + \theta) &\leq \lambda_{\max}(P) \|\phi\|^2 < \gamma \lambda_{\min}(P) \nu \|\phi\|^2 \\ &< \lambda_{\min}(P) \nu \|\phi\|^2, \end{aligned} \quad (24)$$

for $-\tau \leq \theta \leq 0$. We will first prove that

$$\mathcal{W}(t) < \lambda_{\min}(P) \nu \|\phi\|^2, \quad \text{for } t \in (t_0, t_1), \quad (25)$$

via contradiction. Suppose this is not the case; that is, there exists a $t \in (t_0, t_1)$ such that $\mathcal{W}(t) \geq \lambda_{\min}(P)\nu\|\phi\|^2$. Set $t^* = \inf\{t \in (t_0, t_1) : \mathcal{W}(t) \geq \lambda_{\min}(P)\nu\|\phi\|^2\}$; then one has

$$\mathcal{W}(t^*) = \lambda_{\min}(P) \nu \|\phi\|^2, \quad t^* \in (t_0, t_1). \quad (26)$$

Noticing (24), one has $\mathcal{W}(t_0) < \gamma\lambda_{\min}(P)\nu\|\phi\|^2$. Set $\bar{t} = \sup\{t \in (t_0, t^*) : \mathcal{W}(t) \leq \gamma\lambda_{\min}(P)\nu\|\phi\|^2\}$; then one has

$$\mathcal{W}(\bar{t}) = \gamma\lambda_{\min}(P) \nu \|\phi\|^2, \quad \bar{t} \in (t_0, t^*), \quad (27)$$

$$\begin{aligned} \mathcal{W}(t) &\geq \gamma\lambda_{\min}(P) \nu \|\phi\|^2 \geq \gamma \mathcal{W}(t + \theta), \\ \theta &\in [-\tau, 0] \text{ for } t \in (\bar{t}, t^*). \end{aligned} \quad (28)$$

Hence, one has that, for $t \in (\bar{t}, t^*)$,

$$\begin{aligned} \dot{\mathcal{W}}(t) &\leq \mu e^{\mu t} V(t) + e^{\mu t} \dot{V}(t) \\ &\quad + \left(\frac{\alpha}{\gamma} \mathcal{W}(t) - \alpha \mathcal{W}(t - \tau(t)) \right) \\ &\leq e^{\mu t} \left(\bar{e}^T(t) \mu P \bar{e}(t) \right) \\ &\quad + e^{\mu t} \left(\bar{e}^T(t) \left(\frac{1}{\varepsilon} P^2 + \varepsilon \bar{L} \right) \bar{e}(t) + 2\bar{e}^T(t) \right. \\ &\quad \left. \times P((G\mathcal{A}W) \otimes \Gamma) \bar{e}(t - \tau(t)) \right) \\ &\quad + e^{\mu t} \left(\frac{\alpha}{\gamma} \bar{e}^T(t) P e(t) - \alpha e^{-\mu\tau} \bar{e}^T(t - \tau(t)) P e(t - \tau(t)) \right) \\ &\leq e^{\mu t} \xi^T(t) \\ &\quad \times \left[\frac{1}{\varepsilon} P^2 + \varepsilon \bar{L} + \left(\frac{\alpha}{\gamma} + \frac{\ln(\gamma + h)}{\rho} + \mu \right) P \quad P((G\mathcal{A}W) \otimes \Gamma) \right] \\ &\quad \times \xi(t) + \gamma_1 \mathcal{W}(t), \end{aligned} \quad (29)$$

where $\gamma_1 = -\ln(\gamma + h)/\rho, \xi^T(t) = [\bar{e}^T(t), \bar{e}^T(t - \tau(t))]$. Noticing (20), one has

$$\dot{\mathcal{W}}(t) \leq \gamma_1 \mathcal{W}(t), \quad t \in [\bar{t}, t^*]; \quad (30)$$

then

$$\mathcal{W}(t^*) \leq \mathcal{W}(\bar{t}) e^{\gamma_1(t^* - \bar{t})} < \gamma \lambda_{\min}(P) \nu \|\phi\|^2 e^{\gamma_1 \rho}; \quad (31)$$

the last inequality is derived by using (27) and $\bar{t} - t^* < \rho$. Since $\gamma e^{\gamma_1 \rho} < 1$, inequality (31) becomes

$$\mathcal{W}(t^*) < \lambda_{\min}(P) \nu \|\phi\|^2, \quad (32)$$

which contradict to (26). Now we have proved that inequality (25) holds. Next, we assume that

$$\mathcal{W}(t) < \lambda_{\min}(P) \nu \|\phi\|^2, \quad \text{for } t \in [t_0 - \tau, t_m], \quad m \in \mathbb{N}. \quad (33)$$

We want to prove that

$$\mathcal{W}(t) < \lambda_{\min}(P) \nu \|\phi\|^2, \quad \text{for } t \in (t_m, t_{m+1}]. \quad (34)$$

Suppose this is not the case; that is, there exists a $t \in (t_m, t_{m+1}]$ such that

$$\mathcal{W}(t) \geq \lambda_{\min}(P) \nu \|\phi\|^2. \quad (35)$$

Set $t^* = \inf\{t \in (t_m, t_{m+1}] : \mathcal{W}(t) \geq \lambda_{\min}(P) \nu \|\phi\|^2\}$; then

$$\mathcal{W}(t^*) = \lambda_{\min}(P) \nu \|\phi\|^2. \quad (36)$$

From (22) and (33), we have

$$\mathcal{W}(t_m^+) \leq \gamma \mathcal{W}(t_m) < \gamma \lambda_{\min}(P) \nu \|\phi\|^2. \quad (37)$$

Set $\bar{t} = \sup\{t \in (t_m, t^*) : \mathcal{W}(t) \leq \gamma \lambda_{\min}(P) \nu \|\phi\|^2\}$; then $\mathcal{W}(\bar{t}) = \gamma \lambda_{\min}(P) \nu \|\phi\|^2$, and $\mathcal{W}(t) \geq \gamma \lambda_{\min}(P) \nu \|\phi\|^2 \geq \gamma \mathcal{W}(\bar{t} + \theta)$ for $t \in [\bar{t}, t^*]$. One has

$$\begin{aligned} & \dot{\mathcal{W}}(t) \\ & \leq \mu e^{\mu t} V(t) + e^{\mu t} \dot{V}(t) + \left(\frac{\alpha}{\gamma} \mathcal{W}(t) - \alpha \mathcal{W}(t - \tau(t)) \right) \\ & \leq e^{\mu t} \xi^\top(t) \\ & \quad \times \begin{bmatrix} \frac{1}{\varepsilon} P^2 + \varepsilon \bar{L} + \left(\frac{\alpha}{\gamma} + \frac{\ln(\gamma + h)}{\rho} + \mu \right) P & P((G\mathcal{A}W) \otimes \Gamma) \\ * & -\alpha e^{-\mu \tau} P \end{bmatrix} \\ & \quad \times \xi(t) + \gamma_1 \mathcal{W}(t) \\ & \leq \gamma_1 \mathcal{W}(t), \end{aligned} \quad (38)$$

for $t \in [\bar{t}, t^*]$. Hence,

$$\begin{aligned} \mathcal{W}(t^*) & \leq \mathcal{W}(\bar{t}) e^{\gamma_1(t^* - \bar{t})} \leq \gamma \lambda_{\min}(P) \nu \|\phi\|^2 e^{\gamma_1 \rho} \\ & < \lambda_{\min}(P) \nu \|\phi\|^2, \end{aligned} \quad (39)$$

which yields a contradiction to (36). Therefore, inequality (34) holds. By mathematical induction we have

$$\mathcal{W}(t) < \lambda_{\min}(P) \nu \|\phi\|^2, \quad \text{for } t \geq t_0. \quad (40)$$

On the other hand, note that $V(t) \geq \lambda_{\min}(P) \|\bar{e}(t)\|^2$; one has

$$\|\bar{e}(t, t_0, \phi)\|^2 < \nu \|\phi\|^2 e^{-\mu(t-t_0)}; \quad (41)$$

thus from Definition 1, the coupled network (1) is globally synchronized under the distributed controller (9). \square

Remark 5. Theorem 4 outlines the principle of determining the distributed controller gains. However, it does not provide an optimal coupling strength. Next, the sum of all coupling strengths is minimized by solving the following optimisation problem:

$$\min_{P, v_{ij}} \sum_{(i,j) \in \mathcal{E}} v_{ij} \quad (42)$$

subject to (16), (17).

Remark 6. When the coupled network (1) is given, then the coupling strength a_{ij} is known; consequently, A_{ij} is also known. The topology of the distributed controller can be designed as the same with coupled network (1). Only the coupling strength v_{ij} needs to be determined. Our aim is to optimize the coupling strength of the controller and make the sum of all coupling strengths $\sum_{(i,j) \in \mathcal{E}} v_{ij}$ being minimized. Since P and \mathcal{V} are unknown matrices, inequality (17) is not linear matrix inequality and cannot be solved efficiently. We will propose the following algorithm to find a suboptimal solution of the v_{ij} .

Step 1. Let the positive matrix $P = I$, and let β be a small positive scalar.

Step 2. Solve the linear matrix inequality (17); one will have v_{ij} .

Step 3. Using the value of v_{ij} obtained by Step 2, take a positive matrix P that is to be determined. Solving the optimization problem as follows:

$$\begin{aligned} & \max_P \delta \\ & \begin{bmatrix} \varepsilon \bar{L} + \left(\frac{\alpha}{\gamma} + \frac{\ln \gamma}{\rho} \right) P & P((G\mathcal{A}W) \otimes \Gamma) & P \\ * & -\alpha P & 0 \\ * & 0 & -\varepsilon I \end{bmatrix} < 0, \end{aligned} \quad (43)$$

$$l = 1, 2, \dots, r,$$

$$\begin{bmatrix} -\gamma P & (I + (G\mathcal{V}W) \otimes \Gamma)^\top P \\ * & -P \end{bmatrix} < -\delta I,$$

where δ is positive scalar.

Step 4. If $\delta > \beta$, then go back to Step 2; else, terminate the algorithm.

Thus we can obtain the coupling strength v_{ij} with the smallest coupling sum $\sum_{(i,j) \in \mathcal{E}} v_{ij}$ by this iterative algorithm.

4. Illustrative Example

In this section, a numerical example of global exponential synchronization of a coupled network with 5 Lorenz oscillators is provided to illustrate the design procedure of the proposed distributed impulsive controller. The functions of Lorenz oscillators are given by

$$f(x_i) = \begin{bmatrix} -10x_{i1} + 10x_{i2} \\ 28x_{i1} - x_{i2} - x_{i1}x_{i3} \\ x_{i1}x_{i2} - \frac{1}{3}x_{i3} \end{bmatrix}, \quad i = 1, 2, 3, 4, 5, \quad (44)$$

with $x_i = [x_{i1} \ x_{i2} \ x_{i3}]^T$. Let $L = 10$; the inner-coupling matrix is given by $\Gamma = I$ and the coupling delay is set as $0.1 \sin(t)$. The coupling matrix of the given coupled network is given by

$$\mathcal{A} = 0.1 * \begin{bmatrix} -1 & 0 & 1 & 0 & 0 \\ 0 & -1 & 0 & 1 & 0 \\ 0 & 1 & -1 & 0 & 0 \\ 0 & 1 & 0 & -1 & 0 \\ 0 & 0 & 1 & 0 & -1 \end{bmatrix}; \quad (45)$$

then the coupling matrix of distributed controller can be designed as follows:

$$\mathcal{V} = \begin{bmatrix} -v_{13} & 0 & v_{13} & 0 & 0 \\ 0 & -v_{24} & 0 & v_{24} & 0 \\ 0 & v_{32} & -v_{32} & 0 & 0 \\ 0 & v_{42} & 0 & -v_{42} & 0 \\ 0 & 0 & v_{53} & 0 & -v_{53} \end{bmatrix}, \quad (46)$$

such that the sum of coupling strengths $\sum_{(i,j) \in \mathcal{E}} v_{ij}$ is as small as possible. Let $\alpha = 1$, $\rho = 0.01$, and $\gamma = 0.7$. Solving matrix inequalities (16) and (17) by the method proposed in Remark 5, we have $\min \sum_{(i,j) \in \mathcal{E}} v_{ij} = 1.98$. The states of the coupled network without control and with distributed impulsive control are shown in Figures 1 and 2, respectively. From Figure 2, we find that the coupled network (1) is globally exponentially synchronous under the distributed controller.

5. Conclusion

In this paper, we have studied the distributed impulsive controller design for globally exponential synchronization of nonlinear networks with coupling delay. The sum of coupling strengths of the distributed impulsive control is minimized to save the control effort. Some criteria have been derived based on Lyapunov-Razumikhin method to guarantee the global exponential synchronization of the coupled network with distributed impulsive control in terms of matrix inequalities. A numerical example has been presented to demonstrate the usefulness and effectiveness of the proposed approach. Further research directions would include the investigation on more general nonlinear systems.

Conflict of Interests

The authors declare that there is no conflict of interests regarding the publication of this paper.

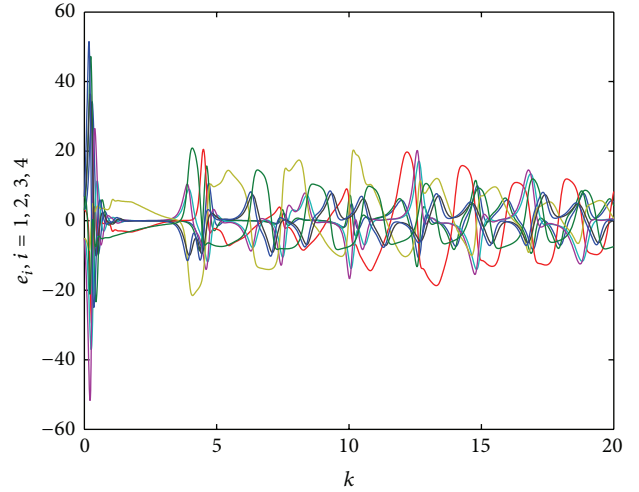


FIGURE 1: The error states of the coupled network without control.

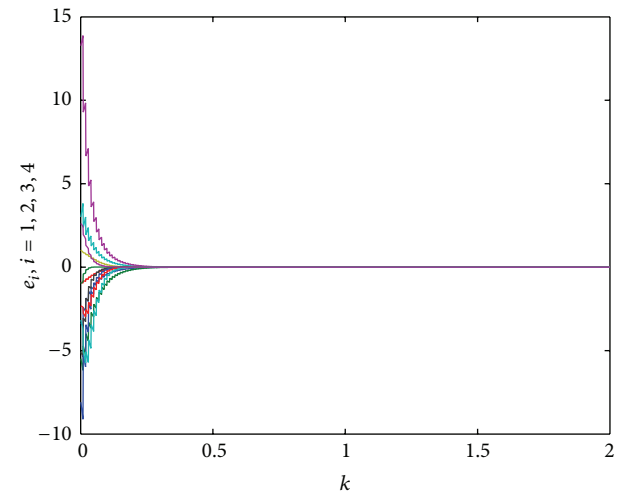


FIGURE 2: The error states of the coupled network with distributed impulsive control.

Acknowledgments

This work is supported by the National Natural Science Foundation of China (61273026, 61004028, 61272064, and 91120308), the Innovation Program of Shanghai Municipal Education Commission (12zz052), and the Fundamental Research Funds for the Central Universities.

References

- [1] H. Li, H. Gao, and P. Shi, "New passivity analysis for neural networks with discrete and distributed delays," *IEEE Transactions on Neural Networks*, vol. 21, no. 11, pp. 1842–1847, 2010.
- [2] B. Shen, Z. Wang, and X. Liu, "Bounded H_∞ synchronization and state estimation for discrete time-varying stochastic complex networks over a finite horizon," *IEEE Transactions on Neural Networks*, vol. 22, no. 1, pp. 145–157, 2011.
- [3] Q. J. Zhang, J. A. Lu, J. H. Lu, and C. K. Tse, "Adaptive feedback synchronization of a general complex dynamical network with

- delayed nodes," *IEEE Transactions on Circuits and Systems II*, vol. 55, no. 2, pp. 183–187, 2008.
- [4] L. Chen, J. A. Lu, and C. K. Tse, "Synchronization: an obstacle to identification of network topology," *IEEE Transactions on Circuits and Systems II*, vol. 56, no. 4, pp. 310–314, 2009.
- [5] J. H. Lü and G. R. Chen, "A time-varying complex dynamical network model and its controlled synchronization criteria," *IEEE Transactions on Automatic Control*, vol. 50, no. 6, pp. 841–846, 2005.
- [6] Q. Song and J. Cao, "On pinning synchronization of directed and undirected complex dynamical networks," *IEEE Transactions on Circuits and Systems I*, vol. 57, no. 3, pp. 672–680, 2010.
- [7] H. Zhang, H. C. Yan, F. W. Yang, and Q. J. Chen, "Quantized control design for impulsive fuzzy networked systems," *IEEE Transactions on Fuzzy Systems*, vol. 19, no. 6, pp. 1153–1162, 2011.
- [8] L. X. Zhang, H. J. Gao, and O. Kaynak, "Network-induced constraints in networked control systems—a survey," *IEEE Transactions on Industrial Informatics*, vol. 9, no. 1, pp. 403–416, 2013.
- [9] H. J. Gao, T. W. Chen, and J. Lam, "A new delay system approach to network-based control," *Automatica*, vol. 44, no. 1, pp. 39–52, 2008.
- [10] H. C. Yan, Z. Z. Su, H. Zhang, and F. W. Yang, "Observer-based H_∞ control for discrete-time stochastic systems with quantisation and random communication delays," *IET Control Theory & Applications*, vol. 7, no. 3, pp. 372–379, 2013.
- [11] H. L. Xu, Y. Q. Chen, and K. L. Teo, "Global exponential stability of impulsive discrete-time neural networks with time-varying delays," *Applied Mathematics and Computation*, vol. 217, no. 2, pp. 537–544, 2010.
- [12] D. Gong, H. Zhang, Z. Wang, and J. Liu, "Synchronization analysis for complex networks with coupling delay based on T-S fuzzy theory," *Applied Mathematical Modelling*, vol. 36, no. 12, pp. 6215–6224, 2012.
- [13] J. Zhou, Q. J. Wu, and L. Xiang, "Pinning complex delayed dynamical networks by a single impulsive controller," *IEEE Transactions on Circuits and Systems I*, vol. 58, no. 12, pp. 2882–2893, 2011.
- [14] F. Sorrentino and E. Ott, "Adaptive synchronization of dynamics on evolving complex networks," *Physical Review Letters*, vol. 100, no. 11, Article ID 114101, 4 pages, 2008.
- [15] Y. Dai, Y. Cai, and X. Xu, "Synchronisation analysis and impulsive control of complex networks with coupling delays," *IET Control Theory & Applications*, vol. 3, no. 9, pp. 1167–1174, 2009.
- [16] Y. W. Wang, M. Yang, H. O. Wang, and Z. H. Guan, "Robust stabilization of complex switched networks with parametric uncertainties and delays via impulsive control," *IEEE Transactions on Circuits and Systems I*, vol. 56, no. 9, pp. 2100–2108, 2009.
- [17] Q. Zhang, J. A. Lu, and J. Zhao, "Impulsive synchronization of general continuous and discrete-time complex dynamical networks," *Communications in Nonlinear Science and Numerical Simulation*, vol. 15, no. 4, pp. 1063–1070, 2010.
- [18] B. Liu, X. Liu, G. Chen, and H. Wang, "Robust impulsive synchronization of uncertain dynamical networks," *IEEE Transactions on Circuits and Systems I*, vol. 52, no. 7, pp. 1431–1441, 2005.
- [19] X. S. Yang, J. D. Cao, and J. Q. Lu, "Synchronization of delayed complex dynamical networks with impulsive and stochastic effects," *Nonlinear Analysis*, vol. 12, no. 4, pp. 2252–2266, 2011.
- [20] J. Q. Lu, D. W. C. Ho, J. D. Cao, and J. Kurths, "Exponential synchronization of linearly coupled neural networks with impulsive disturbances," *IEEE Transactions on Neural Networks*, vol. 22, no. 2, pp. 329–335, 2011.
- [21] J. Q. Lu, D. W. C. Ho, and J. D. Cao, "A unified synchronization criterion for impulsive dynamical networks," *Automatica*, vol. 46, no. 7, pp. 1215–1221, 2010.
- [22] S. G. Peng, "Delay-independent global exponential stabilization for stochastic fuzzy systems with time delay via impulsive fuzzy control," in *Proceedings of the 29th Chinese Control Conference (CCC '10)*, pp. 1049–1052, July 2010.
- [23] C. Wu, "Synchronization in networks of nonlinear dynamical systems coupled via a directed graph," *Nonlinearity*, vol. 18, no. 3, pp. 1057–1064, 2005.
- [24] T. H. Lee, J. H. Park, O. M. Kwon, and S. M. Lee, "Synchronization of a time-varying delayed complex dynamical network with nonidentical nodes and free coupling matrix," in *Proceedings of the International Conference on Control, Automation and Systems (ICCAS '11)*, pp. 1837–1840, October 2011.
- [25] R. Cepeda-Gomez and N. Olgac, "An exact method for the stability analysis of linear consensus protocols with time delay," *IEEE Transactions on Automatic Control*, vol. 56, no. 7, pp. 1734–1740, 2011.
- [26] C. Yoshioka and T. Namerikawa, "Observer-based consensus control strategy for multi-agent system with communication time delay," in *Proceedings of the IEEE International Conference on Control Applications (CCA '08)*, pp. 1037–1042, San Antonio, Tex, USA, September 2008.
- [27] Z. H. Guan, Z. W. Liu, G. Feng, and Y. W. Wang, "Synchronization of complex dynamical networks with time-varying delays via impulsive distributed control," *IEEE Transactions on Circuits and Systems I*, vol. 57, no. 8, pp. 2182–2195, 2010.
- [28] L. Huang, *Linear Algebra in System and Control Theory*, Science Press, Beijing, China, 1984.

Research Article

Metric Learning Method Aided Data-Driven Design of Fault Detection Systems

Guoyang Yan,¹ Jianguan Mei,¹ Shen Yin,¹ and Hamid Reza Karimi²

¹ *Research Institute of Intelligent Control and Systems, Harbin Institute of Technology, Heilongjiang 150001, China*

² *Department of Engineering, Faculty of Engineering and Science, The University of Agder, 4898 Grimstad, Norway*

Correspondence should be addressed to Shen Yin; shen.yin2011@gmail.com

Received 15 December 2013; Accepted 22 January 2014; Published 10 March 2014

Academic Editor: Xudong Zhao

Copyright © 2014 Guoyang Yan et al. This is an open access article distributed under the Creative Commons Attribution License, which permits unrestricted use, distribution, and reproduction in any medium, provided the original work is properly cited.

Fault detection is fundamental to many industrial applications. With the development of system complexity, the number of sensors is increasing, which makes traditional fault detection methods lose efficiency. Metric learning is an efficient way to build the relationship between feature vectors with the categories of instances. In this paper, we firstly propose a metric learning-based fault detection framework in fault detection. Meanwhile, a novel feature extraction method based on wavelet transform is used to obtain the feature vector from detection signals. Experiments on Tennessee Eastman (TE) chemical process datasets demonstrate that the proposed method has a better performance when comparing with existing methods, for example, principal component analysis (PCA) and fisher discriminate analysis (FDA).

1. Introduction

Due to the fact that industrial systems are becoming more complex, safety and reliability have become more critical in complicated process design [1–3]. Traditional model-based approaches, which require the process modeled by the first principle or prior knowledge of the process, have become difficult, especially for large-scale processes. With significantly growing automation degrees, a large amount of process data is generated by the sensors and actuators. In this framework, the data-based techniques are proposed and developed rapidly over the past two decades. Data-driven fault diagnosis schemes are based on considerable amounts of historical data, which take sufficient use of the information provided by the historical data instead of complex process model [4, 5]. This framework can simplify the design procedure effectively and ensure safety and reliability in the complicated processes [6]. Many fault diagnosis techniques have been used in the complicated industrial systems [7–9]. In this framework, PCA [10] and FDA [11] are regarded as the most mature and successful methods in real industrial applications.

PCA aims at dimensionality reduction, which captures the data variability in an efficient way. In PCA method, process variables are projected onto two orthogonal subspaces by carrying out the singular value decomposition on the sample covariance matrix. And cumulative percent variance [12] is the standard to determine the number of principal components. To detect the variability information in two orthogonal subspaces, the squared prediction error (SPE) statistic [13] and the T^2 statistic [14] are calculated. PCA is a sophisticated method. However, PCA determines the lower dimensional subspaces without considering the information between the classes. FDA [15] is a linear dimensionality reduction technique. It has advantages over PCA because it takes into consideration the information between different classes of the data. The aim of FDA is to maximize the dispersion between different classes and minimize the dispersion within each class by determining a group of transformation vectors. In FDA method, three matrices are defined to measure dispersion. The problem of determining a set of linear transformation vectors is equal to the problem of solving generalized eigenvalues [16]. However, FDA has difficulty in dealing with online applications. Motivated by

Input: x_k : a given data sets of n points, s : set of pairs of data in same categories, D : set of pairs of data in different categories, H_0 : a given matrix, s : a given upper bound, b : a given lower bound, β : the slack variable

Output: H : the target Mahalanobis matrix

$$(1) H = H_0, \lambda(i, j) = 0$$

$$(2) m(i, j) = s \text{ when } (i, j) \in S, m(i, j) = b \text{ when } (i, j) \in D$$

(3) Repeat until convergence:

$$(3.1) \text{ Pick a pairs of data } (x_i, x_j)_t \in x_k$$

$$(3.2) l(i, j)_t = 1 \text{ when } (i, j)_t \in S, l(i, j)_t = -1 \text{ when } (i, j)_t \in D$$

$$(3.3) g_t = (x_i - x_j)^T H_t (x_i - x_j)$$

$$(3.4) k_t = l(i, j)_t \cdot \min \left(\lambda(i, j)_t, \frac{l(i, j)_t}{2} \left(\frac{1}{g_t} - \frac{\beta}{m(i, j)_t} \right) \right)$$

$$(3.5) \mu_t = \frac{k_t}{1 - k_t g_t}$$

$$(3.6) m(i, j)_{t+1} = \frac{\beta m(i, j)_t}{\beta + k_t m(i, j)_t}$$

$$(3.7) \lambda(i, j)_{t+1} = \lambda(i, j)_t - \min \left(\lambda(i, j)_t, \frac{l(i, j)_t}{2} \left(\frac{1}{g_t} - \frac{\beta}{m(i, j)_t} \right) \right)$$

$$(3.8) H_{t+1} = H_t + \mu_t H_t (x_i - x_j)(x_i - x_j)^T H_t$$

Return: H

ALGORITHM 1: Learning Mahalanobis matrix by iterative algorithm.

the aforementioned studies, in this paper, we proposed a fault detection scheme based on metric learning which has been used extensively in the pattern classification problem. The purpose of metric learning is to learn a Mahalanobis distance [17] which can represent an accurate relationship between feature vector and categories of instances. The model focuses on the divergence among classes, instead of extracting the principal components. Meanwhile, the Mahalanobis distance learned from the historical data can be utilized in online detection without real-time update. So, metric learning is more suitable than PCA and FDA for fault diagnosis theoretically.

In practice, selecting an appropriate metric plays a critical role in recent machine learning algorithms. Because the scale of the Mahalanobis distance has no effect on the performance of classification, Mahalanobis distance is the most popular one among numerous metrics. Besides, Mahalanobis distance takes into account of the correlations of different features which can build an accurate distance model. A good metric learning algorithm should be fast and scalable. At the same time, a good metric learning algorithm should emphasize the relevant dimensions while reducing the influence of noninformative dimensions [18]. In this paper, we adopt information-theoretic metric learning (ITML) algorithm to learn Mahalanobis distance function [19]. In ITML algorithm, the distances between similar pairs are bounded in a small given value, while the distances between dissimilar pairs are required to be larger than a large given value in the algorithm. The algorithm is expressed as a particular Bregman optimization problem. To avoid overfitting problem, a method based on LogDet divergence to regularize the target matrix to a given Mahalanobis matrix

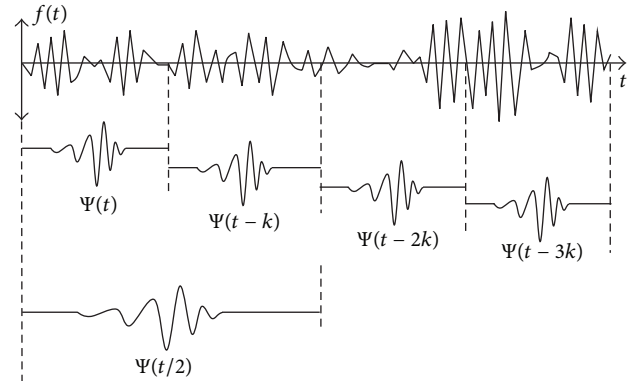


FIGURE 1: Dilating and shifting of wavelet function.

is adopted. It is necessary to remark that a feature extraction method based on wavelet transform is proposed to do the data preprocessing of the algorithm.

The remainder of this paper is organized as follows. In Section 2, we give background knowledge of ITML. Then, wavelet transform is described in Section 3. Section 4 illustrates TE process [20] and gives the experimental results on TE process dataset to demonstrate the good effect of the proposed algorithm. Finally, we draw conclusions and point out future directions in Section 5.

2. Related Work

ITML is a metric learning algorithm without eigenvalue computations or semidefinite programming. And the strategy of

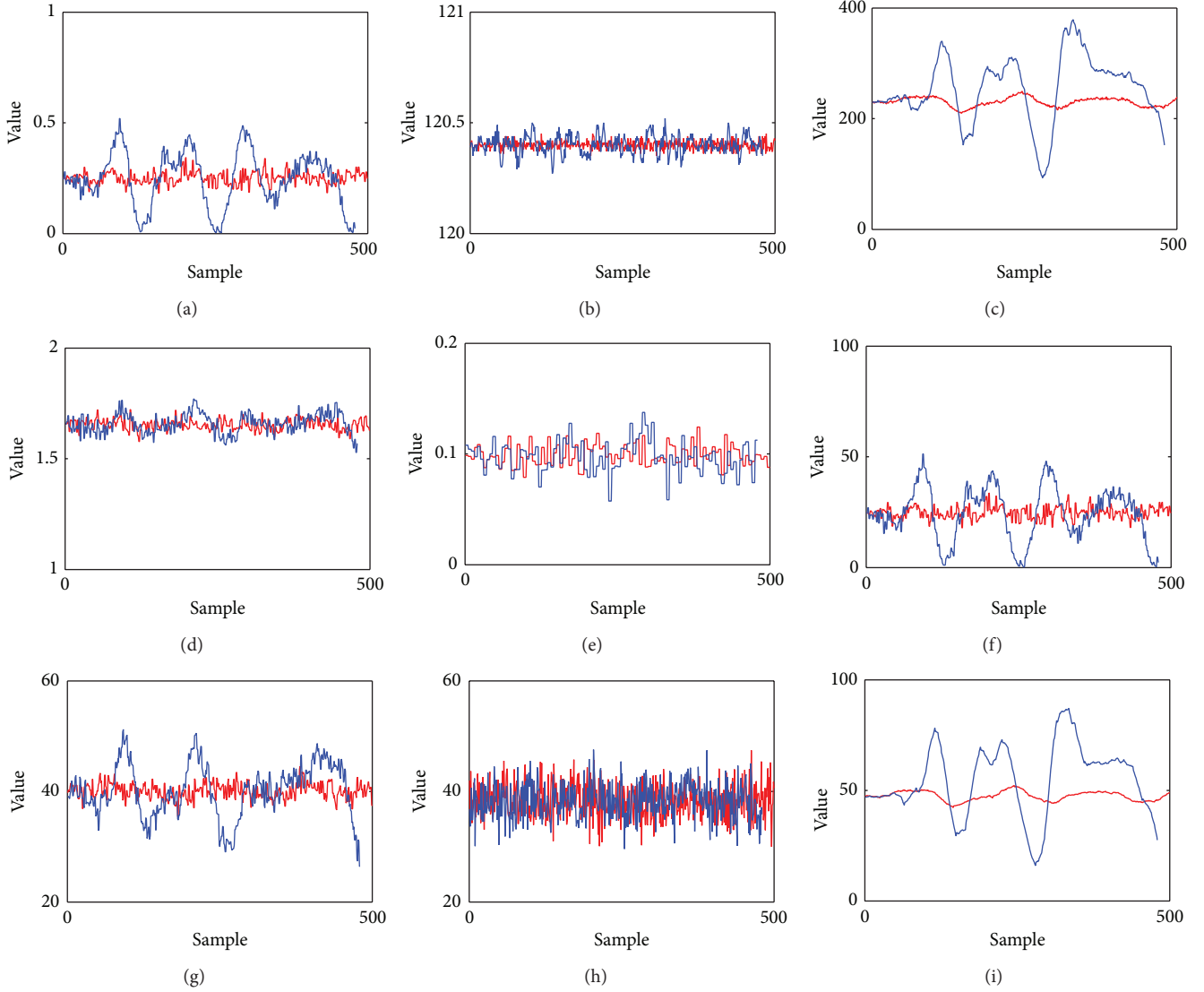


FIGURE 2: Observations of fault 12 in the TE process.

regularizing metric in ITML is to minimize the divergence between the target matrix and a given matrix.

Given a dataset $\{x_k\}$ with $x_k \in R^D$, $k = 1, 2, \dots, n$. The Mahalanobis distance between x_i and x_j can be parameterized by a matrix H as follows:

$$D_H(x_i, x_j) = (x_i - x_j)^T H (x_i - x_j). \quad (1)$$

In ITML, pair constraints are used to represent the relationship of data in the same or different categories. If x_i and x_j are in the same categories, the Mahalanobis distance between them should be smaller than a given value s . Similarly, if x_i and x_j are in different categories, the Mahalanobis distance between them should be larger than a given value b .

The purpose of the ITML is to find a matrix $H \in R^{D \times D}$ which satisfies the following pair constraint sets:

$$\begin{aligned} H &\in R^{D \times D}, \\ \text{s.t. } D_H(x_i, x_j) &\leq s \quad (i, j) \in S, \\ D_H(x_i, x_j) &\geq b \quad (i, j) \in D, \end{aligned} \quad (2)$$

where S and D represent the set of pairs of data in the same and different categories, respectively.

It deserves pointing out that there will be not only one matrix $H \in R^{D \times D}$ which satisfies all the constraints. To ensure the stability of the metric learning, the target matrix H is regularized to a given function H_0 . The distance between H

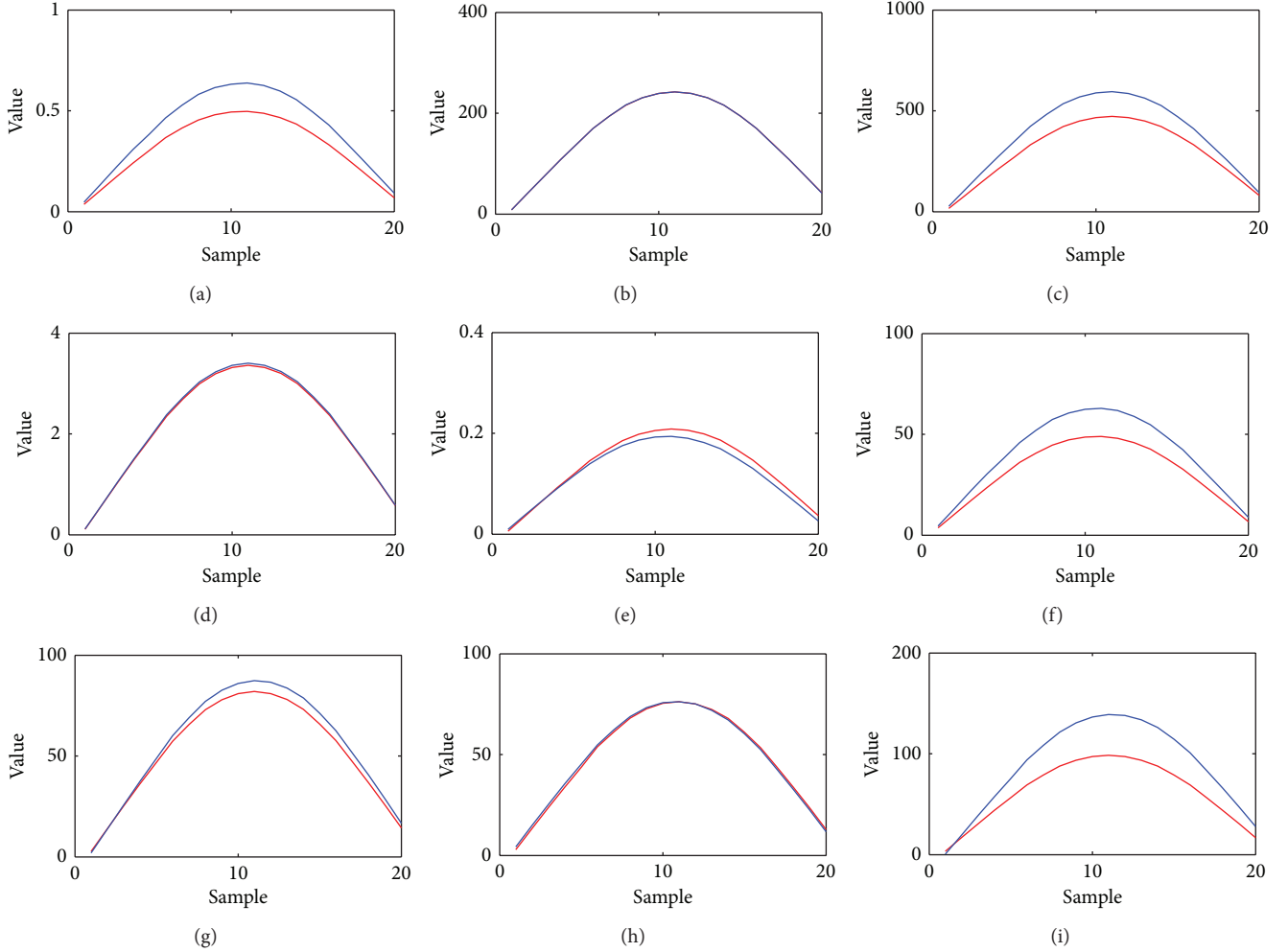


FIGURE 3: Results of the wavelet transform.

and H_0 can be expressed as a type of Bregman matrix divergence [21] as follows:

$$D_\phi(H, H_0) = \phi(H) - \phi(H_0) - \text{tr}((\nabla\phi(H_0))^T (H - H_0)), \quad (3)$$

in which $\text{tr}(H)$ denotes the trace of matrix H and $\phi(H)$ is a given strictly convex differentiable function that plays a determinant role in the properties of the Bregman matrix divergence. Taking the advantages of different differentiable functions into account, $\phi(H)$ is chosen as $\log(\det(H))$. And the corresponding, Bregman matrix divergence $D_\phi(H, H_0)$ is called LogDet divergence. According to the further generalization, the LogDet divergence keeps invariant when performing the invertible linear transformation K , expressed as [22]

$$D_{\text{LD}}(H, H_0) = \text{tr}(HH_0^{-1}) - \log(\det(HH_0^{-1})) - n, \quad (4)$$

$$D_{\text{LD}}(H, H_0) = D_{\text{LD}}(K^T H K, K^T H_0 K).$$

The metric learning problem can be translated into a LogDet optimization problem as follows:

$$\begin{aligned} \min_{H \geq 0} \quad & D_{\text{LD}}(H, H_0), \\ \text{s.t.} \quad & \text{tr}(H(x_i - x_j)(x_i - x_j)^T) \leq s, (i, j) \in S, \\ & \text{tr}(H(x_i - x_j)(x_i - x_j)^T) \geq b, (i, j) \in D. \end{aligned} \quad (5)$$

It is worth pointing out that distance constraints $D_H(x_i, x_j) \leq s$ are equivalent to the linear constraints $\text{tr}(H(x_i - x_j)(x_i - x_j)^T) \leq s$. To guarantee the existence of the feasible solution to (5), Kulis proposed an iterative algorithm which introduce slack variable in it [21]. In this way, an iterative equation to update the Mahalanobis distance function is found as follows:

$$H_{t+1} = H_t + \mu H_t (x_i - x_j)(x_i - x_j)^T H_t, \quad (6)$$

where μ is a parameter mentioned in Algorithm 1. In the algorithm, the slack variable β balanced the satisfaction of $\min_{H \geq 0} D_{\text{LD}}(H, H_0)$ and the linear constraints. Learning the

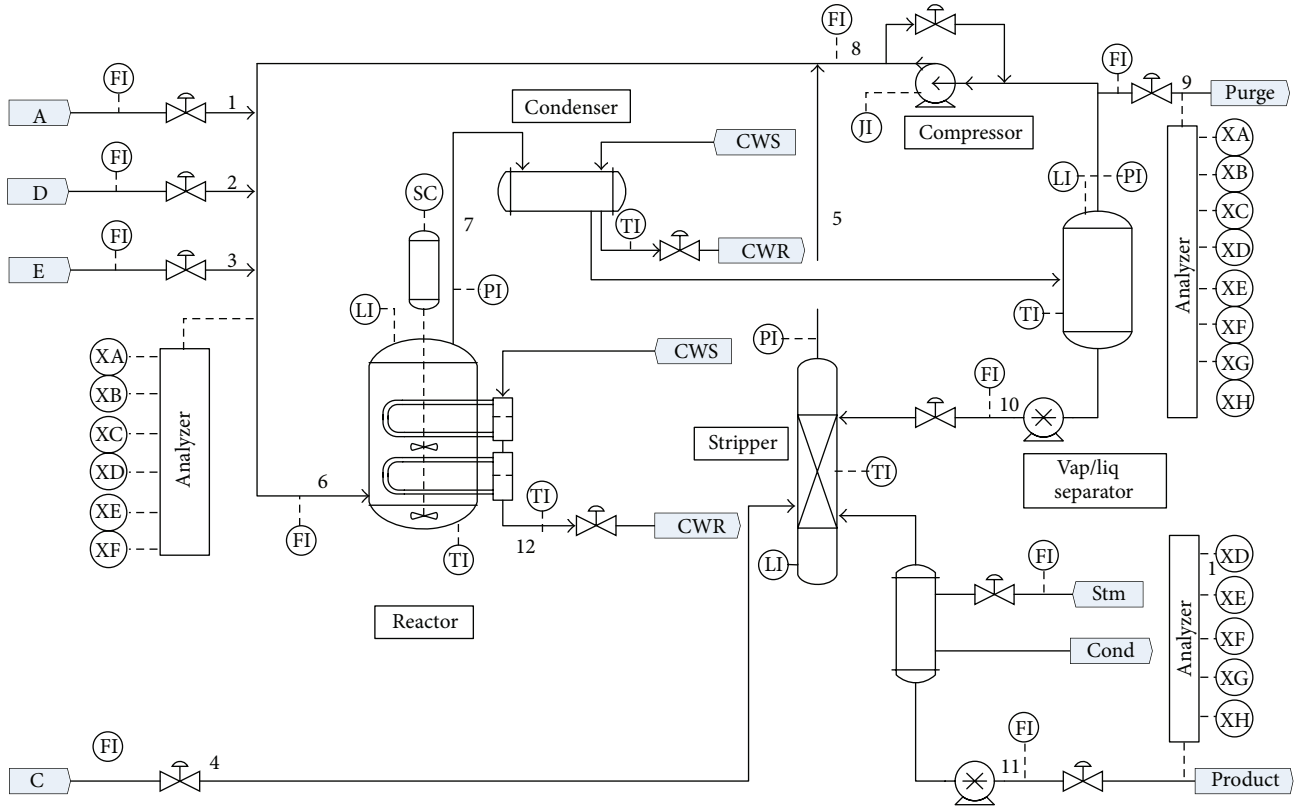


FIGURE 4: The Tennessee Eastman chemical process.

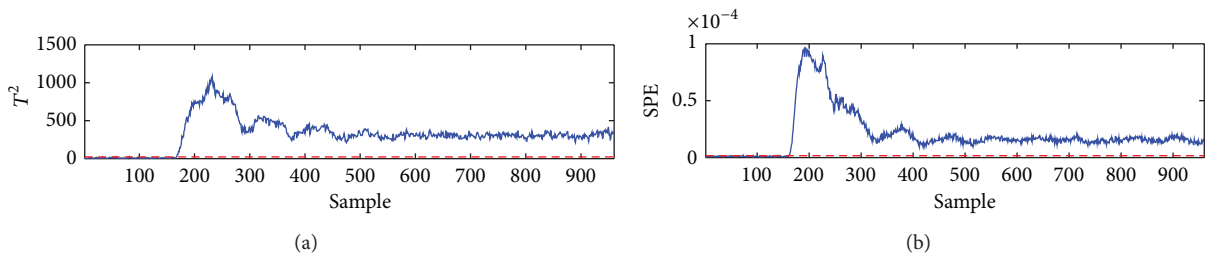


FIGURE 5: The classification accuracy of fault 1 dataset for PCA method.

Mahalanobis matrix H based on the given matrix H_0 , we can classify the data using k -nearest neighbor classifier to realize failure diagnosis.

3. Fault Diagnosis Using ITML

In the data-driven fault diagnosis system based on the ITML, the system is sensitive to values of the datasets. However, the faults are reflected in vibration amplitude or variation tendency in certain situations. Wavelet transform performs multiscale analysis to the dataset by dilating and shifting the wavelet functions. It transforms the discrepancies of vibration amplitude or variation tendency into the discrepancies of values.

Wavelet functions are localized in time and frequency. Wavelet transform has two main advantages. Firstly, the

analysis window changes itself rather than other complex exponential. Secondly, the duration of the analysis window is not fixed. The wavelet functions are created from the wavelet mother function, by dilating and shifting the window. The wavelet mother function $\psi(t)$ is a function with zero mean which has limited duration and salutory duration and amplitude. The wavelet functions can be express as [23]

$$\psi_{a,b}(t) = \frac{1}{\sqrt{a}}\psi\left(\frac{t-b}{a}\right), \quad (7)$$

where a is scaling factor and b is translation factor, with $a, b \in R, a \geq 0$. Through increasing the scaling factor a , the wavelet function is expanded and is conducive to analysis signals with low frequency and long duration. Correspondingly, by reducing the scaling factor a , the wavelet function is shrunk and is conducive to analysis signals with high frequency

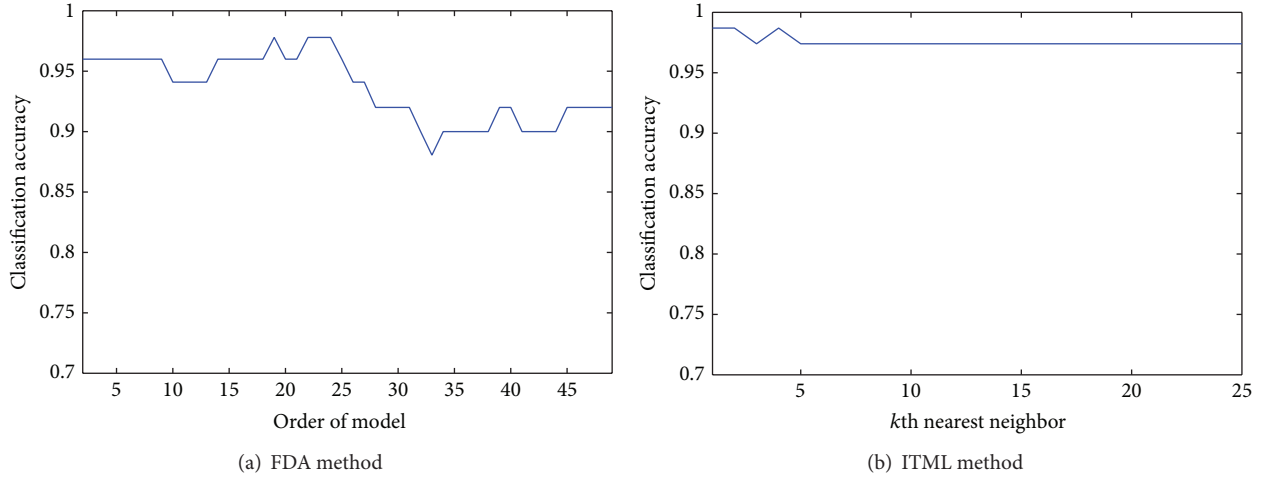


FIGURE 6: The classification accuracy of fault 1 dataset for 2 methods. (a) The experimental results based on FDA method. (b) The experimental results based on ITML method.

and short duration. By changing the translation factor b , the wavelet functions can realize the traversal along the time axis to get the information of time domain. The wavelet transform can study different scale features and information of time domain which can be expressed as in Figure 1.

The wavelet transform aims at getting a linear combination of the wavelet functions to describe the features in the signal. The value of the wavelet transform is generated by different scaling factors and translation factors. The wavelet transform is defined as [23]

$$WT_{a,b} = \frac{1}{\sqrt{a}} \int_{\mathbb{R}} x(t) \psi^* \left(\frac{t-b}{a} \right) dt. \quad (8)$$

Wavelet transform performs multiscale analysis to the dataset which is conducive to the results of ITML. In order to verify this, a wavelet transform to the dataset of TE process is constructed. TE process is introduced in Section 4. Selecting the corresponding 20 consecutive observations of the 9 variables of fault 12 dataset in the TE process randomly, the results of the wavelet transform are shown in Figures 3 and 4. The red lines in Figures 2 and 3 represent the value of fault-free dataset and the blue lines represent the value of fault 12 dataset.

The results of wavelet transform show that features in the signal are converted into the discrepancies of values. Wavelet transform performs well in doing the feature extraction of the ITML.

4. Experimental Results

4.1. Dataset. The designed method of the data-driven fault diagnosis system proposed in this work is applied on the Tennessee Eastman chemical process.

TE process is a chemical plant using as an industrial benchmark process; the schematic flow diagram and instrumentation of which are shown in Figure 4 [24]. TE process gets two products from four reactants. All the 52 variables

TABLE 1: Manipulating variables in TE plant.

Variable number	Variable name
XMV (1)	D feed flow (stream 2)
XMV (2)	E feed flow (stream 3)
XMV (3)	A feed flow (stream 1)
XMV (4)	A and C feed flows (stream 4)
XMV (5)	Compressor recycle valve
XMV (6)	Purge valve (stream 9)
XMV (7)	Separator pot liquid flow (stream 10)
XMV (8)	Stripper liquid product flow (stream 11)
XMV (9)	Stripper steam valve
XMV (10)	Reactor cooling water flow
XMV (11)	Condenser cooling water flow

contained in the process are 11 control variables and 41 measurement variables, respectively, as listed in Table 1 [16] and Table 2 [16].

20 process faults and a valve fault are defined in TE process, as shown in Table 3 [16]. In the work of Chiang et al. [15], a widely used dataset of TE process is given. To copy the measurements of 52 variables for 24 hours, 22 training datasets are contained in the dataset corresponding to the fault-free operating condition and 21 fault operating conditions. Simultaneously, 22 test datasets are contained in the dataset, in which the measurements of 52 variables for 48 hours are collected. It is worth pointing out that the faults in the 22 test datasets are added after 8 simulation hours. The sampling time of both of 22 training datasets and 22 test datasets is 3 minutes.

4.2. Performance Comparing with Classical Methods. To demonstrate the advantages of the proposed fault detection method, we compare it to two classical methods, PCA and FDA. We carried out experiments on the dataset of TE

TABLE 2: Measured variables in TE plant.

Variable number	Variable name
XMEAS (1)	A feed (stream 1)
XMEAS (2)	D feed (stream 2)
XMEAS (3)	E feed (stream 3)
XMEAS (4)	A and C feed (stream 4)
XMEAS (5)	Recycle flow (stream 8)
XMEAS (6)	Reactor feed rate (stream 6)
XMEAS (7)	Reactor pressure
XMEAS (8)	Reactor level
XMEAS (9)	Reactor temperature
XMEAS (10)	Purge rate (stream 9)
XMEAS (11)	Product separator temperature
XMEAS (12)	Product separator level
XMEAS (13)	Product separator pressure
XMEAS (14)	Product separator underflow (stream 10)
XMEAS (15)	Stripper level
XMEAS (16)	Stripper pressure
XMEAS (17)	Stripper underflow (stream 11)
XMEAS (18)	Stripper temperature
XMEAS (19)	Stripper steam flow
XMEAS (20)	Compressor work
XMEAS (21)	Reactor cooling water outlet temperature
XMEAS (22)	Separator cooling water outlet temperature
XMEAS (23)	Component A (stream 6)
XMEAS (24)	Component B (stream 6)
XMEAS (25)	Component C (stream 6)
XMEAS (26)	Component D (stream 6)
XMEAS (27)	Component E (stream 6)
XMEAS (28)	Component F (stream 6)
XMEAS (29)	Component A (stream 9)
XMEAS (30)	Component B (stream 9)
XMEAS (31)	Component C (stream 9)
XMEAS (32)	Component D (stream 9)
XMEAS (33)	Component E (stream 9)
XMEAS (34)	Component F (stream 9)
XMEAS (35)	Component G (stream 9)
XMEAS (36)	Component H (stream 9)
XMEAS (37)	Component D (stream 11)
XMEAS (38)	Component E (stream 11)
XMEAS (39)	Component F (stream 11)
XMEAS (40)	Component G (stream 11)
XMEAS (41)	Component H (stream 11)

process and the classification accuracy of k -nearest neighbor is chosen to evaluate the performance of classification.

The experiments are conducted on 6 datasets in the TE process, fault-free dataset, fault 1 dataset, fault 2 dataset, fault 4 dataset, fault 6 dataset, and fault 7 dataset, respectively. The feature extraction method of the datasets of TE process is selected as wavelet transform. To balance the performance of the feature extraction with the amount of delay, every 7 consecutive samples are collected to do a wavelet transform.

TABLE 3: Process faults in TE plant.

Fault number	Process variable
IDV (1)	A/C feed ratio, B composition constant
IDV (2)	B composition, A/C ration constant
IDV (3)	D feed temperature
IDV (4)	Reactor cooling water inlet temperature
IDV (5)	Condenser cooling water inlet
IDV (6)	A feed loss
IDV (7)	C header pressure loss-reduced availability
IDV (8)	A, B, C feed composition
IDV (9)	D feed temperature
IDV (10)	C feed temperature
IDV (11)	Reactor cooling water inlet temperature
IDV (12)	Condenser cooling water inlet temperature
IDV (13)	Reaction kinetics
IDV (14)	Reactor cooling water valve
IDV (15)	Condenser cooling water valve
IDV (16)	Unknown
IDV (17)	Unknown
IDV (18)	Unknown
IDV (19)	Unknown
IDV (20)	Unknown
IDV (21)	The valve fixed at steady state position

The slack variable used to avoid the overfitting problem is set as $\beta = 10^{-3}$ and all results presented are the average over 10 runs. The experimental results of fault 1 dataset are given in Figures 5 and 6.

Figure 5 shows the result of fault detection of fault 1 dataset for PCA method when fault occurs in both of the two orthogonal subspaces, which can be successfully detected by SPE and T^2 statistics. And the fault detection accuracy of fault 1 dataset for PCA method is 0.99. PCA method provides a satisfactory fault detection rate, but it cannot estimate fault types because it determines the lower dimensional subspaces without considering the information between the classes. Figure 6(a) indicates that the classification accuracy of FDA method float in line with the order of model and the classification accuracy are not totally satisfactory. Figure 6(b) illustrates that the ITML method gives higher fault detection rate than FDA method and it remains stable for different k th nearest neighbor. Furthermore, ITML method takes advantages of PCA method that it can estimate fault types directly.

Experimental results are summarized in Figure 7 and these results reveal that ITML method is more robust than PCA and FDA. Considering the ability of estimating fault types directly, ITML method achieves the best classification accuracy across all datasets. And the performance and effectiveness of the wavelet transform based feature extraction are demonstrated by the results of the experiment.

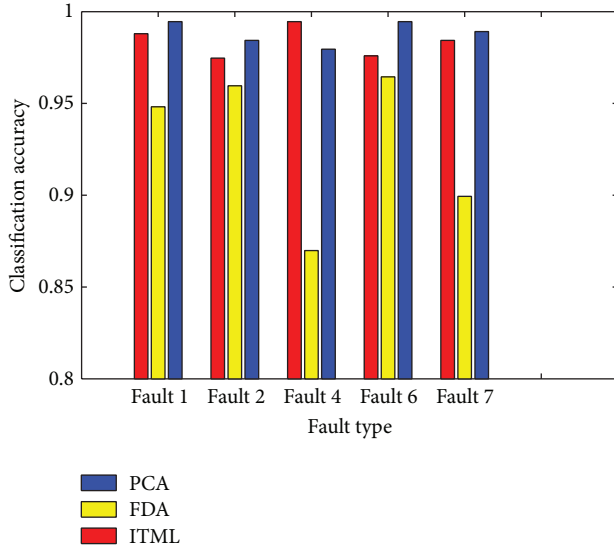


FIGURE 7: The classification accuracy of 5 different datasets for 3 methods.

5. Conclusion

In this paper, we proposed a fault detection scheme based on information-theoretic metric learning. ITML performs well in learning Mahalanobis distance function. In the proposed framework, the feature vector is firstly extracted by applying wavelet transform. After that, we apply the ITML algorithm in fault detection method to improve fault detection accuracy and estimate fault types. Comparing with the fault detection schemes based on PCA and FDA, experiments on TE process dataset demonstrate that the proposed method is more robust. The performance and effectiveness of the wavelet transform-based feature extraction are demonstrated by the results of the experiments at the same time.

Conflict of Interests

The authors declared that there is no conflict of interests regarding the publication of this paper.

Acknowledgments

The authors acknowledge the support of China Postdoctoral Science Foundation Grant no. 2012M520738 and Heilongjiang Postdoctoral Fund no. LBH-Z12092.

References

- [1] Z. Xudong, Z. Lixian, S. Peng, and L. Ming, "Stability and stabilization of switched linear systems with mode-dependent average dwell time," *IEEE Transactions on Automatic Control*, vol. 57, no. 7, pp. 1809–1815, 2012.
- [2] Z. Xudong, Z. Lixian, S. Peng, and L. Ming, "Stability of switched positive linear systems with average dwell time switching," *Automatica*, vol. 48, no. 6, pp. 1132–1137, 2012.
- [3] Z. Xudong and L. Xingwen, "Improved results on stability of continuous-time switched positive linear systems," *Automatica*, 2013.
- [4] S. Yin, S. Ding, A. Haghani, H. Hao, and P. Zhang, "A comparison study of basic datadriven fault diagnosis and process monitoring methods on the benchmark Tennessee Eastman process," *Journal of Process Control*, vol. 22, no. 9, pp. 1567–1581, 2012.
- [5] S. Yin, X. Yang, and H. R. Karimi, "Data-driven adaptive observer for fault diagnosis," *Mathematical Problems in Engineering*, vol. 2012, Article ID 832836, 21 pages, 2012.
- [6] S. Yin, H. Luo, and S. Ding, "Real-time implementation of fault-tolerant control systems with performance optimization," *IEEE Transactions on Industrial Electronics*, vol. 64, no. 5, pp. 2402–2411, 2014.
- [7] R. Dunia, S. J. Qin, T. F. Edgar, and T. J. McAvoy, "Use of principal component analysis for sensor fault identification," *Computers and Chemical Engineering*, vol. 20, pp. 713–718, 1996.
- [8] S. Yin, S. X. Ding, A. H. A. Sari, and H. Hao, "Data-driven monitoring for stochastic systems and its application on batch process," *International Journal of Systems Science*, vol. 44, no. 7, pp. 1366–1376, 2013.
- [9] S. Yin, G. Wang, and H. Karimi, "Data-driven design of robust fault detection system for wind turbines," *Mechatronics*, 2013.
- [10] I. T. Jolliffe, *Principal Component Analysis*, Springer, Berlin, Germany, 1986.
- [11] R. O. Duda, P. E. Hart, and D. G. Stork, *Pattern Classification*, Wiley-Interscience, New York, NY, USA, 2001.
- [12] D. Zumoffen and M. Basualdo, "From large chemical plant data to fault diagnosis integrated to decentralized fault-tolerant control: pulp mill process application," *Industrial and Engineering Chemistry Research*, vol. 47, no. 4, pp. 1201–1220, 2007.
- [13] J. E. Jackson and G. S. Mudholkar, "Control procedures for residuals associated with principal component analysis," *Technometrics*, vol. 21, no. 3, pp. 341–349, 1979.
- [14] N. D. Tracy, J. C. Young, and R. L. Mason, "Multivariate control charts for individual observations," *Journal of Quality Technology*, vol. 24, no. 2, pp. 88–95, 1992.
- [15] L. H. Chiang, E. L. Russell, and R. D. Braatz, "Fault diagnosis in chemical processes using Fisher discriminant analysis, discriminant partial least squares, and principal component analysis," *Chemometrics and Intelligent Laboratory Systems*, vol. 50, no. 2, pp. 243–252, 2000.
- [16] L. H. Chiang, E. L. Russell, and R. D. Braatz, *Fault Detection and Diagnosis in Industrial Systems*, Springer, London, UK, 2001.
- [17] S. Xiang, F. Nie, and C. Zhang, "Learning a mahalanobis distance metric for data clustering and classification," *Pattern Recognition*, vol. 41, no. 12, pp. 3600–3612, 2008.
- [18] L. Meizhu and B. Vemuri, "A robust and efficient doubly regularized metric learning approach," in *Computer Vision—ECCV 2012*, pp. 646–659, Springer, Berlin, Germany, 2012.
- [19] J. V. Davis, B. Kulis, P. Jain, S. Sra, and I. S. Dhillon, "Information-theoretic metric learning," in *Proceedings of the 24th International Conference on Machine Learning (ICML '07)*, pp. 209–216, ACM, June 2007.
- [20] J. J. Downs and E. F. Vogel, "A plant-wide industrial process control problem," *Computers and Chemical Engineering*, vol. 17, no. 3, pp. 245–255, 1993.
- [21] B. Kulis, M. Sustik, and I. Dhillon, "Learning low-rank kernel matrices," in *Proceedings of the 23th International Conference on Machine Learning (ICML '06)*, pp. 505–512, ACM, June 2006.

- [22] J. V. Davis and I. Dhillon, "Differential entropic clustering of multivariate gaussians," *Advances in Neural Information Processing Systems*, vol. 19, p. 337, 2007.
- [23] T. A. Ridsdill-Smith, *The Application of the Wavelet Transform to the Processing of Aeromagnetic Data*, The University of Western Australia, Crawley, Australia, 2000.
- [24] S. Yin, *Data-Driven Design of Fault Diagnosis Systems*, VDI, Dusseldorf, Germany, 2012.

Research Article

A New Mechanism for Network Monitoring and Shielding in Wireless LAN

Jiujun Cheng,^{1,2} Liufei Hu,² Junjun Liu,² Qingyang Zhang,² and Chendan Yan²

¹Department of Computer Science and Technology, Tongji University, Shanghai 201804, China

²Key Laboratory of Embedded System and Service Computing of Ministry of Education, Tongji University, Shanghai 201804, China

Correspondence should be addressed to Liufei Hu; huliufei2008@126.com

Received 5 December 2013; Accepted 21 January 2014; Published 10 March 2014

Academic Editor: Huaicheng Yan

Copyright © 2014 Jiujun Cheng et al. This is an open access article distributed under the Creative Commons Attribution License, which permits unrestricted use, distribution, and reproduction in any medium, provided the original work is properly cited.

Wireless LAN (WLAN) technology is developing rapidly with the help of wireless communication technology and social demand. During the development of WLAN, the security is more and more important, and wireless monitoring and shielding are of prime importance for network security. In this paper, we have explored various security issues of IEEE 802.11 based wireless network and analyzed numerous problems in implementing the wireless monitoring and shielding system. We identify the challenges which monitoring and shielding system needs to be aware of, and then provide a feasible mechanism to avoid those challenges. We implemented an actual wireless LAN monitoring and shielding system on Maemo operating system to monitor wireless network data stream efficiently and solve the security problems of mobile users. More importantly, the system analyzes wireless network protocols efficiently and flexibly, reveals rich information of the IEEE 802.11 protocol such as traffic distribution and different IP connections, and graphically displays later. Moreover, the system running results show that the system has the capability to work stably, and accurately and analyze the wireless protocols efficiently.

1. Introduction

The IEEE 802.11 wireless LAN standard was established in 1989 and was originally intended to seek a wireless equivalent to Ethernet [1]. Since then, wireless technology has been grown tremendously with flexibility. WLAN is a computer local area network using wireless channel as transmission medium and is a combinative product of computer and wireless communication technology. WLAN uses the public electromagnetic waves as a carrier to transmit data signals; thus one of the major issues which needs to be addressed is security. WLAN security technology research has also been rapidly developed with the development and application of wireless LAN.

Many security issues in the IEEE 802.11 WLAN have been identified and demonstrated in many studies [1–7]. The study of Boland and Mousavi [1] in Proceedings of the Canadian Conference on Electrical and Computer Engineering was one of the earlier studies. They introduced the importance of security and proposed several security issues in WLAN. WLAN security system consists of three different

components: authentication, encryption, and WLAN. The issues in encryptions [5] and authentication [6] mechanisms have been demonstrated. In paper [3], they identified and demonstrated two MAC vulnerabilities, identity vulnerability and media access vulnerability. These flaws indicate that wireless shielding technology and protocol analysis are very important for effective network diagnosis.

As wireless LAN technology has many irreplaceable advantages, and its development is very rapid. In recent years, WLAN has been widely used in the family, school, or some places that are not suitable for wiring or enterprises and occasions that need mobile office environment. But it also brings some new attendant issues, such as security issues for wireless networks and management oversight. Many studies [7–13] on measurement and characterization of wireless LANs and wireless monitoring have been performed. The authors in [8] addressed two problems: wireless monitoring technique and its applications in MAC traffic characterization and network diagnosis. They first identified the pitfalls of wireless monitoring and provided two feasible solutions, namely, merging multiple sniffers and their placement. Then,

they applied those techniques to academic research WLAN over two weeks for MAC traffic characterization and network diagnosis.

Wireless monitoring is of prime importance for WLAN security. More importantly, wireless monitoring exposes the characteristics on the wireless network itself so that we can infer more information. Such wireless monitoring allows us to know physical layer header information including signal strength, noise level, and data rate for individual packets. Similarly, it also enables examination of the link layer headers, which include IEEE 802.11 type and control fields. The information can be used to examine network problems and throughput. By analyzing the MAC layer data, we can characterize traffic according to different frame types, namely, data, control, and management frames. The collected data, combined with timestamps, can be used as accurate traces of the IEEE 802.11 link-level operations. Such traces are useful when we want to emulate the protocol or diagnose the problems of wireless networks [8].

In more general wireless environment, in paper [10], a novel 4G multiplatform real-time monitoring system is presented giving emphasis to WLAN part. The main idea of this system is to collect reports from numerous network elements in such way that the system is compatible and operational in any kind of network of any manufacturer and operator. Additionally the system architecture discussed in the paper is capable of accommodating and supporting 4G networks effectively.

In this paper, we focus on proposing a useful mechanism for wireless monitoring and shielding technique based on all the above advantages, implementing an effective wireless monitoring and shielding system, and showing its effectiveness in security monitoring, data sniffer, and protocol analysis. The remainder of this paper is organized as follows. Section 2 presents the proposed wireless monitoring and shielding mechanism and the implement of system. Section 3 shows and discusses the experimental results. Finally, we conclude our works in Section 4.

2. Wireless LAN Monitoring and Shielding Mechanism

Wireless monitoring is an effective mean to understand network performance and behavioral characteristics and improve network efficiency. According to whether inserting probings traffic into network, there are two kinds of wireless monitoring technologies, active monitoring and passive monitoring. To capture the detailed information, wireless monitoring technique can be used.

In this paper we have proposed a new mechanism for wireless LAN monitoring and shielding. Figure 1 illustrates wireless LAN monitoring environment. AP represents wireless access point, and wireless devices mainly include mobile phone and computer.

Figure 2 shows the process of our mechanism for wireless monitoring and shielding. It is user-centered and demonstrates the operating mechanism in detail. The mechanism involves five parts: User, User Interface, Data Buffer, Protocol

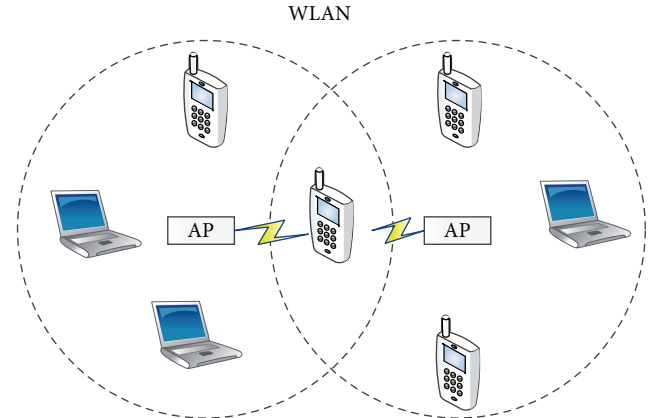


FIGURE 1: Wireless monitoring environment.

Analysis, and Network, which will be introduced in detail in the following section. We give a brief introduction for mechanism process as follows.

- (1) First, the User Interface Module emits a signal to Data Buffer Module every second when no operation happened. Then the Data Buffer Module updates the signal and emits the updated signal to the User Interface Module. Finally, the User Interface Module transforms the data into graphical data and shows them to users (*steps 1-3*).
- (2) In case that the user does not have some operation, whenever it captures a new data packet from network card, the following two tasks will be done. First, the Network Module will send the data packet to the Protocol Analysis Module. Then, the Protocol Analysis Module processes the data and stores the data structure into Data Buffer Module (*steps 4-6*).
- (3) When the user executes an operation or sends a request, the User Interface Module will send a message to the Data Buffer Module to obtain the information; after receiving the message, the Data Buffer Module will start to collect on-demand information and return these information to the User Interface Module; the User Interface Module will transfer the data into graphical data and display them to the user (*steps 7-10*).
- (4) The User Interface Module sends a command signal to Protocol Analysis Module; the Protocol Analysis Module will change analyzing methods based on the received information and process network data packet in different way. At the same time, the Protocol Analysis Module will send a signal to the Data Buffer Module and require it to change its storage format according to the user request. At last, the User Interface Module will update the information which is displayed and provide user with the needed information (*steps 11-15*).

Based on the above mechanism, we implemented a network monitoring and shielding system, which is running

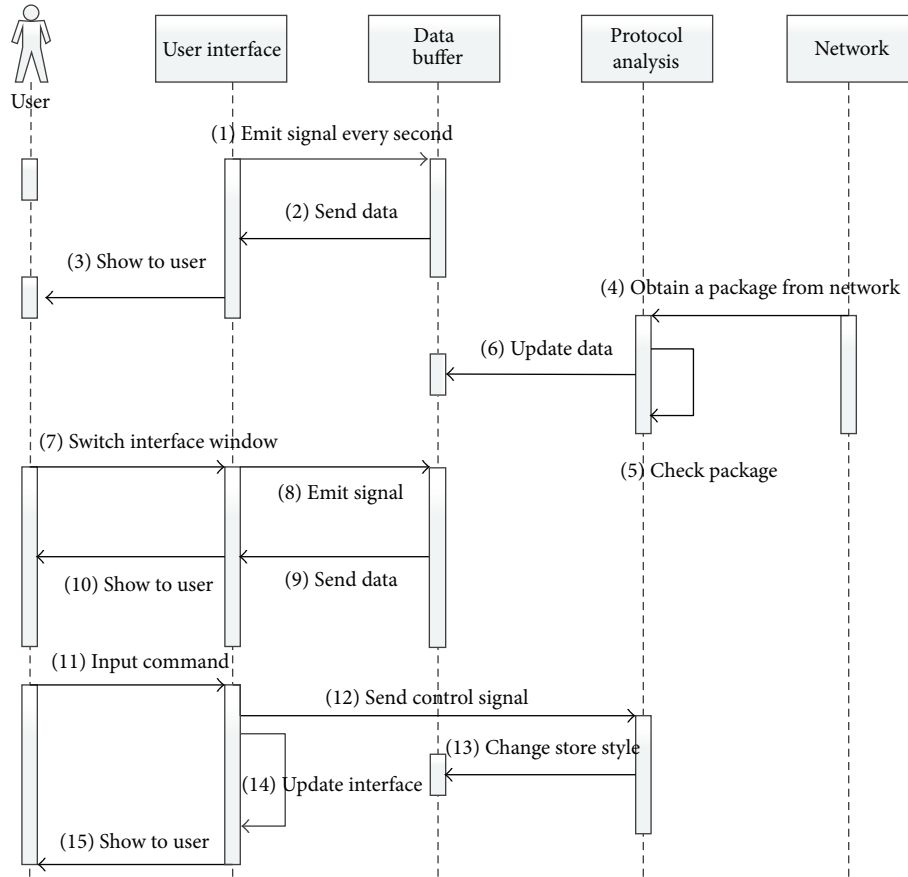


FIGURE 2: Process of mechanism.

on Maemo operating system, a software platform developed by Nokia and then handed over to Hildon Foundation for smartphones and Internet tablets [14] and is named Maemo Shield.

2.1. Maemo Shield Architecture. Maemo Shield is a light-weight network monitoring and shielding system which is run on the mobile and portable devices. To some extent, it can solve the security problems for mobile users. Figure 3 shows the system architecture which consists of Collecting Network Data, System Management, User Interface, and the most important Protocol Analysis Module and so on.

The first step is to collect all the needed data from network stream for the monitoring process. The wireless monitoring system consists of a set of devices which we call sniffers [12, 13], to capture network packets and observe traffic characteristics on the wireless medium. This step collects raw data directly from NIC driver layer taking advantage of sniffer technology, namely, network data capture. We retain whole packets information from raw data, which is the most complete network stream.

After the data collection, the system starts to perform the Protocol Analysis Module, which is the most critical and difficult module. The data packets obtained by previous step will be transferred into Protocol Analysis Module. In this module, all packets headers will be analyzed.

The result of protocol analysis will be stored in the Data Buffer Pool for the use of the latter part and these data will be from the buffer pool after finish the work in protocol analysis procedure. And the released space will be used to store other network data. In order to make these intermediate results be fully utilized, we use the Analyze and Calculate Module to do the secondary analysis and processing.

At this time, the System Management Module is used to coordinate the operating parameters of various analyses and save some configuration. In order to improve the operational efficiency, Maemo Shield uses multithread technology to implement network data capture and protocol analysis. Therefore, it requires a global management module to control the exclusive and parallel processes among threads.

The last but not least is the User Interface. It is the operational interface between system and users. After processing data in detail, the results will be showed to users in the way of diversified image which includes information in text form, in list form, in histogram form, in pie chart form, in grid form, and so on. The system will present dynamic graphical information which is transformed from data by the User Interface to users. At the same time, the User Interface sends the users requests to the management system and these requests will directly responded by the Protocol Analysis Module through processing the captured network data.

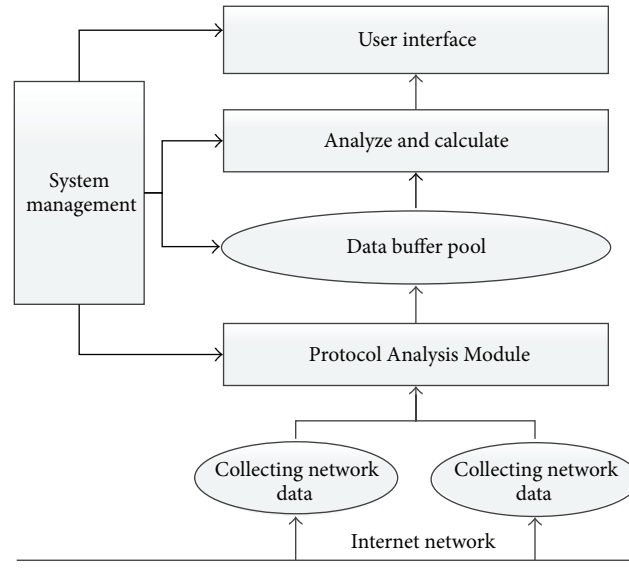


FIGURE 3: System architecture.

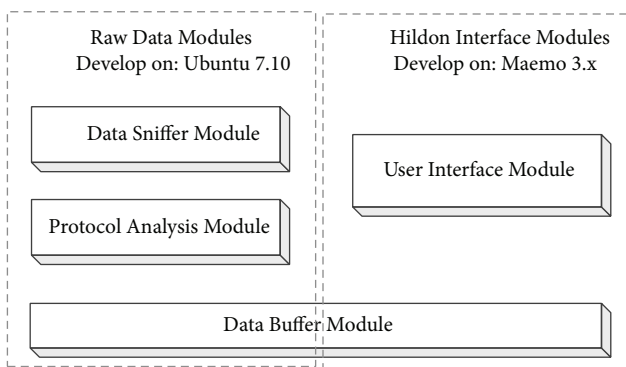


FIGURE 4: System modules.

2.2. The System Modules. Since the operation of the system involves both the network data capturing and the displaying of the high-level Hildon framework, so we will divide the development process of the system into two parts like Figure 4, which demonstrates the system modules, which includes Data Sniffer Module, Protocol Analysis Module, and User Interface Module and gives emphasis to Protocol Analysis Module.

The function of Raw Data Modules is to analyze and control the underlying network data. The system is running on the Nokia's N770/N800/N810 Internet Tablets series. Because the running speed of these devices is relatively slow, if the achievement and analysis of network data of system are developed on these devices directly then the efficiency of the development will be lower and the complexity of system debugging will be higher. Therefore we will extract the common part between those devices and Linux development platform. And we will use the efficient development tools to develop and debug in Linux platform. Then we will modify these modules slightly and inject them into the development system of Nokia.

The function of Hildon Interface Modules is to provide users efficient and dynamic graphics on the Nokia's Maemo development platform. This part will take full advantage of the unique realistic characteristics of Maemo. And all special good features which are not compatible with Linux will be achieved in this part.

- (1) *Data Sniffer Module* obtains full data flow information from NIC directly, which will contain all the data stream packet header and message body.
- (2) *Protocol Analysis Module* analyzes obtained data following different protocols from data linker layer, network layer, transport layer, and application layer. Analysis information will be stored in the data buffer module for secondary analysis and display.
- (3) *Data Buffer Module* is an independent part of the system by constructing and procedures abstract data storage structure to preserve the structure of protocol analysis and to complete the information and data share.
- (4) *User Interface Module* uses GTK +2.0 and Hildon GUI technology to present information in data buffer pool for user, and the user can operate the system with this module.

2.3. Protocol Analysis. Wireless monitoring is widely used in both wireless LAN and wireless LAN security management research. Moreover, wireless monitoring mechanism is also adopted in wireless protocol analysis. Wireless protocol information is very important for security monitoring in the IEEE 802.11 wireless LAN. It is well known that the IEEE 802.11 WLAN has security vulnerability due to the flaws in the MAC protocol [3] and basic features of wireless networks, such as open medium and mobility. To correctly diagnose such security problems we need to monitor wireless network

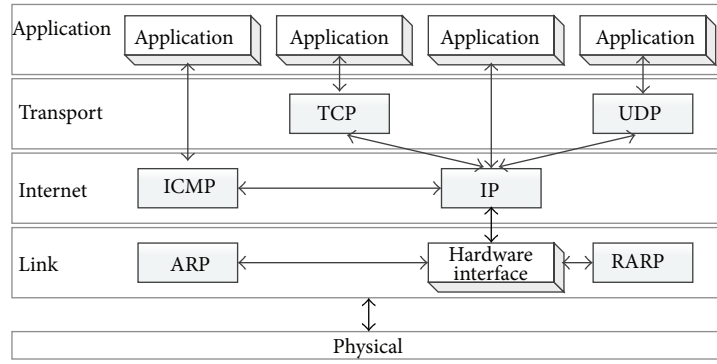


FIGURE 5: TCP/IP protocol stack.

information instantaneously. Therefore, such instantaneous wireless information, security monitoring, and surveillance are very important for effective network security.

The protocol stack used in this system is based on TCP/IP [15, 16] instead of the 7-layer OSI reference model; TCP/IP protocol stack are communication protocols using four-layer structure, each layer invoking network services provided by the next layer to meet their needs (Figure 5). These four layers are as follows.

- (i) *Application layer* is an interapplication communication layer, such as Simple Mail Transfer Protocol (SMTP), File Transfer Protocol (FTP), and Network Remote Access Protocol (Telnet).
- (ii) *Transport layer* provides data transmission services among nodes, such as Transmission Control Protocol (TCP) and User Datagram Protocol (UDP). Its main function is to format data and provide a mechanism for the transmission of data.
- (iii) *Network layer* provides the basic transmission function of data packet and guarantees that packets reach the destination hosts but does not check if received correctly, such as Internet Protocol (IP).
- (iv) *Link layer* manages the actual network media, defines how to use the Internet to transmit data, and is responsible for receiving the network layer datagram and sending through the transmission line.

The transmitted data should be encapsulated through protocol by the system. The first step is to use application layer protocol to encapsulate data, such as HTTP. HTTP protocol is based on TCP protocol. It is encapsulated by the TCP and HTTP as data part of TCP data segment. The TCP protocol is based on the IP protocol. So the TCP segment can be regarded as the payload and added with IP header to be an IP datagram. The IP datagram is Ethernet-based, so this time it is encapsulated into an Ethernet frame, and then the system sends the data by Ethernet frames. After receiving network data, the system will be the decomposer of data packets. Decompose process and encapsulate process on the contrary.

The total process of protocol analysis (Figure 6) begins with the data link layer to analyze and decompose packets,

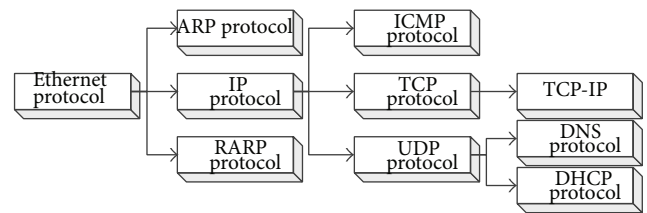


FIGURE 6: Process of protocol analysis.

via the network layer to the transport layer, and ends with the final analysis of application layer.

After obtaining WLAN network source data, first of all, we analyze those data and parse management frame, data frame, and control frame, respectively. Then use statistical data to understand network data composition and structure. In order to implement WLAN protocol analysis, firstly, we should know structure, composition, and topology of wireless LAN; what is more, we must be familiar with the structure of a radio frame, namely, MAC frame format to analyze, and statistic detailed information from frame; in addition, we also need to understand TCP/IP protocol stack to analyze upper level data from the network layer and transport layer; finally, we use these statistics to analyze network data composition and draw and display information.

Protocol Analysis Module is mainly based on the MAC frame format. It respectively parses bits of every field in MAC frame corresponded to every field, respectively, to comprehend the structure of each frame as well as its details and significance. Wireless LAN MAC frame has three kinds of frames, data, control, and management frame. Management frame is used for connection and separation to the site with the access point, timing, synchronization, and authentication; control frame is used for handshake communication and positive confirmation during competition period and ends in noncompetition period; data frame is used for transmitting data between competition period and noncompetition period and combined with acknowledgment (ACK) frame together in the noncompetition period. Therefore, we must distinguish these types of frames before separating and parsing each frame, respectively. After distinguished frame type of each frame, the next step is to handle three types of frames separately.



FIGURE 7: Protocol analysis view.

After the original data was processed and analyzed in accordance with the specific protocol format, User Interface Module gets data from the processed packet buffer and graphically displays the statistic information about packets. See Figure 7, and the details are displayed in Section 3.

3. Analysis of Experimental Results

In this section, we will present our experimental results. The purpose of those experiments is to analyze the wireless monitoring technique in terms of its effectiveness in capturing wireless packets and to present precise statistics information. We set up our device using the Maemo operating system with kernel version 4.1 to capture 802.11 frame information including the IEEE 802.11 header as well as physical layer header and information of higher layer protocols. In the rest of this section we will show the results of our experiment.

3.1. Capture and Analyze Packet Based on Sniffer. The system intercepts every packet through NIC and analyzes bit stream of the data packet. Then it will show the packet information of link layer, network layer, and transport layer in a recognizable manner to the screen in real time.

For example, we will analyze the 135th packet in Figure 8.

=====**Packet 135 (240 bytes)**=====

It indicates that the packet is the 135th packet and length is 240 bytes.

---- Ether header -----

Dest Ether = ff:ff:ff:ff:ff:ff
 Source Ether = 00:15:af:90:70:b6
 Type = 0800

It shows that Ethernet protocol is used in link layer, source Mac address is 00:15:af:90:70:b6, and destination Mac address is ff:ff:ff:ff:ff:ff. The protocol identification of upper layer is 0800.

----- IP header -----

Source IP = 192.168.61.136
 Destination IP = 192.168.61.255

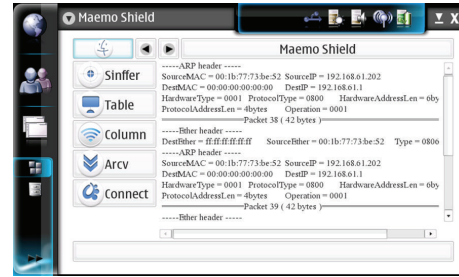


FIGURE 8: Capture and analyze packet.

Version_IHL = 45
 Total Length = 00e2 (226 bytes)
 Identification = 879a
 Time to Live = 80
 Protocol = 11
 Header Checksum = b698

It shows that the network layer using IP protocol source address is 192.168.61.136, and destination address is 192.168.61.255. After removing link layer header, the length of packet is 226 bytes. Network identification number is 879, and the protocol identification of upper layer is 11. Survival time is 80; header checksum is b798.

----- UDP header -----
 Source Port = 008a (138)
 Destination Port = 008a (138)
 Total Length = 00ce (206 bytes)
 Checksum = c799

It says that transport layer uses the UDP protocol, source port is 138, and destination port is 138. After removing linker layer and network layer header, the length of packet is 206 bytes, and packet checksum is c799.

We can get complete information of packet from the data link layer to the network layer through these series data.

3.2. Analysis of Protocol. The system records the recent 20 data records which use ARP, IP, TCP, UDP, and ICMP protocols and displays the protocol header information in list form. Maemo Shield has a buffer buffering the data packet protocol header information of five different protocols, so we can select the switches lower side of the table function panel to view different protocol header information. See Figure 9.

3.3. Protocol and IP Oriented Analysis of Network Stream. The system analyzes network stream by protocol oriented and IP oriented analysis and displays the data in the form of a histogram. In actual operation, the histogram is in the form of dynamic growth from the bottom up, and the whole process is done automatically. Figure 10 demonstrates that Ether protocol datagrams are used at most, followed by the IP datagram should be noted that Level2_Unknown and Level3_Unknown mean, respectively, the system does not

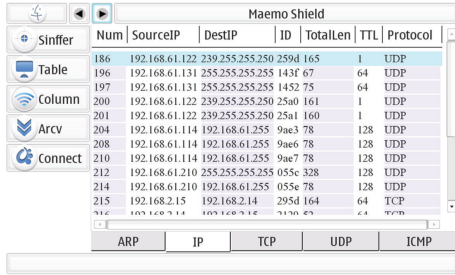


FIGURE 9: Analysis of protocol.

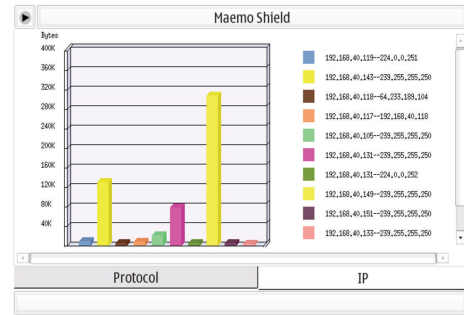


FIGURE 11: IP oriented analysis of network stream.

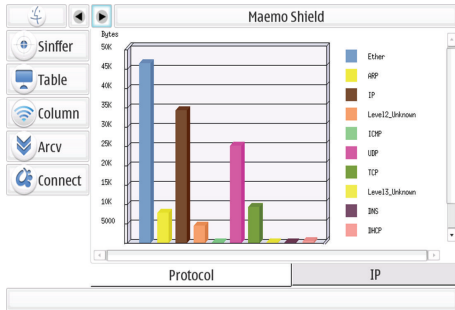


FIGURE 10: Protocol oriented analysis of network stream.

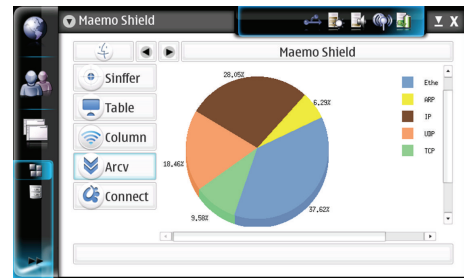


FIGURE 12: Stream distribution based on protocols.

recognize datagram protocol of the network layer and the transport layer. In Figure 11, 192.168.40.148-239.255.255.250 traffic ratio is the highest one among all connections, and 192.168.40.117-192.168.40.118 is the second highest share of traffic. It has four IP connections, whose traffic is relatively stable, while other connection data traffic is relatively small. We can determine that the initial connection to other noise may be invalid connections, while four high-traffic connections are the focus of our attention; they directly related to the process devices.

3.4. Stream Distribution Based on Protocols. Network data stream is divided under the protocols and displayed in pie graph. In the graph, different colors represent different protocols, the larger area occupied sector corresponds to the greater traffic of the protocol, and the percent indicated at its edges represents the percentage in the data stream protocol traffic ratio. In Figure 12, it shows the relative distribution of the data stream protocol: ether share 37.62%, ARP representing 6.29%, IP accounting for 28.05%, UDP accounting for 18.46%, and TCP accounted for 9.58%.

It should be noted that the data represented by these protocols at different levels may be double counted, the share traffic ratio is not a fixed value. For example, 6.29% of ARP and IP is included in the 37.62% of ether. Because ARP and IP protocol used by the data link layer protocols is ether, so their traffic is less than Ether protocol traffic certainly. Similarly, TCP and UDP traffic share values must also be included in the value of IP traffic.

3.5. Connections Related to Device. The system expressed IP connections associated with the device IP connection in the form of mesh. In Figure 13, it shows that there are 10 IP

connections connected to the device in the left panel, and there is a thick orange line in 10 connections, which indicates that the traffic of the current connection is the largest one. The right panel shows these connections clearly and the data transfer volume.

The system running results demonstrate the effectiveness of the mechanism in capturing the packets, presenting statistics, and analyzing protocols. The proposed mechanism has been implemented in the mobile devices. Real packet monitoring has been done and results have been recorded. So the system has the capability to work stably and accurately and analyze the wireless protocols efficiently.

4. Conclusion

In this paper we have researched various issues about wireless security and analyzed numerous problems in implementing the WLAN. We implemented an actual wireless LAN monitoring system to monitor the network data transmission, allowing users to understand the situation of device. What is more, the system analyzes and records ARP, RARP, IP, UDP, TCP, ICMP, and other protocols efficiently and flexibly. In the same time, statistics network data stream allows users to understand the data transmission protocol and type, as well as their share of the network bandwidth, respectively. Moreover, the system monitoring the IP connections allows users to know data communications of connected devices and identify the one communicating with device most frequently. Finally, the system can save the network traffic logs in debug mode. The results show that the system has the capability to work stably and accurately and analyze the wireless protocols efficiently.

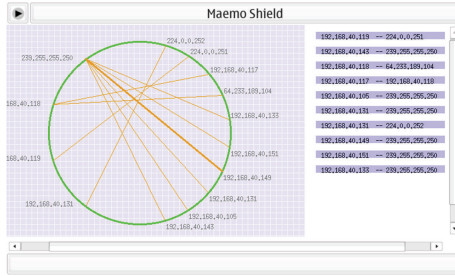


FIGURE 13: Connections related to device.

It is not easy to analyze some wireless network information such as the network running status and operating efficiency because of some features of IEEE 802.11 WLAN. It is now being developed and there are many problems which are worth of in-depth study and research. In this system, besides protocol information, other information can be obtained. We can provide more information of the traffic characteristics and connection status of WLAN. The research needs to propose new and more effective ways to handle those issues.

Conflict of Interests

The authors declare that there is no conflict of interests regarding the publication of this paper.

Acknowledgments

This work was supported in part by Natural Science Foundation Programs of Shanghai Grant no. 13ZR1443100, by ISTCP under Grant 2013DFM10100, by the National Science and Technology Support Plan Grant no. 2012BAH15F03, and by NSFC under Grants 51174210, 61003102, and 61103072.

References

- [1] H. Boland and H. Mousavi, "Security issues of the IEEE 802.11B wireless LAN," in *Proceedings of the Canadian Conference on Electrical and Computer Engineering*, vol. 1, pp. 0333–0336, May 2004.
- [2] IEEE Computer Society LAN MAN Standards Committee, "Wireless LAN Medium Access Control (MAC) and Physical Layer (PHY) Specifications," 1997.
- [3] J. Bellardo and S. Savage, "802.11 Denial-of-service Attacks: real vulnerabilities and practical solutions," in *Proceedings of the USENIX Security Symposium*, pp. 15–28, 2003.
- [4] H. Zhang, H. Yan, F. Yang, and Q. Chen, "Quantized control design for impulsive fuzzy networked systems," *IEEE Transactions on Fuzzy Systems*, vol. 19, no. 6, pp. 1153–1162, 2011.
- [5] S. Fluhrer, I. Mantin, and A. Shamir, "Weaknesses in the key scheduling algorithm of RC4," in *Selected Areas in Cryptography*, pp. 1–24, Springer, Berlin, Germany, 2001.
- [6] B. C. Neuman and T. Ts'o, "Kerberos. An authentication service for computer networks," *IEEE Communications Magazine*, vol. 32, no. 9, pp. 33–38, 1994.
- [7] A. Mishra and W. A. Arbaugh, "An initial security analysis of the IEEE 802.1 X standard," 2002.

- [8] H. Yan, H. Shi, H. Zhang, and F. Yang, "Quantized H_∞ control for networked systems with communication constraints," *Asian Journal of Control*, vol. 15, no. 5, pp. 1468–1476, 2013.
- [9] J. Yeo, M. Youssef, and A. Agrawala, "A framework for wireless LAN monitoring and its applications," in *Proceedings of the ACM Workshop on Wireless Security (WiSe '04)*, pp. 70–79, October 2004.
- [10] D. Nikitopoulos, A. Trakos, I. Popescu, and K. Xenou, "Real-time WLAN monitoring in a 4G multiplatform environment," in *Proceedings of the IEEE 17th International Symposium on Personal, Indoor and Mobile Radio Communications (PIMRC '06)*, pp. 1–5, September 2006.
- [11] K. Thompson, G. J. Miller, and R. Wilder, "Wide-area internet traffic patterns and characteristics," *IEEE Network*, vol. 11, no. 6, pp. 10–23, 1997.
- [12] A. Dabir and A. Matrawy, "Bottleneck analysis of traffic monitoring using wireshark," in *Proceedings of the 4th International Conference on Innovations in Information Technology (IIT '07)*, pp. 158–162, November 2007.
- [13] M. A. Qadeer, M. Zahid, A. Iqbal, and M. Siddiqui, "Network traffic analysis and intrusion detection using packet sniffer," in *Proceedings of the 2nd International Conference on Communication Software and Networks (ICCSN '10)*, pp. 313–317, February 2010.
- [14] S. Ansari, S. G. Rajeev, and H. S. Chandrashekar, "Packet sniffing: a brief introduction," *IEEE Potentials*, vol. 21, no. 5, pp. 17–19, 2002.
- [15] N. Ahmed, N. Ahmed, and A. Q. K. Rajput, "TCP/IP protocol stack analysis using MENE^T," in *Proceedings of the IEEE Conference on Convergent Technologies for the Asia-Pacific Region (TENCON '03)*, vol. 4, pp. 1329–1333, October 2003.
- [16] N. A. Junejo, N. Ahmed, and A. Q. K. Rajput, "Network layer packet analysis using MENE^T," in *Proceedings of the 7th International IEEE Multi Topic Conference (INMIC '03)*, pp. 151–156, 2003.

Research Article

Residual Generator-Based Controller Design via Process Measurements

Zenghui Huang,¹ Shen Yin,¹ and Hamid Reza Karimi²

¹ *Research Institute of Intelligent Control and Systems, Harbin Institute of Technology, Heilongjiang 150001, China*

² *Department of Engineering, Faculty of Engineering and Science, University of Agder, 4898 Grimstad, Norway*

Correspondence should be addressed to Shen Yin; shen.yin2011@gmail.com

Received 15 December 2013; Accepted 28 January 2014; Published 9 March 2014

Academic Editor: Xudong Zhao

Copyright © 2014 Zenghui Huang et al. This is an open access article distributed under the Creative Commons Attribution License, which permits unrestricted use, distribution, and reproduction in any medium, provided the original work is properly cited.

This paper deals with designing the controller of LTI system based on data-driven techniques. We propose a scheme embedding a residual generator into control loop based on realization of the Youla parameterization for advanced controller design. Basic idea of the proposed scheme is constructing the residual generator by using the solution of the Luenberger equations as well as the well-established relationship between diagnosis observer (DO) and the parity vector. Besides, the core of the above idea is straightly using the process measurements to obtain the parity space based on the Subspace Identification Method (SIM), rather than establishing the system model. At last, a simulation based on the numerical model demonstrates the performance and effectiveness of the proposed scheme.

1. Introduction

In the past decades, model-based controller design techniques have been perfectly established and a larger number of schemes have been proposed to design the controllers with the process model given [1–3], especially T-S fuzzy approach [4–6]. However, with the development of the science and technology as well as increasing demands for system performance and product quality, the modern industrial processes become more and more complicated and the traditional model-based approaches have become impractical for being much difficult or even impossible to construct the processes model. Hence, both the data-driven academic research and the data-driven techniques focusing on modern industrial applications have received widespread attention.

Compared with the well-developed model-based techniques, data-driven/data-based approaches, whose core is to extract the significant information contained in process measurements, not only improve the systems performance but also better solve the safety and reliability issues especially on the modern process [7–9]. As a result, over the past two decades, the data-driven methods and techniques have been

rapidly developed and many data-driven approaches have been successfully used in industrial process. For example, PID (proportional-integral-derivative) methods might be the earliest and the most widely used in industrial processes [10, 11]. Principal component analysis (PCA) [12, 13], one of the earliest data-based approaches to lower dimensional principal components, and partial least squares (PLS) aiming to predict key indicator directly from processes measurements are the most famous and successfully used approaches in multivariate statistical analysis which deal with large amounts of highly correlated measured data [14, 15].

In recent years, there are a lot of achievements in the field of fault detection and isolation (FDI) technique based on theory and many schemes to construct FDI systems [16–18]. In the above-mentioned papers, one of the most significant innovations is proposing a scheme that directly uses process measurements to construct residual generators for the purpose of FDI systems design. And several schemes extracting residual signals directly from a feedback control loop, without additional designing and constructing a residual generator based on observers, have been proposed [19, 20]. Ding et al. [21] designed an EIMC structure whose

core is embedding residual generation which aimed for FDI in the feedback control loop and proposed an advanced subspace identification method (SIM) which can generate parity vector directly from process measurements, for the purpose of constructing observer-based residual generator. Besides, Youla parameterization can establish the relationship between all stabilization controllers and observer-based residual generator [16, 22].

Motivated by the aforementioned studies, in this paper, we propose a data-driven scheme using process measurements to design controllers for LTI system, and the basic idea is instructing an observer-based residual generator into feedback control loop. Following the above idea, we first divided the work into three sections based on Youla parameterization and coprime factorizations [22]. Note that the first section is the core of this paper. In this section, to produce residual signals, we design a residual generator with an observer form. Besides, the basis of constructing the generator is the solution of the Luenberger equations [16] from the well-established relationship between diagnosis observer (DO) and the parity vector which are identified directly from the available test data by using the advanced SIM. In addition, we present the scheme proposed in form of algorithms to make it easy to understand.

The structure of remaining content is shown as follows: the basic plant model as well as the system preliminary factorization, in other words, the related work, is explained in Section 2. The first part of the designing controller will be completed in Section 3. In addition, several algorithms are presented to obtain the structure and parameters of the residual generator based on diagnosis observer. And the rest of the parts are studied in Section 4. For the purpose of illustrating the performance and effectiveness of the scheme, a simulation study on an academic model will be presented and discussed in Section 5. At last, we will give some conclusion in Section 6.

2. Related Work

2.1. Process Description. In this paper, we deal with designing the controller of linear time invariant (LTI) system. Without loss of generality, we assume that the discrete state space equation of the system is described by

$$\begin{aligned} x(k+1) &= Ax(k) + Bu(k) + F_d d(k), \\ y(k) &= Cx(k) + Du(k) + F_n n(k), \end{aligned} \quad (1)$$

in which both the plant inputs and outputs are measurable; in other words, the values of them can be obtained at every discrete time point. And they are defined as $u(k) \in R^l$ and $y(k) \in R^m$, respectively. $x(k) \in R^n$ stand for the status variables. It is assumed that $d(k) \in R^n$ and $n(k) \in R^m$ are white noise. And note that values of $d(k)$ and $n(k)$ cannot be measured, and there is no statistical correlation between the noise sequences and the input vectors $u(k)$. In addition, the system matrices and order are unknown parameters.

Based on the well-established relationship between the transfer function matrix and the state space equation, there are some significant points as follows:

$$\begin{aligned} y(z) &= G(z)u(z) + G_1(z)d(z) + F_n n(z), \\ G(z) &= D + C(zI - A)^{-1}B, \\ G_1(z) &= C(zI - A)^{-1}F_d. \end{aligned} \quad (2)$$

As shown in Figure 1, we chose classical output feedback control method to enhance the system performance and robustness [23].

2.2. Left Coprime Factorization and Youla Parameterization. Suppose that there exists a appropriate parameter matrix F , satisfying

$$\max_i |\lambda_i| < 1, \quad (3)$$

where λ_i stands for the eigenvalues of the matrix $A - FC$ and $i = 1, 2, \dots, n$. Then, the left coprime factorization of the system transfer function matrices [22] can be described as follows:

$$G(z) = \widehat{D}^{-1}(z)\widehat{V}(z) \quad (4)$$

$\widehat{V}(z)$ and $\widehat{D}(z)$ are, respectively, defined as $\widehat{V}(z) = D + C(zI - A_F)^{-1}B_F$ and $\widehat{D}(z) = I - C(zI - A_F)^{-1}F$ with $A_F = A - FC$ and $B_F = B - FD$. According to the Youla parameterization, all stable controllers $K(z)$ can be expressed by a unified form for a classical output feedback control loop. Consider

$$K(z) = \left(\widehat{X}(z) - R(z)\widehat{V}(z) \right)^{-1} \left(\widehat{Y}(z) - R(z)\widehat{D}(z) \right). \quad (5)$$

$\widehat{X}(z)$ and $\widehat{Y}(z)$ are, respectively, defined as $\widehat{X}(z) = I - L(zI - A_F)^{-1}B_F$ and $\widehat{Y}(z) = L(zI - A_F)^{-1}F$, in which L is an appropriate parameter matrix and assures a stable $A + BL$. And $R(z)$ is a parameter matrix whose parameter can be chosen according to the requirements of plant performance.

In this paper, we assume that the matrix A is stable to simplify the controller design. Then, letting the matrix L be equal to zero is reasonable. Combining $L = 0$ with (5), we can obtain a simplified controller as follows:

$$K(z) = \left(I - R(z)\widehat{V}(z) \right)^{-1} R(z)\widehat{D}(z). \quad (6)$$

It is well known that the residual signals imply significant information about process and can be used for FDI purpose [17]. Recall that the residual vectors can be described as follows:

$$r(z) = \widehat{D}(z)y(z) - \widehat{V}(z)u(z). \quad (7)$$

Note that the process inputs, that is, outputs of the controller, are expressed as

$$u(z) = K(z)[h(z) - y(z)]. \quad (8)$$

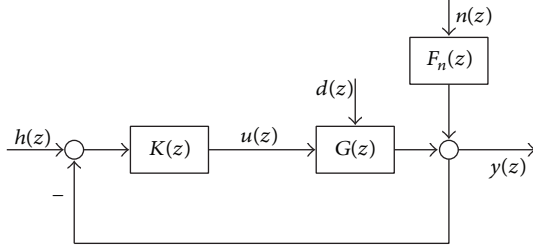


FIGURE 1: The primal system.

Combining (6) and (8), we get

$$u(z) = R(z) \left\{ \widehat{D}(z) h(z) - \left[\widehat{D}(z) y(z) - \widehat{V}(z) u(z) \right] \right\}. \quad (9)$$

Thus, the feedback control loop is restructured as shown in Figure 2.

Observing Figure 2, we notice that the task of designing the controller can be divided into three sections:

- (i) obtaining residual signal through constructing a residual generator,
- (ii) designing the parameter matrix $R(z) \in \mathcal{RH}_\infty$,
- (iii) selecting the prefilter $\widehat{D}(z)$.

3. Residual Generator

This section is the core of the paper. Residual signal represents the difference between the actual observed value and the estimate value, which implies very important information about process. There are many papers which construct residual generator directly using the process inputs and outputs, instead of identifying the system parameter matrixes [12, 17, 18]. The algorithm of constructing generator from inputs and outputs will be given in this section.

3.1. Diagnostic Observer and Parity Space Approach. There are many approaches to generate residual signals. In this subsection, we study two methods of them, which are based on diagnostic observer (DO) and parity space, respectively [16].

The first method is based on DO, and its state space equation is expressed by

$$\begin{aligned} z(k+1) &= A_z z(k) + B_z u(k) + F_z y(k), \\ \widehat{y}(k) &= c_z z(k) + d_z u(k) + g y(k), \end{aligned} \quad (10)$$

where $z \in R^s$, $A_z \in R^{s \times s}$, $B_z \in R^{s \times l}$, $F_z \in R^{s \times m}$, $g \in R^{1 \times m}$, $c_z \in R^{1 \times s}$, and $d_z \in R^{1 \times l}$. Besides, s and T , respectively, represent the order of DO which satisfies $s \geq n$ and the transformation matrix. Besides, the matrixes $A_z, B_z, F_z, g, c_z, d_z$, and T satisfy the Luenberger equations,

$$\begin{aligned} TA - F_z C &= A_z T, & c_z T &= g C, \\ TB - B_z &= F_z D, & d_z &= g D. \end{aligned} \quad (11)$$

The other method studied is based on parity space [24], and we can also obtain the residual signal by using the parity space approach as follows [12]. Assume that the system which is expressed in the related work is observable and the matrix C is row full rank. Then, we can recursively describe the system as

$$\begin{aligned} y(k) &= CA^{s-1} x(k-s+1) + CA^{s-2} Bu(k-s+1) \\ &+ \dots + CBu(k-1) + Du(k). \end{aligned} \quad (12)$$

Using the inputs and outputs to build the following data structure:

$$\begin{aligned} y_s(k) &= \begin{bmatrix} y(k-s) \\ y(k-s+1) \\ \vdots \\ y(k) \end{bmatrix} \in R^{sm}, \\ u_s(k) &= \begin{bmatrix} u(k-s) \\ u(k-s+1) \\ \vdots \\ u(k) \end{bmatrix} \in R^{sl}, \end{aligned} \quad (13)$$

we can get the rewritten system form as follows:

$$y_s(k) = \Gamma_s x(k-s+1) + H_{s,u} u_s(k), \quad (14)$$

in which

$$\Gamma_s = \begin{bmatrix} C \\ CA \\ \vdots \\ CA^s \end{bmatrix}, \quad H_{s,u} = \begin{bmatrix} D & 0 & \dots & 0 \\ CB & D & & \vdots \\ \vdots & \ddots & \ddots & \\ CA^{s-1}B & \dots & CB & D \end{bmatrix}. \quad (15)$$

Equation (14) expresses the relationship between system inputs and outputs using the past plant inputs $u_s(k)$ and past state vectors.

Solving the following equation, we are able to get a parity vector $\gamma_s (\neq 0) \in R^{1 \times (s+1)m}$,

$$\gamma_s \Gamma_s = 0. \quad (16)$$

Hence, γ_s belongs to Γ_s^\perp , which is the parity subspace and satisfies $\Gamma_s^\perp \Gamma_s = 0$.

Note that when both sides of (14) are multiplied by γ_s at the same time, we can obtain a residual signal sequence in the following form:

$$r(k) = \gamma_s (y_s(k) - H_{s,u} u_s(k)). \quad (17)$$

Despite that the diagnostic observer and the parity space approach are in different forms, there have been a well-established relationship between them [16, 25]. For a known

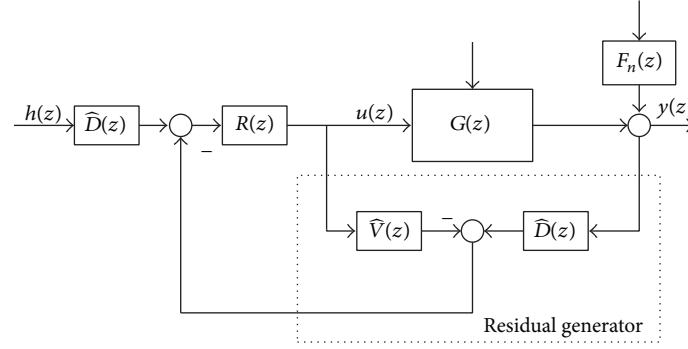


FIGURE 2: The whole control system.

vector, $\gamma_s = [\gamma_{s,0} \ \gamma_{s,1} \ \cdots \ \gamma_{s,s}]$, $\gamma_{s,i} \in R^m$, $i = 0, 1, \dots, s$, the matrixes of the diagnostic observer can be set as follows [17]:

$$A_z = \begin{bmatrix} 0 & 0 & \cdots & 0 \\ 1 & 0 & \cdots & 0 \\ \vdots & \ddots & \ddots & \vdots \\ 0 & \cdots & 1 & 0 \end{bmatrix} \in R^{s \times s}, \quad F_z = - \begin{bmatrix} \gamma_{s,0} \\ \gamma_{s,1} \\ \vdots \\ \gamma_{s,s-1} \end{bmatrix},$$

$$c_z = [0 \ \cdots \ 0 \ 1] \in R^s, \quad g = \gamma_{s,s} \in R^m, \quad d_z = \gamma_s H_{s,s},$$

$$B_z = \begin{bmatrix} \gamma_s H_{s,0} \\ \gamma_s H_{s,1} \\ \vdots \\ \gamma_s H_{s,s-1} \end{bmatrix}, \quad H_{s,\mu} = [H_{s,0} \ \cdots \ H_{s,s}],$$

(18)

$$T = \begin{bmatrix} \gamma_{s,1} & \gamma_{s,2} & \cdots & \gamma_{s,s-1} & \gamma_{s,s} \\ \gamma_{s,2} & \cdots & \cdots & \gamma_{s,s} & 0 \\ \vdots & \cdots & \cdots & \vdots & \vdots \\ \gamma_{s,s} & 0 & \cdots & \cdots & 0 \end{bmatrix} \Gamma_s. \quad (19)$$

Notice that different selected principles of γ_s lead to different system performances. A scheme to select γ_s is proposed, and the scheme can improve the robustness of the residual generator and system performance [26].

3.2. Realization of the Parity Space Approach. Recall the state space of the process expressed in the related work, and suppose that the system matrixes and order are unknown constants which do not change with time, but the process inputs and outputs are available. Constructing data structure as follows:

$$u_p(k) = \begin{bmatrix} u(k-s_p) \\ \vdots \\ u(k) \end{bmatrix}, \quad u_f(k) = \begin{bmatrix} u(k) \\ \vdots \\ U(k+s_f) \end{bmatrix},$$

$$y_p(k) = \begin{bmatrix} y(k-s_p) \\ \vdots \\ y(k) \end{bmatrix}, \quad y_f(k) = \begin{bmatrix} y(k) \\ \vdots \\ y(k+s_f) \end{bmatrix},$$

$$U_p = [u_p(k) \ u_p(k+1) \ \cdots \ u_p(k+N-1)],$$

$$U_f = [u_f(k) \ u_f(k+1) \ \cdots \ u_f(k+N-1)],$$

(20)

in which both s_p and s_f are larger than n , besides, N is user-defined parameters and always much larger than s . To simplify the problem, let both s_p and s_f be equal to s which is user-defined parameters and larger than or equal to n in general. Hence, considering the above-mentioned data structures shown in (20), we can construct matrixes Z_p and Z_f for the process inputs and outputs with Hankel structure:

$$Z_p = \begin{bmatrix} Y_p \\ U_p \end{bmatrix}, \quad Z_f = \begin{bmatrix} Y_f \\ U_f \end{bmatrix}. \quad (21)$$

In the following subsection, we use the subspace identification method (SIM) proposed by Wang and Qin [27] to identify the parity space, that is, finding Γ_s^\perp , $\Gamma_s^\perp H_{s,\mu}$, and Γ_s . Besides, we give this method in the form of an algorithm [28].

Algorithm 1. Consider the following.

Step 1. Construct Z_f and Z_p and calculate $Z_f Z_p^T$.

Step 2. Do SVD on $(1/N)Z_f Z_p^T$

$$\frac{1}{N} Z_f Z_p^T = U_z \begin{bmatrix} \Lambda_{z,1} & 0 \\ 0 & \Lambda_{z,2} \end{bmatrix} V_z^T, \quad (22)$$

in which $U_z \in R^{s_l(s+m) \times s_l(l+m)}$, $V_z \in R^{s_l(s+m) \times s_l(l+m)}$, $U_z = \begin{bmatrix} U_{z,11} & U_{z,12} \\ U_{z,21} & U_{z,22} \end{bmatrix}$, $U_{z,11} \in R^{s_l m \times (s_l l + n)}$, $U_{z,12} \in R^{s_l m \times \zeta}$, $U_{z,22} \in R^{s_l \times \zeta}$, $s_l - 1 = s$, $\zeta = s_l m - n$, and both $\Lambda_{z,1}$ and $\Lambda_{z,2}$ are diagonal matrixes. Note that if d and n are perfect white noise, all eigenvalues of $\Lambda_{z,2}$ are equal to zero, and $\Lambda_{z,1}$ is a nonsingular matrix satisfying $\text{rank}(\Lambda_{z,1}) = s_l l + n$. Hence, the value of n can be determined.

Step 3. Respectively, define Γ_s^\perp and $\Gamma_s^\perp H_{s,\mu}$ as $U_{z,12}^T$ and $-U_{z,22}^T$.

Step 4. Do SVD on Γ_s^\perp

$$\Gamma_s^\perp = U_{\Gamma_s^\perp} \begin{bmatrix} \Lambda_{\Gamma_s^\perp} & 0 \end{bmatrix} V_{\Gamma_s^\perp}^T \quad (23)$$

with $V_{\Gamma_s^\perp} = [V_{\Gamma_s^\perp,1} \ V_{\Gamma_s^\perp,2}]$, $V_{\Gamma_s^\perp,2} \in R^{(s_i+1)m \times n}$, and we can get $\Gamma_s = V_{\Gamma_s^\perp,2}^\perp$.

The necessary conditions have been completely studied in [27, 29], when identifying the parity space by using SIM. This paper assumes that the process measurements used for identifying the parity space meet the above condition, so that we can use Algorithm 1 to identify Γ_s^\perp , $\Gamma_s^\perp H_{s,u}$, and Γ_s . However, when d and n are not absolute white noise, we can use the following method [27] to identify n .

For a sequence of the system order n , for instance, $n \in [0 \cdots 10]$, the order of the system will be the one which makes the following AIC index:

$$\text{AIC}_N(n) = N(m(1 + \ln 2\pi) + \ln |\Phi|) + 2\delta_n \Psi \quad (24)$$

minimum, where

$$\begin{aligned} \Phi &= \frac{1}{N} \sum_{i=1}^N e(i) e(i)^T, \\ e(i) &= (\Gamma_s^\perp)^T [I - H_{s,u}] z_f(i - n), \\ \Psi &= 2nm + \frac{m(m+1)}{2} + nl + ml, \\ \delta_n &= \frac{N}{N - ((M_n/m) + ((m+1)/2))}. \end{aligned} \quad (25)$$

3.3. Design of Residual Generator. After identifying Γ_s^\perp , $\Gamma_s^\perp H_{s,u}$, constructing a residual generator by using the relationship between DO and parity space is just around the corner. Select a parity vector $\gamma_s \in \Gamma_s^\perp$ and $\gamma_s H_{s,u} \in \Gamma_s^\perp H_{s,u}$, with $\gamma_s \in R^{m(s+1)}$, $\gamma_s = [\gamma_{s,0} \ \gamma_{s,1} \ \cdots \ \gamma_{s,s}]$, and $\gamma_{s,i} \in R^m$, $i = 0, 1, \dots, s$; then, we can calculate the parameter matrixes of DO A_z, B_z, F_z, g, c_z , and d_z by solving (18)-(19) and construct a diagnosis observer according to (10).

Note that we can obtain the following residual signal [16] by constructing and using the residual generator (7):

$$r(k) = V(y(k) - \hat{y}(k)) \in R^x, \quad (26)$$

in which V represent parameter matrix satisfying $V \in R^{x \times m}$ and $\hat{y}(k)$ denote an estimate for the process outputs with convergence to the real outputs. To improve the system performance, it is necessary to design a residual generator which can deliver an m -dimensional residual vector. Hence, we need to extend the data-driven based single residual generation to multiple residual generations. In the following section, using Γ_s^\perp and $\Gamma_s^\perp H_{s,u}$ having been identified, we propose a method to construct m -DOs spanning the overall state space to obtain m residual sequences independent from each other [12].

Suppose that Γ_s^\perp and $\Gamma_s^\perp H_{s,u}$ are computed using the above-mentioned method, and choose m parity vectors from Γ_s^\perp , which are linearly independent from each other,

$$\gamma_{s_i} \in \Gamma_s^\perp, \quad i = 1, \dots, m, \quad \gamma_{s_i} = [\gamma_{s_i,0} \ \gamma_{s_i,1} \ \cdots \ \gamma_{s_i,s}] \quad (27)$$

with $\text{rank}([\gamma_{s_1}^T \ \cdots \ \gamma_{s_m}^T]) = m$, and select the corresponding vectors from $\Gamma_s^\perp H_{s,u}$

$$\beta_{s_i} = \gamma_{s_i} H_{s,u} \in \Gamma_s^\perp H_{s,u}, \quad i = 1, \dots, m. \quad (28)$$

Using γ_{s_i} and β_{s_i} , we can design the m -DOs as follows:

$$\begin{aligned} z(k+1) &= A_z z(k) + F_z y(k) + B_z u(k), \\ r(k) &= -C_z z(k) - D_z u(k) + G y(k) \in R^m, \end{aligned} \quad (29)$$

$$A_z = \text{diag}(A_{z_1}, \dots, A_{z_m}), \quad C_z = \text{diag}(c_{z_1}, \dots, c_{z_m}),$$

$$\begin{aligned} B_z &= \begin{bmatrix} B_{z_1} \\ \vdots \\ B_{z_m} \end{bmatrix}, & F_z &= \begin{bmatrix} F_{z_1} \\ \vdots \\ F_{z_m} \end{bmatrix}, \\ D_z &= \begin{bmatrix} d_{z_1} \\ \vdots \\ d_{z_m} \end{bmatrix}, & G &= \begin{bmatrix} g_1 \\ \vdots \\ g_m \end{bmatrix}, \end{aligned} \quad (30)$$

where the matrixes $A_{z_i}, B_{z_i}, c_{z_i}, d_{z_i}$, and F_{z_i} , $i = 1, \dots, m$ are calculated by solving (18)-(19), and the dimensions of the matrix A_z , that is, s , satisfy $s = \sum_{i=1}^m s_i$. Besides, the transformation matrix $T \in R^{s \times n}$ satisfies $\text{rank}(T) = n$, $T = [T_1 \ \cdots \ T_m]$ and note that T_i , $i = 1, \dots, m$, can be got from (19). Then, estimated value of outputs can be generated by the m -DOs,

$$\hat{y}(k) = G^{-1}(C_z z(k) + D_z u(k)). \quad (31)$$

Obviously, when the process is multiple output system, s , the order of the system (29) is significantly larger than n , the order of the process system. Hence, we need to reduce the order of the m -DOs to decrease the amount of calculation and improve the system performance.

Note that the transformation matrix T satisfies $z(k) = T x(k)$, then we can reduce the order of the multiple residual generators as follows [12].

Assume that the multiple residual generators have been constructed, and the transformation matrix T has a pseudoinverse T^- satisfying $T^- T = I$. Thus, we can reconstruct following residual generator:

$$\begin{aligned} \hat{z}(k) &= A_x \hat{z}(k) + B_x u(k) + F_x y(k), \\ r(k) &= -G^{-1} C_x \hat{z}(k) - G^{-1} D_x u(k) + y(k) \in R^m \end{aligned} \quad (32)$$

with $\hat{z}(k)$ being an estimate for the state vector of the system (1), and the matrixes B_x, F_x , and C_x satisfy $B_x = T^- B_z, F_x = T^- F_z$, and $C_x = C_z T$.

Algorithm 2. Consider the following.

Step 1. Identify Γ_s^\perp , $\Gamma_s^\perp H_{s,u}$, and Γ_s .

Step 2. Construct a multiple residual generator as defined in (29).

Step 3. Calculate T_i , $i = 1, \dots, m$,

$$T_i = \begin{bmatrix} \gamma_{s_i,1} & \gamma_{s_i,2} & \cdots & \gamma_{s_i,s-1} & \gamma_{s_i,s} \\ \gamma_{s_i,2} & \cdots & \cdots & \gamma_{s_i,s} & 0 \\ \vdots & \cdots & \cdots & \vdots & \vdots \\ \gamma_{s_i,s} & 0 & \cdots & \cdots & 0 \end{bmatrix} \Gamma_s, \quad (33)$$

Step 4. Reduce the order of the m -DOs as defined in (32).

4. Design of Prefilter $\widehat{D}(z)$ and Parameter Matrix $R(z)$

4.1. *Prefilter $\widehat{D}(z)$ Design.* Noticing that the multiple residual generators which have been constructed and reduced order need to deliver an m -dimensional residual vector. Thus, we construct a residual generator with the state space equation described in (32) which is a little different from (29). According to the well-established relationship between classical and modern control theory, there are some significant equations as follows:

$$r(z) = \widehat{D}(z)y(z) - \widehat{V}(z)u(z),$$

$$\widehat{D}(z) = I - G^{-1}C_x(zI - A_x)^{-1}F_x \quad (34)$$

$$= I - C(zI - A_F)^{-1}F,$$

$$\widehat{V}(z) = G^{-1}(D_x + C_x(zI - A_x)^{-1}B_x) \quad (35)$$

$$= D + C(zI - A_F)^{-1}B_F.$$

Thus, $\widehat{D}(z)$ satisfying (35) can be used in Figure 2. Convenient for using in engineering, we can also design the state equation of $\widehat{D}(z)$.

4.2. *Parameter Matrix $R(z)$ Design.* To accomplish the controller design, the rest of the work is to design the parameter matrix $R(z)$ based on the requirements of the system performance. Suppose that the system error is defined as $e = w - y$ and the requirement of performance is to decrease e . Recall the system structure shown in Figure 2 and notice that the dynamics of the system is subject to the following equation:

$$\widehat{D}(z)y(z) = S(z)h(z) + H(z)\phi(z) \quad (36)$$

in which $S(z) = \widehat{V}(z)R(z)\widehat{D}(z)$, $H(z) = I - \widehat{V}(z)R(z)$, and $\phi(z) = [I \ C(zI - A)^{-1}d(z)]$. Hence, it has become a norm optimization problem to design the parameter matrix $R(z)$ [30]. We can choose a matrix $R(z)$ satisfying that the \mathcal{H}_∞ -norm of the matrix $I - \widehat{V}(z)R(z)$ is minimum. In general, $R(z)$ need meet the conditions of stability and be simple enough to satisfy the practical requirements.

All in all, we can choose $R(z)$ as a constant matrix

$$R = (D_x + C_x(I - A_x)^{-1}B_x)^{-}G \quad (37)$$

with $(\bullet)^{-}$ representing the pseudoinverse. When $D_x + C_x(I - A_x)^{-1}B_x$ is nonsingular, $R = (D_x + C_x(I - A_x)^{-1}B_x)^{-}G$ is equal to $R = (D_x + C_x(I - A_x)^{-1}B_x)^{-1}G$.

5. An Academic Example

In this section, we apply the achieved results to an academic example. Our major purpose is to demonstrate the applicability and effectiveness of the residual generator-based

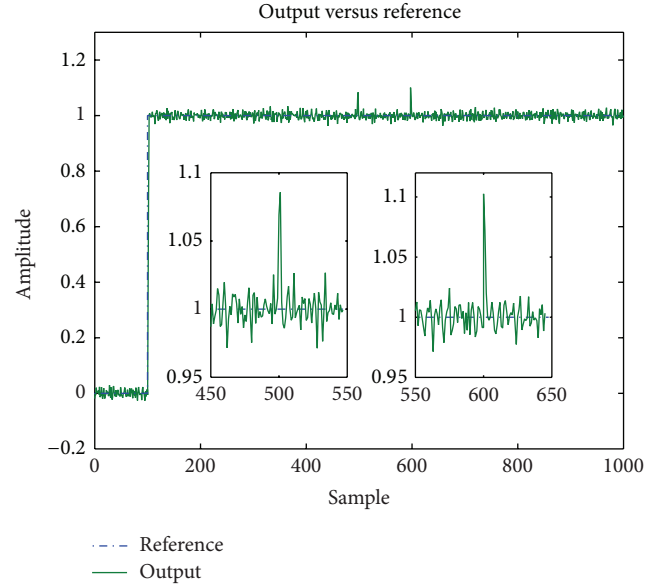


FIGURE 3: The output of system, $s = n = 3$.

controller. We assume the system matrixes in the state space to be as follows:

$$A = \begin{bmatrix} 0 & 0 & -0.006 \\ 1 & 0 & -0.11 \\ 0 & 1 & -0.6 \end{bmatrix}, \quad B = \begin{bmatrix} 1 & 0 \\ 0.18 & 0.33 \\ 0.47 & 0.8 \end{bmatrix}, \quad (38)$$

$$C = [1.6 \ 1.5 \ 0.5], \quad D = \text{zeros}(1, 2),$$

$$d(k) \sim N(0, 0.01^2), \quad n(k) \sim N(0, 0.01^2).$$

$N(\mu, \sigma^2)$ presents normal distribution whose mean is μ and variance is σ^2 . Note that we just use the system model to generate the indispensable inputs and outputs as the available test data, and we do not use the system matrixes A , B , C , and D and the noises to design the controller. The simulation procedure of the data-driven based controller is as follows.

At first, simulate the academic example, and collect 1000 samples of the test data with the reference excitation. Then, identify the parity space using Algorithm 1. Based on the relationship between the parity space and DO, we construct an observer-based residual generator, advanced to design the controller. To demonstrate the application of the controller, we choose the simulation time as $T = 1000$ s and sample time as $T_s = 1$ s. And introduce disturbances $d(k) = 0.1$ and $n(k) = 0.1$, when $t = 500$ s and $t = 600$ s, respectively.

Figure 3 shows the output signal collected from experiment with $s = n$. And, as can be seen from Figure 3, the performance of the controller system is very well, the response speed of unit step is very fast, and disturbances have been suppressed effectively.

More generally, we choose that $s > n$, $s = 5$, for instance, and the output signal is shown in Figure 4. We can learn from Figure 4 that the disturbances have been suppressed effectively; however, when the reference excitation is unit step signal, the overshoot is a bit larger. Thus, we reduce the order

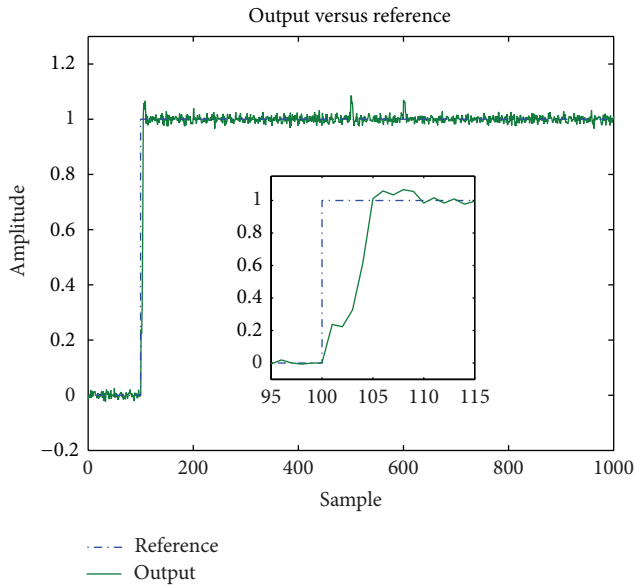


FIGURE 4: The output without order reduced, $s = 5$.

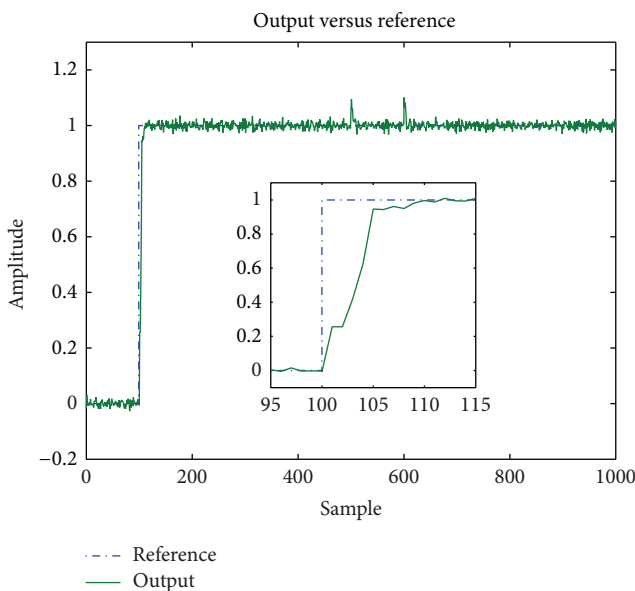


FIGURE 5: The output with order reduced, $s = 5$.

of the residual generator based on Algorithm 2, and then we generate the outputs of the system as Figure 5 shows. It is easy to learn that the overshoot become a smaller one.

6. Conclusion

In this paper, we deal with the controller design for LTI system based on data-driven techniques. The scheme proposed is summarized in the form of several algorithms to be convenient for the readers learning the scheme proposed. The core of this paper is embedding residual generation aiming for FDI in the feedback control loop and structuring the observer-based residual generator based on data-driven approaches

directly identified from available process measurements without generating system model. We constructed the residual generator based on the relationship between DO and the parity vector, obtained directly from process measurements using the advanced SIM. Finally, the applications and effectiveness are demonstrated by applying the scheme and algorithms to an academic example. Besides, our future work is studying a scheme dealing with a real-time system [31, 32].

Conflict of Interests

The authors declare that there is no conflict of interests regarding the publication of this paper.

Acknowledgments

The authors acknowledge the support of China Postdoctoral Science Foundation Grant no. 2012M520738 and Heilongjiang Postdoctoral Fund no. LBH-Z12092.

References

- [1] X. Xie, S. Yin, H. Gao, and O. Kaynak, "Asymptotic stability and stabilisation of uncertain delta operator systems with time-varying delays," *IET Control Theory & Applications*, vol. 7, no. 8, pp. 1071–1078, 2013.
- [2] X. Zhao, L. Zhang, P. Shi, and M. Liu, "Stability and stabilization of switched linear systems with mode-dependent average dwell time," *IEEE Transactions on Automatic Control*, vol. 57, no. 7, pp. 1809–1815, 2012.
- [3] Q. Zhou, S. Peng, X. Shengyuan, and L. Hongyi, "Observer-based adaptive neural network control for nonlinear stochastic systems with time-delay," *IEEE Transactions on Neural Networks and Learning Systems*, vol. 24, pp. 71–80, 2013.
- [4] X. Zhao, L. Zhang, P. Shi, and H. Reza Karimi, "Novel stability criteria for T-S fuzzy systems," *IEEE Transactions on Fuzzy Systems*, vol. 21, no. 6, pp. 1–11, 2013.
- [5] H. Li, J. Yu, C. Hilton, and H. Liu, "Adaptive sliding mode control for nonlinear active suspension vehicle systems using T-S fuzzy Approach," *IEEE Transactions on Industrial Electronics*, vol. 60, pp. 3328–3338, 2013.
- [6] Q. Zhou, P. Shi, J. Lu, and S. Xu, "Adaptive output-feedback fuzzy tracking control for a class of nonlinear systems," *IEEE Transactions on Fuzzy Systems*, vol. 19, no. 5, pp. 972–982, 2011.
- [7] S. Yin, S. Ding, A. Haghani, H. Hao, and P. Zhang, "A comparison study of basic datadriven fault diagnosis and process monitoring methods on the benchmark Tennessee Eastman process," *Journal of Process Control*, vol. 22, pp. 1567–1581, 2012.
- [8] S.-L. Jämsä-Jounela, "Future trends in process automation," *Annual Reviews in Control*, vol. 31, no. 2, pp. 211–220, 2007.
- [9] X. Zhao, P. Shi, and L. Zhang, "Asynchronously switched control of a class of slowly switched linear systems," *Systems & Control Letters*, vol. 61, no. 12, pp. 1151–1156, 2012.
- [10] K. J. Åström, T. Hägglund, and C. C. Hang, "Automatic tuning and adaptation for PID controllers—a survey," *Control Engineering Practice*, vol. 1, no. 4, pp. 699–714, 1993.
- [11] T. Yamamoto, K. Takao, and T. Yamada, "Design of a data-driven PID controller," *IEEE Transactions on Control Systems Technology*, vol. 17, no. 1, pp. 29–39, 2009.
- [12] S. Yin, *Data-Driven Design of Fault Diagnosis Systems*, VDI-Verlag, Düsseldorf, Germany, 2012.

- [13] V. H. Nguyen and J.-C. Golinval, "Fault detection based on Kernel Principal Component Analysis," *Engineering Structures*, vol. 32, no. 11, pp. 3683–3691, 2010.
- [14] G. Lee, C. Han, and E. S. Yoon, "Multiple-fault diagnosis of the Tennessee Eastman process based on system decomposition and dynamic PLS," *Industrial and Engineering Chemistry Research*, vol. 43, no. 25, pp. 8037–8048, 2004.
- [15] R. Muradore and P. Fiorini, "A PLS-based statistical approach for fault detection and isolation of robotic manipulators," *IEEE Transactions on Industrial Electronics*, vol. 59, no. 8, pp. 3167–3175, 2012.
- [16] S. X. Ding, *Mode-Based Fault Diagnosis Techniques*, Springer, Berlin, Germany, 2008.
- [17] S. X. Ding, P. Zhang, A. Naik, E. L. Ding, and B. Huang, "Subspace method aided data-driven design of fault detection and isolation systems," *Journal of Process Control*, vol. 19, no. 9, pp. 1496–1510, 2009.
- [18] A. S. Naik, S. Yin, S. X. Ding, and P. Zhang, "Recursive identification algorithms to design fault detection systems," *Journal of Process Control*, vol. 20, no. 8, pp. 957–965, 2010.
- [19] S. X. Ding, N. Weinhold, P. Zhang, E. L. Ding, T. Jeansch, and M. Schultalbers, "Integration of FDI functional units into embedded tracking control loops and its application to FDI in engine control systems," in *Proceedings of the IEEE International Conference on Control Applications (CCA '05)*, pp. 1299–1304, Toronto, Canada, August 2005.
- [20] N. Weinhold, S. X. Ding, T. Jeansch, and M. Schultalbers, "Embedded model-based fault diagnosis for on-board diagnosis of engine management systems," in *Proceedings of the IEEE Conference on Decision and Control*, pp. 1206–1211, Toronto, Canada, 2005.
- [21] S. X. Ding, G. Yang, P. Zhang et al., "Feedback control structures, embedded residual signals, and feedback control schemes with an integrated residual access," *IEEE Transactions on Control Systems Technology*, vol. 18, no. 2, pp. 352–366, 2010.
- [22] K. Zhou and J. C. Doyle, *Essentials of Robust Control*, Prentice-Hall, Upper Saddle River, NJ, USA, 1998.
- [23] H. Li, X. Jing, and H. R. Karimi, "Output-feedback based H-infinity control for active suspension systems with control delay," *IEEE Transactions on Industrial Electronics*, vol. 61, pp. 436–446, 2014.
- [24] E. Y. Chow and A. S. Willsky, "Analytical redundancy and the design of robust failure detection systems," *IEEE Transactions on Automatic Control*, vol. 29, no. 7, pp. 603–614, 1984.
- [25] P. Zhang and S. X. Ding, "Disturbance decoupling in fault detection of linear periodic systems," *Automatica*, vol. 43, no. 8, pp. 1410–1417, 2007.
- [26] S. Yin, G. Wang, and H. Karimi, "Data-driven design of robust fault detection system for wind turbines," *Mechatronics*, 2013.
- [27] J. Wang and S. J. Qin, "A new subspace identification approach based on principal component analysis," *Journal of Process Control*, vol. 12, no. 8, pp. 841–855, 2002.
- [28] S. X. Ding, S. Yin, and Y. Wang, "Data-driven design of observers and its applications," in *Proceedings of the 18th IFAC World Congress*, Milano, Italy, 2011.
- [29] J. Wang and S. J. Qin, "Closed-loop subspace identification using the parity space," *Automatica*, vol. 42, no. 2, pp. 315–320, 2006.
- [30] S. Yin, H. Luo, and S. Ding, "Real-time implementation of fault-tolerant control systems with performance optimization," *IEEE Transactions on Industrial Electronics*, vol. 64, pp. 2402–2411, 2014.
- [31] S. Yin, S. X. Ding, A. H. A. Sari, and H. Hao, "Data-driven monitoring for stochastic systems and its application on batch process," *International Journal of Systems Science*, vol. 44, no. 7, pp. 1366–1376, 2013.
- [32] S. Yin, X. Yang, and H. R. Karimi, "Data-driven adaptive observer for fault diagnosis," *Mathematical Problems in Engineering*, vol. 2012, Article ID 832836, 21 pages, 2012.

Research Article

Design of a TFT-LCD Based Digital Automobile Instrument

Yunsong Xu,¹ Shen Yin,¹ Jinyong Yu,¹ and Hamid Reza Karimi²

¹ Research Institute of Intelligent Control and Systems, Harbin Institute of Technology, Heilongjiang 150001, China

² Department of Engineering, Faculty of Engineering and Science, The University of Agder, 4898 Grimstad, Norway

Correspondence should be addressed to Shen Yin; shen.yin2011@gmail.com

Received 15 December 2013; Accepted 1 February 2014; Published 5 March 2014

Academic Editor: Xudong Zhao

Copyright © 2014 Yunsong Xu et al. This is an open access article distributed under the Creative Commons Attribution License, which permits unrestricted use, distribution, and reproduction in any medium, provided the original work is properly cited.

The traditional mechanical instrument lacks the ability to satisfy the market with characters of favorable compatibility, easy upgrading, and fashion. Thus the design of a TFT-LCD (thin film transistor-liquid crystal display) based automobile instrument is carried out. With a 7-inch TFT-LCD and the 32-bit microcontroller MB91F599, the instrument could process various information generated by other electronic control units (ECUs) of a vehicle and display valuable driving parameters on the 7-inch TFT-LCD. The function of aided parking is also provided by the instrument. Basic principles to be obeyed in circuits designing under on-board environment are first pointed out. Then the paper analyzes the signals processed in the automobile instrument and gives an introduction to the sampling circuits and interfaces related to these signals. Following this is the functional categorizing of the circuit modules, such as video buffer circuit, CAN bus interface circuit, and TFT-LCD drive circuit. Additionally, the external EEPROM stores information of the vehicle for history data query, and the external FLASH enables the display of high quality figures. On the whole, the accomplished automobile instrument meets the requirements of automobile instrument markets with its characters of low cost, favorable compatibility, friendly interfaces, and easy upgrading.

1. Introduction

As an essential human-machine interface, the automobile instrument provides the drivers with important information of the vehicle. It is supposed to process various information generated by other ECUs and display important driving parameters in time, only in which way can driving safety be secured. However, the traditional mechanical automobile instrument is incompetent to provide all important information of the vehicle. Besides, the traditional instrument meets great challenge with the development of microelectronic technology, advanced materials, and the transformation of drivers' aesthetics [1, 2]. Moreover, the parking of the vehicle is also a problem puzzling many new drivers. Given this, traditional instruments should be upgraded in terms of driving safety, cost, and fashion.

The digital instrument has functions of vehicle information displaying, chord alarming, rear video aided parking, LED indicating, step-motor based pointing, and data storage. The instrument adopts dedicated microcontroller MB91F599, a 7-inch LCD, and two step-motors to substitute

for the traditional instrument. All the information generated by other ECUs can be acquired via not only the sample circuits but also the CAN bus.

The design of the automobile instrument focuses on the following aspects which are also its advantages.

1.1. Friendly Interfaces. The instrument provides interfaces for different types of signals and the CAN bus. All types of signals (such as square wave signal, switching signal, resistance signal, analog voltage signal, etc.) coming from other ECUs can be acquired either from different types of sampling circuits or from the CAN bus. This makes it suitable for both the outdated application where the information from other ECUs can only be acquired via the sampling circuits and the modern application where the information from other ECUs are transmitted via the CAN bus.

1.2. Easy Upgrading and Favorable Compatibility. The CAN bus interface and the 7-inch TFT-LCD make it more convenient to upgrade the instrument without changing

the hardware. If the software needs to be upgraded, we need not bother to take the instrument down and program the MCU. Instead, we can upgrade the instrument via the vehicle's CAN network without taking the instrument down, which makes the upgrading more convenient. Most of the information from other ECUs can be transmitted via the CAN bus; so, we do not have to change the hardware circuits if some of the ECUs' signals are changed in different applications. Besides, since most of the driving parameters are displayed on the TFT-LCD, and the graphical user interface can be designed with great flexibility by programming, only the software needs to be revised to meet different requirements of what kind of driving parameters to display and so forth. These characters, together with the reserved interfaces, enhance the instrument's compatibility in different applications.

1.3. Fault Diagnosing and Information Sharing. It is a trend to incorporate the instrument into the vehicle information system via the CAN bus. The CAN bus interface gives the instrument access to the vehicle CAN network which enables easier fault diagnosing [3, 4] and information sharing. The fault diagnosing could be realized by accomplishing the fault diagnosing protocol above the low-speed CAN bus.

1.4. Low Cost. On the one hand, there are some automobile instruments which adopt 8-bit MCUs or 16-bit MCUs which have limited peripherals, so it is difficult for them to meet some requirements such as rearview video and high real-time data processing performance. And many extra components are needed if the designer wants to accomplish some functions such as video input. On the other hand, there are some advanced automobile instruments which adopt high performance MCUs (such as i.MX 53, MPC5121e, and MPC5123) and run Linux on them. They even use larger TFT-LCDs (such as the 12.3-inch TFT-LCD with a resolution of 1280 × 480 pixels) to display driving parameters. These automobile instruments show higher performances than the instrument in this paper. However, they are more expensive than this automobile. This instrument is able to provide almost all the functions of the advanced automobile instrument with a lower cost.

2. Architecture of the System

The instrument receives signals from other ECUs via the sampling circuits or the CAN bus interface. It can also receive commands from the driver via the button interface. The signals are then processed by the MCU, after which the MCU may send the vehicle information to the LCD or light the LEDs and so forth, according to the results. Therefore, the automobile instrument can be viewed as a carrier of the information flow. And the design of the system can be viewed from two aspects: the hardware system and the information flow based on it.

From the aspect of information flow, the system consists of signal input, signal processing, and signal output, as shown in Figure 1.

From the aspect of hardware system components, the system consists of the MCU MB91F599 and other functional circuits such as sampling circuits and video buffer circuits, as shown in Figure 2.

3. System Hardware Design

3.1. Design Principles. In order to guarantee the performance of the automobile instrument under specific on-board environment and to save the cost of the design, several basic principles must be considered.

3.1.1. Chip Package. SMD components are the first choice due to space limitations of the instrument cluster. And the actual power of these components must be no more than 30% of the rated power.

3.1.2. Overvoltage Protection. Overvoltage protection circuits should be placed at the interfaces of power supply and important signals (such as the CAN bus interface) in case of voltage overshoots.

3.1.3. Generality. Reserved interfaces should be taken into consideration to shorten the development cycle of subsequent similar instruments and optimize the instrument for general use.

3.1.4. Inventories. Reducing the inventories should be kept in mind when selecting electronic components.

3.1.5. Power Consumption. The power consumption of the instrument should be of low level.

3.2. Analysis of Signals Processed on Vehicle. The automobile instrument receives and processes information from other ECUs such as the tachometer, the speedometer, the cooling water temperature gauge, the oil pressure gauge, and the fuel gauge. The signals coming from these ECUs are of different types, according to which different kinds of sampling circuits and interfaces should be designed. Accordingly, a classification of the input signals is first carried out, as shown in Table 1.

3.3. Microcontroller. The microcontroller is essential to the performance of the instrument cluster. Therefore, the microcontroller that suits the system should have rich peripherals to reduce extra components, thus saving the space of the cluster and enhancing the stability of the system. Meanwhile, the operating frequency should be high and the memory size should be large for the demand of speed and accuracy in real-time processing. Besides, various operation modes are needed to lower down the power consumption.

Respecting the above mentioned factors, we finally chose the MB91F599 produced by Fujitsu as the microcontroller. The MB91F599 is particularly well-suited for use in automotive instrument clusters using color displays to generate flexible driver interfaces. It integrates a high performance FR81S CPU core which offers the highest CPU performance level in

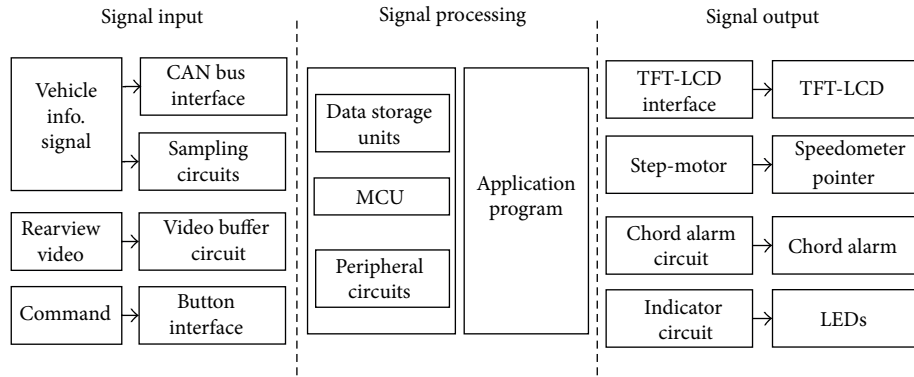


FIGURE 1: Information flow of the system.

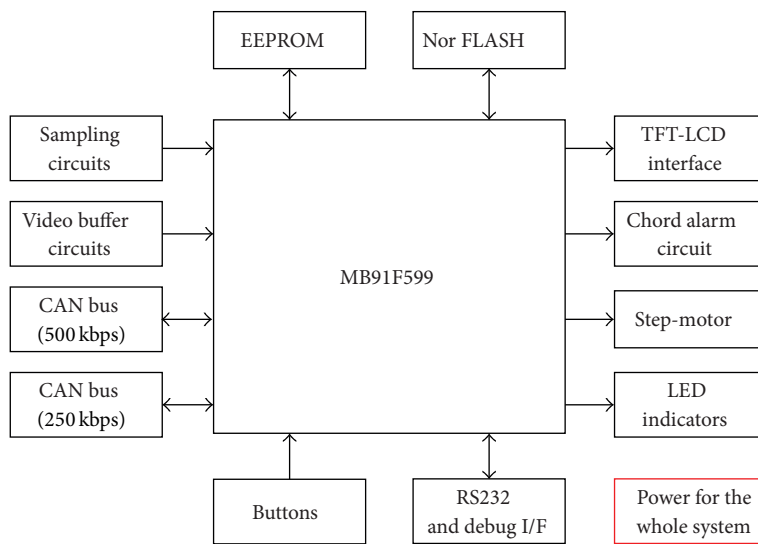


FIGURE 2: Hardware system components.

the industry. Besides, it has a graphics display controller with strong sprite functionality, rendering engine, and external video capture capabilities. These greatly reduce the need for extra components and enhance the stability of the system. The rendering engine can operate in combination with the video capture to enable image manipulation. Overlaid graphics such as needles or parking guidelines can be rendered in conjunction with captured video, which helps to accomplish the aided parking. What is more, multiple built-in regulators and a flexible standby mode enable the MB91F599 to operate with low power consumption.

3.4. Sampling of Square Wave Signal. Square wave signal is the signal that comes from the tachometer. The engine speed, the velocity of the vehicle, and the mileage are proportional to the frequency of the square wave signal. However, the square wave is not “standard” because it is often corrupted by interferences. Besides, the peak voltage of the square wave is +12 V while the I/O voltage of the microcontroller is V_{DD} . The main task for the circuits is to remove the interferences and convert the +12 V voltage to V_{DD} . As shown in Figure 3,

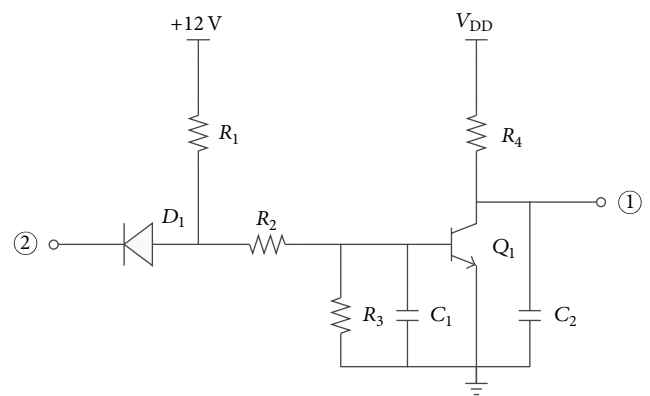


FIGURE 3: Sampling circuit of square wave signal.

the square wave signal is input from node ②; node ① is connected to one pin of the microcontroller.

After the preprocessing of the square wave, the microcontroller detects the positive edge of the “standard” square wave and calculates its frequency. The engine speed, the velocity of

TABLE 1: Classification of input signals.

Signal type	Description of the signal
Square wave signal	Signal coming from the tachometer. It can be of high resistance too.
Switching signal	It acts as a trigger signal to trigger some events such as waking up the MCU.
Resistance signal	Signal of the fuel and air volume.
Analog voltage signal	Signal of battery voltage and air pressure.
Differential signal	Signal on the CAN bus. Information of the tachometer, speedometer, oil pressure, and so forth are all sent to the instrument cluster via CAN bus.

the vehicle, and the mileage can be calculated based on the frequency.

The relationship between the frequency of the square wave and the engine speed can be formulated as:

$$n = \frac{f}{z} \times 60, \quad (1)$$

where n is the engine speed, f is the frequency of the square wave, and z is the number of pulses generated by the tachometer in every circle of the wheel.

The relationship between the frequency of the square wave and the speed of the vehicle can be formulated as:

$$v = \frac{3.6\pi Df}{iN} \times 10^{-2}, \quad (2)$$

where v is the velocity of the vehicle, f is the frequency of the square wave, D is the diameter of the wheel, i is the reduction ratio of the main reducer, and N is the number of pulses generated by the tachometer in every circle of the wheel.

3.5. Sampling of Other Signals. This part includes sampling circuits of switching signal, resistance signal, and analog voltage signal.

The switching signal acts as a trigger signal to trigger some events such as lighting up the backlight and waking up the MCU. It can be categorized into active high and active low according to the ECUs that generate it. Figure 4 offers a complete picture of the sampling circuit of active high signal. The switching signal is input from node ②; node ① is connected to one pin of the microcontroller. Diode D_1 clamps the peak voltage of the switching signal (usually +12 V) to the standard I/O voltage of the microcontroller (V_{DD}) after resistive subdivision. The sampling circuit of active low signal is similar to Figure 4.

The resistance signal is generated by the fuel gauge and the air volume gauge. As shown in Figure 5, the resistance signal R_x is input from node ①; node ② is connected to one pin of the microcontroller. R_1 , R_2 , R_3 , and R_4 have the same value of R and they form a series-parallel network to cut down the power consumption of each resistor to one fourth that of a one-resistor solution.

If the voltage detected at node ② is V , then R_x can be given as:

$$R_x = \frac{R(R_5 + R_6)}{R_6 V_{DD}/V - (R_5 + R_6 + R)}. \quad (3)$$

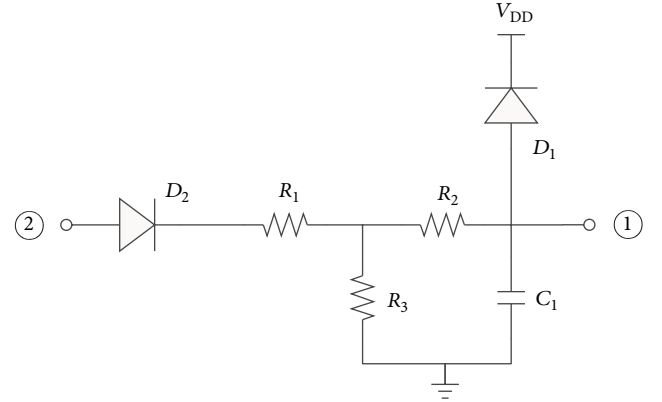


FIGURE 4: Sampling circuit of active high signal.

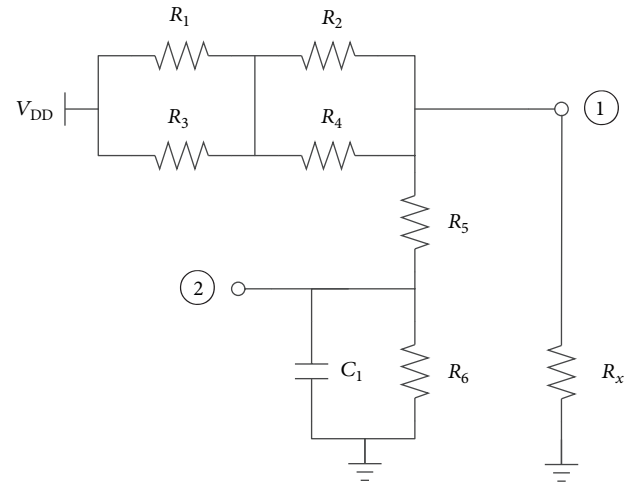


FIGURE 5: Sampling circuit of resistance signal.

The analog voltage signal reflects the battery voltage and the air pressure. The corresponding circuit adopts the resistive subdivision so as to adjust the ratio of the resistors for putting voltage of the signal below the microcontroller's maximum I/O voltage. The value of the resistors should be a little larger to lower down the static power consumption of the resistors. It is unnecessary to go into detail of the circuit.

3.6. Video Buffer Circuit. The rearview video contributes a lot to vehicle backing and parking. The signal coming from the rear camera must be regulated before being processed by

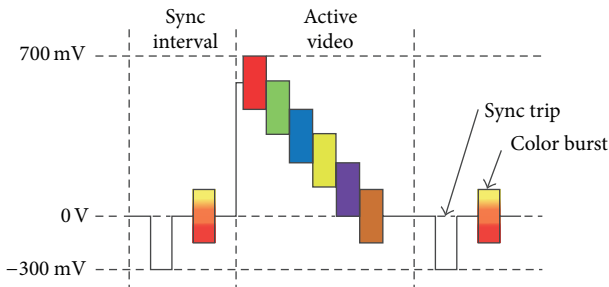


FIGURE 6: RGB with sync in NTSC format.

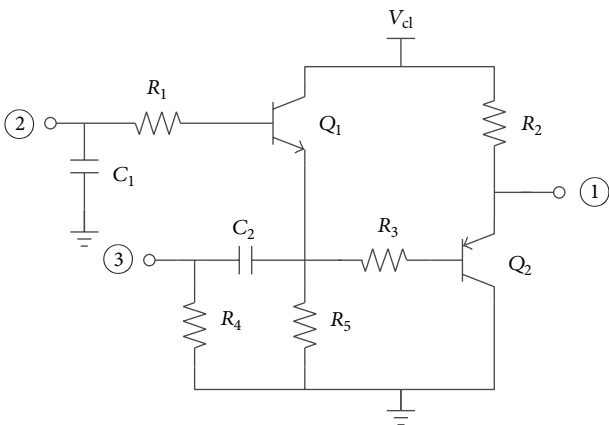


FIGURE 7: Video buffer circuit.

the microcontroller. The rear camera outputs NTSC video. The MB91F599 integrates a video decoder which supports NTSC/PAL video input, which makes the design of the regulatory circuit simple.

Figure 6 shows RGB with sync in NTSC format. The RGB varies in a positive direction from the “black level” (0 V) to 700 mV. Meanwhile, a sync waveform of -300 mV is attached to the video signal. Since the output video signal of the camera is AC-coupled, a clamp circuit is needed to clamp the RGB and sync to a reference voltage and leave the others to vary. If not clamped, the bias voltage will vary with video content and the brightness information will be lost [5].

The video buffer circuit consists of a clamping circuit (R_1 , Q_1 , R_5) and an emitter follower (R_2 , R_3 , Q_2), as shown in Figure 7. Node ① is connected to the NTSC input pin of the microcontroller; node ② is connected to the clamp level output pin of the microcontroller; node ③ is connected to the camera’s signal output. C_2 is the coupling capacitor; R_4 is the matching resistor to realize the 75Ω back termination.

Here, the sync signal is not present, so the clamp level is controlled by the clamp level output pin of the microcontroller, which is called “keyed clamp” [5]. The graphics display controller of the microcontroller let the clamp level output occur in coincidence with the sync pulse; that is, the clamp level output occurs during the sync tip in Figure 6, thus we get the “sync tip clamp” [5].

3.7. Data Storage Units. An EEPROM chip and two non-FLASH chips are used for data storage. The EEPROM is used to store the mileage data permanently. The I²C serial EEPROM 24LC04B is chosen to accomplish this function. It has a memory capacity of 4 K which is enough for the mileage data storage. Besides, the extended temperature range under which it can work reliably meets the demands of on-board environment.

Since the FLASH size of the microcontroller is only 1 MB which is limited for the storage of pictures displayed on the LCD, external FLASH is needed to store different kinds of meaningful pictures such as the background of the dial. Two S29GL256N chips with a memory capacity of 256 Mb are chosen for picture data storage for their high performance and low power consumption. The application circuits of the chips are provided in their datasheets, so it is unnecessary to go into the details of them here.

3.8. CAN Bus Interface. Controller Area Network (CAN) is widely deployed in automobile, industry, and aerospace domains. As a major trend of the technological development of in the automation industry, CAN is now reputed as a local area network in automation [6]. Its low cost and ability to integrate with most microcontroller silicon families have made it a standard for automobile applications [7–9].

The ECUs of engine control, full active suspension control [10, 11], airbag control, traction control, and so forth are nodes of the controller area network and can be controlled via CAN bus in time. Thus a networked control system (NCS) is formed via CAN bus and some results in [12–15] may be useful in the controller design of the communication system. The communication system can be categorized by the requirements of real-time response of each node. The nodes requiring good performance in real-time response and reliability should be designed into high-speed communication network, while others should be designed into low-speed communication network [16].

Full active suspension control, airbag control, traction control, and so forth are incorporated into high-speed communication system since their requirements of real-time response and reliability are critical. Because of less critical requirements, on-board fault diagnosing [17, 18], doors control, windows control, and so forth are incorporated into low-speed communication system. The transmitting rate of the high-speed CAN bus is 500 kbps while that of the low-speed one is 250 kbps. The two kinds of communication systems are connected via a gateway which enables real-time sharing of data. And the data transmitting of the high-speed CAN bus has a higher priority over the low speed CAN bus when a collision occurs.

For this design, only the CAN transceiver and its auxiliary circuit are needed since the MB91F599 is integrated with two CAN controllers, which are connected to the high-speed and low-speed CAN bus, respectively. TJA1040 is chosen as the CAN transceiver for its low consumption in standby mode. Besides, it can also be woken up via CAN bus, which is required by some automobile instruments. Detailed circuit is provided in the datasheet of TJA1040, so the repetitious

details need not be given here. Note that for high-speed CAN, both ends of the pair of signal wires must be terminated. ISO 11898 requires a cable with a nominal impedance of $120\ \Omega$ [19]; therefore, $120\ \Omega$ resistors are needed for termination. Here, only the devices on the ends of the cable need $120\ \Omega$ termination resistors.

3.9. TFT-LCD Interface. The 7-inch TFT-LCD has a resolution of 800×480 pixels and supports the 24-bit for three RGB colors. The interface of the 60-pin TFT-LCD can be categorized into data interface, control interface, bias voltage interface, and gamma correction interface.

The data interface supports the parallel data transmitting of 18-bit (6 bits per channel) for three RGB colors. Thus, a range of 2^{18} colors can be generated. The control interface consists of a “horizontal synchronization” which indicates the start of every scan line, a “vertical synchronization” which indicates the start of a new field, and a “pixel clock.” This part is controlled by the graphics display controller which is integrated in the MB91F599. We just need to connect the pins of the LCD to those of the microcontroller correspondingly.

Bias voltages are used to drive the liquid crystal molecules in an alternating form. The compact LCD bias IC TPS65150 provides all bias voltages required by the 7-inch TFT-LCD. The detailed circuit is also provided in the datasheet of TPS65150.

The greatest effect of gamma on the representations of colors is a change in overall brightness. Almost every LCD monitor has an intensity to voltage response curve which is not a linear function. So if the LCD receives a message that a certain pixel should have certain intensity, it will actually display a pixel which has intensity not equal to the certain one. Then the brightness of the picture will be affected. Therefore, gamma correction is needed. Several approaches to gamma correction are discussed in [20–22]. For this specific 7-inch LCD, only the producer knows the relationship between the voltage sent to the LCD and the intensity it produces. The signal can be corrected according to the datasheet of the LCD before it gets to the monitor. According to the datasheet, ten gamma correction voltages are needed. These voltages can be got from a resistive subdivision circuit.

3.10. Power for the Whole System. The vehicle electric power system is mainly composed of a generator and a battery [23]. The power voltage of a car is +12 V while that of a bus is +24 V. The power supply of the automobile instrument alternates between the generator and the battery. The generator powers the automobile instrument and charges the battery when working. Note that the battery does not power the instrument when the generator is on. If the generator is not working, the instrument is powered by the battery. Figure 9 shows how the power supply alternates. Node ① is connected to the battery; node ② is connected to the generator; node ③ is connected to other circuits. When the generator is on, Q_1 and Q_2 are turned off, which prevents node ③ from getting power from the battery. Then node ③ gets power from the generator via other routes (not shown in the figure). When the generator is off, Q_1 and Q_2 are turned on, so node ③ gets power from the battery.

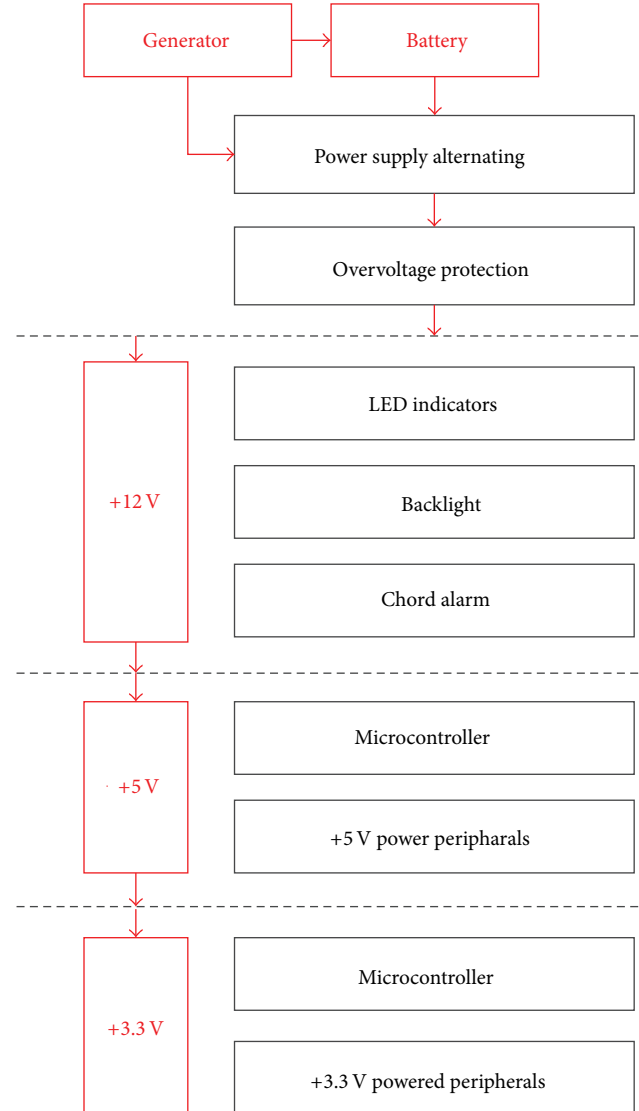


FIGURE 8: Block diagram of the power supply.

For this instrument, the LED indicators, the backlight, and the chord alarm need to be supplied with a voltage of +12 V; the CAN transceiver, the EEPROM, and the buttons need to be supplied with a voltage of +5 V; the video buffer circuit, the external FLASH, and the data interface of the LCD need to be supplied with a voltage of +3.3 V. Besides, the microcontroller needs to be supplied with voltages of +5 V and +3.3 V simultaneously. Figure 8 offers a detailed block diagram of the power supply for the automobile instrument.

4. Software of the System

The main task for the program is to calculate the driving parameters of the vehicle and display them on the TFT-LCD. The calculation is triggered by the input signals via the sampling circuits or the CAN bus. The main program flow chart of the system is shown in Figure 10.

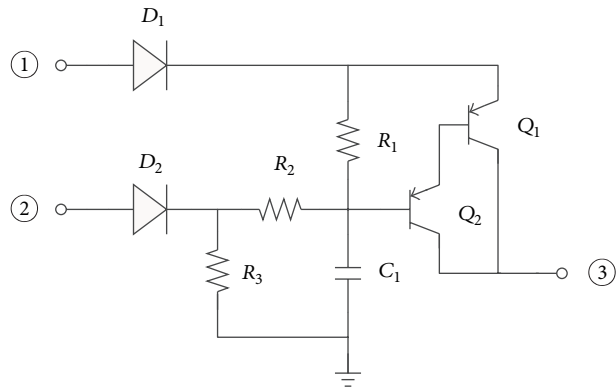


FIGURE 9: Circuit for power supply alternating.

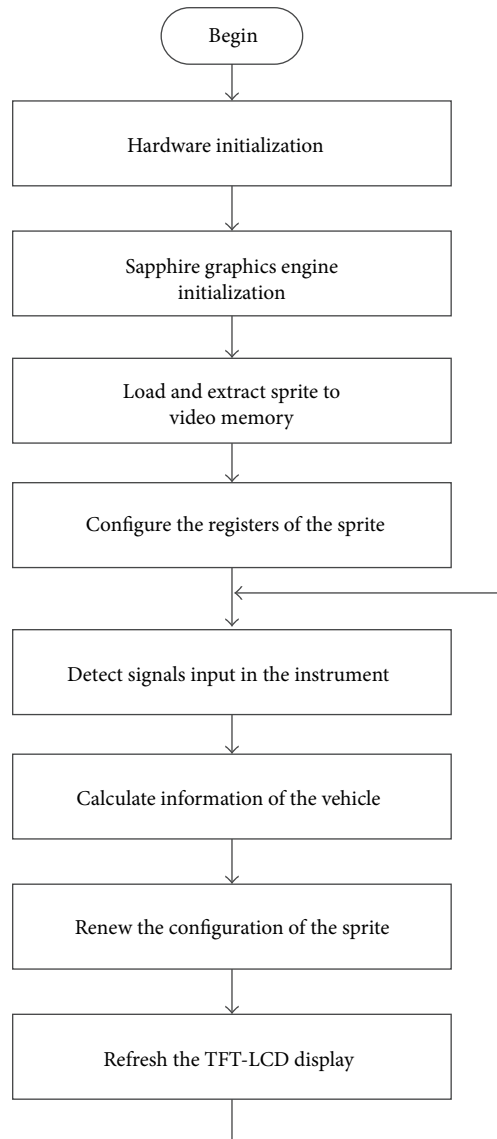


FIGURE 10: Main program flow chart.

5. Conclusion

The design scheme of a TFT-LCD based automobile instrument is carried out from aspects of both the hardware and the main program flow chart. The MB91F599 simplifies the peripheral circuits with its rich on-chip resources and shows high performance in real-time data processing. The automobile instrument is capable of displaying the velocity of the vehicle, the engine speed, the cooling water temperature, the oil pressure, the fuel volume, the air pressure, and other information on the TFT-LCD, which contributes a lot to driving safety and satisfies drivers' aesthetics. Besides, the rearview video makes the parking and backing easier and safer for the driver. Moreover, the CAN bus interface and TFT-LCD make it easier for the upgrading of the instrument without changing the hardware, thus saving the cost.

Conflict of Interests

The authors declare that there is no conflict of interests regarding the publication of this paper.

Acknowledgments

The authors acknowledge the support of China Postdoctoral Science Foundation Grants no. 2012M520738 and no. 2012M520739, Heilongjiang Postdoctoral Fund no. LBH-Z12092, and the support of the Polish-Norwegian Research Programme in the frame of Project Contract no. Pol-Nor/200957/47/2013.

References

- [1] A. Carlosena, C. Macua, and M. Zivanovic, "Instrument for the measurement of the instantaneous frequency," *IEEE Transactions on Instrumentation and Measurement*, vol. 49, no. 4, pp. 783–789, 2000.
- [2] P. Knoll and B. Kosmowski, "Liquid crystal display unit for reconfigurable instrument for automotive applications," *Opto-Electronics Review*, vol. 10, no. 1, pp. 75–78, 2002.
- [3] S. Yin, S. X. Ding, A. Haghani, H. Hao, and P. Zhang, "A comparison study of basic data-driven fault diagnosis and process monitoring methods on the benchmark tennessee eastman process," *Journal of Process Control*, vol. 22, no. 9, pp. 1567–11581, 2012.
- [4] S. Yin, X. Yang, and H. R. Karimi, "Data-driven adaptive observer for fault diagnosis," *Mathematical Problems in Engineering*, vol. 2012, Article ID 832836, 21 pages, 2012.
- [5] B. Stutz, "Get a grip on clamps, bias, and AC-coupled video signals," *Electronic Design*, vol. 52, no. 2, p. 55, 2004.
- [6] T. Gong and H. Yan, "Research on two-speed CAN BUS technique in automobile manufacturing system," *Applied Mechanics and Materials*, vol. 214, pp. 591–595, 2012.
- [7] R. Obermaisser, "Reuse of CAN-based legacy applications in time-triggered architectures," *IEEE Transactions on Industrial Informatics*, vol. 2, no. 4, pp. 255–268, 2006.
- [8] D. Kum, G.-M. Park, S. Lee, and W. Jung, "AUTOSAR migration from existing automotive software," in *Proceedings of the International Conference on Control, Automation and Systems (ICCAS '08)*, pp. 558–562, Seoul, Republic of Korea, 2008.
- [9] R. Obermaisser, "End-to-end delays of event-triggered overlay networks in a time-triggered architecture," in *Proceedings of the 5th IEEE International Conference on Industrial Informatics*, vol. 1, pp. 541–546, Vienna, Austria, 2007.
- [10] H. Li, J. Yu, C. Hilton, and H. Liu, "Adaptive sliding-mode control for nonlinear active suspension vehicle systems using T-S fuzzy approach," *IEEE Transactions on Industrial Electronics*, vol. 60, no. 8, pp. 3328–3338, 2013.
- [11] H. Li, X. Jing, and H. Karimi, "Output-feedback-based control for vehicle suspension systems with control delay," *IEEE Transactions on Industrial Electronics*, vol. 61, no. 1, pp. 436–446, 2014.
- [12] Q. Zhou, P. Shi, J. Lu, and S. Xu, "Adaptive output-feedback fuzzy tracking control for a class of nonlinear systems," *IEEE Transactions on Fuzzy Systems*, vol. 19, no. 5, pp. 972–982, 2011.
- [13] Q. Zhou, P. Shi, S. Xu, and H. Li, "Observer-based adaptive neural network control for nonlinear stochastic systems with time delay," *IEEE Transactions on Neural Networks and Learning Systems*, vol. 24, no. 1, pp. 71–80, 2013.
- [14] X. Xie, S. Yin, H. Gao, and O. Kaynak, "Asymptotic stability and stabilisation of uncertain delta operator systems with time-varying delays," *IET Control Theory & Applications*, vol. 7, no. 8, pp. 1071–1078, 2013.
- [15] S. Yin, S. X. Ding, A. H. A. Sari, and H. Hao, "Data-driven monitoring for stochastic systems and its application on batch process," *International Journal of Systems Science*, vol. 44, no. 7, pp. 1366–1376, 2013.
- [16] Q. Ye, "Research and application of CAN and LIN bus in automobile network system," in *Proceedings of the 3rd International Conference on Advanced Computer Theory and Engineering (ICACTE '10)*, vol. 6, pp. 150–154, Chengdu, China, 2010.
- [17] S. Yin, H. Luo, and S. Ding, "Real-time implementation of fault-tolerant control systems with performance optimization," *IEEE Transactions on Industrial Electronics*, vol. 61, no. 5, pp. 2402–2411, 2014.
- [18] S. Yin, G. Wang, and H. R. Karimi, "Data-driven design of robust fault detection system for wind turbines," *Mechatronics*, 2013.
- [19] International Standards Organization, *11898: Road Vehicle Interchange of Digital Information/Controller Area Network (CAN) for High-Speed Communication*, International Standards Organization, Geneva, Switzerland, 1993.
- [20] M. Brownlow, G. Cairns, C. Dachs, Y. Kubota, H. Washio, and H. Yamashita, "A 6-bit multi-resolution digital to analogue converter for low temperature poly-silicon digital drivers," in *Flat Panel Display Technology and Display Metrology II*, vol. 4295 of *Proceedings of SPIE*, pp. 85–94, San Jose, Calif, USA, 2001.
- [21] G. Cairns, C. Dachs, M. Brownlow, Y. Kubota, H. Washio, and M. Hijikigawa, "9.2: multi-format digital display with content driven display format," *SID Symposium Digest of Technical Papers*, vol. 32, no. 1, pp. 102–105, 2001.
- [22] H. G. Walton, M. Brownlow, J. Lock, M. Rahal, and P. Zebedee, "LCD gamma correction by non-linear digital-to-analogue converter," in *Poly-Silicon Thin Film Transistor Technology and Applications in Displays and Other Novel Technology Areas*, vol. 5004 of *Proceedings of SPIE*, pp. 170–178, Santa Clara, Calif, USA, 2003.
- [23] W. Lee, D. Choi, and M. Sunwoo, "Modelling and simulation of vehicle electric power system," *Journal of Power Sources*, vol. 109, no. 1, pp. 58–66, 2002.

Research Article

Distributed Multitarget Probabilistic Coverage Control Algorithm for Wireless Sensor Networks

Ying Tian,¹ Yang Ou,² Hamid Reza Karimi,³ Yan Tao Liu,¹ and Jian Qun Han¹

¹ College of Engineering, Bohai University, Jinzhou 121000, China

² College of Navigation, Dalian Maritime University, Dalian 116026, China

³ Department of Engineering, Faculty of Engineering and Science, University of Agder, 4898 Grimstad, Norway

Correspondence should be addressed to Ying Tian; tianyingjzh@163.com

Received 23 December 2013; Accepted 13 January 2014; Published 4 March 2014

Academic Editor: Xudong Zhao

Copyright © 2014 Ying Tian et al. This is an open access article distributed under the Creative Commons Attribution License, which permits unrestricted use, distribution, and reproduction in any medium, provided the original work is properly cited.

This paper is concerned with the problem of multitarget coverage based on probabilistic detection model. Coverage configuration is an effective method to alleviate the energy-limitation problem of sensors. Firstly, considering the attenuation of node's sensing ability, the target probabilistic coverage problem is defined and formalized, which is based on Neyman-Pearson probabilistic detection model. Secondly, in order to turn off redundant sensors, a simplified judging rule is derived, which makes the probabilistic coverage judgment execute on each node locally. Thirdly, a distributed node schedule scheme is proposed for implementing the distributed algorithm. Simulation results show that this algorithm is robust to the change of network size, and when compared with the physical coverage algorithm, it can effectively minimize the number of active sensors, which guarantees all the targets γ -covered.

1. Introduction

Wireless sensor networks (WSNs) have attracted a great deal of attention. They are widely used in the fields of military affairs, intelligent family, environment surveillance and commercial management, and so on [1, 2]. However, many applications put on them lots of constraints that make issues in WSNs particularly challenging [3, 4]. Among them, the power constraint of sensor devices imposes many fundamental design limitations in WSNs. According to this problem, coverage control is one of the most effective ways on energy saving for energy-constrained WSNs [5–7], which can make the fewest sensors cover the sensing area or targets in the network.

Recently, many literatures focus on the coverage problems in WSNs. They are generally classified into three types [8]: the first one is the area coverage, where the objective is to cover an area [9–14]; the second one, which our paper also focuses on, is the target coverage, where the objective is to cover a set of targets [15–18]; the last is coverage problems that have the objective to determine the maximal

support/breach path that traverses a sensor field [19]. In the first type, literatures [9–14] introduce different eligibility rules for the WSN based on the problem requirements, such as energy efficiency, area monitoring, and network connectivity. The network activity is organized in rounds, with sensors in the active set performing the area coverage, while all other sensors are in the sleep mode. Different techniques have been proposed to select which sensors will be active in the next round. According to the second type, literatures [15–18] present and develop the target problem. In literature [15], disjoint sensor sets are modeled as disjoint set covers, such that every cover completely monitors all the target points. The disjoint set cover problem [15] is reduced to a maximum flow problem, which is modeled as mixed integer programming. The problem is further extended in literature [16], where sensors are not restricted to participation in only disjoint sets; that is, a sensor can be active in more than one set. Furthermore, literature [17] develops the target coverage problem in [16]. In order to reduce both energy consumption and interference at the MAC layer, the sensing range of the active sensors in [17] can be reduced, while the coverage

requirements are maintained. Literature [18] formalizes the k - (connected) coverage set (k -CCS/ k -CS) problems, develops a linear programming algorithm, and designs two nonglobal solutions for them. In the last type, a different coverage formulation is given in [19]. A path has the worst (best) coverage, if it has the property that, for any point on the path, the distance to the closest sensor is maximized (minimized). Among these papers mentioned above, the sensing range is a critical parameter, which determines the sensing ability of the sensor. In fact, with the increasing of sensing distance between the sensor and the target, the sensing ability of a sensor decays dramatically. We called this kind of sensing model probabilistic detection model. Literatures [13, 14] discuss the area coverage problem based on probabilistic detection model, but the objective of them focuses on area coverage problem. Most of literatures, such as [9–11, 15, 16, 18, 19], make the sensing range fixed. In these papers, a simplified circular sensing model is supposed which follows the yes/no binary detection model, called physical detection model. Obviously, the physical detection model does not obey the signal attenuation characteristic. The adjusted sensing range is adopted by literatures [12, 17], but the sensing ability is still fixed after the sensing range is adjusted.

In this paper we address the multitarget coverage problem based on probabilistic detection model; our contributions are as follows: based on Neyman-Pearson probabilistic detection model, (1) the multitarget probabilistic coverage problem is defined and formalized, (2) the simplified probabilistic coverage judging rule is derived for the distributed coverage control of the network, and (3) using the simplified judging rule, a distributed node schedule scheme is proposed, which not only minimizes the number of active sensors, but also guarantees all the targets monitored at the requirement of coverage probability.

The rest of this paper is organized into the following sections. In Section 2, the problem formulation and preliminaries are given. Section 3 presents the probabilistic coverage judging rule and the distributed coverage control algorithm. Section 4 simulates our algorithm and analyzes the simulation results. In Section 5, conclusions and further research directions are given.

2. Problem Formulation and Preliminaries

In this paper, we deal with the multitarget coverage problem based on Neyman-Pearson probabilistic detection model. The goal is to minimize the number of active sensors while guaranteeing that each target can be covered with the required coverage probability.

We consider a WSN consisting of large number of sensors and a set of targets deployed in the WSN region randomly. To reduce the energy consumption of network, we want to find the minimum number of active sensors with the property that each target is monitored by sensors around it with the required network coverage probability.

2.1. Probabilistic Detection Model. We assume that N sensors, s_1, s_2, \dots, s_N , and M targets, t_1, t_2, \dots, t_M , are distributed

randomly in the monitoring region, with location of the sensor, s_i , $i = 1, 2, \dots, N$ (x_{s_i}, y_{s_i}), and location of the target t_j , $j = 1, 2, \dots, M$, (x_{t_j}, y_{t_j}). Then s_i can make a measurement from the target t_j by the following equation:

$$a_{ij} = \frac{\theta}{d_{ij}^\alpha} + n_i \quad i = 1, 2, \dots, N, \quad j = 1, 2, \dots, M, \quad (1)$$

where θ is the signal strength emitted by the target t_j ; α is the signal decay exponent, $\alpha > 0$; d_{ij} is the distance from the target t_j to the sensor s_i ; that is, $d_{ij} = \sqrt{(x_{s_i} - x_{t_j})^2 + (y_{s_i} - y_{t_j})^2}$. Assuming n_i is the noise at sensor, s_i , and follows a Gaussian distribution with zero mean, that is, $n_i \sim (0, \sigma)$.

For sensor s_i , the binary hypothesis testing problem is presented as follows:

$$H_1: p(z_{ij} | H_1) = \left(\frac{1}{\sqrt{2\pi}\sigma} \right) \exp\left(-\frac{(z_{ij} - a_{ij})^2}{2\sigma^2} \right) \quad (2)$$

$$H_0: p(z_{ij} | H_0) = \left(\frac{1}{\sqrt{2\pi}\sigma} \right) \exp\left(-\frac{z_{ij}^2}{2\sigma^2} \right).$$

Assume that all the sensors use the same detection threshold τ to make a decision; based on Neyman-Pearson detection rule, the relationship between threshold τ and the false alarm rate $P_{f_{ij}}$ is given as follows:

$$P_{f_{ij}} = \int_{\tau}^{\infty} p(z_{ij} | H_0) dz_{ij} = Q\left(\frac{\tau}{\sigma}\right) \quad (3)$$

$$\tau = \sigma \times Q^{-1}(P_{f_{ij}}),$$

where $Q(x)$ is the complementary distribution function of the standard Gaussian; that is

$$Q(x) = \int_x^{\infty} \frac{1}{\sqrt{2\pi}} \exp\left(-\frac{t^2}{2}\right) dt. \quad (4)$$

The detection probability to t_j by s_i is

$$P_{D_{ij}} = \int_{\tau}^{\infty} p(z_{ij} | H_1) dz_{ij} = Q\left(\frac{\tau - a_{ij}}{\sigma}\right) \quad (5)$$

$$= 1 - \Phi\left(\frac{\tau - a_{ij}}{\sigma}\right),$$

where $\Phi(x)$ is the normal distribution function of the standard Gaussian; that is,

$$\Phi(x) = \int_{-\infty}^x \frac{1}{\sqrt{2\pi}} \exp\left(-\frac{t^2}{2}\right) dt. \quad (6)$$

In WSN, many sensors are deployed in the monitoring region to detect the targets. Usually, a target in the monitoring region can be sensed by more than one sensor. The detection probability of t_j by sensors, s_i , $i = 1, 2, \dots, k$, motivated by [20] is

$$P_{D_j} = 1 - \prod_{i=1}^k (1 - P_{D_{ij}}) = 1 - \prod_{i=1}^k \Phi\left(\frac{\tau - (\theta/d_{ij}^\alpha)}{\sigma}\right). \quad (7)$$

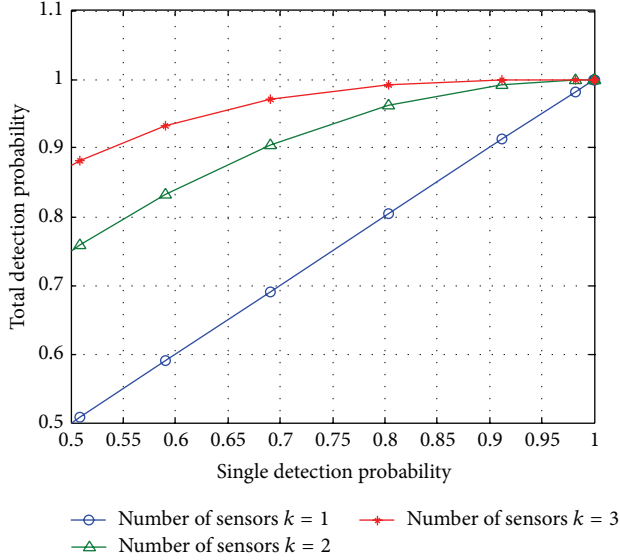


FIGURE 1: Relationship of single detection probabilities and total detection probability with different number of sensing nodes.

The relationship of total detection probability P_{D_j} and single detection probability $P_{D_{ij}}$ with different number of active sensors k is given in Figure 1.

From Figure 1, a target can be detected by three sensors in the same distance with the detection probability of 90% while it can be detected by two sensors with the probability of 84%. At the same condition, the target can be detected by single sensor at the probability of 60%.

2.2. Problem Definitions

Definition 1. γ -Probabilistic Covered. Given M targets and N sensors randomly deployed in the target's vicinity, if one target t_j is detected by k sensors together and the total detection probability is more than γ , that is, $P_{D_j} \geq \gamma$, then the target is γ -probabilistic covered or (γ, k) -probabilistic covered in more detail. For simplicity, we use the notations as γ -covered or (γ, k) -covered.

Definition 2. k -Probabilistic Cover Radius. Assuming the required total detection probability is γ , there are k sensors around one target, the distances between each sensor and the target are the same, denoted as r_k . When these sensors working together, the target can be (γ, k) -covered. Then, the distance r_k is the k -Probabilistic Cover Radius.

Remark 3. From Definition 2, when $d_{1j} = d_{2j} = \dots = r_k$ and (7) is $P_{D_j} = 1 - \Phi^k(\tau - (\theta/r_k^\alpha)/\sigma) = \gamma$, then we can get

$$r_k = \left[\frac{\theta}{\tau - \sigma \Phi^{-1}(\sqrt[k]{1-\gamma})} \right]^{1/\alpha}. \quad (8)$$

Definition 4. Probabilistic Cover Set. If a target t_j can be γ -covered by working together with a set of sensors, denoted by \mathbf{S} , we can say \mathbf{S} is a probabilistic cover set of the target t_j .

Definition 5. Basic Cover Set. If \mathbf{S} is a probabilistic cover set of the target, t_j , and \mathbf{S} will not become the probabilistic cover set when any sensor in \mathbf{S} is not in active, then \mathbf{S} is the basic cover set of target t_j .

3. Multitarget Probabilistic Coverage Control Algorithm

In this section, we first propose a simplified judging rule which can make the sensor judge whether the target can be γ -covered easily; then we present a distributed node schedule scheme which can make the sensor decide whether it needs to be active locally or not, in order to minimize the number of active sensors, while guaranteeing that all the targets can be γ -covered.

3.1. Probabilistic Coverage Judging Rule (PCJ-Rule). The PCJ-Rule is proposed based on Neyman-Pearson probabilistic detection model. In this paper, we assume that each sensor can obtain the distances between itself and the targets in its sensing range.

Theorem 6. Suppose a target t_j is around k active sensors, s_i , $i = 1, 2, \dots, k$, and the distance between t_j and s_i is d_{ij} . If $\sum_{i=1}^k d_{ij} \leq k \cdot r_k$, then target t_j must be (γ, k) -covered.

Proof. Given the requested total detection probability is γ , then from Definition 2, we can obtain

$$\gamma = 1 - \Phi^k \left(\frac{\tau - (\theta/r_k^\alpha)}{\sigma} \right). \quad (9)$$

Let

$$F(d_{ij}) = \Phi \left(\frac{\tau - (\theta/d_{ij}^\alpha)}{\sigma} \right); \quad (10)$$

then $F(d_{ij})$ is a monotonic increasing function about d_{ij} . From (7), (9), and (10), we get

$$\gamma = 1 - F^k(r_k) \quad (11)$$

$$P_{D_j} = 1 - \prod_{i=1}^k F(d_{ij}). \quad (12)$$

Due to the mean value theorem, then

$$\prod_{i=1}^k F(d_{ij}) \leq \left(\frac{\sum_{i=1}^k F(d_{ij})}{k} \right)^k; \quad (13)$$

when $F(d_{1j}) = F(d_{2j}) = \dots = F(d_{kj})$, (13) is found. \square

Considering the fact that $F(d_{ij})$ is a monotonic increasing function about d_{ij} , when $F(d_{1j}) = F(d_{2j}) = \dots = F(d_{kj})$, there must be $d_{1j} = d_{2j} = \dots = d_{kj}$; therefore, we can obtain

$$\prod_{i=1}^k F(d_{ij}) \leq F^k(r), \quad (14)$$

where r is the average value of d_{ij} .

It is assumed in Theorem 6 that $\sum_{i=1}^k d_{ij} \leq k \cdot r_k$; there must be $r \leq r_k$, and we obtain that

$$\prod_{i=1}^k F(d_{ij}) \leq F^k(r) \leq F^k(r_k). \quad (15)$$

From (12), (14), and (15), we have

$$P_{D_j} = 1 - \prod_{i=1}^k F(d_{ij}) \geq 1 - F^k(r_k) = \gamma, \quad (16)$$

where $P_{D_j} = \gamma$ when $d_{ij} = r_k, i = 1, 2, \dots, k$.

Form Theorem 6, a target can be judged whether it satisfied γ -covered or not. However, in order to reduce the amount of data transmission in the network and simplified calculation executed on each sensor, we proposed the PCJ-Rule which simplifies Theorem 6 further and makes the coverage judgment easily. The sensing distance d_{ij} between the sensor s_i and the target t_j can be quantified.

The method of quantification is presented as follows.

Assuming that N sensors s_1, s_2, \dots, s_N and M targets t_1, t_2, \dots, t_M are distributed randomly in the monitoring region, the distance between the sensor s_i and the target t_j is d_{ij} . We set the maximum number of nodes sensing together is k_{\max} ; then from Definition 2 and (8), we can calculate the values of $r_1, r_2, \dots, r_{k_{\max}}$. Because of the constraint of the actual sensing abilities of sensors, we can quantify the d_{ij} is smaller than $r_{k_{\max}}$; that is, $d_{ij} \in [0, r_{k_{\max}}]$, as the quantification distance, notated as d'_{ij} . In this paper, we consider the maximum sensing range as $r_{k_{\max}}$. Then we divided the range of d_{ij} , that is, $[0, r_{k_{\max}}]$, into k_{\max} quantification ranges as $[0, r_1], (r_1, r_2], \dots$, and $(r_{k_{\max}-1}, r_{k_{\max}}]$, and the corresponding quantification values are $r_1, r_2, \dots, r_{k_{\max}}$; then we have $d'_{ij} = r_k$, where $k = 1, 2, \dots, k_{\max}$.

Definition 7. Quantification Coefficient. If a sensing distance d_{ij} can be quantified as d'_{ij} , where $d'_{ij} = r_k$, the quantification coefficient corresponding to d_{ij} is denoted by c_{ij} as follows:

$$c_{ij} = \begin{cases} \frac{1}{k} & \text{if } 0 \leq d_{ij} \leq r_{k_{\max}} \\ 0 & \text{otherwise.} \end{cases} \quad (17)$$

Figure 2 shows an example with one target and four sensors with $k_{\max} = 3$. The distances between t_1 and $S = \{s_1, s_2, s_3, s_4\}$ are $d_{i1} = \{d_{11}, d_{21}, d_{31}, d_{41}\}$; after the

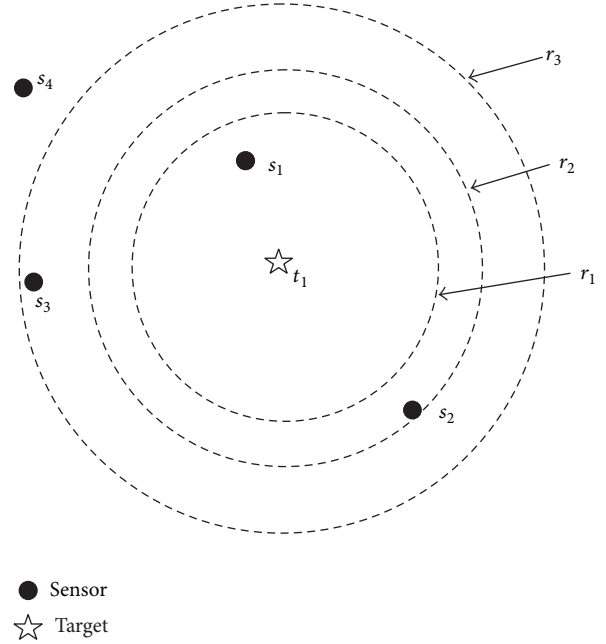


FIGURE 2: Example of quantification with a target t_1 and four sensors; $S = \{s_1, s_2, s_3, s_4\}$, when $k_{\max} = 3$.

quantification, we can get the quantification coefficients as follows:

$$c_{i1} = \{c_{11}, c_{21}, c_{31}, c_{41}\} = \left\{1, \frac{1}{2}, \frac{1}{3}, 0\right\}. \quad (18)$$

Definition 8. Quantification Cover Set. If a sensor set S is a cover set of target t_j , the distances d_{ij} between S and t_j can be quantified as d'_{ij} . If the distances between S' and t_j are d'_{ij} , we can say that the sensor set S' is the quantification cover set of S .

Remark 9. From Definition 8, there must be $d'_{ij} \geq d_{ij}$, where $d'_{ij} \in \{r_1, r_2, \dots, r_{k_{\max}}\}$.

Theorem 10. Suppose S' is the quantification cover set of sensor set S ; if a target t_j can be (γ, k) -covered by S' , the target t_j must be (γ, k) -covered by S .

Proof. Given S' is the quantification cover set of S , where $S = \{s_1, s_2, \dots, s_k\}$, the distances between S and the target t_j are d_{ij} , where $d_{ij} = \{d_{1j}, d_{2j}, \dots, d_{kj}\}$, and the distances between S' and the target t_j are d'_{ij} . From the quantification method, the quantified distance d'_{ij} can be obtained, where $d_{ij} \leq d'_{ij}$ and $d'_{ij} \in \{r_1, r_2, \dots, r_k\}$. \square

As the assumption in Theorem 10 that a target t_j can be (γ, k) -covered by S' , there must be $\sum_{j=1}^k d'_{ij} \leq k \times r_k$; then $\sum_{j=1}^k d_{ij} \leq \sum_{j=1}^k d'_{ij} \leq k \times r_k$. Therefore, the target t_j must be (γ, k) -covered by S .

Corollary 11 (Corollary (PCJ-Rule)). *Suppose there is a target t_j detected by k active sensors \mathbf{S} together, and k_{\max} is the maximum allowable number of sensing nodes working on t_j ; that is, $k \leq k_{\max}$; the corresponding quantification coefficients are c_{ij} , where $c_{ij} \geq 1/k_{\max}$, and the number of nonzero c_{ij} is N_c . If $N_c \geq k_{\max}$, then $\sum_{i=1}^{k_{\max}} c_{ij} \geq 1$, and the target t_j must be (γ, k_{\max}) -covered.*

Proof. Given the distance between sensor, s_i , where $s_i \in \mathbf{S}$ and target, t_j , is d_{ij} , where $i = 1, 2, \dots, k_{\max}$, d'_{ij} is the quantified value of d_{ij} , then $d_{ij} \leq d'_{ij}$, $d'_{ij} \in \{r_1, r_2, \dots, r_{k_{\max}}\}$. Form the Corollary 11, when $N_c \geq k_{\max}$, there must be more than k_{\max} quantification coefficients with $c_{ij} > 0$, so we have the minimum $\sum_{i=1}^{k_{\max}} c_{ij}$ with $(\sum_{j=1}^{k_{\max}} c_{ij})_{\min} = k_{\max} \times (1/k_{\max}) = 1$; therefore, $\sum_{i=1}^{k_{\max}} c_{ij} \geq 1$. \square

When $\sum_{i=1}^{k_{\max}} c_{ij} = 1$, the corresponding quantified distance of the c_{ij} has $d'_{ij} = r_{k_{\max}}$, where $i = 1, 2, \dots, k_{\max}$. And when $\sum_{j=1}^{k_{\max}} c_{ij} > 1$, the corresponding quantified distance of the c_{ij} has $d'_{ij} \leq r_{k_{\max}}$, $i = 1, 2, \dots, k_{\max}$. Because of $d_{ij} \leq d'_{ij}$, we have $d_{ij} \leq d'_{ij} \leq r_{k_{\max}}$; then $\sum_{i=1}^{k_{\max}} d_{ij} \leq \sum_{i=1}^{k_{\max}} d'_{ij} \leq k_{\max} r_{k_{\max}}$. From Theorem 6, when $\sum_{i=1}^{k_{\max}} d_{ij} \leq k_{\max} r_{k_{\max}}$, the target t_j must be (γ, k_{\max}) -covered by \mathbf{S} .

Remark 12. From the proof of Corollary 11, the condition $\sum_{j=1}^{k_{\max}} c_{ij} \geq 1$ is the sufficient condition for judging the target t_j whether it satisfied (γ, k_{\max}) -covered or not.

In our paper, through the information interaction between nodes, a sensor can receive quantification coefficients of the targets in its sensing range. Using Corollary 11, named PCJ-Rule, the sensor will calculate whether the target has been covered by other active sensors and then decide the state of itself in active or others.

3.2. Distributed Node Schedule Scheme. In this section, we design a distributed node schedule scheme, which make the sensor decide the self-working state by local judgment.

The flow chart of the node schedule scheme executed by a sensor locally is shown in Figure 3. When the sensor runs the schedule scheme, there are three working states switched dynamically on each sensor, as shown in Figure 4. They are IDLE state, ACTIVE state, and SLEEP state.

From Figure 3, firstly, a sensor s_i initializes the local information, including the number of targets M in its sensing range and the distances d_{ij} between the node and the targets, where $j = 1, 2, \dots, M$. And then, the node quantifies the sensing distances and calculates the quantification coefficients c_{ij} , where $j = 1, 2, \dots, M$. Finally, the sensor sets the backoff time T_{backoff} based on c_{ij} :

$$T_{\text{backoff}} = \frac{1}{w_1 N_{c_{ij}=1/k} + (1/2) w_2 N_{c_{ij}=1/2} + \dots + (1/k) w_k N_{c_{ij}=1/k}}, \quad (19)$$

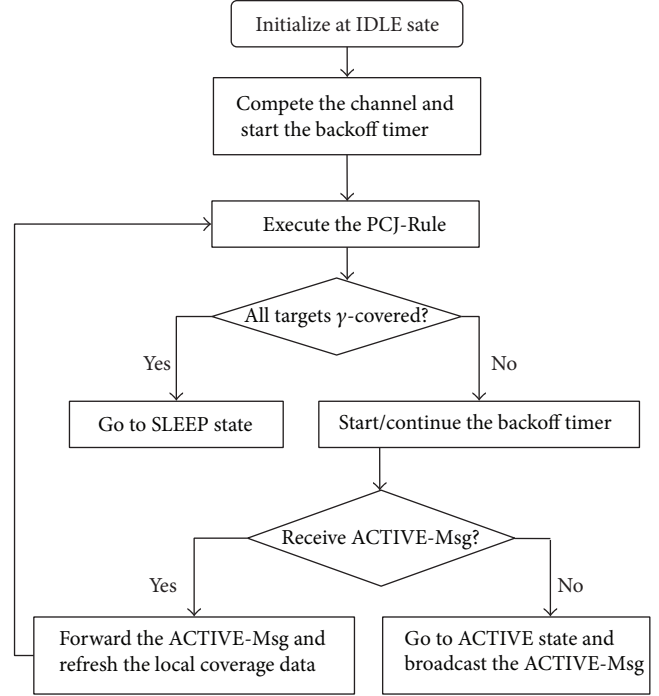


FIGURE 3: Flow chart of the node schedule scheme executed by sensor locally.

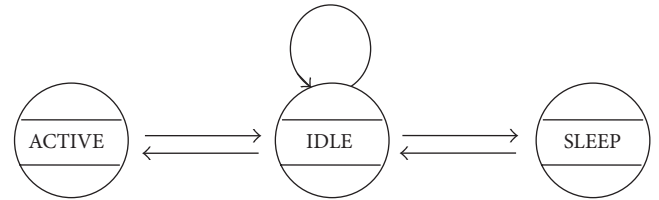


FIGURE 4: Working state transfer diagram on each sensor.

where $N_{c_{ij}=1/k}$ is the number of $c_{ij} = 1/k$ about the sensor s_i ; w_k , called backoff weighted coefficient, is weight of $N_{c_{ij}}$ when $c_{ij} = 1/k$, where $w_1 + w_2 + \dots + w_k = 1$. Therefore, the backoff time of s_i is mainly decided by the quantification coefficients c_{ij} . For example, when $w_1 = 1$, it means that the more a sensor s_i can $(\gamma, 1)$ -cover the targets, the shorter the backoff time of s_i .

After the initialization, if the sensor does not receive any message from the others during the backoff time, it will switch to the ACTIVE state and broadcast the ACTIVE-Msg messages to its neighbor sensors.

The data format of ACTIVE-Msg contains three fields: the local ID, targets' ID in the sensing range of the sensor, and the coverage coefficients c_{ij} about the sensor and targets in its sensing range.

Before the step of "execute the PCJ-Rule" in Figure 3, the sensor should collect the ACTIVE-Msg messages from other active sensors to refresh the local coverage data. Then, based on the PCJ-Rule, the sensor will calculate the value of $\sum_{j=1}^M c_{ij}$ for each target t_j to judge whether the target has been covered

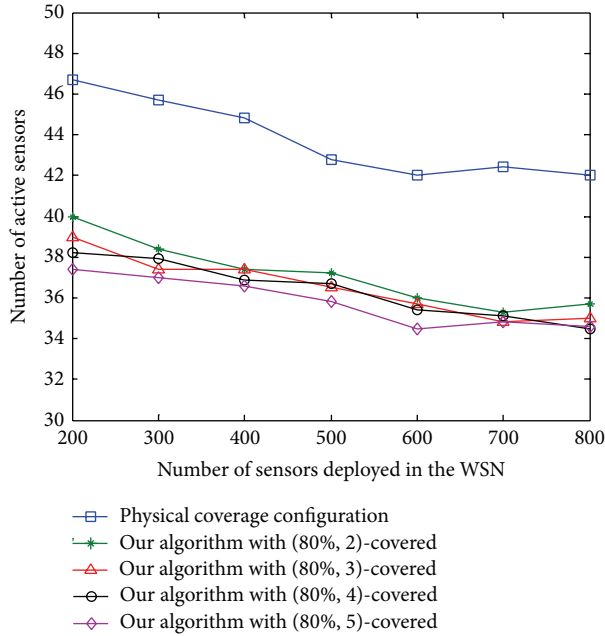


FIGURE 5: Comparison between the physical coverage configuration and the probabilistic coverage configuration with different k .

by other active sensors, where M is the number of targets in the sensing range of s_i . There are three cases of the judgment results described as follows.

Case 1. None of the targets can be γ -covered, and then the sensor will continue the backoff timer; the sensor is still in IDLE state.

Case 2. Some but not all of the targets can be γ -covered; then the sensor will set the $c_{ij} = 0$, where i is the local ID of sensor and j is the ID of target which is γ -covered. The backoff time T_{backoff} will be reset and restarted; the sensor is still in IDLE state.

Case 3. All of the targets are γ -covered; the sensor will be required to switch in SLEEP state, and then the sensor works with low energy consumption, which is still listening to the network for the reconfiguration.

At last of the node schedule scheme, the sensor will work in ACTIVE state or SLEEP state. However, the node schedule scheme can be executed when the topology of network changes. The sensor will return to the IDLE state when the network coverage needs to be reconfigured.

4. Simulation Results and Analysis

In this section, we evaluate the performance of our distributed node schedule scheme. We simulate a stationary network with sensors and targets randomly deployed in a $100 \text{ m} \times 100 \text{ m}$ area. Confidently, all results in this section are from average of 20 runs. In the simulation, some parameters are listed as follows:

- (i) signal strength from the target $\theta = 30$,
- (ii) standard deviation of noise in the channel $\sigma = 1$,
- (iii) signal decay exponent $\alpha = 1.2$,
- (iv) false alarm rate of Neyman-Pearson detection rule $P_{f_i} = 5\%$,
- (v) number of sensors N varied between 200 and 800,
- (vi) number of targets M varied between 100 and 400,
- (vii) maximum node number of sensing together k which varies between 1 and 5,
- (viii) requirement probabilistic coverage probability γ which varies between 70% and 90%,
- (ix) backoff weighted coefficient $w_1 = 1$.

In Figure 5, the numbers of active nodes based on physical detection model and ours based on probabilistic model are compared. The same physical detection model is adopted by literatures [15, 16]; therefore, we call methods in [15, 16] as the physical coverage configuration. In physical detection model, when the target is in the sensing range, it will consider the target is 100% covered, the same as [15, 16]. While, in our simulation, the sensing range of physical coverage is set as the 1-probabilistic cover radius, which means that we consider the physical coverage configuration as the special one of our probability coverage configuration which satisfies (90%, 1)-covered. It is obvious that we relax the requirement of the physical coverage configuration. We set $M = 100$ and $\gamma = 80\%$. Figure 5 shows the following. (1) Our algorithm saves about 12% active nodes comparing with the physical coverage configuration. (2) The number of active sensors that make the network satisfy the coverage requirement becomes smaller with the increasing k , where k is from 2 to 5. However, the number of active sensors decreases slowly when k varies from 2 to 5. Meanwhile, if the bigger k is chosen, there will be a need for more data transfer in network [3, 8]. Therefore, the suitable value of k can make our algorithm the most efficient. Therefore, we choose $k = 3$ in the next simulations. (3) When the maximum number of sensors detects that one target together, that is, the parameter k , is kept, the number of active sensors decreases slightly when the number of sensors deployed increases from 200 to 400, and then the number becomes stable in spite of the increasing of deployed number of sensors. It is because of the fact that when the density of sensors increases, the probability of the sensor deployed on the suitable location increases, where the sensor can make more contribution on sensing multitargets. Figure 5 shows that, in our algorithm, there are less than 40 active nodes required for monitoring all the targets in the WSN under our simulation environment, which is an effective method to save sensors' energy and prolong the network lifetime.

In Figure 6, we compare the number of active sensors which make the network satisfy the (80%, 3)-covered, when the number of targets M is 200, 300, and 400. Obviously, the number of active sensors is stable when the target number is unchanged. In our simulation, there are about 38, 48, 52, and 55 active sensors needed when we deployed 100, 200, 300, and 400 targets in the network. When the number of targets

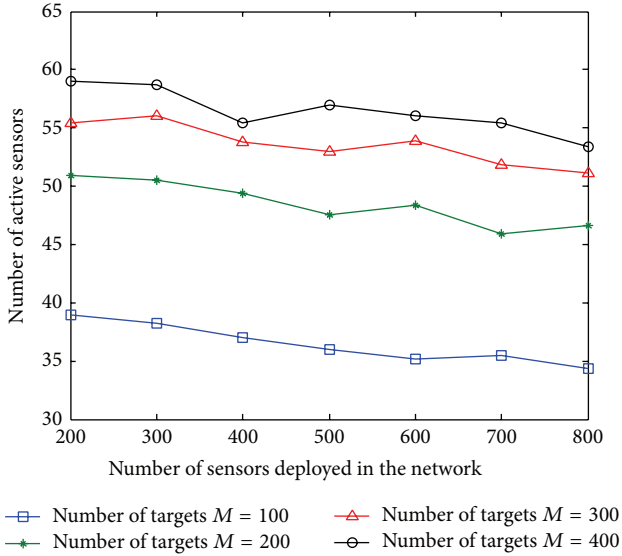


FIGURE 6: Number of active sensors required with different number of targets, which make the network satisfy the (80%, 3) covered.

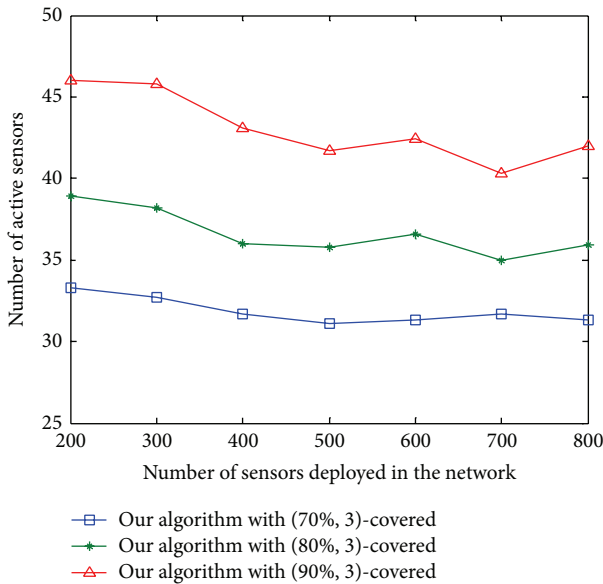


FIGURE 7: Number of active sensors needed which make the network satisfy different requirement detection probabilities.

increased from 100 to 200, there are about 10 active sensors added. And when the number becomes from 200 to 300, only 5 new active sensors increased. It means that the more targets in the network, the more efficiency of our algorithm. In fact, when the number of active sensors increases to the degree that any point in the network can be probabilistic covered, there will no longer need any new active sensor even though the number of targets is increasing in the network.

In Figure 7, our algorithms executed with the requirement detection probability γ as 70%, 80%, and 90% are compared. We set the number of targets $M = 100$ and $k = 3$. It is shown that more sensors are in active state when

the requirement detection probability increases from 70% to 90%. From Figure 7, the number of active sensors is steady at 33 and 38 when the network is (70%, 3)-covered and (80%, 3)-covered; while $\gamma = 90%$, with the increasing of the deployed nodes' number from 200 to 400, the number of active nodes decreases slightly and becomes stable at 42 active nodes at last. It is because of the fact that when $\gamma = 90%$, the network with less than 400 nodes cannot make all the targets γ -covered. At the same time, our algorithm turns off many sensors, which have no contribution to the uncovered targets even though they are in active state. This simulation also indicates that our algorithm can switch a large number of redundant sensors in SLEEP state on the premise of keeping the network coverage degree even though the coverage-hole exists in the network.

The simulation result can be summarized as follows. (1) Our algorithm is robust with the increasing of network size; it needs only a few number of active sensors to guarantee all the targets monitored at the requirement coverage probability. (2) Considering the amount of data transmission in the network, the efficiency of our algorithm can be improved by choosing the proper value of k , where we set $k = 3$. (3) Our algorithm will no longer need the new active sensors with the number of targets increasing, when the density of active sensors increases to the degree that any points in the network can be probabilistic covered. (4) Our algorithm can turn off the redundant sensors on the premise of keeping the network coverage degree, even though the coverage-hole exists in the monitor region.

5. Conclusion

In this paper, based on probabilistic detection model, we propose a distributed probabilistic coverage algorithm for the WSN with multiple static targets. The goal of our work is to find a simplified judging method, which can turn off the redundant sensors and guarantee all the targets covered by active sensors. In this paper, we define and formalize the target probabilistic coverage problems based on Neyman-Pearson probabilistic detection model and propose a distributed node schedule scheme using the simplified judging rule. Simulation results show that our algorithm is robust to the change of network size. When compared with the physical coverage algorithm, the number of active sensors based on probabilistic detection model is smaller than that based on a physical one; at the same time, all the targets can be monitored at the requirement of network coverage probability.

In our future work, we will try to design a distributed and localized protocol that organizes the sensor nodes in disjoint set covers. By this way, the disjoint covers will work in turns, which can avoid sensors judging the local state frequently. Furthermore, we will integrate the sensor network connectivity requirement. The network connectivity is another important requirement of the network quantity of service (Qos), which makes the exchange of information between sensors easy.

Conflict of Interests

The authors declare that there is no conflict of interests regarding the publication of this paper.

References

- [1] I. F. Akyildiz, W. Su, Y. Sankarasubramaniam, and E. Cayirci, "Wireless sensor networks: a survey," *Computer Networks*, vol. 38, no. 4, pp. 393–422, 2002.
- [2] M. Cardei and J. Wu, "Coverage problems in wireless ad hoc sensor networks," in *Handbook of Sensor Networks*, M. Ilyas and I. Mahgoub, Eds., CRC Press, Boca Raton, Fla, USA, 2004.
- [3] S. Yin, S. Ding, A. Haghani, and H. Hao, "Data-driven monitoring for stochastic systems and its application on batch process," *International Journal of Systems Science*, vol. 44, no. 7, pp. 1366–1376, 2013.
- [4] S. Yin, S. Ding, A. Haghani, H. Hao, and P. Zhang, "A comparison study of basic data-driven fault diagnosis and process monitoring methods on the benchmark Tennessee Eastman process," *Journal of Process Control*, vol. 22, no. 9, pp. 1567–1581, 2012.
- [5] S. Yin, H. Luo, and S. Ding, "Real-time implementation of fault-tolerant control systems with performance optimization," *IEEE Transactions on Industrial Electronics*, vol. 64, no. 5, pp. 2402–2411, 2014.
- [6] C.-F. Huang and Y.-C. Tseng, "A survey of solutions to the coverage problems in wireless sensor networks," *Journal of Internet Technology*, vol. 6, no. 1, pp. 1–8, 2005.
- [7] M. Cardei and J. Wu, "Energy-efficient coverage problems in wireless ad-hoc sensor networks," *Computer Communications*, vol. 29, no. 4, pp. 413–420, 2006.
- [8] S. Yin, G. Wang, and H. Karimi, "Data-driven design of robust fault detection system for wind turbines," *Mechatronics*, 2013.
- [9] J. Carle and D. Simplot, "Energy-efficient area monitoring for sensor networks," *IEEE Computer*, vol. 37, no. 2, pp. 40–46, 2004.
- [10] D. Tian and N. D. Georganas, "A coverage-preserving node scheduling scheme for large wireless sensor networks," in *Proceedings of the 1st ACM International Workshop on Wireless Sensor Networks and Applications (WSNA '02)*, pp. 32–41, Atlanta, Ga, USA, September 2002.
- [11] X. Wang, G. Xing, Y. Zhang, C. Lu, R. Pless, and C. D. Gill, "Integrated coverage and connectivity configuration in wireless sensor networks," in *Proceedings of the 1st International Conference on Embedded Networked Sensor Systems (SenSys '03)*, pp. 28–39, Los Angeles, Calif, USA, November 2003.
- [12] J. Wu and S. Yang, "Coverage and connectivity in sensor networks with adjustable ranges," in *Proceedings of the IEEE International Workshop on Mobile and Wireless Networking (MWN '04)*, Montreal, Canada, August 2004.
- [13] J.-P. Sheu and H.-F. Lin, "Probabilistic coverage preserving protocol with energy efficiency in wireless sensor networks," in *Proceedings of the IEEE Wireless Communications and Networking Conference (WCNC '07)*, pp. 2633–2638, Kowloon, China, March 2007.
- [14] Y. Tian, S.-F. Zhang, and Y. Wang, "Distributed probabilistic coverage-preserving configuration protocol for wireless sensor network," *Journal on Communications*, vol. 30, no. 1, pp. 70–75, 2009.
- [15] M. Cardei and D.-Z. Du, "Improving wireless sensor network lifetime through power aware organization," *Wireless Networks*, vol. 11, no. 3, pp. 333–340, 2005.
- [16] M. Cardei, M. T. Thai, Y. Li, and W. Wu, "Energy-efficient target coverage in wireless sensor networks," in *Proceedings of the 24th Annual Joint Conference of the IEEE Computer and Communications Societies (IEEE INFOCOM '05)*, vol. 3, pp. 1976–1984, Miami, Fla, USA, March 2005.
- [17] M. Cardei, J. Wu, M. Lu, and M. O. Pervaiz, "Maximum network lifetime in wireless sensor networks with adjustable sensing ranges," in *Proceedings of the IEEE International Conference on Wireless and Mobile Computing, Networking and Communications (WiMob '05)*, vol. 3, pp. 438–445, Montreal, Canada, August 2005.
- [18] S. H. Yang, F. Dai, M. Cardei, J. Wu, and F. Patterson, "On connected multiple point coverage in wireless sensor networks," *International Journal of Wireless Information Networks*, vol. 13, no. 4, pp. 289–301, 2006.
- [19] S. Meguerdichian, F. Koushanfar, M. Potkonjak, and M. B. Srivastava, "Coverage problems in wireless ad-hoc sensor networks," in *Proceedings of the 20th Annual Joint Conference of the IEEE Computer and Communications Societies (IEEE INFORM '01)*, pp. 1380–1387, Anchorage, Alaska, USA, April 2001.
- [20] N. Ahmed, S. S. Kanhere, and S. Jha, "Probabilistic coverage in wireless sensor networks," in *Proceedings of the 30th Anniversary of the IEEE Conference on Local Computer Networks (LCN '05)*, pp. 672–681, Sydney, Australia, November 2005.

Research Article

The Finding and Dynamic Detection of Opinion Leaders in Social Network

Baocheng Huang,¹ Guang Yu,¹ and Hamid Reza Karimi²

¹ School of Management, Harbin Institute of Technology, Harbin 150001, China

² Department of Engineering, Faculty of Engineering and Science, The University of Agder, 4898 Grimstad, Norway

Correspondence should be addressed to Baocheng Huang; huanghjlhrbin@gmail.com

Received 23 December 2013; Accepted 19 January 2014; Published 4 March 2014

Academic Editor: Xudong Zhao

Copyright © 2014 Baocheng Huang et al. This is an open access article distributed under the Creative Commons Attribution License, which permits unrestricted use, distribution, and reproduction in any medium, provided the original work is properly cited.

It is valuable for the real world to find the opinion leaders. Because different data sources usually have different characteristics, there does not exist a standard algorithm to find and detect the opinion leaders in different data sources. Every data source has its own structural characteristics, and also has its own detection algorithm to find the opinion leaders. Experimental results show the opinion leaders and their characteristics can be found among the comments from the Weibo social network of China, which is like Facebook or Twitter in USA.

1. Introduction

With further study, the definition of opinion leader expands. It involves not only the most influential person but also the most influential commentary. The finding and detection of opinion leader in social network have great commercial and political values. By identifying the most influential person, companies or governments can use this feature for selling or guiding public opinion, respectively. Additionally, detecting the most influential comments is also able to understand the source of public opinion formation process. By building multiple topic networks, this essay can detect opinion leaders with the algorithm of POLD (Positive Opinion Leader Detection). Some researchers had found that some ideas in control field such as data driven [1–6] and robust control [7–13] could be into the study of find and dynamic detection of opinion leaders in social network. However, this idea only stays on the think level. Therefore, this work will propose a Dynamic Opinion Rank algorithm to find the opinion leaders in the comments of Chinese news. By using the methodology, it can find the most influential comments from all the network comments and the most influential users form the entire user network.

2. Problem Formulation

A single theme network based Weibo news consists of three levels. Those levels are themes, comments, and users. There exist some relationship mappings between those different levels. For example, the mapping between themes and comments is 1 divided by n , while the mapping between comments and users is m divided by n . This study will analyze a single topic, build a single view based network and the mathematical model of users, and then find out the most influential comments and users. The structure of those three levels is shown in Figure 1.

As shown in Figure 1, there are three levels. “Layer 1” stands for all the themes of news, “Layer 2” denotes the single-topic network $G_{CN}(V, E)$, which is composed of comments, while “Layer 3” is the single-topic user network $G_{UN}(V, E)$. Based on $G_{CN}(V, E)$, it is possible to find the most influential comments cmt_3 . Then, by using the mapping between comments and users, it can find out U_3 from $G_{UN}(V, E)$.

Definition 1 (the most influential comments). For the comment sets $C = \{C_1, C_2, \dots, C_n\}$, $G_{CN}(V, E)$ is a single point of network theme. After sorting by using some algorithms, there

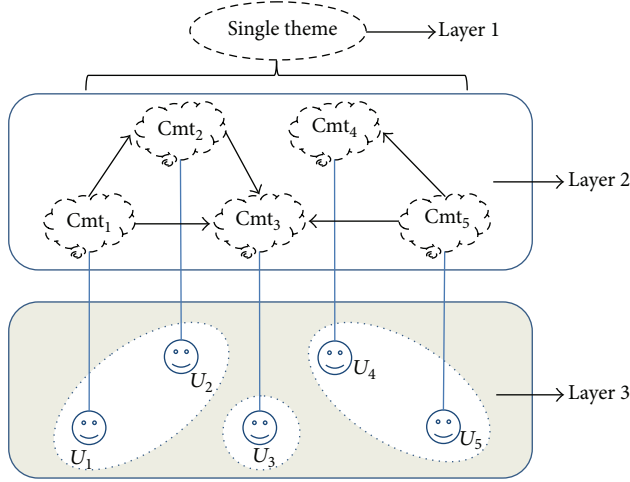


FIGURE 1: The model of single theme network model.

TABLE 1: Sentiment analysis of forum comments.

The contents of the comments	Emotional tendencies
Comment Number 1	Positive
Comment Number 2	Negative
Comment Number 3	Neutral

is sore $C_{i, \text{score}}$ for any comment $C_i \in C$. Based on the sort according to their scores, it can be assumed that $C_{1, \text{score}} > C_{2, \text{score}} > \dots > C_{m, \text{score}}$. Then, the comments with the highest score are defined as the most influential comments; these are also the opinion leaders of comments [14].

Definition 2 (the most influential user). As in Definition 1, for the user set $U = \{u_1, u_2, \dots, u_m\}$, each user $u_i \in U$ has its own score $u_{i, \text{score}}$. Sorting those scores, it follows that $u_{1, \text{score}} > u_{2, \text{score}} > \dots > u_{m, \text{score}}$. Then, the user with the highest score is the most influential one; it is defined as the opinion leader of users [15].

3. Attitude Stabilization Controller Design

3.1. Analysis of Emotions. The work of finding the positive and negative emotion links requires determining the propensity of emotions. Based on the HowNet dictionary, this work will firstly determine the emotional feelings of tendentious comments [16]. Comments are usually classified according to emotional bias: positive (1), negative (-1), and neutral (0); this is shown in Table 1.

According to the preceding definitions, any comments $C_i \in C$ ($1 \leq i \leq n$) can be divided into m statements, such as $\langle S_1, S_2, S_3, \dots, S_m \rangle$. Then, it applies ICTCLAS to split each statement S_j ($1 \leq j \leq m$) into one word, such as $\langle w_1, w_2, w_3, \dots, w_l \rangle$ [17], and it extracts emotion words from emotion dictionary and obtains the number of statistical statements S_j containing negative words, such as "No." Usually, emotional value of words is set as 1, -1, and

0. Finally, accumulating all the emotional words in S_j , it can obtain the emotional value of the statement. Using the parity negative word sentence to correct the statement of emotional tendencies, it yields a final statement $\{-1, 1, 0\}$, while the cumulative review of all statements yields final emotional tendencies $\{1, -1, 0\}$.

3.2. Modeling of Single-Topic Network. By using the explicit and implicit link algorithm, all of the link relationship of the set C is found. Based on the sentiment analysis methods, the algorithm proposed by this work to establish a single theme network is described as in Algorithm 1.

In Algorithm 1, the 1st to 7th line is to traverse the set C and to find out all of the link. The 8th is going to give a certain weight wt_{ij} to the positive and negative links; this weight wt_{ij} is given by

$$wt_{i,j} = \text{tag} \times \text{similarity}(C_i, C_j) \quad (-1 \leq wt_{i,j} \leq 1). \quad (1)$$

In this equation, the function $\text{similarity}(C_i, C_j)$ represents the contents of comments similarity between C_i and C_j and "tag" denotes the emotional consistency between comments. For any reply relationship $C_i \rightarrow C_j$, if the comment is consistent tendency, then this comment is viewed as a positive link; that is, $\text{tag} = 1$. Otherwise, the comment is a negative link and $\text{tag} = -1$. The weight is thus assigned according to the following equation:

$$wt_{i,j} = \begin{cases} 1 & c_j \text{ explicitly links to } c_i \text{ and tag} = 1 \\ -1 & c_j \text{ explicitly links to } c_i \text{ and tag} = -1 \\ \text{Sim}(c_i, c_j) & c_j \text{ implicitly links to } c_i \text{ and tag} = 1 \\ -\text{Sim}(c_i, c_j) & c_j \text{ implicitly links to } c_i \text{ and tag} = -1. \end{cases} \quad (2)$$

In (2), if the connection relationship between C_i and C_j is explicit, then the similarity is equal to 1. If it is an implicit link relationship, the similarity is between the texts. If the emotional tendency between C_i and C_j is consistent, then the weight $wt_{i,j}$ will not be changed, otherwise, its value will become opposite. The above construction procedure can be illustrated as in Figure 2.

In Figure 2(b), the structure of the set $C = \{C_1, C_2, C_3, C_4, C_5\}$ is explicitly evaluated. According to the chronological order release $C_1 < C_2 < C_3 < C_4 < C_5$, and the sequence corresponding to the floors floor₁, floor₂, floor₃, floor₄, and floor₅, the corresponding single topic views networks as shown in Figure 2(a). The serial number of the edge is ranked in ascending order. That represents the link discovery order.

4. Dynamic Detection of Opinion Leaders

Opinion leaders are the most influential comments or persons. This paper will present an approach to find out the most influential comments among a single point of network $G_{CN}(V, E)$ and build a user views the network $G_{UN}(V, E)$ to find out the most influential user.

Input: explicit links and implicit links in C , sentiment orientation O_i of every $C_i \in C$;
 Output: $G_{CN}(V, E)$ //Comment Network of C ;
 Description:
 (1) for each $C_i \in C$
 (2) for each $C_j = C_i \in C$
 (3) if $(C_i \text{ link to } C_j)$ //the link includes explicit and implicit link
 (4) if C_i has the same sentiment orientation with C_j
 (5) C_i positive link to C_j ;
 (6) else
 (7) C_i negative link to C_j ;
 (8) assign weight wt_{ij} for edge $C_i \rightarrow C_j$;

ALGORITHM 1: The algorithm to build comment network.

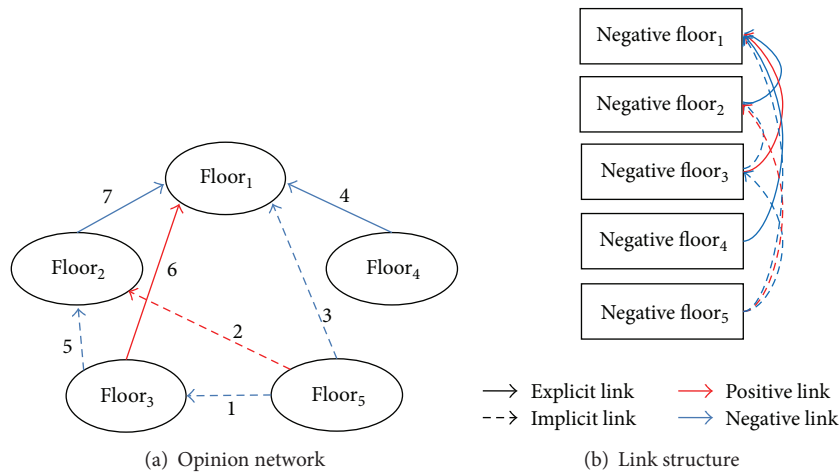


FIGURE 2: Single theme opinion network.

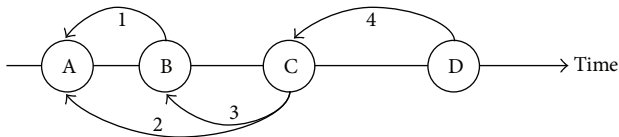


FIGURE 3: Time interval among comments.

4.1. *The Factors of Time.* When reading a review or a comment, the longer the interval to reply is, the weaker its influence is. Hence, the impact of time should be considered [18]. As the above analysis, this section will propose a model to explain the time factor and the comments of the relationship between the strength of influence; this impact of time is shown in Figure 3.

As shown in Figure 3, there is a comment set. The first comments will influence the late comment. For example, “ $B \rightarrow A$ ” represents that the comment B is affected by the comment A. The distance between those two comments denotes the time intervals. The larger the interval is, the weaker the influence is [19]. For example, the distance between A and C is greater than the distance between C and B; thus, the impact of the B on the C is greater than its impact

on A. On the other hand, the influence of comment set C will change over time. Therefore, the link weight between comments not only is related to the similarity wt_{ij} but also gradually changes with time [20].

According to the above analysis, it is found that there is an important relationship between the release time of the comment and the choice of the comment. Defining a function f to reduce the probability of the selection of comment, a function of distance on the time is defined as

$$f(t_1, t_2, D) = D^{|t_2 - t_1| \times K}, \quad (3)$$

where f is a function of time t_1, t_2 , and the damping D . The term t_1 is the time of the respondents comment, t_2 is the time when the replying person proposed a comment. Hence, f is time-varying function. If the reply comment is far away from now, the comment has a smaller probability to be accessed. In (3), D ($0 < D < 1$) is a time-dependent coefficient and K is a control factor. Thus, it can choose an appropriate value of K to enlarge or reduce the time. The larger the distance $|t_2 - t_1|$ is, the smaller the impact becomes. Additionally, f changes with time are shown in Figure 4.

As shown in Figure 4, the function f is gradually changing with the time interval, where $D = 0.85$. Thus, the function f is defined reasonably.

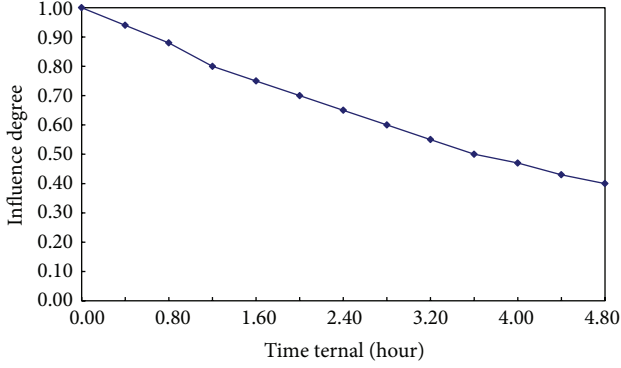


FIGURE 4: The response of the probability function f changing with time.

4.2. *The Detection of the Most Influential Comments.* In a single theme network, if C_i and C_j are explicitly linked, then it leads to $wt_{i,j} = 1$; the impact thus practically exists. If the link relationship is implicit, then $0 \leq |wt_{i,j}| \leq 1$; that is, the impact may exist between comments. For each $wt_{i,j}$, due to the effect of the time can be reduced by using the function f , and then it follows that

$$wt_{i,j}' = f_{i,j} \times wt_{i,j}. \quad (4)$$

To normalize the probability, it needs to normalize the value Sum_i :

$$Sum_i = \sum_{j=1}^n |wt_{i,j}'|. \quad (5)$$

By using (5), the transformed probability can be obtained as

$$wt_{i,j}'' = \frac{wt_{i,j}'}{Sum_i}. \quad (6)$$

Then, the matrix of the improved finite Markov chain can be described as follows.

(a) Step 1

$$A = \begin{bmatrix} wt_{1,1} & \cdots & wt_{1,n} \\ \vdots & & \\ wt_{n,1} & & wt_{n,n} \end{bmatrix}. \quad (7)$$

(b) Step 2

$$A' = \begin{bmatrix} f_{1,1}wt_{1,1} & \cdots & f_{1,n}wt_{1,n} \\ \vdots & & \\ f_{n,1}wt_{n,1} & & f_{n,n}wt_{n,n} \end{bmatrix}. \quad (8)$$

(c) Step 3

$$A'' = \begin{bmatrix} \frac{f_{1,1}wt_{1,1}}{Sum_1} & \cdots & \frac{f_{1,n}wt_{1,n}}{Sum_1} \\ \vdots & \ddots & \\ \frac{f_{n,1}wt_{n,1}}{Sum_n} & & \frac{f_{n,n}wt_{n,n}}{Sum_n} \end{bmatrix}. \quad (9)$$

As shown above, A , A' , and A'' are sequentially linked only considering the time factor and the normalized matrix.

4.3. *The Improved Model of the Finite Markov Chain.* In the field of information retrieval, the PageRank algorithm is widely used. Inspired by this algorithm, a random walk model called Dynamic Opinion Rank is proposed in this section. These algorithms not only take the emotional factors into account but also consider the time factor [21].

From the standpoint view of model use, if a comment gets more positive reviews, then it will be more influential. Moreover, if this comment also replies to other comments, according to the characteristics of the model PageRank, it is reasonable that its influence also will be passed each other. Usually, comments may be affected by the following two cases:

- (1) the comments raised by users are affected by the interested opinion with a probability d ;
- (2) comments may also be subject to random probability $1 - d$ effects.

Based on the above analysis, an algorithm similar to PageRank is proposed as follows:

$$P = \left[(1 - d) \frac{E}{n} + dA^T \right] P, \quad (10)$$

where A is an $n \times n$ improved finite Markov chain transition matrix and n represents the set of comments in the C . Transposing A yields

$$A^T = \begin{bmatrix} a_{11} & \cdots & a_{n1} \\ \vdots & \ddots & \vdots \\ a_{1n} & \cdots & a_{nn} \end{bmatrix}, \quad (11)$$

where any line of of A^T denoted by A^{Ti} ($1 \leq i \leq n$) represents all the cases that C_j links to C_i ($1 \leq i \neq j \leq n$).

For any element $a_{ji} = (f_{j,i} \times wt_{j,i}) / Sum_j$, the ranking score can be calculated by using the following equation:

$$P(i) = (1 - d) + d \sum_{(j,i) \in E} f(t_i, t_j, D) \frac{P(j) \times wt_{ji}}{Sum_j}, \quad (12)$$

where $P(i)$ represents the authority of the value. Following the above methods, it can eventually obtain the score over a period of time. Then, the comment with the maximum

TABLE 2: The changes of opinion leader in the comments.

Number	Content of comment	Ranking score
Number 25	Comment Number 1	6.581
Number 166	Comment Number 2	6.655
Number 25	Comment Number 3	7.187
Number 25	Comment Number 4	7.119

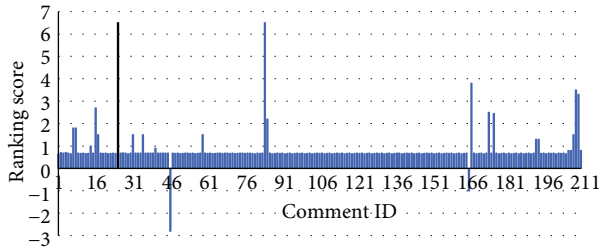


FIGURE 5: Ranking (07:55:17–09:26:46).

authority value can be chosen as the opinion leader. If a comment gets a lot of penetration and most of them are positive emotions consistent link and further the interval time between the comments is not very long, then this comment may get higher ranking scores.

5. Experimental Results and Analysis

To verify the proposed algorithm, experimental analysis is conducted. The data for the experiment is obtained from Weibo news. Through tracking this news within two days (2012-08-17 07:55:17~2012-08-18 05:42:43) and dividing this period of time into four different time periods, each time period was analyzed to identify opinion leaders, and the dynamic change of the opinion leaders was analyzed.

5.1. The Result of Finding Out the Most Influential Comment.

By building a single-topic comments Network $G_{CN}(V, E)$, setting the parameter $d = 0.85$ and $k = 2$, and applying the algorithm proposed in Section 4, the experimental results are shown in Figures 5 and 6. As shown in Figure 6, there are 211 comments in the first time period. It is also easy to find that the comment Number 25 received the highest scores. However, due to the short time, the relationships between comments are not clear. Therefore, opinion leaders may change with time; it leads to the inaccurate opinion leader. As shown in Figure 6, it is found that Number 25 is not the opinion leader, while Number 166 received the highest score. Hence, Number 166 is opinion leader at this time. Some comments received low scores because their views are not accepted by others. Although there has been an increase of the comment number during the second time of period, the relationship between comments still appears to be relatively sparse.

As illustrated in Figure 7, Number 25 becomes opinion leader, while the score of Number 166 decreases with time. Additionally, due to the increasing number of comments,

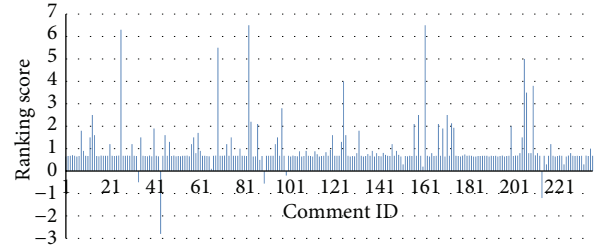


FIGURE 6: Ranking (07:55:17–12:08:44).

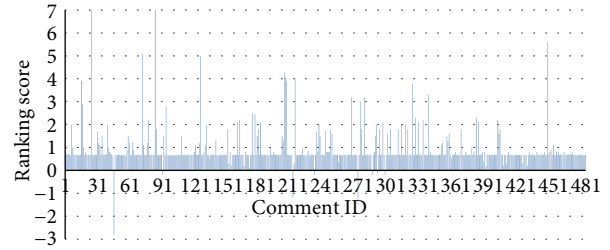


FIGURE 7: Ranking (07:55:17–18:17:19).

the relationship between comments becomes more and more dense and the status of the comments converges to be stable.

It is found in Figure 8 that the number of comments is 560 in the fourth time of period. Now, Number 25 received the highest score, and it is the opinion leader at this time. In comparison with Figure 7, the newly published comment's score grows faster. The result shown in Figure 8 also demonstrates that new comments will get more attention, and it also proves that it is reasonable to take time into account. On the other hand, many comments' scores are growing. Due to the characteristics of news comments, it will get less attention after a period of time. Moreover, the number of comments also will decrease. Hence, the leadership of Number 25 will be maintained for a long time.

The most influential comments and the sort scores are shown in Table 2. We find that opinion leaders are changing over time. Moreover, the rank of opinion leaders is also affected by the time. This also verifies that it is quite necessary to take time into consideration when developing the algorithm.

To evaluate the performance of Dynamic Opinion Rank algorithm, a standard should be proposed to allow the experts to divide comments in each time period into two categories: the strong and weak influence. Then, it needs to measure the time the comment raised, degree centrality, the degree of authority, and the F -Score of several Opinion Rank algorithms. Those comparison results are shown in Figure 9. It is found that the Dynamic Opinion Rank algorithm has much more accuracy and stability than other approaches. It thus verifies the effectiveness of the proposed scheme.

5.2. The Finding of the Most Influential Users. In the process of finding out most influential users, single-topic user network $G_{UN}(V, E)$ should be constructed firstly, and then the

TABLE 3: Clustering results for detection of opinion leader from users.

08:04:37–11:07:11		08:04:07–13:45:49		08:04:37–18:43:22		08:04:37–6:47:08	
Cluster	User count	Cluster	User count	Cluster	User count	Cluster	User count
1	43	1	71	1	117	1	110
2	4	2	11	2	3	2	17
3	2	3	1	3	1	3	1
4	3	4	11			4	
5	1	5					
uid	15928539	uid	15928244		1199491660	uid	15930288

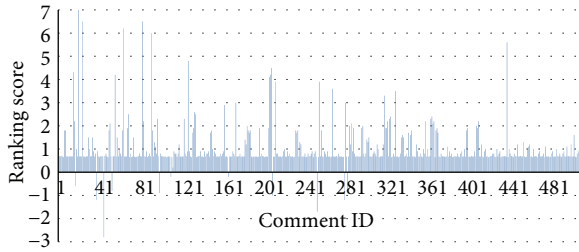


FIGURE 8: Ranking (07:55:17–next day 05:42:43).

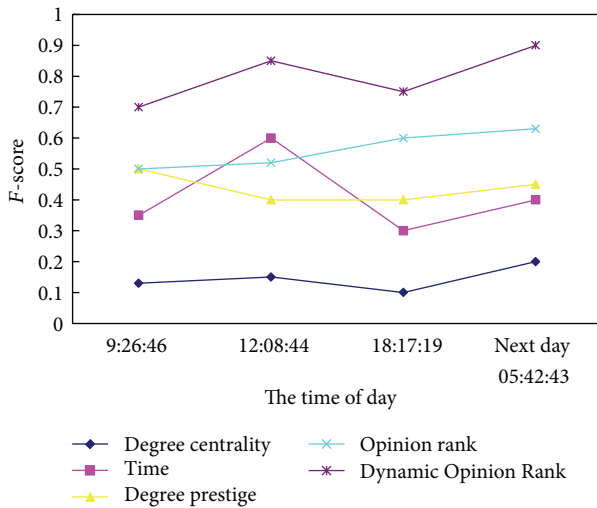


FIGURE 9: F-Score of each method.

proposed algorithm in Section 4 should be applied to detect the most influential users. For the DBSCAN density-based clustering algorithm, the radius range is set between 0.06 and 0.12, and the initial MinPts is chosen as 1. Consequently, there exist some clusters containing noise. With application of the proposed approach, 3~5 clusters are finally obtained, it is shown in Table 3.

From Table 3, we find that the first clusters with most elements can be removed then replaced by clusters with less elements. As $G_{UN}(V, E)$ is sparse, set $w_{PD} = 10$, $w_{CQ} = 0.3$ and $w_{DC} = 10$. Finally, it detects opinion leaders in each period. The result is illustrated in the last line of Table 3. According to the experiment, it reveals that opinion leaders can change with time dynamically.

6. Conclusions

This paper presents a Dynamic Opinion Rank algorithm to find out the opinion leaders in Chinese news. Unlike the existing approaches, the proposed network model explicitly takes explicit and implicit links into account. Moreover, the proposed algorithm was able to conclude that the most influential comments and the opinion leaders were time-varying. Experimental results further verified the effectiveness of the proposed strategy.

Conflict of Interests

The authors declare that there is no conflict of interests regarding the publication of this paper.

Acknowledgments

This work was also supported by the National Natural Science Foundation of China (Project no. 71171068) and the Polish-Norwegian Research Programme (Project no. Pol-Nor/200957/47/2013). The authors highly appreciate the above financial supports.

References

- [1] M. J. Aschwanden, J. P. Wuelser, N. V. Nitta, J. R. Lemen, M. L. DeRosa, and A. Malanushenko, "first three-dimensional reconstructions of coronal loops with the stereo A+B spacecraft. IV: magnetic modeling with twisted force-free fields," *Astrophysical Journal*, vol. 756, no. 2, article 124, 22 pages, 2012.
- [2] S. Yin, S. X. Ding, A. H. A. Sari, and H. Hao, "Data-driven monitoring for stochastic systems and its application on batch process," *International Journal of Systems Science*, vol. 44, no. 7, pp. 1366–1376, 2013.
- [3] S. Yin, S. X. Ding, A. Haghani, H. Hao, and P. Zhang, "A comparison study of basic data-driven fault diagnosis and process monitoring methods on the benchmark Tennessee Eastman process," *Journal of Process Control*, vol. 22, no. 9, pp. 1567–1581, 2012.
- [4] S. Yin, H. Luo, and S. Ding, "Real-time implementation of fault-tolerant control systems with performance optimization," *IEEE Transactions on Industrial Electronics*, vol. 61, no. 5, pp. 2402–2411, 2014.
- [5] S. Yin, G. Wang, and H. R. Karimi, "Data-driven design of robust fault detection system for wind turbines," *Mechatronics*, 2013.

- [6] S. Yin, X. Yang, and H. R. Karimi, "Data-driven adaptive observer for fault diagnosis," *Mathematical Problems in Engineering*, vol. 2012, Article ID 832836, 21 pages, 2012.
- [7] X. Zhao, X. Liu, S. Yin, and H. Li, "Improved results on stability of continuous-time switched positive linear systems," *Automatica*, 2013.
- [8] X. Zhao, P. Shi, and L. Zhang, "Asynchronously switched control of a class of slowly switched linear systems," *Systems & Control Letters*, vol. 61, no. 12, pp. 1151–1156, 2012.
- [9] X. Zhao, L. Zhang, and P. Shi, "Stability of a class of switched positive linear time-delay systems," *International Journal of Robust and Nonlinear Control*, vol. 23, no. 5, pp. 578–589, 2013.
- [10] X. Zhao, L. Zhang, P. Shi, and H. Karimi, "Novel stability criteria for TS fuzzy systems," *IEEE Transactions on Fuzzy Systems*, 2013.
- [11] X. Zhao, L. Zhang, P. Shi, and H. Karimi, "Robust control of continuous-time systems with state-dependent uncertainties and its application to electronic circuits," *IEEE Transactions on Industrial Electronics*, 2013.
- [12] X. Zhao, L. Zhang, P. Shi, and M. Liu, "Stability and stabilization of switched linear systems with mode-dependent average dwell time," *IEEE Transactions on Automatic Control*, vol. 57, no. 7, pp. 1809–1815, 2012.
- [13] X. Zhao, L. Zhang, P. Shi, and M. Liu, "Stability of switched positive linear systems with average dwell time switching," *Automatica*, vol. 48, no. 6, pp. 1132–1137, 2012.
- [14] A. Goyal, F. Bonchi, and L. V. S. Lakshmanan, "Discovering leaders from community actions," in *Proceedings of the 17th ACM Conference on Information and Knowledge Management (CIKM '08)*, pp. 499–508, October 2008.
- [15] F. Bodendorf and C. Kaiser, "Detecting opinion leaders and trends in online communities," in *Proceedings of the 4th International Conference on Digital Society (ICDS '10)*, pp. 124–129, February 2010.
- [16] Z. Hengmin, D. Zeng, and Z. Changli, "Finding leaders from opinion networks," in *Proceedings of the 2009 IEEE International Conference on Intelligence and Security Informatics (ISI '09)*, pp. 266–268, June 2009.
- [17] G. Salton, A. Wong, and C. S. Yang, "A vector space model for automatic indexing," *Communications of the ACM*, vol. 18, no. 11, pp. 613–620, 1975.
- [18] L.-W. Ku and H.-H. Chen, "Mining opinions from the web: beyond relevance retrieval," *Journal of the American Society for Information Science and Technology*, vol. 58, no. 12, pp. 1838–1850, 2007.
- [19] F. Kokkoras, E. Lampridou, K. Ntonas, and I. Vlahavas, "Mopis: a multiple opinion summarizer," in *Artificial Intelligence: Theories, Models and Applications*, pp. 110–122, Springer, 2008.
- [20] L.-W. Ku, H.-W. Ho, and H.-H. Chen, "opinion mining and relationship discovery using CopeOpi opinion analysis system," *Journal of the American Society for Information Science and Technology*, vol. 60, no. 7, pp. 1486–1503, 2009.
- [21] J. Wiebe and E. Riloff, "Creating subjective and objective sentence classifiers from unannotated texts," in *Proceedings of the 6th International Conference (CICLing '05)*, pp. 486–497, February 2005.

Research Article

A Discrete Group Search Optimizer for Hybrid Flowshop Scheduling Problem with Random Breakdown

Zhe Cui and Xingsheng Gu

Key Laboratory of Advanced Control and Optimization for Chemical Process, Ministry of Education, Shanghai 200237, China

Correspondence should be addressed to Xingsheng Gu; xsgu@ecust.edu.cn

Received 5 December 2013; Accepted 24 January 2014; Published 27 February 2014

Academic Editor: Huaicheng Yan

Copyright © 2014 Z. Cui and X. Gu. This is an open access article distributed under the Creative Commons Attribution License, which permits unrestricted use, distribution, and reproduction in any medium, provided the original work is properly cited.

The scheduling problems have been discussed in the literature extensively under the assumption that the machines are permanently available without any breakdown. However, in the real manufacturing environments, the machines could be unavailable inevitably for many reasons. In this paper, the authors introduce the hybrid flowshop scheduling problem with random breakdown (RBHFS) together with a discrete group search optimizer algorithm (DGSO). In particular, two different working cases, preempt-resume case, and preempt-repeat case are considered under random breakdown. The proposed DGSO algorithm adopts the vector representation and several discrete operators, such as insert, swap, differential evolution, destruction, and construction in the producers, scroungers, and rangers phases. In addition, an orthogonal test is applied to configure the adjustable parameters in the DGSO algorithm. The computational results in both cases indicate that the proposed algorithm significantly improves the performances compared with other high performing algorithms in the literature.

1. Introduction

The hybrid flowshop scheduling (HFS) problem, being also referred to as multiprocessor or flexible flowshop, is one kind of production scheduling problems, which has been widely used in the process industry such as the paper, oil, petrochemical, and pharmaceutical industries [1]. In the HFS problem, it is assumed that the jobs have to pass through all stages in the same order and that there is at least one stage that must have multiple machines. Each job is processed on only one machine at each stage. The HFS problem minimizing the makespan or maximum completion time is denoted as $HFc//C_{\max}$ using the three-field notation by Graham et al. [2], and it has been proved to be strongly NP-hard when the number of machines is no less than two [3]. The research efforts on the HFS problem generally presume a static environment and no unexpected events [4]. However, the real natural environments are stochastic and dynamic [5, 6], and the real manufacturing processes tend to suffer a wide range of uncertainties, such as machine breakdown, job cancellation, due-date changes, shortage of materials, and changes in job priority. In this paper, the authors

concentrate only on the hybrid flowshop scheduling problem with random breakdown (RBHFS), which is referred to as $HFc/brkdwn/C_{\max}$. In the RBHFS problem, the breakdown of machines may happen at any time and the job being processed on the machine must be stopped until the machine has been repaired. On the basis of the characters of jobs and the breakdown of machines, the RBHFS problem falls into two categories: the preempt-resume case and the preempt-repeat case. In the preempt-resume case, the completed part of the job will not be lost and the processing time of the job is cumulative after the machine breakdown is repaired. While in the preempt-repeat case, the completed part will be lost so that the operation of the job should be started from the beginning, which is commonly used in the preprocessing phase, for example, the heating and cooling processes.

Compared with a lot of works on the HFS problem, the studies on the RBHFS problem are still in their infancy. Alcaide et al. [7] considered the stochastic flowshop scheduling problem subject to random breakdowns where the objective is to minimize the expected makespan and proposed a dynamic procedure that enables us to consider a random breakdowns stochastic problem as a sequence of

without-breakdowns stochastic problems. In [8] the dynamic scheduling problems in random flexible manufacturing systems subject to machine breakdowns are addressed and an adaptive scheduling approach is proposed to make coupled decisions about the part/machine scheduling and operation/tool assignments on a rolling horizon basis. Allaoui and Artiba [9] studied the hybrid flowshop scheduling problem to minimize flow time and due date based criteria under maintenance constraints. In this model, the setup, cleaning, and transportation time are also considered. Tang et al. [10] studied the single machine stochastic just-in-time scheduling problem subject to machine breakdowns for the preempt-resume and the preempt-repeat. The objective function of the problem is the sum of squared deviations of the job expected completion time from the due date. Gholami et al. [11] examined a heuristic to find schedules minimizing expected makespan in the hybrid flowshop problem with sequence-dependent setups and machines with random breakdowns. This method employed the random keys genetic algorithm approaches (RKGGA) to find the optimum solutions and utilized the simulator algorithm to evaluate the objective function under this condition. From the analysis results of the Taguchi parameter design, the number of job, the number of stage, and the population size play important roles in the algorithm. And the same problem was studied later by Zandieh and Gholami [12]. Based on a clonal selection principle and an affinity maturation mechanism of the immune response, they proposed an immune algorithm (IA) and applied the Taguchi parameter design method to analyze the proposed algorithm. Safari and Sadjadi [13] explored flowshop configuration under the assumption of condition-based maintenance to minimize expected makespan and proposed a condition-based maintenance (CBM) strategy and a hybrid algorithm based on genetic algorithm and simulated annealing. Their simulation results showed its superiority. Wang and Choi [14] proposed a decomposition-based approach that integrates the completely reactive approach with the predictive reactive approach to minimize the makespan of the flexible flowshop scheduling problem under machine breakdown. Mirabi et al. [15] considered a two-stage hybrid flowshop scheduling problem where the machine may not always be available during the scheduling period. The objective is to find the optimal job combinations and the job schedules such that the makespan is minimized.

Recently, a population-based optimization algorithm group search optimizer (GSO) has been proposed by He et al. [16], which is inspired by the animal social foraging behavior and group living theory. Some recent researches indicate that the GSO algorithm is better than some other evolutionary algorithms for solving the large-scale multimodal benchmark functions [17, 18]. At the same time, the GSO algorithm has been successfully applied in a variety of fields, such as artificial neural network training [19, 20], power system [21, 22], and mechanical design [23].

Considering the successes of the GSO algorithm, the authors proposed to use a discrete group search optimizer (DGSO) algorithm for the production scheduling problem. The proposed DGSO algorithm maintains the optimization mechanism of the basic GSO algorithm and abandons the

angle evolution strategy to improve the effectiveness and efficiency of the algorithm. In the DGSO algorithm, an encoding scheme based on the vector representation is introduced in order to adapt the GSO algorithm to the discrete problems. Meanwhile, an improved variable neighborhood search, a novel differential evolution operation, and the destruction and construction procedures are proposed in the producer, scrounger, and ranger phases, respectively. In addition, in order to achieve a good performance of the DGSO algorithm, an orthogonal experiment design is carried out for getting a guideline on tuning of the parameters in the algorithm. In both the preempt-resume case and the preempt-repeat case, our proposed DGSO algorithm shows the state-of-the-art results on benchmarks.

The rest of the paper is organized as follows. In Section 2, the RBHFS problem statement and the approach to dealing with random breakdown are formulated. Section 3 presents the details of the proposed DGSO algorithm. The tests on parameter selection and the simulation results are provided in Section 4. Finally, the authors draw conclusions in Section 5.

2. Problem Statement

2.1. Description of the Problem. The RBHFS problem with makespan criterion can be described as follows. There are n jobs $\mathbf{J} = \{1, 2, \dots, i, \dots, n-1, n\}$ that have to be performed on s stages $\mathbf{S} = \{1, 2, \dots, j, \dots, s-1, s\}$, and each stage j has m_j identical machines. At least one stage j must have more than one machine. Each job consists of s operations, each of which must be sequentially processed at stage 1 to stage s and by exactly one machine at every stage. At any time, a machine can process at most one job and a job can be processed by at most one machine. The processing time required for job i at stage j is given as p_{ij} . These identical machines are not available at all times, and they suffer random breakdown. Once the machine begins to work, it will continue to run until breakdown occurs or all jobs are finished. The setup and release time of all jobs are negligible. Preemption is not allowed and infinite intermediate buffers exist between two successive stages. The scheduling problem is to choose a machine at each stage for each job and determine the sequence of jobs on each machine so as to minimize the makespan [14].

2.2. An Approach to Dealing with Random Breakdown. It is assumed that a machine keeps processing the jobs sequentially until it break down or it has finished all the jobs, and machine breakdowns may arise at any time in working periods. The authors find that the possible positions where the breakdown may happen in are shown in Figure 1, where A means the breakdown happened during machine's processing time interval, B , C , and D represent the breakdown happened during machine's idle time interval.

This paper considers two different cases while dealing with an interrupted job. Case 1 is the preempt-resume case and Case 2 is the preempt-repeat case. In Case 1, after repairing, only the unprocessed part of the interrupted job needs to be processed. And in Case 2, after repairing, the

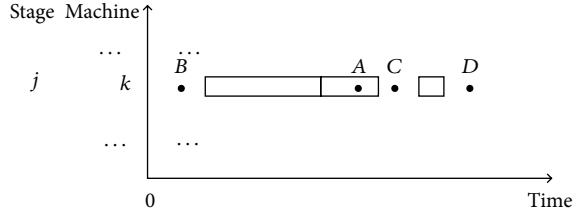


FIGURE 1: The Gantt chart of the RBHFS problem.

whole interrupted job needs to be reprocessed. It is assumed that st_{ijk} and C_{ijk} are the starting time and the completing time of job i on machine k ($k \in \{1, 2, \dots, \sum_{j=1}^s m_j\}$) at stage j , respectively, and r_k denotes the repairing time of machine k . Then C_{ijk} can be calculated as follows:

A: if $st_{ijk} \leq A < C_{ijk}$

Case 1: $st_{ijk} = st_{ijk}, C_{ijk} = st_{ijk} + r_k + p_{ij}$

Case 2: $st_{ijk} = A + r_k, C_{ijk} = st_{ijk} + p_{ij}$

B: if $B < st_{ijk}$

Case 1 and Case 2: $st_{ijk} = \max\{st_{ijk}, B + r_k\}, C_{ijk} = st_{ijk} + p_{ij}$

C: if $C_{(i-1)jk} \leq C < st_{ijk}$

Case 1 and Case 2: $st_{ijk} = \max\{st_{ijk}, C + r_k\}, C_{ijk} = st_{ijk} + p_{ij}$

D: if $D \geq C_{ijk}$

Case 1 and Case 2: $st_{ijk} = st_{ijk}, C_{ijk} = C_{ijk}$.

3. The Discrete Group Search Optimizer (DGSO) for the RBHFS Problem

The basic GSO algorithm adopts the framework of the biological model, Producer-Scrounger (PS) model [24], which uses two foraging strategies within groups: producing and scrounging. In order to avoid entrapment in local minima, GSO also employs rangers foraging strategies which perform random walks [17]. The population of GSO is called a group and each individual in the group is called a member. In the GSO scheme, a group contains three types of members, namely, the producers, the scroungers, and the rangers [18]. Each individual in the group has its own position, search angle, and search direction. At each iteration cycle, the producers perform producing strategy to search for the optimal positions; the scroungers perform scrounging strategy to join resources found by the producers; the remaining members are the rangers which walk randomly in the searching space to find their new positions. In the GSO algorithm, a position of the individual corresponds to a solution of the optimization problem, and the fitness of the position corresponds to the fitness of the solution. The processes of the basic GSO algorithm can be shown in pseudocode as Algorithm 1.

Following the procedure for the continuous function optimization, in this paper the authors propose a discrete version of the GSO algorithm for the RBHFS problem. It is discussed in detail below.

3.1. Individual Representation and Initialization. Owing to its continuous nature, the GSO algorithm does not directly fit for the discrete flowshop scheduling problem. So it is important to find a suitable mapping which can conveniently convert individuals to solutions. In the HFS problem, there are two formats to represent a solution: the matrix representation and the vector representation [25]. In this paper, the RBHFS problem is formulated by the vector representation, which considers the sequence of jobs only at stage one and the sequences of jobs at other stages are decoded by employing the List Scheduling (LS) algorithm [26, 27]. As a result, the vector representation is also adopted in the proposed DGSO algorithm. In such a case, the individual in the DGSO algorithm can be represented by a permutation of jobs at stage one $\pi = \{\pi(1), \pi(2), \dots, \pi(n)\}$. The population size of the proposed DGSO algorithm is determined by parameter PS and the initial population is generated randomly in the search space.

3.2. Producer. Recently, Couzin et al. [28] indicated that the larger the group, the smaller the proportion of informed individuals needed to guide the group, and that only a very small proportion of informed individuals is required to achieve great accuracy. As a result, for the great accuracy and the simplicity, there is only one producer in the DGSO algorithm, which means that the best individual is the producer and the remaining members in the population are scroungers or rangers. Furthermore, considering the efficiency of the algorithm, the producing strategy is executed on the producer only if it is changed after the evolutionary procedure.

Aiming at improving the efficiency of the proposed DGSO algorithm, the authors introduce an improved variable neighborhood search (IVNS) [29] as the producing strategy in this paper. The IVNS contains two structures of neighborhoods: the insert local search and the swap local search. The pseudocodes of the insert local search and the swap local search are given in Algorithm 2. The IVNS keeps doing the insert local search followed by the swap local search until there is no improvement. If the newly generated individual is better than the current producer, the new individual is set to be the producer. Otherwise the old producer is retained.

3.3. Scrounger. In the population, the left individuals except the producer are divided into the scroungers and the rangers. Each individual is set to be scrounger or ranger with the probability of P and $(1 - P)$, respectively.

As for each scrounger, a novel discrete differential evolution scheme is employed for improving the scrounging performance, which consists of three steps: mutation, crossover, and selection.

In the mutation part, the *bestrandinsert* operation [30] is introduced. The procedure of the *bestrandinsert* is described

```

Procedure the GSO algorithm
  Initial population
  While (criterion)
    Choose the producers and perform the producing
    Choose the scroungers and perform the scrounging
    Disperse the rest individuals to perform ranging
    Evaluate the individuals
  End while
End procedure

```

ALGORITHM 1: The procedure of the basic GSO algorithm.

as follows. It first randomly chooses $pr1$ jobs without repetition; then it inserts each chosen job into other $n - 1$ position, and $pr2$ better permutations with relatively smaller makespan are remembered; finally one of the $pr2$ permutations is randomly chosen to replace the incumbent scrounger. For each scrounger, the producer undergoes the *bestrandinsert* operation with a mutation rate (MR) to obtain the mutant individual. On the other hand, the mutant individual is the same as the producer with a probability of about $(1 - MR)$. That is to say, the mutant individual is obtained as

$$V_i^t = \begin{cases} \text{bestrandinsert}(\text{producer}), & \text{if } \text{rand}(0, 1) < \text{MR} \\ \text{producer}, & \text{otherwise,} \end{cases} \quad (1)$$

where V_i^t denotes the mutant individual at generation t and $\text{rand}(0, 1)$ is a random function returning a number between 0 and 1 with uniform distribution.

Next a crossover operation called CRO is employed in the crossover part, and it will be able to work effectively even though the individuals in the population are very close to each other in the later stage of evolution. The crossed individual $U_i^t = \text{CRO}(\text{scrounger}, V_i^t)$. The authors first randomly select a part of job permutation in the scrounger and insert it on the front or back of the mutant individual V_i^t and then delete the jobs in V_i^t which are already in the selected segment. In this case, two valid crossed individuals will be obtained: one is the front one and the other the back one.

Following the crossover operation, the selection is conducted. The best one which has the lowest objective value among the two crossed individuals and the incumbent scrounger is accepted. In other words, if either of these two crossed individuals yields a better makespan than the scrounger, then the better individual becomes the scrounger; otherwise the old scrounger is retained.

3.4. Ranger. In the basic GSO algorithm, the rangers search randomly in the predefined space to increase the population diversity and avoid getting trapped in local optima. Here the rangers employ the destruction and construction procedures of the iterated greedy (IG) algorithm with one parameter: destruction size (d) [31]. Regardless of whether the newly generated individual is better than the original ranger, the ranger is replaced to enhance the global search ability. Throughout

```

(a) the insert local search
  improve = 1;
  while (improve = 1)
  do {
    improve = 0;
    for (i = 1 : n)
      remove job  $j$  at random from producer
       $\pi'$  = best permutation obtained by inserting
      job  $j$  in any possible positions of producer
      if ( $C_{\max}(\pi') < C_{\max}(\text{producer})$ )
        producer =  $\pi'$ ;
        improve = 1;
      endif
    endfor
  }
(b) the swap local search
  improve = 1;
  while (improve = 1)
  do {
    improve = 0;
    for (i = 1 : n)
       $\pi'$  = best permutation obtained by swapping
      job  $j$  with other jobs of producer
      if ( $C_{\max}(\pi') < C_{\max}(\text{producer})$ )
        producer =  $\pi'$ ;
        improve = 1;
      endif
    endfor
  }

```

ALGORITHM 2: The procedure of improved variable neighborhood search.

the course of evolution, once the new individual generated by scroungers or rangers is superior to the producer, the producer will be updated.

3.5. Computational Procedure. Based on the above operations, the procedure of the DGSO algorithm for the RBHFS problem is summarized as follows.

Step 1. Set the algorithm parameters PS, P , MR, $pr1$, $pr2$, and d , and initialize the population.

Step 2. The producer conducts an improved variable neighborhood search to search for a better solution if the producer is changed.

Step 3. The scroungers employ the discrete differential evolution operation to keep searching for the high-quality solutions, which includes mutation, crossover, and selection.

Step 4. The rangers produce new solutions by using the destruction and construction procedures to avoid local optimum.

Step 5. Evaluate each member in the population and utilize the best individual to update the producer.

Step 6. If the given termination criterion is satisfied, end the procedure and return the producer; otherwise go back to Step 2.

Considering the character of the RBHFS problem, some discrete operators are introduced for the producers, scroungers, and rangers. The DGSO algorithm has the producer and the scroungers to play the part of exploitation and employs the rangers to play the part of exploration. Since both the exploitation and exploration are improved and well balanced, it is expected to generate good results for the RBHFS problem under the criterion of makespan minimization. In the next section, the performance of the DGSO algorithm is investigated based on simulation results and comparisons.

4. Simulation Results and Comparisons

4.1. Experimental Setup. To fully examine the performance of the DGSO algorithm, a parameter discussion, a preliminary experiment, and an extensive experimental comparison with other powerful methods are provided. As no test instances are available for the RBHFS problem, some benchmark problems for the HFS problem are modified. Ten benchmark problems proposed by Liao et al. [32] have been selected. In each instance of Liao's benchmark problems, there are 30 jobs and 5 stages. At each stage, the machine number has a uniform distribution in the range of [3, 5]. The processing time in these problems is within [1, 100]. It is assumed that the breakdown time point and repairing time obey the normal distributions and there are five breakdown time points. The mean values of the five breakdown time points are equal to 200, 400, . . . , 1000, respectively, and the variances of all the breakdown points are 10. The mean value of repairing time of each machine is 20, and the variance is 5. All the algorithms were coded in Visual C++ and run on an Intel Pentium 3.06 GHz PC with 2 GB RAM under Windows 7 operating system. The maximum computation time is fixed at 200 seconds for all the parameter tests, the preliminary experiment, and compared algorithms in the following subsections.

4.2. Parameter Discussion. Tuning parameters properly is critical for an evolutionary algorithm to achieve a good

TABLE 1: Factors and levels for orthogonal experiment.

Factor	Level 1	Level 2	Level 3	Level 4	Level 5
PS(1)	10	20	30	40	50
$P(2)$	0.6	0.7	0.8	0.9	1
MR(3)	0.2	0.4	0.6	0.8	1
$pr1(4)$	2	3	4	5	6
$pr2(5)$	1	2	3	4	5
$d(6)$	1	2	3	4	5

performance [33, 34]. In the proposed DGSO algorithm, there are six main parameters: PS, P , MR, $pr1$, $pr2$, and d . All the six parameters are regarded as factors at five different levels, as illustrated in Table 1. If the authors carry out the full factorial experiment design in this case, it requires $5^6 = 15,625$ experiments which is not necessary and economical. Therefore, an orthogonal experiment design [35] is applied to provide a receipt for tuning the adjustable parameters of the DGSO algorithm, which just needs $5^2 = 25$ experiments.

Parameter experiments are conducted on ten Liao's benchmark problems. The breakdowns in the parameter discussion are subject to preempt-resume case (Case 1) for simplicity. Taking the test on instance j30c5e1, for example, Table 2 shows the orthogonal parameter table $L_{25}(5^6)$ including 25 groups of the parameter test samples. Each group of parameters is trialed for ten times. The unabridged result tables similar to Table 2 in other nine instances are omitted here. After the detailed analyses of the orthogonal design, the authors set the parameters PS = 10, $P = 0.6$, MR = 0.8, $pr1 = 4$, $pr2 = 2$, and $d = 2$ in the following experiments.

4.3. Preliminary Experiment. Comparing with the group search optimizer (GSO) algorithm, there are three new elements in the proposed DGSO algorithm: the improved variable neighborhood search in the producer phase, the differential evolution in the scrounger phase, and the destruction and construction procedures in the ranger phase. The following abbreviations represent the variants considered: the GSO-IVNS (GSO with improved variable neighborhood search) and the GSO-IVNS-DE (DHS with improved variable neighborhood search and differential evolution). To verify the effect of each element in the algorithm for solving the RBHFS problem, the authors test four algorithms: GSO, GSO-IVNS, GSO-IVNS-DE, and DGSO in the preempt-repeat case (Case 2). Each method was run twenty times for each Liao's benchmark problem and its performance, including the average and minimum value, was recorded in Table 3.

In Table 3, the overall mean values of AVE and MIN yielded by the DGSO algorithm are equal to 710.9 and 701, respectively, and the DGSO algorithm is the best one among the four variants for all the problems with the same computational time. It is shown that the utilization of the improved variable neighborhood search, the differential evolution, and the destruction and construction procedures is the key to stress the balance of exploration and exploitation so as to improve the performance of GSO algorithm.

TABLE 2: Orthogonal parameter table $L_{25}(5^6)$ and results of j30c5e1.

Test	Factor						Mean value
	PS	P	MR	pr1	pr2	d	
1	10(1)	0.6(1)	0.2(1)	2(1)	1(1)	1(1)	505.7
2	10(1)	0.7(2)	0.4(2)	3(2)	2(2)	2(2)	503.5
3	10(1)	0.8(3)	0.6(3)	4(3)	3(3)	3(3)	504.5
4	10(1)	0.9(4)	0.8(4)	5(4)	4(4)	4(4)	503.8
5	10(1)	1(5)	1(5)	6(5)	5(5)	5(5)	509.8
6	20(2)	0.6(1)	0.4(2)	4(3)	4(4)	5(5)	503.2
7	20(2)	0.7(2)	0.6(3)	5(4)	5(5)	1(1)	506.5
8	20(2)	0.8(3)	0.8(4)	6(5)	1(1)	2(2)	504.7
9	20(2)	0.9(4)	1(5)	2(1)	2(2)	3(3)	505.4
10	20(2)	1(5)	0.2(1)	3(2)	3(3)	4(4)	512.7
11	30(3)	0.6(1)	0.6(3)	6(5)	2(2)	4(4)	503.5
12	30(3)	0.7(2)	0.8(4)	2(1)	3(3)	5(5)	503.4
13	30(3)	0.8(3)	1(5)	3(2)	4(4)	1(1)	506.6
14	30(3)	0.9(4)	0.2(1)	4(3)	5(5)	2(2)	506.3
15	30(3)	1(5)	0.4(2)	5(4)	1(1)	3(3)	512.3
16	40(4)	0.6(1)	0.8(4)	3(2)	5(5)	3(3)	503.4
17	40(4)	0.7(2)	1(5)	4(3)	1(1)	4(4)	506.4
18	40(4)	0.8(3)	0.2(1)	5(4)	2(2)	5(5)	506.0
19	40(4)	0.9(4)	0.4(2)	6(5)	3(3)	1(1)	507.2
20	40(4)	1(5)	0.6(3)	2(1)	4(4)	2(2)	512.0
21	50(5)	0.6(1)	1(5)	5(4)	3(3)	2(2)	504.0
22	50(5)	0.7(2)	0.2(1)	6(5)	4(4)	3(3)	505.3
23	50(5)	0.8(3)	0.4(2)	2(1)	5(5)	4(4)	504.5
24	50(5)	0.9(4)	0.6(3)	3(2)	1(1)	5(5)	507.1
25	50(5)	1(5)	0.8(4)	4(3)	2(2)	1(1)	510.4
k_1	505.46	503.96	507.20	506.20	507.24	507.28	
k_2	506.50	505.02	506.14	506.66	505.76	506.10	
k_3	506.42	505.26	506.72	506.16	506.36	506.18	
k_4	507.00	505.96	505.14	506.52	506.18	506.18	
k_5	506.26	511.44	506.44	506.10	506.10	505.90	
std	0.558	2.946	0.770	0.247	0.554	0.544	

TABLE 3: Performance of HDHS with different versions.

Problem	GSO		GSO-IVNS		GSO-IVNS-DE		DGSO	
	AVE	MIN	AVE	MIN	AVE	MIN	AVE	MIN
j30c5e1	564.2	555	561.9	558	561.3	555	552.7	549
j30c5e2	721.4	716	720.0	716	722.5	716	700.7	697
j30c5e3	752.8	743	741.9	736	740.5	732	723.3	712
j30c5e4	704.5	695	702.5	695	700.5	688	685.3	674
j30c5e5	748.1	726	733.6	726	727.6	726	725.1	709
j30c5e6	743.2	737	737.3	730	731.1	721	718.1	708
j30c5e7	751.9	745	748.0	743	737.2	733	732.1	723
j30c5e8	859.0	824	842.1	801	822.2	788	786.8	771
j30c5e9	799.9	786	796.0	779	791.8	770	766.9	760
j30c5e10	750.2	738	738.4	718	729.6	715	718.5	710
Average	739.5	726	732.2	720	726.4	714	710.9	701

TABLE 4: Comparison results on Liao's benchmark problems of Case 1.

Problem	PSO				RKGa				IA				DGSO			
	AVE	MIN	STD	T (s)	AVE	MIN	STD	T (s)	AVE	MIN	STD	T (s)	AVE	MIN	STD	T (s)
j30c5e1	511.7	507	2.4	50.9	513.0	505	3.9	60.4	509.0	506	1.5	53.6	503.1	501	1.5	64.2
j30c5e2	670.3	670	0.4	29.8	670.5	670	0.8	64.9	670.0	670	0.0	44.9	670.0	670	0.0	1.9
j30c5e3	663.6	657	3.7	66.0	667.5	655	7.5	83.4	659.6	655	1.7	75.9	654.0	651	1.5	72.3
j30c5e4	631.3	628	2.1	85.3	630.7	626	3.1	72.4	629.2	627	1.2	80.4	622.2	621	1.1	82.3
j30c5e5	668.5	666	1.7	64.1	671.7	666	4.5	68.5	662.8	662	0.4	70.0	662.6	662	0.4	33.6
j30c5e6	675.4	670	3.3	67.6	679.0	670	5.6	66.3	669.1	665	2.5	62.7	663.5	661	2.2	52.2
j30c5e7	686.1	684	1.8	49.7	686.0	683	2.5	74.2	683.9	682	0.9	54.8	681.1	681	0.4	47.4
j30c5e8	737.9	732	3.2	95.4	738.3	731	5.1	101.1	734.2	731	1.8	86.3	729.8	729	1.1	64.8
j30c5e9	708.8	705	2.0	89.8	709.8	703	5.1	103.7	705.4	702	1.6	90.2	699.6	698	1.2	99.7
j30c5e10	650.5	641	5.3	82.2	648.8	636	7.2	84.9	642.5	637	2.2	71.2	634.9	631	1.9	83.0
Average	660.4	656	2.6	68.1	661.5	655	4.5	78.0	656.6	654	1.4	69.0	652.1	651	1.1	60.1

TABLE 5: Comparison results on Liao's benchmark problems of Case 2.

Problem	PSO			RKGa			IA			DGSO						
	AVE	MIN	STD	T (s)	AVE	MIN	STD	T (s)	AVE	MIN	STD	T (s)				
j30c5e1	561.6	557	5.1	80.2	562.1	555	8.7	107.0	559.6	554	2.4	87.0	552.7	549	2.7	47.1
j30c5e2	720.0	701	4.4	86.8	723.8	701	7.8	102.3	716.3	701	3.2	97.7	700.7	697	2.7	111.6
j30c5e3	747.5	739	6.0	69.6	748.6	735	6.2	89.0	743.0	736	4.5	77.4	723.3	712	4.6	56.9
j30c5e4	702.2	696	7.5	101.9	701.3	694	8.1	121.6	697.5	688	5.9	69.7	685.3	674	5.9	72.0
j30c5e5	733.7	726	8.7	54.3	734.1	726	13.5	105.3	731.5	726	5.9	54.2	725.1	709	3.8	16.2
j30c5e6	737.1	730	3.6	114.4	737.0	720	6.0	71.8	730.7	718	3.1	101.8	718.1	708	8.8	124.8
j30c5e7	752.2	745	4.3	91.7	751.8	743	6.9	110.1	747.9	741	3.8	84.9	732.1	723	4.7	103.9
j30c5e8	836.7	802	10.4	96.8	839.2	792	14.9	84.6	826.4	790	9.5	83.4	786.8	771	6.7	90.0
j30c5e9	799.4	791	6.8	98.2	800.2	789	15.4	107.3	793.6	788	5.9	106.5	766.9	760	4.8	101.6
j30c5e10	748.9	740	3.2	88.7	746.2	715	11.6	108.8	738.1	712	9.3	93.5	718.5	710	8.7	77.6
Average	733.9	723	6.0	88.3	734.4	717	9.9	100.8	728.5	715	5.4	85.6	710.9	701	5.3	80.2

4.4. *Comparisons among PSO, RKGA, IA, and DGSO in Different Breakdown Cases.* Several metaheuristics have been applied to the RBHFS problem. To evaluate the performance of the proposed DGSO algorithm in solving the RBHFS problem under the criterion makespan, the DGSO algorithm is compared with a PSO algorithm proposed by Liao et al. [32], a RKGA by Gholami et al. [11], and an IA by Zandieh and Gholami [12]. In order to establish more accurate and objective comparisons, the parameters of these algorithms are set following the corresponding literature. All the algorithms were run twenty independent replications for each problem. The comparison results on Liao’s benchmark problems of Case 1 and Case 2 are summarized in Tables 4 and 5. In these two tables, AVE, MIN, STD, and T indicate the values of average, minimum, standard deviation, and the convergence time, respectively.

In Tables 4 and 5, the smallest values of AVE, MIN, STD, and T in the rows are shown in bold. It can be noted that in the preempt-resume case, the overall mean values of AVE, MIN, and STD yielded by the DGSO algorithm are equal to 652.1, 651, and 1.1, respectively, which are much better than those generated by PSO, RKGA, and IA. The DGSO algorithm can converge to better solutions than other three compared algorithms in about the same amount of time, and the same performance is provided in the preempt-repeat case. From these observations, it is concluded that the DGSO algorithm is more effective and efficient in comparison with other methods for the RBHFS problem in both cases.

To confirm whether the observed differences are indeed statistically significant, the authors carry out an analysis of variance (ANOVA). ARE is analyzed by multicompare method using least significant difference (LSD) procedure, where ARE denotes the average relative error to the best solution found by any of the compared algorithms. Obviously, the smaller ARE value is the better result the algorithm yields. The means plots of ARE for all the compared algorithms with LSD intervals at a 95% confidence level in Case 1 and Case 2 are shown in Figures 2 and 3. Note that if the LSD intervals for two means are not overlapping, then the means are significantly different. In Figures 2 and 3, the four algorithms can be divided into two homogenous groups: (PSO, RKGA, and IA) and DGSO, where no statistically significant differences can be found within each group. From these two figures, it is clear that the proposed DGSO algorithm is statistically better than PSO, RKGA, and IA. Considering the stability and robustness [36, 37] of the algorithm, these figures also demonstrate the superiority of the DGSO algorithm under the random breakdown cases.

4.5. *Comparisons of the RBHFS Problem in Different Breakdown Cases.* Figure 4 is the computational result for different breakdown cases of Liao’s benchmark problems, which are achieved by the DGSO algorithm. The authors found that the problem without breakdown takes less time than Case 1, and Case 1 takes less time than Case 2, which is consistent with the theoretical fact. It means that the job without interrupt needs less processing time than the job being interrupted by breakdown, and the job being interrupted by

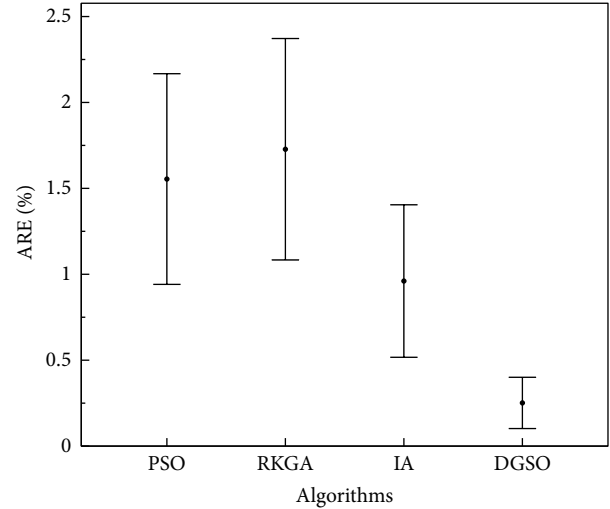


FIGURE 2: Means plot of ARE with 95% LSD intervals for different algorithms in Case 1.

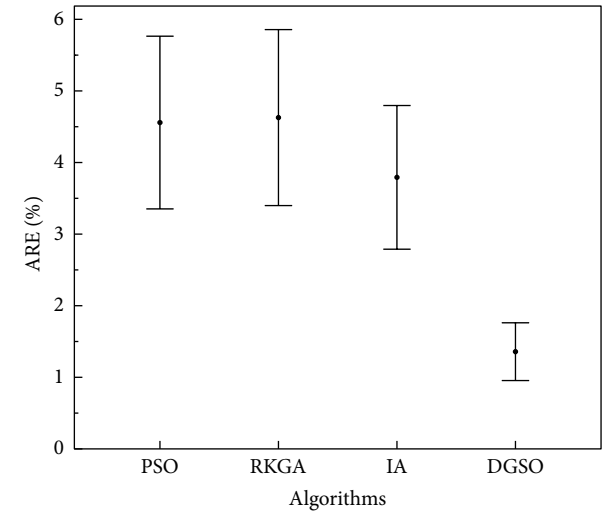


FIGURE 3: Means plot of ARE with 95% LSD intervals for different algorithms in Case 2.

breakdown needs less processing time than the job to be reprocessed. In conclusion, the machine breakdown affects the processing time of the interrupted jobs and influences the scheduling solution, and different breakdown cases have different scheduling schemes.

5. Conclusions

This paper models the hybrid flowshop scheduling problem with random breakdown by analyzing the random breakdown time point and offering an approach to dealing with the breakdown. Then a discrete group search optimizer algorithm is proposed to minimize the makespan of the RBHFS problem. Several efficient operators are introduced for the producers, scroungers, and rangers in the DGSO algorithm. In addition, an orthogonal test is applied to configure the

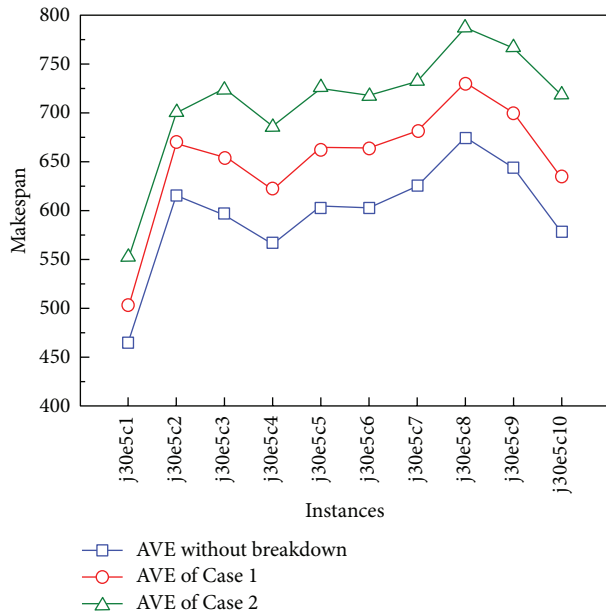


FIGURE 4: The computational results under two breakdown cases and no breakdown case.

algorithm parameters after a small number of experiments. Compared with some state-of-the-art algorithms on the same benchmark problems, the simulation results demonstrate the effectiveness and efficiency of the proposed DGSO algorithm. Future studies can focus on the replication of the DGSO algorithm for other kinds of scheduling problems, such as stochastic scheduling problem and multiobjective scheduling problem.

Conflict of Interests

The authors declare that there is no conflict of interests regarding the publication of this paper.

Acknowledgments

The authors are grateful to the anonymous reviewers for giving us helpful suggestions. This work is supported by National Natural Science Foundation of China (Grant nos. 61174040, 61104178) and Fundamental Research Funds for the Central Universities, Shanghai Commission of Science and Technology (Grant no. 12JC1403400).

References

- [1] M. L. Pinedo, *Scheduling: Theory Algorithms and Systems*, Prentice Hall, Englewood Cliffs, NJ, USA, 2002.
- [2] R. L. Graham, E. L. Lawler, J. K. Lenstra, and A. H. G. Rinnooy-Kan, "Optimization and approximation in deterministic sequencing and scheduling: a survey," *Annals of Discrete Mathematics*, vol. 5, no. 1, pp. 287–326, 1979.
- [3] J. A. Hoogeveen, J. K. Lenstra, and B. Veltman, "Preemptive scheduling in a two-stage multiprocessor flow shop is NP-hard," *European Journal of Operational Research*, vol. 89, no. 1-2, pp. 172–175, 1996.
- [4] R. Ruiz and J. A. Vázquez-Rodríguez, "The hybrid flow shop scheduling problem," *European Journal of Operational Research*, vol. 205, no. 1, pp. 1–18, 2010.
- [5] H. Zhang, Q. Chen, H. Yan, and J. Liu, "Robust H_∞ filtering for switched stochastic system with missing measurements," *IEEE Transactions on Signal Processing*, vol. 57, no. 9, pp. 3466–3474, 2009.
- [6] H. Yan, Z. Su, H. Zhang, and F. Yang, "Observer-based H_∞ control for discrete-time stochastic systems with quantisation and random communication delays," *IET Control Theory & Applications*, vol. 7, no. 3, pp. 372–379, 2013.
- [7] D. Alcaide, A. Rodriguez-Gonzalez, and J. Sicilia, "An approach to solve the minimum expected makespan flow-shop problem subject to breakdowns," *European Journal of Operational Research*, vol. 140, no. 2, pp. 384–398, 2002.
- [8] J. Chen and F. F. Chen, "Adaptive scheduling in random flexible manufacturing systems subject to machine breakdowns," *International Journal of Production Research*, vol. 41, no. 9, pp. 1927–1951, 2003.
- [9] H. Allaoui and A. Artiba, "Integrating simulation and optimization to schedule a hybrid flow shop with maintenance constraints," *Computers and Industrial Engineering*, vol. 47, no. 4, pp. 431–450, 2004.
- [10] H. Tang, C. Zhao, and C. Cheng, "Single machine stochastic JIT scheduling problem subject to machine breakdowns," *Science in China A*, vol. 51, no. 2, pp. 273–292, 2008.
- [11] M. Gholami, M. Zandieh, and A. Alem-Tabriz, "Scheduling hybrid flow shop with sequence-dependent setup times and machines with random breakdowns," *International Journal of Advanced Manufacturing Technology*, vol. 42, no. 1-2, pp. 189–201, 2009.
- [12] M. Zandieh and M. Gholami, "An immune algorithm for scheduling a hybrid flow shop with sequence-dependent setup times and machines with random breakdowns," *International Journal of Production Research*, vol. 47, no. 24, pp. 6999–7027, 2009.
- [13] E. Safari and S. J. Sadjadi, "A hybrid method for flowshops scheduling with condition-based maintenance constraint and machines breakdown," *Expert Systems with Applications*, vol. 38, no. 3, pp. 2020–2029, 2011.
- [14] K. Wang and S. H. Choi, "A decomposition-based approach to flexible flow shop scheduling under machine breakdown," *International Journal of Production Research*, vol. 50, no. 1, pp. 215–234, 2012.
- [15] M. Mirabi, S. M. T. F. Ghomi, and F. Jolai, "A two-stage hybrid flowshop scheduling problem in machine breakdown condition," *Journal of Intelligent Manufacturing*, vol. 24, no. 1, pp. 193–199, 2013.
- [16] S. He, Q. H. Wu, and J. R. Saunders, "A novel group search optimizer inspired by animal behavioural ecology," in *Proceedings of the IEEE Congress on Evolutionary Computation (CEC '06)*, pp. 1272–1278, Vancouver, Canada, July 2006.
- [17] S. He, Q. H. Wu, and J. R. Saunders, "Group search optimizer: an optimization algorithm inspired by animal searching behavior," *IEEE Transactions on Evolutionary Computation*, vol. 13, no. 5, pp. 973–990, 2009.
- [18] L. Wang, X. Zhong, and M. Liu, "A novel group search optimizer for multi-objective optimization," *Expert Systems with Applications*, vol. 39, no. 3, pp. 2939–2946, 2012.

- [19] S. He, Q. H. Wu, and J. R. Saunders, "A group search optimizer for neural network training," in *Computational Science and Its Applications-ICCSA*, Lecture Notes in Computer Science, pp. 934–943, Springer, Berlin, Germany, 2006.
- [20] D. Chen, J. Wang, F. Zou, W. Hou, and C. Zhao, "An improved group search optimizer with operation of quantum-behaved swarm and its application," *Applied Soft Computing*, vol. 12, no. 2, pp. 712–725, 2012.
- [21] Q. H. Wu, Z. Lu, M. S. Li, and T. Y. Ji, "Optimal placement of FACTS devices by a group search optimizer with multiple producer," in *Proceedings of the IEEE Congress on Evolutionary Computation (CEC '08)*, pp. 1033–1039, Hong Kong, June 2008.
- [22] M. Moradi-Dalvand, B. Mohammadi-Ivatloo, A. Najafi, and A. Rabiee, "Continuous quick group search optimizer for solving non-convex economic dispatch problem," *Electric Power Systems Research*, vol. 93, pp. 93–105, 2012.
- [23] H. Shen, Y. Zhu, B. Niu, and Q. H. Wu, "An improved group search optimizer for mechanical design optimization problems," *Progress in Natural Science*, vol. 19, no. 1, pp. 91–97, 2009.
- [24] C. J. Barnard and R. M. Sibly, "Producers and scroungers: a general model and its application to captive flocks of house sparrows," *Animal Behaviour*, vol. 29, no. 2, pp. 543–550, 1981.
- [25] B. Wardono and Y. Fathi, "A tabu search algorithm for the multi-stage parallel machine problem with limited buffer capacities," *European Journal of Operational Research*, vol. 155, no. 2, pp. 380–401, 2004.
- [26] C. Oğuz, Y. Zinder, V. H. Do, A. Janiak, and M. Lichtenstein, "Hybrid flow-shop scheduling problems with multiprocessor task systems," *European Journal of Operational Research*, vol. 152, no. 1, pp. 115–131, 2004.
- [27] C. Oğuz and M. F. Ercan, "A genetic algorithm for hybrid flow-shop scheduling with multiprocessor tasks," *Journal of Scheduling*, vol. 8, no. 4, pp. 323–351, 2005.
- [28] I. D. Couzin, J. Krause, N. R. Franks, and S. A. Levin, "Effective leadership and decision-making in animal groups on the move," *Nature*, vol. 433, no. 7025, pp. 513–516, 2005.
- [29] N. Mladenović and P. Hansen, "Variable neighborhood search," *Computers & Operations Research*, vol. 24, no. 11, pp. 1097–1100, 1997.
- [30] G. L. Deng, Z. Cui, and X. S. Gu, "A discrete artificial bee colony algorithm for the blocking flow shop scheduling problem," in *Proceedings of the 10th World Congress on Intelligent Control and Automation (WCICA '12)*, pp. 518–522, Beijing, China, July 2012.
- [31] R. Ruiz and T. Stützle, "A simple and effective iterated greedy algorithm for the permutation flowshop scheduling problem," *European Journal of Operational Research*, vol. 177, no. 3, pp. 2033–2049, 2007.
- [32] C.-J. Liao, E. Tjandradjaja, and T.-P. Chung, "An approach using particle swarm optimization and bottleneck heuristic to solve hybrid flow shop scheduling problem," *Applied Soft Computing Journal*, vol. 12, no. 6, pp. 1755–1764, 2012.
- [33] R. Zhang and C. Wu, "A hybrid differential evolution and tree search algorithm for the job shop scheduling problem," *Mathematical Problems in Engineering*, vol. 2011, Article ID 390593, 20 pages, 2011.
- [34] H. Zhang, H. Yan, F. Yang, and Q. Chen, "Distributed average filtering for sensor networks with sensor saturation," *IET Control Theory & Applications*, vol. 7, no. 6, pp. 887–893, 2013.
- [35] D. C. Montgomery, *Design and Analysis of Experiments*, John Wiley & Sons, New York, NY, USA, 7th edition, 2008.
- [36] H. Zhang, H. Yan, F. Yang, and Q. Chen, "Quantized control design for impulsive fuzzy networked systems," *IEEE Transactions on Fuzzy Systems*, vol. 19, no. 6, pp. 1153–1162, 2011.
- [37] H. Yan, H. Shi, H. Zhang, and F. Yang, "Quantized H_∞ control for networked systems with communication constraints," *Asian Journal of Control*, vol. 15, no. 5, pp. 1468–1476, 2013.

Research Article

Sampling Based Average Classifier Fusion

Jian Hou,¹ Wei-Xue Liu,¹ and Hamid Reza Karimi²

¹ School of Information Science and Technology, Bohai University, Jinzhou 121013, China

² Department of Engineering, Faculty of Engineering and Science, University of Agder, 4898 Grimstad, Norway

Correspondence should be addressed to Jian Hou; dr.houjian@gmail.com

Received 22 December 2013; Accepted 22 January 2014; Published 24 February 2014

Academic Editor: Xudong Zhao

Copyright © 2014 Jian Hou et al. This is an open access article distributed under the Creative Commons Attribution License, which permits unrestricted use, distribution, and reproduction in any medium, provided the original work is properly cited.

Classifier fusion is used to combine multiple classification decisions and improve classification performance. While various classifier fusion algorithms have been proposed in literature, average fusion is almost always selected as the baseline for comparison. Little is done on exploring the potential of average fusion and proposing a better baseline. In this paper we empirically investigate the behavior of soft labels and classifiers in average fusion. As a result, we find that; by proper sampling of soft labels and classifiers, the average fusion performance can be evidently improved. This result presents sampling based average fusion as a better baseline; that is, a newly proposed classifier fusion algorithm should at least perform better than this baseline in order to demonstrate its effectiveness.

1. Introduction

Object classification is an important task in pattern recognition. Due to the difference in lighting conditions, viewing angles and occlusions, and so forth, there usually exist large intraclass diversity and interclass similarity in real image datasets. This presents great challenges to designing practical object classification systems. While many feature detectors, descriptors, and classification algorithms have been proposed in literature, it is evident that none of these algorithms is able to generate satisfactory classification results for real image datasets. In this case, classifier fusion and feature combination [1] are proposed to combine the decisions of multiple complementary classifiers and produce better performance than any single classifier. In this paper we focus on classifier fusion.

Majority voting is one of the most simple algorithms in classifier fusion. This algorithm uses only the class labeling and discards the probability information of the labels and thus may lead to performance loss. In order to make use of the class probability, average fusion combines the posterior probability of all training classes, that is, the soft labels. Some popular algorithms in this aspect also include weighted sum [2], logistic regression [3], Dempster-Shafer rules [4], and neural networks [5]. In this paper we focus on image

classification. However, the classifier fusion algorithms are also applicable to other domains [6–8].

In proposing a new classifier fusion algorithm, researchers usually choose to compare it with average fusion to show the advantage of the new algorithms. While being simple, average fusion assigns equal weights to all classifiers regardless of their powerfulness. Intuitively this harms the discriminative power of this algorithm and then makes the claimed advantage of newly proposed classifier fusion algorithms less convincing. With this consideration in mind, in this paper we empirically investigate the impact of soft labels and classifiers on classifier fusion performance. As a result, we find that the behaviors of soft labels and classifiers in average fusion can be explained in the framework of kNN classification. This framework gives rise to a sampling based average fusion algorithm, which is shown to outperform the ordinary average fusion evidently in experiments on four diverse image datasets. This result enables us to believe that our sampling based average fusion algorithm explores the potential of average fusion and qualifies as a better baseline. A newly proposed algorithm should be compared with this new baseline to demonstrate its advantage.

The remainder of this paper is organized as follows. In Section 2 we introduce the experimental setups used in our classifier fusion experiments. Sections 3 and 4 present

the details of our work on investigating the behaviors of soft labels and classifiers in average fusion, respectively. In Section 5 we present the sampling based average fusion algorithm based on the experimental results in Sections 3 and 4. Finally, Section 6 concludes the paper.

2. Experimental Setups

We use SVM in classification experiments on four diverse datasets. The regulation parameter C is fixed to be 1000 and the multiclass SVM is trained in a one-versus-all manner. In all experiments we test with 10 different training-testing splits and report the average of recognition rates.

2.1. Datasets. We use the following four datasets in experiments.

The Event-8 dataset [10] contains images from 8 categories of sports events. Each category is composed of 130 to 250 images with different lighting conditions and postures and so forth. Following the experimental setup in [10], we randomly select 70 images per class as training and another 60 images as testing and report the overall recognition rate.

The Scene-15 dataset [11] is composed of images from 15 scene categories with 200 to 400 images in each category. We use the same experimental setup as in [15], that is, randomly selected 100 images per class as training and all the others as testing, and report the mean recognition rate per class.

Oxford Flower-17 dataset [16] consists of 1360 flower images evenly distributed in 17 categories. Similar as in [16], we randomly select 40 images per class as training examples and 20 images as testing images. The overall accuracy is reported as the results.

With the well-known Caltech-101 dataset [15], we use 30 images per class for all the 102 classes in training, and select up to 15 images per class in the remaining for testing. The mean recognition rates per class are reported as the results.

2.2. Features. We use the following features to build the kernels used in SVM classification. These features are popular due to their discriminative power in object classification, for example, in [13, 17, 18]. This makes our conclusions drawn from experiments convincing and meaningful.

PHOG Shape Descriptor. We construct oriented (20 bins) and unoriented (40 bins) PHOG descriptors [19] from level 0 to 3 and obtain 8 descriptors in total. Unlike the implementation in [19], in this paper the descriptor in level L is formed only by its 2^L windows.

Bag-of-SIFT. The SIFT descriptors [20] on patches of radius r with spacing of 8 pixels are extracted and quantized into a 500-bin vocabulary, and we select $r = 4, 8, 12, 16$ to allow for scalability. These descriptors are extracted in gray space for Scene-15 dataset which contains only gray images and, in gray, HSV and CIE-Lab spaces for Flower-17, Event-8, and Caltech-101. We build the visual words histograms from level 0 to 2 and obtain 3 or 9 descriptors.

Locally Binary Patterns. The histograms of the basic locally binary patterns (LBP) [21] are adopted from level 0 to 2.

Gist Descriptor. We extract the global gist descriptor [22] from level 0 to 1.

Self-Similarity Descriptor. The self-similarity descriptors [23] of 30 dimensions (10 orientations and 3 radial bins) are extracted and used to build a 500-bin vocabulary. The histograms are then built from level 0 to 2.

Gabor and RFS Filters. We use two texture features, that is, Gabor and RFS filters [23], to build histograms of 500 bins from level 0 to 2.

Gray Value Histogram. We also use the 64-bin gray value histograms from level 0 to 3.

For all these features, we use χ^2 distance to build kernels in the form of $k(x, y) = \exp(-d_0^{-1}d(x, y))$, where d is the pairwise distances and d_0 is the mean of pairwise distances. Here χ^2 distance is selected due to its great distinctive power, as illustrated in [13, 24–26].

3. Behavior of Soft Labels

In majority voting, each classifier assigns only one label with the largest probability to the testing image. We count the times of each label being selected and adopt the label with the maximum times as the correct one. This approach discards the probability of each label, which may be useful in classifier fusion. Therefore soft labels, that is, the posterior probability of each training label, are proposed to be used in classifier fusion. Between the two extremes, that is, using only the most probable label and using all soft labels in fusion, we are interested to know if it is possible to achieve better performance by adopting a sample of all soft labels.

We evaluate the impact of soft labels sampling on average fusion performance as follows. For each classifier, we sort all labels in descending order according to their posterior probability. Then we use in average fusion only the top k labels, that is, the labels corresponding to k largest probabilities, where k ranges from 1 to the number of all training labels. The experimental results are reported in Figure 1.

It is evident from Figure 1 that, for average fusion, neither adopting only the most probable label nor using all the soft labels is the best choice. Instead, several most probable soft labels generate the best classification results. This is a little similar to the k NN classification framework as the top k most probable soft labels produce the best classification results. Although the best k is different for 4 datasets, $k = 2$ seems an appropriate option as it produces the best or near-best performance for all 4 datasets.

Another interesting observation is that, with the increase of object categories, the performance gain obtained using k most probable soft labels instead of all soft labels is enlarged. From Event-8 to Caltech-101, the performance gain ranges from 0.1 to 10 roughly. This indicates the importance of soft labels sampling, especially for large datasets with a large number of object categories. On the other hand, this

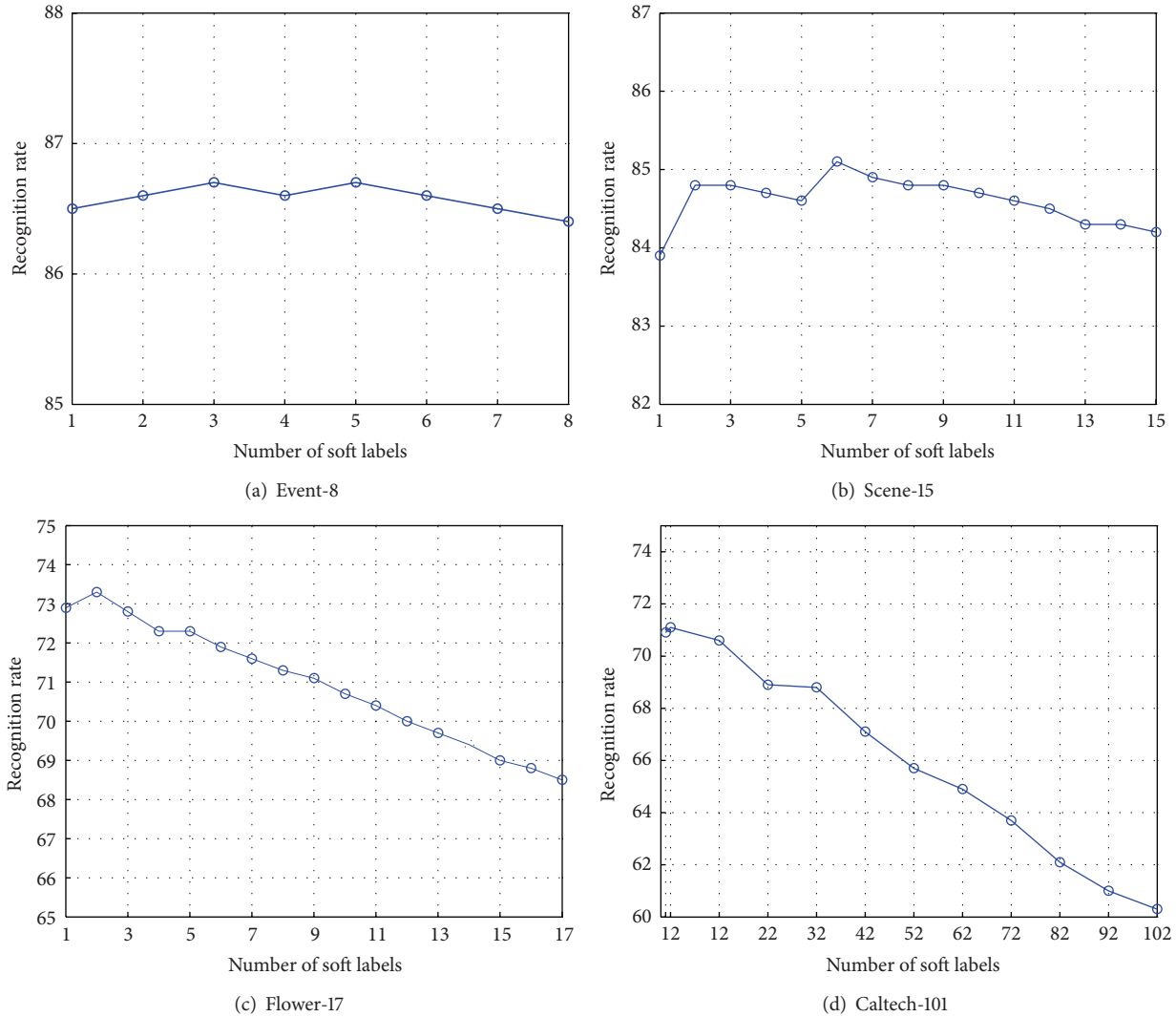


FIGURE 1: Recognition rates from classifier fusion with different numbers of most probable soft labels.

observation highlights the necessity of exploring the potential of average fusion and proposing a better baseline algorithm.

4. Behavior of Classifiers

As classifier fusion is to use multiple classifiers to improve classification performance, another problem of interest is if more classifiers definitely lead to better average fusion performance.

We evaluate the impact of the amount of classifiers on average fusion performance as follows. Firstly, we use the recognition rate of 10-fold cross-validation to estimate the powerfulness of each classifier. In the second step, we sort the classifiers in descending order according to the powerfulness. Then we add the classifiers into fusion one by one and record the fusion performance. The performance with different amounts of classifiers is reported in Figure 2. Note that, in this experiment, we firstly fuse the classifiers from different levels of the same features, for example, all 3 levels of LBP,

and regard the fused decision as of one single classifier. In this way we have 11 classifiers for Caltech-101, Event-8, and Flower-17 and 9 classifiers for Scene-15. This is to compare different classifiers (features) more evidently.

Similar as in the case of soft labels, Figure 2 shows that with average fusion, the best performance is obtained with several most powerful classifiers. Adding more classifiers of less powerfulness into fusion only decreases the final classification performance. It is easy to see that $k = 4$ can be an appropriate selection for the number of classifiers.

5. Sampling Based Average Fusion

In the last two sections we find that using a small sample of most probable soft labels and most powerful classifiers separately helps produce the best fusion performance. Although the optimal number of soft labels, that is, 2, and the optimal number of classifiers, that is, 4, are obtained empirically, they are applied to all the four datasets without special

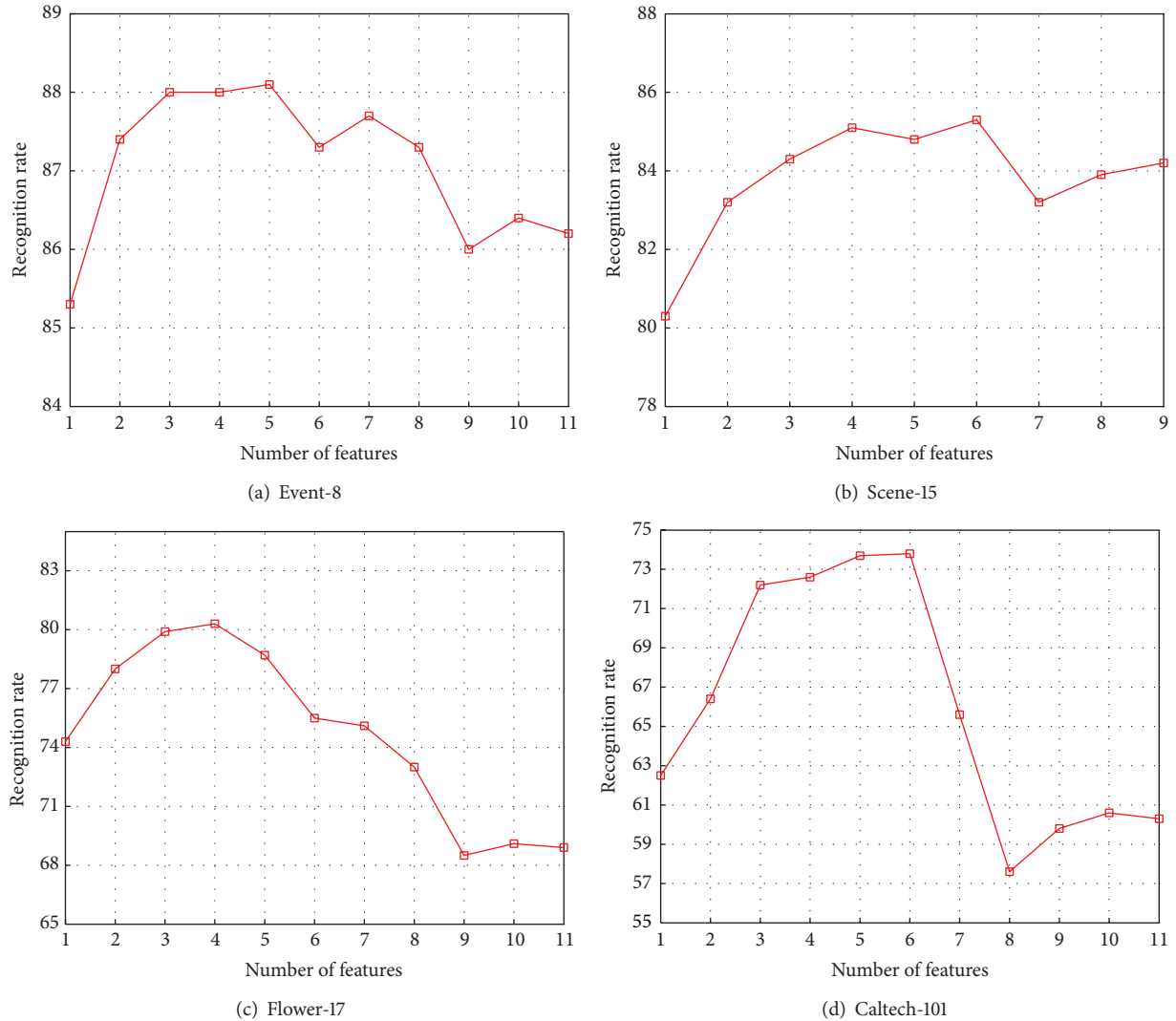


FIGURE 2: Recognition rates from classifier fusion with different numbers of most powerful classifiers.

tuning to individual datasets. Now we test the combined performance of the sampling of both soft labels and classifiers. In experiments on the four datasets, we compare the average fusion performance with and without sampling of soft labels and classifiers and show the results in Tables 1 and 2. In the tables “average1” means recognition rates from average fusion with all classifiers and all soft labels, whereas “average2” indicates corresponding results with sampling of soft labels and classifiers, that is, 2 most probable soft labels and 4 most powerful classifiers. We also compare our algorithm with the state-of-the-art ones on these datasets.

From the comparison we see that, with average fusion, using a small sample of soft labels and classifiers always produces a significant improvement in object classification performance. This means that the sampling based average fusion (SBAF) can serve as a better baseline than ordinary average fusion. Our algorithm performs also comparably to the state-of-the-art ones on these datasets. In fact, on Event-8 and Scene-15 our algorithm produces better results than

TABLE 1: Event-8 and Scene-15 recognition rates and comparison.

Event-8		Scene-15	
Method	Accuracy	Method	Accuracy
Best single	84.6 ± 1.7	Best single	79.3 ± 0.7
Average1	86.4 ± 1.7	Average1	84.2 ± 0.4
Average2	87.9 ± 1.3	Average2	85.0 ± 0.5
[9]	84.2 ± 1.0	[9]	84.1 ± 0.5
[10]	73.4	[11]	81.4 ± 0.5

the state-of-the-art ones, and on Flower-17 and Caltech-101 our results are close to the best ones to date. Noticing that in experiments we only use simple features and average fusion, we believe that this is a very encouraging result which validates the effectiveness of our SBAF algorithm. Since in this paper we present SBAF as a better baseline but not a novel fusion method, we only compare this algorithm with the

TABLE 2: Flower-17 and Caltech-101 recognition rates and comparison.

Flower-17		Caltech-101	
Method	Accuracy	Method	Accuracy
Best single	75.1 ± 1.5	Best single	66.2 ± 1.2
Average1	77.5 ± 1.7	Average1	58.8 ± 1.7
Average2	86.0 ± 1.5	Average2	71.0 ± 1.2
[12]	88.3 ± 0.3	[13]	77.8 ± 0.4
[13]	85.5 ± 3.0	[14]	66.2 ± 0.5

ordinary average fusion and not with other fusion methods, for example, [2, 4].

Another observation from experiments is that the behaviors of soft labels and classifiers can be explained in the framework of k NN classification. Regarding the most probable soft labels and most powerful classifiers as the nearest neighbors, we can explain all the observations from experiments based on the k NN framework easily. This framework provides theoretical support to our following conclusions. Firstly, the best performance of average fusion is not achieved with all soft labels and all classifiers, but with a sample of most probable soft labels and most powerful classifiers. This gives rise to SBAF as a better baseline. Secondly, with a dataset of tens to hundreds of categories, the performance gain of SBAF over average fusion can be rather large (over 10 for Caltech-101). Since in modern time there is an explosive increase in the amounts and categories of images, this observation highlights the importance of soft label and classifier sampling and the necessity to adopt SBAF as the baseline.

Although in this paper we focus our work on image classification, the idea of classifier fusion is also useful to some other related domains, for example, document classification, speech recognition, and fault diagnosis [27–29]. In the next step we plan to explore the possibility of extending the work to more domains [30–32].

6. Conclusion

In this paper we investigated the impact of soft labels and classifiers sampling on average classifier fusion performance through experiments on four diverse datasets. As a result, we found that the behaviors of soft labels and classifiers in average fusion can be elegantly explained in the framework of k NN classification. This framework further gives rise to a sampling based average fusion method, that is, using a sample of most probable soft labels and most powerful classifiers in fusion to obtain the best performance. Experiments indicate that this sampling based average fusion performs evidently better than the ordinary one and thus can serve as a better baseline to be compared with. Our results on the four datasets are also comparable to the state of the art in literature. As the k NN framework elegantly captures the behaviors of soft labels and classifiers in classifier fusion, we believe that it can be helpful in designing novel classifier fusion methods.

Conflict of Interests

The authors declare that there is no conflict of interests regarding the publication of this paper.

Acknowledgments

This work is supported by National Natural Science Foundation of China (Grant no. 61304102), Natural Science Foundation of Liaoning Province of China (Grant no. 2013020002), and Scientific Research Fund of Liaoning Provincial Education Department under Grant no. L2012400.

References

- [1] X. Li, W. Yang, and J. Dezert, "An airplane image target's multi-feature fusion recognition method," *Acta Automatic Sinica*, vol. 38, pp. 1298–1307, 2012.
- [2] C. C. Chibelushi, F. Deravi, and J. S. D. Mason, "Adaptive classifier integration for robust pattern recognition," *IEEE Transactions on Systems, Man, and Cybernetics B*, vol. 29, no. 6, pp. 902–907, 1999.
- [3] T. K. Ho, J. J. Hull, and S. N. Srihari, "Decision combination in multiple classifier systems," *IEEE Transactions on Pattern Analysis and Machine Intelligence*, vol. 16, no. 1, pp. 66–75, 1994.
- [4] L. Xu, A. Krzyzak, and C. Y. Suen, "Methods of combining multiple classifiers and their applications to handwriting recognition," *IEEE Transactions on Systems, Man and Cybernetics*, vol. 22, no. 3, pp. 418–435, 1992.
- [5] D. S. Lee, *Theory of classifier combination: the neural network approach [Ph.D. thesis]*, SUNY, Buffalo, NY, USA, 1995.
- [6] S. Yin, S. Ding, A. Haghani, H. Hao, and P. Zhang, "A comparison study of basic datadriven fault diagnosis and process monitoring methods on the benchmark tennessee eastman process," *Journal of Process Control*, vol. 22, pp. 1567–1581, 2012.
- [7] S. Yin, X. Yang, and H. R. Karimi, "Data-driven adaptive observer for fault diagnosis," *Mathematical Problems in Engineering*, vol. 2012, Article ID 832836, 21 pages, 2012.
- [8] S. Yin, G. Wang, and H. Karimi, "Data-driven design of robust fault detection system for wind turbines," *Mechatronics*, 2013.
- [9] J. X. Wu and J. M. Rehg, "Beyond the Euclidean distance: creating effective visual codebooks using the histogram intersection kernel," in *Proceedings of the IEEE 12th International Conference on Computer Vision (ICCV '09)*, pp. 630–637, October 2009.
- [10] L.-J. Li and L. Fei-Fei, "What, where and who? Classifying events by scene and object recognition," in *Proceedings of the IEEE 11th International Conference on Computer Vision (ICCV '07)*, pp. 1–8, October 2007.
- [11] S. Lazebnik, C. Schmid, and J. Ponce, "Beyond bags of features: spatial pyramid matching for recognizing natural scene categories," in *Proceedings of the IEEE Computer Society Conference on Computer Vision and Pattern Recognition (CVPR '06)*, vol. 2, pp. 2169–2178, June 2006.
- [12] M.-E. Nilsback and A. Zisserman, "Automated flower classification over a large number of classes," in *Proceedings of the 6th Indian Conference on Computer Vision, Graphics and Image Processing (ICVGIP '08)*, pp. 722–729, December 2008.
- [13] P. Gehler and S. Nowozin, "On feature combination for multi-class object classification," in *Proceedings of the IEEE International Conference on Computer Vision*, pp. 221–228, 2009.

- [14] H. Zhang, A. C. Berg, M. Maire, and J. Malik, "SVM-KNN: discriminative nearest neighbor classification for visual category recognition," in *Proceedings of the IEEE Computer Society Conference on Computer Vision and Pattern Recognition (CVPR '06)*, pp. 2126–2136, June 2006.
- [15] L. Fei-Fei, R. Fergus, and P. Perona, "Learning generative visual models from fewtraining examples: an incremental bayesian approach tested on 101 object categories," in *Workshop on Generative-Model Based Vision (CVPR '04)*, p. 178, 2004.
- [16] M.-E. Nilsback and A. Zisserman, "A visual vocabulary for flower classification," in *Proceedings of the IEEE Computer Society Conference on Computer Vision and Pattern Recognition (CVPR '06)*, pp. 1447–1454, June 2006.
- [17] J. Yang, Y. N. Li, Y. H. Tian, L. Y. Duan, and W. Gao, "Group-sensitive multiple kernel learning for object categorization," in *Proceedings of the IEEE 12th International Conference on Computer Vision (ICCV '09)*, pp. 436–443, October 2009.
- [18] J. Hou, W. X. Liu, and H. R. Karimi, "Exploring the best classification from average feature combination," *Abstract and Applied Analysis*, vol. 2014, Article ID 602763, 7 pages, 2014.
- [19] A. Bosch, A. Zisserman, and X. Munoz, "Representing shape with a spatial pyramid kernel," in *Proceedings of the 6th ACM International Conference on Image and Video Retrieval (CIVR '07)*, pp. 401–408, July 2007.
- [20] D. G. Lowe, "Distinctive image features from scale-invariant keypoints," *International Journal of Computer Vision*, vol. 60, no. 2, pp. 91–110, 2004.
- [21] T. Ojala, M. Pietikäinen, and T. Mäenpää, "Multiresolution gray-scale and rotation invariant texture classification with local binary patterns," *IEEE Transactions on Pattern Analysis and Machine Intelligence*, vol. 24, no. 7, pp. 971–987, 2002.
- [22] A. Oliva and A. Torralba, "Modeling the shape of the scene: a holistic representation of the spatial envelope," *International Journal of Computer Vision*, vol. 42, no. 3, pp. 145–175, 2001.
- [23] E. Shechtman and M. Irani, "Matching local self-similarities across images and videos," in *Proceedings of the IEEE Computer Society Conference on Computer Vision and Pattern Recognition (CVPR '07)*, pp. 1–8, June 2007.
- [24] J. Hou, B. P. Zhang, N. M. Qi, and Y. Yang, "Evaluating feature combination in object classification," in *Proceedings of the International Symposium on Visual Computing*, pp. 597–606, 2011.
- [25] J. Hou and M. Pelillo, "A simple feature combination method based on dominant sets," *Pattern Recognition*, vol. 46, pp. 3129–3139, 2013.
- [26] J. Hou, W. X. Liu, E. Xu, Q. Xia, and N. M. Qi, "An experimental study on the universality of visual vocabularies," *Journal of Visual Communication and Image Representation*, vol. 24, pp. 1204–1211, 2013.
- [27] S. Yin, H. Luo, and S. Ding, "Real-time implementation of fault-tolerant control systems with performance optimization," *IEEE Transactions on Industrial Electronics*, vol. 61, pp. 2402–2411, 2014.
- [28] A. Baak, M. Muller, G. Bharaj, H.-P. Seidel, and C. Theobalt, "A data-driven approach for real-time full body pose reconstruction from a depth camera," in *Proceedings of the IEEE International Conference on Computer Vision (ICCV '11)*, pp. 1092–1099, November 2011.
- [29] S. Yin, S. X. Ding, A. H. A. Sari, and H. Hao, "Data-driven monitoring for stochastic systems and its application on batch process," *International Journal of Systems Science*, vol. 44, no. 7, pp. 1366–1376, 2013.
- [30] X. Zhao, L. Zhang, P. Shi, and M. Liu, "Stability and stabilization of switched linear systems with mode-dependent average dwell time," *IEEE Transactions on Automatic Control*, vol. 57, no. 7, pp. 1809–1815, 2012.
- [31] X. Zhao, H. Liu, and J. Zhang, "Multiple-mode observer design for a class of switched linear systems linear systems," *IEEE Transactions on Automation Science and Engineering*, 2013.
- [32] X. Zhao, L. Zhang, P. Shi, and H. R. Karimi, "Novel stability criteria for t-s fuzzy systems," *IEEE Transactions on Fuzzy Systems*, vol. 21, pp. 1–11, 2013.

Research Article

Effects of Surfactants on the Performance of CeO₂ Humidity Sensor

Chunjie Wang,¹ Aihua Zhang,¹ and Hamid Reza Karimi²

¹ College of Engineering, Bohai University, Jinzhou 121013, China

² Department of Engineering, Faculty of Engineering and Science, University of Agder, 4898 Grimstad, Norway

Correspondence should be addressed to Chunjie Wang; cjwang@foxmail.com

Received 25 December 2013; Accepted 18 January 2014; Published 24 February 2014

Academic Editor: Xudong Zhao

Copyright © 2014 Chunjie Wang et al. This is an open access article distributed under the Creative Commons Attribution License, which permits unrestricted use, distribution, and reproduction in any medium, provided the original work is properly cited.

Nanosized CeO₂ powders were synthesized via hydrothermal method with different types of surfactants (polyethylene glycol (PEG), cetyltrimethylammonium bromide (CTAB), and sodium dodecylbenzenesulfonate (SDBS)). X-ray diffraction, Raman spectroscopy, and transmission electron microscopy were utilized to characterize the phase structures and morphologies of the products. The sample with CTAB as surfactant (CeO₂-C) has the largest specific surface area and the smallest particle size among these three samples. The humidity sensor fabricated by CeO₂-C shows higher performance than those used CeO₂-P and CeO₂-S. The impedance of the CeO₂-C sensor decreases by about five orders of magnitude with relative humidity (RH) changing from 15.7 to 95%. The response and recovery time are 7 and 7 s, respectively. These results indicate that the performance of CeO₂ humidity sensors can be improved effectively by the addition of cationic surfactant.

1. Introduction

In recent decades, humidity sensors have received intense interests for their wide applications in environment protection, agriculture, and industrial production driven by the recognized importance of vapor concentration [1–4]. The materials for humidity sensors are generally including organic polymer films and porous ceramic films [5, 6]. The main disadvantages of humidity sensors based on the former are the weak mechanical strength, poor physical and chemical stability, and low operation temperature. For the latter, the dull response and recovery time are the main challenge. In recent years, many efforts have been carried out to explore the materials of humidity sensors, such as SnO₂, TiO₂, ZnO, and BaTiO₃ [7–10]. As one of the candidate materials of sensor, cerium oxide shows large diffusion coefficient for oxygen vacancy and good corrosion resistance to corrosive gases (Cl₂, SO₂ and NO) [11]. Based on the merit mentioned above, CeO₂ becomes heatedly discussed topic in recent years.

In the past few years, several methods have been proposed to prepare fine nanopowders. Hydrothermal method is considered as one of the most promising techniques for the room

temperature manufacture of nanopowders, which can be attributed to the advantages related to the homogeneous nucleation processes and fine grain size. However, due to the high surface energy, nanoparticles are easy to coagulate and difficult to disperse. It is well known that serious agglomeration has an adverse effect on the properties of sensors during the filming process. Kinds of surfactants have been introduced to improve the performance of the materials [12, 13]. Nevertheless, to the best of our knowledge, the systematic investigation of the effects of different types of surfactants (nonionic, cationic, and anionic) on the performance of CeO₂ as humidity sensor has not been reported. To improve the performance of sensing materials, it is essential to make insight into the characteristics with different surfactants.

In this paper, three different kinds of surfactants, that is, PEG (nonionic), CTAB (cationic), and SDBS (anionic), were used as surfactants to prepare CeO₂ nanopowders via hydrothermal process, and the effects of surfactants on the structures and the humidity sensing properties of the corresponding sensors were investigated in detail. The main purpose of this study is to clarify the influence of surfactants on the performance of the CeO₂ humidity sensor.

2. Experimental Details

Based on the conventional hydrothermal method, CeO₂ nanopowders with different surfactants were synthesized as follows: Ce(NO₃)₃·6H₂O (99.99%, Chenghai Chemical of Guangdong), CTAB, PEG, and SDBS (Shanghai Chemicals Ltd.) were used as starting material and surfactants. A certain amount of surfactants (2 wt.%) was added into 50 mL of Ce(NO₃)₃ solution (0.1 M) under magnetic stirring. The pH value of the solution was adjusted to 7 by adding sodium hydroxide solution (2 M). Then, CeO₂ nanopowders were obtained by hydrothermal treatment for the mixed solution at 180 °C for 24 h in a Teflon autoclave. The precipitates were filtered and washed with distilled water and ethanol for several times and dried at 70 °C for 12 h. The same procedure was followed for the preparation of CeO₂ nanocrystalline powders by using CTAB, PEG, and SDBS as surfactants, respectively. In this paper, three produced CeO₂ nanopowders were designated as CeO₂-P, CeO₂-C, and CeO₂-S, respectively.

The crystalline phases of CeO₂ nanocrystalline powders were examined by means of powder X-ray diffraction (XRD, Bruker D8 Focus powder X-ray diffractometer) using Cu K α radiation ($\lambda = 1.5406 \text{ \AA}$) with a scanning rate of $5^\circ \cdot \text{min}^{-1}$. The operation current and voltage were maintained at 40 mA and 40 kV, respectively. The lattice parameters were calculated based on these XRD patterns. The average particle size of nanopowders (D) was determined by Scherrer's equation [14]:

$$D = \lambda \frac{K}{\beta \cos \theta}, \quad (1)$$

where λ is the wavelength of the X-ray radiation, θ is the diffraction angle, K is a constant (0.89), and β is the corrected full-width half maximum (FWHM). The Gaussian-Gaussian relationship [14] was also used for the instrument correction:

$$\beta^2 = B^2 - b^2, \quad (2)$$

where FWHM of the sample and the standard width of reference silicon sample are represented by B and b , respectively.

FT-Raman spectra were recorded on a Thermo Nicolet 960 instrument with an excitation wavelength of 1064 nm, and the measured wave number range is from 100 to 900 cm^{-1} . The specific surface area (S_{BET}) was determined by applying Brunauer-Emmet-Teller (BET) equation [15, 16] with a Micromeritics ASAP2020 instrument. The microstructures, morphologies, and particle sizes of the three samples were examined by a Philips TF-F20 electron transmission microscope.

In order to fabricate the humidity sensors, the CeO₂ nanopowders were dispersed in ethanol by magnetic stirring (30 min). The mixed solution was dropped onto a ceramic substrate (6 cm \times 3 cm, 0.5 cm in thick) with a pair of Ag-Pd interdigital electrodes to form a CeO₂ film with a thickness of 10 μm . Furthermore, the humidity sensors were annealed at 180 °C for 1 h. The characteristic curves of humidity sensitivity were measured on a ZL-5 model LCR analyzer (Shanghai, China). In our study, the voltage was fixed at 1 V. The humidity environments were obtained by

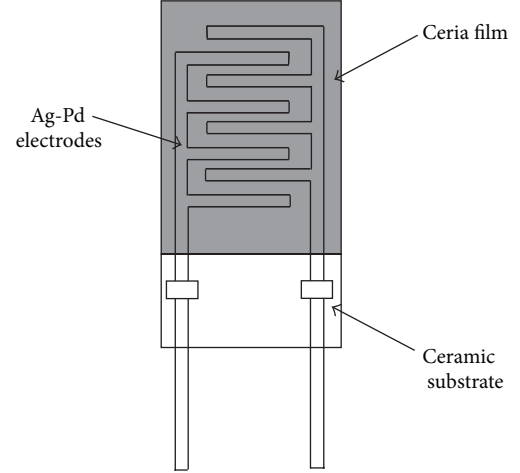


FIGURE 1: Schematic diagram of the sensor structure.

using MgCl₂, Mg(NO₃)₃, NaCl, KCl, and KNO₃ saturated salt solutions, and the corresponding RH values were 33, 54, 75, 85, and 95%, respectively. The humidity of laboratory atmosphere was 15.7% RH controlled by an automatic drier. Figure 1 shows the schematic diagram of the sensor structure.

3. Results and Discussion

The crystal structures of the as-prepared products were examined by XRD, and the corresponding results are shown in Figure 2(a). The XRD patterns of three samples show a face-centered cubic structure of ceria [JCPDS 43-1002]. As shown in Figure 2(a), the peaks at round $2\theta = 29.8^\circ$, 34.6° , 49.6° , 59.2° , and 72.8° are assigned to the (111), (200), (220), (311), and (400) reflections, respectively. It is worth noting that the diffraction peak width of CeO₂-C is wider than those of CeO₂-P and CeO₂-S, implying that the grain size of CeO₂-C is the smallest among the three samples. In addition, the composition of the as-synthesized products was further examined using an energy dispersive X-ray spectrometer (EDS). Figure 2(b) shows the EDS spectrum of CeO₂-C, and only three elements (Ce, O and Si) can be identified in this spectrum. The chemical composition of CeO₂-C is very close to the stoichiometric composition of CeO₂. The presence of Si in the spectrum can be attributed to the Si substrate. Furthermore, the average crystallite sizes, specific surface areas, and lattice parameters of three samples were also investigated, as shown in Table 1. The crystal size was calculated by Scherrer's equation as mentioned in experimental section. For CeO₂-C, the average crystallite size is 17.34 nm, while those of CeO₂-P and CeO₂-S are 19.27 and 21.42 nm, respectively. The lattice parameters are calculated from the XRD patterns using software JADE 5.0, and the determined value of each lattice parameter is the average value of 5 samples. For CeO₂-C, the calculated value is $5.3945 \pm 0.0002 \text{ nm}$, which is higher than those of CeO₂-P ($5.3726 \pm 0.0002 \text{ nm}$) and CeO₂-S ($5.3544 \pm 0.0003 \text{ nm}$). In the case of specific surface area, the values for CeO₂-C, CeO₂-P, and CeO₂-S are 143.45, 116.87, and 99.36 $\text{m}^2 \cdot \text{g}^{-1}$, respectively. For nanomaterials, the crystal

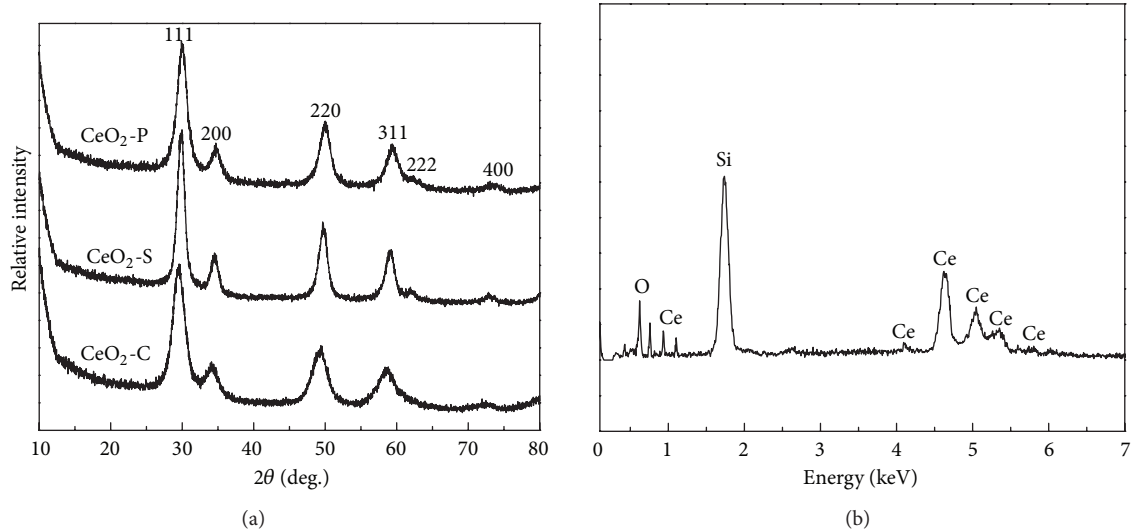


FIGURE 2: XRD patterns of the as-synthesized samples (a) and EDS pattern of as-prepared $\text{CeO}_2\text{-C}$ (b).

TABLE 1: The specific surface areas, crystalline sizes, and lattice parameters for three samples.

Samples	Specific surface area ($\text{m}^2\cdot\text{g}^{-1}$)	Crystallite size (nm)	Lattice parameter (nm)
$\text{CeO}_2\text{-P}$	116.87	19.27	5.3726 ± 0.0002
$\text{CeO}_2\text{-C}$	143.45	17.34	5.3945 ± 0.0002
$\text{CeO}_2\text{-S}$	99.36	21.42	5.3544 ± 0.0003

size is closely related to the specific surface area. The smaller the crystal size is, the higher the specific surface area will be. From the data of average particle sizes mentioned above, the specific surface areas of these three samples should decrease in the following order: $\text{CeO}_2\text{-C} > \text{CeO}_2\text{-P} > \text{CeO}_2\text{-S}$. This trend is coincident with the measurement values in this study. As is well known, the structure, surface area, crystallite size could be influenced by the different elective adsorption processes and the interactions between the surfactant and inorganic precursor molecules during the nucleation process. However, the related mechanism is more complicated and needs to be further investigated.

In order to confirm the phase structure, the as-prepared samples were further examined by Raman spectroscopy in the wave number range of $100\sim 900\text{ cm}^{-1}$, as represented in Figure 3. Careful investigation of the spectra revealed a detailed structure of cubic type. It can be noted from Figure 3 that the main band at 469 cm^{-1} can be attributed to the F_{2g} vibration mode from the space group $Fm\bar{3}m$ of cubic structure [17, 18]. This further confirms that the structures of three samples are cubic phase as mentioned in XRD analysis. Moreover, it can be seen that a small shoulder appeared at about 600 cm^{-1} , which should be assigned as the longitudinal optical mode [19]. In the present case, the intensity of the band at 469 cm^{-1} for $\text{CeO}_2\text{-C}$ is higher than those for the other two samples.

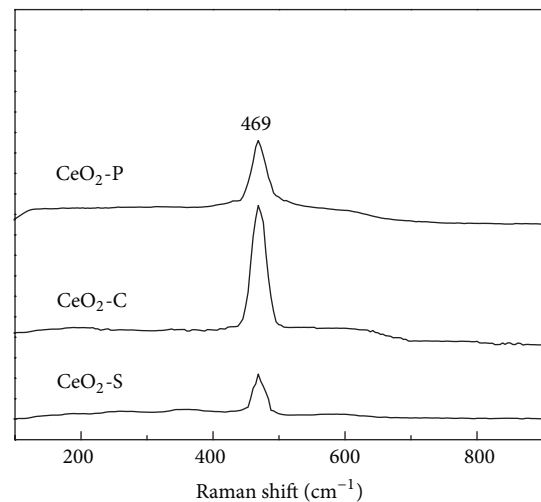


FIGURE 3: Raman spectra of $\text{CeO}_2\text{-P}$, $\text{CeO}_2\text{-C}$, and $\text{CeO}_2\text{-S}$ nanopowders.

The morphologies and particle sizes of three samples were investigated by TEM, as shown in Figure 4. All of these three samples show a monodispersed square shape, and the particle size of $\text{CeO}_2\text{-C}$ is more uniform than those of $\text{CeO}_2\text{-P}$ and $\text{CeO}_2\text{-S}$. The average particle sizes of three samples were also calculated, and the determined particle size was the averaged value of 40 particles selected randomly in the figure. For $\text{CeO}_2\text{-P}$, $\text{CeO}_2\text{-C}$, and $\text{CeO}_2\text{-S}$, the calculated average particle sizes are 19.76, 17.88, and 21.77 nm, respectively. These results are consistent with earlier data in XRD analysis mentioned above.

Figure 5 shows the characteristics of resistance versus relative humidity (RH) of three samples with different surfactants measured at room temperature in the relative humidity range from 15.7 to 95%. In this study, the surfactants obviously have an important influence on the humidity dependence of

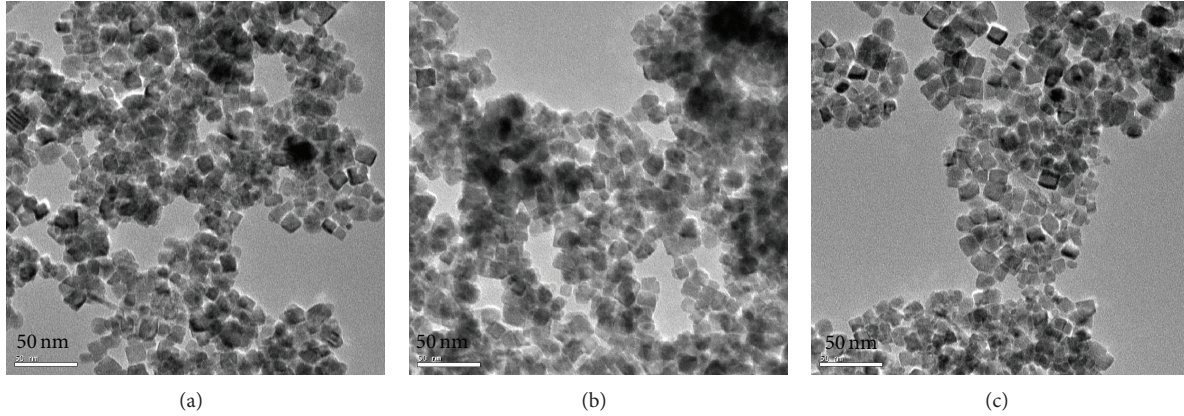


FIGURE 4: TEM image of three as-prepared samples: (a) $\text{CeO}_2\text{-P}$, (b) $\text{CeO}_2\text{-C}$, and (c) $\text{CeO}_2\text{-S}$.

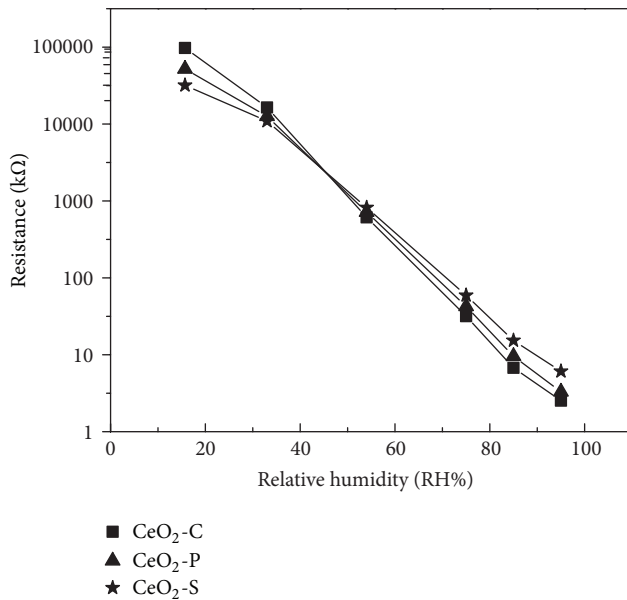


FIGURE 5: Resistance versus RH plots of CeO_2 sensor with different surfactants.

the impedance of sensors. As a comparison among these three samples, the decrease of impedance for $\text{CeO}_2\text{-C}$ is greater than those for $\text{CeO}_2\text{-P}$ and $\text{CeO}_2\text{-S}$. The high humidity sensitivity and the best linearity of the impedance versus RH curve appeared in $\text{CeO}_2\text{-C}$. By contrast, in the case of $\text{CeO}_2\text{-S}$, the situation is just the reverse compared with $\text{CeO}_2\text{-C}$. For $\text{CeO}_2\text{-C}$, moreover, the impedance change is more than five orders of magnitude.

Response and recovery behaviors are the significant characteristics for estimating the performance of humidity sensor. Response time for adsorption process and recovery time in the case of desorption are defined as the time taken by the sensor to achieve 90% variable quantity. Based on the results mentioned above, the response and recovery behaviors of three samples were investigated. The sensor is transferred from initial atmosphere (33% RH) to target atmosphere (95% RH) and transferred back to investigate

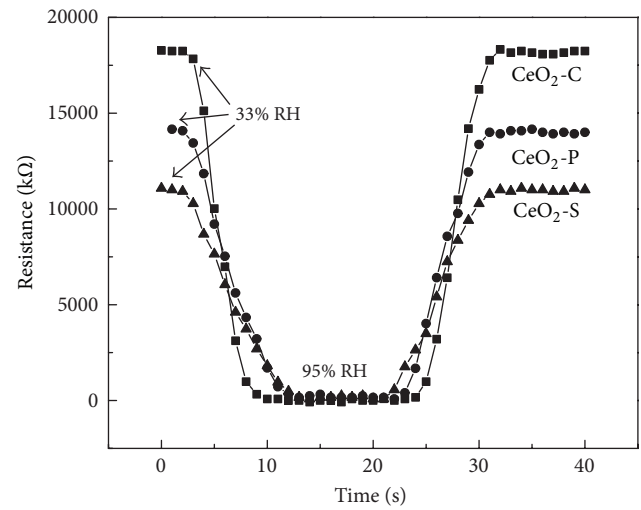


FIGURE 6: Response and recovery characteristics of CeO_2 sensors with different surfactants.

the response and recovery time, respectively. As shown in Figure 6, the humidity sensor fabricated from $\text{CeO}_2\text{-C}$ shows rapid response-recovery characteristics. The response time (humidification from 33 to 95% RH) and the recovery time (desiccation from 95 to 33% RH) are about 7 s and 7 s, respectively. In the cases of $\text{CeO}_2\text{-P}$ and $\text{CeO}_2\text{-S}$, however, the corresponding response and recovery time are 10, 9 s and 12, 11 s, respectively. Such facts indicate that the cationic surfactant (CTAB) has a significant effect on improving the performance of CeO_2 humidity sensors.

It is well known that the humidity sensing is closely related to the adsorption process of water molecules on the surface of the nanoparticles. The number of water molecules adsorbed on the powders has an important effect on electrical response. In the case of low humidity, only a few water molecules can be adsorbed on the surface of the film by the chemisorption mechanism [20–22]. The discontinuous layer of water molecules on the surface of the film leads to the difficulty of electrolytic conduction. According to

Schaub et al. studies [23–25], the high local charge density and a strong electrostatic field result from the tip, defects, and contracts of the powders can promote water dissociation to provide charge carriers. For high humidity, however, more and more water layers can be formed on the surface of nanoparticles by physisorption mechanism. As the dominant charged carriers, H^+ decomposed from water molecules can further decrease the impedance. On the other hand, in our study, the nanosized grains and the high specific surface area also play an important role in the sensor performance. The nanoscale grain size shows much more grain boundaries which produce large amount of active sites available for water molecules to react. Also, the CeO_2 -C nanoparticles have the largest specific surface area among the three samples. The large surface of the nanomaterials makes the water molecules absorbed on the surface of the sensor easily, which can improve the response and recovery characteristics. So the response and recovery time of CeO_2 -C are faster compared with CeO_2 -P and CeO_2 -S. In accordance with the results of the study, a conclusion can be drawn that cationic surfactant (CTAB) has a significant effect on improving the sensibility of CeO_2 humidity sensor compared with nonionic surfactant (PEG) and anionic surfactant (SDBS).

4. Conclusions

CeO_2 nanoparticles with three different types of surfactants were synthesized via hydrothermal method. The CeO_2 -C has the largest specific surface area and the smallest particle size. The performances of the corresponding sensors were also investigated in detail. By comparison, cationic surfactant (CTAB) has a significant effect on improving the performance of humidity sensor compared with the other two surfactants (nonionic (PEG) and anionic (SDBS)). The CeO_2 -C humidity sensor shows a high sensitivity, fast response (7 s), and rapid recovery (7 s) characteristics in the humidity range of 33~95% RH, while the response and recovery time for CeO_2 -P and CeO_2 -S are 10, 9 s and 12, 11 s, respectively.

Conflict of Interests

The authors declare that there is no conflict of interests regarding the publication of this paper.

Acknowledgment

This work was supported by the National Natural Science Foundation of China under Grant no. 11347167.

References

- [1] S. Zampolli, I. Elmi, J. Stürmann, S. Nicoletti, L. Dori, and G. C. Cardinali, "Selectivity enhancement of metal oxide gas sensors using a micromachined gas chromatographic column," *Sensors and Actuators B*, vol. 105, no. 2, pp. 400–406, 2005.
- [2] S. Ehrmann, J. Jüngst, J. Goschnick, and D. Everhard, "Application of a gas sensor microarray to human breath analysis," *Sensors and Actuators B*, vol. 65, no. 1, pp. 247–249, 2000.
- [3] S. Yin, G. Wang, and H. Karimi, "Data-driven design of robust fault detection system for wind turbines," *Mechatronics*, 2013.
- [4] S. Yin, H. Luo, and S. Ding, "Real-time implementation of fault-tolerant control systems with performance optimization," *IEEE Transactions on Industrial Electronics*, vol. 61, no. 5, pp. 2402–2411, 2014.
- [5] X. Q. Fu, C. Wang, H. C. Yu, Y. G. Wang, and T. H. Wang, "Fast humidity sensors based on CeO_2 nanowires," *Nanotechnology*, vol. 18, no. 14, Article ID 145503, 2007.
- [6] S. Yin, S. Ding, A. Haghani, H. Hao, and P. Zhang, "A comparison study of basic data-driven fault diagnosis and process monitoring methods on the benchmark Tennessee Eastman process," *Journal of Process Control*, vol. 22, no. 9, pp. 1567–1581, 2012.
- [7] Q. Kuang, C. Lao, Z. L. Wang, Z. Xie, and L. Zheng, "High-sensitivity humidity sensor based on a single SnO_2 nanowire," *Journal of the American Chemical Society*, vol. 129, no. 19, pp. 6070–6071, 2007.
- [8] G. Garcia-Belmonte, V. Kytin, T. Dittlrich, and J. Bisquert, "Effect of humidity on the ac conductivity of nanoporous TiO_2 ," *Journal of Applied Physics*, vol. 94, no. 8, pp. 5261–5264, 2003.
- [9] Y. Qiu and S. Yang, "ZnO nanotetrapods: controlled vapor-phase synthesis and application for humidity sensing," *Advanced Functional Materials*, vol. 17, no. 8, pp. 1345–1352, 2007.
- [10] J. Wang and G. Song, "Mechanism analysis of $BaTiO_3$ and polymer QAR composite humidity sensor," *Thin Solid Films*, vol. 515, no. 24, pp. 8776–8779, 2007.
- [11] E. B. Várhegyi, I. V. Perczel, J. Gerblinger, M. Fleischer, H. Meixner, and J. Giber, "Auger and SIMS study of segregation and corrosion behaviour of some semiconducting oxide gas-sensor materials," *Sensors and Actuators B*, vol. 19, no. 1–3, pp. 569–572, 1994.
- [12] R. R. Piticescu, C. Monty, D. Taloi, A. Motoc, and S. Axinte, "Hydrothermal synthesis of zirconia nanomaterials," *Journal of the European Ceramic Society*, vol. 21, no. 10–11, pp. 2057–2060, 2001.
- [13] D. K. Smith and B. A. Korgel, "The importance of the CTAB surfactant on the colloidal seed-mediated synthesis of gold nanorods," *Langmuir*, vol. 24, no. 3, pp. 644–649, 2008.
- [14] H. Y. Jin, N. Wang, L. Xu, and S. Hou, "Synthesis and conductivity of cerium oxide nanoparticles," *Materials Letters*, vol. 64, no. 11, pp. 1254–1256, 2010.
- [15] S. Yin, S. Ding, A. Haghani, and H. Hao, "Data-driven monitoring for stochastic systems and its application on batch process," *International Journal of Systems Science*, vol. 44, no. 7, pp. 1366–1376, 2013.
- [16] S. Brunauer, P. H. Emmett, and E. Teller, "Adsorption of gases in multimolecular layers," *Journal of the American Chemical Society*, vol. 60, no. 2, pp. 309–319, 1938.
- [17] Z. D. Dohcevic-Mitrovic, M. J. Šćepanović, M. U. Grujić-Brojčin et al., "The size and strain effects on the Raman spectra of $Ce_{1-x}Nd_xO_{2-\delta}$ ($0 < x < 0.25$) nanopowders," *Solid State Communications*, vol. 137, no. 7, pp. 387–390, 2006.
- [18] S. Patil, S. Seal, Y. Guo, A. Schulte, and J. Norwood, "Role of trivalent La and Nd dopants in lattice distortion and oxygen vacancy generation in cerium oxide nanoparticles," *Applied Physics Letters*, vol. 88, no. 24, Article ID 243110, 2006.
- [19] Z. Xu, S. He, L. He, R. Mu, G. Huang, and X. Cao, "Novel thermal barrier coatings based on $La_2(Zr_{0.7}Ce_{0.3})_2O_7/8YSZ$ double-ceramic-layer systems deposited by electron beam physical

- vapor deposition,” *Journal of Alloys and Compounds*, vol. 509, no. 11, pp. 4273–4283, 2011.
- [20] X. Zhao, X. Liu, S. Yin, and H. Li, “Improved results on stability of continuous-time switched positive linear systems,” *Automatica*, 2013.
- [21] W. M. Qu and W. Wlodarski, “A thin-film sensing element for ozone, humidity and temperature,” *Sensors and Actuators B*, vol. 64, no. 1–3, pp. 42–48, 2000.
- [22] X. Zhao, L. Zhang, P. Shi, and H. Karimi, “Robust control of continuous-time systems with state-dependent uncertainties and its application to electronic circuits,” *IEEE Transactions on Industrial Electronics*, 2013.
- [23] R. Schaub, P. Thostrup, N. Lopez et al., “Oxygen vacancies as active sites for water dissociation on rutile TiO_2 (110),” *Physical Review Letters*, vol. 87, no. 26, Article ID 266104, 4 pages, 2001.
- [24] X. Zhao, L. Zhang, P. Shi, and M. Liu, “Stability of switched positive linear systems with average dwell time switching,” *Automatica*, vol. 48, no. 6, pp. 1132–1137, 2012.
- [25] X. Zhao, L. Zhang, P. Shi, and M. Liu, “Stability and stabilization of switched linear systems with mode-dependent average dwell time,” *IEEE Transactions on Automatic Control*, vol. 57, no. 7, pp. 1809–1815, 2012.

Research Article

A New Three-Dimensional Indoor Positioning Mechanism Based on Wireless LAN

Jiujun Cheng,^{1,2} Yueqiao Cai,² Qingyang Zhang,² Junlu Cheng,² and Chendan Yan²

¹ Department of Computer Science and Technology, Tongji University, Shanghai 201804, China

² Key Laboratory of Embedded System and Service Computing of Ministry of Education, Tongji University, Shanghai 201804, China

Correspondence should be addressed to Yueqiao Cai; caiyueqiao@163.com

Received 9 December 2013; Accepted 15 January 2014; Published 23 February 2014

Academic Editor: Huaicheng Yan

Copyright © 2014 Jiujun Cheng et al. This is an open access article distributed under the Creative Commons Attribution License, which permits unrestricted use, distribution, and reproduction in any medium, provided the original work is properly cited.

The researches on two-dimensional indoor positioning based on wireless LAN and the location fingerprint methods have become mature, but in the actual indoor positioning situation, users are also concerned about the height where they stand. Due to the expansion of the range of three-dimensional indoor positioning, more features must be needed to describe the location fingerprint. Directly using a machine learning algorithm will result in the reduced ability of classification. To solve this problem, in this paper, a “divide and conquer” strategy is adopted; that is, first through k-medoids algorithm the three-dimensional location space is clustered into a number of service areas, and then a multicategory SVM with less features is created for each service area for further positioning. Our experiment shows that the error distance resolution of the approach with k-medoids algorithm and multicategory SVM is higher than that of the approach only with SVM, and the former can effectively decrease the “crazy prediction.”

1. Introduction

With the development of mobile communication technology and the growing demand for new services, location-aware computing especially the Location Based Service (LBS) gradually attracts people's attention, and how to determine the user's location is the core issue in LBS. The global positioning system (GPS) [1] and the cellular network positioning system are location service systems widely used in open outdoor environment [2]. However, these positioning systems in an indoor environment are out of people's satisfaction. And there are already many researches about the indoor positioning technology [3].

Nowadays, various radio techniques have been applied to the indoor positioning, such as UWB (ultra-wide band), RFID (radio-frequency identification), and VHF (ultra-high frequency) technology [4–7]. However, these positioning systems require redeployment of the network and additional signal measurement hardware, and the cost is relatively high, so their application is limited.

In recent years, with the increasing popularity of the application of WLAN, WLAN-based indoor positioning technology has been rapidly developed. The technology can

leverage existing wireless LAN resources without additional network deployments or facilities, which leads to the most attractive advantage, low cost.

WLAN-based indoor positioning technology research mostly uses the location fingerprint method and usually is based on the nearest neighbor search, naive Bayesian statistics, BP neural network or support vector machines [8–13], and other machines learning ideas. The positioning technology based on location fingerprint focuses more on the application of two-dimensional case, and relevant experiments are also conducted in a two-dimensional plane [14]. However, in practice the location systems in large shopping malls, libraries, offices, hospitals, airports, museums, and other places need to provide location information that includes not only the latitude and longitude coordinates, or other two-dimensional representations, but also the height or the room number.

When it comes to three-dimensional indoor positioning environments and the problem begins to be tougher, those methods previously mentioned may not be simply adaptive or scalable, and often a “divide and conquer” strategy acts as a good direction guide.

2. Related Work

Cotroneo et al. [15] proposed a naive partition positioning method that the communication range covered by an AP can be considered as a subregion, and which subregion the mobile terminal belongs to is determined by the signal strength it receives from each AP.

Xu et al. [16] divided the location space into multiple zones and used the distance-loss model choosing different parameters for each region. In the positioning phase, they used the maximum likelihood estimation to determine the location of the mobile terminal.

Nel Samama et al. [17] pointed out that many indoor positioning scenarios often do not require high accuracy and just tell the user some symbolic information, such as which corridor or room the current place is at. They proposed a 3D symbol positioning algorithm that divides the location space into different positioning symbolic subspace and designed a simple rule of symbolic subspace resolution to give the user positioning information.

Gansemmer et al. [18] pointed out that the 3D indoor positioning is more realized by UWB, RFID, and other technologies. They stressed the need for 3D WLAN indoor positioning and proposed a method that extends isolines algorithm [19], used in 2D WLAN indoor positioning to 3D space.

Zhong-liang et al. [20] adopted k-means clustering algorithm to partition a three-dimensional indoor space into multiple regions; namely, location fingerprints with similar Euclidean distance are clustered into one region and the central fingerprint of every region is saved. When in the positioning phase, the fact that the fingerprint received by the mobile terminal is closest to which central fingerprint helps estimate in which area the mobile terminal is located. But they just used this principle to determine which floor the mobile terminal is located on.

Various research works suggest and prove the effectiveness of the partitioning thought which will also be used in this paper. We will first use k-medoids algorithm to cluster the location space into different service areas to achieve coarse positioning and then build a multicategory SVM for each service area to achieve further fine positioning.

3. The Hybrid Indoor Positioning Approach

3.1. Cluster by k-Medoids

Definition 1 (location fingerprint). A location fingerprint is a vector bound to a specified location, which consists of a series of Wi-Fi single strength values received by the mobile terminal from different APs (access point, Wi-Fi hotspot, or WLAN wireless router):

$$LF = [AP_1, AP_2, AP_3, \dots, AP_n]. \quad (1)$$

Definition 2 (record). A record here is a structure consisting of a location representation and a location fingerprint:

$$R = \{\text{location representation, location fingerprint}\}. \quad (2)$$

We adopt k-medoids [21] algorithm to partition the location space into different services areas. Compared to k-means

algorithm, k-medoids algorithm is not sensitive to outliers, which allows us to get a better partition center.

As the complexity of the original implementation of k-medoids (Partitioning around Medoids, PAM [22, 23]) is too high, we need only a method to partition the location space, especially to solve the problem that whether partitioning those locations in stairs into up-floor or down-floor service area is better. Hence, we design our implementation of k-medoids algorithm, as shown in Algorithm 1.

Note. $m_i.\{\}$ is a set of records in i th service area with m_i as its medoid; the initial value of variable *changed* is true; the initial value of variable *count* is 0.

3.2. Classify by Multiclass SVM. The support vector machine (SVM) is a popular classification technique. Professor Chih-Jen Lin has done lots of researches deeply upon SVM for about many years, and he and his fellows or students developed and maintained a very useful SVM library LIBSVM [24].

The standard SVM is a binary classifier, but more often we need a multicategory SVM, especially in the indoor positioning problem, where a location is one category. In the library LIBSVM, there are three methods implementing multicategory SVM, namely, one-against-all, one-against-one, and DAG-SVM [25]. We will choose the DAG-SVM because the testing time of the DAG-SVM is less than the other two and the testing time is an online and time-sensitive operation.

In [26], Hsu et al. also presented some tricks on improving the performance of an SVM, such as scaling on input data and using cross-validation to get proprietary parameters of the RBF kernel.

3.3. Indoor Positioning Approach Combining k-Medoids and Multicategory SVM. The location space that we are now faced with is not limited to the scope of a room or a floor but has been extended to the whole building.

Take our college building as an example; usually there is an AP in a room and there are several APs in a corridor. So the total number of all APs in the whole building is very considerable.

Hence, the number of APs become large, so as the dimension of the location fingerprint. If an SVM is directly applied to classify the location fingerprints with large dimension, the ability to classify will decrease.

In the preparing phase, we will first through k-medoids algorithm use large dimension location fingerprint to partition the location space into several service areas and save a medoid location fingerprint for each service area. Thus, there are a set of location fingerprints (including the medoid itself) bound to each service area. Then we reduce the dimension of fingerprints in every service area through deleting those APs that are shared by none location in that service area. We will create a multicategory SVM upon each set location fingerprints. Detailed processing is shown in Algorithm 2.

In the positioning phase, when the mobile terminal receives many Wi-Fi signals from different APs, some of them are constructed as a fingerprint, and then the medoid

Input: $\{R_1, R_2, \dots, R_n\}$, R_i , i th record, total n records;
 $\{M_1, M_2, \dots, M_k\}$, M_i , i th initial medoid, total k medoids; $maxcount$, maximum iteration time.

Output: $\{m_1, m_2, \dots, m_k\}$, m_i , a record as i th clustered medoid.

- (1) For $i \leftarrow 1$ to k do
- (2) $m_i \leftarrow M_i$
- (3) EndFor
- (4) While $changed \ \&\& \ count < maxcount$ do
- (5) For $i \leftarrow 1$ to n do
- (6) $dist \leftarrow EuclideanDistance(R_i, m_1)$
- (7) $index \leftarrow 1$
- (8) For $j \leftarrow 2$ to k do
- (9) $temp \leftarrow EuclideanDistance(R_i, m_j)$
- (10) If $temp < dist$ do
- (11) $dist \leftarrow temp$
- (12) $index \leftarrow j$
- (13) EndIf
- (14) EndFor
- (15) add R_i to m_{index} .{}
- (16) EndFor
- (17) For $j \leftarrow 1$ to k do
- (18) $centroid \leftarrow Average(m_j)$ {}
- (19) $m_j = record \in m_j$.{nearest centroid
- (20) EndFor
- (21) If $\{m_j\}$ don't change do
- (22) $changed \leftarrow false$
- (23) EndIf
- (24) count++
- (25) EndWhile

ALGORITHM 1: Our implementation of k-medoids.

Input: $\{m_1, \dots, m_k\}$, m_i , set of records in i th service area with m_i as its medoid;
Output: $\{SVM_1, SVM_2, \dots, SVM_k\}$, SVM_i , trained SVM for i th service area;
 $\{AL_1, AL_2, \dots, AL_k\}$, AL_i , AP list of the fingerprints for i th service area.

- (1) For $i \leftarrow 1$ to k do
- (2) For $j \leftarrow 1$ to m_i .length do
- (3) $r \leftarrow m_i$.index[j]
- (4) For $x \leftarrow 1$ to r .fingerprint.length do
- (5) If r .fingerprint[x] $\neq NaN$ do
- (6) add $AP_{r.fingerprint[x]}$ to AL_i
- (7) EndIf
- (8) EndFor
- (9) EndFor
- (10) For $j \leftarrow 1$ to m_i .length do
- (11) $r \leftarrow m_i$.index[j]
- (12) delete $AP \notin AL_i$ from r
- (13) EndFor
- (14) train SVM_i on new m_i with LIBSVM
- (15) EndFor

ALGORITHM 2: Train an SVM for each service area.

fingerprint which is nearest to this finger can help determine which service area the mobile terminal is located in. Finally, the fingerprint modified by reducing dimension is input to the multicategory SVM corresponding to the determined service area, and the fine location is output by the SVM. Detailed processing is shown in Algorithm 3.

4. Experiment and Analysis

4.1. The Experiment Procedure. Our experiment is conducted on the 2nd, 3rd, and 4th floors in the building of the College of Electronics and Information Engineering (CEIE), Jading campus of Tongji University.

Input: fp , fingerprint of certain place;
 $\{m_1, m_2, \dots, m_k\}, m_i$, medoid of i th service area;
 $\{AL_1, AL_2, \dots, AL_k\}, AL_i$, AP list of the fingerprints for i th service area;
 $\{SVM_1, SVM_2, \dots, SVM_k\}, SVM_i$, trained SVM for i th service area.

Output: predicted location representation.

- (1) $dist \leftarrow EuclideanDistance(fp, m_1)$
- (2) $index \leftarrow 1$
- (3) For $j \leftarrow 2$ to k do
- (4) $temp \leftarrow EuclideanDistance(fp, m_j)$
- (5) If $temp < dist$ do
- (6) $dist \leftarrow temp$
- (7) $index \leftarrow j$
- (8) EndIf
- (9) EndFor
- (10) delete AP $\notin AL_{index}$ from fp
- (11) call SVM_{index} with input \leftarrow new fp

ALGORITHM 3: Predict the location of a certain place.

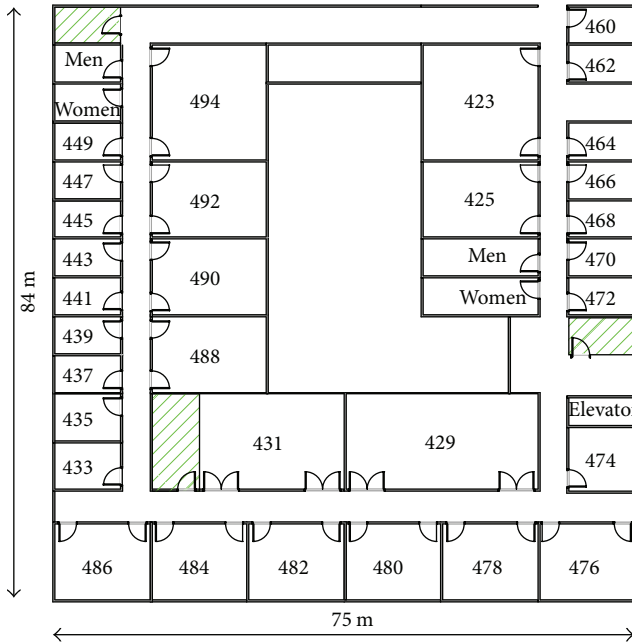


FIGURE 1: Experiment on the 4th floor of CEIE.

Figure 1 shows one of the experiment deployment floor plans, and the other two are similar. 100 sample spots are chosen from the corridor or stairs. These spots are labeled from number 1 to number 100 and every two neighbor spots are 5 m or 8 m or 12 m apart.

Table 1 lists two Wi-Fi info items received from nearby APs by an Android application (Wi-Fi scanner) developed by ourselves when the mobile phone is set in one of sample spots. The application can detect a list of info items (frequently there are more than 10 APs around) every time in the building of CEIE, and the situation can also be found in the library and dormitory buildings of the campus. Although we do not know the location of these APs, the information we can

TABLE 1: Two information items received from near APs.

Address of AP	00:21:29:7a:b2:b6
Network name	tongji419
Channel frequency	2437 MHz
Signal strength	-51 dBm
Address of AP	38:83:45:41:22:24
Network name	ciclab4
Channel frequency	2412 MHz
Signal strength	-58 dBm

get is enough for our experiment, and the “address of AP” and “signal strength” are used to construct a fingerprint of a location.

The main steps of our experiment are shown below.

4.1.1. The Preparing Phase

- (1) At every sample spot, with the mobile phone held in the hand of our tester, run Wi-Fi scanner 5 times for north, west, east, and a random direction, respectively; store the Wi-Fi info items for every time.
- (2) Delete those items with the “address of AP” that do not appear 5 times from the list of Wi-Fi info items, because their signal may be weak or unstable at that sample spot.
- (3) Count the frequency of every “address of AP,” sort those addresses by their frequency, reserve the first 2/3 of the sorted addresses, and discard the rest, 1/3, because we only need the address shared by more sample spots.
- (4) Shuffle the 2/3 of sorted addresses, and store them as a set of index indicators of a fingerprint, called Index Set.
- (5) Construct 5 fingerprints for every sample spot received from every 5 lists of Wi-Fi info items using

the principle that if the item has the “address of AP” in Index Set, the “signal strength” is assigned to the corresponding element with the same index of a fingerprint (the initial value of all elements is -100.0dBm), and these 5 fingerprints are bounded to the sample spot as one location or category for below SVM.

- (6) We get a set of fingerprints, and the size of this set is large. Because these data are collected from 9 corridors of 3 floors, we choose a fingerprint in every middle corridor to get 9 initial medoids; then we use Algorithm 1 with the input (the set of fingerprints, the 9 initial medoids, $maxcount = 100$) to partition them into 9 subsets for every subset as a service area and store the output (9 clustered medoids).
- (7) As every service area does not need so many “addresses of AP” we can discard those addresses shared by none sample spot in every subset; in other words, we can reduce the dimension of the fingerprint in that service area.
- (8) Use the multicategory SVM of LIBSVM to train the data on every service area; then finally we get 9 SVMs for 9 service areas, respectively.

4.1.2. The Positioning Phase

- (1) Run Wi-Fi scanner at a testing spot; get a list of Wi-Fi info items; use the same method mentioned in the preparing phase to construct a new fingerprint.
- (2) Compare this new fingerprint with every clustered medoid (totally 9 medoids); choose the medoid nearest to the new fingerprint with Euclidean distance, and the testing spot is located corresponding to service area.
- (3) According to the subset of fingerprints of the service area, reduce the dimension of the new fingerprint and input the dimension-reduced fingerprint to the corresponding SVM; we finally get the category or location of the testing spot.

4.2. Testing and Analysis. We consider two testing scenarios to evaluate the performance of the hybrid indoor positioning approach.

One is in-place testing scenario and the other is middle-place testing scenario, as is shown Figure 2. The left and right circles represent two sample spots. In the in-place testing scenario, we choose every testing spot that is almost the same with certain sample spot; while in the middle-place testing scenario, we choose every testing spot that is in the middle of two neighbor sample spots.

In these two scenarios, the hybrid k-medoids + SVM approach is compared with the only SVM approach which does not have partitioning and reducing dimension steps and directly trains all fingerprints with one multicategory SVM.

Figure 3 shows the cumulative distribution function (CDF) of the error distance for the hybrid k-medoids + SVM and only SVM approaches methods in the in-place scenario,

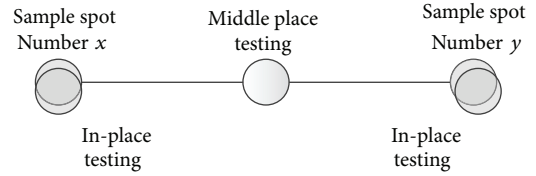


FIGURE 2: In-place and middle-place testing scenarios.

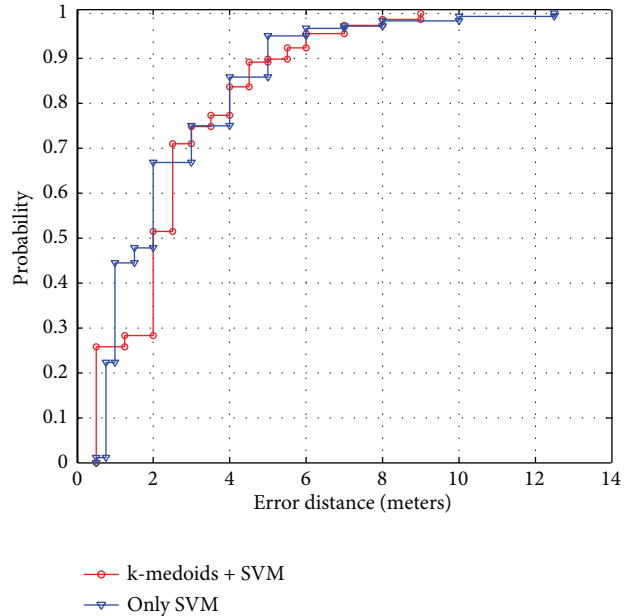


FIGURE 3: CDF of error distance/in-place scenario.

TABLE 2: The performance of two approaches.

Approach	50th percentile	75th percentile	Crazy prediction
k-medoids + SVM	6 m	8 m	0
Only SVM	7.5 m	9.3 m	3 times

while Figure 4 shows the counterpart in the middle-place scenario.

From Figure 3, in the in-place scenario, taking the 75th percentile for example, the error distance is less than 3.25 m with k-medoids + SVM approach and is less than 3.5 m with only SVM. We find that the difference between the performances of the two approaches is not very obvious. This is not hard to expect, because the in-place scenario represents an ideal situation, in which two approaches both achieve their best performance.

From Figure 4, we can easily find that the k-medoids + SVM approach performs better than only SVM approach in the middle-place scenario. The comparison in this scenario is listed in Table 2.

In Table 2, compared with only SVM approach, the k-medoids + SVM approach improves more than 1 m both in terms of the 50th percentile and 75th percentile of the error distance. Because the distance between two neighbor sample

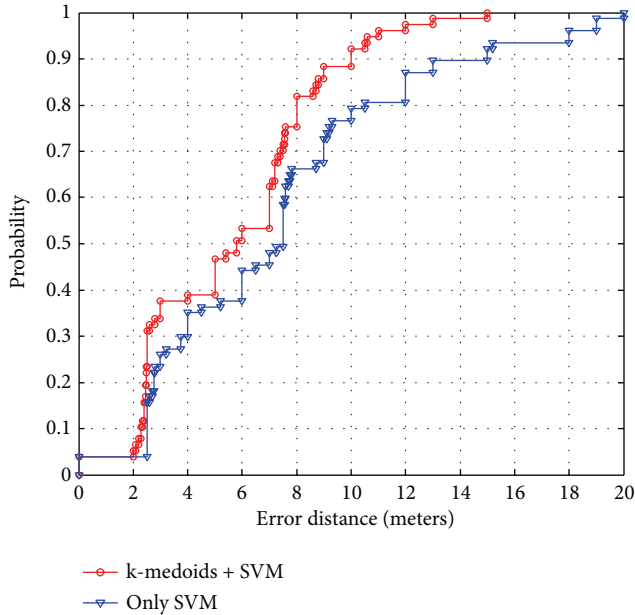


FIGURE 4: CDF of error distance/middle-place scenario.

spots in our experiment is 5 m, 8 m, or 12 m, the error distance hence becomes a little large. But indoor positioning resolution is not the key point we are concerned about in this paper. It is worth mentioning that with only SVM approach there occurs 3 times “crazy prediction,” for instance, that an actual spot on the 3rd floor is predicted on the 2nd floor or 4th floor. The k-medoids + SVM approach can well-reduce and even avoid this kind of “crazy prediction,” which also meets the requirement of indoor positioning, especially in 3D space.

5. Conclusions

A hybrid approach is proposed in this paper. The hybrid approach uses k-medoids algorithm to partition the set of fingerprints into several subsets, reduces the dimension of fingerprints of every subset, and trains a multicategory SVM on each subset data. The hybrid approach outperforms the approach just using SVM to train on all large-dimension fingerprints, in terms of error distance resolution. In addition, the hybrid approach with k-medoids algorithm and multicategory SVM can effectively reduce “crazy prediction.” Finally, we conclude that the hybrid approach can be used to solve 3D WLAN indoor positioning problem with a better performance.

Conflict of Interests

The authors declare that there is no conflict of interests regarding the publication of this paper.

Acknowledgments

This work was supported by the Natural Science Foundation Programs of Shanghai (Grant no. 13ZR1443100), by the 973

Program of China (under Grant 2010CB328101), by ISTCP (under Grant 2013DFM10100), by the National Science and Technology Support Plan (Grant no. 2012BAH15F03), and by NSFC (under Grants 51034003 and 51174210).

References

- [1] P. K. Enge, “The global positioning system: signals, measurements and performance,” *International Journal of Wireless Information Networks*, vol. 1, no. 2, pp. 83–105, 1994.
- [2] J. J. Caffery Jr. and G. L. Stüber, “Overview of radiolocation in CDMA cellular systems,” *IEEE Communications Magazine*, vol. 36, no. 4, pp. 38–45, 1998.
- [3] K. Pahlavan, X. Li, and J.-P. Mäkelä, “Indoor geolocation science and technology,” *IEEE Communications Magazine*, vol. 40, no. 2, pp. 112–118, 2002.
- [4] R. J. Fontana, E. Richley, and J. Barney, “Commercialization of an ultra wideband precision asset location system,” in *Proceedings of the IEEE Conference on Ultra Wideband Systems and Technologies*, pp. 369–373, Reston, Va, USA, November 2003.
- [5] M. N. Lionel, Y. Liu, Y. C. Lau, and A. P. Patil, “LANDMARC: indoor location sensing using active RFID,” *Wireless Networks*, vol. 10, no. 6, pp. 701–710, 2004.
- [6] J. Werb and C. Lanzl, “Designing a positioning system for finding things and people indoors,” *IEEE Spectrum*, vol. 35, no. 9, pp. 71–78, 1998.
- [7] H. Zhang, H. Yan, F. Yang, and Q. Chen, “Quantized control design for impulsive fuzzy networked systems,” *IEEE Transactions on Fuzzy Systems*, vol. 19, no. 6, pp. 1153–1162, 2011.
- [8] P. Bahl and V. N. Padmanabhan, “RADAR: an in-building RF-based user location and tracking system,” in *Proceedings of the 19th Annual Joint Conference of the IEEE Computer and Communications Societies (INFOCOM '00)*, pp. 775–784, March 2000.
- [9] M. A. Youssef, A. Agrawala, and A. U. Shankar, “WLAN location determination via clustering and probability distributions,” in *Proceedings of the 1st IEEE International Conference on Pervasive Computing and Communications (PerCom '03)*, pp. 143–150, Fort Worth, Tex, USA, March 2003.
- [10] R. Battiti, T. L. Nhat, and A. Villani, “Location-aware computing: a neural network model for determining location in wireless LANs,” Tech. Rep DIT-02-0083, 2002.
- [11] M. Brunato and R. Battiti, “Statistical learning theory for location fingerprinting in wireless LANs,” *Computer Networks*, vol. 47, no. 6, pp. 825–845, 2005.
- [12] H. Zhang, H. Yan, F. Yang, and Q. Chen, “Distributed average filtering for sensor networks with sensor saturation,” *IET Control Theory & Applications*, vol. 7, no. 6, pp. 887–893, 2013.
- [13] H. Yan, Z. Su, H. Zhang, and F. Yang, “Observer-based H_∞ control for discrete-time stochastic systems with quantisation and random communication delays,” *IET Control Theory & Applications*, vol. 7, no. 3, pp. 372–379, 2013.
- [14] H. Liu, H. Darabi, P. Banerjee, and J. Liu, “Survey of wireless indoor positioning techniques and systems,” *IEEE Transactions on Systems, Man and Cybernetics C*, vol. 37, no. 6, pp. 1067–1080, 2007.
- [15] D. Cotroneo, S. Russo, F. Corneville, M. Ficco, and V. Vecchio, “Implementing positioning services over an ubiquitous infrastructure,” in *Proceedings of the 2nd IEEE Workshop on Software*

- Technologies for Future Embedded and Ubiquitous Systems*, pp. 14–18, May 2004.
- [16] F.-Y. Xu, L.-B. Li, and Z.-X. Wang, “New WLAN indoor localization system based on distance-loss model with area partition,” *Journal of Electronics and Information Technology*, vol. 30, no. 6, pp. 1405–1408, 2008.
- [17] Nel Samama, “Symbolic 3D WiFi indoor positioning system: a deployment and performance evaluation tool,” in *Proceedings of the 13th World Congress of the International Association of Institutes of Navigation (IAIN '09)*, Stockholm, Sweden, October 2009.
- [18] S. Gansemer, S. Hakobyan, S. Püschel, and U. Großmann, “3D WLAN indoor positioning in multi-storey buildings,” in *Proceedings of the 5th IEEE International Workshop on Intelligent Data Acquisition and Advanced Computing Systems: Technology and Applications (IDAACS '09)*, pp. 669–672, September 2009.
- [19] U. Großmann, M. Schauch, and S. Hakobyan, “The accuracy of algorithms for WLAN indoor positioning and the standardization of signal reception for different mobile devices,” *International Journal of Computing*, vol. 6, no. 1, pp. 103–109, 2007.
- [20] D. Zhong-liang, W. Wen-jie, and X. Lian-ming, “A K-means based method to identify floor in WLAN indoor positioning system,” *Computer Engineering & Software*, vol. 33, no. 12, pp. 114–117, 2012.
- [21] L. Kaufman and P. J. Rousseeuw, “Clustering by means of medoids,” in *Statistical Data Analysis Based on the L_1 -Norm and Related Methods*, Y. Dodge, Ed., pp. 405–416, North-Holland, 1987.
- [22] S. Theodoridis and K. Koutroumbas, *Pattern Recognition*, 3rd edition, 2006.
- [23] H. Yan, H. Shi, H. Zhang, and F. Yang, “Quantized H_∞ control for networked systems with communication constraints,” *Asian Journal of Control*, vol. 15, no. 5, pp. 1468–1476, 2013.
- [24] C.-C. Chang and C.-J. Lin, “LIBSVM: a Library for support vector machines,” *ACM Transactions on Intelligent Systems and Technology*, vol. 2, no. 3, article 27, 2011.
- [25] C.-W. Hsu and C.-J. Lin, “A comparison of methods for multiclass support vector machines,” *IEEE Transactions on Neural Networks*, vol. 13, no. 2, pp. 415–425, 2002.
- [26] C.-W. Hsu, C.-C. Chang, and C.-J. Lin, “A practical guide to support vector classification,” Technical Report, Department of Computer Science, National Taiwan University, 2003.

Research Article

Impulsive Consensus Tracking of Multiagent Systems with Quantization and Input Delays Using Position-Only Information

Hong Zhou, Yu-Zhen Qin, Kuo Feng, Wen-Shan Hu, and Zhi-Wei Liu

Department of Automation, Wuhan University, Wuhan 430072, China

Correspondence should be addressed to Zhi-Wei Liu; liuzw@whu.edu.cn

Received 2 December 2013; Accepted 15 January 2014; Published 20 February 2014

Academic Editor: Huaicheng Yan

Copyright © 2014 Hong Zhou et al. This is an open access article distributed under the Creative Commons Attribution License, which permits unrestricted use, distribution, and reproduction in any medium, provided the original work is properly cited.

This paper investigates the consensus tracking problem for second-order multi-agent systems without/with input delays. Randomized quantization scheme is considered in the communication channels, and impulsive consensus tracking algorithms using position-only information are proposed for the consensus tracking of multi-agent systems. Based on the algebraic graph theory and stability theory of impulsive systems, sufficient and necessary conditions for consensus tracking are studied. It is found that consensus tracking for second-order multi-agent systems without/with input delays can be achieved by appropriately choosing the sampling period and control gains which are determined by second/third degree polynomials. Simulations are performed to validate the theoretical results.

1. Introduction

During the last two decades, the consensus problem in multiagent systems has attracted considerable attention due to its broad applications including synchronization [1], formation control [2], flocking [3], and sensor networks [4]. The main objective of consensus problem in multiagent systems is to design distributed control that enables all agents in a network to reach an agreement with a certain characteristic.

Recently, the leader-following structure containing one leader and some followers has been introduced into the consensus. Particularly, consensus with a static leader is named *consensus regulation* problem, and consensus with an active leader is named *consensus tracking* problem [5]. In the consensus tracking problem, a portion of the followers can obtain the leader's information while other followers can only obtain their neighbors' information. The task of consensus tracking is to make all the followers track the leader. Many valuable results on consensus tracking have been obtained in the existing literatures with different features including variable topology [6, 7], coupling time delays [8], and network-based communication [9].

It is worthwhile to mention that most of the consensus tracking algorithms proposed in the above-mentioned literatures require both position and velocity information among

neighbouring agents. Unfortunately, in order to reduce equipment costs and network traffic, the agents might not be equipped with velocity sensors in many applications such as some robots and air vehicles systems. Thus the velocity of each agent may not be obtained in these special multiagent systems. To address the limitation, consensus algorithms without any velocity information are proposed in [10–12].

On the other hand, in all of the aforementioned works, one major shortcoming of the proposed algorithms for the consensus tracking of multiagent systems is the reliance on the exchange of analog data. It demands quite a broad bandwidth and enough communication power in the information interaction. But in practical situations, communication channels are always with finite bandwidth and finite power so that only a finite number of bits can be transmitted [13–15]. When the constraints are considered, communication with unquantized data is impractical [16, 17]. The authors proposed distributed algorithms in which the agents utilize quantized communication information to communicate with each other [14, 18–20]. The probabilistic quantization scheme was adopted in the agents interaction [14, 18]. In [21], logarithmic quantizer was used to quantize the state of agents in the multiagent systems.

Inspired by the above discussion, randomized quantization scheme is considered in the communication channels in this paper. At the sampling instant, the states of agents are sampled and quantized utilizing this scheme before being transmitted to their neighbors. Since the impulsive control strategy is proved to be a very effective control strategy in many fields due to its various advantages such as smaller control effort (only operates at sampling times), less information required (only needs the information at sampling times), and simple implementation [22–25], it is taken into consideration in our work. In conclusion, the main contribution of this paper includes the following two aspects: (1) the design of impulsive consensus tracking algorithms using the position-only information for the multiagent systems without/with input delays; (2) the introduction of randomized quantization scheme which is applied to the quantization of agents' information before communication, which is different from our previous works on impulsive algorithms [22, 24, 26]. It is worth pointing out that studying the effect of time delays on the consensus of multiagent systems is meaningful. Generally, there are two kinds of time delays in multiagent systems: *communication delays* and *input delays*. Communication delays are related to communication among agents while input delays are related to processing and connecting time for the packets arriving at each agent [27]. Input delay is studied in this paper. It is shown that the second-order multiagent systems without/with input delays can reach quantized consensus tracking if the sampling period and control gains are appropriately designed from polynomials with different orders.

The rest of the paper is organized as follows. In Section 2, preliminaries and problem formulation are given. The impulsive consensus tracking algorithms utilizing quantized communication for second-order multiagent systems without/with time delays are presented in Section 3 and the quantized consensus tracking is proved to be reached. In Section 4, numerical examples are given to illustrate the theoretical analysis. Conclusions are finally drawn in Section 5.

2. Preliminary and Problem Formulation

In this section, some basic concepts used throughout this paper are introduced. Let \mathbb{R} denote the set of real numbers and let $\mathbb{N} = \{1, 2, 3, \dots\}$. $\mathbf{1}_n = (1, 1, \dots, 1)^T$ is the column vector. I_n is the identity matrix of order n . $0_{n \times m}$ denotes the matrix with all elements equal to zero.

2.1. Preliminaries in Graph Theory. For a multiagent system with n agents, let $\mathcal{G} = \{\mathcal{V}, \mathcal{E}, \mathcal{A}\}$ be a directed graph with the set of vertices $\mathcal{V}(\mathcal{G}) = \{v_1, v_2, \dots, v_n\}$, the set of edges $\mathcal{E}(\mathcal{G}) \subseteq \mathcal{V}(\mathcal{G}) \times \mathcal{V}(\mathcal{G})$, and a weighted adjacency matrix $\mathcal{A}(\mathcal{G}) = (a_{ij})_{n \times n}$. An edge of \mathcal{G} is denoted by $\theta_{ij} = (v_j, v_i)$, where v_j is called the parent vertex of v_i and v_i the child of v_j . The adjacency elements associated with the edges are nonnegative. For $i, j \in \mathcal{V}$, $\theta_{ij} \in \mathcal{E}(\mathcal{G}) \Leftrightarrow a_{ij} > 0$, and assume that $a_{ii} = 0$. The set of neighbors of node v_i is denoted by $\mathcal{N}_i = \{v_j \in \mathcal{V}(\mathcal{G}) \mid (v_j, v_i) \in \mathcal{E}(\mathcal{G}), j \neq i\}$. The Laplacian

matrix $L = (l_{ij})_{n \times n}$ is defined as $l_{ij} = \sum_{k=1, k \neq i}^n a_{ik}$, for $i = j$, and $l_{ij} = -a_{ij}$, for $i \neq j$, where $i, j = 1, 2, \dots, n$.

2.2. Definitions and Notations. For a multiagent system, an agent is called a leader if the agent has no neighbor and an agent is called a follower if the agent has neighbors. In this paper, we will consider a multiagent system consisting of one active leader and n followers. Let \mathcal{G} denote the interaction topology of the followers and L be Laplacian matrix of \mathcal{G} . Let $\tilde{\mathcal{G}}$ denote the interaction topology of the multiagent system containing the followers and the leader. Let $B = (b_i)_{n \times n}$ describe the connection between follower i and the leader. $b_i > 0$ if and only if there exists a direct path from the leader to the follower; otherwise, $b_i = 0$. The multiagent system with n followers and one leader can be described by

$$\begin{aligned} \dot{\xi}_0(t) &= \zeta_0(t), \\ \dot{\zeta}_0(t) &= a(t), \\ \dot{\xi}_i(t) &= \zeta_i(t), \\ \dot{\zeta}_i(t) &= a(t) + u_i(t), \end{aligned} \quad (1)$$

where $\xi_i(t) \in \mathbb{R}$ and $\zeta_i(t) \in \mathbb{R}$, $i = 1, 2, \dots, n$, are the position and velocity of agent i and $u_i(t)$ is control input at time t . $\xi_0(t) \in \mathbb{R}$, $\zeta_0(t) \in \mathbb{R}$, and $a(t)$ are the position, velocity, and the acceleration of the dynamic leader, respectively. The followers aim to track the leader in this paper. It is assumed that the communication among agents only occurs at sampling instants, and the sampling intervals are periodic with period h . The sampling information needs to be quantized before being transmitted to the neighbor agents.

Randomized Quantization Scheme. In the following, a quantization scheme adopted in this paper is introduced. Suppose that the scalar value ξ_i is quantized by a uniform quantizer with quantization interval δ . Obviously, there exists an integer k such that $\xi_i \in [k\delta, (k+1)\delta)$. Inspired by [14, 28], the data can be quantized by the probabilistic manner:

$$\Pr\{\xi_i = k\delta\} = 1 - \chi, \quad \Pr\{\xi_i = (k+1)\delta\} = \chi, \quad (2)$$

where $\chi = (\xi_i - k\delta)/\delta$. Define $\mathbb{Q}(\cdot)$ as the quantization operation. One has expectation and variance in the following form:

$$E(\mathbb{Q}(\xi_i)) = \xi_i, \quad E((\mathbb{Q}(\xi_i) - \xi_i)^2) \leq \frac{\delta^2}{4}. \quad (3)$$

In this scheme, the randomized quantized value is equal to the original unquantized value in expectation. Let $\varepsilon_i = \mathbb{Q}(\xi_i) - \xi_i$ be the quantization error; the above formula can be rewritten as $E(\varepsilon_i^2) \leq \delta^2/4$.

Definition 1. The quantized consensus tracking in the multi-agent system (1) is said to be achieved if, for any initial state,

$$\begin{aligned} \lim_{t \rightarrow \infty} E \left(|\xi_i(t) - \xi_0(t)|^2 \right) &\leq p(\delta), \\ \lim_{t \rightarrow \infty} E \left(|\zeta_i(t) - \zeta_0(t)|^2 \right) &\leq q(\delta), \end{aligned} \quad (4)$$

$$i = 1, 2, \dots, n,$$

where $p(\delta), q(\delta)$ are monotonously increasing functions satisfying $\lim_{\delta \rightarrow 0} p(\delta) = 0, \lim_{\delta \rightarrow 0} q(\delta) = 0$.

Before presenting the consensus tracking analysis, we first give the following lemmas which will be used in our work.

Lemma 2 (see [29]). *\mathcal{G} has a spanning tree if and only if L has a simple eigenvalue 0 together with the other eigenvalues whose real parts are all real ones. Therefore, $\tilde{\mathcal{G}}$ contains a spanning tree if and only if all the eigenvalues of $L+B$, $\mu_i, i = 1, 2, \dots, n$, have positive real parts.*

Lemma 3 (see [30]). *Consider a complex polynomial $R(s) = s^2 + (a+bi)s + c + di$, where a, b, c , and d are real constants. Then $R(s)$ is Hurwitz stable if and only if $a > 0$ and $abd + a^2c - d^2 > 0$.*

Lemma 4 (see [31]). *Matrix A and $\varepsilon > 0$ are given. There exists a matrix norm $\|\cdot\|_p$ such that*

$$\rho(A) \leq \|A\|_p \leq \rho(A) + \varepsilon. \quad (5)$$

3. Consensus Tracking with Impulsive Algorithm

3.1. Impulsive Algorithm Utilizing Quantization Communication without Input Delays. Assume sampling period in the multiagent system is a positive constant h , the sampling time sequence can be noted as a set $\Phi = \{0, t_1, \dots, t_k, \dots\}, k = 1, 2, \dots$. On count of the velocities $\zeta_i(t), \zeta_0(t), i = 1, 2, \dots, n$, cannot be obtained; we propose the following impulsive algorithm for system (1):

$$\begin{aligned} \dot{\xi}_i(t) &= \zeta_i(t), \\ \dot{\zeta}_i(t) &= a(t) + u_i(t), \quad t \in (t_k, t_{k+1}], \\ \Delta \zeta_i(t) &= -\beta_1 \phi_i(t_k) - \beta_2 \bar{z}_i(k), \\ z_i(k+1) &= -\alpha_1 \phi_i(t_k), \quad i = 0, 1, 2, \dots, n, \end{aligned} \quad (6)$$

where

$$\begin{aligned} \phi_i(t_k) &= b_i (\xi_i(t_k) - \xi_0(t_k)) + \sum_{j \in \mathcal{N}_i} l_{ij} (\xi_j(t_k) - \xi_i(t_k)), \\ \bar{z}_i(k) &= b_i z_i(k) + \sum_{j \in \mathcal{N}} l_{ij} (z_j(k) - z_i(k)), \end{aligned} \quad (7)$$

$u_i(t) = 0, \Delta \zeta_i(t) = \zeta_i(t_k^+) - \zeta_i(t_k), \zeta_i(t_k^+) = \lim_{t \rightarrow t_k^+} \zeta_i(t), i = 1, 2, \dots, n$. What is worth pointing out is that $\xi_i(t_k) = p_i(t_k) + \varepsilon_i(t_k)$, where $p_i(t_k)$ are the position information which are not

quantized, and $\varepsilon_i(t_k)$ are denoted as the quantization error of agent i at the time $t = t_k$ satisfying $E(\varepsilon_i^2) \leq \delta^2/4$, where δ is the quantization interval of each agent in the system. Assume that $\zeta_i(t)$ is left-hand continuous at $t = t_k$. $\alpha_1 > 0, \beta_1 > 0$, and $\beta_2 > 0$ are the control gains that need to be designed.

Denote $\zeta_i(t_k^+) = \zeta_i(t_{k+1})$. From system (6), one can easily get

$$\begin{aligned} \xi_i(t_{k+1}) &= \xi_i(t_k) + h \zeta_i(t_{k+1}), \\ \zeta_i(t_{k+1}) &= \zeta_i(t_k) - \beta_1 \phi_i(t_k) - \beta_2 \bar{z}_i(k), \\ \phi_i(t_k) &= b_i (\xi_i(t_k) - \xi_0(t_k)) \\ &\quad + \sum_{j \in \mathcal{N}_i} l_{ij} (\xi_j(t_k) - \xi_i(t_k)) + e_i(k), \end{aligned} \quad (8)$$

where $e_i(k) = b_i(\varepsilon_i(t_k) - \varepsilon_0(t_k)) + \sum_{j \in \mathcal{N}_i} l_{ij}(\varepsilon_j(t_k) - \varepsilon_i(t_k))$. Let $x_i(t) = \xi_i(t) - \xi_0(t), y_i(t) = \zeta_i(t) - \zeta_0(t)$, for $i = 1, 2, \dots, n$. Assume that $y_i(t)$ is left-hand continuous at $t = t_k$. Let $y_i(t_k^+) = \lim_{t \rightarrow t_k^+} y_i(t)$. Then for Definition 1, the quantized consensus tracking is achieved if and only if

$$\lim_{t \rightarrow +\infty} E(|x_i(t)|^2) \leq p(\delta), \quad \lim_{t \rightarrow +\infty} E(|y_i(t)|^2) \leq q(\delta). \quad (9)$$

For $t \in (t_k, t_{k+1}]$, one has

$$\begin{aligned} y_i(t) &= y_i(t_k) - \beta_1 b_i x_i(t_k) \\ &\quad - \beta_1 \sum_{j \in \mathcal{N}_i} l_{ij} (x_j(t_k) - x_i(t_k)) - \beta_2 b_i z_i(k) \\ &\quad - \beta_2 \sum_{j \in \mathcal{N}} l_{ij} (z_j(k) - z_i(k)) - \beta_1 e_i(k), \\ x_i(t) &= x_i(t_k) + (t - t_k) y_i(t_k) - (t - t_k) \beta_1 b_i x_i(t_k) \\ &\quad - (t - t_k) \beta_1 \sum_{j \in \mathcal{N}_i} l_{ij} (x_j(t_k) - x_i(t_k)) \\ &\quad - (t - t_k) \beta_2 b_i z_i(k) \\ &\quad - (t - t_k) \beta_2 \sum_{j \in \mathcal{N}} l_{ij} (z_j(k) - z_i(k)) \\ &\quad - (t - t_k) \beta_1 e_i(k), \\ z_i(k+1) &= -\alpha_1 b_i x_i(t_k) \\ &\quad - \alpha_1 \sum_{j \in \mathcal{N}_i} l_{ij} (x_j(t_k) - x_i(t_k)) - \alpha_1 e_i(k). \end{aligned} \quad (10)$$

Let $\Psi_i(k) = (x_i(t_k), y_i(t_k), z_i(k))^T, \Phi(k) = (\Psi_1^T(k), \Psi_2^T(k), \dots, \Psi_n^T(k))^T$, and $\Omega(k) = (e_1(k), e_2(k), \dots, e_n(k))^T$. Then controlled system (6) can be rewritten into a matrix form as

$$\Phi(k+1) = F\Phi(k) + D\Omega(k), \quad (11)$$

where $F = (I_n \otimes A - (L + B) \otimes C)$,

$$A = \begin{pmatrix} 1 & h & 0 \\ 0 & 1 & 0 \\ 0 & 0 & 0 \end{pmatrix}, \quad C = \begin{pmatrix} h\beta_1 & 0 & h\beta_2 \\ \beta_1 & 0 & \beta_2 \\ \alpha_1 & 0 & 0 \end{pmatrix}, \quad (12)$$

$$D = -I_n \otimes \begin{pmatrix} h\beta_1 \\ \beta_1 \\ \alpha_1 \end{pmatrix}.$$

Lemma 5. *The controlled system (6) can achieve the quantized consensus tracking if and only if $\rho(F) < 1$, where $\rho(\cdot)$ denotes the spectral radius of a matrix.*

Proof. Define $\gamma(k) = E(\Phi(k) \otimes \Phi(k))$ and thus the quantized consensus tracking of system algorithm (6) can be studied by analyzing $\gamma(k)$ since

$$E(\|\Phi(k)\|_2^2) \leq \|\gamma(k)\|_1 \leq 3nE(\|\Phi(k)\|_2^2), \quad (13)$$

where $\|\cdot\|_1, \|\cdot\|_2$ denote the 1-norm and 2-norm, respectively. Then from (11), one has

$$\gamma(k+1) = (F \otimes F) \gamma(k) + (D \otimes D) E(\Omega(k) \otimes \Omega(k)). \quad (14)$$

Necessity. If $\rho(F) \geq 1$, the system (14) must be diverging and the system (6) cannot achieve the quantized consensus tracking since $\rho(F \otimes F) \geq 1$.

Sufficiency. If $\rho(F) < 1$, then $\rho(F \otimes F) < 1$. According to Lemma 4, there exist a matrix norm $\|\cdot\|_p$ and a constant $\omega < 1$ satisfying

$$\|F \otimes F\|_p = \omega < \rho(F \otimes F) + \varepsilon < 1, \quad (15)$$

provided that ε is small enough. And then from (14), one has

$$\|\gamma(k+1)\|_p \leq \omega^{k+1} \|\gamma(0)\|_p + \sum_{i=0}^k \omega^i \tilde{\delta}, \quad (16)$$

where $\tilde{\delta} = 12n^2 \|D \otimes D\|_p \delta$, δ is the quantized interval. It is easy to know that $\lim_{k \rightarrow \infty} \|\gamma(k+1)\|_p \leq \tilde{\delta}/(1-\omega)$ since $\omega < 1$. Therefore, there exists a positive constant $I \geq 0$ such that

$$E(\|\Phi(k)\|_2^2) \leq \frac{I\tilde{\delta}}{(1-\omega)}. \quad (17)$$

Obviously, there exist constants $M > 0$ and $N > 0$ satisfying $\lim_{t \rightarrow \infty} E(\|x_i(t)\|_2^2) \leq M\tilde{\delta}/(1-\omega)$, $\lim_{t \rightarrow \infty} E(\|y_i(t)\|_2^2) \leq N\tilde{\delta}/(1-\omega)$; that is,

$$\lim_{t \rightarrow \infty} E(|\xi_i(t) - \xi_0(t)|^2) \leq M\tilde{\delta},$$

$$\lim_{t \rightarrow \infty} E(|\zeta_i(t) - \zeta_0(t)|^2) \leq N\tilde{\delta}, \quad i = 1, 2, \dots, n. \quad (18)$$

According to Definition 1, it is easy to obtain that the quantized consensus tracking in the controlled system (6) can be achieved. Then this lemma is proved. \square

Theorem 6. *The controlled system (6) can reach quantized consensus tracking if and only if the directed graph $\tilde{\mathcal{G}}$ has a spanning tree and the polynomial*

$$g_i(\sigma) = (h\beta_1\mu_i - h\alpha_1\mu_i^2\beta_2)\sigma^2 + 2h\alpha_1\mu_i^2\beta_2\sigma + 4 - h\alpha_1\mu_i^2\beta_2 - h\beta_1\mu_i \quad (19)$$

is Hurwitz stable, where $\mu_i, i = 1, 2, \dots, n$, are the eigenvalues of $L + B$.

Proof. Let

$$F_i = \begin{pmatrix} 1 - h\beta_1\mu_i & h & -h\beta_2\mu_i \\ -\beta_1\mu_i & 1 & -\beta_2\mu_i \\ -\alpha_1\mu_i & 0 & 0 \end{pmatrix}, \quad (20)$$

where $\mu_i, i = 1, 2, \dots, n$, are the eigenvalues of $L + B$. Assume that $L + B$ have m different eigenvalues $\mu_j, j = 1, 2, \dots, m$. There exists a invertible matrix P such that $L + B = P^{-1}JP$, where $J = \text{diag}(J_1, J_2, \dots, J_m)$ and

$$J_j = \begin{pmatrix} \mu_j & 1 & 0 & 0 \\ 0 & \mu_j & 1 & 0 \\ 0 & 0 & \mu_j & 1 \\ 0 & 0 & 0 & \mu_j \end{pmatrix}_{N_j \times N_j}, \quad (21)$$

where N_j is the algebraic multiplicity of $\mu_j, j = 1, 2, \dots, m$. Motivated by [30, 32], one has

$$X(k+1) = (P \otimes I_3) F (P^{-1} \otimes I_3) X(k)$$

$$= (I_n \otimes A - J \otimes C) X(k) + H\Omega(k)$$

$$= \begin{pmatrix} \tilde{J}_j & 0 & 0 & 0 \\ 0 & \tilde{J}_j & \cdots & 0 \\ \vdots & \vdots & \ddots & 0 \\ 0 & 0 & 0 & \tilde{J}_j \end{pmatrix} X(k) + H\Omega(k), \quad (22)$$

where $\tilde{J}_j = I_n \otimes A - J_j \otimes C, H = D$. According to Lemma 5, the quantized consensus tracking can be reached if and only if $\rho(\tilde{J}_j) < 1, j = 1, 2, \dots, m$.

Note that

$$\tilde{J}_j = I_n \otimes A - J_j \otimes C$$

$$= \begin{pmatrix} A - \mu_j C & C & 0 & 0 \\ 0 & A - \mu_j C & \cdots & 0 \\ 0 & \ddots & \ddots & C \\ 0 & 0 & 0 & A - \mu_j C \end{pmatrix},$$

$$|\lambda I_{N_j} - \tilde{J}_j|$$

$$= \begin{pmatrix} \lambda - A + \mu_j C & -C & 0 & 0 \\ 0 & \lambda - A + \mu_j C & \cdots & 0 \\ 0 & \ddots & \ddots & -C \\ 0 & 0 & 0 & \lambda - A + \mu_j C \end{pmatrix}$$

$$= |\lambda - A + \mu_j C|^{N_j}. \quad (23)$$

This implies that $\rho(\tilde{F}_j) < 1$, $j = 1, 2, \dots, m$ if and only if $\rho(A - \mu_j C) < 1$, $j = 1, 2, \dots, m$. As $F_i = A - \mu_i C$, the controlled system (6) can reach the quantized consensus tracking if and only if $\rho(F_i) < 1$, $i = 1, 2, \dots, n$. Note that

$$|\lambda I_3 - F_i| = \lambda^3 + (h\beta_1\mu_i - 2)\lambda^2 + (1 - h\alpha_1\mu_i^2\beta_2)\lambda. \quad (24)$$

Let $f_i(\lambda) = \lambda^2 + (h\beta_1\mu_i - 2)\lambda + (1 - h\alpha_1\mu_i^2\beta_2)$, $i = 1, 2, \dots, n$. $\rho(F_i) < 1$ holds if and only if the polynomial $f_i(\lambda)$ is Schur stable.

Let

$$\begin{aligned} g_i(\sigma) &= (\sigma - 1)^2 f_i\left(\frac{\sigma + 1}{\sigma - 1}\right) \\ &= (h\beta_1\mu_i - h\alpha_1\mu_i^2\beta_2)\sigma^2 \\ &\quad + 2h\alpha_1\mu_i^2\beta_2\sigma + 4 - h\alpha_1\mu_i^2\beta_2 - h\beta_1\mu_i. \end{aligned} \quad (25)$$

Obviously, the polynomial $f_i(\lambda)$ is Schur stable if and only if the polynomial $g_i(\sigma)$ is Hurwitz stable. And, then, the controlled system (6) can reach the quantized consensus tracking if and only if $g_i(\sigma) = (h\beta_1\mu_i - h\alpha_1\mu_i^2\beta_2)\sigma^2 + 2h\alpha_1\mu_i^2\beta_2\sigma + 4 - h\alpha_1\mu_i^2\beta_2 - h\beta_1\mu_i$ is Hurwitz stable. Then Theorem 6 is proved. \square

Remark 7. In Theorem 6, a necessary and sufficient condition for the quantized consensus tracking for the controlled system (6) without input delays is established as a polynomial with order two. For a given topology, whether directed or undirected, one could choose appropriate control gains $\alpha_1, \beta_1, \beta_2$ and sampling period h such that condition (19) is satisfied.

Theorem 8. Assume that \mathcal{G} is a directed graph. The controlled system (6) can achieve the quantized consensus tracking if and only if the directed graph $\tilde{\mathcal{G}}$ contains a spanning tree and

$$\begin{aligned} \operatorname{Re}(\mu_i)(\beta_1 - \alpha\beta_2 \operatorname{Re}(\mu_i)) - \operatorname{Im}^2(\mu_i)\alpha\beta_2 > 0, \\ abd + a^2c - d^2 > 0 \end{aligned} \quad (26)$$

holds, where

$$\begin{aligned} a &= \operatorname{Re}\left(\frac{2h\alpha_1\mu_i\beta_2}{(h\beta_1 - h\alpha_1\mu_i\beta_2)}\right), \\ b &= \operatorname{Im}\left(\frac{2h\alpha_1\mu_i\beta_2}{(h\beta_1 - h\alpha_1\mu_i\beta_2)}\right), \\ c &= \operatorname{Re}\left(\frac{(4 - h\alpha_1\mu_i^2\beta_2 - h\beta_1\mu_i)}{(h\beta_1\mu_i - h\alpha_1\mu_i^2\beta_2)}\right), \\ d &= \operatorname{Im}\left(\frac{(4 - h\alpha_1\mu_i^2\beta_2 - h\beta_1\mu_i)}{(h\beta_1\mu_i - h\alpha_1\mu_i^2\beta_2)}\right). \end{aligned} \quad (27)$$

Proof. According to Theorem 6, note that

$$\begin{aligned} \hat{g}_i(\sigma) &= \frac{g_i(\sigma)}{(h\beta_1\mu_i - h\alpha_1\mu_i^2\beta_2)} \\ &= \sigma^2 + \frac{2h\alpha_1\mu_i\beta_2}{(h\beta_1 - h\alpha_1\mu_i\beta_2)}\sigma + \frac{4 - h\alpha_1\mu_i^2\beta_2 - h\beta_1\mu_i}{(h\beta_1\mu_i - h\alpha_1\mu_i^2\beta_2)}. \end{aligned} \quad (28)$$

From Lemma 2, if the directed graph $\tilde{\mathcal{G}}$ has a spanning tree, then $\operatorname{Re}(\mu_i) > 0$, $i = 1, 2, \dots, n$. According to Lemma 3, the complex polynomial $\hat{g}_i(\sigma)$ is Hurwitz stable if and only if $a > 0$, and $abd + a^2c - d^2 > 0$. It is easy to prove that $a > 0$ is equivalent to $\operatorname{Re}(\mu_i)(\beta_1 - \alpha\beta_2 \operatorname{Re}(\mu_i)) - \operatorname{Im}^2(\mu_i)\alpha\beta_2 > 0$. Then this proof is completed. \square

Corollary 9. Assume that \mathcal{G} is an undirected graph. The controlled system (6) can achieve the quantized consensus tracking if and only if the $\tilde{\mathcal{G}}$ contains a spanning tree and

$$\begin{aligned} h < \frac{4}{\mu_{\max}(\beta_1 + \alpha_1\mu_{\max}\beta_2)}, \\ \beta_1 - \alpha_1\mu_i\beta_2 > 0 \end{aligned} \quad (29)$$

holds, where μ_{\max} is the maximum eigenvalue of $L + B$.

Proof. According to Lemma 2, if the undirected graph $\tilde{\mathcal{G}}$ has a spanning tree, then $\mu_i > 0$, $i = 1, 2, \dots, n$. As this corollary is a special case of Theorem 8 where $\operatorname{Re}(\mu_i) = \mu_i$ and $\operatorname{Im}(\mu_i) = 0$, one can easily obtain the condition (29) by a simple calculation. Then Corollary 9 is proved. \square

3.2. Impulsive Algorithm Utilizing Quantization Communication with Input Delays. In some practical situations, the input time delays always exist, which cannot be ignored. When the time delays τ (assume that $\tau < h$ is time-invariant) are introduced into the protocol, one can consider the impulsive algorithm as

$$\dot{\xi}_i(t) = \zeta_i(t),$$

$$\dot{\zeta}_i(t) = a(t) + u_i(t), \quad t \in (t_k, t_{k+1}], \quad (30)$$

$$\Delta\zeta_i(t) = -\beta_1\phi_i(t_k) - \beta_2\bar{z}_i(k),$$

$$z_i(k+1) = -\alpha_1\phi_i(t_k), \quad i = 0, 1, 2, \dots, n,$$

where

$$\begin{aligned} \phi_i(t_k) &= b_i(\xi_i(t_k - \tau) - \xi_0(t_k - \tau)) \\ &\quad + \sum_{j \in \mathcal{N}_i} l_{ij}(\xi_j(t_k - \tau) - \xi_i(t_k - \tau)), \end{aligned} \quad (31)$$

$$\bar{z}_i(k) = b_i z_i(k) + \sum_{j \in \mathcal{N}} l_{ij}(z_j(k) - z_i(k)).$$

Similar to the above analysis, it is easy to obtain that, for $t \in (t_k, t_{k+1}]$,

$$\begin{aligned} y_i(t) &= y_i(t_k) - \beta_1 b_i x_i(t_k - \tau) \\ &\quad - \beta_1 \sum_{j \in \mathcal{N}_i} l_{ij} (x_j(t_k - \tau) - x_i(t_k - \tau)) - \beta_2 b_i z_i(k) \\ &\quad - \beta_2 \sum_{j \in \mathcal{N}} l_{ij} (z_j(k) - z_i(k)) - \beta_1 e_i(t_k - \tau), \end{aligned}$$

$$\begin{aligned} x_i(t) &= x_i(t_k) + h y_i(t_k) - h \beta_1 b_i x_i(t_k - \tau) \\ &\quad - h \beta_1 \sum_{j \in \mathcal{N}_i} l_{ij} (x_j(t_k - \tau) - x_i(t_k - \tau)) \\ &\quad - h \beta_2 b_i z_i(k) \\ &\quad - h \beta_2 \sum_{j \in \mathcal{N}} l_{ij} (z_j(k) - z_i(k)) - h \beta_1 e_i(t_k - \tau), \end{aligned}$$

$$\begin{aligned} z_i(k+1) &= -\alpha_1 b_i x_i(t_k - \tau) \\ &\quad - \alpha_1 \sum_{j \in \mathcal{N}_i} l_{ij} (x_j(t_k - \tau) - x_i(t_k - \tau)) \\ &\quad - \alpha_1 e_i(t_k - \tau), \end{aligned} \quad (32)$$

where

$$\begin{aligned} e_i(t_k - \tau) &= b_i (\varepsilon_i(t_k - \tau) - \varepsilon_0(t_k - \tau)) \\ &\quad + \sum_{j \in \mathcal{N}_i} l_{ij} (\varepsilon_j(t_k - \tau) - \varepsilon_i(t_k - \tau)). \end{aligned} \quad (33)$$

Let

$$\begin{aligned} \omega(k) &= [e_1(t_k - \tau), e_2(t_k - \tau), \dots, e_3(t_k - \tau)]^T, \\ \Xi(k) &= [\Xi_1(k), \Xi_2(k), \dots, \Xi_n(k)]^T, \end{aligned} \quad (34)$$

where

$$\Xi_i(k) = [x_i(t_k), y_i(t_k), x_i(t_k - \tau), y_i(t_k - \tau), z(k)]^T; \quad (35)$$

then the controlled system (30) can be rewritten as

$$\Xi(k+1) = \widehat{F} \Xi(k) + \widehat{D} \omega(k), \quad (36)$$

where $\widehat{F} = (I_n \otimes \widehat{A} - (L+B) \otimes \widehat{C})$,

$$\begin{aligned} \widehat{A} &= \begin{pmatrix} 1 & h & 0 & 0 & 0 \\ 0 & 1 & 0 & 0 & 0 \\ 1 & h - \tau & 0 & 0 & 0 \\ 0 & 1 & 0 & 0 & 0 \\ 0 & 0 & 0 & 0 & 0 \end{pmatrix}, \\ \widehat{D} &= I_n \otimes \begin{pmatrix} -h\beta_1 \\ -\beta_1 \\ -(h-\tau)\beta_1 \\ -\beta_1 \end{pmatrix}, \\ \widehat{C} &= \begin{pmatrix} 0 & 0 & h\beta_1 & 0 & h\beta_2 \\ 0 & 0 & \beta_1 & 0 & \beta_2 \\ 0 & 0 & (h-\tau)\beta_1 & 0 & (h-\tau)\beta_2 \\ 0 & 0 & \beta_1 & 0 & \beta_2 \\ 0 & 0 & \alpha_1 & 0 & 0 \end{pmatrix}. \end{aligned} \quad (37)$$

Lemma 10. *When the input delays are considered, the controlled system (30) can achieve quantized consensus tracking if and only if $\rho(\widehat{F}) < 1$.*

Proof. It is easy to prove this lemma in a way that is similar to what is used in Lemma 5. Define $\widehat{\gamma}(k) = E(\Xi(k) \otimes \Xi(k))$. Analogously, one has $\lim_{k \rightarrow \infty} E(\|\Xi(k)\|_2^2) \leq \widehat{I} \widehat{\delta} / (1 - \widehat{\omega})$, where $\widehat{\omega} = \|\widehat{F} \otimes \widehat{F}\|_2$. There exist positive constants $\widehat{M}, \widehat{N} > 0$ such that $\lim_{k \rightarrow \infty} E(\|x_i(t_k)\|_2^2) \leq \widehat{M} \widehat{\delta}$, $\lim_{k \rightarrow \infty} E(\|y_i(t_k)\|_2^2) \leq \widehat{N} \widehat{\delta}$, so one has

$$\begin{aligned} \lim_{t \rightarrow \infty} E(|\xi_i(t) - \xi_0(t)|^2) &\leq \widehat{M} \widehat{\delta}, \\ \lim_{t \rightarrow \infty} E(|\zeta_i(t) - \zeta_0(t)|^2) &\leq \widehat{N} \widehat{\delta}, \quad i = 1, 2, \dots, n. \end{aligned} \quad (38)$$

And then this proof is completed. \square

Theorem 11. *The controlled (30) can achieve quantized consensus tracking if and only if the directed graph $\widetilde{\mathcal{G}}$ has a spanning tree and the polynomial*

$$\begin{aligned} \widehat{g}_i(\sigma) &= (1 + a_2 + a_1 + a_0) \sigma^3 + (3 + a_2 - a_1 - 3a_0) \sigma^2 \\ &\quad + (3 - a_2 - a_1 + 3a_0) \sigma + (1 - a_2 + a_1 - a_0) \end{aligned} \quad (39)$$

is Hurwitz stable, where $\mu_i, i = 1, 2, \dots, n$, are the eigenvalues of $L+B$, $a_2 = h\mu_i\beta_1 - \tau\mu_i\beta_1 - 2$, $a_1 = 1 + \tau\mu_i\beta_1 - h\mu_i^2\alpha_1\beta_2 + \tau\mu_i^2\alpha_1\beta_2$, $a_0 = -\tau\mu_i^2\alpha_1\beta_2$.

Proof. Let

$$\widehat{F}_i = \begin{pmatrix} 1 & h & -\mu_i h \beta_1 & 0 & -\mu_i h \beta_2 \\ 0 & 1 & -\mu_i \beta_1 & 0 & -\mu_i \beta_2 \\ 1 & h - \tau & -\mu_i (h - \tau) \beta_1 & 0 & -\mu_i (h - \tau) \beta_2 \\ 0 & 1 & -\mu_i \beta_1 & 0 & -\mu_i \beta_2 \\ 0 & 0 & -\mu_i \alpha_1 & 0 & 0 \end{pmatrix}, \quad (40)$$

where $\mu_i, i = 1, 2, \dots, n$ are the eigenvalues of $L+B$. According to Lemma 10, it is easy to know that the controlled system

(30) can achieve quantized consensus tracking if and only if $\rho(\widehat{F}_i) < 1$, $i = 1, 2, \dots, n$. Note that

$$\begin{aligned} & |\lambda I_5 - \widehat{F}_i| \\ &= \lambda^2 (\lambda^3 + (h\mu_i\beta_1 - \tau\mu_i\beta_1 - 2)\lambda^2 \\ & \quad + (1 + \tau\mu_i\beta_1 - h\mu_i^2\alpha_1\beta_2 + \tau\mu_i^2\alpha_1\beta_2)\lambda - \tau\mu_i^2\alpha_1\beta_2). \end{aligned} \quad (41)$$

Let

$$\begin{aligned} \widehat{f}_i(\lambda) &= \lambda^3 + (h\mu_i\beta_1 - \tau\mu_i\beta_1 - 2)\lambda^2 \\ & \quad + (1 + \tau\mu_i\beta_1 - h\mu_i^2\alpha_1\beta_2 + \tau\mu_i^2\alpha_1\beta_2)\lambda \\ & \quad - \tau\mu_i^2\alpha_1\beta_2, \end{aligned}$$

$$a_2 = h\mu_i\beta_1 - \tau\mu_i\beta_1 - 2,$$

$$a_1 = 1 + \tau\mu_i\beta_1 - h\mu_i^2\alpha_1\beta_2 + \tau\mu_i^2\alpha_1\beta_2, \quad a_0 = -\tau\mu_i^2\alpha_1\beta_2, \quad (42)$$

and then one has $\widehat{f}_i(\lambda) = \lambda^3 + a_2\lambda^2 + a_1\lambda + a_0$. Let

$$\widehat{g}_i(\sigma) = (\sigma - 1)^3 f\left(\frac{\sigma + 1}{\sigma - 1}\right). \quad (43)$$

It can be rewritten in the following form:

$$\begin{aligned} \widehat{g}_i(\sigma) &= (1 + a_2 + a_1 + a_0)\sigma^3 + (3 + a_2 - a_1 - 3a_0)\sigma^2 \\ & \quad + (3 - a_2 - a_1 + 3a_0)\sigma + (1 - a_2 + a_1 - a_0). \end{aligned} \quad (44)$$

Obviously, polynomial $\widehat{f}_i(\lambda)$ is Schur stable if and only if polynomial $\widehat{g}_i(\sigma)$ is Hurwitz stable. It is easy to conclude that the controlled system (30) can achieve the quantized consensus tracking if and only if $\widehat{g}_i(\sigma)$ is Hurwitz stable. Then this theorem is proved. \square

Remark 12. Similar to Theorem 6, a necessary and sufficient condition for the quantized consensus tracking for the controlled system (30) is derived as a polynomial with order three in Theorem 11. For a given topology with determinate input delays τ , whether directed or undirected, one could also choose appropriate control gains $\alpha_1, \beta_1, \beta_2$ and sampling period h such that condition (39) is satisfied.

Corollary 13. Assume that the \mathcal{G} is an undirected graph. The controlled system (30) can achieve quantized consensus tracking if and only if the $\widetilde{\mathcal{G}}$ consists of a spanning tree and

$$\beta_1 > \mu_i\alpha_1\beta_2,$$

$$(h - 2\tau)\beta_1 + (h + 2\tau)\mu_i\alpha_1\beta_2 > 0, \quad (45)$$

$$4 - h\mu_i\beta_1 + (h - 4\tau)\mu_i^2\alpha_1\beta_2 > 0,$$

$$4 + (2\tau - h)\mu_i\beta_1 + (2\tau - h)\mu_i^2\alpha_1\beta_2 > 0,$$

$$1 + a_2a_0 - a_0^2 - a_1 > 0 \quad (46)$$

hold.

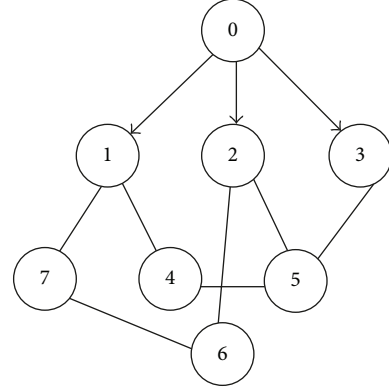


FIGURE 1: The interaction graph.

Proof. While the $\widetilde{\mathcal{G}}$ is the undirected graph, μ_i , $i = 1, 2, \dots, n$ are all real numbers. Thus a_2, a_1, a_0 are all real numbers too. According to Routh's stability criterion, $\widehat{g}_i(\sigma)$ is stable if and only if $1 + a_2 + a_1 + a_0 > 0$, $3 + a_2 - a_1 - 3a_0 > 0$, $3 - a_2 - a_1 + 3a_0 > 0$, $1 - a_2 + a_1 - a_0 > 0$, and $(3 - a_2 - a_1 + 3a_0)(3 + a_2 - a_1 - 3a_0) - (1 + a_2 + a_1 + a_0)(1 - a_2 + a_1 - a_0) > 0$. By solving the first four polynomials, one obtains condition (45). The fifth polynomial can be rewritten as condition (46). Therefore, quantized consensus tracking in controlled system (30) can be reached. This proof is completed. \square

4. Numerical Simulations

In this section, some numerical simulations are given to demonstrate the theorem analysis. Consider a multiagent system with 8 agents (a leader and 7 followers) which is shown in Figure 1. The Laplacian matrix L is

$$L = \begin{pmatrix} 2 & 0 & 0 & -1 & 0 & 0 & -1 \\ 0 & 2 & 0 & 0 & -1 & -1 & 0 \\ 0 & 0 & 1 & 0 & -1 & 0 & 0 \\ -1 & 0 & 0 & 2 & -1 & 0 & 0 \\ 0 & -1 & -1 & -1 & 3 & 0 & 0 \\ 0 & -1 & 0 & 0 & 0 & 2 & -1 \\ -1 & 0 & 0 & 0 & 0 & -1 & 2 \end{pmatrix}, \quad (47)$$

where $B = \text{diag}(1, 1, 1, 0, 0, 0, 0)$, $b = (1, 1, 1, 0, 0, 0, 0)^T$, and $a(t) = 0.1 \sin(t/10)$. Choose quantized interval $\delta = 0.2$. By simple calculation of L , one has $\mu_{\max} = 4.7384$. Choose $\alpha_1 = 0.2$, $\beta_2 = 1$, and $\beta_1 = 1.2$. According to Theorem 8, the quantized consensus tracking can be reached if and only if $h < 0.3931$. Let $h = 0.39$, as it is shown in Figure 2, the quantized tracking consensus can be achieved. While $h = 0.40$, it cannot be achieved, which is shown in Figure 3.

When input delays are taken into consideration, choose $\alpha_1 = 0.2$, $\beta_1 = 1$, $\beta_2 = 1$, $h = 0.4$, and $\tau = 0.02$, which satisfies Theorem 11. As it is shown in Figure 4, the quantized consensus tracking can be achieved. But when $\alpha_1 = 0.2$, $\beta_1 = 1$, $\beta_2 = 1$, $h = 0.4$, and $\tau = 0.06$, the system cannot achieve the consensus tracking, which is shown in Figure 5.

Remark 14. As a matter of fact, the quantized consensus tracking is clearly not a strict consensus; that is, all agents

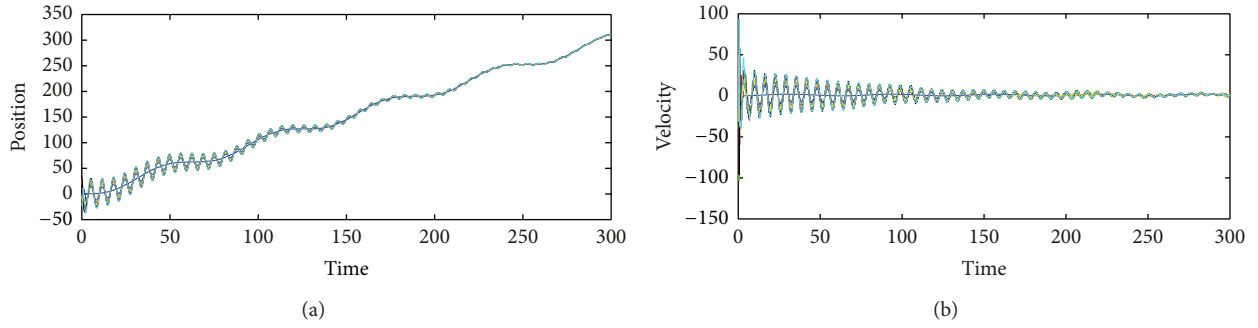


FIGURE 2: Position (a) and velocity (b) states of agents, where $h = 0.39$ and $\delta = 0.2$.

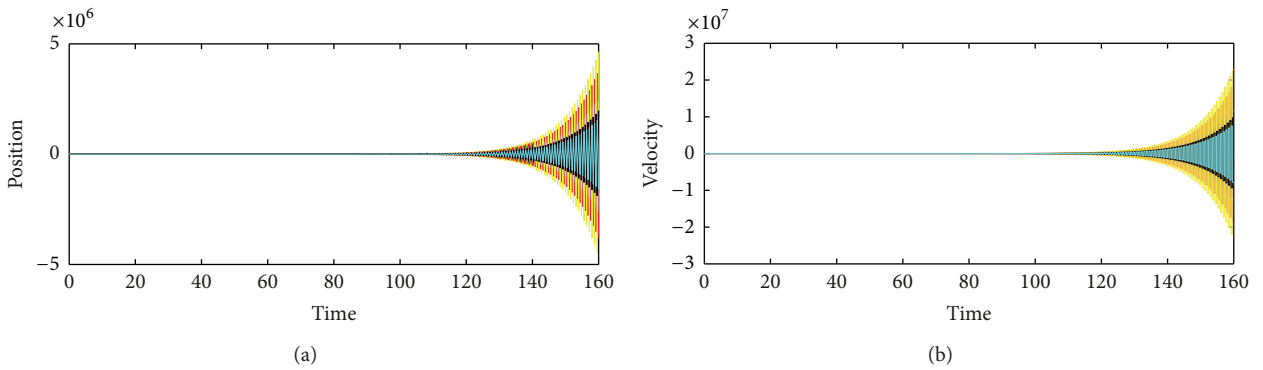


FIGURE 3: Position (a) and velocity (b) states of agents, where $h = 0.40$ and $\delta = 0.2$.

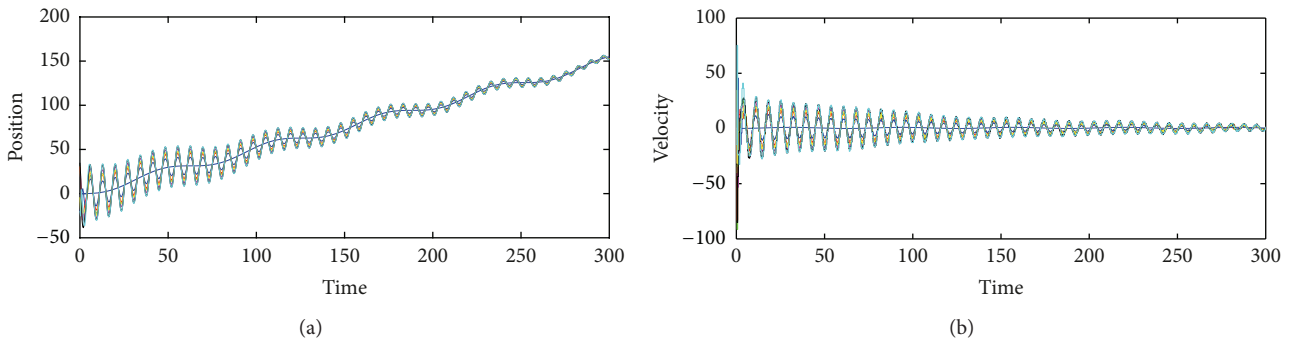


FIGURE 4: Position (a) and velocity (b) states of agents, where $h = 0.4$, $\tau = 0.02$, and $\delta = 0.2$.

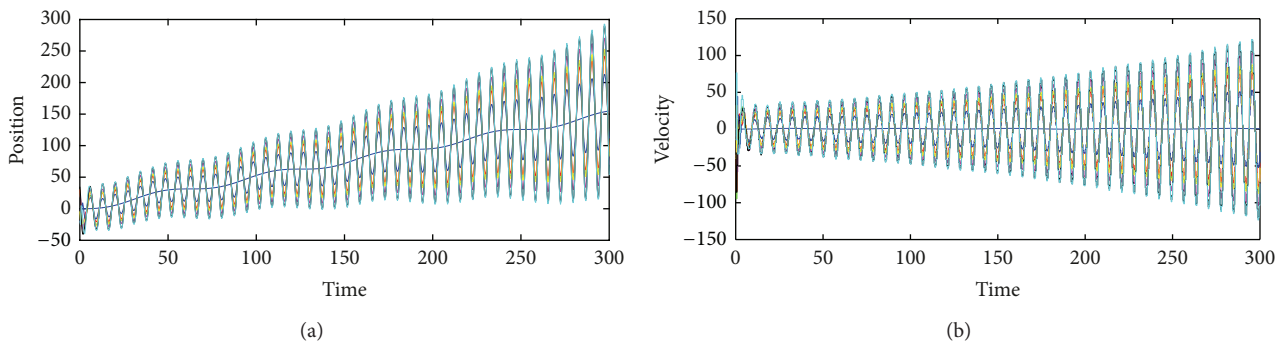


FIGURE 5: Position (a) and velocity (b) states of agents, where $h = 0.4$, $\tau = 0.06$, and $\delta = 0.2$.

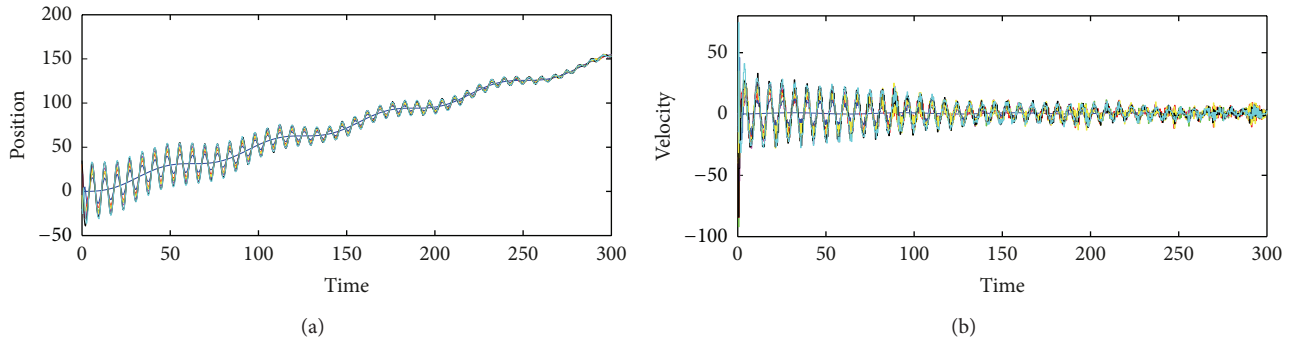


FIGURE 6: Position (a) and velocity (b) states of agents, where $h = 0.4$, $\tau = 0.02$, and $\delta = 1$.

in the network do not have the same value as the leader. There are still some errors in quantized consensus tracking which can be found in the simulation results of Figures 4 and 6. According to Definition 1, this phenomenon is easily explained because the consensus quality is closely related to the quantized interval δ or even determined by it. Comparing Figure 4 with Figure 6, it can be found that the later errors ($\delta = 1$) are bigger than the former ($\delta = 0.2$) under the same control gains, sampling interval, and time delay. Therefore, in order to achieve a more accurate quantized consensus tracking, smaller quantized interval should be taken into account in practical applications.

5. Conclusions

In this paper, the consensus tracking problems for second-order multiagent systems without/with input delays are studied. We propose impulsive consensus tracking algorithms without velocity measurements. Considering the constraints of communication channels with finite bandwidth and finite power, randomized quantization scheme is introduced in our work. Information of agents in the multiagent systems is quantized using this scheme before being transmitted to their neighbors. Some sufficient and necessary conditions for consensus tracking are obtained. By appropriately choosing the sampling period and control gains such that this condition holds, the second-order multiagent systems without/with input delays can achieve quantized consensus tracking. Finally, numerical simulations are given to illustrate the theoretical analysis. Furthermore, future efforts will focus on adaptive and output feedback extensions of the developed controllers to reduce the required amount of state and model knowledge.

Conflict of Interests

The authors declare that there is no conflict of interests regarding the publication of this paper.

Acknowledgments

This work was supported in part by the National Natural Science Foundation of China (61304152, 61374064, and

61364017), National Key Technology Research and Development Program of the Ministry of Science and Technology of China (2013BAA01B01), and the China Postdoctoral Science Foundation funded project (2013T60738).

References

- [1] Z. Li, Z. Duan, G. Chen, and L. Huang, "Consensus of multiagent systems and synchronization of complex networks: a unified viewpoint," *IEEE Transactions on Circuits and Systems*, vol. 57, no. 1, pp. 213–224, 2010.
- [2] Z. Lin, B. Francis, and M. Maggiore, "Necessary and sufficient graphical conditions for formation control of unicycles," *IEEE Transactions on Automatic Control*, vol. 50, no. 1, pp. 121–127, 2005.
- [3] R. Olfati-Saber, "Flocking for multi-agent dynamic systems: algorithms and theory," *IEEE Transactions on Automatic Control*, vol. 51, no. 3, pp. 401–420, 2006.
- [4] R. Olfati-Saber and J. S. Shamma, "Consensus filters for sensor networks and distributed sensor fusion," in *Proceedings of the 44th IEEE Conference on Decision and Control, and the European Control Conference (CDC-ECC '05)*, pp. 6698–6703, Seville, Spain, December 2005.
- [5] Z. Meng, W. Ren, Y. Cao, and Z. You, "Leaderless and leader-following consensus with communication and input delays under a directed network topology," *IEEE Transactions on Systems, Man, and Cybernetics B*, vol. 41, no. 1, pp. 75–88, 2011.
- [6] Y. Hong, J. Hu, and L. Gao, "Tracking control for multi-agent consensus with an active leader and variable topology," *Automatica*, vol. 42, no. 7, pp. 1177–1182, 2006.
- [7] W. Ni and D. Cheng, "Leader-following consensus of multi-agent systems under fixed and switching topologies," *Systems & Control Letters*, vol. 59, no. 3–4, pp. 209–217, 2010.
- [8] J. Hu and Y. Hong, "Leader-following coordination of multi-agent systems with coupling time delays," *Physica A*, vol. 374, no. 2, pp. 853–863, 2007.
- [9] L. Ding, Q.-L. Han, and G. Guo, "Network-based leader-following consensus for distributed multi-agent systems," *Automatica*, vol. 49, no. 7, pp. 2281–2286, 2013.
- [10] H. Su, X. Wang, and G. Chen, "A connectivity-preserving flocking algorithm for multi-agent systems based only on position measurements," *International Journal of Control*, vol. 82, no. 7, pp. 1334–1343, 2009.
- [11] J. Mei, W. Ren, and G. Ma, "Distributed coordination for second-order multi-agent systems with nonlinear dynamics

- using only relative position measurements,” *Automatica*, vol. 49, no. 5, pp. 1419–1427, 2013.
- [12] Z.-W. Liu, Z.-H. Guan, X. Shen, and G. Feng, “Consensus of multi-agent networks with aperiodic sampled communication via impulsive algorithms using position-only measurements,” *IEEE Transactions on Automatic Control*, vol. 57, no. 10, pp. 2639–2643, 2012.
- [13] A. Kashyap, T. Başar, and R. Srikant, “Quantized consensus,” *Automatica*, vol. 43, no. 7, pp. 1192–1203, 2007.
- [14] T. C. Aysal, M. Coates, and M. Rabbat, “Distributed average consensus using probabilistic quantization,” in *Proceedings of the 14th IEEE/SP Workshop on Statistical Signal Processing (SSP '07)*, pp. 640–644, Madison, Wis, USA, August 2007.
- [15] H. Yan, Z. Su, H. Zhang, and F. Yang, “Observer-based H_∞ control for discrete-time stochastic systems with quantisation and random communication delays,” *IET Control Theory & Applications*, vol. 7, no. 3, pp. 372–379, 2013.
- [16] H. Zhang, H. Yan, F. Yang, and Q. Chen, “Quantized control design for impulsive fuzzy networked systems,” *IEEE Transactions on Fuzzy Systems*, vol. 19, no. 6, pp. 1153–1162, 2011.
- [17] Z.-H. Guan, C. Meng, R.-Q. Liao, and D.-X. Zhang, “Consensus of second-order multi-agent dynamic systems with quantized data,” *Physics Letters A*, vol. 376, no. 4, pp. 387–393, 2012.
- [18] T. C. Aysal, M. J. Coates, and M. G. Rabbat, “Rates of convergence for distributed average consensus with probabilistic quantization,” in *Proceedings of the Allerton Conference on Communication, Control, and Computing*, Urbana, Ill, USA, September 2007.
- [19] Z.-W. Liu, Z.-H. Guan, T. Li, X.-H. Zhang, and J.-W. Xiao, “Quantized consensus of multi-agent systems via broadcast gossip algorithms,” *Asian Journal of Control*, vol. 14, no. 6, pp. 1634–1642, 2012.
- [20] T. C. Aysal, M. J. Coates, and M. G. Rabbat, “Distributed average consensus with dithered quantization,” *IEEE Transactions on Signal Processing*, vol. 56, no. 10, pp. 4905–4918, 2008.
- [21] D. V. Dimarogonas and K. H. Johansson, “Stability analysis for multi-agent systems using the incidence matrix: quantized communication and formation control,” *Automatica*, vol. 46, no. 4, pp. 695–700, 2010.
- [22] Z.-H. Guan, Z.-W. Liu, G. Feng, and M. Jian, “Impulsive consensus algorithms for second-order multi-agent networks with sampled information,” *Automatica*, vol. 48, no. 7, pp. 1397–1404, 2012.
- [23] H. Zhang, H. Yan, T. Liu, and Q. Chen, “Fuzzy controller design for nonlinear impulsive fuzzy systems with time delay,” *IEEE Transactions on Fuzzy Systems*, vol. 19, no. 5, pp. 844–856, 2011.
- [24] Z.-W. Liu, H. Zhou, Z.-H. Guan, W.-S. Hu, L. Ding, and W. Wang, “Distributed impulsive consensus of the multiagent system without velocity measurement,” *Abstract and Applied Analysis*, vol. 2013, Article ID 825307, 8 pages, 2013.
- [25] H. Zhang, Z.-H. Guan, and G. Feng, “Reliable dissipative control for stochastic impulsive systems,” *Automatica*, vol. 44, no. 4, pp. 1004–1010, 2008.
- [26] Z.-H. Guan, Z.-W. Liu, G. Feng, and Y.-W. Wang, “Synchronization of complex dynamical networks with time-varying delays via impulsive distributed control,” *IEEE Transactions on Circuits and Systems*, vol. 57, no. 8, pp. 2182–2195, 2010.
- [27] Y.-P. Tian and C.-L. Liu, “Consensus of multi-agent systems with diverse input and communication delays,” *IEEE Transactions on Automatic Control*, vol. 53, no. 9, pp. 2122–2128, 2008.
- [28] Y. Zhang and Y.-P. Tian, “Consensus of data-sampled multi-agent systems with random communication delay and packet loss,” *IEEE Transactions on Automatic Control*, vol. 55, no. 4, pp. 939–943, 2010.
- [29] F. Bullo, J. Cortés, and S. Martínez, *Distributed Control of Robotic Networks: A Mathematical Approach to Motion Coordination Algorithms*, Princeton University Press, Princeton, NJ, USA, 2009.
- [30] W. Yu, W. X. Zheng, G. Chen, W. Ren, and J. Cao, “Second-order consensus in multi-agent dynamical systems with sampled position data,” *Automatica*, vol. 47, no. 7, pp. 1496–1503, 2011.
- [31] R. A. Horn and C. R. Johnson, *Matrix Analysis*, Cambridge University Press, Cambridge, UK, 2012.
- [32] W. Yu, L. Zhou, X. Yu, J. Lu, and R. Lu, “Consensus in multi-agent systems with second-order dynamics and sampled data,” *IEEE Transactions on Industrial Informatics*, vol. 9, no. 4, pp. 2137–2146, 2012.

Research Article

Bayes Network Based Collaborating Control Algorithm in Active Multicamera Network with Applications to Object Tracking

Rui Zhao,^{1,2} Zhihua Wei,^{1,3} Yan Wu,^{1,3} Cairong Zhao,^{1,3} and Duoqian Miao^{1,3}

¹ Department of Computer Science and Technology, Tongji University, Shanghai 201804, China

² The Third Research Institute of the Ministry of Public Security, Shanghai 201204, China

³ Key Laboratory of Embedded System and Service Computing, Ministry of Education, Tongji University, Shanghai 201804, China

Correspondence should be addressed to Zhihua Wei; zhihua_wei@tongji.edu.cn

Received 16 December 2013; Accepted 13 January 2014; Published 20 February 2014

Academic Editor: Huaicheng Yan

Copyright © 2014 Rui Zhao et al. This is an open access article distributed under the Creative Commons Attribution License, which permits unrestricted use, distribution, and reproduction in any medium, provided the original work is properly cited.

Intelligent video surveillance network has many practical applications such as human tracking, vehicle tracking, and event detection. In this paper, an active multicamera network framework is designed for human detection and tracking by optimizing the cameras collaborating control. A multicamera collaborating control algorithm is proposed based on Bayes network to minimize the number of PTZ cameras with control and optimize the cameras' field of view. Hybrid human local feature transform selected by AdaBoost algorithm is adopted to improve the tracking precision. Experimental results on real world environment indicate the effectiveness and efficiency of proposed framework and algorithm.

1. Introduction

Monitoring and tracking mobile objects in public region such as subway stations, square, railway station, and commercial center are the most important function of surveillance [1–3]. Though a large amount of cameras have been installed, it is hard to obtain high-quality and widely covered surveillance videos in real world environment because the station cameras have their fixed Fields Of View (FOV) and some obstacles are likely to occlude the objects. With the rapid growing of sensor network, camera network including both station cameras and active pan/tilt/zoom (PTZ) cameras is possible to be constructed to solve this problem. PTZ cameras could change their angles to interest objects according to control instructions.

However, with the size of camera network increasing, it becomes infeasible for administrators to observe many cameras and discover interest events. Regarding the control of each PTZ camera, such as calibrating and zooming out to a moving object, it is hard to image. Consequently, it is a practical research to design intelligent camera network which could turn to interest objects automatically or semiautomatically

according to control instructions in order to observe given targets.

Such surveillance systems face two difficulties: (1) how could cameras automatically direct to the center of given objects? and (2) what is an effective scheme of multicamera collaborating tracking?

As far as the multicamera network concerned, the premier problem is to calibrate the cameras to the center of an interest object. To achieve robust detection and tracking results, cameras should be calibrated to a good viewpoint to ensure the high quality of captured videos. Some definitions about projective rotations were proposed in [4, 5]. Some methods to determine the intrinsic and extrinsic parameters were proposed in [6, 7]. In [8], a kind of image-ground-plane transformation of each camera was proposed based on a ground-plane coordinate system which was nearly independent of object location change. Some researchers have proposed camera network calibration strategies for both stationary and actively controlled camera nodes from multiple viewpoints [9, 10]. Above works lay more emphasis on independent camera calibration. With the prevalence of camera network, some researches began to take the effect

of relation among cameras into consideration when they design camera calibration strategies. For example, Collins et al. [11] and Zhou et al. [1] employed a stationary wide-FOV camera to control an PTZ camera. More recent works reflect the consideration of content-awareness transmission strategy and transmission delay in their control strategy [2, 12].

In multicamera network, researches on strategies of scheduling multicameras to recognize and track one or more moving objects have attracted many researchers' attention. One scenario is described as tracking moving objects in an environment covered by multiple cameras with overlapping FOV. In this scenario, the tracking problem should be defined as "consistent labeling of objects" which aims at establishing correspondence between tracks of the same object, seen in different cameras, to recover complete information about the object [3]. Another scenario considers the linkage among multiple cameras which is usually applied to schedule, coordinate, and control the network of active cameras to focus on and observe given targets at high resolution. In this case, the targets' information such as location and moving direction is usually utilized to predict cameras which are likely to observe the targets. This paper will focus on this kind of problem.

Considering multicamera collaborating, most works focus on the control strategy in a fully observable surveillance environment, where the locations and directions of targets could be directly observed and their velocity could be estimated by using station cameras or configuring one or more active PTZ cameras to zoom out to them. In [13], an adaptive algorithm was proposed to provide automated control of a PTZ camera by using the captured visual information only. In [14], an image-based PTZ camera control method was proposed based on projective rotations for automated multicamera surveillance systems. The work in [15] focused on the control of a set of PTZ cameras for acquiring close-up views of subjects based on the output of a set of fixed cameras. Reference [16] described using the color model of objects to integrate information from multiple cameras. Reference [17] evaluated various strategies for scheduling a single active camera to acquire biometric imagery.

However, with some uncertainty, dynamic factors often affect the surveillance quality. For example, when multiple pedestrians are present in the scene, it is a difficult work for camera to decide which one should be focused on. More general scenario is partially observable [18]. That is, the exact locations of the objects may not always be observed completely by the cameras. Purely adding station cameras or PTZ cameras does not help the matter because their measured locations become less accurate regardless of the calibration method when the objects move further away from the cameras. More intelligent coordination method should be explored.

Recently, some researchers began to integrate some estimating algorithms into multicamera coordination to deal with the uncertainty of multicamera surveillance system. Zhang et al. [19] proposed a kind of quantized control design for fuzzy network system. Zhou et al. [1] tracked pedestrians using an active camera. When multiple people are present

in the scene, the person who is closest to the last tracked person is chosen. In another view, Hampapur et al. [20] deal with the issues by deciding how cameras should be assigned to various people present in the scene. Ostland et al. [21] used a Markov Chain Monte Carlo approach for object detection and tracking in a multicamera system. In [2], both video transmission and its impact on the accuracy of camera control were considered and content-aware transmission strategy was designed. In [22], missing measurements were considered in their control system. In [23], a principled Partially Observable Markov Decision Process-based approach was proposed to coordinate and control a network of active cameras for tracking and observing multiple mobile objects. These works help to eliminate the dependency on FOV of cameras for tracking the objects' locations by exploiting probability framework to model the multicamera network. Our work is partially illuminated by these works.

Nevertheless, most of above works consider a virtual or simulated environment for their algorithm designing and experiment conducting. It is different from the real world environment to some extent. For example, the distance between cameras in a large region (e.g. a district) should be computed according to the route between cameras which may be not straight line. The objects' movement between different cameras is dynamic. Occlusion phenomenon is general in this environment. All of these factors make the real world surveillance a more complicated problem. In this work, we propose an algorithm for real world video surveillance with PTZ cameras, where the multicamera collaboration scheme is constructed based on Bayes Network by taking into account the GIS information and camera action into models. It is likely to work in a wide region surveillance system with high efficiency.

The remainder of the paper is organized as follows. In Section 2, we present the system model. In Section 3, we propose a multicamera coordinating algorithm in probability framework. In Section 4, the experimental results are introduced and discussed. Section 5 concludes and proposes future research topics.

2. Proposed System Model

The proposed multicamera surveillance network model is shown in Figure 1, where the camera node works as an agent who codes the captured videos and transmits the coded packets to SCC (Surveillance Control Center) over a wireless network. Videos from all cameras' nodes are decoded, in which the interest targets will be detected. Once the interest target is found in videos from a camera, the SCC will send control decision to camera which is likely to capture the targets. We assign the computation of detection and controlling at SCC because it has more powerful computational capability which is necessary for video search tasks. Therefore, based on the video analysis at the SCC, the control model will send instructions to related cameras and these cameras will turn to targets and prepare for transmitting videos. In this process, we mainly address

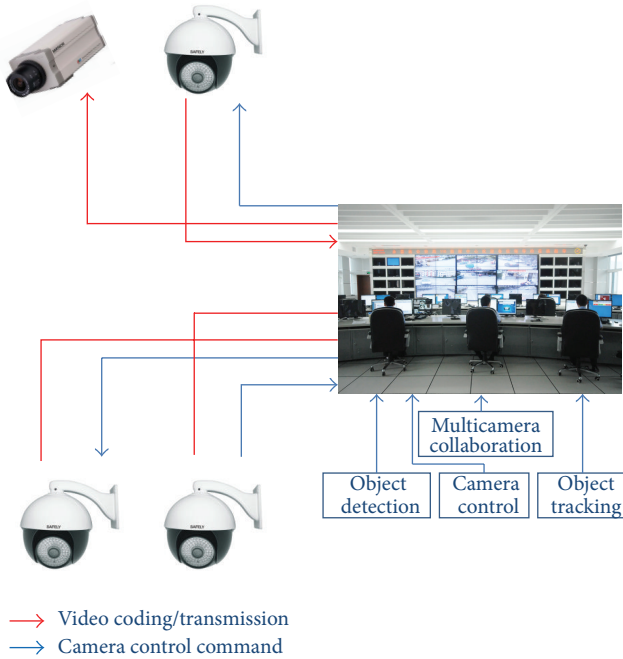


FIGURE 1: Proposed surveillance system model with active multi-cameras.

the following factors to advance the intelligence and efficiency of surveillance system.

(a) *Content-Aware Transmission.* Although videos are coded before being transmitted to SCC, they still severely occupy node resource. Since the captured video frame can be regarded as the combination of target and its background, the target could be coded and transmitted with a higher priority than the background. We adopt a content-aware approach that assigns the limited network resource to interest target firstly and processes the background in a best-effort fashion. In order to extract the target region in a frame, some background-foreground separation methods should be selected. Taking the tradeoff between the separating accuracy and computing complexity at the camera node, the strategy proposed in [2] is conducted in our system.

(b) *Video Content Detection.* Taking human tracking as example, we consider the problem as detecting the certain human in given video volumes. Some front-view image and some rotated images of certain person are taken as labeled examples. The SCC detects the same person or suspected persons in videos by using a hybrid feature that combines several local transform features by means of AdaBoost feature selection method proposed in [24]. In this style, the best local transform feature among several local transform features having the lowest classification error is sequentially selected until the classification performance is satisfied. This hybridization makes human detection robust to changes of external environment and high efficiency.

(c) *Multicamera Collaboration.* A controller in SCC is responsible for the interaction between the PTZ cameras and

detection results in SCC. Once the suspect target is detected in the videos from Camera C_i , the controller needs to decide which camera should be zoomed out and (or) be rotated to focus on the suspected target. Next camera which is possible to capture the target is uncertain and is determined by object's moving direction, velocity, and camera distribution. In real world conditions, occlusion phenomenon or the blind area of camera often affects the tracking results. In this work, we propose a multicamera collaborating algorithm based on Bayes network. The GIS information of cameras is merged to estimate the probability of target location. The detailed algorithm will be addressed in Section 3.

(d) *PTZ Camera Control.* Only when the control decision from SCC becomes the parameter of camera motor, camera could zoom out and change its view to the center of target. In this process, the PTZ cameras are instructed to observe the human and a look-up table is computed for each PTZ camera, which associates the (x, y) location of the person with the corresponding camera settings. The cameras being controlled send high quality videos to SCC and the tracking model of SCC will begin to track target in these videos. The cameras will recover to original status after a given time. The delay estimating algorithm in [2] is borrowed here because it can resolve the time delay in our system successfully.

(e) *Targets Tracking.* As soon as the cameras are controlled to turn to targets, the tracking model begins to work on the video sequences transmitted from these cameras. In tracking model, TLD (Tracking-Learning-Detection) is adopted due to its high performance and robust to some unpredictable factors [25]. TLD decomposes the tracking task into tracking, learning, and detection. The tracker follows the object from frame to frame. The detector localizes the location of object in frame and corrects the tracker if necessary. The learning estimates detector's errors and updates it to avoid these errors in the future. If the target is successfully found in these videos, they will be selected for user's application.

The conducting procedure of each module including object detection, camera election, camera control, and object tracking could be described as Algorithm 1. Where, C_list represents the candidate camera list in $t = k + 1$ and $V_j^{t=k+1}$ represent the videos captured by camera C_j at time $t = k + 1$. All videos captured by assigned cameras consist of the set of candidate videos V_list . If the object T_j is successfully tracked in $V_j^{t=k+1}$, it will be put into V_list which represents the final video set including given objects.

3. Multicamera Collaborative Tracking Based on Bayes Network

The collaboration of cameras is affected by various factors from target such as the location, the moving direction, and the velocity. The cameras' geographical distribution should also be concerned because it is the direct factor for calculating the target's moving time among cameras. Their relations could be modeled by Bayes network. This section

```

Surveillance process with active camera control:
Initialization: at  $t = t_0$ , object  $T_i$  is observed in camera  $C_j$ 
(1) manually label object  $T_i$ 
(2) for (each  $t = k, t_0 \leq k \leq n$ )
(3) { clear C_list
(4)   if  $\text{fov}(C_j) \supset T_i^{t=k+1}$  add  $C_j$  into C_list
(5)   for each  $C_j \in \text{C\_list}$  do
(6)     { send PTZ control instruction to  $C_j$ ;
(7)        $C_j$  conduct instruction;
(8)        $C_j$  transmit videos  $V_j^{t=k+1}$  to SCC;
(9)     }
(10)  conduct tracking algorithm in  $V_j^{t=k+1} \in V$ ;
(11)  if  $T_i$  is found in  $V_j^{t=k+1}$  add  $V_j^{t=k+1}$  into V_list
(12) }

```

ALGORITHM 1: The conducting procedure of each model.

will show the model definition and parameter estimation in the network.

A multicamera interactive network concerning target moving and camera actions is defined as a triple (S, A, P) , where the set S represents the states pairs of PTZ cameras and targets in surveillance system, A represent the action of the PTZ camera, and P is transitional function which defines the transfer relations from state S_i to S_i' .

The state $S \in \mathbb{R}$ is defined as a pair of (T_i, C_j) , where $T_i \in T$ ($i = 1, 2, \dots, m$) represents the target to be observed, $C_j \in C$ ($j = 1, 2, \dots, n$) represents the PTZ camera, and $T \times C$ consist of all possible combination of targets and cameras. For any target T_i , it can be described as a triple (T_i^l, T_i^d, T_i^v) . Further, T is defined on $T^l \times T^d \times T^v$ to represent target's location, moving direction, and velocity, respectively. The state space of PTZ camera is a set of positions. For each camera C_j , $\text{fov}(C_j)$ represents the cover region of camera C_j which can be linked to targets by judging the relation between $\text{fov}(C_j)$ and T_i^l . Once the target is near to the FOV of camera C_j , a control instruction of adjusting the PTZ parameters should be sent to camera C_j to obtain better view.

There are two assumptions in our system as follows.

- (1) Given the state C_j and action A_j , camera j 's next state C_j' is conditionally independent of the other cameras' states and any target's state in current time.
- (2) Given the target T_i , its next state T_i' is conditionally independent of the other targets' states and any camera's state in current time.

Then, the transition model could be simplified as in the following formula:

$$P(S_i' | S_i, A_j) = \prod_{i=1}^m P(T_i' | T_i) \prod_{j=1}^n \delta_{\tau(C_j, A_j)}(T_i'), \quad (1)$$

where $\tau(C_j, A_j) = C_j'$ represent the next state of C_j by executing action A_j . δ function is defined as in the following formula:

$$\delta_{\tau(C_j, A_j)}(T_i') = \begin{cases} 1, & \text{fov}(C_j') \supset T_i^{l'} \\ 0, & \text{otherwise.} \end{cases} \quad (2)$$

The next state of target T_i' is conditionally dependent on the current (T_i^l, T_i^d, T_i^v) . That is, the target's location in next state is decided by the current location, its direction, and velocity. So, $P(T_i' | T_i)$ could be expressed as in the following formula:

$$\begin{aligned} P(T_i' | T_i) &= P(T_i^{l'}, T_i^{d'}, T_i^{v'} | T_i^l, T_i^d, T_i^v) \\ &= P(T_i^{l'} | T_i^l, T_i^d, T_i^v) \\ &\quad \times P(T_i^{d'} | T_i^d) P(T_i^{v'} | T_i^v). \end{aligned} \quad (3)$$

It is supposed that the target's direction and velocity obey Gaussian distribution $N(\mu_d, \sigma_d)$ and $N(\mu_v, \sigma_v)$, respectively. μ_d and μ_v are the direction and velocity in current state, respectively. σ_d and σ_v are the variance of direction and velocity which could be estimated from a large amount of targets' individual behaviors. The transition probability $P(T_i^{l'} | T_i^l, T_i^d, T_i^v)$ could be computed according to the general velocity-direction motion model proposed in [26].

For a large surveillance region, the camera's GIS information which is reserved on SCC will be regarded as the location of targets once the targets enter the FOV of some camera. GIS information will be used to compute the target's moving time from one camera to another.

In Bayes paradigm, the event of "which camera should be controlled" is changed as a problem of "which camera has much more probability to cooccur with given target." We could obtain a candidate camera list by computing the probability of $P(S_i' | S_i, A_i)$. The SCC will send control command to the top n camera node according to the real task requirement.



FIGURE 2: An example of multicamera coordinate tracking.

4. Experiments and Discussions

4.1. Experimental Setting. Experiments of video surveillance were performed in a subway interchange station in Shanghai with 20 exits and more than 100 cameras including 60 active PTZ cameras (200 million pixel). The performance of network is evaluated in terms of the effectiveness of camera coordinating and PTZ control. The PTZ camera is normally installed at the exits, especially the place where there is a large pedestrian flow. We tested our coordinating strategy by setting different autonomous person and different number of targets. For each trail, the target is selected in the videos transmitted from a station camera. Once it is decided as the tracking object, our coordinating algorithm began to work.

All captured video frames except the first one were coded as inter frames. Each video frame was segmented into a foreground part and a background part by the Mixture Gaussians model and was separately coded. Based on the received videos, the target's location was labeled according to the GIS information of corresponding camera and its future location was estimated at SCC by using the Mean Shift algorithm for PTZ camera control decision making.

In the experiments, we adopt a hybrid feature that combines several local transform features by means of the AdaBoost method proposed in [24], where the best feature having the lowest classification error is sequentially selected until we obtain the required classification performance. The features include local gradient patterns (LGP) and binary histograms of oriented gradients (BHOG) and local binary patterns (LBP). LBP is robust to global illumination changes, LGP is robust to intensity changes, and BHOG could resist the effect of local pose change. Their hybridization makes face and human detection robust to various environment changes.

4.2. Collaborated Tracking Process. The process of multicamera collaborating example is indicated in Figure 2, where a suspicious man is found in the video from camera number 1 at 1st Exit (the image on the top middle in Figure 2); a user in SCC selects this target with a red frame and adds some pictures of this person which have been provided by users, the collaborating process starts. Camera number 1 on the access of 1st Exit receives the PTZ (pan, tilt, and zoom) control command from SCC, conducts rotation and zoom operations, and transmits videos zoomed out to SCC. Meanwhile, other possible cameras which is estimated by

our algorithm receive control instructions also and conduct similar operations. From Figure 2, we could observe that camera number 2 at 11th Exit (the image on the top right corner in Figure 2) takes over the observing task, which in turn is taken over by camera number 1 at 9th Exit (the image on the lower right corner in Figure 2) and camera number 2 at 9th Exit (the image on the lower left corner in Figure 2). In Figure 2, three cameras obtained the zoomed out videos and the first camera could not obtain it because the target had left its FOV when the control command arrived. Target's faces are occluded manually in the picture as they involve the problem of personal privacy protection.

4.3. Multicamera Collaboration Performance Analysis. The overall performance is evaluated by the $\text{Percent}_{\text{obs}}$ which is proposed in [23].

$$\text{Percent}_{\text{obs}} = \frac{100}{\tau M_{\text{tot}}} \sum_{i=1}^{\tau} M_{\text{obs}}^i, \quad (4)$$

where τ is the total number of time step in a trial of experiments, M_{obs}^i is the total number of targets tracked by PTZ cameras at time step i , and M_{tot} is the real time steps that targets present in the experiment environment. This metric indicates the average observed time by the PTZ camera network compared to target's real present time.

In fact, the time of targets presenting in front of each camera is different from others because cameras are various in FOV and the environment is also different. The metric $\text{Percent}_{\text{obs}}$ is likely to be affected by the performance of some major cameras. For example, if a target presents in front of a camera with a good view and the camera has captured it for a long time, the overall evaluation by using this metric is prone to be better. Another case is that a target stayed in front of camera C_j for a long time and passed by other cameras rapidly. As a result, the overall performance is dominated by the performance of camera C_j . In order to reflect the average level of cameras, metric $\text{MacroAvg_Percent}_{\text{obs}}$ is proposed here to consider each camera equally as shown in the following formula:

$$\text{MacroAvg_Percent}_{\text{obs}} = \frac{1}{m} \sum_{j=1}^m \text{Percent}_{\text{obs}}(C_j). \quad (5)$$

The performance evaluated by two metrics, respectively, is shown in Table 1, where “number of camera_R” represents the number of cameras that the targets really pass and “number of camera_O” represents the number of cameras having observed targets. To distinguish the two metrics, the $\text{Percent}_{\text{obs}}$ is renamed as $\text{MicroAvg_Percent}_{\text{obs}}$ which reflects the average level of time span.

From Table 1, we could observe that the proposed algorithm correctly assigned PTZ cameras in most cases. The most important reason for falsely assignment is the occlusions by other pedestrian when there was a crowded pedestrian flow. In experiment 4 and experiment 6, there is one camera which could not capture the targets, respectively. However, the mistake mainly resulted from failed tracking instead of multicamera coordinating algorithm. As

TABLE 1: Coordinating tracking experimental results comparisons.

Experiment number	Time (s)	Number of targets	Number of camera _R	Number of camera _O	MicroAvg_Percent _{obs}	MacroAvg_Percent _{obs}
Exp. 1	95	1	4	4	98.5	98.1
Exp. 2	106	1	5	5	96.3	96.0
Exp. 3	84	2	5	5	92.7	92.2
Exp. 4	112	2	6	5	90.3	82.5
Exp. 5	90	3	5	5	90.7	89.8
Exp. 6	121	3	6	5	87.6	80.3

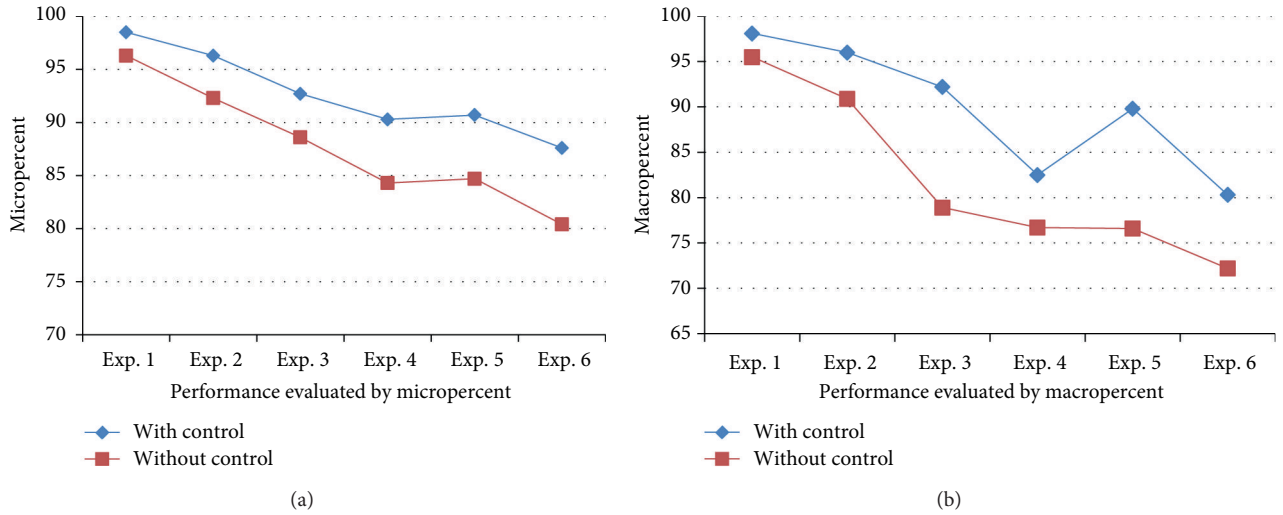


FIGURE 3: Performance comparison between with PTZ control and without PTZ control on cameras.

the number of pedestrian grows, the occlusion problem is more and more serious and the tracking results are not satisfied. The false tracked target will consequently affect the tracking performance of other cameras. The design of model keeps the control decision made by SCC, which could avoid this problem to some extent because a heuristic search could be reinitiated by SCC once the loss track occurs.

We could also find that the $\text{MacroAvg_Percent}_{\text{obs}}$ is a little lower than corresponding $\text{MicroAvg_Percent}_{\text{obs}}$ if all the cameras successfully observed the targets. If some cameras failed to observe the targets, the $\text{MacroAvg_Percent}_{\text{obs}}$ is obviously lower than its $\text{MicroAvg_Percent}_{\text{obs}}$ value.

According to the proposed multicamera collaborating algorithm, once the tracking targets are selected, the algorithm will decide which camera should be controlled. The possible cameras estimated by the algorithm are initiated to participate tracking process. Supposed there is no estimating process, the camera selecting process may depend on the neighbor search. As a result, all the neighboring cameras of current camera will be controlled and the tracking model will work on more videos from all these cameras. In fact, only the cameras in the target's moving direction may be useful for tracking task. In our experiments, the time cost in the case

of our collaborating algorithm is generally no more than one third of the time cost working on all neighboring cameras.

4.4. Effect of Camera Control. In this subsection, we will analyze the effect of camera control model by comparing the results without camera PTZ operations. In Figure 3, we could observe that the overall performance of camera network is decreased when there is no pan-tilt-zoom control on cameras. The reason is that the PTZ control on cameras could enlarge the FOV of cameras and then the cameras could capture target in a longer period. The zoom operation helps to obtain the clear target's image even when it is a little far from the camera. As we all know, clear image can be detected with less ambiguity.

5. Conclusion and Future Works

In this paper, an active camera network framework is designed for video surveillance by jointly considering the cameras collaborating control and effective targets tracking. To maximize the FOV of targets being observed and minimize the number of cameras being controlled, a Bayes network based collaborating control algorithm is proposed

with estimation of the target's location in next time step. The hybrid human feature selection is also concerned to improve the tracking precision. Experimental results on real world environment indicate the efficacy of proposed framework and algorithm. Nevertheless, with the pedestrian flow growth, system performance will be decreasing. The tracking performance is also affected by the number of targets which resulted from the relatively low precision of multiobject tracking problem. Future research will focus on these problems and improve the adaptability of system.

Conflict of Interests

The authors declare that there is no conflict of interests regarding the publication of this paper.

Acknowledgments

This work was partly supported by the National Natural Science Foundation of China under Grant nos. 61202170, 61203247, and 61273304 and the Fundamental Research Funds for the Central Universities under Grant no. 0800219226 and the opening project of Shanghai Key Laboratory of Digital Media Processing and Transmission (no. 2011KF03).

References

- [1] X. Zhou, R. T. Collins, T. Kanade, and P. Metes, "A masterslave system to acquire biometric imagery of humans at distance," in *Proceedings of the 1st ACM SIGMM International Workshop on Video Surveillance*, pp. 113–120, New York, NY, USA, 2003.
- [2] D. Wu, S. Ci, H. Luo, Y. Ye, and H. Wang, "Video surveillance over wireless sensor and actuator networks using active cameras," *IEEE Transactions on Automatic Control*, vol. 56, no. 10, pp. 2467–2472, 2011.
- [3] S. Khan and M. Shah, "Consistent labeling of tracked objects in multiple cameras with overlapping fields of view," *IEEE Transactions on Pattern Analysis and Machine Intelligence*, vol. 25, no. 10, pp. 1355–1360, 2003.
- [4] A. Zisserman, P. A. Beardsley, and I. D. Reid, "Metric calibration of a stereo rig," in *Proceedings of the IEEE Workshop on Representation of Visual Scenes*, pp. 93–100, Cambridge, Mass, USA, June 1995.
- [5] A. Ruf and R. Horaud, "Projective rotations applied to a pan-tilt stereo head," in *Proceedings of the IEEE Computer Society Conference on Computer Vision and Pattern Recognition (CVPR '99)*, pp. 144–150, June 1999.
- [6] P. M. Ngan and R. J. Vulkenhurg, "Calibrating a pan-tilt camera head," in *Proceedings of the Image and Vision Computing Workshop*, New Zealand, 1995.
- [7] R. T. Collins and Y. Tsing, "Calibration of an outdoor active camera system," in *Proceedings of the IEEE Computer Society Conference on Computer Vision and Pattern Recognition (CVPR '99)*, pp. 528–534, Fort Collins, Colo, USA, June 1999.
- [8] G. A. Jones, J. P. Renno, and P. Remagnino, "Auto-calibration in multiple-camera surveillance environments," in *Proceedings of the IEEE International Workshop on Performance Evaluation and Surveillance*, 2002.
- [9] F. Pedersini, A. Sarti, and S. Tubaro, "Accurate and simple geometric calibration of multi-camera systems," *Signal Processing*, vol. 77, no. 3, pp. 309–334, 1999.
- [10] T. Gandhi and M. M. Trivedi, "Calibration of a reconfigurable array of omnidirectional cameras using a moving person," in *Proceedings of the ACM Second International Workshop on Video Surveillance and Sensor Networks*, pp. 12–19, New York, NY, USA, October 2004.
- [11] R. T. Collins, A. J. Lipton, H. Fujiyoshi, and T. Kanade, "Algorithms for cooperative multisensor surveillance," *Proceedings of the IEEE*, vol. 89, no. 10, pp. 1456–1477, 2001.
- [12] H. C. Yan, Z. Z. Su, H. Zhang, and F. W. Yang, "Observer-based H_∞ control for discrete-time stochastic systems with quantization and random communication delays," *IET Control Theory and Applications*, vol. 7, no. 3, pp. 372–379, 2013.
- [13] P. Petrov, O. Boumbarov, and K. Muratovski, "Face detection and tracking with an active camera," in *Proceedings of the 4th International IEEE Conference Intelligent Systems*, pp. 1434–1439, Varna, Bulgaria, September 2008.
- [14] S. Lim, A. Elgammal, and L. S. Davis, "Image-based pan-tilt camera control in a multi-camera surveillance environment," in *Proceedings of the International Conference on Machine Intelligence (ICML '03)*, pp. 645–648, 2003.
- [15] N. Krahnstoeber, T. Yu, S. Lim, and K. Patwardhan, "Collaborative control of active cameras in large-scale surveillance," in *Multi-Camera Networks-Principles and Applications*, H. Aghajan and A. Cavallaro, Eds., Elsevier, Amsterdam, The Netherlands, 2009.
- [16] J. Orwell, P. Remagnino, and G. A. Jones, "Multi-camera color tracking," in *Proceedings of the 2nd IEEE Workshop on Visual Surveillance*, pp. 14–21, Fort Collins, Colo, USA, 1999.
- [17] C. J. Costello, C. P. Diehl, A. Banerjee, and H. Fisher, "Scheduling an active camera to observe people," in *Proceedings of the 2nd ACM International Workshop on Video Surveillance and Sensor Networks*, pp. 39–45, New York, NY, USA, October 2004.
- [18] L. P. Kaelbling, M. L. Littman, and A. R. Cassandra, "Planning and acting in partially observable stochastic domains," *Artificial Intelligence*, vol. 101, no. 1-2, pp. 99–134, 1998.
- [19] H. Zhang, H. C. Yan, F. W. Yang, and Q. J. Chen, "Quantized control design for impulsive fuzzy networked systems," *IEEE Transactions on Fuzzy Systems*, vol. 19, no. 6, pp. 1153–1162, 2011.
- [20] A. Hampapur, S. Pankanti, A. Senior, Y. L. Tian, L. Brown, and R. Bolle, "Face cataloger: multi-scale imaging for relating identity to location," in *Proceedings of the IEEE Conference on Advanced Video and Signal Based Surveillance*, pp. 13–21, Washington, DC, USA, 2003.
- [21] M. Ostland, H. Paula, S. Russell, and Y. Ritov, "Tracking many objects with many sensors," in *Proceedings of the International Joint Conferences on Artificial Intelligence (IJCAI '99)*, Stockholm, Sweden, 1999.
- [22] H. Zhang, Q. J. Chen, H. C. Yan, and J. H. Liu, "Robust H_∞ filtering for switched stochastic system with missing measurements," *IEEE Transactions on Signal Processing*, vol. 57, no. 9, pp. 3466–3474, 2009.
- [23] P. Natarajan, T. N. Hoang, K. H. Low, and M. Kankanhalli, "Decision-theoretic coordination and control for active multi-camera surveillance in uncertain, partially observable environments," in *Proceedings of the 6th International Conference on Distributed Smart Cameras (ICDSC '12)*, pp. 1–6, Hong Kong, 2012.
- [24] B. Jun, I. Choi, and D. Kim, "Local transform features and hybridization for accurate face and human detection," *IEEE*

Transactions on Pattern Analysis and Machine Intelligence, vol. 35, no. 6, pp. 1423–1436, 2013.

- [25] Z. Kalal, K. Mikolajczyk, and J. Matas, “Tracking-learning-detection,” *IEEE Transactions on Pattern Analysis and Machine Intelligence*, vol. 34, no. 7, pp. 1409–1422, 2012.
- [26] P. Natarajan, T. N. Hoang, K. H. Low, and M. Kankanhalli, “Decision theoretic approach to maximizing observation of multiple targets in multi-camera surveillance,” in *Proceedings of the 11th International Conference on Autonomous Agents and MultiAgent Systems (AAMAS '12)*, pp. 155–162, 2012.

Research Article

Attitude Stabilization Control of a Quadrotor UAV by Using Backstepping Approach

Xing Huo,¹ Mingyi Huo,² and Hamid Reza Karimi³

¹ College of Engineering, Bohai University, Jinzhou 121000, China

² Department of Control Science and Engineering, Harbin Institute of Technology, Harbin 150001, China

³ Department of Engineering, Faculty of Engineering and Science, The University of Agder, N-4898 Grimstad, Norway

Correspondence should be addressed to Xing Huo; hmyi888@163.com

Received 29 December 2013; Accepted 13 January 2014; Published 19 February 2014

Academic Editor: Xudong Zhao

Copyright © 2014 Xing Huo et al. This is an open access article distributed under the Creative Commons Attribution License, which permits unrestricted use, distribution, and reproduction in any medium, provided the original work is properly cited.

The modeling and attitude stabilization control problems of a four-rotor vertical takeoff and landing unmanned air vehicle (UAV) known as the quadrotor are investigated. The quadrotor's attitude is represented by the unit quaternion rather than Euler angles to avoid singularity problem. Taking dynamical behavior of motors into consideration and ignoring aerodynamic effect, a nonlinear controller is developed to stabilize the attitude. The control design is accomplished by using backstepping control technique. The proposed control law is based on the compensation for the Coriolis and gyroscope torques. Applying Lyapunov stability analysis proves that the closed-loop attitude system is asymptotic stable. Moreover, the controller can guarantee that all the states of the system are uniformly ultimately bounded in the presence of external disturbance torque. The effectiveness of the proposed control approach is analytically authenticated and also validated via simulation study.

1. Introduction

In the past decade, the small UAV market has grown rapidly. Small UAVs are applied in various areas such as surveillance, reconnaissance, and aerial photography. In particular, quadrotor helicopters are an emerging rotorcraft concept for UAV platforms. The particular interest of the research community in the quadrotor design can be linked to two main advantages over comparable vertical takeoff and landing (VTOL) UAVs, such as helicopters. First, quadrotors do not require complex mechanical control linkages for rotor actuation, relying instead on fixed pitch rotors and using variation in motor speed for vehicle control. This simplifies both the design and maintenance of the vehicle. Second, the use of four rotors ensures that individual rotors are smaller in diameter than the equivalent main rotor on a helicopter, relative to the airframe size. Consequently, the last decade has seen many successfully developed platforms of micro-UAVs, especially the quadrotor UAV, such as Australia National University's X-4 flyer aircraft prototype [1], the Stanford University's STARMAC quadrotor [2], the Swiss Federal Institute's OS4

aircraft prototype [3], and the University of Pennsylvania's Grasp micro-UAV test bed [4].

To guide a quadrotor to accomplish the planned mission, a control system needs to be designed. It consists of position control for translational motion and attitude control for rotation motion. In this study, the design of controller for attitude control is investigated. One distinct feature of attitude dynamics of a quadrotor is that its configuration manifold is not linear; it evolves on a nonlinear manifold, referred to as the special orthogonal group. This yields important and unique properties that cannot be observed from dynamic systems evolving on a linear space. As a result, the attitude control problem of a rigid body has been investigated by several researchers, and a wide class of controllers based on classic or modern control theory has been proposed. For instance, based on the conventional proportional-integer-derivative (PID) approach, an model-independent PD controller by using quaternion-based feedback was proposed to stabilize the quadrotor attitude system [5]. In [6], the design of a PID control algorithm for the quadrotor attitude system was presented. The model of the vehicle was modified to simplify

the controller design. Considering faults occurring on the mounted motors, a control strategy by using gain scheduling incorporating PID was developed in [7]. It successfully achieved attitude and position control even in the presence of actuator faults. In another recent work [8], the problem of stabilization and disturbance rejection of attitude subsystem of a quadrotor was addressed. The controller was designed in the framework of PID control scheme; similar control methods also can be found in [9–13].

In addition to the above PID-based attitude control design, many modern control approaches have also been applied to quadrotor attitude controller design. In [14], an attitude control law was proposed for triple tilting rotor mini-UAV. It was robust with respect to dynamical couplings and adverse torques. The work in [15] investigated the application of model reference adaptive control for quadrotor even in the presence of actuator uncertainties. An adaptive law and control laws based on adaptive technique were developed and applied for quadrotor UAV in case of actuator partial loss of effectiveness faults [16]. In [17], the problem of fault tolerant control for quadrotor was addressed by using backstepping control approach. In [18], the output-feedback control system design for a quadrotor was discussed. The position and attitude control was designed by using model reference control and nonlinear control allocation techniques. The position control of vertical take-off and landing UAV without linear velocity measurements was also investigated in [19]. In [20], an adaptive nonlinear attitude stabilization control scheme was synthesized for a quadrotor. The problem of parametric uncertainties in the quadrotor model was investigated, and the controller was designed based on model reference adaptive control technique. In [21], an attitude free position control design was proposed for a quadrotor by using dynamic inversion. In another related study [22], an adaptive law was designed to asymptotically follow an attitude command without the knowledge of the inertia matrix. The proposed control was verified by using a quadrotor UAV model. In [23], a quaternion-based feedback was developed for the attitude stabilization of quadrotor. The control design took into account a priori input bound and is based on nested saturation approach. It forced the closed-loop trajectories to enter in some a priori fixed neighborhood of the origin in a finite time and remain thereafter.

The sliding mode control (SMC) is a powerful theory for controlling uncertain systems [24]. The main advantages are that the SMC system has great robustness with respect to uncertain parameters and external disturbances. Hence, applying SMC to design attitude control for quadrotor has been intensively carried out in recent years. In [25] integral SMC and reinforcement learning control were presented as two design techniques for accommodating the nonlinear disturbances of an outdoor quadrotor. In [26], SMC was used to control a quadrotor UAV in the presence of disturbance and actuator fault. The proposed approach was able to achieve disturbance rejection in the fault-free condition and also able to recover some of performances when a fault occurred. To regulate the attitude angle of a quadrotor to the desired signals, an SMC-based attitude controller was proposed in [27]. In that approach, an adaptive estimator was incorporated, and

the adaptive technique was used to estimate the upper bound of the virtual command. The work in [28] explained the developments of the use of SMC for a fully actuated subsystem of a quadrotor to obtain attitude control stability. In [29], an SMC attitude controller was developed for a quadrotor. It allowed for a continuous control robust to external disturbance and model uncertainties to be computed without the use of high control gain. In another work [30], an augmented SMC-based fault-tolerant control was designed theoretically, implemented practically, and tested experimentally in a quadrotor. The problems of propeller damage and actuator fault conditions for tracking control were discussed. Moreover, many other nonlinear control techniques based controller design were also proposed for quadrotor, as suggested in [31–33].

Based on the results available in the literature, this work will investigate the attitude control design of a quadrotor UAV. The attitude orientation of the quadrotor is represented by using unit quaternion. Backstepping technique is adopted to develop the controller. It is shown that the controller can asymptotically stabilize the attitude system. Explicitly taking external disturbance torque acting on the quadrotor into consideration, the controller is able to guarantee the uniformly ultimately bounded stability of the attitude system. All the states of the closed-loop attitude system are governed to be uniformly ultimately bounded. The remainder of this paper is organized as follows. In Section 2, mathematical model of a quadrotor UAV attitude system and problem statement are summarized. A backstepping-based attitude control approach is presented in Section 3, and also the stability of closed-loop system is provided. In Section 4, simulation results with the application of the designed control scheme to a quadrotor are presented. Section 5 presents some concluding remarks and future work.

2. Mathematical Model and Control Problem Statement

2.1. Attitude Dynamic Model of a Quadrotor. The quadrotor UAV under consideration consists of a rigid cross frame equipped with four rotors as shown in Figure 1. Those four rotors are divided into front (M_2), back (M_4), left (M_1), and right (M_3) motors. Motors M_2 and M_4 rotate in counterclockwise direction, while the other two in clockwise direction. All of the movements can be controlled by the changes of each rotor speed. If a yaw motion is desired, one has to reduce the thrust of one set of rotors and increase the thrust of the other set while maintaining the same total thrust to avoid an up-down motion. Hence, the yaw motion is then realized in the direction of the induced reactive torque. To accomplish roll motion, it should decrease (increase) the speed of motor M_3 and increase (decrease) the speed of motor M_1 . On the other hand, pitch motion can be maneuvered by decreasing (increasing) the speed of motor M_1 while increasing (decreasing) the speed of motor M_4 .

Let $\mathcal{F}_i(X_I, Y_I, Z_I)$ fixed with the Earth denote an inertial frame, and let $\mathcal{F}_b(X_B, Y_B, Z_B)$ denote a frame rigidly attached to the quadrotor body as shown in Figure 1. The vector

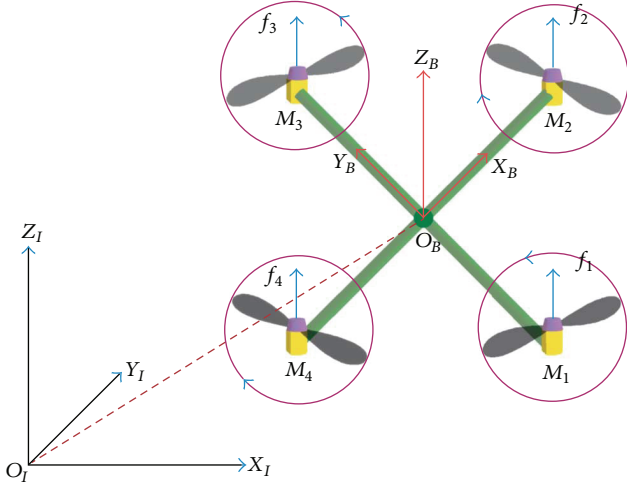


FIGURE 1: The structure of quadrotor UAV and its coordinate reference frames.

$\Theta = [\phi \ \theta \ \psi]^T$ is the orientation of body frame \mathcal{F}_b with respect to \mathcal{F}_i called Euler angles. These angles are bounded as follows:

$$-\frac{\pi}{2} < \phi < \frac{\pi}{2}, \quad -\frac{\pi}{2} < \theta < \frac{\pi}{2}, \quad -\frac{\pi}{2} < \psi < \frac{\pi}{2}. \quad (1)$$

When using Euler angles to represent quadrotor attitude, direction cosine matrix will be used to describe the kinematic motion of attitude. However, one of the drawbacks with application of the direction cosine matrix is the inherent geometric singularity. It is known that the four-parameter description of the orientation called the quaternion representation can be applied to avoid that drawback. Consequently, the unit quaternion will be used in this work for attitude representation of quadrotor UAV. Ignoring aerodynamic effect, the mathematical model of quadrotor attitude system can be described as follows [5]:

$$\dot{q}_0 = -\frac{1}{2} \mathbf{q}^T \boldsymbol{\omega} \quad (2)$$

$$\dot{\mathbf{q}} = \frac{1}{2} [q_0 \mathbf{E}_3 + \mathbf{S}(\mathbf{q})] \boldsymbol{\omega} \quad (3)$$

$$\mathbf{I} \dot{\boldsymbol{\omega}} = -\mathbf{S}(\boldsymbol{\omega}) \mathbf{I} \boldsymbol{\omega} - \mathbf{G}_a + \mathbf{u} \quad (4)$$

$$I_{m_i} \dot{\omega}_i = \tau_i - f_i, \quad i = 1, 2, 3, 4, \quad (5)$$

where $\mathbf{Q} = [q_0 \ \mathbf{q}^T]^T \in \mathbb{R}^4$ with $\mathbf{q} \in \mathbb{R}^3$ is the unit quaternion denoting the attitude of quadrotor with respect to the inertial frame \mathcal{F}_i . It is subject to the equation $q_0^2 + \mathbf{q}^T \mathbf{q} = 1$. $\boldsymbol{\omega} \in \mathbb{R}^3$ denotes the angular velocity of the quadrotor with respect to \mathcal{F}_i and expressed in \mathcal{F}_b . $\mathbf{I} \in \mathbb{R}^{3 \times 3}$ is the positive-definite, symmetric inertia matrix of the UAV. $I_{m_i} \in \mathbb{R}$ and $\omega_i \in \mathbb{R}$ are the moment of inertia and the speed of the rotor M_i , respectively. $\mathbf{G}_a \in \mathbb{R}^3$ denotes the gyroscope torques due to the combination of the rotation of the quadrotor and the four motors; it is given by

$$\mathbf{G}_a = \sum_{i=1}^4 I_{m_i} (\boldsymbol{\omega} \times \mathbf{e}_i) (-1)^{i+1} \omega_i \quad (6)$$

and $\mathbf{e}_i = [0 \ 0 \ 1]^T$ denotes the unit vector in \mathcal{F}_i . The matrix $\mathbf{S}(\mathbf{x})$ is a skew-symmetric matrix such that $\mathbf{S}(\mathbf{x})\mathbf{y} = \mathbf{x} \times \mathbf{y}$ for any vector for $\mathbf{x}, \mathbf{y} \in \mathbb{R}^3$, where “ \times ” denotes the vector cross-product. \mathbf{E}_3 denotes the 3×3 identity matrix.

In (4), $\mathbf{u} = [u_1 \ u_2 \ u_3]^T \in \mathbb{R}^3$ is the total torque acting on the UAV, and it is generated by four motors.

Consider the following:

$$\mathbf{u} = \begin{bmatrix} db(\omega_3^2 - \omega_1^2) \\ db(\omega_2^2 - \omega_4^2) \\ \kappa(\omega_2^2 + \omega_4^2 - \omega_1^2 - \omega_3^2) \end{bmatrix}, \quad (7)$$

where $d \in \mathbb{R}$ is the distance from the rotors to the center of mass of the quadrotor and $b \in \mathbb{R}$ and $\kappa \in \mathbb{R}$ are two positive parameters depending on the density of air, the radius of the propeller, the number of blades and the geometry, lift, and drag coefficients of the blades [34]. The reaction torque $f_i \in \mathbb{R}$ in (5) generated in free air by the motor M_i due to motor drag is given by

$$f_i = \kappa \omega_i^2. \quad (8)$$

Moreover, the four-control input of the attitude system is τ_i , $i = 1, 2, 3, 4$, which denotes the torques produced by the rotors.

2.2. Problem Statement. Given any initial attitude \mathbf{Q} and angular velocity $\boldsymbol{\omega}$, the control objective to be achieved can be stated as: consider the quadrotor UAV attitude dynamics described by (2) and (5); design a control law τ_i for the motor M_i , $i = 1, 2, 3, 4$, to stabilize the resulting closed-loop attitude system; that is,

$$\lim_{t \rightarrow \infty} \mathbf{Q}(t) = [1 \ 0 \ 0 \ 0]^T, \quad \lim_{t \rightarrow \infty} \boldsymbol{\omega}(t) = [0 \ 0 \ 0]^T. \quad (9)$$

3. Attitude Stabilization Control Design

Define new state variables as $\mathbf{x}_1 = [1 - |q_0| \ \mathbf{q}^T]^T$, $\mathbf{x}_2 = \boldsymbol{\omega}$, and $\mathbf{x}_3 = [\omega_1^2 \ \omega_2^2 \ \omega_3^2]^T$. Then, the attitude system equations (2)–(5) can be rewritten as follows:

$$\dot{\mathbf{x}}_1 = [-\text{sgn}(q_0) \dot{q}_0 \ \dot{\mathbf{q}}^T]^T \quad (10)$$

$$\mathbf{I} \dot{\mathbf{x}}_2 = -\mathbf{S}(\mathbf{x}_2) \mathbf{I} \mathbf{x}_2 - \mathbf{G}_a + \mathbf{u} \quad (11)$$

$$\mathbf{I}_m \dot{\mathbf{x}}_3 = \mathbf{X}(\boldsymbol{\tau} - \mathbf{f}), \quad (12)$$

where $\mathbf{I}_m = \text{diag}(I_{m1}, I_{m2}, I_{m3})$, $\mathbf{X} = \text{diag}(2\omega_1, 2\omega_2, 2\omega_3)$, $\boldsymbol{\tau} = [\tau_1 \ \tau_2 \ \tau_3]^T$, $\mathbf{f} = [f_1 \ f_2 \ f_3]^T$, and $\text{sgn}(y)$ is defined as the nonzero sigum function as follows:

$$\text{sgn}(y) = \begin{cases} -1, & y < 0 \\ 1, & y \geq 0. \end{cases} \quad (13)$$

For the transformed system equations (10)–(12), backstepping control technique will be applied in this section to

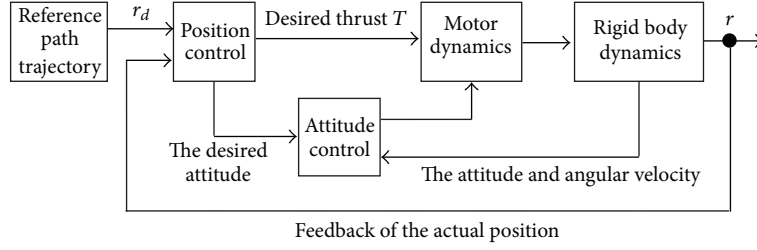


FIGURE 2: The control structure of the quadrotor UAV.

design attitude controller, and the following change of coordinates will be firstly introduced:

$$\mathbf{z}_1 = \mathbf{x}_1 \quad (14)$$

$$\mathbf{z}_2 = \mathbf{x}_2 - \boldsymbol{\alpha}_1 \quad (15)$$

$$\mathbf{z}_3 = \mathbf{x}_3 - \boldsymbol{\alpha}_2, \quad (16)$$

where $\boldsymbol{\alpha}_1 \in \mathfrak{R}^3$ and $\boldsymbol{\alpha}_2 \in \mathfrak{R}^N$ are virtual control inputs to be designed later.

Based on the preceding coordinates changes, the following procedures can be followed to design a controller to stabilize the attitude of the considered quadrotor UAV.

Step 1. We start with (14) by considering \mathbf{x}_2 as the control variable. It is obtained from (2), (3), and (10) that

$$\begin{aligned} \dot{\mathbf{z}}_1 &= \frac{1}{2} \left[\text{sgn}(q_0) \mathbf{q}^T \boldsymbol{\omega} [q_0 \mathbf{E}_3 + \mathbf{S}(\mathbf{q})]^T \boldsymbol{\omega}^T \right]^T \\ &= \frac{1}{2} \begin{bmatrix} \text{sgn}(q_0) \mathbf{q}^T \\ q_0 \mathbf{E}_3 + \mathbf{S}(\mathbf{q}) \end{bmatrix} \boldsymbol{\omega} \\ &= \mathbf{P}(\mathbf{Q}) \boldsymbol{\omega}, \end{aligned} \quad (17)$$

where $\mathbf{P}(\mathbf{Q}) = (1/2) \begin{bmatrix} \text{sgn}(q_0) \mathbf{q}^T \\ q_0 \mathbf{E}_3 + \mathbf{S}(\mathbf{q}) \end{bmatrix}$.

The task in this step is to design a virtual control law $\boldsymbol{\alpha}_1$ to guarantee $\lim_{t \rightarrow \infty} \mathbf{z}_1(t) = \mathbf{0}$. Choose a Lyapunov candidate function as $V_1 = (1/2) \mathbf{z}_1^T \mathbf{z}_1$, and design the virtual control $\boldsymbol{\alpha}_1$ as $\boldsymbol{\alpha}_1 = -l_1 \mathbf{P}^T(\mathbf{Q}) \mathbf{z}_1$, where $l_1 \in \mathbb{R}$ is a positive scalar. Then, applying (15) and (17) yields

$$\begin{aligned} \dot{V}_1 &= \mathbf{z}_1^T \mathbf{P}(\mathbf{Q}) \boldsymbol{\omega} \\ &= \mathbf{z}_1^T \mathbf{P}(\mathbf{Q}) (\mathbf{z}_2 - l_1 \mathbf{P}^T(\mathbf{Q}) \mathbf{z}_1) \\ &= -l_1 \mathbf{z}_1^T \mathbf{P}(\mathbf{Q}) \mathbf{P}^T(\mathbf{Q}) \mathbf{z}_1 + \mathbf{z}_1^T \mathbf{P}(\mathbf{Q}) \mathbf{z}_2. \end{aligned} \quad (18)$$

Hence, if $\mathbf{z}_2 = \mathbf{0}$, then $\dot{V}_1 = -l_1 \mathbf{z}_1^T \mathbf{P}(\mathbf{Q}) \mathbf{P}^T(\mathbf{Q}) \mathbf{z}_1 = -l_1 \|\mathbf{P}^T(\mathbf{Q}) \mathbf{z}_1\|^2 < 0$ for all $\mathbf{P}^T(\mathbf{Q}) \mathbf{z}_1 \neq \mathbf{0}$. By using Lyapunov stability theory [35], it can prove that

$$\lim_{t \rightarrow \infty} \|\mathbf{P}^T(\mathbf{Q}) \mathbf{z}_1\| = \mathbf{0}. \quad (19)$$

On the other hand, it can be obtained from the definition of $\mathbf{P}(\mathbf{Q})$ that

$$\begin{aligned} \mathbf{P}^T(\mathbf{Q}) \mathbf{z}_1 &= \frac{1}{2} \begin{bmatrix} \text{sgn}(q_0) \mathbf{q}^T \\ q_0 \mathbf{E}_3 + \mathbf{S}(\mathbf{q}) \end{bmatrix}^T [1 - |q_0| \mathbf{q}^T]^T \\ &= \frac{1}{2} \text{sgn}(q_0) \mathbf{q}. \end{aligned} \quad (20)$$

Hence, it leaves (19)-(20) as $\lim_{t \rightarrow \infty} \text{sgn}(q_0) \mathbf{q} = \mathbf{0}$. Then, using (13) leads to $\lim_{t \rightarrow \infty} \mathbf{q} = \mathbf{0}$.

The quadrotor UAV actually is an underactuated system because it has six degrees of freedom while it has only four inputs. The collective input (or throttle input) is the sum of the thrusts of each motor. Hence, the control structure of an rigid quadrotor is illustrated in Figure 2. Position control and attitude control are included. Assumed that the desired total thrust supplied by the position control is T , which is generated by the four rotors and given by

$$T = b \sum_{i=1}^4 \bar{\omega}_i^2. \quad (21)$$

Accordingly, the desired speed of the four motors can be obtained from (7) and (21); that is, $\boldsymbol{\eta} = \mathbf{N} \mathbf{x}_3$ with $\boldsymbol{\eta} = [u_1 \ u_2 \ u_3 \ T]^T$ and

$$\mathbf{N} = \begin{bmatrix} 0 & db & 0 & -db \\ db & 0 & -db & 0 \\ \kappa & -\kappa & \kappa & -\kappa \\ b & b & b & b \end{bmatrix}, \quad (22)$$

where \mathbf{N} is nonsingular as long as $db\kappa \neq 0$.

Step 2. From (22), one has $\mathbf{u} = \boldsymbol{\Xi} \mathbf{N} \mathbf{x}_3$, where

$$\boldsymbol{\Xi} = \begin{bmatrix} 1 & 0 & 0 & 0 \\ 0 & 1 & 0 & 0 \\ 0 & 0 & 1 & 0 \\ 0 & 0 & 0 & 0 \end{bmatrix}. \quad (23)$$

We now differentiate the second error, \mathbf{z}_2 , using (15) to give

$$\dot{\mathbf{I}} \mathbf{z}_2 = \dot{\mathbf{I}} \mathbf{x}_2 - \dot{\mathbf{I}} \boldsymbol{\alpha}_1 = -\mathbf{S}(\mathbf{x}_2) \mathbf{I} \mathbf{x}_2 - \mathbf{G}_a + \boldsymbol{\Xi} \mathbf{N} \mathbf{x}_3 - \dot{\mathbf{I}} \boldsymbol{\alpha}_1. \quad (24)$$

Choose another Lyapunov candidate function $V_2 = V_1 + (1/2) \mathbf{z}_2^T \mathbf{I} \mathbf{z}_2$, and design the virtual control law $\boldsymbol{\alpha}_2$ as

$$\boldsymbol{\alpha}_2 = (\boldsymbol{\Xi} \mathbf{N})^\dagger \left[\mathbf{S}(\mathbf{x}_2) \mathbf{I} \mathbf{x}_2 - \mathbf{P}^T(\mathbf{Q}) \mathbf{z}_1 - l_2 \mathbf{z}_2 + \mathbf{G}_a + \dot{\mathbf{I}} \boldsymbol{\alpha}_1 \right], \quad (25)$$

where $l_2 \in \mathbb{R}$ is a positive constant and $(\cdot)^\dagger$ denotes the pseudo inverse of a full-row rank matrix.

Differentiating both sides of V_2 and inserting (24) and (25) yield

$$\begin{aligned}\dot{V}_2 &= \dot{V}_1 + \mathbf{z}_2^T \mathbf{I} \dot{\mathbf{z}}_2 \\ &= -l_1 \mathbf{z}_1^T \mathbf{P}(\mathbf{Q}) \mathbf{P}^T(\mathbf{Q}) \mathbf{z}_1 + \mathbf{z}_1^T \mathbf{P}(\mathbf{Q}) \mathbf{z}_2 \\ &\quad + \mathbf{z}_2^T [-\mathbf{S}(\mathbf{x}_2) \mathbf{I} \mathbf{x}_2 - \mathbf{G}_a + \mathbf{E} \mathbf{N}(\mathbf{z}_3 + \boldsymbol{\alpha}_2) - \mathbf{I} \dot{\boldsymbol{\alpha}}_1] \\ &= -l_1 \mathbf{z}_1^T \mathbf{P}(\mathbf{Q}) \mathbf{P}^T(\mathbf{Q}) \mathbf{z}_1 - l_2 \mathbf{z}_2^T \mathbf{z}_2 + \mathbf{z}_2^T \mathbf{E} \mathbf{N} \mathbf{z}_3.\end{aligned}\quad (26)$$

Again, if $\mathbf{z}_3 = \mathbf{0}$, one has $\dot{V}_2 = -l_1 \|\mathbf{P}^T(\mathbf{Q}) \mathbf{z}_1\|^2 - l_2 \|\mathbf{z}_2\|^2$, and thus both \mathbf{z}_1 and \mathbf{z}_2 will converge to zero asymptotically.

According to the analysis in Steps 1 and 2, if \mathbf{z}_3 can be driven to zero by designing an appropriate controller, then \mathbf{z}_1 and \mathbf{z}_2 will also be governed to zero, and thus the quadrotor attitude will be stabilized. In the following theorem, we summarize our control solution to drive \mathbf{z}_3 to zero by incorporating backstepping-based control action.

Theorem 1. Consider the quadrotor attitude system described by (2)–(5); design a nonlinear backstepping controller as follows:

$$\boldsymbol{\tau} = \mathbf{X}^{-1} [-(\mathbf{E} \mathbf{N})^T \mathbf{z}_2 - l_3 \mathbf{z}_3 + \mathbf{I}_m \dot{\boldsymbol{\alpha}}_2] + \mathbf{f}, \quad (27)$$

where $l_3 \in \mathbb{R}$ is an positive control gain. Then, the closed-loop attitude system is asymptotically stable; that is, $\lim_{t \rightarrow \infty} \mathbf{q}(t) = [0 \ 0 \ 0]^T$, $\lim_{t \rightarrow \infty} \boldsymbol{\omega}(t) = [0 \ 0 \ 0]^T$.

Proof. It can be obtained from (12) and (16) that

$$\mathbf{I}_m \dot{\mathbf{z}}_3 = \mathbf{I}_m \mathbf{x}_3 - \mathbf{I}_m \dot{\boldsymbol{\alpha}}_2 = \mathbf{X}(\boldsymbol{\tau} - \mathbf{f}) - \mathbf{I}_m \dot{\boldsymbol{\alpha}}_2. \quad (28)$$

Consider another candidate Lyapunov function V_3 as follows:

$$V_3 = V_2 + \frac{1}{2} \mathbf{z}_3^T \mathbf{I}_m \mathbf{z}_3. \quad (29)$$

Differentiating (29) and inserting (26) and (28) result in

$$\begin{aligned}\dot{V}_3 &= \dot{V}_2 + \mathbf{z}_3^T \mathbf{I}_m \dot{\mathbf{z}}_3 \\ &= -l_1 \mathbf{z}_1^T \mathbf{P}(\mathbf{Q}) \mathbf{P}^T(\mathbf{Q}) \mathbf{z}_1 - l_2 \mathbf{z}_2^T \mathbf{z}_2 \\ &\quad + \mathbf{z}_2^T \mathbf{E} \mathbf{N} \mathbf{z}_3 + \mathbf{z}_3^T [\mathbf{X}(\boldsymbol{\tau} - \mathbf{f}) - \mathbf{I}_m \dot{\boldsymbol{\alpha}}_2].\end{aligned}\quad (30)$$

With the developed controller equation (27), (30) can be simplified into the following form:

$$\dot{V}_3 = -l_1 \mathbf{z}_1^T \mathbf{P}(\mathbf{Q}) \mathbf{P}^T(\mathbf{Q}) \mathbf{z}_1 - l_2 \mathbf{z}_2^T \mathbf{z}_2 - l_3 \mathbf{z}_3^T \mathbf{z}_3 \leq 0. \quad (31)$$

Investigating of V_3 in (29) shows clearly that $V_3 > 0$ for all \mathbf{z}_i , $i = 1, 2, 3$ and also that $V_3 \rightarrow \infty$ when $\mathbf{z}_i \rightarrow \infty$. Therefore, in accordance with LaSalle-Yoshizawa's theorem [35], \dot{V}_3 from (31) fulfills

$$\dot{V}_3 \leq -W(\mathbf{z}_1, \mathbf{z}_2, \mathbf{z}_3) \leq 0, \quad (32)$$

where $W(\mathbf{z}_1, \mathbf{z}_2, \mathbf{z}_3)$ is a continuous function. Then, all solution $\mathbf{z}_i(t)$ are uniformly globally bounded and

$$\lim_{t \rightarrow \infty} W(\mathbf{z}_1, \mathbf{z}_2, \mathbf{z}_3) = 0. \quad (33)$$

Hence, the controller is uniformly globally asymptotically stable since additionally $W(\mathbf{z}_1, \mathbf{z}_2, \mathbf{z}_3) > 0$. Moreover, it can be concluded from (31)–(33) that

$$\lim_{t \rightarrow \infty} \mathbf{z}_i(t) = \mathbf{0}. \quad (34)$$

To this end, it can be obtained from (14)–(16), the definition of $\boldsymbol{\alpha}_1$ and $\boldsymbol{\alpha}_2$, and (34) that

$$\lim_{t \rightarrow \infty} \mathbf{q}(t) = [0 \ 0 \ 0]^T, \quad \lim_{t \rightarrow \infty} \boldsymbol{\omega}(t) = [0 \ 0 \ 0]^T. \quad (35)$$

Summarizing the above analysis, it can come to the conclusion that the closed-loop attitude system of the considered quadrotor UAV is asymptotically stable. Thereby the proof is completed here. \square

The result obtained from Theorem 1 can only be guaranteed when the quadrotor UAV is free of external disturbance. However, this case will never be true in practical flying, especially when the quadrotor flies outdoor. Assume that the external disturbance torque acting on the quadrotor is $\mathbf{u}_d \in \mathbb{R}^3$; then the dynamics of the quadrotor equation (4) or (11) will be changed as follows:

$$\mathbf{I} \dot{\mathbf{x}}_2 = -\mathbf{S}(\mathbf{x}_2) \mathbf{I} \mathbf{x}_2 - \mathbf{G}_a + \mathbf{u} + \mathbf{u}_d. \quad (36)$$

Although the disturbance torque \mathbf{u}_d is inevitable, it is always bounded in practice. Hence, it is reasonable to assume that there exists a positive scalar $d_{\max} \in \mathbb{R}$ such that $\|\mathbf{u}_d\| \leq d_{\max}$.

Theorem 2. Consider the quadrotor attitude system described by (2)–(5) in the presence of external disturbance torque \mathbf{u}_d , with application of the controller equation (27); suppose that the control gain l_2 is chosen to satisfy

$$l_2 - \varepsilon > 0, \quad (37)$$

where $\varepsilon \in \mathbb{R}$ is a positive scalar specified by the designer. Then, the closed-loop attitude system is uniformly ultimately bounded stable.

Proof. Using the almost the same analysis as in the proof of Theorem 1, one has

$$\dot{V}_2 = -l_1 \mathbf{z}_1^T \mathbf{P}(\mathbf{Q}) \mathbf{P}^T(\mathbf{Q}) \mathbf{z}_1 - l_2 \mathbf{z}_2^T \mathbf{z}_2 + \mathbf{z}_2^T \mathbf{E} \mathbf{N} \mathbf{z}_3 + \mathbf{z}_2^T \mathbf{u}_d. \quad (38)$$

Then, it leaves \dot{V}_3 in (30) as

$$\dot{V}_3 = -l_1 \mathbf{z}_1^T \mathbf{P}(\mathbf{Q}) \mathbf{P}^T(\mathbf{Q}) \mathbf{z}_1 - l_2 \mathbf{z}_2^T \mathbf{z}_2 - l_3 \mathbf{z}_3^T \mathbf{z}_3 + \mathbf{z}_2^T \mathbf{u}_d. \quad (39)$$

Applying the Young's inequality, the following inequality can be established:

$$\mathbf{z}_2^T \mathbf{u}_d \leq \varepsilon \|\mathbf{z}_2\|^2 + \frac{1}{4\varepsilon} \|\mathbf{u}_d\|^2 \leq \varepsilon \|\mathbf{z}_2\|^2 + \frac{1}{4\varepsilon} d_{\max}^2. \quad (40)$$

TABLE 1: Quadrotor UAV model parameters.

Parameters	Description	Value	Units
g	Gravity	9.81	m/s ²
m	Mass	0.468	kg
d	Distance	0.225	m
$I_{mi}, i = 1, 2, 3$	Rotor inertia	3.4×10^{-5}	kgm ²
I_x	Roll inertia	4.9×10^{-3}	kgm ²
I_y	Pitch inertia	4.9×10^{-3}	kgm ²
I_z	Yaw inertia	8.8×10^{-3}	kgm ²
R_a	Motor resistance	0.67	Ω
k_m	Motor constant	4.3×10^{-3}	Nm/A
k_g	Gear ratio	5.6	
b	Proportionality constant	2.9×10^{-5}	
κ	Proportionality constant	1.1×10^{-6}	

It is thus obtained from (40) that \dot{V}_3 is bounded by

$$\begin{aligned} \dot{V}_3 &= -l_1 \mathbf{z}_1^T \mathbf{P}(\mathbf{Q}) \mathbf{P}^T(\mathbf{Q}) \mathbf{z}_1 - l_2 \mathbf{z}_2^T \mathbf{z}_2 - l_3 \mathbf{z}_3^T \mathbf{z}_3 + \mathbf{z}_2^T \mathbf{u}_d \\ &\leq -l_1 \mathbf{z}_1^T \mathbf{P}(\mathbf{Q}) \mathbf{P}^T(\mathbf{Q}) \mathbf{z}_1 - (l_2 - \varepsilon) \mathbf{z}_2^T \mathbf{z}_2 - l_3 \mathbf{z}_3^T \mathbf{z}_3 + \frac{1}{4\varepsilon} d_{\max}^2. \end{aligned} \quad (41)$$

With the choice of control gains in (37), it leads to

$$\dot{V}_3 \leq -2\bar{l}V_3 + \frac{d_{\max}^2}{4\varepsilon}, \quad (42)$$

where $\bar{l} = \min\{l_1 \lambda_{\min}(\mathbf{P}(\mathbf{Q})\mathbf{P}^T(\mathbf{Q})), (l_2 - \varepsilon)/\lambda_{\max}(\mathbf{I}), l_3/\lambda_{\max}(\mathbf{I}_m)\}$, $\lambda_{\min}(\cdot)$ and $\lambda_{\max}(\cdot)$ denote the minimum and the maximum eigenvalue of matrix, respectively. Using Theorem 4.18 (page 172) in [35], it can be concluded from (42) that V_3 is uniformly ultimately bounded together with the states \mathbf{z}_i , $i = 1, 2, 3$. More precisely, there exists a finite-time $\bar{t}_0 \in \mathcal{R}_+$ such that $\|\mathbf{z}_i(t)\| \leq \varepsilon_1^*$, $\|\mathbf{z}_a(t)\| \leq \varepsilon_1^*$ for any $\varepsilon_1^* > d_{\max}/2\sqrt{\bar{l}\varepsilon}$ and $t \geq \bar{t}_0$, $i = 1, 2, 3$. In other words, the closed-loop attitude system is uniformly ultimately bounded stable. Hence, the proof of Theorem 2 is completed. \square

4. Numerical Example

In this section the properties of the proposed attitude stabilization approach is evaluated and simulated numerically by the quadrotor model presented in [5]. The physical parameters of this model are listed in Table 1. At time $t = 0$, the initial attitude of the quadrotor is $\Theta(0) = [35 \ -45 \ 18]^T$ deg, corresponding to the unit quaternion values $\mathbf{q}(0) = [0.3315 \ -0.3170 \ 0.0242]^T$; the initial angular velocity is of $\omega(0) = [0 \ 0 \ 0]^T$ rad/sec. The control gains for the controller equation (27) are chosen as $l_1 = 0.02$, $l_2 = 0.075$, and $l_3 = 0.008$. Moreover, attitude and angular velocity sensor noises (σ_p^2): $0.0001(1\sigma)$ are modeled as zero-mean Gaussian random variables with variance σ_p^2 .

In the ideal case that the quadrotor is free of external disturbance torques, with application of the controller equation

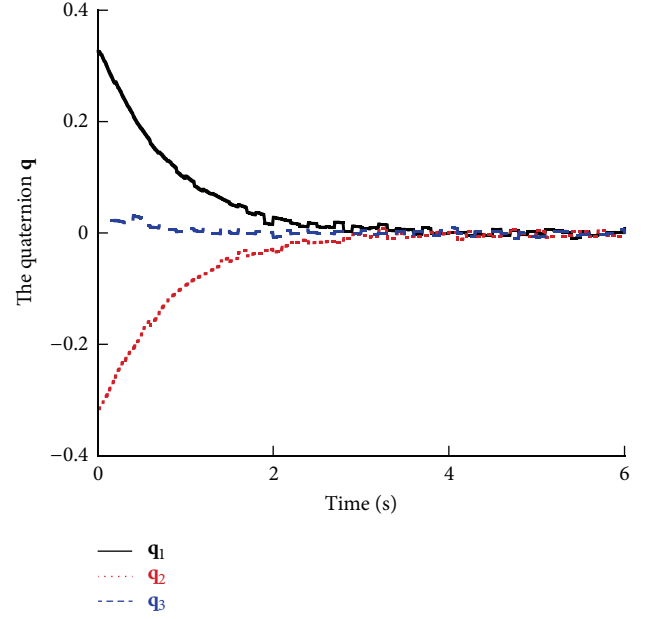


FIGURE 3: The response of the unit quaternion \mathbf{q} in the absence of external disturbances.

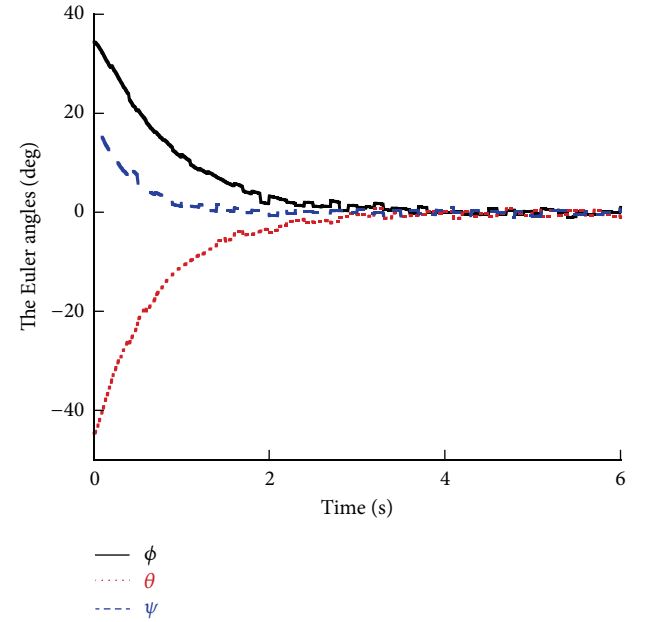


FIGURE 4: The response of Euler attitude angles in the absence of external disturbances.

(27), it leads to the control performance shown in Figures 3–5. It is observed from the response of the unit quaternion and the Euler attitude angles shown in Figures 3 and 4, respectively, that the attitude is successfully accomplished, while the resulted angular velocity is illustrated in Figure 5.

For a quadrotor flying outdoor, it is always under the effect of external disturbances such as induced by wind. Therefore, simulation is further carried out in the presence of external disturbances. Here, disturbances are introduced on

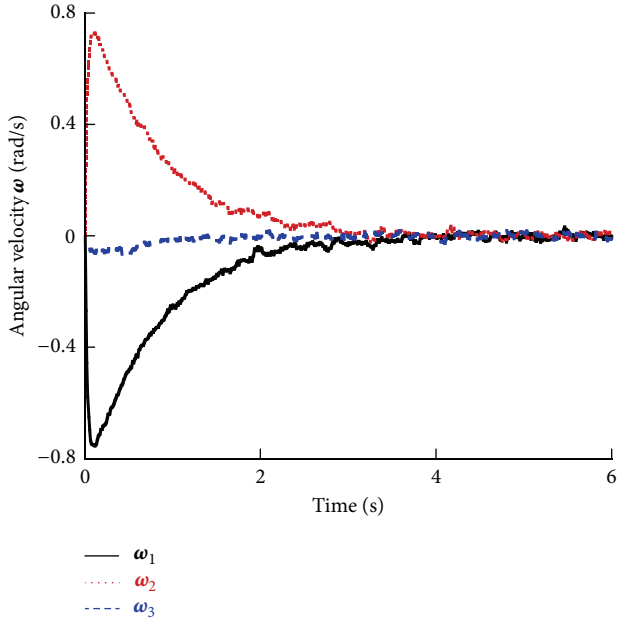


FIGURE 5: The angular velocity ω in the absence of external disturbances.

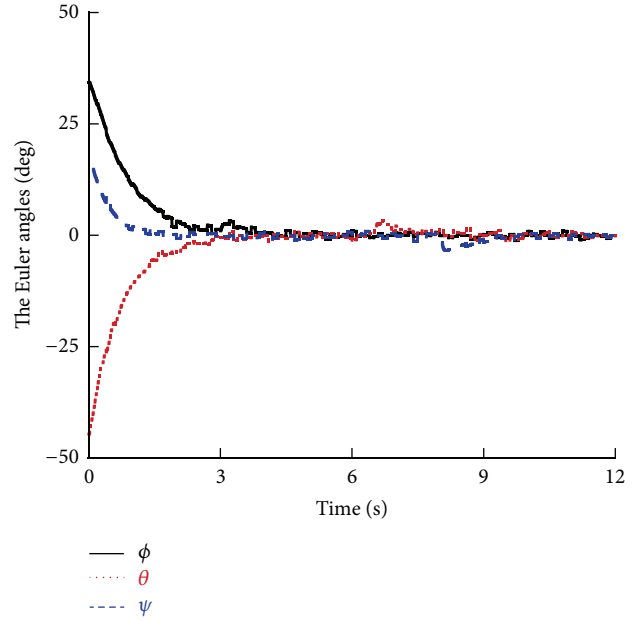


FIGURE 7: The response of Euler attitude angles in the presence of external disturbances.

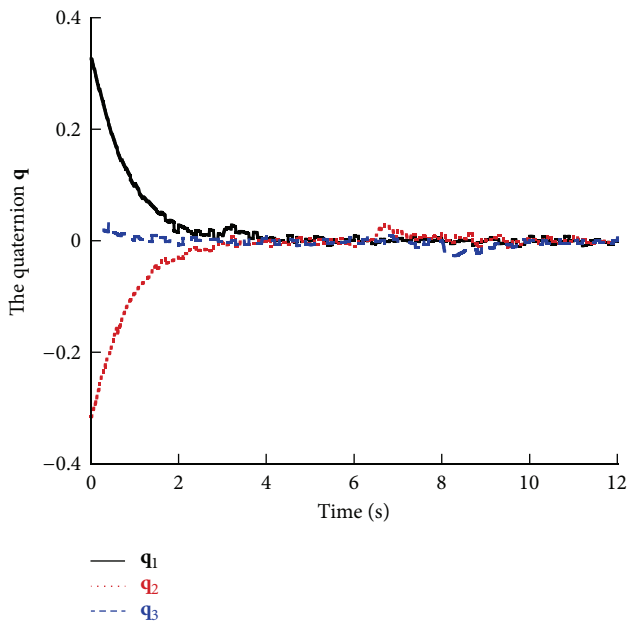


FIGURE 6: The response of the unit quaternion q in the presence of external disturbances.

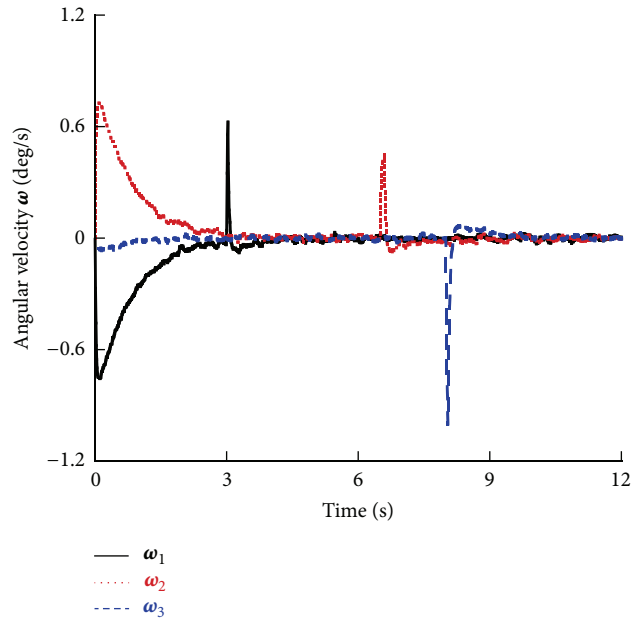


FIGURE 8: The angular velocity ω in the presence of external disturbances.

the pitch, roll, and yaw at the 3th, 6.5th, and the 8th seconds, respectively. The attitude control performance obtained from the developed controller equation (27) is shown in Figures 6–8. From Figures 6–7, it is known that the disturbance torque has little effect on the performance of the attitude and that is because the controller equation (27) is able to guarantee the uniformly ultimately bounded stability of the closed-loop system in the presence of disturbance. It is seen in Figure 8 that although there exists some overshoot for the angular

velocity when disturbance is introduced to the quadrotor, the angular velocity can be stabilized soon.

5. Conclusions

In this work, the design of a quadrotor UAV attitude stabilization controller using quaternion feedback and integrator backstepping was presented. With appropriate choice of integrator backstepping variables, both equilibrium points in

the closed-loop system are proved to be asymptotically stable. Furthermore, taking external disturbance torque into consideration, the attitude and the angular velocity of the quadrotor were governed to be uniformly ultimately bounded by the proposed controller. Simulations of a quadrotor UAV were also presented to illustrate the performance of the controller and that the attitude of the UAV was regulated to the closest equilibrium point. Future work will emphasize the position or path following control of the quadrotor even in the presence of external disturbance.

Conflict of Interests

The authors declare that there is no conflict of interests regarding the publication of this paper.

Acknowledgments

This present work was supported partially by National Natural Science Foundation of China (Project no. 61304149) and Natural Science Foundation of Liaoning, China (Project no. 2013020044). The authors highly appreciate the above financial supports.

References

- [1] C. Shen, Z. J. Rong, and M. Dunlop, "Determining the full magnetic field gradient from two spacecraft measurements under special constraints," *Journal of Geophysical Research A*, vol. 117, no. 10, 2012.
- [2] W. C. Tu, S. R. Elkington, X. L. Li, W. L. Liu, and J. Bonnell, "Quantifying radial diffusion coefficients of radiation belt electrons based on global MHD simulation and spacecraft measurements," *Journal of Geophysical Research A*, vol. 117, no. 10, 2012.
- [3] Y. D. Song and W. C. Cai, "New intermediate quaternion based control of spacecraft: part I—almost global attitude tracking," *International Journal of Innovative Computing Information and Control*, vol. 8, no. 10, pp. 7307–7319, 2012.
- [4] G. M. Li and L. D. Liu, "Coordinated multiple spacecraft attitude control with communication time delays and uncertainties," *Chinese Journal of Aeronautics*, vol. 25, no. 5, pp. 698–708, 2012.
- [5] F. Pantellini, S. Belheouane, N. Meyer-Vernet, and A. Zaslavsky, "Nano dust impacts on spacecraft and boom antenna charging," *Astrophysics and Space Science*, vol. 341, no. 2, pp. 309–314, 2012.
- [6] X. Y. Gao, K. L. Teo, and G. R. Duan, "Robust H_∞ control of spacecraft rendezvous on elliptical orbit," *Journal of the Franklin Institute*, vol. 349, no. 8, pp. 2515–2529, 2012.
- [7] H. R. Williams, R. M. Ambrosi, N. P. Bannister, P. Samaratna, and J. Sykes, "A conceptual spacecraft radioisotope thermoelectric and heating unit (RTHU)," *International Journal of Energy Research*, vol. 36, no. 12, pp. 1192–1200, 2012.
- [8] S. Laborde and A. Calvi, "Spacecraft base-sine vibration test data uncertainties investigation based on stochastic scatter approach," *Mechanical Systems and Signal Processing*, vol. 32, pp. 69–78, 2012.
- [9] S. Yin, S. X. Ding, A. H. A. Sari, and H. Hao, "Data-driven monitoring for stochastic systems and its application on batch process," *International Journal of Systems Science*, vol. 44, no. 7, pp. 1366–1376, 2013.
- [10] S. Yin, S. X. Ding, A. Haghani, H. Hao, and P. Zhang, "A comparison study of basic data-driven fault diagnosis and process monitoring methods on the benchmark Tennessee Eastman process," *Journal of Process Control*, vol. 22, no. 9, pp. 1567–1581, 2012.
- [11] S. Yin, H. Luo, and S.-X. Ding, "Real-time implementation of fault-tolerant control systems with performance optimization," *IEEE Transactions on Industrial Electronics*, vol. 61, no. 5, pp. 2402–2411, 2013.
- [12] S. Yin, G. Wang, and H. R. Karimi, "Data-driven design of robust fault detection system for wind turbines," *Mechatronics*, 2013.
- [13] S. Yin, X. Yang, and H. R. Karimi, "Data-driven adaptive observer for fault diagnosis," *Mathematical Problems in Engineering*, vol. 2012, Article ID 832836, 21 pages, 2012.
- [14] E. V. Morozov and A. V. Lopatin, "Design and analysis of the composite lattice frame of a spacecraft solar array," *Composite Structures*, vol. 94, no. 10, pp. 3106–3114, 2012.
- [15] F. Nemeč, O. Santolik, M. Parrot, and J. S. Pickett, "Magnetospheric line radiation event observed simultaneously on board Cluster 1, Cluster 2 and DEMETER spacecraft," *Geophysical Research Letters*, vol. 39, no. 18, 2012.
- [16] L. Palin, C. Jacquey, J. A. Sauvaud et al., "Statistical analysis of dipolarizations using spacecraft closely separated along Z in the near-Earth magnetotail," *Journal of Geophysical Research A*, vol. 117, no. 9, 2012.
- [17] Y. Miyake, H. Usui, H. Kojima, and H. Nakashima, "Plasma particle simulations on stray photoelectron current flows around a spacecraft," *Journal of Geophysical Research A*, vol. 117, no. 9, 2012.
- [18] M. J. Aschwanden, J. P. Wuelser, N. V. Nitta, J. R. Lemen, M. L. DeRosa, and A. Malanushenko, "First three-dimensional reconstructions of coronal loops with the STEREOA+B spacecraft: IV. Magnetic modeling with twisted force-free fields," *The Astrophysical Journal*, vol. 756, no. 2, article 124, 2012.
- [19] R. E. Denton, B. U. Ö. Sonnerup, J. Birn et al., "Test of Shi et al. method to infer the magnetic reconnection geometry from spacecraft data: MHD simulation with guide field and antiparallel kinetic simulation," *Journal of Geophysical Research A*, vol. 117, no. 9, 2012.
- [20] K. D. Bilimoria and E. R. Mueller, "Handling qualities of a capsule spacecraft during atmospheric entry," *Journal of Spacecraft and Rockets*, vol. 49, no. 5, pp. 935–943, 2012.
- [21] H. Lu, Y.-H. Li, and C.-L. Zhu, "Robust synthesized control of electromechanical actuator for thrust vector system in spacecraft," *Computers & Mathematics with Applications*, vol. 64, no. 5, pp. 699–708, 2012.
- [22] S.-J. Dong, Y.-Z. Li, J. Wang, and J. Wang, "Fuzzy incremental control algorithm of loop heat pipe cooling system for spacecraft applications," *Computers & Mathematics with Applications*, vol. 64, no. 5, pp. 877–886, 2012.
- [23] A. T. Basilevsky, "Analysis of suspicious objects in TV panorama taken by Venera-9 spacecraft," *Solar System Research*, vol. 46, no. 5, pp. 374–378, 2012.
- [24] C. Edwards and S. Spurgeon, *Sliding Mode Control: Theory and Applications*, Taylor & Francis, Boca Raton, Fla, USA, 1998.
- [25] K. B. McCoy, I. Derecho, T. Wong et al., "Insights into the extremotolerance of *Acinetobacter radioresistens* 50v1, a gram-negative bacterium isolated from the Mars Odyssey spacecraft," *Astrobiology*, vol. 12, no. 9, pp. 854–862, 2012.

- [26] K. Yong, S. Jo, and H. Bang, "A modified rodrigues parameter-based nonlinear observer design for spacecraft gyroscope parameters estimation," *Transactions of the Japan Society For Aeronautical and Space Sciences*, vol. 55, no. 5, pp. 313–320, 2012.
- [27] J. X. Fan and D. Zhou, "Nonlinear attitude control of flexible spacecraft with scissored pairs of control moment gyros," *Journal of Dynamic Systems Measurement and Control*, vol. 134, no. 5, Article ID 054502, 5 pages, 2012.
- [28] Y. C. Xu and Q. Chen, "Minimization of mass for heat exchanger networks in spacecrafts based on the entransy dissipation theory," *International Journal of Heat and Mass Transfer*, vol. 55, no. 19-20, pp. 5148–5156, 2012.
- [29] H.-T. Cui and X.-J. Cheng, "Anti-unwinding attitude maneuver control of spacecraft considering bounded disturbance and input saturation," *Science China Technological Sciences*, vol. 55, no. 9, pp. 2518–2529, 2012.
- [30] A.-M. Zou, K. D. Kumar, and Z.-G. Hou, "Attitude coordination control for a group of spacecraft without velocity measurements," *IEEE Transactions on Control Systems Technology*, vol. 20, no. 5, pp. 1160–1174, 2012.
- [31] R. P. Praveen, M. H. Ravichandran, V. T. S. Achari, V. P. J. Raj, G. Madhu, and G. R. Bindu, "A novel slotless Halbach-array permanent-magnet brushless dc motor for spacecraft applications," *IEEE Transactions on Industrial Electronics*, vol. 59, no. 9, pp. 3553–3560, 2012.
- [32] K. G. Klein, G. G. Howes, J. M. TenBarge, S. D. Bale, C. H. K. Chen, and C. S. Salem, "Using synthetic spacecraft data to interpret compressible fluctuations in solar wind turbulence," *The Astrophysical Journal*, vol. 755, no. 2, article 159, 2012.
- [33] G. M. Chen, J. Y. Xu, W. B. Wang, J. H. Lei, and A. G. Burns, "A comparison of the effects of CIR- and CME-induced geomagnetic activity on thermospheric densities and spacecraft orbits: case studies," *Journal of Geophysical Research A*, vol. 117, no. 8, 2012.
- [34] Z. Y. Tan, L. Dong, and F. L. Tang, "Monte Carlo calculations of characteristic quantities of low-energy electron irradiation to spacecraft dielectrics," *Nuclear Instruments & Methods in Physics Research Section B*, vol. 285, pp. 86–93, 2012.
- [35] H. K. Khalil, *Nonlinear Systems*, Prentice Hall, Upper Saddle River, NJ, USA, 3rd edition, 2002.

Research Article

New Strategy for Analog Circuit Performance Evaluation under Disturbance and Fault Value

Aihua Zhang,¹ Yongchao Wang,¹ Chen Chen,¹ and Hamid Reza Karimi²

¹ College of Engineering, Bohai University, Jinzhou 121013, China

² Department of Engineering, Faculty of Engineering and Science, The University of Agder, Grimstad 4898, Norway

Correspondence should be addressed to Aihua Zhang; jsxinxi_zah@163.com

Received 23 December 2013; Accepted 6 January 2014; Published 13 February 2014

Academic Editor: Xudong Zhao

Copyright © 2014 Aihua Zhang et al. This is an open access article distributed under the Creative Commons Attribution License, which permits unrestricted use, distribution, and reproduction in any medium, provided the original work is properly cited.

Focus on this issue of disturbance and fault value is inevitable in data collection about analog circuit. A novel strategy is developed for analog circuit online performance evaluation based on fuzzy learning and double weighted support vector machine (DWMK-FSVM). First, the double weighted support vector regression machine is employed to be the indirect evaluation means, relied on the college analog electronic technology experiment to evaluate analog circuit. Second, the superiority of fuzzy learning also is addressed to realize active suppression to the fault values and disturbance parameters. Moreover, the multikernel RBF is employed by support vector regression machine to realize more flexibility online such as the bandwidths tuning. Numerical results, supported by the college analog circuit experiments, adopted OTL performance eight indexes, which were obtained via precision instrument evaluation in two years to construct training set and are then to be evaluated online based on DWMK-FSVM. Simulation results presented not only highlight precision of the evaluation strategy derived here but also illustrate its great robustness.

1. Introduction

Analog circuits are one of the fundamental parts of modern electromechanic systems. Much digital electronic technology has swarmed into our lives; it seems that all the analog circuits are going to decline, but there still exists a need to use analog circuits [1]. Such as analog circuit is still used to convert speech signals to digital signals, sensor signals are inputted to microprocessors, and digital outputs are converted to analog signals. Furthermore, all the digital systems cannot divorce from ultimately analog circuits [2].

The presence of analog circuit detection capability is vital when focusing on the status discussed above. Physical damage, manufacturing faults, aging, radiation, temperature changes, and power surges are possible reasons; therefore the performance evaluation should be done beforehand. If the system has no performance evaluation part, there is a high risk possibility, especially when the analog circuit is on the status of radical performance degradation. Even worse, analog circuits have been widely used for the autonomous systems working without the intervention of human operators in remote and hazardous environments. The purpose

of analog circuits performance evaluation is to prevent catastrophic accidents and give a caution to the system. In the previous studies, there have been a lot of works about the automation of the process, especially with evolutionary computation [3–5]. Evolutionary computation includes a set of methodologies mimicking the natural evolution phenomena: neural network [6–9], genetic algorithm [6, 10], fuzzy logic [11, 12], switch system [13–16] and data driven [17–20]. Zhang and Yu [20] attempted to evolve analog circuits performance evaluation strategy using support vector regression based on data information about normal analog circuits such as four indexes, input resistance, input voltage, output resistance, and output voltage. This method has presented some advantages such as well evaluation accuracy, portability, and low cost; however, this design has ignored the reality status that the processing of the data collection includes fault value or disturbance value. The low convergence rate could not meet the online evaluation requirement. Literature [21] focused the singularity issue proposed weighted LSSVM algorithm. Based on the idea discussed in literature [21], fuzzy clustering idea is also drawn into LSSVM which guarantees the robust via weighting for each sample [22]. Although there have been

several works on declining singularity effect to this evaluation accuracy with weight to obtain the robustness the weighted value is constant which is susceptible to be influenced by the parameter selection. In fact, Kawamura et al. have leded robust RBF net to robust LSSVR in early years, yet the selection and structure determination of the weight initial value is still the most difficult problem [23].

In this paper, we argue that the evolutionary computation can be useful to realize analog circuit online performance evaluation under disturbance and fault value based on fuzzy learning theory and double weighted support vector machine, and the kernel function of which employs the multikernel RBF. Numerical results, supported by the college analog circuit experiments, adopted OTL performance eight indexes, which were obtained via precision instrument evaluation in two years to construct training set, and are then to be evaluated online based on DWMK-FSVM. Simulation results presented not only highlight speed ability of the evaluation strategy derived here but also illustrate its great precision and robustness.

2. OTL Technical Index

The main technical index of OTL includes gain, transmission bands, center frequency, upper/lower cut-off frequency, maximum output extent, as the important technical index, nonlinear distortion coefficient, input/output resistance, and maximum output power. In addition, aiming at different situation, as the other technical index, power capacity, anti-interference ability, signal to noise ratio, weight, volume, working temperature, and so forth may be proposed. During this technical index, gain embodies the amplified ability, transmission bands give out the response ability to the input signal, and upper/lower cut-off frequency gives out the input/output signal frequency band threshold. When the quiescent point of OTL is confirmed, the four technical indexes such as gain, transmission bands, and upper/lower cut-off frequency are the important.

3. Analog Circuit Performance Evaluation Strategy

3.1. Fuzzy Support Vector Machine (FSVM). The development of SVM came from the best optimum hyperplane which has the linearly separable property. For one training set with classification markers, (x_i, y_i) , $x_i \in R^n$ and $y_i \in \{+1, -1\}$, $i = 1, \dots, l$, if hyperplane $\tilde{\omega} \cdot x + b = 0$ could divide the samples into two types correctly; the best optimum hyperplane would make the sums of the two types to the hyperplane distance be the maximum. The best optimum hyperplane may be obtained via solving the following optimization problem:

$$\begin{aligned} \min \quad & \frac{1}{2} \|\tilde{\omega}\| + C \sum_{i=1}^l \xi_i \\ \text{s.t.} \quad & y_i [(\tilde{\omega} \cdot x_i) + b] \geq 1 - \xi_i, \quad \xi_i \geq 0, \quad i = 1, \dots, l, \end{aligned} \quad (1)$$

where ξ_i is error expression and C is penalty factor.

The solving problem of best optimum hyperplane above may be transformed into dual problem via utilizing Lagrange multiplier method.

Consider

$$\begin{aligned} \max \quad & \sum_{i=1}^l a_i - \frac{1}{2} \sum_{i,j=1}^l a_i a_j y_i y_j (x_i \cdot x_j) \\ \text{s.t.} \quad & \sum_{i=1}^l a_i y_i = 0, \quad 0 \leq a_i \leq C, \quad i = 1, \dots, l, \end{aligned} \quad (2)$$

where a_i is the Lagrange multiplier of x_i . Equation (2) is a typical optimal problem of quadratic function, therefore there will be a guarantee for the existence of a unique solution. That is $a_i \neq 0$ and the corresponding samples are support vector. So the decision function should be

$$f(x) = \text{sign} \left(\sum_{i=1}^l a_i y_i (x_i \cdot x) + b \right). \quad (3)$$

For the nonseparable problem, we can solved this issue via high dimensional mapping $\phi : R^n \rightarrow H$, and the linear classification would be realized in the feature space. By defining the function $k(x_i, x_j) = \phi(x_i) \cdot \phi(x_j)$, the dual programming of formula (2) would be

$$\begin{aligned} \max \quad & \sum_{i=1}^l a_i - \frac{1}{2} \sum_{i,j=1}^l a_i a_j y_i y_j k(x_i \cdot x_j) \\ \text{s.t.} \quad & \sum_{i=1}^l a_i y_i = 0, \quad 0 \leq a_i \leq C, \quad i = 1, \dots, l. \end{aligned} \quad (4)$$

The corresponding decision function would be

$$f(x) = \text{sign} \left(\sum_{i=1}^l a_i y_i k(x_i \cdot x) + b \right), \quad (5)$$

where $k(x_i, x_j) = \phi(x_i) \cdot \phi(x_j)$ is the kernel function; the selection of kernel function should make it to be one of its feature space inner product. The common kernel function includes polynomial kernel function (6); Gauss RBF kernel function (7), and sigmoid kernel function (8), which are expressed as follows:

$$k(x_i, x_j) = (x_i \cdot x_j + 1)^d, \quad d = 1, 2, \dots, n; \quad (6)$$

$$k(x_i, x_j) = \exp(-\gamma \|x_i - x_j\|^2), \quad (7)$$

$$k(x_i, x_j) = \tanh(b(x_i \cdot x_j) + c), \quad b > 0, \quad c < 0. \quad (8)$$

Like SVM, the aim of the FSVM [24] is to find an optimal separating hyperplane that separates the sample points into two classes with the maximal margin. The quadratic optimization problem for classification is considered as the solution to

$$\begin{aligned} \min \quad & \frac{1}{2} \|\tilde{\omega}\| + C \sum_{i=1}^l s_i \xi_i \\ \text{s.t.} \quad & y_i [(\tilde{\omega} \cdot x_i) + b] \geq 1 - \xi_i, \quad \xi_i \geq 0, \quad i = 1, \dots, l. \end{aligned} \quad (9)$$

For considering the effect under the feature strong or weak, the weighted idea has been employed.

3.2. Double Weighted Multikernel FSVM (DWMK-FSVM). Double weighted FSVM (DW-FSVM) is one method that should not only consider the sample number difference and sample importance difference, but also give attention to influence above two characteristics of the feature strong and weak at the same time. DW-FSVM improved the classification precision and conformed FSVM to have better robustness. For illustrative purposes, the DW-FSVM constructed steps [25, 26] are presented as follows.

Step 1. Let source dataset be R , where $R = \{x_i, x_j\}_{i=1}^j$, $x_i \in R^n$, $x_j \in \{-1, +1\}$ and training the FSVMs via R .

Step 2. Based on FSVMs' training result, we eliminated the samples and obtained the dataset S ,

$$x_i^+ \in \text{positive example}, \quad f(x_i^+) > 1 \text{ or } f(x_i^+) < 0, \quad (10)$$

$$x_i^+ \in \text{negative example}, \quad f(x_i^+) < -1 \text{ or } f(x_i^+) > 0. \quad (11)$$

Step 3. We eliminated the redundancy samples of S , obtained the support vector dataset P which included part redundancy samples:

$$P = \{x_i^+, 1\}_{i=1}^{l^+} \cup \{y_j^-, -1\}_{j=1}^{l^-}, \quad (12)$$

where $x_i \in R^n$, l^+ is the positive example number of database P , l^- is the negative example number of database P , x_i^+ is the positive example, and y_j^- is the negative example.

Step 4. we calculated the essentiality weight of P via (13), and the sample error variance value, which is needed during the calculation, can be obtained by initial training FSVMs

$$ml_i^+ = 1 - \frac{\xi_i^+ - \min_i \xi_i^+}{\max_i \xi_i^+ - \min_i \xi_i^+} + \varepsilon, \quad (13)$$

$$ml_j^- = 1 - \frac{\xi_j^- - \min_j \xi_j^-}{\max_j \xi_j^- - \min_j \xi_j^-} + \varepsilon,$$

where ε is a little positive number and category weight may be obtained via $S^+/S^- = l^-/l^+$.

Step 5. The samples of dataset P were described by feature dataset $\{cf, uc\}$, where cf is the class label feature and $uc = (u_1, u_2, \dots, u_n)$ is the nonclass label feature set.

Step 6. We calculated feature uc_i ($1 \leq i \leq n$) information gain, constructed feature weight vector ω and linearity transform diagonal matrix DM :

$$\omega = \sqrt{G} = \left(\sqrt{\text{Gain}(uc_1)}, \dots, \sqrt{\text{Gain}(uc_n)} \right) \quad (14)$$

$$DM = \text{diag}(\omega),$$

where $DM_{kk'} = \omega_k \delta_{kk'}$.

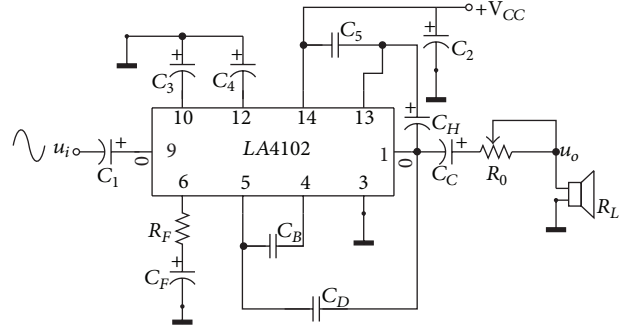


FIGURE 1: The OTL Power Amplifier with Bootstrap Circuit.

Step 7. We replaced FSVM kernel function formulas (6)–(8) with feature weight kernel (15) and selected the appropriate model and training arithmetic to construct classification decision function for dataset P as follows

$$\begin{aligned} k_p(x_i, x_j) &= (x_i^T P \cdot x_j^T P + 1)^d \\ &= (x_i^T P P^T x_j + 1)^d, \quad d = 1, 2, \dots, \\ k_p(x_i, x_j) &= \exp\left(-\gamma \|x_i^T P - x_j^T P\|^2\right) \\ &= \exp\left(-\gamma (x_i - x_j)^T P P^T (x_i - x_j)\right), \\ k_p(x_i, x_j) &= \tanh\left(b (x_i^T P \cdot x_j^T P) + c\right) \\ &= \tanh\left(b (x_i^T P P^T x_j) + c\right), \quad b > 0, c < 0. \end{aligned} \quad (15)$$

In this paper, the feature weighted Gauss RBF kernel function is employed. And the multikernel idea [27] is also imported in this part which can make itself have more flexibility to the kernel function online such as the bandwidths tuning. And the multikernel RBF is defined by

$$\ker(x_i, x_j) = \sum_{m=1}^p \frac{k_m \exp(-d_{i,j}/2\sigma_m^2)}{\sum_{z=1}^p k_z}. \quad (16)$$

4. Experiment Results and Analysis

Experiment based on the test circuit OTL, which is a typical bootstrap circuit shown in Figure 1, and the experiment data, eight indexes, are obtained by precise instrument evaluation in two years. The sample number is 400×100 which is recorded as dataset R . Before verifying the proposed method in this paper, the first thing to be done is establishing datasets of training and testing. However, the disturbance value and fault value in the data set which were caused by industry field influence and other noncircuit fault factors will have great effects on model performance of SVM, especially the dataset, which include the strangeness value, are still used for modeling. Hence, a normalization of the data is required before presenting the input patterns to any statistical machine

TABLE 1: Result of data feature and comparative experiment of regression problem on experiment data.

TRSN	TESN	FN	Method	Parameter ($\sigma, \varepsilon, \gamma$)	SVN	TRMSE	TEMSE	CPU/s
259×100	59×100	8	MKALSSVR	(200, 0.1, 0.75)	30	$1.6982e - 014$	$1.7001e - 028$	0.021
259×100	59×100	8	LSSVR	(200, 0.1, /)	1376	$4.5544e - 015$	$4.2437e - 012$	2.981
259×100	59×100	8	ε -SVR	(200, 0.1, /)	1607	$5.4003e - 017$	$5.3025e - 004$	0.062

SVN denotes the number of support vector, TRSN denotes the number of training support vector, TESN denotes the number of testing support vector, FN denotes the number of the data feature, TEMSE denotes the testing data mean square error, and TDMSE denotes the training data mean square error.

learning algorithm. In this experiment, 0-1 normalization method, denoted by (17), is utilized to preprocess.

$$x_i^n = \frac{x_i^a - x_i^{\min}}{x_i^{\max} - x_i^{\min}}, \quad (17)$$

where x_i^a and x_i^n are the i th components of the input vector before and after normalization, respectively, and x_i^{\max} and x_i^{\min} are the maximum and minimum values of all the components of the input vector before the normalization.

After the above data selection and data normalization, 250×100 samples are selected randomly to be the training samples, the rest data samples are to be a test sample. To validate the superior evaluation performance of the proposed DWMK-FSVM to evaluate the analog circuit performance online, the different methods such as LSSVR, ε -SVR, and the precision instrument are also carried out for the comparison purpose while the analog circuit performance evaluation is on. Meanwhile several parameters needs to be introduced before applying the three SVM algorithms. First of all, it is required to denote three parameters namely, error insensitive zone (ε), penalty factor γ and kernel specific parameters σ . Problem regarding the choice of ε , γ and σ was studied by several researchers [28, 29]. The penalty factor γ controls the smoothness or flatness of the approximation function. If we set the value γ to be large, the objective is only to minimize the empirical risk, which makes the learning machine more complex. On the contrary, if we set the value γ to be small, the objective is to cause the errors to be excessively tolerated yielding a learning machine with poor approximation [30]. In this study, SVM models have been constructed with γ and ε which are the empirical values given by [31, 32]. Via some testing, the parameters γ and ε have been varied over a specific corresponding range in order to obtain better coefficient of correlation value, and the correlation value, denoted Re, is determined by (18). The kernel specific parameters σ is restricted since the value shown in Table 1 gives the better prediction for these models. The three values for each model are shown in the following table. This study adopts RBF (16) where σ is width of RBF, this is also known as kernel function. The adopted γ , ε and σ values for the three models are shown in Table 1.

Consider

$$Re = \frac{\sum_{i=1}^n (D_{ai} - \bar{D}_a)(D_{pi} - \bar{D}_p)}{\sqrt{\sum_{i=1}^n (D_{ai} - \bar{D}_a)^2} \sqrt{\sum_{i=1}^n (D_{pi} - \bar{D}_p)^2}}, \quad (18)$$

where D_{ai} and D_{pi} are the actual and predicted values, respectively, \bar{D}_a and \bar{D}_p are mean of actual and predicted D values corresponding to n patterns.

And MSE is defined by

$$MSE = \sqrt{\frac{1}{K} \sum_{i=1}^K (Y_i - \bar{Y}_i)^2}, \quad (19)$$

where Y_i is the real value, \bar{Y}_i is the predicted value, and K is a testing sample number.

To validate the superior evaluation performance of the proposed DWMK-FSVM, the other two different methods, LSSVR and ε -SVR, are also employed in this part. The sharp contrast about the time response of the three methods are presented in Figure 2. We take one period of testing time of LSSVR as comparison, and the other two performance evaluation methods are also employed to realize comparison in the same testing time. Via this testing comparing, we can see clearly that the testing speed is superiorly greater than the other two methods. In Figure 2, we can see that the support vector density is closely bound up the curvature. If the curvature is bigger, the support vector density is also bigger; on the contrary, while in the position of the relatively smooth, the support vector density is relatively small.

For further analysis, the maximum absolute error is presented by

$$MAE = \max |Y_i - \bar{Y}_i|. \quad (20)$$

From the experimental data given in Tables 2 and 3, we can find the excellent capacity of the proposed DWMK-FSVM to deal with the disturbance and fault values. And Table 4 shows the further proof that the proposed method has better evaluation performance than the other two methods.

To validate the superior evaluation performance of the proposed DWMK-FSVM, we also give out the local regression effect comparison curve of U_O with/without fault values and disturbances under DWMK-FSVM, LSSVR, and ε -SVR. The sharp contrast about the time responses of the three methods are presented in Figures 2 and 3. The proposed method has the well ability to deal with the disturbance value and fault value, and the other ones do not. At the same time, the proposed method also has the same evaluation precision as the other two methods. For the same purpose, the regression effect comparison curves of A_u with/without fault values and disturbances under DWMK-FSVM, LSSVR, and ε -SVR are presented in Figures 4 and 5. From the four figures, we can see that the regression effect of the proposed

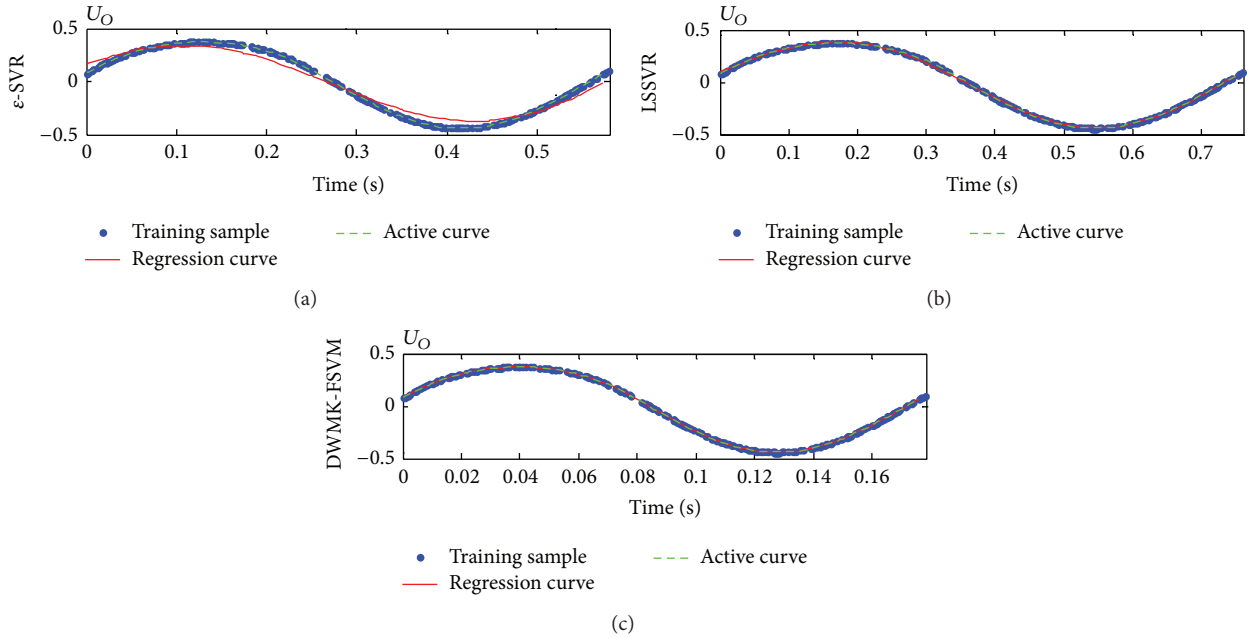


FIGURE 2: The local regression effect comparison curve of U_O without fault values and disturbances under three algorithms.

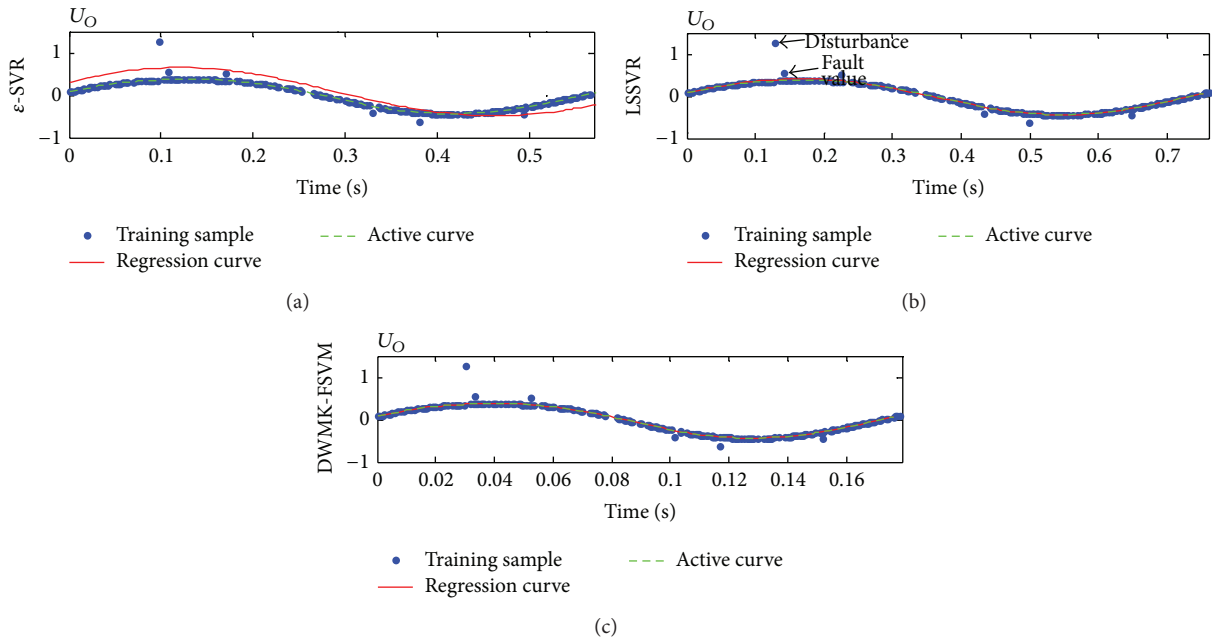


FIGURE 3: The local regression effect comparison curve of U_O with fault values and disturbances under three algorithms.

TABLE 2: Result of data feature and comparative error of training sample.

TRSN	Method	Training MAE				Training MSE			
		A_u	U_{om}	U_s	U_N	A_u	U_{om}	U_s	U_N
250 × 100	DWMK-FSVM	0.0467	0.0985	0.0894	0.2691	0.0091	0.0164	0.0094	0.0485
250 × 100	LSSVR	0.1164	0.3110	0.3225	0.6492	0.0780	0.0768	0.0734	0.2692
250 × 100	ϵ -SVR	0.1659	0.2217	0.2326	0.6618	0.2777	0.2576	0.2528	0.2678

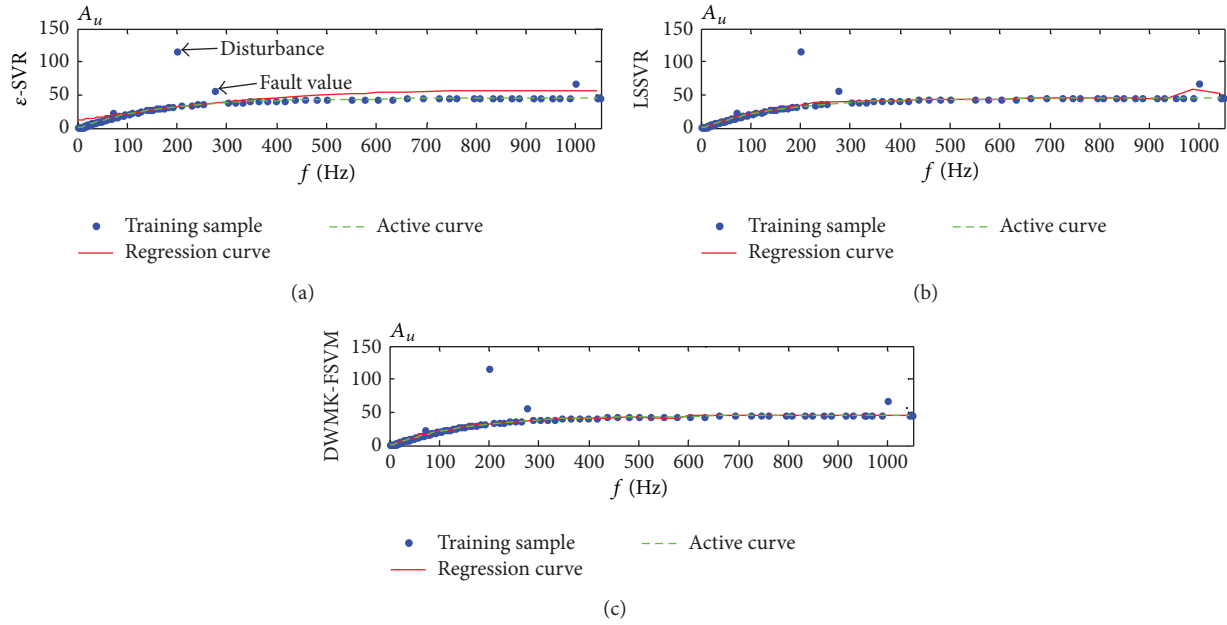


FIGURE 4: The regression effect comparison curve of A_u with fault values and disturbances under three algorithms.

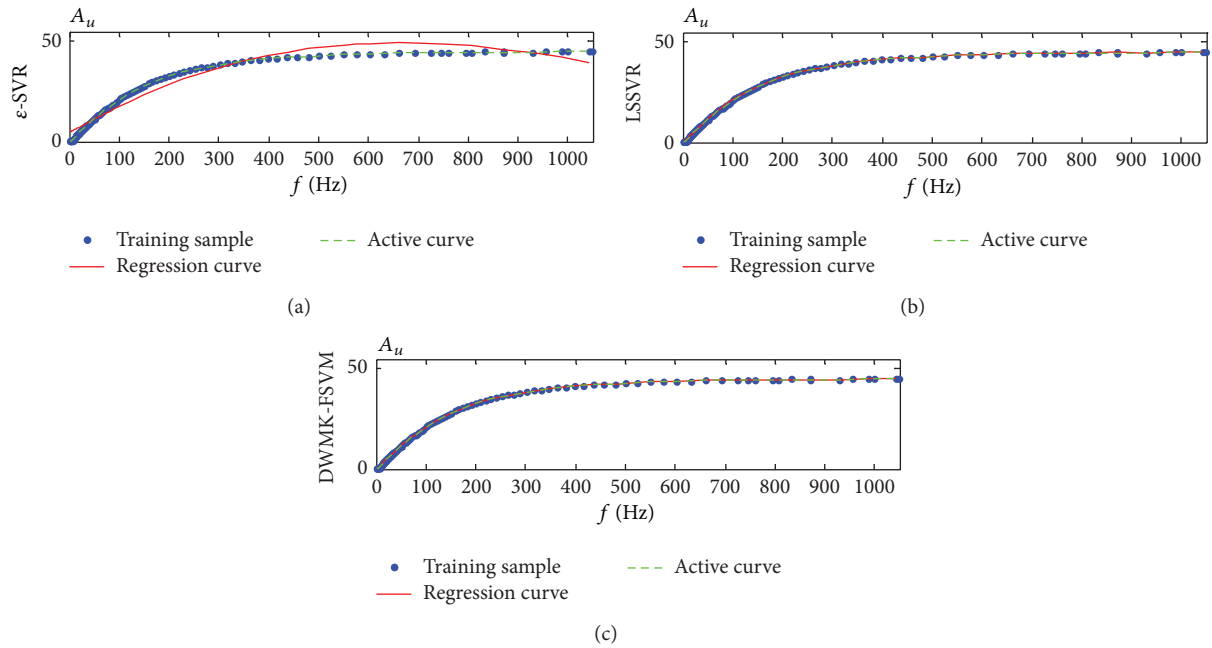


FIGURE 5: The regression effect comparison curve of A_u without fault values and disturbances under three algorithms.

TABLE 3: Result of data feature and comparative error of testing sample.

TSSN	Method	Test MAE				Test MSE			
		A_u	U_{om}	U_s	U_N	A_u	U_{om}	U_s	U_N
100 × 100	DWMK-FSVM	0.0667	0.1035	0.1128	0.1933	0.0201	0.0103	0.0114	0.0993
100 × 100	LSSVR	0.7127	0.3069	0.2369	0.2309	0.1402	0.1026	0.0765	0.2774
100 × 100	ϵ -SVR	0.7277	0.3478	0.2860	0.2662	0.2895	0.2719	0.2657	0.2951

TABLE 4: Result of comparative assessment.

Method	A_{μ}	f_{BW} (MHz)	f_L (Hz)	f_H (MHz)	U_{om} (V)	P_{om} (mW)	U_s (mV)	U_N (pV)	CPU/s
DWMK-FSVM	46.044	3.8002	201.991	3.7041	0.4602	25.9489	10.063	6.2934	0.2056
LSSVR	51.8757	3.9809	173.7801	3.9811	0.4983	20.3304	10.5239	10.6661	0.7614
ε -SVR	56.5644	2.2906	336.7359	2.2909	0.6472	51.0814	16.3679	16.458	0.5796
Test theory value	46.0000	3.7939	203.0921	3.7941	0.4600	25.8049	10.0000	6.3840	—

method is obvious better than the others, and the ability of dealing with disturbance and fault values is more remarkable than the other ones.

5. Conclusion

For the shortcomings of traditional analog circuit performance evaluation method for processing the wrong values, this paper presents an evaluation method based on analog circuit performance of DWMK-FSVM. Using standard SVM, combine fuzzy learning advantages with double weighted SVM to efficiently deal with the dataset that contains the wrong value. Moreover, taking into account the traditional offline evaluation strategy results in the issues that the model cannot adjust timely when the data sample of the sample group is increased or decreased; then the multi-kernel design is employed which has the ability to change the RBF width timely. And this makes the evaluation have the online processing ability. In engineering practice, considering the low-cost development, excellent accuracy evaluation, high operation speed, easy implementation and other features of evaluation methods in DWMK-FSVM, the evaluation strategy deserves development and implementation.

Conflict of Interests

The authors declare that there is no conflict of interests regarding the publication of this paper.

Acknowledgments

This present work was supported partially by the National Natural Science Foundation of China (Project no. 61304149), the Natural Science Foundation of Liaoning, China (Project no. 2013020044), and the Polish-Norwegian Research Programme (Project no. Pol-Nor/200957/47/2013). The authors highly appreciate the above financial supports.

References

- [1] P. Kabisatpathy, A. Barua, and S. Sinha, *Fault Diagnosis of Analog Integrated Circuits*, vol. 30, Springer, New York, NY, USA, 2005.
- [2] J. R. Koza, F. H. Bennett III, D. Andre, M. A. Keane, and F. Dunlap, "Automated synthesis of analog electrical circuits by means of genetic programming," *IEEE Transactions on Evolutionary Computation*, vol. 1, no. 2, pp. 109–128, 1997.
- [3] A. E. Akadi, A. Amine, A. E. Ouadighi, and D. Aboutajdine, "A two-stage gene selection scheme utilizing MRMR filter and GA wrapper," *Knowledge and Information Systems*, vol. 26, no. 3, pp. 487–500, 2011.
- [4] W. Song and S. C. Park, "Latent semantic analysis for vector space expansion and fuzzy logic-based genetic clustering," *Knowledge and Information Systems*, vol. 22, no. 3, pp. 347–369, 2010.
- [5] J. Martinez-Gil and J. F. Aldana-Montes, "Evaluation of two heuristic approaches to solve the ontology meta-matching problem," *Knowledge and Information Systems*, vol. 26, no. 2, pp. 225–247, 2011.
- [6] C.-W. Chen, P.-C. Chen, and W.-L. Chiang, "Modified intelligent genetic algorithm-based adaptive neural network control for uncertain structural systems," *Journal of Vibration and Control*, vol. 19, no. 9, pp. 1333–1347, 2013.
- [7] S. K. Shevade, S. S. Keerthi, C. Bhattacharyya, and K. R. K. Murthy, "Improvements to the SMO algorithm for SVM regression," *IEEE Transactions on Neural Networks*, vol. 11, no. 5, pp. 1188–1193, 2000.
- [8] B. Xiao, Q. L. Hu, and Y. M. Zhang, "Adaptive sliding mode fault tolerant attitude tracking control for flexible spacecraft under actuator saturation," *IEEE Transactions on Control Systems Technology*, vol. 20, no. 6, pp. 1605–1612, 2011.
- [9] B. Xiao, Q. L. Hu, and G. Ma, "Adaptive sliding mode backstepping control for attitude tracking of flexible spacecraft under input saturation and singularity," *Proceedings of the Institution of Mechanical Engineers G*, vol. 224, no. 2, pp. 199–214, 2010.
- [10] S. Sra, S. Nowozin, and S. J. Wright, *Optimization for Machine Learning*, 2011.
- [11] S. Abdulla and M. Tokhi, "Fuzzy logic based FES driven cycling by stimulating single muscle group," in *Converging Clinical and Engineering Research on Neurorehabilitation*, pp. 173–182, Springer, New York, NY, USA, 2013.
- [12] S. Yin, H. Luo, and S. Ding, "Real-time implementation of fault-tolerant control systems with performance optimization," *IEEE Transactions on Industrial Electronics*, vol. 61, no. 5, pp. 2402–2411, 2013.
- [13] X. Zhao, L. Zhang, P. Shi, and H. Karimi, "Robust control of continuous-time systems with state-dependent uncertainties and its application to electronic circuits," *IEEE Transactions on Industrial Electronics*, 2013.
- [14] X. Zhao, L. Zhang, P. Shi, and M. Liu, "Stability of switched positive linear systems with average dwell time switching," *Automatica*, vol. 48, no. 6, pp. 1132–1137, 2012.
- [15] X. Zhao, X. Liu, S. Yin, and H. Li, "Improved results on stability of continuous-time switched positive linear systems," *Automatica*, 2013.
- [16] X. Zhao, L. Zhang, P. Shi, and M. Liu, "Stability and stabilization of switched linear systems with mode-dependent average dwell time," *IEEE Transactions on Automatic Control*, vol. 57, no. 7, pp. 1809–1815, 2012.
- [17] S. Yin, S. X. Ding, A. H. A. Sari, and H. Hao, "Data-driven monitoring for stochastic systems and its application on batch

- process,” *International Journal of Systems Science*, vol. 44, no. 7, pp. 1366–1376, 2013.
- [18] S. Yin, S. X. Ding, A. Haghani, H. Hao, and P. Zhang, “A comparison study of basic data-driven fault diagnosis and process monitoring methods on the benchmark Tennessee Eastman process,” *Journal of Process Control*, vol. 22, no. 9, pp. 1567–1581, 2012.
- [19] S. Yin, X. Yang, and H. R. Karimi, “Data-driven adaptive observer for fault diagnosis,” *Mathematical Problems in Engineering*, vol. 2012, Article ID 832836, 21 pages, 2012.
- [20] A. Zhang and Z. Yu, “Research on amplifier performance evaluation based on support vector regression machine,” *Chinese Journal of Scientific Instrument*, vol. 29, no. 3, pp. 618–622, 2008.
- [21] K.-H. Park, Z. Bien, and D.-H. Hwang, “A study on the robustness of a PID-type iterative learning controller against initial state error,” *International Journal of Systems Science*, vol. 30, no. 1, pp. 49–59, 1999.
- [22] P. R. Ouyang, W. J. Zhang, and M. M. Gupta, “An adaptive switching learning control method for trajectory tracking of robot manipulators,” *Mechatronics*, vol. 16, no. 1, pp. 51–61, 2006.
- [23] S. Kawamura, F. Miyazaki, and S. Arimoto, “Realization of robot motion based on a learning method,” *IEEE Transactions on Systems, Man and Cybernetics*, vol. 18, no. 1, pp. 126–134, 1988.
- [24] C.-F. Lin and S.-D. Wang, “Fuzzy support vector machines,” *IEEE Transactions on Neural Networks*, vol. 13, no. 2, pp. 464–471, 2002.
- [25] M. Hall, E. Frank, G. Holmes, B. Pfahringer, P. Reutemann, and I. H. Witten, “The WEKA data mining software: an update,” *ACM SIGKDD Explorations Newsletter*, vol. 11, no. 1, pp. 10–18, 2009.
- [26] D. E. Lee, J.-H. Song, S.-O. Song, and E. S. Yoon, “Weighted support vector machine for quality estimation in the polymerization process,” *Industrial and Engineering Chemistry Research*, vol. 44, no. 7, pp. 2101–2105, 2005.
- [27] A. Zhang, C. Chen, and H. R. Karimi, “A new adaptive LSSVR with online multikernel RBF tuning to evaluate analog circuit performance,” *Abstract and Applied Analysis*, vol. 2013, Article ID 231735, 7 pages, 2013.
- [28] V. N. Vapnik, *The Nature of Statistical Learning Theory*, Statistics for Engineering and Information Science, Springer, New York, NY, USA, 2000.
- [29] S. R. Gunn, “Support vector machines for classification and regression,” ISIS Technical Report 14, 1998.
- [30] S. Rajasekaran, S. Gayathri, and T.-L. Lee, “Support vector regression methodology for storm surge predictions,” *Ocean Engineering*, vol. 35, no. 16, pp. 1578–1587, 2008.
- [31] P.-S. Yu, S.-T. Chen, and I.-F. Chang, “Support vector regression for real-time flood stage forecasting,” *Journal of Hydrology*, vol. 328, no. 3–4, pp. 704–716, 2006.
- [32] Z. Liang and Y. Li, “Incremental support vector machine learning in the primal and applications,” *Neurocomputing*, vol. 72, no. 10–12, pp. 2249–2258, 2009.

Research Article

Whether and How to Select Inertia and Acceleration of Discrete Particle Swarm Optimization Algorithm: A Study on Channel Assignment

Min Jin,¹ Xiangyuan Zhong,¹ and Xudong Zhao^{2,3}

¹ School of Information Science and Engineering, Hunan University, Changsha, Hunan 410082, China

² College of Information Science and Technology, Bohai University, Jinzhou 121013, China

³ College of Information and Control Engineering, China University of Petroleum, Qingdao 266555, China

Correspondence should be addressed to Min Jin; jinmin@hnu.edu.cn

Received 12 September 2013; Accepted 11 December 2013; Published 5 January 2014

Academic Editor: Lixian Zhang

Copyright © 2014 Min Jin et al. This is an open access article distributed under the Creative Commons Attribution License, which permits unrestricted use, distribution, and reproduction in any medium, provided the original work is properly cited.

There is recently a great deal of interest and excitement in understanding the role of inertia and acceleration in the motion equation of discrete particle swarm optimization (DPSO) algorithms. It still remains unknown whether the inertia section should be abandoned and how to select the appropriate acceleration in order for DPSO to show the best convergence performance. Adopting channel assignment as a case study, this paper systematically conducts experimental filtering research on this issue. Compared with other channel assignment schemes, the proposed scheme and the selection of inertia and acceleration are verified to have the advantage to channel assignment in three respects of convergence rate, convergence speed, and the independency of the quality of initial solution. Furthermore, the experimental result implies that DPSO might have the best convergence performance when its motion equation includes an inertia section in a less medium weight, a bigger acceleration coefficient for global-search optimum, and a smaller acceleration coefficient for individual-search optimum.

1. Introduction

The ever-increasing popularity of mobile communication services gives rise to the need for efficient use of the limited frequency spectrum [1, 2]. The channel assignment problem (CAP) is to obtain a conflict-free channel assignment scheme, which satisfies both the electromagnetic compatibility (EMC) constraints and regional demand for channel. Generally, there are three types of electromagnetic compatibility constraints. The cochannel constraint (CCC) restricts the assignment of the same channel to certain pairs of cells simultaneously. The adjacent channel constraint (ACC) restricts the assignment of channels adjacent in number to adjacent cells simultaneously. The cosite constraint (CSC) specifies that any pair of channels assigned to the same cell must be separated by a certain number.

Currently, much effort has been made to solve the CAP, such as neural network (NN), simulated annealing (SA), and genetic algorithm (GA). However, NN based algorithms

typically yield only suboptimal solutions. The SA approach, although it may be more flexible, is easily trapped in a local minimum, which cannot escape without spending a lot of computation time [3]. GA can effectively locate the neighborhood of the global optimum, but it has the problem of converging to the optimum itself. In other words, the algorithms mentioned above are not particularly efficient in local search [4, 5]. Particle swarm optimization (PSO) is an intelligent algorithm introduced by [6]. It does not have the complex genetic operator and thus the computation complexity is reduced greatly. Moreover, due to the parallel computation of particle swarms, the convergence speed of PSO is much faster than GA.

In [7], a discrete particle swarm optimization (DPSO) based approach is applied to solve the CAP. The particle's position is defined as an N -dimensional vector to represent the call orderings (N is the total number of calls in the cellular system). The velocity of particle is defined as a sequence of movements from source particle to target particle, which is

randomly selected to update the particle's position according to the preset inertia factor and acceleration factor. This representation describes the distance between particles properly and reflects the mechanism of evolution. That means the new position is updated by the particle's inertia position, the particle's historical best position, and the swarm's best position. As the swarm's best acceleration has more influence on the new velocity than the particle's inertia velocity and historical best acceleration in the motion equation, the global search performs better than the local search. For this reason, a strategy of local search is introduced during the process of iteration to speed up the convergence. However, the computation complexity is increased and more iteration is needed.

In whole, there are two major problems in terms of the application of DPSO to CAP. On one hand, the selection of inertia section and acceleration coefficients has a significant effect on the performance in the motion equation. However, some selection experiences in other fields [8–12] may not be suitable for the CAP. On the other hand, the scheme of frequency exhaust assignment (FEA), a call orderings based strategy, can firstly assign channels to the most difficult cells. Thus, FEA has been proved to be an efficient scheme to solve the CAP with large and unevenly distributed traffic demand. In [5], a call orderings based strategy is proposed. From the result of several benchmark instants for CAP, the assigned channel number is disordered, while the channel number for each cell is sorted in ascending manner by FEA.

Adopting channel assignment as a case study, this paper systematically conducts experimental filtering research on the selection of inertia and acceleration in the motion equation in order for DPSO to show the best convergence performance. The rest of this paper is organized as follows. Section 2 introduces the mathematical model of CAP and the eight well-known benchmark problems. Section 3 describes the proposed channel assignment scheme which integrates the optimal DPSO with the FEA strategy in order to meet the usually large and unevenly distributed channel demand in many regions. With the experiments on the eight well-known benchmark problems, the results of the inertia choice and the acceleration adjustment are deeply analyzed and a comparison between the proposed scheme and other channel assignment schemes is further made in Section 4. A conclusion is given in Section 5.

2. Mathematical Formulation and Benchmark Problems

The CAP is specified by the triple (X, D, C) , where X is a cell system, D is a demand vector, and C is an $n \times n$ symmetric compatibility matrix. Each element d_i in D represents the number of channels required by cell i . Each element c_{ij} in C represents the minimum separation distance between any two frequencies assigned to cell i and cell j . The solution space F is represented as an $n \times m$ binary matrix, where m is the total number of available channels and n is the number of cells. Each element f_{ij} in the matrix is either 1 or 0 if $f_{ij} = 1$ indicates the channel j is assigned to cell i . So,

TABLE 1: Specific description of the benchmark problems.

Instant	Cell	Channel	C	D
1	4	11	C_1	d_1
2	25	73	C_1	d_2
3	21	381	C_3	d_3
4	21	533	C_4	d_3
5	21	533	C_5	d_3
6	21	221	C_3	d_4
7	21	309	C_4	d_4
8	21	309	C_5	d_4

the mathematical formulation is to minimize z under the following constrains:

$$\begin{aligned} \sum_{i=1}^n f_{i,j} &= d_i \quad i \in [1, n], \\ |p - q| &\geq c_{i,j} \quad p, q \in [1, z], \quad i, j \in [1, n] \\ &\text{when } f_{p,i} = f_{q,j} = 1. \end{aligned} \quad (1)$$

In order to prove the performance of the algorithm, some well-known benchmark problems are simulated. Table 1 is the specific description of the benchmark problems, and all C and D used here can be found in [13].

3. DPSO and FEA Combined Channel Assignment Scheme

3.1. *FEA*. Compared with the method of minimum cost function [14–16], FEA has been proved to be an efficient scheme to solve the CAP with large and unevenly distributed traffic demand [17–19]. Denote the number of available frequencies by z and the total number of calls in the system by m with $m = \sum_{i=1}^n d_i$. The ordered call list can then be identified with a corresponding vector L which contains m different call numbers described as

$$\begin{aligned} L &= (l_i) \quad i \in [1, m], \\ l_i &\neq l_j \quad \text{for } i \neq j. \end{aligned} \quad (2)$$

FEA starts with the first call in the ordered list. Each call with unsatisfied channel requirement is assigned a channel with the lowest rank so that the assignment satisfies all constraints with previous assignment. The pseudocode illustrating the algorithm of FEA is presented in Algorithm 1. After applying FEA, the number of blocked calls c is computed to evaluate the fitness of the ordered list.

3.2. DPSO

3.2.1. *Position of the Particle*. Represent the ordered list of n calls as the position of the particle by vector X with $X = (x_1, x_2, \dots, x_i, \dots, x_n)$, where $x_i \in \{1, 2, \dots, n\}$, and $i \neq j$ when $x_i \neq x_j$.

```

Loop (L1) for each call  $l_i$  in list  $L$ 
  Loop (L2) for each frequency  $f$  of all  $z$  frequencies (sorted in increasing order)
    If assign the current frequency  $f$  to  $l_i$  without violation of any EMC constraints
      assign  $f$  to  $l_i$ 
    Else
      continue;
  End (L2)
End (L1)

```

ALGORITHM 1: Algorithm of FEA.

3.2.2. Velocity of the Particle. The best call ordering is determined by applying FEA to the list and evaluating the number of blocked calls. The velocity, used to update the particle's position to inflect the call orderings, is defined as transfer to particle's position. Denote the velocity by vector $V = (v_1, v_2, \dots, v_i, \dots, v_n)$, where $v_i \in \{1, 2, \dots, n\}$.

3.2.3. Sum of Position and Velocity. The sum of position and velocity is denoted as $X_2 = X_1 + V$, where X_2 is the new position, X_1 is the original position, and V is the velocity. When the particle's position is updated, if $v_i \neq 0$, exchange the v_i th call and the x_i th call in the list and guarantee the feasibility of new position; else keep the i th call unchanged.

3.2.4. Subtraction of Position and Velocity. The result of subtraction of two positions is velocity, denoted as $V = X_2 - X_1$. For each dimension of X_2 and X_1 , compare $x_{1,i}$ and $x_{2,i}$ one by one. If they are identical, let v_i equal 0; else let v_i equal $x_{2,i}$.

3.2.5. External Multiplication of a Coefficient by a Velocity. The external multiplication of a coefficient by a velocity is represented as $V_2 = c \cdot V_1$, where c is a constant between 0 and 1. For each dimension $v_{1,i}$ of V_1 , a uniformly distributed random number between 0 and 1 is generated, denoted as rand . If $\text{rand} \geq c$, $v_{2,i} = v_{1,i}$; else $v_{2,i} = 0$.

3.2.6. Sum of Velocities. The result of sum of two velocities is a new velocity, denoted as $V = V_1 + V_2$. The new velocity is defined by the equation:

$$v_i = \begin{cases} v_{1,i}, & v_{1,i} \neq 0, v_{2,i} = 0 \\ v_{1,i}, & v_{1,i} \neq 0, v_{2,i} \neq 0, \text{rand} < 0.5 \ (i = 1, 2, \dots, n) \\ v_{2,i}, & \text{others.} \end{cases} \quad (3)$$

3.2.7. Motion Equation. Since the peculiarity of CAP, a motion equation is proposed based on [20], in which the inertia section is determined by experience and the coefficients are adjusted finely. Here, is the motion equation

$$V = wV + c_1 (X_{pbest} - X) + c_2 (X_{gbest} - X), \quad (4)$$

$$X = X + V, \quad (5)$$

where X_{pbest} is the particle's historical best position, X_{gbest} is the swarm's best position, w is the inertia weight, and c_1 and

c_2 are learning factors. When w equals 0, the inertia section is canceled.

With the encoding scheme of call orderings, the upper defined operations can guarantee the feasibility of particle's position. Meanwhile, the formulation still reflects the optimal mechanism for PSO.

3.2.8. Stopping Criteria. The stopping criterion for DPSO is that the best call ordering meeting all requirements (the number of blocked calls is 0 after applying FEA) is found or the max number of iteration is reached. If the max number is reached and the optimal solution is not found, the algorithm does not converge.

3.3. Flowchart of DPSO and FEA Combined Channel Assignment Scheme. The working principle and steps of DPSO and FEA combined channel assignment scheme are described as follows.

Step 1. Input parameters. The parameters are divided into two categories. One is the parameters of PSO, including the size of particle swarm, denoted by $size$, the maximum number of iterations, denoted by $iteration$, inertia weight, denoted by w , and learning factors, denoted by c_1 and c_2 . The other is the parameters of CAP, including the number of cells in cellular system, denoted by N , the number of channels, denoted by M , the matrix of EMC, denoted by C , and the demand vector, denoted by d .

Step 2. Initialize the position and velocity of particles randomly. If the number of calls is n , the initial position is an n dimension vector which represents a randomly ordered call list; and the initial velocity is also an n dimension vector where the i th component v_i equals $\text{rand}(n+1)$. $\text{rand}(n+1)$ is a random number between $(0, 1]$.

Step 3. Evaluate the fitness of each particle in the swarm. After applying FEA, the number of blocked calls is computed and the fitness is evaluated. Each particle's current position and fitness is stored in $pbest$, and the best of all $pbests$ is stored in $gbest$. If the stopping criteria are met, output the call ordering represented by $gbest$ and stop the algorithm.

Step 4. Update the velocity and position of each particle by (4) and (5).

Step 5. Evaluate the fitness of each particle in the swarm by computing the number of blocked calls.

Step 6. Compare the fitness of each particle with its *pbest*. If the current fitness is better, update its *pbest* with the particle's current position.

Step 7. Compare each particle's *pbest* with the swarm's *gbest*, update *gbest*.

Step 8. If the stopping criteria are met, output the call orderings represented by *gbest* and stops the algorithm, else go to Step 4.

4. Filtering Experiments and Result Analysis

4.1. Inertia Choice and Acceleration Adjustment. The algorithm is written in C#. In order to prove the performance of the algorithm, some well-known benchmark problems are simulated, which can be found in [13]. The efficiency of algorithm is evaluated by the convergence rate (CR) and the convergence speed (CS). The CR is defined as the number of times that the optimum solution is found by executing the algorithm 100 times. The CS is defined as the average number of iteration that the optimum solution is found by executing the algorithm 100 times. Generally, the selection of inertia and acceleration in motion equation and whether to include inertia may affect the algorithm's performance greatly. In this simulation, the algorithm is performed and evaluated without inertia and with inertia. The value of the inertia weight and the learning factors (namely the acceleration coefficients) c_1 , c_2 are also determined based on these two conditions by experiment.

4.1.1. Without Inertia ($w = 0$ in (4)). A group of coefficient pairs between $[0, 1]$ is selected to determine the best acceleration coefficients c_1 , c_2 by applying this algorithm to single benchmark Problem 8. Table 2 is the CR and CS of Problem 8.

From Table 2, we can draw two conclusions. One is the algorithm cannot reach 100% CR when c_2 equals 1.0. The other is, when c_1 keeps constant, the CS becomes faster as c_2 increases. When c_2 equals 0.8, the CS is fastest. However, the situation is invalid in two marginal cases (0.0 and 1.0). When c_2 keeps constant, the selection of c_1 has no certain impact on CS. When c_1 equals 0.4, the average number of iteration is smallest (1.455) except for c_2 equals 0.0 and 1.0. When the coefficients c_1/c_2 select 0.8/0.8, the best CS is obtained (1.19).

As the result is obtained by only one benchmark problem, we select a group of coefficients pairs between $[0.2, 0.8]$, apply these coefficients to all benchmark problems (except for the simple Problem 1 and 2) and execute all the 6 problems for 5 trials to obtain the best average CS under different coefficients. The CS of each problem under different coefficient is shown in Figure 1 and the average CS of Problem 8 for each trial is listed in Table 3.

From Figure 1, we can conclude the following three conclusions. First, for complex problems, like Problems 5 and 8 which are denoted as blue and purple lines, when c_2 keeps constant, the average number of iteration increases as c_1

TABLE 2: CS and CR of Problem 8 without inertia.

c_1	c_2						
	0.0	0.2	0.4	0.6	0.8	1.0	
0.0	CR	68	100	100	100	100	67
	CS	48.68	1.65	1.45	1.42	1.39	50.17
0.2	CR	100	100	100	100	100	68
	CS	2.24	2.01	1.59	1.22	1.39	48.68
0.4	CR	100	100	100	100	100	75
	CS	2.81	1.66	1.47	1.39	1.3	38.25
0.6	CR	100	100	100	100	100	76
	CS	2.2	2.12	1.37	1.52	1.31	36.76
0.8	CR	100	100	100	100	100	67
	CS	2.88	3.1	1.61	1.59	1.19	50.17
1.0	CR	66	100	100	100	100	70
	CS	51.66	24.87	26.4	5.56	5.59	45.7

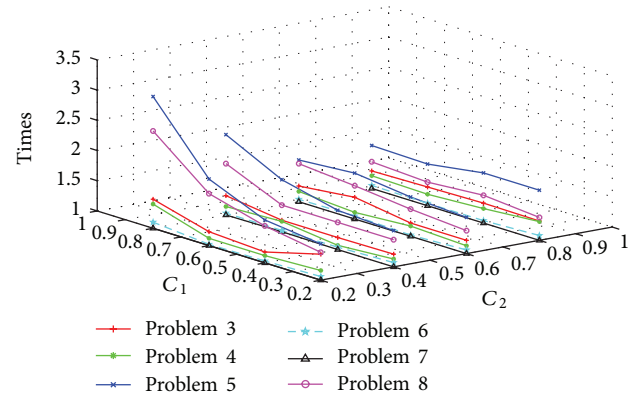


FIGURE 1: Average CS of all problems.

increases. While c_2 equals 0.8, this situation is different. Second, for complex problems like Problem 5 and 8, when c_1 keeps constant, the number of iteration decreases as c_2 increases. Third, for other simple problems, the feature is not obvious as the number of iteration is smaller. From Table 3, we can conclude the following two conclusions. First, for all the benchmark problems, when the coefficient pair c_1/c_2 selects 0.4/0.4, the least average number of iteration (1.16) is obtained. Second, the largest average number of iteration (1.60) is obtained when c_1 equals 0.8 and c_2 equals 0.2. The same conclusion that the average number of iteration increases as c_1 increases when c_2 keeps constant is obtained as the conclusion obtained from Figure 1.

Thus, for single benchmark problem and all benchmark problems, the algorithm performs best when the coefficient pair c_1/c_2 selects 0.2/0.8 and w equals 0. This selection means that the convergence speed can be improved by choosing bigger acceleration coefficient to control the global-search optimum and choosing smaller acceleration coefficient to control the individual-search optimum without inertia section in motion equation for CAP.

TABLE 3: Average CS of Problem 8 without inertia.

c_1/c_2	Trial					avg
	1	2	3	4	5	
0.2/0.2	1.28	1.19	1.17	1.23	1.23	1.22
0.2/0.4	1.25	1.14	1.17	1.13	1.22	1.18
0.2/0.6	1.17	1.17	1.18	1.12	1.20	1.17
0.2/0.8	1.18	1.16	1.27	1.27	1.29	1.23
0.4/0.2	1.15	1.22	1.21	1.23	1.27	1.21
0.4/0.4	1.22	1.16	1.12	1.13	1.18	1.16
0.4/0.6	1.20	1.16	1.19	1.21	1.17	1.19
0.4/0.8	1.18	1.27	1.26	1.19	1.26	1.23
0.6/0.2	1.37	1.31	1.19	1.32	1.33	1.30
0.6/0.4	1.23	1.20	1.24	1.27	1.18	1.22
0.6/0.6	1.26	1.14	1.27	1.23	1.19	1.22
0.6/0.8	1.16	1.19	1.22	1.24	1.14	1.19
0.8/0.2	1.51	1.68	1.53	1.75	1.55	1.60
0.8/0.4	1.38	1.23	1.33	1.36	1.41	1.34
0.8/0.6	1.23	1.14	1.20	1.19	1.37	1.23
0.8/0.8	1.21	1.21	1.27	1.19	1.17	1.21

TABLE 4: CS of all problems with inertia.

w	Benchmark problem							
	1	2	3	4	5	6	7	8
0.0	1.00	1.00	1.32	1.31	1.83	1.05	1.00	1.37
0.2	1.00	1.00	1.11	1.02	1.35	1.02	1.00	1.27
0.4	1.00	1.00	1.11	1.03	1.35	1.01	1.00	1.21
0.6	1.00	1.00	1.23	1.06	1.37	1.03	1.00	1.27
0.8	1.00	1.00	1.15	1.07	1.63	1.02	1.00	1.33
1.0	1.00	1.00	1.33	1.18	1.72	1.04	1.01	1.45

4.1.2. *With Inertia ($w \neq 0$ in (4)).* From the results obtained above, the acceleration coefficients c_1, c_2 are set to be 0.2 and 0.8, respectively. A group of coefficients between $[0, 1]$ are selected to determine the best inertia weight w by applying this algorithm to all benchmark problems. Table 4 is the result for average CS obtained when w equals 0.0, 0.2, 0.4, 0.6, 0.8, and 1.0, respectively.

From Table 4, when w equals 0.4, the algorithm performs best for all benchmark problems and does better than it performs when w equals 0.0 (without inertia).

In summary, in the simulation, this algorithm defines a motion equation with inertia section and when $w, c_1,$ and c_2 select 0.4, 0.2, and 0.8, respectively, the algorithm performs best. Besides, the swarm size of this algorithm is 10 and the max number of iteration is set to be 150 in the simulation.

4.2. *Comparison of CS and CR.* The quality of initial solution has an important influence on the CR and the CS for DPSO. To eliminate the initial solution's impact and evaluate the algorithm's performance objectively, we compute the results with one time and more than one time of iteration respectively, and compare these results with the results obtained from the latest literatures where literature [5] is based on DPSO, literature [21] is based on culture algorithm, and

TABLE 5: Comparison of CS and CR.

Method	Benchmark Problem							
	1	2	3	4	5	6	7	8
One								
CS#	1	1	1.11	1.03	1.35	1.01	1	1.21
CR%	100	100	100	100	100	100	100	100
>one								
CS#	1	1.4	2	3	3.44	4	2.6	3
CR%	100	100	100	100	100	100	100	100
[6]								
CS#	1	5	30	40	55	60	50	60
CR%	100	100	100	100	100	100	100	100
[18]								
CS#	1	2	2	2	2.25	2.75	3.52	4
CR%	100	100	100	100	100	100	100	100
[19]								
CS#	1	2284.6	34.7	12.0	—	136.5	20.2	1977.0
CR%	100	100	100	100	—	100	100	98

literature [22] is based on genetic algorithm. Table 5 is the result.

The result shows that the proposed algorithm achieves 100 percent convergence rate for all benchmark problems. In the experiment, for simple problems, like Problems 1, 2, and 7, the optimum can be obtained by only one time of iteration. Even for the complex problems like Problems 5 and 8, the algorithm achieves a fast convergence speed. Excluding the impact of initial population on the algorithm, 100 percent convergence rate is still achieved for all benchmark problems and the optimum solution is obtained after 5 times of iteration at most.

The result is better than that in [5], where the new velocity is defined as sequential sum of three movement components in the motion equation. For this reason, extra computation is needed and the movement will influence each other, which slows down the CS. The result is also better than culture algorithm and genetic algorithm based approaches which proves that the DPSO and FEA combined scheme with the selection of inertia and acceleration is an efficient approach for CAP.

5. Conclusion

Adopting the channel assignment on the eight well-known benchmark problems as a case study, this paper systematically conducts experimental filtering research on the selection of inertia and acceleration in the motion equation of DPSO. A channel assignment scheme integrating the optimal DPSO with frequency exhaust assignment (FEA) strategy was proposed to meet the usually large and unevenly distributed channel demand in many regions. Compared with other channel assignment schemes, the proposed scheme with the optimal inertia weight and acceleration coefficients achieves 100 percent convergence rate for all benchmark problems and the convergence speed is faster than others without

dependence on the quality of initial solution. For cellular systems with high number of cells, this proposed scheme with the optical inertia weight and acceleration coefficients can also be efficiently applied to find the exact solution in an acceptable time of computation. Furthermore, the filtering result on the eight well-known benchmark problems demonstrates that the optimal inertia weight is 0.4 and the two optimal acceleration coefficients are 0.2 and 0.8, respectively. This result implies that DSPO might be of the best convergence performance when its motion equation includes an inertia section in a less medium weight, a bigger acceleration coefficient for global-search optimum, and a smaller acceleration coefficient for individual-search optimum.

Conflict of Interests

The authors declare that there is no conflict of interests regarding the publication of this paper.

Acknowledgments

This work is supported by the National Natural Science Foundation of China (Grant no. 61374172), National Scientific and Technological Achievement Transformation Project of China (Grant no. 201255), Electronic Information Industry Development Fund of China (Grant no. 2012407), the Military Technology Proliferation Program of China, and the Fundamental Research Funds for the Central Universities, Hunan University.

References

- [1] G. K. Audhya, K. Sinha, and K. Mandal, "A new approach to fast near-optimal channel assignment in cellular mobile networks," *IEEE Transactions on Mobile Computing*, vol. 12, no. 9, pp. 1814–1827, 2013.
- [2] S. Avallone, "An energy efficient channel assignment and routing algorithm for multi-radio wireless mesh networks," *Ad Hoc Networks*, vol. 10, no. 6, pp. 1043–1057, 2012.
- [3] R.-H. Cheng, C. W. Yu, and T. K. Wu, "A novel approach to the fixed channel assignment problem," *Journal of Information Science and Engineering*, vol. 21, no. 1, pp. 39–58, 2005.
- [4] S.-S. Kim, A. E. Smith, and J.-H. Lee, "A memetic algorithm for channel assignment in wireless FDMA systems," *Computers and Operations Research*, vol. 34, no. 6, pp. 1842–1856, 2007.
- [5] K. N. Zhou and Y. L. Hu, "Improvement of computational efficiency for genetic algorithms," *Control Theory & Applications*, vol. 19, no. 5, pp. 812–814, 2002.
- [6] J. Kennedy, "Minds and cultures: particle swarm implications for beings in sociocognitive space," *Adaptive Behavior*, vol. 7, no. 3-4, pp. 269–288, 1999.
- [7] L. Benameur, J. Alami, and A. El Imrani, "A new discrete particle swarm model for the frequency assignment problem," in *Proceedings of the 7th IEEE/ACS International Conference on Computer Systems and Applications*, pp. 139–144, Rabat, Morocco, May 2009.
- [8] Y.-W. Zhong and R.-Y. Cai, "Discrete particle swarm optimization algorithm for QAP," *Acta Automatica Sinica*, vol. 33, no. 8, pp. 871–874, 2007.
- [9] J. D. Zhang, C. S. Zhang, and S. B. Liang, "The circular discrete particle swarm optimization algorithm for flow shop scheduling problem," *Expert Systems with Applications*, vol. 37, no. 8, pp. 5827–5834, 2010.
- [10] H.-F. Xiao and G.-Z. Tan, "A novel particle swarm optimizer without velocity: Simplex-PSO," *Journal of Central South University of Technology*, vol. 17, no. 2, pp. 349–356, 2010.
- [11] L. X. Zhang, H. J. Gao, and O. Kaynak, "Network-induced constraints in networked control system—a survey," *IEEE Transactions on Industrial Informatics*, vol. 9, no. 1, pp. 403–416, 2013.
- [12] L. X. Zhang and P. Shi, "Stability, l2-gain and asynchronous H_∞ control of discrete-time switched systems with average dwell time," *IEEE Transactions on Automatic Control*, vol. 54, no. 9, pp. 2192–2199, 2009.
- [13] N. Funabiki and Y. Takefuji, "A neural network parallel algorithm for channel assignment problems in cellular radio networks," *IEEE Transactions on Vehicular Technology*, vol. 41, no. 4, pp. 430–437, 1992.
- [14] G. Chakraborty and B. Chakraborty, "A genetic algorithm approach to solve channel assignment problem in cellular radio networks," in *Proceedings of the 1999 IEEE Midnight-Sun Workshop on Soft Computing Methods in Industrial Application*, pp. 34–39, Kuusamo, Finland, 1999.
- [15] C. Y. Ngo and V. K. Li, "Fixed channel assignment in cellular radio networks using a modified genetic algorithm," *IEEE Transactions on Vehicular Technology*, vol. 47, no. 1, pp. 163–172, 1998.
- [16] M. Asvial, B. G. Evans, and R. Tafazolli, "Evolutionary genetic DCA for resource management in mobile satellite systems," *Electronics Letters*, vol. 38, no. 20, pp. 1213–1214, 2002.
- [17] D. Beckmann and U. Killat, "A new strategy for the application of genetic algorithms to the channel-assignment problem," *IEEE Transactions on Vehicular Technology*, vol. 48, no. 4, pp. 1261–1269, 1999.
- [18] X. N. Fu, A. G. Bourgeois, and P. Z. Fan, "Using a genetic algorithm approach to solve the dynamic channel-assignment problem," *International Journal of Mobile Communications*, vol. 4, no. 3, pp. 333–353, 2006.
- [19] K. L. Yeung and T. P. Yum, "Fixed channel assignment optimization for cellular mobile networks," *IEICE Transactions on Communications*, vol. E83-B, no. 8, pp. 1783–1791, 2000.
- [20] J. S. Hu, C. X. Guo, B. Ye, H. M. Duan, and Y. J. Cao, "Application of discrete particle swarm optimization to transmission network expansion planning," *Automation of Electric Power Systems*, vol. 28, no. 20, pp. 31–36, 2004.
- [21] J. Alami and A. E. Imrani, "Using cultural algorithm for the fixed-spectrum frequency assignment problem," *Journal of Mobile Communications*, vol. 2, no. 1, pp. 1–9, 2008.
- [22] M.-L. Li, Y.-N. Wang, L. Du, and G.-X. Wang, "Channel assignment problem in cellular networks using genetic algorithms," *Journal of Northeastern University*, vol. 24, no. 3, pp. 213–216, 2003.

Research Article

State Feedback Control for Stochastic Feedforward Nonlinear Systems

Liang Liu¹ and Ming Gao²

¹ College of Engineering, Bohai University, Liaoning 121013, China

² College of Mathematics and Physics, Bohai University, Liaoning 121013, China

Correspondence should be addressed to Liang Liu; smithll@163.com

Received 13 October 2013; Accepted 13 December 2013

Academic Editor: Xudong Zhao

Copyright © 2013 L. Liu and M. Gao. This is an open access article distributed under the Creative Commons Attribution License, which permits unrestricted use, distribution, and reproduction in any medium, provided the original work is properly cited.

This paper considers the state feedback stabilization problem for a class of stochastic feedforward nonlinear systems. By using the homogeneous domination approach, a state feedback controller is constructed to render the closed-loop system globally asymptotically stable in probability. A simulation example is provided to show the effectiveness of the designed controller.

1. Introduction

Consider the following stochastic feedforward nonlinear systems described by

$$\begin{aligned} dx_1 &= x_2 dt + f_1(\bar{x}_3, u) dt + g_1^T(\bar{x}_2, u) d\omega, \\ &\vdots \\ dx_{n-2} &= x_{n-1} dt + f_{n-2}(\bar{x}_n, u) dt + g_{n-2}^T(\bar{x}_{n-1}, u) d\omega, \\ dx_{n-1} &= x_n dt + f_{n-1}(u) dt + g_{n-1}^T(\bar{x}_n, u) d\omega, \\ dx_n &= u dt, \end{aligned} \quad (1)$$

where $x = (x_1, \dots, x_n)^T \in R^n$ and $u \in R$ are the system state and input, respectively. $\bar{x}_i = (x_i, \dots, x_n)$, $i = 2, \dots, n$. ω is an m -dimensional standard Wiener process defined on the complete probability space $(\Omega, \mathcal{F}, \{\mathcal{F}_t\}_{t \geq 0}, P)$ with Ω being a sample space, \mathcal{F} being a σ -field, $\{\mathcal{F}_t\}_{t \geq 0}$ being a filtration, and P being a probability measure. $f_i : R^{n-i+1} \times R \rightarrow R$ and $g_i : R^{n-i} \times R \rightarrow R^m$ are assumed to be locally Lipschitz with $f_i(0, 0) = 0$ and $g_i(0, 0) = 0$, $i = 1, \dots, n-1$.

Since the stochastic stability theory was established, the stabilization problems for stochastic lower-triangular nonlinear systems have made a great number of achievements in recent years; see, for example, [1–16] and the other references.

Feedforward system is another important class of nonlinear systems. From the theoretical viewpoint, they are not feedback linearizable and cannot be stabilized by the conventional backstepping method; to some extent, the control problem of these systems is more difficult than feedback systems. On the other hand, some simple physical models, for example, the cart-pendulum system in [17] and the ball-beam with a friction term in [18], can be described by equations with the feedforward form. In recent papers on feedforward systems, [19] studied delay-adaptive feedback for linear systems. The input delay compensation for forward complete and strict-feedforward nonlinear systems was solved by [20]. Reference [21] considered the adaptive stabilization problem for feedforward nonlinear systems with time delays by taking a nested saturation feedback. The global output feedback stabilization problem for system (1) without stochastic noise was addressed by [22]. Reference [23] investigated the state and output feedback control for a class of feedforward nonlinear time-delay systems. For high-order nonlinear feedforward systems, [24] considered global stabilization problem by using the generalized adding a power integrator method and a series of nested saturation functions, [25, 26] respectively dealt with the state feedback control for this kind of systems with time delay, but all these results are limited to deterministic systems. Due to the special form of this system, there are few results on stochastic feedforward systems at present.

The purpose of this paper is to solve the state feedback stabilization problem of system (1) by using the homogeneous domination approach in [22]. The underlying idea of this approach is that the homogeneous controller is first developed without considering the drift and diffusion terms, and then a low gain is introduced to the state feedback controller to dominate the drift and diffusion terms. By adopting this method, a state feedback controller is explicitly constructed to render the closed-loop system globally asymptotically stable in probability.

The paper is organized as follows. Section 2 provides some preliminary results. The design and analysis of state feedback controller is given in Sections 3 and 4, following a simulation example in Section 5. Section 6 concludes this paper.

2. Preliminary Results

The following notations, definitions, and lemmas are to be used throughout the paper.

R_+ denotes the set of all nonnegative real numbers and R^n denotes the real n -dimensional space. For a given vector or matrix X , X^T denotes its transpose, $\text{Tr}\{X\}$ denotes its trace when X is square, and $|X|$ is the Euclidean norm of a vector X . \mathcal{C}^i denotes the set of all functions with continuous i th partial derivatives. \mathcal{K} denotes the set of all functions: $R_+ \rightarrow R_+$, which are continuous, strictly increasing, and vanishing at zero; \mathcal{K}_∞ denotes the set of all functions which are of class \mathcal{K} and unbounded; \mathcal{KL} denotes the set of all functions $\beta(s, t): R_+ \times R_+ \rightarrow R_+$, which are of \mathcal{K} for each fixed t and decrease to zero as $t \rightarrow \infty$ for each fixed s .

Consider the following stochastic nonlinear system:

$$dx = f(x)dt + g^T(x)d\omega, \quad x(0) = x_0 \in R^n, \quad (2)$$

where $x \in R^n$ is the system state and ω is an m -dimensional standard Wiener process defined on the complete probability space $(\Omega, \mathcal{F}, \{\mathcal{F}_t\}_{t \geq 0}, P)$. The Borel measurable functions $f: R^n \rightarrow R^n$ and $g: R^n \rightarrow R^{m \times n}$ are locally Lipschitz with $f(0) = 0$ and $g(0) = 0$.

Definition 1 (see [1]). For any given $V(x) \in \mathcal{C}^2$ associated with stochastic system (2), the differential operator \mathcal{L} is defined as

$$\mathcal{L}V = \frac{\partial V}{\partial x} f(x) + \frac{1}{2} \text{Tr} \left\{ g(x) \frac{\partial^2 V}{\partial x^2} g^T(x) \right\}. \quad (3)$$

Definition 2 (see [1]). For system (2), the equilibrium $x = 0$ is globally asymptotically stable (GAS) in probability if for any $\epsilon > 0$, there exists a class \mathcal{KL} function $\beta(\cdot, \cdot)$ such that $P\{|x(t)| < \beta(|x_0|, t)\} \geq 1 - \epsilon$ for any $t \geq 0$ and $x_0 \in R^n \setminus \{0\}$.

Definition 3 (see [22]). For fixed coordinates $(x_1, \dots, x_n) \in R^n$ and real numbers $r_i > 0, i = 1, \dots, n$.

- (i) The dilation $\Delta_\epsilon(x)$ is defined by $\Delta_\epsilon(x) = (\epsilon^{r_1}x_1, \dots, \epsilon^{r_n}x_n)$ for any $\epsilon > 0$ and r_1, \dots, r_n are called the weights of the coordinates. For simplicity, we define dilation weight as $\Delta = (r_1, \dots, r_n)$.

- (ii) A function $V \in \mathcal{C}(R^n, R)$ is said to be homogeneous of degree τ if there is a real number $\tau \in R$ such that $V(\Delta_\epsilon(x)) = \epsilon^\tau V(x_1, \dots, x_n)$ for any $x \in R^n \setminus \{0\}, \epsilon > 0$.

- (iii) A vector field $h \in \mathcal{C}(R^n, R^n)$ is said to be homogeneous of degree τ if there is a real number $\tau \in R$ such that $h_i(\Delta_\epsilon(x)) = \epsilon^{\tau+r_i}h_i(x)$ for any $x \in R^n \setminus \{0\}, \epsilon > 0, i = 1, \dots, n$.

- (iv) A homogeneous p -norm is defined as $\|x\|_{\Delta, p} = (\sum_{i=1}^n |x_i|^{p/r_i})^{1/p}$ for any $x \in R^n$, where $p \geq 1$ is a constant. For simplicity, in this paper, we choose $p = 2$ and write $\|x\|_\Delta$ for $\|x\|_{\Delta, 2}$.

Lemma 4 (see [1]). Consider system (2) and suppose that there exist a \mathcal{C}^2 function $V(x)$, class \mathcal{K}_∞ functions α_1 and α_2 , and a class \mathcal{K} function α_3 such that

$$\alpha_1(|x|) \leq V(x) \leq \alpha_2(|x|), \quad \mathcal{L}V \leq -\alpha_3(|x|). \quad (4)$$

Then there exists an almost surely unique solution on $[0, \infty)$, the equilibrium $x = 0$ is GAS in probability, and $P\{\lim_{t \rightarrow \infty} |x(t)| = 0\} = 1$.

Lemma 5 (see [22]). Given a dilation weight $\Delta = (r_1, \dots, r_n)$, suppose that $V_1(x)$ and $V_2(x)$ are homogeneous functions of degrees τ_1 and τ_2 , respectively. Then $V_1(x)V_2(x)$ is also homogeneous with respect to the same dilation weight Δ . Moreover, the homogeneous degree of $V_1 \cdot V_2$ is $\tau_1 + \tau_2$.

Lemma 6 (see [22]). Suppose that $V: R^n \rightarrow R$ is a homogeneous function of degree τ with respect to the dilation weight Δ ; then

- (i) $\partial V / \partial x_i$ is homogeneous of degree $\tau - r_i$ with r_i being the homogeneous weight of x_i ;

- (ii) there is a constant c such that $V(x) \leq c\|x\|_\Delta^\tau$. Moreover, if $V(x)$ is positive definite, then $V(x) \geq c\|x\|_\Delta^\tau$, where c is a positive constant.

Lemma 7 (see [4]). Let c and d be positive constants. For any positive number $\bar{\gamma}$, then $|x|^c|y|^d \leq (c/(c+d))\bar{\gamma}|x|^{c+d} + (d/(c+d))\bar{\gamma}^{-c/d}|y|^{c+d}$.

3. Design of State Feedback Controller

3.1. Assumption. For system (1), we need the following Assumption.

Assumption 8. For $i = 1, \dots, n-1$, there exist positive constants a_1 and a_2 such that

$$\begin{aligned} |f_i(\bar{x}_{i+2}, u)| &\leq a_1(|x_{i+2}| + \dots + |x_n| + |u|), \\ |g_i(\bar{x}_{i+1}, u)| &\leq a_2(|x_{i+1}| + \dots + |x_n| + |u|), \end{aligned} \quad (5)$$

where $x_{n+1} = 0$.

Remark 9. Obviously, system (1) satisfying Assumption 8 is a stochastic feedforward nonlinear system. As discussed in the deterministic feedforward references such as [21–26], that

is, $g_i(\cdot) \equiv 0$ for $i = 1, \dots, n-1$, and stochastic feedforward reference [27], Assumption 8 is a general and frequently used condition.

Due to the special form of stochastic feedforward system, almost all the existing methods fail to be applicable to solve the stabilization problem of system (1). Based on this reason, the objective of this paper is to design a state feedback controller for system (1) such that the equilibrium of the closed-loop system is globally asymptotically stable in probability.

To achieve this objective, we first introduce the following coordinate transformation:

$$\eta_i = \frac{x_i}{\kappa^{i-1}}, \quad v = \frac{u}{\kappa^n}, \quad i = 1, \dots, n, \quad (6)$$

where $0 < \kappa < 1$ is a designed constant. With the help of (6), (1) can be rewritten as

$$\begin{aligned} d\eta_1 &= \kappa\eta_2 dt + \bar{f}_1(\bar{\eta}_3, v) dt + \bar{g}_1^T(\bar{\eta}_2, v) d\omega, \\ &\vdots \\ d\eta_{n-2} &= \kappa\eta_{n-1} dt + \bar{f}_{n-2}(\bar{\eta}_n, v) dt + \bar{g}_{n-2}^T(\bar{\eta}_{n-1}, v) d\omega, \quad (7) \\ d\eta_{n-1} &= \kappa\eta_n dt + \bar{f}_{n-1}(v) dt + \bar{g}_{n-1}^T(\bar{\eta}_n, v) d\omega, \\ d\eta_n &= \kappa v dt, \end{aligned}$$

where $\bar{f}_i = f_i/\kappa^{i-1}$ and $\bar{g}_i = g_i/\kappa^{i-1}$, $i = 1, \dots, n-1$.

3.2. State Feedback Control of Nominal Nonlinear System. We construct a state feedback controller for the following nominal nonlinear system of (7):

$$\begin{aligned} d\eta_i &= \kappa\eta_{i+1} dt, \quad i = 1, \dots, n-1, \\ d\eta_n &= \kappa v dt. \end{aligned} \quad (8)$$

Step 1. Introducing $\xi_1 = \eta_1$ and choosing $V_1(\eta_1) = (1/4)\xi_1^4$, by (3) and (8), it can be verified that $\mathcal{L}V_1 = \kappa\xi_1^3\eta_2$. The first virtual controller

$$\eta_2^* = -c_{11}\xi_1 =: -\alpha_1\xi_1, \quad c_{11} > 0 \quad (9)$$

leads to $\mathcal{L}V_1 \leq -\kappa c_{11}\xi_1^4 + \kappa\xi_1^3(\eta_2 - \eta_2^*)$.

Step i ($i = 2, \dots, n$). In this step, one can obtain the similar property for the i th subsystem, which is presented by the following lemma.

Lemma 10. Suppose that at Step $i-1$ there are a set of virtual controllers $\eta_1^*, \dots, \eta_i^*$ defined by

$$\begin{aligned} \eta_1^* &= 0, \quad \xi_1 = \eta_1 - \eta_1^* = \eta_1, \\ \eta_k^* &= -\alpha_{k-1}\xi_{k-1}, \quad \xi_k = \eta_k - \eta_k^*, \quad k = 2, \dots, i, \end{aligned} \quad (10)$$

such that the $(i-1)$ th Lyapunov function $V_{i-1}(\bar{\eta}_{i-1}) = (1/4)\sum_{j=1}^{i-1}\xi_j^4$ satisfies

$$\mathcal{L}V_{i-1} \leq -\kappa\sum_{j=1}^{i-1}c_{i-1,j}\xi_j^4 + \kappa\xi_{i-1}^3(\eta_i - \eta_i^*), \quad (11)$$

where $\alpha_j, c_{i-1,j}$, $j = 1, \dots, i-1$, are positive constants. Then there exists a virtual control law $\eta_{i+1}^* = -\alpha_i\xi_i$ such that

$$\mathcal{L}V_i \leq -\kappa\sum_{j=1}^i c_{ij}\xi_j^4 + \kappa\xi_i^3(\eta_{i+1} - \eta_{i+1}^*), \quad (12)$$

where $V_i(\bar{\eta}_i) = (1/4)\sum_{j=1}^i \xi_j^4$.

Proof. From (3), (8), (10), and (11), it follows that

$$\begin{aligned} \mathcal{L}V_i &\leq -\kappa\sum_{j=1}^{i-1}c_{i-1,j}\xi_j^4 + \kappa\xi_i^3\eta_{i+1} \\ &\quad + \kappa\xi_{i-1}^3\xi_i - \kappa\xi_i^3\sum_{k=1}^{i-1}\frac{\partial\eta_i^*}{\partial\eta_k}\eta_{k+1}. \end{aligned} \quad (13)$$

We concentrate on the last two terms on the right-hand side of (13).

Using (10) and Lemma 7, one obtains

$$\begin{aligned} \xi_{i-1}^3\xi_i &\leq l_{i,i-1,1}\xi_{i-1}^4 + \rho_{i1}\xi_i^4, \\ -\xi_i^3\sum_{k=1}^{i-1}\frac{\partial\eta_i^*}{\partial\eta_k}\eta_{k+1} &\leq |\xi_i|^3\left|\sum_{k=1}^{i-1}\alpha_{i-1}\cdots\alpha_k(\xi_{k+1} - \alpha_k\xi_k)\right| \\ &\leq |\xi_i|^3\left(\sum_{k=1}^{i-1}(\alpha_{i-1}\cdots\alpha_{k-1} \right. \\ &\quad \left. + \alpha_{i-1}\cdots\alpha_{k+1}\alpha_k^2)|\xi_k| + \alpha_{i-1}|\xi_i|\right) \\ &\leq \sum_{k=1}^{i-1}l_{ik2}\xi_k^4 + \rho_{i2}\xi_i^4, \end{aligned} \quad (14)$$

where $l_{i,i-1,1}, l_{ik2}$ ($k = 1, \dots, i-1$), ρ_{i1} , and ρ_{i2} are positive constants, $\alpha_0 = 0$.

Choosing

$$c_{ij} = \begin{cases} c_{i-1,j} - l_{ij2} > 0, & j = 1, \dots, i-2, \\ c_{i-1,i-1} - l_{i,i-1,1} - l_{i,i-1,2} > 0, & j = i-1, \end{cases} \quad (15)$$

$$\eta_{i+1}^* = -(c_{ii} + \rho_{i1} + \rho_{i2})\xi_i =: -\alpha_i\xi_i, \quad c_{ii} > 0,$$

and substituting (14)-(15) into (13), one gets the desired result. \square

At Step n , choosing $V_n(\bar{\eta}_n) = (1/4)\sum_{i=1}^n \xi_i^4$ and

$$v = \eta_{n+1}^* = -\alpha_n\xi_n = -(\bar{\alpha}_n\eta_n + \bar{\alpha}_{n-1}\eta_{n-1} + \cdots + \bar{\alpha}_1\eta_1), \quad (16)$$

by (3), (12), and (16), one gets

$$\mathcal{L}V_n \leq -\kappa\sum_{i=1}^n c_{ni}\xi_i^4 + \kappa\xi_n^3(v - \eta_{n+1}^*) = -\kappa\sum_{i=1}^n c_{ni}\xi_i^4, \quad (17)$$

where $\xi_n = \eta_n - \eta_n^*$, $\bar{\alpha}_i = \alpha_n \cdots \alpha_i$, c_{ni} , and $i = 1, \dots, n$, are positive constants. The system (7) and (16) can be written as

$$d\eta = \kappa E(\eta) dt + F(\eta, v) dt + G^T(\eta, v) d\omega, \quad (18)$$

where $\eta = \bar{\eta}_n = (\eta_1, \dots, \eta_n)^T$, $E(\eta) = (\eta_2, \dots, \eta_n, v)^T$, $F(\eta, v) = (\bar{f}_1, \dots, \bar{f}_{n-1}, 0)^T$, and $G(\eta, v) = (\bar{g}_1, \dots, \bar{g}_{n-1}, 0)$. Introducing the dilation weight $\Delta = (\underbrace{1, 1, \dots, 1}_{\text{for } \eta_1, \dots, \eta_n})$, by (10) and

$V_n(\eta) = (1/4) \sum_{i=1}^n \xi_i^4$, one obtains

$$\begin{aligned} V_n(\Delta_\varepsilon(\eta)) &= \frac{1}{4} \sum_{i=1}^n (\varepsilon \eta_i + \alpha_{i-1} \varepsilon \eta_{i-1} + \cdots + \alpha_{i-1} \cdots \alpha_1 \varepsilon \eta_1)^4 \\ &= \varepsilon^4 V_n(\eta), \end{aligned} \quad (19)$$

from which and Definition 3, we know that $V_n(\eta)$ is homogeneous of degree 4.

4. Stability Analysis

We state the main result in this paper.

Theorem 11. *If Assumption 8 holds for the stochastic feedforward nonlinear system (1), under the state feedback controller $u = \kappa^n v$ and (16), then*

- (i) *the closed-loop system has an almost surely unique solution on $[0, \infty)$;*
- (ii) *the equilibrium at the origin of the closed-loop system is GAS in probability.*

Proof. We prove Theorem 11 by three steps.

Step 1. Since f_i and g_i are assumed to be locally Lipschitz, so the system consisting of (7) and (16) satisfies the locally Lipschitz condition.

Step 2. By Lemma 6 and (17), there exists a positive constant c_{01} such that

$$\frac{\partial V_n}{\partial \eta} \kappa E(\eta) \leq -c_{01} \kappa \|\eta\|_\Delta^4. \quad (20)$$

By Assumption 8, (6), (16), and $0 < \kappa < 1$, one has

$$\begin{aligned} |\bar{f}_i(\bar{\eta}_{i+2}, v)| &\leq \frac{a_1 (\kappa^{i+1} |\eta_{i+2}| + \cdots + \kappa^{n-1} |\eta_n| + \kappa^n |v|)}{\kappa^{i-1}} \\ &\leq a_1 \kappa^2 (|\eta_{i+2}| + \cdots + |\eta_n| + |v|) \\ &\leq \lambda_1 \kappa^2 \|\eta\|_\Delta, \end{aligned} \quad (21)$$

where λ_1 is a positive constant. According to Lemmas 5–6 and (21), one obtains

$$\frac{\partial V_n}{\partial \eta} F(\eta, v) = \sum_{i=1}^{n-1} \frac{\partial V_n}{\partial \eta_i} \bar{f}_i(\bar{\eta}_{i+2}, v) \leq c_{02} \kappa^2 \|\eta\|_\Delta^4, \quad (22)$$

where c_{02} is a positive constant. Similar to (21), there is a positive constant λ_2 such that

$$|\bar{g}_i(\bar{\eta}_{i+1}, v)| \leq \lambda_2 \kappa \|\eta\|_\Delta, \quad (23)$$

from which and Lemmas 5–6, one leads to

$$\begin{aligned} &\frac{1}{2} \text{Tr} \left\{ G(\eta, v) \frac{\partial^2 V_n}{\partial \eta^2} G^T(\eta, v) \right\} \\ &\leq \frac{1}{2} m \sqrt{m} \sum_{i,j=1}^{n-1} \left| \frac{\partial^2 V_n}{\partial \eta_i \partial \eta_j} \right| |\bar{g}_i(\bar{\eta}_{i+1}, v)| |\bar{g}_j(\bar{\eta}_{j+1}, v)| \\ &\leq c_{03} \kappa^2 \|\eta\|_\Delta^4, \end{aligned} \quad (24)$$

where c_{03} is a positive constant. By (3), (18), (20), (22), and (24), one has

$$\begin{aligned} \mathcal{L}V_n &= \frac{\partial V_n}{\partial \eta} \kappa E(\eta) + \frac{\partial V_n}{\partial \eta} F(\eta, v) \\ &\quad + \frac{1}{2} \text{Tr} \left\{ G(\eta, v) \frac{\partial^2 V_n}{\partial \eta^2} G^T(\eta, v) \right\} \\ &\leq -c_{01} \kappa \|\eta\|_\Delta^4 + (c_{02} + c_{03}) \kappa^2 \|\eta\|_\Delta^4 \\ &= -\kappa (c_{01} - (c_{02} + c_{03}) \kappa) \|\eta\|_\Delta^4. \end{aligned} \quad (25)$$

Since c_{01} is a constant independent of c_{02} and c_{03} , by choosing

$$0 < \kappa < \kappa^* =: \min \left\{ 1, \frac{c_{01}}{c_{02} + c_{03}} \right\}, \quad (26)$$

(25) becomes $\mathcal{L}V_n \leq -c_0 \|\eta\|_\Delta^4$, where c_0 is a positive constant.

By Steps 1–2 and Lemma 4, the system consisting of (7) and (16) has an almost surely unique solution on $[0, \infty)$, $\eta = 0$ is GAS in probability, and $P\{\lim_{t \rightarrow \infty} |\eta| = 0\} = 1$.

Step 3. Since (6) is an equivalent transformation, the closed-loop system consisting of (1), $u = \kappa^n v$, and (16) has the same properties as the system (7) and (16). Theorem 11 holds. \square

Remark 12. This paper extends the homogeneous domination idea from deterministic systems to stochastic system (1) and explicitly constructs a state feedback controller. It should be emphasized that the rigorous proof of Theorem 11 is not an easy work.

5. A Simulation Example

Consider the following stochastic nonlinear system:

$$\begin{aligned} dx_1 &= x_2 dt + \frac{1}{30} u dt + \frac{1}{5} \sin x_2 d\omega, \\ dx_2 &= u dt. \end{aligned} \quad (27)$$

It is easy to verify that Assumption 8 is satisfied with $a_1 = 1/30$ and $a_2 = 1/5$.

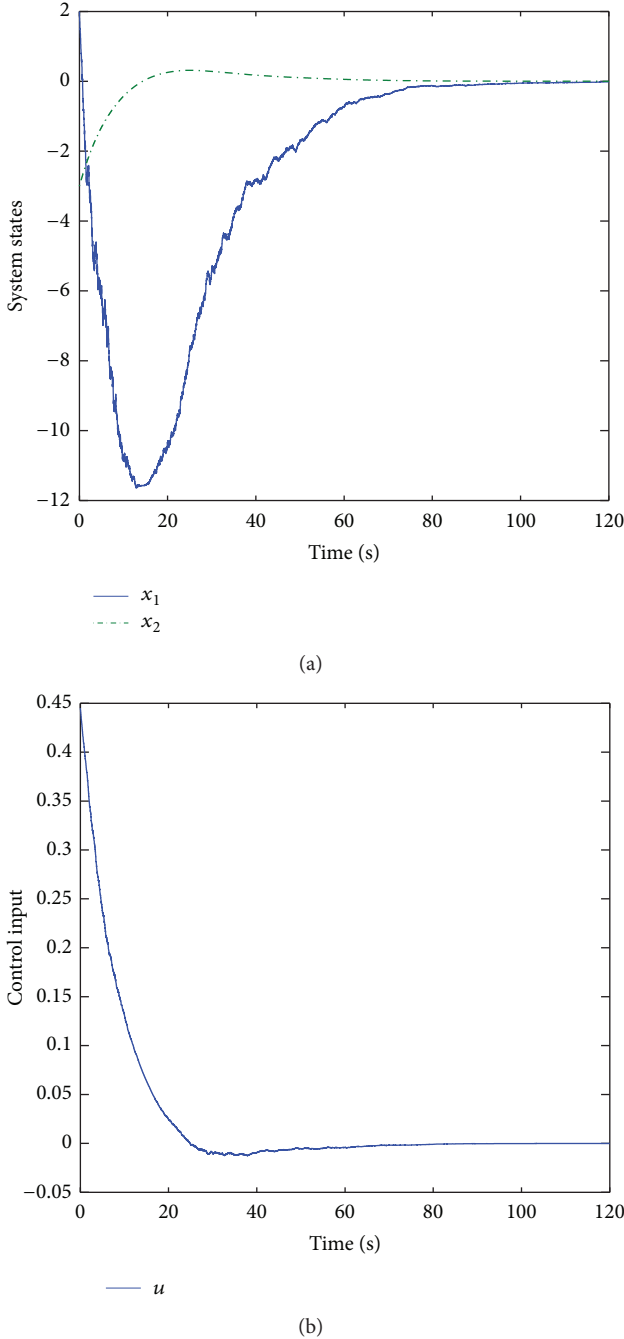


FIGURE 1: The responses of the closed-loop system (27) and (34).

Now, we give the controller design of system (27). Introducing the coordinate transformation

$$\eta_1 = x_1, \quad \eta_2 = \frac{x_2}{\kappa}, \quad v = \frac{u}{\kappa^2}, \quad (28)$$

system (27) becomes

$$\begin{aligned} d\eta_1 &= \kappa\eta_2 dt + \frac{\kappa^2}{30} v dt + \frac{1}{5} \sin \kappa\eta_2 d\omega, \\ d\eta_2 &= \kappa v dt. \end{aligned} \quad (29)$$

Choosing $\xi_1 = \eta_1$ and $V_1(\eta_1) = (1/4)\xi_1^4$, we obtain $\mathcal{L}V_1 \leq -2\kappa\xi_1^4 + \kappa\xi_1^3(\eta_2 - \eta_2^*)$, where $\eta_2^* = -2\eta_1 =: -\alpha_1\xi_1$. By $\xi_2 = \eta_2 - \eta_2^*$ and $V_2(\bar{\eta}_2) = V_1(\eta_1) + (1/4)\xi_2^4$, a direct calculation leads to

$$\mathcal{L}V_2 \leq -2\kappa\xi_1^4 + \kappa\xi_1^3\xi_2 + \kappa\xi_2^3v + \kappa\alpha_1\xi_2^3\eta_2. \quad (30)$$

By Lemma 7, one has

$$\xi_1^3\xi_2 \leq \frac{1}{2}\xi_1^4 + \frac{27}{32}\xi_2^4, \quad (31)$$

$$\alpha_1\xi_2^3\eta_2 \leq \frac{1}{2}\xi_1^4 + (3\sqrt[3]{2} + 2)\xi_2^4.$$

Choosing

$$v = -\left(3 + 3\sqrt[3]{2} + \frac{27}{32}\right)\xi_2 =: -\alpha_2\xi_2, \quad (32)$$

and substituting (31) into (30), it leads to

$$\mathcal{L}V_2 \leq -\kappa(\xi_1^4 + \xi_2^4). \quad (33)$$

By (28) and (32), one obtains the actual controller

$$u = -\alpha_2(\kappa x_2 + \alpha_1\kappa^2 x_1). \quad (34)$$

Defining $\|\eta\|_\Delta = (\eta_1^2 + \eta_2^2)^{1/2}$, one gets $\mathcal{L}V_2 \leq -\kappa\|\eta\|_\Delta^4$. From (22) and (24), it follows that

$$\begin{aligned} \frac{\partial V_2}{\partial \eta_1} \cdot \frac{\kappa^2}{30} v &\leq 46.7133\kappa^2\|\eta\|_\Delta^4, \\ \frac{1}{2} \frac{\partial^2 V_2}{\partial \eta_1^2} \cdot \frac{1}{25} \sin^2 \kappa\eta_2 &\leq 2\kappa^2\|\eta\|_\Delta^4. \end{aligned} \quad (35)$$

By (29), one has $\mathcal{L}V_2 \leq -\kappa(1 - 48.7133\kappa)\|\eta\|_\Delta^4$, from which one obtains $\kappa^* = 0.0205$.

In simulation, we choose the initial values $x_1(0) = 2$, $x_2(0) = -3$, and $\kappa = 0.02$. Figure 1 demonstrates the effectiveness of the state feedback controller.

6. A Concluding Remark

In this paper, the homogeneous domination approach is introduced to solve the state feedback stabilization problem for the stochastic feedforward nonlinear system (1). There still exist some problems to be investigated. One is to consider the more general switched stochastic feedforward nonlinear systems by adopting average dwell time method in [28]. Another is to consider stochastic feedforward networked or fuzzy systems (similar to [29–33]).

Acknowledgments

The authors would like to express their sincere gratitude to the editor and reviewers for their helpful suggestions in improving the quality of this paper. This work was partially supported by the National Natural Science Foundation of China (nos. 61304002, 61304003, 61203123, and 61304054), the Fundamental Research Funds for the Central Universities of China (no. 11CX04044A), the Shandong Provincial Natural Science Foundation of China (no. ZR2012FQ019), and Doctoral Start-up Fund of Bohai University.

References

- [1] M. Krstic and H. Deng, *Stabilization of Uncertain Nonlinear Systems*, Springer, New York, NY, USA, 1998.
- [2] Y. Li, "Exponential stability results of discrete-time stochastic neural networks with time-varying delays," *Mathematical Problems in Engineering*, Article ID 486257, 10 pages, 2013.
- [3] L. Liu and N. Duan, "State-feedback stabilization for stochastic high-order nonlinear systems with a ratio of odd integers power," *Nonlinear Analysis: Modelling and Control*, vol. 15, no. 1, pp. 39–53, 2010.
- [4] L. Liu and X. J. Xie, "Output-feedback stabilization for stochastic high-order nonlinear systems with time-varying delay," *Automatica*, vol. 47, no. 12, pp. 2772–2779, 2011.
- [5] L. Liu and X. J. Xie, "State-feedback stabilization for stochastic high-order nonlinear systems with SISS inverse dynamics," *Asian Journal of Control*, vol. 14, no. 1, pp. 207–216, 2012.
- [6] S. J. Liu, J. F. Zhang, and Z. P. Jiang, "Decentralized adaptive output-feedback stabilization for large-scale stochastic nonlinear systems," *Automatica*, vol. 43, no. 2, pp. 238–251, 2007.
- [7] S. J. Liu, Z. P. Jiang, and J. F. Zhang, "Global output-feedback stabilization for a class of stochastic non-minimum-phase nonlinear systems," *Automatica*, vol. 44, no. 8, pp. 1944–1957, 2008.
- [8] Y. G. Liu and J. F. Zhang, "Practical output-feedback risk-sensitive control for stochastic nonlinear systems with stable zero-dynamics," *SIAM Journal on Control and Optimization*, vol. 45, no. 3, pp. 885–926, 2006.
- [9] L. Wu, P. Shi, and H. Gao, "State estimation and sliding-mode control of Markovian jump singular systems," *IEEE Transactions on Automatic Control*, vol. 55, no. 5, pp. 1213–1219, 2010.
- [10] Z. J. Wu, X. J. Xie, and S. Y. Zhang, "Adaptive backstepping controller design using stochastic small-gain theorem," *Automatica*, vol. 43, no. 4, pp. 608–620, 2007.
- [11] X. J. Xie and L. Liu, "Further results on output feedback stabilization for stochastic high-order nonlinear systems with time-varying delay," *Automatica*, vol. 48, no. 10, pp. 2577–2586, 2012.
- [12] X. J. Xie and L. Liu, "A homogeneous domination approach to state feedback of stochastic high-order nonlinear systems with time-varying delay," *IEEE Transactions on Automatic Control*, vol. 58, no. 2, pp. 494–499, 2013.
- [13] X. Yu and X. J. Xie, "Output feedback regulation of stochastic nonlinear systems with stochastic iISS inverse dynamics," *IEEE Transactions on Automatic Control*, vol. 55, no. 2, pp. 304–320, 2010.
- [14] L. Zhang, E. K. Boukas, and J. Lam, "Analysis and synthesis of Markov jump linear systems with time-varying delays and partially known transition probabilities," *IEEE Transactions on Automatic Control*, vol. 53, no. 10, pp. 2458–2464, 2008.
- [15] C. R. Zhao, X. J. Xie, and N. Duan, "Adaptive state-feedback stabilization for high-order stochastic nonlinear systems driven by noise of unknown covariance," *Mathematical Problems in Engineering*, Article ID 246579, 13 pages, 2012.
- [16] X. Zhao, M. Ling, and Q. Zeng, "Delay-dependent robust control for uncertain stochastic systems with Markovian switching and multiple delays," *Journal of Systems Engineering and Electronics*, vol. 21, no. 2, pp. 287–295, 2010.
- [17] F. Mazenc and S. Bowong, "Tracking trajectories of the cart-pendulum system," *Automatica*, vol. 39, no. 4, pp. 677–684, 2003.
- [18] R. Sepulchre, M. Janković, and P. V. Kokotović, *Constructive Nonlinear Control*, Springer, London, UK, 1997.
- [19] N. Bekiaris-Liberis and M. Krstic, "Delay-adaptive feedback for linear feedforward systems," *Systems & Control Letters*, vol. 59, no. 5, pp. 277–283, 2010.
- [20] M. Krstic, "Input delay compensation for forward complete and strict-feedforward nonlinear systems," *IEEE Transactions on Automatic Control*, vol. 55, no. 2, pp. 287–303, 2010.
- [21] X. Ye, "Adaptive stabilization of time-delay feedforward nonlinear systems," *Automatica*, vol. 47, no. 5, pp. 950–955, 2011.
- [22] C. Qian and J. Li, "Global output feedback stabilization of upper-triangular nonlinear systems using a homogeneous domination approach," *International Journal of Robust and Nonlinear Control*, vol. 16, no. 9, pp. 441–463, 2006.
- [23] X. Zhang, L. Baron, Q. Liu, and E. K. Boukas, "Design of stabilizing controllers with a dynamic gain for feedforward nonlinear time-delay systems," *IEEE Transactions on Automatic Control*, vol. 56, no. 3, pp. 692–697, 2011.
- [24] S. Ding, C. Qian, S. Li, and Q. Li, "Global stabilization of a class of upper-triangular systems with unbounded or uncontrollable linearizations," *International Journal of Robust and Nonlinear Control*, vol. 21, no. 3, pp. 271–294, 2011.
- [25] X. Zhang, E. K. Boukas, Y. Liu, and L. Baron, "Asymptotic stabilization of high-order feedforward systems with delays in the input," *International Journal of Robust and Nonlinear Control*, vol. 20, no. 12, pp. 1395–1406, 2010.
- [26] X. Zhang, Q. Liu, L. Baron, and E. K. Boukas, "Feedback stabilization for high order feedforward nonlinear time-delay systems," *Automatica*, vol. 47, no. 5, pp. 962–967, 2011.
- [27] L. Liu and X. J. Xie, "State feedback stabilization for stochastic feedforward nonlinear systems with time-varying delay," *Automatica*, vol. 49, no. 4, pp. 936–942, 2013.
- [28] L. Zhang and H. Gao, "Asynchronously switched control of switched linear systems with average dwell time," *Automatica*, vol. 46, no. 5, pp. 953–958, 2010.
- [29] H. Gao and T. Chen, " H_∞ estimation for uncertain systems with limited communication capacity," *IEEE Transactions on Automatic Control*, vol. 52, no. 11, pp. 2070–2084, 2007.
- [30] H. Gao, T. Chen, and J. Lam, "A new delay system approach to network-based control," *Automatica*, vol. 44, no. 1, pp. 39–52, 2008.
- [31] H. Gao and T. Chen, "Network-based H_∞ output tracking control," *IEEE Transactions on Automatic Control*, vol. 53, no. 3, pp. 655–667, 2008.
- [32] H. Gao, X. Meng, and T. Chen, "Stabilization of networked control systems with a new delay characterization," *IEEE Transactions on Automatic Control*, vol. 53, no. 9, pp. 2142–2148, 2008.
- [33] X. D. Zhao, L. X. Zhang, P. Shi, and H. R. Karimi, "Novel stability criteria for T-S fuzzy systems," *IEEE Transactions on Fuzzy Systems*, vol. 21, no. 6, pp. 1–11, 2013.